An Introduction to the
Chemistry of Natural and
Engineered Aquatic Systems

WATER
CHEMISTRY

PATRICK L. BREZONIK
WILLIAM A. ARNOLD

Water Chemistry

This page intentionally left blank

Water Chemistry

An Introduction to the Chemistry of Natural
and Engineered Aquatic Systems

Patrick L. Brezonik and William A. Arnold

OXFORD
UNIVERSITY PRESS

OXFORD
UNIVERSITY PRESS

To our extended families:

Leo and Jeannette Brezonik (deceased)
Carol Brezonik
Craig and Laura
Nicholas and Lisa
and Sarah, Joe, Billy, Niko, and Peter

Thomas and Carol Arnold
Maurice and Judith Colman; Lola Arnold (deceased)
Eric and Carly Arnold
Lora Arnold
and Alex and Ben

This page intentionally left blank

Contents

Preface

In deciding whether to write a new textbook in any field, authors must answer two questions: (1) is there a need for another text in the field, and (2) how will their text be different from what is already available? It is obvious from the fact that this book exists that we answered yes to the first question. Our reasons for doing so are based on our answers to the second question, and they are related to the broad goals we set for coverage of topics in this book. Although previous introductory water chemistry textbooks provide excellent coverage on inorganic equilibrium chemistry, they do not provide much coverage on other topics that have become important aspects of the field as it has developed over the past few decades. These include nonequilibrium aspects (chemical kinetics) and organic chemistry—the behavior of organic contaminants and the characteristics and behavior of natural organic matter. In addition, most water chemistry textbooks for environmental engineering students focus their examples on engineered systems and either ignore natural waters, including nutrient chemistry and geochemical controls on chemical composition, or treat natural waters only briefly. This is in spite of the fact that environmental engineering practice and research focuses at least as much on natural systems (e.g., lakes, rivers, estuaries, and oceans) as on engineered systems (e.g., water and wastewater treatment systems and hazardous waste processing). Most existing textbooks also focus on solving inorganic ionic equilibria using graphical and manual algebraic approaches, and with a few exceptions, they do not focus on the use of computer programs to solve problems.

This book was written in an effort to address these shortcomings. Our overall goals in this textbook are to provide readers with (1) a fundamental understanding of the chemical and related processes that affect the chemistry of our water resources and (2) the ability to solve quantitative problems regarding the behavior of chemical substances in water. In our opinion, this requires knowledge of both inorganic and organic chemistry and the perspectives and tools of both chemical equilibria and kinetics. The book thus

takes a broader approach to the subject than previous introductory water chemistry texts. It emphasizes the use of computer approaches to solve both equilibrium and kinetics problems. Algebraic and graphical techniques are developed sufficiently to enable students to understand the basis for equilibrium solutions, but the text emphasizes the use of computer programs to solve the typically complicated problems that water chemists must address.

An introductory chapter covers such fundamental topics as the structure of water itself, concentration units and conversion of units, and basic aspects of chemical reactions. Chapter 2 describes the chemical composition of natural waters. It includes discussions on the basic chemistry and water quality significance of major and minor inorganic solutes in water, as well as natural and human sources and geochemical controls on inorganic ions. Chapters 3–7 cover important fundamentals and tools needed to solve chemical problems. The principles of thermodynamics as the foundation for chemical equilibria are covered first (Chapter 3), followed by a separate chapter on activity-concentration relationships, and a chapter on the principles of chemical kinetics. Chapter 6 provides basic information on the structure, nomenclature, and chemical behavior of organic compounds. Engineers taking their first class in water chemistry may not have had a college-level course in organic chemistry. For those that have had such a course, the chapter serves as a review focused on the parts of organic chemistry relevant to environmental water chemistry. Chapter 7 develops the basic tools—graphical techniques, algebraic methods, and computer approaches—needed to solve and display equilibria for the four main types of inorganic reactions (acid-base, solubility, complexation, and redox). The equilibrium chemistry and kinetics of these major types of inorganic reactions are presented as integrated subjects in Chapters 8–11.

Of the remaining eight chapters, six apply the principles and tools covered in the first 11 chapters to specific chemicals or groups of chemicals important in water chemistry: oxygen (12), disinfectants and oxidants (13), minor metals, silica, and silicates (15), nutrients (16), natural organic matter (18), and organic contaminants (19). The other two chapters describe two important physical-chemical processes that affect and sometimes control the behavior or inorganic and organic substances in aquatic systems: Chapter 14 describes how solutes interact with surfaces of solid particles (sorption and desorption), and Chapter 17 describes the principles of photochemistry and the role of photochemical processes in the behavior of substances in water.

The book includes more material and perhaps more topics than instructors usually cover in a single-semester course. Consequently, instructors have the opportunity to select and focus on topics of greatest interest or relevance to their course; we recognize that the "flavor" and emphasis of water chemistry courses varies depending on the program and instructor. Those wishing to emphasize natural water chemistry, for example, may wish to focus on Chapters 12, 15, 16, and 18 after covering the essential material in Chapters 1–11; others who want to focus on engineered systems and contaminant chemistry may want to focus more on Chapters 13, 14, and 19. Within several chapters, there also are *Advanced Topic* sections that an instructor may or may not use. With supplementary material from the recent literature, the book also may be suitable for a two-quarter or two-semester sequence.

A strong effort was made to write the text in a clear, didactic style without compromising technical rigor and to format the material to make the book inviting and accessible to students. We assume a fairly minimal prior knowledge of chemistry (one

year of general chemistry at the college level) and provide clear definitions of technical terms. Numerous in-chapter examples are included to show the application of theory and equations and demonstrate how problems are solved, and we have made an effort to provide examples that are relevant to both natural waters and engineered systems. The problems included at the end of most of the chapters generally are ordered in terms of difficulty, with the easiest problems coming first. Finally, we encourage readers to visit the book's companion Web site at www.oup.com/us/WaterChemistry, which contains downloadable copies of several tables of data, an interface for the kinetics software, Acuchem, additional problems and figures, and other useful information.

Patrick L. Brezonik and William A. Arnold
University of Minnesota
February 2010

This page intentionally left blank

Acknowledgments

Symbols and Acronyms

Symbols

[ ]	mass or molar concentration
{ }	activity
$\equiv M$	metal center attached to a solid surface
$\equiv S$	surface site
‰	parts per thousand
α_i	fraction of X_T present as species i
α_λ	beam attenuation coefficient of light at wavelength λ
β	cumulative stability (formation) constant
β	buffering capacity (Chapter 8)
β	Bunsen coefficient (Chapter 12)
γ	activity coefficient
$\gamma_\pm$	mean ionic activity coefficient of a salt
γ	interfacial energy or surface tension (Chapters 3, 14)
Δ_O	ligand field splitting parameter
Θ	temperature coefficient in kinetics
Θ_A	macroscopic binding parameter for sorbate A (Chapter 14)
κ	transmission coefficient (Chapter 5 only)
κ^{-1}	radius of ionic atmosphere (Debye parameter), and characteristic thickness of the electrical double layer
λ	wavelength
μ	chemical potential
ν	stoichiometric coefficient
ν	kinematic viscosity ($m^2\ s^{-1}$) (Chapter 12)

ν_f	fundamental frequency factor
$\overline{\nu}$	Scatchard equation variable ($= [ML/L_T]$)
ξ	extent of reaction
ρ	density
ρ	susceptibility factor (Chapter 19)
ρ_w	flushing coefficient for water in a reactor ($= Q/V$)
σ	Hammett constant
τ	characteristic time
Φ	quantum yield
Ψ_0	electrostatic surface potential
ω	electrostatic interaction factor
a_λ	light absorption coefficient at wavelength λ
a_i	activity of i
$\mathbf{a}_i$	size parameter for ion i in Debye-Hückel equation
A	preexponential or frequency factor in Arrhenius equation
at. wt.	atomic weight
at. no.	atomic number
b.p.	boiling point
c, C	concentration
c	correction factor (Chapter 19)
C_p	heat capacity
ΔC_p	change in heat capacity for a reaction
D_λ	wavelength-dependent distribution function for scattered light (Chapter 17)
D	diffusion coefficient
D	distribution coefficient (Chapter 19)
$\boldsymbol{D}$	dielectric constant (relative static permittivity)
$\boldsymbol{D}_o$	permittivity in a vacuum
D_{obs}	observed distribution coefficient (Chapter 4)
D_{theor}	thermodynamic distribution coefficient (Chapter 4)
Da	daltons (molecular weight units)
ΔE	change in internal energy
e_g	type of molecular orbital
e_{aq}^-	a hydrated electron
E°	electrical (reduction) potential under standard conditions
E_{act}	energy of activation
E_{bg}	band gap energy
$E_0(\lambda,0)$	scalar irradiance just below the water surface
esu	electrostatic units
f	fraction of a substance in a specific phase (Chapter 19)
f_i	fugacity of substance i
f_i	fragment constants for fragment i (Chapter 19)
f_{oc}	fraction of organic carbon
F	Helmholtz free energy
F	Faraday, unit of capacitance (Chapter 14)
F_1	Gran function (used in alkalinity titrations)
$\mathcal{F}$	Faraday's constant

G	Gibbs free energy
$G(\lambda)$	total irradiance (sun + sky) at the Earth's surface
G_f°	free energy of formation under standard conditions
ΔG°	change in free energy (or free energy of reaction under standard conditions)
$\Delta G^{\neq}$	free energy of activation
h	Planck's constant
H	enthalpy
H	Henry's law constant ($= K_H^{-1}$)
i	current
i_0	exchange current
I	ionic strength
$I_a(\lambda)$	(wavelength-dependent) number of photons absorbed per unit time
J	joule
kPa	kilopascals (unit of pressure)
k	Boltzmann constant (gas constant per molecule)
k_i°	molar compressibility of i
k	rate constant
K_{λ}	diffuse attenuation coefficient of light at wavelength λ
K	thermodynamic equilibrium constant (products and reactants expressed in terms of activity)
$^c K$	equilibrium constant expressed in terms of concentrations of products and reactants
K_d	solid-water partition coefficient
K_H	Henry's law coefficient ($= H^{-1}$)
K_L	gas transfer coefficient (units of length time^{-1})
K_L	Langmuir sorption constant
K_{oc}	organic carbon-water coefficient
K_{ow}	octanol-water partition coefficient
K_w	ion product of water
l	(light path) length
L_0	ultimate (first-stage) biochemical oxygen demand
m	molal concentration
M	molar concentration
M_T	total mass
m/z	mass-to-charge ratio
n	number (of molecules, atoms, or molecular fragments)
n	nuclophilicity constant (Chapter 19)
N	normality (equivalents/L)
$N(K)$	probability function for equilibrium constant K
N_A	Avogadro's number
pε	negative logarithm of relative electron activity; a measure of the free energy of electron transfer, pronounced "pea epsilon"
pH	negative logarithm of hydrogen ion activity
pH_{PZC}	pH of point of zero charge on surfaces
pH_{ZNPC}	pH of zero net proton charge
pX	negative logarithm of X
P	pressure

P	primary production (Chapter 12)
q	heat
q	charge density in diffuse layer (Chapter 14)
Q	hydraulic flow rate
r	ratio of peak areas determined via gas chromatography
R	gas constant
R	respiration (Chapter 12)
R	rate
s	substrate constant (Chapter 19)
s_λ	wavelength-dependent light-scattering coefficient
S	entropy
S	saturation ratio
Sc	dimensionless Schmidt number (kinematic viscosity/diffusion coefficient)
t_{2g}	type of molecular orbital
$t_{1/2}$	half-life
t_c	critical time (time to achieve maximum DO deficit in Streeter-Phelps model)
T	temperature
TOTX	total concentration of X in all phases of a system
U_{10}	wind velocity 10 m above the surface
V	volume
V_i°	standard molar volume for i
w, W	work
X_T	total concentration of all species of X in solution
X_{max}	maximum sorption capacity
y	amount of O_2 consumed at any time in biochemical oxygen demand test
z	depth (Chapter 17)
z, Z	charge (on an ion)
Z_{AB}	collision frequency between A and B

Acronyms

2,4-D	2,4-dichlorophenoxyacetic acid
AAS	atomic absorption spectrophotometry
ACD	Ahrland-Chatt-Davies classification system
ACP	actual concentration product
ACT	activated complex theory
AHM	aquatic humic matter
ANC	acid-neutralizing capacity (= alkalinity)
AOP	advanced oxidation process
APase	alkaline phosphatase
BCF	bioconcentration factor
BET	Brunauer-Emmet-Teller sorption equation

BNC	base neutralizing capacity
BOD	biochemical oxygen demand
BTEX	benzene, toluene, ethylbenzene, and xylene
CAS	Chemical Abstract Service
CB	conduction band
CCM	constant capacitance model
CD-MUSIC	charge distribution multisite complexation (model)
CFSTR	continuous-flow stirred tank reactor
cgs	centimeter-gram-second, system of measure
CDOM	colored (or chromophoric) dissolved organic matter
CH	carbonate hardness
COD	chemical oxygen demand
CP-MAS NMR	cross-polarization-magic angle spinning nuclear magnetic resonance (spectroscopy)
CUAHSI	Consortium of Universities for the Advancement of Hydrologic Science, Inc.
DBP	disinfection by-product
DCE	dichloroethylene
DDT	dichlorodiphenyltrichloroethane
DEAE	diethylaminoethyl (functional group)
DFAA	dissolved free amino acid
DHLL	Debye-Hückel limiting law
DIC	dissolved inorganic carbon
DLM	double-layer model
DMF	2,5-dimethylfuran
DMG	dimethylglyoxime
DO	dissolved oxygen
DOC	dissolved organic carbon
DOM	dissolved organic matter
DON	dissolved organic nitrogen
DOP	dissolved organic phosphorus
EAWAG	German acronym for Swiss Institute for Water Supply, Pollution Control, and Water Protection
EDHE	extended Debye-Hückel equation
EDTA	ethylenediaminetetraacetic acid
EfOM	effluent organic matter
EPC	equilibrium phosphorus concentration
EPICS	equilibrium partitioning in closed systems
EPI Suite	Estimation Programs Interface Suite
EXAFS	extended x-ray absorption fine structure spectroscopy
FA	fulvic acid
FFA	furfuryl alcohol
FITEQL	nonlinear data fitting program
FMO	frontier molecular orbital (theory)
FT-ICR MS	Fourier transform ion cyclotron resonance mass spectrometry
GC-MS	gas chromatography-mass spectrometry

GCSOLAR	public domain computer program to calculate light intensity and rates of direct photolysis
HA	humic acid
HAA	haloacetic acid
HAc	acetic acid
HMB	heteropoly-molybdenum blue
HMWDON	high-molecular-weight dissolved organic nitrogen
HOMO	highest occupied molecular orbital
HPLC	high-performance liquid chromatography
HRT	hydraulic residence time
HSAB	(Pearson) hard-soft acid-base (system)
IAP	ion activity product
IC	ion chromatography
ICP	inductively coupled plasma
IHSS	International Humic Substances Society
IMDA	imidodiacetic acid
IP	inositol phosphate
IR	infrared
is	inner sphere (complex)
IUPAC	International Union of Pure and Applied Chemistry
LC-MS	liquid chromatography-mass spectrometry
LED	light-emitting diode
LFER	linear free energy relationship
LFSE	ligand-field stabilization energy
LMCT	ligand-to-metal charge transfer (process)
LUMO	lowest unoccupied molecular orbital
MCL	maximum contaminant level
MEMS	microelectromechanical system
MINEQL	computer program to calculate mineral equilibria
MINEQL+	commercially available equilibrium computer program based on MINEQL
MINTEQA2	public domain computer program based on MINEQL
MW	molecular weight
NADP	National Atmospheric Deposition Program
NCH	noncarbonate hardness
NDMA	N-nitrosodimethylamine
NMR	nuclear magnetic resonance (spectroscopy)
NOM	natural organic matter
NTA	nitrilotriacetic acid
NTU	nephelometric turbidity unit
os	outer sphere (complex)
PAH	polycyclic aromatic hydrocarbon
PBDE	polybrominated diphenylether
PCB	polychlorinated biphenyl
PCDD/Fs	polychlorinated dibenzodioxins/furans
PCE	perchloroethylene or tetrachloroethylene
PCU	platinum-cobalt color unit (Hazen unit)

PES	potential energy surface
PFOA	perfluorooctanoic acid
PFOS	perfluorooctane sulfonic acid
PFR	plug-flow reactor
PON	particulate organic nitrogen
POP	persistent organic pollutant
PP	particulate phosphorus
PPC	products of proton consumption
PPCPs	pharmaceutical and personal care products
PPR	products of proton release
RPHPLC	reverse-phase high-performance liquid chromatography
S	salinity
SC	specific conductance (same as EC)
SD	standard deviation
SEC	size-exclusion chromatography
SII	specific ion interaction
SMILES	Simplified Molecular Input Line Entry System
SMP	soluble microbial products
SRFA	Suwannee River fulvic acid
SRP	soluble reactive phosphate (expressed as P)
STP	standard temperature and pressure
SUVA	specific ultraviolet absorption
TCE	trichloroethylene
TCP	2,4,6-trichlorophenol
TDP	total dissolved phosphorus
TDS	total dissolved solids
TH	total hardness
THM	trihalomethane
ThOC	threshold odor concentration
TLM	triple-layer model
TMA	trimethylamine
TNT	trinitrotoluene
TOC	total organic carbon
TON	total organic nitrogen
TP	total phosphorus
TST	transition state theory
UF	ultrafiltration
U.S. EPA	U.S. Environmental Protection Agency
USGS	U.S. Geological Survey
UV	ultraviolet
VB	valence band
VOC	volatile organic compound
WWTP	wastewater treatment plant
XANES	x-ray absorption near-edge spectroscopy

This page intentionally left blank

Units and Constants

Units for physical quantities

Fundamental quantities

Quantity	SI units
Length	meter, m
Mass	kilogram, kg
Time	second, s
Electric current	ampere, A
Temperature	Kelvin, K
Amount of material	mole, mol

Some derived quantities

Quantity	SI units
Force	newton ($kg \cdot m \cdot s^{-2}$)
Volume	cubic meters (m^3)*
Electric charge	coulomb, $C = A \cdot s$
Power	watt, $W = J \cdot s^{-1}$
Electric potential	volt, $V = W \cdot A^{-1}$
Electric resistance	ohm, $\Omega = V \cdot A^{-1}$
Conductance	Siemens, $S = A \cdot V^{-1}$

Important constants

Atomic mass unit	1.6605×10^{-27} kg
Avogadro's constant (number)	6.022×10^{23} mol^{-1}
e (the "natural" number)	2.71828
Electron charge	1.602×10^{-19} coulombs (C) or 4.803×10^{-10} esu
Electron mass	9.109×10^{-31} kg

*The liter (L) is not an SI unit but is widely used as the unit of volume in freshwater studies. $1 \text{ L} = 10^{-3} \text{ m}^3$ = 1 dm^3. Some scientific journals use SI units only and use m^3 for volumetric measurements.

Fundamental frequency, v_f (reciprocal of molecular vibration period)	6.2×10^{12} s^{-1}
Faraday, $\mathcal{F}$	96,485 C mol^{-1}
Gas constant per mole, R	8.314 J mol^{-1} K^{-1} or 1.987 cal mol^{-1} K^{-1}
Gas constant per molecule, **k**, called the Boltzmann constant	1.3805×10^{-23} J K^{-1}
Gravitation constant (of the Earth)	9.806 m s^{-2}
Melting point of water	0°C or 273.15 K
Molar volume of an ideal gas at 0°C and 1 atm	22.414 L mol^{-1} or 22.414×10^3 cm^{-3} mol^{-1}
Molecular vibration period	1.5×10^{-13} s
Permittivity of a vacuum, ε_0	8.854×10^{-12} J^{-1} C^2 m^{-1}
π	3.14159
Planck's constant, h	6.626×10^{-34} J s
Relative static permittivity of water, **D**, also called the dielectric constant)	80 (dimensionless) at 20°C
Speed of light (in a vacuum), c	2.998×10^8 m s^{-1}

Conversion Factors

Energy-related quantities

1 newton (unit of force) $= 1 \text{ N} = \text{kg m s}^{-2}$

1 joule (unit of energy) $= 10^7 \text{ erg} = 1 \text{ N m} = \text{kg m}^2 \text{ s}^{-2} = 1$ volt coulomb (V C) $=$
    0.239 calories (cal) $= 9.9 \times 10^{-3} \text{ L atm}^{-1} = 6.242 \times 10^{18} \text{ eV}$

1 cal $= 4.184 \text{ J}$

1 watt $= 1 \text{ kg m}^2 \text{ s}^{-3} = 1 \text{ J s}^{-1} = 2.39 \times 10^{-4} \text{ kcal s}^{-1} = 0.86 \text{ kcal h}^{-1}$

1 entropy unit $= 1 \text{ cal mol}^{-1} \text{ K}^{-1} = 4.184 \text{ J mol}^{-1} \text{ K}^{-1}$

Pressure

1 atm $= 760 \text{ mm Hg} = 1.013 \times 10^5 \text{ Pa}$ (pascals) $= 1.013$ bars

1 mm Hg $= 1$ torr

1 Pa $= 10^{-5} \text{ bars} = 1 \text{ N m}^{-2}$

Some useful relationships

RT ln x $= 2.303 \text{RT log x} = \textbf{5.709 log x}$ (kJ mol^{-1}) $= 1.364 \text{ log x}$ (kcal mol^{-1}) at 25°C
    (298.15 K)

(RT/F) ln x $= 2.303 \text{RT/F log x} = \textbf{0.05916 log x}$ (V at 25°C, or 59.16 mV at 25°C)

This page intentionally left blank

Water Chemistry

This page intentionally left blank

I

Prologue

This page intentionally left blank

1

■■ Introductory Matters

■■ Objectives and scope of this chapter

This chapter sets the stage for the rest of the book by addressing four main topics. First, a brief introduction to the history of water chemistry and its relationship to other branches of environmental chemistry provides context for the topics treated in this book. Second, a description of the unique properties of water and their relationship to its molecular and macroscopic structure provides an appreciation for the complexity of the medium that supports the chemistry we wish to understand. Third, many different units—some common, some standard chemical units, and some unique to environmental engineering and chemistry—are used to report concentrations of chemicals in water. We introduce these units and show how to use them and make interconversions among them as a first step in describing the chemistry of water quantitatively. Finally, we introduce the major types of chemical reactions occurring in natural and engineered water systems and briefly describe the kinds of equations used to quantify the equilibrium conditions to which they tend and rates at which they occur.

■■ Key concepts and terms

- The "overlapping neighborhoods" of water chemistry, geochemistry, biogeochemistry, soil chemistry, and many other branches of the environmental sciences
- The unique and extreme physical-chemical properties of water
- Liquid water as a structured fluid caused by extensive hydrogen bonding to form water "clusters"

- Common mass units of concentration: parts per million (ppm) and parts per billion (ppb); milligrams per liter (mg/L), micrograms per liter (μg/L)
- Chemical concentration units: moles/liter (molarity, M), moles/kilogram of water (molality, m), equivalents/liter, normality (N), mole fraction
- Concentration units unique to water chemistry: mg/L as $CaCO_3$; mg/L as N, P, Cl, or other elemental (atomic) components of ions and molecules
- Associative reactions: acid-base, solubility (precipitation and dissolution), complex formation and dissociation
- Redox processes: oxidation as a loss of electrons; reduction as a gain in electrons
- Sorption: a phase-transfer process
- Gas transfer and Henry's law

1.1   Origins and scope of water chemistry

As a recognized field of inquiry, water chemistry developed in the mid-twentieth century (late 1950s and early 1960s) at the dawn of the "environmental era." Its origins as subareas of specialization in many other disciplines date back, however, to the early twentieth century and even before. For example, the chemical composition of lakes and the oceans has been of interest to limnologists and oceanographers since the early development of those sciences in the late nineteenth century. Similarly, geochemists long have been interested in the composition of natural waters, in addition to long-standing interests in the composition of geosolids. Water chemistry also was a significant component of the field of environmental engineering (or sanitary engineering, as it was known prior to about 1960), in part because of the important role of chemical processes in drinking water treatment. In all these examples, however, chemistry played a supporting rather than a central role. Analytical and descriptive aspects of chemistry were the prime considerations, and chemistry was viewed primarily as a *tool* to be used by scientists and engineers in the above disciplines rather than a subject worthy of intellectual inquiry in its own right.

One of the seminal papers in the transformation of water chemistry from its supporting role in science to a science having its own intellectual merit is "The Physical Chemistry of Seawater,"[1] written in 1960 by Lars Gunner Sillen (1916–1970), a prominent inorganic coordination chemist from Sweden. In this paper Sillen examined the geochemical origins of seawater and insightfully described the chemistry of seawater as resulting from a "geotitration" of basic rocks by volatile acids, such as carbon dioxide and acids from volcanic emissions. This descriptive model led to many other articles on the geochemical origins of natural waters and to the long-held interests of aquatic chemists and geochemists in chemical models[2] and weathering processes.[3] Sillen's paper also described the "speciation" of a wide variety of metal ions in seawater—that is, the nature of the chemical complexes in which they occur in seawater. Those ideas led to many further studies to quantify and explain the chemical composition of natural waters, and these efforts ultimately resulted in the development of computer codes used to calculate chemical speciation in complicated aquatic systems.

At the same time, the field of environmental engineering was evolving from its narrower predecessor field, sanitary engineering, which had been focused on

drinking water and wastewater treatment, to encompass the broader goals of understanding environmental *systems* (including atmospheric and terrestrial components) and developing the technical tools to manage, protect, and, where necessary, restore environmental quality. Leaders of this emerging field realized that a more fundamental scientific approach was needed to develop the understanding needed to provide sound scientific underpinnings for environmental policy and management. To the considerable extent that the field of water chemistry was developed by scientists and engineers working in or associated with environmental engineering programs, these considerations also played an important role in developing the new science of water chemistry. Academic programs initiated around 1960, like the ones led by Werner Stumm (see Box 1.1) at Harvard University and G. Fred Lee at the University of Wisconsin, espoused a fundamental approach to water chemistry that emphasized scientific rigor and quantitative approaches, involving the two cornerstones of physical chemistry—thermodynamics and kinetics. These programs also emphasized the commonality of chemical principles across all kinds of natural and engineered water systems and forged links with marine chemists, limnologists, soil chemists, and scientists in other related fields. Thus, water chemistry is linked to a wide range of earth and environmental sciences (Figure 1.1). Moreover, a multidisciplinary perspective that includes the principles of chemistry but is not limited to them is now understood to be essential for a holistic understanding of the *biogeochemical* processes that affect the composition of aquatic environments.

No field of science can exist for long without an organizing framework articulated in a textbook. Building upon an important foundation provided by an earlier geochemistry text by Garrels and Christ,[4] Stumm and Morgan provided this broad perspective in 1970 in the first text of the field, *Aquatic Chemistry*.[5] Through three editions, the most recent published in 1996, *Aquatic Chemistry* continued to set a high standard for the field. In the sense of being quantitative and focused on both understanding systems *and* solving problems, the text has an engineering orientation, but it also provides a multidisciplinary approach to understanding the chemistry of water in natural and engineered environments. Several other textbooks, modeled to greater or lesser extents after Stumm and Morgan's text, have been published over the past quarter century.[6–11] Some provide a more didactic approach suitable for students with limited academic backgrounds in chemistry,[6,11] and all focus mostly (or exclusively) on inorganic equilibrium chemistry.

In contrast to the focus of water chemistry textbooks on inorganic and equilibrium chemistry, as the field itself has continued to develop and mature, increasing emphasis has been placed on two other major subjects: (1) the kinetics of chemical reactions—natural waters as *dynamic* systems, and (2) the behavior of organic compounds that contaminate natural waters as a result of their production and use by humans. The list of such compounds is too long to enumerate, but categories of current interest include pesticides, polyhalogenated aromatic compounds, chlorinated solvents, polycyclic aromatic hydrocarbons, and more recently, a variety of pharmaceuticals, antibiotics, personal care products, and perfluorinated compounds. Despite the importance of these contaminants for water quality and ecosystem health and the massive amounts of research undertaken for more than 40 years by environmental engineers and scientists to understand the behavior, fate, and effects of these compounds, the book

Box 1.1   Werner Stumm

Werner Stumm (1924–1999) is widely considered to be the founding father of water chemistry. His contributions to the development of the field are both broad and deep, not only in terms of the span of his research contributions, but equally important as the mentor of many students who became leaders in the field and his authorship (with James Morgan, his first Ph.D. student) of the important textbook *Aquatic Chemistry* (1970). Stumm was born in Switzerland and received his Ph.D. in inorganic chemistry from the University of Zurich in 1952 under G. Schwarzenbach, a coordination chemist who pioneered in the use of complexing agents (e.g., EDTA) in analytical chemistry. Stumm spent 15 years at Harvard University (1956–1970), where he developed a strong research and teaching program, mentoring many of the future leaders of water chemistry and environmental engineering. He returned to Switzerland in 1970 as a professor at the Swiss Federal Institute of Technology and Director of EAWAG, the Swiss Institute for Water Supply, Pollution Control, and Water Protection, which he led until his retirement in 1992. Under his direction, EAWAG became the preeminent research institute for aquatic sciences in the world, recruiting outstanding scientists and engineers to its staff and attracting numerous scientists for sabbatical visits. Stumm's approach to aquatic chemistry was fundamental and multidisciplinary. He emphasized molecular-level studies and application of the principles of physical chemistry to develop both an understanding of chemical processes in natural systems and science-based applications in water technology. Stumm emphasized an ecosystem perspective that integrates the understanding of chemical, geochemical, biological, and physical processes occurring within aquatic systems. He was the author, coauthor, or editor of 300 research publications and 16 books during his illustrious career, and his research spanned most of the field of water chemistry: ionic equilibria, kinetics of iron and manganese oxidation, corrosion chemistry, coagulation and flocculation processes, evolution of the chemical composition of natural waters, phosphorus cycling and eutrophication, acid rain and its effects of chemical weathering and lake chemistry, and chemical processes at water-solid interfaces (aquatic surface chemistry). He received many awards during his life, including honorary doctorates, the Tyler Prize, Stockholm Water Prize, and the Goldschmidt Medal.
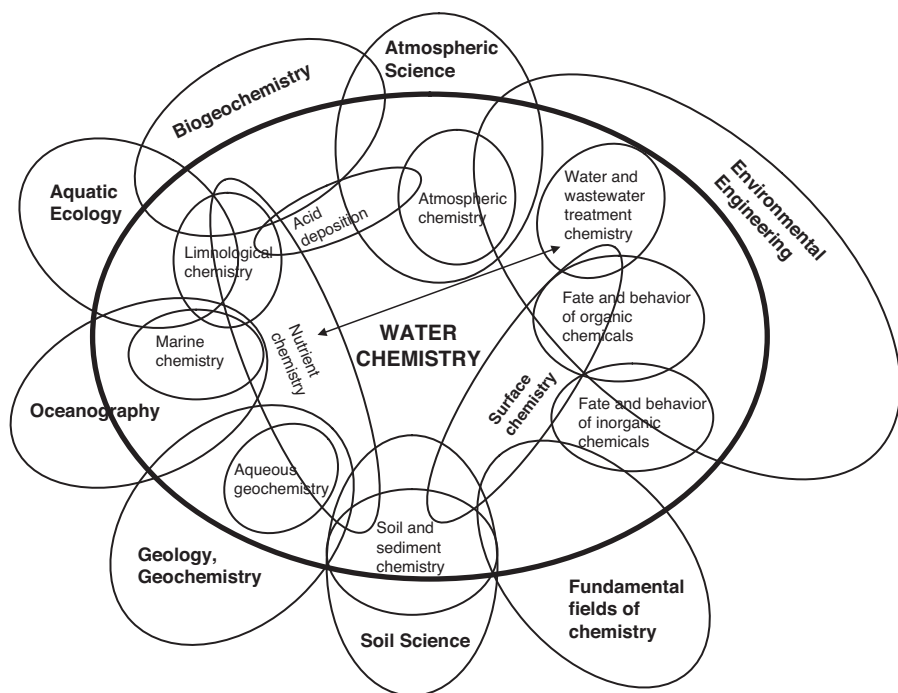
Figure 1.1 Overlapping neighborhoods of the subfields in water chemistry and related disciplines. The size of the ovals is not intended to indicate the importance of a given subfield or discipline, and the extent (or lack) of overlap of ovals reflects drawing limitations more than the extent of concordance among subfields and disciplines. In the interest of clarity, not all active and potential interactions are illustrated; the double-headed arrow shows one obvious interaction not otherwise indicated in the diagram—between nutrient chemistry and environmental engineering and its subfield of water/wastewater treatment.

by Schwarzenbach et al.[12] is the only comprehensive text on the environmental aquatic chemistry of organic contaminants (although a few earlier books and monographs dealt with components of the subject).

By design, the scope of the present book is broader than other introductory water chemistry texts. As described above, environmental organic contaminant chemistry is a major focus of research in water chemistry and environmental engineering, and a substantial fraction of professional practice in these fields involves cleanup or remediation of sites degraded by organic chemicals. Consequently, the authors believe it is important for an introductory textbook on water chemistry to cover this subject matter and to describe the types of chemical reactions, including photochemical processes, whereby such compounds are transformed in aquatic environments. Similarly, because water chemistry has expanded beyond its origins in equilibrium chemistry, we cover the principles of chemical kinetics in some detail and devote significant portions of the text to describing the rates at which processes occur in water, as well as the equilibrium conditions toward which they are headed.

1.2   Nature of water

Water is by far the most common liquid on the Earth's surface, and its unique properties enable life to exist. Water is usually regarded as a public resource—a common good—because it is essential for human life and society. However, water also is an economic resource and is sold as a commodity, and water rights in the American West are continuous source of conflict. Beyond these perspectives, water holds a special place in human society. It is not an exaggeration to speak of its mystical and transcendent properties. Water has spiritual values in many cultures and is associated with birth, spiritual cleansing, and death. The fact that about 70% of the Earth's surface is covered by water and only 30% by land makes one wonder whether "Planet Earth" more properly might be named "Planet Water." For chemists, water is a small, simple-looking, and common molecule, H_2O, but they also know it has many unusual and even unique properties, as discussed below. For civil engineers, water is a fluid to be transported via pipes and channels, and when it occurs in rivers and streams, it is viewed partly as an obstacle to transportation, for which bridges need to be designed and constructed, and partly as an energy-efficient means of transportation and shipping. Scientists in many other disciplines have their own viewpoints about water that reflect how it interacts with their science.

Water is the medium for all the reactions and processes that comprise the focus of this book. In this section we focus on the properties of water itself. We then describe its molecular structure and show how that structure leads to the macroscopic structures of liquid, solid and gaseous water and their unusual physicochemical properties.

Compared with other small molecules, water has very high melting and boiling point temperatures:[13]

Compound	Formula	Mol. wt.	Freezing pt., °C	Boiling pt., °C
Methane	CH_4	16	−182.5	−161.6
Ammonia	NH_3	17	−77.7	−33.3
Water	H_2O	18	0	100
Carbon monoxide	CO	28	−205	−191.5
Nitric oxide	NO	30	−163.6	−150.8

Moreover, as Figure 1.2 shows, water does not follow the trend of decreasing melting and boiling points with decreasing atomic weight shown by the other Group VI hydrides.

Among common liquids, water has the highest heat capacity, heat conduction, heats of vaporization and fusion, and dielectric constant (or "relative static permittivity"); see Table 1.1. The latter characteristic measures the attenuation rate of coulombic forces in a solvent compared to attenuation in a vacuum, and it is important for the dissolution of salts in water. The high dielectric constant of water permits like-charged ions to approach each other more closely before repulsive coulombic forces become important than is the case in solvents with low dielectric constants. Consequently, it is a key property enabling water to be such a good solvent for salts.

In general, the unusual physical properties of liquid water reflect the fact that water molecules do not behave independently. Instead, they are attracted to each other and to many solutes by moderately strong "hydrogen bonds." The hydrogen bonds in ice and
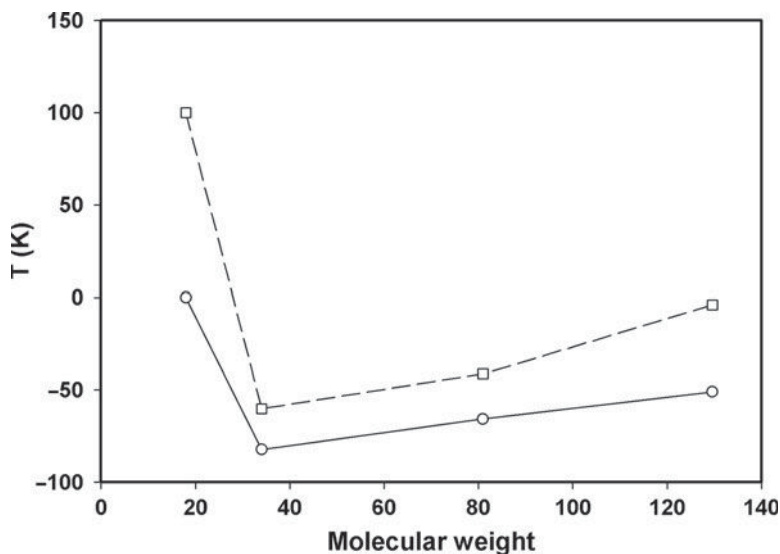
Figure 1.2 Trends in melting point (solid line) and boiling point data[13] for the Group VI hydrides.

liquid water, $\sim$21 kJ/mol,[14] are much weaker than the O-H bond of water (464 kJ/mol), but they are stronger than London-van der Waals forces ($<$ 4 kJ/mol). In addition, the hydrogen bonds in water are stronger than those in NH_3 (13 kJ/mol) but much weaker than those in HF (155 kJ/mol). The differences in H-bonding strengths among these molecules can be explained in terms of the electronegativity of the non-H atom. The importance of hydrogen bonds in promoting structure in ice and water is enhanced by the fact that water has two hydrogen atoms and two pairs of electrons on oxygen, thus allowing each water molecule to have a potential of four hydrogen bonds. In contrast, each HF can have only three bonds (because each HF has only one hydrogen atom), and the importance of hydrogen bonding in NH_3 is lessened by the fact that the N atom has only one pair of electrons available to form such a bond.

Hydrogen bonding is a consequence of the basic molecular structure of water. The angle between the two O–H bonds (105°) in water is greater than the 90° expected for perpendicular p-orbitals (Figure 1.3). This is caused by repulsion between the hydrogen atoms and indicates that there is some hybridization of the s and p orbitals in the electron shell of the oxygen atom. Oxygen's four remaining valence electrons occupy two orbitals opposite the hydrogen atoms in a distorted cube arrangement. This explains the molecule's large dipole moment. These electron pairs attract hydrogen atoms of adjacent water molecules and form hydrogen bonds with lengths of 1.74 angstroms (measured in ice by x-ray diffraction), which leads to the three-dimensional structure found in ice and liquid water.

The structure of ice is known with great accuracy.[14] Ice-I_h, the form that occurs under environmental conditions, has a structure in which each water molecule is surrounded by the oxygen atoms of four adjacent water molecules in a tetrahedral arrangement (Figure 1.4). Extending this arrangement in three dimensions gives rise to a fairly

Table 1.1 Physical properties of water[*]

Property	Value	Comparison with other liquids	Environmental importance
State at room temperature	Liquid	Rather than a gas like H_2S and H_2Se	Provides medium for life
Heat capacity (specific heat)	1.0 cal/g°C 4.18 J/g°C	Very high	Moderates climate
Latent heat of fusion 330 J/g	79 cal/g	Very high	Moderating effect; stabilizes air temperatures
Latent heat of Evaporation	540 cal/g 2257 J/g	Very high	Moderating effect; important in hydrology for precipitation-evaporation balances
Density	1.0 g/cm³ at 4°C	High; anomalous maximum at 4°C	Causes freezing to occur from air-water surface; controls temperature distribution and water circulation in lakes and oceans
Surface tension	72.8 dyne/cm at 20°C 72.8 mN/m	Very high	Affects adsorption, wetting, and transport across membranes
Dielectric constant[§]	80.1 at 20°C (dimensionless)	Very high	Makes water a good solvent for ions; shields electric fields of ions
Dipole moment	1.85 debyes	High compared with organic liquids	Cause of above characteristics and solvent properties of water
Viscosity	1.0×10^{-3} Pa·s 1 centipoise (cP) at 20°C	2–8 × higher than organic liquids	Slows movement of solutes
Transparency	High	Especially in midvisible range	Allows thick zone for photosynthesis and photochemistry
Thermal conductivity	0.6 W m^{-1} K^{-1}	High compared with organic liquids	Critical for heat transfer in natural and engineered systems

[*] Adapted from Horne.[14]
[§] Also called relative static permittivity.
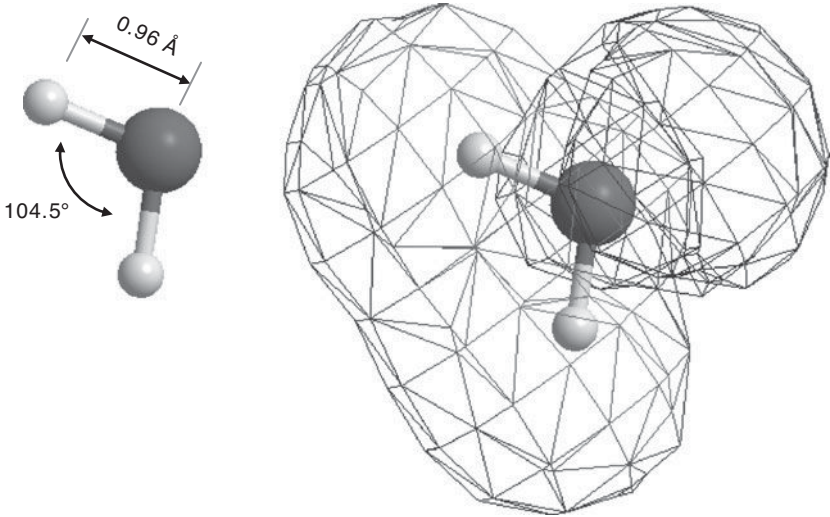
Figure 1.3 H-O bond angle and lengths in the H_2O molecule (left) lead to high polarity of the molecule with the hydrogen atoms (right: positive, light gray mesh) on one side and the unshared electron pairs (right: negative, dark gray mesh) on the opposite side. (See color insert at end of book for a color version of this figure.)
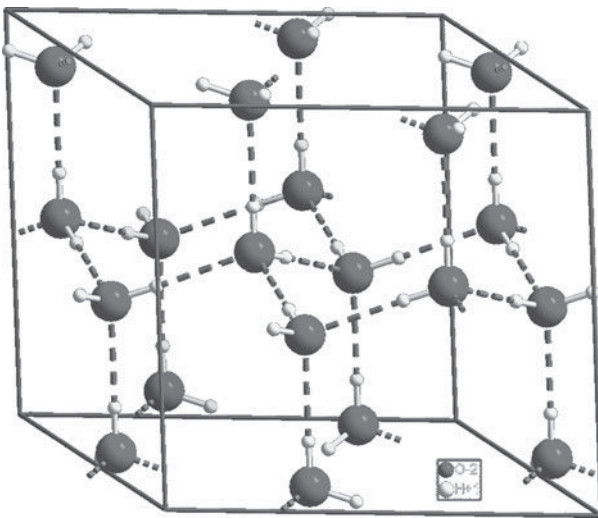
Figure 1.4 Tetrahedral arrangement of hydrogen-bonded water molecules in ice leads to an open hexagonal ring structure in crystalline ice-I_h. Source: Wikimedia Commons, file Hex ice.GIF (public domain). (See color insert at end of book for a color version of this figure.)

open—i.e., low-density—crystalline structure of repeating hexagonal rings (hence the subscript h in I_h), each of which contains six water molecules. The density of ice calculated from measured bond lengths and the three-dimensional structure agrees with the measured density of ice.

    In contrast to the rigid crystalline structure of ice, gaseous water has no structure beyond that of the individual water molecules themselves, except for occasional,

ephemeral dimers. In the gas phase, each water molecule behaves independently, and when two water molecules collide, they do not stick together but simply bounce off each other and continue their independent existences.

The degree of structure in liquid water is intermediate between crystalline ice and the absence of structure in gaseous water. Models of the structure of water must account for the properties in Table 1.1, which suggest that water is a structured medium, and variations in these properties with temperature. The higher density of water than ice and the density maximum at 4°C also must be explained. The heat of fusion of ice (330 J/g)—the energy required to convert ice at 0°C to liquid water at 0°C—suggests that only ~15% of the hydrogen bonds in ice are lost upon melting. In addition, studies using a variety of methods have reported that the average molecule in liquid water participates in ~3.6 hydrogen bonds. The structure of water has been a subject of inquiry for many years, and many models have been proposed, including a "relic ice" model and another in which water molecules exist in a clathrate or cagelike structure.[14]

The flickering-cluster model described by Frank and Wen[15] in 1957 became widely accepted as a reasonable if not exact description for the structure of liquid water. According to this model, water molecules form clusters of hydrogen-bonded molecules of indeterminate structure (Figure 1.5). The clusters have very short lives ($\sim 10^{-10}$ s) and are constantly forming and disintegrating with thermal fluctuations at the microscale. Although the lifetime of clusters may seem trivially short, it is about a thousand times longer than the time between molecular vibrations ($\sim 10^{-13}$ s), and clusters thus have a real, if very ephemeral, existence. Because of dipole effects on individual water molecules, the formation of hydrogen bonds is a cooperative phenomenon, and formation of one bond facilitates formation of the next. Consequently, rather large clusters are formed. The average cluster has 65 molecules at 0°C but only 12 at 100°C. Because the number of clusters increases with temperature, the fraction of molecules in clusters
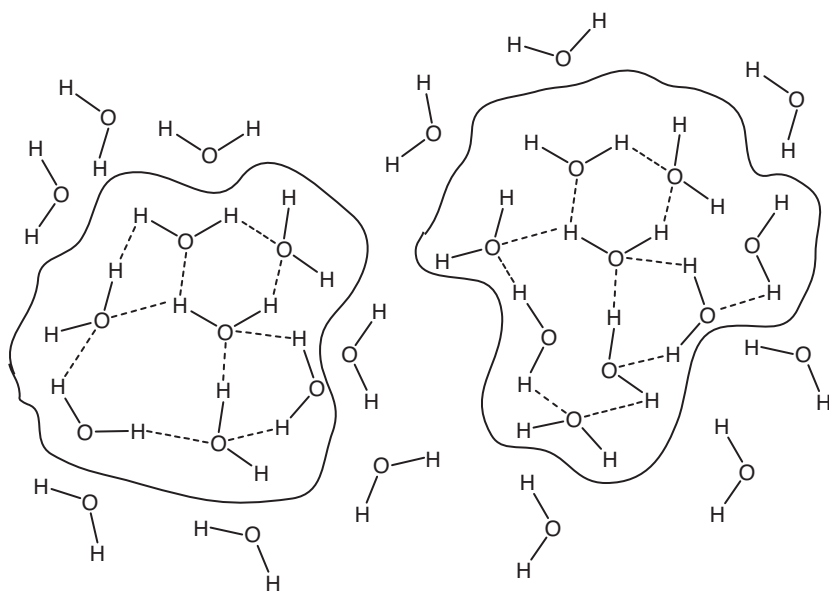

Figure 1.5 The flickering cluster model of liquid water.

decreases much more slowly (from ∼75% at 0°C to ∼56% at 100°C).[14] Unclustered water is considered to be "free."

Frank and Wen did not propose a specific structural arrangement for water in clusters. According to Stillinger,[16] liquid water consists of a random, macroscopic network of hydrogen bonds. The anomalous properties of water are thought to arise from a competition between the relatively bulky ways of connecting molecules via the ideal tetrahedral angles arising from the structure of water molecules and more compact arrangements that have more bond strain and broken bonds. The alternatives should be considered as a continuum of structural possibilities. However, some structures can be ruled out by experimental evidence. For example, if the clusters were relic ice structures, the polygons formed by hydrogen bonding would reflect the hexagonal structure of ice and contain an even number of molecules. It can be shown that breaking a hydrogen bond in the three-dimensional hexagonal ring structure of ice yields a 10-membered ring; loss of a second hydrogen bond yields a 14-membered ring. According to Stillinger,[16] the frequency distribution of polygon sizes in water shows no evidence for rings from relic ice structures, and the most common polygons found in molecular dynamics simulations (five-member rings) are not possible products of ice-I_h.

Although the larger scale structure of clustered water is not specified by the Frank-Wen model, recent molecular dynamics modeling[17] and measurements by femtosecond IR spectroscopy and x-ray absorption spectroscopy[18] suggest that much less extensive hydrogen bonding occurs in liquid water than previously thought. Although earlier molecular dynamics simulations predicted ∼3.3–3.6 hydrogen bonds per water molecule, which agrees with estimates based on the low heat of fusion of ice, recent studies suggest an average of 2.2 ± 0.5 H-bonds (one donating and one accepting) per water molecule at 25°C and 2.1 ± 0.5 bonds at 90°C. The smaller number of H-bonds was reconciled to the small heat of fusion of ice by quantum mechanical calculations indicating that the H-bonds in the proposed configuration are stronger than those in the tetrahedral (four-fold H-bonding) configuration, such that the larger number of weak or broken H-bonds in liquid water causes only a small change in energy. It is likely that the last word has not yet been written on this topic.

Addition of solutes to pure water distorts its general structure. The nature of the interactions between solutes and solvent water depends on whether the solute is a cation, anion, or nonelectrolyte. Solvation of cations results in relatively tight binding of water molecules in the "primary sphere of hydration" (Figure 1.6). Water molecules in the hydration sphere no longer act as solvent molecules, and tight binding results in a loss of volume compared to water in the bulk solvent; this phenomenon is known as **electrostriction**. In some models, unstructured transition zones exist between hydrated ions and the clustered water in the rest of the solvent. In contrast to cations, anions are not solvated and instead occupy interstices or "holes" in the overall solvent structure. Changes in viscosity upon addition of salts to water are used to infer changes in the degree of solvent structure. Most salts are "structure-makers" that increase viscosity, but a few salts (e.g., KCl and $CaSO_4$) are structure-breakers that decrease viscosity. It is interesting to note that the viscosity of pure water[19] (Figure 1.7) and aqueous salt solutions[20] generally decreases with increasing pressure, reaching a minimum value at pressures of ∼400–800 kg/cm^2 (depending on salt content and temperature). Viscosity then increases if pressure continues to increase. Horne[14] explained this phenomenon as resulting from a breakdown in the cluster structure of water as pressure increases such that the unclustered water molecules are arranged more compactly than occurs in
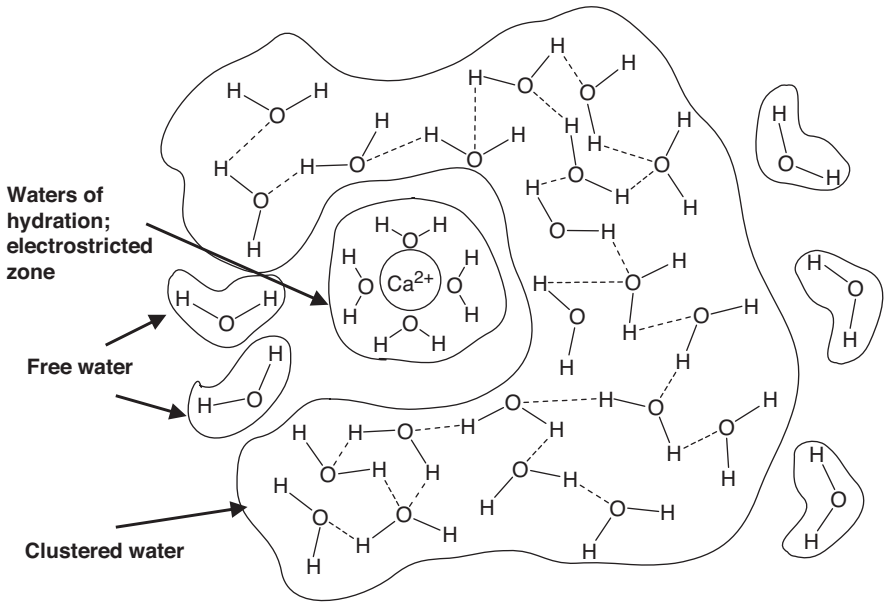
Figure 1.6 Cation hydration leads to an "electrostricted zone" surrounded by clustered and free water.
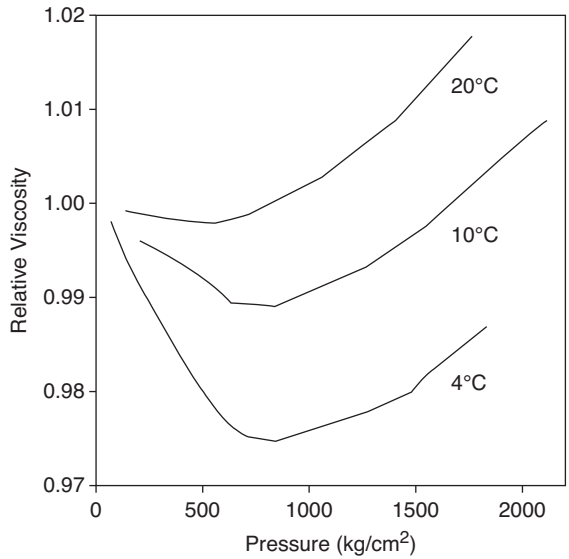
Figure 1.7 Relative viscosity of pure water versus pressure. Drawn from data in Horne and Johnson.[19]
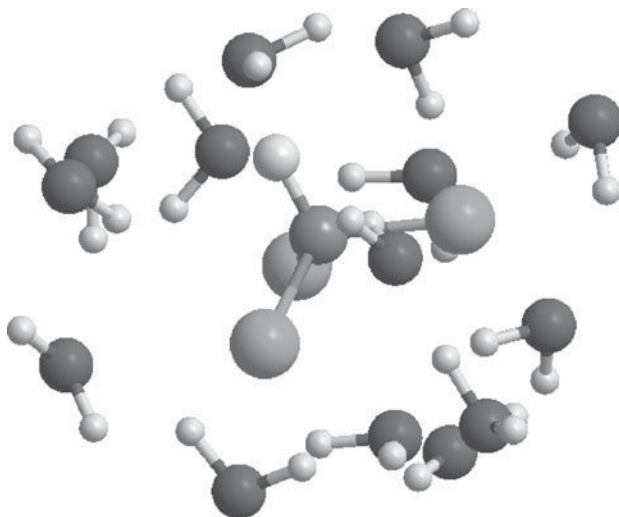
Figure 1.8 Structure of an organic (nonpolar) solute, chloroform, in liquid H_2O computed by energy minimization with MM2 force field in ChemBio3D Ultra 12.0. (See color insert at end of book for a color version of this figure.)

the cluster state. Once the cluster structure is lost—at the viscosity minimum—further increases in pressure pack the water molecules more tightly, and viscosity increases because of increasing friction as the molecules move past each other.

Nonpolar solutes also reside in the interstices between water clusters (Figure 1.8), with water molecules surrounding the solute maintaining their hydrogen bonds.[21] Overall, this may promote structure in liquid water and limit the freedom of the organic molecule as well.[12] Consequently, nonpolar solutes have high negative entropies of solution (see Chapter 3 for a description of the concept of entropy). Water molecules at the air-water interface all are oriented with the oxygen atoms facing the interface and the hydrogen atoms facing the solution (Figure 1.9). This distorts the three-dimensional structure of clustered water in the bulk solution, and as a result, the interfacial region has somewhat different physical properties from bulk water. The highly ordered arrangement of water molecules at the air-water interface also explains the high surface tension of water (surface tension defines the energy needed to break the surface). An analogous situation occurs at solid-water interfaces. Water in the first few molecular layers from a solid-water interface has different physical properties (e.g., low dielectric constant) from the bulk solution. This has important implications for the behavior of solutes at interfaces, as discussed in Chapter 14.

1.3 Concentration units

1.3.1 Introduction

A variety of units are used to express concentrations of substances dissolved or suspended in natural waters. This situation reflects the diversity of substances in these systems, the
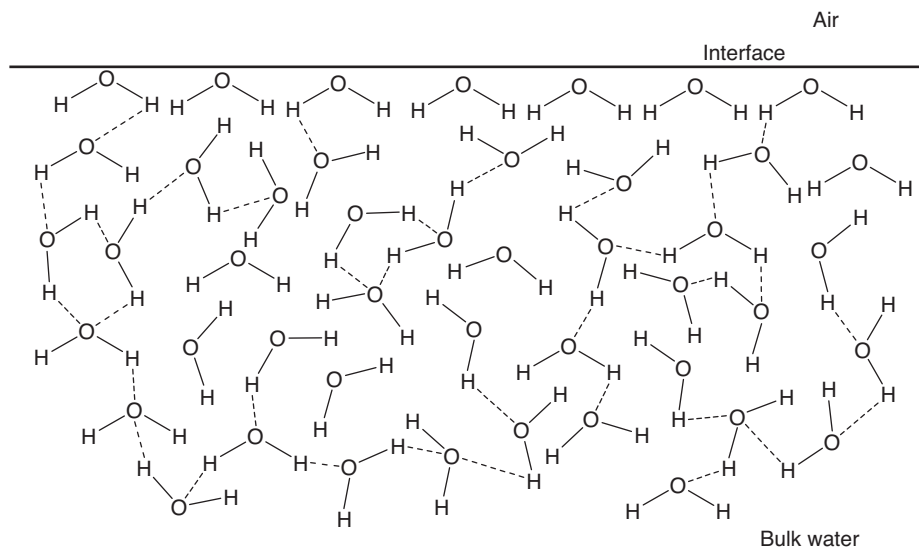
Figure 1.9 The structure of liquid water is perturbed near interfaces, as the O atoms orient toward the interface.

wide range of concentrations at which they are found, and the multidisciplinary origins of water chemistry. An important first step in studying the chemistry of natural waters is to learn about the different concentration units and how they are related to each other.

In general, concentrations of substances in water can be expressed in two principal ways: mass per unit volume of solution and mass per unit mass of water. Mass/volume units more accurately reflect the way that we prepare and analyze solutions, i.e., based on a certain volume of solution rather than a certain weight, but they have the disadvantage of being slightly temperature dependent—because the density (mass per volume) of water varies with temperature. In contrast, mass/mass concentrations are temperature invariant. For accurate work one should express mass/volume concentrations at a standard temperature, but for routine purposes, the differences caused by temperature usually can be ignored. Volumetric glassware is calibrated to contain the nominal volume at 20°C. In either mass/volume or mass/mass units, the mass of solutes and water may be expressed in common units (normally metric or SI units) or chemical units, as described in the following sections.

1.3.2 Common units of concentration

Both mass per unit volume of solution (mass/volume) and mass per unit mass of solvent (mass/mass) are used widely, often interchangeably, to express concentrations of dissolved and suspended substances in water (Table 1.2). For major ions in freshwater, the most convenient mass/volume unit is mg/L because major ions generally occur in the range of a few mg/L to a few hundred mg/L. The corresponding mass/mass unit is parts per million (ppm). For practical purposes, the terms are interchangeable for freshwater

Table 1.2 Common concentration units used in water analysis

Mass/volume	Symbol	Multiple of g	Equivalent mass/mass unit*	Substances for which units are used
Gram/liter	g/L	1	Part per thousand, ppt (%)	Major ions in brackish water and seawater
Milligram/L	mg/L	10^{-3}	Part per million, ppm	Major ions in freshwater
Microgram/L	μg/L	10^{-6}	Part per billion, ppb	Nutrients, minor and trace metals, many organic contaminants
Nanogram/L	ng/L	10^{-9}	Part per trillion†	Trace organic pollutants and some trace metals
Picogram/L	pg/L	10^{-12}	Not used	Ultratrace contaminants, e.g., methylmercury
Femtogram/L	fg/L	10^{-15}	Not used	Not commonly used

* This direct conversion is possible only because the density of water is 1, and so 1 L = 1 kg. This direct relationship does not hold for other solvents.
† To avoid ambiguity, the abbreviation "ppt" should not be used; ppt has been used for parts per thousand by marine scientists for many decades.

because 1 mg $= 10^{-3}$ g and 1 liter of water $= 1$ kg (10^3 g); for solutions in other solvents, see Example 1.1. Thus, we can write

1 mg of substance in 1 L of water $\times$ 1 L water/1 kg water $=1$ mg substance/1 kg water

or

$$1 \text{ g substance}/10^6 \text{ g water } = 1 \text{ part per million.}$$

This assumes that the dissolved substance does not affect the density of the water or contribute a significant amount to the total mass. If that were the case, the equivalency of mg/L and ppm no longer would hold. The salt content of seawater is sufficient for there to be a slight difference between concentrations expressed in mg/L of solution and concentrations expressed in ppm, and the differences become more pronounced in hypersaline waters (see Example 1.2). Many substances of interest in aquatic systems occur at concentrations much less than 1 mg/L, and the major ions of seawater and brines occur at much greater concentrations. Consequently, a series of concentration units are used, as shown in Table 1.2. Also, as analytical capabilities have enhanced our ability to detect and measure ever lower concentrations of inorganic ions and organic compounds in water, use of mass/volume units with the prefixes micro-, nano-, and pico- have become increasingly common. Mass/mass units generally are not used for concentrations of trace and ultratrace contaminants. Because of ambiguities associated with such terms as trillion, quadrillion, and even billion,* their use in expressing concentrations should be avoided.

*A "billion" in the United States is a thousand million (10^9), but a billion in Europe is a million million (10^{12}).

EXAMPLE 1.1 Conversion between mass/volume and mass/mass units: You have 1 ppb standards of the pesticide alachlor in water and in hexane ($\rho = 0.66$ g/mL). What is concentration of each standard in μg/L?

Answer: For water, the answer is straightforward:

$$1 \text{ ppb} = \frac{1 \text{ } \mu\text{g alachlor}}{kg \text{ water}} \times \frac{1 \text{ kg water}}{1 \text{ L water}} = \frac{1 \text{ } \mu\text{g alachlor}}{\text{L water}}$$

For hexane, the density alters the answer:

$$1 \text{ ppb} = \frac{1 \mu\text{g alachlor}}{\text{kg hexane}} \times \frac{0.66 \text{ kg hexane}}{1 \text{ L hexane}} = \frac{0.66 \text{ } \mu\text{g alachlor}}{\text{L hexane}}$$

1.3.3 Chemical units

Use of chemical units to express solute concentrations is becoming more widespread in aquatic sciences, especially in limnology and oceanography, but also in environmental engineering. The fundamental mass/volume unit is ***molarity*** (moles of solute per liter of solution), abbreviated mol/L or M (but never M/L):

$$\begin{aligned}
\textit{Molarity} \text{ (M)} &= \frac{\textit{grams of solute}}{\textit{g formula wt.} \text{ (g/mol)} \times \textit{ vol. of solution} \text{ (L)}} \\
&= \frac{\textit{grams of solute}}{\textit{vol. of solution} \text{ (L)}} \times \frac{1}{\textit{g formula wt.} \text{ (g/mol)}} \quad (1.1)
\end{aligned}$$

Major ions in fresh water generally are in the millimolar and submillimolar (mM) range; minor constituents and nutrients generally are in the micromolar (μM) range.

A ***mole*** of a substance is simply a defined quantity or number of units of the substance, specifically 6.022×10^{23} units of the substance, based on the number of atoms in exactly 12 grams of carbon-12 (^{12}C). This number is given the symbol N_A and is called ***Avogadro's constant*** (see Box 1.2). The term ***mole*** is used mostly with reference to molecules (and ions), and a mole of a molecule is the mass, in grams, equal to the molecular weight of the substance (the sum of the ***atomic weights*** (at. wt.) of the atoms in the formula of the molecule). This quantity, the molecular or formula weight in grams, is called the ***gram-molecular weight*** or gram-formula weight of a compound. As indicated above, it contains 6.022×10^{23} molecules (or formulas) of the compound. However, the term "mole" can be used to express this number of anything—atomic particles, grains of sand, stars in the sky. A mole of electrons is 6.022×10^{23} electrons, and this is known as a coulomb. A mole of photons is called an einstein. A gram-atomic weight of an element (its atomic weight in grams) contains 6.022×10^{23} atoms and is a mole of the element.

Box 1.2   Avogadro and his number

Avogadro's constant (or number), N_A, is arguably the most fundamental constant in chemistry. Although N_A is named for Amedeo Avogadro (1776–1856), an Italian scientist born in Turin, he did not measure its value or even define it precisely in conceptual terms. Instead, Avogadro hypothesized in 1811 that equal volumes of all gases at the same temperature and pressure contain the same number of molecules. The Austrian physicist Johann Loschmidt is credited as the first person to evaluate the constant. Using the kinetic theory of gases, he actually computed the number of particles per unit volume of an ideal gas (the number of particles per cubic centimeter of gas at standard conditions), which is proportional to but not the same as N_A. The French Nobelist Jean Perrin was the first to propose naming the constant in honor of Avogadro, but it was not until the 1930s that use of the term became common in textbooks. The precise value of N_A was not known until fairly recently. Estimates reported in the late nineteenth and early twentieth century ranged from Kelvin's estimate of 5×10^{23} to Perrin's estimate of $6.5–6.9 \times 10^{23}$. The currently accepted value is $6.02214179 \pm 0.00000030 \times 10^{23}$. In 1960, Avogadro's number was defined as the number of atoms in exactly 12 g of the ^{12}C isotope of carbon, and a mole was defined as one Avogadro number of atoms or molecules (or any other entity). The International System of Units (SI) adopted the mole as a fundamental unit in 1971 and reversed the above the definitions: a mole was defined as the number of atoms in 12 g of ^{12}C, with a dimension of "amount of substance," and Avogadro's number became a physical constant with units of reciprocal moles (mol^{-1}).

It is also useful to recall here that the atomic weight of any element approximately is equal to the sum of the number of protons plus the number of neutrons in the nucleus of atoms of the element. The number of protons defines the element's identity and is called the **atomic number** (at. no.). Fractional atomic weights for some elements result from the contributions of several **isotopes**, i.e., atoms having the same number of protons but different numbers of neutrons. For example, chlorine (at. no. 17) is a mixture primarily of two stable (i.e., not radioactive) isotopes: ~76% ^{35}Cl and ~24% ^{37}Cl; hence, its atomic weight is 35.45.

The standard mass/mass concentration unit in chemistry is **molality** (m):

$$molality~(m) = \frac{g~of~solute}{g~formula~wt. ~\times~ kg~of~solvent} \tag{1.2}$$

This unit is used rarely in freshwater chemistry, but it is the unit of choice for careful measurements in marine chemistry and chemical thermodynamics. For dilute solutions, molarity and molality essentially are equivalent, but in solutions as concentrated as seawater (and higher), the equivalency breaks down (see Example 1.2). Molality is temperature invariant, but molarity is not.

EXAMPLE 1.2 Molarity and molality of chloride in seawater: The salt content, or salinity (S), of "mean standard" seawater is 35.00‰ (i.e., 35.00 g/kg seawater). The chlorinity (chloride content) of seawater is related to salinity by the formula: S‰ = 0.03 + 1.805 × Cl‰. What is the molality and molarity of chloride in average seawater at 25°C?

Answer: From above, we find $[Cl^-] = (35.00 - 0.03)/1.805 = 19.374$‰, or 19.374 g Cl^-/kg seawater.

The density of seawater at 25°C is 1.02334 kg/L.[22] The volume occupied by 1 kg of seawater thus is

$$1.000 \text{ kg} \div 1.02334 \text{ kg/L} = 0.97719 \text{ L (or 977.19 mL).}$$

On a volume basis, $[Cl^-]$ thus is 19.374 g/0.97719 L = 19.826 g/L, and the molar concentration is

$$[Cl^-] = \frac{19.826 \text{ g/L}}{35.45 \text{ g/mol}} = 0.5593 \text{ mol/L or } \mathbf{0.5593 \ M}.$$

Because molality is moles of solute per kilogram of water, we need to find how many moles of H_2O are in 1 kg of seawater. From above, it is clear that 1 kg of seawater contains 35 g of salt. Thus, 1 kg of seawater contains $1000 - 35 = 965$ g H_2O. Because we calculated that 1 kg of seawater contains 19.374 g Cl^-, the molality of Cl^- thus is

$$[Cl^-] = \frac{19.374 \text{ g}}{0.965 \text{ kg } H_2O \ \times 35.45 \text{ g/mol}} = 0.5663 \text{ mol/kg } H_2O \text{ or } \mathbf{0.5663 \ m}.$$

The difference between the molar and molal concentrations thus is 0.007, or about 1.2%.

It is simple to convert between common and chemical units of concentration: one multiplies chemical units (M, mol/L) by the gram formula weight of the substance (g/mol) to obtain common units (g/L) and divides common units by the formula weight to get chemical units (see Example 1.3). For example, sulfate ion (SO_4^{2-}) has a formula weight of 96 g/mol (or 96 mg/mmol) (S = 32; O = 16). A water containing 24 mg/L of sulfate thus has 24 mg/L divided by 96 mg/mmol = 0.25 mmol/L of sulfate. Usually, we say the sulfate concentration is 0.25 millimolar (mM).

Another mass/mass unit of concentration is the ***mole fraction***. For any substance X, the mole fraction of X in a system is simply the moles of X divided by the total moles of all substances in the system:

$$\text{mole fraction of } i = \frac{\text{moles of } i}{\sum\limits_{i=1}^{n} \text{moles of } i} \tag{1.3}$$

For example, for a 1.0 M solution of NaCl in water, the mole fraction of NaCl is $\sim 1/(1 + 55.5)$, where 55.5 is the number of moles of water in a liter (1 L × 1000 g/L × mol/18 g = 55.5 mol). Mole fraction units are not common in inorganic solution chemistry but often are used in the solubility of organic substances in water and in thermodynamic treatment of solid phases associated with natural aquatic systems.

An additional mass/volume chemical unit of considerable importance is *normality* (N). This unit is similar to molarity except that the amount of the substance is based on its reactive capacity with regard to some type of chemical reaction. For acid-base reactions, the basis is the quantity of substance that can accept or donate one mole of hydrogen ions. For oxidation-reduction reactions, it is the amount that can accept or release one mole of electrons. This quantity of a substance is called an *equivalent*, and a solution containing one equivalent (of any substance) per liter has a concentration of one normal (1 N):

$$Normality\ (N) = \frac{grams\ of\ solute}{g\ eq.\ wt.\ of\ solute \times\ volume\ of\ solution\ (L)} \tag{1.4}$$

The *equivalent weight* of a substance is equal to the molecular (or formula) weight divided by its reactive capacity, r_c:

$$Equivalent\ weight\ (g) = \frac{Molecular\ (formula)\ weight\ (g)}{reactive\ capacity,\ r_c} \tag{1.5}$$

r_c is the number of H^+ ions a substance can gain or lose in acid-base reactions or the number of electrons a substance can gain or lose in redox reactions. For electroneutrality (charge-balance) calculations, r_c is the absolute value of the charge on the ion. Because these quantities may differ for a given substance, equivalent weight is a potentially ambiguous term, and the basis for calculation should be specified.

Normality is used in chemistry to express concentrations of titrants. For example, the concentration of an acid used to titrate a basic solution is expressed in terms of normality (N or eq/L). *Alkalinity*, which is defined as the sum of the "titratable bases in water," may be expressed in milliequivalents per liter (meq/L) or microequivalents per liter (μeq/L), if levels are low. In the older literature, *equivalents per million* (epm), which is the same as milliequivalents per liter (meq/L), is sometimes used.

EXAMPLE 1.3 Interconversion among common and chemical concentration units: The major ion concentrations of "global-average" river water[3] are reported in mg/L in the first row of numbers below, and the atomic or formula weights of the ions (in grams per mole (g/mol) or milligrams per millimole (mg/mmol)) are given in the next row. Convert the mass concentrations to molar and (charge) equivalent concentrations.

Ion	Na^+	K^+	Mg^{2+}	Ca^{2+}	HCO_3^-	SO_4^{2-}	Cl^-
Concentration (mg/L)	9.0	1.4	5.0	21	68	20	8
Atomic or formula weight	22.99	39.10	24.30	40.08	61.02	96.07	35.45

Answer: To convert from mg/L to mol/L, we divide the concentrations in mg/L by the atomic or formula weights (g/mol or mg/mmol) to get mmol/L. For example, for Mg^{2+},

(1)   5.0 mg/L ÷ 24.3 mg/mmol = 0.206 mmol/L or 0.206 mM.

Results for all the major ions are shown in the first row of numbers below. Similarly, to convert the concentrations to a charge equivalent basis (meq/L), we divide the mass

concentration by the equivalent weight, which for each ion is its atomic (or formula) weight divided by the absolute value of the charge on each ion. Again, for Mg^{2+}, we have

$$(2) \quad 5.0 \text{ mg/L} \div \frac{24.3 \text{ mg/mmole}}{2 \text{ meq/mmole}} = 5.0 \text{ mg/L} \div 12.15 \text{ mg/meq} = 0.412 \text{ meq/L}.$$

Results for all ions are given in the second row of numbers below.

Ion	Na^+	K^+	Mg^{2+}	Ca^{2+}	HCO_3^-	SO_4^{2-}	Cl^-
mmol/L	0.391	0.0358	0.206	0.524	1.114	0.208	0.226
meq/L	0.391	0.0358	0.412	1.048	1.114	0.416	0.226

According to the ***electroneutrality constraint***, all waters are electrically neutral. That is, the sum of the concentrations of the cations must be equal to the sum of the anion concentrations when both are expressed on a charge equivalents basis. Application of this concept to the results in Example 1.3 yields the following:

$$\text{Sum of cation concentrations: } \sum \text{Cations} = 0.391 + 0.0358 + 0.412 + 1.048$$
$$= 1.877 \text{ meq/L}$$
$$\text{Sum of anion concentrations: } \sum \text{Anions} = 1.114 + 0.416 + 0.226 = 1.756 \text{ meq/L}$$

The cation equivalents thus exceed the anion equivalents by $1.877 - 1.756 = 0.121$ meq/L, or about 6% of the total equivalent concentration of cations. This magnitude of difference usually is considered acceptable in routine water analyses and probably can be accounted for by analytical errors in the measured values of the cations and anions. Other possible explanations are that (1) the analysis did not include all the major inorganic ions (the concentration of one or more important inorganic ions is not reported), or (2) unmeasured charged moieties such as carboxylate groups on natural organic matter accounts for the anion deficit. The former explanation is unlikely; in most cases the seven ions listed in the table account for the vast majority of the inorganic ions in natural waters.

EXAMPLE 1.4 Calculations using chemical concentration units:
(A) Preparation of acid reagents

(1) Concentrated sulfuric acid has a density of 1.83 g/mL. If the concentrated acid is 97% H_2SO_4, what is its molarity and normality?

Answer: The formula weight of H_2SO_4 is 98 ($2 + 32 + 4 \times 16$). One liter of acid contains

$$0.97 \times 1830 \text{ g/L} = 1775 \text{ g/L}$$

and

$$1775 \text{ g/L} \div 98 \text{ g/mol} = 18.1 \text{ mol/L or } \sim \textbf{18 M}.$$

Because each mole of H_2SO_4 can release two moles of H^+, the normality of the acid is twice its molarity. Thus concentrated H_2SO_4 is **36 N**.

(2) If 2.0 mL of concentrated H_2SO_4 is diluted with distilled water to 250 mL in a volumetric flask, what is the resulting concentration in units of molarity and normality?

Answer: The 2.0 mL of concentrated H_2SO_4 contains

$$2 \text{ mL} \times 0.97 \times 1.83 \text{ g/mL} \div 98 \text{ g/mol} = 0.0362 \text{ moles}.$$

The solution thus is 0.0362 moles/250 mL $\times$ 1000 mL/L = **0.145 M** and **0.290 N**.

(3) What is the volume of the solution in (2) that should be diluted with distilled water to make a 0.025 N solution of sulfuric acid?

Answer: For this problem we can use the ***fundamental dilution formula***:

$$V_1N_1 = V_2N_2,$$

where V_1 and N_1 are the volume and normality of the initial (or "stock") solution and V_2 and N_2 are the volume and normality of the diluted solution. Thus,

$$(0.29 \text{ N}) V_1 = (0.025 \text{ N}) (1000 \text{ mL}),$$

or

$$V_1 = \textbf{86.2 mL}.$$

Note: reagent grade concentrated sulfuric acid is not pure acid and contains 96–98% H_2SO_4. A solution containing an exact concentration of acid thus cannot be prepared by simple dilution. It is necessary to determine the exact normality by ***titrating*** the acid with a basic solution whose normality is known exactly. This process is called ***standardization***. Because of this, one would not bother to measure the stock solution (V_1) to three-place accuracy; instead, one would measure out ~85 mL by pipette (or graduated cylinder) and determine the exact normality of the diluted acid by titration (see Chapter 8).

(B) Preparation of standard solutions of oxidizing agents

Potassium dichromate is a strong oxidizing agent used in the analysis of "chemical oxygen demand" (COD), a method used by environmental engineers to estimate the total organic matter in wastewater samples.[23] In the process of oxidizing the organic matter, dichromate ion, $Cr_2O_7^{2-}$, is reduced to two chromic ions, Cr^{3+}, which involves transfer of six electrons to dichromate:

$$Cr_2O_7^{2-} + 14H^+ + 6e^- \rightarrow 2Cr^{3+} + 7H_2O$$
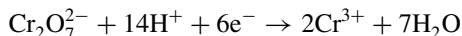
Exactly how many grams of reagent-grade $K_2Cr_2O_7$ must be weighed out and added to water to prepare a 1.0 L of a solution that is exactly 0.25 N $K_2Cr_2O_7$, and what is its molarity?

Answer: The formula weight of $K_2Cr_2O_7$ is $2 \times 39.1 + 2 \times 52 + 7 \times 16 = 294.2$. Its equivalent weight thus is $294.2 \div 6 = 49.033$ g. To make a 1.0 L solution containing 0.250 eq/L of dichromate, we need to weigh out 0.250 eq$\times 49.033$ g/eq $=$ **12.258 g**. The molarity of the solution is 0.25 eq/L $\div$ 6 eq/mol $=$ **0.04167 mol/L**.

1.3.4 Other concentration units used in environmental chemistry

The units described in the previous sections are the preferred ways to express concentrations of chemicals in water and generally are the most commonly encountered units today. However, a few other units are used widely in environmental engineering and water chemistry. We describe and define these units below.

mg/L as calcium carbonate ($CaCO_3$).   This unit formerly was used in natural water chemistry to express concentrations of alkalinity, hardness, and ions related to these terms. Although it now is used only rarely in scientific literature, the unit still is used widely within the water treatment industry. *Alkalinity* is defined as the sum of the concentration of bases titratable with strong acid, and it is closely related to the bicarbonate concentration in most natural waters (see Chapter 8). *Hardness* is the sum of the divalent cations (generally Ca^{2+} and Mg^{2+}, but occasionally Fe^{2+} and Mn^{2+}), which cause problems with soap precipitation and buildup of $CaCO_3$ scale in pipes (see Chapter 10).

The unit *mg/L as $CaCO_3$* is based on the fact that $CaCO_3$ has a formula weight of 100 $(40 + 12 + 3 \times 16)$ and an equivalent weight of 50, in terms of its reacting capacity with H^+ and the charge equivalents of its constituent ions. Thus, 50 g of $CaCO_3$ yields 0.5 moles of carbonate and requires 1.0 moles of H^+ to be titrated to CO_2; 50 g of $CaCO_3$ also yields one equivalent (or one mole) of cationic and anionic charges. The unit expresses concentrations of Ca^{2+}, Mg^{2+}, hardness, or alkalinity as if the constituents all have an equivalent weight of 50. As a "pseudo-equivalents per liter" or "pseudo-normal" unit, it is convenient in that concentrations expressed this way can be added in a meaningful way. For example, Ca + Mg (expressed in mg/L as $CaCO_3$) $\approx$ total hardness (in mg/L as $CaCO_3$). In contrast, Ca + Mg (expressed in mg/L) is not chemically meaningful.

Grains per gallon is a unit still used for hardness in the water utility industry (but nowhere else in environmental engineering or water chemistry). One grain is an old English unit equal to 64.8 mg of $CaCO_3$. A grain per gallon thus is equivalent to 64.8 mg $CaCO_3$/gal $\div$ 3.78 L/gal or **17.1 mg/L as $CaCO_3$**.

To convert from the preferred chemical units of alkalinity (meq/L) to mg/L as $CaCO_3$, we multiply the former by the equivalent weight of $CaCO_3$:

$$\textit{Alkalinity (mg/L as } CaCO_3) = \textit{Alkalinity (meq/L)} \times (50 \text{ mg } CaCO_3/\text{meq of } CaCO_3)$$
$$(1.5)$$

or

$$\textit{Alkalinity (mg/L as } CaCO_3) = \textit{Alkalinity (μeq/L)} \times (0.050 \text{mg/μeq of } CaCO_3)$$
$$(1.6)$$

Conversely,

$$Alkalinity \ (\mu eq/L) = 20 \times Alkalinity \ (mg/L \ as \ CaCO_3) \qquad (1.7)$$

To convert between units of mg/L for Ca^{2+} and Mg^{2+} and units of mg/L as $CaCO_3$, we divide the former by the equivalent weight of the atom (to obtain the number of equivalents of Ca or Mg) and multiply by the equivalent weight of $CaCO_3$:

$$\mathbf{Ca^{2+}}(mg/L \ as \ CaCO_3) = \frac{mg/L \ as \ Ca}{20 \ mg/meq \ of \ Ca} \times 50 \ mg/meq \ of \ CaCO_3 \qquad (1.8)$$

$$\mathbf{Mg^{2+}}(mg/L \ as \ CaCO_3) = \frac{mg/L \ as \ Mg}{12.15 \ mg/meq \ of \ Mg} \times 50 \ mg/meq \ of \ CaCO_3 \qquad (1.9)$$

EXAMPLE 1.5 Conversion of alkalinity and hardness units: (a) The sensitivity of surface waters toward acidification from atmospheric acid deposition is inversely related to the water body's alkalinity (also called acid-neutralizing capacity (ANC)). Water with an alkalinity less than 200 μeq/L is considered "acid sensitive." What is this alkalinity value in mg/L as $CaCO_3$?

Answer: 200 μeq/L$\times$50 mg $CaCO_3$/meq$\times 10^{-3}$ meq/μeq = **10 mg/L as $CaCO_3$**

   (b) Lake Okeechobee in south Florida is a large, shallow, hardwater lake with high concentrations of Ca^{2+} and Mg^{2+}, typical values of which in the lake are $[Ca^{2+}]$ = 45 mg/L and $[Mg^{2+}]$ = 18 mg/L. Convert these values to concentrations in mg/L as $CaCO_3$ and evaluate the total hardness of the lake.

Answer:

   $[Ca^{2+}]$ = 45 mg/L $\div$ 40 mg/mmol = 1.125 mmol/L of Ca^{2+}

   1.125 mmol/L $\times$ 2 meq/mmol = 2.25 meq/L of Ca^{2+}

   $[Ca^{2+}]$ = 2.25 meq/L $\times$ 50 mg/meq $CaCO_3$ **= 112.5 mg/L as $CaCO_3$**

   $[Mg^{2+}]$ = 18 mg/L $\div$ 24.3 mg/mmol = 0.74 mmol/L of Mg^{2+}

   0.74 mmol/L $\times$ 2 meq/mmol = 1.48 meq/L of Mg^{2+}

   $[Mg^{2+}]$ = 1.48 meq/L $\times$ 50 mg/meq $CaCO_3$ **= 74 mg/L as $CaCO_3$**

   Total hardness = $[Ca^{2+}]$ + $[Mg^{2+}]$(both in mg/L as $CaCO_3$) = 112.5 + 74

      = 186.5 mg/L as $CaCO_3$

mg/L as N or P (or mg N/L; mg P/L).   These units are used in water quality and limnological studies and express concentrations of various chemical forms of nitrogen or phosphorus in terms of the amount of elemental N or P present. This is a useful convention for several reasons. From a nutritional point of view, one is not interested in the concentration of nitrate or ammonium ion, for example, but in the amount of N in

the nitrate or ammonium, the actual part of the ion needed by organisms. Also, because these are pseudo-molar units, we can add concentrations of various species if they are expressed in terms of N (or P), but we cannot meaningfully add concentrations of ammonium and nitrate, for example, when they are expressed in mg/L of the ions themselves. A related term used to express concentrations of N and P forms in the older marine chemistry literature, *µg-at./L* (**microgram-atoms per liter**), is equivalent to a micromolar quantity of some N or P form; 1 µg-at N = µg N/14; 1 µg-at P = µg P/31.

To convert from mg/L of some N-containing species to mg/L as N, one divides the former by the formula weight of the species and multiplies the result by 14, the atomic weight of nitrogen. For nitrate,

$$NO_3^- \text{ (mg/L as N)}$$

$$= \frac{\text{mg/L of } NO_3^-}{62 \text{ mg/mmol}} \times (14 \text{ mg/mg-atom}) \times (1 \text{ atom N/molecule of } NO_3^-) \qquad (1.10)$$

For ammonium,

$$NH_4^+ \text{ (mg/L as N)}$$

$$= \frac{\text{mg/L of } NH_4^+}{18 \text{ mg/mmol}} \times (14 \text{ mg/mg-atom}) \times (1 \text{ atom N/molecule of } NH_4^+) \qquad (1.11)$$

Similarly, for phosphate,*

$$PO_4^{3-} \text{ (mg/L as P)}$$

$$= \frac{\text{mg/L of } PO_4^{3-}}{95 \text{ mg/mmol}} \times (31 \text{ mg/mg-atom}) \times (1 \text{ atom P/molecule of } PO_4^{3-}). \qquad (1.12)$$

Care must be taken in reporting nutrient concentrations to ensure that no ambiguity exists with regard to concentration units. This is an issue because the units commonly used to report nutrient concentrations have varied over recent decades, and publications are not always clear about what units were used.

EXAMPLE 1.6 Conversions among nutrient concentration units: The drinking water standard for nitrate is 10 mg/L as N (i.e., drinking waters should not exceed this value). What quantity of nitrate ion does this concentration represent?

Answer:

(10 mg/L as N) ÷ 14 mg N/mg atom = 0.714 mg-atom N/L

0.714 mg-atom N/L × 1 mg-atom N/mmol NO_3^- × 62 mg/mmol NO_3^- = **44.3 mg/L**

---

*The actual form (degree of protonation) of inorganic phosphate in water depends on pH. PO_4^{3-} is important only at very high pH values. Consequently, phosphate usually is reported as "dissolved inorganic P" or "soluble reactive phosphate" (SRP), reflecting the operational nature of the analytical results (see Chapter 16).

Chlorine.   Concentrations of chlorine species and related chemicals used for disinfection or oxidation of contaminants are reported in mg/L as elemental chlorine (mg/L as Cl). The chlorine is assumed to have an equivalent weight equal to the atomic weight of Cl; i.e., a one-electron transfer to form chloride, Cl^-, is the assumed reaction. The concentration of other oxidized chlorine species in terms of Cl equivalents is obtained by multiplying the molar concentration of the species by its reactive capacity, n, i.e., the number of electrons the species accepts in being reduced to chloride (Cl^-, the thermodynamically stable form of chlorine in water), and then multiplying this result by the atomic weight of chlorine. For example, chlorine in hypochlorite, OCl^-, and in hypochlorous acid, HOCl, has an oxidation state of +1, and thus there is a two-electron transfer when these forms are reduced to chloride. Thus, for hypochlorite ion,

$$\mathbf{OCl^-}\text{ (mg/L as Cl)} = \text{mM of } OCl^- \times 2 \times 35.45. \qquad (1.13)$$

Chlorine concentrations are also commonly expressed in units of mg/L as Cl_2. Because Cl_2, the form in which chlorine in its elemental form exists, represents twice the oxidizing capacity of a single Cl atom but also has exactly twice the mass of a single Cl atom, the net effect is just a trivial modification of the above equation, and the answer is the same:

$$\mathbf{OCl^-}\text{ (mg/L as } Cl_2) = \text{mM of } OCl^- \times 70.9 \qquad (1.14)$$

EXAMPLE 1.7 Conversion of chlorine concentration units: Household bleach is $\sim$5% NaOCl by weight. (1) What is the molar concentration of the chlorine solution and (2) what is its concentration in mg/L as Cl? Note: NaOCl is not a primary standard and is not available in pure enough form to compute the exact concentration of a weighed quantity.

Answer: (1) The bleach contains 5 g of bleach per 95 g of water, giving a concentration of 5 g/0.095 L = 52.6 g/L. The formula weight of NaOCl is 74.5 (23 + 16 + 35.5). The approximate molarity of the solution thus is

$$52.6 \text{ g/L} \div 74.5 \text{ g/mol} = \mathbf{0.706 \text{ M or } 706 \text{ mM}}.$$

(2) Concentration in mg/L as Cl:

$$706 \text{ mM} \times 2 \text{ meq/mmol} \times 35.45 \text{ mg/meq Cl} = 50{,}055 \text{ mg/L as Cl, or}$$

$$\sim \mathbf{50{,}000 \text{ mg/L as Cl}}$$

or

$$706 \text{ mM} \times 70.9 \text{ mg/mmol } Cl_2 = 50{,}055 \text{ mg/L as } Cl_2, \text{ or } \sim \mathbf{50{,}000 \text{ mg/L as } Cl_2}.$$

1.3.5 Concentration units for gases and solids

Concentrations of gases in gas phases usually are expressed in terms of pressure (in atmospheres, atm). Concentrations of gases dissolved in water often are expressed in common units (mg/L) or chemical units (mmol/L). They also can be expressed, however,

in terms of the pressure of the gas in the atmosphere that would produce (at equilibrium) the observed concentration in water, based in Henry's law: $S_w = K_H P_g$, where $S_w =$ the equilibrium concentration (solubility) of the gas in water at its pressure (P_g) in the atmosphere and K_H is called the Henry's law constant (see Section 1.4.3).

Two types of units are used to express gas concentrations in atmospheric science: mixing ratios and mass per volume. The former units are expressed as parts per million (ppm) or billion (ppb), depending on concentration, and effectively represent the fractional contribution of the gas to the total pressure of the atmosphere. The latter units are expressed as milligrams or micrograms per cubic meter (mg/m^3 or $\mu g/m^3$). These two concentration units are related to each other by the perfect gas law: $PV = nRT$, where P is pressure (atm), V is volume (L), n is the number of moles of the gas, T is absolute temperature (K), and R is called the gas constant (in units of L·atm K^{-1} mol^{-1}, R has a value of 0.08205). This equation is derived in Chapter 3, and details concerning R are described there. Here we rearrange the equation to show the relationship between mixing ratios and mass/volume concentration units. Dividing by V yields

$$P = RT\frac{n}{V} = RTC_M, \tag{1.15}$$

where C_M ($= n/V$) is the molar concentration of the gas in the atmosphere (moles per liter of air). Multiplying both sides of the equation by the molecular weight of the gas (M_w) gives the gas concentration in g/L, and multiplying by a factor of 10^6 converts the concentration to mg/m^3:

$$P_{(atm)}M_w = 10^6\ RTC_{(mg\ m^{-3})} \tag{1.16}$$

or

$$P_{(atm)} = 10^6 RT\frac{C_{(mg\ m^{-3})}}{M_w} \tag{1.17}$$

If we divide both sides of Eq. 1.17 by the factor 10^6 we can express the pressure of the gas in parts per million by volume (ppm_v):

$$ppm_v = C_{(mg\ m^{-3})}\frac{RT}{M_w} \tag{1.18}$$

Concentration units for substances in solids found in natural waters (e.g., suspended solids or bottom sediments) usually are expressed in common units (e.g., mg/g or $\mu g/g$). For solid phases that consist of only a few components, such as solid solutions of metal carbonates the concentrations of the components are expressed as mole fractions. For example, $Ca_{0.95}Mg_{0.05}CO_{3(s)}$ represents a 5% random substitution of Mg^{2+} ions for Ca^{2+} ions in solid calcium carbonate. The mole fraction concentration of $MgCO_{3(s)}$ is 0.05 and the mole fraction concentration of $CaCO_{3(s)}$ is 0.95.

1.4 Major categories of reactions in natural waters

Although the number of reactions in natural and engineered waters is huge—perhaps incalculable, the inorganic reactions in water can be grouped into four major types of chemical transformations plus two types of phase transformations. Similarly, many thousands of organic reactions exist, but they can be grouped into only a few major reaction types. This section describes these reaction types and presents examples of the relationships used to define their equilibrium status and rates at which they occur.

1.4.1 Chemical reactions and related equilibrium and kinetic expressions

Consider a generalized reaction

$$a\mathrm{A} + b\mathrm{B} \rightleftharpoons c\mathrm{C} + d\mathrm{D}, \tag{1.19}$$

where A and B are reactants, C and D are products, and a–d are "stoichiometric coefficients," i.e., the relative number of molecules of the reactants and products participating in the reaction. For any reaction at equilibrium, the product of the concentrations of the reaction products, each raised to the power of their stoichiometric coefficient, divided by the product of the concentrations of the reactants, raised to the power of their stoichiometric coefficients, is a constant at a given pressure and temperature. The ratio is given the symbol K and called the ***equilibrium constant***. For general reaction 1.19, we can write

$$K = \frac{[\mathrm{C}]^c[\mathrm{D}]^d}{[\mathrm{A}]^a[\mathrm{B}]^b}, \tag{1.20}$$

where brackets, $[i]$, denote molar concentration. This equation is the basis for solving all equilibrium problems and is used extensively in this book. The concept of equilibrium and the relationship between equilibrium constants and reaction energetics (chemical thermodynamics) is developed in Chapter 3. Strictly speaking, concentrations used in equilibrium constant relationships are not molar values but "thermodynamically ideal" concentrations, known as ***activities***, denoted in the rest of the book by braces, i.e., $\{i\}$. Relationships between activity and molar concentration are developed in Chapter 4.

Reactions approach equilibrium at rates that normally depend on the concentrations of one or more of the reactants involved in the reaction. If the reaction proceeds strongly to the right, such that there is little or no tendency for products to react backward to re-form the reactants, then product concentrations do not affect the overall reaction rate. In contrast to the situation describing chemical equilibrium, we cannot predict the exact form of a reaction's rate equation from its overall stoichiometry. This subject is dealt with in Chapter 5; for now we simply note that rate equations for reactions are written as ordinary differential equations in terms of the rate of reactant, A, loss or product, P, formation with respect to time as some function of reactant concentrations:

$$-d[\mathrm{A}]/dt = d[\mathrm{P}]/dt = k_{for}\mathrm{f}([\mathrm{A}] \dots), \tag{1.21}$$

where k_{for} is a rate constant (or rate coefficient) for the reaction, f([A] ...) represents a function of the concentration of one or more of the reactants. Examples are given in Section 1.4.2.

1.4.2 Major inorganic reaction types

Inorganic ions participate in four major types of chemical reactions: (1) acid-base, (2) solubility (or precipitation/dissolution), (3) complexation, and (4) oxidation-reduction (or redox). Examples of each are given below with corresponding equilibrium and kinetic expressions and a brief description of their roles in defining the chemistry of aquatic systems.

Acid-base reactions

Reaction   **Equilibrium expression**

(1a) $HB + H_2O \rightleftharpoons H_3O^+ + B^-$ $K_a = \dfrac{\{H_3O^+\}\{B^-\}}{\{HB\}\{H_2O\}} = \dfrac{\{H_3O^+\}\{B^-\}}{\{HB\}}$

(1b) $HB \rightleftharpoons H^+ + B^-$ $K_a = \dfrac{\{H^+\}\{B^-\}}{\{HB\}}$

(2) $B^- + H_2O \rightleftharpoons HB + OH^-$ $K_b = \dfrac{\{HB\}\{OH^-\}}{\{B^-\}\{H_2O\}} = \dfrac{\{HB\}\{OH^-\}}{\{B^-\}}$

(3) $H_2O \rightleftharpoons H^+ + OH^-$ $K_w = \{H^+\}\{OH^-\}$

Acids and bases are defined in several ways, as discussed in Chapter 8. Here we use the "Brønsted definition," which says that *acids* are substances that release protons (i.e., H^+), and *bases* are substances that accept protons. According to this definition, an acid does not react by itself but reacts with a base (and vice versa). In reaction 1a, acid HB reacts with water, which is acting as a base; the products are the (weaker) acid H_3O^+ and B^-, the "conjugate base" of acid HB. This reflects our understanding that free protons, H^+, do not exist in aqueous solution but always are donated to a base (here H_2O). Although it is common to write acid reactions in water as simple dissociations, as shown in reaction 1b, this is a matter of convenience rather than accuracy; it is easier to write H^+ than H_3O^+. Mathematically, the two are equivalent, because $H^+ = H_3O^+$ and, by definition, the activity of water, H_2O, $= 1$ (see Chapter 4). However, reaction 1a is a better description of the chemistry that occurs when an acid releases a proton in water. K_a, the *acid dissociation constant*, is the *equilibrium constant* for acid dissociation reactions 1a and 1b. Acid-base reactions are rapid and usually reach equilibrium in times of subseconds to a few seconds. Consequently, we generally do not need to worry about the kinetics of acid-base reactions.

In reaction 2, base B^- reacts with water, which now is acting as an acid, to accept a proton, forming conjugate acid HB and hydroxide ion, OH^-, from the water molecule. Although we wrote the base here as an anion (as the conjugate base of acid HB), bases are not necessarily ionic. Ammonia, NH_3, is an example of a nonionic base; it accepts a proton from water to form OH^- and its conjugate acid, ammonium ion (NH_4^+). K_b is the *base dissociation constant* for base B^-.

It is apparent from reactions 1 and 2 that water is both an acid and a base; substances that behave this way are called ***amphoteric*** or ***amphiprotic***. Reaction 3, which is written more properly as $2H_2O \rightleftharpoons H_3O^+ + OH^-$, illustrates this dual nature. The equilibrium constant for reaction 3, K_w, is called the ***ion product of water***. Because water is the solvent and because pure solvents have unit activity, as described in Chapter 4, we do not include it in the ion product for water, and it can be eliminated from the K values in reactions 1a and 2. It also can be seen that the sum of reactions 1b and 2 gives reaction 3. Moreover, the product of the equilibrium constants for 1b and 2 is equal to the equilibrium constant for reaction 3:

$$K_a K_b = \frac{\{H^+\}\{B^-\}}{\{HB\}} \times \frac{\{HB\}\{OH^-\}}{\{B^-\}\{H_2O\}} = \{H^+\}\{OH^-\} = K_w$$

In general, for any acid and its conjugate base, we can say that

$$K_a K_b = K_w. \tag{1.22}$$

An important generalization from reactions 1–3 is that ***whenever two reactions are added, K for the resulting reaction is the product of the K values for the reactants that were added together***.

The primary acid-base system in natural waters is the CO_2-bicarbonate (HCO_3^-)-carbonate (CO_3^{2-}) system, usually just called the carbonate system. The relative concentrations of the acid-base forms in this system control the alkalinity and pH of most natural waters (see Chapter 8). pH is defined as the negative logarithm of the proton activity, i.e., $pH = -\log\{H^+\}$. It is one of the two primary variables defining ion speciation and controlling a myriad of chemical and biological processes in water.

Solubility/dissolution reactions

Reaction	**Equilibrium expression**
(4) $MA_{(s)} + H_2O \rightleftharpoons M^+_{(aq)} + A^-_{(aq)}$	$K_{s0} = \{M^+\}\{A^-\}$
(5) $MA_{(s)} + H^+ \rightleftharpoons M^+_{(aq)} + HA$	$K_{s1} = \dfrac{\{M^+\}\{HA\}}{\{H^+\}}$
(6) $M^{n+} + nH_2O \rightleftharpoons M(OH)_{n(s)} + nH^+$ $K_n = \dfrac{\{H^+\}^n}{\{M^{n+}\}}$	

Subscripts $_{(s)}$ and $_{(aq)}$ denote solid and aqueous phase constituents, respectively, and numerical subscripts in the Ks refer to the number of H^+ reacting to dissolve the solid. As was the case for water in acid-base equilibria, we usually do not write terms for solid phases in solubility equilibrium constants because they have unit activity (if they are pure). Reaction 4 is the simple dissolution or precipitation of a sparingly soluble salt, MA. Reaction 5 is the acid-promoted dissolution of the salt. Reaction 6 is the ***hydrolysis*** of metal ion M^{n+}. Multivalent metal ions (e.g., ferric ion, Fe^{3+}) generally are insoluble at

neutral pH because they react with water to form insoluble hydroxides (e.g., $Fe(OH)_{3(s)}$ or ferric hydroxide). Precipitation reactions control the concentrations of many metal ions in natural waters. The most common of these reactions is the formation of calcium carbonate ($CaCO_{3(s)}$), which causes the build up of marl ($CaCO_3$-rich) sediments in lakes and the oceans and limestone (scale) deposits in water distribution systems. Dissolution of $CaCO_3$ is a major source of Ca^{2+} ions and carbonate alkalinity in natural waters. Solubility reactions also control the concentrations of Fe, Al, and many trace metals in natural waters.
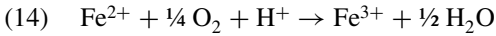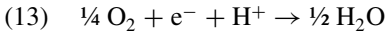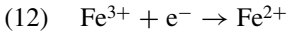
Complexation reactions

Reaction	**Equilibrium expression**
(7) $M^{m+} + L^- \rightleftharpoons ML^{+m-1}$	$K_{stab\ 1} = \dfrac{\{ML^{+m-1}\}}{\{M^{m+}\}\{L^-\}}$
(8) $M^{m+} + nL^- \rightleftharpoons ML_n^{+m-n}$	$\beta_n = \dfrac{\{ML_n^{+m-n}\}}{\{M^{n+}\}\{L^-\}^n}$
(9) $ML_n^{+m-n} \rightleftharpoons M^{m+} + nL^-$	$K_{diss\ n} = \dfrac{\{M^{n+}\}\{L^-\}^n}{\{ML_n\}} = \beta_n^{-1}$
(10) $M^{m+} + HL \rightleftharpoons ML^{+m-1} + H^+$	$^*K_1 = \dfrac{\{ML^{+n-1}\}\{H^+\}}{\{M^{n+}\}\{HL\}}$
(11) $M^{m+} + nH_2O \rightleftharpoons M(OH)_n^{+m-n} + nH^+$	$^*\beta_n = \dfrac{\{M(OH)_n^{+m-n}\}\{H^+\}^n}{\{M^{m+}\}}$

Complexation is the formation of a "complex" species from components capable of independent existence in solution. All complexes contain a central metal ion (electron-pair acceptor or **Lewis acid**) and one or more ligands (electron-pair donors or **Lewis bases**). Ligands contain an electronegative atom that has one or more pairs of electrons available for sharing (bond formation); they may be anions (e.g., Cl^-, SO_4^{2-}) or neutral molecules (e.g., NH_3). Both inorganic and organic ligands, such as carboxylic acids and compounds with amino groups, are important in complex formation in natural waters. Reaction 7 defines the first "stepwise" stability (or formation) constant for metal ion M^{n+} with ligand L^-; reaction 8 defines the "cumulative" stability constant, β_n, to form ML_n from M and n L. From the earlier comment on the addition of reactions, it should be apparent that $\beta_n = K_1 \cdot \cdot K_2 \cdots K_n$. Reaction 9, the reverse of the cumulative formation of ML_n, defines the dissociation (or *instability*) constant for the complex. When a protonated free ligand reacts with a metal ion to form a complex in which the ligand is deprotonated, we use a superscript * before the K or β, as for reaction (10) with HL and cumulative reaction (11), where the protonated ligand, water, forms hydroxide complexes with metal ions, releasing H^+ as a product. Many trace metals exist in natural waters primarily as complexed species; complexation is less important for the major cations, especially the monovalent ones, Na^+ and K^+. Complexation affects metal ion solubility and reactivity toward oxidation, as well as metal bioavailability to aquatic organisms.

Oxidation-reduction (redox) reactions

Reaction	**Equilibrium expression**

(12) $Fe^{3+} + e^- \rightarrow Fe^{2+}$ $E_{12}^\circ = 0.771$ V

(13) $\frac{1}{4} O_2 + e^- + H^+ \rightarrow \frac{1}{2} H_2O$ $E_{13}^\circ = 1.224$ V

(14) $Fe^{2+} + \frac{1}{4} O_2 + H^+ \rightarrow Fe^{3+} + \frac{1}{2} H_2O$ $E_{net}^\circ = 0.453$ V;

$$K_{net} = \frac{\{Fe^{3+}\}}{\{Fe^{2+}\}\{H^+\}P_{O_2}^{1/4}} = 10^{7.67}$$

Oxidation involves a loss of electron(s) by a species; reduction involves a gain in electron(s). Because free electrons cannot build up in a system, whenever a species is oxidized (gives up electrons), other species must be reduced (accepting those electrons). Nonetheless, it is convenient to separate the steps in a net redox reaction and write the separate "half-reactions" for oxidation and reduction. We combine them by appropriate addition or subtraction, multiplying the half-reactions, as necessary, to ensure that each half-reaction involves the same number of electrons—so there is no loss or gain of electrons in the net reaction. The tendency for half-reactions to occur is defined quantitatively in terms of reduction potentials, E°, in volts, V, or the related dimensionless term $p\varepsilon^\circ$, described in Chapter 11. The potential for the net reaction is the difference between E° for the oxidation and reduction steps: $E_{net}^\circ = E_{red}^\circ - E_{ox}^\circ$. In turn, E_{net}° and $p\varepsilon_{net}^\circ$ are related to the energetics of the reaction and to its equilibrium constant.

The reactions shown above represent the reduction potentials (half-reactions) for the ferric-ferrous iron couple and the oxygen-water couple. Subtraction of reaction 12 from reaction 13 yields the net reaction (14)—the oxidation of ferrous iron, Fe^{II}, to ferric iron, Fe^{III}, by molecular oxygen.* Ferric ion is insoluble at neutral pH and forms ferric hydroxide, $Fe(OH)_{3(s)}$. The standard potential for the net reaction is: $E_{net}^\circ = E_{red\,(O_2)}^\circ - E_{ox\,(Fe(II))}^\circ = 1.224 - 0.771 = 0.453$ V. Details regarding the relationship between E_{net}° and K_{net} and other aspects of redox chemistry are described in Chapter 11. Redox potential (E) and related term $p\varepsilon$ represents the second "master variable" (along with pH) defining the chemical composition of natural waters and associated sediments. Dissolved oxygen often is considered a surrogate variable for redox conditions and plays a major role in defining the chemical composition of aquatic systems.

In contrast to acid-base reactions, which achieve equilibrium in seconds or less, redox reactions have a very wide range of rates. Some are nearly instantaneous, but others are exceedingly slow. For many redox reactions, rates depend strongly on solution conditions, such as pH. For example, reaction 14 reaches equilibrium in seconds at pH 9 but requires months or years for completion at pH 3–4. Oxidation of ferrous iron by molecular oxygen, called the ***autoxidation*** of iron, has a rate equation of the form

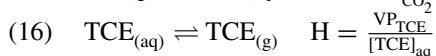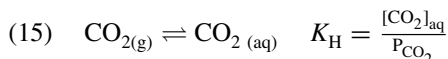$$-d[Fe^{II}]/dt = k_{obs}[Fe^{II}]P_{O_2}\{OH^-\}^2. \tag{1.23}$$

*The oxidation state of an element, regardless of its exact ionic form, is given by Roman numerals using either of two conventions: in parentheses after the element, or as superscripts. In this book we use the latter convention.

Because a one unit increase in pH represents a 10-fold increase in the activity $\{OH^-\}$, the $\{(OH^-\}^2$ term in Eq. 1.23 means that the reaction rate increases 100-fold per unit increase in pH. Assuming other factors remain constant, over the pH range of 5–9, the rate of Fe^{II} autoxidation increases by a factor of 10^8! Reasons for the high sensitivity of this reaction to $\{OH^-\}$ are discussed in Chapter 15.

1.4.3 Phase transfers

Chemicals in aquatic systems undergo two important phase transfers: (1) gas or vapor dissolution into water or volatilization from water, and (2) sorption of substances (called *sorbates*) from solution onto solid surfaces (called *sorbents*), or desorption of substances from surfaces to the solution phase. Mathematically, these processes are treated like chemical reactions and described by equilibrium constants and rate equations. In fact, sorbate interactions with sorbents involve a gradient from weak physical binding by van der Waals forces to electrostatic attractions between ions and charged surface sites, and stronger chemisorption processes in which the sorbate is chemically transformed.

Gas transfer

(15) $CO_{2(g)} \rightleftharpoons CO_{2\,(aq)}$ $K_H = \dfrac{[CO_2]_{aq}}{P_{CO_2}}$

(16) $TCE_{(aq)} \rightleftharpoons TCE_{(g)}$ $H = \dfrac{VP_{TCE}}{[TCE]_{aq}}$

Equilibrium constants for gas solubility, K_H, are called Henry's law constants. In general, K_H (and gas solubility) decreases as water temperature increases. Henry's law also applies to air-water transfers of volatile organic compounds (VOCs) like trichloroethylene (TCE) in reaction 16, but then the process usually is written in reverse direction (water to air) from that for fixed gases and given the symbol H. Obviously, $H = K_H^{-1}$ for any given compound. Care must be taken to recognize which convention is being used when reading the literature on phase transfers of gases and volatile organic compounds.

Sorption

(17) $TCE_{(aq)} + X_{(sfc)} \rightleftharpoons TCE_{(sfc)}$ $K_{sorp} = \dfrac{[TCE]_{(sfc)}}{[TCE]_{(aq)}[X_{sfc}]}$

Our example is the volatile organic pollutant TCE adsorbing onto a solid surface, e.g., activated carbon or natural organic matter. Sorption of ions to mineral surfaces is an important process that receives similar mathematical treatment. $[X_{sfc}]$ represents the concentration of surface sites available for sorption of TCE. It is difficult to measure $[X_{sfc}]$ directly, and the equilibrium condition thus is not solvable when written as in Eq. 17. A common way to portray sorption equilibria is by the ***Langmuir equation***, which is based on a simple physical model for sorption but in practice is largely an empirical formulation:
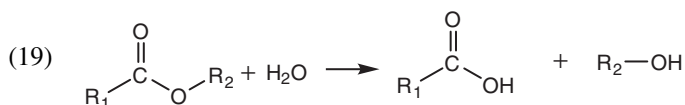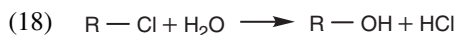
$$X = \frac{X_m K_L C}{1 + K_L C} \tag{1.24}$$

where X is the amount of sorbate sorbed per unit of sorbent (e.g., $\mu g/g$), X_m is the sorption capacity ($\mu g/g$), K_L is a constant related to binding energy ($L/\mu g$), and C is the equilibrium sorbate concentration in solution. Many other models, ranging from empirical formulas to complicated, multiequation formulations with many fitting parameters, are used to describe sorption equilibria (Chapter 14).

1.4.4 Reactions of organic compounds

Some of the chemical reactions and phase transformations described in the preceding sections involve organic compounds, as well as inorganic species, as reactants and products. Many natural and synthetic organic compounds act as acids and bases, e.g., compounds with carboxylic acid ($-COOH$) and/or amino ($-NH_2$) functional groups. Such organic compounds also act as ligands and form complexes with metal ions in aquatic systems. In addition, gas-liquid and liquid-solid phase transfers are important in the environmental processing of many organic compounds. The number and variety of reactions for organic compounds is extremely large, reflecting the huge diversity of such compounds. This is especially true if we include reactions involved in organic synthesis, but if we limit ourselves to aqueous-phase reactions related to the breakdown of organic compounds, we need to consider just three kinds of reactions: hydrolysis, photolysis, and redox (electron transfer) reactions.

Hydrolysis

(18) $R-Cl + H_2O \longrightarrow R-OH + HCl$

(19)

$$R_1 \overset{O}{\underset{C}{\parallel}} O-R_2 + H_2O \longrightarrow R_1 \overset{O}{\underset{C}{\parallel}} OH + R_2-OH$$

In a general sense, hydrolysis involves the reaction of organic compounds with water. The products typically have hydroxyl or acid functional groups and are more polar than the reactants and more susceptible to biodegradation. Two examples are the hydrolysis of organic halides (reaction 18) and the hydrolysis of esters (reaction 19). R in these reactions stands for some organic structure, the nature of which need not concern us here. R-Cl is an organochlorine compound, and R-OH is an alcohol. The organic reactant in reaction 19, an ester, hydrolyzes to a carboxylic acid, R_1COOH, and an alcohol, R_2OH. All organic compounds are thermodynamically unstable, and we cannot write equilibrium expressions for reactions 18 and 19. Instead, we are interested in the kinetics of these reactions. Many hydrolysis reactions are catalyzed by acids or bases, and a typical rate equation for hydrolysis reaction 18 is

$$-d(R-Cl)/dt = k_{hyd}[R-Cl]\{H^+\}. \tag{1.25}$$

The rate constant k_{hyd} is specific for a given compound, RCl, and varies with temperature and other solution conditions. The $\{H^+\}$ term in the rate expression reflects catalysis by hydrogen ions. Essentially, this means that H^+ participates in the mechanism to facilitate

the reaction and increase the rate, but there is no net consumption (or production) of H^+ (see Chapter 5).

Photolysis

(20)

Atrazine   Hydroxyatrazine

(21)
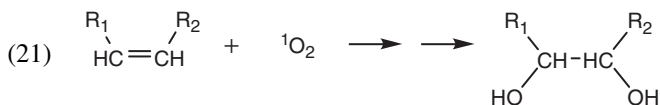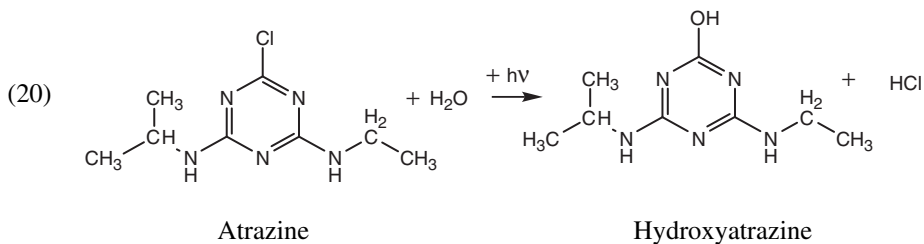
Light, the energy source that activates molecules into a reactive state in photolysis, is denoted in reaction 20 by $h\nu$. This term derives from Planck's law, which relates the energy of light to its frequency (ν). In direct photolysis, the compound of interest absorbs a photon, becomes activated, and forms a product. Atrazine, a common herbicide, undergoes direct photolysis (reaction 20) in which a Cl atom is replaced by an $-OH$ group to form hydroxyatrazine. This essentially is a light-induced hydrolysis reaction. In indirect photolysis, the substance that absorbs a photon transfers its energy to another compound that undergoes chemical reaction (Chapter 19). Atrazine also is degraded by several indirect photolysis mechanisms. Reaction 21 is an example of an indirect photolysis reaction. Singlet oxygen, $^1O_2$, the first excited state of molecular oxygen, is formed when ground-state O_2 collides with another molecule (called a sensitizer molecule) that has been excited by absorbing a photon of light. $^1O_2$ reacts readily with certain classes of organic molecules, including compounds with carbon-carbon double bonds to form glycols (dialcohols), as shown in reaction 21.

Electron transfer (redox) reactions

(22)

(23)

(24)

$$\text{phenolate} + 4Mn^{III} + H_2O \longrightarrow \text{quinone} + 4Mn^{II} + 2H^+$$

(25)

$$\text{(TCE)} + Fe^0_{(s)} + H^+ \longrightarrow \text{(DCE)} + Fe^{2+} + Cl^-$$

(26)

$$\text{nitrobenzene} + 6Fe^{II} + 6H^+ \longrightarrow \text{aniline} + 6Fe^{III} + 2H_2O$$
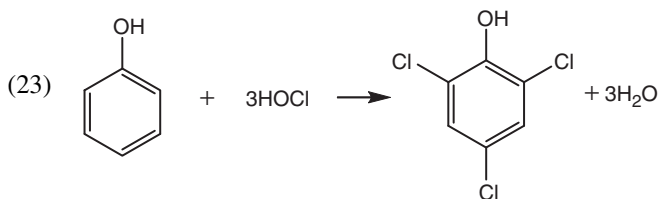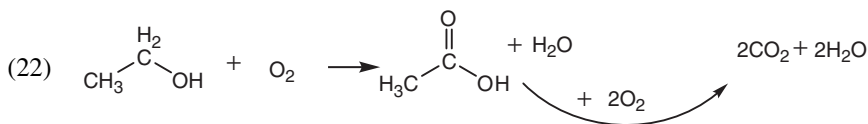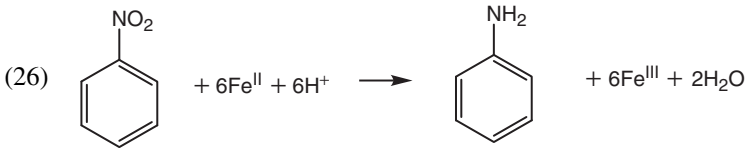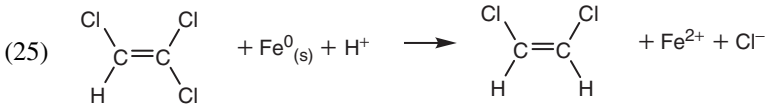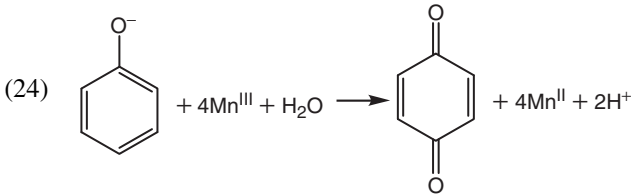
Electron transfer (redox) processes are important in transforming organic compounds in aquatic systems. These reactions involve a highly diverse set of organic reactants, inorganic oxidants and reductants, and both abiotic (chemical) and biotic mechanisms. Reaction 22 shows the oxidation of ethanol to acetic acid by molecular oxygen, which is mediated by many microorganisms, and the subsequent oxidization (mineralization) of acetic acid to carbon dioxide and water. Neither step in reaction 22 occurs directly by abiotic (chemical) reaction under normal environmental conditions. Reaction 23 shows the chlorination of phenol, an abiotic oxidation that occurs in water treatment plants using chlorine for disinfection. Phenolate (deprotonated phenol) also is oxidized by manganese minerals, leading to quinones (reaction 24). Degradation pathways for organic compounds also may involve reduction steps. Reaction 25 shows the reductive dechlorination of trichloroethylene (TCE) to dichloroethylene (DCE) by zero-valent iron (iron in its metallic state), a step in some remediation processes to remove chlorinated solvents from contaminated ground water. The reduction of a nitroaromatic compound, a common structural component in pesticides and explosives, by ferrous iron (Fe^{II}) to form an aniline is shown in reaction 26.

References

1. Sillen, L. G. 1961. The physical chemistry of seawater, pp. 549–581 in *Oceanography*, M. Sears (ed.), Amer. Assoc. Adv. Sci., Washington, D.C.

2. Stumm, W. (ed.). 1967. *Equilibrium concepts in natural water systems*, Adv. Chem. Ser. **67**, Amer. Chem. Soc., Washington, D.C.

3. Holland, H. D. 1978. *The chemistry of the atmosphere and oceans*, Wiley-Interscience, New York.

4. Garrels, R. M., and C. L. Christ. 1965. *Solutions, minerals, and equilibria*, Harper & Row, New York.

5. Stumm, W., and J. J. Morgan. 1970. *Aquatic chemistry*, Wiley-Interscience, New York; 2nd ed., 1980; 3rd ed., 1996.

6. Snoeyink, V. L., and D. Jenkins. 1980. *Water chemistry*, J. Wiley & Sons, New York.

7. Pankow, J. F. 1991. *Aquatic chemistry concepts*, Lewis Publ., Chelsea, Mich.

8. Drever, J. 1982. *Geochemistry of natural waters*, Prentice-Hall, Englewood Cliffs, N.J.

9. Morel, F. M. M., and J. G. Hering. 1993. *Principles and applications of aquatic chemistry*, J. Wiley & Sons, New York.

10. Benjamin, M. M. 2002. *Water chemistry*, McGraw-Hill, New York.

11. Jensen, J. N. 2003. *A problem-solving approach to aquatic chemistry*, J. Wiley & Sons, New York.

12. Schwarzenbach, R. P., P. M. Gschwend, and D. M. Imboden. 1993. *Environmental organic chemistry*, J. Wiley & Sons, New York; 2nd ed., 2003.

13. Wikipedia. available online at http://en.wikipedia.org; entries for the compounds listed in the text were accessed September 9, 2010.

14. Horne, R. A. 1969. *Marine chemistry*, Wiley-Interscience, New York.

15. Frank, H. S. and W. Y. Wen. 1957. Structural aspects of ion-solvent interaction in aqueous solutions: a suggested picture of water structure. *Disc. Faraday Soc*. **24**: 133–140.

16. Stillinger, F. H. 1980. Water revisited. *Science* **209**: 451–457.

17. Wernet, P., D. Nordlund, U. Bergmann, M. Cavalleri, M. Odelius, H. Ogasawara, L. Å. Näslund, T. K. Hirsch, L. Ojamäe, P. Glatzel, L. G. M. Pettersson, and A. Nilsson. 2004. The structure of the first coordination shell in liquid water. *Science* **304**: 995–999.

18. Woutersen, S., U. Emmerichs, and H. J. Bakker. 1997. Femtosecond mid-IR pump-probe spectroscopy of liquid water: evidence for a two-component structure. *Science* **278**: 658–660.

19. Horne, R. A., and D. S. Johnson. 1966. The viscosity of water under pressure. *J. Phys. Chem*. **70**: 2182–2190.

20. Horne, R. A., and D. S. Johnson. 1966. The viscosity of compressed seawater. *J. Geophys. Res*. **71**: 5275–5277.

21. Blokzijl, W., and J. B. F. N. Engberts. 1993. Hydrophobic effects—opinions and facts. *Angew. Chem. Int. Ed.* **32**: 1545.

22. Dept. of Energy. 1997. Physical and thermodynamic data. In *Handbook of methods for the analysis of the various parameters of the carbon dioxide system in seawater,* ver. 2.1, A. G. Dickson and C. Goyet (eds.), ORNL/CDIAC-74, Chap. 5, p. 6 (available online at http://cdiac.esd.ornl.gov/ftp/cdiac74/, accessed January 2009).

23. Eaton, A. D., L. S. Clesceri, E. W. Rice, and A. E. Greenberg (eds.) 2005. *Standard methods for the examination of water and wastewater*, 21st ed., Amer. Pub. Health Assoc., Washington, D.C.

2

Inorganic Chemical Composition of Natural Waters

Elements of Aqueous Geochemistry

Objectives and scope

This chapter addresses four questions about the chemical composition of natural waters:

(1) What is the nature of the dissolved or suspended substances in water?
(2) What are the natural and human-derived sources of these materials?
(3) How do these sources and the natural hydrologic cycle control the chemical composition of water?
(4) Can we develop simple conceptual models to describe or predict the composition of natural waters?

We describe the major and minor ions whose behavior forms the basis for the chemical composition of natural waters. Natural weathering processes, the role of atmospheric transport and transformation processes, and human activities are described as sources of those ions. The characteristics of hard and soft waters are summarized, and examples of the chemical composition of freshwaters, seawater, and hypersaline waters are presented. We describe the hydrologic cycle as cycling of water between major global reservoirs such as the atmosphere, surface streams, rivers and lakes, and ground-water aquifers, and we illustrate how important chemical reactions and processes affect the chemical composition of water as it moves among these major reservoirs. Controls on the composition of natural waters are explained in the context of simple geochemical models. Information is presented on accessing water chemistry data through online databases, and ways to portray water chemistry data graphically are described. Finally, we briefly discuss analytical methods by which major and minor inorganic solutes are measured.

Key terms and concepts

- The seven major ions: Na^+, K^+, Mg^{2+}, Ca^{2+}, HCO_3^-, SO_4^{2-}, Cl^-; minor solutes: Al, B, Fe, Mn, F, Si
- Hardness, hard and soft waters
- Salinity and chlorinity, hypersaline water
- Electroneutrality and ion balances
- Primary and secondary aluminosilicate minerals, congruent and incongruent dissolution, weathering
- Hydrologic and hydrochemical cycles
- Maucha diagrams, trilinear (Piper) diagrams

2.1   Introduction

As stated in Chapter 1, this book is mostly about what is in water rather than water itself. Although water may not completely deserve its common label as "universal solvent," nonetheless it is a very good solvent, especially for ions and polar substances. Some have argued that every element in the Periodic Table (at least those with stable isotopes) can be found in water. At some level, that is true, but many elements—in fact, the majority—occur at vanishingly small concentrations and are of little concern to environmental chemists and engineers. However, concentrations of many elements are high enough to be of interest, and that makes water chemistry a complicated and challenging subject.

The Periodic Table in Figure 2.1 highlights the elements of interest in water chemistry. By our reckoning, 43 of the first 94 elements are in this category. Several others could be added to the list; e.g., isotopes of ^{6}Be, ^{90}Y, and ^{210}Po are used for dating sediments and water, and some noble gases (e.g., Ar; see Section 16.2.2) are used as reference substances. Nine elements are classified as major elements in natural waters and four as minor elements—that is, common in freshwater but generally present at concentrations < 1 mg/L. Three elements (C, N, P) are classified as major nutrients, but many other elements, including most of the major and minor elements and many trace elements, are essential in the nutrition of aquatic organisms. Our classification of some trace elements as pollutants is somewhat arbitrary in that many trace elements not so classified (e.g., Cu, Zn) also cause problems if present in elevated concentrations, although they are benign or even essential nutrients at low concentrations. Those elements labeled "pollutant" (e.g., Cd, Pb) have no apparent beneficial effects even at very low concentrations and are found in natural waters primarily as the result of human activity. Considering that most elements exist in water as several chemical species (ions or molecules) and some (e.g., C, N, P) occur in numerous ions and compounds, it is easy to see why the chemistry of natural waters is a complicated subject.

Table 2.1 lists the common physical and chemical variables used to describe the composition and quality of water and indicates which chapter discusses the variable. Table 2.1 provides another perspective on the complexity of natural waters. Of course, not every variable needs to be measured to obtain an understanding of the chemical behavior of a water body or whether it is fit for human use or various ecosystem services, but it is safe to say that "more is better" and that water chemists invariably rely on many

Figure 2.1 Periodic Table with the size and font for the elements keyed to categories of interest in water chemistry. (See color insert at end of book for a color version of this figure.)

kinds of chemical measurements, as well as several physical properties, to define aquatic systems.

2.2   Inorganic chemical composition of natural waters

2.2.1 Major and minor ions and their chemical behavior

In spite of the emphasis made above on the chemical diversity of natural waters, one important feature that freshwaters share is the identity of the ions that constitute their inorganic solutes. In nearly all cases, just seven ions (four cations and three anions) and one un-ionized species (silica, which exists as $Si(OH)_4$ at the pH of most natural waters) constitute 95–99% of the total dissolved inorganic solutes of natural waters. The seven ions are as follows:

Major cations   Major anions
$Ca^{2+}, Mg^{2+}, Na^+, K^+$ HCO_3^-, SO_4^{2-}, Cl^-

The near-ubiquitous status of these species as major ions in water stems from their relative abundance in the Earth's crust and the fact that their salts are moderately to very soluble. The proportion of total ionic solutes represented by a given ion depends on local geochemical conditions, but a few general trends can be stated. First, although many exceptions occur, the order of the ions in the lists reflects the most common order of abundance in natural waters. Within the cations, $[Ca^{2+}]$ almost always is larger than $[Mg^{2+}]$, and $[Na^+]$ is larger than $[K^+]$, which usually is the least abundant of the major cations. In water bodies not affected by human activities and located away

Table 2.1 Important physical and chemical measures of water quality

Variable	Measure	Chapter	Units
Physical			
Color	Absorbance of light	17, 18	platinum-cobalt units (PCU)
Specific conductance (SC)	Electric carrying capacity	4	micro-Siemens per cm (μS/cm)
Dissolved solids	Concentration of solids < a given filter pore size		mg/L
Suspended solids	Concentration of particles > given filter pore size		mg/L
Temperature	Thermal energy	3, 16	°C (or K)
Transparency	Light transmission (e.g., Secchi depth)	17	m
Turbidity	Light scattering (related to suspended solids)	17	nephelometric turbidity units (NTU)
Chemical			
Aggregate	Alkalinity (acid neutralizing capacity)	7, 8	μeq/L, meq/L, or mg/L as $CaCO_3$
	Biochemical oxygen demand (BOD)	1, 12	mg/L
	Chemical oxygen demand (COD)	12	mg/L
	Dissolved/total organic carbon (DOC/TOC)	18	mg/L
	Dissolved inorganic carbon (DIC or C_T)	7, 8	Same as alkalinity
	Hardness: $\sum$(divalent cations) $\approx [Ca^{2+}]+[Mg^{2+}]$	2, 9, 10	meq/L or mg/L as $CaCO_3$
Inorganic	Major cations: Ca^{2+}, Mg^{2+}, Na^+, K^+	2, 10	meq/L or mg/L as $CaCO_3$
	Major anions: HCO_3^-, SO_4^{2-}, Cl^-	2, 7, 8, 9	mg/L or meq/L
	Minor ions, e.g., Al, Fe, Mn, F^-	2, 15	mg/L, μg/L or meq/L, μeq/L
	H^+ (pH)	7, 8	mol/L (no units for pH)
Dissolved gases	O_2 (DO), N_2, CO_2 ($H_2CO_3^*$)	8, 12, 16	mg/L, mL/L
Nutrients	NH_4^+/NH_3 (ammonium/ammonia)	8, 9, 16	mg/L as N
	NO_3^- (nitrate), NO_2^- (nitrite)	16, 17–19	mg/L as N
	Dissolved (or total) organic N (DON, TON)	16	mg/L as N
	Orthophosphate ($H_2PO_4^-$/HPO_4^{2-})	7, 8, 16	mg/L or μg/L as P
	Total (dissolved) phosphate (TDP, TP)	16	mg/L or μg/L as P
	Silica ($Si(OH)_4$)	2, 15	mg/L as Si or as SiO_2
Contaminants	Heavy metals, e.g., Cd, Cu, Hg, Ni, Pb, Zn	9–11, 18	pg/L to μg/L
	Persistent organic pollutants (POPs): numerous classes, thousands of compounds	6, 19	pg/L to μg/L

from coastal areas, Cl^- usually is the least abundant anion in inland waters with humid climates. Chloride salts are so soluble that they do not persist in soil formations in humid environments. Natural sources of Cl^- are somewhat geographically restricted, but halite (NaCl) crystals are commonly found within sedimentary rocks of marine origin.

The above order of abundance does not apply at the extremes of ionic strength. Brackish and saline waters have higher concentrations of Na^+ than of the divalent cations because of solubility constraints on the divalent ions, especially Ca^{2+}; Cl^- is high in such waters for analogous reasons. Generalizations about order of abundance are difficult to make for waters of very low ionic strength. Such waters tend to occur in regions with poor, noncalcareous soils and slow-to-weather granitic bedrock.

The chemistry of the major cations is relatively simple. None participates in redox reactions, and as strong base cations (i.e., they form soluble salts, rather than complexes and insoluble minerals with hydroxide), their acid-base behavior is limited. However, the divalent cations, especially Mg^{2+}, do react with OH^- at high pH, which is important in removing hardness from waters. Na^+ behaves nearly conservatively in natural waters; that is, it is only slightly reactive and once in water tends to stay in it. Na^+ engages in ion exchange reactions with clays, but this reaction is more important as a source for Na^+ in water than a sink. However, high ratios of Na^+ to the sum of Ca^{2+} and Mg^{2+} soil solutions can cause "sodification," the replacement of divalent cations in clays by Na^+, causing them to swell and become impervious.[1] This can be a problem in irrigated agricultural soils. In general, K^+ has a stronger tendency to sorb onto clays and soil particles, accounting for its more limited concentration range in freshwaters. Salts of both Na^+ and K^+ are highly soluble (precipitation is not an issue in freshwaters), and complexation reactions are not very important for these cations, especially in freshwaters.

Ca^{2+} and Mg^{2+} are much more reactive—hence nonconservative in natural waters. Complexation with organic ligands and even with some major anions can be important for both cations. The concentration of Ca^{2+} in freshwater and seawater usually is limited by the solubility of $CaCO_{3(s)}$, which depends on pH because bicarbonate, HCO_3^-, increasingly dissociates to form CO_3^{2-}, a moderately strong base, as pH increases. The removal of dissolved CO_2 from water by photosynthesis causes pH to increase, and precipitation of $CaCO_3$ in productive lakes and is the source of $CaCO_{3(s)}$ deposits (called ***marl***) in lake sediments. Over geological timescales, marl deposits turn into limestone. The solubility of $CaCO_{3(s)}$ decreases with temperature, giving rise to scale problems in hot water pipes where the water is high in Ca^{2+} and HCO_3^- (see Chapter 10). $MgCO_3$ is much more soluble than $CaCO_3$, and Mg^{2+} solubility is limited by $Mg(OH)_{2(s)}$, which also depends on pH. Ca^{2+} usually is more abundant than Mg^{2+} in freshwaters because mineral sources of Ca^{2+} are more abundant, but this trend does not continue at higher ionic strengths, because there are fewer chemical controls on Mg^{2+} concentrations. As described in Section 2.2.4, Mg^{2+} exceeds Ca^{2+} in seawater and hypersaline waters. All four major cations are taken up by aquatic organisms, but this does not represent a significant sink for the ions.

Of the major anions, bicarbonate (HCO_3^-) has the most complicated chemistry, including acid-base, solubility, complexation, and redox reactions that are central to the chemistry of natural waters. Details are provided in Chapters 7–11. Here we simply note that HCO_3^- is the first acid dissociation product ($pK_{a1} = 6.35$) of carbonic acid (H_2CO_3), which is formed by hydration of dissolved CO_2, and HCO_3^- dissociates further ($pK_{a2} = 10.33$) to form carbonate ions (CO_3^{2-}). At circumneutral pH, HCO_3^- is the predominant species of the CO_2–H_2CO_3–HCO_3^-–CO_3^{2-} acid-base system (hereafter

referred to as the ***carbonate system***). Because HCO_3^- can accept and donate protons, it is important in buffering pH and constitutes the great majority of the ***alkalinity*** (acid neutralizing capacity; see Chapter 8) of natural waters.

In contrast, chloride, the least reactive major anion, usually is considered to be a conservative substance in water. It does not participate in acid-base, solubility, or redox reactions in freshwaters or seawater and does not form complexes with the major cations. However, it is taken up by plants and thus is not entirely conservative. It is an important complexing agent for a few trace metals. The dominant forms of Cd^{II} and Zn^{II} in seawater are chloro-complexes (see Chapter 9).

Sulfate has a richer chemistry than chloride. It serves as a microbial electron acceptor under anoxic conditions and is reduced to sulfide, which also has a rich chemistry and is an important minor or possibly even major ion in anoxic aquatic systems. Sulfide, a weak acid ($pK_{a1} = 7.02$), limits the concentrations of many heavy metal ions in anoxic waters. Sulfate is a stronger ligand than chloride, and sulfato-complexes constitute a few percent of the speciation of the major cations in seawater (Chapter 9). Sulfate salts of the monovalent cations are very soluble, and $MgSO_4$ also is quite soluble ($K_{s0} = 10^{-2.13}$). However, solid forms of calcium sulfate (anhydrite ($CaSO_4$), $K_{s0} = 10^{-4.36}$, and gypsum ($CaSO_4 \cdot 2H_2O$), $K_{s0} = 10^{-4.61}$) limit the solubility of these ions in brackish waters, forming evaporite deposits of these minerals in arid areas of the western United States. Sulfur is an essential element for biota, and sulfate is the main source for microorganisms, which reduce it *in vivo* to sulfide (S^{-II}), the main oxidation state for S in organisms. Sulfate is rarely limiting for microbial growth in natural waters, and the amounts required for growth are small relative to ambient concentrations such that biological uptake is not a major sink for sulfate.

Silica, SiO_2, occurs in water as the hydrated species $Si(OH)_4$ ($pK_{a1} = 9.84$), primarily a result of weathering of clays and aluminosilicate minerals in soils. Concentrations are variable depending on the ease of weathering of local soils and rocks and range from sub-mg/L values in dilute (soft) waters to tens of mg/L in many rivers and ground waters. Because silica is a required nutrient for some algae (diatoms), concentrations vary seasonally in surface waters, with minimum concentrations occurring during summer.

Four elements in Figure 2.1 are considered minor constituents in fresh waters: Al, Fe, Mn, and F. For seawater we may add the minor species boron (present as boric acid, $B(OH)_3$), strontium, and bromide, which are trace elements in freshwaters. The minor elements rarely constitute more than a few percent of the inorganic solutes of water bodies, and their concentrations usually are below 1 mg/L in freshwaters. The minor nonmetals occur in the low mg/L range in seawater. The three metals (Al, Fe, and Mn) are insoluble at circumneutral pH in oxic waters. Under these conditions Fe and Al are in the +III oxidation state, and Mn is +IV, and they occur in the μg/L to tens of μg/L range ($\sim 10^{-7}$ to 10^{-6} M). Under anoxic conditions, the reduced oxidation states (+II) of Fe and Mn are more soluble, and concentrations may rise to many tens to hundreds of μg/L ($\sim$1–10 μM). Al has only one oxidation state (+III), and regardless of redox status its solubility is limited to the submicromolar range at pH > 5 by the low solubility of $Al(OH)_{3(s)}$. Elevated dissolved Al concentrations can occur in acidic waters, and this is a concern regarding lake and stream acidification by acid deposition because of toxic effects on biota.

Fluoride occurs naturally at trace (ppb) levels in most freshwaters, but concentrations > 1 mg/L are found in some arid regions of the western United States. Fluoride often is

added to drinking water at levels of 0.7–1 mg/L to help prevent tooth decay.* Because of this widespread practice, which is still controversial, municipal wastewater effluent usually has elevated F^- concentrations ($\sim$1 mg/L), and F^- concentrations in waters receiving wastewater effluent are correspondingly elevated.

2.2.2 Hard versus soft waters

Hardness is defined as the sum of the concentrations of divalent cations in water. In most cases, it is essentially the sum of Ca^{2+} and Mg^{2+}, both expressed in mg/L as $CaCO_3$ (see Section 1.3.4). Various other chemical conditions, however, are associated with hardness and its converse, ***softness***. Hardness and alkalinity are usually closely correlated because they are derived in large part from a common source—dissolution of limestone ($CaCO_3$). Hard waters tend to be high in total dissolved solids (TDS) and have relatively high pH (> 7). Soft waters tend to have low TDS and lower pH. They also tend to be more corrosive to metals and more susceptible to acidification by atmospheric acid deposition (because they have less buffering capacity; Chapter 8). We will use the terms ***hard water*** and ***soft water*** as shorthand way of describing these broader chemical characteristics. Waters often are classified according to hardness as follows:

Hardness	meq/L	mg/L as $CaCO_3$
Soft	< 1	< 50
Moderately hard	1–3	50–150
Hard	3–6	150–300
Very Hard	> 6	> 300

2.2.3 Water quality significance of the major and minor ions

The major ions generally do not have negative ecological effects over the concentration ranges at which they occur in fresh water, although elevated salt levels in waters of arid climates can cause problems for agriculture. However, many aquatic organisms do have preferences for certain chemical conditions. Some aquatic plants and species of algae prefer hard (or soft) water—so much so that indices have been developed that predict various chemical characteristics of water (pH, alkalinity, nutrient concentrations) based on the species composition of algae or major classes of algae (e.g., diatoms).[2]

Similarly, none of the major ions causes serious health issues for humans within the ranges found in fresh waters, but several ions raise concerns related to human health and drinking water quality. Sodium is implicated in cardiovascular disease. Although food rather than drinking water is usually the major source of sodium in human diets, high levels of sodium in water softened by ion exchange (see below) may be of concern to persons on restricted-salt diets. Chloride causes a salty taste in drinking water, and the federal secondary ***drinking water standard***[†] for Cl^- is 250 mg/L. Sulfate also causes taste problems (bitter or astringent taste) and has a laxative effect at

---

*The mineral fluorapatite ($Ca_5(PO_4)_3F$) is more resistant to dissolution and decay than is the main ingredient of tooth enamel, carbonated hydroxyapatite, which is $Ca_5(PO_4)_3OH$ with some –OH groups replaced by carbonate groups.

[†]***Secondary standards*** are nonenforceable guidelines based on aesthetics; ***primary drinking water standards***, usually called MCLs (maximum contaminant levels), are legally enforceable values based on human health issues.

high concentrations. This can cause diarrhea problems for travelers to areas with much higher sulfate concentrations in drinking water than found in their home environments (and also for infants living in such areas), and the federal secondary drinking water standard for sulfate is 250 mg/L.

Calcium, magnesium, and potassium are essential mineral nutrients for humans and aquatic organisms, and the presence of these ions in water is considered beneficial for human health. The hardness cations, primarily Ca^{2+} and Mg^{2+}, nonetheless cause household problems—soap precipitation causing poor lathering and ineffective cleaning, mineral deposits on glassware, and buildup of limestone scale in hot water heaters and pipes. As a result, if high hardness is not removed by a central (municipal) water treatment plant, consumers often choose to remove it from their water by point-of-use ion-exchange softeners, which replace each Ca^{2+} and Mg^{2+} ion with two Na^+ ions. Central water treatment plants usually remove hardness by the lime-soda softening process (see Chapter 10).

As mentioned above, the addition of fluoride to drinking water to prevent tooth decay is controversial. The controversy has two aspects, and a huge literature exists on this topic. First, fluoride has well-known negative effects at higher concentrations. At concentrations only slightly above the optimum for tooth protection, it causes dental *fluorosis*—mottling that ranges from mild discoloration to strong staining and pitting of tooth enamel. At higher concentrations it causes a condition called skeletal fluorosis, leading to joint stiffness, arthritic symptoms, and increased risk of bone weakening and fracture. Severe cases generally are associated with high F^- concentrations (> 10 mg/L), but a recent review[3] concluded that the U.S. EPA's current MCL of 4 mg/L in drinking water should be lowered because of increased risk of dental fluorosis, bone fracture, and skeletal fluorosis at concentrations between $\sim$2.5 and 4 mg/L. The second aspect of the fluoridation controversy is a philosophical difference between proponents and opponents regarding the appropriate balance of government actions that benefit many but may infringe on individual rights. Fluoridation is one of many examples of such public policy conflicts. Some opponents argue that fluoridation is a medical treatment and that it is unethical to practice it without medical supervision or informed consent. Proponents view it as an appropriate public intervention that just replicates the benefits of naturally fluoridated water. They argue that it provides the greatest benefits to those least able to help themselves and that it would be unethical to withhold treatment.[4] The chemistry and water quality significance of the other minor elements are described in Chapter 15.

2.2.4 Sources of major and minor ions

Sources of the inorganic species in natural waters can be divided into two broad categories: natural and human derived. In turn, natural sources can be divided into terrestrial and atmospheric. The former involve *weathering* reactions of rocks, minerals, and soils in the catchment of a water body or solid matrix of an aquifer. The latter represent a transport mechanism rather than an ultimate source. Except for the fixed gases (e.g., O_2 and N_2), atmospherically derived materials in natural waters originate in terrestrial or in some cases aquatic (mainly marine) environments, although they may undergo chemical transformation while in the atmosphere.

In a simple sense, weathering is just the dissolution of minerals. There are two main types of mineral dissolution processes: ***congruent*** and ***incongruent***. In the former, the solid phase dissolves to form only soluble species, and no new solid phase is formed. Dissolution of simple salts, including metal sulfates and carbonates, behaves this way. For example, limestone (impure calcium carbonate) dissolves to form only calcium and bicarbonate ions:

$$CaCO_{3(s)} + H_2O + CO_{2(aq)} \rightarrow Ca^{2+} + 2HCO_3^- \tag{2.1}$$
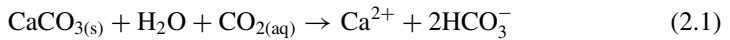
Primary silicate minerals such as feldspars and secondary aluminosilicate clay minerals dissolve incongruently, forming a secondary mineral phase, in addition to releasing ions to solution. Recalling Sillen's geotitration model (Chapter 1), we can write a generalized weathering equation:

$$\text{basic rocks/minerals} + \text{acidic rain} \rightarrow \text{base cations} + \text{alkalinity} + \text{silica} + \text{clay minerals} \tag{2.2}$$
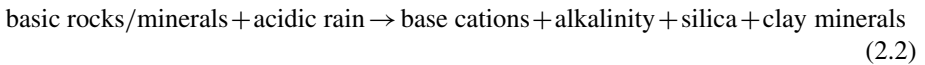
For example, albite, a sodium feldspar, reacts as follows:

$$\underset{\text{albite}}{NaAlSi_3O_{8(s)}} + H_2O + CO_{2(aq)} \rightarrow \underset{\text{all in solution}}{\underline{Na^+ + HCO_3^- + 2Si(OH)_{4(aq)}}} + \underset{\text{kaolinite}}{Al_2Si_2O_5(OH)_{4(s)}} \tag{2.3}$$

Aluminosilicate weathering is complicated (see Chapter 14 for details). Here we mention a few important features. First, weathering is 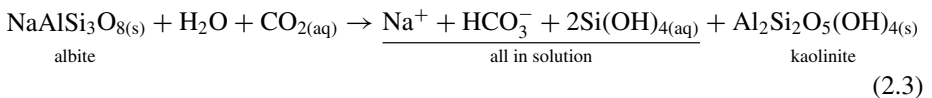essentially an acid-base reaction, and some source of acid—carbonic acid from atmospheric CO_2, mineral acids (H_2SO_4 or HCl) from acid rain or volcanic activity, or organic acids from humic matter—is needed to accelerate the process. Water itself can act as an acid, but it is so weak that weathering is very slow in pure water. Second, the process occurs as two steps: the mineral being weathered is broken down first to soluble species, and the secondary mineral is formed separately. Third, many primary and secondary silicate minerals—with varying susceptibilities toward weathering—can serve as the reactant, and various clays are formed as the solid-phase products. The products, however, always have a higher Al:Si ratio than the reactants because of the production of dissolved silica in the weathering process. Fourth, the HCO_3^- produced from dissolved CO_2 by weathering is a major source of alkalinity. Fifth, although aluminosilicate weathering is slow, it is energetically favorable and essentially irreversible—i.e., reactions like Eq. 2.3 have a strong tendency to proceed to the right and do not go in the opposite direction. Finally, the nature of the base cation(s) produced depends on the composition of the minerals undergoing weathering, but such reactions do yield all four major cations.

Globally, atmospheric transport contributes major ions to freshwaters from marine aerosols formed when sea spray evaporates. These aerosols can travel great distances in the atmosphere and are an important source of major ions in rainfall over terrestrial areas. Because Cl^- is the most abundant ion in seawater (almost twice as high by weight as Na^+, the next most abundant ion) and because terrestrial sources of Cl^- are not abundant (absent human activities), atmospheric (or ***cyclic***) chloride is a relatively important source of the ion. On a local scale, wind-blown dust and soil also contributes ions to water bodies.

Table 2.2 Effects of some human activities on chemical composition of natural waters

Activity	Effects
Municipal water treatment	Ca^{2+} and Mg^{2+} (−); Na^+ (possible +); F^- (+); Cl^- (+)*; HPO_4^{2-} (corrosion inhibitor) (+); suspended solids and NOM (−)
Home water treatment	Ca^{2+} and Mg^{2+} (−); Na^+ (+) by ion-exchange softening
Wastewater treatment	Suspended solids, organic matter and some nutrients (−); Cl^- and SO_4^{2-} (+)*
Food processing/cooking	Na^+, Cl^-, other major ions (+); trace elements (+)
Domestic cleaning materials	Surfactants (soaps, detergents), HPO_4^{2-}, NH_4^+, various organic chemicals (+)
Street deicing	Na^+ and Cl^- (+)
Agriculture	N and P forms and K^+ from fertilizer (+); suspended solids from soil erosion (+); organic chemicals (pesticides) (+)
Mining activities	SO_4^{2-} from pyrite oxidation (+)
Chemical manufacturing	Cl^-, SO_4^{2-} (from HCl and H_2SO_4) (+); Na^+ (from NaOH) (+)
Construction activities	Ca^{2+}, HCO_3^- from concrete (+); Ca^{2+}, SO_4^{2-} from gypsum (+)

* Cl^- is not added directly but is a product of the reaction of Cl_2 or NaOCl added as disinfecting agents; SO_4^{2-} is a product of sulfite added to wastewater effluent as a dechlorinating agent.

The atmosphere is an important proximate source, via rainfall and dry deposition, of inorganic nitrogen (ammonium (NH_4^+), and nitrate (NO_3^-)) and sulfate to surface waters. Although all three ions occur in pristine rain, their concentrations have been increased greatly over the past 50–75 years by human activities. Volatilization from feedlots and waste treatment lagoons and loss of applied fertilizer from fields are large sources of atmospheric NH_3. Nitrogen oxides (NO and NO_2, together referred to as NO_x), from fossil fuel combustion—both stationary sources, such as electric power plants, and mobile sources, such as cars and trucks—are oxidized by photochemical reactions to form nitric acid vapor, $HNO_{3(g)}$, in the atmosphere.[5] SO_2, mainly from combustion of coal and oil, similarly is oxidized to sulfuric acid, H_2SO_4, in the atmosphere. The timescale for these reactions is on the order of many hours ($<$ one day to a few days), and the spatial scale of transport is hundreds to thousands of kilometers. Volatilized NH_3 reacts with sulfuric and nitric acid in the atmosphere to form ammonium sulfate and ammonium nitrate aerosols, which settle onto terrestrial surfaces by "dry deposition" or act as nuclei for raindrop formation.

Human activities contribute significant quantities of all seven major ions to natural waters, as summarized in Table 2.2. Many impacts are associated with the treatment of water for domestic use and its use for cooking in homes and commercial establishments, but industrial uses of mineral acids and bases, agricultural activities, mining, and construction practices also make important contributions.

2.2.5 Chemical composition of natural waters: some examples

Table 2.3 summarizes the ionic composition, including inorganic nutrients where available, of freshwaters across a range of ionic strength and hardness, along with

background information on conductivity and pH. The waters listed include low ionic-strength rainfall, soft- and hard-water lakes, springs, and ground water from limestone and igneous aquifers. An estimate of the average composition of North American river water also is given. Differences in chemical composition between rainfall and the surface and ground waters—even those with low ionic strength—are readily apparent. Ammonium and nitrate, primarily from human activities, are a much higher fraction of the total ions in rainfall than in surface waters, and because rainfall is acidic (pH is < 6), bicarbonate is absent. The most abundant anion in rain usually is sulfate, derived from atmospheric oxidation of anthropogenic SO_2 emissions or sea-salt aerosols. Concentrations of the major ions in surface and ground waters of calcareous regions are in the range of tens of mg/L (mM range); major ions in rainfall and very soft waters generally are ≤ 1 mg/L.

The oceans cover 70% of the Earth's surface. On a volume basis, seawater represents an even greater proportion of the Earth's water resources (~96.5%; see Table 2.4). Moreover, about half of the inland water (lakes, rivers, ground water) is saline. Freshwater thus provides only a small fraction (< 0.8%) of the Earth's total water resources. An emphasis on understanding the chemistry of freshwater is appropriate for environmental engineers and scientists, given the essential role of freshwaters as agricultural and drinking water supplies, the wide range of ecosystem services they provide, the impacts humans have on freshwaters (including overuse), and the great lengths humans have gone in order to engineer/attempt to control freshwaters (diversions, dams, reservoirs). Nonetheless, the abundance of saline waters globally suggests the need for balance in our coverage. Moreover, we should be mindful that saline inland waters also provide ecosystem services and benefits to human society, and the importance of the oceans hardly needs to be stated. Beyond these considerations, saline waters have many unusual chemical features that make them worthy of attention.

Table 2.5 lists the chemical composition of seawater and a few hypersaline water bodies. Although the dissolved salt content of seawater (i.e., its salinity) varies somewhat around the world's oceans and seas, the relative chemical composition, especially of the major constituents, is remarkably uniform. Most ocean water has a salinity of ~35‰ (~97% is between 33‰ and 37‰),[16] and standard seawater is defined to have a salinity of 35.00. Until 1978 salinity was defined in reference to an artificial seawater standard maintained in Copenhagen, and the salinity of a seawater sample was determined from the ratio of its conductivity to that of the standard seawater. Since 1978, oceanographers have defined salinity on the ***Practical Salinity Scale*** as the ratio of the conductivity of a sample to that of a standard solution containing 32.4356 g of KCl in 1 kg of solution (0.4452 m KCl). As a ratio of conductivity values, salinity is dimensionless, and the symbol ‰ is no longer used by oceanographers. An alternative unit called practical salinity units similarly has been disdained.[17] Nonetheless, salinity still serves, at least for persons who are not marine scientists, primarily as a measure of the dissolved inorganic solids in a seawater sample, even if it no longer is tied directly to the way dissolved solids content is measured. For this reason, we will continue to use the symbol ‰ to express salinity values in this book.

It is apparent from Table 2.5 that the predominant ions in seawater are Na^+ and Cl^-. The second-most abundant ions are Mg^{2+} and SO_4^{2-}. The much lower concentrations of Ca^{2+} and HCO_3^- are explained by solubility constraints; calcium carbonate minerals

Table 2.3 Chemical composition of atmospheric deposition and some freshwaters

A. Variable*	Atmospheric precipitation[†]				Lakes[‡]				Rivers[§]			
	Gainesville, Fla., 1976–1977	Trout Lake, Wisc., 2005	Sagehen Creek, Calif., 2005	Whiteface Mt., N.Y., 2005	Little Rock, Vilas Co., Wisc.	Harriett, Minneapolis, Minn.	Mendota, Madison, Wisc.	Tahoe, Calif., Nev.	Colorado River, Az.	Salt River, Az.	North America average	Global average
SC	—	8.01	2.38	11.39	12.4	484	350	92	966	1337	—	—
pH	4.53	5.12	5.44	4.72	6.16	7.3	7.9	7.3	8.3	8.07	—	—
Ca^{2+}	0.41	0.139	0.014	0.052	0.84	40	31	8.4	70.9	52.9	21.2	14.7
Mg^{2+}	0.12	0.018	0.003	0.008	0.29	13	25.5	2.5	27.7	15.8	4.9	3.7
Na^+	0.44	0.027	0.023	0.024	0.18	50	6.3	6.0	92.7	188	8.4	7.2
K^+	0.20	0.031	0.004	0.020	0.60	5.6	4.0	1.6	4.4	5.4	1.5	1.4
NH_4^+	0.129	0.344	0.024	0.166	0.024	0.064	—	0.004	—	—	—	—
HCO_3^-	—	—	—	—	1.32	131	200	56	161	153	72.3	53.0
SO_4^{2-}	2.05	0.783	0.067	0.932	2.73	9	24	2.0	243	64.2	18.0	11.5
Cl^-	0.98	0.048	0.044	0.051	0.37	97	7.9	2.0	80.3	300	9.2	8.3
NO_3^-	0.84	0.828	0.121	0.727	0.123	0.044	—	0.033	1.2	0.55	—	—
F^-	0.01	—	—	—	0.02	0.15	0.17	—	0.3	—	—	—
$Si(OH)_4$	—	—	—	—	—	—	0.8	22.1	8.8	—	7.2	10.4

B. Variable*	Springs[¶]			Ground water[£]				
	Silver Ocala, Fla.	Blue Seminole, Fla.	Apopka Winter Garden, Fla.	Floridan aquifer (1)	Floridan aquifer (2)	Well-water, Pennsylvania	Near Lake Tomahawk, Wisc., unconfined aquifer	Kenora, Ont., unconfined aquifer
SC	440	2120	255	458	—	—	50.1	—
pH	7.2	7.2	7.8	7.48	7.69	7.47	6.3	6.3
Ca^{2+}	76	77.8	31.5	80	56	55	9.9	4.8
Mg^{2+}	9.4	35.9	8.6	19.4	12	28	1.8	1.54
Na^+	6.8	307	6.3	8.5	7.9	3.1	1.46	2.07
K^+	0.59	10.3	1.4	1.3	1.0	0.6	0.70	0.59
NH_4^+	0.1	0.09	—	—	—	—	—	—
HCO_3^-	231	185.4	100	207.4	160	265	45.0	24.0
SO_4^{2-}	26	82	12	8.2	53	20	0.46	1.1
Cl^-	9.6	550	14	35	12	10	0.68	0.6
NO_3^-	1.1	0.36	4.5	0.02	—	—	0.02	—
F^-	0.19	0.091	0.073	0.4	—	—	0.05	—
$Si(OH)_4$	10	8	5	14	—	—	15.0	22.1

* Specific conductance (SC) in $\mu S/cm$; all ions in mg/L as the stated species; silica in mg/L as SiO_2.

[†] All sites are wet-only precipitation; Gainesville from Hendry and Brezonik[6]; other sites from National Atmospheric Deposition Program.[7] Data are volume-weighted annual average values.

[‡] Little Rock and Harriett data from the author (P.L.B.); Mendota median values from 1966–1967, courtesy of J. Delfino,[8] , Univ. of Florida; Tahoe data compiled from various sources, courtesy of C. Goldman and P. Arneson, University of California–Davis.

[§] Salt River, Arizona, at Lake Roosevelt (reservoir); Colorado River at Granite Reef in Colorado-Arizona Project canal. Data compiled by and courtesy of Larry Baker, University of Minnesota; North American and global average values from Berner and Berner[9] based on data of Meybeck.[10]

[¶] Spring data for various dates in 2002–2008 compiled by St. Johns River Water Management District (SJRWMD) from various sources; courtesy of E. Lowe, SJRWMD, Palatka, Fla.

[£] Floridan aquifer and Pennsylvania wells are in dolomitic limestone; Kenora aquifer is in igneous rock; aquifer near Lake Tomahawk is in glacial till. (1) from Gainesville regional utility courtesy of J. Delfino and P. Chadik, University of Florida; well near Lake Tomahawk, unpublished data of the author (P.L.B.); other columns from Freeze and Cherry.[11]

Table 2.4 Distribution of Earth's water resources[12]

Source	Volume (km^3)	Percent of total	Residence time
Oceans and seas	1.338×10^9	96.5	~ 4000 years
Ice caps, glaciers, permanent snow	2.406×10^7	1.74	10–1000 years
Ground water	2.304×10^7	1.7	2 weeks-10,000 years
Freshwater	1.053×10^7	0.76	
Saline water	1.287×10^7	0.94	
Ground ice and Permafrost	3.0×10^5	0.022	
Lakes	1.764×10^5	0.013	~ 10 years
Fresh	9.10×10^4	0.007	
Saline	8.54×10^4	0.006	
Soil moisture	1.65×10^4	0.001	2 weeks-1 year
Atmosphere	1.29×10^4	0.001	~ 10 days
Swamps	1.15×10^4	0.0009	1–10 years
Rivers	2.12×10	0.0002	~ 2 weeks

Table 2.5 Chemical composition of seawater and some hypersaline water bodies*

Constituent	Seawater[†]	Great Salt Lake[‡]	Mono Lake[‡]	Dead Sea[§]
pH	8.1	8.5	9.65	6.3
Na^+	10.76	15.6	32.0	39.2
K^+	0.399	1.22	1.71	7.3
Ca^{2+}	0.412	0.13	0.0064	16.9
Mg^{2+}	1.294	1.73	0.0405	40.7
Sr^{2+}	0.0079	—	—	—
Cl^-	19.35	28.3	10.05	212.4
SO_4^{2-}	2.712	3.45	5.44	0.5
HCO_3^-	0.145	0.43	40.30**	0.2
Br^-	0.067	—	—	4.2
F^-	0.0013	—	—	—
$B(OH)_3$ as B	0.0046	—	—	—
$Si(OH)_4$ as Si	0.0029	—	—	—

* Concentrations in g/kg for seawater and g/L for other waters except for pH (dimensionless).
[†] From Holland.[13]
[‡] From Domagalski et al.[14]
[§] From Nissenbaum.[15]
** Based on reported average alkalinity of 660 meq/L and stated pH.

(calcite and aragonite) are close to saturation in seawater, which is important for species that have shells (see Chapter 10). The ionic content of seawater sometimes is expressed in terms of its chloride content, or **chlorinity**, which for standard seawater is 19.4‰. A simple formula relates chlorinity and salinity:

$$\text{Salinity}(‰) = 0.03 + 1.805 \times \text{chlorinity}(‰) \tag{2.4}$$

An extreme example of a hypersaline water body is the Dead Sea (Israel-Jordan), which is located in a closed basin at the lowest location on the Earth's surface not covered by water or ice (480 m below sea level). (*Hypersaline* refers to conditions

more saline than seawater.) With a salt content of $\sim$320 g/L, about nine times that of seawater, it is the Earth's second saltiest water body. It has an unusually high density 1.23 g/mL, providing much more buoyancy than seawater or freshwaters (Figure 2.2a), and its chemical composition is markedly different from that of seawater, being depleted in sulfate and bicarbonate but elevated in Br^-. It is said to have the highest Br^- concentration of any water body on Earth. Its water is saturated with $NaCl$,[18] and halite crystals occur on rocks around its shoreline (Figure 2.2b). Mono Lake (California-Nevada), an alkaline brine, is quite different from the Dead Sea and seawater in chemical composition. The order of abundance of cations is $Na^+ \gg K^+ \gg Mg^{2+} > Ca^{2+}$,

(a)

(b)

Figure 2.2 (a) The buoyancy of the Dead Sea is seen by how high in the water the chemist's body floats. (b) Halite crystals on rocks along the Dead Sea shoreline. (a) Courtesy of Carol Brezonik; (b) by author (P.L.B.), August 1998. (See color insert at end of book for a color version of this figure.)

Figure 2.3 Mono Lake (California-Nevada), showing tufa towers of calcium carbonate formed in situ when the lake level was higher. Photo by author (P.L.B.), December 1999. (See color insert at end of book for a color version of this figure.)

and the concentration of Ca^{2+} is lower than found in typical hard waters of limestone regions. The low Ca^{2+} concentrations allow high HCO_3^- concentrations in Mono Lake, and the water is described geochemically as a $Na–CO_3–Cl–SO_4$ brine. In spite of the low Ca^{2+} concentrations, the lake is at or near saturation with respect to $CaCO_{3(s)}$, and spectacular limestone formations called tufa towers are formed in the lake (Figure 2.3). In contrast to Mono Lake, Great Salt Lake (Utah) is a low-alkalinity $Na–Mg–Cl–SO_4$ brine. Its two main basins (separated by a manmade causeway) differ in salinity, which overall, has varied significantly over historical times, reflecting cycles of lower or higher precipitation and corresponding changes in lake stage. More information on the chemistry of these interesting water bodies is provided in the references cited in Table 2.5.

2.3 The hydrologic and hydrochemical cycles

The *hydrologic cycle* involves the cyclic movement of water on a global scale: (1) evaporation from surface waters, especially the oceans, to the atmosphere; (2) transport as water vapor and clouds; (3) precipitation on land as rain and snow; (4) subsequent runoff into streams and rivers or (5) percolation into aquifers, which provide (6) base flow for downgradient rivers and streams; (7) storage in lakes and reservoirs; (8) appropriation by humans from surface and subsurface storages and conduits for use in agriculture, industry, and cities; and (9) ultimate return to the oceans by rivers and ground water discharge. The above numbers are keyed to portrayal of processes in the cycle
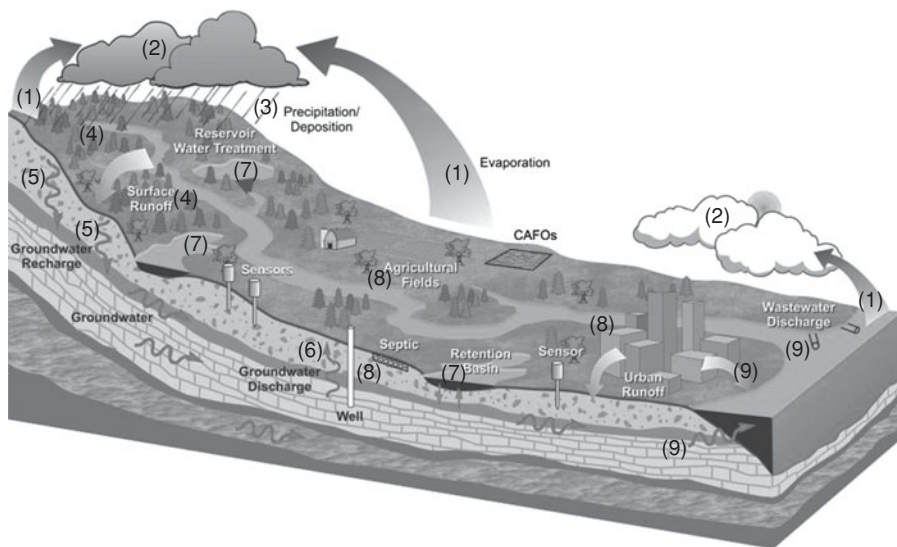
Figure 2.4 Schematic representation of the hydrologic cycle illustrating the role of human activities in the cycle and related hydrochemical cycle. See text for explanation of numbers. From NSF WATERS Network initiative, courtesy of Jerald Schnoor, University of Iowa. (See color insert at end of book for a color version of this figure.)

in Figure 2.4. In a broader sense, the hydrologic cycle involves the transport not just of water, but also numerous dissolved and suspended constituents that accumulate in water at steps in the cycle. This idea leads to the concept of the ***hydrochemical cycle***. The chemical composition of water varies dramatically in different parts of the cycle, as a result of interactions with the atmosphere, soil and subsurface solids, natural biological processes, and human activities. The residence times of the water in different compartments (see Table 2.4) also are important in this regard. Although the residence time of water in the atmosphere is short, gas-water exchange is rapid, and atmospheric water can be assumed to be in equilibrium with surrounding gases. Ground water often has high levels of dissolved solids, in part because of the long water-mineral contact times. Minerals that dissolve in streams and rivers as they flow through landscapes accumulate in the oceans. Concentrations of some species in surface waters (e.g., oxygen and carbon dioxide) are dynamic because of biochemical processes in sunlight exposed waters. With reference to the reaction types described in Section 1.4 and previous discussions in this chapter, the major processes affecting global hydrochemistry are described below.

When water vapor condenses into cloud droplets in the atmosphere, it absorbs reactive gases, such as CO_2, NH_3, SO_2, and NO_x, and aerosols formed photochemically from the reactive gases, as well as aerosols from salt residues when seawater droplets evaporate. Although the chemical composition of cloud water and rainwater is complicated, it is dilute compared to most water bodies (Table 2.3). Because of the absorption of acidic gases and aerosols, rainfall is a weakly acidic solution of sulfuric, nitric, and carbonic acids with a pH of $\sim$4.0–5.5 across most of the United States. The acidity of precipitation promotes mineral weathering of soils and rocks

on the Earth's surface. Rocks and minerals (including clays) of varying composition participate in the weathering reaction, which accounts for most of the silica and much of five major ions in natural waters (the four cations and bicarbonate). "Cyclic salts" from marine aerosols account for some of the nonanthropogenic Cl^- and SO_4^{2-}. Dissolution of calcium sulfate minerals is a source of natural SO_4^{2-} in arid environments.

As water percolates through soils and aquifers, weathering reactions continue. In calcareous regions the dissolution of limestone and dolomite, $CaMg(CO_3)_2$, is an important source of divalent cations and bicarbonate. Oxidative dissolution of sulfide minerals adds sulfate, iron, and other heavy metals to the water. Biological processes also affect the chemical composition as water moves through the landscape. Primary production raises the pH because it removes the weak acid $CO_{2(aq)}$, and this causes $CaCO_3$ to precipitate. Natural organic ligands produced by aquatic microorganisms form complexes with major cations and trace metals produced by weathering reactions. Organic matter of plants exerts an oxygen demand as it decomposes to more refractory forms, adding dissolved organic matter (DOM, measured as DOC) to the water. This may induce anoxic conditions in ground water and bottom layers of lakes, thus stimulating a range of redox reactions, including the reductive dissolution of iron and manganese oxides.

Thus far, we have not mentioned the effects of human activities on hydrochemistry. A century or so ago, the above overview would have been satisfactory as a simple explanation of the global hydrochemical cycle. We are not implying that human activities had no effects on water chemistry prior to the last century or two, but the smaller global population and lower use of fossil fuels and other minerals meant that human impacts were limited to local areas or small regions. Today, human impacts at the scale of continental- or global-average concentrations cannot be ignored. Impacts on the hydrochemical cycle start in the atmosphere, where SO_2 and NO_x emissions from fossil fuel combustion lead to higher acidity in rainfall than occurs naturally, accelerating weathering reactions in landscapes. Major human interventions in hydrochemistry occur when rainwater or stored water is used to irrigate crops and when water is captured behind dams (both large and small). Numerous other hydrologic modifications caused by human activities—conversion of wetlands to uplands, drainage of agricultural soils by tile drains, stormwater management practices and other hydrologic modifications in urban areas—all have implications for aquatic biogeochemistry. Pumping groundwater at rates faster than it is recharged or pumping "fossil" ground water (where recharge, if any, is extremely low) also is a human alteration of the hydrochemical cycle. Modern industrial-scale agriculture consumes large quantities of fertilizer, herbicides, insecticides, antibiotics, and other chemicals to produce impressive yields of grains, vegetables, fruits, and livestock, but excess nutrients and synthetic organic chemicals— unintended by-products of these operations—contaminate streams and ground water in agricultural regions.

The appropriation of water by cities changes water chemistry and quality significantly. In treating water for drinking purposes, chemicals are added to remove turbidity. Softening removes Ca^{2+} and Mg^{2+} but adds Na^+. Disinfection adds chlorine to the water. Use of treated water by domestic and industrial consumers adds various salts to water, and road salt (mainly NaCl) used for deicing in cold climates affects the chemistry of urban runoff. Domestic use of water adds large amounts of organic matter and related nutrients (N and P) to water. Most but not all of the organic matter is removed by wastewater

treatment plants before discharge into a receiving water body. Finally, domestic use of personal-care and household products, as well as consumer use of pharmaceuticals and antibiotics and industrial production and use of synthetic organic chemicals, adds a potpourri of organic compounds to water draining from urban areas. Many of these compounds are slow to degrade and remain a part of the water cycle for long times. The low solubility of many organic chemicals in water promotes their partitioning to solids and settling from water to the bottom sediments. Other important processes that remove organic contaminants from the water environment include photolysis, hydrolysis and oxidation/reduction.

The hydrochemical changes described in preceding paragraphs are exemplified by water chemistry data for a series of sampling sites in the Upper Mississippi River Basin (Table 2.6). Sites were selected to illustrate the effects of major natural processes and human interventions on water chemistry. Differences in water chemistry can be seen (1) between the headwaters (Lake Itasca) and conditions down river, (2) as the river passes through the urban area of Minneapolis and St. Paul, Minnesota, and (3) between a tributary draining a largely forested basin (the St. Croix River) and a tributary draining a large agricultural region (the Minnesota River). In addition, large effects of treatment processes and human use of water are readily evident in the water chemistry/quality data from the drinking water and primary and secondary wastewater effluent samples from a wastewater treatment plant (WWTP).

2.4   Models of the chemical composition of natural waters

2.4.1 Introduction

Although Tables 2.3, 2.5, and 2.6 represent just a very small sample of available water chemistry data, the diversity in chemical composition found in the world's natural waters is readily apparent. The two previous sections provide qualitative explanations for that diversity, but we understand how readers might be tempted at this point to conclude that the expression "anything goes" applies to water chemistry. That is not the case, however. In this section we describe evidence that the inorganic chemical composition of natural waters can be explained by relative simple relationships and models.

We start with empirical evidence for constraints on the chemical composition of natural waters. Figure 2.5, cumulative frequency distributions of concentrations for ions in the then-available literature, has been widely cited since it was published more than 40 years ago.[19] The plot encompasses concentrations over a range of five orders of magnitude (10^{-2} to 10^3 mg/L), but distributions for individual ions generally occupy only a small part of the range. For example, nearly 80% of the K^+ data are in the range of 1–5 mg/L, and silica values are narrowly distributed around 10 mg/L, probably because of chemical controls on them (e.g., K^+ tends to sorb onto clays in soils). Less reactive ions, such as Na^+ and Cl^-, tend to have wider distributions than do more reactive ions like Ca^{2+}. Taken at face value, the plots indicate that the composition of natural waters is not amorphous—"anything goes" does *not* apply—and suggest that there are limits to compositional variation and explanations for those limits.

A second line of evidence for constraints is provided by log-log plots of ion concentrations in rivers of the United States versus annual runoff per unit area (expressed

Table 2.6 Chemical composition of waters in the Upper Mississippi River Basin near Minneapolis-St. Paul, MN*

Constituent[†]	1 Lake Itasca	2 Miss. R., above Minneapolis	3 Minnesota River	4 Miss. R., St. Paul center	5 Miss. R., at Lock and Dam no. 2	6 St. Croix River	7 Miss. R., below Prescott, Wisc.	8 Minneapolis drinking water	9 St. Paul drinking water	10 Metro WWTP primary effluent	11 Metro WWTP final effluent
Major ions											
Na^+	6.2	11.3	51.4	21.0	31.4	5.65	24.6	12.6	16.0	165	163
K^+	1.9	3.0	6.5	3.8	4.3	1.2	3.4	2.7	2.6	17.3	14.4
Ca^{2+}	40.8	50.4	72.8	55.8	51.1	28.9	44.0	16.6	24.8	66.2	67.5
Mg^{2+}	16.5	18.1	38.8	22.6	20.1	11.4	17.9	4.4	3.4	21.9	20.6
HCO_3^-	210	198	266	215	198	127	172	24	57	349	172
Cl^-	1.7	26.6	65.1	31.2	43.1	8.8	34.5	26.6	30.1	235	235
SO_4^{2-}	0.9	28.3	134	51.8	46.1	6.3	34.3	28.3	23.1	78.9	79.6
General											
pH	7.92	8.37	8.16	8.24	8.35	8.65	8.32	8.02	8.10	7.12	7.42
SC	174	315	628	387	397	185	344	174	191	1064	985
Turbidity	0.6	3.9	55	35	9.3	1.8	8.9	0.26	0.06	65	1.6
Color	63	79	58	58	42	71	29	12	–	323	96
Alkalinity	172	162	218	176	162	104	141	19.5	47	286	141
DOC	2.98	8.97	11.2	9.93	10.8	5.11	8.6	5.1	4.8	59.7	13.9
Minor ions											
Fe	0.002	0.003	0.010	0.006	0.006	0.004	0.003	0.018	0.016	0.088	0.028
Mn	0.0005	0.0003	0.002	0.0006	0.001	0.0002	0.0006	0.001	0.001	0.419	0.002
Sr	0.086	0.115	0.312	0.16	0.14	0.05	0.114	0.065	0.062	0.15	0.15
F^-	0.09	0.15	0.26	0.18	0.20	0.08	0.16	0.83	1.02	1.06	0.93
Br^-	0.006	0.04	0.109	0.047	0.057	0.008	0.040	0.032	0.020	0.24	0.22

Nutrients

NO_3^- -N	0.11	0.84	1.73	0.96	1.39	0.28	0.94	0.69	0.75	0.46	16.5
Total dissolved phosphorus[g]	0.013	0.098	0.166	0.116	0.123	0.017	0.101	0.319	0.005	5.78	0.21
SiO_2	11.6	13.3	17.8	13.7	11.8	6.6	10.1	5.6	6.4	15.8	17.8

*Sketch of sample locations in the metropolitan area of Minneapolis-St. Paul, Minnesota:
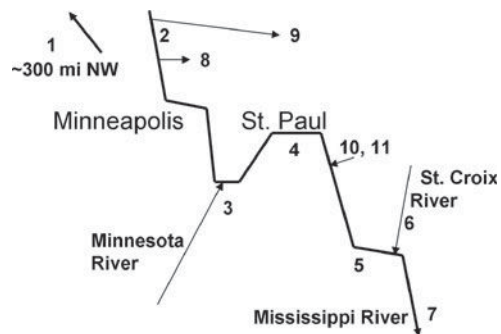
Note: the City of St. Paul takes its drinking water from a combination of the Mississippi River, a drainage basin northeast of the metro area, and ground water.

[†]Concentrations in mg/L except pH (no units), conductivity (μS/cm), turbidity (NTU, [nephelometric turbidity units]), color (PCU [platinum-cobalt units]), and alkalinity (mg/L as $CaCO_3$).
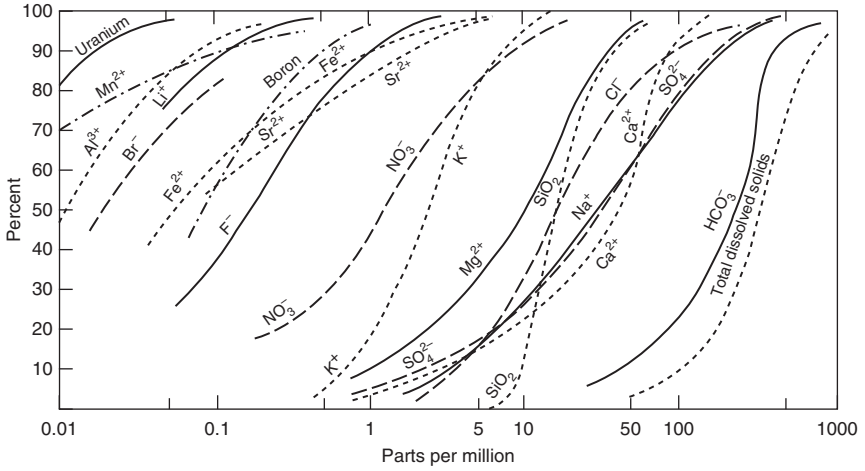
Figure 2.5 Cumulative frequency distributions for concentrations of inorganic solutes in natural waters; data mostly from the United States. Reprinted with permission from Stumm and Morgan[16] (original from Davies and DeWiest[19]), copyright by John Wiley & Sons, Inc.
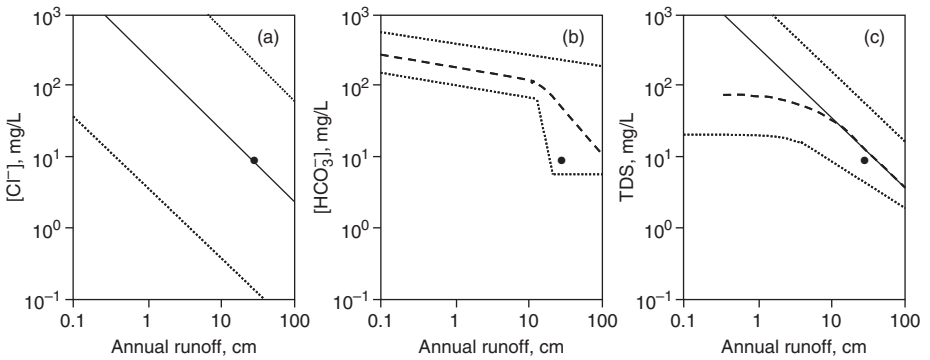
Figure 2.6 Conceptualized plots of (a) chloride, (b) bicarbonate, and (c) total dissolved solid (TDS) concentrations (mg/L) versus annual areal runoff (in cm) in the catchments of U.S. rivers based on plots in Holland.[13] Dotted lines represent approximate ranges of observed data; solid lines in (a) and (c) with slope of −1 represent the "constant source" model: $[i] \times \text{runoff} = \text{constant}$. Dashed lines in (b) and (c) represent general trend in observed data, and the black data point represents world average concentration and annual runoff.

in cm) in the drainage basin (Figure 2.6). Although there is much scatter in such plots, chemically unreactive ions like Cl^- (Figure 2.6a) have a slope of −1. Holland[13] interpreted the general trend as reflecting simple dilution of a constant (atmospheric) source of a highly soluble compound by increasing runoff. The high scatter reflects the importance of other natural and human-influenced sources of Cl^- for individual water bodies. For example, small amounts of halite (NaCl) crystals found in sedimentary rocks of marine origin are thought to be a more important source, on average, of Na^+ and Cl^-

than is cyclic salt.[9] Plots for Na^+ and SO_4^{2-} also have slopes of -1. In contrast, the slope for a reactive species like HCO_3^- (Figure 2.6b) is much flatter (less negative), and the scatter in the data at low annual runoff ($<\sim15$ cm) is lower than the scatter at higher runoff. Plots for Ca^{2+}, Mg^{2+}, and SiO_2 have the same features, and the plots suggest there are solubility constraints on these ions in arid (low runoff) regions.[13] In addition, a log-log plot of total dissolved solids (TDS, mg/L) versus annual runoff (cm; Figure 2.6c) shows a mixture of the trends for conservative and reactive species: a slope of -1 at annual runoff > 10 cm and a flatter slope (approaching a value of zero, suggestive of solubility constraints) at lower runoff. The slope of -1 implies that the annual load of TDS per unit area, i.e., TDS concentration (g/m^3) times flow (m^3) per unit area (m^2), is independent of runoff amount at values > 10 cm/yr.

2.4.2 A simple model for the inorganic chemical composition of natural waters: does it work?

Based on an analysis of data for 135 water bodies around the world, Gibbs[20] proposed an appealingly simple conceptual model to explain the world's water chemistry (Figure 2.7a). Gibbs found that the waters were distributed within "boomerang-shaped"
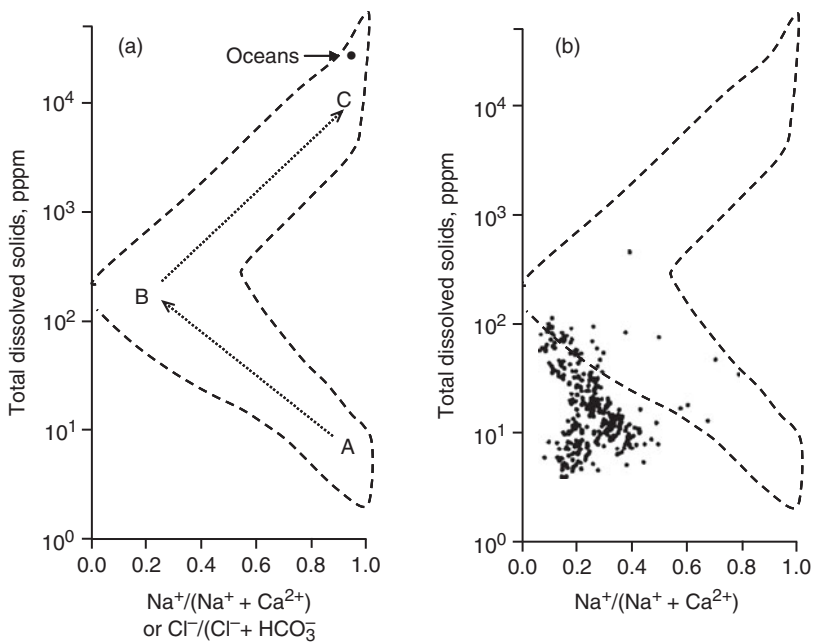

Figure 2.7 (a) Conceptual model of world water chemistry: total dissolved solids (TDS) versus cation and anion ratios based on figures in Gibbs.[20] Waters in region A are dominated by atmospheric precipitation, in region B by rocks (mineral weathering), and in C by evaporation-crystallization (chemical precipitation). (b) Data for 300 soft-water lakes in northeast Minnesota and north-central Wisconsin from Eilers et al.[23] superimposed on conceptual plot from (a).

envelopes on plots of TDS versus the ratio of $Na^+: (Na^+ + Ca^{2+})$ and $Cl^-: (Cl^- + HCO_3^-)$ and concluded that the distribution reflected the relative importance of three underlying processes—atmospheric precipitation, rock dominance, and evaporation-crystallization—over three ranges of TDS. At low TDS, the chemical composition of natural waters was presumed to be dominated by atmospheric precipitation, which in turn is dominated (in terms of major ions) by the chemistry of seawater—via the role of sea-salt aerosols in rainfall chemistry. Low-TDS waters ($<\sim$40 mg/L) thus should have high ratios of $Na^+: (Na^+ + Ca^{2+})$ and $Cl^-: (Cl^- + HCO_3^-)$. At medium values of TDS ($\sim$40–1000 mg/L), Gibbs argued for "rock dominance" on water chemistry, and given the preponderance of easily weathered limestone, dolomite, and other minerals rich in divalent ions, he concluded this should lead to low values of the two ratios. As TDS values continue to rise (through a combination of weathering and evaporation), solubility constraints are reached for divalent metals and carbonate (especially $CaCO_3$), leading to increasing values of the ratios (high proportions of Na^+ and Cl^-) as TDS continues to rise above $\sim$1000 mg/L (upper arms of the boomerang in Figure 2.7a). Because of its simplicity and seemingly rational basis, the model has been widely cited.

It now is evident, however, that the "real world" does not follow the Gibbs model and that his proposed mechanisms are not the correct explanation for the composition of some natural waters. For example, some low-TDS South American waters in the high $Na^+: (Na^+ + Ca^{2+})$ arm were found to be the result of watershed weathering processes rather than atmospheric input of cyclic salts from marine aerosols.[9,21] Numerous waters have been found not to fit in the envelope proposed by Gibbs. Kilham[22] demonstrated that surface waters in tropical Africa occupy a much broader envelope than Gibbs proposed, and Eilers et al.[23] showed that the model does not fit data from several large surveys of dilute, acid-sensitive lakes (Figure 2.7b). These findings do not diminish the general importance of the mechanisms Gibbs proposed as drivers of the chemical composition of natural waters, but they indicate that the mechanisms have little power to predict the ratios of cations and anions as a function of TDS.

2.4.3 Stoichiometric models of chemical provenance

Many papers were published in the early days of water chemistry that attempted to explain the chemical composition of a water body by stoichiometrically forming again the minerals that are presumed to have weathered in the catchment to produce the composition of the water body. The approach is based on Sillen's seminal paper on the origin of seawater.[24] For example, Garrels and MacKenzie[25] accounted for the chemical composition of springs in the Sierra Nevada Mountains by this method (Table 2.7). For such models to be more than academic accounting exercises, evidence should exist that the minerals and products occur in the catchment. Because the primary mineral plagioclase, a feldspar of mixed Na^+ and Ca^{2+} content, is common in the region of the springs and is easily weathered, it made sense for the authors to convert as much Na^+ and Ca^{2+} as possible back to that mineral (a "reverse weathering" calculation). The variable cation composition of plagioclase allows a fair amount of flexibility in varying the amounts of Na^+ and Ca^{2+} used to form the mineral. Potassium feldspar (orthoclase) and biotite, a mica-type of silicate mineral, also are found in bedrock of the region containing the springs.

Table 2.7 Stoichiometric source model for Sierra Nevada springs*

Reaction	Na^+	K^+	Ca^{2+}	Mg^{2+}	HCO_3^-	SO_4^{2-}	Cl^-	$Si(OH)_4$	Products
Initial concentrations	1.34	0.28	0.78	0.29	3.28	0.10	0.14	2.73	
Minus concentrations in snow	1.10	0.20	0.68	0.22	3.10	0.00	0.00	2.70	Derived from rock

Change kaolinite back into plagioclase

$$1.23\ \underset{\text{kaolinite}}{Al_2Si_2O_5(OH)_4} + 1.10\ Na^+ + 0.68\ Ca^{2+} + 2.44\ HCO_3^- + 2.20\ Si(OH)_4 \rightarrow$$
$$1.77\ \underset{\text{plagioclase}}{Na_{0.62}Ca_{0.38}Al_{1.38}Si_{2.62}O_8} + 2.44\ CO_2 + 8.07\ H_2O$$

| Minus plagioclase | 0.00 | 0.20 | 0.00 | 0.22 | 0.64 | 0.00 | 0.00 | 0.50 | 1.77 $Na_{0.62}Ca_{0.38}$ feldspar |

Change kaolinite back into biotite

$$0.37\ \underset{\text{kaolonite}}{Al_2Si_2O_5(OH)_4} + 0.073\ K^+ + 0.22\ Mg^{2+} + 0.15\ Si(OH)_4 + 0.51\ HCO_3^- \rightarrow$$
$$0.073\ \underset{\text{biotite}}{KMg_3AlSi_3O_{10}(OH)_2} + 0.51\ CO_2 + 0.56\ H_2O$$

| Minus biotite | 0.00 | 0.00 | 0.00 | 0.13 | 0.13 | 0.00 | 0.00 | 0.35 | 0.073 biotite |

Change kaolinite back into orthoclase (K-feldspar)

$$0.065\ \underset{\text{kaolinite}}{Al_2Si_2O_5(OH)_4} + 0.13\ K^+ + 0.13\ HCO_3^- + 0.26\ Si(OH)_4 \rightarrow$$
$$0.13\ \underset{\text{K-feldspar}}{KalSi_3O_8} + 0.13\ CO_2 + 0.715\ H_2O$$

| Minus orthoclase | 0.00 | 0.00 | 0.00 | 0.00 | 0.00 | 0.00 | 0.00 | 0.12 | 0.13 K-feldspar |

* Concentrations of reactants and products in 10^{-4} mol/L. From Garrels and MacKenzie.[25]

An interesting result of the calculations is that only a small fraction of the initial dissolved silica remained after aluminosilicates were formed from the available cations. This suggests that the main source of silica in the spring water is weathering of aluminosilicate minerals, not dissolution of quartz. This finding agrees with other stoichiometric modeling studies, including Sillen's model for seawater. A more recent development on this topic—a spreadsheet calculation model that solves for the stoichiometric coefficients in the source-reaction equations simultaneously—has been used to apply the "reverse weathering" approach more broadly to water bodies across the United States.[26] Although this type of model generally has good explanatory power, it has little predictive power. Such models can "hindcast" what happened to form the water but are unable to predict the composition of an unmeasured water body in a catchment from a given set of rocks and mineral—because they are unable to predict how much weathering will occur. Weathering rates depend not just on the nature of the minerals but also on concentrations of weathering agents (acids, ligands) and on flow paths and rates of travel of water through mineral assemblages (see Chapter 15).

Holland[13] used a general accounting approach to calculate the sources of inorganic solutes in global-average river water. He based these values on estimates by Livingstone[27] for the composition of major rivers on each continent and took the simple average for the global value. His calculations (Table 2.8) show that about two-thirds of the Ca^{2+} was attributed to weathering of carbonate rocks (limestone and dolomite), and ~20% comes from weathering of silicate minerals. A greater fraction (~57%) of the Mg^{2+} is derived from silicates (e.g., olivine and biotite), and only 37% comes from dissolution of carbonates (dolomite). Nearly all the K^+ is derived from silicate weathering, but only half of the Na^+ is; the other half comes from NaCl. Holland attributed 40% of the sulfate in global average river water to atmospheric sources, and a large fraction of that was considered to be anthropogenic. Sulfate and sulfide minerals were thought to contribute the remaining 60% in equal amounts. Only about a third of the

Table 2.8 Holland's attribution of solute sources in global average river water*

Source	Anions (meq/kg)			Cations (meq/kg)				Neutral (mmol/kg)
	HCO_3^-	SO_4^{2-}	Cl^-	Ca^{2+}	Mg^{2+}	Na^+	K^+	$Si(OH)_4$
Atmosphere	0.58	0.09	0.06	0.01	≤ 0.01	0.05	≤ 0.01	< 0.01
Weathering or dissolution of								
Silicates	0	0	0	0.14	0.20	0.10	0.05	0.21
Carbonates	0.31	0	0	0.50	0.13	0	0	0
Sulfates	0	0.07	0	0.07	0	0	0	0
Sulfides	0	0.07	0	0	0	0	0	0
Chlorides	0	0	0.16	0.03	≤ 0.01	0.11	0.01	0
Organic matter	0.07	0	0	0	0	0	0	0
Total								
(meq/kg)	0.96	0.23	0.22	0.75	0.35	0.26	0.07	0.22
(mg/L)	58.6	11	7.8	15	4.3	6	2.7	13.2

* From Holland[13]

Table 2.9 Sources of major solutes (in percent of total concentration) in global river water according to Berner and Berner[*]

Solute	Weathering					
	Concentration (mg/L)	Atmospheric cyclic salt	Carbonates	Silicates	Evaporites[†]	Human activities
Ca^{2+}	14.7	0.1	65	18	8	9
Mg^{2+}	3.7	2	36	54	< 1	8
Na^+	7.2	8	0	22	42	28
K^+	1.4	1	0	87	5	7
HCO_3^-	53	< 1	61[§]	37[§]	0	2
SO_4^{2-}[‡]	11.5	2	0	0	22	43
Cl^-	8.3	13	0	0	57	30
$Si(OH)_4$	10.4	< 1	0	99+	0	0

[*] From Berner and Berner.[9]

[†] Includes NaCl from shales and thermal springs.

[§] For carbonates, 34% is from calcite and dolomite and 27% from atmospheric (soil) CO_2 (as driver of carbonate dissolution (equation 2.1); for silicates, all 37% is from atmospheric CO_2 (as the driver of silicate weathering, equation 2.3). Total HCO_3^- from atmosphere (soil) CO_2 is 64%.

[‡] Other sources also are important for sulfate: natural biogenic emissions to atmosphere (delivered to land by rain), 17%; volcanic activity, 5%; pyrite weathering, 11%.

HCO_3^- in river water was attributed to carbonate rocks, but this is misleading. As Eq. 2.1 shows, $CaCO_{3(s)}$ dissolution requires one molecule of CO_2 (or other acid) for every Ca^{2+} produced; i.e., the HCO_3^- is derived equally from carbonate rock and atmospheric CO_2. In this sense, $CaCO_{3(s)}$ dissolution is responsible for 0.62 meq/kg (65% of the total HCO_3^-). Similarly, the production of major cations by silicate weathering is associated with consumption of CO_2 and production of HCO_3^- (Eq. 2.3), and silicate weathering accounts for the remaining 0.27 meq/kg of atmospheric CO_2.

A similar analysis of solute sources in global average river water by Berner and Berner[9] (Table 2.9) used a more recent estimate of global average river concentrations[10] that separates natural and anthropogenic contributions. These are significant for three major ions: Na^+, Cl^- (ultimately mined from rock salt), and especially SO_4^{2-} (mostly from combustion of fossil fuels). This analysis included CO_2 used from the atmosphere (or soil air) to dissolve carbonate and silicate minerals in the contributions of those minerals to river HCO_3^-, and that accounts for most of the difference with Holland's estimates for these minerals. The importance of silicates and atmospheric sources for other ions are generally similar between Tables 2.8 and 2.9, once we consider that human activities are treated as a separate source in Table 2.9 and not in Table 2.8.

2.5 Data sources and the analysis of chemical composition

2.5.1 Sources of water chemistry data and online databases

Water chemistry data increasingly are becoming available online. Students should become familiar with these resources because they provide easy-to-exploit opportunities

to examine what already has been measured on water bodies. Such information is useful in putting new data into context. In some cases, historical data may be sufficient for one's needs—eliminating the need for expensive and time-consuming sample collection and analysis. An important first step in planning *any* sampling program is to gather information on what already is known about the water bodies of interest. Online data bases help in that task, but readers are cautioned not to fall into the trap of assuming that if it is not available on the Internet, it simply does not exist. This is especially true for older data, which is important in analyzing temporal trends.

Two federal agencies have important online databases. The national water information system of the U.S. Geological Survey (USGS (http://waterdata.usgs.gov/nwis) provides information for more than 1.5 million sites in the United States, including stream flow records and lake and ground water levels, and water quality data (basic water chemistry, nutrients, trace metals, organic contaminants). The site also provides access to monitoring sites that produce real-time flow data and near real-time continuous data on a few basic water quality variables (conductivity, pH, dissolved oxygen). The U.S. Environmental Protection Agency (U.S. EPA) is a major repository for national water quality data related to pollution in two STORET (short for STOrage and RETrieval) databases. A legacy system (http://www.epa.gov/storpubl/legacy/gateway.htm) contains data collected before 1999, and a modernized system (http://www.epa.gov/storet/dw_home.html) has all data collected since then. Both systems contain physical, chemical, and biological data on surface and ground water collected by government agencies, volunteer groups, and academic institutions for the 50 states plus the territories and other jurisdictions of the United States. Monitoring data related to discharge permits for wastewater treatment and drinking water facilities also can be accessed through STORET. Because of the size and complexity of these sites, finding information can take some effort, but the sites are reasonably easy to navigate. Many state water management agencies also maintain extensive Web-based databases that include chemistry and other water quality information on water resources within their jurisdiction. The Consortium of Universities for the Advancement of Hydrologic Science Inc. (CUAHSI) has developed a search engine to find information on water quality and hydrology in such databases (covering ~2 million sites in the United States), which can be accessed via http://www.hydroseek.org.

For information on the chemistry of atmospheric precipitation at 323 U.S. sites, some since the 1970s (not all still active), the National Atmospheric Deposition Program (NADP; http://nadp.sws.uiuc.edu/) provides raw and time-averaged data, as well as isopleths maps showing how the concentrations and deposition of ammonium, nitrate, and sulfate vary annually across the continental United States.

2.5.2 Graphical display of chemical composition

As we have seen, the chemical composition of natural waters is complicated. Even if we consider only the major ions, we still are faced with a large variety of concentrations and ratios among the ions. Graphical displays of major ion composition can help to gain a "quick picture" of the nature of a water body or differences between waters. Stacked bar graphs and pie charts (Figure 2.8a,b) are common ways to display major ion chemistry. In the former case, one bar is used for cations and another for anions, and concentrations are given in milliequivalents per liter (meq/L). Because of the
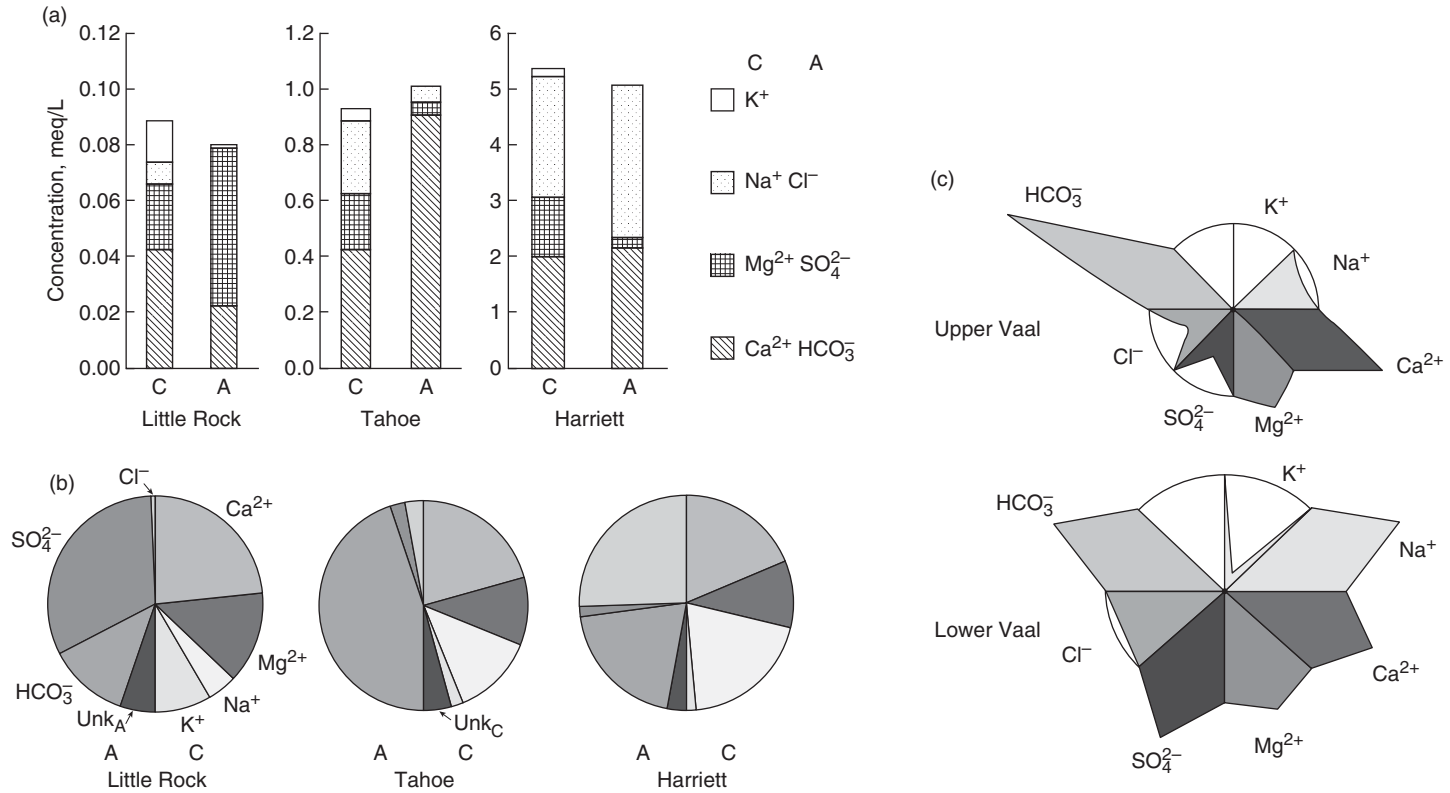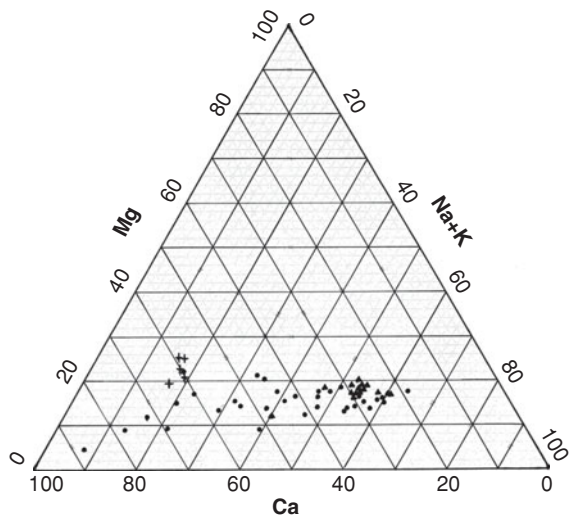
Figure 2.8 (a) Stacked bar graphs showing the major ion composition of three freshwater lakes: Little Rock, Vilas County, Wisc.; and Harriett, Minneapolis, Minn. (see table 2.3). C = cations; A = anions. (b) Major-ion pie charts for the same lakes; Little Rock and Harriett have cation deficiencies that are compensated for by an unknown anion (Unk_A), probably natural organic matter (NOM); Tahoe has an anion deficiency compensated for by an unknown cation (Unk_C), but this probably indicates analytical error. (c) Maucha diagrams from Silberbauer and King[29] for the Upper and Lower Vaal River in South Africa with sizes proportional to total ionic content. (See color insert at end of book for a color version of this figure.)

electroneutrality constraint, a difference in the magnitude of the bars signals that the analysis is in error or incomplete. Similarly, pie charts are divided into one semicircle for cations and another for anions. In comparing waters, the area of the pie chart may be made proportional to total ionic concentration (although, for reasons of clarity, that was not done in Figure 2.8b). Differences in relative chemical composition among the three lakes are easily discerned from both types of charts.

Maucha diagrams,[28] which are eight-sided, star-shaped diagrams, are a variant on the pie chart approach used in limnology to show differences in the chemical composition of lakes and rivers (Figure 2.8c). The original format of the diagrams has concentrations of the four major cations on the right side, and the major anions Cl^-, SO_4^{2-}, and HCO_3^-, plus carbonate, CO_3^{2-} are on the left side. More recent versions[29] combine HCO_3^- and CO_3^{2-} because the latter usually is small and the proportion of total inorganic carbon between these forms varies with pH. Although Maucha diagrams are tedious to draw by hand, they are easy to interpret—the areas of the quadrilaterals for each of the major ions are proportional to their percentage contribution to the total ionic equivalents. Instructions on drawing the diagrams are available elsewhere,[30] and a computer program is available to simplify the process.[31] Maucha diagrams also can be scaled so that their size is proportional to the total ionic concentration.[30]

Trilinear diagrams have been used in geochemistry for decades to portray the major ion composition of natural waters.[1] Each axis on such a diagram (e.g., Figure 2.9) represents the relative concentration of a major cation (or anion) expressed as a percentage of the total meq/L of cations (or anions). Because the sum of values on the three axes must add up to 100, only two axis values are independent, and specifying any two axis values fixes the value for the third. For the major cations, aggregation is necessary because four cations are important. Concentrations of K^+ usually are the lowest and least variable of the four cations, and by convention concentrations of K^+ and Na^+ are combined. Trilinear diagrams are useful to portray the composition of water bodies from a given region to see whether there are patterns or "clusters" of

Figure 2.9 Trilinear diagram for major cations in 55 lakes of north-central Florida. Circles, lakes in Alachua County surrounding the city of Gainesville; pluses, Ocklawaha chain of lakes in central Florida; triangles, softwater lakes in sand-hill Trail Ridge region northeast of Gainesville. Unpublished data from the author (P.L.B.).

DISSOLVED SOLIDS
MILLIGRAMS PER LITER

0
100
500
1000
5000
10,000

SCALE OF DIAMETERS

80   80
SO₄ + Cl 60   60 Ca + Mg
40   40
20   20

15–1   17–3
12–6   10

80   20   80
60   40   Na + K 40   CO₃ + HCO₃ 40   60
40   60   60   80
20   80   80   20

Mg   SO₄

12–6   10

17–3

15–1   10   15–1 12–6   17–3

80   80   40   20   20   40   60   80
Ca   Cl
CATIONS   ANIONS

PERCENT OF TOTAL
MILLIEQUIVALENTS PER LITER

Figure 2.10 Piper diagram showing cation and anion composition in trilinear diagrams at bottom left and right. Circles in the central quadrilateral have areas proportional to the dissolved solids concentration and are located by extending the points in the triangles to the point of intersection. From Hem,[1] who provided information on sample locations.

differing types. For example, the drainage lakes in the Ocklawaha Chain in central Florida are clustered together and have a distinctly different composition from the seepage lakes in the Trail Ridge region of north-central Florida (Figure 2.9). In contrast, 33 lakes of mixed hydrologic character in the county surrounding Gainesville show a wide range in Ca/(Na + K), but a common feature of all the lakes of the three regions is a low fraction of Mg (generally 10–20% of cationic equivalents). Trilinear diagrams also can be used to illustrate how the composition of water develops or changes along a hydrologic pathway. It is interesting to note that if two waters A and B with different compositions are plotted on a trilinear diagram, the composition of any mixture of the two waters lies on a straight line connecting points A and B.[1] A common variant of these diagrams by Piper[32] projects the cation and anion loci from trilinear plots onto a tetrahedron between the two triangles (Figure 2.10).

2.5.3 Chemical analysis of major and minor ions

Although this book is primarily about the chemical behavior of solutes in water rather methods to measure them, it is important for readers to have some understanding of how water chemistry data are obtained. Chemists have used various analytical methods over previous decades for major ion analyses. These are described in *Standard Methods for the Examination of Water & Wastewater*,[33] a compendium of analytical methods for water and wastewater produced on a regular basis by three professional societies. The U.S. federal agencies with major responsibilities for water research (USGS) and protection (U.S. EPA) also have water analysis manuals.[34,35] It is important to note that changes in analytical methods over time create difficulties in evaluating long-term trends in water chemistry and quality. Although different methods intended to measure the same chemical constituent ideally should give the same results, this ideal often does not reflect reality. Consequently, readers must exercise caution in downloading and using historical data.

In the past, Cl^- was determined by titration with silver nitrate (AgCl is insoluble), and sulfate was determined by adding barium chloride to a sample to precipitate $BaSO_4$, which was measured by filtering, drying and weighing the precipitate (i.e., gravimetrically) or by the increase in turbidity caused by the $BaSO_4$ particles. Both methods suffered from lack of sensitivity. During the 1970s, colorimetric methods[33] became available for both SO_4^{2-} and Cl^-, which greatly improved measurement capabilities for low ionic-strength waters. More recently, analysis of major and minor anions has been performed by ion chromatography, which has the advantage of providing results simultaneously for Cl^-, SO_4^{2-}, F^-, and NO_3^- on one small sample with virtually no preprocessing required. The only major anion not measured this way is HCO_3^-, which still is determined by acid-base titration; HCO_3^- is a weak base and can be titrated with strong acid, as described in Chapter 8.

Reliable wet-chemical methods are not available for Na^+ and K^+, and prior to the 1960s they were measured by flame emission spectrophotometry (FES). When the ions are aspirated into a flame they go into an excited electronic state, and when the electrons drop back to their ground states, the atoms emit light at characteristic wavelengths. The amount of light emitted at those wavelengths is proportional to the concentration of the ions in a sample. Titration methods for Ca^{2+} and Mg^{2+} and their sum as hardness using the chelating agent ethylenediaminetetraacetic acid (EDTA) were developed in the 1940s, and these methods still are used in small laboratories. In the 1960s, atomic absorption spectrophotometry (AAS) became commercially available and quickly became the method of choice for major cations, as well as for minor and trace metals. AAS is still used widely for major cation and trace metal analyses, but large research and commercial laboratories now use a variation on FES called inductively coupled plasma-optical emission spectroscopy (ICP-OES). The ICP alternatively can be coupled with a mass spectrometer (ICP-MS) which allows the detection of different isotopes of metal ions. ICP is able to measure a wide suite of metals simultaneously on one small sample. ICP instruments have sufficient sensitivity to measure trace metals at the ng/L range (ICP-MS) or μg/L (ICP-OES) at the same time that their wide dynamic range permits measurement of major cations in the mg/L range.

Problems

2.1. The major ions in a ground-water sample were found to be as follows:

Species	(mg/L)	Species	(mg/L)
Ca^{2+}	75	HCO_3^-	300
Mg^{2+}	40	Cl^-	10
Na^+	10	SO_4^{2-}	109

(a) Determine concentrations in mol/L and meq/L of each ion.
(b) In any water sample, the sum of the positive charges must equal the sum of the negative charges (electroneutrality). Is this water electrically neutral? If not, name two ions not listed in the table that are likely to represent the imbalance.
(c) Calculate the total dissolved solids in the sample (based on the data above only).

2.2. Consider the major ion data for the natural waters in Table 2.3. Convert the ion concentrations from mg/L into molar units (mM) and tabulate the results for the following waters: Trout Lake rainfall, Little Rock Lake, Lake Harriet, average North American river water, and Silver Springs. Briefly discuss differences among the waters and note the difference in the chemistry of rainfall compared to the other waters. Note: to facilitate solving this problem a spreadsheet version of Table 2.3 is available on the textbook's companion Web site.

2.3. Perform ion balances on the five waters in problem 2.2 by summing up the total concentration of cationic charges (expressed in meq/L or μeq/L) and the total concentration of anionic charges (also in meq/L or μeq/L) and compare the difference as a percent of the sum of the cationic charges. Write a paragraph discussing your findings and make conclusions about the overall accuracy and/or completeness of the major ion data for each water.

2.4. As a member of the student chapter of Protect Our Lake Ecosystems (POLE), you obtained the following results on a water sample from a local lake; all units are in mg/L except pH (no units) and SC (μS/cm):

Measurement	Value	Measurement	Value
SC	484	NO_3^-	0.044
pH	7.3 (none)	NH_4^+	0.064
H^+	5×10^{-5}	HCO_3^-	131
Na^+	50	Cl^-	97
K^+	5.6	SO_4^{2-}	9
Ca^{2+}	40	F^-	0.15
Mg^{2+}	13		

Note: SC = specific conductance.

Perform the following calculations:

(a) Convert the given concentrations to mol/L and meq/L.

(b) Calculate an ion balance (Σcations – Σanions, in meq/L). What is the likely cause of any observed imbalance?

(c) Convert the bicarbonate data to mg/L as $CaCO_3$ and the ammonium and nitrate data to mg/L as N.

2.5. (a) Convert the concentrations of nitrate and ammonium for the atmospheric precipitation sites and lake waters in Table 2.3 from the given units (mg/L) to μg/L as N.

(b) Convert the concentrations of bicarbonate (HCO_3^-), Ca^{2+}, and Mg^{2+} from mg/L to mg/L as $CaCO_3$ and estimate the total hardness (TH) of the springs and ground-water samples in mg/L as $CaCO_3$.

2.6. Prepare stacked bar and pie chart graphs of the major ion data in Table 2.3 for Little Rock Lake, Lake Tahoe, Lake Mendota, average North American river water, and Silver Spring, and write a paragraph describing what the graphs show.

References

1. Hem, J. D. 1985. *Study and interpretation of the chemical characteristics of natural water*, 3rd ed., Wat. Suppl. Pap. 2254, U.S. Geol. Surv., Reston, Va.

2. There is a large literature on this topic. A few relevant references include ter Braak, C. J. F., and H. van Dam. 1989. Inferring pH from diatoms: a comparison of old and new calibration methods. *Hydrobiol.* **178**: 209–223; Ponader, K. C., D. F. Charles, and T. J. Belton. 2007. Diatom-based TP and TN inference models and indices for monitoring nutrient enrichment of New Jersey streams. *Ecol. Indic.* **7**: 79–93; Whitmore, T. J. 1989. Florida diatom assemblages as indicators of trophic state and pH. *Limnol. Oceanogr.* **34**: 882–895.

3. National Research Council. Committee on Fluoride in Drinking Water. 2006. *Fluoride in drinking water: A scientific review of EPA's standards*, National Academies Press, Washington, D.C.

4. Wikipedia. Water fluorination (available online at http://en.wikipedia.org/wiki, accessed February 2009); McNally, M., and J. Downie. 2000. The ethics of water fluoridation. *J. Can. Dent. Assoc.* **66**: 592–593.

5. Seinfeld, J. H., and S. N. Pandis. 2006. *Atmospheric chemistry and physics: From air pollution to climate change*, 2nd ed., J. Wiley, New York.

6. Hendry, C. D., and P. L. Brezonik. 1980. Chemistry of precipitation at Gainesville, Florida. *Environ. Sci. Technol.* **14**: 843–849.

7. National Atmospheric Deposition Program (available online at http://nadp.sws.uiuc.edu/, accessed March 2009).

8. Delfino, J. J. 1968. Aqueous environmental chemistry of manganese. Ph.D. thesis, University of Wisconsin, Madison.

9. Berner, E. K., and R. A. Berner. 1987. *The global water cycle*, Prentice-Hall, Englewood Cliffs, N.J.

10. Meybeck, M. 1979. Concentrations des eaux fluviales en éléments majeurs et apports en solution aux océans. *Rev. Géol. Dyn. Géogr. Phys.* **21**: 215–246.

11. Freeze, R. A., and J. A. Cherry. 1979. *Groundwater*, Prentice-Hall, Englewood Cliffs, N.J.

12. Gleick, P. H. 1996. Water resources. In *Encyclopedia of climate and weather*, vol. 2, S. H. Schneider (ed.), Oxford University Press, New York, 817–823,.

13. Holland, H. D. 1978. *The chemistry of the atmosphere and oceans*, Wiley-Interscience, New York.

14. Domagalski, J. L., W. H. Orem, and H. P. Eugster. 1989. Organic geochemistry and brine composition in Great Salt, Mono, and Walker Lakes. *Geochim. Cosmochim. Acta* **53**: 2857–2872.

15. Nissenbaum, A. 1975. The microbiology and biogeochemistry of the Dead Sea. *Microb. Ecol.* **2**: 139–161.

16. Stumm, W., and J. J. Morgan. 1996. *Aquatic chemistry*, 3rd ed. Wiley-Interscience, New York.

17. Salinity does not have physical units. Exchange of comments, available online at http://www.oceanographers.net/forums/showthread.php?t=902, accessed March 2009).

18. Steinhorn, I. 1983. In situ salt precipitation at the Dead Sea. *Limnol. Oceanogr*. **28**: 580–583.

19. Davies, S. N., and R. C. N. DeWiest. 1965. *Hydrogeology*. J. Wiley, New York.

20. Gibbs, R. J. 1970. Mechanisms controlling world water chemistry. *Science* **170**: 1088–1090.

21. Stallard, R. F., and J. M. Edmond. 1983. Geochemistry of the Amazon. 2: The influence of the geology and weathering environment on the dissolved load. *J. Geophys. Res.* **86** (C10): 9844–9858.

22. Kilham, P. 1990. Mechanisms controlling the chemical composition of lakes and rivers: data from Africa. *Limnol. Oceanogr*. 3**5**: 80–83.

23. Eilers, J. M., D. F. Brakke, and A. Henriksen. 1992. The inapplicability of the Gibbs model of world water chemistry for dilute lakes. *Limnol. Oceanogr*. **37**: 1335–1337.

24. Sillen, L. G. 1961. The physical chemistry of seawater. In *Oceanography*, M. Sears (ed.), Amer. Assoc. Adv. Sci., Washington, D.C., 549–581.

25. Garrels, R. M., and F. T. MacKenzie. 1967. Origin of the chemical composition of some springs and lakes. In *Equilibrium concepts in natural water systems*, W. Stumm (ed.), Adv. Chem. Ser. **67**, Am. Chem. Soc., Washington, D.C., 222–242.

26. Bowser, C. J., and B. F. Jones. 2002. Mineralogic controls on the composition of natural waters dominated by silicate hydrolysis. *Am. J. Sci.* **302**: 582–662.

27. Livingstone, D. A. 1963. Chemical composition of rivers and lakes. In *Data of geochemistry*, 6th ed., Prof. Pap. 440-G, U.S. Geol. Surv., Reston, Va.

28. Maucha, R. 1932. Hydrochemische Methoden in der Limnologie. *Binnengewasser* **12**: 1–173.

29. Silberbauer, M. J., and J. M. King. 1991. Geographical trends in the water chemistry of wetlands in the south-western Cape Province, South Africa. *S. African J. Aquatic Sci.* **17**: 82–88 (available online at http://www.dwaf.gov.za/iwqs/gis_apps/maucha.pdf, accessed February 2009.

30. Broch, E. S., and Yake. 1969. A modification of Maucha's ionic diagram to include ionic concentrations. *Limnol. Oceanogr.* **14**: 933–935.

31. Hassell, A. L., and D. F. Martin. 1995. A computer-generated (Q-BASIC) program to construct Maucha diagrams. *Fla. Sci.* **58**: 300–312.

32. Piper, A. M. 1944. A graphic procedure in the geochemical interpretation of water analyses. *Amer. Geophys. Union Trans*. **25**: 914–923.

33. Eaton, A. D., L. S. Clesceri, E. W. Rice, and A. E. Greenberg (eds.). 2005. *Standard methods for the examination of water & wastewater*, 21st ed., Amer. Pub. Health Assoc., Amer. Water Works Assoc., Water Environ. Fed., Washington, D.C.

34. U.S. Geological Survey. 2009. Processing of water samples. In *National field manual for the collection of water-quality data*, TWRI Book 9, ver. 2.2, chap. A5 (available online at http://water.usgs.gov/owq/pubs.html).

35. U. S. Environmental Protection Agency. 2009. *Clean Water Act analytical methods. Approved general-purpose methods* (available online at http://www.epa.gov/waterscience/ methods/method/).

This page intentionally left blank

II

Theory, Fundamentals, and Important Tools

This page intentionally left blank

3

■■ The Thermodynamic Basis for Equilibrium Chemistry

■■ Objectives and scope

This chapter provides a basic understanding of chemical thermodynamics, which is the basis for all of chemical equilibria. We describe the basic concepts, principal functions of state, and laws of thermodynamics and show how these concepts are used to define the equilibrium conditions for chemical processes. The effects of temperature and pressure on thermodynamic functions of state and on chemical equilibria also are developed, and examples are provided throughout the chapter to illustrate applications of important thermodynamic principles and equations.

■■ Key terms and concepts

- Thermodynamic systems: isolated, adiabatic, closed, open
- Thermodynamic functions of state: internal energy (E), enthalpy (H), entropy (S), Gibbs free energy (G)
- Zeroth, first, second, and third laws of thermodynamics and the functions of state that they define
- Gibbs free energy functions: chemical potential (μ), free energy of formation (G_f°), free energy of reaction (ΔG_r)
- The gas constant R and its relationship to thermal energy
- Relationship between free energy and chemical equilibrium: $\Delta G_r^\circ = -RT \ln K_{eq}$
- Effect of temperature on chemical equilibria: the van't Hoff equation, relationship with enthalpy and heat capacity
- Effect of pressure on chemical equilibria: change in molar volume of reaction, molar compressibility

3.1   Introduction

This chapter provides the basis for understanding the concepts of chemical equilibrium and solving equilibrium problems. As the chapter title indicates, that basis is the field of thermodynamics. Stripped to its essentials, thermodynamics provides two major kinds of information:

(1) whether a particular process is possible; i.e., can it proceed spontaneously (without the input of energy) under specified conditions; and
(2) the composition of a reacting system at equilibrium.

The unifying concept on which decisions related to these two issues are based is that of entropy production. Entropy is produced in any natural process; at thermodynamic equilibrium, the rate of entropy production is zero.

Although the field of thermodynamics has a reputation for being highly theoretical and laden with abstract and sometimes complicated mathematics, in fact the important concepts of thermodynamics are based on experimental observations, and the laws and functions derived from these observations have highly practical applications. This chapter takes a relatively informal approach to the subject. We avoid, as much as possible, derivations of equations in the text (although a few are provided in boxes) and instead focus on describing basic concepts and the principal functions and laws discovered by thermodynamics. After introducing the laws of thermodynamics and the properties they define, we show how they are related to the equilibrium constants for chemical reactions. Lastly, we discuss the effects of the two most important physical variables, temperature and pressure, on the values of key thermodynamic functions and equilibrium constants for chemical reactions.

3.2   Thermodynamic and other systems

Physical systems that we may wish to analyze can be grouped into four types according to the degree to which they are isolated from their surroundings.

	Type	Example
(1)	*Isolated systems* cannot exchange heat, work, or matter with their surroundings	Entire universe
(2)	*Adiabatic systems* cannot exchange heat or matter with their surroundings but can exchange work	A rising parcel of air, which expands and thus does work
(3)	*Closed systems* can exchange energy but not matter with their surroundings and can have changes in chemical composition	A laboratory beaker or microcosm
(4)	*Open systems* can exchange both energy and matter with their surroundings	Environmental systems: lakes, rivers, oceans

We can predict the chemical composition of isolated, adiabatic, and closed systems from the laws of thermodynamics, but the last of these is by far of greatest interest

to chemists since it alone (among those systems) allows the possibility of chemical change. To predict the composition of an open system, we must have additional, i.e., *extrathermodynamic*, information: rates of input and outflow of matter from the system and rates of chemical reaction within the system. Open systems thus must be analyzed from a *kinetic* perspective. In reality, all aquatic systems that we may consider in the natural environment are open systems—some more so than others. A segment of a river obviously is more open than a lake; in turn, a lake is more open than a bedrock aquifer. "Openness" is a matter of degree–a matter of the *rate* of exchange of material with the surrounding environment, but no natural system is completely closed. Exchange of matter with a natural system's surroundings always occurs, even if at a very slow rate. Consequently, in a strict sense, real natural systems cannot be analyzed as thermodynamic entities.

We get around the above constraint by defining "abstractions" or models of real (open) systems as closed systems. These model systems contain only the chemical constituents that meet the assumption implicit in thermodynamic treatment, i.e., behavior as a closed system. From a thermodynamic perspective, an open system behaves as if it were closed if the rates of material exchange are slow compared with the rates of chemical reaction that are tending toward an equilibrium condition. For example, reactions involving the common inorganic acids and bases found in natural waters are very rapid (timescales for completion are on the order of a small fraction of a second to a few seconds) compared with the timescales for exchange of these materials with surrounding systems by hydrologic inflows and outflows. Thus, the inorganic acid-base system in natural waters can be treated as an equilibrium system using thermodynamic principles. In contrast, many chlorinated organic compounds such as polychlorinated biphenyls (PCBs) and many pesticides degrade very slowly in aquatic environments even though they are not stable thermodynamically; they are subject to spontaneous decomposition and eventually will decompose to an equilibrium system containing carbon dioxide, water, and chloride ions. Rates of degradation for some of these compounds have timescales of thousands of years—much longer than the timescales of water renewal and exchange for any surface freshwater body. Consequently, water bodies cannot be treated as equilibrium systems with respect to these chemicals.

It may seem an extreme statement, but it can be shown that no natural water body is ever at complete equilibrium with respect to all its chemical constituents.[*] Therefore, thermodynamic principles are not applied to water bodies in a holistic sense, but they are applied to the many chemical components of water bodies that fit the assumptions implicit in thermodynamic models. Finally, it is pertinent to note that the time-invariant condition for closed systems, the *equilibrium state*, is defined by thermodynamics, but the time-invariant condition for open systems, the *steady state*, is defined by kinetics.

---

[*]No organic compound is thermodynamically stable in the presence of oxygen, but a wide variety of natural and synthetic organic compounds are found in natural waters. In addition, N_2 and O_2 are not stable in the presence of each other, although they coexist because of a large kinetic barrier. At true equilibrium in an atmosphere-water system, nearly all the oxygen would be consumed by reacting with some of the N_2 and water to form nitric acid.

3.3 Thermodynamic variables

From a thermodynamic perspective, two kinds of variables are used to define the equilibrium properties of a system: (1) fundamental variables and (2) characteristic thermodynamic functions of state. The nature of the former variables is taken as understood, or at least not subject to derivation by mathematics or experimental observations. The latter variables are derived from the fundamental variables by the laws of thermodynamics, which, it must be emphasized, are based on empirical data, i.e., physical evidence from laboratory experiments. Most thermodynamics texts regard the following as fundamental variables:

Intensive properties	Extensive properties
T (temperature)	V (volume)
P (pressure)	n (number of moles)

The value of an intensive property does not depend on the size of or quantity of material in a system, but the value of an extensive property does depend on these factors.

The primary characteristic thermodynamic functions of state are as follows:

E (internal energy)	G (Gibbs free energy)
H (enthalpy)	S (entropy)
F (Helmholtz free energy)	

All these functions of state are extensive properties. The goal of thermodynamics is to define *equations of state* that describe these properties as functions of the fundamental variables (P, T, and V). Simply put, thermodynamics seeks to explain the energetics of closed systems using the fewest possible fundamental variables (i.e., variables we assume we understand and do not derive from experimental evidence). Scientists do not agree completely regarding the classification of the above variables. For example, some have described entropy as a fundamental variable (although it is defined by the second law of thermodynamics); others consider temperature to be a characteristic function of state.

3.4 States and processes

Before proceeding to describe the laws of thermodynamics based on the fundamental variables and functions of state described in the previous section, we take pause to define some important terms related to states of systems and thermodynamic processes.

(1) In a thermodynamic context, the *state of a system* is said to be defined when each of its fundamental properties has a definite value.

(2) *Processes* bring about a change in the state of a system. We monitor processes by keeping track of the energy passing into and out of a system.

(3) *Adiabatic processes* occur when the boundary between a system and its surroundings is a pure insulator such that no heat is transferred across the boundary.

(4) *Isothermal processes* involve the transfer of heat between a system and its surroundings such that both are always at the same temperature.

(5) A *cyclic process* returns a system to its original state.

(6) A *reversible process* is considered to be the limit of a sum of infinitesimal processes such that equilibrium is maintained at every step of the process.

(7) In an *irreversible process*, equilibrium is not maintained at every step. All naturally occurring (i.e., spontaneous) processes are irreversible.

(8) *Heat*, symbolized as **q** (or **Q**), added to a system from its surroundings is positive; if a system releases heat to its surrounding, q is negative.

(9) *Work* (**w** or **W**) is done by a system on its surroundings, expressed in terms of the energy transferred by the system to the surroundings without an accompanying transfer of entropy (S). For example, expansion of a gas represents pressure × (volume) work.

The basic laws of thermodynamics were derived from experiments involving measurements of heat and mechanical work (expansion or pressure × volume work). However, at least four other types of work can be considered, and the total work done by a system, expressed in differential form, can be written as

$$dw_{tot} = PdV + \mu dn_i + Ede + Mgdh - \gamma_{sur}dA, \qquad (3.1)$$

where

$$
\begin{aligned}
PdV &= \text{(pressure)} \times \text{d(volume)} = \text{expansion (mechanical) work} \\
&\quad \text{Pa} (= \text{N/m}^2) \times \text{m}^3 = \text{N-m} = \text{J} \\
\mu dn_i &= \text{(chemical potential)} \times \text{d(moles of chemical i)} = \text{chemical work} \\
&\quad \text{J/mol} \times \text{mol} = \text{J} \\
Ede &= \text{(electrical potential)} \times \text{d(charge)} = \text{electrical work} \\
&\quad \text{V} (= \text{J/C}) \times \text{C} = \text{J} \\
Mgdh &= \text{(mass)} \times \text{(grav. accel.)} \times \text{d(height)} = \text{gravitational work} \\
&\quad \text{kg} \times \text{m/s}^2 \times \text{m} = \text{N-m} = \text{J} \\
\gamma_{sur}dA &= \text{(surface tension)} \times \text{d(area)} = \text{surface work} \\
&\quad \text{J/m}^2 \times \text{m}^2 = \text{J}
\end{aligned}
$$

EXAMPLE 3.1: Vigorous exercise burns about 300 Calories per hour. What is the rate of energy use in watts?

Answer: Energy (i.e., heat or work) usually is expressed in units of joules (J) or calories (1 cal = 4.184 J). Food (or exercise) energy units are Calories, where 1 Calorie = 1000 calories:

300 Calories × (1000 calories/Calorie) × (4.184 J/calorie) = 1,255,200 J = 1,255 kJ

A watt (W) is a J/s, and so the number of watts is

$$1,255,200 \text{ J}/3600 \text{ s} = 348 \text{ W}.$$

This is the equivalent of two to three incandescent light bulbs!

3.5   The laws or principles of thermodynamics

3.5.1 "Zeroth" law

According to most thermodynamics texts, there are three laws of thermodynamics. The first and second laws define the important functions, internal energy (E) and entropy (S), respectively, and the third provides a basis for determining the absolute amount of entropy in a substance. Denbigh, a physical chemist, argued that a "zeroth" law preceding the first and second laws defines temperature.[1] In his view, the state of a system is determined by the two fundamental variables P and V. He argued that from experimental knowledge a function, $T = f(P,V)$, called temperature, can be derived that determines whether two bodies are in thermal equilibrium or not. The present authors find this argument somewhat circular since the law still requires the assumption that the nature of "thermal equilibrium" is understood.

3.5.2 First law

The first law of thermodynamics is a statement for the conservation of energy. It is based on experiments by Joule in the 1840s showing that heat and work are interconvertible quantities. In turn, Joule's work was based on earlier qualitative work by an American-born scientist, spy, and international raconteur, Benjamin Thompson (see Box 3.1). In simple form, the first law states that the total work expended on a body in an *adiabatic* process depends only on the initial and final states and not on the pathways between these states. The latter condition is a definition of a *function of state*. This work is expressed as equal to the change in the internal energy, E, which also is a function of state: $E = f(P,V) = f'(T,P)$. As defined above, an adiabatic process is one in which there is no change in the heat content of a system. The mathematical form of the first law derives from the above ideas:

$$dE = dq - dw, \tag{3.2}$$

where q = heat absorbed *by* a system *from* its environment, and w = work done by a system on its environment. Thus, internal energy, E, is the algebraic sum of heat and work.

3.5.3 Second law

This law derives the function of state called entropy, S, from observations that some changes are possible under adiabatic conditions and others are not (e.g., mixtures of gases never "demix" spontaneously). The word *entropy* comes from the Greek word for change. The possibility or impossibility of the change $A \rightarrow B$ depends on a characteristic of states A and B, namely, the entropy function. If $S_B \geq S_A$, then the change $A \rightarrow B$ is possible in an adiabatic enclosure. If $S_B < S_A$, the change is impossible under adiabatic conditions, but it can occur under nonadiabatic conditions, i.e., if there is a change in the heat content of the system. The second law stems from general conclusions drawn from experience about a key difference between heat energy and work (mechanical energy). Work always can be converted completely to heat energy, but the converse is not possible in the absence of other change.

Box 3.1   Benjamin Thompson: an American original

Born in colonial Massachusetts in 1753, Thompson was knighted by George III of Great Britain in the 1790s and later became a noble known as Count Rumford in the Holy Roman Empire. Considered a brilliant scientist but an utter scoundrel, Thompson proposed to found the U.S. Military Academy at West Point, but his having supported the British side in the Revolutionary War put a quick end to that effort. However, he did establish the French military school at St. Cyr. In 1804 he married and then divorced the widow of Lavoisier, taking half of her inheritance in the divorce. Lavoisier, the French discover of oxygen and hydrogen and in some respects Thompson's scientific rival, was a nobleman scientist who had the misfortune of being guillotined in the French Revolution. Thompson is credited with doing groundbreaking experiments with cannons that showed heat is a form of motion and that refuted Lavoisier's caloric theory of heat, which had posited that heat is a substance. In turn, Joule based his work leading to the first law on Thompson's experiments. Thompson also is credited with developing the science of ballistics and inventing a photometer to measure light, as well as developing many other innovations to practical devices, including the coffee percolator, central heat and smokeless chimneys, and a nutritious soup for the poor. On the negative side, he is thought to have stolen large amounts of public funds during his varied European careers. He died in Paris in 1814. More detailed accounts of his life are available elsewhere.[2,3]

   The key observation that led to the second law is that it is not possible to convert heat into work by means of an isothermal cyclic process. In contrast, it is possible to obtain work from a nonisothermal process, such as the flow of heat from a high temperature T_2 to a lower temperature T_1. Moreover, the greater the difference between T_2 and T_1, the greater the fraction of q_2 (the heat content at T_2) that can appear as work, as Carnot demonstrated with heat engines in the 1820s. A quantitative measure of the *unavailability* of heat energy for work is q_{rev}/T, which has the properties of a function of state; i.e., it is independent of the pathway taken between the initial and final states. This leads to the quantitative definition of entropy:

$$dS = dq_{rev}/T, \tag{3.3}$$

where dq_{rev} is the change in heat absorbed by a system from the surrounding environment under reversible conditions, and T is absolute temperature.

3.5.4 Third law

This law states that the entropy of a pure crystalline solid is zero at 0 K. It can be deduced by arguments that relate the concepts of entropy and randomness, i.e., the probability that molecules are in a given energy state. The existence of the third law allows us to calculate the entropy of a substance (in absolute terms) at other temperatures by using thermochemical methods.

3.6 Further definitions of entropy

From a chemical perspective, an increase in entropy is the fundamental driving force for spontaneous chemical change; for a broader perspective on the concept of entropy, see Box 3.2. The total entropy change for a system is composed of two components:

$$dS = d_{sys}S + d_{sur}S, \tag{3.4}$$

where dS is the total entropy change, $d_{sys}S$ is the change in entropy *inside* the system, and $d_{sur}S$ is the flow of entropy between (to) a system and (from) the surrounding environment.

Box 3.2 The transcendent concept of entropy

Entropy is possibly the most elusive and philosophical entity in chemistry, and its use extends far beyond the physical sciences into the biological and even the social sciences. Entropy is commonly identified as measuring the "randomness" of a system: an increase in entropy means a system is less ordered. An alternative way of expressing this concept is that an increase in entropy means there is a decrease in the probability that all the molecules will be in a given (energy) state. The identification of entropy with randomness has led to use of the concept in such disparate fields as ecology, economics, information science, astrophysics and cosmology, among others. From the perspective of information content, an increase in entropy (or randomness) means that a system is less well known—or that more conditions (parameter values) must be specified to completely define it—than would be the case if it had lower entropy.

In their classical textbook on physical chemistry, Lewis and Randall[3] showed that $d_{sur}S$ must be equal to dq/T (Eq. 3.3). Many texts on physical chemistry give Eq. 3.3 as an underived axiom. For a reversible process, $d_{sys}S = 0$, and thus dS = dq/T. For an irreversible process, $d_{sys}S > 0$, and thus dS ≥ dq/T. Because dq = 0 for adiabatic processes (by definition), dS ≥ 0. That is, dS = 0 for an adiabatic reversible process, and dS > 0 for an adiabatic irreversible process. As noted in Section 3.4, "reversible" and "irreversible" have special meanings in thermodynamics. Reversible processes are idealized phenomena involving change induced by infinitesimal driving forces, in which equilibrium conditions are maintained; irreversible changes are associated with nonequilibrium conditions. *All* natural processes are irreversible, and thus dS > dq/T for all natural processes, and dS > 0 for adiabatic processes.

3.7 Other thermodynamic state functions

Ultimately, everything in thermodynamics can be described in terms of the functions of state derived from the zeroth, first, and second laws: T, E, and S (temperature, internal

energy and entropy). However, many expressions would become cumbersome. For convenience, several other thermodynamic functions are defined in terms of T, E, S, and fundamental variables P and V. The most important of these derived variables are as follows:

Enthalpy

$$\mathbf{H} = E + PV \tag{3.5}$$

Helmholtz free energy

$$\mathbf{F} = E - TS \tag{3.6}$$

Gibbs free energy

$$\mathbf{G} = H - TS = F + PV \tag{3.7}$$

These three new functions all apply to closed systems at equilibrium. Some extensions of the concept of free energy to other fields are described in Box 3.3.

Box 3.3   Free energy, exergy, and emergy

Chemists and chemical engineers have used Gibbs free energy to solve thermodynamic problems for many decades, but like entropy, this concept also has broader implications for other sciences. Workers in the fields of industrial ecology, ecological economics, and ecological engineering recently have used the related term ***exergy***,[4] which also has units of joules, to quantify the maximum amount of energy available for work in a given process. Calculations involving exergy play a role in studies on efficient use of energy in the context more sustainable management of natural resources. In contrast to Gibbs free energy, however, exergy depends on both the state of the system and the environment.

   Emergy, another energy term used widely in systems ecology and ecological engineering, does not have an exact counterpart in thermodynamics. In general, emergy represents "embodied energy" and is a contraction of those words, but there is a divergence of opinion among several schools of thought in energy analysis and ecological engineering on the precise definition. For our purposes we define it as the sum over time of the energy required either to (1) generate a certain energy flow or (2) generate a product or service, including ecosystem products and services. In the latter context, the systems ecologist H. T. Odum and his collaborators were the originators and developers of the idea.[5,6] A large literature exists on this topic.[4–7]

 Equation 3.5 is essentially a restatement of the first law, and enthalpy (H) thus is closely related to the heat content of a substance (or system). H is used for constant pressure systems and is defined by T and P. In contrast, internal energy, E, is defined by

T and V. The Gibbs free energy (see Box 3.4) is a measure of the free or *available* work energy or the maximum chemical work possible at constant T and P. The Helmholtz free energy gives the maximum ***total*** work (mechanical plus chemical) possible at constant T. In general, at equilibrium, $dS = dG = dF = 0$, and S is at a minimum consistent with given values of E and T. Also at equilibrium, F is at a minimum for a given values of T and V, and G is at a minimum for given values of T and P. Helmholtz free energy is useful in describing equilibrium conditions for systems where volume is fixed but pressure can vary; Gibbs free energy is used to describe equilibrium conditions in systems of fixed pressure, where volume can vary. In environmental systems, we usually are interested in defining equilibrium at fixed temperature and pressure, and Gibbs free energy is the most widely used free energy function.

Box 3.4 J. Willard Gibbs: reclusive founding father of physical chemistry

Josiah Willard Gibbs (1839–1903) is one of the giants of American science.[8] His work laid the foundation for chemical thermodynamics and many other components of physical chemistry. Except for a three-year postdoctoral study period in the laboratories of leading scientists in Europe, he spent his entire career at Yale University, where he received his bachelor's and Ph.D. degrees. Gibbs never married and lived most of his life with a sister and brother-in-law in his boyhood home. He apparently had little social life and his life revolved around his work, at which he was amazingly productive. A list of his major accomplishments includes the concepts of chemical potential and free (available) energy and the Gibbs-Helmholtz equation, Gibbs phase rule, Gibbs adsorption equation, Gibbs-Duhem equation, and Gibbs-Donnan effect. He wrote the first book on chemical thermodynamics and also developed vector analysis as a tool to advance mathematical physics. His work influenced many Nobel-winning scientists, including van der Waals and Planck. Even the American economist Paul Samuelson acknowledged his academic lineage to Gibbs in his Nobel Prize lecture, *Maximum Principles in Analytical Economics*.[9]

Although Gibbs received several awards during his career, he was generally not well known outside of a narrow scientific circle, partly because his papers were not widely accessible. It was not until two decades after his death, when Lewis and Randall[9] published their book on chemical thermodynamics that the importance of his many contributions became more widely recognized.

3.8 Combined statements of the first and second laws: differentials of E, H, and G

The differential form of Eq. 3.5, which defines enthalpy, is

$$dH = dE + VdP + PdV. \tag{3.8}$$

According to the first law in differential form (Eq. 3.2), $dE = dq - dw$. Pressure-volume work (dw in this equation) can be written as PdV. If we substitute this for dE in Eq. 3.8, we see that

$$dH = dq + VdP. \tag{3.9}$$

According to the second law (Eq. 3.3), $dS = dq/T$, or $TdS = dq$. Hence, we can restate Eq. 3.9 as

$$dH = TdS + VdP. \tag{3.10}$$

Similarly, when the only work done by a system is expansion (mechanical work), $dw = PdV$, and it is easy to show that Eqs. 3.2 and 3.3 combine to yield

$$dE = TdS - PdV. \tag{3.11}$$

Finally, the full differential of the Gibbs free energy function (Eq. 3.7) is $dG = dH - SdT - TdS$. If we substitute Eq. 3.10 for dH into this expression, we obtain

$$dG = -SdT + VdP. \tag{3.12}$$

Equations 3.10–3.12 are all statements of the combined first and second laws. As stated, they apply to systems of constant composition (i.e., no chemical change or other kinds of work are allowed). Equation 3.12 is of special interest because it quantifies the change in available work energy (dG) in relation to temperature and pressure. As such, it provides the basis for evaluating effects of T and P on chemical equilibria (see Sections 3.15–3.17).

3.9 Chemical potential

Equation 3.12 is the fundamental relationship between the thermodynamic functions of state Gibbs free energy (G) and entropy (S) in closed systems of fixed composition when only P-V work is involved. Extension of the thermodynamic state functions to open systems or to systems of variable composition requires addition of a term to account for energy changes in the system resulting from changes in chemical content. This term is based on a thermodynamic variable μ, called chemical potential, and it changes Eq. 3.12 to

$$dG = -SdT + VdP + \sum \mu_i dn_i, \tag{3.13}$$

where μ_i is the chemical potential of the ith component and dn_i is the infinitesimal change in the number of moles of i in the system.

Chemical potential is defined mathematically as a partial molar quantity:

$$\mu_i = \left(\frac{\partial E}{\partial n_i} \right)_{S, V, n_j} = \ldots = \left(\frac{\partial G}{\partial n_i} \right)_{T, P, n_j} = G_i \tag{3.14}$$

For a one-component phase (a pure substance), μ is simply the Gibbs free energy per mole. For mixtures, μ_i is the increase in Gibbs free energy of a phase at constant T and

P on adding one mole of i to an infinitely large sample of the phase. We define μ in this manner so that the composition of the phase does not change.

3.10 Chemical reactions and equilibrium: derivation of $\triangle$G

The general condition for equilibrium in a system at constant temperature and pressure is

$$\sum \mu_i \, dn_i = 0. \qquad (3.15)$$

This is obtained from Eq. 3.13 by remembering that $dG = 0$ at equilibrium. Equation 3.15 is too abstract and "compact" to be directly useful in solving equilibrium problems, but it provides the basis for expressions that are useful. Consider a general chemical reaction

$$\nu_A A + \nu_B B + \ldots \rightleftharpoons \nu_C C + \nu_D D + \ldots , \qquad (3.16)$$

where the ν_i are stoichiometric coefficients—the relative number of moles of reactants or products. By convention, $\nu_i > 0$ for products and < 0 for reactants; i.e., the stoichiometric coefficient is positive for products and negative for reactants. With this definition of ν, we can rewrite Eq. 3.16 in shorthand form as $\sum \nu_i M_i = 0$, where M_i is the molecular weight of component i. This is a simple statement of the law of mass conservation. The change in Gibbs free energy resulting from changes in the number of moles of each component in Eq. 3.16 is

$$dG = \sum \mu_i \, dn_i; \qquad (3.17)$$

that is, the rate of change in G is equal to the sum of the product of the chemical potentials for all reactants and products times the rate of change in the quantities (number of moles) of these substances. We now introduce a new variable ξ, called the extent of reaction, defined by the relationship:

$$dn_i = \nu_i \, d\xi \qquad (3.18a)$$

and

$$n_i = n_{io} + \nu_i \xi, \qquad (3.18b)$$

where n_i is the number of moles of i at any values of ξ, and n_{io} is the initial number of moles of i. Substituting Eq. 3.18a into Eq. 3.17, we obtain

$$dG = \sum_i \mu_i \nu_i d\xi \qquad (3.19)$$

The quantity $\sum_i \nu_i \mu_i$ is called the *Gibbs free energy of reaction* and is given the symbol $\triangle \mathbf{G}$. This is an intensive state variable—that is, the quantity does not depend

on the extent of the system. This fact can be seen readily by rearranging Eq. 3.19:

$$dG/d\xi = \sum_i \mu_i \nu_i = \Delta G \tag{3.20}$$

The free energy of reaction, ΔG, thus is the ***rate of change of Gibbs free energy of the system with respect to the extent of reaction***. The closely related term $\mathbf{\Delta G°}$ is the free energy of reaction when all reactants and products are present in their "standard states." For now we define this term simply as the state at which the effective (or thermodynamic) concentration of a substance is unity (see Chapter 4 for details). It is important to note the formal similarity between the free energy of reaction, ΔG (or $\Delta G°$), and chemical potential, μ. Both functions are intensive properties, and both are expressed in energy units (e.g., kJ/mol). However, μ is a partial molal quantity referred to a *single component*, and ΔG is the change in free energy with respect to a reacting *system*. For a one-component system, μ is the molar Gibbs free energy, G_i.

3.11   Free energy of formation

This quantity, symbolized $G°_{f,i}$ for species i, also has molar energy units (kJ/mol) and is defined as the molar free energy of a substance in its standard state compared with the free energy of the elements from which it is made. It is not possible to measure the absolute amount of Gibbs free energy (or for that matter, many other thermodynamic quantities) for any substance. Instead, we can measure only *differences* in G between states. To circumvent this problem, the convention was established that G = 0 for the most stable form of any element. Values of $G°_f$ have been measured or calculated for numerous inorganic and organic compounds and ions; the Appendix lists $G°_f$ values for common species in aquatic systems.

The concept of free energy of formation is especially useful in calculating standard-state free energies of reaction ($\Delta G°$) of reactions for which this quantity has not been measured. This is based on the relationship

$$\Delta G° = \sum G°_{f,products} - \sum G°_{f,reactants}. \tag{3.21}$$

Note that ***stoichiometry must be taken into account*** and that the $G°_f$ of a given species must be multiplied by the stoichiometric coefficient for the species in the balanced reaction. Similar arguments apply to the concept of enthalpy changes; that is, the standard-state enthalpy of reaction can be computed from the algebraic difference:

$$\Delta H° = \sum H°_{f,products} - \sum H°_{f,reactants}, \tag{3.22}$$

where $H°_f$ is the standard state enthalpy of formation of a compound from its elements, which by convention have zero enthalpy. In practice, enthalpies of reaction for many organic chemical reactions are calculated from the enthalpies of combustion for the individual reactants and products, which are determined experimentally in bomb calorimeters.

An additional convention that $G_f^\circ = 0$ and $H_f^\circ = 0$ for H^+ allows us to calculate values of G_f° and H_f° for single ions in solution and thus ΔG° and ΔH° for reactions involving ions in solution. Without this important convention (or a similar one), we would not be able to calculate free energies or enthalpies of formation for single ions because they cannot exist in solution by themselves but only as pairs of cations and anions.

EXAMPLE 3.2 What is ΔG_r° for the acid-mediated dissolution of calcite?: Although ΔG_r° values are tabulated for many reactions (either directly or as equilibrium constants or K values; see Section 3.14), it is possible to determine ΔG° for *any* reaction, as long as G_f° values are known for all reactants and products of the reaction.

Answer: The acid-mediated dissolution of calcite is defined by the reaction

$$CaCO_{3(s)} + H^+ \rightleftharpoons Ca^{2+} + HCO_3^-.$$
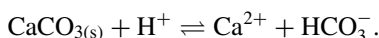
From tabulated G_f° values in the Appendix, we find G_f° for $CaCO_{3(s)} = -1128.8$ kJ/mol; G_f° for $H^+ = 0$ kJ/mol (by convention); G_f° for $Ca^{2+} = -553.54$ kJ/mol; and G_f° for $HCO_3^- = -586.8$ kJ/mol.

$$\Delta G^\circ = \sum G_{f,products}^\circ - \sum G_{f,reactants}^\circ$$

$$\Delta G^\circ = G_{f,\ Ca^{2+}}^\circ + G_{f,\ HCO_3^-}^\circ - G_{f,\ CaCO_3}^\circ - G_{f,\ H^+}^\circ$$

$$\Delta G^\circ = -553.54 + -586.8 - (-1128.8) - 0 \text{ kJ/mol}$$

$$\mathbf{\Delta G^\circ = -11.54 \text{ kJ/mol}}$$

As we will see below, the fact that ΔG° is negative means that the dissolution of calcite proceeds spontaneously if H^+, Ca^{2+}, and HCO_3^- are all present at unit activity (i.e., 1 mol/L). Note that minerals of different crystal structure often have the same chemical form (e.g., calcite and aragonite), and care must be taken to use the correct G_f° value when calculating ΔG°.

3.12 Variations of G and ΔG with extent of reaction, ξ

There are important distinctions for the Gibbs free energy functions G and ΔG between reacting systems composed of pure phases and those composed of phases with variable composition. Examples of the former category are phase changes of a compound (e.g., ice $\rightleftharpoons H_2O_{liq}$) or changes from one crystalline form of a compound to another (e.g., aragonite $\rightleftharpoons$ calcite for $CaCO_3$). For such reactions, G varies linearly with ξ—increasing for endergonic reactions and decreasing with ξ for exergonic reactions. For multiphase systems at equilibrium, G is independent of the amount present in each phase. Similarly, ΔG is independent of ξ; that is, it stays at a constant value regardless of the value of ξ in phase-change reactions. In contrast, G and ΔG vary nonlinearly with ξ for reactions in systems of variable composition, such as solution-phase reactions, where reactant concentrations decrease and product concentrations increase with ξ. In such cases, G decreases with ξ when reaction conditions are favorable, reaches a minimum value at equilibrium, and rises with ξ as the reaction continues beyond the equilibrium point.

For spontaneous reactions, ΔG is more negative when the system is far from equilibrium and gradually approaches a value of zero at equilibrium. If reactions in such systems are forced to continue beyond this point, ΔG becomes positive and continues to increase with increasing distance (ξ) from the equilibrium point. Of course, the only way nonspontaneous reactions can occur is via an input of free energy from some other source.

3.13 Driving force for chemical change

As explained in Box 3.5, the driving force for chemical change is $\Delta G < 0$. Because the change in free energy is the sum of an enthalpy term and entropy term ($\Delta G = \Delta H - T\Delta S$), the driving force can arise from a negative ΔH, positive ΔS, or both. If $\Delta H < 0$ and $\Delta S > 0$, the reaction is spontaneous at all T, and if $\Delta H > 0$ and $\Delta S < 0$, the reaction is not spontaneous at any temperature. However, if $\Delta H < 0$ and $\Delta S < 0$, or if $\Delta H > 0$ and $\Delta S > 0$, then the possibility of spontaneity depends on temperature.

In some cases, entropy changes are small, and the primary driving force for chemical reaction is a change in enthalpy. For other aquatic reactions, the enthalpy change is small,

---

Box 3.5 Another derivation of ΔG

According to the second law of thermodynamics,

(1) ΔS_{sur} = heat absorbed by surroundings/T

or

(2) $\Delta S_{sur} = -\Delta H_{sys}/T$.

For a spontaneous change under thermodynamically irreversible conditions in a closed system (with constant T and P), the following condition applies:

(3) $\Delta S_{universe} = \Delta S_{sys} + \Delta S_{sur} > 0$

Substituting eq. (2) into eq. (3) yields

(4) $\Delta S_{univ} = \Delta S_{sys} - \Delta H_{sys}/T$,

or

(5) $-T\Delta S_{univ} = \Delta H_{sys} - T\Delta S_{sys} < 0$.

Equation (5) gives the condition for spontaneous change in a closed system. For simplicity, we will omit the subscript "sys" hereafter and assume that unsubscripted thermodynamic functions refer to the value for a system. Because ΔH and ΔS are changes in thermodynamic functions of state, the term $\Delta H - T\Delta S$ (i.e., $-T\Delta S_{univ}$) is a measure of change in another function of state. We call this function Gibbs free energy and thus can write

(6) $\Delta G = \Delta H - T\Delta S = -T\Delta S_{univ}$.

The criterion for spontaneity in a closed system is $T\Delta S_{univ} > 0$, or $\Delta G < 0$. The criterion for equilibrium is $\Delta G = 0$.

and the primary driving force is a change in entropy. Complex formation between major cations and anions in natural waters frequently fits in the latter category. As mentioned above, entropy often is equated with the randomness of a system. For reactions with a decrease in the number of molecules from the reactant to the product side, ΔS thus should be negative; for reactions with more product molecules than reactants, ΔS should be positive. *A priori*, we would predict that complex formation reactions should have $\Delta S < 0$, and mineral (salt) dissolution reactions should have $\Delta S > 0$. This is not always the case, however, because of the release or binding of solvent (H_2O) molecules by cations involved in these reactions, as explained in Chapter 9.

3.14   Derivation of the equilibrium constant

G.N. Lewis defined chemical potential in the following way:

$$\mu_i = \mu_i^\circ + RT \cdot \ln a_i \tag{3.23}$$

Superscript $^\circ$ refers to the standard state for substance i, R is the gas constant (see Box 3.6), T is absolute temperature (K), and a_i is the **activity** of i. Although R was derived as part of the perfect gas law and is called the **gas** constant, the term has much broader applicability and in this sense is misnamed. The product RT, which has units of energy per mole, often is referred to as the thermal energy per mole. The concept of RT as thermal energy per mole applies to substances in solution and to solids, as well as to gases. At 25°C, $RT = 8.314$ (J mol^{-1} K^{-1}) $\times$ 298.15 K = 2479 J mol^{-1}. Table 3.1 lists values of R in other common units; care must be taken to make sure that the appropriate units are used for R in various equations and problems (compare Examples 3.3 and 3.5).

Activity is sometimes referred to as the "thermodynamic concentration" of a substance, meaning that it is the way concentration is expressed in thermodynamic (equilibrium) relationships. Although the activity of a substance represents an idealized concentration or "reactivity," it is important to recognize that activity is a dimensionless quantity. This can be seen by conducting a dimensional analysis of Eq. 3.23. Activities are dimensionless because they actually represent a ratio of the actual reactivity of a substance to its reactivity in a standard state. The nature of the standard states for substances in solution and for solids and liquids is explained in Chapter 4, along with relationships between activity and measured concentrations (e.g., in mol/L). By the above definition, the activity of any substance in its standard state is unity (a = 1). Equation 3.23 thus states that the actual chemical potential of a substance (its free energy per mol) is equal to its chemical potential in its standard state corrected for its actual state.

Substituting Eq. 3.23 into Eq. 3.20, which relates ΔG and chemical potential, yields

$$\Delta G = \sum \mu_i v_i = \sum v_i \mu_i^\circ + RT \sum v_i \cdot \ln a_i, \tag{3.24}$$

or

$$\Delta G = \Delta G^\circ + RT \ln \Pi \, a_i^{v_i}. \tag{3.25}$$

Box 3.6   The gas law and R, the gas constant

The ideal gas law was developed from the seventeenth-century observations of Boyle that the product PV is approximately constant and that for two sets of P and V at a given temperature, $P_1V_1 = P_2V_2$. A century later, Charles noted that the value of PV depends on temperature; that is,

   (1) $PV_m = f(T)$,

where V_m is the volume occupied by one mole of gas. Still later, Gay-Lussac (1805) found that the function was approximately linear:

   (2) $f(T) = b + Rt$,

where t is temperature in Celsius. When P was expressed in atm and V_m in liters (per mole), b was found to have a value of 22.41 at 0°C. The slope of the relationship, R, was found to be 0.08206. Thus,

   (3) $PV_m = 22.41 + 0.08206t$,

or

   (4) $PV_m = 0.08206(273.15 + t)$.

Defining a new temperature scale, $T = 273.15 + t$ (called the Kelvin or absolute temperature scale), yields

   (5) $PV_m = 0.08206T = RT$.

or

   (6) $PV = nRT$,

where n is the number of moles and V is the volume of the gas. The units and value of gas constant R depend on the units in which P, V, and T are expressed (see Table 3.1).

   Equations 5 and 6 are forms of the ideal gas law. They apply to most real gases at pressures up to about 1 atm. Deviations from the law at high P result from the fact that the law treats gas molecules as if they have no volume. This is satisfactory at low P, at which the molecules occupy a small fraction of the total volume, but the volume of the molecules must be taken into account at high P. Also, the ideal gas law assumes that molecules act as hard spheres with no attractive forces, but there are limits under which this approximation holds.

$\Delta G° = \sum v_i \mu_i°$ thus is the Gibbs free energy of reaction when all reactants and products are in their standard states; Π is the mathematical symbol for multiplication (analogous to $\sum$ as the symbol for addition). For the generalized chemical reaction (Eq. 3.16), Eq. 3.25 becomes

$$\Delta G = \Delta G° + RT \ln \left[\frac{a_C^{v_C} \, a_D^{v_D}}{a_A^{v_A} \, a_B^{v_B}} \right], \tag{3.26a}$$

Table 3.1 Units for the gas constant, R

Units	R
$L\ atm\ mol^{-1}\ K^{-1}$	0.08206
$cm^3\ atm\ mol^{-1}\ K^{-1}$	82.06
$cm^3\ bar\ mol^{-1}\ K^{-1}$	83.15
$cal\ mol^{-1}\ K^{-1}$	1.987
$joule\ mol^{-1}\ K^{-1}\ (J\ mol^{-1}\ K^{-1})$	8.314

or

$$\Delta G = \Delta G^\circ + RT \ln Q, \qquad (3.26b)$$

where Q = reaction coefficient $\Pi a_i v_i$.

At equilibrium, $\Delta G = 0$. By definition, the value of Q at $\Delta G = 0$ is called K, the equilibrium constant. Then from Eq. 3.26b, we can write

$$\Delta G^\circ = -RT \ln K \qquad (3.27a)$$

or

$$K = \exp(-\Delta G^\circ / RT) \qquad (3.27b)$$

and

$$\Delta G = RT \ln Q/K. \qquad (3.28)$$

Equation 3.27 is an important statement in that it provides a direct relationship between a fundamental thermodynamic quantity, the free energy of reaction, and the equilibrium constant for a reaction, the primary parameter used to solve chemical equilibrium problems. For an alternative derivation of equilibrium constants based on mass action (kinetic) principles, see Box 3.7.

EXAMPLE 3.3: What is the equilibrium constant at 25°C for the acid-mediated dissolution of calcite?

Answer: From Example 3.2 we know that $\Delta G^\circ = -11.54$ kJ/mol for this reaction, $CaCO_{3(s)} + H^+ \rightleftharpoons Ca^{2+} + HCO_3^-$. From Eq. 3.27 we can write

$$-11{,}540\ (J\ mol^{-1}) = -8.314\ (J\ mol^{-1}\ K^{-1}) \times 298.15\ (K) \times \ln K_{eq}$$

$$\ln K_{eq} = 4.655$$

or

$$K_{eq} = 105.2 = 1.05 \times 10^2$$

Box 3.7 A kinetic (mass-action) derivation of equilibrium constants

It is ironic that the original derivation of the concept of equilibrium constants was not obtained from thermodynamic principles but from kinetics. Berthelot and other chemists in the mid-nineteenth century noted that equilibrium was not a static phenomenon but actually resulted from a counterbalancing of forward and reverse reactions; i.e., at equilibrium the forward rate is equal to the rate of the reverse reaction. Reaction rates were expressed by mass action principles such that for general reaction $A + B \rightleftharpoons C + D$, the forward and reverse rates were expressed as

$$R_f = k_f[A][B],$$
$$R_r = k_r[C][D].$$

At equilibrium, $R_f = R_r$, or

$$k_f/k_r = [C][D]/[A][B] = K.$$

This gives rise to the description of K as a "mass action" equilibrium constant. Rates of reactions are not always exact functions of the concentrations of reactants as expressed in the stoichiometric equation. The form of the rate expression for a reaction depends on the reaction pathway or mechanism. However, the above derivation does hold for elementary reactions—those that proceed in a single step.

EXAMPLE 3.4: What concentration of protons is necessary to dissolve calcite?

Answer: Again from Example 3.2, we know $\Delta G°$ for the acid-mediated dissolution of calcite, $CaCO_{3(s)} + H^+ \rightleftharpoons Ca^{2+} + HCO_3^-$. From the stoichiometry we see that we can calculate the concentration of H^+ necessary for the reaction to proceed if we know the concentrations of Ca^{2+} and HCO_3^-. Here we will assume that both are present at 1 mmol/L.

To solve this problem we can use Eq. 3.26a:

$$\Delta G = \Delta G° + RT \ln \left[\frac{a_C^{\nu_C} \times a_D^{\nu_D}}{a_A^{\nu_A} \times a_B^{\nu_B}} \right].$$

For the reaction to proceed spontaneously, $\Delta G < 0$, and we can write

$$\Delta G = \Delta G° + RT \ln \left[\frac{a_{Ca^{2+}} \times a_{HCO_3^-}}{a_{CaCO_3} \times a_{H^+}} \right] < 0.$$

Using concentrations to represent the activities of the dissolved species and $a = 1$ for solid phase calcite:

$$-11{,}540 + (8.314)(298) \ln \left[\frac{(1 \times 10^{-3})(1 \times 10^{-3})}{(H^+)} \right] < 0$$

Solving for H^+ yields $(H^+) > 9.49 \times 10^{-9}$ mol/L, or

$$\textbf{pH} < \textbf{8.02.}$$

Thus, if the concentration of protons exceeds this value or pH < 8.02, calcite will dissolve spontaneously. Note that this is true only for the stated concentrations of Ca^{2+} and HCO_3^-. As calcite dissolves, concentrations of these species increase, changing the answer above and eventually halting dissolution, as a new equilibrium is established.

EXAMPLE 3.5 What is the equilibrium state of a closed chemical system?: A 0.5 mole sample of the mineral wustite ($FeO_{(s)}$) is place in a closed room containing 1000 L of air at 25°C. The initial partial pressure of oxygen is 0.21 atm and that of carbon dioxide is 3.16×10^{-4} atm. Given the following reactions, determine the final composition of the system.

$$FeO_{(s)} + CO_{2(g)} \rightleftharpoons FeCO_{3(s)} \text{ (siderite)}$$

$$2FeO_{(s)} + \tfrac{1}{2}O_{2(g)} \rightleftharpoons Fe_2O_{3(s)} \text{ (hematite)}$$
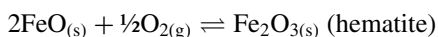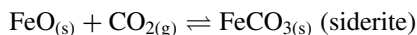
Answer: Beginning with the first reaction, we can determine ΔG°:

$$\Delta G^\circ = G^\circ_{f,\ FeCO3} - G^\circ_{f,\ FeO} - G^\circ_{f,\ CO_2} = -666.7 - (-251.1) - (-394.37)$$
$$= -21.23 \text{ kJ/mol} = -21{,}230 \text{ J/mol}$$

Now we can write out K (at equilibrium when $\Delta G = 0$):

$$\Delta G^\circ = -RT \ln K, \text{ and rearranging gives } K = e^{-\Delta G^\circ / RT}$$

So,

$$K = e^{-(-21{,}230/(8.314 \times 298))} = 5{,}265.$$

We also can relate K to the activities of the chemical species of the reaction:

$$K = \frac{a_{FeCO_3}}{a_{FeO} a_{CO_2}}$$

Using $a = 1$ for pure solids and $a = P$ for gases, we find that

$$K = \frac{1}{P_{CO_2}}.$$

Thus,

$$P_{CO_2} = \frac{1}{5,265} = 1.9 \times 10^{-4} \text{ atm.}$$

Using the ideal gas law, we can determine the number of moles of CO_2 that have reacted:

$$\Delta n = \Delta PV/RT = (3.16 \times 10^{-4} - 1.9 \times 10^{-4})(1000)/(0.0821)(298) = 0.005 \text{ moles}$$

Thus, if this reaction dictates the equilibrium of the system, the final state will have 0.495 moles of $FeO_{(s)}$ and 0.005 moles of $FeCO_{3(s)}$.

Similar calculations for the reaction forming $Fe_2O_{3(s)}$ yield

$$\Delta G^\circ = G^\circ_{f, \text{ Fe2O}_3} - 2G^\circ_{f, \text{ FeO}} - \tfrac{1}{2}G^\circ_{f, \text{ O}_2} = -742.7 - 2(-251.1) - \tfrac{1}{2}(0)$$

$$= -240.5 \text{ kJ/mol} = -240,500 \text{ J/mol.}$$

Note the multiplication of the number of $FeO_{(s)}$ by 2 and the number for O_2 by $\tfrac{1}{2}$ to account for the stoichiometry:

$$K = e^{-(-240,500/(8.314 \times 298))} = 1.44 \times 10^{42}$$

$$K = \frac{a_{Fe_2O_3}}{a_{FeO}a^{1/2}_{O_2}}$$

$$K = \frac{1}{P^{1/2}_{O_2}}.$$

$$P_{O_2} = \left(\frac{1}{1.44 \times 10^{42}}\right)^2 = 4.85 \times 10^{-85}\text{atm}$$

Essentially all of the oxygen would be consumed at equilibrium. The 0.21 atm of O_2 is equivalent to 8.58 moles of oxygen (via the ideal gas law). Thus there is a large excess of oxygen compared with wustite, and the reaction cannot proceed to equilibrium (because all of the wustite will react first). If this reaction dictates the final state of the system, there would be 0.25 moles of $Fe_2O_{3(s)}$ (one mole of this is produced per 2 moles of $FeO_{(s)}$).

We now know that both reactions are favorable and $FeO_{(s)}$ will react, but will the final state of the system have $Fe_2O_{3(s)}$ or $FeCO_{3(s)}$? The answer is easily determined by logic. If $FeO_{(s)}$ reacts with CO_2 until equilibrium is reached, there is still $FeO_{(s)}$ remaining (in fact 99% of it). Because the second reaction shows that $FeO_{(s)}$ is unstable in the presence of oxygen, all the remaining $FeO_{(s)}$ will react to $Fe_2O_{3(s)}$, and it stands to reason that the $FeCO_{3(s)}$ will be converted to $Fe_2O_{3(s)}$ as well. It is left to the reader to perform the thermodynamic calculation to prove this last point.

3.15   Effect of temperature and pressure on G and ΔG

We showed in Section 3.8 that the differential of Gibbs free energy is

$$dG = -SdT + VdP \tag{3.11}$$

We now consider simplifications of Eq. 3.11 for restricted conditions.
   (A) If $dP = 0$ (we hold pressure constant), $\partial G_P = -S\partial T$, or

$$\left(\frac{\partial G}{\partial T}\right)_P = -S \tag{3.29}$$

A similar relationship applies to reactions with their associated ΔG:

$$\left(\frac{\partial \Delta G}{\partial T}\right)_P = \Delta S \tag{3.30}$$

where ΔS is the entropy of reaction. Equation 3.30, called the ***Gibbs-Helmholtz equation***, serves as the starting point to evaluate the effects of temperature on chemical equilibria.
   (B) If $dT = 0$ (we hold temperature constant), $\partial G_T = V\partial P$, or

$$\left(\frac{\partial G}{\partial P}\right)_T = V \tag{3.31}$$

and similarly, for a reaction

$$\left(\frac{\partial \Delta G}{\partial P}\right)_T = \Delta V \tag{3.32}$$

where V is the volume of the system and $\mathbf{\Delta V}$ is the ***change in molar volume*** (cm^3 mol^{-1}) for the reaction, which is obtained as the sum of the molar volumes of the reaction products minus the sum of the molar volumes for the reactants.
   The change in Gibbs free energy with respect to a change in temperature at constant pressure thus is equal to the decrease in entropy, and the change in Gibbs free energy with respect to a change in pressure at constant temperature is equal the change in (molar) volume. Finally, when both T and P are constant, $dG = -TdS$ (see Eq. (6) in Box 3.5), or

$$dS = -\frac{dG}{T} \tag{3.33}$$

The increase in internal entropy thus is equal to the decrease in Gibbs free energy divided by absolute temperature.

3.16   Effects of temperature on equilibria

As stated in the previous section, the starting point to evaluate the effects of temperature on equilibria is the Gibbs-Helmholtz equation (Eq. 3.30). By itself, this equation is not very useful in solving problems related to temperature effects on equilibria, but we can use it to derive equations that are useful in this regard. Before doing that, it is useful to define one more thermochemical property: heat capacity.

3.16.1 Heat capacity, C_p

For a system at constant pressure, heat capacity is defined as

$$C_P = \left(\frac{dq}{dT} \right)_P = \left(\frac{dH}{dT} \right)_P. \tag{3.34}$$

The second equality in Eq. 3.34 holds because $dH = dq + VdP$ (Eq. 3.9), and at constant pressure, the term VdP is zero. Heat capacity thus is simply the rate of change in the enthalpy of a substance with respect to temperature. It has the same units as entropy (e.g., $J\,mol^{-1}\,K^{-1}$), but it is *not* the same as entropy, which was defined by Eq. 3.7 as the difference between enthalpy and Gibbs free energy divided by temperature $((H - G)/T)$. Also recall that $dS = dH/T$. Enthalpy and entropy thus vary with temperature according to the following equations:

$$H_{T_2} = H_{T_1} + \int_{T_1}^{T_2} C_p \, dT \tag{3.35}$$

$$S_{T_2} = S_{T_1} + \int_{T_1}^{T_2} C_p \, d \ln T \tag{3.36}$$

We can define ΔC_p as the ***change in heat capacity for a reaction***, i.e., the difference between the sum of the heat capacities for the products and the sum of the heat capacities for the reactants. This variable is useful in predicting the effects of temperature on chemical equilibria.

3.16.2 Equilibrium with respect to changes in T and P: the Clapeyron equation

Recall that at equilibrium, $dG = 0$. The differential of Gibbs free energy at equilibrium thus can be written as $dG = -SdT + VdP = 0$. By rearranging, we obtain

$$\frac{dP}{dT} = \frac{S}{V}. \tag{3.37}$$

Consider a phase change $A \rightleftharpoons B$. The differential of Gibbs free energy for each phase is

$$dG_A = V_A dP - S_A dT,$$

$$dG_B = V_B dP - S_B dT,$$

where all subscripted variables are molar quantities (V_A and V_B are molar volumes of A and B). When the phases are in equilibrium with each other, $dG_A = dG_B = 0$, and thus $V_A dP - S_A dT = V_B dP - S_B dT$. Rearranging yields

$$\frac{dP}{dT} = \frac{S_B - S_A}{V_B - V_A} = \frac{\Delta S}{\Delta V} \qquad (3.38)$$

From the combined first and second laws, $\Delta G = \Delta H - T\Delta S$, and the fact that $\Delta G = 0$ at equilibrium, we find that $\Delta S = \Delta H/T$. Substituting this relationship into Eq. 3.38 yields

$$\frac{dP}{dT} = \frac{\Delta H}{T\Delta V} \qquad (3.39)$$

This is called the Clapeyron equation, and it applies to any phase transformation—gas to liquid, solid to liquid, or solid to another solid.

3.16.3 The Clausius-Clapeyron equation

This approximation, derived from Eq. 3.39, is useful in solving equilibrium problems involving vapor and liquid phases (e.g., vapor pressure of a liquid as a function of temperature). In such cases, ΔV of Eq. 3.39 represents the difference between the molar volume of the vapor phase and that of the liquid phase: $\Delta V = V_v - V_l$. Because V_l is small compared with V_v, we can ignore it as a first approximation, and Eq. 3.39 becomes $dP/dT \approx \Delta H/TV_v$. From the perfect gas law, $PV_v = RT$ (where V_v is the molar volume of the vapor phase), we obtain $V_v = RT/P$. Substituting this expression into Eq. 3.39 and rearranging yields the Clausius-Clapeyron equation:

$$\frac{dP_{VP}}{P_{VP}dT} = \frac{d \ln P_{VP}}{dT} \approx \frac{\Delta H_{vap}}{RT^2} \qquad (3.40)$$

where subscript "VP" means that the pressure is an (equilibrium) vapor pressure, and ΔH_{vap} is the enthalpy (or heat) of vaporization. The approximately equal sign reflects the simplification made in arriving at this equation. The integrated form of the equation (assuming is ΔH_{vap} is not a function of temperature) is

$$\ln \frac{P_{T_2}}{P_{T_1}} = \frac{\Delta H_{vap}(T_2 - T_1)}{RT_1 T_2} \qquad (3.41)$$

EXAMPLE 3.6 Effect of temperature on the vapor pressure of liquid organic compounds: The vapor pressure of many organic compounds is highly temperature dependent. In this example, calculations are performed with n-hexane and toluene. Note that one must ensure that the compound is a *liquid* in the range of temperatures for which the data is given for the calculation performed. Calculations also can be performed for solids (i.e., with vapor pressures below the melting point temperature), but the relevant parameter is then the heat of sublimation, which is the sum of the heat of vaporization and the heat of fusion [melting].

(a) Given that the vapor pressure of n-hexane (melting point $-95.3°C$) at $0°C$ is 0.0564 atm and ΔH_{vap} is 34.1 kJ/mol, what is the vapor pressure at $30°C$?

Answer: This problem is solved using Eq. 3.41, but temperatures must be in K and ΔH_{vap} in J/mol:

$$\ln\frac{P_{T_2}}{P_{T_1}} = \frac{\Delta H_{vap}(T_2 - T_1)}{RT_1T_2}$$

$$P_{T_2} = P_{T_1}e^{\frac{\Delta H_{vap}(T_2 - T_1)}{RT_1T_2}} = 0.0564 \text{ atm} \times e^{\frac{34,100\frac{J}{mol}(303.15 - 273.15)K}{8.314\frac{J}{mol-K}(303.15)(273.15)K^2}} = 0.249 \text{ atm}$$

(b) Given the following data,[10] determine the ΔH_{vap} of toluene (melting point $-95°C$).

T (°C)	−26.7	6.4	31.8	51.9	89.5
P (mm Hg)	1	10	40	100	400

Answer: Based on Eq. 3.41, the dependence of pressure on temperature is $\ln P = -\Delta H_{vap}/RT + C$. Plotting $\ln P$ versus $1/T$ gives a line with slope $\Delta H_{vap}/R$. To get the proper units, we first put temperature in K and pressure in atm:

T (K)	246.45	279.55	304.95	325.05	362.65
P (atm)	0.0013	0.0132	0.0526	0.1316	0.5263

Plotting $\ln P$ versus $1/T$ (see Figure 3.1) yields a slope of –4626.3. Thus,

$$\Delta H_{vap} = 4623.3 \text{ K} \times 8.314 \text{ J/mol} - \text{K} \times \text{kJ}/1000 \text{ J} = 38.4 \text{ kJ/mol}.$$
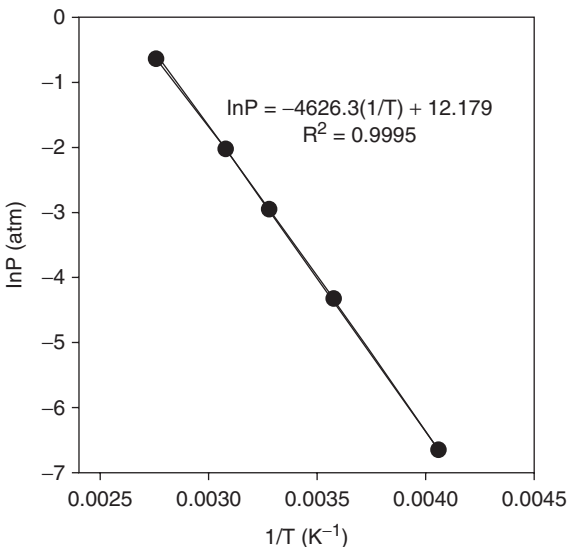
Figure 3.1 Plot of toluene vapor pressure versus temperature.

3.16.4 Effect of T on ΔG for reactions of solids and pure liquids

From the combined first and second laws, $\Delta G = \Delta H - T\Delta S$, it is clear that ΔG is a function of temperature. If ΔH and ΔS are not themselves functions of temperature, then ΔG is a linear function of T, and one can estimate ΔG at any temperature from values of ΔH and ΔS determined at one temperature. This situation is often assumed for solids and pure liquids, and the following equation is used to estimate ΔG_T:

$$\Delta G_T = \Delta H_{298K} - T\Delta S_{298} \tag{3.42}$$

3.16.5 Effect of T on chemical equilibria: the van't Hoff equation

This is the most widely used equation to quantify the effects of temperature on chemical equilibria, and it relates changes in the equilibrium constant (K) for a reaction with temperature to the standard enthalpy of reaction, $\Delta H°$. The equation can be derived readily from the function $\Delta G°/T$ (see Box 3.8). In differential form the equation is

$$\left[\frac{\partial \ln K}{\partial T}\right]_P = \frac{\Delta H°}{RT^2} \tag{3.43}$$

Box 3.8   Derivation of the van't Hoff equation

The differential of the function $\Delta G°/T$ with respect to T at fixed P is

$$(1) \quad \left[\frac{\partial(\Delta G°/T)}{\partial T}\right]_P = -\frac{\Delta G°}{T^2} + \frac{1}{T}\left[\frac{\partial \Delta G°}{\partial T}\right].$$

If we substitute the Gibbs-Helmholtz equation (eq. 3.30) into equation (1), we obtain

$$(2) \quad \left[\frac{\partial(\Delta G°/T)}{\partial T}\right]_P = -\frac{\Delta G°}{T^2} + \frac{\Delta S}{T}.$$

Further substituting $\Delta G° = \Delta H° - T\Delta S°$ into equation (2) and simplifying yields

$$(3) \quad \left[\frac{\partial(\Delta G°/T)}{\partial T}\right]_P = -\frac{\Delta H°}{T^2} + \frac{T\Delta S°}{T^2} - \frac{\Delta S}{T} = -\frac{\Delta H°}{T^2}.$$

Recalling that $\Delta G° = -RT \ln K$ and substituting this into equation (3) yields the differential form of the van't Hoff equation:

$$(4) \quad \left[\frac{\partial \ln K}{\partial T}\right]_P = \frac{\Delta H°}{RT^2}$$

The integrated form of this equation depends on whether $\Delta H°$ is constant or a function of temperature. Three possibilities exist:

(1) $\Delta H°$ is constant; $\Delta C_p = 0$; Eq. 3.43 integrates simply to

$$\ln \frac{K_{T_2}}{K_{T_1}} = \int_{T_1}^{T_2} \frac{\Delta H°}{RT^2} dT = \frac{\Delta H°}{R} \left[\frac{1}{T_1} - \frac{1}{T_2} \right] = \frac{\Delta H°(T_2 - T_1)}{RT_1 T_2}, \qquad (3.44)$$

or

$$\ln K = -\frac{\Delta H°}{RT} + \text{constant.} \qquad (3.45)$$

The indefinite integral form, Eq. 3.45, is useful for plotting purposes. It is clear that if a plot of $\ln K$ versus $1/T$ yields a straight line, the data fit Eq. 3.45 and $\Delta H°$ is constant with temperature. Moreover, the slope of the line $= -\Delta H°/R$. If the slope is positive, $\Delta H°$ is negative, and the reaction is said to be *exothermic*. If the slope is negative, $\Delta H°$ is positive, and the reaction is *endothermic*.

(2) ΔC_p is a (nonzero) constant. Then $\Delta H°$ is a linear function of T, and Eq. 3.43 integrates to

$$\ln \frac{K_{T_2}}{K_{T_1}} = \frac{\Delta H_1°}{R} \left[\frac{1}{T_1} - \frac{1}{T_2} \right] + \frac{\Delta C_P°}{R} \left(\frac{T_1}{T_2} - 1 - \ln \frac{T_1}{T_2} \right) \qquad (3.46)$$

(3) ΔC_p is a function of temperature. In this case, $\Delta H°$ is a nonlinear function of T, and a more complicated expression results (see Stumm and Morgan,[11] p. 53).

Figure 3.2 shows plots of $\ln K$ versus $1/T$ for the solubility of oxygen (O_2) in water and for chemical reactions involving the carbonate system in water. Although there is a very slight curvature in the data, the solubility of O_2 fits closely to a straight line with a positive slope, meaning that the dissolution of $O_{2(g)}$ into water is an exothermic process and $\Delta H°$ is approximately constant over the plotted temperature range. From the slope we find $\Delta H° = -14.16 \, \text{kJ/mol}$. Similarly, the slope for the Henry's law constant for the solubility of CO_2 in water is positive and the data fit closely to a straight line (with only very slight curvature apparent over the range of 0–50°C. The calculated heat of dissolution ($\Delta H°$), $-20.07 \, \text{kJ/mol}$, is somewhat higher than that for O_2. The data for ionization of dissolved CO_2 ($CO_{2(aq)} \rightleftharpoons H^+ + HCO_3^-$, K_{a1}) and for ionization of HCO_3^- ($HCO_3^- \rightleftharpoons H^+ + CO_3^{2-}$, K_{a2}) both have negative slopes (i.e., they are endothermic reactions) with a small amount of curvature (more for K_{a1} than for K_{a2}) over the temperature range of 0–50°C. Ignoring the curvature, we find $\Delta H°$ values of $+9.78$ and $+15.31 \, \text{kJ/mol}$ for K_{a1} and K_{a2}, respectively. The solubility products of calcite, aragonite, and vaterite, three crystalline forms of calcium carbonate ($CaCO_{3(s)} \approx Ca^{2+} + CO_3^{2-}$, K_{s0}), all have positive slopes, and thus all are exothermic processes. Because the lines are curved, $\Delta H°$ is not constant over the plotted temperature range but becomes increasingly positive (more exothermic) as temperature increases. Note that one can estimate $\Delta H°$ at any given temperature from the tangent to the curve at that temperature.

EXAMPLE 3.7: What is the difference in the equilibrium constant for the acid-mediated dissolution of calcite at 25°C and 45°C?
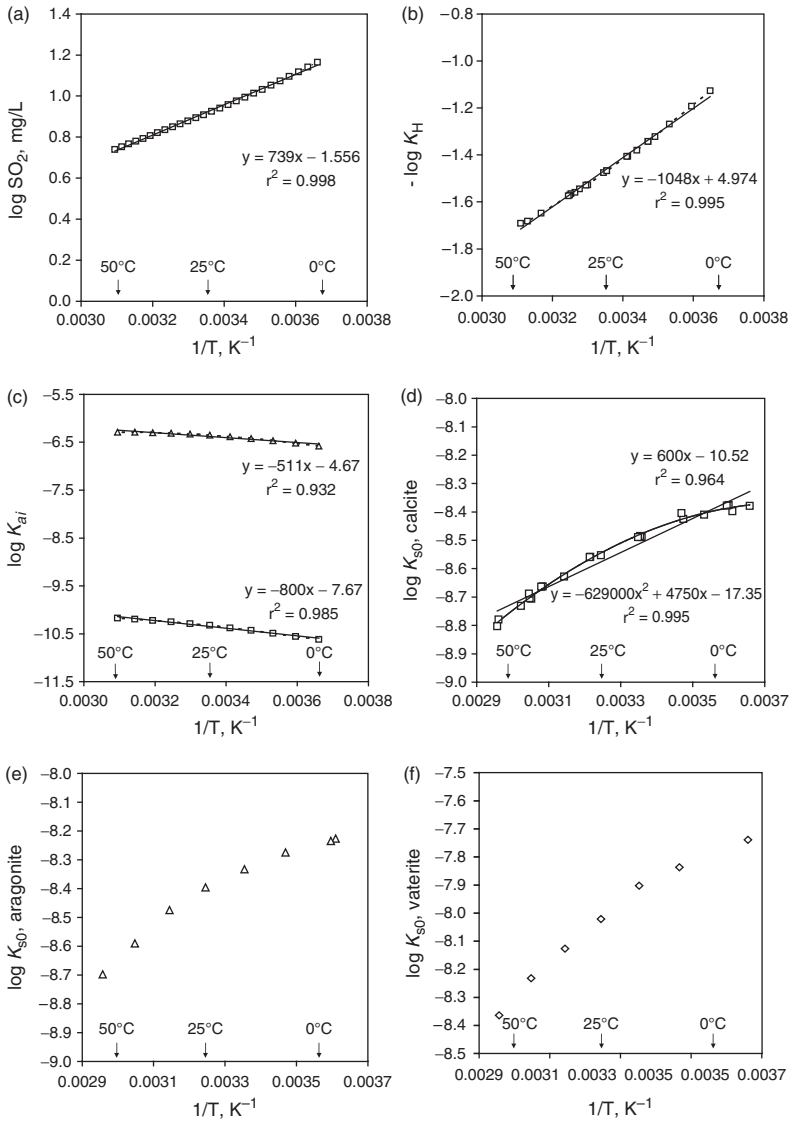
Figure 3.2 Van't Hoff plots for O_2 solubility in water (a); reactions in the carbonate system: Henry's law constant for CO_2 (b); dissociation constants K_{a1} (top) and K_{a2} (bottom) for carbonic acid (c); and solubility of calcium carbonate solid phases: calcite (d), aragonite (e), and vaterite (f). Data for (a) from *Standard Methods*[12]; data for (b)–(f) from Plummer and Busenberg.[13]

Answer: In the absence of information to the contrary, we will assume that $\Delta H°$ is constant and use Eq. 3.44. First we need to determine K at 25°C and $\Delta H°$. Recalling that $\Delta G° = -11.54$ kJ/mol at 25°C,

$$K = e^{-\Delta G°/RT} \quad K = e^{-(-11,540/(8.314\times298))} = 105.4,$$

$$\Delta H° = \sum H°_{f,\ products} - \sum H°_{f,\ reactants}$$

$$= H°_{f,\ Ca^{2+}} + H°_{f,\ HCO_3^-} - H°_{f,\ CaCO_3} - H°_{f,\ H^+},$$

and

$$\Delta H°_f = -542.83 + -692.0 - (-1207.4) - 0\ \text{kJ/mol}$$

$$= -27.43\ \text{kJ/mol}.$$

Remembering to use temperature in Kelvin,

$$\ln\frac{K_{T_2}}{K_{T_1}} = \frac{\Delta H°(T_2 - T_1)}{RT_1 T_2},$$

or

$$\ln\frac{K_{T_2}}{K_{T_1}} = \frac{-27430(318 - 298_1)}{(8.314)(318)(298)}.$$

Thus,

$$K_{T_2} = 52.5$$

Note that one *may not* simply use $T = 318$ K and calculate K from the given $\Delta G°$ value via Eq. 3.27 because the $\Delta G°$ value determined from tabulated $G°_f$ data is valid only at 25°C or 298 K.

3.17 Advanced topic: effects of pressure on chemical equilibria

Pressure effects become important only at pressures of hundreds of atmospheres, which occur at great depths in the oceans. In contrast, temperature changes of 10°C or even less usually have measurable effects on chemical equilibria. Consequently, temperature always must be considered in evaluating chemical equilibria. Pressure has insignificant effects on equilibria in freshwaters, but it must be taken into account in evaluating equilibrium conditions at the ocean bottom.

    Pressure effects on equilibria are conveyed by the fundamental thermodynamic variable V (volume), as described in Eq. 3.32; i.e., $(\partial G/\partial P)_T = V$. The forms of the equations describing pressure effects on free energy (see Box 3.9) and equilibria are similar to those describing temperature effects, except that entropy terms are replaced by volume terms. Table 3.2 lists the important relationships

between pressure and chemical equilibria. The usual convention for standard states of compounds (where its thermodynamic activity is defined to be unity) usually is defined to be at P = 1 atm. This leads to difficulties in describing effects of pressure on equilibria and to avoid these difficulties, a variable-pressure standard state convention was used to derive the equations in Table 3.2. Use of this convention does not affect chemical potentials (μ_i) or the equilibrium composition with pressure.

Box 3.9 Derivation of an equation relating ΔG and P for gases

Based on eq. 3.31, we can write the following equation for the change in G with pressure at constant temperature:

(1) $\int dG = \Delta G = \left(\int V dP \right)_T$

ΔG is the molar free energy change and V is the molar volume. For an ideal gas, V = RT/P, and thus eq. (1) becomes

(2) $\Delta G = \int \dfrac{RT}{P} dP = RTd \ln P$

or

(3) $G_2 - G_1 = RT \ln \dfrac{P_2}{P_1}$

If we let $P_1 = 1$ atm and define that as the "standard state" for the gas, at which its free energy is defined to be $G°$, we can rewrite eq. (3) as

(4) $G = G° + RT \ln P$

Equation (4) applies to an ideal gas. A similar equation can be written for nonideal gases and vapors. In this case, we substitute an idealized vapor pressure called the fugacity, f, for P:

(5) $G = G° + RT \ln f$

Fugacity has units of pressure (most commonly, atm). The term often is described as a measure of the "escaping tendency" of a substance. Although fugacity was defined above in terms of gases, it is a perfectly general concept and applies equally to liquids and solids (which have vapor pressures). The importance of fugacity in defining the activity of any substance i, a_i, is described in chapter 4.

The effect of pressure on the free energy of reaction for standard conditions, $\Delta G°$, and thus on K_{eq}, is exerted through $\Delta V°$, the difference between the sums of the standard-state

Table 3.2 Equations defining pressure effects on equilibrium properties

Chemical potential of any substance:

(1) $(\partial \mu_i / \partial P)_T = V_i$

Change in free energy of reaction:

(2) $(\partial \Delta G / \partial P)_T =) V = \sum V_{prod} - \sum V_{react}$

Activities of solutes, solids, and liquids:

(3a) $(\partial \ln a_i / \partial P)_T = V_i / RT$

or

(3b) $\ln(a_{i,P} / a_{i,1 \text{ atm}}) = (1/RT) \int V_i dP$

If k_i° is independent of P and $\neq 0$, then $V_i = f(P) = k_i^\circ P + V_i^\circ$, and

(4) $RT \ln(a_{i,P} / a_{i,1 \text{ atm}}) = V_i^\circ (P - 1) + \frac{1}{2} k_i^\circ (P - 1)^2$

Equilibrium constants for reactions:

(5) $(\partial \ln K / \partial P)_T = -\Delta V^\circ / RT$

When ΔV° is independent of P ($\Delta k^\circ = 0$), equation (5) integrates to

(6) $\ln(K_P / K_{1 \text{ atm}}) = -\Delta V^\circ (P - 1) / RT$

When Δk° is constant but $\neq 0$, integration of equation (5) yields more complicated expression:

(7) $\ln(K_P / K_1) = \{-\Delta V^\circ (P - 1) + \frac{1}{2} \Delta k^\circ (P - 1)^2\}$

molar volumes of the products and reactants:

$$\Delta V^\circ = \sum V_{prod}^\circ - \sum V_{react}^\circ \tag{3.47}$$

$$\Delta V = \sum v_i V_i \text{(for actual conditions)} \tag{3.48}$$

V_i, which has units of cm^3/mol, has a simple physical interpretation. Difficulties arise regarding values of V_i for ions in solution, however. We cannot determine volumes for single ions, just as we cannot measure enthalpies or free energies of single ions, because we cannot produce solutions containing only one kind of ion. To circumvent this problem, the volume of one ion must be defined arbitrarily. By convention, the standard molar volume for H$^+$ is taken to be zero: $V^\circ_{H^+} = 0$. This convention leads to

Table 3.3 Partial molar volumes and compressibilities for inorganic ions in water*

Ion	V° (pure water), $cm^3\ mol^{-1}$		V (seawater), $cm^3\ mol^{-1}$		k° (pure water), $-10^{-3}\ cm^3$ $mol^{-1}\ bar^{-1\dagger}$		k (seawater), $-10^{-3}\ cm^3$ $mol^{-1}\ bar^{-1\dagger}$	
	$0°C$	$25°C$	$0°C$	$25°C$	$0°C$	$25°C$	$0°C$	$25°C$
H^+	0	0	0	0	0	0	0	0
OH^-	−7.58	−3.98	−2.01	−0.05	6.41	3.86	4.24	2.32
Na^+	−3.46	−1.21	−1.90	−0.72	5.13	3.94	3.64	3.66
K^+	7.26	9.03	8.73	9.61	4.36	3.37	2.92	2.87
Mg^{2+}	−22.32	−21.15	−18.65	−19.67	7.83	8.01	5.73	7.23
Ca^{2+}	−19.69	−17.83	−15.93	−16.00	7.43	7.61	5.82	6.89
F^-	−3.05	−1.16	−0.02	1.91	5.57	3.02	3.91	2.56
Cl^-	16.37	17.82	17.85	19.64	2.51	0.74	1.31	−0.04
HCO_3^-	21.07	24.29	24.72	27.76	5.30	2.75	3.01	1.08
CO_3^{2-}	−8.74	−3.78	7.4	13.20	11.04	7.35	7.88	3.70
SO_4^{2-}	9.26	13.98	17.98	22.38	10.43	6.74	7.54	3.36

* Summarized from Millero.[14,15]
† One bar = 0.987 atm.

some strange-looking (negative) values of V_i, as shown in Table 3.3. Obviously, no real substance can have a negative volume; the negative values simply mean that an ion has a smaller molar volume than does H^+.

It is important to realize that molar volumes for ions in aqueous solution reflect not only the intrinsic volume of the ions themselves but also the effects of the ion on the structure (hence, volume) of the solvent water. Insofar as an ion binds water molecules to itself, as all cations do, it removes the water molecules from the relatively loose solvent structure and decreases the overall volume of the system (see Chapter 1). In many cases, the contribution of the ion to increased solvent binding has a larger effect on its molar volume than does the volume of the ion itself. It is apparent from Table 3.3 that V varies with ionic content of the solution and its temperature—partial molar volumes for ions are smaller in pure water than in seawater and at 0°C than at 25°C or 50°C; however, the trend with temperature is not linear.

The molar volumes of many ions and compounds vary with pressure. Partial **_molar compressibility_** (k_i°) is the term that quantifies this variation in V_i:

$$k_i^\circ = \left(\frac{\partial V_i^\circ}{\partial P}\right)_T \tag{3.49}$$

Similarly, Δk°, the compressibility of reaction, is the difference in the sums of k_i° for the products and reactants, all in their standard states. Both k° and Δk° usually are assumed to be independent of pressure. For reactions involving only ionic reactants and products, Δk° is small (because values of k° tend to be of similar magnitudes for various ions), and effects of compressibility on predicted equilibrium conditions can be ignored. Compressibilities of solid minerals generally are much lower than those of ions (by a factor of 10 or more), and the magnitude of compressibility

for ions is sufficient that significant errors will be made in computing ΔV and related thermodynamic variables (ΔG, K) for mineral dissolution and precipitation processes at the bottom of the oceans, if ion compressibility is not taken into account.[15]

The mean depth of the oceans is $\sim$6500 m, and the pressure at this depth is about 650 atm; at the maximum depth of the ocean ($\sim$10,000 m), the pressure is about 1000 atm. At this depth, the activity of water is $\sim$2.1, compared with a value of 1.0 for pure water at 1 atm. Similarly, the ion product of pure water (K_w) at 5°C and 1000 atm is 2.8 times the value at 1 atm.[16] In general, ΔV is negative for ionization processes, including dissolution of minerals like $CaCO_3$. Equations 6 and 7 of Table 3.2 indicate that solubility products for mineral salts (K_{s0}) generally increase with pressure.

EXAMPLE 3.8 Effect of pressure on solubility product of calcite: $\Delta V°$ for dissolution of calcite ($CaCO_3$) at 0°C in pure water is computed from $V°$ for calcite (36.93 cm^3 mol^{-1}) and the partial molar volumes of Ca^{2+} and CO_3^{2-} (Table 3.3) as

$$\Delta V° = V_{Ca^{2+}} + V_{CO_3^{2-}} - V_{CaCO_3} = -19.69 - 8.74 - 36.93 = -65.36 \text{ cm}^3\text{mol}^{-1}.$$

If we assume that k° for calcite is zero and use k° values for Ca^{2+} and CO_3^{2-} from Table 3.3, we find that $\Delta k° = -7.43 + -11.04 - 0 = -18.47 \times 10^{-3}$ cm^3 mol^{-1} bar^{-1} or -18.72×10^{-3} cm^3 mol^{-1} atm^{-1} at 0°C. Using Eq. (7) of Table 3.2, we find that the solubility product of calcite at 0°C and 1000 atm ($K_{s0, \ 1000 \ atm}$) is $\sim$12 $\times$ higher than that at 1 atm:

$$\ln(K_P/K_1) = \{-\Delta V°(P - 1) + \tfrac{1}{2}\Delta k°(P - 1)^2\}/RT$$

$$\ln(K_{s0, \ 1000 \ atm}/K_{s0, \ 1 \ atm}) = \{65.36(1000 - 1) + 2(-18.72 \times 10^{-3}) \times$$

$$(1000 - 1)^2\}/82.05(273) = 2.46$$

or

$$K_{s0, \ 1000 \ atm}/K_{s0, \ 1 \ atm} = 11.7$$

Note: we use a value for R, the gas constant, of 82.05 cm^3 atm K^{-1} mol^{-1} in this problem to match the units of ΔV, $\Delta k°$, and P. The calculated value agrees with measured effects of P on calcite solubility. Corresponding values for seawater at 0°C are $\Delta V = -45.46$ cm^3 mol^{-1}, $\Delta k = 13.70$ cm^3 mol^{-1} bar^{-1} (13.88 cm^3 mol^{-1} atm^{-1}), and $K_{sw, \ 1000atm}/K_{sw, \ 1 \ atm} = 5.57$. The smaller effect of P in seawater results primarily from a much larger value of V for CO_3^{2-} in seawater compared with pure water, which results in a smaller value of ΔV in seawater.

If the compressibility of the ions is not considered (Δk assumed to be 0), use of Eq. (6) from Table 3.2 leads to $K_{s0, \ 1000 \ atm}/K_{s0, \ 1 \ atm} = 17.7$ and $K_{sw, \ 1000 \ atm}/K_{sw, \ 1 \ atm} = 7.58$. The larger error for pure water reflects the fact that ions generally have smaller compressibility values in seawater, as shown in Table 3.3.

Problems

3.1. Determine the standard Gibbs free energy change of reaction, ΔG_r°, and the equilibrium constants, K_{eq}, for the following reactions using the tabulated values for $\overline{G}_f^\circ$ in the Appendix:

(a) $AgBr_{(s)} \rightleftharpoons Ag^+ + Br^-$
(b) $PO_4^{3-} + H^+ \rightleftharpoons HPO_4^{2-}$
(c) $HPO_4^{2-} + H^+ \rightleftharpoons H_2PO_4^-$
(d) $AgBr_{(s)} + Cl^- \rightleftharpoons AgCl_{(s)} + Br^-$

3.2. You are studying the hydration of compound X, which is represented by the reaction $X + H_2O \rightleftharpoons X - H_2O$. For this reaction $\Delta G_f^\circ = -28.23$ kJ/mol.

(a) Using a spectroscopic technique, you establish that a solution contains 3×10^{-3} M of X and 3.7×10^{-4} M of $X - H_2O$ at 25°C. What is ΔG_f for the reaction under these conditions? In which direction is the reaction proceeding?
(b) What is the final, equilibrium composition of the solution?

3.3. Plot the data for K_w given in Table 8.1 as a van t'Hoff plot and determine whether the reaction is endothermic or exothermic. If the plot is linear, determine ΔH° for the reaction from the slope of the plot.

3.4. (a) Using the standard Gibbs free energies of formation in the Appendix, find ΔG_r°, and the equilibrium constant, K_{eq}, for the following reaction:

$$CaCO_{3(s)} \rightleftharpoons CaO_{(s)} + CO_{2(g)}.$$

For K_{eq}, give both its numerical value and the mass action expression involving any variable reactants and products.
(b) A dry mixture containing 1 g of each solid is on a lab bench in contact with the atmosphere, which contains CO_2 at a partial pressure of $10^{-3.4}$ atm. Does the driving force of the reaction favor conversion of one of the solids into the other, or are the solids equilibrated with each other?

3.5. Consider the reaction

$$CaCO_{3(s)} + 2H_{(aq)}^+ \rightleftharpoons CO_{2(g)} + H_2O_{(l)} + Ca_{(aq)}^{2+},$$

where $CaCO_3$ is calcite. Answer the following:

(a) What is ΔG° for this reaction at 25°C?
(b) What is K at 25°C?
(c) What is K at 40°C?
(d) Is the reaction exothermic or endothermic?
(e) If a solution has $[H^+] = 1 \times 10^{-7}$ M, $P_{CO_2} = 10^{-3.5}$ atm, and calcite is present, what is the concentration of Ca^{2+} at equilibrium at 25°C?

3.6. A geologist has found a sample of celestite (strontium sulfate). He decides to clean the mineral in a solution containing 10^{-3} M CO_3^{2-} and 10^{-7} M SO_4^{2-}. Considering the following reaction,

$$SrSO_{4(s)} + CO_3^{2-} \rightleftharpoons SrCO_{3(s)} + SO_4^{2-}$$
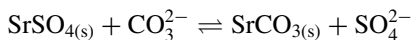
(a) Calculate ΔG° and ΔG. In which direction does the reaction proceed?
(b) What will be the ratio of SO_4^{2-} and CO_3^{2-} at equilibrium?
(c) Assuming the concentration of CO_3^{2-} can be held constant at 10^{-3} M, what concentration of SO_4^{2-} must be added to solution to reverse the direction of the reaction?

Potentially useful information:

Mineral	Formula	G_f° (in kJ/mol)
Strontianite	$SrCO_{3(s)}$	-1137.6
Celestite	$SrSO_{4(s)}$	-1341.0

3.7. Driving along the freeway through Minneapolis, you notice your battery light is on. Worried that something might be wrong, you pull off at the next exit and find the Arnold-Brezonik Car House and Emporium of Mechanics (AB-CHEM). While testing your battery, the proprietors ask you to perform some chemistry-related calculations. The overall reaction that takes place in the lead battery is

$$Pb_{(s)} + PbO_{2(s)} + 2H^+_{(aq)} + 2HSO^-_{4\ (aq)} \rightleftharpoons 2PbSO_{4(s)} + 2H_2O_{(l)}.$$

Because the battery can be recharged, the reaction is (and must be) reversible.

(a) What is the equilibrium constant (K) for the above reaction?
(b) If all three solids are present, $[HSO_4^-] = 1 \times 10^{-2}$ M, and $[H^+] = 1 \times 10^{-2}$ M, in which direction is the reaction proceeding?
(c) If all the protons present originally come from H_2SO_4, what are the equilibrium concentrations of H^+ and HSO_4^- in the system?

Potentially useful information:

Species	G_f° (kJ/mol)	Species	G_f° (kJ/mol)
$Pb_{(s)}$	0	$HSO^-_{4\ (aq)}$	-756
$PbO_{2(s)}$	-217.4	$PbSO_{4(s)}$	-813.2
$H^+_{(aq)}$	0	$H_2O_{(l)}$	-237.18

3.8. While searching an online auction site for rare minerals, you come across someone selling a sample of cerussite ($PbCO_{3(s)}$). This is the only lead mineral you are missing from your collection, so you are excited. You are concerned, however, that it may not have been stored properly. An inquiry to the seller reveals that the cerussite was left in an open room ($P_{O_2} = 0.208$ atm, $P_{CO_2} = 10^{-3.5}$ atm, relative humidity = 30%). Given the following information, which Pb-bearing solid is most stable?

Species	G_f^0 (kJ/mol)
$PbCO_{3(s)}$	−625.5
$PbO_{(s)}$	−187.9
$PbO_{2(s)}$	−217.4
$Pb(OH)_{2(s)}$	−452.2
$O_{2(g)}$	0
$CO_{2(g)}$	−394.37
$H_2O_{(g)}$	−228.57

References

1. Denbigh, K. 1966. *The principles of chemical equilibrium*, 2nd ed., Cambridge Univ. Press, London.
2. Adamson, A. W. 1979. *A textbook of physical chemistry*, 2nd ed., Academic Press, New York.
3. Lewis, G. N., and M. Randall. 1925. *Thermodynamics*, McGraw-Hill, New York.
4. Exergy; available online at http://en.wikipedia.org/Exergy, accessed 12/2008.
5. Odum, H. T. 1988. Self-organization, transformity, and information. *Science* **242**: 1132–1139.
6. Brown, M., and Ulgiati. 2004. Energy quality, emergy, and transformity: H.T. Odum's contributions to quantifying and understanding systems. *Ecol. Model.* **178**: 201–213.
7. Scienceman, D. M. 1997. Emergy definition. *Ecol. Eng.* **9**: 209–212.
8. Wheeler, L. P. 1952. *Josiah Willard Gibbs, the history of a great mind*, Yale Univ. Press, New Haven, Conn.
9. http://nobelprize.org/nobel_prizes/economics/laureates/1970/samuelson-lecture.pdf, accessed September 9, 2010.
10. Lide, D. R. (ed.). 2008. *CRC Handbook of chemistry and physics*, 89th ed., CRC Press, Boca Raton, Fla.
11. Stumm, W., and J. J. Morgan. 1996. *Aquatic chemistry*, 3rd ed., Wiley-Interscience, New York.
12. Eaton, A. D., L. S. Clesceri, E. W. Rice, and A. E. Greenberg (eds.). 2005. *Standard methods for the examination of water and wastewater*, 21st ed., Amer. Pub. Health Assoc., Amer. Water Works Assoc., Water Environ. Fed., Washington, D.C.
13. Plummer, N. L., and E. Busenberg. 1982. The solubilities of calcite, aragonite, and vaterite in CO_2-H_2O solutions between 0 and 90°C, and an evaluation of the aqueous model for the system $CaCO_3$-CO_2-H_2O. *Geochim. Cosmochim. Acta* **46**: 1011–1140.

14. Millero, F. J. 1982. The effect of pressure on the solubility of minerals in water and seawater. *Geochim. Cosmochim. Acta* **46**: 11–22.
15. Millero, F. J. 2001. *Physical chemistry of natural waters*, Wiley-Interscience, New York.
16. Owen, B. B., and S. R. Brinkley. 1941. Calculation of the effect of pressure upon ionic equilibria in pure water and in salt solutions. *Chem. Rev.* **29**: 461–474.

4

▉▉ Activity-Concentration Relationships

▉▉ Objectives and scope

In this chapter you will learn about the relationships between thermodynamically ideal concentrations, called activities, and the standard ways we measure and report chemical concentrations. In general, activities and concentrations are related by "activity coefficients." Relationships are described for gases, liquids, ionic and nonionic solutes in water, and mixtures of solids (called solid solutions). Ion activity coefficients normally are calculated as a function of "ionic strength" by one of several forms of the Debye-Hückel equation, and you will learn about the limiting conditions under which these equations apply.

▉▉ Key terms and concepts

- Standard and reference states; Raoultian and Henryan behavior; fugacity
- Activity coefficients for gases, liquids, solutes, and solids
- Ionic strength: definition and methods to estimate it
- Debye-Hückel equation: limiting law, extended equation; Guntelberg approximation; Davies equation
- Mean-salt and single-ion activities
- Salting coefficients for nonelectrolytes
- Ideal and regular solid solutions

4.1 Introduction

We saw in Chapter 1 that solving problems of chemical equilibria involves the use of equilibrium constants (mass-action expressions), K_{eq}. In Chapter 3 we learned about

the relationship between such constants and the free energy of a reaction, $\Delta G°$, a thermodynamic function. We also learned that the equilibrium concentrations defined by K_{eq} expressions are idealized concentrations called activities. In this chapter we describe the relationships between activities of various kinds of chemical components—solvents, solutes, gases, and solids—and the concentration units (e.g., mol/L) used to report the results of chemical analyses.

4.2   Reference and standard states

We cannot measure the absolute activity of any substance, only its relative activity, that is, its activity relative to that of some *reference state*. In fact, as noted in Chapter 3, activity is a dimensionless quantity because it is defined as a ratio of a behavioral trait of a substance at some state (set of conditions) to the value of that trait in the reference state. The behavioral trait used to define activity is called *fugacity*, which physically is described as defining the "escaping tendency of a substance from its given state." At equilibrium, all substances in a reacting system have the same escaping tendency; i.e., their fugacities are equal.[*] In general, we can write

$$a_i = \frac{f_{i,\text{actual}}}{f_{i,\text{ref}}}. \tag{4.1}$$

At a given temperature and pressure, we define the reference state of substance i as the state where $f_i = a_i = c_i$ and $\gamma_i = 1$; a_i stands for the activity (thermodynamic or effective concentration) of i, c_i stands for the actual concentration of i (usually in mole fraction or mol L^{-1}), and γ_i is the activity coefficient or proportionality factor relating a_i and c_i in the general relationship

$$a_i = \gamma_i c_i. \tag{4.2}$$

Two conventions are needed to define all possible reference states. For solids and liquids, **Raoultian behavior** states that $a \to c$ as $c \to 1$, and $\gamma \to 1$ as $c \to 1$. In words, this statement says that the limiting behavior of solids and liquids approaches ideal behavior as they approach unit mole fraction; that is, as they become a pure (single component) phase. For Raoultian behavior, if the solute is dissolved in another phase (i.e., water) the nonideal interactions lead to increasing values of γ (i.e., $\gamma > 1$). This is the convention used for noncharged organic solutes (see Section 4.7). The idea of ionic solutes in water approaching unit mole fraction makes no physical sense, however, and consequently, for charged solutes we use **Henryan behavior**, where $a \to c$ as $c \to 0$, and $\gamma \to 1$ as $c \to 0$. In words, this says that a Henryan-type substance approaches ideal behavior as its molar or mole fraction concentration approaches zero. Thus for solutes, the reference state is the dilute solution limit, where $a = c$, and $\gamma = 1$ (and $c \to 0$). For Henryan behavior, γ ranges between 0 and 1. Some texts say that the first convention should be selected where possible and the second where necessary.

---

[*]Not surprisingly, fugacity is related to Gibbs free energy: $\ln f_i = G_i/RT + \text{constant}$, or in differential form, $d \ln f_i = dG_i/RT$ (at constant temperature).[1]

To be exact, Eq. 4.2 is not dimensionally correct. Because activity is dimensionless and activity coefficients also are dimensionless, concentration must be dimensionless. This is the case if we express c in mole fraction, but not if we express it in mol/L, as is the more common case. We can get around this problem by noting that the more exact equation[2] is

$$a_i = \gamma_i \frac{c_{i,\text{actual}}}{c_{i,\text{std}}},\tag{4.3}$$

where $c_{i,\text{std}}$ is the "standard state" concentration of i. By definition, $c = 1$ in the standard state, which generally is defined as the state where $c = 1$, $a = 1$, and $\gamma = 1$. The standard state is a real state for solids and liquids; it is given as the pure liquid or solid at 1 atm pressure. For solutes, the standard state usually is defined as $c = 1$ mol/L at 1 atm pressure. For actual solutes, $a \neq 1.0$ at $c = 1$ mol/L, and so the standard state for solutes is a hypothetical state. For gases, the standard state usually is defined so that $a = f$, and $a/P = 1$, which occurs when $P = 0$. Under these hypothetical conditions, the gas behaves as an ideal gas and $a° = f° = 1$ when $P = 0$.[1]

To designate whether concentrations or activities are being specified, different symbols are used. To specify that a concentration of species i is being given, the notation is [i]. To show that the activity (i.e., $\gamma_i c_i$) is being given, the notation is {i}.

4.3 Activities of liquids

As noted above, the reference (and standard) state for liquid water is pure water at $P = 1$ atm and a specified temperature. Here $a = c = \gamma = 1$. There is no general theoretical expression to compute γ (and a) when the mole fraction of water (or any other liquid) decreases from unity. Instead, these values must be measured from the behavior of colligative properties of the solution, such as vapor pressure or freezing point. For example, the activity of water in brine solutions has been measured from the decrease in vapor pressure (or boiling point elevation) of the solution as its salt content increases. Similar effects are seen on the freezing point of the liquid, and this why salt is added to roads in the winter. From the discussion in Section 4.2, it is clear that the activity of water is given by the ratio of its fugacity in a given state to the fugacity of pure water. In turn, this ratio of fugacities is equal to the ratio of vapor pressures for the respective systems:

$$a_{H_2O} = \frac{f_{H_2O,\text{sol}}}{f^*_{H_2O}} = \frac{P_{H_2O,\text{sol}}}{P^*_{H_2O}}\tag{4.4}$$

The superscript "*" refers to pure water and subscript "sol" refers to water containing solutes. According to Robinson and Stokes,[3] the activity of water in solutions of NaCl varies in the following way:

Molality of NaCl, m	0	0.10	0.30	0.50	0.70	1.00
a_{H_2O}	1.000	0.9966	0.9901	0.9836	0.9769	0.9669
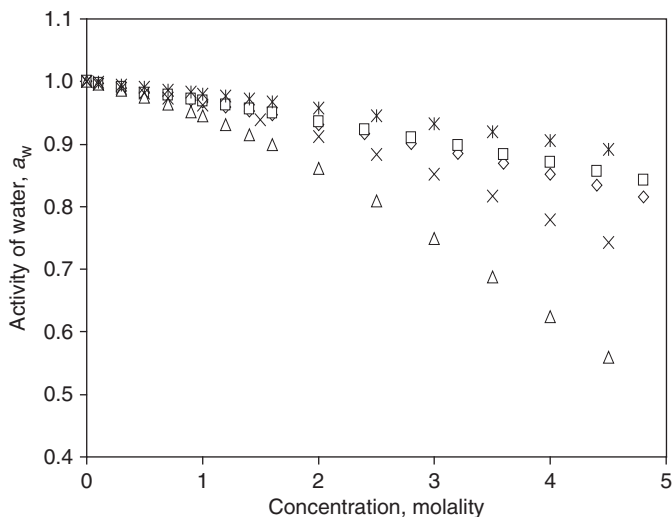
Figure 4.1 Activity of water in solutions of various solutes: $\triangle$, $CaCl_2$; $\times$, H_2SO_4; $\diamond$, NaCl; $\square$, KCl; $\ast$, sucrose. Data from Robinson and Stokes.[3]

The activity of water in seawater is $\sim$0.98, and this value is used in careful equilibrium calculations for seawater when water appears as a product or reactant. At a given concentration, the identity of the solute has an effect on a_w (Figure 4.1), but for practical purposes, we can assume that the activity of water in dilute solutions ($m < 0.1$), such as natural freshwater, is unity.

4.4   Ion activity coefficients

4.4.1   Overview

In solving ionic equilibrium problems involving mixtures of salts, we need to know values of the activity coefficients for each ion that appears in an equilibrium constant expression. Most commonly, these values are *computed* from a theoretical relationship—the Debye-Hückel equation, the forms of which are described in Sections 4.4.3 and 4.4.4. This theory assumes that ion activity coefficients in dilute solutions do not depend on the composition of the solution but only on the total ionic strength (defined below). This assumption becomes increasingly untenable as ion concentrations increase. Single ion activities and activity coefficients can be *measured* from colligative properties of solutions only if an extrathermodynamic assumption is made, but mean salt activities and activity coefficients can be measured experimentally with no extrathermodynamic assumption (see Section 4.4.5).

4.4.2   Ionic strength: definition and approximations

The concept of ionic strength, I, is critically important in predicting activity-concentration relationships for ions in aqueous solutions. Lewis introduced the concept in 1921 and

proposed that the activity coefficient of an ion in dilute solution is the same in all solutions of the same ionic strength. Activity coefficients in dilute solutions thus do not depend on the composition of a solution but merely on the total concentration. Debye and Hückel developed a theoretical relationship between ion activity coefficients and ionic strength in 1923.

The exact definition of ionic strength is

$$I = \frac{1}{2} \sum_i m_i Z_i^2, \tag{4.5}$$

where m_i is the molality of the ith ion, Z_i is the integer number of charges on the ith ion, and the summation is over all ions. For practical purposes, concentrations in natural waters may be expressed in molarity with no loss in accuracy. The importance of ionic charge in contributing to ionic strength is notable. For monovalent salts, $I = m$, but for a divalent cation, monovalent anion, $M^{2+}X_2^-$, or monovalent cation/divalent anion, $M_2^+X^{2-}$, we find that $I = 3 \times m$, and for the salt of a divalent cation and anion ($M^{2+}X^{2-}$), $I = 4 \times m$.

The range of ionic strength of freshwaters generally is slightly more than 10^{-4} to slightly more than 10^{-2}; the lower limit applies to softwater systems such as surface streams and lakes in granitic regions, and the upper limit applies to hard waters, such as ground water in calcareous regions. Pristine rainfall in continental areas (away from the influence of sea salts) has an ionic strength of about 1×10^{-4}. The ionic strength of seawater itself is 0.699.

The only rigorous way to compute I for a solution is to know the concentrations of all ions and apply Eq. 4.5. This means that one must have a complete water analysis and also know the extent to which ions are complexed with each other rather than present as individual entities. Because the complete ionic composition of natural waters often is not known, aquatic chemists have developed equations to estimate I from readily available information, such as electrical conductivity and/or total dissolved solids. The earliest of these approximations is by Langelier:[4]

$$I = 2.5 \times 10^{-5} \times TDS, \tag{4.6}$$

where TDS is total dissolved solids concentration in mg/L. This relationship is based on the assumption that the relative ionic composition of natural waters is fairly constant. Ponnamperuma et al.[5] related I to specific conductance:

$$I = 1.6 \times 10^{-5} \times SC \quad \text{(for I < 0.06),} \tag{4.7a}$$

where SC is specific conductance in μS/cm. Griffin and Jurinak[6] extended the range of the relationship between I and SC and found a lower proportionality factor between I and SC over that range:

$$I = 1.3 \times 10^{-5} \times SC \quad \text{(for I < 0.5),} \tag{4.7b}$$

Equations 4.6 and 4.7 imply that a correlation should exist between dissolved solids concentration and specific conductance, and in fact, there is a rough correlation between

these variables. *Standard Methods*[7] long has provided the approximate formula:

$$\text{TDS} \approx b \times \text{SC}, \tag{4.8}$$

where b is in the range from 0.55 to 0.70, as a test of whether TDS results are reasonable.

Finally, errors in predicting I from either TDS or SC are caused by the variable ionic composition of natural waters,[8] that is, varying ratios of divalent to monovalent ions and varying ratios of lighter ions (Na^+, Mg^{2+}) to heavier ions (K^+, Ca^{2+}) . The accuracy of estimates obtained from these equations, however, usually is satisfactory for purposes of calculating activity coefficients by the Debye-Hückel equation.

EXAMPLE 4.1 Calculating and estimating ionic strength: (1) Your field measurement of a stream sample gave a specific conductance of 100 µS/cm, and your analysis of the water gave concentrations of Na^+, Ca^{2+}, Cl^-, and HCO_3^- of 9, 21, 6, and 45 mg/L, respectively. Are these measurements consistent?

Answer: Using Eq. 4.7, $I = 2.5 \times 10^{-5} \times 100 = 2.5 \times 10^{-3}$. To use Eq. 4.5, we must first convert the concentration into mol/L and then multiply by the square of the charge on each ion:

Ion	*mg/L*	*Mol. wt.*	*mol/L*	*charge*	$C_i Z_i^2$
Na^+	9	23	3.91×10^{-4}	1	3.91×10^{-4}
Ca^{2+}	21	40	5.25×10^{-4}	2	2.10×10^{-3}
Cl^-	6	35.45	1.69×10^{-4}	1	1.69×10^{-4}
HCO_3^-	45	61	7.38×10^{-4}	1	7.38×10^{-4}
				Sum =	3.40×10^{-3}
				I	1.70×10^{-3}

The results are not consistent, most likely because the measurement of the ions in the water sample is incomplete and needs to include, at a minimum, Mg^{2+}, K^+, and SO_4^{2-}.

(2) Treated drinking water for the city of St. Paul, Minnesota, was found to have a total dissolved solids (TDS) of 165 mg/L and a specific conductance (SC) of 205 µS/cm. Estimate the ionic strength of the water from the TDS and SC and determine whether the water fits the usual relationship between TDS and SC.

Answer: From Eq. 4.6, $I = 2.5 \times 10^{-5} \times 165 = \mathbf{4.13 \times 10^{-3}}$ based on TDS. From Eq. 4.7, $I = 1.6 \times 10^{-5} \times 205 = \mathbf{3.28 \times 10^{-3}}$ based on SC. The two estimates are only in fair agreement. From the TDS and SC values and Eq. 4.8, we find that $b = 0.80$, which is above the range for b reported in *Standard Methods* and may explain the discrepancy between the two estimates of I from TDS and SC. Probably one of the measurements (most likely TDS) is in error.

4.4.3 The Debye-Hückel equation

Debye and Hückel based their theoretical development of ion activity coefficients on two basic laws that describe interactions among ions in electrolyte solutions: (1) Coulomb's inverse square law for electrostatic attraction between particles of unlike sign and electrostatic repulsion for particles of like sign, and (2) the Boltzmann distribution law, which describes the tendency of thermal energy to counteract the effects of electrostatic attraction and repulsion. The discussion of these laws in Box 4.1 is based on descriptions of the theory by Laitinen and Harris[9] and Adamson.[10]

Box 4.1   Coulomb's Law and the Boltzmann distribution: the basis for the Debye-Hückel equation

In the cgs system of units, Coulomb's law is written as:

$$(1) \ f = \frac{z_1 z_2}{d^2} \ \text{(in vacuum)}, \quad \text{or} \quad f = \frac{z_1 z_2}{D d^2} \ \text{(in a medium)},$$

where f is the force, z is the charge (in esu), d is the interparticle distance (cm), and D is the dielectric constant of the medium. In a vacuum, $f = 1$ dyne for charges of 1 esu at a distance of 1 cm.* It is apparent that $1/D$ is the fraction by which the electrostatic force is reduced in a medium. Water has a high D (80.1 at 25°C) and thus a large shielding effect on electrostatic forces between ions.

The Boltzmann law relates the distribution of ions in solution to the electric potentials caused by ionic charges:

$$(2) \ C_i = C_i^\circ \exp\left(\frac{-Z_i e \Psi}{kT}\right),$$

where C_i is the concentration of the ith ion at potential Ψ, C_i° is the concentration of that ion at an electrically neutral point, Z_i is the integer value of charge (positive or negative) for the ion, e is the charge of an electron (4.803×10^{-10} esu), and $\mathbf{k}$ is the gas constant per molecule (R/N_A, where N_A is Avogadro's number), known as the Boltzmann constant. According to this law, the concentration of like-charged ions is lower near a given ion and the concentration of unlike-charged ions is higher, forming an "ion atmosphere." Because the solution as a whole is electrically neutral, the net charge of the "shielding ions" in the ion atmosphere is equal to and opposite of that of the central ion. Boltzmann's law states that this charge drops off exponentially with distance (or potential). It depends on temperature because thermal energy tends to counteract the attractive and repulsive forces between ions.

* Because a dyne has dimensions of $g\ cm\ s^{-2}$, the dimensions of the cgs unit of charge, esu (now known as a statcoulomb), are $g^{1/2}\ cm^{3/2}\ s^{-1}$.

In the simplest derivation of the Debye-Hückel equation, the ions are assumed to behave as point charges, and the equation has the form

$$\ln \gamma_i = -\frac{Z_i^2 e^2 \kappa}{2D\mathbf{k}T}, \tag{4.9}$$

where γ_i is the activity coefficient of the ith ion; ; e is the charge of an electron (4.803×10^{-10} esu); D is the dielectric constant of the solvent; $\mathbf{k}$ is the gas constant per molecule (the Boltzmann constant); and κ is defined as the reciprocal of the radius of the "ionic atmosphere." The value of κ depends on the ionic strength of the solution:

$$\kappa = \sqrt{8\pi e^2 N/1000 D\mathbf{k}T} \times \sqrt{I} = B\sqrt{I} \tag{4.10}$$

Constant B has a value of 0.33×10^8 in water at 25°C. According to Millero,[1] it varies with $(D\text{T})^{-1/2}$; $B = 50.29 \times 10^8 \times (D\text{T})^{-1/2}$; D itself also deceases with temperature. Substituting Eq. 4.10 for κ into Eq. 4.9 and simplifying leads to the usual form of the Debye-Hückel limiting law (DHLL):

$$-\log \gamma_i = AZ_i^2 \sqrt{I} \tag{4.11}$$

Constant A varies with $(D\text{T})^{-3/2}$: $A = 1.8248 \times 10^6 \times (D\text{T})^{-3/2}$ and has a value of 0.511 at 25°C. Table 4.1 lists values of A and B over a range of natural water temperatures.

The assumption that ions behave as point charges imposes limitations on the DHLL, which is accurate only at low solute concentrations. This assumption causes errors in describing the distribution of shielding ions in the ionic atmosphere; for physical reasons, the approach cannot be closer than the actual size of the ions. As a result, the DHLL overcompensates for the effects of ionic attraction and repulsion, producing values of γ that are too small. The error increases with ionic strength, and the DHLL should not be used when $I > \sim 0.005$. Debye and Hückel introduced a variable $\mathbf{a}$, which they called the mean distance of approach of the ions. This variable subsequently became known as the "ion size parameter," and it leads to the extended form of the Debye-Hückel equation (EDHE):

$$-\log \gamma_i = \frac{Z_i^2 A \sqrt{I}}{1 + B\mathbf{a}_i \sqrt{I}}, \tag{4.12}$$

Table 4.1 Effect of temperature on Debye-Hückel constants A and B*

Temp. (°C)	A	B
0	0.492	0.325×10^8
10	0.552	0.326×10^8
20	0.507	0.328×10^8
25	0.511	0.329×10^8
30	0.515	0.329×10^8
35	0.520	0.330×10^8

* Summarized from Pitzer and Brewer.[11a]

Table 4.2 Values of the ion size parameter, a, for the extended Debye-Hückel equation (EDHE)*

a $(10^{-8}$ cm)	Ion
3	K^+, Ag^+, Cl^-, NH_4^+, OH^-, NO_3^-, HS^-, I^-, ClO_4^-
4	Na^+, HCO_3^-, SO_4^{2-}, $H_2PO_4^-$,
	HPO_4^{2-}, PO_4^{3-}, CH_3COO^-
5	CO_3^{2-}, Sr^{2+}, Ba^{2+}, Pb^{2+}
6	Ca^{2+}, Cu^{2+}, Fe^{2+}, Mn^{2+}, Zn^{2+}, Sn^{2+}
8	Mg^{2+}, Be^{2+}
9	H^+, Fe^{3+}, Al^{3+}, La^{3+}, Ce^{3+}

* Values from Keilland.[12]

where constant B is the same as that in Eq. 4.10. Note that **a** is not truly the size of an ion but represents the nearest approach of other ions to the ion of interest. Consequently, **a** cannot be measured directly and instead is a "fitting parameter."

Values of **a** for common ions in aqueous solutions were determined by Kielland[12] (see Table 4.2). Values for most ions are in the range of $3-9 \times 10^{-8}$ cm, and except for H^+, which has one of the largest values of listed in the table (9×10^{-8}), most of the ions with $\mathbf{a} > 4 \times 10^{-8}$ are multivalent cations. It is important to recognize that **a** applies not only to the ion whose activity coefficient is being calculated by the EDHE but also to the shielding ions in the ionic atmosphere surrounding it. The EDHE thus applies strictly only to solutions of relatively simple composition—where the ion of interest and the "shielding ions" have the same ion size. With this constraint, the EDHE is considered accurate up to I = 0.1.

Because $\mathbf{a} \approx 3 \times 10^{-8}$ for many ions, the factor $B\mathbf{a} \approx 1$, and the EDHE can be simplified to

$$ -\log \gamma_i = \frac{Z_i^2 A \sqrt{I}}{1 + \sqrt{I}}, \tag{4.13} $$

Equation 4.13 is the "Guntelberg approximation," and it gives accurate estimates of activity coefficients for many ions up to $I \approx 0.1$. This equation is considered to be the most appropriate version of the Debye-Hückel theory for solutions containing a mixture of several electrolytes.

The importance of ionic charge on the value of activity coefficients is illustrated in Table 4.3, and the trends in γ with varying I are shown in Figure 4.2. The table and figure also show that the importance of using the appropriate version of the Debye-Hückel equation and the correct value of **a** is greater for divalent ions than for monovalent ions and is more pronounced at higher ionic strength. All three equations and the full range of **a** yield values of γ within a range of 0.003 for monovalent ions at I = 0.001 (comparable to many lakes and streams in noncalcareous regions; see Chapter 2). The range for divalent ions at I = 0.001 is larger but probably still negligible for most equilibrium calculations. For I = 0.01, comparable to waters in calcareous regions and those affected by sewage effluents, the range of γ for monovalent ions is 0.024, and that for divalent ions is 0.071. Table 4.3 also shows that the DHLL yields very different values of γ than the EDHE and Guntelberg equations at their limit of applicability (I = 0.1).

Table 4.3 Values of γ calculated by the three Debye-Hückel equations

I	Z_i	Guntelberg*	DHLL	EDHE	
				$\mathbf{a} = 6 \times 10^{-8}$	$\mathbf{a} = 9 \times 10^{-8}$
0.001	1	0.964	0.965	0.966	0.967
0.01	1	0.889	0.899	0.907	0.913
0.1	1	0.689	0.754	0.800	0.825
0.001	2	0.862	0.866	0.869	0.873
0.01	2	0.625	0.652	0.676	0.696
0.1	2	0.226	0.323	0.400	0.464

* Equivalent to the EDHE at $\mathbf{a} = 3 \times 10^{-8}$ cm.
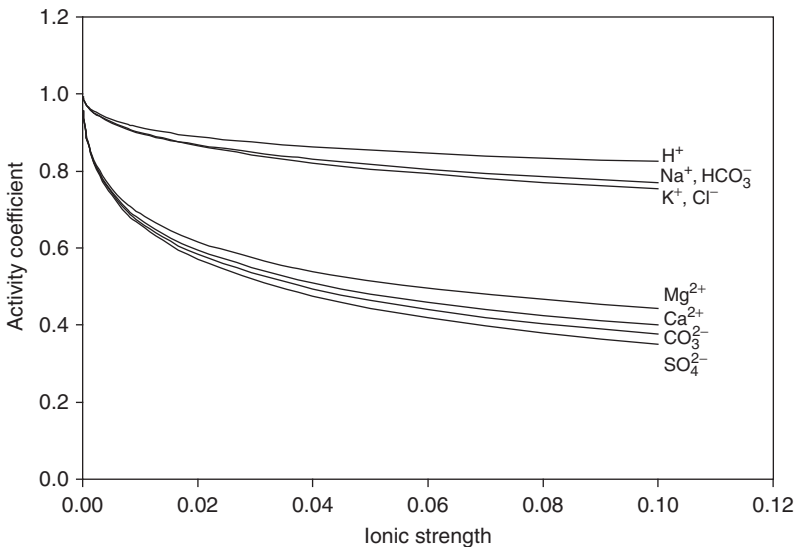
Figure 4.2 Effect of ionic strength on activity coefficient values calculated by the EDHE for common monovalent and divalent ions.

Moreover, uncertainty about which value of $\mathbf{a}$ to use at this value of I would produce an unacceptably large uncertainty in the value of γ, especially for divalent ions.

EXAMPLE 4.2 Calculating ion activity coefficients: Calculate γ for Na^+ and SO_4^{2-} in a solution with a total ionic strength of 0.06 M at 20°C using the EDHE.

Answer: Because the ionic strength is given, the appropriate parameters need to be taken from Tables 4.1 and 4.2. For Na^+,

$$- \log \gamma_{Na^+} = \frac{Z_{Na^+}^2 A \sqrt{I}}{1 + B a_{Na^+} \sqrt{I}} = \frac{1^2 (0.507)\sqrt{0.06}}{1 + (0.328 \times 10^8)(4 \times 10^{-8})\sqrt{0.06}} = 0.094$$

or $\gamma_{\mathbf{Na^+}} = 10^{-0.094} = \mathbf{0.805}$

and for SO_4^{2-},

$$-\log \gamma_{SO_4^{2-}} = \frac{Z_{SO_4^2}^2 A\sqrt{I}}{1 + Ba_{SO_4^{2-}}\sqrt{I}} = \frac{2^2(0.507)\sqrt{0.06}}{1 + (0.328 \times 10^8)(4 \times 10^{-8})\sqrt{0.06}} = 0.376$$

or $\gamma_{SO_4^{2-}} = 10^{-0.376} = \mathbf{0.421}$.

4.4.4 Estimating ion activity coefficients in high ionic-strength solutions

The EDHE and Guntelberg equation apply up to $I \sim 0.1$, well above the ionic strength of freshwaters, but in brackish or estuarine waters, seawater ($I = 0.699$), and brine solutions, these equations do not give accurate results because they do not account for "specific ion interactions" that occur in concentrated solutions. By this term, we mean interactions that depend on the *nature* of the ions and that are not accounted for by the general Debye-Hückel theory. Several approaches have been used to overcome the difficulties in estimating ion activity coefficients for concentrated solutions; for example, (1) extension of the EDHE by empirical correction factors, (2) development of ion association models to account for specific ion interactions, and (3) definition of a more useful reference state than the infinite-dilution convention used heretofore. In this section, we describe some extensions of the EDHE and the use of an alternative reference state for seawater.

Empirical approach: the Davies equation. Hückel was the first (in 1925) to add an empirical term to the EDHE to extend its range to higher ionic strength. By far the most widely used equation of this type is due to Davies:[13]

$$-\log \gamma_i = AZ_i^2 \left(\frac{\sqrt{I}}{1 + \sqrt{I}} - 0.2I \right), \tag{4.14}$$

which is the Guntelberg expression with an empirical correction factor added. This equation yields accurate results up to $I = \sim 0.5$. As Figure 4.3 shows, the Davies expression gives values that deviate increasingly at $I > 0.1$ from results of the Guntelberg expression. Also, the empirical correction term causes activity coefficient values to reach a minimum value around $I = 0.5$ and then to increase as I continues to rise. This trend agrees at least qualitatively with experimental findings at high ionic strength and also with results for more complicated models, as described below.

Advanced topic: Stokes and Robinson "single-parameter" model. A more complicated semiempirical equation that holds for solutions of a single salt, AB, at high concentrations (> 1 molal) was described by Stokes and Robinson:[14]

$$\log \gamma_{\pm} = -\frac{AZ_A Z_B \sqrt{I}}{1 + Ba\sqrt{I}} - \frac{n}{v} \log a_w - \log\{1 - 0.018(n - v)m\}, \tag{4.15}$$
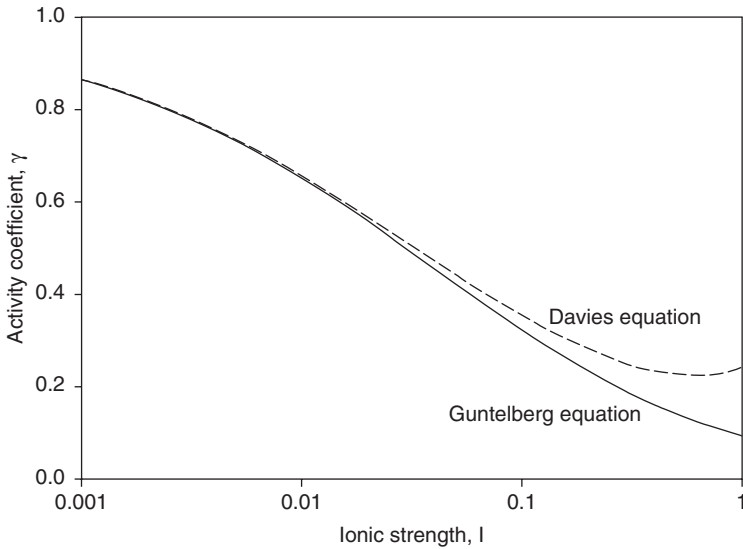
Figure 4.3 Comparison of activity coefficient trends for a divalent ion calculated by the Guntelberg expression (solid line) and the Davies equation (dashed line) up to I = 1.0.

where $\gamma_{\pm}$ is the mean activity coefficient of salt AB (see Section 4.4.5); n is the number of water molecules bound by one "molecule" (i.e., one formula weight) of the solute salt; ν is the number of ions per "molecule" of solute; m is the molality of the solute; and a_w is the activity of water. The first term on the right side of Eq. 4.15 is the EDHE; and the second term accounts for the decreased activity of water in a concentrated electrolyte solution. The third term, called a "scale factor," takes into account hydration of the ions—the binding of n water molecules by ν ions to remove them from acting as solvent molecules. The Stokes-Robinson equation has two fitted parameters, the ion size parameter, **a**, and hydration parameter, n. The rest of the variables are known from the nature of the solute or from experimental data (a_w). Stokes and Robinson found an empirical relationship* to estimate **a** from n, thus reducing the number of parameters that need to be fitted to just one (n). Stokes and Robinson achieved excellent agreement between the fitted equation and experimental data for I up to $\sim$4, as shown in Figure 4.4. In general, the equation breaks down when n $\times$ m > 10–15 (n $\times$ m represents the number of moles of water bound by solute per kg of water). Because only 55.5 moles of water are present in a kg of water, the equation holds up to the point where only $\sim$75% of the water molecules are available to act as a solvent. The Stokes-Robinson equation applies

---

*According to Stokes and Robinson,[14] $\mathbf{a} = \{ [(3/4\pi)(30n + V_+)]^{1/3} + r_- - \Delta \}$, where V_+ is the cation volume (Å^3), r_- is the crystallographic radius of the anion, and Δ is an empirical factor called the penetration distance. In turn, $V_+ = V_{app} - 6.47z_1 r_-^3$, where V_{app}, the apparent molal volume of the salt, $= 6.47(r_+^3 + r_-^3)$; z_1 is the cation valence; and r_+ is the crystallographic radius of the cation (Å). The term Δ was found to be 0.7 Å for alkali halides and 1.3 Å for alkaline earth halides. Values of r_+ and r_- were obtained from Pauling.[15]
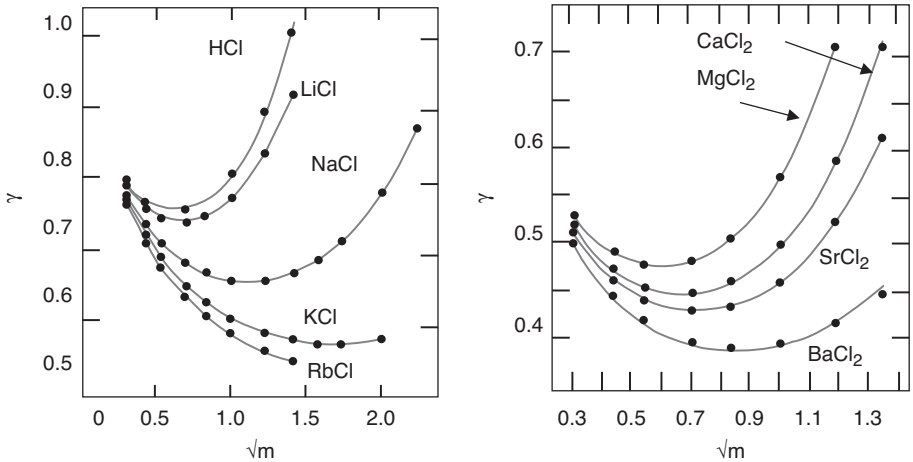
Figure 4.4 Comparison of experimental values of activity coefficients (points) of monovalent (left) and divalent cations (right) of chloride with values (solid lines) predicted by eq. 4.15. Redrawn from Stokes and Robinson[14] and used with permission of the American Chemical Society.

only to solutions of a single salt, however, and not to concentrated solutions of mixed electrolytes such as seawater and brines.

Advanced topic: Ion association models. Guggenheim[16] was the first to develop a specific ion interaction term to extend the EDHE to higher I, and many others contributed to the development of this approach since then (Millero[1] provided a review). Today, the specific ion interaction (SII) model of Pitzer and coworkers[17] is most commonly used to estimate activity coefficients (γ_{SII}) at high ionic strength. The basic form of this complicated model is

$$\log \gamma_{SII} = -\frac{AZ^2\sqrt{I}}{1 + Ba\sqrt{I}} + \sum_j B_{ij}m_j, \qquad (4.16)$$

The first term on the right side is the EDHE, and the second accounts for specific ion interactions. B_{ij}, the specific interaction term between ions i and j, has been determined experimentally for the major ions in natural waters. Unfortunately, the B_{ij} vary with ionic strength, but they have been evaluated for many pairs of ions over a range of I.[11] According to Baes and Mesmer,[18] B_{ij} generally varies linearly with the function of I, $F(I) = \{1 - (1 + 2I^{1/2} - 2I)\exp(-2I^{1/2})\}/4I$. The basic SII model (Eq. 4.16) can yield accurate values of γ up to m $\approx$ 4; a more complicated model with additional terms extends the calculations to even higher ionic strengths.

Alternative reference states.   Finally, another approach to avoid large corrections in concentration-activity relationships is to redefine the reference state. For example, one could define a reference state to have the same composition and ionic concentrations

as standard seawater. Then by definition, $a_i = c_i$, and $\gamma_i = 1$. This would simplify equilibrium calculations for seawater, and because the values of activity coefficients would not change greatly for small changes in total ionic concentration, calculated equilibrium values would be reasonably accurate across the range of salinity (thus, ionic strength) one finds across the world's oceans. Of course, it would be problematic to develop an equation to compute changes in activity coefficients over a broader range of salinity (I), such as encountered in estuarine environments, and perhaps because of this, this approach is not commonly used. It is simple, however, to relate activity coefficients in the alternative reference states (infinite dilution and seawater). For example, for the infinite dilution reference state, γ of sulfate (SO_4^{2-}) is 1.0 at $I = 0$ and ~0.16 in seawater. If a seawater reference state is used, γ in seawater now is 1.0, and γ at $I = 0$ would be $1.0/0.16 = 6.18$. This is because the relative activities of SO_4^{2-} in the two solutions is the same, regardless of the scale (or reference system) used to quantify activity.[2]

EXAMPLE 4.3 Concentration versus activity of the proton: A common misconception is that a pH meter measures proton concentration, when in fact, it measures proton activity. What is the difference between the readings of the pH meter for a solution containing $[H^+] = 10^{-6}$ mol/L and a counterion at the same concentration but no other ionic solutes present and that containing the same proton concentration and 0.25 M NaCl?

Answer: In the first case, if we assume the solution is essentially infinitely dilute, $\gamma = 1$ and $\{H^+\} = [H^+] = 10^{-6}$. The pH meter will read 6.00 (pH $= -\log\{H^+\}$), which is both the concentration-based value (p^cH) and the activity-based value (p^aH). In the second case, $I = 0.25$, and using Eq. 4.14 for H^+,

$$-\log \gamma_i = \frac{1^2(0.511)\sqrt{0.25}}{1 + \sqrt{0.25}} - 0.2(0.25) = 0.120$$

$$\gamma_i = 10^{-0.120} = 0.758$$

So, although $[H^+]$ is 1.00×10^{-6} ($p^cH = 6.00$), $\{H^+\} = 0.758 \times 10^{-6}$, giving $p^aH = 6.12$ and a pH meter reading of 6.12.

The answer in the absence of the NaCl ignores the small contribution to ionic strength of the proton (and counterion). To be fully correct, the ionic strength of this solution should be calculated and an activity coefficient determined.

4.4.5 Mean salt and single ion activities

It is not possible to measure single ion activities without recourse to "extrathermo-dynamic" assumptions because it is not possible to have a solution containing only one kind of ion. Instead, one always has an electrically neutral solution containing equal numbers of cations and anions (on a charge equivalent basis). Consequently, what chemists actually measure is the ***mean ionic activity***, $a_\pm$, and the mean ionic activity coefficient, $\gamma_\pm$ of a salt MX. Mean ionic activity coefficients ($\gamma_\pm$) can be determined by measuring a solution's colligative properties: freezing point depression, boiling point elevation, vapor pressure, or osmotic pressure. These properties depend solely on the effective concentrations of solutes in solution (i.e., on the total activity of the solutes)

rather than on the type of chemical species present. One also can determine activity coefficients by making solubility measurements. All measurements are based on the assumption that $\gamma_\pm = 1$ in infinitely dilute solutions; i.e., $a_{MX} = m_{MX}$ as $m_{MX} \to 0$.

For any simple monovalent salt, MX, that dissolves completely to form M^+ and X^-, the following relationships apply:

$$a_+ = \gamma_+ \, m_+, \text{ or } \quad \gamma_+ = a_+/m_+$$

$$a_- = \gamma_- \, m_-, \text{ or } \quad \gamma_- = a_-/m_-$$

$$\gamma \to 1 \text{ as } m \to 0;$$

$$a_+ \to m_+ \text{ as } m \to 0;$$

$$a_- \to m_- \text{ as } m \to 0$$

Thus,

$$a_+ \to a_-, \text{ as } m \to 0.$$

Subscripts "+" and "−" refer to the cation and anion, respectively. For a simple salt, MX, $a_\pm$ and $\gamma_\pm$ are defined as follows:

$$a_\pm = (a_+ \, a_-)^{1/2} = a_s^{1/2} \tag{4.17}$$

$$\gamma_\pm = (\gamma_+ \, \gamma_-)^{1/2} = \left[\frac{a_+ \, a_-}{m_+ \, m_-} \right]^{1/2} = \frac{a_\pm}{m_s}, \tag{4.18}$$

where $m_s = m_+ = m_-$.

For unsymmetrical salts, $M_a X_b$, we still have $\gamma_\pm = a_\pm/m_\pm$, but $m_\pm$ is defined as

$$m_\pm = m_s \{a^a b^b\}^{1/(a+b)} \tag{4.19}$$

and

$$(\gamma_\pm)^{(a+b)} = (\gamma_+)^a (\gamma_-)^b. \tag{4.20}$$

For example, for $CaCl_2$, $m_\pm = m_s \{1^1 2^2\}^{1/3} = 4^{1/3} m_s$, and $\gamma_\pm = \{\gamma_{Ca} \gamma_{Cl}^2 \}^{1/.3}$.

In solving ionic equilibrium problems that involve mixtures of salts, mean ionic activity coefficients are of little direct use; we need to know the activity coefficient for each ion in a mass action (equilibrium constant) expression. Normally, these values are computed from some version of the Debye-Hückel equation, described earlier, but it is useful to be able to determine individual ion activity coefficients, if for no other reason than to evaluate the accuracy of results from theoretical expressions. Individual ion activity coefficients can be estimated from experimental values of $\gamma_\pm$ by the ***mean salt method***, which does not suffer from the limitations of the Debye-Hückel equation at high ionic strength but does require an "extrathermodynamic" assumption. We must assume that $\gamma_+ = \gamma_-$ for some standard univalent salt over the ionic strength of interest. The salt used for this purpose is KCl, and various lines of evidence, including similar

ion sizes, ionic mobilities, and equivalent conductivities, indicate that γ_{K^+} and γ_{Cl^-}. have very similar values. Nonetheless, there is no way to prove that they have exactly the same values. If we accept this extrathermodynamic assumption, we can write

$$\gamma_{\pm, KCl} = [(\gamma_{K^+})(\gamma_{Cl^-})]^{1/2} = \gamma_{K^+} = \gamma_{Cl^-}. \tag{4.21}$$

Box 4.2 Use of solubility measurements to determine $\gamma_\pm$

The change in solubility of sparingly soluble salts with varying concentrations of an unreactive electrolyte (salt) can be used to determine $\gamma_\pm$ for the salt. Choice of the electrolyte is based on three characteristics: (a) it does not have a common ion with the salt of interest; (b) it does not form precipitates or soluble complexes with the salt of interest (or other solutes in the system); and (c) it dissociates completely so that I can be determined exactly. KNO_3 and $KClO_4$ both fit these conditions.

Let the solubility of MX be S_o in pure water and S in water with added electrolyte, and let $\gamma_{\pm o}$ and $\gamma_\pm$ be the mean ionic activity coefficients in pure water and electrolyte, respectively. As electrolyte is added and I increases, $\gamma_\pm$ decreases, and MX becomes more soluble. Because $a_i = \gamma_i m_i$, and $(a_i)^2 = K_{s0}$, which is constant, m_i must increase if γ_i decreases. We express this as:

In pure water:

(1) $K_{s0} = a_i^2 = m_{Mo}\gamma_{Mo}m_{Xo}\gamma_{Xo} = S_o^2\gamma_{\pm o}^2$

With electrolyte:

(2) $K_{s0} = a_i^2 = m_M\gamma_M m_X\gamma_X = S^2\gamma_\pm^2$

Thus

(3) $S_o^2\gamma_{\pm o}^2 = S^2\gamma_\pm^2$

or

(4) $S_o\gamma_{\pm o} = S\gamma_\pm$

Taking logs, we get

(5) $\log S + \log \gamma_\pm = \log S_o + \log \gamma_{\pm o}$

or

(6) $\log S = \log S_o\gamma_{\pm o} - \log \gamma_\pm$

We thus can obtain $\gamma_\pm$ at any I from the solubility (S) of MX if we know $S_o\gamma_{\pm o}$, which is obtained from the y-intercept of a plot of $\log S$ versus $\sqrt{I}$ (where $\sqrt{I} = 0$). At $I = 0$, $\log S = \log S_o\gamma_{\pm o}$ (because $\gamma_{\pm o} = 1$ and $\log \gamma_{\pm o} = 0$ at $I = 0$). Once $\log S_o\gamma_{\pm o}$ is known, we can determine $\log \gamma_\pm$ and thus $\gamma_\pm$ at any I by subtracting $\log S_o\gamma_{\pm o}$ from $\log S$, which is measured directly.

Using this relationship, we can derive values for other ions from mean ionic activity coefficients measured *at the same ionic strength* as the values for $\gamma_{\pm KCl}$. For example, for a monovalent chloride salt, MCl,

$$\gamma_{\pm,MCl} = [(\gamma_{M^+})(\gamma_{Cl^-})]^{1/2} = [(\gamma_{M^+})(\gamma_{\pm KCl})]^{1/2} \tag{4.22}$$

or

$$\gamma_{M^+} = \frac{(\gamma_{\pm MCl})^2}{\gamma_{\pm KCl}}. \tag{4.23}$$

4.5 Activity coefficients for nonelectrolyte solutes

Activity coefficients of uncharged solutes in waters with varying salt content often are assumed to be unity, and solute activity is taken to be equal to its molar concentration. In fact activity coefficients for nonelectrolyte solutes do vary with ionic strength, but the rate of change is much less than that for ions. The general relationship between activity coefficients for nonelectrolytes, γ_{ne}, and ionic strength is called the Setschenow equation:

$$\log \gamma_{ne} = \log \frac{S_{ne\,o}}{S_{ne}} = kI. \tag{4.24}$$

S_{ne} is the solubility of the nonelectrolyte, and $S_{ne\,o}$ is its solubility at $I = 0$. Note that some books use total molality or molarity instead of I. The proportionality constant k is called the "salting coefficient." Values of k generally are small, vary with temperature, and depend on the nature of both the solute and solvent. Equation 4.24 holds up to $I \approx 5$ M for nonelectrolyte solute concentrations up to $\sim$0.1 M.

If a nonelectrolyte solute has a dielectric constant, D, lower than the solvent, which is the case if water is the solvent, then k is positive, and $\gamma_{ne} > 1$ at $I > 0$. Furthermore, γ_{ne} increases as I increases. The activity of the nonelectrolyte thus is greater than its concentration, and activity increases as I increases at a given concentration. This leads to a decreasing solubility for the nonelectrolyte solute as I increases, a phenomenon known as "salting out." This process is commonly observed with dissolved gases (Figure 4.5). For example, the solubility of O_2 in seawater ($I = 0.699$) is only 79% of that in pure water.[6]

According to Laitinen and Harris,[9] k generally ranges from $\sim$0.01 to 0.1. Therefore, for I up to about 0.2, $\log \gamma_{ne} \leq (0.01 - 0.1) \times 0.2 \leq 0.02$, or γ_{ne} is less than $\sim$1.05, and we usually can ignore activity coefficient corrections for nonelectrolyte solutes in freshwaters, for which $I \ll 0.1$.

Several possible reasons can be cited for changes in γ_{ne} with increasing I. First, there might be specific chemical interactions between the nonelectrolyte molecules and ions, although this is considered unlikely. Second hydration of ions leaves less H_2O to solvate nonelectrolytes. Nonelectrolytes, however, are not thought to be solvated; instead, they exist in "cavities" within the solvent structure; see Chapter 1). Third, addition of ions changes the dielectric constant of water. Finally, the quantity of free (i.e., solvent)
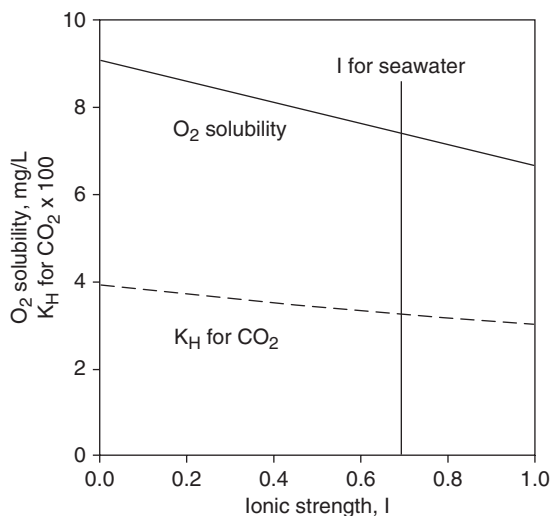
Figure 4.5 Effect of ionic strength on solubility of O_2 (solid line) and Henry's law constant for CO_2 at 20°C (dashed line).

water decreases as I increases, and this effectively increases the concentration of the nonelectrolyte in the remaining solvent.

4.6 Activities of ideal and real gases

The behavior of ideal (or perfect) gases is defined by the ideal gas law (see Box 3.6 for a derivation):

$$PV = nRT \tag{4.25}$$

The activity of an ideal gas is defined as numerically equal to pressure, P, in atm; i.e., $a = P$, and

$$\mu_g = \mu_g^\circ + RT \ln P_g, \tag{4.26}$$

where μ_g is the actual chemical potential of the gas and μ_g° is the standard chemical potential of the gas, i.e., the chemical potential of the gas in its reference state. Box 3.9 derives this relationship. For an ideal gas, the reference state is a given temperature and $P = 1$ atm. In this state, $a = P = 1$, and $\gamma = 1$.

Most gases of environmental interest behave ideally (or close to it) up to about 1 atm pressure at ambient temperatures. At high P, gases do not behave as predicted by the ideal gas law for two important reasons: (1) the derivation of the ideal gas law assumes that gases behave as points (i.e., they occupy no volume), and (2) it assumes that the gas molecules behave as hard (inert) spheres that have no attractive or repulsive tendencies toward other molecules. Neither assumption is exactly true. As P increases, the volume fraction of a gaseous system occupied by gas molecules increases. As the gas molecules become packed together more tightly, the importance of intermolecular

attractive forces (London-van der Waals forces) likewise increases. The net effect of these attractive forces is to make the gas molecules behave less independently than they otherwise would.

To have Eq. 4.26 apply to real gases, Lewis replaced P by an idealized pressure, f, called the fugacity and described as the "escaping tendency" for a substance from its particular state:

$$\mu_g = \mu_g^\circ + RT \ln f_g \qquad (4.27)$$

where $f \to P$ as $P \to 0$. In general, $f = \gamma_g P$, where γ_g is a gas activity coefficient. As $P \to 0$, $\gamma_g \to 1$, and as noted earlier, the standard state for real gases is defined as $f = a = 1$ at $P = 0$. Nonetheless, for most common real gases, $\gamma_g \approx 1$ at $P = 1$ atm. The effective (or thermodynamic) concentration of real gases at high P tends to be less than their actual concentration for reasons described above, and γ_g thus becomes < 1 as P becomes $>\sim 1$ atm. Although fugacity was defined originally as an idealized property of gases, it is a general property, and as discussed in Section 4.2, it is used for solutes, liquids, and solids.

4.7 Activities of solids

4.7.1 Ideal and regular solid solutions

The reference and standard state of a solid is the pure substance at $P = 1$ atm and a specified temperature. Here $a = c = \gamma = 1$. Mineral solids in nature usually are not pure, however, but consist of *solid solutions*. For example, one of the most common mineral phases associated with natural waters, calcite, $CaCO_{3(s)}$, often has a small amount of magnesium ions substituted randomly in the crystal lattice in place of Ca^{2+} ions; e.g., $Ca_{0.95}Mg_{0.05}CO_3$ is a 5% "***magnesian calcite***." The $MgCO_3$ can be considered to be dissolved in the $CaCO_3$ matrix.

Although pure solids have unit activity, the components of solid solutions (e.g., $CaCO_3$ and $MgCO_3$ in the above case) do not, and this has important implications regarding the solubility (equilibrium concentrations of ions in solution) for solid solution phases. Two possibilities exist for the behavior of components in solid solutions:

$$\text{ideal solutions}: \qquad a_i = N_i, \qquad (4.28)$$

$$\text{regular solutions}: \qquad a_i = \gamma_i N_i, \qquad (4.29)$$

where N_i is the mole fraction of component i. Equation 4.29 is Raoult's law; ideal solutions are a subset of regular solutions where $\gamma_i = 1$. Ideal behavior is often assumed to apply to the major components of solid solutions (where $N_i \to 1$), but deviations from ideal behavior can occur at N fairly close to 1 (e.g., N $<\sim 0.95$). Minor components of solid solutions follow Raoult's law with $\gamma \neq 1$; in fact, γ can be far from unity for minor components, and this leads to large deviations in the predicted composition of aqueous solutions in equilibrium with solid solutions that are assumed to behave ideally.

Activity coefficients for components of regular binary solutions, such as $(Ca,Mg)CO_3$, can be predicted from the following equation:

$$\log \gamma_i = \left(\frac{\beta}{2.3RT} \right) (1 - N_1)^2 = \beta'(1 - N_1)^2, \tag{4.30}$$

where β is a constant for a given mineral solution that is independent of the actual concentrations (N_1 and N_2). According to Garrels and Christ,[19] values of β' for common mineral solid solutions range between -5 and $+5$. Significant deviations from ideal behavior ($\gamma = 1$) can occur for major components even at $N > 0.9$. For example, if $\beta' = 5$ and $N_1 = 0.9$, $\log \gamma_1 = 0.05$ or $\gamma_1 = 1.12$.

4.7.2 Advanced topic: solid solution equilibria and activity coefficients of solid phases

Consider a solid solution of MY in MX, where MX is the major component and MY is the minor component, in equilibrium with an aqueous solution. Then we can write

$$MX_{(s)} + Y^- \leftrightarrow MY_{(s)} + X^-. \tag{4.31}$$
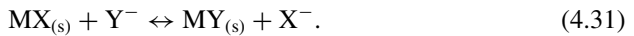
By convention, the reaction is always written with the major component as reactant and minor component as the product. The equilibrium constant for this reaction is normally expressed as D, the distribution coefficient. It is easy to show that D corresponds to the ratio of the solubility products for MX and MY:

$$D = K_{eq} = \frac{\{MY_{(s)}\}\{X^-\}}{\{MX_{(s)}\}\{Y^-\}} = \frac{K_{s0,MX}}{K_{s0,MY}}, \tag{4.32}$$

where $\{i\}$ refers to the activity of substance i. This is so because

$$\frac{K_{s0,MX}}{K_{s0,MY}} = \frac{\dfrac{\{M^+\}\{X^-\}}{\{MX_{(s)}\}}}{\dfrac{\{M^+\}\{Y^-\}}{\{MY_{(s)}\}}} = \frac{\{MY_{(s)}\}\{X^-\}}{\{MX_{(s)}\}\{Y^-\}}. \tag{4.33}$$

Although we cannot measure activities of components in solid phases directly and thus cannot measure D, it can be computed from the ratio of the solubility products (K_{s0} values). If we assume that the solid behaves as a regular solution, then $\{MX_{(s)}\} = \gamma_{MX} N_{MX}$ and $\{MY_{(s)}\} = \gamma_{MY} N_{MY}$, and Eq. 4.33 can be written as:

$$D = \frac{\{X^-\}\{MY_{(s)}\}}{\{Y^-\}\{MX_{(s)}\}} = \frac{\{X^-\}}{\{Y^-\}} \frac{N_{MY}}{N_{MX}} \frac{\gamma_{MY}}{\gamma_{MX}} = D_{obs} \frac{\gamma_{MY}}{\gamma_{MX}}, \tag{4.34}$$

where D_{obs} is the ratio of measurable components only (activities of solutes and mole fractions of solid solution components). It thus is referred to as the *observable* distribution coefficient. Because D can be computed from the ratio of solubility product constants (K_{s0}) and D_{obs} can be measured, the ratio of activity coefficients for the

Table 4.4 D and D_{obs} for some solid solutions*

Solid solution	D	D_{obs}	$T\,(°C)$
AgBr in AgCl	315.7	211.4	30
$MnCO_3$ in calcite	525	17.4	25
$SrCO_3$ in calcite	10	0.14	25
$MgCO_3$ in calcite	0.16	0.02	20

* Summarized from Stumm and Morgan.[20]

components of binary solid solutions can be determined simply as the ratio D/D_{obs}. Furthermore, if $D = D_{obs}$, it is apparent that the ratio of activity coefficients is unity. The simplest inference then is that both components behave ideally ($\gamma = 1$). Table 4.4 lists values of D and D_{obs} for a few binary solid solutions of interest in aquatic systems.

EXAMPLE 4.4 Equilibrium activities of solutes that are minor components of solid solutions: A solid solution of 10% AgBr in 90% AgCl is in equilibrium with an aqueous solution containing $\{Cl^-\} = 10^{-3.0}M$. What is the equilibrium activity of Br^- and Ag^+ in the aqueous solution?

(a) From Table 4.4, $D/D_{obs} = \gamma_{AgBr}/\gamma_{AgCl} = 315.7/211.4 = 1.5$. If we assume that $\gamma_{AgCl} \approx 1.0$ (because it is the major component, $N_{AgCl} = 0.9$), then $\gamma_{AgBr} = 1.5$.

(b) From Eq. 4.34,

$$315.7 = \frac{\{Cl^-\}N_{AgBr}\gamma_{AgBr}}{\{Br^-\}N_{AgCl}\gamma_{AgCl}} = \frac{10^{-3.0} \times 0.1 \times 1.5}{\{Br^-\} \times 0.9 \times 1.0}$$

or

$$\{Br^-\} = 5.27 \times 10^{-7} \text{ or } 10^{-6.28} \text{ M}.$$

(c) K_{s0} for AgCl is $10^{-9.70}$ and K_{s0} for AgBr is $10^{-12.20}$. We can compute $\{Ag^+\}$ from either of these equilibrium constants:

$$K_{s0} = \frac{\{Ag^+\}\{Cl^-\}}{\{AgCl_{(s)}\}} = 10^{-9.7} = \frac{\{Ag^+\} \times 10^{-3.0}}{0.90}, \text{ or } \{Ag^+\} = 1.80 \times 10^{-7} \text{ M}$$

The activity of solid AgCl is assumed to be equal to its mole fraction ($\gamma_{AgCl} = 1.0$). Note that in most equilibrium calculations involving solubility products, the solid phase is assumed to be pure ($N = a = 1.0$) and is not considered explicitly. Correction for the (nonunit) activity of the solid phase is small for AgCl, the major component but is much larger for minor components. For AgBr, the ion activity product (IAP) is calculated as

$$IAP = \{Ag^+\}\{Br^-\} = 10^{-6.74} \times 10^{-6.28} = 10^{-13.02}.$$

This is considerably smaller than $K_{s0\,AgBr}$ ($10^{-12.20}$), and if we ignored the solid phase composition, the aqueous solution would appear to be undersaturated with respect to AgBr:

$$\frac{IAP}{K_{s0}} = \frac{10^{-13.02}}{10^{-12.20}} = 10^{-0.82} = 0.15$$

It is clear from the above relationships that the ratio $IAP/K_{s0} = \{AgBr\}$, the activity of solid phase AgBr. The calculated value of the ratio agrees with the product $N_{AgBr}\gamma_{AgBr} = \{AgBr\}$; that is, $0.1 \times 1.5 = 0.15$.

EXAMPLE 4.5 Calculation of D and estimation of γ for the minor component in a solid solution: Consider a solid solution of strontianite ($SrCO_3$) in calcite (the major component). K_{s0} values for strontianite and calcite are $10^{-9.35}$ and $10^{-8.35}$, respectively. Calculate D and compare it to the value in Table 4.4. Also estimate the activity coefficient for $SrCO_3$ in the solid solution.

(a)

$$D = \frac{K_{s0,\,CaCO_3}}{K_{s0,\,SrCO_3}} = \frac{10^{-8.35}}{10^{-9.35}} = 10$$

This agrees with the value for D in Table 4.4.

(b) According to Table 4.4, $D_{obs} = 0.14$. From Eq. 4.33 we write

$$D = D_{obs}\frac{\gamma_{SrCO_3}}{\gamma_{CaCO_3}}, \text{ or } 10 = 0.14\frac{\gamma_{SrCO_3}}{\gamma_{CaCO_3}}.$$

If we assume that γ_{CaCO_3}. 1.0, we find that $\gamma_{SrCO_3} = 10/0.14 = 71$! The minor component $SrCO_3$ thus has a much higher effective concentration (i.e., activity) than one would surmise from its mole fraction concentration in calcite. This decreases the solubility of $SrCO_3$ in the solid phase but increases the solubility of $SrCO_3$ in the liquid phase (beyond that expected from its mole fraction in the solid phase).

4.8 Activity coefficients for neutral organic compounds

As mentioned in Section 4.2, Raoultian behavior is used for organic compounds. In this case, the pure substance (i.e., pure organic liquid) is the reference state with $\gamma = 1$. When the compound is placed into water, nonideal interactions of the hydrophobic organic compounds lead to unfavorable energy interactions that are quantified using the activity coefficient. Details of such derivations can be found in Schwarzenbach et al.[21] For our purposes here, it is sufficient to note that for organic compounds that are *liquids* at standard temperature and pressure:

$$\gamma_i^{sat} = \frac{1}{x_i^{sat}} \tag{4.35}$$

That is, the activity coefficient of an organic solute in water is the inverse of the mole fraction of the compound at saturation. Thus, the less soluble the compound, the greater

the activity coefficient—meaning that the solute-solvent interactions are less than ideal. This is converted to a concentration basis using the molar volume of water ($V_w = 1/55.5$ mol/L = 0.018 L/mol):

$$\gamma_i^{sat} = \frac{1}{V_w C_i^{sat}} \tag{4.36}$$

Of course, organic pollutants are rarely present at saturation, but this is a reasonable estimate of activity coefficients for neutral organic compounds (i.e., within ± 10–20% of the value at infinite dilution).

For organic compounds that are solids or gases under standard conditions, correction factors are necessary for the energy costs associated with melting (solids) or condensation (gases). For solids,

$$\gamma_i^{sat} = \frac{1}{x_i^{sat}(s)} e^{-56.5(T_m - T)/RT}, \tag{4.37}$$

where $x_i^{sat}(s)$ is the solubility of the substance on a mole fraction basis, T_m is the melting point of the compound and T is the temperature of interest (both in K). The value $56.5(T_m - T)$ is a *rough estimate* of the free energy of fusion (ΔG_{fus}) of organic compounds in J/mol. Obviously, not all compounds have the same free energy of fusion, and more refined estimates can be made if more accuracy is desired.[21]

For gases,

$$\gamma_i^{sat} = \frac{1}{x_i^{1bar}} \cdot \frac{1}{p_{iL}}, \tag{4.38}$$

where x_i^{1bar} is the mole fraction of compound i when its vapor pressure above the water is 1 bar (i.e., at saturation at standard temperature and pressure), and p_{iL} is the vapor pressure of a "hypothetical liquid" at the temperature of interest. This hypothetical pressure may be estimated by extending the vapor pressure versus temperature data for the liquid (readily available for many volatile organic compounds) beyond the boiling point to the temperature of interest. There are several other ways to estimate the hypothetical vapor pressure based on the compound's boiling point and/or its molecular structure.[21] Both the solid and gas mole fractions are also converted to a mol/L basis using the molar volume of water.

Finally, it is worth noting that salts have a similar "salting out" effect on organic compounds in water to that observed for other neutral solutes:[21]

$$\log \frac{\gamma_{i, salt}^{sat}}{\gamma_i^{sat}} = \log \frac{C_i^{sat}}{C_{i, salt}^{sat}} = K_s[salt]_{total} \tag{4.39}$$

K_s values generally range from 0.15 to 0.3 L/mol for seawater and can be measured for any specific salt solution by investigating the effect of salt on the air-water or solvent-water partitioning. Note that rather than ionic strength used in Eq. 4.24, K_s values for organic compounds have been determined on the basis of the total concentration of salt. This means that K_s values need to be determined for each salt added and differ among

salts (i.e., K_s is different for NaCl and Na_2SO_4). This effect is of practical use when extracting organic compounds from water samples with an immiscible organic solvent for analysis. The addition of salt increases the activity coefficient (decreasing solubility) and provides added driving force for the compound to move from the aqueous to the organic phase.

EXAMPLE 4.6 Determination of activity coefficients for organic compounds: Chlorinated ethanes are common pollutants in groundwater systems. Given the following information, determine the activity coefficient for the following three compounds at 25°C:

Chloroethane (C_2H_5Cl)	m.p. $= -139°C$	b.p. $= 12.3°C$	$C_{iw}^{1bar}(25°C) = 0.104$ mol/L
1,1,2,2-Tetrachloroethane			
($CHCl_2–CHCl_2$)	m.p. $= -36°C$	b.p. $= 146°C$	$C_{iw}^{sat}(25°C) = 0.017$ mol/L
Hexachloroethane	(C_2Cl_6)	m.p $= 187°C$	$C_{iw}^{sat}(25°C) = 2.11 \times 10^{-4}$ mol/L

Answer: For each compound, whether it is a solid, liquid or gas at the relevant temperature must first be determined. At 25°C chloroethane is a gas, 1,1,2,2-tetrachloroethane is a liquid, and hexachloroethane is a solid.

Beginning with the easiest calculation for 1,1,2,2-tetrachlorethane, we use Eq. 4.36:

$$\gamma_i^{sat} = \frac{1}{0.018 \times 0.017} = 3268$$

For hexachloroethane, we first convert C_{iw}^{sat} to a mole fraction:

$$x_i^{sat} = V_w C_i^{sat} = (0.018)(2.11 \times 10^{-4}) = 3.80 \times 10^{-6}$$

We then use Eq. 4.37:

$$\gamma_i^{sat} = \frac{1}{3.80 \times 10^{-6}} e^{-56.5(460.15-298.15)/(8.314 \times 298.15)} = 6555$$

For chloroethane, we require the vapor pressure of the hypothetical liquid at 25°C. Plotting the following vapor pressure data[22] [ln P (atm) vs. 1/T (K^{-1})]:

T(°C)	-89.8	-65.8	-47.0	-32.0	-3.9
P (mm Hg)	1	10	40	100	400

Taking the regression, and extending to 298.15 K, we find that p_{iL} is 1.97 atm. Using Eq. 4.38, we find that

$$x_i^{sat} = V_w C_i^{sat} = (0.018)(0.104) = 1.87 \times 10^{-3},$$

$$\gamma_i^{sat} = \frac{1}{1.87 \times 10^{-3}} \cdot \frac{1}{1.97} = 271.$$

Problems

4.1. Compute the ionic strength (I) the waters listed in Table 2.3 using the rigorous formula for I. Note: to facilitate solving this problem a spreadsheet version of Table 2.3 is available on the textbook's companion Web site.

4.2. Estimate I for the waters listed in Table 2.3 with available specific conductance (SC) data using Eq. 4.7a. Prepare a graph showing the relationship between I computed by the rigorous formula and estimated from SC and determine the correlation coefficient. Comment on the accuracy (or lack of accuracy) of this way to estimate I.

4.3. Calculate values of the activity coefficients for Ca^{2+} and Cl^- in each of the waters the four lakes and first two river waters in Table 2.3 based on the ionic strength (I) calculated in problem 1 using

(a) the Debye-Hückel Limiting Law (DHLL), and
(b) the extended Debye Hückel Equation (EDHE).

Comment on the accuracy of the DHLL compared with the EDHE (assume that the values obtained from the EDHE are accurate).

4.4. As a member of the student chapter of Protect Our Lake Ecosystems (POLE), you obtained the following results on a water sample from a local lake; all units are in mg/L except pH (no units) and SC (μS/cm):

Measurement	Value	Measurement	Value
SC	484	NO_3^-	0.044
pH	7.3	NH_4^+	0.064
H^+	5×10^{-5}	HCO_3^-	131
Na^+	50	Cl^-	97
K^+	5.6	SO_4^{2-}	9
Ca^{2+}	40	F^-	0.15
Mg^{2+}	13		

Note: SC = specific conductance

Perform the following calculations:

(a) Compute the ionic strength for this water and determine the activity coefficients for Na^+ and SO_4^{2-} using the extended Debye-Hückel equation and the Davies equation.
(b) You accidentally spilled NaCl in the water and now the total ionic strength is 0.1 mol/L. Recalculate the activity coefficients for Na^+ and SO_4^{2-}.

4.5. Estimate the activity coefficient and activity of 1.0×10^{-5} M Fe^{3+} in 0.01 M HNO_3

4.6. The solubility of O_2 at 20°C is 9.07 mg/L in freshwater (I ~0) and 7.37 mg/L in seawater. Estimate the activity coefficient of O_2 in seawater.

4.7. Estimate the activity coefficient of $MgCO_3$ in a 4% magnesian calcite (i.e., $Ca_{0.96}Mg_{0.04}CO_{3(s)}$).

4.8. Cad4U, a local metal processing facility, is currently violating its discharge permits for dissolved cadmium, Cd^{2+}. The regulations are based on activity rather than concentration, and so the savvy (or unethical) chief chemist decides to alter the ionic strength to meet the discharge regulations. Currently the Cd^{2+} is discharged in very low ionic strength water (I << 0.001 M). Three salts are available: $MgBr_2$ ($5/mol), $MgSO_4$ ($10/mol), and NaCl ($3/mol). If the Cd^{2+} activity must be lowered by at least 40%, which salt is the most economical choice?

4.9. The following data were obtained for a rainfall sample collected at a site on your campus:

Ion	Molecular weight g/mol	Concentration mg/L
Na^+	23	0.15
K^+	39	0.09
Ca^{2+}	40	0.83
Mg^{2+}	24	0.08
NH_4^+	18	0.32
SO_4^{2-}	96	4.96
NO_3^-	62	2.88
Cl^-	35.5	0.47

The measured p^aH of the solution was 4.05 using a glass electrode. Using the composition data, estimate the molar concentration of H^+ in the rainfall assuming that H^+ and OH^- are the only two species present that are not listed above. Determine the activity coefficient for H^+ in the sample based on the calculated ionic strength, and compare the calculated p^aH value to that measured by the electrode.

4.10. Your advisor, Dr. Gettowerk, has given you the task of making a 1-liter of a solution with a calcium ion activity $\{Ca^{2+}\}$ of 1.3×10^{-4} M, and he wants you to make it in three different ways: one solution made in distilled water, one in 0.05 M KCl, and one in 0.1 M $MgCl_2$. How much $CaCl_2$ do you need to add to 1-L of water (or the appropriate salt solution) to make each solution and achieve the desired activity? Assume that all of the salts completely dissociate. Use the Davies equation for activity coefficients.

4.11. Using Figure 4.1 and the compositional data in Table 2.5, estimate the activity of water in the Dead Sea. For simplicity assume that the water is an equimolar solution of NaCl and $MgCl_2$ and the $MgCl_2$ behaves like $CaCl_2$.

4.12. Changes in the solubility of sparingly soluble salts with varying concentrations of an inert electrolyte (salt) can be used to determine $\gamma_\pm$ for the salt. The inert salt must have three characteristics: (a) it does not have a common ion with the salt of interest; (b) it does not form precipitates or soluble complexes with the salt of interest; and (c) it dissociates completely so that I can be determined exactly. KNO_3 and $KClO_4$ fit these conditions and are the salts of choice for such experiments. Let the solubility of MX be S_o in pure water and S in water with added salt, and let $\gamma_{\pm o}$ and $\gamma_\pm$ be the mean ionic activity coefficients in pure water and salt solutions, respectively. As more salt is added and I increases, $\gamma_\pm$ decreases, and MX becomes more soluble. Derive an expression that quantifies the relationship between S_o and S and allows you to evaluate $\gamma_\pm$.

References

1. Millero, F. J. 2001. *Physical chemistry of natural waters*, Wiley-Interscience, New York.
2. Benjamin, M. M. 2002. *Water chemistry*, McGraw-Hill, New York.
3. Robinson, R. A., and R. H. Stokes. 1959. *Electrolyte solutions*, 2nd ed. Butterworths, London.
4. Langelier, W. F. 1936. The analytical control of anti-corrosion water treatment. *J. Am. Water Wks. Assoc.* **28**: 1500.
5. Ponnamperuma, F. N., E. M. Tianco, and T. A. Loy. 1966. Ionic strengths of the solutions of flooded soils and other natural aqueous solutions from specific conductance. *Soil Sci.* **102**: 408–413.
6. Griffin, R. A., and J. J. Jurinak. 1973. Estimation of activity coefficients from the electrical conductivity of natural aquatic systems and soil extracts. *Soil Sci.* **116**: 26–30.
7. Eaton, A. D., L. S. Clesceri, E. W. Rice, and A. E. Greenberg. 2005. *Standard methods for the examination of water & wastewater*, 21st ed., Amer. Pub. Health Assoc., Amer. Water Works Assoc., Water Environ. Fed., Washington, D.C., 1–21.
8. Polemio, M., S. Bufo, and S. Paoletti. 1980. Evaluation of ionic strength and salinity of groundwaters: effect of the ionic composition. *Geochim. Cosmochim. Acta* **44**: 809–814.
9. Laitinen, H. A., and W. E. Harris. 1975. *Chemical analysis; an advanced text and reference*, 2nd ed., McGraw-Hill, New York.
10. Adamson, A. W. 1979. *A textbook of physical chemistry*, 2nd ed., Academic Press, New York.
11. Pitzer, K. S., and L. Brewer. 1961. *Thermodynamics*, 2nd ed. (revision of the text by G. N. Lewis and M. Randall), McGraw-Hill, New York.
12. Kielland, J. 1937. Individual activity coefficients of ions in aqueous solutions at 25°C and 1 atmosphere. *J. Am. Chem. Soc.* **59**: 1675–1678.
13. Davies, C. W. 1961. *Ion association*, Butterworths, London.
14. Stokes, R. H., and R. A. Robinson. 1948. Ionic hydration and activity in electrolyte solutions. *J. Am Chem. Soc*. **70**: 1870–1878.
15. Pauling, L. 1944. *The nature of the chemical bond*, 2nd ed., Cornell Univ. Press, Ithaca, N.Y.
16. Guggenheim, E. A. 1935. Thermodynamic properties of aqueous solutions of strong electrolytes. *Philos. Mag*. **19**: 588–643.
17. Pitzer, K. S. 1975. Thermodynamics of electrolytes. V. Effects of higher order electrostatic terms. *J. Solution Chem*. **4**: 249–265.
18. Baes, C. F., Jr., and R. E. Mesmer. 1976. *The hydrolysis of cations*, Wiley-Interscience, New York.

19. Garrels, R. M., and C. L. Christ. 1965. *Solutions, minerals, and equilibria*, Harper & Row, New York.
20. Stumm, W., and J. J. Morgan. 1981. *Aquatic chemistry*, 2nd ed., Wiley-Interscience, New York.
21. Schwarzenbach, R. P., P. M. Gschwend, and D. M. Imboden. 2003. *Environmental organic chemistry*, 2nd ed., J. Wiley & Sons, New York.
22. Lide, D. R. 2008. *CRC handbook of chemistry and physics*, 89th ed., CRC Press, Boca Raton, Fla.

5

█████ Fundamentals of Chemical Kinetics

█████ Objectives and scope

This chapter presents the principles and equations of kinetics, the branch of chemistry that deals with rates of chemical processes, factors affecting rates, and mechanisms by which reactions proceed. Starting with definitions of important terms and concepts, the chapter introduces the elements of chemical kinetics needed to analyze and interpret water chemistry and quality and focuses on three topics: (1) rate equations, including solutions for simple reactions, fitting data to equations to obtain rate constant values, and use of the equations to predict concentrations of reactants and products over time in reacting systems; (2) basic theory of how chemical reactions occur, focusing on transition state and activated complex theory; and (3) effects of physical factors—temperature, pressure, ionic strength, and pH on reaction rates and rate constants.

█████ Key terms

- Elementary reactions, reaction order and molecularity
- Rate equations and their analytical solutions: zero, first, second, third, and mixed-order equations
- Rate constants (coefficients), reactant half-lives ($t_{1/2}$), characteristic times, and other fractional lives
- Consecutive reactions, multistep mechanisms and the steady-state assumption
- Michaelis-Menten and Monod kinetics
- Chemical reactors: continuous-flow stirred tank reactors (CFSTRs) and plug-flow reactors (PFRs)
- Catalysts and catalyzed reactions
- Activation energy, E_{act}; frequency factor, A; and the Arrhenius equation

- Diffusion-encounter theory and diffusion-controlled versus chemical-controlled reactions
- Collision theory, absolute reaction rate or transition state theory, activated complex theory
- Free energy, enthalpy, entropy, and volume of activation ($\Delta G^{\neq}$, $\Delta H^{\neq}$, $\Delta S^{\neq}$, $\Delta V^{\neq}$, respectively)

5.1   Introduction and basic concepts

Kinetics is a mature science, and kinetic principles actually were used to develop early equilibrium concepts. In the mid-1800s chemical equilibrium was shown to involve a balance between forward and reverse rates of reaction. The law of mass action, which expresses reaction rates as proportional to reactant concentrations, was used to derive the concept of equilibrium constants, and in the late 1800s van't Hoff showed that the ratio of rate constants for the forward and reverse reactions is equal to the equilibrium constant for a reaction, i.e., $K_{eq} = k_f / k_r$.

Reaction rates generally increase with the concentration of one or several reactant(s) in a stoichiometric equation. The only exceptions—zero-order reactions—are only apparent contradictions of the rule, as explained in Section 5.2.4. Chemical reactions can be divided into two classes based on the pathways by which they proceed. **Elementary reactions** proceed in one step, and product(s) are formed directly when reactants collide with proper orientation and sufficient energy. No intermediates are involved, and rates follow the law of mass action. Only simple transformations can take place in a single collision: electron transfer, formation of a bond between atoms that have electrons and orbitals available for sharing, and breaking of a bond between two atoms. Chemical reactions involving more extensive changes proceed by a series of elementary steps that together define the mechanism of a **multistep reaction**. The sum of the steps determines the stoichiometry of the reaction. Although rates of multistep reactions depend on some reactant concentrations, overall stoichiometry is not a good predictor of the form of the rate equation.

The first step in analyzing the kinetics of a reaction is to fit measured data to an empirical rate equation. Rates of most reactions can be described by equations of the general form

$$\text{Rate} = -\frac{d[A]}{dt} = \frac{d[P]}{dt} = k[A]^a [B]^b \dots, \tag{5.1}$$

where A and B are reactants and P is a product. The exponent for a given reactant usually is a small integer (1 or 2 for elementary reactions), and k is called the **rate constant**. The sum of the exponents in the rate equation defines the **reaction order**, and the individual exponents define the order for a given reactant. For example, reactions that fit the rate equation $-d[A]/dt = k[A]$ are first order in A and first order overall, regardless of the number of reactants in the stoichiometric equation. Reactions that fit the equation $-d[A]/dt = k[A][B]$ are second order overall and first order in A and B. The order of reactants and rate equations for multistep reactions need not be integer values but may be fractional or even zero. Order is determined by empirical fit of data to a rate equation. In contrast, a reaction's **molecularity** is given by the number of

molecules acting as reactants. This concept applies only to elementary reactions; in multistep reactions, individual elementary steps each may have different molecularities. The value of k in Eq. 5.1 depends on temperature and other physical conditions (but not on time); thus, k more properly is called a rate coefficient than a rate "constant." The units of k depend on the order of the equation. In general, k has units of $[C]^{1-n} t^{-1}$, where n is the overall order of the rate equation.

EXAMPLE 5.1: What is the reaction order in A and the overall reaction order of the following equations?

(a) $-\dfrac{d[A]}{dt} = k[B]$

(b) $-\dfrac{d[A]}{dt} = k[A]^2$

(c) $-\dfrac{d[A]}{dt} = k[A]^{1.5}[B]$

Answers: (a) zero order in A, first order overall; (b) second order in A, second order overall; (c) 1.5 order in A, 2.5 order overall.

Fitting kinetic data for a reaction to a rate equation requires determining the value of the rate constant and the orders of the reactants. This is usually done with integrated forms of rate equations that give reactant concentrations, [C], as functions of time. Integrated expressions of simple rate equations can be written such that rate constants can be evaluated graphically from a plot of a function of [C] versus time. These expressions then can be used to compute [C] for a reactant or product at any desired time. For simple rate equations, standard integrated forms are available, as described in following sections. Rate equations for complicated (sequences of) reactions often cannot be solved analytically, and in such cases, numerical methods (computer programs) are used to solve the rate equations and evaluate [C] as a function of time. In multistep reactions, one elementary step usually is much slower than the others and limits the overall rate. The stoichiometry of this step usually has a strong influence on the overall reaction order. For example, if this step involves two molecules, the reaction likely will follow second-order kinetics, at least over some range of concentrations. Although reaction mechanisms determine rate equations and reaction order, the converse is not true; many mechanisms may lead to the same rate equation and reaction order.

5.2 Simple rate equations and their solutions

5.2.1 First-order kinetics

A reaction follows first-order kinetics if its rate depends linearly on the concentration of a single reactant. If we let the initial concentration of reactant A be $[A]_o$, and the amount that has reacted (per unit volume) at any time t be x, then $([A]_o - x) = [A]$, the concentration remaining at time t. The rate is given by the following equation:

$$-\frac{d[A]}{dt} = \frac{dx}{dt} = k_1[A] = k_1([A]_o - x) \tag{5.2}$$

Equation 5.2 is valid if the reaction is irreversible; i.e., it proceeds only in a forward direction, and there is no tendency for the product to react back to form the reactant. The integrated form of Eq. 5.2 is

$$\frac{[A]}{[A]_o} = \exp(-k_1 t), \tag{5.3a}$$

or the linearized version,

$$\ln\frac{[A]}{[A]_o} = \ln\frac{([A]_o - x)}{[A]_o} = -k_1 t. \tag{5.3b}$$

The reaction progress can be followed by measuring either the amount of reactant remaining or product formed at as a function of time. The left sides of equations 5.3a and 5.3b are dimensionless ratios, and thus the right sides also must be dimensionless. Therefore, the units of k_1 are reciprocal time. The common unit is s^{-1}, but any convenient time unit may be used. In first-order reactions, the value of the rate constant is not affected by the units in which the reactant concentration is expressed. Because rates vary with temperature, the temperature at which k_1 was measured should be specified.

For graphical solutions, we write Eq. 5.3b in natural log form as

$$\ln[A] = -k_1 t + \ln[A]_o, \tag{5.4}$$

and a plot of $\ln[A]$ versus t yields a straight line if a reaction follows first-order kinetics (Figure 5.1a). The y-intercept gives the initial reactant concentration, $\ln[A]_o$, and the slope gives the value of k_1. If the data are plotted on base-10 log paper, $k_1 = -2.303 \times$ slope.
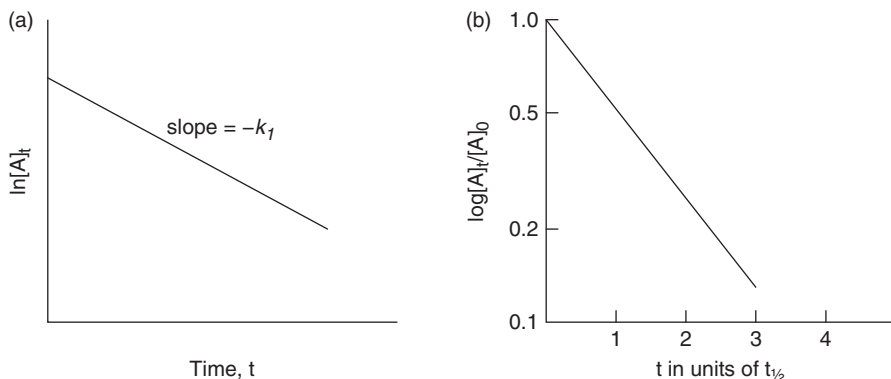
Figure 5.1 (a) Plot of $\ln[A]_t$ versus time yields a straight line with slope $= -k_1$ for first-order reactions; (b) dimensionless plot of log fraction [A] remaining versus time in units of $t_{1/2}$ also is a straight-line relationship for first-order reactions.

A useful concept for first-order reactions is the ***half-life***, $t_{1/2}$, which is defined as the time required for half of the reactant to react. From Eq. 5.3 we can readily derive

$$t_{1/2} = \frac{1}{k_1} \ln \frac{[A]_o}{0.5[A]_o} = \frac{\ln 2}{k_1} = \frac{0.693}{k_1}. \tag{5.5}$$

It is apparent that the half-life of a first-order reaction does not depend on the initial concentration; a constant fraction of reactant is lost in successive time periods of equal length. Half of the initial concentration remains at $t = t_{1/2}$, one-fourth at $t = 2t_{1/2}$, one-eighth at $t = 3t_{1/2}$, and so on. Plots of $\log[A]/[A]_o$ versus time expressed in units of $t_{1/2}$ thus yield straight lines (Figure 5.1b).

Other fractional lives can be calculated and are useful in some circumstances. In general, if $t_{1/i}$ is the time required for A to decrease to $1/i$th of its initial value,

$$t_{1/i} = -\frac{1}{k_1} \ln \frac{1}{i} = \frac{\ln i}{k_1} \tag{5.6}$$

When $i =$ e (the natural number, 2.718), $t_{1/i}$ has the symbol τ, and Eq. 5.6 becomes $\tau = 1/k_1$. τ is called the ***characteristic time*** of a reaction. It is analogous to τ_w, the hydraulic residence time in water bodies and treatment process reactors, and to τ_s, the substance residence time, in completely mixed reactors. τ represents the *average time* before a molecule reacts. From the nature of the exponential function, [A] is $1/e$th (0.37) of $[A]_o$ at $t = \tau$. From the equation for $t_{1/2}$ and the fact that $k = 1/\tau$, we see that $t_{1/2} = 0.69\tau$.

Radioisotope decay follows first-order kinetics, and decay rates usually are expressed in half-lives rather than rate constants. Die-off rates of microorganisms also usually follow first-order kinetics, and the decline in microbial populations at constant concentration of disinfectant is first order in microbe concentration. A common term in disinfection kinetics is t_{99}, the time required for 99% die-off, which unfortunately is also symbolized as the ambiguous term $t_{.01}$, the time required for the initial concentration to be 1% of the initial value. From Eq. 5.6,

$$t_{99} = -\frac{1}{k_1} \ln \frac{1}{100} = \frac{4.605}{k_1}. \tag{5.7}$$

Many processes in natural waters follow first-order kinetics under some circumstances even if they are mechanistically complex. Examples include loss rates of nutrients and trace metals from lakes even though several processes, including biological uptake, chemical precipitation, and adsorption onto suspended solids, may be involved. The chemical residence times of substances in water bodies generally are calculated from chemical reactor theory,[1,2] with first-order kinetics assumed. Growth of microorganisms also follows first-order kinetics under many circumstances. Finally, reactions whose rates depend on concentrations of several reactants can be made ***pseudo-first order*** by holding the concentrations of all but one reactant constant. One simple way to achieve this is to make their concentrations much higher than that of the so-called variable reactant. Dissolved gas concentrations can be held constant by sparging the solution with a gas mixture containing a fixed partial pressure of the reactant gas. Reactions

in which the solvent is a reactant often are pseudo-first order; hydrolysis reactions of organic compounds are examples. The observed rate constant (k_{obs}) in pseudo-first-order reactions is the product of an intrinsic higher-order rate constant and the concentration(s) of the reactants whose concentrations were held constant in measuring k_{obs}; e.g., $k_{obs} = k_2[X]_{fr}$, where $[X]_{fr}$ stands for the concentration of the "fixed reactant."

EXAMPLE 5.2 Rate constant for oxidation of Fe^{2+}: Over a wide range of pH ($\sim$5–9), the autoxidation of Fe^{II} (i.e., oxidation by O_2) is described by the rate equation $-d[Fe^{II}]/dt = k[Fe^{II}]P_{O_2}[OH^-]^2$. The rate thus is highly pH dependent. If rate measurements are made in buffered solutions at fixed pH and if the partial pressure of oxygen is held constant (e.g., by sparging the solution with a gas having a fixed P_{O_2}), the reaction becomes pseudo-first order ($-d[Fe^{II}]/dt = k_{obs}[Fe^{II}]$).

The following data on $[Fe^{II}]$ were obtained using the phenanthroline colorimetric method in solutions with an ionic strength of 0.0010 buffered to pH 7.00 with P_{O_2} held at 0.21 atm by sparging with clean air. Compute

   (a) k', the observed (pseudo-first-order) rate constant for the reaction;
   (b) the half-life of Fe^{II} under the reaction conditions; and
   (c) k, the rate constant for the complete rate equation, in its usual units (M^{-2} atm^{-1} min^{-1}) and compare the result to the literature value given in Chapter 13.

Time (min)	0	10	20	30	40	60
$[Fe^{II}]$ ($\mu g/L$)	500	320	200	130	80	35

(a) A first-order plot of the data, $\ln [Fe^{II}]$ versus time (graph below), yields a straight line with a slope of -0.0446; that is, $k' = 4.46 \times 10^{-2}$ **min^{-1}**.

$y = -0.0446x + 6.203$
$r^2 = 0.999$
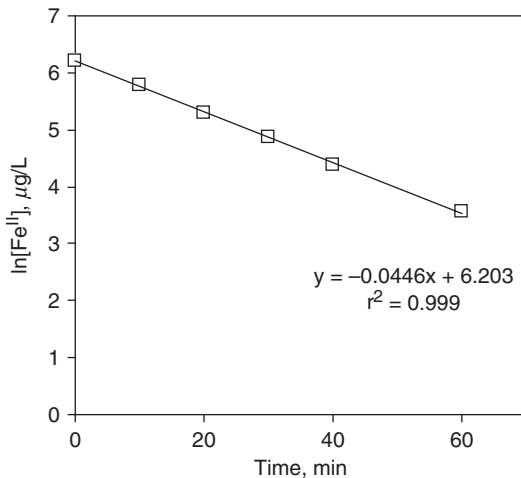
(b) The half-life of Fe^{II} under the measurement conditions is

$$t_{1/2} = 0.693/k' = 0.693/4.46 \times 10^{-2} \text{ min}^{-1}, \text{ or } \mathbf{t_{1/2} = 15.54 \text{ min}}$$

(c) The pseudo-first-order rate constant is related to the rate constant for the full rate equation as follows:

$$k' = kP_{O_2}[OH^-]^2$$

At pH 7.00, $\{OH^-\} = 1.00 \times 10^{-7}$, and from Table 4.3 we find $\gamma_{OH^-} = 0.965$ at $I = 0.001$. From $a_i = \gamma_i c_i$, we find that

$$[OH^-] = 1.036 \times 10^{-7} \text{ M.}$$

Therefore,

$$k = k' \div P_{O_2}[OH^-]^2 = 4.46 \times 10^{-2} \text{ min}^{-1} \div (0.21 \text{ atm} \times (1.036 \times 10^{-7} \text{ M})^2),$$

or

$$\boldsymbol{k = 1.98 \times 10^{13} \text{ M}^{-2} \text{ atm}^{-1} \text{ min}^{-1}.}$$

In Chapter 13 we find that a wide range is reported for k in the literature, in part because the reaction rate can be accelerated or inhibited by many ions and organic substances), but in synthetic media without interfering substances the range is about 1.5–$3.0 \times 10^{13} \text{ M}^{-2} \text{ atm}^{-1} \text{ min}^{-1}$.[3] The above results thus fit well within this range.

5.2.2 Second-order kinetics

Two types of elementary reactions have second-order kinetics, and many reactions with multistep mechanisms fit second-order expressions under limited conditions. Elementary reactions of the types $A + B \rightarrow P$ and $2A \rightarrow P$ are second order. For the first type, if $[A]_o$ and $[B]_o$ are initial concentrations and x is the concentration of each that has reacted at time t, the rate equation is

$$\frac{dx}{dt} = k_2[A][B] = k_2([A]_o - x)([B]_o - x). \tag{5.8}$$

By convention, elementary reactions are written as unidirectional; the reverse reaction, if it occurs, is considered as a separate elementary reaction. Consequently, an implicit assumption for Eq. 5.8 to apply is that the reaction is irreversible. If $x = 0$ at $t = 0$ and $[A]_o \neq [B]_o$, the integrated form of this equation is

$$\frac{1}{[A]_o - [B]_o} \ln \frac{[B]_o([A]_o - x)}{[A]_o([B]_o - x)} = \frac{1}{[A]_o - [B]_o} \ln \frac{[B]_o[A]}{[A]_o[B]} = k_2 t. \tag{5.9}$$

The rate constant, k_2, has units of t^{-1} conc.$^{-1}$, and the magnitude of k_2 thus depends on the units of t and concentration, as well as the nature of the reaction and physical conditions like temperature. For reactions in solution, concentrations are usually in mol L^{-1} (M), and k_2 commonly is in $M^{-1} s^{-1}$ (or $L \text{ mol}^{-1} s^{-1}$).
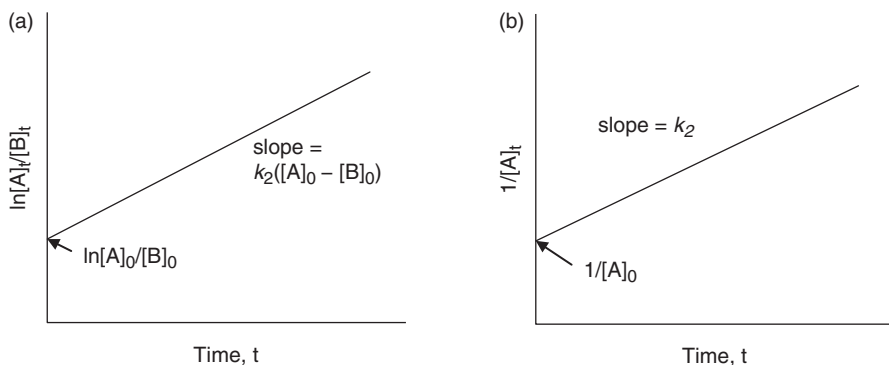
Figure 5.2 (a) General second-order plot showing slope and intercept values; (b) second-order plot with slope and intercept values for $2A \rightarrow P$ or $A + B \rightarrow P$ when $[A]_o = [B]_o$.

Graphical solutions are obtained by rearranging Eq. 5.9:

$$\ln\frac{[A]}{[B]} = k_2([A]_o - [B]_o)t + \ln\frac{[A]_o}{[B]_o} \tag{5.10}$$

In a given experiment, $[A]_o$ and $[B]_o$ are constant. A plot of $\ln[A]/[B]$ versus t thus is a straight line for second-order reactions (Figure 5.2a), and k_2 is obtained from the slope $k_2 = (\text{slope})/([A]_o - [B]_o)$. If the data are plotted on base-10 log paper, this expression must be multiplied by 2.303 to obtain k_2. In reactions of the type $2A \rightarrow P$ and also when $[A]_o = [B]_o$ in reactions of type $A + B \rightarrow P$, eqs. 5.8–5.10 are indeterminate. The rate expression for these cases is given by

$$\frac{dx}{dt} = k_2[A]^2 = k_2([A]_o - x)^2, \tag{5.11}$$

which integrates to

$$\frac{1}{[A]} = \frac{1}{[A]_o - x} = k_2 t + \frac{1}{[A]_o}. \tag{5.12}$$

For this reaction type, plots of $1/[A]$ versus t are linear, and the slope is directly equal to k_2 (Figure 5.2b). Plots of Eq. 5.12 are simpler than those of Eq. 5.10, and setting initial reactant concentrations equal is a convenient way to simplify the analysis of second-order reactions.

In studying second-order reactions, one may hold the concentration of one reactant constant by making its concentration much higher than that of the other reactant. The rate constant thus obtained is **pseudo-first order**, because Eq. 5.8 then integrates to a first-order-like equation: $-d[A]/dt = k_2[A][B] = k'[A]$, where $k' = k_2[B]$ and B is the fixed reactant. The value of the apparent first-order rate constant, k', depends on the concentration of the fixed reactant. In many environmental reactions, species B is water, which is always present in excess, or H^+ or OH^-, which are approximately constant due

to pH buffering, allowing pseudo-first-order kinetics to be applied. Second-order rate constants often are determined by measuring k' at multiple values of [B] and plotting k' versus [B] to get slope k_2.

The half life of a second-order reaction is an ambiguous concept if $[A]_o \neq [B]_o$ because the two reactants then have different times for half of the initial concentration to react. If $[A]_o = [B]_o$ or the two reactants are the same, the half life is inversely proportional to the initial reactant concentration:

$$t_{1/2} = \frac{1}{k_2[A]_o} \tag{5.13}$$

Rate equations are sometimes written in terms of stoichiometric coefficients. With this convention, second-order reactions like $2A \rightarrow P$ have the rate expression $-d[A]/dt = 2k_2[A]^2$, which integrates to Eq. 5.12 except for a factor 2 before k_2. It is apparent that in this convention k_2 has half the value of k_2 in Eq. 5.12. Both conventions are used in the literature, and caution must be used to determine which convention was used for a published value.

EXAMPLE 5.3 Oxidation of bromide by HOCl: a second-order reaction: HOCl, hypochlorous acid, is the major form of free chlorine in water at pH < 7.5. It reacts rapidly ($k_2 = 1.3 \times 10^3$ M^{-1} s^{-1}) with bromide ions to form HOBr, hypobromous acid, and Cl$^-$: HOCl + Br$^- \rightarrow$ HOBr + Cl$^-$. A slightly acidic (pH = 6.2) ground water being used for drinking water has a bromide concentration of 80 ppb and is dosed with chlorine to yield a free chlorine residual concentration of 1 mg/L as Cl. What is the concentration of HOBr in the water after 1 minute of reaction?

Answer: $[Br^-]_o = 80$ ppb $\div$ 79.9 g/mol $= 1 \times 10^{-6}$ M; $[HOCl]_o = 1$ mg/L as Cl $\div$ 35.45 g/mol $= 2.82 \times 10^{-5}$ M.

Substituting into Eq. 5.9 and solving for x, the concentration of Br$^-$ that has reacted, readily yields

$$\frac{1}{2.82 \times 10^{-5} - 1 \times 10^{-6}} \ln \frac{1 \times 10^{-6}(2.82 \times 10^{-5} - x)}{2.82 \times 10^{-5}(1 \times 10^{-6} - x)} = 1.3 \times 10^3 \times 60,$$

or

$$x = 8.84 \times 10^{-7} \text{ M} = [HOBr];$$

that is, about 88% of the initial bromide has reacted in 1 minute.

Many reactions in aqueous systems are second order, including oxidation of sulfide and chlorination reactions. Many of these reactions are complicated by competing reactions or catalytic effects, however, and simple second-order formulations do not fully describe them.

5.2.3 Third-order kinetics

Third-order elementary reactions are fairly uncommon, except where catalysis is involved. This is reasonable given that reactions occur when molecules collide. The probability of simultaneous collision of three or more reactants is much smaller than the probability of bimolecular collisions. Rate equations for third-order processes are written in ways analogous to equations for first- and second-order rate processes. Analytical solutions of rate equations for third-order reactions are not widely used in environmental chemistry but are available in kinetics textbooks.[1,2]

Many reactions with complicated pathways have third-order or higher rate equations. Oxidation of Fe^{II} by O_2 is first order in Fe^{II} and P_{O2} and second order in OH^-, or fourth order overall. The development of rate equations and rate constants for such reactions involves isolating one reactant at a time as a variable and fixing concentrations of all others, for example, by making their concentrations much higher than that of the variable reactant or, in the case of H^+ and OH^- as reactants, by adding a buffer.

5.2.4 Zero-order reactions

We stated earlier that reaction rates depend on the concentration of reactants, as required by the law of mass action. Despite this statement, zero-order reactions, whose rates are independent of concentration, are fairly common. Rate expressions of such reactions may be considered to contain concentration to the zero power:

$$-\frac{d[A]}{dt} = \frac{dx}{dt} = k_o[A]^0 = k_o, \tag{5.14}$$

the integrated form of which is

$$[A] = [A]_o - k_o t, \tag{5.15a}$$

or

$$[P] = [P]_o + k_o t. \tag{5.15b}$$

Plots of concentration versus time thus are linear for such reactions (Figure 5.3). The violation of mass-action principles is only apparent, however, and has at least three explanations: (1) Some reactions seem to be zero order simply because reactant concentrations did not change sufficiently in an experiment to cause curvature in a plot of concentration versus time. (2) If the reacting system is open, the influx of reactant from outside the system may be sufficient to maintain a steady concentration. (3) If the reaction occurs only as a catalyzed process, e.g., by an enzyme or a surface with reactive sites, and if the attraction of the reactant to catalytic sites is strong, these sites will be completely occupied by reactant over a broad range of its concentrations in solution. The rate then will be independent of solution concentrations. The fraction of occupied sites will decrease only when the solution concentration gets sufficiently low, but this may not always be reached in a given experiment. Except for explanations (1) and (2), reactions with zero-order kinetics involve multistep mechanisms; otherwise, single-step (elementary) reactions cannot exhibit zero-order kinetics.
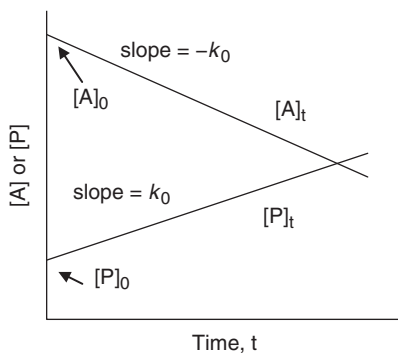
Figure 5.3 Zero-order reactions have simple linear plots of [A] or [P] versus time.

5.3   More complicated reactions

5.3.1 Consecutive reactions

Many reactions involve a sequence of steps with intermediate products that build up to measurable concentrations and then decline as they undergo further reaction. Rate equations and analytical solutions for the simplest (two-step) first-order consecutive sequence, $A \rightarrow B \rightarrow C$, are given in Table 5.1. The shapes of the concentration-time curves for appearance and disappearance of A, B, and C depend on the relative magnitudes k_i and k_{ii} for the two steps. As Figure 5.4 shows, when $k_i > k_{ii}$ (Figure 5.4a), B tends to reach higher concentrations than when $k_i < k_{ii}$ because B tends to react more quickly than it is formed in the latter case (Figure 5.4c). In addition, there is a greater lag (called the ***induction period***) in the buildup of product C (Figures 5.4b and 5.4c) when $k_i > k_{ii}$ than vice versa. The time at which [B] reaches its maximum, $t_{B_{max}}$, also depends on the relative sizes of k_i and k_{ii} and is given by

$$t_{B_{max}} = \frac{1}{k_i - k_{ii}} \ln \frac{k_i}{k_{ii}}. \tag{5.16}$$

$[B]_{max}$ itself is given by

$$[B]_{max} = \frac{k_i}{k_{ii}}[A]_o \exp(-k_i t_{B_{max}}). \tag{5.17}$$

Table 5.1 Rate equations for the first-order sequence A → B → C

Rate equations	*Analytical solutions*
$d[A]/dt = -k_i[A]$	$[A] = [A]_o \exp(-k_i t)$
$d[B]/dt = k_i[A] - k_{ii}[B]$	$[B] = \dfrac{k_i[A]_o}{k_{ii} - k_i} \{\exp(-k_i t) - \exp(-k_{ii} t)\}$
$d[C]/dt = k_{ii}[B]$	$[C] = \dfrac{k_i[A]_o}{k_{ii} - k_i} \{k_{ii}(1 - \exp(-k_i t)) - (1 - \exp(-k_{ii} t))\}$
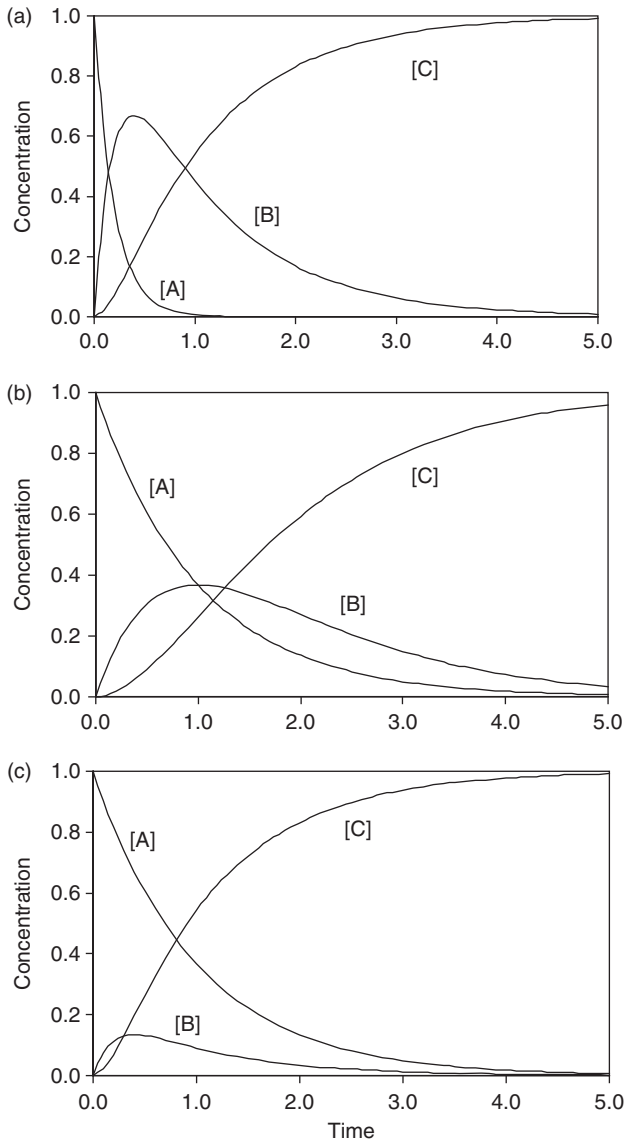
Figure 5.4 Concentration versus time for the two-step, first-order sequence $A \rightarrow B \rightarrow C$, with $[A]_0 = 1$ and $[B]_0 = [C]_0 = 0$. (a) $k_i = 5$ t^{-1}, $k_{ii} = 1$ t^{-1}; (b) $k_i = k_{ii} = 1$ t^{-1}; (c) $k_i = 1$ t^{-1}, $k_{ii} = 5$ t^{-1}. Simulations done in Acuchem.[6]

Equations 5.16 and 5.17 can be derived from the rate equations in Table 5.1. We also can show that the ratio of [A] to [B] is given by the following equation:

$$\frac{[B]}{[A]} = \frac{k_i}{k_{ii} - k_i}\{1 - \exp(-(k_{ii} - k_i)t\} \tag{5.18a}$$

When $k_{ii} > k_i$, [B]/[A] reaches a steady-state value called **secular equilibrium** (see Box 5.1) at $t \gg t_{\text{max,B}}$:

$$\lim \frac{[B]}{[A]} = k_i/(k_{ii} - k_i) \tag{5.18b}$$

Box 5.1   Secular equilibrium in radioisotope decay

Secular equilibrium is common in the decay sequences of radioisotopes. For example, radium-226 (^{226}Ra) decays slowly ($t_{\frac{1}{2}} = 1620$ yr; $k_i = 4.28 \times 10^{-4}$ yr^{-1}) to radon-222 (^{222}Rn), which decays rapidly ($t_{\frac{1}{2}} = 3.8$ days, $k_{ii} = 66$ yr^{-1}) to polonium-218 (^{218}Po). ^{222}Rn is a useful tracer for sediment-water exchange processes in natural waters. This application relies on the fact that ^{226}Ra occurs in much greater quantities in sediments than in overlying waters, and sediments thus act as a source of ^{222}Rn (by diffusion and gas ebullition). It is necessary to determine both the total ^{222}Rn activity in water samples and the fraction that arises from secular equilibrium with ^{226}Ra in the water column. This is done by purging a water sample with an inert gas, collecting the ^{222}Rn in a liquid N$_2$ trap, and measuring the Rn activity by alpha spectroscopy. The purged sample is set aside for several weeks to allow ^{226}Ra in the water to reach a new secular equilibrium with ^{222}Rn. From eq. 5.18a, we can compute that the activity ratio {Rn}/{Ra} is 92% of the limiting value after 14 days and 98% after 21 days. Purging after 21 days and measuring the ^{222}Rn thus yields its activity in secular equilibrium with dissolved ^{226}Ra. Subtraction of this activity from the initial activity gives the {Rn} arising sediment-water exchange processes. Similar procedures are used to determine levels of ^{90}Sr, ^{226}Ra, and ^{210}Pb in water and sediment samples because their daughter products (^{90}Y, ^{222}Rn, and ^{210}Po, respectively) can be isolated conveniently from interfering matrices. The disequilibrium of ^{90}Y and ^{90}Sr in treated drinking water has been used as a novel means of estimating water age in distribution systems (J. Waples, unpublished data, University of Wisconsin-Milwaukee, 2007).

Nitrification, a microbially mediated two-step process, can be modeled by the equations in Table 5.1, and chlorination of phenol is an example in water treatment chemistry of a longer sequence of consecutive reactions that includes several branching or competing reactions. Chlorination of acetic acid is another example. Analytical solutions of the rate equations for straight-chain sequences as long as A $\rightarrow$ B$\rightarrow$ C $\rightarrow$ D $\rightarrow$ E $\rightarrow$ F are available,[4] but simulation of such sequences by numerical methods is a more widely used method of solution.

5.3.2 Reversible reactions

The reactions discussed previously in this chapter were assumed to proceed only in the forward direction; that is, the product had no tendency to react back to form the reactant. In many reactions relevant to natural waters, measurable quantities of reactant and product exist at equilibrium, and the net effect is that the reaction is ***reversible***; that is, the backward reaction proceeds at a significant rate relative to that of the forward direction. Kinetic expressions for reversible reactions are complicated by addition of a term for the back reaction, and analytical solutions soon become intractable as reaction order increases. We consider here only the simplest reversible reaction, $A \rightleftharpoons P$, which is first order in both directions. Taking the back reaction into account, the net change in $[A]$ is $-d[A]/dt = rate_{for} - rate_{rev}$, or

$$-\frac{d[A]}{dt} = k_f[A] - k_r[P], \tag{5.19a}$$

or

$$\frac{dx}{dt} = k_f([A]_o - x) - k_r([P]_o + x), \tag{5.19b}$$

where k_f and k_r are first-order rate constants for the forward and reverse reactions and x is the concentration of A that has reacted (or concentration of P formed) at any time. The analytical solution for Eq. 5.19b is

$$\ln\frac{(k_f[A]_o - k_r[P]_o)}{k_f([A]_o - x) - k_r([P]_o + x)} = (k_f + k_r)t = k^*t, \tag{5.20}$$

where $k^* = k_f + k_r$. If $[P]_0 = 0$, then $[P] = [A]_o - [A]$, and Eq. 5.20 becomes

$$\ln\frac{k_f[A]_o}{k^*[A] - k_r[A]_o} = k^*t \tag{5.21}$$

or

$$[A] = \frac{[A]_o}{k^*}\{k_r + k_f\exp(-k^*t)\} \tag{5.22}$$

Equation 5.22 can be written in terms of the equilibrium constant for the reaction, $K = k_f/k_r = [P]_{eq}/[A]_{eq}$. Again, if $[P]_o$, is 0, then $[P]_{eq} = [A]_o - [A]_{eq}$, and the following equations can be derived:[2]

$$\frac{[A]}{[A]_{eq}} = 1 + K\exp(-k^*t) \tag{5.23a}$$

or

$$\frac{[A] - [A]_{eq}}{[A]_o - [A]_{eq}} = \exp(-k^*t) \tag{5.23b}$$

Equation 5.23b is similar to the first-order equation (Eq. 5.3a) for irreversible reactions, except that $[A]$ is corrected for equilibrium concentration, $[A]_{eq}$, and the reaction
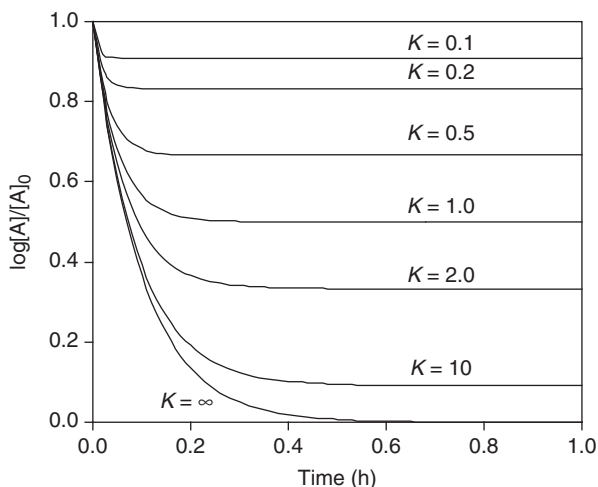
Figure 5.5 Effect of equilibrium constant $K(= k_f/k_r)$ on shape of fractional reactant disappearance curves for reversible first-order reactions. Time in units of h; k_f was fixed at 10 h^{-1}, and k_r was varied to give the values of K associated with each curve.

approaches equilibrium (Figure 5.5) with a rate constant k^* equal to the *sum* of the forward and back rate constants. Equation 5.23b applies to air-water exchange rates of gases, to the kinetics of two-box compartment models,[2,5] and to continuous-stirred tank reactors in which a step change in input has occurred.[1,2] Because of the mathematical complexity of reversible reactions, they usually are studied by isolating one reaction (forward or reverse) by setting product concentration(s) for that reaction equal to zero and measuring initial rates so that product concentrations remain small and the reverse reaction is insignificant.

Analytical solutions of rate equations are not available for reaction sequences much more complicated than those described above. Determination of concentrations versus time for reactants, intermediates, and products in such cases is achieved by computer simulation with programs that solve sets of simultaneous differential equations. Acuchem[6] is a public-domain computer program designed for kinetic analysis of chemical reaction sequences.*

5.3.3 Rate equations for reactions with multistep mechanisms

As mentioned at the beginning of this chapter, many reactions of interest in natural waters involve multistep mechanisms. From a practical perspective, the difference between such reactions and the sequential reactions described in Section 5.3.1 is a matter of degree rather than kind. In the sequential reactions described previously, concentration profiles

---

*Acuchem is a DOS-based program in the public domain. Although the program has a powerful algorithm to simulate the kinetics of complicated reaction sequences, its DOS interface limits its usability. The program itself and a Windows-based interface that facilitates the input of data on reaction sequences and the transfer of output data to spreadsheet files are available on the companion Web site for this book at www.oup.com/us/WaterChemistry. A brief tutorial on Acuchem and use of the interface program also is found at that site.

of intermediate products were of interest because they built up to significant levels during timescales of interest relative to the overall reaction sequence.[†] In reactions with multistep mechanisms, intermediates also are formed, but because they are so reactive, they usually do not reach concentrations that can be measured easily and do not contribute significantly to a mass balance for the reactants and (final) products. Consequently, we want to write a rate equation for product formation in terms of only the main reactants—not including the unmeasured/unmeasurable intermediates. We can do this by two different techniques that require a simplifying assumption. In both cases, the slowest step, called the rate-limiting step, is the bottleneck for the overall reaction. In the ***equilibrium assumption*** approach, the rapid (non-rate-limiting) steps are assumed to reach equilibrium, so that the concentration of an intermediate involved in such a step can be defined by an equilibrium constant and concentrations of the main reactants. In the more robust ***steady-state assumption*** approach, the rapid reactions do not necessarily attain equilibrium, but the concentration of (unmeasured) intermediate, $[I]$, is assumed to reach a constant (steady-state) value. In this circumstance, the rate equation becomes an algebraic equation that can be solved for $[I]$ in terms of rate constants and concentrations of measured reactants. This assumption generally produces more accurate expressions for the rate of product formation than the equilibrium constant approach does. Use of the steady-state assumption to produce rate equations for two important multistep reactions is illustrated in Boxes 5.2 and 5.3.

Development of rate equations from known mechanisms, as described in Boxes 5.2 and 5.3, may be termed the "forward problem." If a mechanism is reasonably compact (a few steps and small number of reactants, intermediates and products), development of the rate equation is straightforward. In terms of everyday activity in environmental

---

Box 5.2   The Lindeman mechanism

A basic tenet of kinetics is that reactions do not occur until reactants gain sufficient energy to overcome an "activation barrier" (section 5.5). In photochemical reactions, the energy is provided by absorption of light, but in all other reactions (called "thermochemical" reactions) the activation energy is obtained from the kinetic energy provided when molecules collide. First-order kinetics, where rates depend only on the concentration of a single reactant raised to the first power, seem to violate this tenet. Lindeman[7] described a two-step mechanism that explains how

---

[†]There is no absolute dividing line between these situations. Whether one considers a reaction to be a sequential set of reactions or one reaction with a multistep mechanism depends on such factors as whether one is interested in or able to measure the intermediates, the overall timescale for the reaction, and one's goals in studying the reaction.

reactions with a single reactant (A) can fit first-order kinetics and not violate the above principle. The mechanism is

(1) $A + A \underset{k_{-i}}{\overset{k_i}{\rightleftharpoons}} A + A^*$

(2) $A^* \xrightarrow{k_{ii}} P$
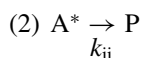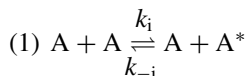
Some fraction of the collisions of A molecules transfers energy to one of the A molecules to produce activated state A^* (reaction 1). Although A^* has the energy for reaction, the energy may not be focused in the correct part of the molecule, and reaction 2 to form P must wait for the energy to be redistributed into that part (e.g., a bond that will break). During this time, A^* could collide with another molecule of A, causing deactivation of A^* (reverse of reaction 1). Rate equations for changes in [A], $[A^*]$, and [P] are

(3) $-d[A]/dt = k_i[A]^2$,

(4) $d[A^*]/dt = \sum \text{rate}_{form} - \sum \text{rate}_{loss} = k_i[A]^2 - k_{-i}[A][A^*] - k_{ii}[A^*]$,

(5) $d[P]/dt = k_{ii}[A^*]$.

Invoking the steady-state assumption for $[A^*]$ means that $d[A^*]/dt = 0$. Solving the resulting algebraic equation for $[A^*]$ leads to

(6) $[A^*] = \dfrac{k_i[A]^2}{k_{-i}[A] + k_{ii}}$.

Substituting eq. (6) into the rate of product formation, eq. (5), leads to an expression for the rate of formation of P that does not depend on the concentration of unmeasured intermediate A^*:

(7) $d[P]/dt = \dfrac{k_i k_{ii}[A]^2}{k_{ii} + k_{-i}[A]}$

If A^* deactivates much faster than it reacts to form product, then $k_{-i}[A] >> k_{ii}$, and eq. (7) reduces to a first-order expression:

(8) $d[P]/dt = k_{ii}K_i[A] = k_{obs}[A]$,

where k_{obs} is the observed (measured) rate constant. $K_i = k_i/k_{-i}$ is the equilibrium constant for the first step (reaction 1), and $K_i[A]$ is the equilibrium concentration of A^*. When [A] is sufficiently small, $k_{-i}[A] < k_{ii}$, and $d[P]/dt \approx k_i[A]^2$. Reactions following the above mechanism thus become second order at low reactant concentrations. Of course, many reactions with much more complicated mechanisms and stoichiometry also fit first-order kinetics, and readers should not infer that the above mechanism is the only explanation for first-order kinetics.

Box 5.3   Reaction of a single reactant with a recyclable catalyst

Catalysts are substances that affect the rate of a reaction but do not participate in the reaction in a net sense; that is, they interact with reactants but are recycled to form fresh catalyst somewhere in the overall reaction mechanism. The simplest reaction with a recycled catalyst involves a single reactant in the following mechanism:

(1) $A + C \underset{k_{-i}}{\overset{k_i}{\rightleftharpoons}} X \overset{k_{ii}}{\rightarrow} P + C,$
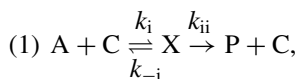
where the net reaction is $A \rightarrow P$, C is the catalyst, and X is an intermediate consisting of the reactant sorbed onto or complexed with the catalyst. Rate equations for sequence (1) are

(2) $-d[A]/dt = k_i[A][C] - k_{-i}[X],$

(3) $d[C]/dt = (k_{-i} + k_{ii})[X] - k_i[A][C],$

(4) $d[X]/dt = k_i[A][C] - (k_{-i} + k_{ii})[X],$

(5) $d[P]/dt = k_{ii}[X].$

An analytical solution is not possible for eqs. (2)–(5), but they can be solved by invoking the steady-state assumption for [X]; that is, $d[X]/dt = 0 = k_i[A][C] - (k_{-i} + k_{ii})[X]$:

(6) $[X] = \dfrac{k_i[A][C]}{k_{-i} + k_{ii}}$

Equation (6) contains [C], the concentration of free catalyst, which may not be measurable, but a mass balance can be written for the catalyst:

(7) $[C]_T = [C] + [X],$

where subscript $_T$ denotes the total catalyst in the system. Solving eq. (7) for [C], substituting into eq. (6), and solving for [X] yields

(8) $[X] = \dfrac{k_i[A][C]_T}{k_i[A] + k_{-i} + k_{ii}}.$

Substitution of eq. (8) into eq. (5) yields the rate of product formation:

(9) $\dfrac{d[P]}{dt} = \dfrac{k_i k_{ii}[A][C]_T}{k_i[A] + k_{-i} + k_{ii}} = \dfrac{k_{ii}[A][C]_T}{\frac{(k_{-i} + k_{ii})}{k_i} + [A]},$

which can be simplified to

(10) $v = \dfrac{V[A]}{K_A + [A]},$

where v is the rate of formation of product P; V ($= k_{ii}[C]_T$) is interpreted as the maximum reaction rate, which occurs when all the catalyst is bound as intermediate X; and $K_A = (k_{-i} + k_{ii})/k_i$ is called the half-saturation constant because its value is numerically equal to the concentration of A when $v = \frac{1}{2}V$.

Figure 5.6a shows how the reaction rate varies with [A] at constant $[C]_T$ and demonstrates that the reaction is a mixed-order process with two limiting cases. When $[A] >> K_A$, the reaction is zero order in [A], and $v = V$. When $[A] << K_A$, the equation simplifies to a first-order expression at constant $[C]_T$. Equation (10) is mathematically equivalent to the Michaelis-Menten equation for enzyme-catalyzed reactions and the Monod expression for microbial growth. Figure 5.6b shows how a linear transformation of eq. (10) is used to obtain the two parameters of the rate equation (K_A and V).
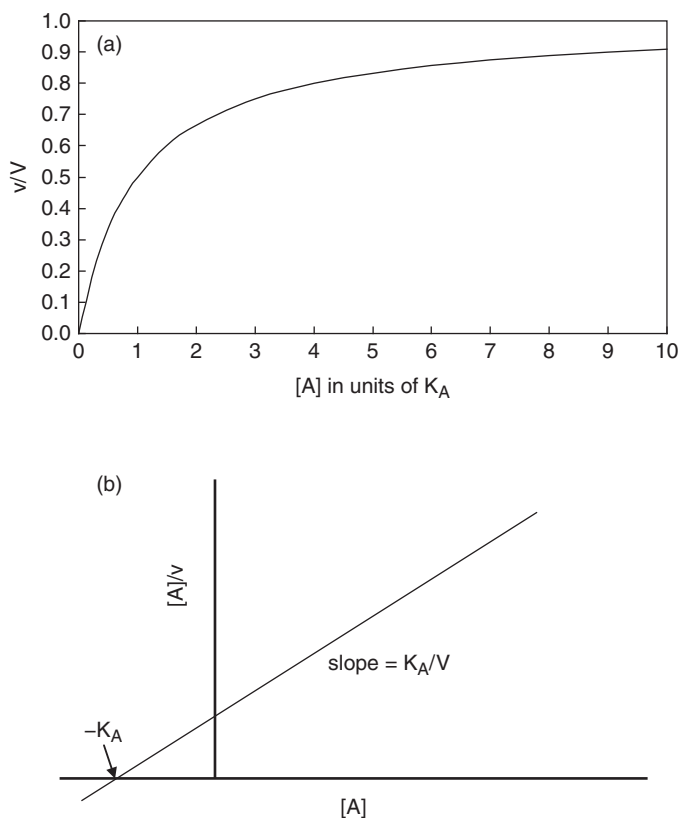
Figure 5.6 (a) Normalized reaction rate v/V for a reactant, A, with a recyclable catalyst; [A] is expressed in units of the "half-saturation constant," K_A. (b) Transformation of eq. (10) (box 5.3) yields a straight-line plot where K_A and V can be obtained from the slope and intercept.

water chemistry, the opposite, so-called "inverse problem"—fitting experimental data to a rate equation and then inferring a mechanism—is much more common and also much more difficult. It is fair to say that fit of data to a particular rate equation is not sufficient evidence that a reaction follows a particular mechanism, and additional information usually is needed to make inferences about reaction mechanisms. This topic is beyond the scope of this chapter and largely beyond the scope of this book, but a few examples are given in later chapters.

5.4 Chemical reactors and reactor theory

5.4.1 Introduction

The rate equations developed in preceding sections apply to closed systems, such as laboratory reactors, in which reactant concentrations are highest at the start of an experiment. Because terms for material input and outflow can be ignored, the rate equations include just a reaction term. Some aquatic systems like lakes can be treated as closed systems, particularly if the timescale for reaction is short compared to the timescale for water renewal, but material inflows and outflows often must be considered—i.e., the systems must be treated as "open." Engineered reactors like water and wastewater treatment plants usually are operated as continuous-flow open systems. Reactor analysis is a complicated topic—the subject of whole textbooks.[1,2] This section provides an introduction to the kinetics of two common kinds of open reactors: plug-flow and completely-mixed systems.

Three types of chemical reactors can be considered based on flow: (1) no-flow (batch), (2) continuous-flow, and (3) intermittent flow. Continuous-flow reactors may have variable or constant flow rates, but here we consider only systems with constant inflow/outflow rates. In terms of physical shape, most reactors can be classified as tubes or tanks. The former behave ideally as plug-flow reactors (*PFRs*), in which entering fluid moves as a discrete entity through the system. Tank reactors ideally are well mixed with uniform concentrations of reactants and products throughout their volume. Such systems usually are called *continuous-flow stirred tank reactors* (*CFSTRs*). Concentrations of reactants and products in the outflow of a CFSTR thus are the same as those throughout the reactor. If the CFSTR is effective as a reactor, reactant concentrations in the tank will be much lower than the inflow concentrations, and influent concentrations are diluted to effluent values essentially instantly. Reactors may be joined in series for flexibility in process control in engineered systems, and staged reactors also occur in nature. A series of river reaches may behave like a series of PFRs, and a chain of lakes may behave like a series of CFSTRs. A series of PFRs is equivalent to a single PFR with a volume equal to the total volume of the PFRs in series, and as the number of CFSTRs in series increases, the system approaches the characteristics of a PFR with a volume equal to the total of the CFSTRs.

5.4.2 Hydraulic and mass balance characteristics of reactors

Hydraulic residence time (*HRT* or τ_w) is an important characteristic of continuous-flow reactors; $\tau_w = V/Q_{in}$, where V is the reactor volume (m^3) and Q_{in} is the hydraulic inflow

rate (m^3 per time). The reciprocal of residence time, $1/\tau_w = Q/V = \rho_w$ ($time^{-1}$), is called the ***flushing coefficient***; ρ_w is equivalent to a first-order rate constant for fluid flow. Another useful variable for tank reactors is the ***areal hydraulic loading rate***, also called the "overflow rate," which is the fluid inflow rate divided by reactor surface area, $q_a = Q/A$. This is a design parameter for sedimentation tanks in water and wastewater treatment and also is used in CFSTR models of lakes.

The primary tool used by environmental engineers to analyze reactor behavior is the mass balance. For any reacting system the general mass balance is

$$\Delta S = F_{in} - F_{out} + R \tag{5.24}$$

Rate of accumulation = Rate of reactant – Rate of reactant + Rate of reaction
in system   inflow   outflow   in system

Mass balances are based on one of the most fundamental concepts in science: conservation of mass. To use Eq. 5.24 for calculations, each term must be expressed in a functional form. The general equation is simpler for some reactor types: input and output terms are not needed for batch reactors, and the accumulation term disappears for continuous-flow reactors at steady state. For CFSTRs, a single mass balance equation applies to the whole reactor, but reactant concentrations in PFRs depend on position in the reactor. In PFRs, a mass balance is written for an "element of volume," in which concentrations are considered homogeneous, and this is integrated over the entire reactor.

5.4.3 Rate equations for CFSTRs

CFSTRs are tanks stirred continuously to achieve uniform composition (Figure 5.7). This has two important implications. First, inflowing fluid has an equal probability of being anywhere in the reactor after entry, and all fluid elements have equal probabilities of leaving the reactor at any time. This leads to a broad distribution of
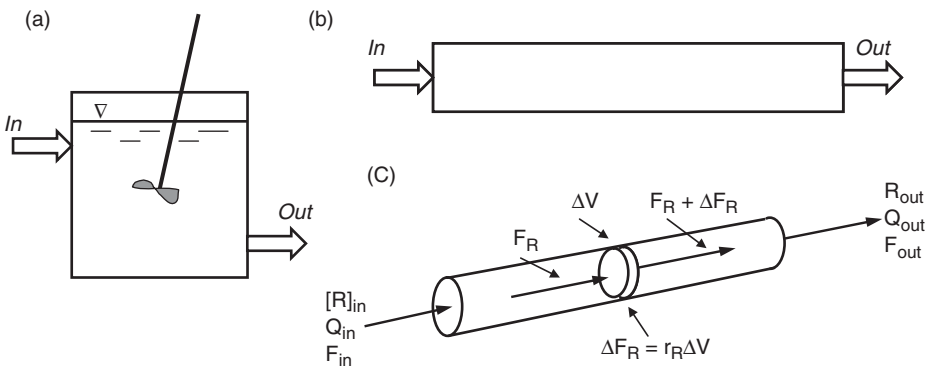
Figure 5.7 (a) Schematic diagram of a CFSTR; (b) schematic diagram of a PFR; (c) details of reactant and fluid flow in a PFR illustrating the concept of an element of volume, ΔV.

substance residence times in CFSTRs. The *average* residence time of a conservative substance is the same as that of the fluid, but only a small fraction of molecules is in the reactor for this time. Second, the outflow composition is the same as the reactor fluid, and this has implications regarding reaction rates in CFSTRs versus rates in PFRs.

The non-steady-state mass balance for reactant R in a CFSTR is essentially the general mass balance equation (Eq. 5.24), written for the entire reactor volume V (because the CFSTR composition is uniform):

$$\text{Accumulation} = \text{Inflow} - \text{Outflow} + \text{Reaction} \tag{5.25a}$$

$$V\frac{d[R]}{dt} = Q[R]_{in} - Q[R] + R_R V \tag{5.25b}$$

If the input is constant over time and if the reaction term is first order ($R_R = -k_1[R]$), we can write

$$\frac{d[R]}{dt} + \{k_1 + Q/V\}[R] = (Q/V)[R]_{in} \tag{5.26a}$$

or

$$\frac{d[R]}{dt} + \varphi[R] = \rho_w[R]_{in} \tag{5.26b}$$

where $\phi = k_1 + \rho_w$ is called the "total elimination" coefficient. ϕ is the sum of reaction plus hydraulic washout. Equation 5.26b is mathematically equivalent to the rate equation for a reversible first-order reaction (Eq. 5.19), which has a standard integral form (analogous to Eq. 5.22). The non-steady-state solution for reactant R in a CFSTR thus is

$$[R] = [R]_{out} = \frac{\rho_w}{\varphi}[R]_{in}\{1 - \exp(-\varphi t)\} + [R]_o\exp(-\varphi t) \tag{5.27a}$$

The steady-state solution for [R] in CFSTRs can be obtained from Eq. 5.27a by setting $t = \infty$, which eliminates all exponential terms (they approach zero):

$$[R] = \frac{\rho_w}{\varphi}[R]_{in} = \frac{1}{\tau_w(k_1 + \rho_w)}[R]_{in} = \frac{1}{1 + k_1\tau_w}[R]_{in} \tag{5.27b}$$

The steady-state solution also can be obtained from the mass balance equation by setting accumulation to zero and solving for [R]. As Eq. 5.27b shows, reaction rates in CFSTRs can be determined directly from influent and effluent concentrations if the reactor volume and flow rate are known. In addition, analytical solutions for CFSTRs are available for various simple input functions (e.g., step changes in input, instantaneous spikes of input) for substances that react by first-order processes.[2,8,9]

5.4.4 Kinetic equations for PFRs

In an ideal plug-flow (tube) reactor (Figure 5.7), fluid flows with no longitudinal dispersion and is perfectly mixed from the wall to center of the tube. For flow at constant rate, the mass balance for reactant R on an element of volume, ΔV, is

$$\text{Accumulation of R} = \text{Inflow rate of R} - \text{Outflow rate of R} + \text{Reaction of R,} \tag{5.28a}$$

$$\Delta V \frac{\partial [R]}{\partial t} = F_R - (F_R + \Delta F_R) + R_R \Delta V \tag{5.28b}$$

Mass inflow rate F_R is the product of flow rate Q times the inflow concentration of R: $Q[R]$. The change in flow of R across, ΔF_R, is $= Q\Delta[R]$, where $\Delta[R]$ is the change in $[R]$ from the inlet side to outlet side of the volume element. Finally, $\Delta V = A\Delta x$, where A is the cross-sectional area and Δx is the length of the volume element. Substituting these relationships into Eq. 5.28b and taking the limit as $\Delta x \rightarrow 0$ yields

$$\frac{\partial [R]}{\partial t} = -\frac{Q}{A}\frac{\partial [R]}{\partial x} + R_R. \tag{5.28c}$$

At steady state, accumulation is zero, and $\partial [R]/\partial t = 0$. Simplifying and rearranging Eq. 5.28c yields

$$\frac{A dx}{Q} = \frac{d[R]}{R_R}. \tag{5.28d}$$

Integrating over the reactor length gives an equation defining the residence time needed to obtain a given outflow concentration, $[R]_{out}$, that i.e., the residence time needed for a given conversion of R to product:

$$\frac{Ax}{Q} = \frac{V}{Q} = \tau_w = \int_{[R]_{in}}^{[R]_{out}} \frac{d[R]}{R_R} \tag{5.29a}$$

Use of Eq. 5.29a requires a functional relationship for R_R to solve the integral. When R_R is first order, $R_R = -k[R]$, and the equation integrates to

$$k\tau_w = -\ln\frac{[R]_{out}}{[R]_{in}} \tag{5.29b}$$

or

$$[R]_{out} = [R]_{in}\exp\{-k\tau_w\}, \tag{5.29c}$$

which is mathematically equivalent to the first-order kinetic equation for batch systems (Eq. 5.3a).

5.4.5 Comparative behavior of CFSTRs and PFRs

If the extent of reaction is large, [R] in a CFSTR is small compared with $[R]_{in}$. Reaction rates decrease over distance in a PFR as the reactant is consumed, but rates are constant in a CFSTR. For equal extents of reaction, the rate in a CFSTR is equal to the lowest rate (i.e., that at the outlet) in a comparable PFR. Therefore, to obtain the same extent of reaction, a CFSTR must be larger than a PFR. The extra volume needed can be decreased by putting several CFSTRs in series, and if many CFSTRs are in series, the system approaches plug flow behavior, with each CFSTR equivalent to an element of volume in a PFR. Nonetheless, CFSTRs have several advantages over PFRs. Because some fluid elements have short residence times in CFSTRs, $[R]_{out}$ responds rapidly to changes in inlet conditions, and CFSTRs are easier to control. The rate equations for CFSTRs are simpler than those of PFRs, and it is easier to analyze kinetic data from CFSTRs.

5.5 Effects of temperature on reaction rates

Four main factors affect reaction rates in aqueous systems by influencing rate constants: temperature, pressure, ionic strength, and pH. Of these, temperature is the most important, affecting nearly all chemical reactions even over small changes in temperature. In almost all cases, rates of chemical reactions increase with increasing temperature. Within physiological limits, biological processes increase with temperature, and physical processes such as diffusion also are temperature dependent. The sensitivity of process rates to temperature varies widely. Physical processes increase by a factor of ~1.1–1.4 for a 10°C rise; increases by factors of 1.5–3.0 are common for chemical and biological reactions over a 10°C rise.

5.5.1 The Arrhenius equation

The van't Hoff equation (Eq. 3.46) expresses the effect of temperature on chemical equilibria and relates K to T as a function of ΔH_r°. Based on the idea that K for a reaction is equal to the ratio of the rate constants for the forward and reverse steps, Arrhenius in 1889 proposed a similar equation for the relationship between rate constants and temperature:

$$\frac{d \ln k}{dT} = \frac{E_{act}}{RT^2} \qquad (5.30)$$

where E_{act}, the ***activation energy*** of a reaction, is considered to be the energy reactants must absorb to react. For Eq. 5.30 to be useful in predicting the effects of T on k, E_{act} must be constant (or a simple function of T). For most reactions E_{act} in fact is nearly constant over wide temperature ranges, and Eq. 5.30 integrates to

$$\ln k = \frac{E_{act}}{RT} + \ln A, \qquad (5.31a)$$

or
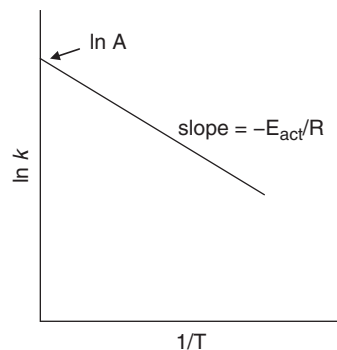
Figure 5.8 The slope of an Arrhenius plot of ln k versus 1/T yields E_{act}.

$$k = A \exp\left(\frac{-E_{act}}{RT}\right). \qquad (5.31b)$$

A is called the ***preexponential*** or ***frequency factor***. Between T_1 and T_2, equation 5.30 integrates to

$$\ln \frac{k_{T_2}}{k_{T_1}} = \frac{E_{act}(T_2 - T_1)}{RT_1 T_2}, \qquad (5.32)$$

which is similar to Eq. 3.47 for chemical equilibria. Equations 5.30–5.32 are forms of the Arrhenius equation. A plot of $\ln k$ versus 1/T gives a straight line if the Arrhenius equation is obeyed (Figure 5.8). This provides a convenient method to evaluate E_{act} and thus to estimate k at other temperatures.

Although the concept of E_{act} was developed to explain the effect of temperature on single-step chemical reactions, it is widely used to quantify temperature effects on multistep chemical reactions, as well as physical and biological processes. When applied to such processes, the term ***apparent activation energy*** should be used.

EXAMPLE 5.4 Use of the Arrhenius equation to estimate rate constants at different temperatures: Vogel and Reinhard[10] measured hydrolysis rate constants for 1,2-dibromopropane at elevated temperatures to obtain data in a reasonable time. The following first-order rate constants were measured at pH 7:

T (°C)	k_{obs} (s^{-1})
81	1.30×10^{-5}
61	0.21×10^{-5}

Estimate the rate constants and $t_{1/2}$ at 25°C.

Answer: From the integrated form of the Arrhenius equation (Eq. 5.32), we obtain

$$\ln \frac{1.3 \times 10^{-5}}{0.21 \times 10^{-5}} = \frac{E_{act}(354 - 334)}{8.314 \times 354 \times 334}, \text{ or } E_{act} = 89,600 \text{ J mol}^{-1} \ (89.6 \text{ kJ mol}^{-1}).$$

Substituting the calculated value of E_{act} back into Eq. 5.32 and solving for k at 25°C (298 K) yields

$$\ln \frac{1.3 \times 10^{-5}}{k_{25^\circ}} = \frac{89,600(354 - 298)}{8.314 \times 354 \times 298}, \text{ or } \mathbf{\mathit{k}_{25^\circ} = 4.26 \times 10^{-8} s^{-1}}.$$

From $t_{1/2} = 0.693/k_1$, we find $t_{1/2} = 0.693/4.26 \times 10^{-8} s^{-1}$ i.e., $\mathbf{t_{1/2} = 1.63 \times 10^7}$ **s or 188 days** at 25°C.

5.5.2 Physical interpretation of activation energy

Figure 5.9 illustrates the idea that reactants do not turn directly into products but first must become activated and form an intermediate "transition state." In exothermic reactions the reactants have higher enthalpies than the products, and the difference is the enthalpy of reaction, ΔH_r. The transition state has a higher energy than the reactants, thus requiring absorption of some energy (E_{act}). As noted in Box 5.2, this energy is obtained from kinetic energy when reactants collide (except in photochemical reactions). Once the transition state is formed, it proceeds spontaneously to form products and releases energy equal to $E_{act} + \Delta H_{for}$. The concept of microscopic reversibility, which states that reactions proceed by the same path in both directions, implies that the activation energy of the reverse reaction, $E_{act,rev}$, must be $E_{act,for} + \Delta H_{rev}$, and $\Delta H_{rev} = -\Delta H_{for}$.

ΔH can be positive (endothermic) or negative (exothermic), but activation energies of elementary reactions always are positive (or zero in some cases). If the measured E_{act} is negative, it can be assumed that the reaction has several steps and that the negative E_{act} is the sum of a negative ΔH for a rapid first step and a smaller positive E_{act} for a later step. Apparent activation energies for biochemical processes are positive only within physiological limits; denaturation of enzymes at higher temperatures causes rates to decrease, producing negative apparent E_{act} values above the temperature optimum.
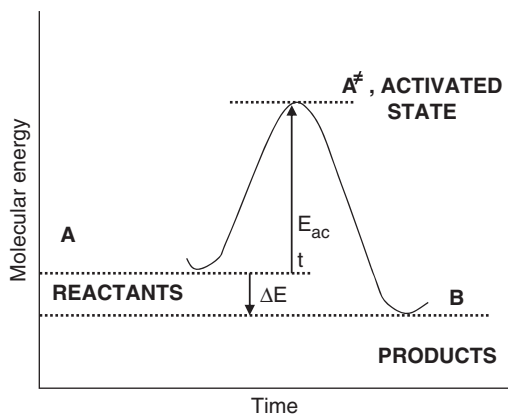
Figure 5.9 Time-energy course for an exergonic reaction, showing the concept of activation energy and activated (transition) state. The difference in energy states between reactant A and product B is shown here as the change in internal energy, ΔE, but this is closely related to the change in enthalpy, ΔH (see Chapter 3).

5.5.3 An empirical expression for temperature effects

A simple expression used by environmental engineers to express the effect of temperature on rates of biological processes is

$$k_{T_2} = k_{T_1} \Theta^{(T_2 - T_1)}, \tag{5.33}$$

where Θ is an empirical constant that typically has a value in the range 1.03 to 1.10; a value of 1.07 is equivalent to a doubling of k over a 10°C rise in temperature. Over narrow temperature limits, such as those of interest for most microbial processes in the environment, Eq. 5.33 closely approximates the Arrhenius equation. Θ can be estimated from k values at two temperatures: $\log \Theta = (\log k_{T_2} - \log k_{T_1})/(T_2 - T_1)$.

5.6 Advanced topic: how reactions occur—some fundamental kinetic theories

5.6.1 Collision theory for gas-phase reactions

As noted above, Arrhenius proposed that E_{act} is the minimum energy that reactants must attain for reaction. The exponential factor in his equation represents the fraction of molecules having this energy, and it is known as the Maxwell-Boltzmann distribution:

$$n/N = \exp(-E/RT), \tag{5.34}$$

where n is the number of molecules with energy $\geq$ E at temperature T and N is the total number of molecules in the system. When E (or E_{act}) is large, n/N is very small; increasing T at constant E increases the fraction of molecules with energy > E. Increasing T thus increases the fraction that can react and increases the rate of reaction.

Further development of kinetic theory came early in the twentieth century, when the preexponential factor in the Arrhenius equation was quantified as the frequency of collisions between gaseous reactants. Rates of bimolecular gas-phase reactions thus were expressed as

$$\text{Rate} = \begin{bmatrix} \text{Number of collisions of} \\ \text{reactants per unit time} \end{bmatrix} \times \begin{bmatrix} \text{Fraction of collisions whose} \\ \text{impact pairs have E} > E_{act} \end{bmatrix}. \tag{5.35}$$

Collision frequencies (Z_{AB}) of gases can be computed from the kinetic theory of gases, which is described in physical chemistry texts.[11] According to this theory, Z_{AB} depends on the square root of temperature, some physical constants, and the concentration, diameter, and mass of the colliding molecules. The latter two variables are constant for a given reaction. Thus, $Z_{AB} = (A')T^{1/2}[A][B]$, where Z_{AB} is the number of collisions per cm^3 per second between two kinds of molecules and A' is a constant for a given reaction. For gases at standard conditions, there are 10^{10} to 10^{11} collisions per molecule per second or a total of $\sim 10^{28}$ collisions cm^{-3} s^{-1}. Substituting the expression

for Z_{AB} and the Maxwell-Boltzmann term into Eq. 5.35 gives the following expression for rates of bimolecular gas-phase reactions:

$$\text{Rate} = A'T^{1/2} \exp(-E_{act}/RT)[A][B] \qquad (5.36)$$

Dividing both sides of Eq. 5.36 by the reactant concentrations gives an expression for the rate constant (in $M^{-1} s^{-1}$) based on collision theory of gases:

$$k = A'T^{1/2} \exp(-E_{act}/RT) \qquad (5.37)$$

The result of collision theory is an equation similar to the Arrhenius expression (Eq. 5.31b) except that it implies the Arrhenius factor A varies with temperature ($A = A'T^{1/2}$), while the Arrhenius equation assumes that A is constant. Plots of log k versus 1/T thus are not perfectly linear, but because the factor $T^{1/2}$ is small compared with the exponential term, deviations from linearity are small.

Collision theory yielded accurate predictions of reaction rates for a few simple gas-phase reactions, but measured rates for most reactions are lower than predicted values, in some cases by factors up to 10^6. Efforts to overcome this problem included addition of an empirical "steric factor" to account for the idea that reactants must have a spatial orientation at collision that allows energy and group transfers to take place. Steric factors of 10^{-1} to 10^{-2} are easily explained on this basis, but much larger factors are difficult to explain by solely steric effects. A major shortcoming of collision theory is that it considers reacting molecules as structureless hard spheres and assumes that only E_{act} and a collision frequency determine the rate of reaction. However, not all collisions with enough energy and the right spatial orientation lead to reactions between molecules because many other possibilities exist for energy dissipation.

The fact that many reactions are first order also posed difficulties for classical collision theory, which assumes that E_{act} comes from the kinetic energy of colliding reactants; first-order kinetics implies that the rate does not depend on collision frequency. As described in Box 5.2, Lindeman[7] explained this by postulating a two-step mechanism with a time lag between activation and reaction. Major advances have occurred in collision theory since it was developed. The RRK models (named after the last initials of their developers) derived in the 1920s[12] showed that the energy for the activated state could come from both the energy of collision and a molecule's internal energy by vibrational redistribution. A later, more sophisticated RRKM model[12] uses statistical mechanics to predict rates at which excited molecules, A^*, with sufficient energy to react are converted to $A^{\neq}$ (excited molecules with the proper configuration to react).

5.6.2 Diffusion and encounter of solutes

Classical collision theory does not apply to reactions in liquids because dissolved reactants are not as free to move around as gas molecules are. Instead, descriptions of reactions in solution must consider that reactants are surrounded by solvent molecules and that collisions between reactants require displacement of solvent molecules. The standard model for such reactions views reactant molecules existing in a low-energy "solvent cage" (Figure 5.10a). The reactants vibrate rapidly against the cage walls and every so often escape to adjacent positions. The frequency at which two reactant

(a)

(b)
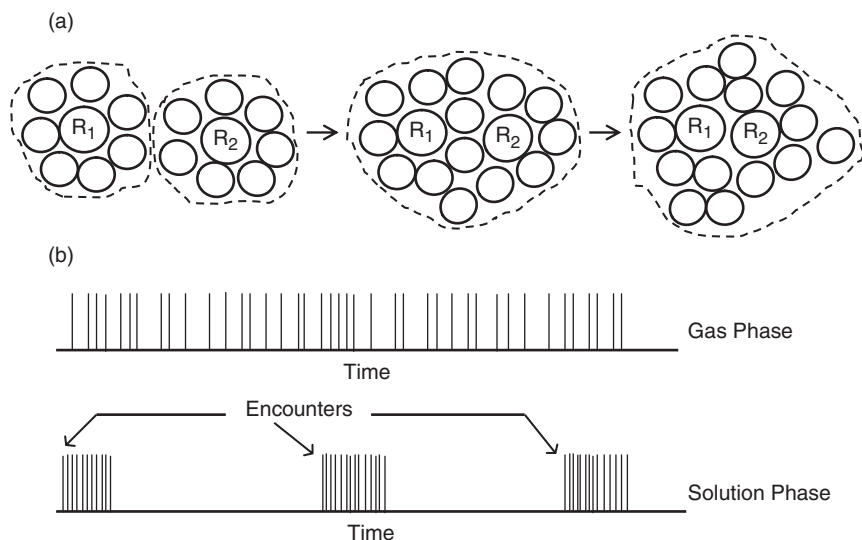
Figure 5.10 (a) Cage-encounter model brings together two reactants R_1 and R_2 from separate solvent cages through diffusion of solvent molecules in a series of elementary "jump steps"; (b) comparison of time course of reactant collisions in gas and liquid phases (timescale and number of collisions per encounter not intended to be exact). Adapted from Adamson.[11]

molecules come into the same solvent cage was derived[11] from principles of random molecular diffusion, which is assumed to occur by elementary jumps of distance $\lambda = 2r$, where r is the molecular radius. The Einstein-Smoluchowski equation defines diffusion coefficients in terms of λ:

$$D = \lambda^2/2\tau; \quad \text{or} \quad \tau = \lambda^2/2D \qquad (5.38a)$$

where D is the molecular diffusion coefficient ($cm^2 s^{-1}$) and τ is the average time between jumps. Equation 5.38a assumes a continuous medium. For a liquid with a semicrystalline structure such as water, a more accurate relationship is[11]

$$D = \lambda^2/6\tau; \quad \text{or} \quad \tau = \lambda^2/6D \qquad (5.38b)$$

The diffusion coefficient of water is $\sim 1 \times 10^{-5}$ $cm^2 s^{-1}$, and λ for water molecules is about 4×10^{-8} cm (4 Å). The length of time a water molecule spends in a given solvent cage, τ, thus is $\sim 2.5 \times 10^{-11}$ s. We can compare this to the vibrational frequency of molecules based on thermal energy:

$$\nu_f = \mathbf{k}T/h, \qquad (5.39)$$

where ν_f is frequency (s^{-1}), $\mathbf{k}$ is the Boltzmann constant (i.e., the gas constant per molecule), and h is Planck's constant. At 25°C, $\nu_f = 6.2 \times 10^{12}$ s^{-1}, and so the average

time between vibrations is $\sim 1.5 \times 10^{-13}$ s. The average water molecule thus vibrates about $2.5 \times 10^{-11}/1.5 \times 10^{-13}$, or 150 times in its solvent cage before jumping to a new position.

A similar analysis done for two solute reactants, A and B, leads to the following equation for the frequency at which molecules of reactant A and B encounter each other in the same solvent cage:

$$1/\tau = 25 r_{AB} D_{AB} n_B, \tag{5.40}$$

where r_{AB} is the sum of the radii of A and B, D_{AB} is their effective diffusion coefficient $(= D_A + D_B)$, and n_B is the mole fraction of reactant B in the solution. Derivation of Eq. 5.40[2,11] is based on several simplifying assumptions about the shapes and sizes of reactant molecules and the geometry of solvent cages for water. The number of encounters of A and B per cm^3 per second is given by Eq. 5.40 multiplied by the number of molecules of A per cm^3. If [A] and [B] are expressed in mol L^{-1}, we can multiply by $N_A/1000$ (N_A = Avogadro's number), and the encounter frequency becomes (M s^{-1}):

$$Z_{e,AB} = 2.5 \times 10^{-2} r_{AB} D_{AB} N_o [A][B] \tag{5.41}$$

Dividing both sides of Eq. 5.41 by [A][B] gives the frequency factor, A_e—the encounter frequency per unit concentration of A and B, which has units (M^{-1} s^{-1}) of a second-order rate constant. A_e is equivalent to the rate constant (k_D) for a diffusion-controlled reaction—one that occurs on every encounter. $Z_{e,AB}$, the rate of such a reaction, is equal to A_e when the reactant concentrations are 1 M. The value of A_e depends on the diffusion coefficients and radii of the reactants. For small molecules it is in the range of $\sim 10^9$ to 10^{10} M^{-1} s^{-1}. For example, if $D_A = D_B = 1 \times 10^{-5}$ cm^2 s^{-1} and $r_{AB} = 4 \times 10^{-8}$ cm, then $A_e = 1.2 \times 10^{10}$ M^{-1} s^{-1}. A more rigorous derivation of k_D based on diffusion toward the surface of a sphere around the reacting molecule leads to an equation[12] that gives values about half those of Eq. 5.41. Given the assumptions involved in these derivations, the discrepancies between the two equations must be considered negligible.

Several difficulties arise in applying the above models to encounter rates of ions and molecules in water. First, they ignore long-range electrostatic interactions between reactants. Second, they assume that each reactant behaves as a stationary sink around which a concentration gradient of the other reactant is established; however, in reality all molecules are moving simultaneously. Third, they treat the solvent as continuous and unstructured, but aqueous solutions are neither. Modifications to overcome these assumptions result in much more complicated models. As described below, coulombic interactions between ions can be accounted for, but quantifying forces between nonionic reactants is difficult. The most serious difficulty in improving diffusion-encounter models is in describing the effects of solvent structure on reacting molecules as they approach each other.

When the electrostatic forces between reacting ions are taken into account, Eq. 5.41 becomes[12]

$$k_D = \frac{-4\pi D_{AB} z_A z_B r_o N_o}{1000[1 - \exp(z_A z_B r_o/R)]}, \tag{5.42}$$

where r_o is an electrostatic factor with units of length; $r_o = e^2/DkT = 7.1 \times 10^{-8}$ cm at 25°C. Values of k_D computed by Eq. 5.42 for diffusion-limited reactions between oppositely charged ions are in good agreement with observed rate constants. For example, for acid-recombination reactions ($H^+ + B^- \rightarrow HB$),[12]

Base	$k_{D,obs}$, M^{-1} s^{-1}	$k_{D,calc}$, M^{-1} s^{-1}
SO_4^{2-}	10×10^{10}	6.5×10^{10}
HS^-	7.5×10^{10}	9.0×10^{10}
NH_3	4.3×10^{10}	4.0×10^{10}

Note that NH_3 is not an ion, but it is a highly polar molecule. The diffusion-encounter model for solutions produces patterns of reactant collisions different from those of the collision model for gas-phase reactions. If colliding gas-phase reactants do not react, they immediately separate and move on independently. The frequency factor for gas-phase collisions is about 10^{11} M^{-1} s^{-1}. For the same concentrations, reactants in solution encounter each other less frequently (10^9–10^{10} M^{-1} s^{-1}; Figure 5.10b), but because of the solvent cage effect, they remain together as an "encounter complex" for $\sim 2.5 \times 10^{-11}$ s and collide with each other ~ 150 times. When E_{act} is high, the probability of reaction on any given collision is very small, and the difference in collision patterns between gas- and solution-phase reactions does not affect reaction rates. However, when activation energies are low or zero, reaction occurs after one or a few collisions and every encounter leads to reaction. Such reactions are *diffusion controlled*—their rates are limited by rates of encounter. Nonetheless, rates of diffusion-controlled encounters are temperature dependent, with $E_{act} = 12$–17 kJ/mol, corresponding to the apparent E_{act} for viscous flow. The existence of solvent cages has consequences for free radicals formed by photoactivation in solution. Because radicals are highly reactive and have low activation energies for recombination, a pair formed in a solvent cage may recombine before the radicals can diffuse apart.

The encounter-reaction process in solution essentially is a two-step sequence with two rate constants: k_D for diffusion encounter and k_c for chemical reaction. When $k_D >> k_c$, reaction controls the process, and the overall rate constant (k_r) approaches k_c. Conversely, when $k_c >> k_D$, diffusion controls and k_r approaches k_D. When k_D and k_c are of comparable size, both must be considered. In analogy to electrical resistances in series, the total resistance for the reaction is the sum of the resistances for individual steps. Resistance is the inverse of conductance, and rate constants are analogous to conductivities; thus,

$$\frac{1}{k_r} = \frac{1}{k_D} + \frac{1}{k_c} \quad \text{or} \quad k_r = \frac{k_D k_c}{k_D + k_c}. \tag{5.43}$$

Substitution of Eq. 5.42 into 5.43 yields an equation for the overall rate constant of rapid ionic reactions.

5.6.3 Transition state and activated complex theory

Deficiencies in collision theory led to the development of more fundamental theories of reaction kinetics. *Transition state theory* (TST) was developed in the mid-1930s by

Eyring and colleagues,[13-15] who used quantum and statistical mechanics to quantify energy states of reactants and intermediates. They considered the "transition state" as a very short-lived but real intermediate with definable properties in the process of converting reactants to products. The transition state often is described as the *reactant configuration of no return*; that is, once reactants reach this configuration, they proceed to form products. It is an artificial concept in that reactants are continuously changing rather than static. Even aside from this problem, transition states are so short-lived that problems arise in assigning equilibrium properties to it; the lifetime of transition states is in the subpicosecond ($< 10^{-12}$ s) range. Nonetheless, ultra-short-pulse laser techniques have enabled transition state configurations to be observed by "femtosecond transition-state spectroscopy," which has provided experimental verification of theoretical calculations on transition states.[16]

The nature of the transition state often is described in terms of potential energy surfaces (PES) for reactions. The reactants and products exist at the bottom of "potential energy wells," meaning that they are stable species, and the potential energy increases as reactants approach each other. An infinite number of approach pathways exist, but the one with the smallest energy increase is favored. The maximum position on this pathway is at the "saddle point" of the PES. This point defines the transition state, and at it the surface is at a maximum in the direction of the reaction but increases in all other directions.

Statistical mechanics quantifies the energy states of molecules and defines the probability that a molecule is in a given energy state (including the transition state). Until recently, exact (*ab initio*) calculations of the potential energies of reactants along possible reaction pathways were feasible only for very simple molecules such as H_2. The expansion of computing power over the past few decades and development of efficient algorithms now allows estimation of the PES for many reactions of environmental interest by numerically solving the Schrodinger wave equation using certain assumptions to constrain the problem and solution space. Several programs that run on personal computers (e.g., Gaussian[17] and Schrodinger's Jaguar[18]) are available for such calculations. A critical assumption is that only atoms within a few atoms' distance of the reaction center affect the potential energy of the transition state. This simplifies the problem to computations involving a reasonable number of atoms and allows the analysis of transition state conditions for reactions of environmental interest. For example, Lasaga and coworkers[19] calculated the shape and interatomic distances of transition states for water- and ion-induced dissolution of quartz.

An easy-to-understand approach to TST based on thermodynamic formalisms[11] is presented below. Because some simplifying assumptions in this approach violate the tenets of TST, it is given the separate name ***activated complex theory*** (ACT). Building on Lindeman's model, we can describe the transition state $A^{\neq}$ or $AB^{\neq}$ as a species "in equilibrium" with the reactants; e.g., for bimolecular reactions,

$$A + B \rightleftharpoons AB^{\neq} \quad K^{\neq} = \frac{[AB^{\neq}]}{[A][B]}, \tag{5.44a}$$
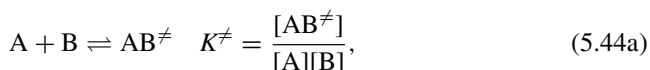
or

$$[AB^{\neq}] = K^{\neq}[A][B]. \tag{5.44b}$$

The rate of reaction is controlled by dissociation of the intermediate to form products and thus is proportional to its concentration and its frequency of dissociation to products, $AB^{\neq} \rightarrow$ products:

$$\text{Forward rate} = \left[\begin{array}{c} \text{Concentration of} \\ \text{activated complex} \end{array} \right] \times \left[\begin{array}{c} \text{Frequency of its dis-} \\ \text{sociation to product} \end{array} \right] \quad (5.45)$$

The activated complex (or transition state) breaks down to products when the potential energy of its reacting bond becomes equal to the bond's vibrational energy. $AB^{\neq}$ is not just the energized molecule of collision theory (although both have the same activation energy) but a special species in which one "vibrational degree of freedom" continues movement along the reaction coordinate converting $AB^{\neq}$ into products with the release of the energy of the activated state (E_{act}) plus the energy of reaction.

The potential and vibrational energies of the reacting bond are quantified as follows. Vibrational energy is related to vibrational frequency by Planck's law: $E_{vib} = h\nu$, where h is Planck's constant (6.62×10^{-27} erg s) and ν is frequency (s^{-1}). The bond being broken in the activated complex is weak compared with the ground state molecule, and by definition it will break on the next vibration, without further energy input. Although thermodynamics does not allow us to calculate the energy of the (weakened) bond exactly, it at least must have thermal energy. Thus, $E_{pot} \approx \mathbf{k}T$, where $\mathbf{k}$ is the Boltzmann constant (gas constant per molecule). When $E_{vib} = E_{pot}$, $h\nu = \mathbf{k}T$, or $\nu_f = \mathbf{k}T/h$ (cf. Eq. 5.39); i.e., ν_f is the dissociation frequency of the activated complex (transition state) to products. At 25°C, $\mathbf{k}T/h = 6.2 \times 10^{12}$ s^{-1}, and ν_f is called the fundamental frequency. According to ACT, ν_f is the same for all reactions (except some electron transfer reactions). The reciprocal of ν_f, $\sim 1.6 \times 10^{-13}$ s, defines the lifetime of the transition state and also is the time period for one molecular vibration at 25°C.

The concentration of transition state complex $AB^{\neq}$ is given by Eq. 5.39b, and its dissociation frequency is given by ν_f. From these we can parameterize the word equation for the ACT-derived rate (Eq. 5.45):

$$\text{Rate} = [AB^{\neq}](\nu_f) = K^{\neq}[A][B](\mathbf{k}T/h) \quad (5.46)$$

Given that the conventional second-order rate equation is $-d[A]/dt = k[A][B]$, it is apparent that

$$k = \frac{\text{Rate}}{[A][B]} = \frac{\mathbf{k}T}{h}K^{\neq} \quad (5.47)$$

The above derivation is not rigorous in several respects.[11] First, for several reasons, $K^{\neq}$ is not a true (thermodynamic) equilibrium constant for the reaction $A + B \rightleftharpoons AB^{\neq}$. Second, Eq. 5.46 is an approximation because $E_{pot} = \mathbf{k}T$ is only a minimal estimate, and consequently, ν_f is not really a *universal frequency* of activated complex decomposition. Finally, a correction factor, κ, called the "transmission coefficient," should be added to Eq. 5.47 ($k = \kappa\nu K^{\neq}$) to account for processes not covered by the theory. κ ranges from ~ 0.1 to 1 for solution-phase reactions at ambient temperatures.[20] Equation 5.47 is derived more rigorously using statistical mechanics.[15]

The usefulness of Eq. 5.47, the fundamental relationship of ACT, is limited by the fact that $K^{\neq}$ cannot be measured by conventional equilibrium methods because $AB^{\neq}$ is so ephemeral. From Chapter 3, however, we know that $\Delta G^{\circ} = -RT \ln K$ (or $K = \exp(-\Delta G^{\circ}/RT)$) and $\Delta G^{\circ} = \Delta H^{\circ} - T\Delta S^{\circ}$. Substituting the latter relationship for ΔG° into the exponential expression for K leads to

$$K = \exp\left(\frac{\Delta S^{\circ}}{R}\right) \exp\left(\frac{-\Delta H^{\circ}}{RT}\right). \tag{5.48}$$

Identifying K with $K^{\neq}$, changing the corresponding thermodynamic functions, and substituting into Eq. 5.47 yields

$$k = \frac{kT}{h} \exp\left(\frac{-\Delta G^{\neq}}{RT}\right) = \frac{kT}{h} \exp\left(\frac{\Delta S^{\neq}}{R}\right) \exp\left(\frac{-\Delta H^{\neq}}{RT}\right), \tag{5.49}$$

where $\Delta G^{\neq}$, $\Delta S^{\neq}$, and $\Delta H^{\neq}$, the free energy, entropy, and enthalpy of activation, respectively, represent the difference in each thermodynamic variable between the transition state and the reactants, when all are in their standard states (at unit concentration). It is apparent from Eq. 5.49 that k for a reaction is related exponentially to $\Delta G^{\neq}$. The larger $\Delta G^{\neq}$ is, the slower the reaction will be.

The experimental activation energy, E_{act}, is related to the internal energy of activation $\Delta E^{\neq}$ and thus to the enthalpy of activation $\Delta H^{\neq}$. For solution-phase reactions, $\Delta E^{\neq} \approx \Delta H^{\neq}$, and it can be shown[2,14] that

$$E_{act} = \Delta H^{\neq} + RT. \tag{5.50}$$

Substituting this relationship into Eq. 5.49 and simplifying leads to the following expression for rate constants of solution-phase reactions:

$$k = \left(\frac{ekT}{h}\right) \exp\left(\frac{\Delta S^{\neq}}{R}\right) \exp\left(\frac{-E_{act}}{RT}\right), \tag{5.51}$$

where e is the natural number (2.718). The similarity between Eq. 5.51 and the Arrhenius equation is apparent. Moreover, it is clear that factor A in the latter equation is related to the frequency of dissociation of the transition state and the exponential of the activation entropy: $A = (ekT/h)\exp(-\Delta S^{\neq}/R)$. $\Delta S^{\neq}$ is analogous to the concept of ΔS° for chemical equilibria—it is a measure of disorder in the transition state compared with the reactant state.

EXAMPLE 5.5 Calculating values of the kinetic activation parameters for the hydration of CO₂: The primary hydration reaction for CO_2 at circumneutral pH is $CO_{2(aq)} + H_2O \rightarrow H_2CO_{3(aq)}$. Given $k_h = 3.7 \times 10^{-2}$ s^{-1} at 25°C and 3.66×10^{-3} s^{-1} at 5°C,[21] compute the values of E_{act}, the preexponential factor, A, $\Delta G^{\neq}$, $\Delta H^{\neq}$, and $\Delta S^{\neq}$.

Although the reaction is bimolecular, the rate constant is reported as a *pseudo*-first-order value because reactant H_2O is the solvent. It is necessary to convert these values to second-order rate constants. This is done by dividing k_h by the concentration of water, 55.5 M, because $k_h = k_2[H_2O]$. Thus, $k_2 = 6.67 \times 10^{-4}$M^{-1} s^{-1} at 25°C and

$6.60 \times 10^{-5} M^{-1} s^{-1}$ at 5°C. We assume that the transmission coefficient $\kappa = 1$ and that $\nu_f = kT/h = 6.2 \times 10^{12} s^{-1}$ applies to the reaction. All the requested parameters can be computed directly from equations presented in previous sections.

From Eq. 5.32,

$$\mathbf{E_{act}} = RT_1 T_2 \times \ln\{k_{T_2}/k_{T_1}\}/(T_2 - T_1)$$
$$= 8.31(278)(298)\{\ln(6.67 \times 10^{-4}/6.60 \times 10^{-5})\}/20 = \mathbf{79{,}600 \ J/mol}.$$

From Eq. 5.31b,

$$\mathbf{A} = k_2/\exp(-E_{act}/RT) = 6.67 \times 10^{-4}/\{\exp(-79{,}600/8.31 \times 298)\}$$
$$= \mathbf{6.13 \times 10^{10} M^{-1} s^{-1}}.$$

From Eq. 5.49,

$$k_2 = (\mathbf{k}T/h)\exp(-\Delta G^{\neq}/RT), \ \text{or} \ \Delta G^{\neq}_{25C} = RT\{ln(\mathbf{k}T/h) - \ln k_2\},$$
$$\Delta G^{\neq}_{25\,C} = 8.31(298)\{\ln(6.2 \times 10^{12}) - \ln(6.67 \times 10^{-4})\}$$
$$= 91{,}050 \ J/mol \ \text{or} \ \mathbf{91.05 \ kJ/mol}.$$

From Eq. 5.50,

$$\Delta \mathbf{H}^{\neq} = E_{act} - RT = 79{,}600 - 8.31(298) = 77{,}150 \ J/mol \ \text{or} \ \mathbf{77.15 \ kJ/mol}.$$

From Eq. 5.51,

$$k_2 = (\mathbf{e}\mathbf{k}T/h)\exp(\Delta S^{\neq}/R)\exp(-E_{act}/RT), \ \text{or}$$
$$\Delta S^{\neq} = E_{act}/T + R\{\ln k_2 - \ln(e) - \ln(\mathbf{k}T/h)\},$$
$$\Delta \mathbf{S}^{\neq} = 79{,}600/298 + 8.31\{\ln(6.67 \times 10^{-4}) - 1 - \ln(6.2 \times 10^{12})\}$$
$$= \mathbf{-46.7 \ J \ K^{-1} mol^{-1}}.$$

Alternatively, once $\Delta G^{\neq}$ and $\Delta H^{\neq}$ are known at a given temperature, one can compute $\Delta S^{\neq}$ from the thermodynamic relationship $\Delta G^{\neq} = \Delta H^{\neq} - T\Delta S^{\neq}$, or $\Delta S^{\neq} = (\Delta H^{\neq} - \Delta G^{\neq})/T = (77{,}150 - 91{,}050)/298 = \mathbf{-46.7 \ J \ K^{-1} \ mol^{-1}}$.

Comments on calculated values

The value of k_2 is much smaller (by a factor of about 5×10^{-14}) than k values for diffusion-controlled reactions. The value of A is near the "normal" range $(10^{11} M^{-1} s^{-1})$, as expected for a reaction between uncharged reactants. The negative value of $\Delta S^{\neq}$ suggests that the transition state is more ordered than the reactant state; this probably reflects the coming together of the two reactants to form the transition state.

One might think that $\Delta S^{\neq}$ is always negative in bimolecular reactions because bringing two reactants together to form an activated complex decreases the randomness of the system. This ignores, however, the contributions of solvent structure on entropy. Although $\Delta S^{\neq}$ often is negative for associative reactions, changes in solvent structure often are large enough to produce positive values of $\Delta S^{\neq}$ for reactions of ions and polar molecules. If ions of opposite sign react, the activated complex has a lower charge density than either of the reactants, which tends to loosen waters of hydration surrounding the activated complex, increasing entropy. Conversely, if the reacting ions have the same sign, the activated complex has a higher charge density than the reactants, which causes electrostriction (see Figure 1.7) and tighter binding of water molecules in the hydration sphere. The net effect is a decrease in entropy. Similarly, formation of transition states that are more polar than the reactants decreases $\Delta S^{\neq}$, and formation of less polar complexes increases $\Delta S^{\neq}$. Hydrolysis of esters produces more polar transition states; such reactions have $\Delta S^{\neq} < 0$ and thus low values of A. In general, effects on $\Delta S^{\neq}$ are lower for polar molecules than for ions, and because transition states are intermediates between reactants and products, $\Delta S^{\neq}$ typically is less than $\Delta S°$ for reactions. The ratio $\Delta S^{\neq}/\Delta S°$ can be used to estimate of the extent to which transition states resemble reactants or products.

5.7   Other physical factors affecting rate constants

5.7.1 Advanced topic: pressure

The effects of pressure on reaction rates are not important for freshwater systems. Even at great depths in the oceans effects on rate constants are fairly small. Pressure effects are of interest, however, insofar as they provide useful information for understanding reaction mechanisms, and consequently, we examine pressure effects briefly.

Analogous to the effects of P on chemical equilibria, the effects of P on reaction rates are exerted through a variable called the volume of activation, $\Delta V^{\neq}$, which is simply the difference in molar volume of the transition state compared to the reactant state. In general,

$$\left(\frac{\partial \ln k}{\partial P} \right)_{T} = \frac{-\Delta V^{\neq}}{RT}. \tag{5.52}$$

Tangents to curves of $\ln k$ versus P have slopes of $-\Delta V^{\neq}/RT$ at any given value of P, and if the curves are straight lines, we can infer that $\Delta V^{\neq}$ is constant with P. In that case, Eq. 5.52 integrates to

$$\ln \frac{k_{P}}{k_{1\ atm}} = \frac{\Delta V^{\neq}(P-1)}{RT}. \tag{5.53}$$

Plots of $\ln k$ versus P usually are not linear, however, meaning that $\Delta V^{\neq}$ is not constant with P. This implies that the reactants and transition states have different molar compressibilities. Values of $\Delta V^{\neq}$ are reported to range between -20 and $+20\ cm^3\ mol^{-1}$, which allows us to estimate the range of $k_P/k_{1\ atm}$ at various pressures.[2]

Figure 5.11   Crater Lake, Oregon, the deepest lake in the United States, early June 1978. Photo by the author (P.L.B.). (See color insert at end of book for a color version of this figure.)

For example, at the average depth of the world's oceans ($\sim$4000 m), P = $\sim$400 atm, and $k_P/k_{1\text{ atm}}$ ranges from 0.70 to 1.42 for $\Delta V^{\neq}$ ranging from -20 to $+20$ cm^3 mol^{-1}. For the deepest water bodies in North America (Crater Lake, Oregon (Figure 5.11) and Great Slave Lake, Canada; z_{max} = 610 m, P_{max} = 61 atm for both), the range is 0.95–1.05, that is, roughly a 5% effect, which is negligible compared with the effects of other environmental factors on reaction rates.

Values of $\Delta V^{\neq}$ for a reaction are the result of two processes: (1) changes in reactant volumes as the transition state is formed ($\Delta V_{str}^{\neq}$) and (2) changes in the solvent ($\Delta V_{solv}^{\neq}$) resulting from conversion of reactants to the transition state. If a bond is being broken, $\Delta V_{str}^{\neq}$ generally is positive; if two reactants are coming together to form the transition state, $\Delta V_{str}^{\neq}$ is negative. A correlation was found between $\Delta V_{solv}^{\neq}$ and $\Delta S^{\neq}$ by Laidler and Chen.[22] Factors that lead to tighter binding of solvent molecules by transition states (compared with the reactants) result in negative $\Delta V_{solv}^{\neq}$ and $\Delta S^{\neq}$, and such reactions have abnormally low frequency factors (A $<<$ 10^{11} M^{-1} s^{-1} for bimolecular reactions). Conversely, factors that lead to looser binding of solvent molecules by transition states result in positive $\Delta V_{solv}^{\neq}$ and $\Delta S^{\neq}$ and abnormally high values of A ($>>$ 10^{11} M^{-1} s^{-1}). Finally, reactions with negative $\Delta V^{\neq}$ and $\Delta S^{\neq}$ tend to be slow (because A is small), but k increases with P. In contrast, reactions with positive $\Delta V^{\neq}$ and $\Delta S^{\neq}$ tend to be rapid (because A is large), and k decreases with P.

5.7.2 Effect of ionic strength on rate constants

For nonionic reactions, shifts in ionic strength (I) have negligible effects on reaction rates. For ionic reactions, log k varies with ionic strength as a result of variations in ion

activity with I. The Brønsted-Bjerrum equation expresses this quantitatively:

$$\log k_2 = \log k_2^o + 1.02 Z_A Z_B \sqrt{I} \qquad (5.54a)$$

This form of the equation is based on the Debye-Hückel limiting law (Chapter 3), which applies to $I < 0.005$. With the Guntelberg form of the Debye-Hückel equation the equation becomes

$$\log k_2 = \log k_2^o + 1.02 Z_A Z_B \frac{\sqrt{I}}{1 + \sqrt{I}} \qquad (5.54b)$$

Equations 5.54a and 5.54b predict that plots of $\log k_2$ versus $I^{1/2}$ (or $I^{1/2}/(1 + I^{1/2})$) are linear with slopes nearly equal to the product of reactant ionic charges, $Z_A Z_B$ (Figure 5.12). If both ions are positive or negative, the product is positive and k_2 increases with I. If the ionic charges have opposite signs, the product is negative and k_2 decreases with I. Rate constants in Figure 5.12 are normalized to $k_2°$, the value at $I = 0$, so that they plot on the same scale, but reactions with negative slopes have much higher k values than those with positive slopes—because electrostatic attraction accelerates collisions for oppositely charged reactants and electrostatic repulsion inhibits collisions for like-charged reactants. The equations have a simple physical interpretation: increasing ionic strength shields ionic reactants, thus decreasing the distance over which their charges exert coulombic attraction or repulsion. Many studies (e.g., Weston and Schwarz[12]) have verified that ionic reactions fit the Brønsted-Bjerrum relationship and plots like Figure 5.12.

Reactions between ions and solid surfaces also are affected by I. The electric double layer surrounding solid particles is compressed as I increases. This affects transport of
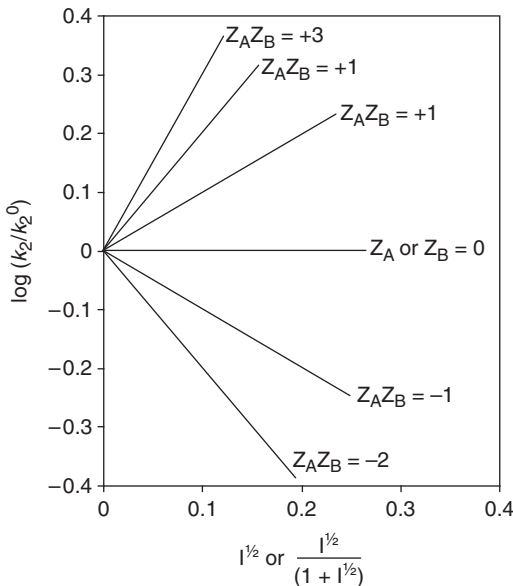
Figure 5.12 Brønsted-Bjerrum plot showing effect of ionic strength on rate constants for bimolecular reactions of two ions. Slopes of the lines for $\log(k_2/k_2^0)$, where k_2^0 is the rate constant at $I = 0$, are approximately equal to the product of the charges on the reactant ions. If one of the reactants is nonionic, the slope is approximately zero.

ions to and from the surface, allowing like-charged ions and particles to approach more closely before being influenced by electrostatic repulsion.

5.7.3 pH

Effects of pH are twofold. First, H^+ and OH^-, as well as Brønsted acids, HB, and bases, B (see Chapter 8), act as catalysts for many reactions. In general, catalysts are substances that participate in (and accelerate) reactions but are not consumed. Catalysis by H^+ and OH^- is called ***specific acid*** and ***specific base catalysis***, respectively, and catalysis by Brønsted acids and bases is called ***general acid/base catalysis***. A large number of possibilities involving combinations of these four processes exist, giving rise to a variety of patterns by which rate constants for catalyzed reactions change with pH; these are described elsewhere.[2] Here we consider the effects of H^+ and/or OH^- catalysis on the nature of the rate equation for a few simple cases. The hydrolysis of esters is catalyzed by H^+, and the rate equation under varying acidic conditions is written as

$$-d[E]/dt = k_{h,H^+}[E][H^+], \qquad (5.55a)$$

where E stands for some ester (which can be hydrolyzed to its component carboxylic acid and alcohol). In a given experiment, one can control the pH by adding a buffer, in which case $[H^+]$ is constant and can be embedded into the rate coefficient, $k'_h = k_h[H^+]$, making the reaction pseudo-first order.

Under circumneutral pH conditions, the uncatalyzed hydrolysis reaction may occur at a significant rate, and at higher (alkaline) pH, the hydrolysis may be catalyzed by OH^-. This leads to the possibility of a multiterm rate equation:

$$-d[E]/dt = k_{h,H^+}[E][H^+] + k_{h,H_2O}[E] + k_{h,OH^-}[E][OH^-] \qquad (5.55b)$$

At low pH, the concentration of OH^- is so low that the third term in Eq. 5.55b does not contribute significantly to the overall rate of reaction, and the magnitude of k_{h,H_2O} generally is small compared with k_{h,H^+} and k_{h,OH^-}, so the uncatalyzed term becomes important (if at all) only when both H^+ and OH^- are low in concentration (i.e., at circumneutral pH). Consequently, in many cases a plot of the observed rate versus pH may exhibit three separate regions, as illustrated in Figure 5.13: an H^+-catalyzed region, an uncatalyzed region, and an OH^--catalyzed region.

The second reason why pH affects rates of chemical reactions is that the acid-base forms (degree of deprotonation) for some substances have different inherent reactivities. In general, autoxidation (i.e., oxidation by O_2) of reduced inorganic substances is pH dependent because the more deprotonated form(s) of the substance being oxidized are more reactive. For example, H_2S has a smaller rate constant than HS^- for oxidation by O_2. The autoxidation of Fe^{II} and Mn^{II} are highly pH dependent because the free cations are unreactive toward O_2 compared with the metal hydroxide complexes MOH^+ and especially $M(OH)_2^0$ (Chapter 15). Similarly, oxidation of bisulfite (HSO_3^-) by ozone is much slower than oxidation of sulfite (SO_3^{2-}) by O_3.
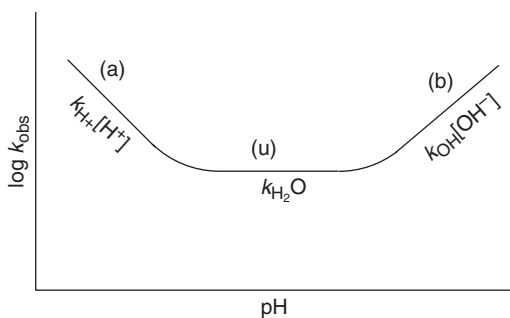
Figure 5.13 Schematic diagram of the effect of pH on the observed rate constant for a reaction catalyzed by H^+ in region (a), by OH^- in region (b), and occurring by an uncatalyzed reaction in region (u).

5.8   Linear free energy relationships

A universal relationship does not exist between the thermodynamics of reactions and the rates at which they occur. This is understandable from TST, which states that reaction rates are controlled by the energy difference between reactants and a transition state rather than by the energy difference between reactants and products. Nonetheless, reaction rates for many *sets of related compounds* are correlated with corresponding data on the energetics of related reactions. Such relationships are called **linear free energy relationships** (**LFERs**) because they are linear correlations between logarithms of rate constants (k_i) and logarithms of equilibrium constants (K_i) for reactions of the compounds.[*] From TST (Eq. 5.49), we know that $\ln k_i$ is linearly related to $\Delta G^{\neq}$, and from thermodynamics (Eq. 3.27) we know that $\ln K_i$ is linearly related to ΔG°_i. If two reactions have an LFER, we can write[2]

$$\ln k_2 - \ln k_1 = \alpha\{\ln K_2 - \ln K_1\},$$

or

$$\{-\Delta G_2^{\neq} + \Delta G_1^{\neq}\}/RT = \alpha\{-\Delta G_2^{\circ} + \Delta G_1^{\circ}\}/RT, \tag{5.56}$$

where α is a constant of proportionality between the kinetic and equilibrium terms. For sets of reactants and reactions having LFERs, the free energy of activation thus is a constant fraction of the free energy of reaction for a series of reactants, $\Delta G_i^{\neq}/\Delta G^{\circ}_i = \alpha$. The basis for this can be understood qualitatively from potential energy diagrams, which show that if the energy curves for related reactions have similar shapes (which is reasonable), then geometry dictates that the change in E_{act} must be proportional to the change in overall reaction energetics: $\Delta(\Delta E^{\neq}) \propto \Delta(\Delta E^{\circ})$.[2]

For a series of related reactants undergoing the same reaction, we can generalize Eq. 5.56 to

$$\ln k_i = \alpha \ln K_i + C, \ \text{ or } \ \Delta G_i^{\neq} = \alpha\Delta G^{\circ}_i + C, \tag{5.57a}$$

[*]Correlations of equilibrium constants for related sets of compounds also are LFERs; e.g., stability constants for metal ion complexes with different ligands often are correlated with constants of another metal for the same ligands.

where subscript i refers to the ith reactant in a series of related compounds, and constant C is a function of $\Delta G^{\neq}$ and ΔG° for a reference compound. Linear relationships may apply even if the reactions on the kinetic and equilibrium sides of the equation are different (for examples, see Chapter 19). For a series of i reactants and related reactions j and k,

$$\ln k_{ij} = \alpha \ln K_{ik} + C, \text{ or } \Delta G_{ij}^{\neq} = \alpha \Delta G_{ik}^{\circ} + C. \tag{5.57c}$$

Kinetic LFERs are used to predict reaction rates from more easily measured or more readily available equilibrium properties, but they also provide valuable insights into reaction mechanisms. They are used in organic chemistry to quantify the effects of substituent groups on the kinetics of reactions for sets of related compounds. Such groups influence the reactivity of organic compounds by altering the electron density at reaction sites. For example, reactions favored by a low electron density at the reacting site are accelerated by electron-withdrawing (electronegative) substituent groups like $-Cl$ and $-NO_2$.

As Eq. 5.49 shows, $\Delta G^{\neq}$ has entropy and enthalpy terms. The former is associated with A in the Arrhenius equation and the latter with E_{act}. In some reactions, like the alkaline hydrolysis of benzoic acid esters, substituents affect primarily E_{act} (or $\Delta H^{\neq}$) and ΔH°. Thus, $\Delta G^{\neq}$ (and $\ln k$) and E_{act} covary, and $\ln k$ varies linearly with ΔG°. In other cases, $\Delta G^{\neq}$ (and $\ln k$) and ΔG° (and $\ln K$) are linearly related despite variations in both A and E_{act}. In these cases, values of $\Delta H^{\neq}$ and $\Delta S^{\neq}$ are correlated, and because $\Delta G^{\neq} = \Delta H^{\neq} - T\Delta S^{\neq}$, the changes are compensating, and the change in k is less than if E_{act} or A changed alone. Similar relationships are observed in ΔH° and ΔS°, and the net effect is a linear relationship between $\Delta G^{\neq}$ and ΔG°.

Problems

5.1. A graduate student has collected the following data for the reaction of an organic pollutant with a naturally occurring mineral surface:

Time (h)	Concentration (μM)
1.5	137
18	98.6
42.5	68
71.5	38.4
91.5	23.7
115	12.2
138.5	8.4

Determine the reaction order and a rate constant for this disappearance of this pollutant.

5.2. Vogel and Reinhard[10] measured hydrolysis rate constants for 1,2-dibromopropane and several other halogenated aliphatic compounds. Experiments were conducted at elevated temperatures to obtain data in a reasonable time. Given the following observed (first-order) rate constants, estimate the first-order rate constants and half-life at 25°C at pH 9 and 11 (values for pH 7 are given in Example 5.4). Is the rate pH dependent, and how strong is the evidence, if any, for base (OH^-) catalysis?

1,2-Dibromopropane,	k_{obs} (10^{-5}) s^{-1}	
pH	81°C	61°C
7	1.3	0.21
9	1.3	0.21
11	3.7	0.51

5.3. A glass vial contains 0.4% potassium by weight. The natural abundance of ^{40}K, which decays by β^- emission, is 0.0117%, and its half-life is 1.248×10^9 yr. If the vial weighs 20 g, calculate the rate of β^- production by the vial in dpm (disintegrations per minute).

5.4. Derive the overall rate equation for product formation for the following mechanism:

$$A + A \underset{k_{-1}}{\overset{k_1}{\leftrightarrow}} A^* + A$$

$$A^* + B \overset{k_2}{\to} P$$
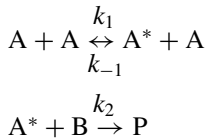
A^* is an excited intermediate of reactant A formed by collision with another molecule of reactant A (i.e., by absorbing the kinetic energy from the collision). Use the steady-state assumption to solve the rate equation for A^*.

5.5. Pyrophosphate ($H_2P_2O_7^{2-}$), a component of some detergents, hydrolyzes to orthophosphate ($H_2PO_4^-$) as a pseudo-first-order process at constant pH ($H_2P_2O_7^{2-}$ + $H_2O \to 2H_2PO_4^-$). The half-life of pyrophosphate is 140 h at 75°C and 13 h at 100°C. Compute the apparent activation energy, E_{act}, for the reaction and estimate the time required for 99% hydrolysis of a pyrophosphate solution at 20°C.

5.6. Uptake of inorganic nutrients by phytoplankton often is modeled using the Michaelis-Menten equation. The half-saturation constant for uptake of both ammonium and nitrate by the alga *Asterionella formosa* (a diatom), K_S, is ~1 μM. Estimate the concentrations of ammonium and nitrate at which uptake of these N forms is 90 and 95% of the alga's maximum uptake rate.

5.7. Monochloromethylamine, a possible disinfection by-product, can react to form dichloromethylamine and methylamine: $2CH_3NHCl \to CH_3NCl_2 + CH_3NH_2$. The reaction may proceed either directly as written or by a two-step mechanism:

$$CH_3NHCl + H_2O \to CH_3NH_2 + HOCl \quad \text{(slow)}$$
$$CH_3NHCl + HOCl \to CH_3NCl_2 + H_2O \quad \text{(fast)}$$
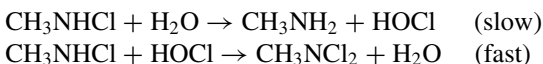
The first mechanism leads to a second-order rate equation; the second leads to a first-order rate equation. An experiment at pH 3.5 with $[CH_3NHCl] = 5.5 \times 10^{-4}$ M yielded the following results:

Time (min)	0	10	20	30	40
$[CH_3NHCl]$ (10^{-4} M)	5.0	3.12	2.28	1.79	1.47

Determine the reaction order and thus the apparent mechanism of the reaction and also determine the rate constant under the above conditions.

5.8. Using Acuchem, simulate the following reaction scenarios:

(a) $A \xrightarrow{k_1} B \xrightarrow{k_2} C$; scenarios: (i) $k_1 = k_2 = 0.1$; (ii) $k_1 = 0.1$, $k_2 = 0.5$; (iii) $k_1 = 0.5$, $k_2 = 0.1$

(b) $A \xrightarrow{k_1} B$ and $A \xrightarrow{k_2} C$; scenarios: (i) $k_1 = k_2 = 0.1$; (ii) $k_1 = 0.1$, $k_2 = 0.5$; (iii) $k_1 = 0.5$, $k_2 = 0.1$

(c) $A \xrightarrow{k_1} B$ and $A \xrightarrow{k_2} C$ and $B \xrightarrow{k_3} D$; scenarios: (i) $k_1 = k_2 = k_3 = 0.1$; (ii) $k_1 = 0.1$, $k_2 = 0.5$, $k_3 = 0.5$; (iii) $k_1 = 0.5$, $k_2 = 0.1$, $k_3 = 0.5$.
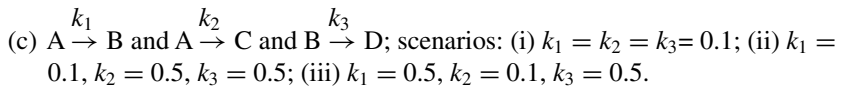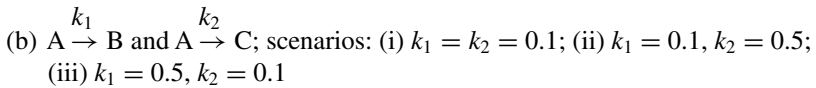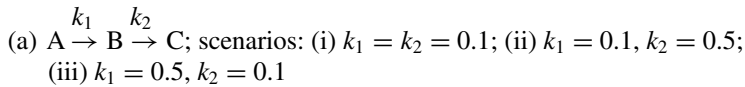
In each case plot the results. For sequence (a), which scenario produces secular equilibrium?

5.9. Consider sequence (a) in problem 5.8 where $A = {}^{90}Sr$ ($t_{1/2} = 29$ y), $B = {}^{90}Y$ (yttrium; $t_{1/2} = 64$ h), and C is ${}^{90}Zr$, which is stable. Sr (and thus ${}^{90}Sr$) occurs at low concentrations in natural waters, and measurement of its daughter product has been proposed as a means of age-dating water in municipal water distributions systems. If ${}^{90}Y$ is removed from water during the treatment process but ${}^{90}Sr$ is not removed, ${}^{90}Y$ activity in the water will increase over time, eventually reaching secular equilibrium with the ${}^{90}Sr$ in water when it enters the distribution system. Alum treatment, a common practice in treating surface waters, has been found to remove ${}^{90}Y$ efficiently but does not remove ${}^{90}Sr$ (J. Waples, University of Wisconsin–Milwaukee, personal communication, 2007). Based on the above information, estimate the length of time required for ${}^{90}Y$ to reach 90% of its secular equilibrium value under the above conditions, and comment on how your computed value may provide an upper time range for the use of ${}^{90}Y$ measurements to estimate the age of water in a distribution system.

5.10. A CFSTR is operating with a volume of 10 m³ and flow rate of 0.1 m³/h. In the influent, chemical X enters with a concentration of 5 mg/L and reacts with a rate constant of 0.02 h^{-1}.

(a) If the reactor is running at steady state, what is the effluent concentration?
(b) You desire to obtain 90% transformation of X. You can either change the flow rate or volume of the reactor (leaving the other unchanged). Determine the new volume (with the same flow rate) or the new flow rate (with the same volume) required.

(c) For a PFR operating under the same conditions described above, what is the effluent concentration?

5.11. Based upon the data below, determine the activation energy for the reaction and the preexponential factor:

T (°C)	rate constant (s^{-1})
0	9.16×10^{-3}
20	0.12919
40	1.2993
50	3.7017
70	25.017

5.12. Develop a plot that shows how a rate constant is affected by changes in temperature for $E_{act} = 10, 20, 40,$ and 80 kJ/mol.

5.13. The rate constant for reaction of bromoacetate ($BrCH_2COO^-$) with thiosulfate ($S_2O_3^{2-}$) at zero ionic strength is $\sim 5 \times 10^{-3}$ M^{-1} s^{-1}. Estimate the value of the rate constant at ionic strengths of 0.01 and 0.1.

References

1. Hill, C. G., Jr. 1977. *An introduction to chemical engineering kinetics and reactor design*, J. Wiley & Sons, New York.
2. Brezonik, P. L. 1994. *Chemical kinetics and process dynamics in aquatic systems*. CRC Press, Boca Raton, Fla.
3. Davidson, W., and G. Seed. 1983. The kinetics of oxidation of ferrous iron in synthetic and natural waters. *Geochim. Cosmochim. Acta* **47**: 67–79.
4. Ja'far, A., P. H. Gore, E. F. Saad, D. N. Water, and G. F. Moxon. 1983. Kinetic analysis of an extended single-path sequence of first-order reactions. The reaction of mesitonitrile in sulfuric acid. *Int. J. Chem. Kinetics* **15**: 697–703.
5. Lasaga, A. C. 1980. The kinetic treatment of geochemical cycles. *Geochim. Cosmochim. Acta* **44**: 815–828.
6. Braun, W., J. T. Herron, and D. K. Kahaner. 1988. Acuchem: a computer program for modeling complex chemical reaction systems. *Int. J. Chem. Kinetics* **6**: 51–62.
7. Lindeman, F. A. 1922. Discussion on the "radiation theory of chemical action." *Trans. Faraday Soc.* **17**: 598–599.
8. Chapra, S. C., and K. H. Reckhow. 1983. *Engineering approaches for lake management*, Vol. 2: *Mechanistic modeling*, Butterworth Publ., Boston.
9. Thomann, R. V., and J. A. Mueller. 1987. *Principles of surface water quality modeling and control*, Harper and Row, New York.
10. Vogel, and M. Reinhard. 1986. Reaction products and rates of disappearance of simple bromoalkanes, 1,2-dibromopropane and 1,2-dibromoethane in water. *Environ. Sci. Technol.* **20**: 992–997.

11. Adamson, A. W. 1979. *A textbook of physical chemistry*, 2nd ed., Academic Press, New York.

12. Weston, R. E., Jr., and H. A. Schwarz. 1972. *Chemical kinetics*, Prentice-Hall, Englewood Cliffs, N.J.

13. Eyring, H. 1935. The activated complex in chemical reactions. *J. Chem. Phys.* **3**: 107–115.

14. Glasstone, S., K. J. Laidler, and H. Eyring. 1941. *The theory of rate processes*, McGraw-Hill, New York.

15. Eyring, H., S. H. Lin, and S. M. Lin. 1980. *Basic chemical kinetics*, Wiley-Interscience, New York.

16. Zewail, A. H. 1988. Laser femtochemistry. *Science* **242**: 1645.

17. Gaussian09, Gaussian, Inc., Wallingford. Conn., available online at http://www.gaussian.com.

18. Schrödinger, LLC. 2010. Jaguar available online at http://www.schrodinger.com/products/14/7/.

19. Lasaga, A. C., and G. V. Gibbs. 1990. *Ab initio* quantum mechanical calculations of surface reactions—a new era? In *Aquatic chemical kinetics*, W. Stumm (ed.), Wiley-Interscience, New York, 259–289.

20. Pacey, P. D. 1981. Changing conceptions of activation energy. *J. Chem. Ed.* **58**: 612–614.

21. Johnson, K. S. 1982. Carbon dioxide hydration and dehydration kinetics in seawater. *Limnol. Oceanogr.* **27**: 849–855.

22. Laidler, K. J., and D. T. Y. Chen. 1959. Pressure and temperature effects on the kinetics of the alkaline fading of organic dyes in aqueous solution. *Can. J. Chem.* **37**: 599–612.

6

▰ Fundamentals of Organic Chemistry for Environmental Systems

▰ Objectives and scope

This chapter describes the basic principles of organic chemistry needed to understand the behavior of organic contaminants in aquatic environments. We start with a description of the nature of chemical bonds in carbon compounds and a summary of the major categories of organic compounds, including the main classes of aliphatic and aromatic compounds. We then deal with the common types of functional groups that affect the physical, chemical, and biological behavior of organic compounds. Rules are given for naming aliphatic and aromatic compounds based on their structural features, and different ways of drawing structures of organic compounds are presented. Next, the nature and significance of stereoisomers and optical isomers are explained as background for a description of the chemical nature of biomolecules—the building blocks of organisms that control the cycling of carbon and other biogenic elements in aquatic environments. Finally, we describe some important properties used to make predictions about the behavior and fate of organic compounds in the environment. In particular, we focus on three equilibrium constants: (1) K_{ow}, the octanol-water partition coefficient, as the major variable to predict partitioning of compounds between polar (water) environments and less polar phases in biota and sediments; (2) K_H (or its converse, H), the Henry's law constant, to predict the volatilization of compounds into the atmosphere; and (3) K_a, acid dissociation constants, to predict the pH conditions under which many organic compounds exist as un-ionized versus ionized species.

▰ Key terms and concepts

- sp^3, sp^2, and sp hybrid orbitals of carbon atoms; sigma (σ) and pi (π) bonds

- Electron delocalization; aromaticity
- Aliphatic compounds; hydrocarbons and substituted hydrocarbons
- Heterocyclic compounds
- Synthetic organic compounds and refractory or persistent organic compounds (POPs)
- Major functional groups: alcohols, aldehydes, ketones, ethers, carboxylic acids, amines, amino acids, nitro compounds, thiols, sulfides (thioethers), sulfonates, sulfates, phosphonates, thiophosphonates, phosphates, halides
- Stereoisomers; *cis* and *trans* substituents; asymmetric carbons, chirality, enantiomers, and diastereomers
- K_{ow} (octanol-water partition coefficient)
- K_H and H (Henry's law constant)
- Nucleophiles and electrophiles, nucleophilic and electrophilic substitution.

6.1   Introduction

Organic compounds play a vital role in the chemistry of natural waters and engineered aquatic systems, and for the past several decades much research in these fields has focused on the environmental behavior of human-derived organic chemicals and natural organic matter (NOM). This chapter provides the basic information that aquatic chemists and engineers need to work in these fields, to understand the rich literature that is still developing on organic aquatic chemistry, and to be prepared for the treatment of organic matter and organic compounds in later chapters of this book. The chapter is not intended to be a substitute for a college-level course in organic chemistry,[1] but it does not assume that readers of this book will have taken such a course. It covers the fundamentals of organic chemistry structure, functional groups and their characteristics, and basic organic nomenclature, and it concludes with a description of the most important properties of organic compounds used to predict their environmental behavior.

6.2   Electron orbital and bonding configurations of carbon

Carbon (atomic number = 6) is a tetravalent element. Its outer shell of electrons is half-filled—two electrons complete the spherical 2s orbital, and one each is in two of the three orthogonal "dumbbell-shaped" p orbitals. The electron configuration of a ground-state carbon atom thus is $1s^2\,2s^2\,2p^2$. To complete their octet of electrons, carbon atoms always seek four more electrons by sharing them in bonds with other atoms. Often, the bonds are "single bonds"; that is, they involve pairs of electrons shared between the carbon atom and some other atom, but in some cases they are "double bonds," involving four electrons (two pairs of electrons), or "triple bonds," involving six electrons (three pairs of electrons).

In cases where carbon atoms form four single bonds, the outer shell electron s and p orbitals "hybridize" into four spherical "sp^3" orbitals arranged tetrahedrally around the carbon atom, as shown below in the structures for methane (Figure 6.1).

Carbon atoms with double bonds have sp^2 hybridization; that is, the 2s orbital and two of the 2p orbitals hybridize to form three σ orbitals arranged around the carbon nucleus in a plane at angles of 120° from each other (>C—). The remaining 2p orbital
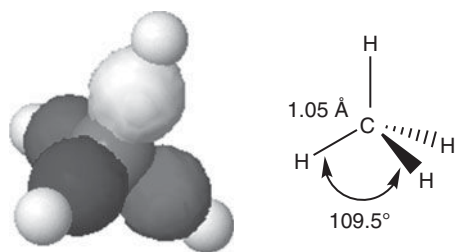
Figure 6.1 Methane molecule showing tetrahedral sp^3 hybrid orbitals and bond angles and lengths. Small white spheres attached to larger orbital spheres represent attached H atoms. Readers should interpret the solid triangle-shaped bonds as extending out of the plane of the page toward the reader, triangular dashed-line bonds as extending beyond the plane of the page away from the reader, and solid-line bonds in the plane of the paper. (See color insert at end of book for a color version of this figure.)
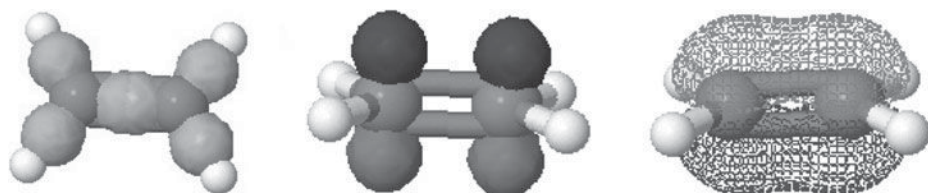
Figure 6.2 Hybrid orbitals for ethylene: left, sp^2 orbitals; center, p orbitals; right, mesh represents π orbitals above and below plane of ethylene molecule. (See color insert at end of book for a color version of this figure.)
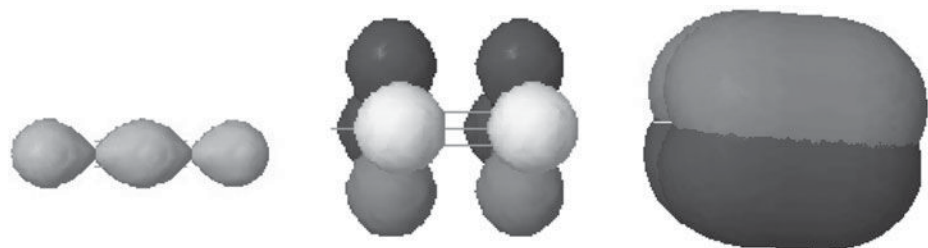
Figure 6.3 Hybrid orbitals for acetylene: left, sp orbitals; center, two sets of p orbitals; right, cylinder of π orbitals. (See color insert at end of book for a color version of this figure.)

forms a π bond above and below the plane of the sp^2 orbitals, as shown for ethylene ($CH_2{=}CH_2$) in Figure 6.2.

In carbon atoms with triple bonds, the $2s$ orbital and one $2p$ orbital hybridize to form two sp orbitals that are 180° apart ($-C-$), and the remaining two $2p$ orbitals form two π bonds producing a cylindrical electron cloud, as shown for acetylene ($HC{\equiv}CH$) in Figure 6.3.

A special case arises when carbon-carbon double bonds occur in "conjugated" fashion, i.e., alternating double and single bonds, in ring compounds. Benzene, a six-carbon ring (C_6H_6), is the prime example. In such cases, the double and single bonds can be written in two alternative and wholly equivalent ways, as shown in Figure 6.4a.
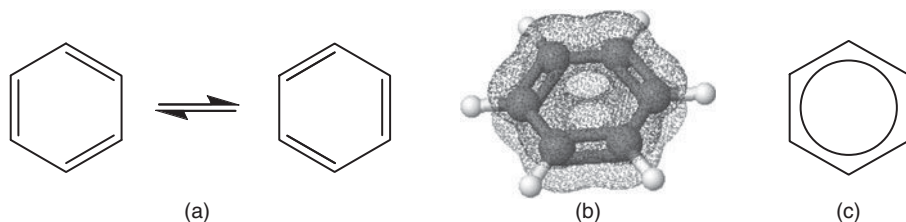
Figure 6.4 (a) Equivalent ways of writing the conjugated double bonds in benzene; (b) rings of delocalized π electrons above and below the plane of the benzene ring; (c) alternative way of drawing the benzene structure to emphasize the delocalized nature of the π bonds. (See color insert at end of book for a color version of this figure.)

In fact, however, neither structure is correct because the electrons are ***delocalized*** and shared equally by the six carbons, leading to a ring of π electrons above and below the plane of the carbon ring (Figure 6.4b). This electron delocalization, usually shown as a circle inside the benzene ring (Figure 6.4c), stabilizes the ring leading to starkly different characteristics for benzene and similar compounds compared with organic compounds not exhibiting these features. For example, such "aromatic" compounds (so-called because they often have an odor) undergo substitution reactions (replacement of an H atom attached to the ring by some other atom or molecular group) much more readily than "addition reactions" that would destroy the electron delocalization.

6.3   Major categories of organic compounds

The richness of subject matter in organic chemistry is based largely on the ability of carbon atoms to form covalent bonds with each other, leading to a great diversity of structures, but it also reflects the fact that carbon forms stable covalent bonds with other elements, especially oxygen, nitrogen, sulfur, and the halides. Classification of the millions of organic compounds thus should be expected to be complicated. Here we define major categories used to classify organic compounds; it is important to recognize that the categories are not mutually exclusive. The subsequent section examines organic compound classification in more detail based on "functional groups" attached to basic carbon skeletons.

At a high level of categorization, organic compounds can be placed into three broad (and very diverse) classes: aliphatic, aromatic, and heterocyclic. ***Aliphatic compounds*** consist of compounds with the carbon atoms arranged both in chains—straight or branched—and in ring structures. They can be further divided into ***saturated compounds***, where all the carbon bonds are single bonds, and ***unsaturated compounds***, where two or more carbon atoms have double or triple bonds. ***Aromatic compounds*** have conjugated double bonds in rings—usually six-member rings or condensed multiples thereof—whereby the π electrons are delocalized, that is, not associated with a single pair of carbon atoms, and form a π cloud above and below the ring, as shown in Figure 6.4b. ***Heterocyclic compounds*** have ring structures in which one (or more) of the carbon atoms is replaced by an N, O, or S atom. Some heterocyclic compounds have an aromatic character because of the conjugated nature of their double bonds, but because

the heteroatoms have a different number of electrons than carbon, complete electron delocalization usually does not occur in these compounds.

Hydrocarbons are compounds that contain only carbon and hydrogen. They may be aliphatic or aromatic. The term also is used with a modifier to describe substituted groups in compounds that otherwise contain only C and H—e.g., chlorinated hydrocarbons have one or more Cl atoms in addition to C and H atoms.

The term *synthetic organic compounds* refers to compounds that are not found in nature, except for the effects of human activities, and are not synthesized by organisms.* Instead, they have been synthesized in laboratory or industrial chemical reactors. The term *anthropogenic organic compounds* generally has the same meaning. Many synthetic organic compounds, especially those containing halogens, are difficult for microorganisms to degrade, and once released to the natural environment as a result of human activities, they remain there for long periods of time. Such compounds are said to be *refractory* or *persistent*; often they are referred to as persistent organic pollutants (*POPs*).

In contrast, *natural organic matter* (*NOM*) refers to organic material in water, soil, or sediment derived from the activities of plants and animals (other than humans) in the natural environment. A related term, *dissolved organic matter* (*DOM*), refers to the fraction of NOM that is dissolved or colloidal, i.e., the fraction that passes through a filter of a selected pore size (usually 0.45 or 0.1 μm). DOM usually is measured (e.g., in mg/L) in terms of its carbon content and reported as dissolved organic carbon (DOC). *CDOM* (*colored dissolved organic matter*) is the portion of DOM that absorbs visible light and thus appears colored (usually yellow to brown). *Humic* and *fulvic acids* (more generally, *humic substances*), the major components of CDOM, are derived from the decomposition of plant materials and play important roles in the chemistry and ecology of natural waters (see Chapter 18).
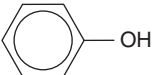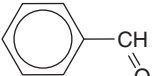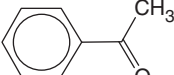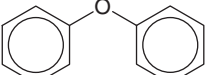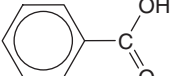
Organic compounds formed by organisms and constituting the metabolic products and structural components of cells often are called *biomolecules*. Small biomolecules important as metabolites include sugars, fatty acids, amino acids, and short-chain carboxylic acids. The main categories of small biomolecules that serve as building blocks of biological macromolecules are amino acids, sugars, phosphonucleotides, and fatty acids, and the corresponding macromolecules they form are proteins, carbohydrates (including starch and cellulose), nucleic acids, and lipids. Section 6.7 describes the important classes of biomolecules.
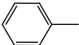
6.4   Organic functional groups

Tables 6.1–6.3 show the major functional groups found in organic compounds and give examples of aliphatic and aromatic compounds containing the groups. Together with overall size and three-dimensional configuration, the presence of such groups determines the physical, chemical, and biological behavior of organic compounds. For example, the addition of oxygen functional groups (Table 6.1) to hydrocarbons increases their polarity,

---

*This class is not quite as distinct as was thought a decade or more ago. Recent studies have shown that chlorinated and brominated organic compounds, including some polychlorinated biphenyls (PCBs) and other persistent organic compounds (POPs), occur as natural products.

Table 6.1 Oxygen functional groups
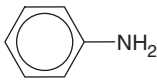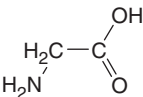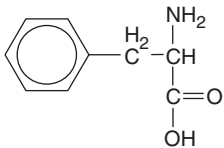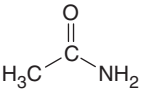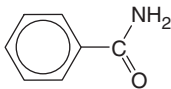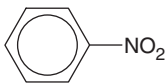
Type	Structure	Aliphatic example	Aromatic example*
Alcohol; -anol	R−OH	CH$_3$CH$_2$OH, ethanol	Φ−OH, phenol
Aldehyde	R−CHO	CH$_3$CHO, acetaldehyde	Φ−CHO, benzaldehyde
Ketone	R$_1$(CO)R$_2$	CH$_3$(CO)CH$_2$CH$_3$, methylethyl ketone	Φ−(CO)CH$_3$, methylphenyl ketone
Ether	R−O−R	(C$_2$H$_5$)O(C$_2$H$_5$), diethyl ether	Φ−O−Φ, diphenylether (a diaryl ether)
Carboxylic acid	R−COOH	CH$_3$COOH, acetic acid	Φ−COOH, benzene carboxylic acid or benzoic acid

* Φ− is used as a symbol for the phenyl group .

solubility in water, and susceptibility to biodegradation. The presence of oxygen also increases the oxidation state of the carbon atom to which the oxygen is attached, but not all oxygen groups have equal effects in this regard. For single-carbon compounds, the oxidation state of the carbon increases according to the trend CH$_4$ (methane) < CH$_3$OH (methanol) < CH$_2$O (formaldehyde) < HCOOH (formic acid) < CO$_2$ (i.e., alkane < alcohol < aldehyde < carboxylic acid < carbon dioxide); a quantitative approach to defining the oxidation state of organic compounds is described in Chapter 11.

Aliphatic alcohols are very weak acids (pK_a values typically in the range 15–18), indicating that the hydrogen in the –OH group is strongly bound and that H$^+$ has little tendency to dissociate in aqueous solutions. In contrast, electron delocalization in the benzene ring of phenols allows the negative charge resulting from H$^+$ dissociation to be accommodated more easily. Consequently, phenols are much more acidic (pK_a generally
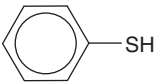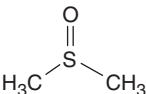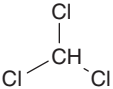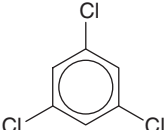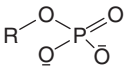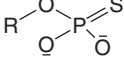
Table 6.2 Nitrogen functional groups
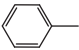
Type	Structure	Aliphatic example	Aromatic example
Amine; amino	$R-NH_2$	H_3C-NH_2 methylamine	aniline
Amino acid	$R-CH(NH_2)-COOH$	glycine	phenylalanine
Amide	$R-(C=O)-NH_2$	acetamide	benzamide
Nitro	$R-C-NO_2$	Not common	nitrobenzene
Nitroso	$R-C-NO$	Not common in small compounds	Not common in small compounds
Nitrile	$R-C\equiv N$	acetonitrile	Not common

in the range 5–10). The presence of electron-withdrawing groups on the aromatic ring (e.g., electronegative groups like $-NO_2$) stabilizes the phenolate anion and increases the acidity of such substituted phenols (e.g., $pK_a = 9.99$ for phenol, 7.17 for 2-nitrophenol, and an amazingly low 0.38 for 2,4,6-trinitrophenol,[1] which is called picric acid). Carboxylic acid groups are weak Brønsted acids (although much stronger than alcoholic groups), and pK_a values range from about 2 to 6. Again, the presence of electron withdrawing groups on a compound tends to stabilize the anionic charge and increases the compound's acidity.

Because the nitrogen atom in amine groups $(-NH_2)$ has an unshared pair of electrons available to form a bond with H^+, amines (Table 6.2) are weak bases. Amino acids, which combine a weak base and weak acid in close proximity, exhibit both acidic and basic properties. Carboxylic acid groups are stronger acids (hence their conjugate base is weaker) than amino groups (which are stronger bases). This results in the interesting property of "self-acid-base reaction," whereby at circumneutral pH amino acids exist as *zwitterions* with the carboxylic acid group in its base form and the amino group in its acidic form: $RCH(NH_3^+)COO^-$. Nitro and nitroso groups are not common in natural organic compounds but are found in some synthetic organic compounds that are environmental pollutants.

Table 6.3 Sulfur, halide, and phosphorus functional groups

Type	Structure	Aliphatic example	Aromatic example*
Sulfur			
Thiol; thioalcohol mercaptan	R−SH	H_3C — SH methyl mercaptan or methyl thiol	thiophenol
Organosulfide	R−S−R	H_3C S CH_3 dimethyl sulfide	Not common
Disulfide	R−S−S−R	proteins	
Sulfoxide	R−SO−R	H_3C S($=O$) CH_3 dimethylsulfoxide	Not common
Sulfone	R−SO$_2$−R	Found in pesticides, polymers, and pharmaceuticals	
Sulfonate	R−SO$_3^-$ H$^+$	Not common	$CH_3(CH_2)_{15}\Phi-SO_3^-$ H$^+$ linear alkylbenzene sulfonate (surfactant)
Sulfate	R−O−SO$_3^-$ H$^+$	$CH_3(CH_2)_{10}CH_2-OSO_3^-$ NH$_4^+$ ammonium lauryl sulfate (surfactant)	
Halides			
Halide	R−X (X = F, Cl, Br, I)	H_3C —Br methyl bromide chloroform	1,3,5-trichlorobenzene
Phosphorus			
Phosphate	R−O−PO$_3^{2-}$	Found in many biomolecules (see section 6.7) and some pesticides	Found in pesticides
Thiophosphate	R−O−PSO$_2^{2-}$	Found in some pesticides	
Phosphonate	R−C−PO$_3^-$	Found in pesticides	Found in pesticides

* $\Phi-$ is used as a symbol for the phenyl group.

The sulfur functional groups of low oxidation state, thiols and organosulfides (Table 6.3), are analogues of the oxygen groups, alcohols and ethers, respectively. Thiols (also called mercaptans) are stronger acids than alcohols; pK_a values in the range of 10–12 are common, and much lower values are known for some thiophenols with electron-withdrawing substituents. Both thiols and organosulfides form very strong bonds with certain metal ions known as "Class B" or "soft" metals (see Chapter 9), of which mercuric (Hg^{2+}) and lead (Pb^{2+}) ions are prime examples. Thiol and sulfide groups in humic matter are thought to be major binding sites for mercury in organic-rich soils and bottom sediments. Disulfide linkages found in biomolecules are formed by amino acids that have thiol groups.

The oxidized sulfur groups, sulfonates and organosulfates, are strong acids. In sulfonates the S atom is attached directly to a carbon atom, but in sulfates an oxygen atom provides the linkage (Table 6.3). A similar pattern occurs in phosphonates and organophosphates. These four types of organic compounds are important environmental chemicals. Sulfonates and organosulfates are widely used as surfactants in detergents. Many organophosphate compounds are important biomolecules (see Section 6.7). A variety of synthetic organophosphates, thiophosphates, and phosphonates have been used widely as pesticides in the past. Because of the high toxicity of some of these compounds to humans and other animals, many of the phosphorus-containing pesticides are no longer used in the United States.

6.5   Organic nomenclature and structures

6.5.1 Introduction

Given the huge diversity of organic compounds and the fact that many of them have complicated structures, readers should not be surprised to learn that naming of organic compounds is sometimes difficult. Our goal in this section is not to make you an expert in organic nomenclature; it *is* to provide the basic information whereby you can visualize (and draw) the structures of relatively simple and common organic molecules and name a compound if given its structure. Our focus is on organic compounds relevant to environmental chemistry, which still is a very large number of compounds.

6.5.2 Aliphatic compounds

Aside from the common names used for some (usually small) aliphatic compounds, the process of naming compounds of this type is based on a few simple rules. First, the longest chain of carbon atoms provides the root of the name. By convention, the following roots are used for chains up to 20 carbons long:

# of C	root	# of C	root	# of C	root
1	meth-	8	oct-	15	pentadec-
2	eth-	9	non-	16	hexadec-
3	prop-	10	dec-	17	heptadec-
4	but-	11	undec-	18	octadec-
5	pent-	12	dodec-	19	nonadec-
6	hex-	13	tridec-	20	eicos-
7	hept-	14	tetradec-		

Second, one of the following suffixes is added to the root to identify the type of compound:

-ane	saturated hydrocarbon
-ene	unsaturated hydrocarbon, one double bond
-diene	unsaturated hydrocarbon, two double bonds
-yne	unsaturated hydrocarbon, one triple bond
-anol	alcohol (R—OH)
-anal	aldehyde (R—CHO)
-anoic acid	carboxylic acid (R—COOH)

Ethers (R_1—O—R_2) and ketones (R_1—(C=O)—R_2) are named by placing the names of the two alkyl (or aryl) groups first, followed by the word ether or ketone (see Table 6.1). The suffix "-yl" added to a root denotes an alkyl group of the given carbon chain length that is attached to some other atom; for example, "methyl" refers to the group CH_3—, ethyl to the group CH_3CH_2—, propyl to the group $CH_3CH_2CH_2$—, and so on. Thus, CH_3Cl becomes methyl chloride, and CH_3CH_2OH becomes ethyl alcohol (or ethanol).

Third, the position of substituents on the main carbon chain is denoted by numbering the carbon atoms in the chain starting with 1 for the terminal carbon containing the functional group (if there is one) that provided the suffix. Often there are at least two choices in numbering carbon atoms and locating substituent groups. A general rule is that the carbon atoms are numbered in a way to use the smallest numbers. An example is illustrated below.

The above compound is correctly named 2,3-dichloropentane, not 3,4-dichloro-pentane (although the incorrect name yields the same structure as the correct name). Note also that in naming compounds we run the substituent group name, root, and suffix all together. Also, we separate the numbers denoting locations of substituents by commas and connect the numbers to the name of the substituent group by a hyphen. For ease in drawing (and viewing) organic compounds, it often is convenient to show only the bonds linking carbon atoms and other atoms (except for hydrogen atoms

attached to carbon). The structure of 2,3-dichloropentane drawn in this manner is shown above.

Some other simple structures drawn in the "stick bond" style and their names are illustrated below:
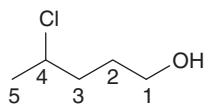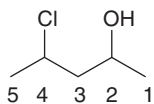
4-Chloro-1-pentanol   4-Chloro-2-pentanol   Pentanoic acid
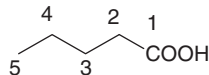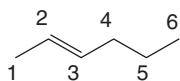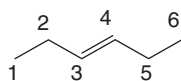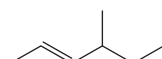
2-Hexene   3-Hexene   4-Methyl-2-hexene   2-Methyl-3-hexene
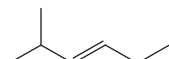
Finally, many C_{1-4} compounds and some larger ones have common names. Many biomolecules, including all common sugars, amino acids, and di- and tri-carboxylic acids important in cellular metabolism, also have common names (see Section 6.7). Especially for the smallest compounds and biomolecules, the common name is used almost exclusively in preference to the proper chemical name. Important examples are

C_1: HCOOH, formic acid; H_2CO, formaldehyde; CH_3OH methyl alcohol; $CHCl_3$, chloroform; CCl_4, carbon tetrachloride; CF_2Cl_2, Freon-12 (it can be argued whether the latter two are really organic compounds)
C_2: CH_3COOH, acetic acid; CH_3CHO, acetaldehyde; CH_3CO-, acetyl group
C_3: CH_3CH_2COOH, propionic acid (instead of propanoic acid)
C_4: $CH_3CH_2CH_2COOH$, butyric acid (instead of butanoic acid)

EXAMPLE 6.1 Example 6.1 Name that compound (round 1): Name the six compounds below:
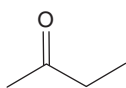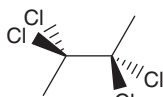
1   2   3
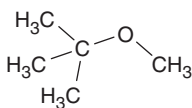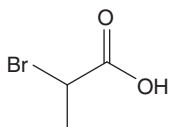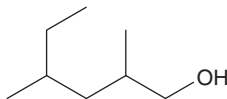
4   5   6

Answers: (1) 2-butanone (common name: methyl ethyl ketone); (2) 2,2,3,3-tetrachlorobutane; (3) cyclohexane; (4) methyl *tert*-butyl ether; (5) 2-bromoproanoic acid; (6) 2,4-dimethyl-1-hexanol.
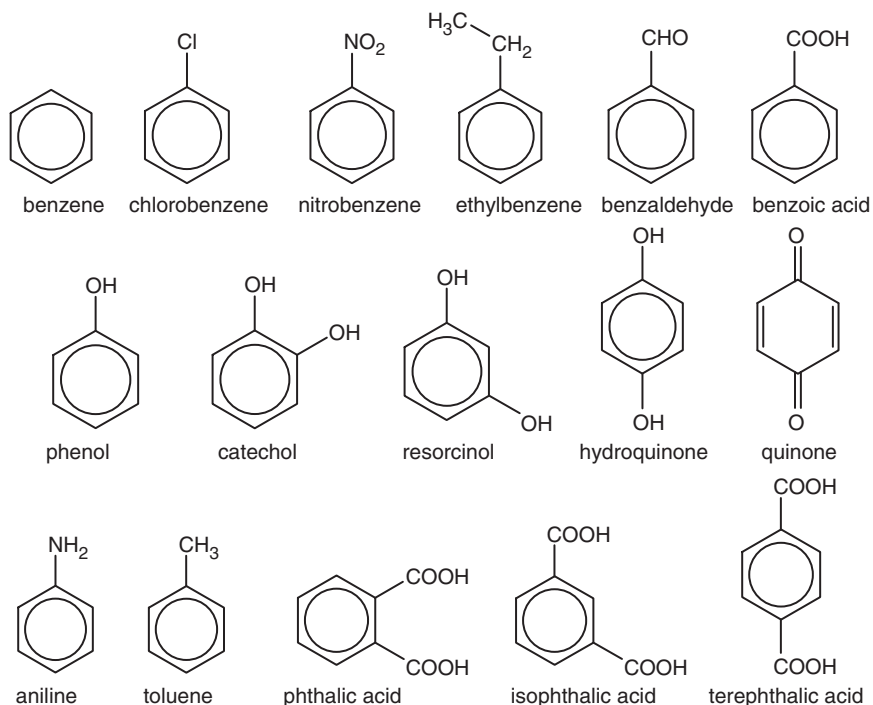
Figure 6.5 Structures and names of simple substituted benzene compounds.

6.5.3 Single-ring aromatic compounds

Many simple single-ring aromatic compounds use the word benzene as the root name (e.g., nitrobenzene; Figure 6.5), but many simple substituted benzenes have common names not based on benzene (e.g., phenol; Figure 6.5). The three possible dihydroxyl-substituted benzenes have distinct names, and quinone is the oxidized form of hydroquinone. The three dicarboxylic acids also have different names based on the root name phthalic acid. However, for most aromatic compounds with multiple substitution, we need to indicate the positions of the substituents on the benzene ring. For disubstituted aromatic compounds, the terms *ortho-*, *meta-* and *para-* (symbolized *o-*, *m-*, and *p-*) can be used to indicate substituents on benzene carbons respectively one, two, and three carbons away from the carbon to which the primary substituent is attached. For example, for chlorophenols and cresols (which are hydroxyl-substituted toluenes),
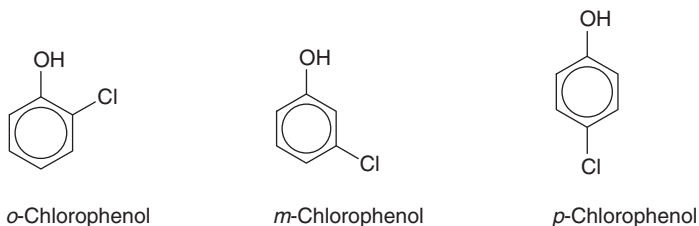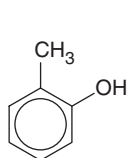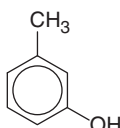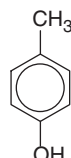
o-Cresol   m-Cresol   p-Cresol

Alternatively, for aromatic compounds with two or more substituents, we number the atoms in the ring from 1 to 6, with the carbon to which the primary substituent is attached (if there is one) being carbon 1:
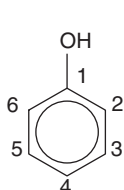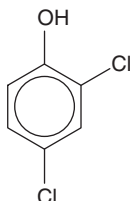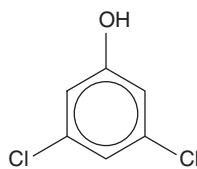
Phenol   2,4-Dichlorophenol   3,5-Dichlorophenol
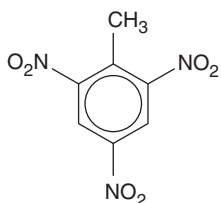
2,4,6-Trinitrotoluene (TNT)   2,4-Dichlorophenoxyacetic acid
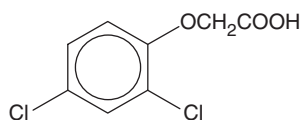
In cases where one or more benzene or phenol rings are attached to a complicated aliphatic chain, it often is simpler to name the compound using the aliphatic chain as the root. In such cases benzene rings are identified as *phenyl* groups, and phenols as *phenoxy* groups (if the linkage of the aromatic ring to the aliphatic chain occurs via the phenolic group). For example, the widely used herbicide 2,4-D (2,4-dichlorophenoxyacetic acid) has the structure shown above.

EXAMPLE 6.2 Name that compound (round 2): Name the following four aromatic compounds:
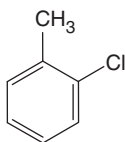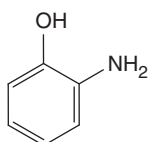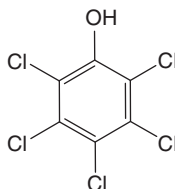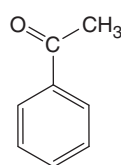
1   2   3   4

Answers: (1) 1-methyl-2-chlorobenzene (or 2-chlorotoluene); (2) 2-aminophenol (or 2-hydroxyaniline); (3) pentachlorophenol (or 2,3,4,5,6-pentachlorophenol); (4) 1-phenylethanone (common name: acetophenone).

6.5.4 Aromatic compounds with multiple and fused rings

The simplest aromatic compound with more than one benzene ring is biphenyl, the parent compound of the notorious pollutants PCBs (polychlorinated biphenyls). The carbon atoms in the rings are numbered as shown below:

Biphenyl   3,3′,4,4′-Tetrachlorobiphenyl   2,2′6,6′-Tetrachlorobiphenyl
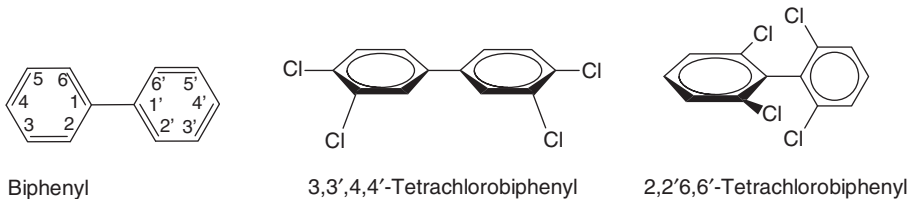
There are 209 possible ***congeners*** of PCBs having from one to a maximum of 10 Cl atoms substituted into the rings. Two examples of tetra-substituted biphenyls are shown above. In the first, the chlorine atoms are located in the *meta* (i.e., 3, 3′, 5, and 5′) and *para* (i.e., 4 and 4′) positions relative to the carbons linking the two rings. Although the rings are free to rotate about this bond, the energetically favorable position has the rings coplanar. In contrast, because of steric considerations, substitution of chlorine atoms in the 2, 2′, 6, and 6′ positions of the rings, that is, the positions *ortho* to bond connecting the rings, leads to restricted rotation about that bond, and the energetically favorable situation has the rings perpendicular to each other. These differences have important effects on the toxicity and environmental behavior of PCB congeners (see Chapter 19).

Compounds with more than two fused benzene rings are called ***polycyclic aromatic hydrocarbons*** (***PAHs***). These common environmental pollutants arise largely from incomplete combustion of fossil fuels and wood. The simplest aromatic compound with fused benzene rings, naphthalene, an ingredient once used in mothballs, is not considered to be a PAH but is a bicyclic aromatic hydrocarbon. According to the IUPAC definition, anthracene and phenanthrene are the simplest PAHs. Structures of a few common PAHs are illustrated in Figure 6.6. Benzo[a]pyrene is highly carcinogenic.

6.5.5 Heterocyclic compounds

By definition, these compounds have one or more hetero-atoms in a ring of carbon atoms. Both five- and six-member heterocyclic compounds are important, and N, O, and S are common hetero-atoms. Hetero-N and -S groups can be involved in proton exchange reactions at environmentally relevant pH values (i.e., they act as weak acids or bases). Of most importance are unsaturated heterocyclic compounds that behave similar to aromatic compounds. Because the heteroatom has a different number of electrons than carbon, complete electron delocalization usually is not possible, but substantial delocalization and aromatic character are found in the compounds shown in
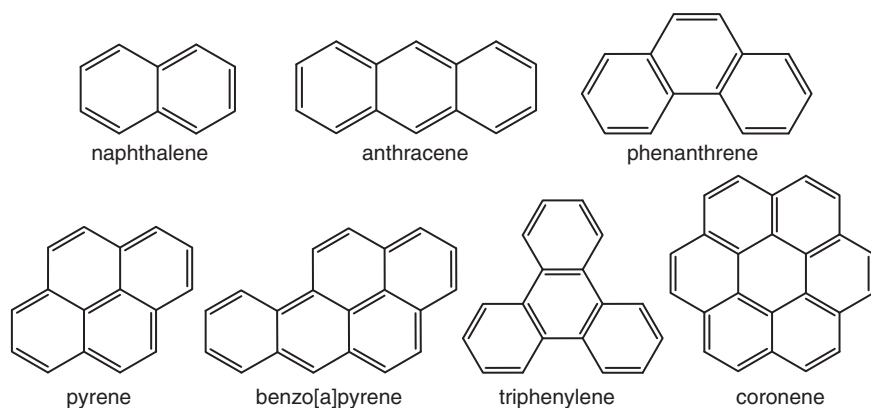
Figure 6.6 Structures of naphthalene and some common PAHs.
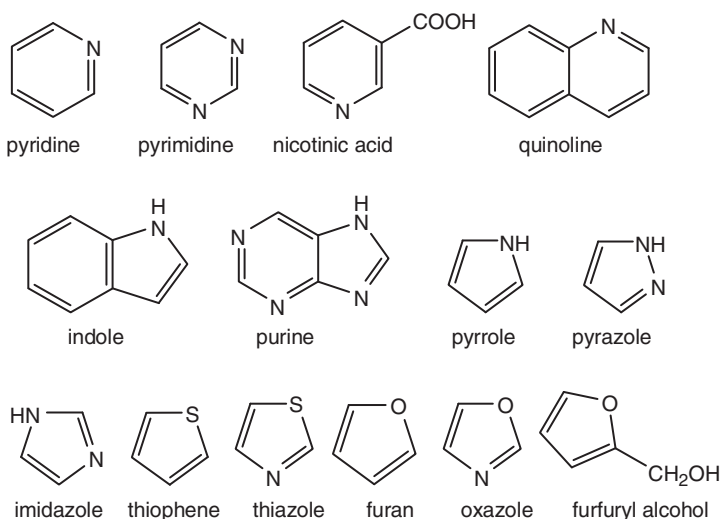
Figure 6.7 Heterocyclic compounds with aromatic character.

Figure 6.7. Many of the heterocyclic compounds in Figure 6.7 are important components of biomolecules: purines and pyrimidines are found in nucleic acids, and indole and imidazole are components of the amino acids tryptophan and histidine. Nicotinic acid is the vitamin niacin and a relative of the narcotic nicotine. Thiophene units are common in agricultural pesticides and in various pharmaceuticals. Pyrrole rings are units in larger porphyrin (tetrapyrrole) rings, from which both chlorophyll and hemoglobin are derived.

Dibenzodioxins are an environmentally important class of condensed heterocyclic compounds because of the high toxicity of some chloro derivatives. Their structures are

similar to anthracene except that the carbon atoms on the center ring are replaced by oxygen atoms:
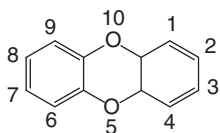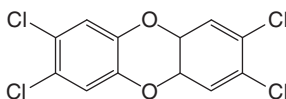
Dibenzodioxin   2,3,7,8-Tetrachlorodibenzodioxin (TCDD)

Numbering of the atoms in the three dibenzodioxin rings, which formally are called dibenzodioxin, is shown above. The unnumbered carbon atoms do not have any hydrogens attached and thus are not available for substitution; 2,3,7,8-TCDD, the compound shown above right, is the congener of greatest concern because of its high toxicity to humans. Dibenzodioxins sometimes are referred to informally as dioxins.

6.6   Stereochemistry: geometric isomers and chirality

Multiple arrangements of the same stoichiometric collection of carbon, hydrogen, and other atoms are of course possible. Such sets of compounds are called ***isomers***. In this section we focus on two kinds of isomers—geometric stereoisomers and optical stereoisomers—that are important in environmental organic chemistry.

6.6.1 Geometric isomers: *cis* and *trans* forms of alkenes

Rotation around carbon-carbon double or triple bonds would require the π bond(s) to be broken. In contrast to the generally free rotation of carbon-carbon single bonds, rotation around such bonds is restricted. As a result, substituents on such carbons can occur in two distinct configurations. We illustrate this using the simplest alkene, ethylene:
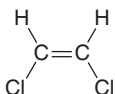
cis-1,2-Dichloroethene   *trans*-1,2-Dichloroethene
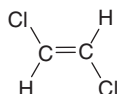
In the above examples, chlorine atoms bonded to the adjacent carbon atoms are either on the same side of the C=C bond or on opposite sides; the prefixes *cis*- and *trans*- are used, respectively, to denote these configurations. The two structures are ***isomers*** of the same basic compound (1,2-dichloroethene, commonly called 1,2-dichloroethylene). Because the only difference between them is in their three-dimensional configuration— they otherwise have the same number and types of bonds and functional groups—they are called ***stereoisomers***, in particular, ***geometric*** stereoisomers. Because of their structural similarities, we can expect that such compounds will exhibit similar physical and chemical behavior. Nonetheless, some differences may occur as a result of differences

in polarity and related factors. For example, the *cis* form is more polar, and thus we might expect it to have higher melting and boiling points than the *trans* form. It turns out that both isomers have the same melting point ($-81°C$), but the boiling point of the *cis* compound is 60.3°C, whereas that of the *trans* compound is only 47.5°C.

6.6.2 Optical isomers or chiral compounds

A second, more subtle, and potentially even more important type of stereoisomerism occurs in compounds with one or more asymmetric carbons. A carbon atom is said to be asymmetric if four different constituent groups are attached to it, as shown below:

As the above examples show, in cases of asymmetry, the constituent groups can be arranged around the carbon atom in two ways that are "mirror images." The center and right forms are the same structure, with the first being the direct mirror image of the species on the left and the second rotated around the A–C bond to show the placement of the substituents. The mirror image forms are not interconvertible without the bonds being broken and reformed. Such compounds are called ***enantiomers*** or ***optical isomers*** because they cause polarized light to be rotated to the right or to the left. Compounds with asymmetric carbons that exhibit optical activity are said to be ***chiral***.

   Although chirality is common in organic chemistry, it is not a major factor in the environmental chemistry of organic contaminants. Enantiomers behave identically, except toward optically active reagents, and have identical physical properties (except for the direction of rotation of polarized light). Chirality is, however, of profound importance in biology. Both carbohydrates and amino acids exhibit chirality, and this has implications for their bioactivity. For example, the active sites of enzymes are sensitive to the stereochemistry of the molecules whose reactions they catalyze. Except for the simplest amino acid, glycine, all natural amino acids are optically active. Although they can occur in two forms (D and L),[†] those in organisms almost always are in the L-form:

L-Amino acid   D-Amino acid
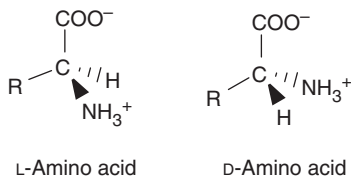
[†]The prefixes "D" and "L" stand for "dextrorotatory" (right) and "levorotatory" (left), respectively, and refer to the direction of rotation of polarized light by a given enantiomer. This terminology is used for optically active compounds in biochemistry, but organic chemists use the corresponding symbols "R" and "S."

In contrast, the biologically active forms of sugar molecules, which have multiple asymmetric carbons, are the D forms (see Section 6.7.4). Compounds with more than one asymmetric carbon have as many pairs of enantiomers as they have asymmetric carbons. The stereoisomers of a given formula that are not enantiomers are called *diastereomers*. In contrast to enantiomers, diastereomers have different physical properties and chemical reactivities. They are given different names and treated as different compounds.

6.7   Types and structures of organic biomolecules

6.7.1 Introduction

A huge variety of organic compounds are "biologically active" in the sense of being subject to microbially mediated transformations. This includes many synthetic organic compounds, even chlorinated compounds such as PCBs—compounds that generally do not occur in the natural environment except for the fact that they are synthesized and used by humans. We do not consider all biologically active molecules to be "biomolecules," however, and reserve the term for molecules that form the basic structures of cells or are active in normal cellular metabolism. Four major kinds of small biomolecules—amino acids, sugars, fatty acids, and heterocyclic bases—are the building blocks of the macromolecules of cells; in general, these building blocks are linked in regular fashion (often by simple dehydration (i.e., abstraction of a water molecule) to form the polymeric macromolecules that make up cells. Proteins consist of chains of amino acids bound by amide linkages (see Table 6.2); complex carbohydrates (cellulose and starch) consist of chains of simple sugars; and nucleic acids consist of chains of monomeric *nucleotides* composed of sugar molecules, phosphate ions, and heterocyclic bases (purines and pyrimidines). Here we provide a brief introduction to the structures and chemistry of biomolecules.

6.7.2 Sugars and carbohydrates

Common sugars generally have a like number of carbon and oxygen atoms. A typical stoichiometry is $C_nH_{2n}O_n$, where n = 5 or 6, but in some cases there is one fewer O than C. One of the oxygen atoms is an aldehyde or ketone, and the rest are –OH groups (each on a different carbon), The suffix "-ose" indicates that a compound is a sugar; combined with the above comments on carbon length and oxygen groups, this gives rise to several generic names for sugars: aldoses and ketoses, hexoses and pentoses. Glucose, a hexose and aldose, is possibly the most common organic compound on the planet, given that it is the monomeric unit of all celluloses and starches. Its basic formula is shown below (left), but for more than 100 years it has been known that the aldehyde group is not free but rearranged to form the six-membered "pyranose" ring shown second from left. Because the carbon containing the aldehyde group is asymmetric in the ring form, two enantiomers exist—the α and β forms shown on the right; note the numbering of the carbon atoms, as shown in the α form.

Fisher projection   Crude ring structure   α-Pyranose   β-Pyranose
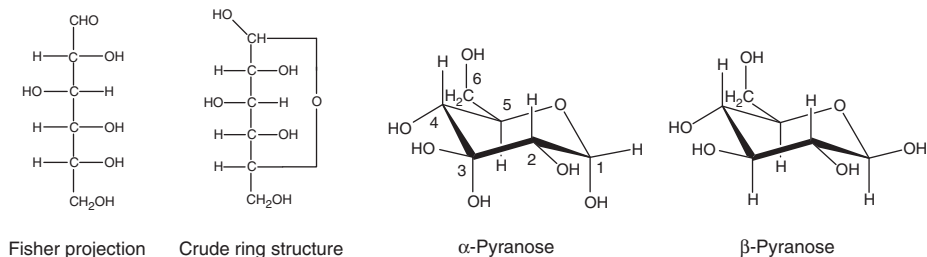
Other common aldoses with six carbons also have the basic pyranose structure and differ from glucose primarily in conformations of the –OH groups (whether they are axial (above or below the plane of the ring) or equatorial (in the plane of the ring)). The hexose fructose has an –OH group on C1, and C2 contains a ketone group ($>C=O$). This gives rise to a five-membered (furanose) ring structure analogous to that for glucose. Five-carbon aldoses such as ribose also have furanose ring structures. It is obvious from the abundance of –OH groups that sugars are polar substances; as such, we can expect that they are relatively soluble in water. With their basic stoichiometry of $C_nH_{2n}O_n$, they also are rather oxidized compounds, especially compared with fatty acids.

As mentioned above, glucose forms two highly important polymers: starches and cellulose. In the simplest starch, amylose, the glucose units are linked by eliminating an H_2O molecule from the C1 and C4 carbons of adjacent molecules , and the C1 carbon has the α conformation (i.e., the linkage is axial to the plane of the ring). In contrast, the 1,4 linkages of cellulose have the C1 carbon in the β form (equatorial position).

The α linkage between C1 and C4 carbons of adjacent glucose units in amylose, the simplest starch. Note: the disaccharide shown is maltose.	The β linkage between C1 and C4 carbons of adjacent glucose units in cellulose.
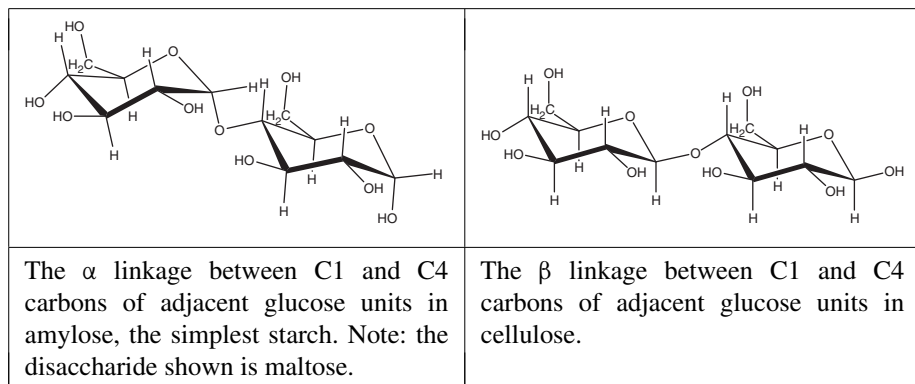
The differences in biodegradability that these contrasting bonding arrangements yield are impressive. The β-1,4 linkage in cellulose leads to rigid structures with high tensile strength suitable for fibers, and the monomeric glucose units are unavailable for cellular metabolism. Cellulase enzymes found only in certain microorganisms are needed to break this linkage. In contrast, the α-1,4 linkage in starch leads to more flexible structures that are easily hydrolyzed by enzymes found in all cells (and even nonenzymatically by mild acid). Starches also have glucose units connected in 1,6 fashion (see above α-glucose figure for carbon numbering), which leads to cross-linked three-dimensional structures called amylopectin. Macromolecular carbohydrates have two major biological functions. Starches serve as readily available energy reserves

for cells. Celluloses act as structural components of macroscopic plants, and combined with proteins as "glycopoteins" they serve a structural role within cells. In addition, the sugars ribose and deoxyribose are major components of nucleic acids.

6.7.3 Amino acids and proteins

There are 20 common amino acids, and they constitute a highly diverse set of structures (Figure 6.8). All are α-amino acids, meaning that the amino group is on the carbon atom next to the carboxylic acid group, and have the generic formula $RCH(NH_2)COOH$, except for proline, in which the amino group becomes an imino ($>NH$) group in a five-membered ring. The nature of R varies widely, however, and includes simple hydrocarbon groups; hydroxyl-substituted hydrocarbons (i.e., alcohols); sulfur-substituted groups; groups with additional acidic moieties and the amides of those compounds; groups with additional basic ($-NH_2$) moieties; and aromatic and heterocyclic groups. These differences impart very different chemical behaviors to the amino acids; more important, as discussed below, they lead to different chemical environments within the macromolecular proteins that amino acids form. Aside from their role as the components of proteins, amino acids are of interest in water chemistry because they occur at low concentrations in surface waters and are involved in microbial metabolism. Some free amino acids are important ligands in trace metal complexation (see Chapter 9).

Amino acids are called the building blocks of life because they are the units that form proteins, which are major structural components and metabolic catalysts in cells. Proteins consist of chains of amino acids connected by amide linkages (also called peptide bonds):
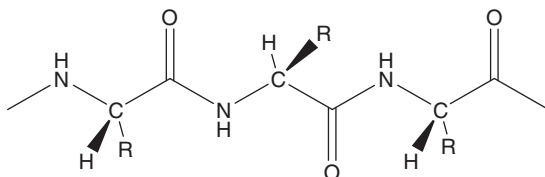
Chains of amino acids, called polypeptides, generally do not have a simple linear shape. Proteins consist of one or more polypeptides held together by nonamide covalent bonds that link amino acids of adjacent polypeptides or by hydrogen bonding. The chemical differences in amino acids resulting from differences in the "R" group are critically important determinants of protein structures and functions. For example, amino acids with unsubstituted aliphatic and aromatic groups can form hydrophobic pockets in proteins; S-containing amino acids can form –S–S– cross-linkages in or between peptide chains, contributing to peptide folding and the three-dimensional structure of proteins; and amino acids with extra carboxylate groups (glutamate, aspartate) may act as sites for binding of heavy metals, which in turn may form the "active sites" in enzymes where catalysis of reactions takes place.

Proteins come in a wide range of sizes (MW from $< 10^4$ to $> 10^6$ Da) and shapes (globular, sheetlike, rodlike), and they have many structural and metabolic functions. All enzymes are proteins, but as noted above, some enzymes have a small, nonprotein

Hydrocarbon

$H_2C–COOH$
|
NH_2
glycine

$CH_3–CH–COOH$
|
NH_2
alanine

$CH_3–CH–CH–COOH$
| |
CH_3 NH_2
valine

Alcohol

$CH_3–CH–CH–COOH$
| |
OH NH_2
threonine

$CH_3–CH–CH_2–CH–COOH$
| |
CH_3 NH_2
leucine

$CH_3–CH_2–CH–CH–COOH$
| |
CH_3 NH_2
isoleucine

$HO–CH_2–CH_2–CH–COOH$
|
NH_2
serine

Sulfur

$CH_3–S–CH_2–CH_2–CH–COOH$
|
NH_2
methionine

$HS–CH_2–CH–COOH$
|
NH_2
cysteine

Acidic

$HOOC–CH_2–CH–COOH$
|
NH_2
aspartic acid

$HOOC–CH–CH_2–S–S–CH_2–CH–COOH$
| |
NH_2 NH_2
cystine

$HOOC–CH_2–CH_2–CH–COOH$
|
NH_2
gluatmic acid

Basic

$H_2N–CH_2–CH_2–CH_2–CH_2–CH–COOH$
|
NH_2
lysine

$H_2N–C–NH–CH_2–CH_2–CH_2–CH–COOH$
‖ |
NH NH_2
arginine

Amide

$HN–C–CH_2–CH–COOH$
‖ |
O NH_2
aspargine

$HN–C–CH_2–CH_2–CH–COOH$
‖ |
O NH_2
glutamine

Heterocyclic

Aromatic

$CH_2–CH–COOH$
|
NH_2
phenylalanine

$CH_2–CH–COOH$
|
NH_2
histidine

CH_2
|
$H_2N–CH–COOH$
tryptophan

Non-α-amino-N

COOH

HN

proline

HO—⟨ring⟩—$CH_2–CH–COOH$
|
NH_2
tyrosine

Figure 6.8 The common amino acids grouped on the basis of the nature of R–, the group attached to the carbon with the amino group.

component (e.g., sometimes a metal ion) called a coenzyme that usually is the active site, that is, the site where catalysis of reactions takes place.

6.7.4 Carboxylic acids

Two types of carboxylic acids are important as biomolecules: long-chain compounds called fatty acids and short-chain mono-, di-, and tricarboxylic acids that are involved

(a)

(b)

stearic acid

trans-oleic acid

cis-oleic acid

trans-linoleic acid

palmitic acid
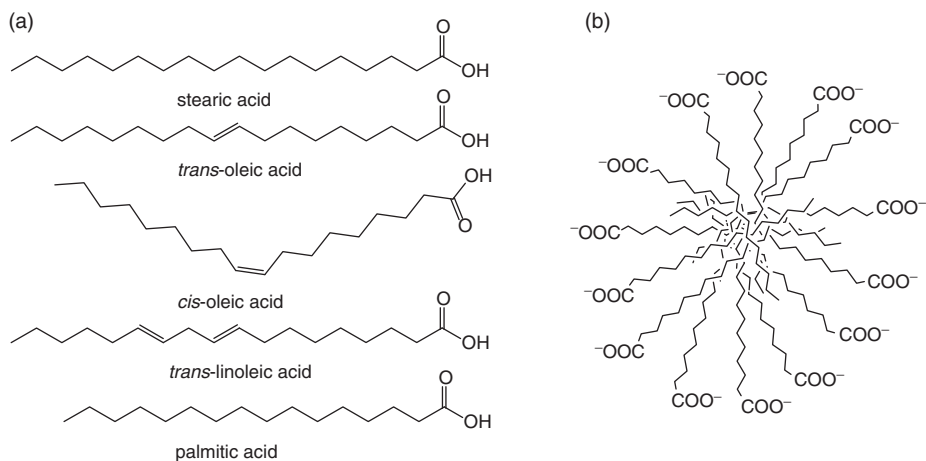
Figure 6.9 (a) Some common fatty acids: The top four are all C_{18}, and the bottom is C_{16}; (b) hydrophobic chains of ionized fatty acids form nonpolar micelles with the ionized carboxylate groups facing the aqueous phase.

in intermediary metabolic processes. Most fatty acids have even numbers of carbon atoms because they are synthesized from acetyl (C_2) units. Although chain lengths can range from C_4 to C_{28}, common fatty acids are in the range of C_{14} to C_{18} (Figure 6.9a). Note that the *trans* forms of unsaturated acids are straight chains, but the *cis* forms are curved, and this difference has important physiological implications. The long aliphatic chains of fatty acids are hydrophobic, but the carboxylic acid groups are hydrophilic, especially when dissociated. This leads to a behavior called micelle formation. When concentrations exceed a critical value called the "critical micelle concentration," the hydrophobic "tails" clump together to create a spherical hydrophobic environment, and the terminal carboxylate groups remain in the aqueous phase on the exterior of the sphere (Figure 6.9b). Nonpolar substances and dirt are solubilized within micelles, making them useful as cleaning agents (this is the basis for the cleaning action of soaps).

Some short-chain acids are important in metabolites in the breakdown of fats, carbohydrates, and proteins to CO_2 and H_2O (which generates energy for organisms) and the formation of some amino acids and structural components of cells. Structures of some carboxylic acids important in these processes are shown in Figure 6.10a. Many of these acids participate in the citric acid cycle (Figure 6.10b), which is responsible for oxidizing acetate to CO_2 and H_2O in aerobic respiration.

6.7.5 Nucleic acids

The molecular biology revolution of recent decades has had major impacts on the ways that environmental scientists and engineers study microbial processes in aquatic systems. A brief description of the chemical composition of genetic material thus is appropriate here. Deoxyribonucleic acid (DNA), which comprises cellular genetic material, consists of two very long polymers that occur as complementary strands of a double helix (Figure 6.11a). For example, the genome of the common bacterium *E. coli* has 4.6×10^6
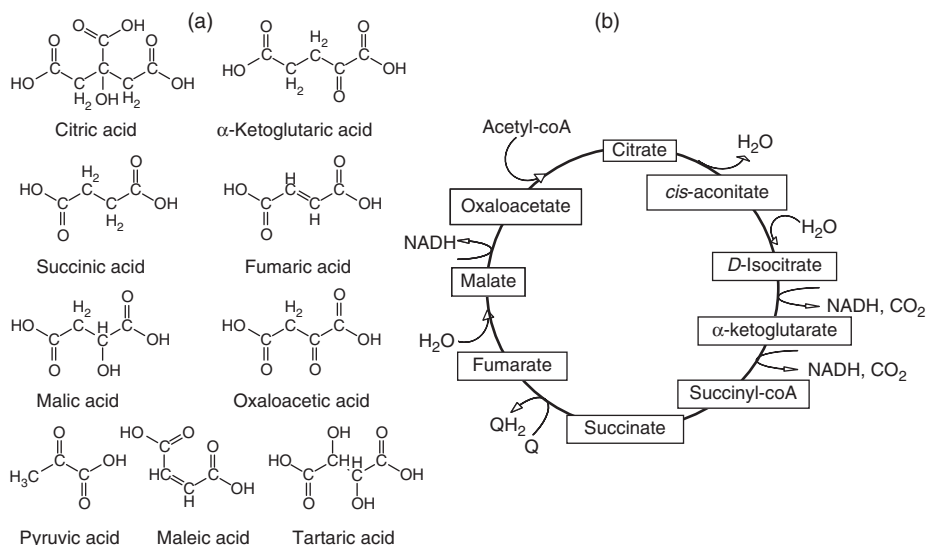
Figure 6.10 (a) Structures of some common carboxylic acids involved in intermediary metabolism; (b) summary sketch of the citric acid cycle, which is of central importance in aerobic metabolism. NAD$^+$ (nicotinamide adenine dinucleotide) and Q (coenzyme Q10) are coenzymes that function as electron (or H) carriers in cellular redox processes; coenzyme A (CoA) functions as a carrier of acetyl groups.
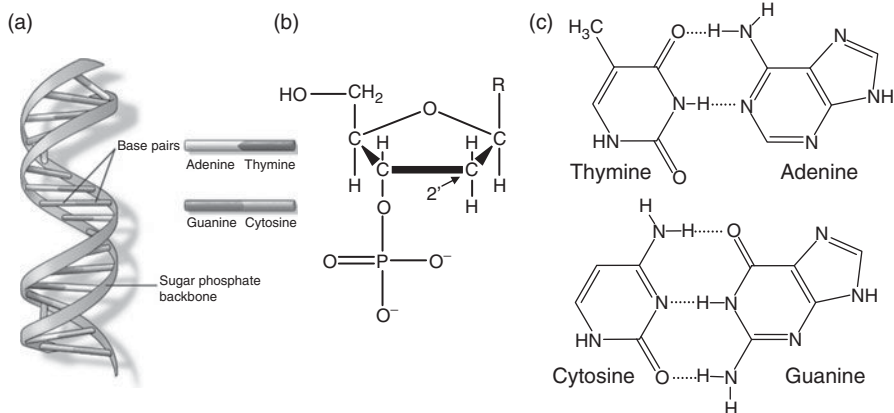
Figure 6.11 (a) The double helix structure of DNA. (b) Structure of nucleotides, the basic units in DNA. The polymer is formed by linking the HO-group from one unit to the phosphate (a phosphoester) of another unit. (c) R in the nucleotide structure is one of these four bases. (a) from U.S. National Library of Medicine (public domain). (See color insert at end of book for a color version of this figure.)

monomeric units in each strand. The polymers consist of combinations of four basic monomers called nucleotides (Figure 6.11b), each of which is composed of a five-carbon sugar, deoxyribose, to which is attached a phosphate group and one of four bases: adenine (A), guanine (G), cytosine (C), and thymine (T) (Figure 6.11c) The sugar and phosphate form the backbone of the polymer, and the sequence of bases encodes information. Specifically, triplet combinations of the bases form the "genetic code"; i.e., sequences of three bases "code" for individual amino acids. For example, AGC codes for serine; GGA codes for glycine; CTC for leucine, and so forth. The bases also exhibit pairwise attractions such that A forms hydrogen bonds with T and G with C, but for steric reasons A has little attraction for C, and G has little attraction for T. The two strands in DNA are complementary in the sense that the bases in one strand are pairwise complements of the bases in the other strand. For example, if one strand has a sequence AGCGGACTC, the other strand has the complementary sequence TCGCCTGAG. This critically important feature enables cells to make faithful copies of their DNA.

Ribonucleic acid (RNA) plays essential roles in translating information from DNA into the synthesis of proteins in cells and also is the genetic material in some viruses. Several kinds of RNA molecules provide these services, but they all differ from DNA in the same respects. First, instead of deoxyribose, the sugar in the basic nucleotide unit of RNA is ribose, which has an –OH group in the 2′ position where deoxyribose has an –H (Figure 6.11b). Second, RNA usually occurs in single strands rather than double helices. Third, the base thymine in DNA is replaced in RNA by the base uracil, which is thymine without the methyl group. Finally, RNA molecules usually are much shorter than DNA.

6.8   Key properties of organic compounds to predict their environmental behavior

6.8.1 Introduction

To completely describe the physical, chemical, and biological behavior of any organic compound would require knowledge of innumerable property values, coefficients, and constants. However, with respect to understanding and interpreting the observed environmental behavior of most organic compounds and predicting how the compounds will behave in the environment, we are in the fortunate situation of being able to rely on a few key constants that in many cases can be measured directly by relatively straightforward procedures. For compounds where direct measurements are difficult or impractical, we frequently can estimate values for these constants based on established correlations with other easily measurable characteristics such as molecular weight, melting or boiling point, and aqueous solubility. We focus here on three equilibrium constants:

(1) K_a, acid dissociation constants for compounds having acid-base properties (or corresponding K_b values), to quantify/predict the pH conditions under which such compounds exist as un-ionized versus ionized species
(2) K_H (or its converse, H), the Henry's law constant, which defines a compound's volatility and serves as a predictor of the partitioning of a compound between water and the atmosphere

(3) K_{ow}, the octanol-water partition coefficient, the major explanatory/predictor variable for the partitioning of compounds between polar (water) environments and less polar phases in biota and sediments—this property is particularly important for understanding the behavior of neutral (i.e., relatively nonpolar) organic compounds

To be sure, many other physical-chemical properties of organic compounds are useful in describing or predicting how compounds react chemically or biologically, including their susceptibility to chemical or biological degradation and toxicity to organisms. However, the above constants are in a class by themselves relative to usefulness in predicting the behavior of organic contaminants in aquatic systems.

Regarding K_a and K_b values, we need to say little beyond the comments already made in Section 6.4.1, other than the fact that values of these constants are available in the open literature for almost all organic compounds of environmental interest that act as Brønsted or Lewis acids or bases (see, e.g., Schwarzenbach et al.[2]). Whether a compound occurs in an ionized state (e.g., as a carboxylate anion or protonated cationic amine) versus an un-ionized state (e.g., a fully protonated carboxylic acid) has an obvious effect on the volatility of the compound. However, the degree of ionization also may affect its chemical reactivity toward oxidation/reduction or substitution, its tendency to sorb onto or desorb from various kinds of surfaces, and its ability to be taken up by microorganisms.

6.8.2 Henry's law constants (H)

As described in Chapter 1, the solubility of a gas (or volatile compound) in water, S_w, is defined by Henry's law, which states that solubility is directly proportional to the partial pressure of the gas (P) in the atmosphere with which the water is equilibrated:

$$S_w = K_H P \tag{6.1}$$

For organic compounds at temperatures below their boiling point, P represents the vapor pressure of the compound at the temperature of interest. The proportionality constant, K_H, depends on temperature, ionic strength, and the nature of the gas/volatile compound. Henry's law constants for classes of organic contaminants have been compiled by various authors.[2,3] K_H commonly is expressed in mol/L atm or sometimes as mg/L atm.

A more common convention for organic contaminants expresses Henry's law in reverse manner:

$$H S_w = P \tag{6.2}$$

$H(= K_H^{-1})$ has units of atm L mol^{-1} or bar L mol^{-1}. Care must be taken when using Henry's law constants from various sources, because the definitions of K_H and H may vary from source to source (so watch the units!). The gas phase content also can be expressed on the basis of mass (or mole) per volume in the same units as S_w, in which case H is "dimensionless." From the ideal gas law, $PV = nRT$, or $P = RT(n/V)$.

The relationship between concentration in air C_a (in mol/L) and the partial pressure is thus

$$C_a = \frac{P}{RT},$$ (6.3)

where R is the gas constant (0.0821 L atm K^{-1} mol^{-1}) and T is the temperature at which the vapor pressure is measured. This leads to a "dimensionless" Henry's law constant of the form

$$H' = \frac{C_a}{S_w}$$ (6.4)

H' is not truly dimensionless, however; it has units of (mol/L$_{air}$)/(mol/L$_{water}$).

Values of H or for organic compounds are calculated from the measured (or calculated) aqueous solubility and the corresponding measured vapor pressure. Alternatively, H' may be determined by introducing a known mass of a compound into a sealed system and measuring the concentration in one phase and determining the other by difference. This is usually done by equilibrating a water sample multiple times with air[4] or by using a series of vials with different air-water ratios.[5] Dynamic (gas stripping methods) also are used, because the rate at which a compound is stripped from water is a function of Henry's law constant.[6] Correlation methods also are used to estimate S_w and H from other properties of the compounds.[2,7] Estimates based on the structure of molecule also are possible.[8,9] These experimental and estimation methods are discussed in greater detail in Chapter 19.

Values of H are large for fixed gases (e.g., methane), moderately small for volatile organic compounds (e.g., tetrachloroethylene), and very low for large, chlorinated compounds like PCBs (range of about 0.5–7 × 10^{-6} atm L^{-1} mol^{-1} for various PCB mixtures). Values of H for some common gases and organic contaminants are given Table 6.4.

6.8.3 Octanol-water partition coefficients, K_{ow}

In general, a partition coefficient is the ratio of the equilibrium concentrations of a compound in two phases. The partition coefficient of a compound between n-octanol

Table 6.4 Henry's law constants for common gases and organic contaminants[2,10]

Common gases	H (atm L mol^{-1} at 25°C)	Organic compounds	H (atm L^{-1} mol^{-1} at 25°C)
N_2	1513	Carbon tetrachloride	21.8
H_2	1260	Tetrachloroethylene	18.5
CO	1047	Trichloroethylene	9.7
O_2	794	Toluene	5.9
CH_4	775	Benzene	5.4
CO_2	29.5	Chloroform	3.7
H_2S	9.5	Naphthalene	0.46
SO_2	0.8	DDT	0.012262

(o) and water (w) is considered to be the standard measure of a compound's **lipophilicity**, that is, its tendency to "prefer" being dissolved in a nonpolar rather than a polar solvent:

$$K_{ow} = C_o/C_w \qquad (6.5)$$

Remembering the adage "like dissolves like," we can conclude that nonpolar compounds generally prefer* nonpolar solvents and polar compounds prefer to be surrounded by polar solvents. The relative lipophilic/hydrophilic character of a molecule (i.e., preference for being in a nonpolar versus a polar (aqueous) environment) is a major predictor of its environmental behavior, including its tendency to "partition" into suspended and bottom sediments (particularly the relatively low-polar organic fraction), its potential for bioaccumulation, and its bioavailability (in terms of both toxicity and biodegradability).[†]

In theory, measurement of K_{ow} is straightforward; one simply measures a compound's concentration in both phases after equilibration in a shaken flask. In practice, the situation is complicated because K_{ow} for aquatic contaminants ranges over many orders of magnitude—from $\log K_{ow} \approx 1$ (e.g., aniline) to > 8 (e.g., highly chlorinated PCBs). Measurement of K_{ow} by flask methods is not practical for compounds with $\log K_{ow} > \sim 5$ because the equilibrium concentrations of such compounds in the aqueous phase are too low to be measured accurately. Column methods[12] extend measurements to $\log K_{ow} > 8$. Substantial variations (0.5–2.0 log units) exist among measured values of aquatic contaminants even at $\log K_{ow} < 5$, e.g.,[13]

Benzene	1.56–2.15	Hexachlorobenzene	4.13–7.42	2-Chlorobiphenyl	3.90–4.59
Naphthalene	3.01–4.70	Pentachlorophenol	3.32–5.86	*p,p'*-DDT	3.98–6.36

A widely used technique to estimate K_{ow} involves its correlation with retention indices (k') measured by reverse-phase high-performance liquid chromatography (RPHPLC).[14] This method is attractive because of the speed and ability of HPLC to separate large numbers of closely related compounds that are difficult to isolate (e.g., PCB congeners). One experiment can provide K_{ow} values over about 6 log units. The mobile phase in RPHPLC usually is a mixture of polar solvents, commonly 70–95% methanol/water, and the stationary phase consists of nonpolar, long-chain (C_{18}) hydrocarbons bonded to an inert support. In RPHPLC, solutes elute from the chromatographic column in order of increasing lipophilicity. Compounds are detected by UV absorbance or mass spectrometry, and a calibration curve is constructed for a given set of experimental conditions by measuring k' for a series of compounds with known K_{ow} values.

Like Henry's law constants, K_{ow} can be estimated using correlations or estimates based on the structure of molecule.[15,16] S–K correlations have some basis in theory.[17] As Eq. 4.35 shows, S_w is inversely proportional to γ_w, and K_{ow} has been shown to

---

*Here we use the word "prefer," which has an admitted anthropocentric connotation, to indicate an energetically favorable condition.

[†]Interest in lipophilic/hydrophilic partitioning of organic compounds extends back more than a century to studies showing a correlation between olive oil/water partition coefficients and the narcotic action of organic compounds.[11]

be proportional to γ_w.[18] Thus, we expect an inverse correlation between K_{ow} and S_w of organic compounds. K_{ow} is a measure of the relative solubility of a compound in a nonpolar and a polar solvent, and hydrophobicity (i.e., low S_w) is a major driving force for solute partitioning into octanol. Hydrophobicity and lipophilicity, however, are not *exactly* the same phenomenon. Correlation and estimation methods for K_{ow} are discussed in detail in Chapter 19.

6.8.4 Nucleophilic and electrophilic substitution reactions

As a general rule, the unequal sharing of electrons between more electronegative elements like N, O, and S and more electropositive elements like C and H in organic molecules leads to enhanced possibilities for chemical reactions. A brief discussion of two types of organic substitution reactions is necessary here so that material in later chapters is put into proper context. A **nucleophile** is a nucleus or positive-charge-"loving" species. Nucleophiles have a pair of electrons that are available to form a chemical bond. Nucleophiles most often are negatively charged species, but they also may contain a lone pair of electrons, such as those on an amino group. Nucleophiles are abundant in aquatic systems because water itself is a nucleophile having two lone pairs of electrons on the oxygen atom. Nucleophilic reactions with organic molecules are categorized as substitution and elimination reactions.

A classic nucleophilic substitution reaction is the reaction of methyl bromide with water:

$$H-\ddot{O}H \quad H_3C-Br \quad \longrightarrow \quad HO-CH_3 \ + \ H^+ + Br^- \tag{6.6}$$

Here the bromine atom is replaced (or substituted) by a hydroxyl group, giving methanol as the product. Because bromine is more electronegative than carbon, it pulls electron density away from the carbon center. Thus, the carbon has a slight positive charge and the bromine a slight negative charge (i.e., the compound is a dipole), the carbon is subject to reaction with an electron-rich species (i.e., a nucleophile). Water actually is a weak nucleophile (see Chapter 19), but this reaction occurs because the concentration of water (55.5 mol/L) is so much higher than that of the product, bromide (8×10^{-4} M in seawater; $< 10^{-6}$ M in freshwaters). In water with a high concentration of chloride, the following reaction also could occur:

$$Cl^- \quad H_3C-Br \quad \longrightarrow \quad Cl-CH_3 \ + \ Br^- \tag{6.7}$$

Here, chloromethane (methyl chloride) is the product, with chlorine replacing bromine. The kinetics and reaction products of nucleophilic substitution reactions are indicative of the reaction mechanism, and this is discussed in Chapter 19.

An **electrophile** is an "electron-loving" (or electron-poor) species that reacts with electron-rich species. These species usually react rapidly in water if electron-rich nucleophiles and other species (e.g., NOM) are present to react with them. Electrophilic

reactions require controlled conditions (e.g., biological systems), chemical addition (e.g., water treatment), or energy input (e.g., biological or photochemical systems) because electrophiles are generally not long-lived. A representative electrophilic reaction is the chlorination of a carbon-carbon double bond with hypochlorous acid (i.e., bleach):

$$+ \quad H_2O \tag{6.8}$$
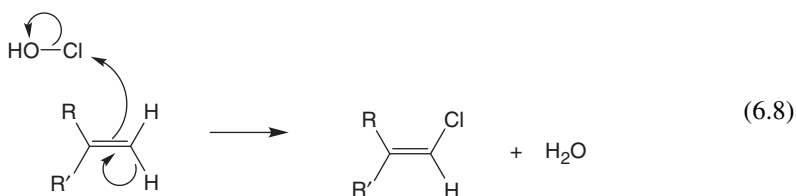
In hypochlorous acid, the oxygen atom is more electronegative than the chlorine. The chlorine thus is electron deficient (thus an electrophile) and can react with an electron-rich species.

Problems

6.1. Name the following compounds from the given structures:

(a)

(b)

(c)

(d)

(e)

(f)

(g) $H_2C=CHCH_2CH_2Cl$

(h) $H_2C=CHCH_2CH_2CH=CH_2$

(i) $H_3C(CH_2)_{16}COOH$

(j)
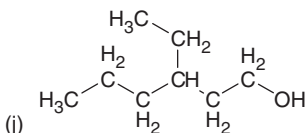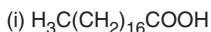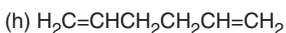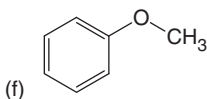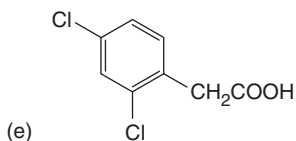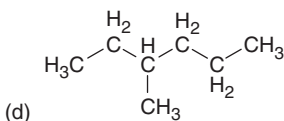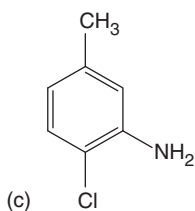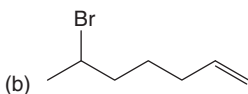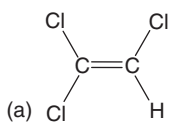
6.2. Draw the structures of the following compounds given their names:

(a) 2-Chlorobutanol   (f) 2-Ethoxy-4-nitrophenol
(b) 4-Fluoronitrobenzene   (g) 2,2′,4,4′-Tetrachlorobiphenyl
(c) 2-Pentyne   (h) 4-Methyl-5-chloro-2-octene
(d) 1,5-Dipentanoic acid   (i) Ethyl-*m*-chlorophenylether
(e) Methylethylketone   (j) 2-Amino-butyl-1-thiol

6.3. Name the following structures, which are either important organic solvents/common ground-water pollutants or disinfection byproducts:
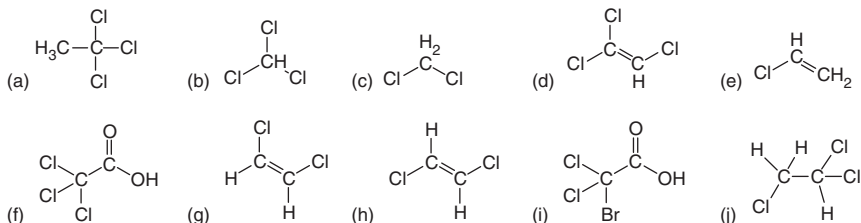
6.4. The K_{ow} of 1,2,4-trichlorobenzene is 10^4 (mol/L octanol)/(mol/L water), and the Henry's law constant K_H is 0.112 mol L^{-1} atm^{-1}. If you have 1 L of water, 500 mL of octanol and 100 mL of air in a sealed flask, what fraction of the 1,2,4-trichlorobenzene will be in the aqueous phase?

Notes: (1) The mass of 1,2,4-trichlorobenzene in phase j is $M_j = C_j \times V_j$, where C is concentration and V is volume. Total 1,2,4-trichlorobenzene mass $= \sum M_j$. (2) $K_{ow} = C_{oct}/C_{water}$. (3) $K_H = C_{water}/P$.

6.5. What is the difference between geometric stereoisomerism and optical isomerism? Draw the structures of some compounds that illustrate what is meant by these two terms and in what way(s) might these phenomena be important relative to the environmental behavior of organic compounds?

6.6. Describe what is meant by the terms nucleophile and electrophile and give examples (structures) of both types of substances using any of the molecular structures in Chapter 6 that you think are appropriate.

6.7. Find a research article from the last 10 years in the journal *Environmental Science & Technology* (or another journal of your instructor's choice) that presents new findings on the relationship between K_{ow} and other structural or physical-chemical properties of organic contaminants (or some class of organic contaminants), or alternatively uses K_{ow} as a predictor variable for some "behavioral trait" of organic contaminants like bioaccumulation or sorption to sediments. Write a 200–250 word summary and critique of the article.

References

1. Wade, L. G. 2006. *Organic chemistry*, 6th ed., Addison-Wesley, Boston.
2. Schwarzenbach, R. P., P. M. Gschwend, and D. M. Imboden. 2003. *Environmental organic chemistry*, 2nd ed., Wiley-Interscience, New York.

3. Mackay, D., W.-Y. Shiu, K. T. Valsaraj, and L. J. Thibodeaux. 1990. *Air-water transfer: the role of partitioning*. In *Air water mass transfer*, J. Gulliver and S. Wilhelm (eds.), American Society Civil Engineering, New York, 34–56.

4. McAuliffe, C. D. 1971. GC determination of solutes by multiple phase equilibration. *Chem. Tech.* **1**: 46–51.

5. Gosset, J. M. 1987. Measurement of Henry's law constants for C1 and C2 chlorinated hydrocarbons. *Environ. Sci. Technol.* **21**: 202–208.

6. Mackay, D., W. Y. Shiu, and R. P. Sutherland. 1979. Determination of air-water Henry's law constants for hydrophobic pollutants. *Environ. Sci. Technol.* **13**: 333–337.

7. Lyman, W. J., W. F. Reehl, and D. H. Rosenblatt. 1982. *Handbook of chemical property estimation methods. Environmental behavior of organic compounds*, McGraw-Hill, New York.

8. Hine, J., and P. K. Mookerjee. 1975. The intrinsic hydrophilic character of organic compounds. Correlations in terms of structural contributions. *J. Org. Chem.* **40**: 292–298.

9. Meylan, W. M., and P. H. Howard. 1991. Bond contribution method for estimating Henry's law constants. *Environ. Toxicol. Chem.* **10**: 1283–1293.

10. Stumm, W., and J. J. Morgan. 1996. *Aquatic chemistry*, 3rd ed., Wiley-Interscience, New York.

11. Meyer, H. 1899. *Arch. Exp. Pathol. Pharmakol.* **42**: 110; Overton, E. 1901. *Studien über die Narkose*. Fischer Publ., Jena, Germany.

12. Woodburn, K. B., W. J. Doucette, and A. W. Andren. 1984. Generator column determination of octanol/water partition coefficients for selected polychlorinated biphenyl congeners. *Environ. Sci. Technol.* **18**: 457–459.

13. Brezonik, P. L. *Chemical kinetics and process dynamics in aquatic systems*, CRC Press, Boca Raton, Fla.

14. Ruepert, C., A. Grinwis, and H. Govers. 1985. Prediction of partition coefficients of unsubstituted polycyclic aromatic hydrocarbons from C_{18} chromatographic and structural properties. *Chemosphere* **14**: 279–291.

15. Hansch, C., and A. Leo. 1979. *Substituent constants for correlation analysis in chemistry and biology*, Wiley, New York.

16. Meylan, W. M., and P. H. Howard. 1995. Atom/fragment contribution method for estimating octanol-water partition coefficients. *J. Pharm. Sci.* **84**: 83–92.

17. Mackay, D., R. Mascarenhas, W. Y. Shiu, S. C. Valvani, and S. H. Yalkowsky. 1980. Aqueous solubility of polychlorinated biphenyls. *Chemosphere* **9**: 257–264.

18. Arbuckle, W. B. 1983. Estimating activity coefficients for use in calculating environmental parameters. *Environ. Sci. Technol.* **17**: 537–542.

7

▅▅ Solving Ionic Equilibria Problems

In this chapter you will learn how to use the three main types of tools environmental scientists and engineers use to solve problems involving ionic equilibria in water: graphical, algebraic, and numerical (computer-based) techniques. The types of equations applicable to all three approaches are defined and described, along with the important concept of α as the fraction of the total (analytical) concentration of a substance present in a particular chemical form. Construction and interpretation of single "master-variable" diagrams (e.g., pC-pH diagrams) are explained, and their use to solve acid-base equilibrium problems is illustrated through examples. Construction of two-master-variable (predominance-area) diagrams (e.g., pH-log P_{CO_2} diagrams) and their use to illustrate mineral/phase equilibria also are described. The basic concepts and techniques used to solve ionic equilibria by algebraic techniques are developed through simple examples, with an emphasis on understanding the conditions under which it is appropriate to make simplifying assumptions. Because many "real-world" problems involving ionic equilibria in aquatic systems are too complicated to solve conveniently through graphical or manual algebraic techniques, emphasis is placed on the use of computer-based solutions for equilibrium problems. After a brief description of the history of computer solutions for ionic equilibria and the fundamental principles by which such programs operate, example-based instructions are given for use of the program MINEQL+.

Key terms and concepts

- Mass-action (equilibrium) expressions, mass-balance equations: X_T and TOTX, charge-balance (electroneutrality) equations, proton-balance equations
- α_i, fraction of X_T present as species i
- Master variables, pC $= -\log$ C, pC-pH diagrams, system points
- Predominance-area diagrams
- Eight-step approach for manual algebraic solution of ionic equilibria
- Components and various types of species in computer-based equilibrium programs

7.1 Introduction

A large part of aquatic chemistry involves the solution of ***ionic equilibrium*** problems. Such problems are important, for example, in water treatment chemistry, in describing the chemical composition of natural waters, and in analytical aspects of aquatic chemistry. Although the term "ionic equilibria" implies an exclusive focus on ions, as used here, the term is not meant to be so restrictive. Some ionic equilibria involve dissolved gases (e.g., CO_2 and O_2) and *air-water equilibria* of gases. Some important *acid-base and complexation equilibria* for aquatic systems involve organic compounds, particularly organic acids and bases. Finally, *solubility equilibria* involve solid (mineral) phases that are not ionic.

   This chapter describes three basic approaches—graphical, algebraic, and numerical (computer-based) methods—to solve and/or display chemical equilibria involving the kinds of species and equilibrium processes italicized above: gas transfer, acid-base, complexation, and mineral solubility reactions. All three approaches rely on the same set of mathematical expressions that define chemical equilibrium and associated constraints. Solutions for a fifth process, oxidation-reduction (redox) reactions, rely on similar types of expressions and similar graphical, algebraic, and numerical approaches. However, solving redox problems requires some additional understanding about redox fundamentals and additional equations and terms, and so we defer discussion of solving redox equilibria until Chapter 11.

7.2 Equations used to define and constrain ionic equilibria

Five types of equations or relationships are used to define chemical equilibria: mass-action (or equilibrium-constant, the term we use to refer to mass action) expressions, two kinds of mass-balance expressions (X_T and TOTX), charge-balance expressions based on the electroneutrality constraint, and proton balances, which are analogous to charge balances but are based on balancing the products resulting from the release of protons and the products of consumption (or acceptance) of protons. The goal is to use these equations to obtain an equal number of equations and unknowns and thus have a solvable problem. To illustrate the development of these equations, we will use the carbonic acid-bicarbonate-carbonate system (hereafter referred to simply as the "carbonate system") because of its importance in defining the acid-base chemistry and chemical composition of natural waters. Figure 7.1 is a schematic of important processes in the carbonate system; Chapter 8 discusses the carbonate system in more detail (see Section 8.5).

$CO_{2(g)}$

$K_H = 3.39\times10^{-2}$ M atm^{-1} = $10^{-1.47}$

∇

$K_h = 2.5\times10^{-3}$ $K_{a0} = 2\times10^{-4}$ $K_{a2} = 4.7\times10^{-11} = 10^{-10.33}$

$H_2O + CO_{2(aq)} \rightleftharpoons H_2CO_3 \rightleftharpoons H^+ + HCO_3^- \rightleftharpoons H^+ + CO_3^{2-}$

Ca^{2+}

$K_{s0} = 3.8\times10^{-9}$

$K_{a1} = 4.45\times10^{-7} = 10^{-6.35}$

$H_2CO_3^*$

$CaCO_{3(s)}$
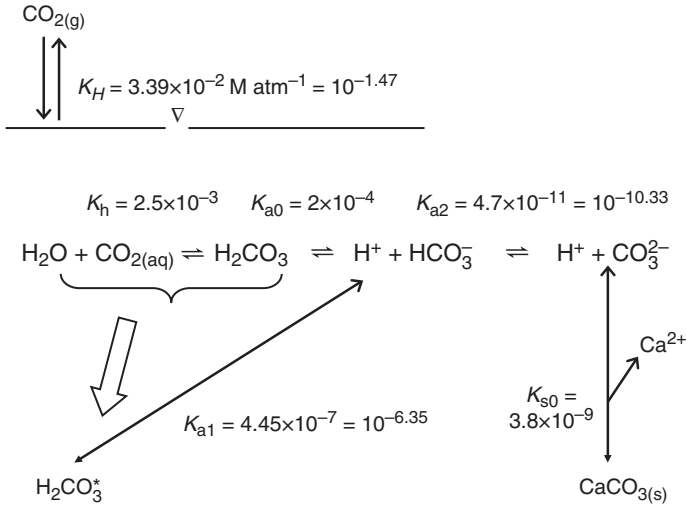
Figure 7.1 Schematic representation of the main equilibria involved in the CO_2-carbonate system. $H_2CO_3^*$ is the sum of $CO_{2(aq)}$ and H_2CO_3 (true carbonic acid). K_{a0} is the acid dissociation constant for true carbonic acid, and K_{a1} is the acid dissociation constant for the composite species $H_2CO_3^*$. K values are for 25°C.

7.2.1 Equilibrium constant or mass-action expressions

These are based on stoichiometric relationships defined by chemical reactions or phase-transfer processes. For a general reaction, $aA + bB \rightleftharpoons cC + dD$, where the lowercase letters are stoichiometric coefficients, the equilibrium expression is

$$K_{eq} = \frac{\{C\}^c\{D\}^d}{\{A\}^a\{B\}^b},$$

(7.1)

where $\{i\}$ stands for the activity of species i. Recall that the equilibrium constant is related to $\Delta G°$ of the reaction ($\Delta G° = -RT \ln K$). As described in Chapter 4, under some circumstances we can approximate the activity terms using molar concentrations:

$$^cK_{eq} = \frac{[C]^c[D]^d}{[A]^a[B]^b}$$

(7.2)

From the general relationship between activity and concentration, $\{i\} = \gamma_i[i]$, we can see that the concentration-based equilibrium constant $^cK_{eq}$ for the general reaction $aA + bB \rightleftharpoons cC + dD$ is related to the thermodynamic (activity-based) constant as follows:

$$^cK_{eq} = K_{eq} \times \frac{\gamma_A{}^a\gamma_B{}^b}{\gamma_C{}^c\gamma_D{}^d}$$

(7.3)

Important equilibrium constant expressions for the carbonate system (Figure 7.1) include acid dissociation constants (K_{a1} and K_{a2}), air-water equilibria (K_H for CO_2), and the solubility product, K_{s0}, for calcium carbonate.

Three important issues need to be discussed regarding the use of equilibrium constant expressions in solving ionic equilibrium problems. First, it frequently is useful to write these expressions in log form. The general example (Eq. 7.2) then becomes

$$^c \log K_{eq} = c \log[C] + d \log[D] - a \log[A] - b \log[B]. \tag{7.4}$$

As we shall see, such logarithmic expressions are particularly useful for graphical solutions, which usually involve logarithmic plots of variables.

Second, if equilibrium constants are expressed as thermodynamic values (i.e., in terms of activities), there is an inconsistency between them and the other kinds of equations available to solve equilibrium problems, which are written in molar or equivalent concentrations. Several ways around this problem are described in Section 7.4 on algebraic solutions.

Third, in solving ionic equilibria, one frequently encounters equilibrium expressions for which the value of K is unknown. Sometimes, K can be computed from tabulated values of $G°_f$ (free energy of formation) of the products and reactants, as described in Chapter 3 (see Section 3.11). In other cases, K for the reaction of interest can be obtained by adding or subtracting other reactions for which K values are known. This approach is used in several examples later in this chapter. A simple example here illustrates the basic idea. Consider the following expression for the dissolution of calcium carbonate:

$$CaCO_{3(s)} + H^+ \rightleftharpoons Ca^{2+} + HCO_3^- \tag{7.5}$$

This expression is used in water treatment chemistry and is the basis for the Langelier index of calcium carbonate saturation (see Sections 10.2 and 10.4). Most tabulations, however, of equilibrium constants for the carbonate system do not list this specific reaction. Inspection of the reaction suggests that it can be derived by adding two well-known reactions for which K values are available: the solubility product for calcium carbonate, and reverse reaction for the second acid dissociation of carbonic acid. The equilibrium constant for the net reaction is obtained by multiplying the K values for the two reactions:

$$CaCO_{3(s)} \rightleftharpoons Ca^{2+} + CO_3^{2-} \qquad K_{s0} = 10^{-8.35}$$
$$\underline{CO_3^{2-} + H^+ \rightleftharpoons HCO_3^- \qquad K_{a2}^{-1} = 10^{10.33}}$$

Net:

$$CaCO_{3(s)} + H^+ \rightleftharpoons Ca^{2+} + HCO_3^- \quad K_{net} = K_{s0}K_{a2}^{-1} = 10^{-8.35} \times 10^{10.33} = 10^{1.98}$$
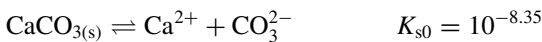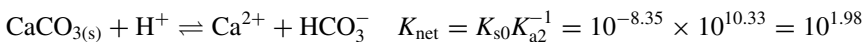
It is mathematically equivalent to write the second reaction as the dissociation of HCO_3^- and subtract it from the solubility expression for $CaCO_3$. In that case, we *divide K_{s0}* by K_{a2} (where $K_{a2} = 10^{-10.33}$).

The above example can be formulated as a general rule: **When two reactions are added, the equilibrium constant for the net reaction is the *product* of the**

K values for the individual reactions; when a reaction is subtracted from another, K for the net reaction is obtained by *dividing K for the reaction being subtracted into K for the other reaction.* The basis for this rule is the fact that equilibrium constants are exponentially related to free energies of reaction. Multiplying K values is equivalent to adding $\log K$ values, and the latter is equivalent to adding free energies of reaction ($\Delta G°_r$).

7.2.2 Mass-balance (X_T) expressions

In many equilibrium problems, information is given about the total concentration of an acid-base system or some other substance that can exist as multiple species in solution, for which concentrations (or activities) of the individual species are not known. A mass-balance equation (sometimes called a "mole-balance equation") then can be written as a constraint on the system. In general, we can write

$$X_T = \sum_i [X]_i, \tag{7.6}$$

where X is the species/element of interest, concentrations are in molar units, subscript $_T$ stands for total dissolved, and the summation is over all chemical species of the substance in solution. For a simple carbonic acid-carbonate system, X is carbon, and thus C_T is

$$C_T = [H_2CO_3^*] + [HCO_3^-] + [CO_3^{2-}], \tag{7.7}$$

where $H_2CO_3^*$ is the sum of dissolved CO_2 and true carbonic acid, as shown in Figure 7.1:

$$[H_2CO_3^*] = [CO_2]_{aq} + [H_2CO_3] \tag{7.8}$$

Routine analytical methods do not distinguish between true carbonic acid and dissolved CO_2, so it is convenient to lump the two species together into the "composite species" $H_2CO_3^*$. The expression in Eq. 7.7 assumes that from a mass-balance perspective there are no significant soluble complexes involving bicarbonate or carbonate ions, which usually is the case in freshwater systems. C_T for the carbonate system can be measured by several analytical techniques and thus is a common item of information in problems involving this system.

7.2.3 *TOT*X expressions

For systems in which both dissolved and gaseous or precipitated species affect the mass balance, the total amount present is X_T plus any material in the solid or (occasionally) gaseous phases. For example, in a closed system containing calcium carbonate,

$$TOTC = [CaCO_{3(s)}] + [H_2CO_3^*] + [HCO_3^-] + [CO_3^{2-}], \tag{7.9}$$

and

$$TOTCa = [CaCO_{3(s)}] + [Ca^{2+}], \tag{7.10}$$

Although these equations are useful in determining the total mass in the system or for completing total mass balances (i.e., fraction of metal precipitated), they are not often used as one of the equations in solving equilibrium problems.

7.2.4 The last equation

At this point, the equilibrium expressions (including that for the dissociation of water) and the mass-balance equations for the relevant species provide us with n unknowns but generally only $n-1$ equations. Thus, one more equation usually is needed, and there are three choices for this final expression: the charge-balance, the proton-balance, and the $TOTH$ equation. In the end, each is a different way of expressing the same equation/concept and the choice depends on which makes most sense to the solver of the problem. That said, understanding of the $TOTH$ equation is necessary to understand and use most computer-based solution programs.

7.2.4.1 Charge-balance (electroneutrality) expressions

All solutions are electrically neutral. Thus, the sum of the cation concentrations must equal the sum of the anion concentrations when both are expressed on a charge equivalents basis—that is, as the molar concentration times the integer value of the charge on each ion (ignoring the sign of the charge). In general, this constraint can be expressed as

$$\sum \text{cation equivalents} = \sum \text{anion equivalents,}$$

$$\sum_i v_i \left[M^{v_i+} \right] = \sum_j v_j \left[A^{v_j-} \right]. \tag{7.11}$$

The concentrations of cations (M) and anions (A) are expressed in moles per liter, and v_i and v_j are the absolute values of the integer charges on each cation and anion, respectively. Because one mole of a substance with a ± 2 charge contributes two moles of charge, it is important to remember to multiply by the factor of 2. For a solution of sodium bicarbonate ($NaHCO_3$) in pure water, the charge-balance equation is

$$[H^+] + [Na^+] = [HCO_3^-] + 2[CO_3^{2-}] + [OH^-], \tag{7.12}$$

and for a solution of carbon dioxide in pure water, the charge balance is

$$[H^+] = [HCO_3^-] + 2[CO_3^{2-}] + [OH^-]. \tag{7.13}$$

The starting substance ($CO_{2(aq)}$) does not appear in the charge balance because it is not an ion; only the ionic products of its reaction with water and ionic products of the dissociation of water appear in the expression.

7.2.4.2 Proton-balance expressions

These equations represent a special case of the electroneutrality condition, and they apply primarily to problems dealing with acid-base equilibria. For any acid that dissociates and releases a proton, another substance (a base) must accept the proton. The sum of the concentrations of all the products of proton release in an acid-base system thus must equal the sum of the concentrations of the products of proton consumption (or proton acceptance). This is because free protons do not exist in aqueous solution. As discussed in Chapter 8, when acids dissociate in water, the proton is accepted by a base; if no other base is available, water itself acts as a base, accepting the proton to become H_3O^+. Thus we can write the general proton-balance expression as

$$\sum PPC = \sum PPR, \tag{7.14}$$

where PPC stands for products of proton consumption (or proton acceptance) and PPR stands for products of proton release. The simplest proton balance is for water itself. When it dissociates, the product of proton release is hydroxide ion, OH^-; the product of proton consumption is the hydronium ion, H_3O^+. Therefore, the proton balance for water is

$$\sum PPC = \sum PPR,$$
$$[H_3O^+] = [OH^-]. \tag{7.15}$$

For simplicity we usually ignore the fact that H^+ is attached to H_2O and write it just as H^+. The proton balance thus becomes

$$\sum PPC = \sum PPR$$
$$[H^+] = [OH^-]. \tag{7.16}$$

Equation 7.16 is the starting point for *all* proton-balance expressions of aqueous solutions; that is, $[H^+]$ is always a product of proton consumption (because it represents H_3O^+), and OH^- is always a product of proton release in such proton balances. Proton balances for some carbonic acid-carbonate systems are given in the following examples. In Example 7.2, note that it is always possible to convert a charge balance to a proton balance (and vice versa).

EXAMPLE 7.1 Dissolution of CO$_2$ in water: As shown in Figure 7.1, dissolved CO_2 becomes hydrated to form true carbonic acid, H_2CO_3, which then dissociates to form a bicarbonate ion, HCO_3^-, and one H^+ (again, really H_3O^+). In turn, HCO_3^- can dissociate to form a carbonate ion, CO_3^{2-}, and another H^+. However, $CO_{2(aq)}$ and its hydration product H_2CO_3 (the sum of which, as we noted above, is $H_2CO_3^*$) cannot accept another proton. The proton-balance expression thus is

(1) $\sum PPC = \sum PPR,$
$[H^+] = [HCO_3^-] + 2[CO_3^{2-}] + [OH^-].$

Note that the reactant (CO_2 or $H_2CO_3^*$) is not a part of the proton balance. This is a general rule for proton balances; only the products of reaction are a part of the expression. Note also that the only product of proton consumption is H^+ itself, from the dissociation of water, carbonic acid, and bicarbonate. The factor of 2 multiplying the CO_3^{2-} concentration derives from the stoichiometric fact that for every CO_3^{2-} formed from H_2CO_3, two H^+ are produced. Finally, it is pertinent to note that the proton-balance equation in this case is the same as the charge-balance equation.

EXAMPLE 7.2 Dissolution of sodium bicarbonate ($NaHCO_3$) in water: Sodium is a strong base cation and has no significant tendency to react with water or its dissociation products. Therefore, it does not contribute to the proton balance. In contrast, bicarbonate is both a weak acid and a weak base. It can accept a proton to form carbonic acid and can release a proton to form carbonate ion. The proton-balance expression for $NaHCO_3$ and water thus is

(2) $$\sum PPC = \sum PPR,$$
$$[H^+] + [H_2CO_3^*] = [CO_3^{2-}] + [OH^-].$$

Recall that $C_T = [H_2CO_3^*] + [HCO_3^-] + [CO_3^{2-}]$. Rearranging, we obtain $[H_2CO_3^*] = C_T - [HCO_3^-] - [CO_3^{2-}]$. Also note that because for each unit of bicarbonate added to the solution, one unit of sodium is added, so $C_T = [Na^+]$. Substituting $[H_2CO_3^*]$ into the proton balance,

$$[H^+] + [Na^+] - [HCO_3^-] - [CO_3^{2-}] = [CO_3^{2-}] + [OH^-].$$

Combining the anions on the right hand side gives the charge balance:

$$[H^+] + [Na^+] = [HCO_3^-] + 2[CO_3^{2-}] + [OH^-].$$

Thus, either the charge balance or the proton balance (but not both) can be used in solving a problem.

7.2.4.3 TOTH expressions

In development of the *TOT*H expression, the acid/base groups must be categorized. For each group, one must be chosen as the reference species. For the example of adding sodium bicarbonate to water, the groups are (1) H^+, OH^-, H_2O; (2) $H_2CO_3^*$, HCO_3^-, and CO_3^{2-}; and (3) Na^+. The choice of the reference species is arbitrary, but it is convenient if the reference species is chosen as the one that will be dominant in the system. Here we will choose H_2O and HCO_3^-. All species are now related to the reference species:

$$
\begin{aligned}
1\ H_2O + 0\ H^+ &\rightleftharpoons 1\ H_2O \\
0\ H_2O + 1\ H^+ &\rightleftharpoons 1\ H^+ \\
1\ H_2O - 1\ H^+ &\rightleftharpoons 1\ OH^- \\
1\ Na^+ + 0\ H^+ &\rightleftharpoons 1\ Na^+ \\
1\ HCO_3^- + 1\ H^+ &\rightleftharpoons H_2CO_3^* \\
1\ HCO_3^- + 0\ H^+ &\rightleftharpoons 1\ HCO_3^- \\
1\ HCO_3^- - 1\ H^+ &\rightleftharpoons 1\ CO_3^{2-}
\end{aligned}
$$
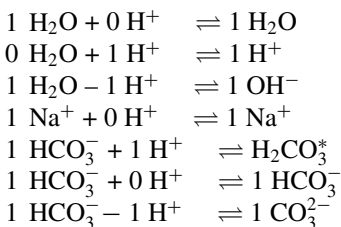
The coefficients on the protons (n_i) indicate the excesses or deficiencies of H^+ in the product species relative to the reference species. For example, the proton (or H_3O^+) contains one more proton that water so $n = 1$. Hydroxide contains one less proton than water, and thus n for hydroxide is -1. The $TOTH$ at equilibrium ($TOTH_{eq}$) is $\sum\limits_i n_i\,[X_i]$ for all X:

$$TOTH_{eq} = [H_2O] \times 0 + [H^+] \times 1 + [OH^-] \times (-1) + [Na^+] \times 0$$

$$+ [H_2CO_3^*] \times 1 + [HCO_3^-] \times 0 + [CO_3^{2-}] \times (-1) \qquad (7.17a)$$

$$TOTH_{eq} = [H^+] - [OH^-] + [H_2CO_3^*] - [CO_3^{2-}] \qquad (7.17b)$$

The expression that arises is dependent on the choice of reference species. If H^+ and CO_3^{2-} are chosen as the reference species, one will not obtain the same equation as shown in Eq. 7.17b.

To complete the $TOTH$ expression, the proton concentration added ($TOTH_{in}$) relative to the reference species needs to be determined. If Na_2CO_3 is added, the contribution to $TOTH_{in}$ is the negative of the concentration of the sodium carbonate added (i.e., if 1×10^{-3} M is added, $TOTH_{in} = -1 \times 10^{-3}$), because CO_3^{2-} is proton deficient ($n = -1$) compared to the reference species HCO_3^-. If NaOH is added, the contribution is again the negative of the concentration added ($n = -1$) because hydroxide is proton deficient relative to water. If $NaHCO_3$ is added in any amount, the contribution to $TOTH_{in}$ is 0 (because HCO_3^- is the reference). The equation is completed by setting $TOTH_{in} = TOTH_{eq}$, which is the general form of the $TOTH$ expression.

If we add only $NaHCO_3$ to the solution, $TOTH_{in} = 0$, and thus substituting in this value and the expression for $TOTH_{eq}$ (Eq. 7.17b) into $TOTH_{in} = TOTH_{eq}$ gives

$$0 = [H^+] - [OH^-] + [H_2CO_3^*] - [CO_3^{2-}]. \qquad (7.18a)$$

This equation can be rearranged to give

$$[H^+] + [H_2CO_3^*] = [CO_3^{2-}] + [OH^-], \qquad (7.18b)$$

which, of course, is the proton balance shown in Example 7.2, and we already know that this is equivalent to the charge balance. Thus, the charge-balance, the proton-balance, and the $TOTH$ equations are three different ways of looking at the same equation.

7.2.5 α_i as the fraction of X_T present as species i

The alpha (α) notational system is widely used in ionic equilibria to express the fraction of the total analytical concentration of an acid-base system present as a particular ionic species. In general,

$$\alpha_i = \frac{[i]}{X_T}, \qquad (7.19)$$

where $[i]$ is the molar concentration of the ith species and X_T is the sum of the molar concentrations of all species in the system. For the carbonate system illustrated in

Figure 7.1 and its C_T, as represented in Eq. 7.7, we can write

$$\alpha_0 = \frac{[H_2CO_3^*]}{[H_2CO_3^*] + [HCO_3^-] + [CO_3^{2-}]} = \frac{[H_2CO_3^*]}{C_T}, \qquad (7.20a)$$

$$\alpha_1 = \frac{[HCO_3^-]}{[H_2CO_3^*] + [HCO_3^-] + [CO_3^{2-}]} = \frac{[HCO_3^-]}{C_T}, \qquad (7.20b)$$

$$\alpha_2 = \frac{[CO_3^{2-}]}{[H_2CO_3^*] + [HCO_3^-] + [CO_3^{2-}]} = \frac{[CO_3^{2-}]}{C_T}. \qquad (7.20c)$$

By convention, for all acid-base systems α_0 is the fraction of C_T present as the completely protonated acid; α_1 is the fraction of C_T present as the first dissociation product of the acid; α_2 is the fraction of C_T present as the second dissociation product of the acid, and α_n is the fraction of C_T present as the completely deprotonated form of an n-protic acid. By simple rearrangement of Eqs. 7.18–7.20, we have

$$[H_2CO_3^*] = \alpha_0 C_T, \qquad (7.21)$$

$$[HCO_3^-] = \alpha_1 C_T, \qquad (7.22)$$

$$[CO_3^{2-}] = \alpha_2 C_T. \qquad (7.23)$$

The usefulness of the α notation lies in the fact that the α values can be expressed in terms solely of equilibrium constants and $\{H^+\}$. Values of α for a given species thus can be calculated and tabulated as a function of pH, independent of the concentration of individual acid-base species or of C_T for the system of interest. For any diprotic acid, the expressions for α_0, α_1, and α_2 can be derived readily from the corresponding expressions for C_T, K_{a1}, and K_{a2} (see Example 7.3):

$$\alpha_0 = \frac{\{H^+\}^2}{\{H^+\}^2 + \{H^+\}K_{a1} + K_{a1}K_{a2}} \qquad (7.24)$$

$$\alpha_1 = \frac{\{H^+\}K_{a1}}{\{H^+\}^2 + \{H^+\}K_{a1} + K_{a1}K_{a2}} \qquad (7.25)$$

$$\alpha_2 = \frac{K_{a1}K_{a2}}{\{H^+\}^2 + \{H^+\}K_{a1} + K_{a1}K_{a2}} \qquad (7.26)$$

Equations 7.24–7.26 can be generalized for a *n*-protic acid as follows:

$$\alpha_i = \frac{DT_i}{\{H^+\}^n + \{H^+\}^{n-1}K_{a1} + \{H^+\}^{n-2}K_{a1}K_{a2} + \ldots + \{H^+\}K_{a1}\ldots K_{an-1} + K_{a1}\ldots K_{an}}, \qquad (7.27)$$

where DT_i stands for the corresponding denominator term for species *i*. Note that $\{H^+\}^n$ is the denominator term for the fully protonated species H_nB, and that $K_{a1}\ldots K_{an}$ is the

Table 7.1 Alpha (α) expressions for triprotic acids

$$\alpha_0 = \frac{\{H^+\}^3}{\{H^+\}^3 + \{H^+\}^2 K_1 + \{H^+\} K_1 K_2 + K_1 K_2 K_3}$$

$$\alpha_1 = \frac{\{H^+\}^2 K_1}{\{H^+\}^3 + \{H^+\}^2 K_1 + \{H^+\} K_1 K_2 + K_1 K_2 K_3}$$

$$\alpha_2 = \frac{\{H^+\}^2 K_1 K_2}{\{H^+\}^3 + \{H^+\}^2 K_1 + \{H^+\} K_1 K_2 + K_1 K_2 K_3}$$

$$\alpha_3 = \frac{K_1 K_2 K_3}{\{H^+\}^3 + \{H^+\}^2 K_1 + \{H^+\} K_1 K_2 + K_1 K_2 K_3}$$

term for the fully deprotonated species B^{n-}. For a monoprotic acid, HB, Eq. 7.27 thus yields

$$\alpha_0 = \frac{[HB]}{C_T} = \frac{\{H^+\}}{\{H^+\} + K_{a1}} \tag{7.28}$$

and

$$\alpha_1 = \frac{[B^-]}{C_T} = \frac{K_{a1}}{\{H^+\} + K_{a1}}. \tag{7.29}$$

Expressions for α_0 to α_3 for triprotic acids are given in Table 7.1.

EXAMPLE 7.3 Derivation of α expressions for diprotic acids: Derivations of α expressions for any acid-base system starts with writing the basic expression as in Eqs. 7.17–7.20 and then solving the acid dissociation constants to express all the components of the denominator in terms of the numerator term. For example, for α_0,

(1) $\alpha_0 = \dfrac{[H_2B]}{C_T} = \dfrac{[H_2B]}{[H_2B] + [HB^-] + [B^{2-}]}.$

The acid dissociation (equilibrium) constants are*

(2) $K_1 = \dfrac{\{H^+\}[HB^-]}{[H_2B]},$ (3) $K_2 = \dfrac{\{H^+\}[B^{2-}]}{[HB^-]}.$

Solving K_1 for $[HB^-]$ and solving K_2 for $[B^{2-}]$ yields

(4) $[HB^-] = \dfrac{K_1[H_2B]}{\{H^+\}},$ (5) $[B^{2-}] = \dfrac{K_2[HB^-]}{\{H^+\}},$

---

*For consistency here we write K_{a1} and K_{a2} as mixed constants with H^+ expressed as activity and other terms in molar concentrations (because pH is a measure of the log of H^+ activity and the other constituents are expressed in molar concentration in X_T). Values of the equilibrium constants thus are not the true "thermodynamic" values but apply only to a particular ionic strength. See Eq. 7.3 for the relationship between these Ks and the thermodynamic values.

which is not quite what we need. However, if we substitute Eq. (4) for $[HB^-]$ into Eq. (5), we obtain an expression for $[B^{2-}]$ in terms of $[H_2B]$:

(6) $[B^{2-}] = \dfrac{K_1K_2[H_2B]}{\{H^+\}^2}$

Substituting Eqs. (4) and (6) into Eq. (1) yields

(7) $\alpha_0 = \dfrac{[H_2B]}{[H_2B] + K_1[H_2B]/\{H^+\} + K_1K_2[H_2B]/\{H^+\}^2}.$

We can eliminate the term $[H_2B]$ from Eq. (7) because it appears in every term in the numerator and denominator. Furthermore, we can simplify the result by multiplying the numerator and denominator by $\{H^+\}^2$ to obtain

(8) $\alpha_0 = \dfrac{\{H^+\}^2}{\{H^+\}^2 + K_1\{H^+\} + K_1K_2}.$

For α_1, we solve K_1 and K_2 for $[H_2B]$ and $[B^{2-}]$, respectively, in terms of $[HB^-]$ and substitute the results into the denominator of the α_1 expression:

(9) $[H_2B] = \dfrac{\{H^+\}[HB^-]}{K_1},$ (10) $[B^{2-}] = \dfrac{K_2[HB^-]}{\{H^+\}},$

(11) $\alpha_1 = \dfrac{[HB^-]}{[H_2B]+[HB^-]+[B^{2-}]} = \dfrac{[HB^-]}{\{H^+\}[HB^-]/K_1+[HB^-]+K_2[HB^-]/\{H^+\}}.$

Again, we can eliminate the term $[HB^-]$ from the right side of Eq. (11) and simplify by multiplying the numerator and denominator by the term $K_1\{H^+\}$ to get

(12) $\alpha_1 = \dfrac{K_1\{H^+\}}{\{H^+\}^2 + K_1\{H^+\} + K_1K_2}.$

Finally, for α_2 we solve K_2 for $[HB^-]$ in terms of $[B^{2-}]$ and substitute that into K_1 to get $[H_2B]$ in terms of $[B^{2-}]$ and then substitute both results into the denominator of the α_2 expression:

(13) $[HB^-] = \dfrac{\{H^+\}[B^{2-}]}{K_2},$

(14) $[H_2B] = \dfrac{\{H^+\}[HB^-]}{K_1} = \dfrac{\{H^+\}^2[B^{2-}]}{K_1K_2},$

and

(15) $\alpha_2 = \dfrac{[B^{2-}]}{[H_2B]+HB^-]+[B^{2-}]} = \dfrac{[B^{2-}]}{\{H^+\}^2[B^{2-}]/K_1K_2+\{H^+\}[B^{2-}]/K_2+[B^{2-}]},$

which upon simplification yields

(16) $\alpha_2 = \dfrac{K_1K_2}{\{H^+\}^2 + K_1\{H^+\} + K_1K_2}.$

Finally, we note that the concept of α values is not limited to acids and bases but also is used for metal ions and their complexes with various ligands. For example, for metal M

and ligand L we can write

$$\alpha_M = \frac{[M^{m+}]}{M_{TM}}, \quad \alpha_{ML} = \frac{[ML^{+m-1}]}{M_{TM}}, \quad \ldots \alpha_{ML_n} = \frac{[ML_n^{+m-n}]}{M_{TM}}, \tag{7.30}$$

where $M_{TM} = [M^{m+}] + [ML^{+m-1}] + \ldots + [ML_n^{+m-n}]$, and the equilibrium constants used in the expressions are stepwise complex dissociation constants.

7.3 Graphical methods of displaying ionic equilibria and solving equilibrium problems

7.3.1 Introduction

Many types of graphs are used to display ionic equilibrium, but two types are by far the most common and are the focus of this chapter. The first involves plots of the log of concentration of various ionic species versus some independent variable, most commonly pH. Because the negative log of concentration is denoted pC, and because ionic concentrations in natural waters generally have negative log values, such plots often are called pC-pH diagrams. The independent variable sometimes is referred to as a "master variable," and the plots also are called "single master-variable diagrams." The second type involves plots of master variables on both axes, e.g., log P_{CO_2} versus pH or redox potential, E_h versus pH. These are often called "predominance-area" diagrams because the lines on such plots delimit regions in which a given species (ionic form or mineral phase) is the predominant species in the system.

7.3.2 pC-pH diagrams

Equilibrium expressions for acid-base reactions have multiplicative terms, and concentrations of reactants and products vary over many orders of magnitude over the pH range of 0–14, which itself is a range of 14 orders of magnitude for $\{H^+\}$. Consequently, it is not feasible to graph concentrations of acid-base species as a linear function of pH. A more useful way is to plot concentrations on a log scale ($-\log C$ or pC) versus pH ($-\log\{H^+\}$). This results in generally simple, straight line relationships. The following paragraphs and equations describe how such diagrams are developed from acid-base equilibrium and mass-balance relationships.

Consider the monoprotic acid, acetic acid (HAc):

$$K_a = \frac{\{H^+\}\{Ac^-\}}{\{HAc\}} = 1.8 \times 10^{-5}; pK_a = 4.76 \tag{7.31}$$

For ease in developing the equations for pC-pH diagrams, we will ignore differences between activity and concentration, and from here forward will use brackets, [i], to denote either. We can write the mass-balance expression:

$$Ac_T = [HAc] + [Ac^-] \tag{7.32}$$

Solving Eq. 7.31 in terms of $[Ac^-]$ and $[HAc]$, we obtain

$$[HAc] = \frac{[H^+][Ac^-]}{K_a}, \tag{7.33}$$

and

$$[Ac^-] = \frac{K_a[HAc]}{[H^+]}. \tag{7.34}$$

Substituting Eq. 7.33 and 7.34 into Eq. 7.32 and solving for $[HAc]$ and $[Ac^-]$, we obtain

$$Ac_T = [HAc] + K_a[HAc][H^+] \tag{7.35a}$$

or

$$[HAc] = \frac{Ac_T[H^+]}{[H^+] + K_a}, \tag{7.35b}$$

and

$$Ac_T = [Ac^-] + [H^+][Ac^-]/K_a \tag{7.36a}$$

or

$$[Ac^-] = \frac{Ac_T K_a}{[H^+] + K_a}. \tag{7.36b}$$

Furthermore, we know that

$$K_w = [H^+][OH^-]. \tag{7.37}$$

For the system HAc and water, we have four unknowns: $[HAc]$, $[Ac^-]$, $[H^+]$, and $[OH^-]$. We wish to plot the unknowns versus pH, or more precisely, plot $-\log X$ versus pH, where X is one of the unknown concentrations. From equations 7.35b, 7.36b, and 7.37, we can do this—plotting $-\log X$ on the ordinate versus pH on the abscissa. It is apparent from Eqs. 7.35b and 7.36b that we need to know the values of Ac_T and K_a to draw the diagram. Figure 7.2 shows the pC-pH diagram for acetic acid ($pK_a = 4.76$) at $Ac_T = 1.0 \times 10^{-2}$ M ($pAc_T = 2.0$). Instructions on how the lines are developed are as follows.

(1) $[H^+]$.   By definition, $pH = -\log[H^+]$ since we are ignoring differences between activity and concentration. This defines a line with a slope of -1 and an intercept of $pH = 0$:

$$\mathbf{pC = -\log[H^+] = pH}; \tag{7.38}$$

At $pH = 0$, $pC = 0$; that is, $[H^+] = 1.0$.
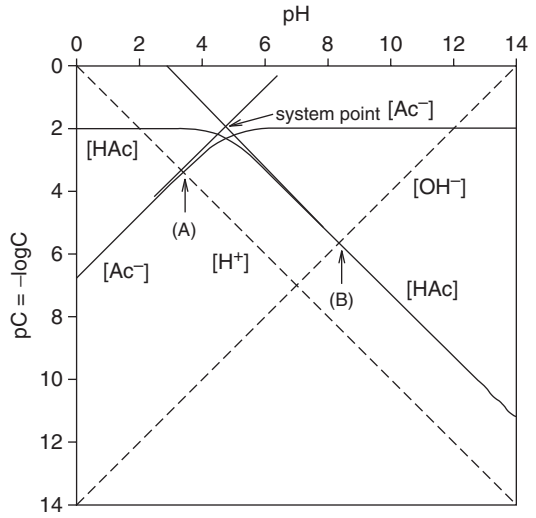
Figure 7.2 pC-pH diagram for
1.0×10^{-2} M acetic acid.

(2) [OH$^-$]. From Eq. 7.37, $\log K_w = -14.0 = \log[H^+] + \log[OH^-]$, or $pC = -\log[OH^-] = 14 + \log[H^+]$,

or

$$pC = 14 - pH, \tag{7.39}$$

which defines a line for $-\log[OH^-]$ with a slope of $+1$ and an intercept of $\log[OH^-] = 0$ when pH $= 14$.

(3) [HAc].   When pH $< pK_a$, that is, when $[H^+] >> K_a$, the denominator in Eq. 7.20b approaches $[H^+]$ and [HAc] approaches Ac_T:

$$[HAc] = Ac_T[H^+]/\{[H^+] + K_a\} \approx Ac_T[H^+]/[H^+] \approx Ac_T$$

or

$$p[HAc] = -\log[HAc] = pAc_T \quad \text{when pH} < pK_a \tag{7.40}$$

Thus, for pH $< pK_a$, $\log[HAc]$ is a straight line parallel to the pH axis at $pC = -\log[HAc] = 2.0$.

If pH $> pK_a$, $[H^+] << K_a$, and Eq. 7.35b becomes

$$[HAc] = Ac_T[H^+]/\{[H^+] + K_a\} \approx Ac_T[H^+]/K_a,$$

or

$$p[HAc] = -\log[HAc] = -\log Ac_T - \log[H^+] + \log K_a,$$

$$p[HAc] = -\log[HAc] = pAc_T - pK_a + pH. \tag{7.41}$$

Equation 7.41 defines a line with a slope of -1 for log[HAc] in the region pH $> \mathrm{p}K_a$. It can be constructed from the slope by assuming that it intersects the line $-$log[HAc] $= \mathrm{pAc_T} = 2.0$ (Eq. 7.40) at pH $= \mathrm{p}K_a$.

(4) [Ac$^-$].   Similarly, Eq. 7.36b can be represented by two asymptotes. If pH $> \mathrm{p}K_a$, then $K_a >> [\mathrm{H}^+]$, and

$$[\mathrm{Ac}^-] \approx \mathrm{Ac_T} K_a / K_a = \mathrm{Ac_T},$$

or

$$\mathbf{p[Ac^-] = -log[Ac^-] = pAc_T}; \qquad (7.42)$$

that is, the line is parallel to the pH axis at pC $= 2.0$. If pH $< \mathrm{p}K_a$, then $[\mathrm{H}^+] >> K_a$, and

$$[\mathrm{Ac}^-] \approx \mathrm{Ac_T} K_a / [\mathrm{H}^+], \text{ or } \mathrm{p}[\mathrm{Ac}^-] = -\log[\mathrm{Ac}^-] = -\log \mathrm{Ac_T} - \log K_a + \log[\mathrm{H}^+],$$

or

$$\mathbf{p[Ac^-] = -log[Ac^-] = pAc_T + pK_a - pH}, \qquad (7.43)$$

which has a slope of $+1$ and intersects the line $\mathrm{p}[\mathrm{Ac}^-] = \mathrm{pAc_T}$ (Eq. 7.42) at pH $= \mathrm{p}K_a$.

Finally, it is clear from the nature of Eqs. 7.35b and 7.36b that both denominator terms must be taken into account when the pH is close to $\mathrm{p}K_a$ and that the lines are curved in this region. At pH $= \mathrm{p}K_a$, p[HAc] $=$ p[Ac$^-$] $=$ p(Ac$_T$/2) $=$ pAc$_T$ $-$ log 2 $=$ pAc$_T$ $-$ 0.3. The exact curves for [HAc] and [Ac$^-$] thus intersect at this point. The pC-pH diagram thus should be completed by hand drawing curved lines through this point and connecting asymptotically to the horizontal lines for p[HAc] and p[Ac$^-$] $=$ pAc$_T$ and the sloping lines for p[HAc] and p[Ac$^-$]. The size of the curved region for each species should be approximately one log unit above and below pH $= \mathrm{p}K_a$. This can be seen from the Henderson-Hasselbach equation:

$$\mathrm{pH} = \mathrm{p}K_a + \log \frac{[\mathrm{X}^-]}{[\mathrm{HX}]} \qquad (7.44)$$

When the pH is one unit greater than $\mathrm{p}K_a$ (i.e., at pH 5.76 for acetic acid), log[Ac$^-$]/[HAc] $= 1.0$. Thus, the ratio [Ac$^-$]/[HAc] $= 10$, and [Ac$^-$] approaches Ac$_T$. Conversely, when the pH is one unit less than $\mathrm{p}K_a$ (i.e., pH 3.76 for acetic acid), log[Ac$^-$]/[HAc] $= -1.0$. Thus, the ratio [Ac$^-$]/[HAc] $= 0.10$, and [HAc] approaches Ac$_T$.

7.3.3 Simple approach to drawing pC-pH diagrams

Although it is useful to derive equations 7.40–7.43 at least once to understand the basis for the diagrams, it is not necessary to go through all the algebraic manipulations described in the preceding section to draw a pC-pH diagram for any acid-base system. Once you have this understanding, the only information you need to draw a pC-pH diagram is

Table 7.2 Step-by-step instructions for drawing pH-pC diagrams.

1. Draw and label the axes as a "fourth quadrant" graph with x-axis at top of graph labeled "pH" and the y-axis extended downward labeled "−log C" or "pC."
2. Draw identity lines for pH = −log[H$^+$] and pOH = −log[OH$^-$]. For H$^+$, draw straight line with slope −1 intercepting pC = 0 at pH = 0; for OH$^-$, draw a straight line with slope +1 intercepting pC = 0 at pH = 14.
3. Draw (lightly) a horizontal line parallel to and across the range of the pH axis at pC = − log X$_T$.
4. Insert a "system point" at pC = pX$_T$ and pH = pK_a.
5. Insert another point 0.3 log units below the system point.
6. **For HX,** at pH < pK_a, p[HX] = pX$_T$; this is the line drawn in #3; label it "[HX]."
    At pH > pK_a, p[HX] is a straight line with slope = −1 that intersects the system point. Draw the line lightly and label it.
7. **For X$^-$,**k at pH > pK_a, p[X$^-$] = pX$_T$; this is the line drawn in #3; label it "[X$^-$]."
    At pH < pK_a, p[X$^-$] is a straight line with slope = +1 that intersects the system point. Draw this line lightly and label it.
8. For pH = pK_a±1, lines for p[HX] and p[X$^-$] are curved. They intersect at pH = pK_a and the point 0.3 log units below the system point. The line for p[HX] approaches pX$_T$ at pH ≈ pK_a − 1.0. The line for p[X$^-$] approaches pX$_T$ at pH ≈ pK_a + 1.0. Sketch these curved lines to connect asymptotically with the horizontal and sloping lines for p[HX] and p[X$^-$] and darken all lines.
9. For polyprotic acids, repeat steps 4–8 for p$K_{2,3}$. .... Slopes for the acid-base species change across the pH range as follows. For diprotic acids: p[H$_2$X] has a slope of −2 in the pH region above pK_2, and p[X^{2-}] has a slope of +2 in the pH region below pK_1. For triprotic acids, p[H$_3$X] has a slope of −3 for pH > pK_3, and p[X^{3-}] has a slope of +3 for pH < pK_1. Similar changes in slope apply to higher order polyprotic acids.

(1) the pK_a of the acid (or the pK_a values for polyprotic acids), (2) the total analytical concentration (X$_T$) of the acid, and (3) the simple instructions given in Table 7.2.

Alternatively, it is easy to use a spreadsheet program to generate the pC-pH diagram. This is accomplished by first making a column of pH values (e.g., from 0 to 14). In the next column of cells, generate the corresponding [H$^+$] concentrations (e.g., [H$^+$] = 10^{-pH} or in spreadsheet notation, = 10^-A1, where A1 is cell you are referencing). Subsequent columns for [HAc], [Ac-], and [OH$^-$] are generated using Eqs. 7.35b, 7.36b, and 7.37. In spreadsheet notation with Ac$_T$ = 10^{-3} M, [HAc] would be =((10^-3)*B1)/(B1+ 10^-4.767), where cell B1 contains the [H$^+$] concentration based on the pH in cell A1. Dragging these formulas down for all pH values will generate the concentrations at each pH value. The logarithms of these values are needed to generated the pC-pH diagram, and these can be obtained using the log function in the spreadsheet program.

7.3.4 Use of pC-pH diagrams to solve acid-base equilibrium problems

pC-pH diagrams like that in Figure 7.2 are useful not only for gaining a quick visual perspective of the equilibrium concentrations of acid and base species as a function of pH but also for quantitatively solving simple to moderately complicated

acid-base equilibrium problems. We illustrate this problem-solving capability with Examples 7.4–7.8, the first two of which rely on the acetic acid/acetate diagram in Figure 7.2. In some cases (e.g., Examples 7.4 and 7.5), equilibrium conditions can be inferred directly from the stoichiometry of the reaction. In all the examples, we write and analyze the proton-balance expression. In most cases (and in *all* cases we shall analyze), the proton-balance expression can be simplified to only two important species (one on each side of the $\sum PPC = \sum PPR$ expression, and this tells us that the equilibrium condition (e.g., the equilibrium pH) can be found on the pC-pH diagram where the lines for these two species intersect (i.e., where their concentrations are equal).

EXAMPLE 7.4 Dissolution of 1.0×10^{-2} M acetic acid in pure water: The equilibrium reaction for this case is

$$HAc + H_2O \rightleftharpoons H_3O^+ + Ac^- \text{ or } HAc \rightleftharpoons H^+ + Ac^-.$$

From stoichiometric considerations, we see that $[H^+]$ must equal $[Ac^-]$ at equilibrium, and therefore the equilibrium pH must occur where the lines for $[H^+]$ and $[Ac^-]$ intersect.

The proton-balance expression is

$$\sum PPC = \sum PPR$$

$$[H^+] = [Ac^-] + [OH^-].$$

From the pC-pH diagram in Figure 7.2, we see that $[OH^-]$ is negligibly small compared with $[Ac^-]$ except at high pH ($>> 7$). Because we are adding a weak acid to pure water, we know that the equilibrium pH must be < 7.0. Consequently, we can ignore the term for $[OH^-]$ in the proton balance, and we find the equilibrium condition at $[H^+] \approx [Ac^-]$, which agrees with the conclusion from the stoichiometry of the reaction expression. This condition occurs at the intersection of the lines for $[H^+]$ and $[Ac^-]$, which occurs at pH = 3.4 (point (A) in Figure 7.2).

EXAMPLE 7.5 Dissolution of 1.0×10^{-2} M sodium acetate in pure water: The   equilibrium reaction is

$$Ac^- + H_2O \rightleftharpoons HAc + OH^-.$$
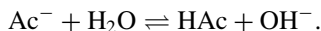
Thus, from stoichiometry, we see that at equilibrium $[HAc] = [OH^-]$ (assuming that the above reaction is the only significant source of both HAc and OH^-).

The proton-balance expression is

$$\sum PPC = \sum PPR,$$

$$[H^+] + [HAc] = [OH^-].$$

From Figure 7.2, we see that the line for $[H^+]$ is much lower than the line for $[HAc]$, except at low pH, which we would not expect to be the equilibrium situation since we are adding a weak base to pure water. Thus, $[H^+]$ can be assumed to be negligible in the proton balance, and the equilibrium condition is defined by $[HAc] = [OH^-]$, that is,

the intersection of these lines on the diagram. This occurs at pH $\sim$ 8.4 (point (B) in Figure 7.2).

EXAMPLE 7.6 Dissolution of 1.0×10^{-3} M sodium bicarbonate (NaHCO$_3$) in pure water: To solve this problem we drew the pC-pH diagram for the carbonic acid (H$_2$CO$_3^*$)-bicarbonate-carbonate system (pK_1 = 6.35, pK_2 = 10.33) for C_T = 1.0×10^{-3} M (Figure 7.3) using the procedures described in Table 7.1. Note the change in slope for p[H$_2$CO$_3^*$] at pH > pK_{a2} and p[CO$_3^{2-}$] at pH < pK_{a1}. The proton-balance expression is (see Example 7.2)

$$\sum \text{PPC} = \sum \text{PPR},$$

$$[\text{H}_2\text{CO}_3^*] + [\text{H}^+] = [\text{CO}_3^{2-}] + [\text{OH}^-].$$

From the pC-pH diagram (Figure 7.3), we see that $[\text{H}_2\text{CO}_3^*] \gg [\text{H}^+]$ and $[\text{CO}_3^{2-}] >$ $[\text{OH}^-]$ in the circumneutral pH range where we expect the equilibrium condition to occur. The reader may ask, How can we make this inference?

The answer is that we know that we have added to pure water a substance (HCO$_3^-$) that acts as both a very weak acid and a weak base; that is, it can release a proton becoming CO$_3^{2-}$ and it also can accept a proton becoming H$_2$CO$_3^*$. Thus, we do not expect the solution to be highly acidic or highly basic, and the equilibrium pH should not be very high or very low. Given the above inequalities, we conclude that the equilibrium condition is defined approximately as $[\text{H}_2\text{CO}_3^*] = [\text{CO}_3^{2-}]$, and the pH is defined by the intersection of these lines (pH = 8.3; point (A) in Figure 7.3). We note that [OH$^-$] is not totally negligible compared with [CO$_3^{2-}$]; careful analysis of the figure will show that it is about one-fifth the concentration of [CO$_3^{2-}$]. Consequently, use of the term "is defined approximately" is appropriate in the previous sentence.
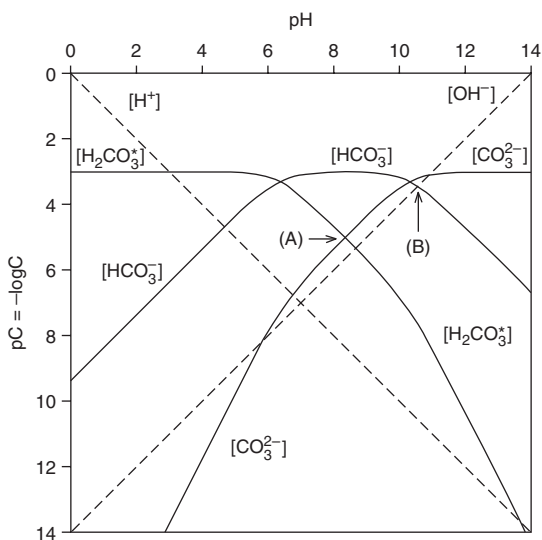
Figure 7.3 pC-pH diagram for the carbonate system at C_T = 1×10^{-3}M. Point (A) gives the pH if NaHCO$_3$ is added to water and point (B) gives the pH if Na$_2$CO$_3$ is added to water as described in Examples 7.6 and 7.7.

EXAMPLE 7.7 Dissolution of 1.0 × 10⁻³ M sodium carbonate (Na₂CO₃) in pure water: We can use the same diagram (Figure 7.3) to solve this problem. Here the proton balance is defined as

$$\sum PPC = \sum PPR,$$

$$2[H_2CO_3^*] + [H^+] + [HCO_3^-] = [OH^-].$$

Note that the factor of 2 multiplying the concentration of $[H_2CO_3^*]$ arises because for every molecule of $H_2CO_3^*$ formed from the starting species (CO_3^{2-}), two H^+ are consumed. From the pC-pH diagram we see that both $[H_2CO_3^*]$ and $[H^+]$ are small compared with $[HCO_3^-]$. Therefore, the proton balance simplifies to $[HCO_3^-] \approx [OH^-]$, and the equilibrium pH is defined by the intersection of the lines for these species: pH $\approx$ 10.8 (point (B) in Figure 7.3).

EXAMPLE 7.8 Dissolution of equimolar NH₄Cl and NaHCO₃ (both at 2.0 × 10⁻² M) in water: Because Na^+ and Cl^- constitute a neutral salt, the additions effectively represent addition of NH_4HCO_3 (ammonium bicarbonate) to water. To solve this diagram we need to superimpose the pC-pH diagrams for the carbonate system (as in Figure 7.3) and the ammonium-ammonia system, where both C_T and $N_T = 2 \times 10^{-2}$M, on the same graph, as shown in Figure 7.4.

The proton balance is the sum of the proton balances for the two acid-base substances $(NH_4^+$ and $HCO_3^-)$:

$$\sum PPC = \sum PPR,$$

$$[H_2CO_3^*] + [H^+] = [CO_3^{2-}] + [NH_3] + [OH^-].$$

From the combined pC-pH diagram, we see that $[H_2CO_3^*] >> [H^+]$, and $[NH_3] >>$ $[CO_3^{2-}] >> [OH^-]$ for almost the entire pH range shown in the figure. Therefore,
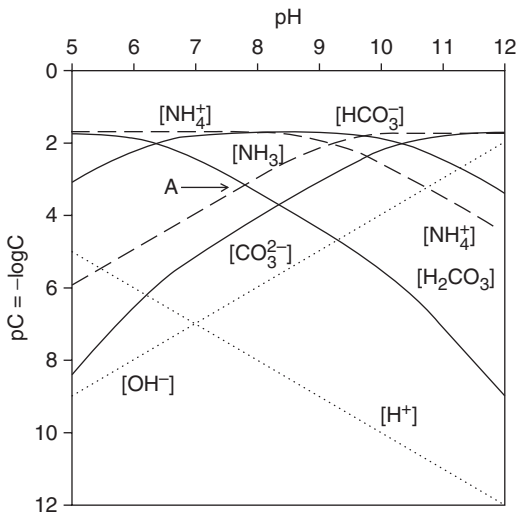
Figure 7.4 pC-pH diagram for ammonium bicarbonate at $C_T = 2 \times 10^{-2}$ M. Point (A) gives the pH if equimolar NH₄Cl and NaHCO₃ are added to water as described in Example 7.8.

$[H_2CO_3^*] \approx [NH_3]$, and the equilibrium pH occurs where the lines for these species intersect (pH = 7.8, point A in Figure 7.4).

7.3.5 pC-pH diagrams for metal hydroxide solubility

In addition to displaying conventional acid-base equilibria, pC-pH diagrams can be used to display the effects of pH on some metal hydroxides like $Al(OH)_3$ and $Fe(OH)_3$. Construction of such diagrams, although similar to the approach used for the diagrams described in the previous section, differs in several important respects. A brief summary of the general procedure for drawing such diagrams is as follows.

(1) First, identify all the soluble forms of the metal ion that can exist in equilibrium with the solid metal hydroxide. These include the free metal ion and various metal-hydroxide (M-OH) complexes.
(2) Write an equilibrium equation relating (as a function of pH) the concentration (or activity) of each soluble metal form to the solid phase metal hydroxide, and draw the lines representing these equations on a pC-pH diagram.
(3) Sum up the concentrations of the various soluble species at a given pH ($X_{T,M}$ for M, hereafter referred to as M_T), and draw the line representing M_T versus pH.

Figure 7.5 shows the pC-pH solubility diagram for amorphous ferric hydroxide ($Fe(OH)_{3\,am}$, ferrihydrite) for an assumed maximum $M_T = 1$ M. Example 7.9 lists the equilibrium expressions for the soluble Fe^{III} species and describes how they are used to define lines for the species.

Step 3 sounds like a formidable task, but it usually is easy to do because only one metal ion species is important in the mass-balance expression for M (M_T) over wide
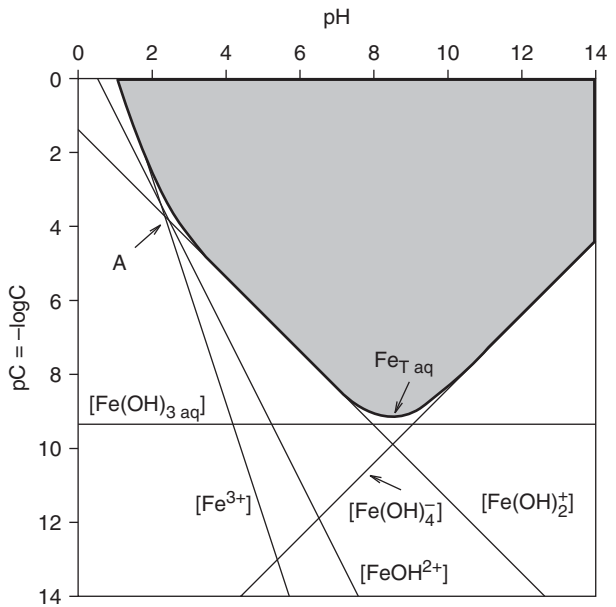
Figure 7.5 Solubility diagram (pC-pH) for ferrihydrite (amorphous ferric hydroxide) in water. The shaded area is the region of supersaturation, where solid $Fe(OH)_3$ will precipitate spontaneously. See Example 7.9.

ranges of pH, and it is unusual for more than two species to contribute significantly to M_T. When two species are important, the largest impact on M_T occurs where the lines intersect. At this point, M_T is 0.3 log unit greater than the value of either species at that pH; that is, pM_T is 0.3 units less than the value of pM at the intersection point. When the pH is more than one unit higher or lower than the pH at the intersection, the line for pM_T approaches the pM line for the more soluble species at that pH. Where three species are approximately coequal in concentration, as in point A in Figure 7.5, where $p[Fe^{3+}] \approx p[FeOH^{2+}] \approx p[Fe(OH)_2^+]$, the line for pFe_T is three times higher than the point of intersection, or ~0.5 log units higher. Consequently, the line for pM_T can be sketched on the diagram easily once the lines for the individual species are drawn.

EXAMPLE 7.9 Derivation of the lines for Fe species in Figure 7.5: We need equilibrium relationships for the following Fe^{III} species with solid $Fe(OH)_{3\ am}$ (ferrihydrite): Fe^{3+}, $FeOH^{2+}$, $Fe(OH)_2^+$, $Fe(OH)_3^0$, and $Fe(OH)_4^-$. There are several other soluble Fe^{III} species, such as $Fe_2(OH)_2^{4+}$, but they generally do not contribute significantly to Fe_T. In the interests of simplicity, we will not consider them here in drawing the solubility diagram. Also, for simplicity we will not consider effects of ionic strength on activity and we equate activity to molar concentration.

For Fe^{3+}, the simple solubility product is

$$Fe(OH)_{3\ am} = Fe^{3+} + 3OH^-; K_{s0} = 1.55 \times 10^{-39}; \log K_{s0} = -38.81.$$
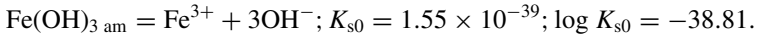
Thus,

$$K_{s0} = [Fe^{3+}][OH^-]^3,$$

or

$$\log K_{s0} = -38.81 = \log[Fe^{3+}] + 3\log[OH^-] = \log[Fe^{3+}] - 3pOH,$$

or

$$\mathbf{pFe^{3+}} = 38.81 - 3(14.00 - pH) = \mathbf{-3.19 + 3pH}.$$

The line of pFe^{3+} thus has a slope of 3 and crosses the pH-axis (where $pFe^{3+} = 0$) at pH = 3.19/3, or pH 1.06.

For $FeOH^{2+}$ we cannot find a direct equilibrium expression with $Fe(OH)_{3\ am}$, but we can obtain it from K_{s0} and K_1, the first acidity constant of Fe^{3+}:

$$Fe(OH)_3 = Fe^{3+} + 3OH^-; \quad K_{s0} = 10^{-38.81}$$

$$Fe^{3+} + H_2O = FeOH^{2+} + H^+; \quad K_1 = 10^{-2.19}$$

$$\underline{H^+ + OH^- = H_2O; \quad K_w^{-1} = 10^{14.00}}$$

Net:
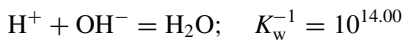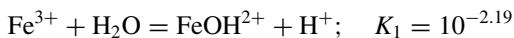
$$Fe(OH)_{3\ am} = FeOH^{2+} + 2OH^-; \quad K = K_{s0}K_1K_w^{-1} = 10^{-38.81} \times 10^{-2.19} \times 10^{14.00}$$

$$= 10^{-27.00}$$

Thus, we can write

$$\log[\text{FeOH}^{2+}] + 2\log[\text{OH}^-] = \log K = -27.00,$$

or

$$\text{pFeOH}^{2+} = 27.00 - 2(\text{p}K_w - \text{pH}) = 27.00 - 28.00 + 2\text{pH},$$

or

$$\textbf{pFeOH}^{2+} = \textbf{2pH} - \textbf{1}.$$

The line for pFeOH^{2+} thus has a slope of 2 and crosses the pH-axis at pH $= 0.5$

Similarly, for Fe(OH)_2^+, we can obtain an equilibrium expression with $\text{Fe(OH)}_{3 \text{ am}}$ as follows:

$$\text{Fe(OH)}_3 = \text{Fe}^{3+} + 3\text{OH}^-; \quad K_{s0} = 10^{-38.81}$$

$$\text{Fe}^{3+} + 2\text{H}_2\text{O} = \text{Fe(OH)}_2^+ + 2\text{H}^+; \quad K_2 = 10^{-4.59}$$

$$\underline{2\text{H}^+ + 2\text{OH}^- = 2\text{H}_2\text{O}; \quad K_w^{-2} = 10^{28.00}}$$

Net:
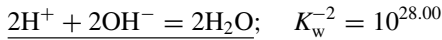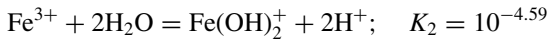
$$\text{Fe(OH)}_{3 \text{ am}} = \text{Fe(OH)}_2^+ + \text{OH}^-; \quad K = K_{s0}K_2K_w^{-2} = 10^{-38.81} \times 10^{-4.59} \times 10^{28.00}$$

$$= 10^{-15.40}$$

We can write

$$\log[\text{Fe(OH)}_2^+] + \log[\text{OH}^-] = \log K = -15.40.$$

or

$$\textbf{pFe(OH)}_2^+ = 15.4 - (\text{p}K_w - \text{pH}) = \textbf{1.4} + \textbf{pH}.$$

The line for pFe(OH)_2^+ thus has a slope of 1 and crosses the pH-axis at pH $= -1.4$.

For the un-ionized soluble species $Fe(OH)_3^0$, a similar exercise yields the following relationship:

$$Fe(OH)_3 = Fe^{3+} + 3OH^-; \quad K_{s0} = 10^{-38.81}$$

$$Fe^{3+} + 3H_2O = Fe(OH)_3^0 + 3H^+; \quad K_3 = 10^{-12.56}$$

$$\underline{3H^+ + 3OH^- = 3H_2O; \quad K_w^{-3} = 10^{42.00}}$$

Net:
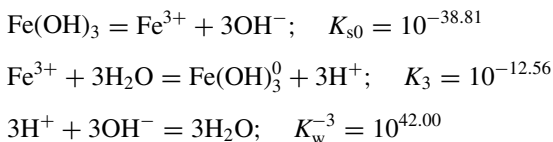
$$Fe(OH)_{3 \text{ am}} = Fe(OH)_3^0; \quad K = K_{s0}K_3K_w^{-3} = 10^{-38.81} \times 10^{-12.56} \times 10^{42.00}$$

$$= 10^{-9.37}$$

We thus can write

$$\mathbf{pFe(OH)_3^0 = pK = 9.37}.$$

Note that the line for this species is not pH dependent; instead, it is a horizontal line at pC = 9.37.

Finally, for $Fe(OH)_4^-$, a similar exercise leads to

$$Fe(OH)_3 = Fe^{3+} + 3OH^-; \quad K_{s0} = 10^{-38.81}$$

$$Fe^{3+} + 4H_2O = Fe(OH)_4^- + 4H^+; \quad K_4 = 10^{-21.59}$$

$$\underline{4H^+ + 4OH^- = 4H_2O; \quad K_w^{-4} = 10^{56.00}}$$

Net:
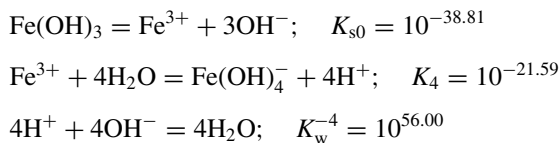
$$Fe(OH)_{3 \text{ am}} + OH^- = Fe(OH)_4^-; \quad K = K_{s0}K_4K_w^{-4} = 10^{-38.81} \times 10^{-21.59} \times 10^{56.00}$$

$$= 10^{-4.4}$$

We can write

$$\log[Fe(OH)_4^- - \log[OH^-] = \log K = -4.4.$$

or

$$\mathbf{pFe(OH)_4^- = 4.4 + (pK_w - pH) = 18.4 - pH}.$$

The line for $pFe(OH)_4^-$ has a slope of -1 and intersects with the right y-axis (at pH 14) at pC = 4.4.

In summary, the equations for all the Fe lines in the diagram are

$$pFe^{3+} = -3.19 + 3pH,$$

$$pFeOH^{2+} = 2pH - 1,$$

$$pFe(OH)_2^+ = 1.4 + pH,$$

$$pFe(OH)_3^0 = 9.37,$$

and

$$pFe(OH)_4^- = 18.4 - pH.$$

Finally, we note that the lines have meaning only where solid $Fe(OH)_{3\ am}$ exists. Because we limited Fe_T to 1 M (maximum $pFe_T = 0$), the lines at pH $<\sim 1.2$ (where we start to exceed the mass-balance constraint) are not meaningful.

Diagrams like Figure 7.5 are useful in illustrating how the solubility of a metal hydroxide varies with pH, but they generally are not used to solve problems as are the pC-pH diagrams in Figures 7.2–7.4. Interpretation of solubility diagrams is straightforward. Any combination of pH and pM_T values that falls within the shaded envelope in Figure 7.5 represents supersaturated conditions with respect to the solubility of $Fe(OH)_{3\ am}$, and the precipitation reaction will proceed spontaneously (although the figure implies nothing about the rate at which that may occur). Any combination of pH and pM_T values that falls outside the shaded envelope in Figure 7.5 represents undersaturated conditions with respect to the solubility of $Fe(OH)_{3\ am}$, and if solid phase $Fe(OH)_{3\ am}$ is present, it will tend to dissolve. The gray line denoted Fe_T in Figure 7.5 represents the equilibrium condition—the total solubility of $Fe(OH)_{3\ am}$ expressed in terms of Fe as a function of pH.

7.3.6 Predominance-area diagrams

These diagrams involve master variables on both axes. Examples include plots of (1) log P_{CO_2} versus pH for carbonate and hydroxide mineral solubility and (2) redox potential, E_h versus pH to describe the effects of those variables on the speciation of an element. They are called "predominance-area" diagrams because the lines on such plots delimit regions in which a given species (ionic form or mineral phase) is predominant in the system. The lines themselves represent one of three possibilities—the locations (combination of values of the master variables) at which

(1) two mineral phases coexist at equilibrium;
(2) a mineral (solid) phase coexists in equilibrium with some (arbitrarily defined) concentration of a free ion component of the solid; or
(3) two different soluble species of the element coexist at the same concentration (or a specified ratio of concentrations).

Construction of E_h-pH diagrams is covered in Chapter 11; here we describe how to construct and interpret predominance-area diagrams for mineral solubility as controlled
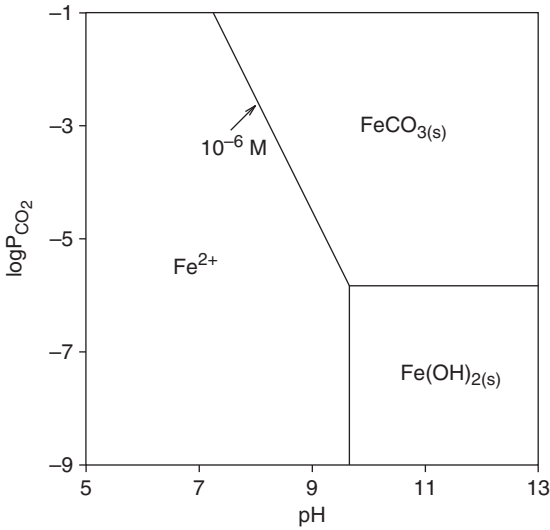
Figure 7.6 Log P_{CO_2}-pH predominance-area diagram for $FeCO_3$ and $Fe(OH)_2$.

by the master variables pH and P_{CO_2}. Our example is a simple ferrous iron system, for which we consider one soluble species, Fe^{2+}, and two solid phases: $FeCO_3$, siderite, and $Fe(OH)_2$, wustite (Figure 7.6).

Predominance-area diagrams usually are constructed with pH on the abscissa and the other master variable (in this case log P_{CO_2}) on the ordinate. Three kinds of lines can be defined in relation to the axis variables, and Figure 7.6 has one of each kind. Horizontal lines are pH-independent and log P_{CO_2}-dependent. The equilibrium between $FeCO_{3(s)}$ and $Fe(OH)_{2(s)}$ is an example; it depends on P_{CO_2} but not on pH. Vertical lines are pH-dependent and P_{CO_2}-independent. The solubility of $Fe(OH)_{2(s)}$ is an example. Finally, sloping equilibria depend on both pH and P_{CO_2}; the solubility of $FeCO_3$ is an example. In order to define lines representing equilibria between a solid phase and a dissolved species, we must specify a concentration of the dissolved species that we want the line to represent. In Figure 7.6 the lines represent $[Fe^{2+}] = 1 \times 10^{-6}$ M, which is close to the drinking water standard for iron and in the range of values for Fe^{2+} in anoxic waters (where Fe^{II} is the stable species). Given the above information, we now are ready to write the equations defining the lines in Figure 7.6.

Horizontal line.   This line defines the conditions under which siderite and wustite can coexist at equilibrium. The line is defined by the equilibrium relationship:

$$FeCO_{3(s)} + H_2O \rightleftharpoons Fe(OH)_{2(s)} + CO_2,$$

$$K = 1.48 \times 10^{-6} = 10^{-5.83} = P_{CO_2} \qquad (7.45)$$
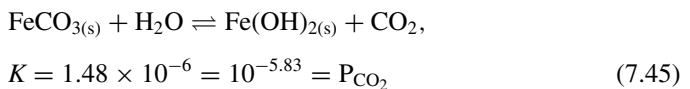
The value of the equilibrium constant for Eq. 7.45 was derived by adding and subtracting reactions for which K values are known (Box 7.1). Because the minerals and water are

---

Box 7.1   Derivation of equilibrium constant for eq. 7.45

$$FeCO_{3(s)} \rightleftharpoons Fe^{2+} + CO_3^{2-} \quad K_{s0 \text{ siderite}} = 10^{-10.68}$$

$$Fe^{2+} + 2OH^- \rightleftharpoons Fe(OH)_{2(s)} \quad (K_{s0 \text{ wustite}})^{-1} = 10^{14.70}$$

$$CO_3^{2-} + H^+ \rightleftharpoons HCO_3^- \quad K_2^{-1} = 10^{10.33}$$

$$HCO_3^- + H^+ \rightleftharpoons H_2CO_3^* \quad K_1^{-1} = 10^{6.35}$$

$$H_2CO_3^* \rightleftharpoons CO_{2(g)} \quad K_H^{-1} = 10^{1.47}$$

$$\underline{2H_2O \rightleftharpoons 2H^+ + OH^- \quad K_w^2 = 10^{-28.00}}$$

Net: $FeCO_{3(s)} \rightleftharpoons Fe(OH)_{2(s)} + CO_{2(g)};$
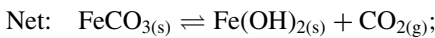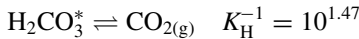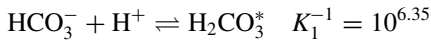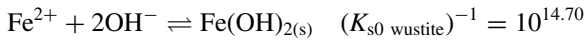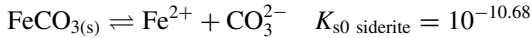
$$K = K_{s0 \text{ sid}} \times K_{s0 \text{ wus}}^{-1} \times K_2^{-1} \times K_1^{-1} \times K_H^{-1} \times K_w^2$$

or $K = 10^{-10.68+14.70+10.33+6.35+1.47-28.00} = 10^{-5.83}$

---

pure phases for which $a = 1$ (by definition), the equilibrium constant has only one variable component—the pressure of CO_2. That is, equilibrium between the minerals is specified by that pressure of CO_2. The equilibrium is pH-independent within the pH range that the two components exist.

Vertical line.   This line defines the conditions under which wustite exists in equilibrium with dissolved Fe^{2+} at the concentration we selected (1×10^{-6} M). The line is defined by the solubility relationship

$$Fe(OH)_{2(s)} \rightleftharpoons Fe^{2+} + 2OH^- \quad K_{s0} = 2 \times 10^{-15} = 10^{-14.70}. \qquad (7.46a)$$

The equilibrium constant written in log form is

$$\log[Fe^{2+}] + 2\log[OH^-] = \log K_{s0} = -14.70, \qquad (7.46b)$$

or

$$\log[Fe^{2+}] - 2(pK_w - pH) = -14.70. \qquad (7.46c)$$

Solving for pH and substituting in the value of $[Fe^{2+}]$ yields

$$pH = 14 - \tfrac{1}{2}\{14.70 + \log[Fe^{2+}]\}$$

$$= 14 - \tfrac{1}{2}\{14.70 - 6.0\} = 9.65 \qquad (7.46d)$$

Thus $Fe(OH)_2$ is in equilibrium with 1×10^{-6} M Fe^{2+} at pH 9.65.

Sloping line.   This line defines the conditions under which siderite exists in equilibrium with dissolved Fe^{2+} at the concentration we selected (1×10^{-6} M). The solubility of siderite is given by

$$FeCO_{3(s)} \rightleftharpoons Fe^{2+} + 2CO_3^{2-} \quad K_{s0} = 2.09 \times 10^{-11} = 10^{-10.68}. \quad (7.47a)$$
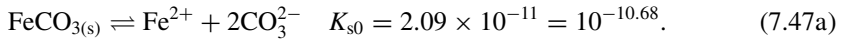
To obtain the line of interest, we need to express this relationship in terms relevant to the axes of the diagram, i.e., in terms of CO_2 and H^+:

$$FeCO_{3(s)} + 2H^+ \rightleftharpoons Fe^{2+} + CO_2 + H_2O \quad K = 2.95 \times 10^7 = 10^{7.47} \quad (7.47b)$$
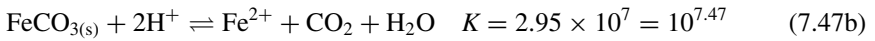
Derivation of Eq. 7.47b is illustrated in Box 7.2. In log form the equilibrium constant for Eq. 7.47 is

$$\log[Fe^{2+}] + \log P_{CO_2} - 2\log[H^+] = \log K = 7.47, \quad (7.48a)$$

or

$$\log P_{CO_2} = 7.47 - \log[Fe^{2+}] - 2pH. \quad (7.48b)$$

Box 7.2   Derivation of K for eq. 7.47b

$$FeCO_{3(s)} \rightleftharpoons Fe^{2+} + CO_3^{2-} \quad K_{s0 \text{ siderite}} = 10^{-10.68}$$

$$CO_3^{2-} + H^+ \rightleftharpoons HCO_3^- \quad K_2^{-1} = 10^{10.33}$$

$$HCO_3^- + H^+ \rightleftharpoons H_2CO_3^* \quad K_1^{-1} = 10^{6.35}$$

$$\underline{H_2CO_3^* \rightleftharpoons CO_{2(g)} \quad K_H^{-1} = 10^{1.47}}$$

Net:

$$FeCO_{3(s)} + 2H^+ \quad \rightleftharpoons Fe^{2+} + CO_{2(g)} + H_2O;$$
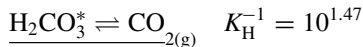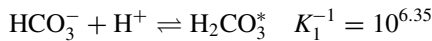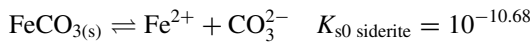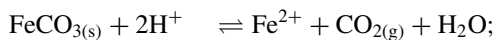
$$K = K_{s0 \text{ sid}} \times K_2^{-1} \times K_1^{-1} \times K_H^{-1}$$

or

$$K = 10^{-10.68+10.33+6.35+1.47} = 10^{7.47}$$

Substituting in the selected value of $[Fe^{2+}] = 1 \times 10^{-6}$ M and simplifying yields the equation we need:

$$\log P_{CO_2} = 13.47 - 2pH \quad (7.48c)$$

The line expressing the equilibrium of $FeCO_3$ with 1×10^{-6} M Fe^{2+} thus has a slope of -2. Substituting a value of $\log P_{CO_2} = -5.83$ into Eq. 7.48c yields a pH of 9.65, and

thus the sloping line intersects the horizontal and vertical lines at the common point log $P_{CO_2} = -5.83$ and pH $= 9.65$.

7.4 Algebraic approaches to solving ionic equilibrium problems

7.4.1 Introduction

As noted at the beginning of this chapter, the algebraic approach to solving ionic equilibrium problems involves the solution of a set of simultaneous algebraic equations. As many equations must be written as there are species with unknown concentrations in the system. If sufficient equations cannot be found, the system is underspecified and cannot be solved. If more equations are available than needed, the system is overspecified, which generally means that two (or more) species have the same concentration or at least do not behave as independent variables.

A simple eight-step general approach for the algebraic solution of ionic equilibria is as follows:

(1) List and count the number of unknown species, including H^+ and OH^-, in the solution.
(2) Write a set of equations equal in number to the number of unknowns specified in step 1 using the possible equation types described in Section 7.2.
(3) Resolve discrepancies between activities and concentrations in the different types of equations by assuming $a_i = c_i$ ($\gamma_i = 1.0$) if ionic strength (I) is not known or by computing the γ_i values if I is known and correcting the thermodynamic values of the equilibrium constants to corresponding ^cK values.
(4) Simplify the equations by eliminating terms of negligible value (concentration).
(5) Solve the simplified simultaneous equations by substitution, usually in terms of $[H^+]$ (or $[M^{n+}]$) by substituting expressions for each species as functions of $[H^+]$ or $[M^{n+}]$ into the mass-balance or charge-balance equation to obtain a polynomial equation in one unknown (e.g., $[H^+]$).
(6) Replace the various constants with their numerical values, and solve for the unknown concentration by trial and error. Once that is known, substitute the result into equilibrium constants and/or other equations derived in step 5 to obtain values for all other unknown species.
(7) Check the reasonableness of the simplifying assumptions made in step 4 and re-solve if necessary.
(8) Calculate the ionic strength of the solution (if that is not given in the original problem conditions), compute activity coefficients for the ionic species, correct the thermodynamic values of the equilibrium constants to ^cK values and repeat step 6. Repeat this step as necessary to achieve convergence of the solution.

In theory, the above process is "foolproof"; in practice, the ease with which it can be achieved depends strongly on the number of equations (i.e., number of unknown species) and complexity of the mass-balance, charge-balance and proton-balance equations. Consequently, in most practical situations, step 4 is critically important in determining whether the set of equations can be solved easily by hand or not. One also may use

the more complicated equation and solve it using the "solver" utility in a spreadsheet program.

7.4.2 Application to acid-base equilibria

We illustrate the above general approach first for a simple case: dissolution of a known amount of a monoprotic acid, HB, in pure water. In this case we have four unknowns: [HB], $[B^-]$, $[OH^-]$, and $[H^+]$ (which can be converted to $\{H^+\}$ and hence to pH once the ionic strength of the solution is known). Thus, we need four equations. We have K_1 for the dissociation of HB and K_w for the dissociation of water:

$$K_1 = \frac{\{H^+\}\{B^-\}}{\{HB\}}, \quad \text{and} \quad K_w = \{H^+\}\{OH^-\} \tag{7.49}$$

We also can write the mass-balance and charge-balance equations:

$$B_T = [HB] + [B^-], \quad \text{and} \quad [H^+] = [B^-] + [OH^-] \tag{7.50}$$

In this case the charge-balance equation is the same as the proton-balance equation. We now have four equations for four unknowns. We will make an initial assumption that activities and concentrations are the same. We can solve K_w for $[OH^-]$, substitute the result into the charge-balance equation and solve for $[B^-]$:

$$[B^-] = [H^+] - K_w/[H^+] \tag{7.51}$$

In turn, we can solve K_1 for [HB], substitute Eq. 7.51 into it for $[B^-]$ and substitute the result and Eq. 7.51 into the mass-balance expression, yielding an equation with only $[H^+]$ as an unknown variable:

$$B_T = \frac{[H^+]\left([H^+] - \frac{K_w}{[H^+]}\right)}{K_1} + [H^+] - \frac{K_w}{[H^+]} \tag{7.52}$$

Rearranging yields the following polynomial equation in terms of $[H^+]$:

$$[H^+]^3 + K_1[H^+]^2 - (K_w + K_1 B_T)[H^+] - K_w K_1 = 0 \tag{7.53}$$

If K_1 and B_T are known, Eq. 7.53 can be solved for $[H^+]$ by trial and error. Substituting the answer into Eq. 7.51 yields $[B^-]$, and further substituting these results into K_1 yields [HB].

It must be admitted that Eq. 7.53 is rarely used to find the equilibrium conditions for simple monoprotic acid problems. The term for $[OH^-]$ in the charge-balance equation derives from the contribution of the dissociation of water itself to the ionic balance, but in almost all cases of practical interest, this term is very small—negligible—compared with the concentration of $[B^-]$ when HB is the species added to the system. The charge balance thus can be simplified to $[H^+] = [B^-]$. This simplification effectively results in the removal of all terms involving K_w in Eq. 7.53 (because the substitution of $K_w/[H^+]$ for

[OH$^-$] in the charge balance is the origin of all these terms. Applying this simplification to Eq. 7.53 yields

$$[H^+]^2 + K_1[H^+] - K_1 B_T = 0. \tag{7.54}$$

Equation 7.54 can be solved by the quadratic formula

$$[H^+] = \frac{-b \pm \sqrt{b^2 - 4ac}}{2a} = \frac{-K_1 \pm \sqrt{K_1^2 - 4(-K_1 B_T)}}{2}. \tag{7.55}$$

While there are two roots (solutions) to the equation, only the positive one gives a real answer.

Finally, the situation can be simplified one step further in cases where [B$^-$] is very small compared with [HB]. In such cases, B$_T \approx$ [HB], and since we noted above that [H$^+$] = [B$^-$], the problem simplifies to working simply with K_1:

$$K_1 = \frac{[H^+]^2}{B_T}, \quad \text{or} \quad [H^+] = \sqrt{K_1 B_T} \tag{7.56}$$

In solving simple monoprotic acid problems, one can make this assumption initially, calculate [H$^+$] and [B$^-$], and compare the latter to B$_T$ to determine whether the assumption holds. If [B$^-$] is < 5% of B$_T$, the assumption usually can be accepted without compromising the calculated value of [H$^+$] (and pH).

EXAMPLE 7.10 Algebraic solution for diprotic acids: Consider the dissolution of a known concentration of a diprotic acid H$_2$B into pure water. The system has five unknowns: [H$_2$B], [HB$^-$], [B^{2-}], [H$^+$], and [OH$^-$]; thus, we need five equations. We have three mass-action expressions:

(1) $K_1 = \dfrac{\{H^+\}\{HB^-\}}{\{H_2B\}}$;   (2) $K_2 = \dfrac{\{H^+\}\{B^{2-}\}}{\{HB^-\}}$;   (3) $K_w = \{H^+\}\{OH^-\}$.

In addition, we can write the mass-balance expression and charge-balance equation (which is the same as the proton-balance equation):

(4) Mass balance: $B_T = [H_2B] + [HB^-] + [B^{2-}]$

(5) Charge balance: $[H^+] = [HB^-] + 2[B^{2-}] + [OH^-]$

Initially we assume that activities and concentrations are the same ($\gamma_i = 1.0$) and solve the equilibrium constant expressions for the components of the mass-balance expression in terms of [HB$^-$], K_1, K_2, and [H$^+$]:

(6) $B_T = \dfrac{[H^+][HB^-]}{K_1} + [HB^-] + \dfrac{K_2[HB^-]}{[H^+]} = [HB^-]\left\{ \dfrac{[H^+]}{K_1} + \dfrac{K_2}{[H^+]} + 1 \right\}$

We can perform a similar set of operations on the charge-balance equation, yielding

(7) $[H^+] = [HB^-] + \dfrac{2[HB^-]K_2}{[H^+]} + \dfrac{K_w}{[H^+]}$,

or

(8) $[H^+] + \dfrac{K_w}{[H^+]} = [HB^-]\left\{1 + \dfrac{2K_2}{[H^+]}\right\}$.

Inspection of Eqs. (6) and (8) shows that we can eliminate $[HB^-]$ by dividing the former by the latter:

(9) $\dfrac{B_T}{[H^+] - \dfrac{K_w}{[H^+]}} = \dfrac{[HB^-]\left\{\dfrac{[H^+]}{K_1} + \dfrac{K_2}{[H^+]} + 1\right\}}{[HB^-]\left\{1 + \dfrac{2K_2}{[H^+]}\right\}} = \dfrac{\dfrac{[H^+]}{K_1} + \dfrac{K_2}{[H^+]} + 1}{1 + \dfrac{2K_2}{[H^+]}}$,

which can be rearranged to

(10) $[H^+]^4 + K_1[H^+]^3 + (K_1K_2 - K_w - K_1B_T)[H^+]^2 - (K_1K_w + 2K_1K_2B_T)[H^+] - K_1K_2K_w = 0$.

There is no analytical solution for this quartic equation, but it can be solved for $[H^+]$ by trial and error if B_T is known. Once this is done, substitution of $[H^+]$ into Eq. (6) or (8) yields $[HB^-]$, and then concentrations of the other species can be obtained from Eqs. (1)-(3). The ionic strength of the solution then can be computed; activity coefficients can be calculated from the Debye-Hückel equation; and the equilibrium constants can be corrected to corresponding ^cK values. Equation (10) then can be solved again using those values. If the computed ionic strength after this second iteration differs sufficiently from the initial value, the process can be completed again (and again) until the solutions converge, but usually one obtains sufficient accuracy with the second iteration.

Alternatively, we can make some simplifying assumptions as follows:

(i) Neglect contributions of $[H^+]$ and $[OH^-]$ from the dissociation of water. This is equivalent to dropping all terms containing K_w from Eq. (10), and it yields a cubic equation:

(11) $[H^+]^3 + K_1[H^+]^2 + (K_1K_2 - K_1C_T)[H^+] - 2K_1K_2B_T = 0$

This also can be solved by trial and error.

(ii) In many cases, $K_1 \gg K_2$. If that is the case, we can ignore terms involving K_2 in Eq. (11):

(12) $[H^+]^2 + K_1[H^+] - K_1B_T = 0$

Readers will recognize Eq. (12) as the same as Eq. 7.54 derived earlier for monoprotic acids.

Spreadsheets and other calculation programs available on computers and calculators make it possible to solve cubic equations (Eq. 7.53) or quartic equations (example 7.10) using a solver tool. This involves typing out the appropriate equation and using the tool to adjust the variable (e.g., iterate) until a solution is found. There are, of course, some

potential pitfalls. These equations have multiple roots, and thus one has to make sure the reported value makes physical sense (i.e., concentrations can't be negative!). Getting the solver to converge on a value of zero may cause problems for some fitting algorithms. This could be avoided by moving the $K_w K_{a1}$ term to the right side of Eq. 7.53 and then iterating to solve for $[H^+]$, but the value of $K_w K_{a1}$ often is on the order of 10^{-18} or lower. Numerical convergence to such small values also is difficult. Although it is possible to use a spreadsheet program or calculator to iterate to a solution of such equations, it is recommended that readers use software designed for solving chemical equilibrium problems (see Section 7.5) if it is not possible to simplify the equation to a form readily solvable by hand.

7.4.3 Application to mixed equilibria

The approach to solving ionic equilibria presented in Section 7.4.1 also applies to problems involving more the one kind of equilibrium process, e.g., acid-base, solubility and complexation equilibria. Such problems are very common in water chemistry. Examples 7.11 and 7.12 illustrate the use of algebraic methods to solve two cases involving the solubility of calcium carbonate (calcite, $CaCO_{3(s)}$), which also involve acid-base equilibria in the carbonate system. The examples involve six species and thus require six equations. Manual solution is facilitated by making some simplifying assumptions. For problems much more complicated than these examples, solution of the simultaneous equations can be quite tedious, and the ready availability of computer-based solution methods (see Section 7.5) makes it unnecessary to use manual algebraic methods for such problems.

EXAMPLE 7.11 Dissolution of calcite ($CaCO_3$) in pure water: The basic reaction involved in the dissolution of calcite is $CaCO_{3(s)} \rightleftharpoons Ca^{2+} + CO_3^{2-}$. Carbonate ion is a moderately strong base that undergoes reactions with water to form other species in the carbonic acid-carbonate system: $CO_3^{2-} + H_2O \rightleftharpoons HCO_3^- + OH^-$; and $HCO_3^- + H_2O \rightleftharpoons H_2CO_3^* + OH^-$. The system thus has six unknowns: Ca^{2+}, CO_3^{2-}, HCO_3^-, $H_2CO_3^*$, H^+, and OH^-. $CaCO_{3(s)}$ is not an unknown because, as a pure solid, its activity is defined to be unity (see Chapter 4 for more details). If we assume that the system is closed to the atmosphere, we also do not need to consider P_{CO_2}. Consequently, to solve this problem algebraically, we need six equations. Four mass-action (equilibrium constant) expressions are available:

(1) $K_{s0} = 10^{-8.48} = \{Ca^{2+}\}\{CO_3^{2-}\}$;   (2) $K_{a1} = 10^{-6.35} = \{H^+\}\{HCO_3^-\}/\{H_2CO_3^*\}$

(3) $K_{a2} = 10^{-10.33} = \{H^+\}\{CO_3^{2-}\}/\{HCO_3^-\}$;   (4) $K_w = 10^{-14.00} = \{H^+\}\{OH^-\}$

Values for K_{s0}, K_{a1}, and K_{a2} are from Figure 7.1. We also can write a mass-balance equation for the dissolution of calcite and a charge balance for the solution:

(5) $C_T = [Ca^{2+}] = [CO_3^{2-}] + [HCO_3^-] + [H_2CO_3^*]$

(6) $2[Ca^{2+}] + [H^+] = 2[CO_3^{2-}] + [HCO_3^-] + [OH^-]$

For the initial solution we ignore the difference between activity and concentration (i.e., assume I $\approx$ 0 and activity coefficients are 1.0) and solve the six simultaneous equations in terms of $[H^+]$.

First, we can simplify Eqs. (5) and (6) to eliminate terms that are negligible in size compared to the other terms. Because the dissolution of calcite produces a base (CO_3^{2-}) and that reacts with water to produce OH^-, we can assume that the resulting solution will be alkaline (pH > 7). Consequently, $[H^+]$ and $[H_2CO_3^*]$ can be assumed to be small compared to the other species. This yields

(7) $[Ca^{2+}] = [CO_3^{2-}] + [HCO_3^-]$,

and

(8) $2[Ca^{2+}] = 2[CO_3^{2-}] + [HCO_3^-] + [OH^-]$.

There are several ways to proceed in solving Eqs. (1)–(4), (7), and (8), but one convenient way is to notice that if we multiply Eq. (7) by two and subtract the result from Eq. (8), we get

(9) $[HCO_3^-] = [OH^-]$.

The net effect of eliminating $H_2CO_3^*$ and combining Eqs. (7) and (8) to yield the equality between $[HCO_3^-]$ and $[OH^-]$ in Eq. (9) is to decrease the dimensionality of the problem. Relating this finding to Eq. (4) yields

(10) $[OH^-] = K_w/[H^+] = [HCO_3^-]$.

Solving Eq. (3) for $[CO_3^{2-}]$ and substituting Eq. (10) for $[HCO_3^-]$ yields

(11) $[CO_3^{2-}] = K_{a2}[HCO_3^-]/[H^+] = K_{a2}K_w/[H^+]^2$.

Substituting Eq. (11) into Eq. (1) and solving for $[Ca^{2+}]$ yields

(12) $[Ca^{2+}] = K_{s0}/[CO_3^{2-}] = K_{s0}[H^+]^2/K_{a2}K_w$.

Finally, we can substitute Eqs. (10)–(12) into Eq. (7) to obtain an equation solely in terms of $[H^+]$ and constants:

(13) $K_{s0}[H^+]^2/K_{a2}K_w = K_{a2}K_w/[H^+]^2 + K_w/[H^+]$

or

(14) $10^{15.85}[H^+]^4 - 10^{-14.00}[H^+] - 10^{-24.33} = 0$

No simple analytical solution exists for Eq. (14), but it can be solved by trial and error, yielding $[H^+] = 10^{-9.90}$, or pH $\approx$ 9.90. Back substituting for the other terms yields: $[Ca^{2+}] = 10^{-3.95}$; $[CO_3^{2-}] = 10^{-4.53}$; $[HCO_3^-] = [OH^-] = 10^{-4.10}$; and $[H_2CO_3^*] = 10^{-7.65}$. Our assumption in solving the equations that $[H^+]$ and $[H_2CO_3^*]$ could be ignored in comparison to the other terms in Eqs. (5) and (6) thus is justified. The ionic strength can be computed to be 3.6×10^{-4}. From the Debye-Hückel limiting law we find $\gamma_{Ca^{2+}} = \gamma_{CO_3^{2-}} = 0.91$; $\gamma_{HCO_3^-} = \gamma_{OH^-} = \gamma_{H^+} = 0.98$. Correcting the various K values for the γ values to obtain ^cK values and solving again does not result in any significant changes in $[H^+]$ or any other species. The equilibrium pH is calculated to be 9.91 when $[H^+]$ is converted to $\{H^+\}$.

EXAMPLE 7.12 Dissolution of calcite in a system open to the atmosphere: We now open the system in Example 7.11 to the ambient atmosphere at a partial pressure of CO_2

of $\sim 10^{-3.5}$ atm. This problem has many similarities to Example 7.11, and Eqs. (1)–(4) and (6) there still apply. However, the mass-balance equation does not apply because there now are two sources of inorganic carbon in the water: dissolution of $CaCO_3$ and absorption of CO_2 from the atmosphere. However, an additional equilibrium expression does apply: the Henry's law equation for CO_2:

(15) $K_H = 10^{-1.47} = \dfrac{[H_2CO_3^*]}{P_{CO_2}}$

Note that for simplicity, we continue with the numbering of equations started in Example 7.11. From the specified P_{CO_2}, we find that $[H_2CO_3^*] = 10^{-1.47} \times 10^{-3.5} = 10^{-4.97}$.

Given this information, we can solve K_{a1}, K_{a2}, and K_{s0} for the components of Eq. (8) in terms of constants and $[H^+]$:

From K_1,   (16) $[HCO_3^-] = K_{a1} \times 10^{-4.97}/[H^+]$

From K_2,   (17) $[CO_3^{2-}] = K_{a2}[HCO_3^-]/[H^+] = 10^{-4.97}K_{a1}K_{a2}/[H^+]^2$

From K_{s0},   (18) $[Ca^{2+}] = K_{s0}/[CO_3^{2-}] = K_{s0}[H^+]^2/10^{-4.97}K_{a1}K_{a2}$

If we assume that the solution will be alkaline (pH > 7) because carbonate is a fairly strong base, Eq. (8) still applies:

(8) $2[Ca^{2+}] = 2[CO_3^{2-}] + [HCO_3^-] + [OH^-]$

We can check the validity of this assumption once we solve the set of equations. Substituting Eqs. (4) and (16)–(18) into Eq. (8) yields

(19) $2K_{s0}[H^+]^2/10^{-4.97}K_{a1}K_{a2} = 2 \times 10^{-4.97}K_{a1}K_{a2}/[H^+]^2$
$+K_{a1} \times 10^{-4.97}/[H^+] + K_w/[H^+],$

or

(20a) $10^{13.47}[H^+]^4 = 10^{-11.32}[H^+] + 10^{-14.00}[H^+] + 10^{-21.35},$
(20b) $[H^+]^4 - 10^{-24.79}[H^+] - 10^{-34.82} = 0.$

Solving by trial and error yields $[H^+] = 10^{-8.26}$, or pH ≈ 8.26, and back-substituting yields: $[Ca^{2-}] = 10^{-3.35}$; $[HCO_3^-] = 10^{-3.06}$; $[CO_3^{2-}] = 10^{-5.13}$; and $[OH^-] = 10^{-5.74}$. It is apparent that the simplifying assumption that the solution would have a pH > 7 is valid.

The ionic strength of the solution (1.34×10^{-3}) is higher than that in Example 7.11. Using the extended Debye-Hückel equation (EDHE) to compute activity coefficients yields $\gamma_{Ca^{2+}} = \gamma_{CO_3^{2-}} = 0.85$; $\gamma_{HCO_3^-} = \gamma_{OH^-} = \gamma_{H^+} = 0.96$. Correcting the K values for the γ values yields the following ^cK values: $^cK_1 = 10^{-6.31}$; $^cK_2 = 10^{-10.26}$; $^cK_{s0} = 10^{-8.28}$; and $^cK_w = 10^{-13.96}$. Solving Eq. (19) again using these values yields a small change in $[H^+]$ ($10^{-8.26}$; pH = 8.28 when $[H^+]$ is corrected to $\{H^+\}$) and only small changes in other constituents: $[Ca^{2+}] = 10^{-3.32}$; $[HCO_3^-] = 10^{-3.02}$; and $[CO_3^{2-}] = 10^{-5.02}$. These changes are small enough not to affect the initially computed ionic strength, and hence we do not need another iteration.

Comparison of the results from Examples 7.11 and 7.12 shows that opening the system to the atmosphere makes a huge difference in the solubility of calcium carbonate.

The equilibrium pH drops from 9.91 to 8.28 when the system is opened to the atmosphere; Ca^{2+} increases more than fourfold—from 1.12×10^{-4} M to 4.79×10^{-4} M; and the ionic strength of the solution increases almost fourfold. More realistic examples involving the dissolution of calcite in water that include consideration of ionic complexes formed by ions are presented in Chapter 10, but such problems are difficult to solve using manual methods. The following section describes how complicated problems can be solved by using computer programs.

7.5 Computer-based solutions of ionic equilibria

7.5.1 Historical introduction

Modeling the chemical speciation of natural waters has been an interest of water chemists since the earliest days of the field as a recognized discipline. The seminal papers by Sillen[1] on the chemistry of seawater and Garrels and Thompson[2] on major ion speciation in seawater are important examples. Both efforts, published in the early 1960s, preceded the availability of computer programs to expedite calculations, and their results were produced by manual solutions of the algebraic equations. Garrels and Thompson[2] used a manual method of successive approximations to solve a system of 17 simultaneous equations. Efforts to develop computer programs to solve ionic equilibrium problems began soon thereafter, and Sillen's group produced a prototype general program, HALTAFALL,[3] in the late 1960s. Metal ion speciation studies using "ad hoc" computer algorithms written for specific studies also were reported.[4] The first general calculation program for aqueous chemical equilibria that was widely used in the United States, REDEQL, was published by Morel and Morgan[5] in 1972. A FORTRAN program for mainframe computers, it used a Newton-Raphson algorithm to solve sets of nonlinear simultaneous equations. Although it represented a major advance in analytical capabilities, by today's standards it was slow, cumbersome, and not user friendly.

REDEQL was supplanted by MINEQL[6] in 1976. This program had a more compact mainframe code based on a Gaussian elimination algorithm and was easier and more flexible to use. Through various versions it has remained highly popular for solving ionic equilibrium problems, including evaluation of the chemical speciation of waters based on total analytical (X_T) concentrations. When personal computers became popular in the 1980s, MINEQL was adapted to run on PCs and Macs. For example, MINTEQA2, developed by the U.S. EPA in the 1980s but updated and still available,[7] provides a menu-driven interface program (PRODEFA2) that simplifies the formulation of problems and provides capabilities for doing multiple equilibrium calculations (e.g., titrations) in a single set-up. MINTEQA2 also provides some capabilities for graphing output. Recent versions of MINEQL, for example, MINEQL+[8] and Visual MINTEQ,[9] are Windows-based programs, in which problems are formulated and executed and output is accessed all within a single operating environment. Both versions provide graphical and tabular display of output and easy exporting of results to spreadsheet programs. In addition, both programs provide capabilities to model more complicated problems involving surface complexation, adsorption phenomena, metal binding by aquatic humic material, and biotic ligand models.

Many other programs have been developed over the past 30 years to solve ionic equilibrium and related problems. Nordstrom et al.[10] reviewed over 30 equilibrium programs available in the late 1970s to calculate aqueous chemical equilibria and reported a comparison of 13 such programs. Good agreement was found among the programs for major species, but agreement was poor for minor species. Differences in the thermodynamic data bases used by the programs were the major cause of discrepancies in the results. Most of the programs described by Nordstrom et al. are no longer available or no longer widely used. A few examples of other important equilibrium programs include GEOCHEM,[11] which was developed from REDEQL to solve equilibria involving trace metals in contaminated soil solutions, and WATEQ[12] and its successors (e.g., WATEQ2[13] and WATEQ4F[14]), which were developed by the U.S. Geological Survey to characterize major and minor element speciation and mineral equilibria in natural waters. The latest version, WATEQ4F, is still used. PHREEQC and PREEQCI,[15] also developed by the U.S. Geological Survey, are successors of a series of programs that started with PATHI[16] to simulate reaction pathways in mineral dissolution and rock weathering processes. Such programs are used to analyze problems related to ground-water chemistry. WHAM[17] was developed primarily to analyze trace metal equilibria in surface waters containing humic substances.

7.5.2 How the programs work

Two related programming approaches have been taken to solve ionic equilibria: either the problem is formulated to minimize free energy subject to mass-balance constraints, or the set of equilibrium constant equations is solved simultaneously subject to mass-balance constraints. Because of the intrinsic relationship between free energy changes and equilibrium constants (Eq. 3.27), the two approaches ultimately are equivalent, but for mathematical reasons, the algorithms used in the two approaches are different. The more widely used equilibrium constant approach (used in MINEQL and related programs) solves the matrix of nonlinear equations by Newton-Raphson, Gaussian elimination, or successive approximation. The less widely used free energy approach allows use of various optimization techniques such as linear programming and gradient methods.[10]

Of more interest to environmental scientists and engineers than the numerical algorithm used to solve the equations is the general framework used to set up equilibrium problems. MINEQL+, VMINTEQ and related programs use a framework in which chemicals are divided into six types, as described below.

Type I substances, *components*, are defined (with a few exceptions) as free (aquo) cations and the completely dissociated (deprotonated) forms of inorganic anions and organic ligands. The exceptions include water itself (H_2O), a default component added automatically in all problem formulations. Substances that never exist in completely deprotonated form are added either as the fully protonated species (e.g., silica as $Si(OH)_4$ and borate as $B(OH)_3$) or as the most deprotonated form that does exist in water (e.g., sulfide as HS^-; $pK_{a2} >> 14$ for H_2S). A few metals that exist in water as only as oxycations (some oxidation states of U and V) are added in that form, e.g., $U^VO_2^+$. It is interesting to note that although H^+ is a component in these programs, OH^- is not. Instead, OH^- is treated as a soluble species derived from the dissociation of H_2O,

and its composition is given in terms of those components as $H_2O(1)$, $H^+(-1)$, that is, as component water minus component H^+, which is defined by the inverse of the dissociation constant K_w. MINEQL+ has 145 predefined components and 55 "null" components. The latter are available for users to add new components to the database.

Type II substances—*aqueous species*—consist of all soluble species derived from combinations of components. They include soluble complexes formed from metal ions and ligands, including uncharged species like $CaCO_3^0$, as well as partially and totally protonated acids formed from the completely deprotonated acid anions and component H^+. Type III substances are *fixed entities*, such as gases (fixed at a selected partial pressure), solids, and pH. Type IV substances are *precipitated solids* (these exist only as "output variables"), and type V substances are *dissolved solids*—substances that have the potential to precipitate. Finally, type VI substances are species or solids not considered in a given problem. For example, you could define a problem involving the components Ca^{2+} and CO_3^{2-}, and if you do not want to allow $CaCO_3$ to precipitate, you can define calcite (and other solid forms of $CaCO_3$) as type VI species. Type II, III, V, and VI species are described by the program in a *tableau*, which consists of a table listing the relevant species of each type, the components from which they are made, the stoichiometric coefficients that define the composition of the species, and log K and enthalpy of reaction values for the formation reaction for each species; Table 7.3 is a simple example. The thermodynamic data can be modified by the user, and users can define new species by inserting a name, stoichiometric coefficients for its components, and log K for the formation reaction.

7.5.3 Setting up problems

Formulation of problems in MINEQL+ and VMINTEQ varies with the nature of the problem to be solved, and generic instructions are not very useful. Instead, we will use a few simple examples here and provide additional information in later chapters focused on particular kinds of reactions. The examples used here refer to problems earlier in this chapter in the sections on graphical and algebraic methods. Further details are available in the programs' user manuals and Help menus in the programs.

Table 7.3 Example of a MINEQL+ tableau for aqueous species associated with the components H_2O, H^+, Ca^{2+}, and CO_3^{2-} (type II, aqueous species)*

Name	(Charge)	H2O	H(+)	Ca(2+)	CO3(2-)	log K[†]	Delta H[§]
OH–	(−1)	1	−1	0	0	−13.997	13.339
CaOH+	(+1)	1	−1	1	0	−12.697	15.323
CaHCO3	(+1)	0	1	1	1	11.599	1.291
H2CO3 (aq)	(0)	0	2	0	1	16.681	−5.679
HCO3–	(−1)	0	1	0	1	10.329	−3.490
CaCO3 (aq)	(0)	0	0	1	1	3.200	3.824

*The program does not use subscripts and superscripts, and the table mimics the appearance of the program on a computer screen.

[†]Equilibrium constant at 25°C for the formation reaction of the species from its components.

[§]Standard enthalpy of reaction, $\Delta H°$.

EXAMPLE 7.13 What is the pH of a 1 × 10⁻² M solution of acetic acid?: This is the same as Example 7.4, which was solved from the pC-pH diagram using the proton-balance expression. To solve this problem using MINEQL+, one follows the steps:

(1) On the initial screen (component selection module), check the box for component acetate (Ac^-); components H^+ and H_2O are added by default.

(2) Click the button to scan the thermodynamic database, which collects the thermodynamic data (log K) for all species involving the selected components.

(3) In the calculation wizard screen insert the total concentration of Ac^- (1×10^{-2} M, typed as 1E-2).

(4) In the pH tab of the wizard, click the option for the program to calculate pH and insert a total concentration of 1×10^{-2} M for H^+ (same as the concentration of Ac^-). Alternatively, you can add no H^+ and check the box to instruct the program to solve for pH based on electroneutrality. (In the latter case, the program iteratively adds H^+ until it reaches a stable solution.)

(5) In the "RunTime Manager" screen, insert a name for the output file, select the option for calculating ionic strength (for activity coefficient corrections), and run the program.

(6) The "Output Manager" screen appears once the calculations are complete, and various options for viewing the output are available on it. In this simple case, we suggest clicking on the button labeled "Special Reports" and then the "View" button. Scrolling in the box that then appears to report type "Summary of All Species for a Single Run" yields a table of output values and gives a pH of 3.38, which agrees with the result in Example 7.4

EXAMPLE 7.14 What is the solubility of calcite ($CaCO_3$) in pure water, and what is the: equilibrium pH of a pure water-calcite system?: This is the same problem as Example 7.11. Solving this problem in MINEQL+ can be approached in two ways. In the first (and perhaps more intuitive) method we add the two components Ca^{2+} and CO_3^{2-} in concentrations that exceed the solubility of calcite and allow the program to precipitate them until equilibrium is achieved. This involves the following steps:

(1) Add the components Ca^{2+} and CO_3^{2-} in the component selection module and scan the thermodynamic database.

(2) In the calculation wizard, specify total concentrations of the two components that exceed the solubility of $CaCO_{3(s)}$. Of course, *a priori*, you do not know what such values are, so you may need to proceed iteratively—that is, guess at supersaturated values, run the problem, and see whether calcite has precipitated. If it has not, increase the initial concentrations and rerun the problem until calcite does precipitate. Because the process is so fast, this approach is not a significant drain on one's time. Here we use initial values of Ca^{2+} and $CO_3{}^{2-}$ of 1×10^{-3} M, which are sufficient to cause calcite precipitation.

(3) In the CO_2 tab of the wizard (where the total carbonate concentration is added), select the option for a calculation closed to the atmosphere (no CO_2).

(4) In the pH tab of the calculation wizard, select the option to let pH be calculated by MINEQL+ and check the box to calculate by the electroneutrality condition.

(5) In the "solids mover" tab of the wizard, select the options to ignore other solids (aragonite, lime, and portlandite). Note that in this case the same answer

is obtained whether they are included or not because they all are more soluble than calcite and are not thermodynamically stable in a system where calcite is allowed.

(6) In the RunTime Manager, check the button to calculate ionic strength, insert a name for the output file, and click run.

(7) The results obtained from the output manager (see previous example) are $[Ca^{2+}] = 10^{-3.93}$ M, $[CO_3^{2-}] = 10^{-4.47}$, $[HCO_3^-] = [OH^-] = 10^{-4.08}$, pH = 9.908, which agree closely with those obtained manually in Example 7.11. Slight differences in the results reflect the fact that the computer output includes results for some soluble complexes ($CaHCO_3^+$, $CaOH^+$, $CaCO_3^0$) that were not included in the manual calculations.

The second method converts calcite to a Type III "fixed species." This forces solid calcite and its solubility equilibria to remain in the calculations. The program iteratively increases Ca^{2+} and CO_3^{2-} concentrations until equilibrium is reached. This involves the following steps:

(1) Add the components Ca^{2+} and CO_3^{2-} in the component selection module and scan the thermodynamic database.

(2) In the Type V – Dissolved Solids Tableau, sequentially move lime, portlandite, and aragonite to be Type VI (species not considered) by clicking on the "Move" button at the top of the tableau and clicking the Type VI option. Then move calcite to become Type III (fixed species) by the same approach.

(3) In the calculation wizard, specify initial values of Ca^{2+} and CO_3^{2-} of 0. (Actually, you can put in any numbers you wish, as long as they are the same for both components.)

(4) In the CO_2 tab of the wizard (where the total carbonate concentration is added), select the option for a calculation closed to the atmosphere (no CO_2).

(5) In the pH tab of the calculation wizard, select the option to let pH be calculated by MINEQL+ and check the box to calculate by the electroneutrality condition.

(6) In the RunTime Manager, check the button to calculate ionic strength, insert a name for the output file, and click run.

The same values are obtained by this method as given above for the first method. It is important to note that formulation of this problem in VMINTEQ must be done in a way similar to the second approach described above to obtain the correct answer. In VMINTEQ one adds calcite as an "infinite solid phase" (equivalent to a Type III species). It is not necessary to add the components Ca^{2+} and CO_3^{2-} explicitly or specify their initial concentrations; one obtains the correct answer whether they are added or not.

Examples 7.13 and 7.14 are simple enough that they can be solved by hand. The true power of computer-based solutions is that they allow determination of equilibrium concentrations of multiple species in systems that are too complicated to solve by hand. As we progress through the remainder of the book, computer-based solutions will be used to solve such problems.

7.5.4 Generating pC-pH diagrams with MINEQL+

Truth be told, the pC-pH diagrams presented earlier in this chapter (Figures 7.2–7.5) all were drawn using MINEQL+! Of course, they could have been drawn by hand,

but doing them in MINEQL+ allowed the production of an "editable" graphics file that could be inserted into the word-processing package used in writing the book. The "multirun" functionality of MINEQL+ and related programs was used to generate the data for pC-pH diagrams, related pε-pC diagrams in redox equilibria, acid-base and complexation titration curves, and other plots of equilibrium conditions as a function of some "master variable." The exact procedure depends on the nature of the desired plot and the computer program used. Rather than trying to cover all possibilities here, we provide specific details later in the text where such diagrams are used.

Problems

7.1. EDTA (ethylenediaminetetraacetic acid), a widely used complexing agent, is a tetraprotic acid with the following pK_a values: $pK_{a1} = 2.16$; $pK_{a2} = 3.12$; $pK_{a3} = 6.27$; $pK_{a4} = 10.95$. Write the expressions for $\alpha_0, \alpha_1, \alpha_2, \alpha_3$, and α_4 and determine the numerical value of each at pH 7.0.

7.2. Derive the α expressions for the triprotic acid H_3AsO_3, also written as $As(OH)_3$, arsenious acid. The pK_a values for this acid are 9.29, 12.04, and 13.34. Evaluate and plot the values of $\alpha_0, \alpha_1, \alpha_2$, and α_3 at half-unit pH values over the range 8–13 and plot the results. Note: do not attempt to do this problem by hand calculations; use a spreadsheet program to insert the α_i formulas and to plot the results.

7.3. From the following pC-pH diagram for hypochlorous acid-hypochlorite ($HOCl/OCl^-$) system at $Cl_T = 1 \times 10^{-3}$ M, determine (a) the pH of a solution containing pure water and 1×10^{-3} M HOCl, and (b) pure water and 1×10^{-3} M NaOCl. (c) Estimate the pK_a for HOCl from the graph. In each case, describe the position on the graph where the answer occurs.
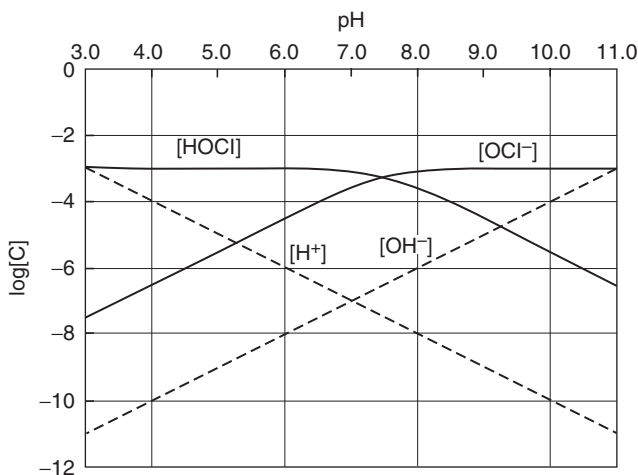
7.4. Solve algebraically for the pH of a solution of 5×10^{-3} moles of NaOCl in 1 L of water. Write the relevant equations starting with the mass-action and mass-balance

expressions. For your "last equation," write the charge-balance, proton-balance, and *TOT*H equations, and then choose one of them to use to solve the problem.

7.5. Construct a pC-pH diagram for the propionic acid/propionate (Pr) system ($pK_a =$ 4.87) at $Pr_T = 1 \times 10^{-3}$ M. Draw the lines as accurately as you can and include the lines for H^+ and OH^- on the graph. Using the graph and the appropriate proton-balance expression, determine the pH of a solution of water with enough propionic acid added to yield $Pr_T = 1 \times 10^{-3}$ M. Similarly, determine the pH of a solution of water with enough sodium propionate added to yield $Pr_T = 1 \times 10^{-3}$ M.

7.6. Solve for the pH of the HPr system in problem 7.5 using an algebraic approach. You may use the charge-balance, proton-balance, or *TOT*H equation.

7.7. Sketch the pC-pH diagram for the HCN/CN$^-$ system with $[CN]_T = 1 \times 10^{-3}$ M. If you add 1×10^{-3} moles of HCN to one liter of water, what is the pH (solve graphically)? If you add 1×10^{-3} moles of NaCN to one liter of water, what is the pH (solve graphically)?

7.8. In past years, there has been intense scrutiny of the tobacco industry. One specific charge is that cigarette manufacturers have manipulated tobacco chemically to make the cigarettes more addictive. The component in cigarettes that causes physical addiction is nicotine. Nicotine occurs in two forms:
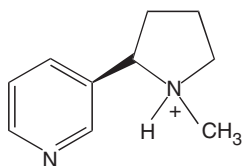
Acid form (nicotine-H$^+$)   Basic form (nicotine)
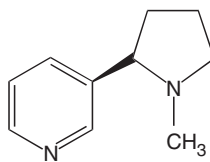
The acidic form is not volatile and cannot be taken up into the body from cigarette smoke. The free base form is volatile and is easily taken up through the lungs from cigarette smoke. (Note: the term "free basing" comes from adding a base to a drug to make it volatile so that it can be smoked.) The charge against cigarette manufacturers is that ammonia (a base) is added to change the form of the nicotine to make it absorbable. Given the equation nicotine-H$^+$ $\rightleftharpoons$ nicotine + H$^+$, $pK_a =$ 8.0, answer the following questions (ignore the fact that nicotine is volatile).

(a) Calculate ΔG° for the above reaction at 25°C.
(b) Calculate ΔG° for the above reaction at 60°C, assuming that $\Delta H^\circ = +25$ kJ/mol.
(c) What is the ratio of nicotine in the free base form to that in the protonated form (nicotine-H$^+$), at pH 5, 6, 7, 8, and 9?

7.9. You add the following chemicals to water to make a 1-L solution: 1×10^{-3} moles of acetic acid, 1×10^{-3} moles of NaOCl, 2×10^{-3} M KBr, and 1×10^{-3} moles of NaHCO$_3$. Set up the equations necessary to solve the problem. While you only need the charge-balance, proton-balance, or *TOT*H equation, set up all three of them.

7.10.   (a) Write the equations to solve for the pH of a solution to which you add
1×10^{-3} moles of the triprotic phosphoric acid (H_3PO_4) to water to
make a 1-L solution.

(b) Solve the system in part (a) using MINEQL+ or an alternative computer
equilibrium program.

(c) Write the equations to solve for the pH of a solution to which you add
1×10^{-3} moles of Na_2HPO_4 to 1 L of water.

(d) Solve the system in part (c) using MINEQL+ or an alternative computer
equilibrium program.

(e) Assume that 0.5×10^{-3} moles of HCl is added to the solution in part (b)
without changing the total volume. What is the resulting pH? Solve using
MINEQL+ or an alternative computer equilibrium program.

References

1. Sillen, L. G. 1961. The physical chemistry of seawater. In *Oceanography*, M. Sears (ed.),
   Amer. Assoc. Adv. Sci., Washington, D.C., 549–581.
2. Garrels, R. M., and M. E. Thompson. 1962. A chemical model for seawater at 25°C and one
   atmosphere total pressure. *Am. J. Sci.* **260**: 57–66.
3. Ingri, N., W. Kalowicz, L. G. Sillen, and B. Warnquist. 1967. High-speed computers as a
   supplement of graphical methods. V. HALTAFALL, a general program for calculating the
   composition of equilibrium mixtures. *Talanta* **14**: 1261–1286.
4. Zirino, A., and S. Yamamoto. 1972. A pH-dependent model for the chemical speciation of
   copper, zinc, cadmium, and lead in sea water. *Limnol. Oceanogr.* **17**: 661–671.
5. Morel, F. M. M., and J. J. Morgan. 1972. A numerical method for computing equilibria in
   aqueous chemical systems. *Environ. Sci. Technol.* **6**: 58–67.
6. Westall, J. C., J. L. Zachary, and F. M. M. Morel. 1976. MINEQL, a computer program for
   the calculation of chemical equilibrium composition of aqueous systems. Technical Note 18,
   Dept. of Civil Engineering, Mass. Inst. Technol., Cambridge, Mass.
7. U.S. EPA. 2006. MINTEQA2 (ver. 4.03). (available at http://www.epa.gov/ceampubl/
   mmedia/minteq/index.htm).
8. Anonymous. 2008. MINEQL+ ver. 4.6, a chemical equilibrium modeling system.
   Environmental Research Software, Hallowell, Maine. Also see http://www.mineql.com.
9. Gustafsson, J. P. 2007. Visual MINTEQ, ver. 3.0, Department of Land and Water Resources
   Engineering, Royal Institute of Technology—KTH, Stockholm, Sweden (available at
   http://www.lwr.kth.se/English/OurSoftware/vminteq/).
10. Nordstrom, D. K., et al. 1979. A comparison of computerized chemical models for
    equilibrium calculations in aqueous systems. In *Chemical modeling in aqueous systems*,
    E. A. Jenne (ed.), Amer. Chem. Soc. Symp. Ser. **93**, Amer. Chem. Soc., Washington, D.C.,
    857–892.
11. Mattigod, S. V., and G. Sposito. 1979. Chemical modeling of trace metal equilibria in
    contaminated solid solutions using the computer program GEOCHEM. In *Chemical
    modeling in aqueous systems*, E. A. Jenne (ed.), Amer. Chem. Soc. Symp. Ser. **93**, Amer.
    Chem. Soc., Washington, D.C., 837–856.
12. Truesdell, A. H., and B. F. Jones. 1973. WATEQ, a computer program for calculating
    chemical equilibria of natural waters. NTIS Technical Rep. PB2-20464, Springfield, Va.
13. Ball, J. W., E. A. Jenne, and D. K. Nordstrom. 1979. WATEQ2—a computerized chemical
    model for trace and major element speciation and mineral equilibria of natural waters.

In *Chemical modeling in aqueous systems*, E. A. Jenne (ed.), Amer. Chem. Soc. Symp. Ser. **93**, Amer. Chem. Soc., Washington, D.C., 815–835.

14. Ball, J. W., and D. K. Nordstrom. 1991. Users manual for WATEQ4F, with revised thermodynamic database and test cases for calculating speciation of major, trace, and redox elements in natural waters. U.S. Geol. Surv. Open File Rep. 91–183, Reston, Va (available at http://water.usgs.gov/software/lists/geochemical).
15. Parkhurst, D., S. Charlton, and A. Riggs. 2008. Reaction-transport modeling in ground-water systems. PHREEQC version 2—a computer program for speciation, batch-reaction, one-dimensional transport, and inverse geochemical calculations. U.S. Geol. Surv., Reston, Va (available at http://wwwbrr.cr.usgs.gov/projects/GWC_coupled/phreeqc/.) Note: PhreeqcI, also available from the U.S. Geological Survey, is a graphical user interface that allows operation of PRHEEQC in a Windows operating environment.
16. Helgeson, H. C., T. H. Brown, A. Nigrini, and T. A. Jones. 1970. Calculation of mass transfer in geochemical processes involving aqueous solutions. *Geochim. Cosmochim. Acta* **34**: 569–592.
17. Tipping, E. 1994. WHAM—a chemical equilibrium model and computer code for waters, sediments, and soils incorporating a discrete site/electrostatic model of ion-binding by humic substances. *Comput. Geosci.* 20: 973–1023; Tipping, E. 1998. Humic ion binding model VI: an improved description of the interactions of protons and metal ions with humic substances. *Aquat. Geochem.* **4**: 3–48.

This page intentionally left blank

III

Inorganic Chemical Equilibria and Kinetics

This page intentionally left blank

8

██ Acid-Base Systems

██ Objectives and scope

In this chapter you will learn the basic concepts of acids and bases, including different ways to define acids and bases, the differences between strong and weak acids and bases, and the relevant equilibrium expressions. The equations used to solve acid/base problems are described using the graphical and algebraic methods described in Chapter 7, and computer-based solutions of acid-base problems also are presented. Examples are used to demonstrate acid-base titrations and buffering capacity, and this knowledge then is used to discuss acid-base systems in natural waters, especially the carbonate system, and associated concepts, such as factors affecting pH and alkalinity, and Gran titrations. Other acid-base systems relevant to natural waters (ammonia, phosphate, and sulfide) also are discussed, and the kinetics of acid-base reactions is briefly described.

██ Key terms and concepts

- Arrhenius, Brønsted, and Lewis acids and bases
- pH, pOH, pK_a, pK_b
- Henderson-Hasselbach equation
- Titration curves
- Open and closed carbonate systems
- Carbonate, bicarbonate, and total alkalinity; acidity
- Gran titrations

8.1 Introduction

The concentration (or activity) of protons in water (i.e., the pH) is often the critical variable determining water quality and chemistry in both natural systems, such as lakes and rivers, and engineered systems, such as drinking water distribution systems. The speciation of many dissolved species, solubility of many minerals, and association (sorption) of dissolved species with solid surfaces all are controlled by pH. For example, the base ammonia ($NH_{3(aq)}$) is toxic to fish, but its concentration versus that of its acidic counterpart, ammonium (NH_4^+), depends on a solution's pH. Acid deposition (acid rain) lowers the pH of lakes and streams and promotes the dissolution of aluminosilicate minerals in poorly buffered soils resulting in high concentrations of dissolved aluminum that can be toxic to fish. In drinking water, pH is critically important because the acid form of the disinfectant, free chlorine (hypochlorous acid, HOCl), is much more potent than the basic form (hypochlorite, OCl^-). This must be balanced by the fact that a lower pH can lead to dissolution of metal pipes carrying the water and cause taste, odor, and toxicity problems for consumers. Thus, it is important to calculate the pH changes that occur when species that increase proton concentrations (acids) or decrease proton concentrations (bases) are added to waters. This chapter has two main parts. The first part (Sections 8.2–8.4) covers the fundamental concepts of acid-base chemistry; the second part (Sections 8.5–8.7) covers the applications of these principles to the acid-base chemistry of natural and engineered water systems.

PART 1. PRINCIPLES OF ACID-BASE CHEMISTRY

8.2 Properties of acids and bases

8.2.1 Water as an acid and base

As a starting point, we first consider pure water. In absolutely pure water, which in practice is extremely difficult to obtain because carbon dioxide from the atmosphere readily dissolves in water, only three species exist, protons (H^+), hydroxide ions (OH^-), and water (H_2O), and the only relevant equilibrium expression is

$$K_w = \{H^+\}\{OH^-\}, \tag{8.1}$$

which is for the reaction

$$H_2O \rightleftharpoons H^+ + OH^-. \tag{8.2}$$

The value of K_w is temperature dependent, as shown in Table 8.1. At 25°C the value of K_w is $\sim 1 \times 10^{-14}$, and in most situations rounding to this value is acceptable. Therefore, in pure water, $\{H^+\}\{OH^-\} = 10^{-14}$. Because protons and hydroxide are the only charged species (ions) present, $\{H^+\} = \{OH^-\}$, and the activity (or ignoring activity corrections, concentrations) of each species is 1×10^{-7} M. Thus, the pH (and pOH) of pure water is 7.00. Of course, this is neutral water. If $\{H^+\}$ increases, the pH decreases, leading to an

Table 8.1 Temperature dependence of K_w

Temperature, °C	K_w
0	0.114×10^{-14}
10	0.292×10^{-14}
20	0.681×10^{-14}
25	1.008×10^{-14}
30	1.47×10^{-14}
40	2.92×10^{-14}
50	5.5×10^{-14}
100	55.0×10^{-14}

acidic solution, which by definition has a pH < 7. If $\{H^+\}$ decreases, the pH increases, leading to a basic solution with a pH > 7. It is now necessary to show how to identify a species as an acid or base.

8.2.2 Defining acids and bases

Two common definitions of acids and bases are used today—***Brønsted*** and ***Lewis*** acids and bases—along with an older, narrower definition by ***Arrhenius*** that defines acids as substances that release protons (H^+) in water and bases as substances that release OH^-.

The Brønsted concept of acids and bases is not limited to aqueous solutions, and a ***Brønsted acid*** simply is defined as a ***proton donor***, and a ***Brønsted base*** is a ***proton acceptor***. Any reaction in this concept involves both an acid and a base; that is, a donated proton from an acid must be accepted by a proton acceptor (or base). When a Brønsted acid is added to water, water acts as the base and accepts the proton released from the acid. Examples include hydrochloric acid,

$$HCl + H_2O \rightleftharpoons H_3O^+ + Cl^-, \tag{8.3}$$

and acetic acid,

$$CH_3COOH(HAc) + H_2O \rightleftharpoons H_3O^+ + CH_3COO^-(Ac^-). \tag{8.4}$$
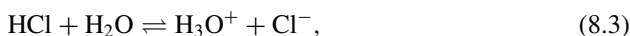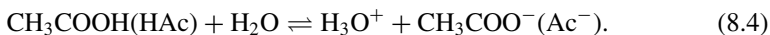
For simplicity in aqueous acid-base reactions, we normally write H_3O^+ simply as H^+ and ignore the water molecule as a reactant (base) in the acid-base reaction, but it is important to remember that free protons (H^+) actually do not exist in water. The species formed from Brønsted acids by release of a proton (e.g., Cl^- and Ac^-) are known as ***conjugate bases*** or Brønsted bases. Other examples include ammonia,

$$NH_3 + H_3O^+ \rightleftharpoons NH_4^+ + H_2O, \tag{8.5a}$$

or

$$NH_3 + H^+ \rightleftharpoons NH_4^+, \tag{8.5b}$$

and phosphate,

$$PO_4^{3-} + H_3O^+ \rightleftharpoons HPO_4^{2-} + H_2O, \tag{8.6a}$$

or

$$PO_4^{3-} + H^+ \rightleftharpoons HPO_4^{2-}. \tag{8.6b}$$
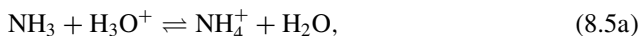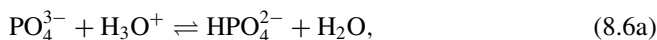
In these examples, NH_4^+ and HPO_4^{2-} are the ***conjugate acids*** of NH_3 and PO_4^{3-}, respectively, and as described above for acid dissociation reactions, we usually ignore the H_2O molecule and write the reactions as in Eqs. 8.5b and 8.6b.

Many species are both Brønsted acids and Brønsted bases; e.g., bicarbonate:

$$HCO_3^- \rightleftharpoons H^+ + CO_3^{2-} \text{ or } HCO_3^- + H^+ \rightarrow H_2CO_3^* \tag{8.7}$$
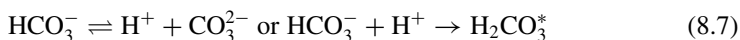
Many metal ions also act as Brønsted acids. For example, when sufficient ferric iron (Fe^{3+}) is added to water, the following reaction can occur:

$$Fe^{3+} + 3H_2O \rightleftharpoons Fe(OH)_{3(s)} + 3H^+ \tag{8.8}$$
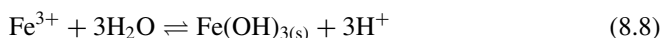
Thus, three units of protons are released per mole of iron added. However, Fe^{3+} does not itself release protons. Instead, we need to remember that metal ions exist as hydrated species in water, and Fe^{3+} actually exists as $Fe(H_2O)_6^{3+}$ in water. What happens is that one of the hydrated water molecules releases a proton. For example, in the first step the following reaction occurs:

$$Fe(H_2O)_6^{3+} \rightleftharpoons FeOH(H_2O)_5^{2+} + H^+ \tag{8.9}$$
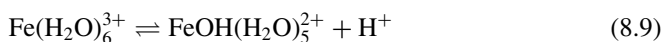
In this case the highly positive aqueous Fe^{3+} ion attracts electron pairs from hydrated water molecules so strongly that the electron pair of an O–H bond is drawn toward the electronegative oxygen atoms, thus facilitating the release of an H^+.

According to the Lewis theory a ***Lewis acid*** is an electron acceptor, and a ***Lewis base*** is an electron donor. This concept can be illustrated using the reaction of ammonia:

$$H^+ + :NH_3 \rightleftharpoons H-NH_3^+ \tag{8.10}$$

The lone pair of electrons on ammonia is donated to the proton, making ammonia a Lewis base; H^+, the electron pair acceptor, is a Lewis acid. All Lewis acids (or bases) are Brønsted acids (or bases), but not all Brønsted acids (or bases) are Lewis acids (or bases). A classic example is

$$H_3N: + BF_3 \rightleftharpoons H_3N-BF_3, \tag{8.11}$$
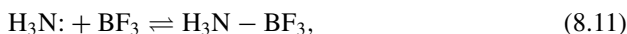
in which ammonia is a Lewis base and boron trifluoride is a Lewis acid. Because a proton is not exchanged, the Brønsted definitions do not apply.

The Brønsted definition works well for a wide variety of aqueous species, but the Lewis definition is more comprehensive and allows additional insight into processes such as metal-ion complexation (Chapter 9).

8.2.3 Strong and weak acids and bases

Of course, some species give up their protons (i.e., accept electrons) more readily than others. This allows us to categorize acids and bases based on this propensity. We already saw in Chapters 1 and 7 that the dissociation of an acid is written as $HA \rightarrow H^+ + A^{-*}$ with an equilibrium constant:

$$K_a = \frac{\{H^+\}\{A^-\}}{\{HA\}} \tag{8.12}$$

Subscript a often is used to denote an acid dissociation. For a diprotic acid, where $H_2A \rightarrow H^+ + HA^- \rightarrow H^+ + A^{2-}$, we have

$$K_{a1} = \frac{\{H^+\}\{HA^-\}}{\{H_2A\}}, \tag{8.13}$$

and

$$K_{a2} = \frac{\{H^+\}\{A^{2-}\}}{\{HA^-\}}. \tag{8.14}$$

Each acid has its own equilibrium constant, which is commonly referred to as the ***acid dissociation constant*** or ***acidity constant***. K_a values for common acids are tabulated in Table 8.2. Of course, if the data are available, the K_a values may be calculated from appropriate G_f° values. The magnitude of K_a determines the extent to which an acid dissociates at equilibrium. The larger K_a is (or the smaller pK_a is), the greater the concentrations must be in numerator of the equilibrium expression (at equilibrium), and thus the more dissociation occurs. By definition, ***strong acids*** are completely dissociated in water. The conjugate bases of strong acids are strongly electronegative and thus can easily carry full negative charge(s). The conjugate bases of strong acids thus are always ***weak bases***; that is, they have little propensity to accept a proton. Examples include Cl^-, NO_3^-, and SO_4^{2-}; the corresponding strong acids are HCl, HNO_3, and H_2SO_4. As a rule of thumb, strong acids have pK_a values of 2 or less. Note that the hydronium ion (H_3O^+) has a pK_a of 0. Thus, any acid with a $pK_a < 0$ will donate its proton to water, making H_3O^+ the strongest acid that can exist in aqueous solution. This is known as the ***leveling effect of water***.

Weak acids do not dissociate completely in water and have pK_a values of $\sim$3 or higher. The difference between strong and weak acids is exemplified by the different pH values observed upon adding 10^{-2} moles of the strong acid hydrochloric acid (HCl; $pK_a = -3$) and acetic acid (HAc; $pK_a = 4.76$) to a liter of water. The HCl

---

*Because the reaction is reversible, for accuracy we normally use bidirectional arrows ($\rightleftharpoons$). Here we are focusing just on the forward reaction, and so the forward arrow is acceptable.

Table 8.2 Acidity constants (pK_a) for some common acids*

Formula	Name	pK_{a1}	pK_{a2}	pK_{a3}	pK_{a4}
$HClO_4$	Perchloric acid	−7			
H_2SO_4	Sulfuric acid	−3	1.92		
HCl	Hydrochloric acid	−3			
HNO_3	Nitric acid	−1.30			
CCl_3COOH	Trichloroacetic acid	−0.5			
H_3O^+	Hydronium ion	0			
H_2CrO_4	Chromic acid	0.86	6.51		
HOOCCOOH	Oxalic acid	0.9	4.20		
	nitrilotriacetic acid	2.00	2.94	10.28	
H_3PO_4	phosphoric acid	2.15	7.20	12.38	
	EDTA	2.16	3.12	6.27	10.95
$Fe(H_2O)_6^{3+}$	Aquo ferric ion	2.20			
H_3AsO_4	Arsenic acid	2.24	6.76	11.60	
$C_6H_4OHCOOH$	Salicylic acid	3.10			
$C_3H_4OH(COOH)_3$	citric acid	3.13	4.76	6.40	
HF	Hydrofluoric acid	3.17			
HCOOH	Formic acid	3.75			
C_6H_5COOH	Benzoic acid	4.20			
CH_3COOH	Acetic acid	4.76			
$Al(H_2O)_6^{3+}$	Aquo aluminum ion	4.90			
$H_2CO_3^*$	Total un-ionized CO_2	6.35	10.33		
H_2S	Hydrogen sulfide	7.02	>>14		
HOCl	Hypochlorous acid	7.50			
HOBr	Hypobromous acid	8.63			
HCN	Hydrogen cyanide	9.21			
$B(OH)_3$	Boric acid	9.24			
NH_4^+	Ammonium ion	9.25			
H_3AsO_3	Arsenious acid	9.29			
$Si(OH)_4$	Silica; silicic acid	9.84			
C_6H_5OH	Phenol	9.99			

* Values selected to agree with MINEQL+ database where possible.

solution has a pH of 2.0 (i.e., complete dissociation occurs), but the pH of HAc is 3.4 (see Example 7.1), which indicates that only a small fraction of the protons are released from HAc.

Before discussing **strong and weak bases**, it is necessary to discuss the **basicity constant**, K_b. The K_b value for the conjugate base of an acid is related to the K_a for the acid and K_w, as shown by the following example using acetate and acetic acid. The base reaction of acetate is

$$Ac^- + H_2O \rightleftharpoons HAc + OH^- \qquad K_b =? \qquad (8.15)$$

A little chemical intuition shows that we can derive K_b from K_a and K_w by writing the acid dissociation reaction in reverse and adding the dissociation of water to it; recall that

when reactions are added, their equilibrium constants are multiplied together to yield the equilibrium constant for the new reaction:

$$H^+ + Ac^- \rightleftharpoons HAc \qquad K_a^{-1} = 10^{4.76}$$

$$H_2O \rightleftharpoons OH^- + H^+ \qquad K_w = 10^{-14.00}$$

$$Ac^- + H_2O \rightleftharpoons HAc + OH^- \qquad K_b = 10^{-9.24} \qquad (8.16)$$
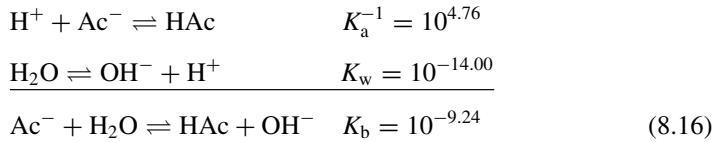
where

$$K_b = \frac{\{HA\}\{OH^-\}}{\{Ac^-\}}.$$

Note that for any acid/conjugate base pair,

$$K_a \times K_b = K_w, \qquad (8.17a)$$

and

$$pK_a + pK_b = pK_w = 14, \qquad (8.17b)$$

Thus, if we know either K_a or K_b for an acid/conjugate base pair, we readily can compute the other constant from Eq. 8.17.

The same rule of thumb applies to define **strong bases** as for strong acids. A strong base has a pK_b of 2 or less. Strong bases include OH^- (by far the most common strong base; added as NaOH or KOH, which dissociate completely), PO_4^{3-}, and S^{2-}.* For many species, the acid is a weak acid and the base is a weak base, but in general the stronger the acid (i.e., the lower the pK_a), the weaker the base (i.e., the higher the pK_b), and vice versa. As we saw in Chapter 7, pC-pH diagrams, algebraic solutions, and computer-based solutions can give the pH of system when an acid or base is added to solution.

EXAMPLE 8.1: Hypochlorous acid (HOCl) is commonly used as a disinfectant. If 5 mL of a 10 g/L solution of HOCl is diluted to a total volume of 1 L using distilled water, what is the resulting pH? (Ignore activity corrections.)

Answer: Because activity corrections are being ignored, the problem can be solved on a concentration basis. We have four species (not including H_2O), H^+, OH^-, HOCl, OCl^-, and thus need four equations.

Equilibrium constants:

(1) From Table 8.2: $HOCl \rightleftharpoons H^+ + OCl^- \qquad K_a = 10^{-7.60} = \dfrac{[H^+][OCl^-]}{[HOCl]}$

(2) $K_w = [H^+][OH^-] = 10^{-14}$

---

*Indeed, the latter ion is such a strong base that it does not exist in water at pH ≤ 14; the pK_a of its conjugate acid (HS^-) is not known with accuracy (values as high as 17 and 19 have been reported) but it is much higher than 14.

Mass balance:

(3) $OCl_T = [HOCl] + [OCl^-]$, but what is OCl_T?

We have

$$5 \text{ mL} \times \frac{1 \text{ L}}{1000 \text{ mL}} \times \frac{10 \text{ g HOCl}}{\text{L}} \times \frac{\text{mol HOCl}}{52.45 \text{ g HOCl}} = 9.5 \times 10^{-4} \text{ mol HOCl added,}$$

and thus $OCl_T = 9.5 \times 10^{-4}$ M.

Charge balance:

(4) $[H^+] = [OH^-] + [OCl^-]$

Note that the charge balance and proton balance are the same for this problem. We now have four equations and four unknowns. Because we have added an acid to the water, it is reasonable to assume that the pH will be less than 7 and that $[OH^-]$ is negligible. Thus, $[H^+] = [OCl^-]$.

Using Eq. (1),

$$[HOCl] = \frac{[H^+][OCl^-]}{K_a}.$$

Substituting into Eq. (3) gives

$$OCl_T = \frac{[H^+][OCl^-]}{K_a} + [OCl^-] = [OCl^-]\left(1 + \frac{[H^+]}{K_a}\right),$$

or

$$[OCl^-] = \frac{OCl_T K_a}{K_a + [H^+]}.$$

Substituting into the simplified charge balance gives

$$[H^+] = \frac{OCl_T K_a}{K_a + [H^+]} \text{ or } [H^+]^2 + K_a[H^+] - OCl_T K_a = 0.$$

Using the quadratic equation to solve for $[H^+]$ gives $[H^+] = 4.9 \times 10^{-6}$ (which, as indicated above, is also the concentration of OCl^-) and **pH = 5.31**. Checking the assumption that $[OH^-] << [OCl^-]$ was correct, we find $[OH^-] = 2.04 \times 10^{-9}$ at pH 5.31, and the assumption is valid.

Below is an example using ammonia in which two different questions are asked.

EXAMPLE 8.2: Two beakers each contain 0.1 M NaCl. To the first beaker 10^{-3} M NH_3 is added, and to the second beaker, NH_3 is added until the $p^cH = 10.5$. What is the pH in beaker 1, and how much ammonia was added to beaker 2?

Answer: In each beaker, the same set of equations applies. First write out the species and the relevant equilibrium constants. For species:

$$H^+, OH^-, Na^+, Cl^-, NH_3, NH_4^+$$
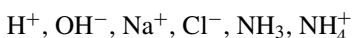
Equilibrium constants:

(1) $^aK_w = \{H^+\}\{OH^-\} = 10^{-14}$ and (2) $^aK_a = \dfrac{\{H^+\}\{NH_3\}}{\{NH_4^+\}} = 10^{-9.25}$

Mass balance:

(3) $N_T = [NH_3] + [NH_4^+]$

We now need either the charge balance,

(4) $[Na^+] + [NH_4^+] + [H^+] = [OH^-] + [Cl^-]$,

or proton balance,

(5) $[NH_4^+] + [H^+] = [OH^-]$.

Note that these are the same, because $[Na^+] = [Cl^-] = 0.1$ M.

   For this solution, we may not ignore activity corrections, and to solve the problem it is most convenient to convert the ^aK_a values to ^cK_a values. The ionic strength is 0.1 M, and from the Davies equation (Eq. 4.14), $\gamma_\pm = 0.776$:

(6) $^aK_w = \gamma_\pm [H^+] \gamma_\pm [OH^-] = (\gamma_\pm^2)^cK_w$,

so

(7) $^cK_w = 10^{-14}/(0.776^2) = 10^{-13.78}$,

(8) $^aK_a = \dfrac{\gamma_\pm[H^+][NH_3]}{\gamma_\pm[NH_4^+]} = \dfrac{[H^+][NH_3]}{[NH_4^+]} = {}^cK_a = 10^{-9.25}$.

For beaker 1, we added a base, and so we can assume that pH > 7 and $[H^+]$ is negligible. Equation (5) thus becomes

(9) $[NH_4^+] = [OH^-]$,

which leads to

$$\dfrac{[H^+]N_T}{[H^+] + {}^cK_a} = \dfrac{{}^cK_w}{[H^+]},$$

or

(10) $N_T[H^+]^2 - {}^cK_w[H^+] - {}^cK_w{}^cK_a = 0$.

Solving the quadratic equation gives

$[H^+] = \mathbf{9.98}$.

For beaker 2, $[H^+]$ is known, and N_T is unknown. Substituting into Eq. (10) gives

(11) $N_T(10^{-10.5})^2 - (10^{-13.78})(10^{-10.5}) - (10^{-13.78})(10^{-9.25}) = 0$,

or

$N_T = \mathbf{9.86 \times 10^{-3}}$ **M**.

We leave it to the reader to verify using MINEQL+ that adding this amount of ammonia gives a pH of 10.5. Note that (1) the reference species in MINEQL+ is NH_4^+, and so $TOTH_{in}$ will be -9.86×10^{-3} M, and (2) rather than adding Na^+ and Cl^- to set the ionic strength, the ionic strength can be set to 0.1 M before running the calculation. Approximate answers to both problems also can be obtained using a pC-pH diagram.

8.2.4 The Henderson-Hasselbach relationship and the concept of buffers

As the above examples illustrate, with the concepts of K_a and K_b in hand and the methods described in Chapter 7, it is possible to determine the concentrations of acids and bases in solution (as well as the pH). Before moving on to more complicated acid-base relationships, we need to demonstrate another simple means to display relative concentrations of acids and bases as a function of pH. We start with the acid dissociation constant (and ignore activity corrections):

$$K_a = \frac{[H^+][A^-]}{[HA]} \tag{8.18}$$

Taking the negative logarithm of both sides yields

$$-\log K_a = pK_a = -\log[H^+] - \log\frac{[A^-]}{[HA]} = -\log[H^+] + \log\frac{[HA]}{[A^-]},$$

and rearranging,

$$pH = pK_a - \log\frac{[HA]}{[A^-]}. \tag{8.19}$$

Equation 8.19 is known as the **Henderson-Hasselbach** equation. Although it is not used to solve complicated problems, it is very useful for simple problems involving weak acids and their conjugate bases. Collectively, such systems are known as **buffers**, because they resist or minimize changes in pH when strong acids or bases are added to such solutions. The Henderson-Hasselbach equation also is useful for displaying relative concentrations of an acid and its conjugate base. Taking ammonium/ammonia ($pK_a = 9.25$) as an example, Table 8.3 demonstrates that (1) when $pH = pK_a$, the concentrations of the acid and conjugate base are equal (as seen in the pC-pH diagrams in Chapter 7), and (2) for unit change in pH, the relative amounts of the acidic and basic forms change by one order of magnitude.

8.3   Titrations of acids and bases

In the previous section, the examples showed how to determine the pH of system once an acid or base has been added and how to determine how much of an acid or base to add to achieve the desired pH. In many situations, a water sample is collected, and it is not known which acid and bases are present. By adding strong acid or base to such

Table 8.3 Speciation of ammonium/ammonia using the Henderson-Hasselbach equation

pH	$log \frac{[HA]}{[A^-]}$	$\frac{[HA]}{[A^-]}$
6.25	3	1000
7.25	2	100
8.25	1	10
9.25	0	1
10.25	−1	0.1
11.25	−2	0.01
12.25	−3	0.001

a solution and monitoring changes in pH, it is possible to gather information about the acids and bases in the solution. This process is known as ***titration***, and the resulting data (pH as a function of acid or base added) is a ***titration curve***. The most important example of an acid-base titration in water chemistry involves the addition of strong acid to water samples to determine the concentrations of carbonate forms and other weak bases; this is known as alkalinity (see Section 8.7).

In many situations, it is desirable to control the pH of a system. That is, one wants the pH to change very little if strong or weak acid or strong or weak base is added. If such additions do not cause pH to change much, the system is said to be ***buffered***. Titration curves are used to determine the ***buffering capacity*** (i.e., how much acid or base can be absorbed with out dramatic pH change) of a system. A more exact mathematical definition of this term is provided in Section 8.4.

8.3.1 Titration of a strong acid with a strong base

The simplest titrations involve pure water with a strong acid or base added. In any titration, the system is titrated with the opposite species; i.e., if acid had been added, one titrates with base, and vice versa. For example, consider a 1-L beaker of pure water to which 1×10^{-2} moles of HCl has been added. HCl is a strong acid, and the initial pH thus is 2.0. Increments of strong base are now added. We will assume that the volumes of NaOH added are negligible so that the volume can be assumed to remain constant at 1 L. The charge balance for this system is (ignoring activity corrections)

$$[Na^+] + [H^+] = [OH^-] + [Cl^-]. \tag{8.20}$$

At any point, the concentration of strong acid, C_A, is equal to the chloride concentration, and the concentration of strong base added, C_B, is equal to the sodium concentration. Thus, we can rewrite the equation as follows:

$$C_B - C_A = [OH^-] - [H^+] = K_w/[H^+] + [H^+] \tag{8.21}$$

Initially C_A is 1×10^{-2} M and C_B is 0. We know that $[H^+] = 1 \times 10^{-2}$ M because HCl is a strong acid, and thus $[OH^-]$ must equal 1×10^{-12} M. Note that the left side of Eq. 8.21 is equal to 10^{-2} M and the right-hand side is $10^{-2} + 10^{-12}$ M. Because this
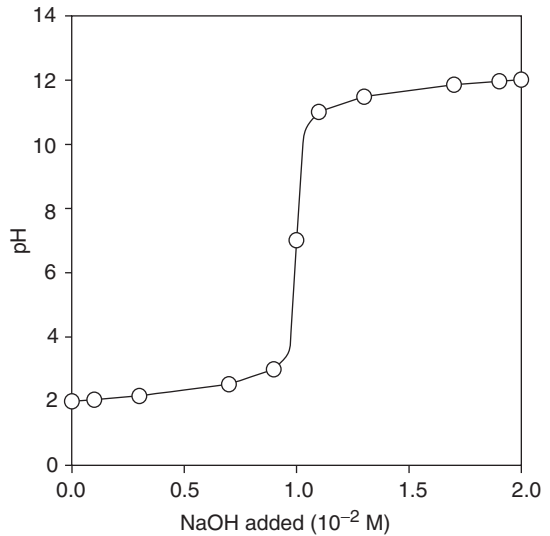
Figure 8.1 Titration of 1×10^{-2} M
HCl with 1×10^{-2} M NaOH.

Table 8.4 Strong acid/strong base titration

C_B	C_A	$[H^+]$	$[OH^-]$	pH
0	10^{-2}	10^{-2}	10^{-12}	2
1×10^{-3}	10^{-2}	9×10^{-3}	1.1×10^{-12}	2.05
3×10^{-3}	10^{-2}	7×10^{-3}	1.4×10^{-12}	2.15
7×10^{-3}	10^{-2}	3×10^{-3}	3.3×10^{-12}	2.52
9×10^{-3}	10^{-2}	1×10^{-3}	1.0×10^{-11}	3
1×10^{-2}	10^{-2}	10^{-7}	10^{-7}	7
1.1×10^{-2}	10^{-2}	1.0×10^{-11}	1×10^{-3}	11
1.3×10^{-2}	10^{-2}	3.3×10^{-12}	3×10^{-3}	11.48
1.7×10^{-2}	10^{-2}	1.4×10^{-12}	7×10^{-3}	11.85
1.9×10^{-2}	10^{-2}	1.1×10^{-12}	9×10^{-3}	11.96
2×10^{-2}	10^{-2}	10^{-12}	10^{-2}	12

inequality is so small, we will not worry about it at this point. When a unit of base is added, the approximate calculation is repeated, as summarized in Table 8.4. When $C_B = C_A$, $[OH^-]$ and $[H^+]$ must be equal, and pH = 7. Once $C_B > C_A$ we can assume that $C_B - C_A \sim [OH^-]$ and use this to estimate the $[H^+]$ concentration. The data are plotted in Figure 8.1, which is the titration curve for a strong acid in water. Note the very sharp change in pH at the equivalence point (around pH 7). This shows that when even small amounts of strong acid or base are added to pure water, the pH changes dramatically.

8.3.2 Titration of a weak acid with a strong base

Weak acids and bases are common in natural waters and thus in drinking water and wastewater systems (which draw their water from natural sources). Titrations are used

to determine the concentration (and in some cases, the identity) of the weak acid/base system present. To illustrate, the titration of a weak acid, ammonium will be used. When conducting a titration of a weak acid, an aliquot of strong acid of known concentration may be added first to ensure all of the weak acid/base system is in the acid form, and the pH is recorded. Then small increments of strong base of known concentration are added and the pH is recorded after each step. One could also add strong base and then titrate with strong acid.

Consider a 1-L solution with an unknown amount of ammonium/ammonium in it. We can determine the concentration using the following procedure. First, 0.01 moles strong acid is added by introducing 5 mL of a 2 M HCl solution. The pH is measured and found to be 2.0. We then begin to add NaOH (a strong base) in increments of 0.0025 moles (0.5 mL of a 5 M solution) as long as the pH changes little and add smaller increments of 0.00125 moles (0.25 mL of the solution) when the pH changes rapidly. Table 8.5 lists the value of $C_B - C_A$ (the "resulting concentration" of strong base added minus the "resulting concentration" of strong acid added) and the resulting pH, and the titration curve generated from these data is shown in Figure 8.2. The titration curve provides information about the system being titrated. There are two inflection points in the graph (where the curvature turns from concave upward to concave downward). These occur at $C_B - C_A = 0$ and $C_B - C_A = 0.01$. The distance along the x-axis between the two inflection points gives the total concentration of the weak acid/base system present (in this case, 0.01 M). This is also true for polyprotic systems (which have multiple inflection points; the distance between any two inflection points gives the concentration of the acid/base system present. At $C_B - C_A = 0$, this is the point at which the pH

Table 8.5 Titration data for ammonium solution

$C_B - C_A$ (added strong base and acid concentration, M)	pH (measured)
−0.01	2.00
−0.0075	2.12
−0.005	2.30
−0.0025	2.60
−0.00125	2.90
0	5.57
0.00125	8.40
0.0025	8.77
0.00375	9.02
0.005	9.24
0.00625	9.46
0.0075	9.71
0.00875	10.03
0.01	10.50
0.0125	11.20
0.015	11.48
0.0175	11.66
0.02	11.78
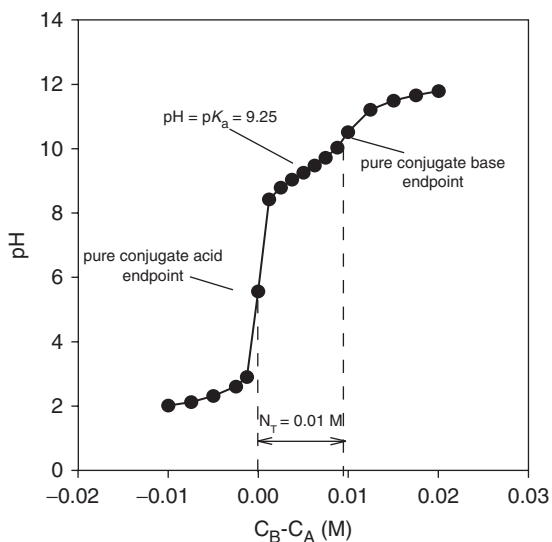
Figure 8.2 Plot of data in Table 8.5 to give a titration curve of a solution containing ammonia/ammonium.

equals that if we had added 0.01 M NH$_4$Cl to the water. Thus, this is the ***pure conjugate acid endpoint*** of the system. When 0.020 moles of base has been added to the system ($C_B - C_A = 0.010$), the ***equivalence point*** is reached. This is the ***pure conjugate base endpoint***. That is, if we initially added NH$_3$ to the solution, the measured pH would be this value. Between the two endpoints, there is a region of shallow slope. The center of this region is the point where the concentration of the ammonia and ammonium are equal, and the pH at this value, which is an inflection point on the curve, is the pK_a. If the acid/base system is unknown, it may be possible to identify it using the pK_a value.

We also can generate a titration curve mathematically via a reverse calculation, in which the pH is specified and concentrations of all other species (and thus $C_B - C_A$) are calculated (see Example 8.3).

EXAMPLE 8.3 Titration of ammonium chloride: To a 1-L beaker, 0.010 moles of ammonium chloride and 0.10 moles of sodium chloride is added. Draw the titration curve when HCl or NaOH is added. From the initial solution, add up to either 0.020 moles of HCl or NaOH.

Answer: We begin in the same way as for Example 8.2. We will assume that the 0.10 M NaCl is sufficient to fix the ionic strength, and that activity coefficients are not dramatically influenced by the addition of acid or base. Species:

$$H_2O, H^+, OH^-, Na^+, Cl^-, NH_3, NH_4^+$$
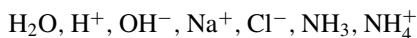
Equilibrium constants:

(1) $^cK_w = 10^{-13.78}$
(2) $^cK_a = 10^{-9.25}$

Mass balance:

(3) $N_T = [NH_3] + [NH_4^+]$

As with the titration of water, we could use the charge balance, but the proton condition allows us to avoid the complication of the having the background electrolyte in the equation:

(4) $[Na^+]_{NaOH} + [H^+] = [OH^-] + [NH_3] + [Cl^-]_{HCl}$

Na^+ appears because it is the product of the acceptance of a proton by NaOH. Similarly, Cl^- is a product of the proton release from HCl. Rearranging the above equation gives

(5) $C_B - C_A = [OH^-] + [NH_3] - [H^+]$.

Writing all species in terms of protons (using the equilibrium constant and mass balance to substitute for ammonia, or equivalently the α_1 value for a monoprotic acid) yields

(6) $C_B - C_A = \dfrac{{}^cK_w}{[H^+]} + \dfrac{{}^cK_aN_T}{[H^+] + {}^cK_a} - [H^+]$

If we were to perform the experiment, we would measure the pH after adding each increment of strong acid or strong base titrant. For calculation purposes we have two choices. The first is the forward calculation, in which the $C_B - C_A$ term is chosen, and $[H^+]$ concentration determined; this is how Figure 8.2 was generated. Although this does allow an iterative calculation to be performed in which ionic strength and activity coefficients are calculated at each value of $C_B - C_A$, it involves solving a cubic equation by hand or using the solver function in a spreadsheet at each step. It is simpler to select the pH value, and then calculate $C_B - C_A$. Figure 8.3 was generated in this manner.
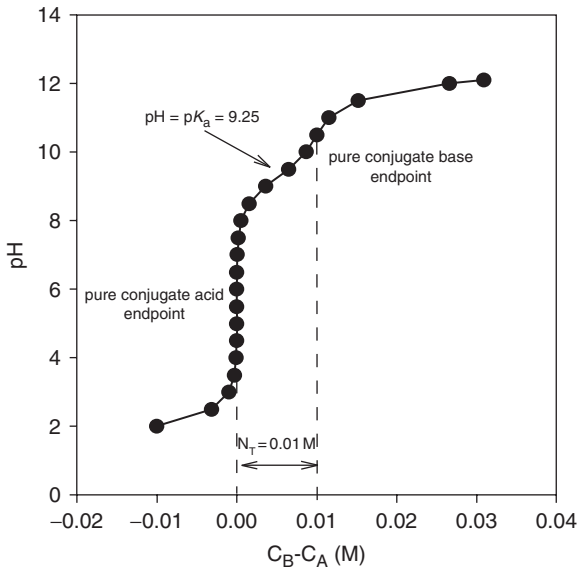
Figure 8.3 Plot of NH_3 titration. This plot was generated by selecting $[H^+]$ and calculating $C_B - C_A$ (reverse calculation).

Note that if we begin with NH_3 rather than NH_4^+, the relevant equations for generating the titration curve are

(7) $C_B - C_A = [OH^-] - [NH_4^+] - [H^+],$

and

(8) $C_B - C_A = \dfrac{{}^cK_w}{[H^+]} - \dfrac{[H^+]N_T}{[H^+] + {}^cK_a} - [H^+]$

The curve generated is identical to that in Figure 8.2 except that the x-axis moves 0.010 units to the right; that is, $C_B - C_A = 0$ will be where $C_B - C_A = 0.010$.

8.4 Buffering and acid/base neutralizing capacities

When $pH = pK_a$ (halfway between the two endpoints of a titration curve), the rate of change of pH with respect to the addition of acid or base is lowest, and the solution has its greatest buffering. The ***buffering capacity*** (or buffering intensity), symbolized as β, at any point along the titration is the inverse of slope of the curve and is defined mathematically as

$$\text{Buffering capacity} = \beta = \frac{d(C_B - C_A)}{d(pH)} \approx \frac{\Delta(C_B - C_A)}{\Delta(pH)} \tag{8.22}$$

In general, for any acid/base system, β is greatest near the pK_a value(s) and smallest at the pure acid and pure conjugate base endpoints. For example, note the flattening of the titration curves in Figures 8.2 and 8.3 near the value of pK_a. Also, β for pure water or for a solution to which NH_4Cl has been added is essentially zero (i.e., the titration curve is nearly vertical, and so the slope approaches infinity).

Two more quantities can be defined by examining the titration curve. Let us assume that we began with a 0.010 M NH_4Cl solution and titrated it to its pure conjugate base end point. Our proton balance would be

$$C_B - C_A = 0.01 = [OH^-] + [NH_3] - [H^+]. \tag{8.23}$$

How much acid would it take to get back to the pure conjugate acid endpoint? The answer, of course, is 0.010 mol/L. The ***acid neutralizing capacity*** of the solution thus is

$$ANC = [OH^-] + [NH_3] - [H^+]. \tag{8.24}$$

That is, the amount of acid that can be consumed by the solution is the sum of the strong bases and the weak bases, minus any protons already in solution. More generally,

$$ANC = \sum [\text{strong bases}] + \sum [\text{weak bases}] - \sum [\text{strong acids}] \tag{8.25}$$

Similarly, the ***base neutralizing capacity*** for the solution of ammonia/ammonium is

$$BNC = [H^+] + [NH_4^+] - [OH^-], \tag{8.26}$$

or

$$BNC = \sum [\text{strong acids}] + \sum [\text{weak acids}] - \sum [\text{strong bases}]. \tag{8.27}$$

Note that these equations are nothing more than another rearrangement of the charge balance, proton balance, or *TOT*H equation. Nonetheless, these concepts are useful in analyzing polyprotic systems, especially the carbonate system, as we shall see in Part 2 of this chapter.

PART 2. THE ACID-BASE CHEMISTRY OF NATURAL AND ENGINEERED WATERS

8.5   The carbonate system

8.5.1 Introduction

Earth's waters are dominated by the carbonate weak acid/base system. For example, there are approximately 7×10^{14} moles of living organic carbon in the oceans, but more than 3×10^{18} moles of dissolved carbonate species in the ocean. As we saw in Figure 7.1, the three dissolved carbonate species are $H_2CO_3^*$, HCO_3^-, and CO_3^{2-}, and total dissolved carbonate is given by $C_T = [H_2CO_3^*] + [HCO_3^-] + [CO_3^{2-}]$. Because concentrations of $CO_{2(aq)}$ and H_2CO_3 (the latter, true carbonic acid, is merely the product of the hydration reaction of $H_2O + CO_{2(aq)}$) cannot be determined individually via titration, we lump them together as $H_2CO_3^*$:

$$CO_2 + H_2O \rightleftharpoons H_2CO_3, K_{hyd} = 2.2 \times 10^{-3} \tag{8.28}$$

$$H_2CO_3 \rightleftharpoons H^+ + HCO_3^-, K_0 = 2.0 \times 10^{-4} \tag{8.29}$$

$$[CO_{2(aq)}] + [H_2CO_3] = [H_2CO_3^*] \tag{8.30}$$
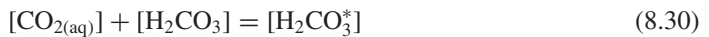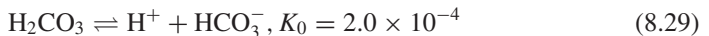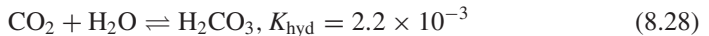
From the above relationships we can see that K_{a1}, the first acid dissociation constant for $H_2CO_3^*$ really is a composite constant involving both K_{hyd}, the equilibrium constant for hydration of $CO_{2(aq)}$, and K_0, the acid dissociation constant for true carbonic acid (H_2CO_3):

$$K_{a1} = \frac{[H^+][HCO_3^-]}{[H_2CO_3^*]} = \frac{[H^+][HCO_3^-]}{[CO_2] + [H_2CO_3]} = \frac{[H^+][HCO_3^-]/[H_2CO_3]}{[CO_2]/[H_2CO_3] + 1}$$

$$= \frac{K_0}{K_{hyd}^{-1} + 1} = \frac{2 \times 10^{-4}}{454 + 1} = 4.4 \times 10^{-7} = 10^{-6.35} \tag{8.31}$$

The relevant equilibrium constants thus are

$$H_2CO_3^* \rightarrow H^+ + HCO_3^-;\ K_{a1} = \frac{[H^+][HCO_3^-]}{[H_2CO_3^*]} = 10^{-6.35}, \qquad (8.32)$$

and

$$HCO_3^- \rightarrow H^+ + CO_3^{2-},\ K_{a2} = \frac{[H^+][CO_3^{2-}]}{[HCO_3^-]} = 10^{-10.33}. \qquad (8.33)$$
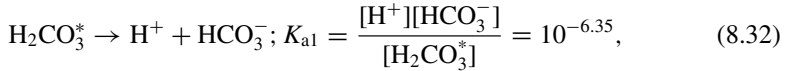
Table 8.6 lists values of the equilibrium constants for the carbonate system at temperatures relevant to natural waters. Examining these species, we see that $H_2CO_3^*$ can neutralize two units of base, and HCO_3^- can neutralize one unit of base. Thus, following Eq. 8.26, the BNC of a carbonate solution is

$$BNC = [Acy] = 2[H_2CO_3^*] + [HCO_3^-] + [H^+] - [OH^-]. \qquad (8.34)$$

This is often called the total acidity, written as [Acy], of the solution.

8.5.2 Alkalinity

Similar to the relationship between BNC and acidity, the acid neutralizing capacity for the carbonate system usually is called the ***alkalinity*** [Alk]:

$$ANC = [Alk] = [HCO_3^-] + 2[CO_3^{2-}] + [OH^-] - [H^+] \qquad (8.35)$$

As discussed below, Eq. 8.35 is an incomplete definition of the total alkalinity of natural waters and is more properly referred to as the ***total carbonate alkalinity***.

Table 8.6 Equilibrium constants for the carbonate system[*]

Temperature °C	log K_H	log K_{a1}	log K_{a2}
0	−1.108	−6.579	−10.629
5	−1.192	−6.516	−10.554
10	−1.269	−6.463	−10.488
15	−1.341	−6.419	−10.428
20	−1.407	−6.382	−10.376
25	−1.468	−6.352	−10.329
30	−1.524	−6.328	−10.288
35	−1.577	−6.310	−10.252
40	−1.625	−6.297	−10.222
50	−1.711	−6.286	−10.174

[*] Values computed from the "best-fit" equations of Plummer et al.[1]:

$\log K_H = 108.3865 + 0.01985076T - 6919.53/T - 40.4154^* \log T + 669365/T^2$

$\log K_{a1} = -356.3094 - 0.06091964T + 21834.37/T + 126.8339^* \log T - 1684915/T^2$

$\log K_{a2} = -107.8871 - 0.03252849T + 5151.79/T + 38.92561^* \log T - 563713.9/T^2$

Also note that

$$[Alk] + [Acy] = 2C_T. \tag{8.36}$$

In a real sense, the alkalinity equation (or the acidity equation) is merely a charge or proton balance. Thus, it can be used as one of the equations when solving carbonate system problems.

Actually, three different definitions of alkalinity are in common use in water chemistry:

(1) **Analytical definition:**   Alkalinity is the sum of titratable bases with strong acid to defined endpoints based on the carbonate system. This definition gives rise to the alternative term for alkalinity: *acid neutralizing capacity* or *ANC*.

(2) **Chemical definition:**

$$ANC = [HCO_3^-] + 2[CO_3^{2-}] + [OH^-] + \sum[B^-] - [H^+], \tag{8.37}$$

where B^- represents any other titratable base. In natural waters, these include borate, which is important in sea water, phosphate, silicate, and humic substances (i.e., the anionic forms of humic and fulvic acids).

(3) **Geochemical or charge-balance definition:**

$$ANC = \sum[BC] - \sum[SA], \tag{8.38}$$

where BC are base cations (principally Na^+, K^+, Ca^{2+}, Mg^{2+}), and SA are strong acid anions (principally Cl^-, SO_4^{2-}).

Of course, the three definitions define essentially the same property of water, but each emphasizes a different aspect of alkalinity, respectively: (1) the way we measure alkalinity; (2) the chemical species that comprise it; and (3) the fact that alkalinity in natural waters arises from an "imbalance" between the biogeochemical processes giving rise to strong base cations and strong acid anions.

As described in the first definition, alkalinity is a *capacity* term: the sum of titratable bases to two endpoints defined in reference to the carbonate system: (1) pH 8.3, where all carbonate has been titrated to bicarbonate and essentially all hydroxide alkalinity, if any was present in the sample, has been converted to water; and (2) pH 4.5–5.1, where all bicarbonate has been titrated to $H_2CO_3^*$. The second endpoint is defined by a pH range because the pH of the equivalence point depends on the concentration of $H_2CO_3^*$ present at that point. In turn, this depends on the initial alkalinity, as well as the extent to which the sample is stirred to release CO_2 to the atmosphere. If operational factors like the degree of stirring are constant, samples with high alkalinity will have high concentrations of $H_2CO_3^*$ at the equivalence point, and the higher $[H_2CO_3^*]$ is, the

lower the pH will be. *Standard Methods*[2] gives the following endpoint pH values for different alkalinities:

Total alkalinity mg/L as $CaCO_3$	meq/L	Endpoint pH
30	0.6	4.9
150	3.0	4.6
500	10.0	4.3

Figure 8.4 shows an idealized titration of the carbonate system for a solution initially containing 1×10^{-3} M Na_2CO_3 and illustrates some important conditions for measuring alkalinity. The quantity of acid required to reach the first endpoint, called V_1, determines the **carbonate alkalinity** of a sample. This quantity sometimes is called the "phenolphthalein alkalinity," in reference to the color indicator commonly used to detect the endpoint. The total quantity of acid required to reach the second end point, called V_2, gives the **total alkalinity** of a sample, and the difference between V_1 and V_2 gives the **bicarbonate alkalinity**. The color indicator usually used to determine V_2 is a mixture of bromcresol green and methyl red (color change from green to pink to red), but V_2 also is determined by (1) plotting the titration curve (as in Figure 8.4) and determining the inflection point, (2) titrating to a fixed pH (see values tabulated above), or (3) Gran plots (see Section 8.5.3). The **total alkalinity** thus is the sum of the carbonate and bicarbonate alkalinity. Waters with pH < 8.3 have no titratable carbonate alkalinity. In these cases, which are very common, the bicarbonate alkalinity is equal to the total alkalinity. It is important to note that the inflection points marking the two endpoints (especially that for the second one) in the carbonate titration are much less sharp than the inflection point for strong acids and bases shown in Figure 8.1. As the carbonate
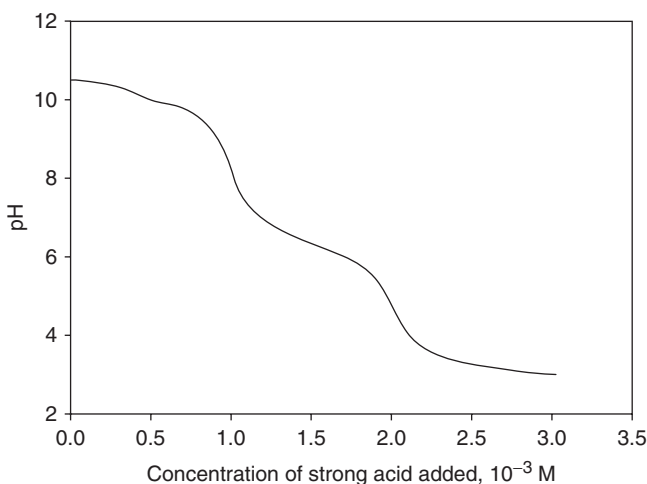
Figure 8.4 Titration of 1×10^{-3} M Na_2CO_3 with strong acid. V_1 occurs at the first inflection point, and V_2 at the second.

concentration decreases, the endpoint sharpness continues to decrease, and it becomes increasingly difficult to measure endpoints accurately in waters with lower and lower alkalinity.

EXAMPLE 8.4 Calculation of alkalinity and related carbonate species from titration data: A 100-mL water sample with an initial pH of 7.20 required 8.4 mL of 0.0205 N HCl to reach the total alkalinity endpoint (V_2). Compute the total alkalinity and determine the equilibrium concentrations of carbonate species.

Answer:

$$\text{Total alkalinity} = 8.4 \text{ mL} \times 0.0205 \text{ meq/mL} \times 1000 \text{ mL/L} \div 100 \text{ mL}$$

$$= \textbf{1.722 meq/L},$$

or

$$1.722 \text{ meq/L} \times 50 \text{ mg CaCO}_3/\text{meq} = \textbf{86.1 mg/L as CaCO}_3.$$

Because the initial pH is < 8.3, there is no carbonate (or phenolphthalein) alkalinity, and all of the total alkalinity is bicarbonate. Thus, $[\textbf{HCO}_3^-] = \textbf{1.722} \times \textbf{10}^{-3} \textbf{ M}$ (or $10^{-2.76}$ M). We can compute $[H_2CO_3^*]$ and $[CO_3^{2-}]$ from the given pH, computed $[HCO_3^-]$, and appropriate acid dissociation constant. Because we do not know the ionic strength of the water, we will ignore activity corrections and use the thermodynamic values for K_{a1} and K_{a2} from Table 8.6. Assume the analyses were done at room temperature (20°C). Then $K_{a1} = 10^{-6.38}$ and $K_{a2} = 10^{10.38}$:

$$[H_2CO_3^*] = [H^+][HCO_3^-]/K_{a1} = 10^{-7.35} \times 10^{-2.76} \div 10^{-6.38} = 10^{-3.73}\text{M or } [\textbf{H}_2\textbf{CO}_3^*]$$

$$= \textbf{1.86} \times \textbf{10}^{-4} \textbf{ M},$$

and

$$[CO_3^{2-}] = K_{a2}[HCO_3^-]/[H^+] = 10^{-10.38} \times 10^{-2.76} \div 10^{-7.35} = 10^{-5.79}\text{M or } [\textbf{CO}_3^{2-}]$$

$$= \textbf{1.62} \times \textbf{10}^{-6} \textbf{ M}.$$

EXAMPLE 8.5: Determine the alkalinity of solution containing 2×10^{-3} M NaHCO$_3$, 3×10^{-3} M Ca(OH)$_2$, 1×10^{-3} M KOH, 1×10^{-3} M H$_2$SO$_4$, and 6×10^{-3} M HCl.

Answer: Note that with the exception of carbonate, the other species added are strong acids or strong bases. While one could solve this as a titration problem, we will take a different approach. Writing out the charge balance,

(1) $[Na^+] + 2[Ca^{2+}] + [K^+] + [H^+] = [HCO_3^-] + 2[CO_3^{2-}] + [OH^-]$
    $+2[SO_4^{2-}] + [Cl^-]$.

The sodium, calcium, potassium, sulfate, and chloride concentrations are known, so rearrange to

(2) $[Na^+] + 2[Ca^{2+}] + [K^+] - 2[SO_4^{2-}] - [Cl^-] = [HCO_3^-] + 2[CO_3^{2-}]$
$+ [OH^-] - [H^+]$.

The right-hand side is [Alk], and thus

(3) $[Alk] = [Na^+] + 2[Ca^{2+}] + [K^+] - 2[SO_4^{2-}] - [Cl^-] = 2 \times 10^{-3}$
$+ 2(3 \times 10^{-3}) + 1 \times 10^{-3} - 2(1 \times 10^{-3}) - 6 \times 10^{-3} = 1 \times 10^{-3} M$.

Using the equations described in Sections 8.5.1–2, the pH of this solution can also be calculated.

Concentrations of the other weak bases listed under the second definition usually are low compared with the carbonate species, and for practical purposes total alkalinity in most natural waters, especially those with moderate levels of hardness and alkalinity, can be considered a measure of the concentrations of the carbonate species (Eq. 8.35). Nonetheless, alkalinity is an "operationally defined" procedure, and caution should be observed in interpreting alkalinity data in terms of concentrations of chemical species.

EXAMPLE 8.6 Contributions of phosphate to alkalinity: "back of the envelope" estimates: Assume the water in Example 8.4 was wastewater sample with a total phosphorus (TP) concentration of 6.2 mg/L (0.2 mM). How important is the contribution of phosphate to the sample's alkalinity?

Answer: If half of the TP were present as orthophosphate, then half of the orthophosphate will be present as HPO_4^{2-} and half as $H_2PO_4^-$ (because the pH of the sample is equal to pK_{a2} for phosphoric acid). The HPO_4^{2-} contributes to alkalinity because it is titrated to $H_2PO_4^-$ within the pH range of the alkalinity titration, but the $H_2PO_4^-$ does not contribute because it is not titrated to H_3PO_4 until the pH is approximately < 3 ($pK_{a1} = 2.15$). The concentration of titratable P then is $0.5 \times 0.5 \times 0.2$ mM $= 0.05$ meq/L, which is 2.9% of the 1.722 meq/L of total alkalinity.

Next, assume the water in Example 8.4 is a eutrophic lake with a pH of 8.7 and that TP $= 62$ μg/L. How important is the contribution of phosphate to the sample's alkalinity?

Answer: As indicated above, TP concentrations are much lower in lakes than in wastewater. Even in eutrophic lakes, a TP concentration of 2 μM is considered high, and usually only a small fraction of TP is present as dissolved orthophosphate. As an extreme case, we will consider all the TP to be orthophosphate and assume that all of it is present as HPO_4^{2-} (which is close to correct, given the high pH). Even then, the contribution of phosphate to the alkalinity would be 0.002/1.722 or only $\sim 0.1\%$ of the total.

It is important to note that dissolved CO_2 (or $H_2CO_3^*$) is not a component in any of the definitions of alkalinity. Therefore, except for the following circumstances, addition or removal of CO_2 has no effect on total alkalinity. This statement is valid as long as CO_2 addition or removal does not form or dissolve solid-phase $CaCO_3$. If suspended

particles of $CaCO_3$ are present in a water sample, CO_2 addition may solubilize them by the reaction $CaCO_{3(s)} + CO_2 + H_2O \rightarrow Ca^{2+} + 2HCO_3^-$, thus increasing alkalinity. Conversely, stripping dissolved CO_2 from a water sample may raise its pH enough to exceed K_{s0} for $CaCO_3$, and its precipitation will decrease the alkalinity. Addition or removal of CO_2 may affect the form of alkalinity, however. If a sample has carbonate alkalinity, adding CO_2 decreases this form and increases the bicarbonate: $CO_2 + CO_3^{2-} + H_2O \rightarrow 2HCO_3^-$ (for no net change in total alkalinity).

8.5.3 Gran titrations

As noted above, difficulties are encountered in measuring endpoints of alkalinity titrations when the starting alkalinity and pH are low, as occurs in acid-sensitive lakes in noncalcareous watersheds. Consider a water sample with an alkalinity of 20 μeq/L. Its pH likely would be < 6.0, and under the standard conditions[2] for performing alkalinity titrations (i.e., 100 mL samples titrated with ~0.020 N sulfuric acid), only 0.1 mL of titrant would be required to reach the equivalence point. No sharp inflection point would be found in such situations, and the pH would just decrease gradually. A useful procedure to determine alkalinity in such cases involves ***Gran titrations***, named after the Swedish chemist who developed them.[3] Gran titrations have two advantages: (1) they do not require measurements close to the equivalence point, and (2) they linearize the titration curve, allowing determination of the equivalence point by extrapolating a fitted straight line to the x-axis of the Gran plot. The theoretical basis for Gran titrations of alkalinity is as follows.

Alkalinity is defined as a "capacity" term by Eq. 8.35, and the way it relates to the carbonate system is illustrated in Figure 8.5a. Other capacities are defined similarly in the figure. For example, hydrogen ion acidity, $[H^+\text{-Acy}]$, is defined as

$$[H^+ - Acy] = [H^+] - [HCO_3^-] - 2[CO_3^{2-}] - [OH^-]. \qquad (8.39)$$

This term defines the quantity of strong base needed to raise the pH of a solution to the equivalence point of the carbonate titration—that is, where all the carbonate has been converted to $H_2CO_3^*$. If the pH of the solution is greater than the point where this occurs (roughly a pH of 5), the water has no H^+-Acy (more precisely, it does not have a positive H^+-Acy).

At any point in the alkalinity titration curve, the following equality exists:

$$(V_{sample} + V)[H^+ - Acy] = (V - V_2)C_{acid}, \qquad (8.40)$$

where V is the volume of strong acid titrant added; V_2 is the second equivalence point in titration of carbonate (where all carbonate has been titrated to $H_2CO_3^*$); C_{acid} is the normality of the titrant; and V_{sample} is the volume of the sample whose alkalinity is being titrated. Note that $[H^+\text{-Acy}]$ is negative when $V < V_2$ and positive when $V > V_2$, i.e., after the equivalence point has been reached.

Beyond V_2, Eq. 8.40 can be simplified:

$$(V_{sample} + V)[H^+] = (V - V_2)C_{acid} \qquad (8.41)$$
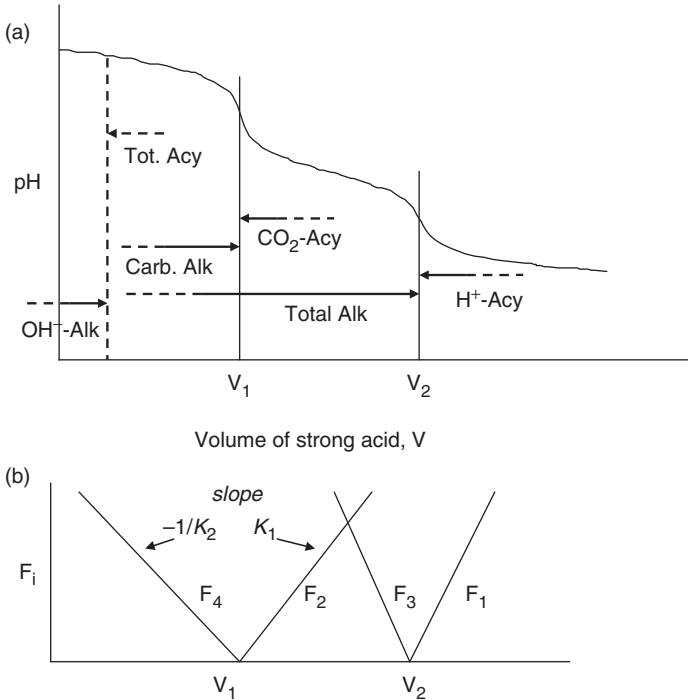
Figure 8.5 (a) Sketch of an alkalinity titration showing how various capacity terms are defined. (b) Gran plot of titration curve (a). Redrawn and modified from Stumm and Morgan.[4]

If we replace $[H^+]$ with the roughly equivalent term, 10^{-pH}, Eq. 8.41 becomes

$$F_1 = (V_{sample} + V)10^{-pH} = (V - V_2)C_{acid}. \qquad (8.42)$$

F_1, called the first Gran function, $= 0$ when $V = V_2$. This means that a plot of F_1 versus V is a straight line for $V \gg V_2$ and crosses the x-axis at $V = V_2$, and extrapolation of the straight-line F_1 function to the x-axis thus yields the amount of acid (V_2) required to titrate the sample to the alkalinity endpoint (see Figure 8.5b). Three other Gran functions (F_2, F_3, and F_4) can be derived (Figure 8.5b).[4] Extrapolation of the F_2 line to the x-axis gives V_1, that is, the first endpoint in the carbonate titration, where all CO_3^{2-} has been converted to HCO_3^-. This endpoint occurs only if the initial pH is > 8.3. Consequently, F_2 is of little practical use in Gran titrations of alkalinity in natural waters because the procedure almost always is used for low-alkalinity waters with initial pH < 7.0. Functions F_3 and F_4 respectively provide redundant estimates of V_2 and V_1. Because they are rarely used, we will not derive them here.

Several cautions must be observed in performing Gran titrations to ensure accurate results. First, data points near the equivalence point should not be included in the regression to obtain F_1 because they violate a basic assumption of the Gran procedure that the sample pH is controlled solely by the amount of strong acid added after the
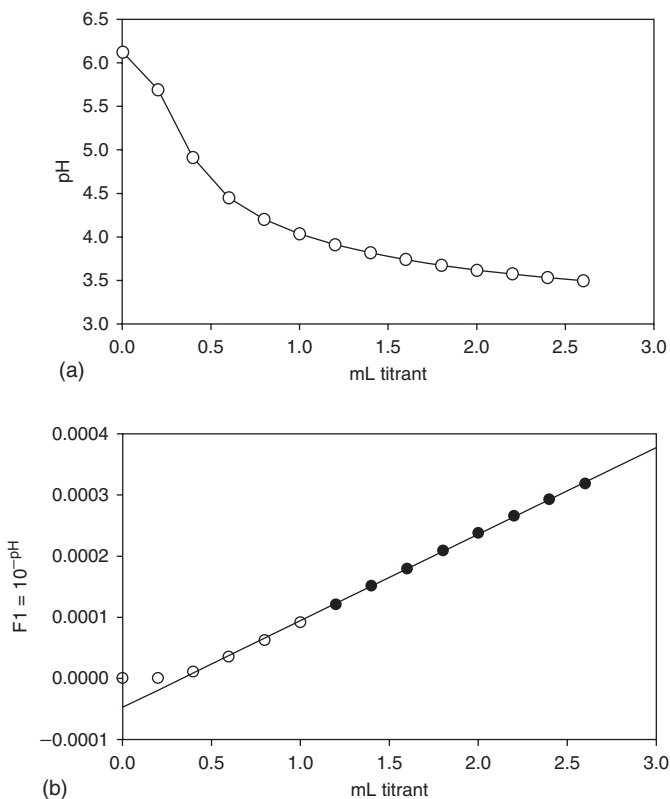
Figure 8.6 Conventional alkalinity titration plot for a typical acid-sensitive lake; (b) Gran plot of same data showing linearity of Gran function F_1 and precision with which the equivalence point (V_2) can be determined. V_2 occurs at the intersection of the regression line for F_1 with the x-axis (where $F_1 = 0$), in this case, $V_2 = 0.33$ mL, and from the titrant normality (0.0212 N), we calculate that the 100 mL sample had an alkalinity of 70 μeq/L. (Unpublished data of the author [P.L.B.] for an unnamed lake in northern Minnesota.)

equivalence point; near the equivalence point, dissociation of $H_2CO_3^*$ is sufficient to cause curvature in the F_1 line. Second, a quantity of NaCl is added to the samples before the titration to maintain a constant ionic strength (thereby allowing a constant [H^+] with 10^{-pH}). If too much acid titrant is added, the ionic strength increases, activity coefficients change, and the relationship between [H^+] and 10^{-pH} is no longer constant. Together, these two issues lead to the recommendation that titration data used to calculate F_1 should be limited to the pH range of 4.00–3.50. Figure 8.6 compares a plot of a conventional alkalinity titration with a Gran plot for a low-alkalinity lake in northern Minnesota. The indistinct inflection point in the conventional plot and the advantage of the Gran plot in estimating the sample's alkalinity are readily apparent.

8.5.4 Closed-system carbonate problems

We begin with closed systems, or systems that are isolated from the atmosphere. These systems are generally not realistic, but they may be applicable to laboratory situations. The advantage of a closed system is that C_T is fixed. To solve a closed system problem, the available equations are those for K_{a1}, K_{a2}, K_w, C_T, and [Alk]. Recall from Section 7.2.5 that

$$[H_2CO_3^*] = \alpha_0 C_T, \tag{8.43}$$

$$[HCO_3^-] = \alpha_1 C_T, \tag{8.44}$$

$$[CO_3^{2-}] = \alpha_2 C_T. \tag{8.45}$$

Thus, we can rewrite the alkalinity equation as follows:

$$[Alk] = \alpha_1 C_T + 2\alpha_2 C_T + K_w/[H^+] - [H^+] \tag{8.46}$$

$$[Alk] = \left(\frac{K_{a1}[H^+] + 2K_{a1}K_{a2}}{[H^+]^2 + [H^+]K_{a1} + K_{a1}K_{a2}} \right) C_T + \frac{K_w}{[H^+]} - [H^+] \tag{8.47}$$

In closed-system problems, three variables are generally sought: C_T, [Alk], and [H$^+$]. If any two are specified, the third one can be calculated. As an example, we consider solutions for three closed systems of pure water to which we add 1×10^{-3} mol/L of one of the three main carbonate forms.

EXAMPLE 8.7: Determine the pH and carbonate speciation in three sealed beakers, each containing 1-L of pure water to which is added 1×10^{-3} moles of one of the following: (1) $H_2CO_3^*$, (2) $NaHCO_3$, or (3) Na_2CO_3.

Answer: First list the relevant chemical species:

OH$^-$, H$^+$, $H_2CO_3^*$, HCO_3^-, CO_3^{2-}, and Na$^+$ (present only in cases 2 and 3)
Equilibrium constants: K_w, K_{a1}, K_{a2}
Mass balances: $C_T = [H_2CO_3^*] + [HCO_3^-] + [CO_3^{2-}] = 1 \times 10^{-3}$ for all three cases

Case 1: [Na$^+$] = 0
Case 2: [Na$^+$] = 1×10^{-3} M = C_T
Case 3: [Na$^+$] = 2×10^{-3} M = $2C_T$

Charge balance: [Na$^+$] + [H$^+$] = $[HCO_3^-]$ + $2[CO_3^{2-}]$ + [OH$^-$]

Rearranging the charge balance yields

(1) [Na$^+$] = [Alk] = $[HCO_3^-]$ + $2[CO_3^{2-}]$ + [OH$^-$] − [H$^+$].

Substituting the equilibrium expressions solved for the various species in terms of [H$^+$] into Eq. (1) yields

$$(2) \quad [Na^+] = \left(\frac{K_{a1}[H^+] + 2K_{a1}K_{a2}}{[H^+]^2 + [H^+]K_{a1} + K_{a1}K_{a2}} \right) C_T + \frac{K_w}{[H^+]} - [H^+]$$

Table 8.7 Equilibrium solutions for the three carbonate problems in Example 8.7

Species added	1×10^{-3} M $H_2CO_3^*$	1×10^{-3} M $NaHCO_3$	1×10^{-3} M Na_2CO_3
Knowns			
C_T	1×10^{-3}	1×10^{-3}	1×10^{-3}
$[Na^+] = [Alk]$	0	1×10^{-3}	2×10^{-3}
Calculated			
$[H^+]$ (pH)	2.09×10^{-5} (4.68)	5.08×10^{-9} (8.29)	2.77×10^{-11} (10.56)
$[OH^-]$	4.83×10^{-10}	1.98×10^{-6}	3.63×10^{-4}
$[H_2CO_3^*]$	9.79×10^{-4}	1.12×10^{-5}	2.26×10^{-8}
$[HCO_3^-]$	2.09×10^{-5}	9.79×10^{-4}	3.63×10^{-4}
$[CO_3^{2-}]$	4.69×10^{-11}	9.04×10^{-6}	6.14×10^{-4}

This can be solved by trial an error for each case, substituting values of $[H^+]$ until the right-hand side equals $[Na^+]$. Once the proton concentration is known, concentrations of OH^- and the carbonate species are determined using the equilibrium constants and C_T values. The results are summarized in Table 8.7.

These problems also can be solved easily (and much more quickly) with MINEQL+ using the following instructions. Select Na^+ and CO_3^{2-} as components (Na^+ actually is not needed for the $H_2CO_3^*$ problem) and enter the sodium concentration in the calculation wizard. In the pH tab, select "pH is calculated by MINEQL+ " and enter the appropriate value of $TOTH$ (2E-3 for $H_2CO_3^*$, 1E-3 for HCO_3^-, and 0 for CO_3^{2-}). In the CO_2 tab, select a closed system and enter the total carbonate concentration. In the RunTime Manager, check the button to calculate ionic strength, insert a name for the output file, and click run. One of the options for displaying the output for 10^{-3} M $NaHCO_3$ is shown in Table 8.8.

8.5.5 Open-system carbonate problems

For open systems, the equations used for closed systems are still valid. Because the system is now open (and assumed to be in equilibrium with the atmosphere), C_T is no longer constant. However, two additional equations are now available. The first is Henry's law:

$$K_H = \frac{[H_2CO_3^*]}{P_{CO_2}} \tag{8.48}$$

The second is an equation for [Alk] expressed in terms of the partial pressure of carbon dioxide. This equation can be derived by solving K_1 and K_2 for $[HCO_3^-]$ and $[CO_3^{2-}]$ and substituting Eq. 8.48 solved in terms of $[H_2CO_3^*]$ into the equations:

$$[HCO_3^-] = K_{a1} \frac{[H_2CO_3^*]}{[H^+]} = \frac{K_{a1} K_H P_{CO_2}}{[H^+]}, \tag{8.49}$$

and

$$[CO_3^{2-}] = K_{a2} \frac{[HCO_3^-]}{[H^+]} = \frac{K_{a1} K_{a2} K_H P_{CO_2}}{[H^+]^2}. \tag{8.50}$$

Table 8.8 MINEQL+ output for single run for 1×10^{-3} M NaHCO$_3$

```
Data Extracted from: NAHCO3.MDO
Run: 1
ID Species Conc. Log C Log K
Type I - COMPONENTS
2 H2O 1.000E+00 0.000 0.000
3 H(+) 5.080E-09 -8.294 0.000
23 CO3(2-) 9.040E-06 -5.044 0.000
45 Na(+) 9.990E-04 -3.000 0.000
Type II - COMPLEXES
3800 OH- (-1) 1.980E-06 -5.703 -14.000
31700 H2CO3 (aq) 1.120E-05 -4.951 16.680
31800 HCO3- (-1) 9.790E-04 -3.009 10.330
32200 NaHCO3 (aq) 5.500E-07 -6.260 10.080
95400 NaCO3- (-1) 1.680E-07 -6.774 1.270
Type III - FIXED ENTITIES
3801 H2O (Solution) 0.000
Type V - DISSOLVED SOLIDS
205900 THERMONATRITE -11.682 -0.640
206000 NATRON -9.734 1.310
Type VI - SPECIES NOT CONSIDERED
175310 pH (+1) 5.080E-02 -1.294 7.000
175300 CO2 (g) 1.030E+00 0.015 21.650
Other Species
900003 Activity of H+ 5.080E-09 -8.294 0.000
```

Substituting into the alkalinity expression gives

$$[\text{Alk}] = \frac{K_{a1}K_{H}P_{CO_2}}{[\text{H}^+]} + \frac{2K_{a1}K_{a2}K_{H}P_{CO_2}}{[\text{H}^+]^2} + \frac{K_w}{[\text{H}^+]} - [\text{H}^+]. \tag{8.51}$$

For open systems, if any two of the four variables [Alk], P_{CO_2}, [H$^+$], and C_T are specified, the other two can be calculated.

EXAMPLE 8.8: Consider the three beakers in Example 8.7 and open them to the atmosphere. Determine the final pH, C_T, and carbonate speciation at equilibrium.

Answer: Once the systems are opened, CO_2 in the atmosphere will equilibrate with the solutions. If we assume P_{CO_2} is $10^{-3.5}$ atm, this means that $[\text{H}_2\text{CO}_3^*] = 1 \times 10^{-5}$ M (Eq. 8.48). We now know one of the four parameters needed to solve the problem. Clearly, we do not know C_T (it changes) or pH, which also must change as CO_2 dissolves or is released. The key to solving the problem is to realize that *alkalinity is constant*. Only CO_2 (i.e., $H_2CO_3^*$) is entering or leaving the system, and because this is a neutral species, the charge balance (i.e., the alkalinity equation) is unaffected. Even though the $H_2CO_3^*$ may dissociate, this creates one unit of positive charge (H$^+$) for each unit of negative charge (HCO$_3^-$), and so [Alk] is unaffected. Thus, we know P_{CO_2} and [Alk], and for each system, [H$^+$] is determined using Eq. 8.51. All the terms on the right-hand side are known except for [H$^+$]. An iterative solution is necessary, choosing different

Table 8.9 Equilibrium solutions for the three open beakers in Example 8.8

Species added	1×10^{-3} M $H_2CO_3^*$	1×10^{-3} M NaHCO$_3$	1×10^{-3} M Na$_2$CO$_3$
Knowns			
$[H_2CO_3^*]$	1.08×10^{-5}	1.08×10^{-5}	1.08×10^{-5}
$[Na^+] = [Alk]$	0	1×10^{-3}	2×10^{-3}
Calculated			
$[H^+]$ (pH)	2.2×10^{-6} (5.66)	4.91×10^{-9} (8.31)	2.51×10^{-9} (8.60)
$[OH^-]$	4.59×10^{-9}	2.05×10^{-6}	4.02×10^{-6}
C_T	1.3×10^{-5}	9.98×10^{-4}	1.97×10^{-3}
$[HCO_3^-]$	2.19×10^{-6}	9.78×10^{-4}	1.92×10^{-3}
$[CO_3^{2-}]$	4.68×10^{-11}	9.33×10^{-6}	3.59×10^{-5}

values of $[H^+]$ until the right-hand side = [Alk]. This is best done with a spreadsheet. The concentrations of HCO_3^-, CO_3^{2-}, and C_T then can be calculated, as summarized in Table 8.9.

Solution by MINEQL+ is simple and fast, but there are some important differences in setting up the problems compared with those in Example 8.7 (closed systems). For all three problems, choose an open system in the CO_2 tab and set log P to −3.5. This will prevent you from specifying a total concentration of component CO_3^{2-}, which will be calculated by the program. For all three problems, leave *TOT*H = 0, and check the box to calculate pH by electroneutrality. For the NaHCO$_3$ case, add Na$^+$ at 1×10^{-3} M and for the Na$_2$CO$_3$ case, add Na$^+$ at 2×10^{-3} M. Specifying the pH calculation by electroneutrality will ensure that the program continues to add CO_2 from the atmospheric reservoir until the solution is electrically neutral (i.e., until HCO_3^- and CO_3^{2-} are high enough to balance all the Na$^+$). It is interesting to observe that almost 99% of the initial $H_2CO_3^*$ in the first beaker is lost to the atmosphere. A very small amount (∼0.2%) is lost to the atmosphere in the NaHCO$_3$ beaker. In contrast, the Na$_2$CO$_3$ beaker nearly doubles its C_T, as CO_2 from the atmosphere effectively titrates most (∼96%) of the CO_3^{2-} to HCO_3^-.

8.5.6 The phase rule

In a closed carbonate system, there are three parameters that describe the system: C_T, [Alk], and $[H^+]$. Knowing (or specifying) any two of the three values allows one to calculate the third. Thus, one cannot arbitrarily set all three. In an open carbonate system, there are four parameters that describe the system: C_T, [Alk], P_{CO_2} and $[H^+]$. In this case, one can specify any two of the four variables and then calculate the other two. One cannot, however, arbitrarily set three or four of the values.

This is an appropriate place to discuss an assumption that has been made throughout the text to this point. It is the ***phase rule*** (formally known as Gibbs phase rule, after its developer, J. Willard Gibbs; see Box 3.4). The phase rule has two parts:

(1) the number of species with fixed activities (e.g., solids, gases at fixed pressure) must be less than the number of components in the chemical system at fixed T and P, and
(2) species with fixed activities must be independent.

Mathematically, this is expressed as

$$F = c + 2 - p, \tag{8.52}$$

where F is number of degrees of freedom (i.e., the number of variables for which arbitrary values can be chosen; two of which will be temperature and pressure of the system), c is the number of components that must be brought together to make the system, and p is the number of phases present (where phases are regions of uniform composition).

The simplest example is a system containing only liquid water. In this case, the chemical potential of the water is a function of the temperature and pressure of the system:

$$\mu_{H_2O} = f(T, P) \tag{8.53}$$

Using the phase rule we have: $F = 1 + 2 - 1 = 2$, meaning we can arbitrarily set T and P. If both liquid water and water vapor are present, their chemical potentials must be equal (i.e., they are in equilibrium). With two phases (liquid and gas) present, $F = 1 + 2 - 2 = 1$, and we can only set T or P, but not both. Finally, if water is present in three forms (solid, liquid, and gas), $F = 1 + 2 - 3 = 0$, and there is only one combination of T and P— i.e., no degrees of freedom—where all three phases can exist (T $= 0.01°C$; $P = 6 \times 10^{-3}$ atm; i.e., the triple point of water).

Returning to the carbonate system, we can consider the closed system first. Here, p $= 1$ (aqueous solution) and c $= 3$. That is, we need three components to make up any possible one-phase carbonate-water system: (1) $H_2O_{(l)}$, (2) H^+, and (3) one of the carbonate components (let's say CO_3^{2-}). There are, of course, other components in the system (OH^-, $H_2CO_3^*$, HCO_3^-), but these can be determined (and "constructed") from the concentrations of H^+ and CO_3^{2-}. The system thus is defined by three components (think of MINEQL+ components, which are H_2O, H^+, and CO_3^{2-} for this system). In this case, $F = 3 + 2 - 1 = 4$, meaning we can specify T, P, and concentrations of two of the three possibilities (C_T, [Alk], [H^+]).

For the open system, p $= 2$ (aqueous solution, gas phase), and c $= 4$ ($H_2O_{(l)}$, H^+, $CO_{2(g)}$, and CO_3^-), and $F = 4 + 2 - 2 = 4$. If T and total P are again specified, only two of the four variables C_T, [Alk], P_{CO_2} and [H^+] can be set arbitrarily. If one violates the phase rule, a system is said to be overspecified.

8.5.7 Deffeyes diagrams

Graphs with variables having conservative properties (like C_T, alkalinity, and acidity) as coordinates can be used to show contours of "nonconservative" variables like pH, [$H_2CO_3^*$], and [HCO_3^-]. Addition or removal of components of the carbonate system on such graphs behave as vectors (as long as solubility constraints are not violated), and they can be used for rapid solution of some carbonate system problems. Deffeyes[5] derived several graphs of this type. Here we describe the most common of his diagrams—a plot of [Alk] versus C_T (Figure 8.7). Ignoring other bases that may contribute to alkalinity
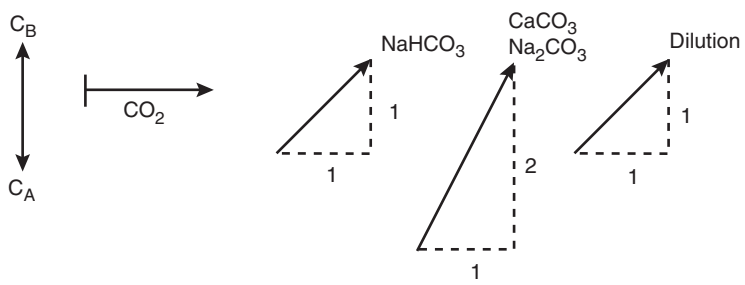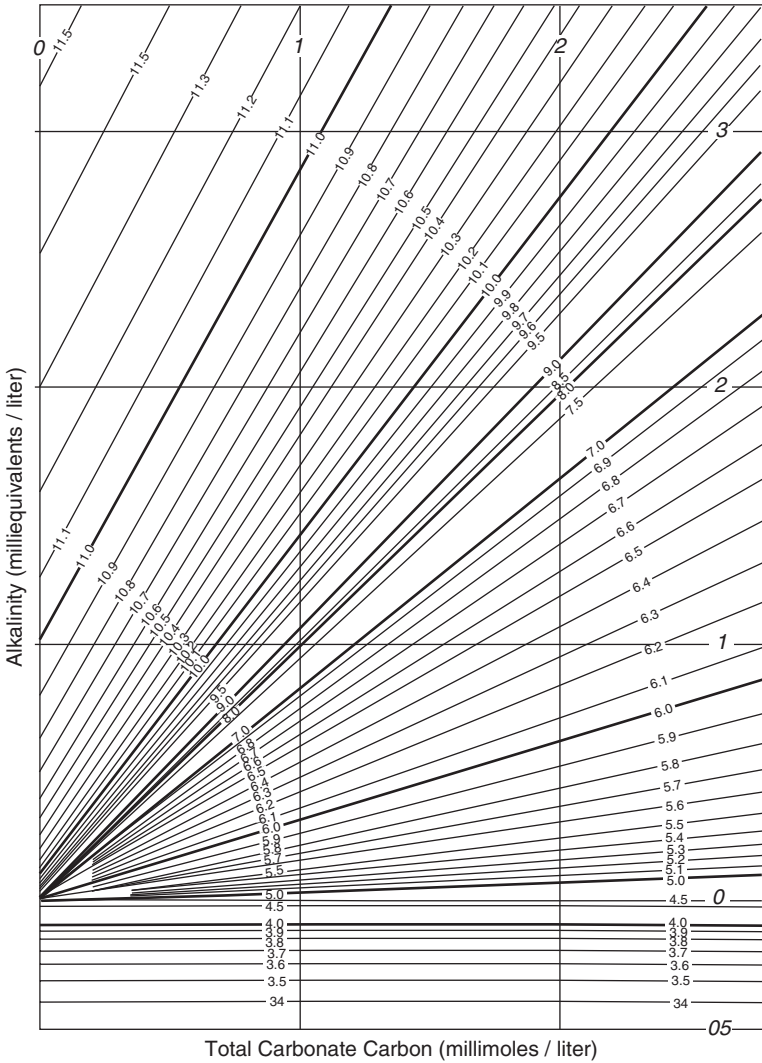
Figure 8.7 pH isolines on a plot of alkalinity versus C_T. Sketches below graph show that the solution composition changes as a vector when the illustrated constituents are added or removed. Modified from Deffeyes[5] and used with permission of the American Society of Limnology and Oceanography.

and restricting our analysis to the carbonate system, we recall that Eq. 8.35 defines [Alk] as

$$[Alk] = [HCO_3^-] + 2[CO_3^{2-}] + [OH^-] - [H^+]. \qquad (8.35)$$

Also, as shown by Eq. 8.46, we can substitute the appropriate α and equilibrium expressions for the first three terms on the right-hand side and obtain an equation expressing [Alk] in terms of pH and C_T:

$$[Alk] = (\alpha_1 + 2\alpha_2)C_T + K_w/[H^+] - [H^+] \qquad (8.46)$$

Equation 8.46 tells us that at a given pH, [Alk] is a linear function of C_T. At any pH, the system thus is completely defined by specifying either [Alk] or C_T. Alternatively, we can state that for each set of [Alk] and C_T values, pH is defined. Using this information, Deffeyes developed a plot of [Alk] versus C_T with a series of isolines for pH spanning the pH range of interest in natural waters (Figure 8.7). On this plot the point defining solution composition moves as a vector when various acid-base and carbonate forms are added or removed. For example, addition of strong base increases [Alk] but does not affect C_T, and addition of strong acid decreases [Alk] but does not affect C_T. Therefore, these additions are defined by vertical vectors. In contrast, addition or removal of CO_2 (e.g., by respiration and photosynthesis) affects C_T but does not affect [Alk], and the line describing this is a horizontal vector. Addition or removal of $NaHCO_3$ affects [Alk] and C_T equally, and the vector for this process has a slope of $+1$. Finally, dissolution of calcite ($CaCO_{3(s)}$) adds two equivalents of alkalinity for every mole of CO_3^{2-} that dissolves.

EXAMPLE 8.9 Use of the Deffeyes diagram to solve problems involving the mixing of waters containing different concentrations of Alk and C_T: Consider two waters with the following compositions: (A) pH = 6.5, [Alk] = 1.0 meq/L; (B) pH = 7.0, [Alk] = 1.8 meq/L. What will the pH be if equal volumes of A and B are mixed together, assuming no CO_2 is lost to or gained from the atmosphere?

Answer: From Figure 8.7, we find C_T = 1.8 mM for A and 2.2 mM for B. The mixture thus has the following composition: [Alk] = (1.0 + 1.8)/2 = 1.4 meq/L; C_T = (1.8 + 2.2)/2 = 2.0 mM. From Figure 8.7 we find **pH = 6.75** for these values of [Alk] and C_T.

8.5.8 Air-water transfer of CO_2

The partial pressure of CO_2 in the atmosphere currently is $\sim 10^{-3.4}$ atm.[*] Partitioning of CO_2 into water must be taken into account in many problems involving the

---

[*]Several water chemistry textbooks[4,6] (including this one) have used a value of $10^{-3.5}$ atm for atmospheric CO_2, but the global average CO_2 in 2009 was estimated to be ~ 387 ppm, which translates to $10^{-3.41}$ atm: and increases the solubility of $H_2CO_3^*$ at 25°C from 1.07×10^{-5} M to 1.32×10^{-5} M. The value is increasing by $\sim 2\%$ per year. When monitoring of atmospheric CO_2 began in 1958 at Mauna Loa, Hawaii (site of the longest record and considered representative of the global average value), the concentration was ~ 315 ppm (or $10^{-3.50}$ atm).

carbonate system. As described in Chapter 1, gas partition reactions may be written in two ways:

$$CO_{2(g)} \rightleftharpoons H_2CO_3^* \quad K_H = \frac{[H_2CO_3^*]}{P_{CO_2}} = 10^{-1.47} \qquad (8.54a)$$

or

$$H_2CO_3^* \rightleftharpoons CO_{2(g)} \quad H = \frac{P_{CO_2}}{[H_2CO_3^*]} = 29.51 \qquad (8.54b)$$
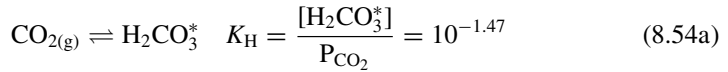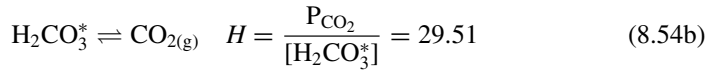
Both Eq. 8.54a and 8.54b are forms for **Henry's Law**. Either is suitable for solving problems, but Eq. 8.54a is used more commonly when dealing with fixed gases like CO_2 and makes calculation of $[H_2CO_3^*]$ more intuitive. Table 8.6 lists K_H values for CO_2 at temperatures of environmental interest.

As discussed in Box 8.1, concentrations of $H_2CO_3^*$ (or $CO_{2(aq)}$) in natural waters typically are not at equilibrium with atmospheric CO_2; freshwaters typically are supersaturated, and ocean waters are undersaturated. This nonequilibrium situation suggests that the kinetics of CO_2 transfer across the air-water interface is of interest. In general, rates of gas transfer across this interface (in either direction) depend on the difference between the actual concentration of the gas in water and its saturation value. Several theories are used to model gas transfer kinetics, including the classic two-film theory and more recent "surface renewal" modifications, which are more realistic. These theories are described in Chapter 12 and developed in depth elsewhere.[13,14] The theories divide gases into two broad categories: (1) unreactive gases, such as O_2 and N_2, for which exchange rates are is limited by transfer through a liquid surface film, and (2) reactive gases, such as NH_3 and SO_2, for which rates are limited by transfer through a surficial gas film. The question is, To which of these classes does CO_2, which we know to be chemically reactive, belong? The answer has varied over past decades, but CO_2 always has been regarded as less reactive (in terms of both rates and equilibria) than the reactive gases mentioned above. Studies in the 1970s indicated that CO_2 transfer rates could be modeled like rates for unreactive gases multiplied by a "chemical enhancement" factor.[13] More recent studies suggest that the chemical enhancement factor is not needed and that CO_2 transfer can be modeled like other unreactive gases, for which transfer rates depend primarily on the wind speed at the air-water surface and the Schmidt number of the gas, which depends on its molecular diffusion coefficient (see Section 12.3.2).

8.5.9 Factors affecting alkalinity and pH in natural waters

As described in Chapter 2, mineral weathering is the primary source of alkalinity in natural waters. Dissolution of carbonate minerals (limestone, dolomite) is important, but so is the incongruent dissolution of silicate minerals (see Table 8.10, reactions 6 and 7). Atmospheric acid deposition of sulfuric and nitric acids can be a significant sink for alkalinity in watersheds with low rates of mineral weathering (typically in regions with thin soils, exposed granitic rock, and no carbonate minerals). Aside from weathering/dissolution reactions and atmospheric inputs, many biochemical processes in water bodies and watersheds also affect pH and alkalinity. Photosynthetic production

Box 8.1 CO_2 disequilibrium in lakes and oceans

Surface waters usually are not in equilibrium with atmospheric CO_2. A widely cited study showed that 87% of lakes around the world were supersaturated with respect to atmospheric CO_2.[7] The likely cause is respiration processes that occur faster than rates of gas transfer, thus elevating CO_2 concentrations in lake waters above the equilibrium concentrations. The world's oceans, however, are undersaturated with respect to CO_2. Given that oceans cover so much of the Earth's surface, this makes oceans an important CO_2 sink, and oceans have been proposed to play an important role in limiting global climate change.

CO_2 emitted by fossil fuel combustion and cement production (estimated as 244×10^{15} g from 1800 to 1994)[8,9] is of primary concern because of its potential to change global climate, but it also is of concern because of potential impacts on the chemistry of the oceans. Recent estimates[8,9] indicate that up to 50% of the anthropogenic CO_2 emitted to the atmosphere has been absorbed by the oceans, which means that atmospheric CO_2 levels would be even higher if not for the oceanic sink. Extensive studies over the past few decades make it clear that humans have altered the global carbon cycle, and recent studies have shown alterations in oceanic chemistry, including a 0.1 decrease in the pH of oceanic surface waters.[10] Although that seems like a small change, the oceans surface layers are supersaturated with respect to $CaCO_3$, and even a small decrease in pH lowers the degree of supersaturation. This affects the ability of marine organisms to precipitate calcium carbonate needed to grow shells and corals.[11] As pH and alkalinity continue to decrease, there is even the potential for shells and corals to begin dissolving. This would have profound effects on oceanic ecosystems.

In 2004, Sabine et al.[9] estimated that anthropogenic CO_2 emissions had consumed about one-third of the ocean's long-term storage potential. However, more recent observations and simulations[12] have suggested that climate change (resulting in an alteration in ocean winds) already has weakened the capacity of the southern ocean to absorb CO_2.

of organic matter (Table 8.10, reaction 1a) and the reverse reaction, respiration, do not affect alkalinity directly, but they do affect pH by consuming and producing CO_2. If these pH changes cause $CaCO_3$ to precipitate or dissolve, then alkalinity is affected. Plant growth involves more than the production of organic carbon, however; proteins also must be formed, and depending on the inorganic source of nitrogen, this can cause either an increase (NO_3^-) or decrease (NH_4^+) in alkalinity.

Other nitrogen cycle reactions also affect pH and alkalinity. Nitrification (Table 8.10, reaction 2) converts the weak acid NH_4^+ ($pK_a = 9.25$) to the strong acid, HNO_3, thus decreasing pH and alkalinity. Denitrification consumes the strong acid, HNO_3, increasing pH and alkalinity. Sulfur cycle redox reactions behave similarly. Sulfide oxidation converts a weak acid, H_2S ($pK_{a1} = 7.0$) to a strong acid, H_2SO_4, and sulfate reduction has the opposite effect. Sulfate reduction in lake sediments is an important pH buffering mechanism in some low-ANC (acid-sensitive) lakes.[15] Because oxidized forms of elements are stronger acids than reduced forms, we can make the

Table 8.10 Biogeochemical processes affecting pH and alkalinity

Process	pH/alkalinity change for forward reaction
Photosynthesis and respiration	
(1a) $nCO_2 + nH_2O \rightarrow (CH_2O)_n + nO_2$	Increase in pH No change in alkalinity
(1b) $106CO_2 + 16NO_3^- + HPO_4^{2-} + 122H_2O + 18H^+$ $\rightarrow \{C_{106}H_{263}O_{110}N_{16}P\} + 138O_2$ "algae"	Increase
(1c) $106CO_2 + 16NH_4^+ + HPO_4^{2-} + 108H_2O$ $\rightarrow \{C_{106}H_{263}O_{110}N_{16}P\} + 107O_2 + 14H^+$	Decrease
Nitrification	
(2) $NH_4^+ + 2O_2 \rightarrow NO_3^- + H_2O + 2H^+$	Decrease
Denitrification	
(3) $5CH_2O + 4NO_3^- + 4H^+ \rightarrow 5CO_2 + 2N_2 + 7H_2O$	Increase
Sulfide and iron sulfide oxidation	
(4a) $HS^- + 2O_2 \rightarrow SO_4^{2-} + H^+$	Decrease
(4b) $FeS_{2(s)} + 3\frac{3}{4}O_2 + 3\frac{1}{2}H_2O \rightarrow Fe(OH)_{3(s)} + 4H^+ + 2SO_4^{2-}$	Decrease
Sulfate reduction	
(5) $2CH_2O + SO_4^{2-} + H^+ \rightarrow 2CO_2 + HS^- + H_2O$	Increase
CaCO₃ dissolution/precipitation	
(6) $CaCO_3 + CO_2 + H_2O \rightarrow Ca^{2+} + 2HCO_3^-$	Increase
*Aluminosilicate mineral weathering**	
(7) $2NaAlSi_3O_{8(s)} + 2CO_2 + 11H_2O$ $\rightarrow Al_2Si_2O_5(OH)_{4(s)} + 2Na^+ + 2HCO_3^- + 4Si(OH)_4$ albite kaolinite	Increase

* There are many aluminosilicate minerals, and they weather to form base cations, bicarbonate, dissolved silica, and a variety of clay mineral products (see chapter 15). The reaction shown is a typical example.

generalization that oxidative biogeochemical processes, such as nitrification, sulfide oxidation, and iron oxidation, consume alkalinity by producing strong acid. Conversely, reductive biogeochemical processes, such as nitrate assimilation, denitrification, and sulfate reduction, produce alkalinity by consuming a strong acid or producing a weak acid from a strong one.

8.6 Acid-base systems in natural waters; ranges and controls on pH

The carbonate system is by far the most important acid-base system in natural waters, controlling pH conditions in the oceans, most inland surface waters and nearly all ground waters. Most waters where the carbonate system is dominant are circumneutral to slightly alkaline in pH, and a pH range of 6–9 often is considered to represent "normal conditions." In fact, ambient water quality standards in most states require the pH to be maintained within this range unless it can be shown that natural processes cause a water body to have a pH outside this range. The pH of surface waters in the oceans generally

falls within a narrow range of $\sim$8.1–8.3. Hardwater lakes have a broader pH range, but values of 8–9 are common. High primary production rates that remove $H_2CO_3^*$ from the water may lead to higher values (range of 9–10), especially during daylight hours in summer. Somewhat lower pH values are found in ground water, even in limestone aquifers, where pH values commonly are in the range of 7–8 (see Table 2.3). Softwater systems generally have still lower pH values; a range of 6–7 or even lower is common. This reflects a relatively greater importance of acidic $H_2CO_3^*$ and lower importance of alkaline CO_3^{2-} in the carbonate distribution of such systems. A further buildup of $CO_{2(aq)}$ from microbial respiration during ice cover can lead to seasonal pH depressions as low as 5.2–5.3, as was found in Little Rock Lake, Wisconsin (Table 2.3).[16] It is interesting to note that the maximum buffering in the CO_2-bicarbonate system occurs at pH $\sim$6.3 (i.e., around pK_{a1} for carbonic acid), but pH values in most carbonate-dominated natural waters do not fall close to this value. Indeed, the pH of seawater and calcareous freshwaters typically is poised closer to the pH where the carbonate system has its minimum buffering capacity (pH 8.3), which is halfway between pK_{a1} and pK_{a2} and represents the equivalence point in the acid titration of CO_3^{2-} to HCO_3^- (and also the equivalence point in the base titration of $H_2CO_3^*$ to HCO_3^-).

Many other acid-base systems occur in aquatic environments, and they do exert at least some influence on pH. Inorganic examples mentioned earlier in this chapter include ammonium/ammonia, phosphate species, boric acid/borate, silica, ferric iron, and in anoxic environments hydrogen sulfide. In many situations these other acid-base systems are too low in concentration compared with the carbonate system to play an effective role in regulating the pH of a water body (see Example 8.6 for phosphate), but exceptions do occur. For example, atmospheric deposition of sulfuric and nitric acid into softwater systems effectively titrates their naturally low levels of alkalinity and decreases the pH, even if day-to-day control of pH and acid-base conditions is still maintained by the carbonate system. If natural processes (e.g., mineral weathering) that produce alkalinity are sufficiently low and atmospheric acid deposition is sufficiently high, the acid neutralizing capacity (ANC) of the system may be overwhelmed, leading to zero or negative alkalinity values and pH of 4–5, or even lower. The control of pH in such acidified waters is exerted by a mixture of mineral acid inputs and biogeochemical processes (see Table 8.10) that generate alkalinity and increase pH. Substantial and costly efforts to control SO_2 emissions in the United States, Canada, and Europe over the past 20 years have made major strides to lessen the occurrence of lake and stream acidification in these countries (although it has not been eliminated), but the problem remains a serious concern in other parts of the world, such as China.

Hydrolysis of ferric iron controls the pH in waters draining from some mines or natural mountain streams where seams of iron sulfide or iron pyrite deposits become exposed to atmospheric oxygen. Most of the acid produced by the oxidative dissolution of FeS and FeS_2 actually is derived from the hydrolysis of Fe^{3+} to $Fe(OH)_{3(s)}$; indeed, three of the four H^+ shown as products of reaction 4b in Table 8.10 are from Fe^{3+} hydrolysis, and only one comes from sulfide (or pyrite) oxidation. Values of pH as low as 1–3 may result from these processes. Such "acid mine drainage" streams are common in parts of the Appalachian Mountains in the eastern United States, as well as in the Colorado Rockies. The biotic diversity of such streams is very restricted—limited mostly to acidophilic iron- and sulfide-oxidizing bacteria. As Box 8.2 describes, these streams do not represent the lowest pH values found in natural aquatic systems, however.

Box 8.2   How low (or high) can it go? Extreme values of pH

Americans, it seems, are especially intrigued by superlatives—the highest this, biggest that, oldest, smallest, fastest—you name it, having an "-est" on lends a certain cachet and piques our interest. So, what is the lowest pH found in the environment? We have been aware for many years of volcanic lakes with pH near 1. Hutchinson[17] described a volcanic lake, Katanuma, in Japan with a pH of 1.7 as having the lowest measured pH and also mentioned Awoe, a crater lake in Indonesia, as having a strong acid content of 0.8–1.3 N, which would imply a pH of 0 or less. Nonetheless, these do not represent the lowest pH values measured in the natural environment. Several pH measurements in the range 0 to −1 were cited by Nordstrom et al.[18] for hot springs and acid crater lakes, but the record for surface waters belongs to some hot springs near the Ebeko Volcano in Russia, where high concentrations of sulfuric and hydrochloric acid lead to pH values as low as −1.7!

However, even that is not the most acidic water ever measured. That "honor" belongs to underground drippings of water in Richmond Mine near Redding, California, where measured pH values of −3.6 were found.[18] Calibration of the pH meter to achieve such low readings required special efforts using the Pitzer ion association theory (see section 4.4.4) because conventional pH buffers do not apply to the high ionic strength and H^+ concentrations encountered. Activity coefficients calculated by the Pitzer theory for H^+ at sulfuric acid concentrations found in the mine samples were much larger than unity, as the following summary from Nordstrom et al.[18] indicates:

H_2SO_4 molality	pH	γ_{H+}
0.146	0.86	0.76
1.497	−0.38	1.28
2.918	−1.07	3.23
4.485	−1.78	11.2
7.622	−3.13	165.4
9.850	−4.09	1200

Less information is available on extreme values at the other end of the pH spectrum. Hutchinson[17] credited a closed alkaline lake in Kenya, with a pH of 12, as having the highest pH, and Hem[19] reported that some spring waters associated with serpentine deposits (a metamorphic magnesium iron silicate) in the western United States also had pH values of 12.

Concentrations of organic (fatty) acids can be sufficient to influence the pH of wastewater, particularly in anaerobic treatment processes. In natural surface waters, humic substances—humic and fulvic acids—are the most important organic acid-base species. Under some conditions—e.g., in wetland bogs and streams draining forested wetlands of noncalcareous regions—they play a dominant role in the acid-base chemistry

of water bodies and may lead to pH values as low as ~3.[17] It should be noted, however, that high concentrations of humic substances in water do not necessarily mean the pH will be acidic. Many examples of highly colored lakes and streams can be found with circumneutral pH values and moderate or even high concentrations of carbonate alkalinity. These cases reflect a complicated provenance for the water itself and its acid-base components.

8.7   Kinetics of acid-base reactions

8.7.1 Rates of acid dissociation and recombination

Acid dissociation is a very rapid elementary reaction, and it is reasonable to assume that equilibrium conditions always apply to acid-base reactions in natural waters. However, rate constants for dissociation actually are proportional to the strength of an acid. This derives from the law of microscopic reversibility, from which we obtain the relationship, $K_a = k_d/k_r$, where k_d is the rate constant for dissociation and k_r is the rate constant for acid recombination. Because acid recombination reactions are very rapid (diffusion-limited; $k_r \approx 4 \times 10^9 M^{-1} s^{-1}$)[13] and independent of the nature of the conjugate base A^-, we can rewrite the above relationship as $k_d = \alpha K_a$, where the coefficient $\alpha = k_r$. This is simple example of a linear free energy relationship, and from it we can estimate values of k_d for some common acids: ~$10^{4.8} s^{-1}$ for acetic acid ($pK_a = 4.78$), ~$10^{2.6} s^{-1}$ for H_2S ($pK_{a1} = 7.02$), and ~$2.2 s^{-1}$ for NH_4^+ ($pK_a = 9.25$).

8.7.2 Kinetics of carbonate system reactions

The rates of carbonate system reactions are of interest because they are so important in the acid-base chemistry of natural waters. Using the above approach, we predict that the dissociation of HCO_3^- ($pK_{a2} = 10.33$ at 25°C) is fairly slow: $k_d \approx 0.2 s^{-1}$. The value of k_d for H_2CO_3 cannot be obtained this way, however, because pK_{a1} is a composite equilibrium constant based on the hydration of aqueous CO_2 and dissociation of carbonic acid, H_2CO_3: $K_{a1} = K_0/(1 + K_{hyd}^{-1})$, where K_0 is the dissociation constant of true carbonic acid (see Eqs. 8.27–8.30). From the value for K_0 (2×10^{-4}) we conclude that the dissociation rate of true carbonic acid is very fast ($k_d = 8 \times 10^5 s^{-1}$). As we saw earlier, however, $CO_{2(aq)}$ is the dominant form in $H_2CO_3^*$, and its hydration to H_2CO_3 is relatively slow (pseudo-first-order rate constant $k_{hyd} = 0.037 s^{-1}$ at 25°C; see Example 5.5). The hydration of CO_2 actually is the sum of two reactions:[20]

$$CO_2 + H_2O \rightarrow H_2CO_3, k_i \tag{8.55a}$$

$$CO_2 + H_2O \rightarrow H^+ + HCO_3^-, k_{ii} \tag{8.55b}$$
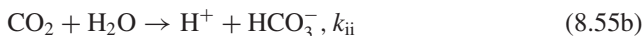
Because H_2CO_3 and HCO_3^- are in rapid equilibrium with each other, the reactions cannot be separated, and $k_{hyd} = k_i + k_{ii}$. Similarly, dehydration is the sum of the reverse reactions for Eqs. 8.55a and 8.55b, and its rate constant, $k_{dehyd} = k_{-i}/K_0 + k_{-ii}$, where k_{-i} and k_{-ii} are rate constants for the reverse reactions of Eqs. 8.55a and 8.55b. At 25°C, $k_{dehyd} = 7.6 \times 10^4 M^{-1} s^{-1}$.[7] At pH > 8, the direct reaction of $CO_{2(aq)}$ with OH^- to produce HCO_3^- is competitive ($k_{OH} = 7.1 \times 10^3 M^{-1} s^{-1}$ at 25°C) with the

two-step path of hydration to H_2CO_3 followed by dissociation. The reverse reaction ($HCO_3^- \rightarrow CO_2 + OH^-$) has a rate constant of 1.8×10^{-4} s^{-1} at 25°C.[20]

The kinetics of $CO_{2(aq)}$ hydration is rapid on the timescale at which we make observations of natural water bodies, and consequently, it still is valid to assume that equilibrium conditions always apply among the dissolved components of the carbonate system ($CO_{2(aq)}$, H_2CO_3, HCO_3^-, and CO_3^{2-}) in bulk solution. Nonetheless, the hydration kinetics of $CO_{2(aq)}$ is slow enough that it can be demonstrated easily in the laboratory,[21] and the rate of hydration may be rate limiting at the scale of CO_2 transfer/uptake at cell membranes.[13] Consequently, it has been proposed that the reaction might limit primary production in some natural waters. The hydration reaction is catalyzed by bases, and the enzyme carbonic anhydrase is an efficient catalyst in organisms. The enzyme once was hypothesized to play a role in CO_2 dynamics in surface waters, but no direct evidence has been found.[22]

Problems

8.1. Compute the pH of the following solutions. In each case ignore the effects of ionic strength and assume that $a_i = c_i$.

(a) 1×10^{-3} M HNO_3
(b) 1×10^{-4} M KOH
(c) 5×10^{-8} M HCl (careful; this is not as easy as it looks!)

8.2. Correct the results in problem 1 for the effects of ionic strength and compare the results to your answers for that problem.

8.3. Compute the pH of the following solutions using the thermodynamic values of K_a given in Table 8.1 corrected to ^cK_a values:

(a) 1×10^{-3} M benzoic acid, 0.1 M NaCl
(b) 1×10^{-4} M sodium formate, 0.05 M $MgCl_2$
(c) 1×10^{-4} M hydrogen sulfide, 0.025 M Na_2SO_4

8.4. What is the pH of the following solutions?

(a) 100 mL of 1×10^{-3} M acetic acid mixed with 50 mL of 4×10^{-3} M sodium acetate
(b) 120 mg of Na_2HPO_4 and 100 mg of NaH_2PO_4 dissolved in 1 L of deionized water
(c) 100 mL of a 1×10^{-3} M solution of sodium hypochlorite (NaOCl) to which 25 mL of 2×10^{-3} M HCl is added

8.5. A 100 mL sample of a lake water is titrated with standardized sulfuric acid solution at 0.01035 N, and 7.45 mL were required to reach the bromcresol green-methyl red endpoint. What is the alkalinity of the lake water. Express your results in meq/L and mg/L as $CaCO_3$.

8.6. Using MINEQL+ or an alternative computer equilibrium program perform titrations of sodium carbonate solutions at starting concentrations of 1.0×10^{-3} M and 1.0×10^{-4} M. Export the data to a spreadsheet and plot the results.

Discuss them in terms of the ability to detect the endpoint. Make sure that you have at least six data points beyond the second equivalence point (V_2) in the titration.

8.7. Using MINEQL+ or an alternative computer equilibrium program titrate a 1×10^{-5} M solution of $NaHCO_3$. Make sure you add enough acid to reach a pH < 3.50. (This is not quite as simple as it may seem; you need to balance the desire to have some data points before the equivalence point with the need to have the titrating acid strong enough to reach pH < 3.5.) Note that the starting solution is not Na_2CO_3 but $NaHCO_3$; how do you obtain that? Plot the results as a conventional titration and comment on whether you could determine the endpoint of the titration accurately. Also plot the data points from near V_2 and beyond (e.g., those $\leq$ pH 5.0) separately as a Gran plot using a spreadsheet or graphics program to do this. Determine the equivalence point of the titration from the Gran plot and express the alkalinity in μeq/L and mg/L as $CaCO_3$. Comment on the usefulness of the Gran method for low-alkalinity samples.

8.8. Plot the following laboratory data in conventional and Gran plots and estimate the ANC for this low-alkalinity Minnesota Lake. The sample volume was 100 mL, and the titrant concentration was 0.0208 M. You may wish to put the data into a spreadsheet and use its graphing capabilities.

mL	pH	mL	pH
0.10	6.12	1.30	3.935
0.20	5.99	1.50	3.792
0.30	5.89	1.70	3.744
0.40	5.69	1.90	3.703
0.50	4.85	2.10	3.623
0.70	4.39	2.30	3.596
0.90	4.21	2.50	3.532
1.10	4.024	2.70	3.514

8.9. The pK_a values for citric acid are 3.13, 4.72, and 6.33. From these you can compute values of α_0, α_1, α_2, and α_3 as a function of pH. This would be tedious to do manually, but MINEQL+ and similar equilibrium programs can make short work of it for you. Use the MultiRun option in MINEQL+ to obtain the data for a plot of the percent distribution of the four species (H_3Cit, H_2Cit^-, $HCit^{2-}$, and Cit^{3-}) versus pH. This essentially is a plot of the α values $\times$ 100. Also plot the conventional pC-pH diagram for citric acid at $Cit_T = 1 \times 10^{-1}$ M. Rather than plotting the species over the entire pH range, use the range pH 1–9, and specify enough increments to clearly define the lines (calculation increments of 0.25 pH units should be sufficient), which are not linear for most of the species within much of this range. Because MINEQL+'s graphing capabilities provide limited flexibility for sizing data points and making a visually attractive and easy-to-read

graph, you may wish to export your results to a spreadsheet/graphics program to produce your diagrams. Provide a one-paragraph summary of the graph.

8.10. According to Benjamin,[6] chromic acid, H_2CrO_4, dimerizes to dichromate, $Cr_2O_7^{2-}$, when added to water, with an equilibrium constant of $\log K = 1.54$ for the reaction

$$2HCrO_4^{2-} \rightleftharpoons Cr_2O_7^{2-} + H_2O; \qquad K = 10^{1.54}.$$
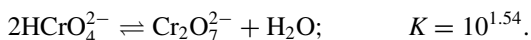
(a) Verify that this value is used in MINEQL+ by computing the equilibrium composition for 0.2 M H_2CrO_4 and using the results to compute K.

(b) Find the equilibrium pH of a 0.2 M solution of Na_2CrO_4 solution and a 0.2 M solution of $NaHCrO_4$ and compare the values to the pH of a 0.2 M solution of H_2CrO_4. Note: you may ignore ionic strength corrections in solving these problems.

8.11. You have flask in your laboratory on which the label is smudged. From what you are able to read, it is a solution of a monoprotic acid (we'll call it HX) at a concentration of 2×10^{-3} M in a 0.05 M NaCl solution. You measure the pH of the solution and get a reading of 3.09. Using this information, do the following:

(a) Determine the pK_a of the acid and the identity of X^- using the information in Table 8.2. Recall that a pH meter measures activity, not concentration of protons.

(b) Determine the pH of a 4×10^{-3} M NaX solution in 0.05 M NaCl.

8.12. (Courtesy of Dan Giammar). You need to prepare 1 L of solution containing the weak acid 2-(n-morpholino)ethanesulfonic acid (MES) at pH 6.0 and a concentration of 0.001 M. The acid has a pK_a of 6.15. You have available the following: pure water, 0.1 M MES made from the fully protonated solid form (write as HMES), a 0.1 M solution of the sodium form of the conjugate base of MES (write as NaMES), and 1 M NaOH.

(a) Develop a recipe to prepare the desired 1 L of solution and show your calculations to demonstrate that it will have the correct concentration and pH.

(b) Without doing any calculations, suggest an alternative recipe to the one that you described in (a), and briefly explain why you know that it will also provide the correct solution.

8.13. The famous explorer and archeologist Illinois Smith also is an expert water chemist. He particularly enjoys mixing waters from exotic locales and determining the resulting changes in water chemistry. He has water samples from Egypt and India. Conducting some quick measurements, he finds the following:

Source	Egypt	India
pH	7.3	8.0
[Alk] eq/L	1.3×10^{-3}	2.6×10^{-3}

If he takes two parts of the Egyptian water and mixes it with one part of the Indian water, what are the resulting values of [Alk] and C_T? Assume a closed system.

8.14. (Courtesy of Dan Giammar). A discharge of acid-mine drainage (AMD) with a flow of 10 ft^3 s^{-1} (cfs) flows into a small stream with a flow-rate upstream of the AMD discharge of 90 cfs. It has the following characteristics:

Acid-mine Drainage: pH $= 3.0$; $C_T = 0$

Stream upstream of discharge: pH $= 8.1$; $C_T = 2 \times 10^{-3}$ M; Alk $= 1.98 \times 10^{-3}$ eq/L

   (a) Calculate the alkalinity of the AMD discharge. Note: it is possible to have negative alkalinity values. Assume that the AMD discharge and stream are closed systems (no exchange with the atmosphere).
   (b) What are the C_T and alkalinity downstream of the discharge point? Assume the discharge is completely mixed in with the stream and that the stream remains a closed system.
   (c) Show an equation that would use the results of part (b) to solve for the pH. You do not actually need to solve for the pH. The pH for this system will be 7.49.
   (d) If the downstream portion of the stream does equilibrate with the atmosphere, will the pH, C_T, and alkalinity increase, decrease, or stay the same?

8.15. (a) Using a spreadsheet program, develop a titration curve for a system containing 10^{-2} M total cyanide ($[CN]_T = 1 \times 10^{-2}$ M). At what pH is the buffer intensity strongest and what is its value?
   (b) Develop a titration curve for the same system using MINEQL+. Assume that 10^{-2} M of NaCN and 10^{-2} M of NaOH was added to the system. We will use MINEQL+ to perform the titration calculation by adding HCl. See the hints below. Explain why hint (2) below is important to conducting the calculation. Print out a copy of your plot. Does it look the same as the one you generated?

Hints:

   (1) For species, select CN^-, Na^+, and Cl^-.
   (2) On the pH tab, select "pH is calculated by MINEQL+" and "Base pH Calculation on electroneutrality."
   (3) On the "Solids Mover" tab, click "All Off."
   (4) Under "MultiRun" select "total concentration of Cl^- as your variable. Justify the starting and ending values you choose.
   (5) To graph, select H^+ as the component, log C as the unit, and click the 1:H(+) box from the list on the right side of the screen.

8.16. EDTA (ethylenediaminetetraacetic acid) is a metal complexing agent often found in food and shampoos to prevent calcium or magnesium from precipitating.

(a) Use MINEQL+ or another computer equilibrium program to titrate a 1×10^{-2} M solution of H_4EDTA (do a base titration). Locate as many pK_a values and inflection points as possible. The pK_a values are 2.16, 3.12, 6.27, and 10.95.

(b) If your shampoo contains 2×10^{-4} M disodium ETDA (Na_2H_2EDTA), what is the pH of your shampoo? Use MINEQL+ to solve. Be sure to use the "Total H" box to add the appropriate number of protons.

8.17. (Courtesy of Dan Giammar). To mitigate CO_2 emissions to the atmosphere, some have suggested injecting CO_2 into deep groundwater. A groundwater initially at pH 8.3 with an alkalinity of 1×10^{-2} M will have CO_2 injected until the groundwater comes to equilibrium with $P_{CO_2} = 10$ bar. Before adding the CO_2, the groundwater behaves as a closed system.

(a) What is the total inorganic carbon (C_T) of the groundwater before CO_2 injection?

(b) What are the alkalinity, total inorganic carbon (C_T), and pH of the groundwater after equilibration with the injected P_{CO_2}?

8.18. You have discovered a subterranean lake deep in a cave that has very limited air exchange with the atmosphere. The partial pressure of CO_2 in the cave is 0.015 atm, and an analysis you perform with your new portable ion chromatograph gives the rather bizarre results listed below for the lake's chemical composition. You also measure the pH of the water and find that it is 6.8.

(a) Assuming the lake water is in equilibrium with the atmosphere in the cave, what are the C_T, [Alk], and [Acy] of the lake?

(b) Your ion chromatograph does not measure carbonate species and you do not have a carbonate analyzer with you. If you assume the water chemistry data are otherwise complete and accurate, what is the bicarbonate concentration in the water and does that value agree with the alkalinity value calculated in part (a)?

Ion	F^-	Cl^-	Br^-	SO_4^{2-}	NO_3^-	Ca^{2+}	Mg^{2+}	Na^+	K^+	Sr^{2+}
Conc. (mM)	0.1	0.3	0.15	0.5	0.2	1.0	2.0	0.75	0.5	0.25

References

1. Plummer, N. L., and E. Busenberg. 1982. The solubilities of calcite, aragonite, and vaterite in CO_2-H_2O solutions between 0 and 90°C, and an evaluation of the aqueous model for the system $CaCO_3$-CO_2-H_2O. *Geochim.Cosmochim. Acta* **46**: 1011–1140.

2. Eaton, A. D., L. S. Clesceri, E. W. Rice, and A. E. Greenberg (eds.). 2005. *Standard methods for the examination of water & wastewater*, 21st ed., Amer. Pub. Health Assoc., Amer. Water Works Assoc., Water Environ. Fed., Washington, D.C.

3. Gran, G. 1952. Determination of the equivalence point in potentiometric titrations. Part II. *Analyst* **77**: 661–671.

4. Stumm, W., and J. J. Morgan. 1996. *Aquatic chemistry*, 3rd ed., Wiley-Interscience, New York.

5. Deffeyes, K. S. 1965. Carbonate equilibria: a graphic and algebraic approach. *Limnol. Oceanogr.* **10**: 412–426.

6. Benjamin, M. M. 2002. *Water chemistry*, McGraw-Hill, New York.

7. Cole, J. J., N. F. Caraco, G. W. Kling, and T. K. Kratz, 1994. Carbon dioxide supersaturation in the surface waters of lakes. *Science* **265**: 1568–1570.

8. Takahashi, T. 2004. The fate of industrial carbon dioxide. *Science* **305**: 352–353.

9. Sabine, C. L., R. A. Feely, N. Gruber, R. M. Key, K. Lee, J. L. Bullister, R. Wanninkhof, C. S. Wong, D. W. R. Wallace, B. Tilbrook, F. J. Millero, T.-H. Peng, A. Kozyr, T. Ono, and A. F. Rios. 2004. The oceanic sink for anthropogenic CO_2. *Science* **305**: 367–371.

10. Interacademy Panel on International Issues. 2009. IAP Statement on Ocean Acidification (available at http://www.interacademies.net/Object.File/Master/9/075/Statement_RS1579_IAP_05.09final2.pdf).

11. Feely, R. A., C. L. Sabine, K. Lee, W. Berelson, J. Kleypas, V. J. Fabry, and F. J. Millero. 2004. Impact of anthropogenic CO_2 on the $CaCO_3$ system in the oceans. *Science* **305**: 362–366.

12. Le Quere, C., C. Roedenbeck, E. T. Buitenhuis, T. J. Conway, R. Langenfelds, A. Gomez, C. Labuschagne, M. Ramonet, T. Nakazawa, N. Metzl, N. Gillett, and M. Heimann. 2007. Saturation of the southern ocean CO_2 sink due to recent climate change. *Science* **316**: 1735–1738.

13. Brezonik, P. L. 1994. *Chemical kinetics and process dynamics in aquatic systems*, CRC Press, Boca Raton, FL.

14. Gulliver, J. S. 2007. *Introduction to chemical transport in the environment*, Cambridge University Press, New York.

15. Baker, L. A., and P. L. Brezonik. l988. Dynamic model of internal alkalinity generation: calibration and application to precipitation-dominated lakes. *Water Resources Res*. **24**: 65–74.

16. Kratz, T. K., R. B. Cook, C. J. Bowser, and P. L. Brezonik. 1987. Winter and spring in northern Wisconsin lakes caused by increases in PCO_2. *Canad. J. Fish. Aquat. Sci*. **44**: 1082–1088.

17. Hutchinson, G. E. 1957. *A treatise on limnology*, Vol. 1: *Geography, physics and chemistry*, J. Wiley & Sons, New York.

18. Nordstrom, D. K., C. N. Alpers, C. J. Ptacek, and D. W. Blowes. 2000. Negative pH and extremely acidic mine waters from Ion Mountain, California. *Environ. Sci. Technol.* **34**: 254–258.

19. Hem, J. D. 1985. Study and Interpretation of the Chemical Characteristics of Natural Water, 3rd ed., Wat. Suppl. Pap. 2254, U.S. Geol. Surv., Reston, VA (available at http://pubs.usgs.gov/wsp/wsp2254/.

20. Johnson, K. S. 1982. Carbon dioxide kinetics of hydration and dehydration in seawater. *Limnol. Oceanogr.* **27**: 849–855.

21. Jones, P., M. L. Haggett, and J. L. Longridge. 1964. The hydration of carbon dioxide: a double clock experiment. *J. Chem. Ed*. **41**: 610–612.

22. Goldman, J. C., and M. R. Dennett. 1983. Carbon dioxide exchange between air and seawater: no evidence for rate catalysis. *Science* **220**: 199–201.

9

Complexation Reactions and Metal Ion Speciation

Objectives and scope

In this chapter we deal with the second "associative" reaction type involved in ionic equilibria: complexation. After presenting definitions and basic concepts related to aqueous complexes, we describe ways to express equilibrium relationships of complexes and their components: metal ions (Lewis acids) and electronegative "ligands" (Lewis bases). The chemical and ecological significance of complexes in natural and engineered waters is summarized, along with the nature of the two major types of complexes—inner sphere and outer sphere. Factors that affect the binding strength of components that form complexes are described, with attention to useful predictive relationships. Methods to solve and display complexation equilibria are explained starting with examples simple enough to solve by manual (algebraic) techniques and then computer-based methods for the complicated situations found in many natural water problems. The roles of inorganic and organic ligands in metal ion speciation are described using examples ranging from dilute soft water to hard waters and high-ionic-strength seawater. The kinetics of complex formation and dissociation is treated next. Although most complex formation reactions are fast, complex dissociation can be observably slow for strong complexes. Some metal-ligand exchange processes are slow enough for nonequilibrium conditions to be maintained for months or even years.

Key terms and concepts

- Central metal ions; coordination number; coordination chemistry; coordinate covalent bonds
- Monodentate, bidentate, multidentate ligands

- Chelates and chelating agents
- Stepwise (K_i) and cumulative (β_i) stability (formation) constants and instability (dissociation) constants
- Inner-sphere and outer-sphere complexes
- Anation; hydrolysis; water exchange rates; labile and inert complexes
- Metal-ligand and ligand-ligand exchange; adjunctive and disjunctive mechanisms

9.1   Introduction

9.1.1 Review of fundamentals

In Chapter 1 we described complexes as ions or neutral molecules in solution that are comprised of components that are capable of existing independently in solution. All complexes consist of a ***central metal ion***, which acts as a Lewis acid (an electron acceptor), and one or more ***ligands***, which act as Lewis bases (electron donors). The central metal ion is characterized by its positive charge and its ***coordination number***, C_N, i.e., the number of ligands with which it is able to form bonds.

Ligands are quite diverse in character, but they all include an electronegative atom that has one or more pairs of electrons available to form bonds with metal ions. Types of ligands include simple monoatomic anions (e.g., Cl^-, Br^-), multiatomic inorganic ions (e.g., OH^-, CO_3^{2-}, CN^-), neutral molecules (e.g., NH_3), and organic bases and anions (e.g., amines and carboxylic acid anions). The most common ligand is water itself, which has oxygen as its electronegative ion. Metal ions do not in fact exist in solution as free species. They are surrounded by four to eight water ligands, and so it would be more appropriate to write $Zn(H_2O)_4^{2+}$ than Zn^{2+}, for example.

Ligands also are classified by the number of binding sites they contain. ***Monodentate ligands*** have one atom with a pair of electrons available to share with a metal ion; ***bidentate ligands*** have two sites; and ***multidentate ligands*** have an unspecified number greater than one. Ligands with two or more sites form ringed structures (Figure 9.1) with metal ions that are called ***chelates*** (after the Greek word for claw), and such multidentate ligands are called ***chelating agents***. In general, the binding strength of chelating agents increases with the number of binding sites on the agent because the agent is able to fill a greater number of bonding orbitals on a metal ion as the number of ligand atoms increases. From a thermodynamic perspective, this phenomenon is explained largely by entropic considerations. For example, consider Zn^{II}, which has a coordination number of 4, reacting with ammonia or tetradentate triethylenetetramine (trien) chelating agent, which contains four amine groups (Figure 9.1). The reactions can be written as

$$Zn(H_2O)_4^{2+} + 4NH_3 \rightleftharpoons Zn(NH_3)_4^{2+} + 4H_2O, \tag{9.1}$$

and

$$Zn(H_2O)_4^{2+} + trien \rightleftharpoons Zn\text{-}trien^{2+} + 4H_2O. \tag{9.2}$$
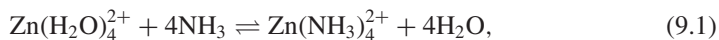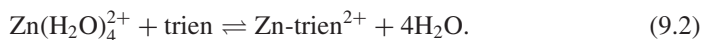
Reactions 9.1 and 9.2 illustrate the fact that complexation reactions actually are substitution reactions (ligands replace a water of hydration) rather than the addition reactions they appear to be when the waters of hydration are not written explicitly.
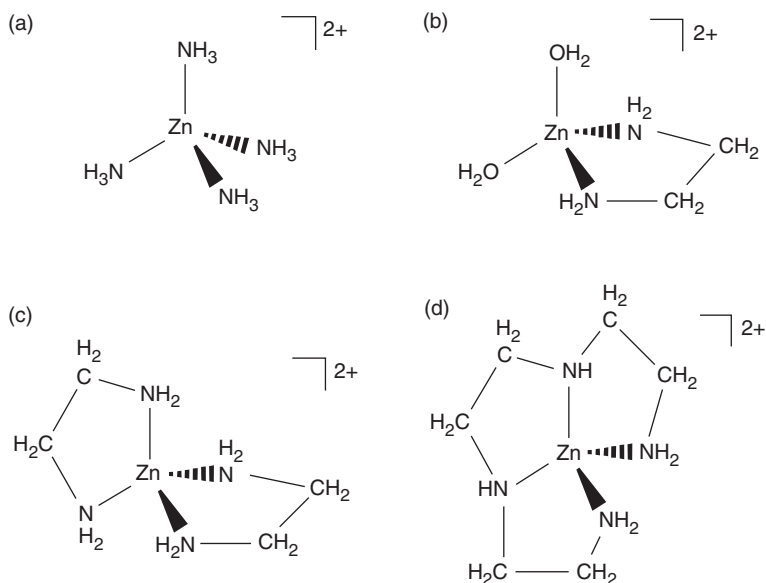
Figure 9.1 Structures of $Zn^{2+}(C_N = 4)$ with the simple monodentate ligand NH_3 (a) and with chelating agents: the bidentate ligand ethylenediamine (b and c) and the tetradentate ligand triethylenetetramine (d).

In reaction 9.1, the number of reactants and products is the same, but in reaction 9.2 there are two reactant species and five product species, when one includes the released waters from the aquated metal ion. The larger number of independent species on the product side of reaction 9.2 increases the randomness of the system and results in a large increase in entropy, as the following thermodynamic data show:[1]

Reaction	Ligand(s)	ΔG_r° (kJ mol^{-1})*	ΔH_r° (kJ mol^{-1})	ΔS_r° (J mol^{-1}K^{-1})
9.1	4 NH_3	−55.54	−61.5	−20.0
9.2	Trien	−66.88	−35.0	+107.0

Values for ΔG_r° were calculated from reported ΔH_r° and ΔS_r°[1] and do not agree exactly with values calculated from the equilibrium constants (given below), which are from the same source.[1]

In contrast, ΔS_r° for reaction 9.1 is slightly negative, probably because the product water molecules do not behave as completely independent species (recall the flickering cluster nature of liquid water; see Chapter 1). The decrease in ΔG_r° for reaction 9.2 compared with reaction 9.1 derives entirely from the large increase in entropy; note that ΔH_r° is actually more negative for the reaction with ammonia than for the reaction with trien. Overall, the equilibrium constant for complexation of Zn^{2+} by trien (reaction 9.2) is $10^{11.95}$, a factor of more than 400× larger than that for the Zn^{2+}-NH_3 reaction.

9.1.2 Chemical and ecological importance of complexation

The importance of complexation in aquatic chemistry is profound. First, complexation plays a major role in metal ion (and ligand) speciation in aquatic systems, and second, speciation affects chemical behavior in myriad ways. As a simple case in point, complexation of metal ions with anionic ligands affects net charge and may transform cations into anions. For example, the predominant forms of gold in seawater are anionic chloride complexes: $AuCl_2^-$ and $AuCl_4^-$ (for the two oxidation states of gold, Au^I and Au^{III}). Thus, if you have ambitions to develop a superselective ion-exchange material to concentrate gold from seawater, you had better think about an anion exchange material, not a cation exchange resin. The native abundance of gold in seawater[2] is very low— about 0.4 ng/L or $10^{-11.7}$ M, but given the huge volume of water in the world's oceans, that still means there is a lot of gold in the oceans!

Complexation affects metal ion reactivity in both thermochemical and photochemical reactions. Some metal ion complexes are less reactive than the free ions regarding oxidation, but others are more reactive. Examples are given for iron and manganese in Chapter 15. From the perspective of biogeochemical cycling, complexation increases the total concentrations of metal ions in solution, and the net effect is to promote transport and cycling of metals in aquatic environments. For example, complexation of ferric iron by humic material greatly increases the amount of Fe in oxygenated solutions and thus promotes the downstream movement of iron in watersheds. Similarly, the presence of soluble complexes imposes limits on metal ion removal by precipitation reactions. The extent to which Ca^{2+} can be removed by lime softening to form $CaCO_{3(s)}$ may be limited in part by soluble complexes of Ca^{2+}.

Finally, complexation plays a major role in the biological availability and toxicity of metal ions in aquatic systems. This is a complicated topic, and the effects can go in either direction (increased or decreased bioavailability and toxicity), depending on circumstances. As noted above, complexation increases total concentrations of metal ions in solution and thus should increase metal bioavailability. In some cases, biota excrete ligands into water to complex metal ions to make them more bioavailable. Siderophores are important examples: they form very strong complexes with Fe^{III}, an otherwise highly insoluble form of iron in natural waters at circumneutral pH. In contrast, complexation decreases the toxicity of metal ions whose predominant toxic species is the free metal ion. An example is Al^{3+}, which is toxic to fish and aquatic invertebrates in acidic waters. The low solubility of $Al(OH)_{3(s)}$ at circumneutral pH means that Al^{3+} concentrations are below toxic levels in such waters, and complexation of Al^{3+} with F^- to form AlF^{2+} and AlF_2^+ mitigates the toxicity of soluble Al in some low-pH waters. Equilibrium considerations explain only part of the story regarding the effects of complexation on metal ion toxicity and bioavailability, however. The kinetics of complex dissociation also plays a role.

9.2   Types and structures of complexes

From a bonding perspective, two kinds of complexes can be distinguished: ***inner-sphere*** or "true" ***complexes*** and ***outer-sphere*** or "ion-pair" ***complexes***. The following sections describe the characteristics and structural differences of these two types of complexes.

9.2.1 Inner-sphere or "true" complexes and metal-ion coordination numbers

In inner-sphere complexes, ligand atoms replace waters of hydration surrounding the central metal ion, and the orbital of an electron-donating ligand (Lewis base) overlaps with an empty bonding orbital of the metal ion (Lewis acid) to form a molecular orbital. Formerly, this was known as a ***coordinate covalent bond***, used to indicate that both bonding electrons come from one atom (the Lewis base or ligand atom), but this terminology no longer is in vogue. Insofar as waters of hydration form bonds with metal ions the same way as other ligands, complexation should be viewed as an exchange reaction (ligand X replacing ligand H_2O). As mentioned above, the number of ligands a metal ion can accommodate defines its coordination number, C_N. For common metal ions, C_N ranges from 2 to 8, but even higher values are known for large metal ions (e.g., C_N is as high as 12 for uranium, U^{IV}). By far, the most common C_N values for metal ions of interest in natural waters are 4 and 6, and odd-numbered coordination numbers are rare. The arrangement of ligands around the metal ion varies with C_N and nature of the orbitals available for bonding (see Figure 9.2a,b), for example, whether the metal has only s and p orbitals or also has d orbitals. Metal ions in the second row of the Periodic Table (Li, Be) have only s and p orbitals and form a maximum of four bonding
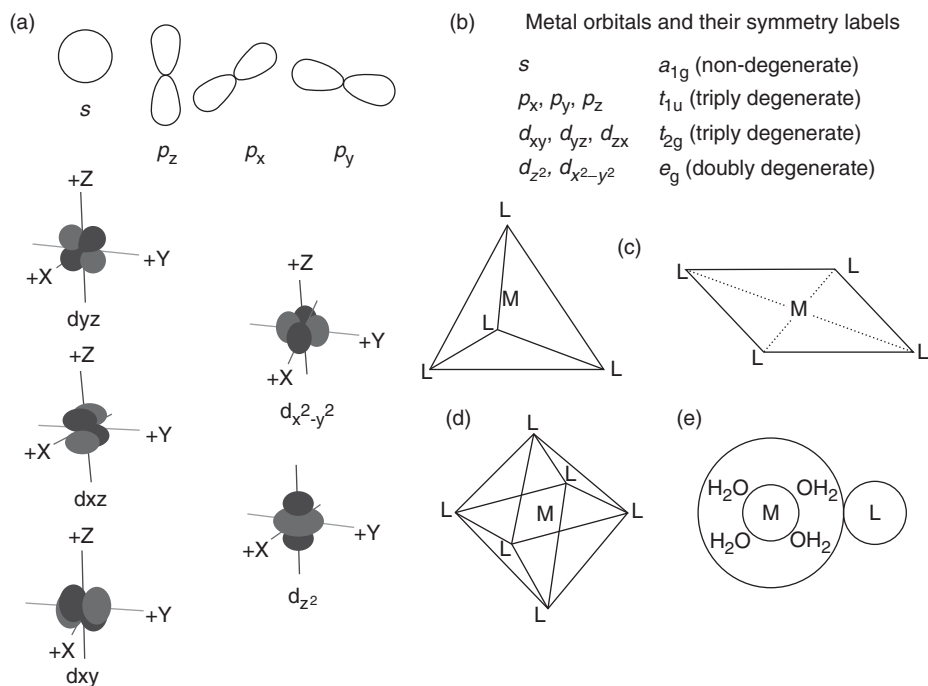
Figure 9.2 (a) Shapes of the three kinds of atomic orbitals involved in bonding: s, p, and d orbitals; (b) symmetry labels associated with the orbitals shown in (a); (c) structures of complexes with $C_N = 4$: tetrahedral and square planar; (d) octahedral complex for $C_N = 6$; (e) schematic structure of an outer-sphere complex. (See insert for color version of figure)

molecular orbitals (involving one *s* and three *p* orbitals). Metals in the third row and beyond have five *d* orbitals in their valence shell that are accessible for bond formation, and they can form a maximum of nine (bonding) molecular orbitals.

Metal ions with $C_N = 2$ form linear complexes. Silver (Ag^I) and gold (Au^I) form such complexes with Cl^- (e.g., $(Cl-Au-Cl)^-$), but these ions are very uncommon in freshwater. (As mentioned above, Au occurs at trace levels in seawater.) The highly toxic $CH_3-Hg^{II}-CH_3$, dimethylmercury, is another example of $C_N = 2$. This usually is considered an organometallic compound rather than a complex, but the same principles apply. Two main structural configurations exist for $C_N = 4$: *tetrahedral*, which are more common, and *square planar* (Figure 9.2c). Nearly all nontransition metals, which form complexes with just *s* and *p* orbitals, form tetrahedral complexes; the metal ion orbitals are hybridized into an sp^3 tetrahedral arrangement that maximizes the separation of ligands. Square planar complexes are formed primarily by d^8 transition metals (those with eight electrons in their *d* orbitals), which include Ni^{2+}, Pd^{2+}, Pt^{2+}, and Au^{3+}. However, other transition metal ions can form square planar complexes with certain organic ligands.[3] The bonding orbitals in square planar complexes are hybrids: either p^2d^2 or sp^2d.[4] Some complexes with $C_N = 4$ (e.g., $CuCl_4^{2-}$) have flattened tetrahedral structures that are intermediate between tetrahedral and square planar. Metal ions with $C_N = 6$ form octahedral complexes, with four ligands oriented in a square plane with the metal ion at the center and two ligands orthogonal to the plane (above and below it; Figure 9.2d). The bonding orbitals in octahedral complexes also are hybrids—in this case sp^3d^2.[4] In some cases the six bonds are symmetric (equivalent in length and strength), but in others the bonding orbitals above and below the plane are longer (or shorter) and have different strengths, especially when two of the ligands differ from the other four.

9.2.2 Outer-sphere or ion-pair complexes

In outer-sphere complexes ligands form long-range electrostatic bonds with intact hydrated metal ions; that is, the metal ion does not lose any waters of hydration, and the ligand's orbitals do not overlap with bonding orbitals of the metal ion (Figure 9.2e). The bonds formed in such cases generally are weak, but we cannot distinguish between ion pairs and true complexes (i.e., inner-sphere (*is*) and outer-sphere (*os*) complexes) based simply on the magnitude of stability constants. (The mathematical relationships describing equilibria for the two types of complexes are identical.) The concept of *os* complexes was developed by the Swedish chemist Bjerrum in the 1920s to explain the nonideal behavior of salt solutions as ionic strength increases; the effect of ion-pair formation is *additional* to the long-range interactions explained by the Debye-Hückel equation. The role of ion pairs in the speciation of major ions in seawater was first described by Garrels and Thompson[5] in 1962 (see Section 9.6).

The strength of *os* bonds can be estimated based on electrostatic principles. An approximate predictor relationship called the ***Fuoss equation*** is[6]

$$K_{os} = (4/3)(\pi N_A a^3 e^{-b}) \times 10^{-3} M^{-1}, \tag{9.3}$$

where N_A is Avogadro's number, *a* is the center-to-center distance between M and L (estimated as $4–5 \times 10^{-8}$ cm), and $b = Z_M Z_L e_0^2 / a\boldsymbol{D}kT$, where e_0 is the electronic charge (4.8×10^{-10} esu in the cgs system of units), $\boldsymbol{D}$ is the dielectric constant (78 for water

at 25°C), and $\mathbf{k}T$ is the thermal energy per molecule, 4.11×10^{-14} erg at 25°C. Equation 9.3 yields values of $K_{os} \approx 1.0$ for $1+, 1-$ complexes and ~ 200 for $2+, 2-$ complexes. For *os* complexes with uncharged ligands, Eq. 9.3 yields $K_{os} \approx 0.1$. Outer-sphere complexes thus are weak, and we would not expect them to be important in dilute solutions like most fresh waters.

Although one cannot infer whether a 1:1 complex between a metal ion and monodentate inorganic ligand is *os* or *is* from the value of the stability constant, there are several other ways to differentiate between the two types of complexes. Formation of *os* complexes involves little change in volume ($\Delta V_r \approx 0$; i.e., the sum of the molar volumes of the products is approximately equal to the molar volumes of the reactants). Consequently, stability constants for *os* complexes do not vary much with pressure. In contrast, formation of *is* complexes involves a change in molar volume ($\Delta V_r \neq 0$; recall the concept of ***electrostriction*** from Chapter 1; see Section 1.2), and their stability constants vary with pressure. In addition, *os* complexes are formed in single-step reactions, but *is* complexes are formed by multistep mechanisms, of which the first step forms an *os* complex (see Section 9.7.2). If kinetic studies are able to show that a complexation reaction occurs by a two-step mechanism (not always an easy task), one can infer that the product is an *is* complex.

9.3 Factors affecting the strength of metal-ligand interactions

Given the thousands of combinations of metal ions and ligands, it should come as no surprise that making sense of the data on stability constants[1] and developing predictive relationships for them has been a major pursuit in coordination chemistry (the branch of chemistry that deals with complexes.) Here we examine the properties of metal ions and ligands that affect binding strengths between metal ions and ligands.

9.3.1 Metal ion properties

Two closely related classification systems for metal ions are useful in explaining broad trends in metal binding with inorganic ligands: the ***Ahrland-Chatt-Davies*** (***ACD***)[7] system, which classifies metals into ***class A***, ***class B***, and ***borderline*** metals, and Pearson's ***Hard and soft acid-base*** (***HSAB***)[8] classification system (Table 9.1).* According to these classification systems, class A (or hard acid) metal ions have electron configurations of inert gases (i.e., completed octets), which are highly stable. Physically, these metal ions are spherical, their electron shells are not easily polarized (i.e., distorted) by the presence of ligands, and they tend to form relatively weak electrostatic bonds with ligands. Given what we know about the factors that affect electrostatic bonding from Coulomb's inverse square law—$f = z_1 z_2 / \boldsymbol{D} d^2$, where f = the force, z_i = charge on the atoms, d = distance between atoms, and $\boldsymbol{D}$ = dielectric constant of the medium (see Box 4.1, Eq. (1))—we can predict that hard metal ions form their strongest bonds with

---

*Hardness is an attribute of elements defined quantitatively by the difference in ionization potentials of the element and its anion.[4] Large differences correspond to high hardness, and small differences to softness, whether one is dealing with a metal ion (Lewis acid) or a ligand (Lewis base).

Table 9.1 Metal classification schemes and trends in ligand preferences

A. Ahrland-Chatt-Davies (ACD) classification of metal ions

Class A	Borderline	Class B
H^+, Li^+, Na^+, K^+, Rb^+, Cs^+, Be^{2+}	Mn^{2+}, Fe^{2+}, Co^{2+}, Ni^{2+} Cu^{2+}, Bi^{3+}, Mn^{3+}, Co^{3+}	Cu^+, Ag^+, Au^+, Tl^+, Hg^{2+}, Hg_2^{2+}
Mg^{2+}, Ca^{2+}, Sr^{2+}, Ba^{2+} Zn^{2+}, Sn^{2+}, Pb^{2+}	1–9 outer-shell electrons; Not spherically symmetric	Rh^+, Pd^{2+}, Pt^{2+}, Tl^{3+}, Cd^{2+}, Au^{3+}
Al^{3+}, Sc^{3+}, La^{3+}, Ga^{3+}, In^{3+}, Sn^{4+}, Ti^{4+}		10–12 outer-shell electrons
Ti^{3+}, V^{3+}, Cr^{3+}		Highly polarizable
Inert gas configuration		

B. Pearson hard and soft acids

Hard acids	Borderline	Soft acids
All A cations plus Sn^{2+}, Fe^{3+}, Co^{3+} Mn^{3+}, minus Cs^+, Zn^{2+}, Pb^{2+}	Bivalent transition metals Metals plus Zn^{2+}, Pb^{2+}	All B cations plus Cs^+, CH_3Hg^+

C. Bonding characteristics and ligand trends for A and B cations

A-type cations	B-type cations
Strongest complexes with first-row ligands; Relatively weak electrostatic bonding; Entropy dominates over enthalpy in energy of reaction	Strongest complexes with heavier ligands in second, third, and fourth rows; Mainly strong covalent bonding; Enthalpy dominates in energy of reaction
$N \gg P > As > Sb$	$N \ll P > As > Sb$
$O \gg S > Se > Te$	$O \ll S \sim Se \sim Te$
$F \gg Cl > Br > I$	$F \ll Cl < Br < I$

D. Irving-Williams order for transition metals

For divalent transition metal ions, the following sequence of complex stability is based on ligand-field stabilization energies, which depends on the number of d orbital electrons:*
$Mn < Fe < Co < Ni < Cu > Zn$

*Some books (e.g., Shriver et al.[4]) give a larger list that includes alkaline earth metals: $Ba^{2+} < Sr^{2+} < Ca^{2+} < Mg^{2+} Mn^{2+} < Fe^{2+} Co^{2+} < Ni^{2+} < Cu^{2+} > Zn^{2+}$. The early part of the order reflects electrostatic effects; the part from Mn^{2+} on reflects ligand field stabilization.

the smallest (i.e., first row) of atoms in a column of the Periodic Table, e.g., for Group VII (halide ligands), $F^- > Cl^- > Br^- > I^-$.

In contrast, class B and soft acid metal ions have 10–12 electrons in their outer shell, and their shapes are more easily distorted (polarized) by ligands. These metal ions tend to form complexes with relatively strong covalent bonds—true sharing of the electron pair forming the bond. Such bonds are stronger when the difference in electron affinity between the atoms forming the bond is minimized. Electron affinity is usually quantified in terms of an element's ***electronegativity***, a concept developed by Linus Pauling. By definition, ligand atoms are electronegative—otherwise they would
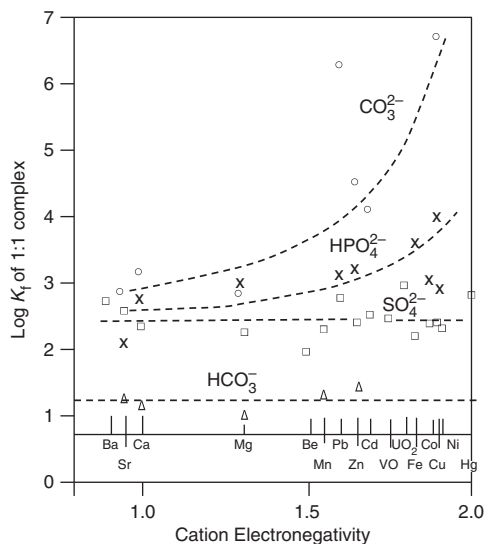
Figure 9.3 Correlations of stability constants for various metal ion complexes versus electronegativity of the metal. Redrawn from Langmuir[9] and used with permission of the American Chemical Society.

not have a pair of electrons to share—and metal ions are electropositive. Thus, we conclude that class B (soft) metals should form the strongest bonds with ligands that are the least electronegative. Because electronegativity decreases going down a column in the Periodic Table, we predict that the order of binding strength is opposite that for electrostatic bonding of hard acids (class A metals). Actual trends in a column of the Periodic Table for class B (soft) metals are not clear cut (Table 9.1), but it is true that the smallest atom in a given group does *not* form the strongest complexes. For example, $F \ll Cl$ is consistent among class B (soft) metals, but $Cl < Br$ is not.

The HSAB concept applies to both metal ions and ligands. Small ligands like F^- are hard spheres and tend to form electrostatic bonds; large ions like I^- are softer (more polarizable) and tend to form covalent bonds.

As the above discussion indicates, the characteristics of metal ions that affect binding strengths depend on whether the bond is primarily covalent or primarily electrostatic.* In addition, the nature of the orbitals involved bonding (*d* vs. *s* and *p*) is important relative to predicting bonding strengths, especially for the borderline (transition) metal ions (see Section 9.3.3). Finally, as noted above, the strength of covalent bonds is greater when the difference in affinity for electrons between the atoms forming the bond is minimized. Given that ligands are electronegative and metal ions are electropositive, we conclude that bonding is stronger as metal ions become more electronegative (or less electropositive). This trend is illustrated in Figure 9.3 for carbonate and hydrogen phosphate ions (HPO_4^{2-}) as ligands with a series of metal ions ranked according to their electronegativity. In contrast, the lack of a trend in binding strength for the same metals with sulfate and bicarbonate ions suggests that these anions form outer-sphere

---

*The idea that a bond must be *either* electrostatic *or* covalent is too simple; there is a range of conditions between the two extremes rather than two simple classes. The same comment applies to the concepts of hardness and softness.

complexes with metal ions. Although normally we want high correlation coefficients (r^2 approaching 1) for predictive relationships, the lack of a statistically significant correlation in these cases is not cause for dismay because the horizontal lines imply that all metal ions of comparable charge and size have stability constants of similar magnitude (log $K = \sim 1.1$ for $MHCO_3^+$ and log $K = \sim 2.4$ for MSO_4^0).

For bonds that are primarily electrostatic, the characteristics of metal ions that affect bond strength are predicted by Coulomb's law: ion size and charge are controlling factors. Bond strength should increase with the charge on the metal ion and decrease with ionic size. (The scatter about the horizontal lines for HCO_3^- and SO_4^{2-} complexes with the metal ions in Figure 9.3 may reflect variations in cation size, as well as uncertainties in the measurements.) Several relationships based on these ideas have been described.

A common relationship (Figure 9.4) is based on the ***polarizing power of the cation***, expressed as z^2/r, where z is the integer charge on the cation and r is its atomic radius. Analogous to the earlier comment that elements exhibit a range of hardness and softness, the idea that metal ions can be classified neatly as either A or B (with attendant binding characteristics) also is too simple. Instead, it is more appropriate to consider "A-ness" and "B-ness" as two ends of a spectrum. The term used to position metal ions along this spectrum is $\Delta\beta$,[11] which is defined as the difference in the stability constants (log K values) for the fluoride and chloride complexes of a metal ion:

$$\Delta\beta_M = \log K_{MF} - \log K_{MCl} \qquad (9.4)$$

Figure 9.5 shows that $\Delta\beta$ ranges from about $+8$ to -8 for metal ions. Turner et al.[10] divided this range into four classes that essentially forms the original A and B classes of
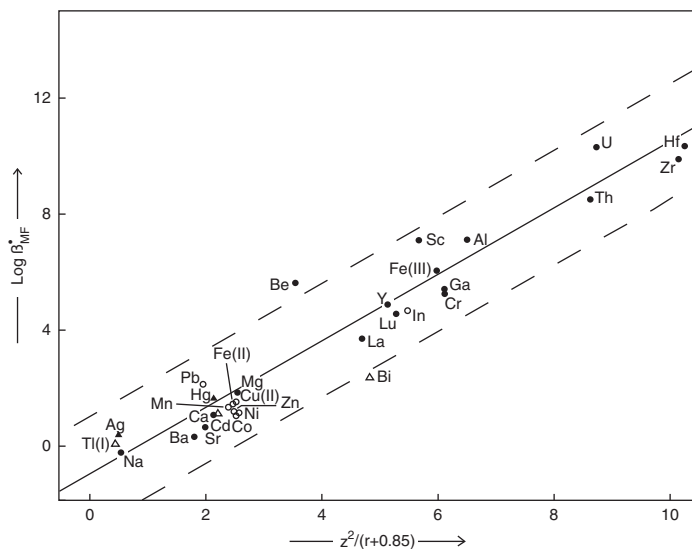
Figure 9.4 Log β_{MF} versus z^2/r, the polarizing power of the cation. The constant 0.85 is an empirical correction factor. From Turner et al.,[10] copyright 1981, and used with permission from Elsevier.
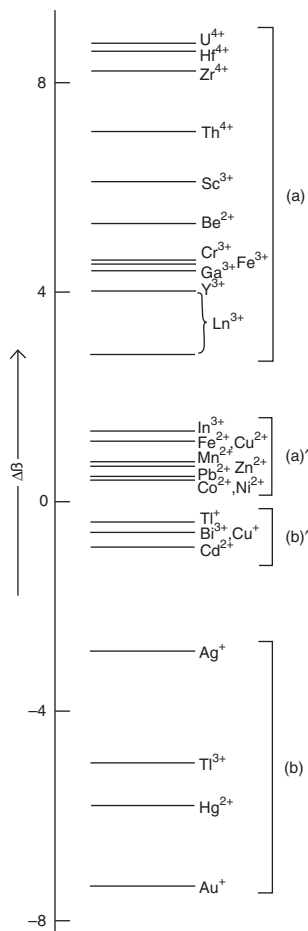
Figure 9.5 Rankings of metal ions according to $\Delta\beta$ of Turner et al.,[10] copyright 1981, and used with permission of Elsevier.

the ACD scheme and divides the borderline metals into two groups, A′ and B′, with $\Delta\beta$ values roughly between +2 and −2. The B′ group includes some class B metals from the ACD scheme.

Turner et al.[10] combined the concepts of $\Delta\beta$ and the polarizing power of the cation (z^2/r) into a bivariate classification scheme for metal ions that considers the ionic and covalent bonding tendencies of metal ions to be orthogonal (independent) variables (Figure 9.6). Four subclasses were considered for each classification variable (I–IV for z^2/r and A, A′, B′, B for $\Delta\beta$). The scheme yielded four general classes of metal ions with relatively distinct complexing tendencies: (1) very weakly complexed cations (IA and IIA), (2) chloro-dominated cations (IBB′, IIBB′), (3) hydrolysis-dominated cations (IIIBB′, IVAA′), and (4) a "residual group" with (unexplained)

$\Delta\beta$

	A	A'	B'	B
I	Li, Na, K, Rb, Cs		Cu^I, Tl^I	Ag, Au^I
II	Mg, Ca, Sr, Ba	Co, Cu^{II}, Fe^{II}, Mn^{II}, Ni, Pb, Zn	Cd	Hg
III	Ln Y		Bi	Tl^{III}
IV	Be, Al, Fe^{III}, Cr^{III}, Sc, Ga, Hf, Th, U^{IV}, Zr	In		

(z^2/r on vertical axis)
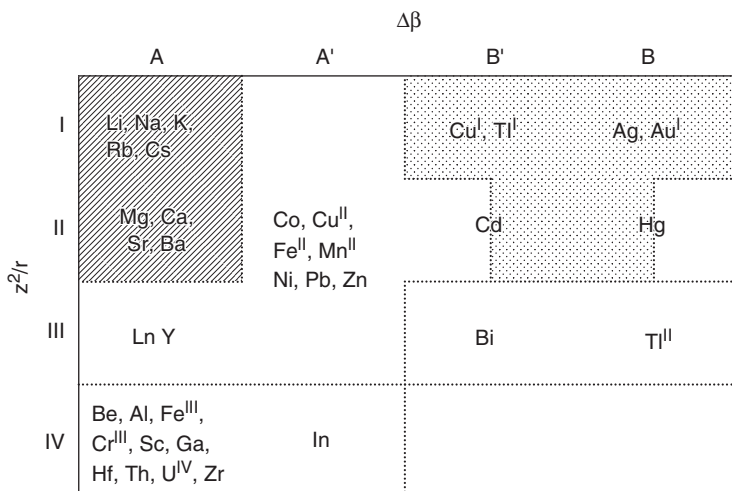
Figure 9.6 Bivariate classification scheme for complexation patterns of metal ions based on ionic and covalent bonding tendencies: cation polarizing power (z^2/r) and $\Delta\beta$. From Turner et al.,[10] © 1981, and used with permission of Elsevier.

variable speciation. Unfortunately the last group contains many of the trace metals of greatest interest in water chemistry.

9.3.2 Ligand properties

In addition to the hard-soft properties of inorganic ligands mentioned previously, three properties of organic ligands have predictive value for trends in stability constants: (1) the number of binding sites (or ligand atoms) on a molecule; (2) the size of the rings formed by chelating agents; and (3) the nature of the ligand atom (e.g., N vs. O). In general, stability constant values increase with increasing number of binding sites on a ligand molecule (and the number of rings it can form with a metal ion). This is called the *chelating effect*, and as noted earlier, it can be explained by entropy effects. Some examples are shown in Table 9.2. Stability constant values for chelating agents that form five-membered rings are generally larger than those for agents forming six-membered rings, and chelates with six-membered rings are stronger than those with seven-membered rings. Steric factors explain this trend; five-membered rings have bond angles that provide optimal overlap of bonding orbitals within the ligand and between the ligand and metal ion. This trend is shown in Figure 9.7 for complexes of the transition metal ions in the Irving-Williams order (Table 9.1D) with dicarboxylic acids forming five-, six-, and seven-membered rings (oxalic, malonic, and succinic acid, respectively).

Finally, the strength of bidentate chelating agents generally decreases in the following pattern: N...N > N...O > O...O. (The bullets between the ligand atoms simply indicate they are part of the same molecule, not that there is a direct bond between them.) Figure 9.7 shows that this trend holds with a few exceptions across the Irving-Williams order. Stability constants with ethylenediamine (N, N ligands) generally are

Table 9.2 Chelating effect and binding strengths of some divalent metal ions*

Name of complex	Number of binding sites	Number of rings	Log K_{CaL}	Log K_{CuL}	Log K_{ZnL}
M-acetate	1	0	0.55	1.79	1.07
M-oxalate	2	1	2.46	4.85	4.00
M-citrate	3	2	3.48	3.8	4.96

*Data from Martell and Smith[1] for I = 0.1.
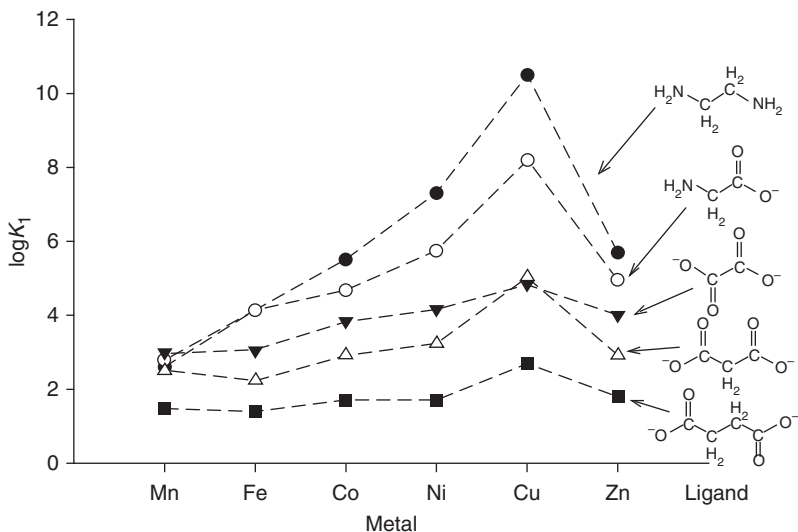
Figure 9.7 Stability constants across the Irving-Williams order generally follow two trends for bidentate ligands: (1) N,N > N,O > O,O, and (2) values decrease with ring size in the order 5 > 6 > 7. Data from Martell and Smith[1] for I = 0.1.

stronger than those for the amino acid glycine (N, O ligands), which in turn are stronger than those for oxalic acid (O, O ligands).

9.3.3 Advanced topic: ligand field and molecular orbital theory for transition metal complexes

The borderline classes in the ACD and HSAB schemes do not fit the patterns of either class A (hard) or class B (soft) metals. The classes are somewhat misnamed in that the metals in them do not behave in a manner simply intermediate between classes A and B. Instead, it is appropriate to say that these metals do not fit the bonding characteristics or ligand preference trends of either A or B metals. A useful trend for some borderline metals is the Irving-Williams order for the second half of the first row of divalent transition metal ions, a group of metals with substantial relevance in aquatic chemistry.

The trends in bond strength defined by the Irving-Williams order (Table 9.1D), which hold for many ligands, are explained by frontier molecular orbital theory (FMO) and

the earlier ligand-field theory. These theories relate the strength of complexes to the stabilization of electrons in the partially filled d orbitals of the metals that results when ligands form bonds with the metal ions. The characteristic that FMO uses to evaluate the stability of an electronic arrangement is the difference between the energy of the highest occupied molecular orbital (HOMO) and that of the lowest unoccupied molecular orbital (LUMO), called the ligand-field stabilization energy (LFSE) In turn, LFSE is related to Δ_0, a parameter called the ***ligand field splitting***:

$$LFSE = (-0.4x + 0.6y)\Delta_O, \tag{9.5}$$

where x is the number of electrons in the triply degenerate t_{2g} orbitals and y is the number of electrons in the doubly degenerate e_g orbitals (see Figure 9.2a,b). Some examples are illustrated in Figure 9.8. Detailed development of ligand field theory is beyond the scope of this chapter and is covered in texts on inorganic chemistry,[3,4] but it is important to understand that not all ligands have the same effect on Δ_0. Some ligands exert a strong
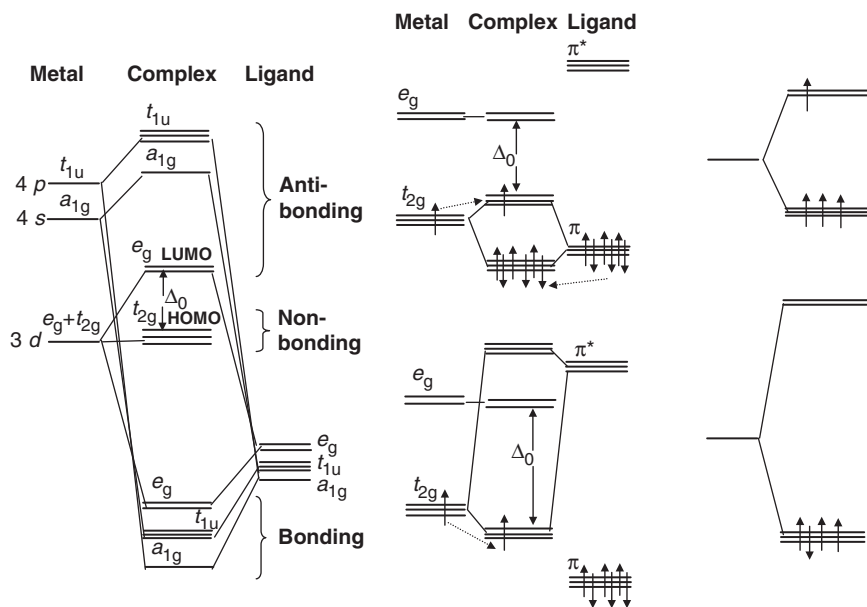
Figure 9.8 Molecular orbital diagrams showing how metal and ligand atomic orbitals combine to form bonding, antibonding, and nonbonding molecular orbitals of a complex: (a) Typical octahedral complex of a transition metal and ligand; Δ_0 shows how the energy level of the five d orbitals (two e_g and three t_{2g}) becomes split by complex formation. The nonbonding t_{2g} orbitals (the highest occupied molecular orbitals or HOMO) are purely metal in character; the antibonding e_g orbitals (lowest unoccupied molecular orbitals or LUMO) are largely metal. (b) Effects of two types of π-bonding ligands on ligand field splitting: top, ligands acting as π bases decrease Δ_0; bottom, ligands acting as π acids increase Δ_0. (c) Effect of ligand field strength on d^4 complexes: top, the weak-field, high-spin $t_{2g}^3 e_g^1$ configuration; bottom, strong-field, low-spin t_{2g}^4 configuration. Redrawn based on diagrams in Shriver et al.[4]

field, and others exert a weak field. The spectrochemical series for ligands (so-called because it is based on spectroscopic (light absorption) measurements) arranges ligands in order of their ligand field strength as follows:[4]

$$I^- < Br^- < S^{2-} < SCN^- < Cl^-, NO_3^- < F^- < C_2O_4^{2-} < H_2O < NCS^-$$
$$< CH_3CN < NH_3 < en < bipy < phen < NO_2^- < PPh_3 < CN^- < CO \qquad (9.6)$$
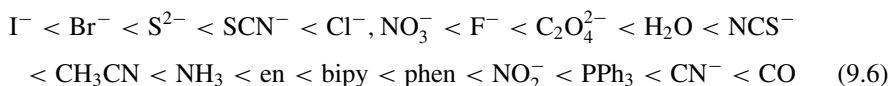
The ligands en, bipy, and phen are ethylenediamine, 2, 2′-dipyridine, and phenanthroline, respectively.

A corresponding spectrochemical series also exists for metal ions:[4]

$$Mn^{2+} < V^{2+} < Co^{2+} < Fe^{2+} < Co^{3+} < Mn^{4+} < Mo^{3+}... \qquad (9.7)$$
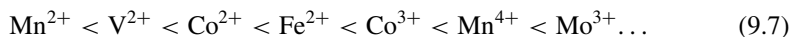
Metal ions following on the right side of the series are not of interest in natural waters (e.g., Rh, Ru, Pd). It is not generally possible to state whether a ligand is "high field" or "low field" without reference to the metal ion, but the extremes of the two series generally follow the expected pattern (i.e., a weak metal ion and weak ligand yield a low-field complex, and strong ligands and metals yield high-field complexes).

9.4   Complexation equilibrium constants

Equilibrium constants for complexation reactions usually are written as formation constants (also called stability or association constants), and two types are used: stepwise (K_i) and cumulative (β_n). The two forms will be derived using hydroxide and ammonia as examples.

9.4.1 Hydroxy complexes

As mentioned above, metal ions in solution are complexed by a varying number of water molecules depending on the size of the ion. When a ligand complexes with a metal, it replaces a water molecule. Hydroxide, having a negative charge, forms stronger complexes with metal ions than water does. Thus, it is logical to assume that hydroxide will displace water if it is in sufficient concentration. (In fact, hydroxide does not displace water, but rather removes a proton from the water ligand, thus creating a hydroxide ligand.) Because this is an acid/base reaction, rates of complexation by hydroxide generally are rapid. Overall, the reaction for generic metal ion Me^{n+} can be written as

$$Me(OH_2)_x^{n+} + OH^- \rightleftharpoons Me(OH)(OH_2)_{x-1}^{(n-1)} + H_2O \qquad (9.8)$$

To simplify, this is usually written as

$$Me^{n+} + OH^- \rightleftharpoons MeOH^{(n-1)} \qquad (9.9a)$$

or

$$Me^{n+} + H_2O \rightleftharpoons MeOH^{(n-1)} + H^+ \tag{9.9b}$$
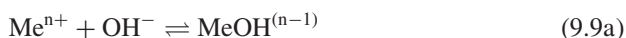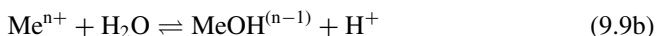
Of course, multiple hydroxy ligands may attach to the metal, as shown below for Zn^{2+}:

$$Zn^{2+} + OH^- \rightleftharpoons ZnOH^+ \qquad K_1 = \frac{[ZnOH^+]}{[Zn^{2+}][OH^-]} = 10^5 \tag{9.10a}$$

$$ZnOH^+ + OH^- \rightleftharpoons Zn(OH)_2^0 \qquad K_2 = \frac{[Zn(OH)_2^0]}{[ZnOH^+][OH^-]} = 10^{5.203} \tag{9.10b}$$

$$Zn(OH)_2^0 + OH^- \rightleftharpoons Zn(OH)_3^- \quad K_3 = \frac{[Zn(OH)_3^-]}{[Zn(OH)_2^0][OH^-]} = 10^{3.697} \tag{9.10c}$$

$$Zn(OH)_3^- + OH^- \rightleftharpoons Zn(OH)_4^{2-} \qquad K_4 = \frac{[Zn(OH)_4^{2-}]}{[Zn(OH)_3^-][OH^-]} = 10^{1.6} \tag{9.10d}$$
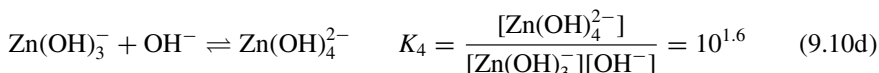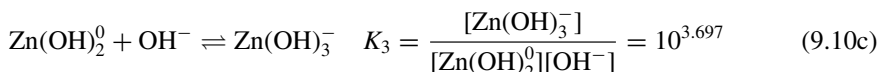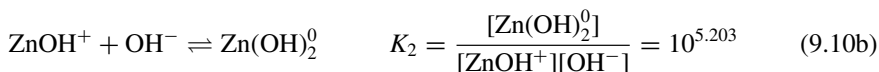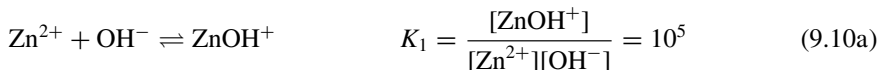
Note that activity corrections are ignored in Eq. 9.10a–e. The total dissolved Zn_T^{II} would be

$$Zn_T^{II} = [Zn^{2+}] + [ZnOH^+] + [Zn(OH)_2^0] + [Zn(OH)_3^-] + [Zn(OH)_4^{2-}]. \tag{9.11}$$

Normally, one would substitute rearranged equilibrium constants into the mass balance expression to solve the problem. One may notice here that this results in a rather cumbersome effort, in that the last complex is dependent on the concentration of the third, which is dependent on the concentration of the second, which is dependent on the concentration of the first. Thus, the expressions get complicated quickly. Also, there are dependencies on the concentration of hydroxide, and our master variable to this point has been protons. A solution to this problem is to rewrite the reaction expressions as follows:

$$Zn^{2+} + OH^- \rightleftharpoons ZnOH^+ \qquad\qquad K_1 = 10^5$$
$$\underline{H_2O \rightleftharpoons H^+ + OH^- \qquad\qquad\qquad K_w = 10^{-13.997}}$$
$$Zn^{2+} + H_2O \rightleftharpoons ZnOH^+ + H^+ \qquad K_w \times K_1 = {}^*\beta_1 = 10^{-8.997} = \frac{[ZnOH^+][H^+]}{[Zn^{2+}]} \tag{9.12a}$$

$$ZnOH^+ + OH^- \rightleftharpoons Zn(OH)_2^0 \qquad K_2 = 10^{5.203}$$
$$Zn^{2+} + H_2O \rightleftharpoons ZnOH^+ + H^+ \qquad {}^*\beta_1 = 10^{-8.997}$$
$$\underline{H_2O \rightleftharpoons H^+ + OH^- \qquad\qquad\qquad K_w = 10^{-13.997}}$$
$$Zn^{2+} + 2H_2O \rightleftharpoons Zn(OH)_2^0 + 2H^+ \quad {}^*\beta_2 = 10^{-17.791} = \frac{[Zn(OH)_2^0][H^+]^2}{[Zn^{2+}]} \tag{9.12b}$$
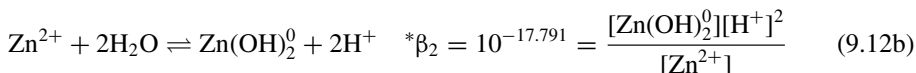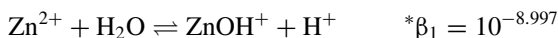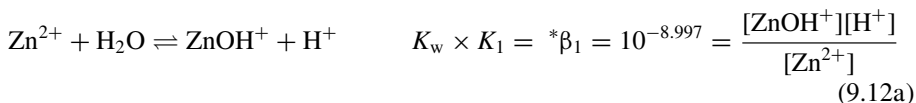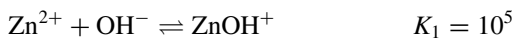
Similarly one may derive

$$Zn^{2+} + 3H_2O \rightleftharpoons Zn(OH)_3^- + 3H^+ \quad {}^*\beta_3 = 10^{-28.091} \tag{9.12c}$$

$$Zn^{2+} + 4H_2O \rightleftharpoons Zn(OH)_4^{2-} + 4H^+ \quad {}^*\beta_4 = 10^{-40.488} \tag{9.12d}$$
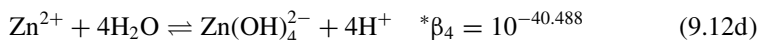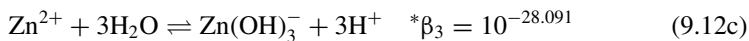
Such reactions represent the reaction of a metal ion with a protonated ligand to form a complex with the deprotonated form of the ligand. In this case, the protonated ligand is water, and OH^- is the deprotonated ligand. As discussed in Section 1.4.2 (see Eqs. 9 and 10), stability constants for such reactions are given a "star" (*) prefix. The term β denotes that all reactions are written using the free metal ion on the left-hand side. These equations have the advantage that the $^*\beta$ constants can be used to express the complex concentration in terms of protons and the free metal ion. For example,

$$\left[Zn(OH)_2^0\right] = \left[Zn^{2+}\right] \frac{{}^*\beta_2}{[H^+]^2}. \tag{9.13}$$

The mass balance expression for Zn_T^{II} then becomes

$$Zn_T^{II} = \left[Zn^{2+}\right]\left(1 + \frac{{}^*\beta_1}{[H^+]} + \frac{{}^*\beta_2}{[H^+]^2} + \frac{{}^*\beta_3}{[H^+]^3} + \frac{{}^*\beta_4}{[H^+]^4}\right). \tag{9.14}$$

Note that there also are stepwise $^*K$ values in which the free metal ion is complexed with water to form the hydroxy complex, and a water molecule is added to the first hydroxy complex to form the second, etc. There are also β values in which the free metal ion is complexed with increasing numbers of hydroxides. For simplicity, Table 9.3 lists only the β and $^*\beta$ values for formation of hydroxy complexes with some common metal ions.

9.4.2 Complexes with other ligands

As described above, metal ions may form complexes with any suitable ligand containing a lone pair of electrons. Common ligands include inorganic ions (e.g., OH^-, CO_3^{2-}, CN^-), neutral molecules (e.g., NH_3), and organic bases and anions (e.g., amines and carboxylic acid anions). The β notation is useful for such complexes, as shown for the Zn^{2+}-NH_3 combination. For example, when considering the complexation of Zn^{2+} by NH_3, we have

$$Zn^{2+} + NH_3 \rightleftharpoons Zn(NH_3)^{2+} \qquad K_1 \text{ and } \beta_1 = 10^{2.31} \tag{9.15a}$$

$$Zn(NH_3)^{2+} + NH_3 \rightleftharpoons Zn(NH_3)_2^{2+} \quad K_2 = 10^{2.46} \tag{9.15b}$$

$$Zn(NH_3)_2^{2+} + NH_3 \rightleftharpoons Zn(NH_3)_3^{2+} \quad K_3 = 10^{2.34} \tag{9.15c}$$

$$Zn(NH_3)_3^{2+} + NH_3 \rightleftharpoons Zn(NH_3)_4^{2+} \quad K_4 = 10^{2.23} \tag{9.15d}$$
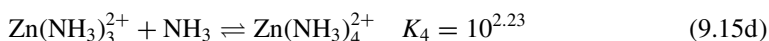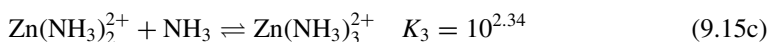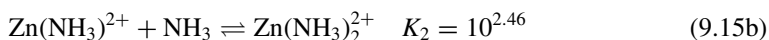
Table 9.3 Stability constants for hydroxy complexes of metals

Metal	i	$\log \beta_i$	$\log {}^*\beta_i$	Metal	i	$\log \beta_i$	$\log {}^*\beta_i$
Ag^+	1	2	-11.997	Fe^{2+}	1	4.6	-9.397
	2	3.987	-24.007		2	7.5	-20.494
Al^{3+}	1	9	-4.997		3	13	-28.991
	2	17.9	-10.094	Fe^{3+}	1	11.81	-2.187
	3	25.2	-16.791		2	23.4	-4.594
	4	33.3	-22.688		3	29.431	-12.56
Ba^{2+}	1	0.64	-13.357		4	34.4	-21.588
Be^{2+}	1	8.6	-5.397	Hg^{2+}	1	10.6	-3.397
	2	14.4	-13.594		2	21.8	-6.194
	3	18.8	-23.191		3	20.9	-21.091
	4	18.6	-37.388	Mg^{2+}	1	2.6	-11.397
Ca^{2+}	1	1.3	-12.697	Mn^{2+}	1	3.4	-10.597
Cd^{2+}	1	3.9	-10.097		3	7.191	-34.800
	2	7.7	-20.294		4	7.7	-48.288
	3	9.486	-32.505	Ni^{2+}	1	4.1	-9.897
	4	8.7	-47.288		2	8.997	-18.997
Co^{2+}	1	4.3	-9.697		3	12	-29.991
	2	9.2	-18.794	Pb^{2+}	1	6.4	-7.597
	3	10.5	-31.491		2	10.9	-17.094
	4	9.7	-46.288		3	13.9	-28.091
Co^{3+}	1	12.706	-1.291		4	16.289	-39.699
Cr^{3+}	1	10.34	-3.657	Sn^{2+}	1	10.6	-3.397
	2	18.425	-9.569		2	20.9	-7.094
	3	24	-17.991		3	25.4	-16.591
	4	28.6	-27.388	Zn^{2+}	1	5	-8.997
Cu^{2+}	1	6.5	-7.497		2	10.2	-17.794
	2	11.8	-16.194		3	13.9	-28.091
	3	15.112	-26.879		4	15.5	-40.488
	4	16.008	-39.980				

All values match the thermodynamic database in MINEQL+ v. 4.6 using $\log K_{\mathrm{w}} = -13.997$.

Note that adding Eqs. 9.15a and 9.15b yields β_2:

$$Zn^{2+} + NH_3 \rightleftharpoons Zn(NH_3)^{2+} \qquad K_1 = 10^{2.31}$$

$$\underline{Zn(NH_3)^{2+} + NH_3 \rightleftharpoons Zn(NH_3)_2^{2+} \qquad K_2 = 10^{2.46}}$$

$$Zn^{2+} + 2NH_3 \rightleftharpoons Zn(NH_3)_2^{2+} \qquad \beta_2 = K_1 K_2 = 10^{4.77} \qquad (9.15e)$$

Similarly,

$$Zn^{2+} + 3NH_3 \rightleftharpoons Zn(NH_3)_3^{2+} \qquad \beta_3 = K_1 K_2 K_3 = 10^{7.11} \qquad (9.15f)$$

$$Zn^{2+} + 4NH_3 \rightleftharpoons Zn(NH_3)_4^{2+} \qquad \beta_4 = K_1 K_2 K_3 K_4 = 10^{9.34} \qquad (9.15g)$$
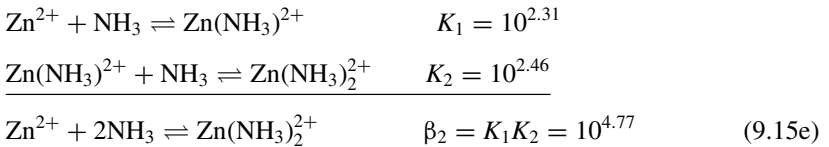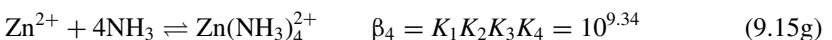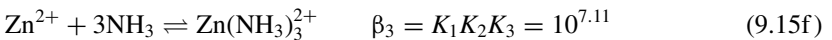
Any complex concentration can now be expressed in terms of the ligand concentration and the free metal ion concentration. For example

$$\beta_2 = \frac{[Zn(NH_3)_2^{2+}]}{[Zn^{2+}][NH_3]^2},$$

and thus

$$Zn(NH_3)_2^{2+} = \beta_2[Zn^{2+}][NH_3]^2. \tag{9.16}$$

Our mass balance expression for total dissolved zinc now becomes

$$Zn_T^{II} = [Zn^{2+}]\left(1 + \frac{^*\beta_1}{[H^+]} + \frac{^*\beta_2}{[H^+]^2} + \frac{^*\beta_3}{[H^+]^3} + \frac{^*\beta_4}{[H^+]^4}\right.$$

$$\left. + \beta_1[NH_3] + \beta_2[NH_3]^2 + \beta_3[NH_3]^3 + \beta_4[NH_3]^4\right). \tag{9.17}$$

Complexation constants for metals with various inorganic ligands are compiled in Table 9.4. As the following example demonstrates, the acid/base speciation of ligands must be considered when determining the speciation of a metal ion.

EXAMPLE 9.1 Speciation of zinc when ammonia is present: For a system containing 10^{-7} M Zn_T^{II} and 10^{-3} M total ammonia (N_T) at pH 9.25, what are the concentrations of free zinc and the eight complexes in equation 9.17? Assume that no solids precipitate.

Answer: We begin with the NH_3/NH_4^+ component of the system. We can treat this component of the system separately, because even if all 10^{-7} mol/L zinc was complexed by four ammonia molecules, only 4×10^{-7} mol/L ammonia would be taken from the total pool, which is a negligible fraction of N_T (10^{-3} M).

The pK_a of ammonium is 9.25, which is the same as the pH of the system. Thus,

$$[NH_3] = [NH_4^+] = 5 \times 10^{-4}M = 10^{-3.3}M.$$

We now substitute into Eq. 9.17 the known equilibrium constants, $[H^+] = 10^{-9.25}$, and the ammonia concentration:

$$Zn_T^{II} = [Zn^{2+}]\left(1 + \frac{10^{-8.997}}{[10^{-9.25}]} + \frac{10^{-17.794}}{[10^{-9.25}]^2} + \frac{10^{-28.091}}{[10^{-9.25}]^3} + \frac{10^{-40.488}}{[10^{-9.25}]^4}\right.$$

$$\left. + 10^{2.31}[10^{-3.3}] + 10^{4.77}[10^{-3.3}]^2 + 10^{7.11}[10^{-3.3}]^3 + 10^{9.34}[10^{-3.3}]^4\right)$$

$$Zn_T^{II} = [Zn^{2+}](1 + 10^{0.253} + 10^{0.706} + 10^{-0.341} + 10^{-3.488}$$

$$+ 10^{-0.99} + 10^{-1.83} + 10^{-2.79} + 10^{-3.86})$$

From the above equation, we see that the first two hydroxy complexes have higher concentrations than Zn^{2+}, and the ammonia complexes have lower concentrations than

Table 9.4 Stability constants for a selection of metal-ligand complexes

	CO_3^{2-}	SO_4^{2-}	Cl^-	F^-	NH_3	PO_4^{3-}	CN^-	HS^-
Ag^+		AgL^- 1.30	AgL^0 3.31; AgL_2^- 5.25; AgL_3^{2-} 5.20; AgL_4^{3-} 5.15	AgL^0 0.40	AgL^+ 3.31; AgL_2^+ 7.22		AgL_2^- 20.48; AgL_3^{2-} 21.7	AgL^0 13.814; AgL_2^- 17.914
Al^{3+}		AlL^+ 3.89; AlL_2^- 4.92		AlL^{2+} 7.00; AlL_2^+ 12.60; AlL_3^0 16.70; AlL_4^- 19.40				
Ca^{2+}	$CaHL^+$ 11.60; CaL^0 3.20	CaL^0 2.36		CaL^+ 1.038	CaL^{2+} 0.1; CaL_2^{2+} −0.3	$CaHL$ 15.035; CaH_2L^+ 20.923		
Cd^{2+}	$CdHL^+$ 10.686; CdL^0 4.358; CdL_2^{2-} 7.228	CdL^0 2.37; CdL_2^{2-} 3.50	CdL^+ 1.98; CdL_2^0 2.60; CdL_3^- 2.40	CdL^+ 1.20; CdL_2^- 1.50		CdL^- 3.9	CdL^+ 6.01; CdL_2^0 11.12; CdL_3^- 15.65; CdL_4^{2-} 17.92	CdL^+ 8.008; CdL_2^0 15.212; CdL_3^- 17.112; CdL_4^{2-} 19.308
Co^{2+}	$CoHL^+$ 12.22; CoL^0 4.228	CoL^0 2.30	CoL^+ 0.539	CoL^+ 1.50	CoL^{2+} 2.08; CoL_2^{2+} 3.71; CoL_3^{2+} 4.81; CoL_4^{2+} 5.53; CoL_5^{2+} 5.75	$CoHL$ 15.413	CoL_3^- 14.312; CoL_5^{3-} 23.00	
Cr^{3+}		CrL^+ 3.368	CrL^+ 0.112; CrL_2^- −0.911	CrL^+ 5.20	CoL_6^{3+} 13.0	CrH_2L^{2+} 22.338		
Cu^{2+}	$CuHL^+$ 12.129; CuL^0 6.77; CuL_2^{2-} 10.2	CuL^0 2.36	CuL^+ 0.20; CuL_2^0 −0.26; CuL_3^- −2.29; CuL_4^{2-} −4.59	CuL^+ 1.80	CuL^{2+} 4.01; CuL_2^2 (5.8); CuL_3^{2+} 10.7; CuL_4^{2+} 14.7; 17.6	$CuHL$ 16.6		CdL_3^- 25.899
Fe^{2+}	$FeHL^+$ 11.429	FeL^0 2.39	FeL^+ 0.90; FeL_2^0 0.04			$FeHL$ 15.975; FeH_2L^+ 22.273	$FeH_2L_6^{2-}$ 42.11; $FeHL_6^{3-}$ 39.71; FeL_6^{4-} 35.40	FeL_2 8.950; FeL_3^- 10.987

Ion								
Fe^{3+}		FeL^+ 4.05 FeL_2^- 5.38	FeL^{2+} 1.48 FeL_2^+ 2.13 FeL_3^0 1.13	FeL^{2+} 6.04 FeL_2^+ 10.468 FeL_3^0 13.617			$FeHL^+$ 22.292 FeH_2L^{2+} 23.852	FeL_6^{3-} 43.60
Hg^{2+}	$HgHL^+$ 16.348 HgL^0 12.078 HgL_2^{2-} 15.578	HgL 2.418	HgL^+ 7.3 HgL^0 14.0 HgL_3^- 15.0 HgL_4^{2-} 15.6	HgL^{2+} 1.569	HgL^{2+} 8.80 HgL_2^{2+} 17.80 HgL_3^{2+} 18.40 HgL_4^{2+} 19.30		HgL^+ 17.0 HgL^0 32.75 HgL_3^- 36.31 HgL_4^{2-} 38.97	HgL^+ 38.322 HgL_2^0 31.928
Mg^{2+}	$MgHL^+$ 11.339 MgL^0 2.92	MgL^0 2.26		MgL^+ 2.05		$MgHL$ 15.175 MgH_2L^+ 21.256 MgL^- 4.654		
Mn^{2+}	$MnHL^+$ 11.629	MnL^0 2.26	MnL^+ 0.10 MnL_2^0 0.25 MnL_3^- −0.31	MnL^+ 1.60				
Ni^{2+}	$NiHL^+$ 12.420 NiL^0 4.572 *NiL_2^{2-} 10.11*	NiL^0 2.30 NiL_2^{2-} 0.82	NiL^+ 0.408 NiL_2^0 −1.89	NiL^+ 1.40	NiL^{2+} 2.73 NiL_2^{2+} 4.89		$NiHL_4^-$ 36.029 $NiH_3L_4^+$ 43.343 $NiH_2L_4^0$ 40.743 NiL_4^{2-} 30.20	
Pb^{2+}	$PbHL^+$ 13.200 PbL^0 6.478 PbL_2^{2-} 9.938	PbL^0 2.69 PbL_2^{2-} 3.47	PbL^+ 1.55 PbL_2^0 2.20 PbL_3^- 1.80 PbL_4^{2-} 1.46	PbL^+ 1.848 PbL^0 3.142 PbL_3^- 3.420 PbL_4^{2-} 3.100			*PbL_4^{2-} 10.6*	PbL_2 15.27 PbL_3^- 16.57
Sn^{2+}			SnL^+ 1.64 SnL_2^0 2.43 SnL_3^- 1.256	SnL^+ 4.488 SnL_2^0 7.292 SnL_3^- 10.112				
Zn^{2+}	$ZnHL^+$ 11.829 ZnL^0 4.760 *ZnL_2^{2-} 9.6*	ZnL^0 2.34 ZnL_2^{2-} 3.28	ZnL^+ 0.40 ZnL_2^0 0.60 ZnL_3^- 0.50 ZnL_4^{2-} 0.199	ZnL^+ 1.30	*ZnL^{2+} 2.31* *ZnL_2^{2+} 4.77* *ZnL_3^{2+} 7.11* *ZnL_4^{2+} 9.34*	*$ZnHL$ 15.7*	*ZnL_2^0 11.07* *ZnL_3^- 16.05* *ZnL_4^{2-} 16.72*	ZnL_2 12.82 ZnL_3^- 16.10

Log β is shown for each complex. Where possible, values are consistent with the thermodynamic database in MINEQL+ v. 4.6. Italicized values are derived from Martell and Smith,[1] Benjamin,[12] or Stumm and Morgan.[13] When an H is included in the formula, an H^+ must be included on the left-hand side of the reaction. For example, $MeHL^0$ would be $Me^{2+} + H^+ + L^{2-} = MeHL^0$.

all but one of the hydroxy complexes. Substituting in the value for Zn_T^{II} and dividing by the term in parentheses (which equals 8.447) gives $[Zn^{2+}] = 1.18 \times 10^{-8}$ M. The complex concentrations are determined by multiplying this value by the appropriate term from the expression in parentheses:

$$[ZnOH^+] = (1.18 \times 10^{-8})(10^{0.203}) = 1.88 \times 10^{-8} M$$

$$[Zn(OH)_2^0] = (1.18 \times 10^{-8})(10^{0.606}) = 4.76 \times 10^{-8} M$$

$$[Zn(OH)_3^-] = (1.18 \times 10^{-8})(10^{-0.491}) = 3.81 \times 10^{-9} M$$

$$[Zn(OH)_4^{2-}] = (1.18 \times 10^{-8})(10^{-3.688}) = 2.42 \times 10^{-12} M$$

$$[Zn(NH_3)^{2+}] = (1.18 \times 10^{-8})(10^{-0.99}) = 1.21 \times 10^{-9} M$$

$$[Zn(NH_3)_2^{2+}] = (1.18 \times 10^{-8})(10^{-1.83}) = 1.74 \times 10^{-10} M$$

$$[Zn(NH_3)_3^{2+}] = (1.18 \times 10^{-8})(10^{-2.79}) = 1.91 \times 10^{-11} M$$

$$[Zn(NH_3)_4^{2+}] = (1.18 \times 10^{-8})(10^{-3.86}) = 1.63 \times 10^{-12} M$$

9.4.3 Linear free energy relationships to predict K_{ML}

Organic ligands with N or O functional groups (e.g., amines, carboxylic acids, and phenols) are important complexing agents. Some are man-made and others are natural. For monodentate ligands with negatively charged oxygen atoms (e.g., phenol, hydroxide, nitrous acid, and carboxylic acids), a recent study showed that equilibrium constants for metal-ligand binding (K_{ML}) in general can be estimated from the K_a (or K_{HL}) of the ligand.[14] The expressions are of the form

$$\log K_{ML} = \alpha_0 \log K_{HL}, \qquad (9.18)$$

which is known as the Irving-Rosotti relationship.[14] Because equilibrium constants are exponentially related to free energies ($\Delta G°$; Eq. 3.27), this is a ***linear free energy relationship*** (***LFER***). Such correlations are useful for predicting a quantity without having to conduct experiments. Values of α_0 range from 0.17 to 0.90 (Table 9.5) and depend on charge of the metal ion and its row in the Periodic Table. Because α_0 is always < 1, this means that if a metal ion and protons are at equal concentration, the activity of the protonated ligand (HL) always will be greater than that of the metal-ligand complex for monodentate ligands with negatively charged oxygen. Many other examples of linear correlations useful to estimate K_{ML} can be found in the literature. For example, stability constants for various metal ion complexes with oxygen-containing carbonate and oxalate ligands are strongly correlated (Figure 9.9), so that knowledge of either $K_{M-carbonate}$ or $K_{M-oxalate}$ allows one to estimate the other value with reasonable accuracy.

Table 9.5 Values of α_0 to predict log K_{ML} from log K_{HL} by eq. 9.18*

Metal ion	α_0	Metal ion	α_0
Mg^{2+}	0.176	Zn^{2+}	0.304
Ca^{2+}	0.194	Fe^{2+}	0.861
Sr^{2+}	0.171	Cr^{3+}	0.818
Mn^{2+}	0.255	Al^{3+}	0.607
Fe^{2+}	(0.287)	Cd^{2+}	0.306
Co^{2+}	0.306	Hg^{2+}	0.796
Ni^{2+}	0.301	Pb^{2+}	0.442
Cu^{2+}	0.466		

*From Carbonaro and DiToro.[14]
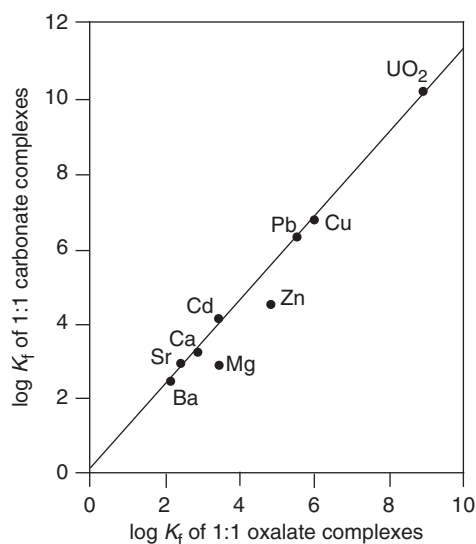
Figure 9.9 Linear free energy relationship (LFER) between log K_f values for metal carbonate and corresponding metal oxalate complexes. Drawn from thermodynamic data in Visual MINTEQ.

9.5 Solving complexation equilibria

9.5.1 Introduction

The manual graphical and algebraic methods described in Chapter 7 and illustrated in Example 9.1 can be used to solve problems involving complexation equilibria, including some that are surprisingly complicated, but many problems involving complexation reactions in environmental water systems are just too difficult to solve readily by manual methods. Such problems usually involve a variety of components, each with several species; in addition, competing acid-base and sometimes solubility equilibria (see Chapter 10) also must be considered. The net effect is that it is impractical to solve such problems manually. Consequently, computer programs such as MINEQL+ and VMINTEQ are used to obtain quantitative solutions and generate the data for graphing complexation equilibria. This section illustrates the solution of complexation equilibria

starting with examples that can be solved manually and then using computer methods to graph and solve more complicated problems.

9.5.2 Complexation of lead by chloride in seawater

The inorganic chemical speciation of trace metals in seawater (and in many freshwaters) is sufficiently simple that we can do the calculations manually, if we can assume that complexation of the metal ions by natural organic matter and trace organic ligands of human origin is unimportant. Because the metal ion concentrations are low (often $\ll 10^{-6}$ M), complexation does not affect the concentrations of the inorganic anionic ligands, which typically occur at concentrations of 10^{-4} to 10^{-3} M in freshwaters (and 10^{-4}–10^{-1} M in seawater). This constrains the problems sufficiently to allow manual solution of the speciation equations. We illustrate this with three examples of the speciation of lead in seawater that sequentially involve an increasing number of potential ligands.

EXAMPLE 9.2 Abundance of monochloro-lead(II) complex in seawater: Lead exists in natural waters primarily as Pb^{II}. Its total concentration in surface layers of the world's oceans is $Pb_T = 14$ ng kg^{-1} ($\sim$14 ng/L, or 7×10^{-11} M). Liam, a new grad student who has a limited chemistry background, is told by his adviser to calculate lead speciation in seawater and is also told that it is dominated by chloride, because the concentration of Cl^- in seawater is so high (0.546 M). Liam proceeds to calculate the fraction of Pb^{II} complexed with chloride in seawater and initially finds a stability constant value for the monochloro-lead complex:

(1) $Pb^{2+} + Cl^- \rightleftharpoons PbCl^+$; $\log K_1 = 1.55$
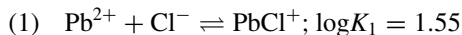
Erroneously thinking that these are the only species that need to be considered, he calculated the distribution of Pb^{II} between Pb^{2+} and $PbCl^+$ as follows. First, he corrected the stability constant to a concentration-based constant by computing activity coefficients for the species in Eq. (1) using the Davies equation. At the ionic strength of seawater (I = 0.699), he found $\gamma = 0.69$ for monovalent ions and $\gamma = 0.23$ for divalent ions. Using these values, he computed that log $^cK_1 = 0.912$ and proceeded to solve the problem:

(2) $^cK_1 = 10^{0.912} = \dfrac{[PbCl^+]}{[Pb^{2+}][Cl^-]} = \dfrac{[PbCl^+]}{[Pb^{2+}] \times 0.546}$

Thus,

(3) $4.459 = \dfrac{[PbCl^+]}{[Pb^{2+}]}$,   or $[PbCl^+] = 4.459[Pb^{2+}]$

He wrote the mass balance expression for lead in seawater and substituted Eq. (3) into it:

(4) $Pb_T = 7.0 \times 10^{-11} = [Pb^{2+}] + [PbCl^+] = [Pb^{2+}] + 4.459[Pb^{2+}] = 5.459[Pb^{2+}]$

Solving for $[Pb^{2+}]$, he found $[Pb^{2+}] = 1.28 \times 10^{-11}$, and by difference he found $[PbCl^+] = 5.72 \times 10^{-11}$.

Based on these calculations, he concluded that 82% of the Pb^{II} in seawater exists as the monochloro-complex.

EXAMPLE 9.3 Abundance of chloro-complexes of Pb^{II} in seawater: Upon showing the above results to his adviser, Liam learned that Pb^{II} can form more than one complex with Cl^- and was told to do more research into stability constants for these complexes. Undaunted, he readily found a tabulation of stability constant values in a reference book and learned that Pb^{II} can form four complexes with Cl^-:

(1) $Pb^{2+} + Cl^- \rightleftharpoons PbCl^+$; $\beta_1 = 10^{1.55} = \{PbCl^+\}/\{Pb^{2+}\}\{Cl^-\}$

(2) $Pb^{2+} + 2Cl^- \rightleftharpoons PbCl_2^0$; $\beta_2 = 10^{2.20} = \{PbCl_2^0\}/\{Pb^{2+}\}\{Cl^-\}^2$

(3) $Pb^{2+} + 3Cl^- \rightleftharpoons PbCl_3^-$; $\beta_3 = 10^{1.80} = \{PbCl_3^-\}/\{Pb^{2+}\}\{Cl^-\}^3$

(4) $Pb^{2+} + 4Cl^- \rightleftharpoons PbCl_4^{2-}$; $\beta_4 = 10^{1.46} = \{PbCl_4^{2-}\}/\{Pb^{2+}\}\{Cl^-\}^4$

Using what he learned in solving the problem the first time, Liam proceeded to correct the β values to concentration-based constants using the activity coefficients he calculated in the previous example using the Davies equation. He found $^c\beta_1 = 10^{0.912}$, $^c\beta_2 = 10^{1.168}$, $^c\beta_3 = 10^{0.839}$, $^c\beta_4 = 10^{0.816}$. Next, he noted that all the β equations can be solved for the concentration of the respective complex in terms of free lead(II) concentration, $[Pb^{2+}]$:

(5) $[PbCl^+] = {}^c\beta_1[Pb^{2+}][Cl^-]$

(6) $[PbCl_2^0] = {}^c\beta_2[Pb^{2+}][Cl^-]^2$

(7) $[PbCl_3^-] = {}^c\beta_3[Pb^{2+}][Cl^-]^3$

(8) $[PbCl_4^{2-}] = {}^c\beta_4[Pb^{2+}][Cl^-]^4$

He wrote the mass balance equation for Pb_T and proceeded to substitute Eqs. (5)–(8) in it for the concentrations of the four chloro-complexes:

(9) $Pb_T = 7 \times 10^{-11} = [Pb^{2+}] + [PbCl^+] + [PbCl_2^0] + [PbCl_3^-] + [PbCl_4^{2-}]$

and

(10) $Pb_T = 7 \times 10^{-11} = [Pb^{2+}] + {}^c\beta_1[Pb^{2+}][Cl^-] + {}^c\beta_2[Pb^{2+}][Cl^-]^2$
$\qquad + {}^c\beta_3[Pb^{2+}][Cl^-]^3 + {}^c\beta_4[Pb^{2+}][Cl^-]^4,$

or

(11) $Pb_T = 7 \times 10^{-11} = [Pb^{2+}](1 + {}^c\beta_1[Cl^-] + {}^c\beta_2[Cl^-]^2 + {}^c\beta_3[Cl^-]^3$
$\qquad + {}^c\beta_4[Cl^-]^4).$

Substituting in values for $[Cl^-]$ and the $^c\beta$s, he obtained

(12) $Pb_T = 7 \times 10^{-11} = [Pb^{2+}](1 + 4.459 + 4.389 + 1.123 + 0.582)$
$\qquad = 11.553[Pb^{2+}].$

Thus, $[Pb^{2+}] = 6.02 \times 10^{-12}$. Liam then multiplied this value by each of the terms within parentheses in Eq. (12) to obtain concentrations of the various chloro-complexes:

$$[PbCl^+] = 6.02 \times 10^{-12} \times 4.459 = 2.702 \times 10^{-11} M;$$

$$[PbCl_2^0] = 6.02 \times 10^{-12} \times 4.389 = 2.66 \times 10^{-11}$$

$$[PbCl_3^-] = 6.02 \times 10^{-12} \times 1.123 = 6.81 \times 10^{-12} M;$$

$$[PbCl_4^{2-}] = 6.02 \times 10^{-12} \times 0.582 = 3.53 \times 10^{-12} M$$

As a check on his calculations, Liam added the concentrations of these four complexes plus that of free Pb^{2+} and found a value of 7.00×10^{-11}, which agrees the reported value of Pb_T.

EXAMPLE 9.4 A comprehensive analysis of Pb^{II} inorganic speciation in seawater: Liam took his newly calculated results for the chloro-complexes of lead in seawater to his adviser, only to hear him say, "Nice try—better than the first one—but don't you realize that lead forms complexes with other major anions in seawater? Try again!" Undismayed— although perhaps a bit weak in chemistry, he was not lacking self-confidence—Liam decided to look at the thermodynamic data base in MINEQL+ and found constants for complexes of lead with Cl^-, SO_4^{2-}, HCO_3^-, CO_3^{2-}, and F^-, as well as values for hydroxide complexes formed by hydrolysis reactions of Pb^{2+}.

Stability constants were found for 19 complexes. Liam decided he could apply the same approach he used in the previous example, and being stubborn, he decided he could solve this system manually instead of relying on the computer program. For ease of working with the large number of reactions and constants, he put his work into tabular form (Table 9.6), with the formation reaction listed in the first column and corresponding stability constant at $I = 0$ in the next column. Using activity coefficients calculated from the Davies equation, he corrected the constants to concentration-based values (column 3). Using data from the marine chemistry literature[13,15] for the concentrations of anions in seawater (Table 9.6B), he computed values of $^c\beta_n[L]^n$ (column four) in a manner comparable to the terms within the parentheses of Eqs. 11 and 12 in Example 9.3. Summing these terms, he found

$$(2) \quad Pb_T = [Pb^{2+}]\left(1 + \sum {}^c\beta_n[L]^n\right) = 7 \times 10^{-11} = [Pb^{2+}](1 + 13.205),$$

or $[Pb^{2+}] = 4.93 \times 10^{-12}$. Multiplying all the terms in column four by this value yielded the concentrations of all the complexes tabulated in the final column. Liam took his tabulated results to his adviser, who was pleased that his new graduate student had finally had figured it out!

It is apparent from Table 9.6 that not all 19 complexes are important in Pb^{II} speciation in seawater. It also should be apparent from the examples that the manual calculation procedure, although time-consuming, is straightforward and can be used even when a trace metal forms complexes with many ligands—provided that the ligand concentrations are not materially affected by complexation with the metal.

9.5.3 Analysis of calcium ion by EDTA titration

EDTA (ethylenediaminetetraacetic acid), commonly written in shorthand as H_4Y, is the most widely used chelating agent in a class of compounds known as aminopolycarboxy-lates. With two nitrogen atoms and four carboxylate groups, EDTA is a hexadentate ligand and thus can completely satisfy the needs of metal ions of coordination number six.

Table 9.6 Speciation of lead(II) in seawater

	$Log\ \beta_i$	$Log\ ^c\beta_i$	$^c\beta_n[L]^n$	$[PbL_n^{2-n}]$
A. Reaction				
$Pb^{2+} + Cl^- = PbCl^+$	1.55	0.912	4.459	2.20×10^{-11}
$Pb^{2+} + 2Cl^- = PbCl_2^0$	2.20	1.168	4.389	2.16×10^{-11}
$Pb^{2+} + 3Cl^- = PbCl_3^-$	1.80	0.839	1.123	5.54×10^{-12}
$Pb^{2+} + 4Cl^- = PbCl_4^{2-}$	1.46	0.816	0.582	2.86×10^{-12}
$Pb^{2+} + F^- = PbF^+$	1.848	1.210	1.1×10^{-3}	5.42×10^{-15}
$Pb^{2+} + 2F^- = PbF_2^0$	3.142	2.181	7.0×10^{-7}	3.45×10^{-18}
$Pb^{2+} + 3F^- = PbF_3^-$	3.42	2.459	9.0×10^{-11}	4.44×10^{-22}
$Pb^{2+} + 4F^- = PbF_4^{2-}$	3.10	2.456	6.1×10^{-15}	3.00×10^{-26}
$Pb^{2+} + Br^- = PbBr^+$	1.70	1.061	9.7×10^{-3}	4.78×10^{-14}
$Pb^{2+} + 2Br^- = PbBr_2^0$	2.60	1.639	3.1×10^{-5}	1.53×10^{-16}
$Pb^{2+} + CO_3^{2-} = PbCO_3^0$	6.478	5.201	0.370	1.82×10^{-12}
$Pb^{2+} + 2CO_3^{2-} = Pb(CO_3)_2^{2-}$	9.938	8.661	2.5×10^{-3}	1.23×10^{-14}
$Pb^{2+} + SO_4^{2-} = PbSO_4^0$	2.69	1.413	0.730	3.55×10^{-12}
$Pb^{2+} + 2SO_4^{2-} = Pb(SO_4)_2^{2-}$	3.47	2.193	0.124	6.11×10^{-13}
$Pb^{2+} + H^+ + CO_3^{2-} = PbHCO_3^+$	13.20	12.562	0.078*	3.85×10^{-13}
	$log^*\beta_i$	$log^{c*}\beta$	$^{c*}\beta_n/[H^+]^n$	
$Pb^{2+} + H_2O = PbOH^+ + H^+$	-7.597	-7.913	1.337	6.59×10^{-12}
$Pb^{2+} + 2H_2O = Pb(OH)_2^0 + 2H^+$	-19.988	-20.304	5.9×10^{-5}	2.91×10^{-16}
$Pb^{2+} + 3H_2O = Pb(OH)_3^- + 3H^+$	-28.091	-28.085	1.1×10^{-4}	5.31×10^{-16}
$Pb^{2+} + 4H_2O = Pb(OH)_4^{2-} + 4H^+$	-39.699	-39.054	1.3×10^{-7}	6.21×10^{-19}
			$\sum = 13.205$	

B. Ligand concentrations (M)

$[Cl^-]$	$[F^-]$	$[Br^-]$	$[SO_4^{2-}]$	$[HCO_3^-]$	$[CO_3^{2-}]$	$[H^+]^\dagger$
0.546	0.0013	0.067	0.0282	1.12×10^{-4}	2.33×10^{-6}	9.14×10^{-9}

*For the bicarbonate complex, this term is $^c\beta_n[L]^n[H^+]$.
†Calculated from pH = 8.2 assuming $\gamma_{H^+} = 0.69$.
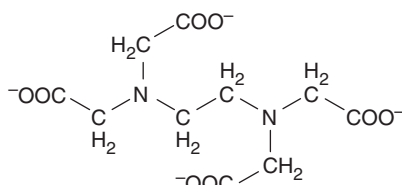
Structure of EDTA:

Not surprisingly, EDTA forms strong complexes with the major divalent metal ions Ca^{2+} and Mg^{2+}, as well as many heavy metal ions, and is used commercially to prevent the precipitation of these ions (e.g, prevent precipitation of fatty acids in food processing). EDTA and related aminopolycarboxylates have been used widely as complexing agents in analytical chemistry. Hardness and its constituents, Ca^{2+} and Mg^{2+}, are still measured by titration with standard EDTA solutions[16] in some water treatment facilities.

As noted earlier, MINEQL+ and other ionic equilibria programs store thermodynamic data (equilibrium constants) as cumulative formation constants. For the

component EDTA^{4-} (Y^{4-}) one finds information on the following species and equilibria in the thermodynamic database:

Name	H+	EDTA^{4-}	LogK	Delta H
H[EDTA] (–3)	1	1	10.948	–5.600
H2[EDTA] (–2)	2	1	17.221	–9.800
H3[EDTA] (–1)	3	1	20.340	–8.500
H4[EDTA]	4	1	22.500	–8.200
H5[EDTA] (+1)	5	1	24.000	–7.700

The first column gives the name and net charge on the species: HY^{3-}, H_2Y^{2-}, H_3Y^-, H_4Y, and H_5Y^+, respectively. The next two columns provide stoichiometric information on the composition of the species in terms of components (in this case H^+ and Y^{4-}). The fourth column gives the log of the cumulative formation constant for each species (log β_i values, but labeled log K in the program), and the fifth column gives the stepwise enthalpy of formation for the reaction, if known, which allows temperature correction of log K (log β). Although EDTA is considered a tetraprotic acid, the "fully protonated" form, H_4Y, can accept still another proton at low pH, becoming the cationic H_5Y^+. Conversion of the cumulative formation constants (log β_i) to conventional acid dissociation constants is straightforward. For example, log K for H[EDTA] in the above list is for the formation reaction

$$H^+ + Y^{4-} \rightleftharpoons HY^{3-} \qquad \log K = 10.948. \qquad (9.19)$$
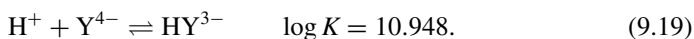
This obviously is just the reverse of the acid dissociation reaction, $HY^{3-} \rightleftharpoons H^+ + Y^{4-}$. Thus $K_{a4} = 10^{-10.948}$, and $pK_{a4} = 10.948$. The information in the second row is for the reaction

$$2H^+ + Y^{4-} \rightleftharpoons H_2Y^{2-} \qquad \log K = 17.221. \qquad (9.20)$$
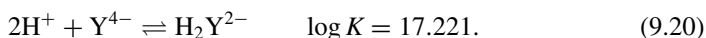
If we subtract Eq. 9.19 from Eq. 9.20, we obtain the stepwise formation reaction

$$H^+ + HY^{3-} \rightleftharpoons H_2Y^{2-} \quad \log K = 6.273 \text{ (i.e., } \log K = 17.221 - 10.948). \qquad (9.21)$$
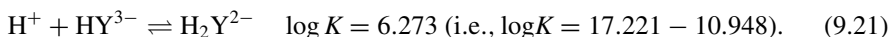
The reverse of Eq. 9.21 is the third acid dissociation constant for EDTA, $K_{a3} = 10^{-6.273}$, or $pK_{a3} = 6.273$. Continuing with this stepwise process leads to $pK_{a2} = 3.119$ (i.e., 20.340 – 17.221) and $pK_{a1} = 2.160$ (i.e., 22.500 – 20.340). Similarly, we find that $pK_{a0} = 1.50$ for the "superprotonated" cationic species H_5Y^+.

The completely deprotonated form Y^{4-} is the preferred ligand for complex formation, especially for metal ions with a coordination number of six, but the partly protonated forms HY^{3-} and to a lesser extent H_2Y^{2-} can form weaker complexes with some metal ions. It is apparent that the extent of complex formation by EDTA depends on pH, and thus it is instructive to consider how EDTA speciation varies with pH.

Although one can use the instructions provided in Table 7.2 to sketch the pH-pC diagram for EDTA, inspection of the pK_a values listed above shows that some are sufficiently close together that we cannot assume the lines are linear (in regions beyond
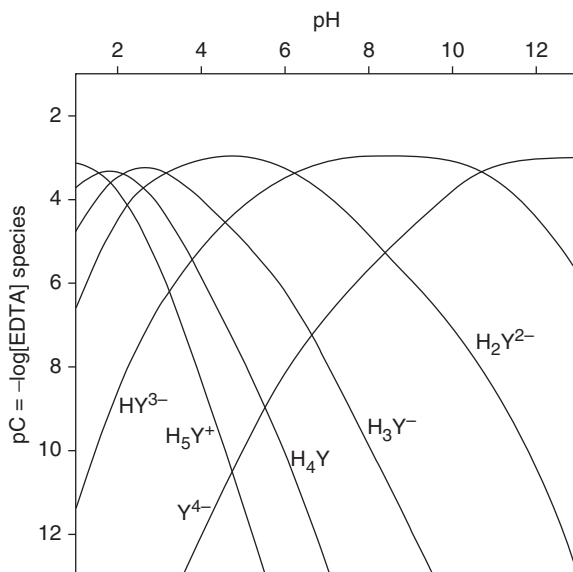
Figure 9.10 pH-pC diagram of 1×10^{-3} M EDTA over the pH range of 1–13. The graph was drawn in Excel using data exported from a multirun series selected in the RunTime Manager of MINEQL+. The run used the "titration mode" with "log K of pH" as titration variable, starting and ending pH values of 1 and 13, and 49 calculation points (every 0.25 pH units). Note that MINEQL+ can produce similar graphs without the need to export the data to a spreadsheet, but the options for editing graphs within MINEQL+ are more limited than those in spreadsheet and graphics programs.

± 1 pH unit of a given pK_a). Consequently, it is easier and more accurate to draw this diagram using the "multirun" capability of computer equilibrium programs. Figure 9.10 shows the result of such an effort and verifies that substantial curvature exists for the species lines at pH < 4. The figure legend provides hints on how to produce the diagram.

Figure 9.10 shows that HY^{3-} is the predominant form of EDTA over the pH range $\sim$6.2–10.9; Y^{4-}, the actual complexing ligand, does not become dominant until the pH exceeds pK_{a4}, or pH > 10.95. This raises a question: over what pH range can one titrate solutions containing Ca^{2+} and still get a sharp endpoint? We note that the standard procedure[16] for measuring water hardness (essentially the sum of Ca^{2+} and Mg^{2+} in most natural waters) calls for titrating water samples buffered to pH 10.0 using a standard EDTA solution. Measurement of Ca^{2+} by itself is achieved by raising the pH to 13, which rapidly precipitates Mg^{2+} as $Mg(OH)_{2(s)}$. Although this high pH causes the solubility of $CaCO_{3(s)}$ to be exceeded, it does not precipitate as rapidly as $Mg(OH)_{2(s)}$.

We can approach an answer to the above question at least semi-quantitatively by performing simulated titrations of Ca^{2+} using MINEQL+ at pH 10 and a few other values and plotting the results. Figure 9.11 illustrates titrations of 1.0×10^{-3} M Ca^{2+} (or 40 mg/L as Ca, a typical concentration for "hard water") at pH values of 5.0, 7.0, and 10.0. Similar to Figure 9.10, Figure 9.11 was generated by exporting the output from MINEQL+ into Excel; details on how the simulation was
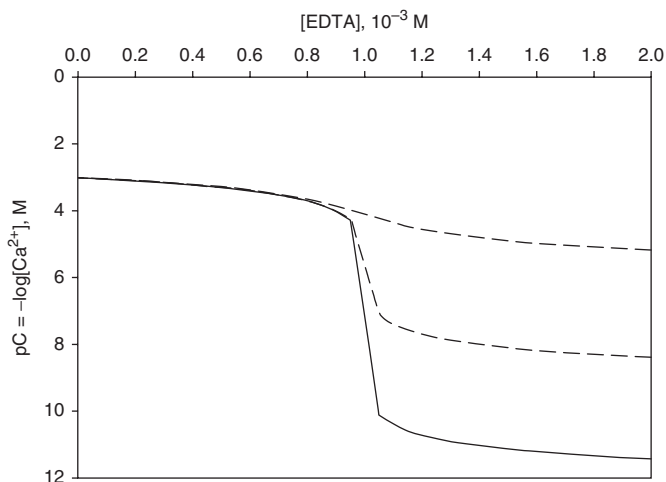
Figure 9.11 Simulated titrations of Ca^{2+} with EDTA at three pH values based on MINEQL+ calculations. Starting conditions for the multiruns were $[Ca^{2+}] = 1.0 \times 10^{-3}$ M; $[EDTA^{-4}] = 0.0$; and pH fixed at one of the three values in the figure. In the RunTime Manager screen, the multirun titration mode was specified, and total concentration of EDTA was selected as the titration variable, with starting and ending values of 0 and 2.0×10^{-3} M and 40 increments of 5×10^{-5} M EDTA.

programmed are in the figure legend. It is apparent from the figure that titration at pH 5 is infeasible because there is no large inflection point in the curve near the equivalence point. In contrast, the activity of free Ca^{2+} decreases dramatically at the equivalence point for titration at pH 10, and the decrease is substantial even at pH 7. Analysis of the computer output from the simulations for EDTA increments just before, at, and just after the equivalence point yields the following values for $\{Ca^{2+}\}$:

[EDTA], M	pH 10	pH 7	pH 5
0.00095	4.99×10^{-5}	5.01×10^{-5}	1.06×10^{-4}
0.00100	6.12×10^{-8}	2.01×10^{-6}	7.77×10^{-5}
0.00105	7.51×10^{-11}	8.00×10^{-8}	5.74×10^{-5}

These results suggest that the decrease in $\{Ca^{2+}\}$ around the equivalence point is large enough to make the titration feasible at pH 10 and 7 but not at pH 5. However, the increments of titrant EDTA used to generate Figure 9.11 were rather large (5×10^{-5} M, or 5% of the initial $[Ca^{2+}]$), which is equivalent to 0.5 mL additions of 0.010 M EDTA to a 100 mL sample containing Ca^{2+}, the typical condition for such titrations in analytical laboratories. A better test of the sharpness of the endpoint (i.e., extent of decrease in $\{Ca^{2+}\}$ near the equivalence point) would be to compare $\{Ca^{2+}\}$ values exactly at the equivalence point and after one additional drop ($\sim$0.05 mL) of titrant. This is equivalent

to adding 5×10^{-6} M EDTA after the equivalence point. Rerunning MINEQL+ for this amount of titrant yields the following values:

[EDTA], M	pH 10	pH 7	pH 5
0.001000	6.12×10^{-8}	2.01×10^{-6}	7.77×10^{-5}
0.001005	7.51×10^{-10}	7.02×10^{-7}	7.53×10^{-5}

At pH 10, one drop of titrant thus decreases $\{Ca^{2+}\}$ by two orders of magnitude, but the decrease at pH 7 is only about a factor of three. Thus it is doubtful whether one could obtain accurate results in titrations of Ca^{2+} by EDTA at pH 7. Similar analyses could be done at pH 8 and 9.

9.5.4 Zinc cyanide complexes

Cyanide ion (CN^-), a moderately strong ligand with transition metal ions and Class B metal ions (Section 9.3.1), is widely used in metal plating and mining operations, and treatment of industrial and mining wastes containing heavy metals like zinc, copper, and cadmium complexed with cyanide has been an interest of environmental engineers for many decades. With $C_N = 4$, Zn^{2+} forms four stepwise complexes with CN^-, as well as two mixed-ligand complexes involving CN^- and OH^-: $ZnCN^+$, $Zn(CN)_2^0$, $Zn(CN)_3^-$, $Zn(CN)_4^{2-}$, $ZnOH(CN)_2^-$, and $ZnOH(CN)_3^{2-}$. Removal of the last four complexes from wastewater can be achieved using anion exchange resins. Because HCN is volatile and highly toxic to humans, industrial operations using cyanide usually are done at high pH ($\geqslant 10$; pK_a for HCN is 9.21). Consideration of the acid-base chemistry of cyanide thus must be included in any analysis of metal-cyanide speciation.

The uncharged species $Zn(CN)_2^0$ possibly could be separated from the ionic complexes by a membrane or solvent-extraction process. For the sake of this example we will assume that the uncharged species is soluble in some nonaqueous solvent but the ionic forms are not. One simple question regarding the feasibility of such approaches concerns the conditions, if any, under which the uncharged species may predominate in solutions containing zinc and cyanide. When a computer run was formulated to examine this question, the authors found that MINEQL+'s thermodynamic database did not include information on zinc cyanide complexes. VMINTEQ includes data for the simple Zn^{2+}-CN^- complexes but not for mixed-ligand (OH^-/CN^-) complexes. An Internet search for information on zinc cyanide complexes produced many links, including recent papers on removal of zinc cyanide complexes from waste streams by ion exchange.[17–19] It is easy to insert new data into MINEQL+'s thermodynamic database; Table 9.7 shows the format of the input data for the six cyanide complexes. Once the data are entered, they can be saved permanently using the File menu. Because the (type I) components that make up the complexes (Zn^{2+} and CN^-) already exist in MINEQL+'s database, there was no need to add components, and the species were added in the "Type II-Aqueous Species" tableau using the "Insert" tool.

With the required thermodynamic data now in the program, we can address the question about $Zn(CN)_2^0$. Using $Zn_T = 1 \times 10^{-3}$ M, we varied $[CN^-]$ from 0 to 5×10^{-3} M at increments of 2×10^{-4} M at pH 10.0 and plotted the results (Figure 9.12). The results show that $[Zn(CN)_2^0]$ reaches a maximum of 56% of Zn_T at $[CN^-] = 2.0 \times 10^{-3}$ M, that is, when the $Zn:CN^-$ ratio is the same as the stoichiometry of the complex.

Table 9.7 Format for addition of zinc cyanide complexes to MINEQL+ thermodynamic database via the Type II-Aqueous Species tableau

Name	H_2O	$H(+)$	$CN(-)$	$Zn(2+)$	$Log\ K^*$
ZnCN (+)	0	0	1	1	5.34
Zn(CN)$_2$	0	0	2	1	11.97
Zn(CN)$_3$ (−1)	0	0	3	1	16.05
Zn(CN)$_4$ (−2)	0	0	4	1	19.62
ZnOH(CN)$_2$ (−1)	0	−1	2	1	0.71
ZnOH(CN)$_3$ (−2)	0	−1	3	1	4.08

Values from Osathaphan et al.[17] Some uncertainties exist in the literature, especially for log β_4; for example, Solis et al.[18] reported a range of 18.62–20.73 for log β_4, and Kim et al.[19] used log β_4 = 21.57. The value used here is that reported[17] for I → 0.
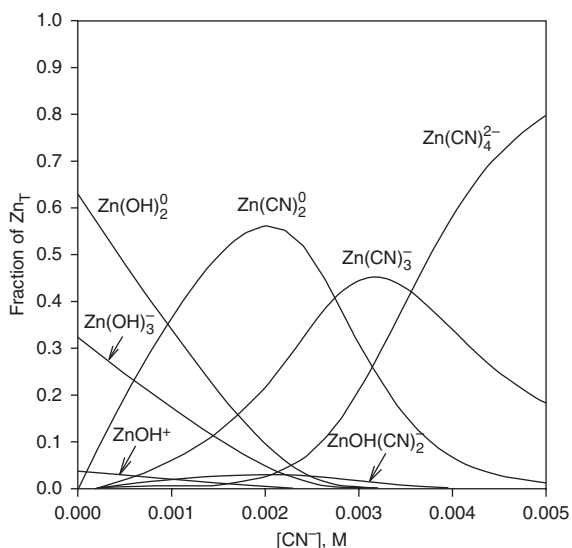
Figure 9.12 Speciation of zinc complexes with cyanide and hydroxide at pH 10.0 versus [CN$^-$] for Zn$_T$ = 1 × 10^{-3} M: results from a MINEQL+ multirun titration at [CN$^-$] in increments of 2 × 10^{-5} M.

Thus, it might be feasible to remove some zinc cyanide from waste streams by membrane-based or solvent extraction processes, but it would not be quantitative, and the Zn:CN$^-$ ratio would need to be controlled to the optimum value of 2.0.

Osathaphan et al.[17] reported successful removal of zinc cyanide complexes from water at pH 10 and 12 by anion exchange resins. They found essentially no breakthrough of soluble Zn from exchange columns for up to 300 bed volumes of waste water passed through the columns. Slight differences noted in the capacities of the columns to remove Zn at the two pH values were attributed differences to changes in Zn speciation with CN$^-$. To evaluate these differences, we calculated the speciation of zinc cyanide systems over a range of pH using Zn$_T$ and CN$_T$ concentrations similar to those used in the column experiments. The results (Figure 9.13) show that Zn(CN)$_4^{2-}$ is by far the predominant Zn species both at pH 10 (93.3%) and at pH 12 (87.3%). Zn(CN)$_3^-$ is the second-most important species at pH 10 (6.1%), but at pH 12 the mixed-ligand complex ZnOH(CN)$_3^{2-}$ assumes that status (6.6%), while Zn(CN)$_3^-$ constitutes 4.5%.
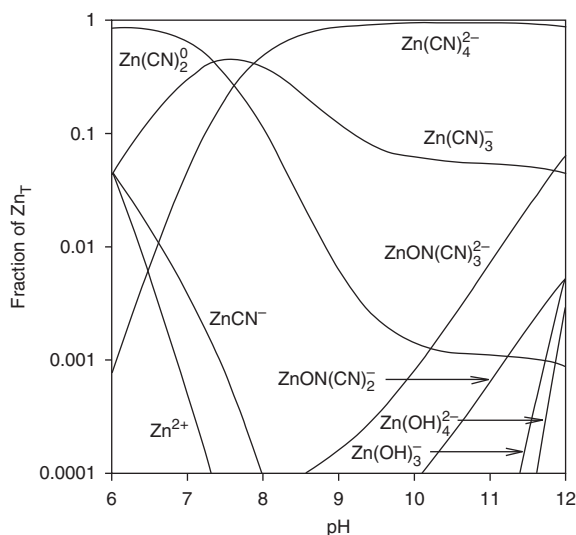
Figure 9.13 Speciation of Zn from pH 6 to 12 for $Zn_T = 1.5 \times 10^{-3}$ M and $CN_T = 1 \times 10^{-2}$ M: graph drawn in Excel using data from a MINEQL+ multirun selected using the titration mode with "log K of pH" as "titration" variable, starting and ending values of 6 and 12, and 25 calculation points (every 0.25 pH units).

The uncharged Zn species, $Zn(OH)_2^0$ and $Zn(CN)_2^0$, constitute negligible fractions of Zn_T at both pH values (~0.01 and < 0.1%, respectively), and cationic complexes and free Zn^{2+} are even less important. Consequently, differences in Zn speciation between pH 10 and 12 are small, and the dominant forms of Zn are anionic complexes. The similarity of removal patterns by anionic exchange resins at the two pH values thus is not surprising; indeed, it is difficult to see how the very small differences in speciation would cause any differences in removal by anionic resins.

9.6 Role of complexation in the speciation of cations and anions in natural waters

9.6.1 Major inorganic ions

As noted in the introduction to this chapter, aquo-complexes are the "default condition" for all metal cations dissolved in water. From that perspective, it is obvious that complexation is a fundamentally important phenomenon in aquatic systems. Anions and uncharged ligands like NH_3 do not form chemical bonds with solvent water molecules although weak van der Waals and dipole interactions occur between them. Here we are interested in examining the extent to which metal ions form soluble complexes with anions and uncharged ligands *other than H_2O* in natural waters. We start with the major ions: $Ca^{2+}, Mg^{2+}, Na^+, K^+, HCO_3^-$ and CO_3^{2-}, Cl^-, and SO_4^{2-}. For sake of completeness, we also consider OH^-, which becomes increasingly important as pH increases.

Based on the classification systems for metals in Table 9.1, we note that the four major cations in natural waters are class A (or hard acid) cations. Consequently, we can predict that they tend to form relatively weak electrostatic bonds with ligands. We also can predict that they will form stronger complexes with F^- than with Cl^-, but because F^- concentrations typically are low compared with Cl^- concentrations, we would not expect

fluoro-complexes to be important. Based on the Fuoss model for stability constants of *os* complexes (see Section 9.2.2 and Eq. 9.3), we should expect stability constants for the monovalent cations Na^+ and K^+ with monovalent anions (Cl^-, HCO_3^-, OH^-) to be around $K_f = \sim 1$. Corresponding values for the divalent cations Ca^{2+} and Mg^{2+} with divalent anions (SO_4^{2-}, CO_3^{2-}) should be $\sim 2 \times 10^2$. Stability constants for divalent cations with monovalent anions and for monovalent cations with divalent anions should be somewhere in the middle of the range of 1–200. These are all small values for stability constants, and this allows us to make three important predictions. First, the major ions should exist primarily as free (hydrated) cations and free anions rather than as complexes with each other in natural waters. Second, to the extent that complexation occurs, it should be more important as ionic strength increases. Third, complexation should be more important for divalent ions than for monovalent ones. The accuracy of these predictions is assessed in the following paragraphs, which describe the results of chemical speciation modeling on a range of typical freshwaters and seawater (Tables 9.8 and 9.9).

Inspection of the results in Table 9.8 for three freshwaters—a very dilute, softwater lake, a hardwater lake, and average North American river water—shows that complexation of the major cations by the major anions (including CO_3^{2-} and OH^-) is not an important factor in speciation of the ions. Chloride has almost no tendency to form complexes with major cations, and MINEQL+ does not have equilibrium constants for Cl^- with the major cations. In general, fluoride, carbonate, and hydroxide are not important ligands for the major cations at the concentrations and pH of the three freshwaters. Although the extent of complexation is small, it does increase with ionic strength (represented here by specific conductance). In Little Rock Lake, with a composition and conductivity approaching that of rainfall, 99–100% of the major cations and anions occur as free ions. Even in hard-water Lake Harriet, 95–100% of the four major cations and 85–100% of the anions are present as the free ions. Ca^{2+} is the major cation with the largest fraction in complexed forms; $CaHCO_3^-$ constitutes $\sim 2.7\%$ of the total dissolved calcium, and $CaSO_4^0$ almost 1%. Among the anions, only $\sim 85\%$ of the sulfate is in free form; more than 10% of the sulfate is present as $CaSO_4^0$, and another 4% occurs as $MgSO_4^0$. Although average North American river water is more dilute and has lower hardness than Lake Harriet, complexation trends generally are similar in the two waters.

Overall, complexation of major ions is more important under the much higher ionic concentrations found in seawater (Table 9.9). As with the two hard-water samples in Table 9.8, OH^- and F^- are unimportant ligands, especially for the monovalent cations, and Cl^- remains 100% free. Na and K still are mostly ($\sim 98\%$) present as the free cations, but the two divalent cations, Ca^{2+} and Mg^{2+}, are only ~ 84 and $\sim 87\%$ free. Strontium, also a major ion in seawater ($Sr_T = 8.1$ mg/L or 9.24×10^{-5} M), is only $\sim 86\%$ free. The dominant ligand for all three divalent cations is sulfate (12–15% for each divalent cation), and the effect on sulfate speciation is startling: only 43% if SO_{4T}^{2-} is present in seawater as the free anion. Although the fractions of the cations occurring as complexes with HCO_3^- is small (<1% in each case), the net effect on the relatively low value of HCO_{3T}^- is significant; only 91% of the HCO_3^- is free. Complexation is much more important for CO_3^{2-}; only 14.5% of the carbonate in seawater is free, and the majority ($\sim 68\%$) is complexed with Mg and Na. Similarly, the low total concentration of F^- prevents it from complexing significant fractions of the major cations, but complexation is important in fluoride speciation; only 11% of the F_T is present as the free anion.

Table 9.8 Speciation of major ions in three freshwater systems determined by MINEQL+*

Cations	M^{z+}	MOH	$MHCO_3$	MCO_3	MSO_4	MF	MCl	Anions	X^{z-}
Little Rock Lake, Wisconsin: pH = 6.16; SC = 12.4 μS cm^{-1}									
Na	7.83E-6 (100)	— —	9.58E-11 (1E-3)	2.18E-13 (3E-6)	1.12E-9 (0.01)	5.03E-12 (6E-5)	— —	HCO_3^-	2.24E-5 (100)
K	1.53E-5 (100)	— —	— —	— —	2.89E-9 (0.02)	— —	— —	Cl^-	1.04E-5 (100)
Mg	1.18E-5 (99.2)	6.57E-11 (6E-4)	2.56E-9 (0.02)	1.39E-11 (1E-4)	5.42E-8 (0.5)	1.31E-9 (0.01)	—	SO_4^{2-}	2.82E-5 (99.3)
Ca	2.08E-5 (99.2)	5.8E-12 (3E-5)	8.2E-9 (0.03)	4.67E-11 (2E-4)	1.2E-7 (0.6)	2.25E-10 (1E-3)	—	F^-	1.05E-6 (100)
Average North American River Water: pH = 7.20; SC = 220 μS cm^{-1}									
Na	3.65E-4 (100)	— —	2.17E-7 (0.06)	5.66E-9 (2E-5)	2.67E-7 (0.07)	— —	— —	HCO_3^-	1.19E-3 (99.2)
K	3.84E-5 (100)	— —	— —	— —	3.7E-8 (0.1)	— —	— —	Cl^-	2.60E-3 (100)
Mg	1.96E-4 (97.0)	1.05E-8 (5E-3)	1.9E-6 (0.9)	1.08E-7 (0.05)	3.87E-6 (1.9)	— —	— —	SO_4^{2-}	1.71E-4 (91)
Ca	5.07E-4 (95.8)	1.36E-9 (3E-4)	8.92E-6 (1.7)	5.33E-7 (0.1)	1.26E-5 (2.4)	— —	— —		
Lake Harriet, Minnesota: pH = 7.30; SC = 484 μS cm^{-1}									
Na	2.17E-3 (99.7)	— —	2.18E-6 (0.1)	7.37E-8 (3E-3)	6.61E-7 (0.03)	8.64E-9 (4E-4)	— —	HCO_3^-	2.13E-3 (98.3)
K	1.43E-4 (100)	— —	— —	— —	5.73E-8 (0.04)	— —	— —	Cl^-	2.74E-3 (100)
Mg	5.22E-4 (97.5)	3.21E-8 (6E-3)	8.01E-6 (1.5)	5.58E-7 (0.1)	3.79E-6 (0.7)	3.1E-7 (0.06)	—	SO_4^{2-}	8.04E-5 (85.8)
Ca	9.60E-4 (96.2)	2.96E-9 (3E-4)	2.68E-5 (2.7)	1.96E-6 (0.2)	8.78E-6 (0.9)	5.55E-8 (6E-3)	—	F^-	7.51E-6 (95.2)

*Rows with numbers in parentheses represent percentages of the total (analytical) concentrations of the cations and anions. Other numbers are molar concentrations. See Table 2.3 for the analytical concentrations of ions in these water bodies and sources of the data. No information was available on the fluoride content of average North American river water.

Table 9.9 Speciation of major ions in seawater at pH = 8.20 and I = 0.699 calculated by MINEQL+*

Cations	M^{+z+}	MOH	$MHCO_3$	MCO_3	MSO_4	MF	MCl	Anions	X^{z-}
Na	4.62E-1	—	2.13E-4	7.39E-5	7.65E-7	8.64E-9	—	HCO_3^-	2.13E-3
	(98.4)	—	(4.5E-2)	(1.6E-2)	(1.6)	(1.8E-6)	—		(91.0)
K	9.81E-3	—	—	—	2.14E-4	—	—	Cl^-	5.47E-1
	(97.9)	—	—	—	(2.1)	—	—		(100)
Mg	4.61E-2	1.05E-2	1.96E-4	8.4E-5	6.59E-3	3.1E-7	—	SO_4^{2-}	1.21E-2
	(86.9)	(2E-2)	(0.37)	(0.16)	(12.4)	(5.8E-4)	—		(43.0)
Ca	8.60E-3	9.81E-8	6.64E-5	2.98E-5	1.55E-3	5.55E-8	—	F^-	7.51E-6
	(83.9)	(9.6E-4)	(0.65)	(0.29)	(15.1)	(5.4E-4)	—		(11.0)
Sr	7.93E-5	3.0E-10	5.33E-7	1.12E-7	1.24E-5	1.96E-9	—	CO_3^{2-}	3.38E-5
	(85.8)	(3.2E-4)	(0.58)	(0.12)	(13.4)	(2.1E-3)	—		(15.1)

*For starting composition (analytical concentrations of the cationic and anionic components, see Table 2.5) Rows with numbers in parentheses represent percentages of the total (analytical) concentrations of the cations and anions. Other numbers are molar concentrations.
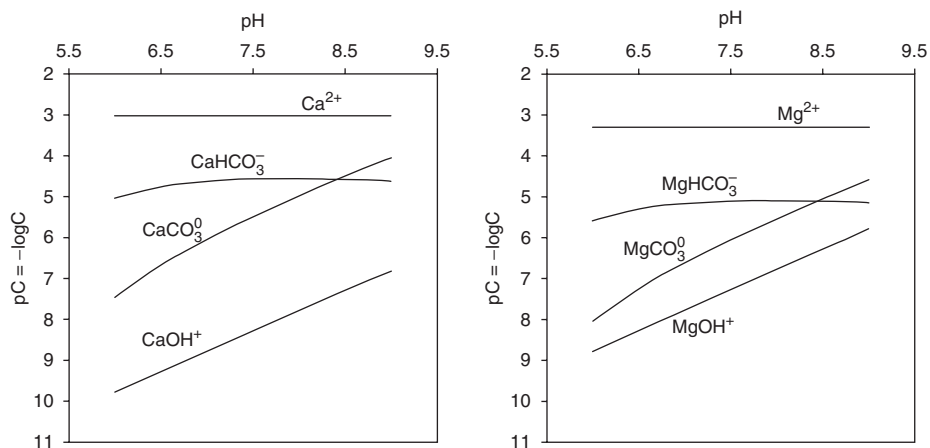
Figure 9.14 pH-pC diagrams showing the importance of hydroxo-, bicarbonato-, and carbonato-complexes of the major divalent cations in natural waters: Ca and Mg. In both cases, the free cations predominate over the pH range for most natural waters (6.0–9.0): $Ca_T = 1 \times 10^{-3}$ M; $Mg_T = 5 \times 10^{-4}$ M; $C_T = 2 \times 10^{-3}$ M. Calculations were performed by MINEQL+. Note that the solubility of calcite is exceeded above pH ~7.7 for the Ca_T and C_T used to draw the figure. All solids were prevented from precipitating (i.e., they were made type VI species) in the MINEQL+ runs.

In a seminal paper from the early days of water chemistry, Garrels and Thompson[5] modeled the major ion speciation in seawater and quantified what they termed "ion-pair" complexation. The values in Table 9.9 differ slightly from Garrels and Thompson's findings because of refinements in stability constants for CO_3^{2-}, HCO_3^-, and SO_4^{2-}, but the trends they described have held up remarkably well.

The results in Tables 9.8 and 9.9 represent "snapshots" of the major ion speciation at a single pH for each water. Because concentrations of the carbonate species and hydroxide are pH-sensitive within the pH range of natural waters, it is useful to examine how pH affects metal ion speciation. Figure 9.14 illustrates these trends for Ca^{2+} and Mg^{2+} over the pH range 6–9, in which most natural waters occur. Values of Ca_T, Mg_T, and C_T used for the figures are typical of moderate hard waters—1×10^{-3} M and 5×10^{-4} M (40 and 12.1 mg/L) for Ca_T and Mg_T, respectively, and 2×10^{-3} M (100 mg/L as $CaCO_3$) for C_T.

The figures show that the free metal ions dominate over the entire pH range. Complexation patterns are similar for both metals, but a few differences are notable. In both cases, the bicarbonato-complex is the second most abundant species up to pH ~8.5, but the carbonato-complex then becomes more important. At its maximum, $CaHCO_3^+$ represents only 3% of Ca_T, and $MgHCO_3^+$ represents even less (1.6%) of Mg_T. At pH 9.0, $CaCO_3^0$ reaches 9% of Ca_T (assuming no precipitation occurs), and $MgCO_3^0$ reaches 5% of Mg_T. The hydroxo-complexes are minor for both metal ions over the entire pH range but more important for Mg than for Ca. Conversely, the carbonato-complexes are more important for Ca, which agrees with the trends in solubility controls, Ca being limited by $CaCO_{3(s)}$ and Mg by $Mg(OH)_{2(s)}$.

9.6.2 Inorganic complexes of minor and trace metals

We start by acknowledging that complexation is much more important in the speciation of minor and trace metals in natural waters than it is for the major cations. Hydroxo-complexes are important for many minor and trace metals, especially trivalent ions like Al^{III} and Fe^{III}. Metal ion hydroxides are formed by hydrolysis—essentially acid-base reactions,

$$M(H_2O)_n^{z+} \rightleftharpoons M(H_2O)_{n-1}OH^{z-1} + H^+, \,^* K_1 \qquad (9.22)$$
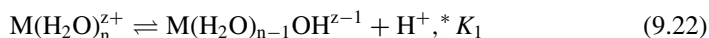
—rather than by reaction of free metal ions with hydroxide ligands, but the net effect, formation of hydroxide complexes, is the same. As Stumm and Morgan[13] noted, the acidity of hydrated water molecules can be much greater than that of bulk solution water, and the acidity of hydrated water varies greatly among cations. As Figure 9.15 illustrates, useful trends in acidity, expressed in terms of $^*K_1$, are related to the term z/d (ratio of charge to metal ion diameter),[20] which is analogous to the polarizing power of the cation (z^2/r) described earlier (see Figure 9.4). Four groups of cations can be distinguished based on the trends in log $^*K_1$ versus z/d. Relative to their size and charge, the group furthest to the right consists of the cations most likely to form ionic M–O bonds; i.e., they are relatively strong base cations. The groups to the left have stronger tendencies to form covalent M–O bonds and tend to hydrolyze according to Eq. 9.8. Within any group, a wide range of log $^*K_1$ values are found, and in all cases the metal ions with the largest negative values are the strongest bases; i.e., they have the smallest tendencies to hydrolyze to form M–OH complexes. In agreement with the trend noted for hydroxo-complexes of the major divalent ions in Figure 9.14, log $^*K_1$ is more negative for $Ca^{2+}(-12.4)$ than $Mg^{2+}(-11.4)$. Values of log $^*K_1$ for many divalent transition
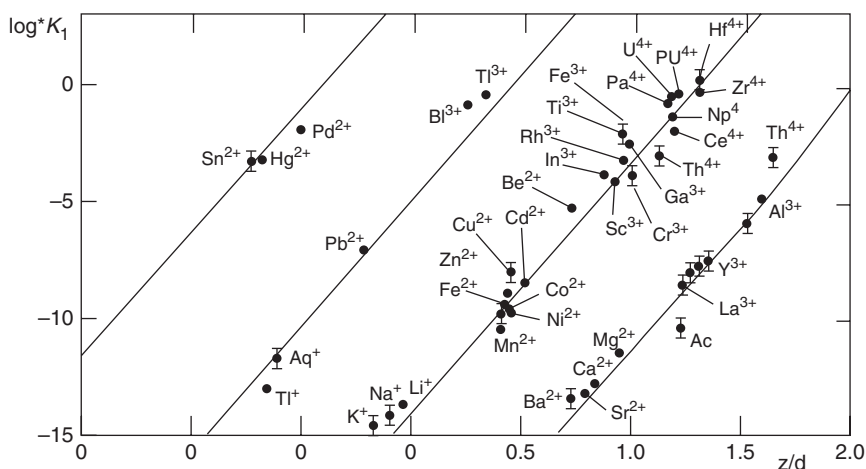
Figure 9.15 Relationship between the first hydrolysis constant, $^*K_1$, of metal ions and the ratio of charge to M–O distance (z/d) for four groups of cations. Note the change in abscissa zero for the different groups. From Baes and Mesmer,[20] copyright 1976, and used with permission of John Wiley & Sons.

metals are less negative than those for Ca^{2+} and Mg^{2+} (e.g., $Cu^{2+} - 7.5$; Zn^{2+}, -9.0; Fe^{2+}, -9.4; Co^{2+}, -9.7; Mn^{2+}, -9.6), suggesting that hydroxo-complexes are more important for these metals in the pH range 6–9 than we found for Ca^{2+} and Mg^{2+}.

We cannot possibly describe all combinations of complexation of minor and trace metals by inorganic ligands in natural aquatic systems; the diversity of metals, ligands, and conditions such as pH and ionic strength are far too great for that. Instead, we illustrate trends over the pH range of 6.0–9.0 in seawater using four heavy metals of interest in aquatic systems that have starkly differing complexation trends with major inorganic ligands: Cu^{II}, Zn^{II}, Pb^{II}, and Cd^{II} (Figure 9.16). The first two metals are important as trace nutrients, but at higher concentrations they are toxic to aquatic organisms. The latter two metals are not nutrients at any concentration, and the primary interest in them relates to their toxicity to humans.
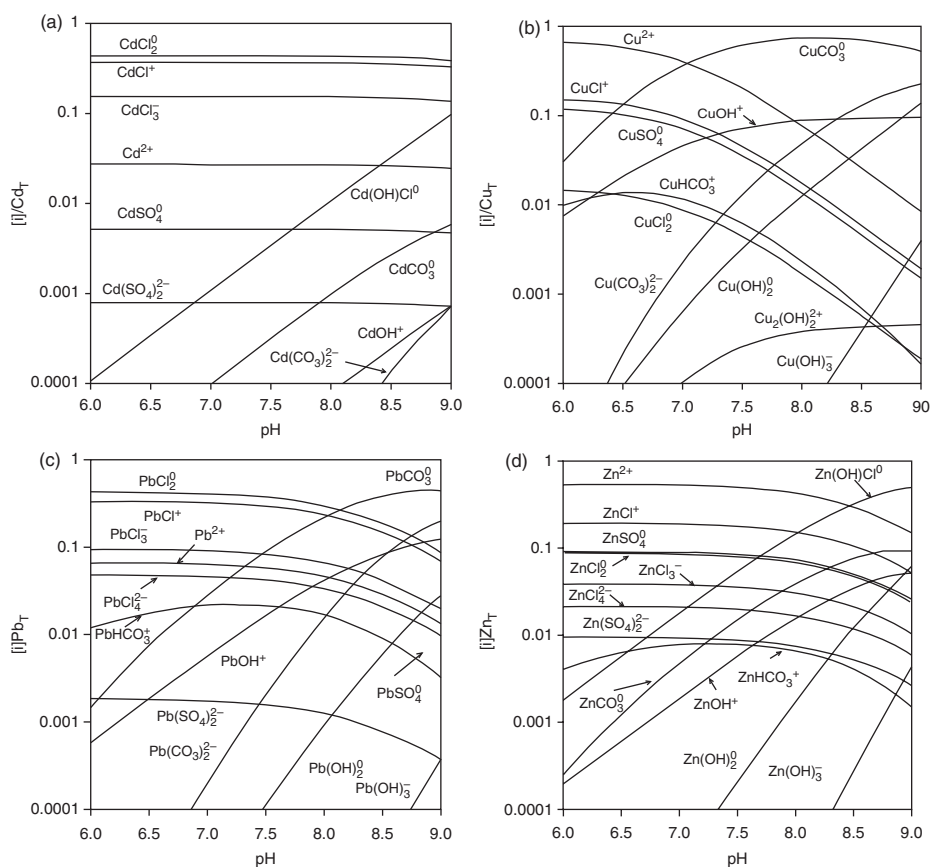
Figure 9.16 pH-pC diagrams of four divalent heavy metals, Cd (a), Cu (b), Pb (c), and Zn (d), in seawater over the pH range of 6.0–9.0. Ordinates represent the fractions of the total metal present as individual species (note logarithmic scale). $M_T = 1 \times 10^{-6}$ M in each case, and the seawater composition in Table 2.5 was used as the input condition for MINEQL+.

Cadmium, a class B (soft) metal ion, forms strong complexes with Cl^-, and three forms ($CdCl_2^0$, $CdCl^+$, and $CdCl_3^-$) together account for $> 95\%$ of Cd_T in seawater over the entire pH range. Free Cd^{2+} is only $\sim 2.7\%$ of Cd_T, and the next most abundant species ($CdSO_4^0$) constitutes only 0.5% of Cd_T. Because no pH-dependent species is important, Cd speciation changes very little over the pH range 6.0 to 9.0. Chloro-complexes also dominate Pb^{II} speciation over pH 6.0–8.0, but the carbonato-complex gradually increases to become dominant at pH > 8.1; by pH 9.0 it represents 43% of Pb_T. The dicarbonato-complex ($Pb(CO_3)_2^{2-}$) also rises rapidly to constitute 20% of Pb_T at pH 9.0. $PbOH^+$ is the third-most abundant species at pH 9.0 (12.5% of Pb_T). The speciation of Pb^{II} in seawater thus varies markedly with pH, shifting from chloro dominance at low pH to dominance by CO_3^{2-} and OH^- at high pH.

The complexation patterns for Cu^{II} differ from those of Cd^{II} and Pb^{II}. Free Cu^{2+} dominates at low pH but cedes that status to $CuCO_3^0$ just above pH 7.0. This species reaches a maximum of $\sim 75\%$ of Cu_T near pH 8.0 and maintains its dominance to pH 9.0. $CuOH^+$ (8.8%) is the second-most abundant species at pH 8.0, and free Cu^{2+} is close behind (7.7%). Chloro-complexes are much less important for Cu^{II} than for Cd^{II} and Pb^{II}. $CuCl^+$ is the second-most abundant Cu^{II} species (15%) at pH 6.0 (followed by $CuSO_4^0$ at 12%), but both decline with increasing pH as the carbonato- and dicarbonato-complexes grow in importance.

Zn^{II} presents still another speciation pattern. Of the four metals, it is the least complexed in seawater, and Zn^{2+} is the dominant species from pH 6.0 (56%) to pH ~ 8.4, where the mixed ligand complex $ZnOHCl^0$ begins to dominate. The chloro- ($\sim 20\%$) and sulfato- ($\sim 10\%$) complexes are the second and third most important species up to pH ~ 7.5–7.8, and the carbonato- and hydroxo-complexes are of minor importance until pH approaches 9.0. Because C_T in seawater is not very different from C_T in calcareous (limestone-rich) watersheds and aquifers, the trends for carbonato and hydroxo species shown in Figure 9.16 are similar to the trends we would expect in many freshwater systems. However, because seawater is much higher in Cl^- and SO_4^{2-} than freshwaters, the chloro- and sulfato-complexes of the four heavy metals should be much less important in the latter systems.

9.6.3 Metal complexation by organic ligands in natural waters

As a general rule, low-molecular-weight organic ligands are not very important in complexation of major, minor, or trace metals in many natural waters. This may seem surprising given that many strong organic chelating agents are known. Thus, it is important to explain the basis for this statement and note the exceptions to the rule. First, we note that stability constants for organic ligands like mono- and dicarboxylic acids are relatively small (log β_1 typically are in the range of 1–5; see Table 9.2), and their concentrations in natural surface waters (e.g., rivers, lakes) are very low ($<< 1~\mu M$) because they are easily are metabolized by aquatic microorganisms. Rearranging the general stability constant expression, we can write: $\beta_1[L] = [ML]/[M]$. Using the above range of values for β_1 and [L], we predict that [ML]/[M] generally is $<< 0.1$ for small carboxylic acids. Bidentate free amino acids, which in some cases have higher log β_1 values, also are found in natural waters generally only at nanomolar concentrations (see Section 16.2.4), and these also are not high enough to dominate the speciation of major or trace metal ions. A few amino acids (e.g., serine, lysine, glycine, alanine) are found at

Table 9.10 Complexation of Cu and Zn with the amino acid serine under freshwater conditions

Input: pH = 7; $[Ca^{2+}] = C_T = 1 \times 10^{-3}$ M; I = 2×10^{-3};
$Cu_T^{II} = 2 \times 10^{-8}$M; $Zn_T^{II} = 1 \times 10^{-7}$; [Serine] = 2×10^{-8}M

Output:	Species	Conc. (M)	% of M_T or L_T
	Cu^{2+}	3.7×10^{-9}	18.5
	$CuSer^-$	8.49×10^{-9}	42
	$Cu(Ser)_2$	1.08×10^{-10}	0.5
	Zn^{2+}	9.5×10^{-8}	95
	$ZnSer^-$	1.7×10^{-10}	0.17*
	$Zn(Ser)_2$	3.5×10^{-14}	3E-5
	Ser^-	1.1×10^{-8}	55

*Value increased to 0.3% when Cu_T was set to zero.

concentrations that potentially affect the speciation of some trace metals. For example, log K_f values for Cu^{2+} and Zn^{2+} with serine are 8.4 and 5.3 (ML) and 14.5 and 9.6 (ML$_2$), respectively.[21] Insertion of these values into the MINEQL+ thermodynamic database yielded the results summarized in Table 9.10 for some hypothetical (but reasonable) concentrations of the metal ions and serine in a typical freshwater, which indicate significant binding of Cu but only minor effects on Zn speciation. Several other amino acids (e.g., alanine, glycine, aspartic acid) have similar K_f values with Cu^{2+} and Zn^{2+},[21] and so the results in Table 9.10 have more general applicability.

Several other important exceptions can be cited. Waters with high concentrations of dissolved organic matter (DOM), such as municipal wastewaters, have high concentrations (perhaps approaching millimolar values) of small organic ligands like amino acids and organic acids arising from microbial metabolism and also much higher concentrations of various heavy metals. In addition, polluted waters commonly have significant concentrations of strong chelating agents like EDTA, which is widely used in food and consumer products. EDTA is found in wastewater at concentrations of around 100–1000 µg/L (~0.3–3.0 µM).[22]

Another exception is the class of natural compounds called siderophores, which have extremely high binding constants with Fe^{III} (in some cases >> 10^{20}). These ligands are excreted into natural waters by microorganisms (fungi and bacteria, including some cyanobacteria) that synthesize them as a means of scavenging Fe, an essential but very insoluble element, from water. Although siderophores as a class constitute a diverse set of structures (Figure 9.17), most of them share the feature of being hexadentate oxygen ligands that form octahedral complexes with Fe^{3+}. The strongest siderophores (e.g., enterobactin and ferrichrome) have three bidentate ligands per molecule. Many studies have found siderophores in the surface waters of the oceans, where they are thought to play important roles in chelating highly insoluble Fe^{III}. Concentrations of dissolved Fe in the open oceans are so low that they limit the rate of primary production. For example, 99.97% of the dissolved Fe^{III} in central North Pacific surface waters was found to be chelated by natural organic ligands (siderophores) present at a total concentration of ~2 nM (much greater than ambient dissolved Fe concentrations).[23]

Figure 9.17 Structures of some common types of iron-complexing siderophores: (a) desferrioxamine B (also called desferal), a hydroxamate; (b) enterobactin, a catecholate (structure on left shows that the three catechol rings serve as actual ligands with Fe^{3+}); (c) ferrichrome, a cyclic hexapeptide formed by three glycine and three modified ornithine molecules.

Similarly, Mawji et al.[24] recently found two hydroxamate siderophores in Atlantic Ocean surface waters to be widely distributed at 3–20 pM levels (a few percent of the Fe in 0.2-μm-filtered seawater). Although the primary function of siderophores is thought to be iron mobilization, the actions of these chelating agents are not specific to Fe. They form strong complexes with Mn^{III} and play a role in the coupled biogeochemical cycles of Mn and Fe.[25] In addition, siderophores excreted by cyanobacteria (formerly called blue-green algae) form strong complexes with Cu^{II} in lake water, and it was speculated that most of the dissolved Cu in lakes with blooms of iron-limited cyanobacteria is chelated by siderophores.[26]

Although small, relatively simple organic compounds usually are not important ligands in natural waters, DOM and especially aquatic humic substances (AHM) are important binding agents for trace heavy metals in natural aquatic systems. The responsible components of DOM and AHM are complicated mixtures of macromolecules, and accurate description of metal complexation by them requires more complicated approaches than the simple stability constant approach used in this chapter. Aquatic

scientists have struggled for decades to develop modeling techniques that balance the reality of DOM and AHM as complicated mixtures with the need for tractable approaches. This subject is treated in Chapter 18.

9.7 Kinetics of complexation reactions

Rates of complexation reactions span many orders of magnitude. Many reactions of environmental interest are essentially instantaneous, but some reach equilibrium on timescales of months or even years. Consequently, we need to consider the kinetics of complexation reactions. Several comprehensive reviews are available.[27,28] We will consider five types of reactions:

(1) Water exchange in the coordination sphere
(2) Complex formation from aquated metal ions and monodentate ligands
(3) Hydrolysis of complexes with monodentate ligands
(4) Complex formation with multidentate ligands
(5) Multidentate ligand-exchange reactions

The first two types typically are very fast, and special techniques are needed to measure them.

9.7.1 Water exchange rates

Water exchange rates are known for all metal ions of interest in aquatic systems (Figure 9.18). Rate constants (k_{-H_2O}) span more than 16 orders of magnitude, from diffusion-limited values ($>10^9$ s^{-1}) to $< 10^{-7}$ s^{-1}. Only a few metal ions have rate constants slower than 1 s^{-1}. Slow exchange rates are measured by isotope dilution and rapid rates usually by spectroscopic (NMR) methods, which are suitable for a wide range of rates. The order of the constants in the first two rows of Figure 9.18 suggests that exchange rates are related to ion size, at least for Group IA and IIA ions. Over a broader range, k_{-H_2O} is correlated with z/d^3, where z is the charge of the metal and d is one-half the sum of the radii of the metal and oxygen atoms.[27] Water exchange rates can be grouped into four classes:

I. $k_{-H_2O} > 10^8$ s^{-1}; i.e., at or near diffusion controlled limits. This includes most Group IA and IIA ions except Be^{2+} and Mg^{2+}, as well as Cd^{2+}, Cu^{2+}, Hg^{2+} and Pb^{2+}.
II. $k_{-H_2O} = 10^4$–10^8 s^{-1}. This includes most first row transition metal divalent ions and Mg^{2+}.
III. $k_{-H_2O} = 1$–10^3 s^{-1}: Al^{3+} and Be^{2+}.
IV. $k_{-H_2O} = 10^{-7}$–10^{-3} s^{-1}: Cr^{3+} and Co^{3+}.

Complexes with exchange half lives > 1 min (*class IV*) are called **kinetically inert**; complexes with shorter half-lives (*classes I–III*) are called **labile**. Obviously, a wide range of reactivity exists for labile complexes. Values of k_{-H_2O} are uncertain for a few metal ions, and the results depend on the measurement method. For example, reported values for Al^{3+} range from 0.5 s^{-1} to 16 s^{-1}. The difference in k_{-H_2O} between Cr^{2+} ($10^{+8.7}$ s^{-1}) and Cr^{3+} (10^{-6} s^{-1}) is astounding considering that we are comparing two
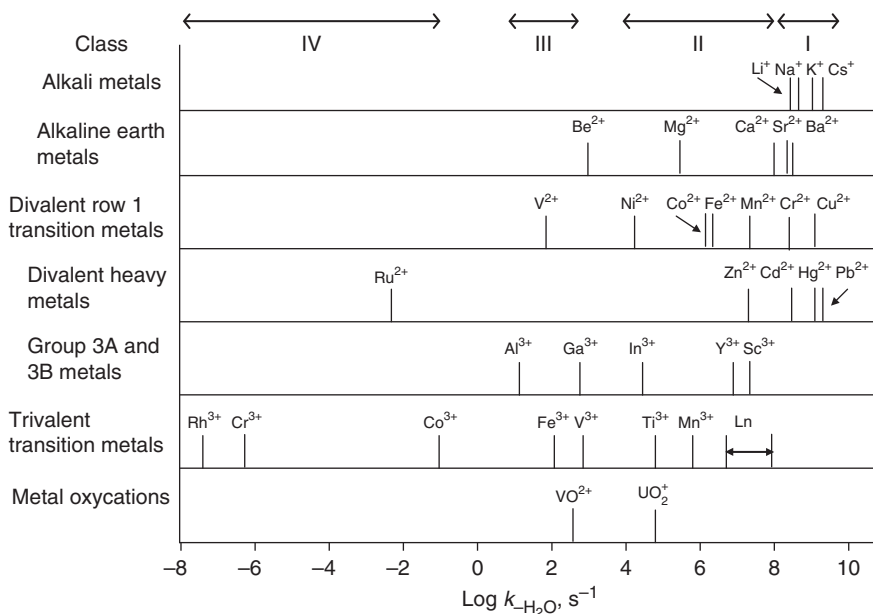
Figure 9.18 Water exchange first-order rate constants for water aquo metal ions. Modified and redrawn from Margerum et al.[27]

states of the same element that differ by just one electron. The difference is explained by configurations of the d electron orbitals in Cr, which result in a highly stable, symmetric octahedral structure for $Cr(H_2O)_6^{3+}$ and a nonsymmetric, elongated octahedral structure for $Cr(H_2O)_6^{2+}$ that is much more labile.[3]

9.7.2 Complex formation rates with monodentate ligands

Rates of reaction of aquated metal ions with monodentate ligands to form 1:1 complexes generally are comparable to their water exchange rates. As noted earlier, formation of true complexes is not an addition but a substitution reaction, where ligand L replaces ligand H_2O in the metal ion's coordination sphere. If L is an anion, the forward reaction is called anation; the reverse is called hydrolysis. Mechanistic studies indicate that anation is a two-step process:

$$M(H_2O)_n^{z+} + L^- \underset{k_r}{\overset{k_f}{\rightleftharpoons}} \{M(H_2O)_n \cdot L\}^{z-1} \tag{9.23a}$$

$$\{M(H_2O)_n \cdot L\}^{z-1} \xrightarrow{k_{-H_2O}} ML(H_2O)_{n-1}^{z-1} + H_2O \tag{9.23b}$$
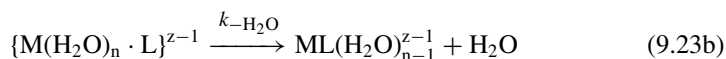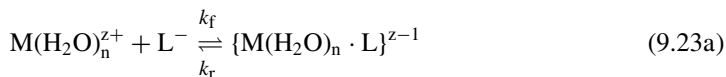
This sequence is called the Eigen mechanism. The first step involves diffusion of a ligand to a metal ion's outer hydration sphere to form an *os* complex. This rapid (diffusion-limited) step is reversible and can be treated as a "pre-equilibrium" step with equilibrium

constant $K_{os} = k_f/k_r$. The rate-controlling step involves loss of a water molecule from the coordination sphere of the metal ion and its replacement by the ligand. There are three possibilities for this step: (1) an associative pathway, in which the ligand enters the coordination sphere before the water molecule leaves, temporarily increasing the coordination number of the complex; (2) a dissociative pathway, in which the H_2O molecule leaves the coordination sphere before the ligand enters; or (3) an interchange pathway, in which H_2O leaves and L enters more or less simultaneously. The latter mechanism could be predominantly associative (I_a) or dissociative (I_d), depending on the importance of bond making or breaking in forming the transition state.

Of the above possibilities, the I_d mechanism best explains anation reactions for metal ions forming cationic octahedral complexes. Associative mechanisms are unlikely for steric reasons. In addition, reaction rates for metal ion M and a series of ligands, L^-, of the same charge do not vary with the basicity of L^- and depend on the nature of M rather than the nature of L^-. This implies that bond formation with L^- is not important in the rate-determining step and rules out associative and I_a mechanisms. Evidence for intermediates of lower coordination number does exist for anation reactions of some anionic octahedral complexes.[28] Although release of H_2O may not be a separate step, overall rates of anation still are highly correlated with water exchange rates of metal ions, as expected for I_d mechanisms, where bond breaking is more important in transition state formation than bond formation is.

Using the equilibrium constant approach (Chapter 5), one can derive the following second-order rate equation for the anation reaction (Eq. 9.23): $d[ML]/dt = k_f[M^{z+}][L^-]$, where $k_f = K_{os}k_{-H_2O}$. If k_f and k_{-H_2O} can be determined independently, one can estimate K_{os} from their ratio.

9.7.3 Hydrolysis of 1:1 complexes

By the principle of microscopic reversibility, hydrolysis and anation occur along the same reaction coordinate in opposite directions:

$$M(H_2O)_{n-1}L^{z-1} + H_2O \underset{\text{anation}, k_f}{\overset{\text{hydrolysis}, k_{hy}}{\rightleftharpoons}} M(H_2O)_n^{z+} + L^- \tag{9.24}$$
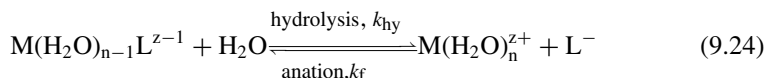
An interesting consequence of this principle is that although anation rates do not depend on the nature of L^-, hydrolysis rates do. This can be understood by considering the equilibrium constant for reaction 9.10: $K_{eq} = k_{hy}/k_f$. For a given metal ion and a series of like-charged ligands, k_f is roughly constant. Therefore, k_{hy} is proportional to K_{eq}. This is another example of a linear free energy relationship. Unless K_{eq} is constant, which is generally not true for related series of *is* complexes), k_{hy} must depend on L^-.

If we consider k_f for complex formation to be approximately $K_{os}k_{-H_2O}$, we can estimate dissociation rates of 1:1 complexes, k_{hy}, as a function of K_f, the stability constant for a complex:

$$M^{n+} + L^- \rightleftharpoons ML^{n-1} + H_2O, \ K_f = \{ML^{z-1}\}/\{M^{z+}\}\{L^-\} = k_f/k_{hy} = K_{os}k_{-H_2O}/k_{hy} \tag{9.25}$$

Thus,

$$k_{hy} \approx K_{os} k_{-H_2O} / K_f. \tag{9.26}$$

Values of K_f for monovalent, monodentate ligands generally range from $< \sim 10^1$ to $\sim 10^3$, and $k_{-H_2O} > 10^6 \text{ s}^{-1}$ for most metals of interest in natural waters. Based on the Fuoss equation (Eq. 9.3), K_{os} is ~ 1 for monovalent cations and ~ 5–10 for divalent ions with monovalent ligands. Dissociation rates of ML^{z-1} complexes that fit the above assumptions thus are rapid ($k_{hy} > \sim 10^3$ to 10^4 s^{-1}), but dissociation rates of Al^{3+} complexes ($k_{-H_2O} \approx 10 \text{ s}^{-1}$) and Fe^{3+} complexes ($k_{-H_2O} \approx 10^2 \text{ s}^{-1}$) are much slower ($\sim 10^{-2}$ to 10 s^{-1}).

9.7.4 Chelate formation and dissociation

Formation rates of complexes with chelating ligands are more variable than those for monodentate ligands. Factors like steric hindrance, electrostatic repulsion and elimination of H^+ from partially protonated multidentate ligands decrease formation rates; electrostatic attraction between metal ions and negative ligands enhances rates. Electrostatic forces can greatly affect K_{os} and k_f. For example, k_f has a range of nearly 10^6 for reactions of Ni^{2+} with ligands ranging in charge from $+3$ to -4.[22] Nonetheless, k_f for many chelates is roughly equal to $K_{os} k_{-H_2O}$, the same as found for monodentate ligands. This implies that the rate-limiting step is formation of a singly-bound intermediate and that further reaction to close the ring is rapid. Once the first ring is formed, formation of additional rings also is rapid. Fully protonated ligands generally are unreactive toward complex formation, but HF and HCN are exceptions for monodentate ligands. For multidentate polyaminocarboxylate ligands like EDTA, less protonated forms react faster than more protonated forms, and $k_{f,L}/k_{f,HL}$ ranges from 10 to ~ 300 for reactions of divalent metals with various organic ligands.[28]

Dissociation rates of chelates typically are much slower than dissociation rates of complexes with monodentate ligands. K_f values for chelates typically are large, often $>> 10^8$. This implies that even if k_f is high, k_d will be low. Dissociation of most chelates is catalyzed by acid, and in the absence of catalysis, half-lives of strong chelates toward dissociation can be on the scale of years. Even in 1 M acid, $t_{1/2}$ for dissociation of the Fe^{3+}-complexing siderophore, desferal, is 5 minutes.[29]

9.7.5 Metal-ligand exchange reactions

Rates of metal-metal exchange with a given chelating agent,

$$ML + M' \rightleftharpoons M'L + M, \tag{9.27}$$

tend to be slow, but some reactions are faster than one would predict for a mechanism in which ML dissociates completely before M'L begins to form. Metal exchange reactions of the type illustrated by Eq. 9.27 have important water quality implications—such as effects on metal toxicity to biota. For example, complexation of Cu^{2+} by EDTA in

seawater* is slow (timescale of minutes to hours). As a result, toxic levels of Cu^{2+} can persist in seawater being prepared as an algal growth medium even after EDTA is added.[†] The slowness of exchange reflects kinetic competition by much higher concentrations of Ca^{2+} and Mg^{2+} rather than intrinsically slow formation of CuY. CaY and MgY complexes form very rapidly, and because their concentrations are much higher they form preferentially (for mass action reasons) over CuY complexes, even when EDTA is added at the same time as Cu^{2+}. Formation of CuY thus proceeds as a metal-metal (M-M′) exchange reaction rather than simple anation.

M-M′ ligand exchange can occur by two pathways: ***disjunctive*** mechanisms, in which ML dissociates stepwise (perhaps catalyzed by acid) to form free or protonated L before M′L begins to form, and ***adjunctive*** mechanisms in which dinuclear intermediates (M-L-M′) are formed. Rates of disjunctive mechanisms are inversely proportional to [M] because higher [M] promotes re-formation of the M-L complex, but rates of adjunctive mechanisms are independent of [M]. M-M′ exchange rates and mechanisms for EDTA and other aminocarboxylate complexes have been studied in detail.[27,30,31] Rates generally conform to the expression

$$\frac{d[M'Y]}{dt} = k_{M'}^{MY}[M'][MY], \tag{9.28}$$

where Y = EDTA, but the reaction order may vary as concentrations of M and M′ change. The second-order expression suggests that a rate-limiting step involving M-Y-M′ as an intermediate (the adjunctive mechanism).

Although the concentration of Mg^{2+} is higher than that of Ca^{2+} in seawater (5×10^{-2} M vs. 1×10^{-2} M), Ca^{2+} forms stronger complexes with EDTA, and it is more important in hindering the formation of Cu-EDTA. As Figure 9.19a shows, Cu-CaY and Cu-MgY exchange rates are independent of [Ca] and [Mg] at the concentrations in seawater, and Cu-MgY exchange is ∼10× faster than Cu-CaY exchange. Second-order rate constants for Ca and Mg increase at lower concentrations, implying that the mechanism shifts from adjunctive to disjunctive. The disjunctive pathway is acid catalyzed, and pH affects $t_{1/2}$ for Cu^{2+} at Ca $< 10^{-2}$ M (Figure 9.19b). For disjunctive pathways, Margerum et al.[30] showed that the ratio of the rate constants, k_{Ca}^{Y}/k_{Mg}^{Y} is the same as the ratio of the stability constants, K_{CaY}/K_{MgY}, which is ∼60.

According to Hering and Morel,[31] the rate of CuY formation from CaY is

$$\frac{-d[Cu]}{dt} = \left(\left[k_{Cu}^{Y} + \frac{k_{Cu}^{HY} K_{HY}\{H^+\}}{K_{CaY}} \right] \frac{1}{[Ca]} + k_{Cu}^{CaY} \right) [CaY][Cu] \tag{9.29}$$

Values of the constants are

$$k_{Cu}^{Y} = 2.3 \times 10^{9} M^{-1} s^{-1}; \; k_{Cu}^{HY} = 5.7 \times 10^{7} M^{-1} s^{-1}; \; k_{Cu}^{CaY} = 1 \times 10^{3} M^{-1} s^{-1};$$

$$K_{HY} = 6.3 \times 10^{9}; \; K_{CaY} = 4.1 \times 10^{10} \text{(at I = 0.1).}$$

---

*The situation also applies to freshwaters with significant hardness, but $[Ca^{2+}]$ in seawater is ∼10× to 20× higher (400 mg/L vs. 20–40 mg/L) than typical values in hard freshwaters.
[†]Cu is essential for algal growth but becomes toxic at concentrations only slightly above the optimum level.
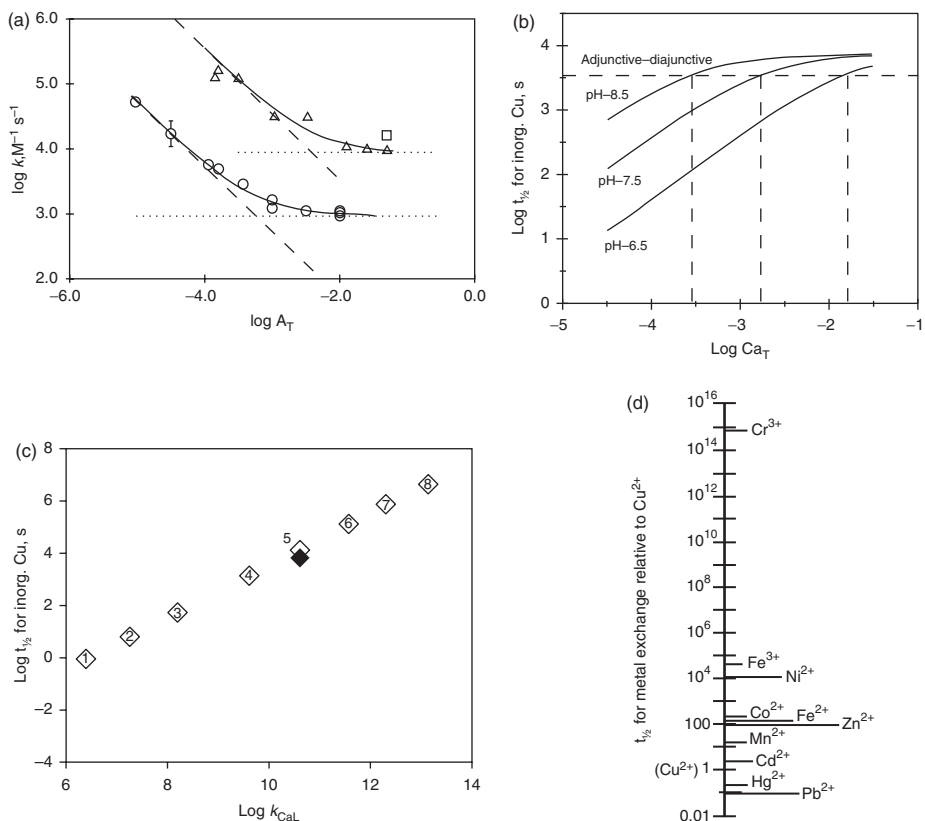
Figure 9.19 (a) Dependence of second-order rate constant for $-d[Cu]/dt = k[EDTA]_T[Cu]$ on $\log[Mg]$ (triangles) or $\log[Ca]$ (circles). (b) Log of pseudo-first-order $t_{1/2}$ for Cu with respect to reaction with 10^{-7} M Ca-EDTA as function of $[Ca]_T$ for three pH values. Vertical dashed lines show $[Ca]_T$ at which adjunctive and disjunctive mechanisms contribute equally to reaction of Cu with Ca-EDTA. (c) Predicted values of log $t_{1/2}$ for Cu in seawater for adjunctive reaction with various Ca-bound ligands at 10^{-7} M L_T, where L = various aminopolycarboxylate chelating agents: 1 = NTA; 5 = EDTA; other ligands identified in Hering and Morel.[31] (d) Predicted $t_{1/2}$ for various metal ions relative to $t_{1/2}$ for Cu for metal exchange reactions. Reprinted from Hering and Morel[31] with permission of the American Chemical Society.

Figure 9.19b shows that hindrance of CuY formation is less important in freshwater with low pH and low $[Ca^{2+}]$. Nonetheless, $t_{1/2}$ still is on the order of minutes at $[Ca^{2+}] \lesssim 10^{-3}$M and circumneutral pH. In contrast, concentrations of Ca and Mg in natural waters have little effect on the formation of Cu-NTA (NTA = nitrilotriacetic acid), which is complete in seawater within 2 minutes (Figure 9.19c).[31] NTA is a much weaker chelating agent ($K_{Ca} = 10^{6.3}$) than EDTA. Theoretical calculations suggest that $t_{1/2}$ is < 1 s for such comparatively weak ligands.

It is interesting to note that exchange rates of M-L to M′-L are proportional to water exchange rates of M′ despite the fact that overall exchange rates are many orders of magnitude slower than water exchange. Thus, we can predict that Ca-M′ exchange rates

of most trace metals for strong ligands are slower than those for Cu because Cu^{2+} has one of the fastest water exchange rates of all metal ions, $k_{-H_2O} \approx 5 \times 10^8$ s^{-1}. Among trace metals of interest in natural waters, only Pb^{2+} (7×10^9) and Hg^{2+} (2×10^9) have higher values (Figure 9.18). Exchange rates for Fe^{2+} and Zn^{2+} should be $\sim 100\times$ slower, and rates for Fe^{3+} should be $> 10^4$ slower (Figure 9.19d). The potential thus exists for long equilibration times (up to months) in waters with neutral to high pH, moderate to high concentrations of Ca, and the presence of strong ligands like EDTA. As mentioned above, the slowness of these reactions has important biological implications. Many free metal ions are toxic to aquatic organisms at low concentrations, but complexes of the metals are not.

Ligand-ligand (L-L$'$) exchange reactions (i.e., ML + L$'$ $\rightarrow$ ML$'$ + L) tend to be fairly rapid when ML$'$ is the more stable complex. Such reactions are faster than M-M$'$ exchange rates and faster than the dissociation rate of the ML complex. Such exchange reactions are faster when L does not satisfy all coordination sites of M than when it does. In the former case, L$'$ can more easily gain a "foothold" for further reaction. Exchange rate constants for metal-aminocarboxylate complexes in the range 10^3–10^5 M^{-1} s^{-1} have been reported.[27] Xue et al.[32] found second-order exchange kinetic constants, k_{exch} of 1.2×10^2 to 5.7×10^3 s^{-1} M^{-1} for ligand exchange of Ni-EDTA with dimethylglyoxime (DMG), a common chelating agent for Ni^{2+} and 5×10^2 and 7×10^3 s^{-1} M^{-1} for exchange of natural ligands with DMG in freshwater samples under similar conditions. Ni ligand exchange between natural ligands and DMG occurred over days with half-lives of 5–95 h.

Problems

9.1. Using the database in MINEQL+ or VMINTEQ, search for values of K_{s0} for divalent metal carbonates ($MCO_{3(s)}$) and K_f for metal carbonate complexes (MCO_3^0). Include in your search the metal ions in the Irving-Williams series and the alkaline earth cations: Mg, Ca, Sr, and Ba. Using metals for which you find values of both constants, determine whether there is a correlation between K_f and K_{s0}. If there is, you have developed an LFER (linear free energy relationship) that could be used to predict K_{s0} or K_f for a metal ion for which one constant has been determined but the other is not available. Using your relationship, estimate K_f for $FeCO_3^0$. K_{s0} for siderite, $FeCO_{3(s)}$ is $10^{-10.24}$. Discuss your findings and speculate on the reliability of your calculated K_f value.

9.2. Using the Fuoss model estimate the stability constant for $Fe^{II}SO_4^0$ and compare it to values that you find in textbooks or MINEQL+. Use your judgment in selecting a value for "a" in the Fuoss equation.

9.3. (a) Use the major ion data (Ca, Mg, Na, K, Cl$^-$, SO_4^{2-}, and HCO_3^-; also include F$^-$, if available) for one of the freshwaters whose chemical composition is given in Table 2.3 or 2.6 to do the following analysis. Insert the data into MINEQL+ or another computer equilibrium program and also insert the following trace metals: Cu (10^{-6} M), Pb (10^{-8}), Cd (10^{-8}), and Zn (10^{-6} M) into the input file (assume all are in the divalent form). Fix the pH at the value given in Table 2.3 or 2.6, and run the program to determine the

equilibrium composition. Repeat the analysis at a pH one unit higher than that in the table. Tabulate the results for the four heavy metals at the two pH values, and write a paragraph describing your results and comparing the speciation at the two pH values. Note: you may wish to prevent the precipitation of solids in running this problem.

(b) Simulate the role of humic substances in complexing the heavy metals by adding 1×10^{-4} M salicylate and 1×10^{-4} M phthalate as components to the input file for part (a) at the ambient pH. Salicylate and phthalate have binding sites similar to the carboxyl and phenolic binding sites in humic matter (see Chapter 18). The total concentration of salicylate and phthalate is roughly comparable to the carboxyl content of $\sim$20 mg/L of DOC. Note: you should check the database of the computer program used to solve the problem to ensure that K_f values are present for complexes of the metals with the organic ligands. Lack of an output value for a metal-organic complex means the K_f is missing from the database and is not an indication that the complex does not exist.

9.4. Determine the speciation of manganese when 2×10^{-6} M Mn(NO$_3$)$_2$ added to water at pH 6 and at pH 9. Assume that the manganese does not participate in any redox reactions but remains wholly as Mn^{II}. Solve manually using the thermodynamic data in Table 9.3 or use MINEQL+ or another computer equilibrium program.

9.5. Repeat problem 4 when 0.1 M NaCl is present. Consider activity corrections.

9.6. Set up the appropriate equations to solve for the speciation of the following system. To a 1-L beaker of water are added 1×10^{-6} moles of NiCl$_2$, 5×10^{-2} moles of NH$_4$Cl, and 2.5×10^{-4} moles of Ca(OH)$_2$. After you set up the necessary equations, solve using MINEQL+. Tabulate your results in summary form and write a short paragraph summarizing what the results show (i.e., do not just print the output from the computer program).

9.7. Free zinc (Zn^{2+}) is toxic to fish at levels above 10^{-7} M, and the well water for your home contains Zn^{II} at a concentration of 65 µg/L (1×10^{-6} M). In an attempt to lower the free zinc concentration in the water he is using for the bowl of his beloved "Goldy Goldfish," your younger brother adds cyanide to complex the zinc. Goldy tragically dies from cyanide poisoning, but you still find the water chemistry aspects of the problem fascinating. Using Tables 9.3 and 9.4, determine the speciation of Zn^{II} and cyanide in a solution at pH 8.1 which contains 1×10^{-6} M of Zn(NO$_3$)$_2$ and 1×10^{-4} M total cyanide (HCN + CN$^-$). You may solve manually or use a computer equilibrium program. If you use MINEQL+, you will need to add the formation constants for the zinc cyanide complexes (from Table 9.7) to the database. (This will be good practice for you!) If you use VMINTEQ, the constants already are in the database. The toxicity of cyanide to fish is complicated, but the U.S. EPA's quality criteria for water indicates that free cyanide concentrations > 50 µg/L are lethal to fish. If you assume this is the case, does this explain why Goldy died?

9.8. Re-solve problem 7 for the case where your brother, in an effort to avoid cyanide toxicity to his new fish, Goldy 2, adds total cyanide at the same concentration as

Zn^{II}, that is, 1×10^{-6} M. You may solve by hand or use a computer equilibrium program. Is this approach likely to have solved the problem?

9.9. Lesser known than their tiger-taming colleagues who once performed at a Las Vegas casino, Riegfried & Soy have been performing daring (some would say stupid) feats of water chemistry for decades at Hank's Casino and Bait Shop. Soy makes a solution by adding 2.5×10^{-6} moles of cadmium (Cd^{2+}) and 1×10^{-3} moles of EDTA to 1 L of water, waits 5 minutes, and then drinks it. He claims that he if waits that long, the complex concentrations reach equilibrium values, and under these conditions, the remaining free Cd^{2+} is nontoxic. You take your pH probe and determine that $[H^+] = 10^{-7.5}$ in the solution. Given the following information, determine the free $[Cd^{2+}]$ in the solution that Soy drinks. You may ignore the potential precipitation of $Cd(OH)_{2(s)}$ and the protonated forms of $EDTA^{4-}$. What do you suppose happens when the solution reaches his stomach (pH = ~1)?

$Cd^{2+} + H_2O = CdOH^+ + H^+$	$^*K_1 = 10^{-10.08}$
$Cd^{2+} + 2H_2O = Cd(OH)_2^0 + 2H^+$	$^*\beta_2 = 10^{-20.35}$
$Cd^{2+} + 3H_2O = Cd(OH)_3^- + 3H^+$	$^*\beta_3 = 10^{-33.30}$
$Cd^{2+} + 4H_2O = Cd(OH)_4^{2-} + 4H^+$	$^*\beta_4 = 10^{-47.35}$
$Cd^{2+} + EDTA^{4-} + H^+ = CdH\text{-}EDTA^-$	$^*K_{HE} = 10^{2.9}$
$Cd^{2+} + EDTA^{4-} = Cd\text{-}EDTA^{2-}$	$^*K_E = 10^{16.28}$
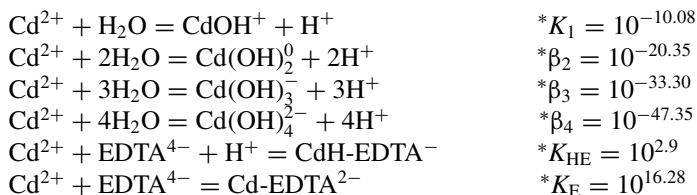
9.10. Estimate the rate constant for hydrolysis of the 1:1 Fe^{III}-acetate complex given that $K_f = 10^{4.02}$ and $k_{-H_2O} = 10^2$ s^{-1}.

9.11. For experiments at constant pH and the metal and ligand concentrations that Hering and Morel[31] used to study CaY-Cu M-L exchange, equation 9.29 effectively becomes a simple second-order rate equation. The entire term in parentheses before the terms for [CaY] and [Cu] is equivalent to an observed rate constant, k_{obs} because the only variable in the parentheses at constant pH is [Ca], which is so high that it does not change during the reaction. You can calculate k_{obs} by inserting values of the constants, the starting value of $[Ca^{2+}]$, and $[H^+]$ from the given pH. You then could use the analytical solution for second-order equations (see Chapter 5) to determine [Cu] at any time of interest or could simulate the time-course using Acuchem by inserting a second-order reaction and the value of k_{obs}. Alternatively, you could use a spreadsheet to solve for $[Cu^{2+}]$, [CuY], and [CaY] versus time.

(a) Given $[Ca^{2+}] = 5 \times 10^{-2}$ M, $[Cu^{2+}]_0 = 1 \times 10^{-7}$ M, $[CuY]_0 = 0$, and $[CaY]_0 = 1.25 \times 10^{-7}$ M, simulate the reaction time-course at pH = 6, 7, and 8 using either Acuchem or a spreadsheet method. Use the rate and equilibrium constants provided in the text. Assume that Y_T (total [EDTA]) is 1.25×10^{-7} M and all the Y remains complexed either by Ca or Cu. Plot your results and discuss the differences found at the three pH values.

Hint: To solve/simulate a well-behaved second-order ordinary differential equation by a spreadsheet, you can use a simple Euler calculation. The approach solves for $[Cu]_t$ iteratively using the general equation: $y_{t+1} = y_t + \Delta t \times (dy/dt)_t$. For this problem, the equation becomes

$[Cu]_{t+1} = [Cu]_t + \Delta t \times (d[Cu]/dt)_t$. Similarly, $[CuY]_{t+1}$ is computed from: $[CuY]_{t+1} = [CuY]_t - \Delta t \times (d[Cu]/dt)_t$, and $[CaY]_{t+1}$ is computed from $[CaY]_{t+1} = [CaY]_t + \Delta t \times (d[Cu]/dt)_t$. The key for accurate solutions is to select a sufficiently small time increment that the slope of the line (i.e., dy/dt) effectively doesn't change over time increment (Δt). For Eq. 9.29 and the conditions in this problem, $\Delta t = 10$ s and a total reaction time of $\sim$250 min work well, but you have some flexibility in choosing these values. An example of a spreadsheet solution for rate equations is available on the book's Web site.

(b) Perhaps more interesting than the reaction time course at constant pH is the effect of [Ca] and pH on k_{obs}. Develop an expression for this relationship from Eq. 9.29 by substituting in values of the constants, and determine how [Ca] affects k_{obs} at the three pH values used in part (a). Use a range of [Ca] of 10^{-5} to 10^{-2} M, and plot your results as a log-log relationship. Compare your plot to Figure 9.19b and discuss the results.

 References

1. A. E. Martell and R. M. Smith (eds.). 2004. NIST Standard Reference Database 46: NIST critically selected stability constants of metal complexes: version 8.0, National Institute of Standards and Technology, Gaithersburg, Md.

2. Goldberg, E. D. 1965. Minor elements in sea water. In *Chemical oceanography*, J. P. Riley and G. Skirrow (eds.), Academic Press, New York, 163–196.

3. Purcell, K. F., and J. C. Kotz. 1977. *Inorganic chemistry*, W. B. Saunders Co., Philadelphia.

4. Shriver, D. F., P. W. Atkins, and C. H. Langford. 1990. *Inorganic chemistry*, W. H. Freeman and Co., New York.

5. Garrels, R. M., and M. E. Thompson. 1962. A chemical model for sea water at 25 C and one atmosphere total pressure. *Am. J. Sci.* **260**: 57–66.

6. Fuoss, R. M. 1958. Ionic association. III. The equilibrium between ion pairs and free ions. *J. Am. Chem. Soc.* **80**: 5059–5061; Eigen, M. 1954. Kinetics of ion reactions in solution. *Z. Phys. Chem.* NF**1**: 176.

7. Ahrland, S., J. Chatt, and N. R. Davies. 1958. The relative affinities of ligand atoms for acceptor molecules and ions. *Quart. Rev.* **11**: 265–276.

8. Pearson, R. G. 1963. Hard and soft acids and bases. *J. Am. Chem. Soc.* **85**: 3533–3539.

9. Langmuir, D. 1979. Techniques of estimating thermodynamic properties for some aqueous complexes of geochemical interest. In *Chemical modeling in aqueous systems*, E. A. Jenne (ed.), Amer. Chem. Soc. Symp. Ser. **93**, Amer. Chem. Soc., Washington, D.C., 353–387.

10. Turner, D. R., M. Whitfield, and A. G. Dickson. 1981. The equilibrium speciation of dissolved components in freshwater and seawater at 25°C and 1 atm pressure. *Geochim. Cosmochim. Acta* **45**: 855–881.

11. Ahrland, S. 1968. Thermodynamics of complex formation between hard and soft receptors and donors. *Struct. Bonding* **5**: 118–149.

12. Benjamin, M. 2002. *Water chemistry*, McGraw-Hill, New York.

13. Stumm, W., and J. J. Morgan. 1996. *Aquatic chemistry*, 3rd ed., Wiley-Interscience, New York.

14. Carbonaro, R. F., and D. M. DiToro. 2007. Linear free energy relationships for metal–ligand complexation: monodentate binding to negatively-charged oxygen donor atoms. *Geochim. Cosmochim. Acta* **71**: 3958–3968.

15. Culkin, F. 1965. The major constituents of sea water. In *Chemical oceanography*, Vol. 2, J. P. Riley and G. Skirrow (eds.), Academic Press, New York, 121–161.

16. Eaton, A. D., L. S. Clesceri, E. W. Rice, and A. E. Greenberg. 2005. *Standard methods for the examination of water & wastewater*, 21st ed., Amer. Pub. Health Assoc., Amer. Water Works Assoc., Water Environ. Fed., Washington, D.C.

17. Osathaphan, K., T. Boonpitak, T. Laopirojana, and V. K. Sharma. 2008. Removal of cyanide and zinc-cyanide complex by an ion-exchange process. *Water, Air, Soil Pollut.* 194: 179–183.

18. Solis, J. S., P. M. May, and G. T. Hefter. 1996. Cyanide thermodynamics. Part 4. Enthalpies and entropies of cyanide complexes of CuI, AgI, ZnII, and CdII. *J. Chem. Soc. Farad. Trans.* **92**: 641–644.

19. Kim, S.-J., K.-H. Lim, K.-H. Joo, M.-J. Lee, S.-G. Kil, and S.-Y. Cho. 2002. Removal of heavy metal-cyanide complexes by ion exchange. *Korean J. Chem. Eng.* **19**: 1078–1084.

20. Baes, C. F., and R. E. Mesmer. 1976. *The hydrolysis of cations*, J. Wiley, New York.

21. Berthon, G. 1995. The stability constants of metal complexes of amino acids with polar side chains. *Pure Appl. Chem.* 67: 1117–1240.

22. Meissner, G., A. Reid, G. Stork. 1997. Investigation of sewage sludge heavy metals and EDTA in municipal wastewater—Part 3: Determination of EDTA and NTA in wastewater with GC/MS and screening methods. *Gas- Wasserfach Wasser Abwasser* **138**: 564–569.

23. Rue, E. L., and K. W. Bruland. 1996. Complexation of iron(III) by natural organic ligands in the central North Pacific as determined by a new competitive ligand equilibration/adsorptive cathodic stripping voltammetric method. *Mar. Chem.* **50**: 117–138.

24. Mawji, E., M. Gledhill, J. A. Milton, G. Tarran, S. Ussher, A. Thompson, G. A. Wolff, P. J. Worsfold, and E. P. Achterberg. 2008. Hydroxamate siderophores: occurrence and importance in the Atlantic Ocean. *Environ. Sci. Technol.* **42**: 8675–8680.

25. Duckworth, O. W., J. R. Bargar, and G. Sposito. 2009. Coupled biogeochemical cycling of iron and manganese as mediated by microbial siderophores. *BioMetals* **22**: 605–613.

26. McKnight, D. M., and F. M. M. Morel. 1980. Copper complexation by siderophores from filamentous blue-green algae. *Limnol. Oceanogr.* **25**: 62–71.

27. Margerum, D. W., G. R. Cayley, D. C. Weatherburn, and G. K. Pagenkopf. 1978. Kinetics and mechanisms of complex formation and ligand exchange. In *Coordination chemistry*, Vol. 2, A. E. Martell (Ed.), ACS Monograph **174**, Am. Chem. Soc., Washington, D.C., pp. 1–220.

28. Brezonik, P. L. 1994. *Chemical kinetics and process dynamics in aquatic systems*, CRC Press, Boca Raton, Fla.

29. Biruš, M., Z. Bradić, G. Krznarić, N. Kujundžic, M. Pribanić, P. C. Wilkins, and R. G. Wilkins. 1987. Kinetics of stepwise hydrolysis of ferrioxamine B and formation of diferrioxamine B in acid perchlorate solution. *Inorg. Chem.* **26**: 1000–1005.

30. Margerum, D. W., D. L. Janes, and H. M. Rosen. 1965. Multidentate ligand kinetics. VII. The stepwise nature of the unwrapping and transfer of ethylenediaminetetraacetate from nickel(II) to copper (II) *J. Am. Chem. Soc*. **87**: 4463–4472.

31. Hering, J. G., and F. M. M. Morel. 1988. Kinetics of trace metal complexation: role of alkaline earth metals. *Environ. Sci. Technol*. **22**: 1469–1478.

32. Xue, H. B., S. Jansen, A. Prasch, and L. Sigg. 2001. Nickel speciation and complexation kinetics in freshwater by ligand exchange and DPCSV. *Environ. Sci. Technol.* **35**: 538–546.

10

� Solubility

Reactions of Solid Phases with Water

▢ Objectives and scope

In this chapter you will learn the basic concepts of solubility. The chapter begins with the relevant thermodynamic expressions and key equations in solving solubility equilibria. pC-pH diagrams are constructed to represent the conditions under which solids form. Carbonate, sulfide, and oxide/hydroxide minerals are emphasized. Water softening is used to demonstrate how solubility is important in engineering practice. The effects of ligands, common ions, and temperature on solubility are presented. Measurement and prediction of the solubility of organic compounds also are discussed. Although solubility is often thought of as a thermodynamically driven process, the concepts of supersaturation and nucleation reveal the importance of kinetics.

▢ Key terms and concepts

- K_{s0}
- Ion activity product
- Precipitation
- Dissolution
- Common ion effect
- Softening reactions
- Molar volume

10.1 Introduction

Solubility is a concept that we routinely encounter. When you put a teaspoon of table salt (sodium chloride; NaCl) into a glass of water, you know it will dissolve. Similarly,

if one adds sand, which is consists of quartz or silica (SiO_2), to a glass of water, the material does not appear to dissolve—at least to the naked eye. Simply put, the table salt is soluble and the sand is not. In the first case, the reaction

$$NaCl_{(s)} \rightarrow Na^+ + Cl^- \tag{10.1}$$

goes to completion, and the solid completely dissolves. If you continue to add teaspoons of NaCl to the water, eventually you reach a point where (even with stirring) the added salt will no longer dissolve. The solid NaCl and the Na^+ and Cl^- in solution are now in equilibrium, and the water is **saturated** with sodium chloride. In the second case, the reaction

$$SiO_{2(s)} + 2H_2O \rightarrow H_4SiO_{4(aq)} \tag{10.2}$$
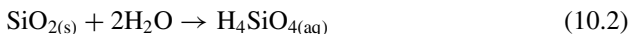
does occur to a limited extent (see Section 15.4 for quantitative information on this), but most of the solid mineral remains. The remaining quartz and dissolved silica are in equilibrium. When a solid is placed into water and dissolves, the process is known as **dissolution**. The process of dissolved constituents leaving solution and forming a solid is known as **precipitation**. For example, if a solution of silver nitrate ($AgNO_3$) is added dropwise to a solution of sodium chloride, silver chloride ($AgCl_{(s)}$) will precipitate when the solution becomes saturated with respect to this solid.

Some "rules of thumb" for the solubility of salts are useful to keep in mind. First, solids containing the alkali metals (Li^+, Na^+, K^+) as cations or nitrate or perchlorate as anions are very soluble. In general, the alkaline earth metal ions (Mg^{2+}, Ca^{2+}, Sr^{2+}) are less soluble than the alkali metals, particularly when considering the carbonates and hydroxides. Many halide-containing salts, including both the alkali and alkaline earth metals are highly soluble, but not all halides are highly soluble (e.g., silver chloride is highly insoluble). Solids containing sulfide (S^{2-}) generally have very low solubility, as do almost all solids containing silver ($AgNO_3$ is an exception and one of the few ways to get silver into solution).

As is likely obvious at this point, the same thermodynamic concepts (Gibbs free energy and equilibrium constants) used to describe acid/base chemistry and complexation reactions are used to describe solubility. In fact, acid-base and complexation chemistries play a critical role in determining solubility in many systems, so be sure to keep those concepts in mind.

10.2 Thermodynamics of solubility, the ion activity product, and the common ion effect

To illustrate the concept of solubility, we begin with the solid anhydrite (calcium sulfate; $CaSO_{4(s)}$). The relevant solubility reaction is

$$CaSO_{4(s)} \rightleftharpoons Ca^{2+} + SO_4^{2-}. \tag{10.3}$$

By convention, dissolution and precipitation reactions are always written with the solid on the left hand side. As we shall see shortly, this often has mathematical convenience.

Using the free energies of formation, we can calculate $\Delta G°$ for this reaction using Eq. 3.21,

$$\Delta G° = \sum_i \nu_i \left. G°_{f,i} \right|_{products} - \sum_i \nu_i \left. G°_{f,i} \right|_{reactants}, \qquad (3.21)$$

and the equilibrium constant with Eq. 3.27a:

$$\Delta G° = -RT\ln K_{s0}, \qquad (3.27a)$$

where K_{s0} is the solubility constant. Subscript "s" denotes this is a solubility equilibrium constant, and the numerical index (the symbol following the s is the number 0, not the letter O) allows us to account for multiple solubility constants, which will be explored later in the chapter. The solubility constant also is written often as K_{sp} (sp = solubility product). Recalling from Chapter 4 that activity coefficients for solids are equal to one, we can write

$$K_{s0} = \{Ca^{2+}\}\{SO_4^{2-}\} \qquad (10.4)$$

Using equations 3.21, 3.27a, and 10.4, we get

$$\Delta G° = G°_{f,CaSO_4} - G°_{f,Ca^{2+}} - G°_{f,SO_4^{2-}}$$

$$= -1321.7\,kJ/mol - (-553.54\,kJ/mol) - (-744.6\,kJ/mol)$$

$$= -23.56\,kJ/mol = 23,560\,J/mol$$

$$K_{s0} = \{Ca^{2+}\}\{SO_4^{2-}\} = e^{-\Delta G°/RT} = e^{-(23,560)/(8.314 \times 298.15)} = 10^{-4.13}$$

The value MINEQL+ gives for this reaction is $10^{-4.36}$; such discrepancies are not uncommon and reflect uncertainties in solubility measurements. We will use the value $10^{-4.36}$ for the rest of our analysis.

　　If we add anhydrite to water, we can determine whether or not it will dissolve. For this salt, dissolution of the solid produces one calcium ion and one sulfate ion; thus, $\{Ca^{2+}\} = \{SO_4^{2-}\} = (K_{s0})^{1/2}$. The solubility of anhydrite thus is 6.60×10^{-3} M when it is added to pure water. This is a special case. Let us now consider the situation in which we would like determine how much anhydrite can dissolve in water that already contains sulfate ions. The concentration of sulfate can be set to any desired value by adding sodium sulfate, which is essentially infinitely soluble. We can then add calcium chloride in any desired amount and evaluate whether or not anhydrite will precipitate. There are three potential cases:

$$\{Ca^{2+}\}\{SO_4^{2-}\} < K_{s0} \text{ undersaturation} \qquad (10.5a)$$

$$\{Ca^{2+}\}\{SO_4^{2-}\} = K_{s0} \text{ equilibrium} \qquad (10.5b)$$

$$\{Ca^{2+}\}\{SO_4^{2-}\} > K_{s0} \text{ supersaturation} \qquad (10.5c)$$

The product $\{Ca^{2+}\}\{SO_4^{2-}\}$ is also known as the **_ion activity product_** (**_IAP_**). If IAP $< K_{s0}$, the condition for solid to be present has not been met. No precipitation

will occur, and the solution has the capacity to dissolve additional solid. If IAP = K_{s0} the first molecule of solid is "ready" to precipitate, and any addition of calcium or sulfate will lead to precipitation. If solid is already present, precipitation of one molecule of the solid is accompanied by dissolution of another at equilibrium. If IAP > K_{s0}, solid will precipitate from solution, decreasing the concentration of ions in solution until equilibrium is reached. It is important to note that supersaturated solutions can be "metastable." If water is heated (which increases the solubility of many solids) and a solid is dissolved in it until is saturated, and the water is then slowly cooled, the solid may not precipitate even though it is supersaturated. Addition of a nucleating surface (a small crystal of the solid or a piece of dust) may lead to rapid precipitation (see Section 10.10 on the kinetics of precipitation/dissolution).

EXAMPLE 10.1 Solubility of lead iodide: This example is given for use as an in-class demonstration. The solubility equilibrium expression for lead iodide is

(1) $PbI_{2(s)} \rightleftharpoons Pb^{2+} + 2I^-$ $K_{s0} = 8.7 \times 10^{-9}$.
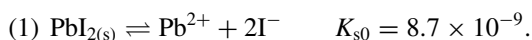
Make a 1-L solution of 0.01 M lead nitrate ($Pb(NO_3)_2$) in a graduated cylinder. Make a separate solution of 0.5 M potassium iodide (KI). Add one drop of the KI solution (0.05 mL). Observe what happens over the course of 1–2 minutes. Explain your observations in terms of an IAP calculated for a 0.5-mL volume (that formed just after the KI drop is added to the $Pb(NO_3)_2$ solution) and for the entire 1-L volume once the system is completely mixed.

Answer: What? Ruin the fun of doing it in class? You are on your own for this one.

It is instructive to examine the three cases given by Eqs. 10.5a–10.5c graphically. Ignoring activity corrections, we know that at equilibrium for any sulfate concentration,

$$[Ca^{2+}] = K_{s0}/[SO_4^{2-}], \tag{10.6}$$

which is plotted in Figure 10.1. The solid line is Eq. 10.6. Above this line (the shaded area), the IAP (i.e., product of calcium and sulfate concentrations) exceeds the solubility constant, and so anhydrite precipitates in this region. In the area below the line, solubility is not exceeded, and the calcium and sulfate remain dissolved.

Note that at only one point on the equilibrium line (at 6.60×10^{-3} M) are the calcium and sulfate concentrations the same. If pure anhydrite is added to water, 6.60×10^{-3} moles per liter of water will dissolve, and this value is the **solubility** of anhydrite in pure water. There are an infinite number of other points on this line, however, meaning that for a given amount of sulfate in solution, calcium (whether from anhydrite or some other salt or solid) can be added only to a certain point until anhydrite precipitates. Note that the higher the sulfate concentration, the lower the amount of calcium that can be put in solution before the anhydrite precipitates. This is known as the **common ion effect**; that is, when an ion is already present in solution, it lowers the solubility (i.e., the total number of moles that can dissolve) of any solid that contains that ion as part of its structure.

EXAMPLE 10.2 The common ion effect: What is the solubility of calcium in a solution containing 10^{-1} M of sulfate?
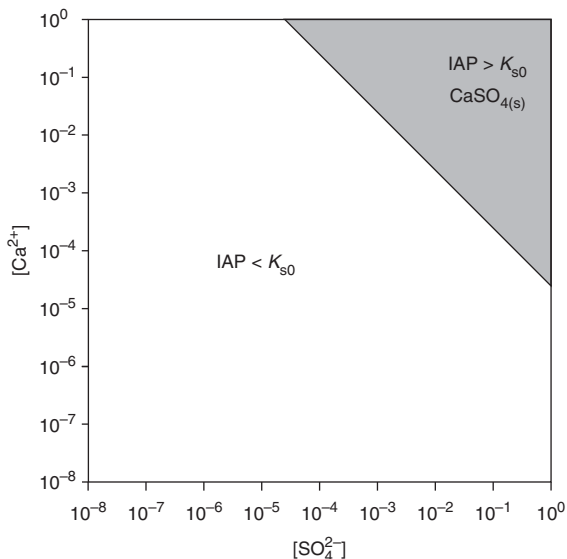
Figure 10.1 Solubility diagram for anhydrite ($CaSO_{4(s)}$).

Answer: If pure anhydrite is added to water, the amount of calcium that can be dissolved is 6.60×10^{-3} mol/L, but if 10^{-1} sulfate is present, this drops to 4.36×10^{-4} mol/L (i.e., $[Ca^{2+}] = K_{s0}/[SO_4^{2-}]$). The presence of sulfate makes anhydrite precipitate at a lower concentration than it does in pure water. This is the common ion effect.

Metal ions form solids with many of the common anions in water (hydroxide, chloride, carbonate, sulfate, sulfide). A list K_{s0} values for several solids is given in Table 10.1. These equilibrium constants can be determined from experiment, as shown in the following example.

EXAMPLE 10.3 Determining K_{s0} from solubility data: When stannous (tin) fluoride (SnF_2) is added to pure water, the solubility is 0.012 g per 100 mL. Using only this information, determine (A) the K_{s0} for SnF_2 and (B) the solubility of SnF_2 in a solution that originally contains 0.8 M sodium fluoride (NaF).

Answer: (A) First we need to convert the dissolved mass to moles,

(1) $0.012g/(118.71 + 2(19))g/mol = 7.66 \times 10^{-5}$ moles,

giving a solubility of 7.66×10^{-5} moles per 0.1 L $= 7.66 \times 10^{-4}$ moles/L. For each Sn^{2+}, there are 2 F^-, and so the concentration of Sn^{2+} is 7.66×10^{-4} M and F^- is 1.53×10^{-3}. We now have the information necessary to calculate K_{s0}:

(2) $SnF_2 \rightleftharpoons Sn^{2+} + 2F^-$; $^cK_{s0} = [Sn^{2+}][F^-]^2 = (7.66 \times 10^{-4})(1.53 \times 10^{-3})^2$
$$= \mathbf{1.80 \times 10^{-9}}$$

Note that because we used concentrations to calculate this value, it is a $^cK_{s0}$. Calculating the ionic strength of the solution and using the appropriate activity coefficients would allow calculation of the thermodynamic value ($^aK_{s0}$).

(B) If a solution contains 0.8 M F^-, the concentration of Sn^{2+} (and thus the number of moles of SnF_2) that can dissolve is

(3) $1.80 \times 10^{-9} = (S)(2S + 0.8)^2$.

This is a cubic equation, and solving for S (the amount that dissolves) gives 2.81×10^{-9} mol/L. Note one can assume that $2S \ll 0.8$, giving $1.80 \times 10^{-9} = 0.64S$, and $S = 2.81 \times 10^{-9}$ mol/L, as well. This again illustrates the common ion effect; the solubility of $SnF_{2(s)}$ is more than five orders of magnitude smaller in 0.8 M NaF solution than in distilled water.

10.3 Solubility of sulfides

One of our common interactions with sulfides is with hydrogen sulfide (H_2S), and its rotten egg smell. In environments depleted of oxygen, bacteria turn to alternative electron acceptors (this is discussed in Chapter 11), one of which is sulfate. In these environments, sulfate is reduced to sulfide. Sulfides are important in dictating metal solubility in anoxic environments, where sulfate reduction to sulfide occurs. As we learned in Chapter 9, hard metals bind preferentially bind with hard ligands, and soft metals preferentially bind with soft ligands. Sulfide is a soft ligand, and thus it forms highly insoluble solids with soft metals such as Cu^+, Pd^{2+}, Ag^+, Cd^{2+}, Pt^{2+}, Au^+, Hg^{2+}, and Tl^+. Note that these are all heavy metals, and part of the reason they are toxic is that they bind to sulfur-containing proteins. Sulfide minerals also are important in dictating the solubility of the borderline metals (i.e., the Irving Williams series: Cr^{2+}, Mn^{2+}, Fe^{2+}, Co^{2+}, Ni^{2+}, Cu^{2+}, and Zn^{2+}), most of which are also micronutrients, in anoxic environments. The K_{s0} values for sulfide minerals in Table 10.1 are somewhat different than those found in previous texts (e.g., Benjamin[1] and Stumm and Morgan[3]). This difference arises from the pK_a value used for the dissociation of bisulfide (HS^-) to sulfide (S^{2-}) (Table 10.2). Stumm and Morgan,[3] for example, used a value of 13.9. This text uses a value of 17.3 (consistent with MINEQL+ and recent literature[2]); HS^- thus is a much weaker acid than previously thought and dissociation of HS^- to S^{2-} effectively does not occur in aqueous solutions even at pH 14.

It is instructive to see why a pK_a value would affect a solubility product constant. Assume you had added $CoS_{(s)}$ to a solution containing 1×10^{-6} M total dissolved sulfide (S_T) and buffered to pH 6.0. Measuring (e.g., via atomic absorption spectroscopy) the Co^{2+} concentration, which dominates the aqueous species at this pH (see Table 9.3) would allow calculation of K_{s0} if one knows $[S^{2-}]$ and ignoring activity corrections. In this situation, $[Co^{2+}] = 9.76 \times 10^{-11}$ M, and the sulfide concentration is

$$[S^{2-}] = \alpha_2 S_T = \frac{K_{a1}K_{a2}}{[H^+]^2 + [H^+]K_{a1} + K_{a1}K_{a2}} S_T \qquad (10.7)$$

The value of K_{a1} is $10^{-7.02}$ and $[H^+]$ is $10^{-6.0}$. Using the two values of K_{a2} gives

$$[S^{2-}] = 1.10 \times 10^{-15} \text{ M for } K_{a2} = 10^{-13.9},$$

Table 10.1 Solubility constants for selected minerals*

Metal	Mineral name	Formula	$Log\ K_{s0}^{\dagger}$ or $log\ ^*K_{s0}$	ΔH kcal/mol	Metal	Mineral name	Formula	$Log\ K_{s0}^{\dagger}$ or $log\ ^*K_{s0}$	ΔH kcal/mol
Ag^+		Ag_2O	12.574	−10.904	Fe^{2+}	Wustite	FeO	11.688	−24.842
	Acanthite	Ag_2S	−53.52§	54.254			$Fe(OH)_2$	13.564	
	Bromyrite	$AgBr$	−12.30	−20.196		Vivianite	$Fe_3(PO_4)_2$	−36	
	Cerarcyrite	$AgCl$	−9.75	−15.583		Mackinawite	FeS	−20.9§	
		Ag_2CO_3	−11.09	−10.074		Siderite	$FeCO_3$	−10.24	−3.824
		Ag_3PO_4	−17.59						
		Ag_2SO_4	−4.82	4.063					
Ba^{2+}	Witherite	$BaCO_3$	−8.57	0.956	Fe^{3+}	Lepidocrocite	γ-FeOOH	1.371	
	Barite	$BaSO_4$	−9.98	5.497		Goethite	α-FeOOH	0.491	−14.48
						Hematite	α-Fe$_2$O$_3$	−1.418	−30.829
						Ferrihydrite	$Fe(OH)_3$	3.191	−17.537
						Maghemite	γ-Fe$_2$O$_3$	6.386	
						Strengite	$FePO_4(H_2O)_2$	−26.4	−2.237
							$Fe_2(SO_4)$	−3.734	−57.846
Ca^{2+}	Lime	CaO	32.699	−46.346	Hg^{2+}	Montroydite	HgO	2.554	−9.297
	Portlandite	$Ca(OH)_2$	22.804	−30.741			$Hg(OH)_2$	2.698	
	Hydroxyapatite	$Ca_5(OH)(PO_4)_3$	−44.333			Cinnabar	HgS	−56.8§	60.65
	Gypsum	$CaSO_4\bullet 2H_2O$	−4.16	0.239			$Hg(CN)_2$	−39.28	
	Anhydrite	$CaSO_4$	−4.36	−1.721			$HgCO_3$	−22.52	
	Aragonite	$CaCO_3$	−8.30	−2.868					
	Calcite	$CaCO_3$	−8.48	−1.912					
Cd^{2+}		$Cd(OH)_2$	13.644	−22.612	Mg^{2+}	Periclase	MgO	21.584	−36.145
	Monteponite	CdO	15.103	−24.713		Brucite	$Mg(OH)_2$	16.844	−27.246
	Greenockite	CdS	−31.66§	13.145		Nesquehonite	$MgCO_3(H_2O)_3$	−4.67	−5.789
	Otavite	$CdCO_3$	−12.00	−0.132		Epsomite	$MgSO_4(H_2O)_7$	−2.126	2.763
		$Cd_3(PO_4)_2$	−32.60			Magnesite	$MgCO_3$	−7.46	4.78
		$CdSO_4$	−0.172	−12.424			$Mg_3(PO_4)_2$	−23.28	

Ion	Mineral	Formula	Value 1	Value 2
Co^{2+}		$Co(OH)_2$	13.094	
		CoS	-28.37§	
		$CoCO_3$	-9.98	-3.05
		$Co_3(PO_4)_2$	-34.688	
		$CoSO_4$	2.802	-18.948
Co^{3+}		$Co(OH)_3$	-2.309	-22.091
Cr^{3+}		$Cr(OH)_3$	10.905	-7.115
Cu^{2+}	Tenorite	CuO	7.644	-15.504
		$Cu(OH)_2$	8.674	-13.485
	Malachite	$Cu_2(OH)_2CO_3$	-33.30	18.255
	Covellite	CuS	-39.60§	23.184
		$Cu_3(PO_4)_2(H_2O)_3$	-35.12	
		$CuCO_3$	-11.5	
		$CuSO_4$	2.94	-17.457
Cu^{+}	Cuprite	Cu_2O	-1.406	-29.642
	Chalcocite	Cu_2S	-51.68§	40.153
	Nantokite	$CuCl$	-6.73	10.196

Ion	Mineral	Formula	Value 1	Value 2
Mn^{2+}	Pyrochroite	$Mn(OH)_2$	15.194	-23.186
		MnS	-17.13§	-7.648
	Rhodochrosite	$MnCO_3$	-10.58	-0.449
		$Mn_3(PO_4)_2$	-23.827	2.12
		$MnSO_4$	2.583	-15.497
Mn^{3+}	Bixbyite	Mn_2O_3	-0.644	-29.754
Ni^{2+}	Bunsenite	NiO	12.446	-23.932
		$Ni(OH)_2$	12.794	-22.935
		NiS	-30.10§	
		$NiCO_3$	-6.87	-9.94
		$Ni_3(PO_4)_2$	-31.3	
Pb^{2+}	Massicot	PbO	12.894	
		$Pb(OH)_2$	8.15	-13.99
	Galena	PbS	-31.27§	19.12
	Cerrusite	$PbCO_3$	-13.13	5.925
	Anglesite	$PbSO_4$	-7.79	2.868
	Hydroxylpyromorphite	$Pb_5(OH)(PO_4)_3$	-62.79	
	Hydrocerrusite	$Pb_2CO_3(OH)_2$	-45.3	
Zn^{2+}	Zincite	ZnO	11.334	-21.42
		$Zn(OH)_2$	12.474	-19.269
	Sphalerite	ZnS	-28.75§	7.17
	Smithsonite	$ZnCO_3$	-10.00	-3.786
	Zincosite	$ZnSO_4$	3.93	-19.738

*Values match the thermodynamic database in MINEQL+ ver. 4.6 except for italicized values, which are from Benjamin.[1]

†Values are for the reaction MeX → Me + X, except for (hydr)oxide solids (i.e., $Me(OH)_x$ or M_xO_y, MeOOH) where the values are $^*K_{s0}$ values (see section 10.5), and the corresponding reactions are

$$Me(OH)_x + xH^+ \rightarrow Me^{x+} + xH_2O,$$

$$Me_xO_y + 2yH^+ \rightarrow Me^{(2y/x)+} + yH_2O,$$

$$MeOOH + 3H^+ \rightarrow Me^{3+} + 2H_2O.$$
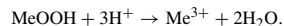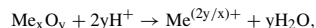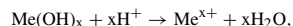
Other solids containing hydroxide release a hydroxide ion for the K values given.

§Solubility constants for sulfide minerals assume $pK_{a2} = 17.3$ for $HS^- \rightarrow H^+ + S^{2-}$, which is the value in MINEQL+ ver. 4.6 and is consistent with recent measurements.[2]

Table 10.2 Effect of K_{a2} value for H_2S on K_{s0} values for mineral sulfides

	Log K_{s0} with $K_{a2} = 13.9$	Log K_{s0} with $K_{a2} = 17.3$
Cd^{2+}	−28.26	−31.66
Co^{2+}	−24.97	−28.37
Cu^{2+}	−36.20	−39.60
Fe^{2+}	−17.50	−20.90
Hg^{2+}	−53.40	−56.80
Mn^{2+}	−13.73	−17.13
Ni^{2+}	−26.70	−30.10
Pb^{2+}	−27.87	−31.27
Zn^{2+}	−25.35	−28.75

and

$$[S^{2-}] = 4.37 \times 10^{-19} \text{ M for } K_{a2} = 10^{-17.3}.$$

Obviously, the product of $[Co^{2+}][S^{2-}]$ will have two different values, each one correct depending on the K_{a2} value used. (Note: when performing any calculation with MINEQL+ involving sulfide, it is necessary to move the species $H_2S_{(g)}$ from "fixed entities" to "species not considered.")

Sulfide obviously is not the dominant species in most sulfide-containing systems. Writing the dissolution reaction in terms of bisulfide involves adding reactions:

$$CoS_{(s)} \rightleftharpoons Co^{2+} + S^{2-} \qquad\qquad K_{s0} = 10^{-28.37}$$

$$\underline{S^{2-} + H^+ \rightleftharpoons HS^- \qquad\qquad 1/K_{a2} = 10^{17.3}}$$

$$CoS_{(s)} + H^+ \rightleftharpoons Co^{2+} + HS^- \qquad {}^*K_{s0} = 10^{-11.07}$$
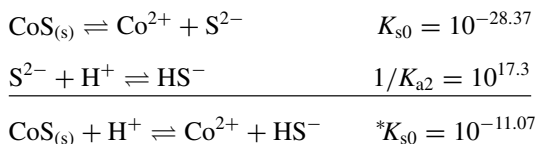
The * designation is used because the reaction is mediated by a proton when written in this form.

EXAMPLE 10.4 $MnS_{(s)}$ versus $MnCO_{3(s)}$: In a solution at pH 9 with values of total sulfide and total carbonate fixed at 10^{-6} M, which solid will control manganese solubility? Assume a closed system.

Answer: The relevant solubility expressions are

(1) $MnS_{(s)} \rightleftharpoons Mn^{2+} + S^{2-}$ $\qquad K_{s0} = \{Mn^{2+}\}\{S^{2-}\} = 10^{-17.13}$,
(2) $MnCO_{3(s)} \rightleftharpoons Mn^{2+} + CO_3^{2-}$ $\qquad K_{s0} = \{Mn^{2+}\}\{CO_3^{2-}\} = 10^{-10.58}$.
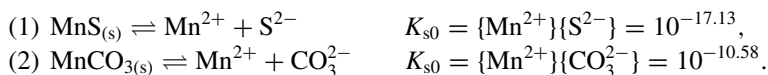
Using the appropriate values of K_{a1} and K_{a2} for the carbonate and sulfide systems and the α_2 expression, one obtains

(3) $\{S^{2-}\} = 4.96 \times 10^{-15} M$,
(4) $\{CO_3^{2-}\} = 1.78 \times 10^{-7} M$.
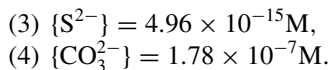
To test the equilibrium concentration of Mn^{2+} in each situation, the K_{s0} value is divided by the concentration (actually activity) of the anion. For MnS,

(5) $\{Mn^{2+}\} = 10^{-17.13}/4.96 \times 10^{-15} = 1.49 \times 10^{-3}M$.

For $MnCO_3$,

(6) $\{Mn^{2+}\} = 10^{-10.58}/1.78 \times 10^{-7} = 1.48 \times 10^{-4}M$.

Thus, $MnCO_{3(s)}$ will control the solubility of Mn^{2+} because it will precipitate when $\{Mn^{2+}\}$ is an order of magnitude smaller than that needed to precipitate $MnS_{(s)}$. Although the K_{s0} for $MnS_{(s)}$ is smaller, the carbonate ion concentration is much higher than sulfide concentration at pH 9 (because of the difference in pK_{a2} values). This makes $MnCO_{3(s)}$ less soluble under these conditions. Note that we have not considered potential oxide or hydroxide solids of manganese, which would need to be considered to fully evaluate the system (see Section 10.5).

10.4 Solubility of carbonates and water softening

Calcium and bicarbonate are two of the major ions in natural waters, and calcium carbonate minerals are vitally important in many aquatic environments. Calcium and magnesium carbonates are important in terms of water treatment, and the shells of many oceanic species consist of calcium carbonates (see Box 8.1). Other carbonate minerals also may form depending on the concentration of the relevant cations. Here our discussion is largely focused on calcium and magnesium carbonates. As in Chapter 8, we must consider both open and closed systems.

10.4.1 Solubility of calcium carbonate

There are three common crystalline forms of $CaCO_{3(s)}$ in aquatic environments: *calcite*, *aragonite*, and *vaterite*; these are called *polymorphs* of $CaCO_{3(s)}$. Calcite is the thermodynamically most stable form (it has the smallest K_{s0} value and lowest solubility), and vaterite is the least stable. Calcite is common in the shells of marine plankton (foraminifera and coccolithophores) and corals, but aragonite is commonly found in shells of mollusks, e.g., clams, oysters, snails (sometimes mixed with calcite). The most reliable measurements of K_{s0} for these polymorphs are those of Plummer and Busenberg,[4] which are summarized as a function of temperature in Table 10.3. It is important to note that the solubility of $CaCO_{3(s)}$ decreases with increasing temperature, and this frequently causes problems of scale build-up (i.e., formation of $CaCO_{3(s)}$ deposits) in hot water pipes and water heaters in regions with hard water. The decrease in $CaCO_{3(s)}$ solubility with temperature makes sense in that one of the ions, CO_3^{2-}, is in equilibrium with $CO_{2(aq)}$, which (as a dissolved gas) has decreasing solubility with temperature.

Mixed crystalline forms of calcite with magnesium as an impurity, called magnesian calcites, also are common in nature, including in shells of aquatic organisms. Magnesian calcites are solid solutions with up to ~20% of the Ca^{2+} in the crystalline lattice replaced randomly by Mg^{2+} ions ($Ca_{1-x}Mg_xCO_{3(s)}$). In general, low Mg-calcites (with x <~0.03–0.04) are thought to be more stable than calcite and aragonite, but high

Table 10.3 Solubility data for common CaCO₃ polymorphs*

Temperature, °C	Log K_{s0}		
	Calcite	Aragonite	Vaterite
0	8.382	8.218	7.737
10	8.411	8.256	7.797
20	8.450	8.307	7.868
25	8.481	8.337	7.908
30	8.511	8.371	7.951
40	8.581	8.447	8.046

Predictive equations (T in Kelvin)

Log $K_{s0(\text{calcite})} = -171.9065 - 0.077993T + 2839.319/T + 71.595\log T$

Log $K_{s0(\text{aragonite})} = -171.9773 - 0.077993T + 2903.293/T + 71.595\log T$

Log $K_{s0(\text{vaterite})} = -172.1295 - 0.077993T + 3074.688/T + 71.595\log T$

$\Delta G°$, kJ mol⁻¹	48.40	47.58	45.17
$\Delta H°$, kJ mol⁻¹	−9.61	−10.83	−15.79
$\Delta S°$, J mol⁻¹ K⁻¹	−194.6	−195.8	−198.7
$\Delta C_p°$, J mol⁻¹ K⁻¹	−295	−295	−295

*Adapted from Plummer and Busenberg.[4]

Mg-calcites are less stable (i.e., more soluble) than calcite and aragonite.[3] Solid solutions of other metal ions (e.g., Sr and Mn) with CaCO₃ also are common, and the formation of such solids has important solubility implications especially regarding the minor cation in the solid solution (see Section 4.7.2 and Examples 4.4 and 4.5). Limestone is largely calcite, usually with other divalent cations (especially Mg; also Sr, Fe^{II}, Mn^{II}) as impurities. (Limestone also contains small amounts of silica as clay, silt, or chert particles mixed with the carbonates, but as separate phases.)

10.4.2 Solubility diagram for calcite

We begin with the solubility expression for calcite:

$$CaCO_{3(\text{calcite})} \rightleftharpoons Ca^{2+} + CO_3^{2-} \qquad K_{s0} = 10^{-8.48} = \{Ca^{2+}\}\{CO_3^{2-}\} \qquad (10.8)$$
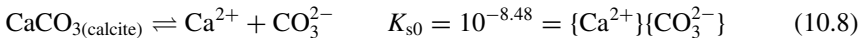
We will assume a C_T value of 1 mM. Thus, we need to keep in mind

$$K_{a1} = \frac{\{H^+\}\{HCO_3^-\}}{\{H_2CO_3^*\}} = 10^{-6.35} \qquad (8.31)$$

$$K_{a2} = \frac{\{H^+\}\{CO_3^{2-}\}}{\{HCO_3^-\}} = 10^{-10.33} \qquad (8.32)$$

When the pH of the system is above pK_{a2}, $\{CO_3^{2-}\} \sim C_T$. Thus,

$$\{Ca^{2+}\} = \frac{K_{s0}}{\{CO_3^{2-}\}}, \text{ or } \log\{Ca^{2+}\} = \log K_{s0} - \log\{CO_3^{2-}\} \qquad (10.9)$$

Substituting the known values of K_{s0} and $\{CO_3^{2-}\}$ gives

$$\log\{Ca^{2+}\} = \log(10^{-8.48}) - \log(10^{-3}) = -8.48 - (-3) = -5.48. \qquad (10.10)$$

Thus, above pH 10.33, a calcium concentration $\geq 10^{-5.48}$ mol/L will cause precipitation of calcite. Between pH 6.35 and 10.33, bicarbonate dominates the carbonate speciation, and calcite solubility can be expressed as

$$CaCO_{3(s)} \rightleftharpoons Ca^{2+} + CO_3^{2-} \qquad\qquad K_{s0} = 10^{-8.48}$$

$$\underline{H^+ + CO_3^{2-} \rightleftharpoons HCO_3^- \qquad\qquad\qquad 1/K_{a2} = 10^{10.33}}$$

$$CaCO_{3(s)} + H^+ \rightleftharpoons Ca^{2+} + HCO_3^- \qquad K_{s1} = 10^{1.85}$$

$$K_{s1} = \frac{\{HCO_3^{2-}\}\{Ca^{2+}\}}{\{H^+\}}, \qquad \text{or} \qquad \{Ca^{2+}\} = \frac{K_{s1}\{H^+\}}{\{HCO_3^{2-}\}} \qquad (10.11)$$
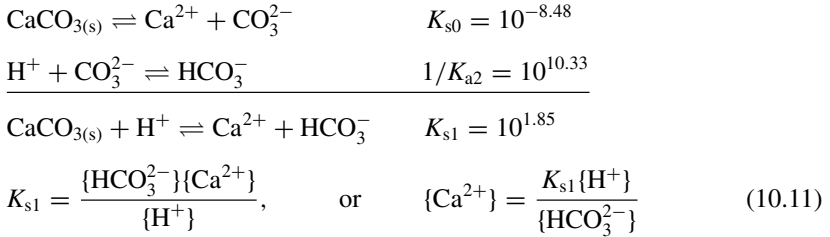
Thus,

$$\log\{Ca^{2+}\} = \log K_{s1} + \log\{H^+\} - \log\{HCO_3^{2-}\}. \qquad (10.12)$$

In this pH range, $\{HCO_3^-\} \approx C_T$, and

$$\log\{Ca^{2+}\} = \log(10^{1.85}) - \log(10^{-3}) - pH = 4.85 - pH. \qquad (10.13)$$

Notice that at pH 10.33, $\log\{Ca^{2+}\} = -5.48$, making this equation consistent with Eq. 10.10.

Finally, we perform the same manipulation for pH < 6.35.

$$CaCO_{3(calcite)} + H^+ \rightleftharpoons Ca^{2+} + HCO_3^- \qquad K_{s1} = 10^{1.85}$$

$$\underline{H^+ + HCO_3^- \rightleftharpoons H_2CO_3^* \qquad\qquad\qquad 1/K_{a1} = 10^{6.35}}$$

$$CaCO_{3(calcite)} + 2H^+ \rightleftharpoons Ca^{2+} + H_2CO_3^* \qquad K_{s2} = 10^{8.2}$$

$$K_{s2} = \frac{\{H_2CO_3^*\}\{Ca^{2+}\}}{\{H^+\}^2}, \text{ or } \{Ca^{2+}\} = \frac{K_{s1}\{H^+\}^2}{\{H_2CO_3^*\}} \qquad (10.14)$$
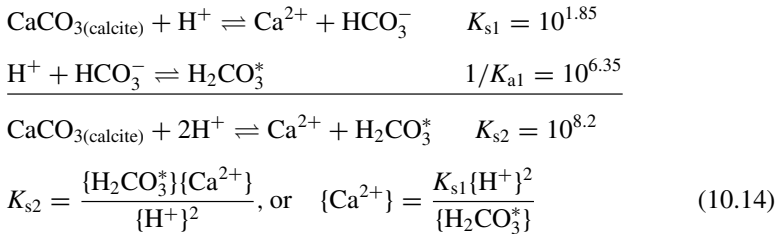
Thus,

$$\log\{Ca^{2+}\} = \log K_{s2} + 2\log\{H^+\} - \log\{H_2CO_3^*\}. \qquad (10.15)$$

In this pH range, $\{H_2CO_3^*\} \approx C_T$, and

$$\log\{Ca^{2+}\} = \log(10^{8.2}) - \log(10^{-3}) - 2pH = 11.2 - 2pH. \qquad (10.16)$$

Equations 10.10, 10.13, and 10.16 may now be plotted on a pC-pH diagram, each in the appropriate pH range, to obtain a solubility diagram for calcium carbonate in a
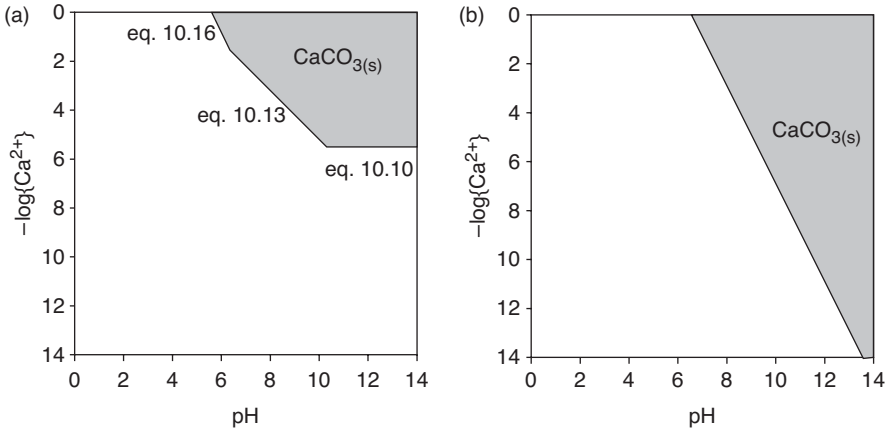
Figure 10.2 (a) Solubility diagram for calcite in a closed system with $C_T = 1$ mM; (b) solubility diagram for calcite in an open system.

closed system containing 1 mM total carbonate. This is shown in Figure 10.2 (recall that $pC = -\log\{C\}$).

In an open system, generating the diagram is somewhat easier because it is unnecessary to specify C_T, which changes with pH. At any pH, however, the carbonate concentration can be calculated using the relationship given in Chapter 8:

$$\{CO_3^{2-}\} = \frac{K_{a1}K_{a2}K_H P_{CO_2}}{\{H^+\}^2} \tag{8.46}$$

Thus,

$$\{Ca^{2+}\} = \frac{\{H^+\}^2 K_{s0}}{K_{a1}K_{a2}K_H P_{CO_2}}, \tag{10.17a}$$

and

$$\log\{Ca^{2+}\} = \log K_{s0} - \log K_{a1}K_{a2}P_{CO_2} + 2\log\{H^+\} \tag{10.17b}$$

or

$$\log\{Ca^{2+}\} = \log(10^{-8.48}) - \log(10^{-21.68}) - 2pH = 13.2 - 2pH \tag{10.17c}$$

This equation is plotted in Figure 10.2b.

10.4.3 Dolomite

Another common carbonate mineral that contains both calcium and magnesium is dolomite, $CaMg(CO_3)_2$. In contrast to magnesian calcites, which are solid solutions with random substitution of Mg atoms in the crystalline matrix, dolomite is a mineral

phase, in which Mg atoms replace the Ca atoms in every other layer of the basic calcite structure. Many limestones of marine origin contain both calcite and dolomite. For many years scientists were unable to form dolomite under laboratory conditions (ambient temperature and pressure) from supersaturated solutions, and it was thought that it formed only at high temperatures ($> 100°C$) in deep sedimentary environments. This "irreversible" behavior led to difficulties in measuring the solubility product for dolomite, $K_{s0(dol)}$, and to large uncertainties in the reported values. In fact, Sherman and Barak[5] reported that published values for $K_{s0(dol)}$ range over almost four orders of magnitude, from $\sim 10^{-15.6}$ to $10^{-19.4}$. Based on careful laboratory experiments, these workers concluded that $K_{s0(dol)}$ is $10^{-17.2 \pm 0.2}$. Although the factors limiting dolomite formation under ambient conditions still are incompletely understood, the high concentration of sulfate in seawater has been shown to be a major limiting factor.[6] Nonetheless, a few recent studies have shown that dolomite is formed at low temperatures and pressures in some hypersaline lakes, and perhaps ironically, the formation process appears to be mediated by actions of sulfate-reducing bacteria.[7] Success in forming dolomite in the laboratory was achieved only in 1999,[8] when it was found that varying the solution pH between supersaturating and undersaturated conditions resulted in net formation of dolomite.

In a clever application of field data, Hsu[9] estimated $K_{s0(dol)}$, from well-water data from Florida. The rock matrix of the Floridan Aquifer, a vast underground reservoir that underlies most of peninsular Florida and extends into Georgia, consists of dolomitic limestone. Hsu found that the ratio of $[Mg^{2+}]/[Ca^{2+}]$ was nearly constant with a value of 0.8 ± 0.1 in well-water samples from the aquifer, despite wide variations in total Ca and Mg concentrations, and he proposed that the reason for the nearly constant ratio is that water in the aquifer is in equilibrium with both calcite and dolomite phases:

$$CaMg(CO_3)_{2(dol)} + Ca^{2+} \rightleftharpoons 2CaCO_{3(cal)} + Mg^{2+}; K_{d \to c} = ? \qquad (10.18)$$
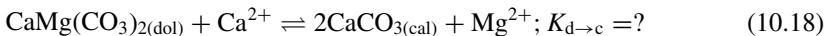
The equilibrium constant for this phase-change reaction is equal to the ratio of $[Mg^{2+}]$ to $[Ca^{2+}]$ and also to the ratio of the solubility product of dolomite to the square of the solubility product of calcite (ignoring activity corrections):

$$K_{d \to c} = \frac{[Mg^{2+}]}{[Ca^{2+}]} = \frac{(K_{s0(dol)})}{K_{s0(cal)}^2} = \frac{[Ca^{2+}][Mg^{2+}][CO_3^{2-}]^2}{[Ca^{2+}]^2[CO_3^{2-}]^2} \qquad (10.19)$$

The reader can readily verify the validity of the relationship involving the K_{s0} terms by writing the K_{s0} expression for dolomite and subtracting the square of the K_{s0} expression for calcite. Because $K_{d \to c}$ was found to have a value of 0.8 from the aquifer data, and $K_{s0(cal)}$ is 3.55×10^{-9} (Table 10.3), we calculate that $K_{s0(dol)} = 1.0 \times 10^{-17}$. This value agrees well with the $K_{s0(dol)}$ value reported by Sherman and Barak,[5] providing independent support for the two estimates.

10.4.4 Water softening

Removal of calcium and magnesium ions by precipitation is an important process in drinking water treatment. **Hardness**, the sum of multivalent cations in water, usually is dominated by Ca^{2+} and Mg^{2+}. The **carbonate hardness** is that portion of the hardness

that can be associated with the bicarbonate and carbonate present in the water. If the carbonate hardness (CH) and total hardness (TH) are equal, the calcium and magnesium often are presumed to be are derived from carbonate minerals.* If TH > CH, the difference is called noncarbonate hardness (NCH), and it reflects the dissolution of calcium and magnesium minerals that contained other anions.

The goal of *water softening* is to remove hardness. Hard water causes scaling in pipes and on fixtures and makes soaps less effective cleaners. (The EDTA present in many shampoos is designed to complex calcium and prevent it from precipitating in your hair and to make rinsing easier!) From Figure 10.2, it is obvious that raising the pH facilitates the precipitation of calcium carbonate. Lime, $Ca(OH)_2$, is the reagent commonly used to raise the pH of waters to precipitate calcium carbonate; the process is known as lime softening. Lime provides two benefits. It raises the pH, but it also raises the Ca^{2+} concentration, aiding precipitation. Obviously, one wants to precipitate much more Ca^{2+} than one adds. In typical lime softening processes, sufficient lime is added to raise the pH of the water to ~11.0. Under these conditions, highly effective removal of Ca^{2+} as $CaCO_{3(s)}$ can be achieved.

Magnesium carbonate (magnesite), $MgCO_3$, is the stable solid that forms in natural waters containing typical concentrations of Mg^{2+} and alkalinity at moderate pH values (see Example 10.5). However, under the normal conditions for lime softening (pH > 10.5), magnesium ions precipitate as brucite, $Mg(OH)_{2(s)}$. As shown in Example 10.6, the pH at which magnesite and brucite can coexist depends on the C_T of the water (i.e., its concentration of CO_3^{2-}), and for typical C_T values ~2 mM, this occurs at pH 10.65. Below this value, magnesite is the stable mineral form of Mg^{2+}, and above this value brucite is the stable form.

In waters without sufficient alkalinity, soda ash (i.e., sodium carbonate) also is added to convert all the NCH to CH. This is known as lime-soda softening. This has the benefit of decreasing carbonate mineral solubility by increasing the concentration of carbonate ions. Table 10.4 presents the stoichiometric equations involved in lime-soda softening for hardness removal. After softening, the water has a high pH (~11) but a low carbonate concentration. The bicarbonate concentration is increased and the pH lowered by bubbling CO_2 through the water, a process called recarbonation. Water needs to have appropriate pH and carbonate levels to prevent damage to concrete or iron pipes.

Alternatively, removal of calcium and magnesium can be accomplished via ion exchange. Most home water softeners (to which sodium chloride pellets or blocks are added) are such exchangers that take up calcium and magnesium in the water and replace it with sodium.

EXAMPLE 10.5 Removal of Mg^{2+} by lime softening: (A) If the magnesium concentration in a water is 50 mg/L as $CaCO_3$, at what pH does Mg^{2+} start to precipitate, and which solid precipitates? Assume a closed system with $C_T = 1$ mM.

---

*This is not always true, however. Recall that the CO_2-induced weathering of aluminosilicate minerals produces both base cations and an equivalent amount of bicarbonate alkalinity. If the mineral being weathered contains Ca or Mg (e.g., a calcium plagioclase), the resulting hardness will be all carbonate hardness (see Eq. 2.3 and Section 2.2.4).

Table 10.4 Stoichiometric equations involved in lime-soda softening[*]

Carbonate hardness (lime is sufficient)

Ca^{2+}: $Ca^{2+} + 2HCO_3^- + Ca(OH)_{2(sl)} \rightarrow 2CaCO_{3(s)} + 2H_2O$

Mg^{2+}: $Mg^{2+} + 2HCO_3^- + 2Ca(OH)_{2(sl)} \rightarrow Mg(OH)_{2(s)} + 2CaCO_{3(s)} + 2H_2O$
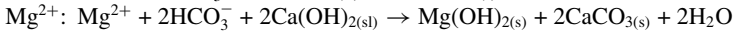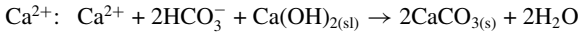
Noncarbonate hardness (requires soda as well)[†]

Ca^{2+}: $Ca^{2+} + 2Cl^- + Na_2CO_{3(sl)} \rightarrow CaCO_{3(s)} + 2Na^+ + 2Cl^-$

Mg^{2+}: $Mg^{2+} + 2Cl^- + Na_2CO_{3(sl)} + Ca(OH)_{2(sl)} \rightarrow Mg(OH)_{2(s)} + CaCO_{3(s)} + 2Na^+ + 2Cl^-$
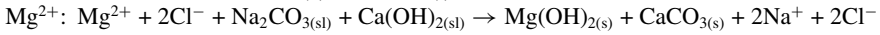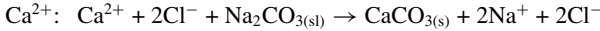
[*]Equations assume pH is high enough for brucite to be the stable phase for Mg^{2+}; subscript "sl" in the equations denotes a slurry for the reagents.

[†]Cl^- shown as counter anion for charge balance purposes, but other ions also may play this role.

Answer: First, convert the concentration of Mg^{2+} to molar units:

$$50 \, mg/L \, as \, CaCO_3 \times 12.15 \, mg \, Mg^{2+}/meq/50 \, mgCaCO_3/meq = 12.15 \, mg/L \, Mg^{2+}$$

$$12.15 \, mg/L \, Mg^{2+} \times 1 \, mmol/24.3 = 0.5 \, mM \, Mg^{2+}$$

The problem is now solved using the titration function in MINEQL+ via the following steps:

(1) Select Mg^{2+} and CO_3^{2-} as species and scan the thermodynamic database.
(2) In the Wizard, set Mg^{2+} to 0.5E-3 and total carbonate (closed system) to 1E-3.
(3) Do not change anything on the pH tab, and leave all solids on. The goal is to see which one precipitates.
(4) Close the Wizard and click "No" on the Tableau Switch dialog.
(5) On the RunTime Manager, click Multirun and select "Titration" for type of calculation.
(6) Click "Select Variable" and set the variable type to log K, and then scroll down and select "log K of pH." Set the starting value as 6 (or some other number low enough to be confident that no precipitation will occur), the ending as 14, and the number of steps as 33 (which will calculate every 0.25 pH units).
(7) After naming the output file, click Run.
(8) Using the graphing function, plot log Mg^{2+} versus pH. This shows that Mg^{2+} begins to decrease around pH 9.5. Selecting "Special Reports" and "Summary of all species for a single run." Select run 14, and then run 15. On run 14, the pH is 9.25, and no solids have precipitated. On run 15, the pH is 9.50, and magnesite ($MgCO_{3(s)}$) has precipitated.

(B) For the water in (A), what is the solid form of Mg^{2+} that precipitates under normal softening operations in water treatment plants?

Answer: As indicated in the text, water treatment plants normally add enough lime or lime-soda to raise the pH to ~11. From the MINEQL+ runs in (A), select the "Special Report" for run 21, where the pH is 11.0. You will find that brucite is the solid phase that has precipitated. You may also use the graphing function and plot log Mg^{2+}, log(brucite) and log(magnesite) versus pH. When log(brucite) reaches a value of zero, the activity of brucite $= 1$, and the solid has begun to form. (The same idea holds for magnesite).

From the graph you can see that magnesite begins to precipitate, i.e., log(magnesite) = 0, around pH 9.5, and brucite begins to precipitate around pH 10.75.

EXAMPLE 10.6: What is the pH at which brucite and magnesite coexist in equilibrium with an Mg^{2+} bicarbonate solution? Ignore activity corrections

Answer: First, we need to specify a C_T value. Here we will use $C_T = 2 \times 10^{-3}$ M, which is in the range typically found for moderately hard waters.

Next, we write the solubility expressions for magnesite and brucite:

(1) $MgCO_{3(s)} \rightleftharpoons Mg^{2+} + CO_3^{2-}$ $K_{s0(m)} = 10^{-7.46}$
(2) $Mg(OH)_{2(s)} \rightleftharpoons Mg^{2+} + 2OH^-$ $K_{s0(b)} = 10^{-11.16}$
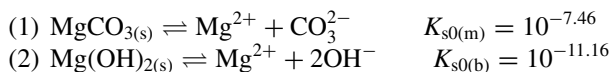
Subtracting Eq. (2) from Eq. (1) yields:

(3) $MgCO_{3(s)} + 2OH^- \rightleftharpoons Mg(OH)_{2(s)} + CO_3^{2-} K_{m \to b} = K_{s0(m)}/K_{s0(b)} = 10^{3.70}$
= $[CO_3^{2-}]/[OH^-]^2$
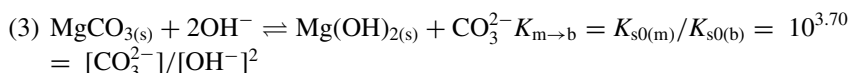
As a first approximation, we will assume that the pH is high enough so the $[CO_3^{2-}]$ = $C_T = 2 \times 10^{-3}$ M. Substituting into the expression for $K_{m \to b}$ and solving for $[OH^-]$ yields $[OH^-] = 10^{-3.20}$, or (ignoring activity corrections) pOH = 3.20, and pH = 10.80. We note that the calculated pH is above pK_{a2} (10.33) for carbonic acid, and thus most (but not all) of the C_T is present as CO_3^{2-} (to be precise, $[CO_3^{2-}] = 2.95[HCO_3^-]$ or $\sim 0.75C_T$). For a more accurate estimate, we can use the method of successive approximations and find that at pH = 10.72 brucite and magnesite can coexist.

10.5 Solubility of metal oxides and hydroxides

The hydroxy complexes of metal ions were discussed in Chapter 9, and such species must be considered when considering the solubility of oxide and hydroxide minerals. The equations used to calculate metal ion solubility are similar to those in Chapter 9, except that an additional solubility equation is included. To demonstrate this, ferrous iron (Fe^{2+}) is used below, and activity corrections are ignored. The relevant complexation equations are

$$Fe^{2+} + H_2O = FeOH^+ + H^+ \qquad *\beta_1 = \frac{[FeOH^+][H^+]}{[Fe^{2+}]} = 10^{-9.397} \qquad (10.20)$$

$$Fe^{2+} + 2H_2O = Fe(OH)_2^0 + 2H^+ \qquad *\beta_2 = \frac{[Fe(OH)_2^0][H^+]^2}{[Fe^{2+}]} = 10^{-20.494} \qquad (10.21)$$

$$Fe^{2+} + 3H_2O = Fe(OH)_3^- + 3H^+ \qquad *\beta_3 = \frac{[Fe(OH)_3^-][H^+]^3}{[Fe^{2+}]} = 10^{-28.991} \qquad (10.22)$$
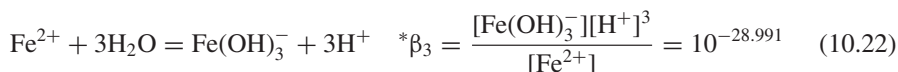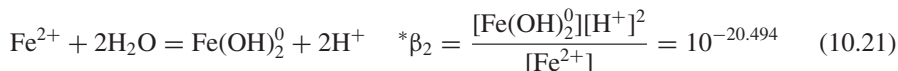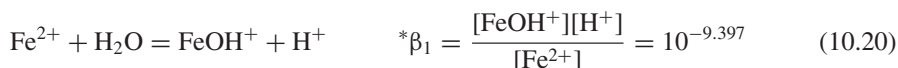
and the relevant solubility equilibrium is

$$Fe(OH)_{2(s)} \rightleftharpoons Fe^{2+} + 2OH^- \qquad K_{s0} = [Fe^{2+}][OH^-]^2 = 10^{-14.43}. \qquad (10.23)$$
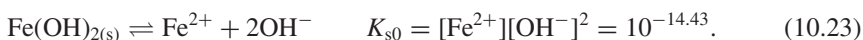
Note that $Fe(OH)_2^0$ denotes the neutral, soluble complex and $Fe(OH)_{2(s)}$ denotes solid ferrous hydroxide. Because the complexation equations are in terms of protons, it is convenient to rewrite the solubility expression to match the value given in Table 10.1 for $*K_{s0}$.

$$Fe(OH)_{2(s)} \rightleftharpoons Fe^{2+} + 2OH^- \qquad\qquad K_{s0} = 10^{-14.43}$$

$$\underline{+\ 2H^+ + 2OH^- \rightleftharpoons 2H_2O \qquad\qquad 1/K_w^2 = 10^{27.994}}$$

$$Fe(OH)_{2(s)} + 2H^+ \rightleftharpoons Fe^{2+} + 2H_2O \qquad *K_{s0} = 10^{13.564} = [Fe^{2+}]/[H^+]^2 \quad (10.24)$$
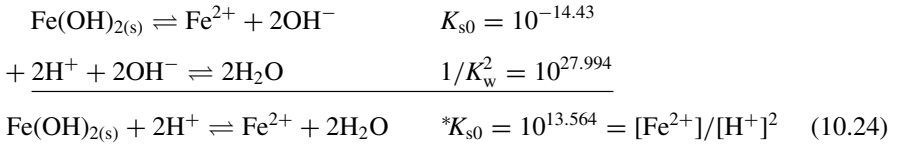
Two questions now can be asked: (1) for a given total Fe^{2+} level $(TOT Fe^{II})^*$ over what pH range will $Fe(OH)_{2(s)}$ precipitate, and (2) if excess solid is present, what is the speciation of Fe^{II} at a given pH?

Taking the first case at $TOT Fe^{II} = 10^{-4}$ M, we can determine whether the solid will precipitate at any pH value. This is not a simple as plugging in 10^{-4} M as $[Fe^{2+}]$ into the $*K_{s0}$ expression and solving for pH because of complexation of the ferrous iron. Recall that

$$Fe_T^{II} = [Fe^{2+}] + [FeOH^+] + [Fe(OH)_2^0] + [Fe(OH)_3^-] \qquad (10.25)$$

and

$$Fe_T^{II} = [Fe^{2+}]\left(1 + \frac{*\beta_1}{[H^+]} + \frac{*\beta_2}{[H^+]^2} + \frac{*\beta_3}{[H^+]^3}\right) \qquad (10.26)$$

For any pH value, $[Fe^{2+}]$ can be calculated (assuming $TOT Fe^{II} = Fe_T^{II}$), followed by the complex concentrations. For each value selected, the IAP must be tested to see if $[Fe^{2+}]/[H^+]^2$ is greater than $10^{13.564}$ (see Eq. 10.24). If it is, the assumption that $TOT Fe^{II} = Fe_T^{II}$ is invalid. Because the solid has precipitated, $[Fe^{2+}]$ then is set by the solubility expression (Eq. 10.24), and the concentrations of the complexes are calculated based on this value. These data are summarized in Table 10.5.

At pH 9 and 11, the IAP exceeds $*K_{s0}$ (based on the numbers that are lined out), and the solid thus precipitates. These numbers tell us that the solubility condition is exceeded and that the calculations for these pH values must be performed again assuming that $Fe(OH)_{2(s)}$ is present, which gives the italicized numbers. Note that at pH 13, the solid redissolves, because the anionic trihydroxy complex, $Fe(OH)_3^-$, dominates. This is a feature for many (hydr)oxide minerals—when anionic hydroxy complexes begin to dominate the speciation, the solubility increases. This is depicted using the data from Table 10.5 to produce Figure 10.3. Note that there is a region in the figure where the total dissolved iron, Fe_T^{II}, is less than the 10^{-4} M added to the system, because $Fe(OH)_{2(s)}$ precipitates. At pH > 11.5 one can see that Fe_T^{II} returns to 10^{-4} M (i.e., this is the concentration of the $Fe(OH)_3^-$ complex), again emphasizing that as pH increases, solids can precipitate and then redissolve.

---

*Note that in previous chapters we used X_T for the total quantity of X because we were dealing only with the amount in solution. (X_T is defined in Section 7.2.2 as the mass balance expression for the sum of all species involving X in solution.) Now we are interested in keeping track not just of the dissolved components of X (here Fe^{II}) but also the quantities that precipitate. ($TOT X$ expressions do this; see Section 7.2.3 for review.)

Table 10.5 Speciation of Fe^{2+} for $TOTFe^{II} = 10^{-4}$ M as a function of pH

pH	$[Fe^{2+}]$	$[FeOH^+]$	$[Fe(OH)_2^0]$	$[Fe(OH)_3^-]$	IAP	Solid Forms?
1	1×10^{-4}	4.01×10^{-13}	3.21×10^{-23}	1.02×10^{-30}	10^{-2}	N
3	1×10^{-4}	4.01×10^{-11}	3.21×10^{-19}	1.02×10^{-24}	10^2	N
5	1×10^{-4}	4.01×10^{-9}	3.21×10^{-15}	1.02×10^{-18}	10^6	N
7	9.96×10^{-5}	3.99×10^{-7}	3.19×10^{-11}	1.02×10^{-12}	10^{10}	N
9	7.07×10^{-5}	2.83×10^{-5}	2.27×10^{-7}	7.22×10^{-7}	$10^{13.85}$	Y
9 (with $Fe(OH)_{2(s)}$)	3.66×10^{-5}	1.46×10^{-5}	1.17×10^{-7}	3.74×10^{-7}		
11	9.73×10^{-9}	3.90×10^{-7}	3.12×10^{-7}	9.93×10^{-5}	$10^{13.99}$	Y
11(with $Fe(OH)_{2(s)}$)	3.66×10^{-9}	1.46×10^{-7}	1.17×10^{-7}	3.74×10^{-5}		
13	9.79×10^{-15}	3.93×10^{-11}	3.14×10^{-9}	1×10^{-4}	$10^{11.99}$	N
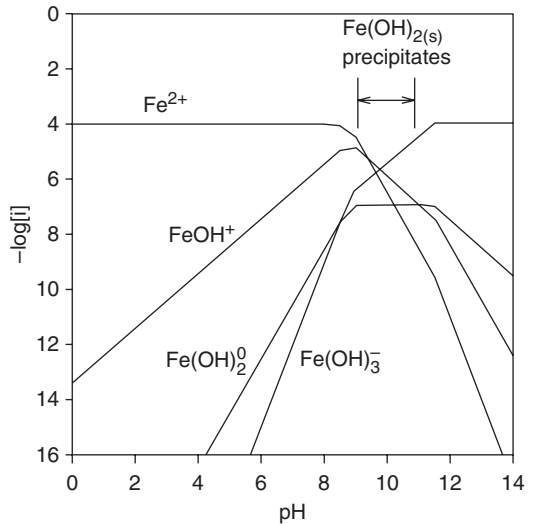
Figure 10.3 pC-pH diagram for $TOTFe^{II}$ of 10^{-4} M.

We now turn to the situation where excess solid is present. For this condition, the $[Fe^{2+}]$ concentration at any pH is dictated by

$$[Fe^{2+}] = {}^*K_{s0}[H^+]^2. \tag{10.27}$$

Taking the logarithm of both sides, we get

$$\log[Fe^{2+}] = \log {}^*K_{s0} + 2\log[H^+] = \log {}^*K_{s0} - 2pH. \tag{10.28}$$

This, of course, is equivalent to a line on a pC-pH diagram. By developing similar lines for the three complexes, $FeOH^+$, $Fe(OH)_{2(aq)}^0$, and $Fe(OH)_3^-$, we can develop a pC-pH diagram that shows the region of $Fe(OH)_{2(s)}$ precipitation (like those for calcium carbonate in Figure 10.2). For example, for $FeOH^+$ we need to develop a relationship

between the concentration of this species and $Fe(OH)_{2(s)}$. We can do this by adding the following equations:

$$Fe^{2+} + H_2O \rightleftharpoons FeOH^+ + H^+ \qquad\qquad {}^*\beta_1 = 10^{-9.5}$$

$$+ \quad \underline{Fe(OH)_{2(s)} + 2H^+ \rightleftharpoons Fe^{2+} + 2H_2O \qquad\qquad {}^*K_{s0} = 10^{13.564}}$$

$$Fe(OH)_{2(s)} + H^+ = FeOH^+ + H_2O \qquad {}^*K_{s1} = 10^{4.064} = [FeOH^+]/[H^+]$$

$$(10.29)$$
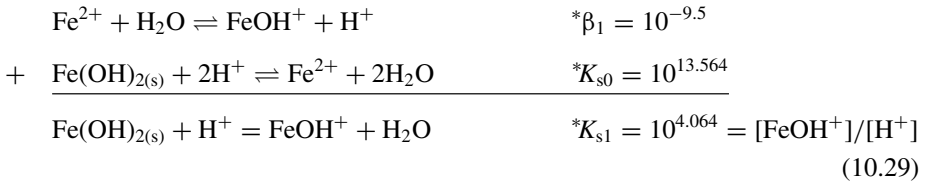
${}^*K_{s1}$ is the solubility constant for solid ferrous hydroxide dissolving to form the first hydroxy complex. Taking the log of the ${}^*K_{s1}$ equation gives

$$\log {}^*K_{s1} = \log[FeOH^+] - \log[H^+], \qquad\qquad (10.30a)$$

or

$$\log[FeOH^+] = \log {}^*K_{s1} - pH. \qquad\qquad (10.30b)$$

The equivalent expressions for the other two complexes can be derived similarly:

$$Fe(OH)_{2(s)} + 2H^+ \rightleftharpoons Fe^{2+} + 2H_2O \qquad {}^*K_{s0} = 10^{13.564}$$

$$+ \quad \underline{Fe^{2+} + 2H_2O \rightleftharpoons Fe(OH)_2^0 + 2H^+ \qquad {}^*\beta_2 = 10^{-20.494}}$$

$$Fe(OH)_{2(s)} \rightleftharpoons Fe(OH)_{2(aq)}^0 \qquad {}^*K_{s2} = 10^{-6.93} \qquad (10.31a)$$

$$\log[Fe(OH)_{2(aq)}^0] = \log {}^*K_{s2} \qquad\qquad (10.31b)$$

$$Fe(OH)_{2(s)} + 2H^+ \rightleftharpoons Fe^{2+} + 2H_2O \qquad {}^*K_{s0} = 10^{13.564}$$

$$+ \quad \underline{Fe^{2+} + 3H_2O \rightleftharpoons Fe(OH)_3^- + 3H^+ \qquad {}^*\beta_3 = 10^{-28.991}}$$

$$Fe(OH)_{2(s)} + H_2O \rightleftharpoons Fe(OH)_3^- + H^+ \qquad {}^*K_{s3} = 10^{-15.427} \qquad (10.32a)$$
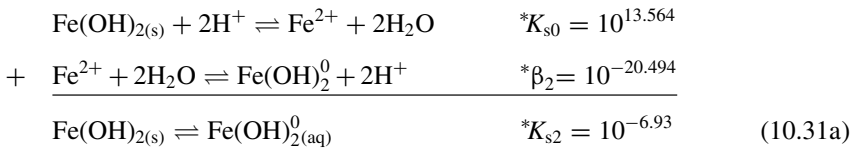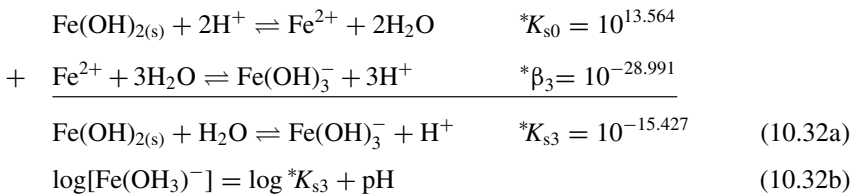
$$\log[Fe(OH)_3)^-] = \log {}^*K_{s3} + pH \qquad\qquad (10.32b)$$

Plotting the equations on a pC-pH diagram gives Figure 10.4. It is interesting to note that when solid $Fe(OH)_2$ is present, the concentration of $Fe(OH)_{2(aq)}^0$ is constant and independent of pH (see Eq. 10.31). This also can be seen in the region of Figure 10.3 where $Fe(OH)_2$ precipitates. This situation is general for all metal ions that form neutral hydroxide complexes with the same formula as the solid, and it also applies to uncharged carbonate complexes (e.g., the concentration of $CaCO_{3(aq)}^0$ is constant over the entire region where solid $CaCO_3$ exists).

Diagrams like Figures 10.3 and 10.4 are useful to illustrate how the solubility of a metal hydroxide and concentrations of hydroxyl complexes vary with pH, but they generally are not used to solve problems as are the pC-pH diagrams described in Chapter 8. Interpretation of solubility diagrams (Figure 10.4) is straightforward. Any combination of pH and pFe_T^{II} values that falls within the shaded region represents supersaturated conditions (i.e., $IAP > {}^*K_{s0}$) with respect to $Fe(OH)_{2(s)}$ solubility, and the
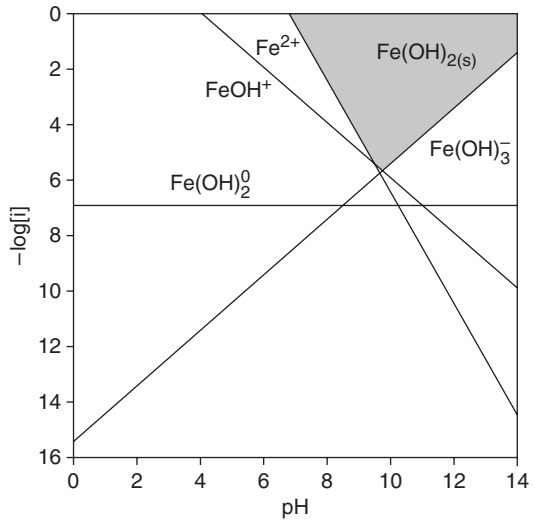
Figure 10.4 pC-pH diagram for a system with $Fe(OH)_{2(s)}$ present. In the shaded region IAP > K_{s0}.

precipitation reaction will proceed spontaneously (although the figure implies nothing about the rate at which that may occur). Note that this region extends indefinitely above the top of the plot, but these are very high (unrealistic) Fe_T^{II} concentrations. Any combination of pH and pFe_T^{II} values that falls outside the shaded region represents undersaturated conditions with respect to the solubility of $Fe(OH)_{2(s)}$, and if solid phase $Fe(OH)_{2(s)}$ is present, it will tend to dissolve. Finally, points along the lines enclosing the shaded area represent the total Fe^{II} that is soluble in equilibrium with $Fe(OH)_{2(s)}$ at a given pH.

10.6 Effects of ligands on solubility

In Section 10.2, we showed that increasing sulfate and fluoride concentrations cause decreased solubility due to the common ion effect. Sections 10.3–10.5 have covered the major anionic species that dictate the solubility of many minerals in natural waters. In this section we explore the effect of other anions (i.e., ligands) on the solubility of metal sulfides, carbonates, and (hydr)oxides. As we saw in Chapter 9, the presence of ligands greatly increases the number of species that are present in solution and can thus increase the total amount of a metal present. As shown in Figure 10.4, increasing the concentration of hydroxide leads to redissolution of a precipitated solid because a new complex becomes more important. Although the concentration of the free metal ion is involved in the K_{s0} expression, solubility is dictated by the total amount of the species that can dissolve. Thus, it is logical to start with the assumption that ligands will increase the total amount of solid that can be dissolved into solution.

EXAMPLE 10.7 A new engineering graduate seeks to impress his boss: Rick has just finished his M.S. with an emphasis in water chemistry and has taken a job with a local consulting firm. His first job is to determine whether pennies thrown into a fish pond at

a local mall have the potential to kill the fish. He was told that the total dissolved copper levels in the pond must be less than 1×10^{-7} M to prevent killing the fish.

Part 1. Rick assumed that tenorite, $CuO_{(s)}$, which likely coats the outside of the pennies, is in excess and dictates copper solubility. He measured the pH of the water found it to be 7.5.

(1) $CuO_{(s)} + 2H^+ \rightleftharpoons Cu^{2+} + H_2O$ $^*K_{s0} = 7.644$
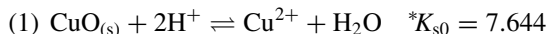
Remembering his graduate school colleague Liam's embarrassment (see Chapter 9), Rick was sure to look up the equilibrium constants for the hydroxy complexes for Cu^{2+}:

(2) $Cu^{2+} + H_2O \rightleftharpoons CuOH^+ + H^+$ $\log{}^*\beta_1 = -7.497$
(3) $Cu^{2+} + 2H_2O \rightleftharpoons Cu(OH)_2^0 + 2H^+$ $\log{}^*\beta_2 = -16.194$
(4) $Cu^{2+} + 3H_2O \rightleftharpoons Cu(OH)_3^- + 3H^+$ $\log{}^*\beta_3 = -26.879$
(5) $Cu^{2+} + 4H_2O \rightleftharpoons Cu(OH)_4^{2-} + 4H^+$ $\log{}^*\beta_4 = -39.980$
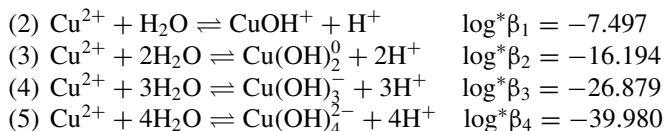
What is the total dissolved copper concentration?

Answer: Assuming tenorite is in excess, Rick calculated the free copper concentration from $^*K_{s0}$:

(6) $10^{7.644} = [Cu^{2+}]/[H^+]^2$ or $[Cu^{2+}] = 10^{7.644}[H^+]^2 = 10^{7.664}(10^{-7.5})^2$
    $= 10^{-7.356}$M,

that is,

$$[Cu^{2+}] = 4.40 \times 10^{-8}M.$$

Using Eq. 10.26 for ferrous iron above and extending it for a fourth hydroxy complex yielded:

(7) $Cu_T^{II} = [Cu^{2+}]\left(1 + \dfrac{{}^*\beta_1}{[H^+]} + \dfrac{{}^*\beta_2}{[H^+]^2} + \dfrac{{}^*\beta_3}{[H^+]^3} + \dfrac{{}^*\beta_4}{[H^+]^4}\right)$

He now calculated Cu_T^{II} (if desired, he also could have calculated the individual copper complex concentrations):

(8) $Cu_T^{II} = 10^{-7.356}\left(1 + \dfrac{10^{-7.497}}{10^{-7.5}} + \dfrac{10^{-16.194}}{10^{-15}} + \dfrac{10^{-26.879}}{10^{-22.5}} + \dfrac{10^{-39.98}}{10^{-30}}\right)$
    $= 9.10 \times 10^{-8}$ M

Part 2. Rick also collected a sample for measurement of dissolved copper, and the measurement gave a value of 1.91×10^{-7} M, a factor of ~2 higher than he calculated, and also higher than the reported safe level for fish. Somewhat embarrassed, Rick returned to the pond to see if he missed something. While sitting and staring at the pond seeking inspiration, a fish jumped up, splashing Rick. The few drops of water that landed on his mouth tasted salty. Taking out his handy chloride-specific electrode and calibration standards, Rick determined that the chloride concentration was 0.5 M (close to that of seawater). Using this additional information, Rick wondered whether the measured and calculated total dissolved copper concentrations would match.

Answer: The copper-chloride complexes must be considered. Ignoring activity corrections, he found

(9) $Cu^{2+} + Cl^- \rightleftharpoons CuCl^+$ $\qquad \log\beta_1 = 0.20$,

(10) $Cu^{2+} + 2Cl^- \rightleftharpoons CuCl_2^0$ $\qquad \log\beta_2 = -0.26$,

(11) $Cu^{2+} + 3Cl^- \rightleftharpoons CuCl_3^-$ $\qquad \log\beta_3 = -2.29$,

(12) $Cu^{2+} + 4Cl^- \rightleftharpoons CuCl_4^{2-}$ $\qquad \log\beta_4 = -4.59$.
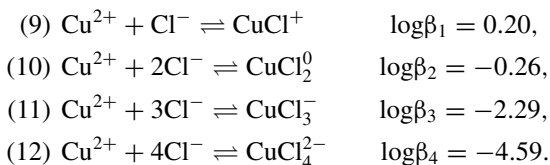
The value of $[Cu^{2+}]$ is unchanged. All that is needed is to include the copper-chloride complexes in the total dissolved copper expression:

(13) $Cu_T^{II} = [Cu^{2+}]$

$$\left(1 + \frac{{}^*\beta_1}{[H^+]} + \frac{{}^*\beta_2}{[H^+]^2} + \frac{{}^*\beta_3}{[H^+]^3} + \frac{{}^*\beta_4}{[H^+]^4} + \beta_1[Cl^-] + \beta_2[Cl^-]^2 + \beta_3[Cl^-]^3 + \beta_4[Cl^-]^4\right)$$

Rick again calculated Cu_T^{II}:

(14) $Cu_T^{II} = 10^{-7.356} \left(\begin{array}{c} 1 + \dfrac{10^{-7.497}}{10^{-7.5}} + \dfrac{10^{-16.194}}{10^{-15}} + \dfrac{10^{-26.879}}{10^{-22.5}} \dfrac{10^{-39.98}}{10^{-30}} + \\[2mm] 10^{0.20}(0.5) + 10^{-0.26}(0.5)^2 + 10^{-2.29}(0.5)^3 + 10^{-4.59}(0.5)^4 \end{array} \right)$

$$= 1.32 \times 10^{-7} \text{ M}$$

Although the chloride complexes increased the total concentration, it was not enough to account for the difference.

Part 3. Seeking to reconcile the differences between the calculation and experiment, Rick called his old friend Liam to ask for advice. After hearing a description of the system, Liam said, "The pond is an open system and exposed to the atmosphere right? You need to consider the carbonate system." Rick quickly did the following "back of the envelope" calculation:

(15) At pH 7.5, $[CO_3^{2-}] = \dfrac{K_{a1}K_{a2}K_H P_{CO_2}}{[H^+]^2} = 2.25 \times 10^{-7} M$

(16) $Cu^{2+} + CO_3^{2-} \rightarrow CuCO_3^0$ $\quad \beta_1 = 10^{6.77} = [CuCO_3^0]/[Cu^{2+}][CO_3^{2-}]$

(17) $[CuCO_3^0] = 10^{6.77}[Cu^{2+}][CO_3^{2-}] = 10^{6.77}(4.40 \times 10^{-8})(2.25 \times 10^{-7})$
$\qquad = 5.85 \times 10^{-8} M$

Adding this value to that from part 2 gives 1.90×10^{-7} M, which is very close to the measured value. The remaining difference possibly could be accounted for by the two other potential carbonate complexes listed in Table 9.4.

As the above example demonstrates, ligands can increase the solubility of metal ions dramatically. This also is illustrated by the following MINEQL+ example.

EXAMPLE 10.8: Determine the solubility of lead carbonate in ultrapure water and seawater at pH 8 using MINEQL+. Assume an open system.

Answer: First, the ultrapure water situation is computed. This is just as if we have added solid lead carbonate to water. In MINEQL+, perform the following steps:

(1) Select Pb^{2+} and CO_3^{2-} as components and click Scan THERMO.
(2) In the Wizard, set the pH to 8, the log PCO_2 to -3.5, and turn off all solids off except for cerrusite ($PbCO_{3(s)}$). Click OK.
(3) Click close and then select "dissolved solids."
(4) Click "Move" and select "Fixed Entities." This tells MINEQL+ that cerrusite is present in excess. Close the dialog box and proceed to the RunTime Manager and run the calculation.
(5) To find the result, select Special Reports and click View. Then select "Total Dissolved Concentration by Component."

This calculation gives a Pb_T^{II} of 3.55×10^{-7} M (with $PbCO_3^0$ as the dominant complex).

We now repeat the calculation, using the information in Table 9.6 to select the appropriate anions and their concentrations. Following the same steps as above (with the additional anions included in steps 1 and 2) gives $Pb_T^{II} = 3.67 \times 10^{-6}$ M, slightly more than a factor of 10 times that for distilled water, with $PbCl_2^0$ as the dominant complex.

10.7 Coexistence of solids and the phase rule

As Table 10.1 shows, many metal ions form minerals with multiple anions, such as (hydr)oxides, carbonates, sulfates, and sulfides. Can multiple solids exist at the same time? If so, what conditions are required? Our explorations here lead back to a fundamental principle of physical chemistry: the Gibbs phase rule.

We will explore the questions using solids of barium (Ba^{2+}). Because Ba^{2+} does not form complexes to an appreciable extent, this simplifies the calculations. Assume that $Ba(NO_3)_2$ is titrated into a closed system at pH 8.0 (held constant) containing 5 mM total carbonate (C_T) and 1 mM total sulfate with a volume of one liter (1 L). As the barium is added, a solid will precipitate. First we will determine which solid forms first, and then we evaluate under what conditions solids can coexist. We will ignore activity corrections and perform the calculation in terms of concentrations.

We need the solubility expressions for $BaCO_{3(s)}$ and $BaSO_{4(s)}$:

$$BaSO_{4(s)} \rightleftharpoons Ba^{2+} + SO_4^{2-} \qquad K_{s0(SO_4)} = [Ba^{2+}][SO_4^-] = 10^{-9.93} \qquad (10.33a)$$

$$BaCO_{3(s)} \rightleftharpoons Ba^{2+} + CO_3^{2-} \qquad K_{s0(CO_3)} = [Ba^{2+}][CO_3^{2-}] = 10^{-7.6} \qquad (10.33b)$$

Also relevant are

$$H_2CO_3^* \rightleftharpoons H^+ + HCO_3^-, \qquad K_{a1} = 10^{-6.35}, \qquad (8.31)$$

$$HCO_3^- \rightleftharpoons H^+ + CO_3^{2-}, \qquad K_{a2} = 10^{-10.33}, \qquad (8.32)$$
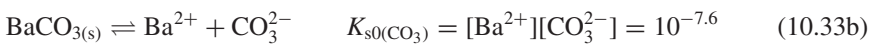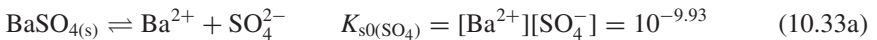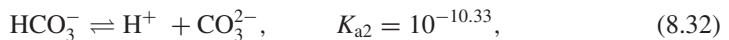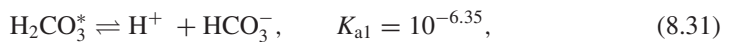
The relevant mass balance equations for the anions are

$$C_T = [H_2CO_3^*] + [HCO_3^-] + [CO_3^{2-}] = 5 \times 10^{-3}, \qquad (10.34)$$

$$S_T = [SO_4^{2-}] = 1 \times 10^{-3}. \qquad (10.35)$$

We now can determine which solid precipitates first. $BaSO_{4(s)}$ precipitates when $[Ba^{2+}][SO_4^{2-}] > 10^{-9.93}$. Because $[SO_4^{2-}] = 1$ mM, this means that the solid will form when

$$[\textbf{Ba}^{2+}] = 10^{-9.93}/10^{-3} = 10^{-6.93} = \textbf{1.17} \times \textbf{10}^{-7}\textbf{M}. \tag{10.36}$$

$BaCO_{3(s)}$ will precipitate when $[Ba^{2+}][CO_3^{2-}] > 10^{-9.93}$. At pH 8.0, $[CO_3^{2-}] = \alpha_2 C_T = (4.55 \times 10^{-3})(5 \times 10^{-3})$M $= 2.275 \times 10^{-5}$ M. This solid thus will form when

$$[\textbf{Ba}^{2+}] = 10^{-7.6}/2.275 \times 10^{-5} = \textbf{1.10} \times \textbf{10}^{-3}\textbf{ M}. \tag{10.37}$$

Clearly, the solubility limit for $BaSO_{4(s)}$ is reached first, and this will be the first solid to precipitate (when Ba^{2+} has been added to make the concentration 1.17×10^{-7} M).

Now we can determine the conditions under which the two solids can coexist. First we need to derive the equation for the equilibrium between the two solids:

$$BaSO_{4(s)} \rightleftharpoons Ba^{2+} + SO_4^{2-} \qquad K_{s0(SO_4)} = [Ba^{2+}][SO_4^{2-}] = 10^{-9.93}$$

$$\underline{Ba^{2+} + CO_3^{2-} \rightleftharpoons BaCO_{3(s)} \qquad 1/K_{s0(CO_3)} = 1/([Ba^{2+}][CO_3^{2-}]) = 10^{7.6}}$$

$$BaSO_{4(s)} + CO_3^{2-} \rightleftharpoons BaCO_{3(s)} + SO_4^{2-} \qquad K_{S \to C} = 10^{-2.33} = [SO_4^{2-}]/[CO_3^{2-}]$$

$$= S_T/\alpha_2 C_T \tag{10.38}$$
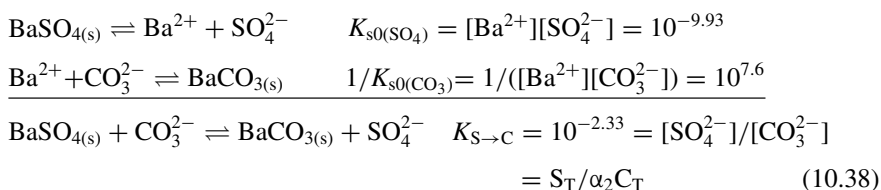
Multiplying $K_{S \to C}$ by α_2 tells us that at pH 8, the solids coexist when $S_T/C_T = 2.13 \times 10^{-5}$. We now need to solve for S_T and C_T right when the $BaCO_{3(s)}$ begins to precipitate. At this point, no carbonate has been removed from solution, and so $C_T = 5 \times 10^{-3}$ M. Thus, S_T must be 1.15×10^{-7} M ($10^{-6.939}$ M).

The total moles of sulfate in the system is

$$TOTS = 1 \times 10^{-3}\text{ M} = \text{moles } BaSO_{4(s)} + \text{moles of } SO_4^{2-}$$

$$= \text{moles } BaSO_{4(s)} + 1.15 \times 10^{-7}\text{ M} \times 1L,$$

or

$$\text{moles } BaSO_{4(s)} = 9.99885 \times 10^{-4}.$$

Thus,

$$[\text{Ba}^{2+}] = K_{s0(SO_4)}/S_T = 10^{-9.93}/10^{-6.939} = 10^{-2.991}\text{ M} \quad \text{or } 1.02 \times 10^{-3}\text{ M}.$$

To achieve this concentration, we have added enough barium to precipitate 9.99885×10^{-4} moles $BaSO_{4(s)}$ (essentially removing all of the sulfate from solution) and then an additional 1.02×10^{-3} moles. In summary, $BaSO_{4(s)}$ begins to precipitate when 1.17×10^{-7} moles of barium has been added and continues to precipitate until 9.99885×10^{-4} moles of $BaSO_{4(s)}$ have precipitated (consuming all of the sulfate). Barium then begins to accumulate in solution, until the concentration reaches 1.02×10^{-3} in solution (2.02×10^{-3} total moles added). $BaCO_{3(s)}$ then precipitates, and both solids continue to coexist as additional barium is added.

This is an appropriate place to return to the phase rule. Recall

$$F = c + 2 - p, \tag{8.52}$$

where F is number of degrees of freedom (i.e., the number of variables for which arbitrary values can be chosen), c is the number of components that must be brought together to make the system, and p is the number of phases present (where phases are regions of uniform composition).

Let us apply this to the above system where $c = 5$ (Ba^{2+}, CO_3^{2-}, SO_4^{2-}, H^+, H_2O). If no solids are present, $p = 1$ (the solution phase), and $F = 6$. Thus, after specifying T and P, we must know (or we can arbitrarily set) concentrations of four of the species to define the system (e.g., Ba^{2+}, SO_4^{2-}, CO_3^{2-}, and H^+). When the first solid begins to precipitate, $p = 2$ and $F = 5$, and we can only specify three of the concentrations (e.g., H^+, SO_4^- and CO_3^{2-}; the Ba^{2+} content would be dictated by the presence of barium sulfate and the SO_4^{2-} concentration). Once the second solid precipitates, $p = 3$ and $F = 4$, and we can only set two of the concentrations (e.g., H^+ and SO_4^{2-}, the solids dictate the Ba^{2+} concentration, and CO_3^{2-} is set by Eq. 10.38).

10.8 Solubility of neutral organic compounds

There is an old adage that oil and water don't mix, and thus often it is thought that organic compounds do not readily dissolve in water. The truth, however, is that neutral organic compounds have a wide range of solubility in water, from complete miscibility (e.g., methanol) to nanomolar or lower concentrations (e.g., some PCB and chlorinated dioxin congeners).

The solubility of neutral organic molecules is driven by how energetically unfavorable it is to remove a molecule from the pure organic phase and place it in an aqueous environment. For any compound i, this energy is called the excess free energy of solution (G_{iw}^E), and it usually is positive (thus unfavorable). The range of G_{iw}^E is ~10–50 kJ/mol for typical organic contaminants (for details see Schwarzenbach et al.[10]). The excess free energy has both enthalpic contributions (H_{iw}^E, ranging from ca. −5 to +25 kJ/mol) and entropic contributions (ca. −10 to −20 kJ/mol for T × S_{iw}^E).

The excess free energy at saturation is related to the activity coefficient of i:

$$G_{iw}^E = -RT\ln\gamma_i^{\text{sat}} \tag{10.39}$$

Recall from Chapter 4 that

$$\gamma_i^{\text{sat}} = \frac{1}{x_i^{\text{sat}}} \tag{4.35}$$

where x_i^{sat} is the mole fraction of compound i in water at saturation. With $V_w = 0.018$ L/mol,

$$\gamma_i^{\text{sat}} = \frac{1}{V_w C_i^{\text{sat}}}. \tag{4.36}$$

Thus, if one knows the activity coefficient, the solubility (C_i^{sat}) can be determined, or vice versa. These equations apply to organic compounds that are liquids at standard temperature and pressure; Chapter 4 describes the corrections needed for solids and gases. In practice, solubility is measured either by equilibrating the compound of interest in water with slow stirring and measuring the concentration in the water or by using a generator column.[11] There are also means to measure the activity coefficient.[12]

Approaches to predict the solubility of neutral organic molecules are somewhat limited, but there are two general relationships. The first correlates solubility with molecular size; G_{iw}^E tends to increase within a compound class as additional hydrophobic groups are added (e.g., hexane to heptane to octane). The other relationship correlates solubility with octanol:water partition coefficients (K_{ow}). Compounds with high K_{ow} have less affinity for water and thus lower solubility. These linear free energy relationships (LFERs) are of the form

$$\log C_i^{sat} = -a(\text{size}) + b \ [\text{or} \log \gamma_i^{sat} = c(\text{size}) + d], \tag{10.40}$$

$$\log C_i^{sat} = -w(\log K_{ow}) + x \ [\text{or} \log \gamma_i^{sat} = y(\log K_{ow}) + z]. \tag{10.41}$$

The relationships also can be expressed in the opposite manner (e.g., $\log K_{ow} = -w' (\log C_i^{sat}) + x'$). For size, the molar volume, V_x, often is used. The molar volume of a compound (the volume in liters of one mole of the compound) is related to its density and molecular weight:

$$V_x(\text{L/mol}) = \frac{\text{MW (g/mol)}}{\rho} \frac{}{\text{(g/L)}} \tag{10.42}$$

If this information is not available, there are means to estimate molar volume based on the structure of a compound.[13] Equations 10.41 and 10.42 hold well only within classes of compounds (e.g., alkanes, chlorobenzenes, PAHs). Values of the slopes and intercepts for such relationships are available, and a selection is presented in Table 10.6. Multiparameter LFERs also have been developed that are not specific to a particular compound class. These account for van der Waals forces, the H-donor and H-acceptor character of the molecule, polarizability of the molecule, and molecular size. This approach allows accurate predictions of activity coefficients, and the only limitation is the availability of the appropriate parameters for the molecule of interest.[10]

Table 10.6 Coefficients for the LFER: $\log K_{ow} = -a' \log C_i^{sat} + b'$*

Compound class	a'	b'	Log K_{ow} range[†]	R^2	n[§]
Alkanes	0.85	0.62	3.0–6.3	0.98	112
Alkylbenzenes	0.94	0.60	2.1–5.5	0.99	15
PAHs	0.75	1.17	3.3–6.3	0.98	11
Chlorobenzenes	0.90	0.62	2.9–5.8	0.99	10
PCBs	0.85	0.78	4.0–8.0	0.92	14

*From Schwarzenbach et al.[10]
[†]Range of values used to establish the relationship.
[§]Number of compounds used to develop the LFER.

10.9 Effects of temperature on solubility

For minerals, the effect of temperature follows the van't Hoff equation (same as for other equilibrium constants):

$$\ln \frac{K_{T_2}}{K_{T_1}} = \int_{T_1}^{T_2} \frac{\Delta H^\circ}{RT^2} dT = \frac{\Delta H^\circ}{R} \left[\frac{1}{T_1} - \frac{1}{T_2} \right] = \frac{\Delta H^\circ (T_2 - T_1)}{RT_1 T_2} \qquad (3.44)$$

This form of the equation assumes that ΔH° is constant with temperature (i.e., $\Delta C_p = 0$), which is reasonable for solids (see Section 3.16.4). For all the solubility constants in Table 10.1, the enthalpy change of reaction (ΔH°) is given in kcal/mol (so watch your units on R!). Temperatures are in Kelvin. Thus, the equilibrium constant can be calculated for solids at any temperature using the data in Table 10.1 and Eq. 3.44. For highly soluble solids, such as salts (like NaCl) or sugars, a common rule of thumb is that increasing temperature increases solubility. Looking at Table 10.1, however, we see that the picture is much more complicated. Some minerals have positive ΔH° values, indicating that solubility increases with increasing temperature, but many have negative values, meaning solubility decreases with increasing temperature. For example, tenorite, CuO, has $\Delta H^\circ = -15.504$ kcal/mol (or -64.90 kJ/mol), and log $^*K_{s0} = 10^{7.644}$ at 25°C. Lowering the temperature to 15°C gives the following change in equilibrium constant:

$$\ln \frac{^*K_{T_2}}{^*K_{T_1}} = \frac{\Delta H^\circ (T_2 - T_1)}{RT_1 T_2}$$

$$^*K_{15°C} = {^*K_{25°C}} \exp \left(\frac{\Delta H^\circ (T_2 - T_1)}{RT_1 T_2} \right) = 10^{7.644} \exp \left(\frac{-64,900(288 - 298)}{8.31(288)(298)} \right) = 10^{8.04}$$

This represents a factor of 2.5 *increase* in solubility for a 10°C decrease in temperature!

For gases that dissolve ideally in water (i.e., inorganic compounds), the effect of increasing temperature is to decrease solubility. The thermodynamic parameter that dictates this behavior is the enthalpy of vaporization, ΔH_{vap}, which defines the change in heat content (enthalpy) of a chemical going from a condensed phase into a gas phase. When a gas dissolves, however, it goes *into* a condensed phase; that is,

$$i_{gas} \rightarrow i_{aqueous}, \qquad (10.43)$$

with Eq. 6.1 defining the equilibrium (Henry's law) constant. The relevant equation to determine the effect of temperature on gas solubility thus is

$$\ln \frac{K_{H,T_2}}{K_{H,T_1}} = \int_{T_1}^{T_2} \frac{-\Delta H_{vap}}{RT^2} dT = \frac{-\Delta H_{vap}}{R} \left[\frac{1}{T_1} - \frac{1}{T_2} \right] = \frac{-\Delta H_{vap}(T_2 - T_1)}{RT_1 T_2}. \qquad (10.44)$$

If we had chosen to define the reaction in reverse (i.e., use H as our Henry's law constant), we then would use ΔH_{vap} instead of $-\Delta H_{vap}$. For a given vapor pressure

of the compound, the solubility of a gas can then be determined using the temperature corrected Henry's law constant.

For organic molecules that are liquids over the temperature range of interest, the relevant thermodynamic parameter is the excess enthalpy of solution, H_{iw}^E. When a pure organic liquid dissolves into water, the relevant reaction is

$$i_{\text{liquid}} \rightarrow i_{\text{aqueous}}, \tag{10.45}$$

and the relevant equilibrium constant is

$$K_{1-\text{aq}} = \frac{x_{i,\text{w}}^{\text{sat}}}{x_{i,1}} \tag{10.46}$$

which is the mole fraction of i in water divided by its mole fraction in the organic liquid. (We could use the concentrations in each by dividing by the molar volume.) The mole fraction in the pure organic liquid, however, is ~ 1 (assuming little water dissolves into the organic phase), and thus $K_{1-\text{aq}} \sim x_{i,\text{w}}$. We can substitute $x_{i,\text{w}}$ into the van't Hoff expression

$$\ln \frac{x_{i,\text{wT}_2}^{\text{sat}}}{x_{i,\text{wT}_1}^{\text{sat}}} = \frac{H_{iw}^E}{R}\left[\frac{1}{T_1} - \frac{1}{T_2}\right] = \frac{H_{iw}^E(T_2 - T_1)}{RT_1T_2} \tag{10.47}$$

This generally is good only for narrow temperature ranges because H_{iw}^E often is temperature dependent. If solubility data are available at different temperatures, H_{iw}^E can be determined from a plot of $\ln x_{i,\text{w}}^{\text{sat}}$ Versus $1/T$:

$$\ln x_{i,\text{w}}^{\text{sat}} = -\frac{H_{iw}^E}{R}\frac{1}{T} + A \tag{10.48}$$

A is a constant (i.e., the intercept of the line). A plot of $\ln C_{iw}^{\text{sat}}$ versus $1/T$ will give the same slope, but a different intercept.

For organic molecules that are gases or solids at the temperature of interest, the "energy cost" for dissolution into water includes the heat of vaporization (gases) or heat of fusion (solids). The appropriate van't Hoff relationships are

$$\ln \frac{x_{i,\text{wT}_2}^{\text{sat}}(g)}{x_{i,\text{wT}_1}^{\text{sat}}(g)} = \frac{H_{iw}^E - \Delta H_{\text{vap}}}{R}\left[\frac{1}{T_1} - \frac{1}{T_2}\right] = \frac{(H_{iw}^E - \Delta H_{\text{vap}})(T_2 - T_1)}{RT_1T_2} \tag{10.49}$$

$$\ln \frac{x_{i,\text{wT}_2}^{\text{sat}}(s)}{x_{i,\text{wT}_1}^{\text{sat}}(s)} = \frac{H_{iw}^E + \Delta H_{\text{fus}}}{R}\left[\frac{1}{T_1} - \frac{1}{T_2}\right] = \frac{(H_{iw}^E + \Delta H_{\text{fus}})(T_2 - T_1)}{RT_1T_2} \tag{10.50}$$

Again, these equations assume that the enthalpies are constant over the temperature range of interest.

EXAMPLE 10.9 Effect of temperature on the solubility of benzene and naphthalene: H_{iw}^E for benzene is 2 kJ/mol. For naphthalene $H_{iw}^E = 9$ kJ/mol and $\Delta H_{\text{fus}} = 19$ kJ/mol. Determine the effect of changing the temperature from 25°C to 15°C on the solubility of these two compounds.

Answer: Not being given the solubility specifically, all we can do is determine the factor by which the solubility changes. For benzene this factor is

$$(1) \quad \exp\left(\frac{H^E_{iw}}{R}\left[\frac{1}{T_1} - \frac{1}{T_2}\right]\right) = \exp\left(\frac{2000}{8.31}\left[\frac{1}{298} - \frac{1}{288}\right]\right) = 0.972$$

and for naphthalene it is

$$(2) \quad \exp\left(\frac{H^E_{iw} + \Delta H_{fus}}{R}\left[\frac{1}{T_1} - \frac{1}{T_2}\right]\right) = \exp\left(\frac{9000 + 19000}{8.31}\left[\frac{1}{298} - \frac{1}{288}\right]\right) = 0.675$$

The larger values of H^E_{iw} and ΔH_{fus} for naphthalene lead to a more dramatic effect of temperature on solubility.

10.10 Kinetics of precipitation and dissolution

10.10.1 Introduction

Natural waters frequently are not at equilibrium with respect to existing or potential solid phases. Probably the most notorious example is the fact that near-surface waters of the world's oceans are consistently supersaturated with respect to calcite, but deeper waters (below a few hundred meters depth) consistently are unsaturated. These facts indicate that rates of precipitation and mineral dissolution are (or at least can be) slow, indicating a need to understand the kinetics of these processes. Precipitation of solids from supersaturated solutions and dissolution of solids into undersaturated phases might be regarded as "two sides of the same coin," but there are some differences between the processes and the factors affecting their rates, just as the two sides of coins are different.

10.10.2 Precipitation kinetics: nucleation mechanisms

The driving force for precipitation is an excess of dissolved species relative to their solubility. For salts this can be expressed quantitatively as $IAP > K_{s0}$, where IAP is the actual ion activity product. The ratio $IAP{:}K_{s0}$ is called the saturation ratio:

$$S = \left(\frac{IAP}{K_{s0}}\right)^{1/x} = \frac{a_a}{a_s} \tag{10.51}$$

where x is the number of ions in the mineral formula (e.g., $x = 2$ for $CaCO_3$ and $x = 9$ for $Ca_5(PO_4)_3OH$), a_a is the actual activity of the solutes, and a_s is the solute activity at saturation. Under limiting conditions explained below, precipitation rates are proportional to some simple function of S. However, the situation is more complicated in the initial stage of precipitation—in supersaturated solutions where no solid particles are present. In fact, the process of precipitation must be viewed as having two distinct steps: ***nucleation*** and ***crystal growth***.[14] Nucleation, the formation of very small (nanoscale) particles (called ***nuclei***), may occur by two pathways: ***homogeneous*** and ***heterogeneous nucleation***.

Homogeneous nucleation is endergonic, even under conditions of supersaturation. For salts, it involves dissolved cations and anions clustering together (forming bonds) to

start a crystal. Initially, when the number of molecular units, n, in the embryonic cluster (or incipient nucleus) is small, perhaps on the order of ~10, most of them will be at its surface. (For a simple salt, MA, the molecular unit consists of one cation, M, and one anion, A.) This means these ions are not fully in a crystalline lattice, and not all the bonds that they ultimately will form with other ions are present. Surface ions exist in a state of excess potential energy (fewer and weaker bonds) compared with interior ions and also are at a disadvantage (compared with solute ions) from an entropy perspective—their freedom of independent movement is limited by the bonds linking them to the growing nucleus. Overall, the free energy involved in forming the nucleus, ΔG_n, can be viewed as having two components:

$$\Delta G_n = \Delta G_{bulk} + \Delta G_{sfc} \tag{10.52}$$

ΔG_{bulk} is the free energy involved in converting solute ions into a solid (crystal lattice), and ΔG_{sfc} is the work required to create the surface (interface) of the solid. For a supersaturated solution, bond formation in the first process makes ΔG_{bulk} negative, but formation of a surface requires energy. Initially, most of the ions are at the surface and have excess energy. Adding ions to a growing nucleus thus will be endergonic; in absolute terms, ΔG_{sfc} will be greater than ΔG_{bulk}, even if the solution is supersaturated. Both energy terms can be expressed in terms of the number of molecular units n in the incipient crystal, and if we assume that the nucleus is spherical, the terms also can be expressed in terms of the volume of the sphere resulting from n units having a molecular volume V_m.[3,14] For ΔG_{bulk} we have

$$\Delta G_{bulk} = -n\mathbf{k}T \ln \frac{a_a}{a_s} = -n\mathbf{k}T \ln S \tag{10.53}$$

or

$$\Delta G_{bulk} = -\left(\frac{4\pi r^3}{3V_m}\right)\mathbf{k}T \ln S \tag{10.54}$$

where $\mathbf{k}$ is Boltzmann's constant, $\mathbf{k}T$ is thermal energy per molecule, and r is the radius of the spherical nucleus. The term in parentheses in Eq. 10.54 represents the conversion between the number of molecular units, n, of volume V_m that constitute the nucleus and the volume of the (spherical) nucleus, $(4/3)\pi r^3$.

For ΔG_{sfc} (again assuming a spherical nucleus), we have

$$\Delta G_{sfc} = A_n \overline{\gamma} = 4\pi r^2 \overline{\gamma} \tag{10.55}$$

where A_n is the surface area of a nucleus of size n and $\overline{\gamma}$ is the interfacial energy. Substituting Eqs. 10.54 and 10.55 into Eq. 10.52 yields

$$\Delta G_n = -\left(\frac{4\pi r^3}{3V_m}\right)\mathbf{k}T \ln S + 4\pi r^2 \overline{\gamma} \tag{10.56}$$

The fact that the exergonic bulk free energy term is a function of r^3, but the endergonic surface free energy term is a function of r^2 suggests that at some value of r (equivalent
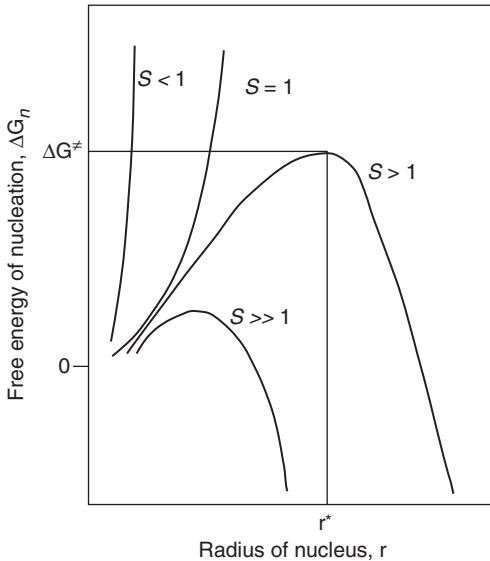
Figure 10.5 Schematic of homogeneous nucleation at several values of S, the saturation ratio for a salt showing how the critical nucleus size and energy input needed to attain that size decrease with increasing S. Based on similar figures in Nielsen[14] and Stumm and Morgan.[3]

to some value of n) the rate of change in the bulk term ($d\Delta G_{bulk}/dn$) will exceed the rate of change in the surface term ($d\Delta G_{sfc}/dn$).[14] At this point, the nucleus has reached a critical size, n^* (with radius r^*). Beyond this point, adding ions to the particle becomes net exergonic ($d\Delta G_n/dn < 0$), meaning that the particle now will grow spontaneously (as long as supersaturation exists). Figure 10.5 illustrates these ideas for different degrees of supersaturation.

The relevance of the above to the kinetics of homogeneous nucleation is that the free energy needed to grow nuclei to critical size n^* (i.e., the difference between ΔG_{bulk} and ΔG_{sfc} at this point) represents the activation barrier, $\Delta G^{\neq}$, the system must overcome for net nucleation and precipitation to occur. Simulations involving Eq. 10.56 and reasonable values of the associated parameters show that both n^* and $\Delta G^{\neq}$, decrease as the saturation ratio S (a_a/a_s) increases.[3] Further calculations indicate that homogeneous nucleation is sufficiently rapid to account for actual precipitation rates only in highly supersaturated solutions ($S > 100$ or even 1000 in the case of $BaSO_4$, as shown by Nielsen[15]). Such conditions may be generated in laboratory or engineered systems (chemical treatment reactors), but they almost never occur in the natural environment. Consequently, homogeneous nucleation is not important in controlling solids formation in freshwater or seawater.

Heterogeneous nucleation is the controlling process to initiate precipitation in natural waters. It involves crystal growth on other mineral nuclei and particles suspended in the solution. Substances that act as heteronuclei in natural waters include inorganic crystals of other salts, sand, silt, and clays, diatom shells, calcium carbonate shells of certain plankton, and biological surfaces. In qualitative terms, heteronuclei act as catalysts and lower the activation energy for nuclei formation (compared with that for homogeneous conditions). Quantitative aspects of heteronucleation are more complicated than described above for homogeneous nucleation and are beyond our

scope. However, one can imagine that the closer the surface of the heteronuclei are morphologically to the structure of the mineral to be precipitated, the more effective they will be—the lower will be the interfacial energy between the two solids, thus allowing nucleation and crystal growth to occur at lower values of S than in the homogeneous case.

As the above discussion indicates, interfacial energy is a primary factor in both the thermodynamics and kinetics of precipitation. The Ostwald step rule, which is useful for predicting the order of precipitation for a series of polymorphs of a given mineral formula (e.g., calcite, aragonite, and vaterite are polymorphs of $CaCO_{3(s)}$), is based on interfacial energetics. It says that the form with the highest solubility, that is, the least stable one, will precipitate first; for $CaCO_{3(s)}$ this indicates that vaterite should be first to precipitate, and that apparently is what occurs in softening operations of water treatment plants (M. Semmens, personal communication, 2009). The Ostwald rule is based on the finding that the interfacial mineral-solution free energy, $\bar{\gamma}$, increases with decreasing solubility.[3,16] Nucleation of the least stable (most soluble) form thus is favored because its $\bar{\gamma}$ is the smallest of the polymorphs.

10.10.3 Crystal growth kinetics

Once stable nuclei are formed, crystal growth can proceed. Various forms of rate equations are used to describe the kinetics of crystal growth, but a common expression is

$$\text{Rate} = k_p(C_a - C_s)^n, \qquad (10.57)$$

where C_a is the actual concentration, C_s is the saturation value of the precipitating ions, and n is the empirical reaction order (usually n = 1 or 2). Four mechanisms may control crystal growth: ***mononuclear***, ***polynuclear***, ***screw dislocation***, and ***diffusion-controlled growth*** (see Figure 10.6a–c).[14] In the first, growth is limited by the rate of formation of new layers on the crystal surface (Figure 10.6a). According to this scenario, it is difficult for precipitating ions to establish a new layer on a flat surface, particularly when S is low, for reasons similar to those described above for the formation of nuclei. Once a new layer is established, it is more favorable energetically for ions to attach to a step or (even better) to the end of a partly completed row—a kink (Figure 10.6d). Kinks are site of excess surface energy because binding of ions to the crystal is less complete there than elsewhere on a surface.[17] Kinks are preferred sites for sorption of impurities, which can inhibit crystal growth or result in the incorporation of impurities in the growing crystal.

In polynuclear growth, surface nucleation (i.e., the start of a new layer) is assumed to be fast, possibly because of strong sorption of precipitating ions to surface sites, compared with growth rates of molecular layers. Growth thus occurs on multiple layers simultaneously (Figure 10.6b). "Screw dislocation" is important for crystal growth, especially at low S. In this process, imperfections on the crystal surface called screw dislocations arise spontaneously, for example, from the presence of foreign nuclei, allowing nearly unlimited spiral growth of the crystal (Figure 10.6c). Finally, diffusion—from the bulk solution to the surface or in the adsorption layer on the surface—may limit crystal growth when the energetics of surface nucleation and chemical attachment to the crystal are particularly favorable and precipitation is rapid.
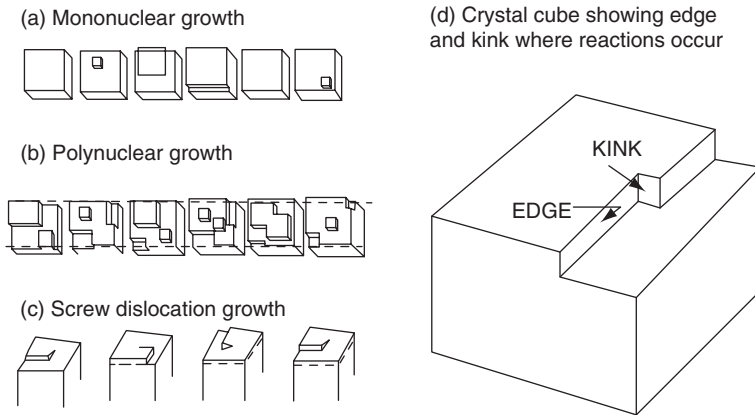
Figure 10.6 Simple cube models showing the nature of (a) mononuclear growth (one layer at a time); (b) polynuclear growth (multiple layers at a time); and (c) screw dislocation growth at crystal imperfections. (d) Sketch of a crystal cube showing nature of edges and kinks, where surface reactions are most likely to occur. (a)–(c) from Stumm and Morgan,[3] © John Wiley & Sons, and used with permission.

10.10.4 Kinetics of dissolution

In simple terms, dissolution can viewed roughly as the reverse of crystal growth, and dissolution of mineral salts follows rate expressions similar to Eq. 10.57. Loss of ions from the crystal surface should occur most readily at sites where the ions have minimal points of attachment to the crystal—that is, at kinks (the same place where crystals grow). According to this so-called "kink" theory,[17] migration of kinks gradually leads to step retreat and crystal dissolution (or step advance and crystal growth). Migration of kinks is viewed as a faster process than the formation of new kinks.

The driving force for dissolution of a solid phase is unsaturated conditions in the solution, and under such circumstances, the process is spontaneous. The kinetics of dissolution, however, may be quite slow under conditions of slight unsaturation and in the absence of solutes that catalyze dissolution. Under such conditions, mineral dissolution sometimes is called "water catalyzed," but this term is somewhat incorrect because water actually acts as a reactant. Metal ions must become hydrated to go into the solution phase. For salt MA, we can write $MA_{(s)} + cH_2O \rightarrow M^{n+}_{(aq)} + A^-$, where $c =$ the coordination number of the metal ion. Various solutes can accelerate dissolution by reacting with the cation or anion (this topic is covered in greater detail for weathering of aluminosilicate minerals in Section 15.5). Again, such solutes often are referred to as catalysts, but usually they are net reactants. Examples include anions that act as ligands, complexing the cation and enhancing its solubility, and acids, including Brønsted acids and H^+. Acids may convert a metal (hydr)oxide to a more soluble acidic form, e.g.,

$$\equiv\text{Me-OH} + H^+ \rightleftharpoons \equiv\text{Me-OH}_2^+, \tag{10.58}$$
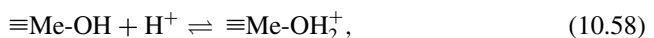
or may protonate the anion of the salt to a more soluble form, e.g., in calcite,

$$\equiv CaCO_3 + H^+ \rightleftharpoons \equiv + Ca^{2+} + HCO_3^-, \tag{10.59}$$
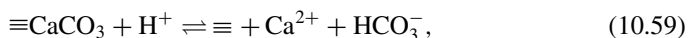
where the bare $\equiv$ represents a site that has lost its surface Ca^{2+} and CO_3^{2-} ions.

At high partial pressures CO_2 accelerates the dissolution of calcium carbonate;[18] its hydrated form reacts with carbonate ions in the crystal surface to produce two bicarbonate ions in solution: $CaCO_{3(s)} + H_2CO_3$ (or $CO_{2(aq)}$) $\rightarrow Ca^{2+} + 2HCO_3^-$. In contrast, sorption of some ions to the crystal surface may inhibit rates of dissolution by blocking reactive sites. For example, phosphate has been shown to be a strong inhibitor of calcite dissolution.[19]

10.10.5 Dissolution and precipitation kinetics of calcium carbonate

Rates of dissolution and precipitation of $CaCO_{3(s)}$ are of interest to aquatic chemists because of its widespread occurrence in nature and of great interest to environmental engineers because of its importance of water treatment (softening) and scale formation in pipes. Dissolution rates of $CaCO_{3(s)}$ depend (nonlinearly) on its degree of unsaturation, S:

$$S = \frac{\text{measured ion product}}{\text{saturation ion product}} = \frac{\text{IAP}}{{}^cK_{s0}} = \frac{[Ca^{2+}]_m[CO_3^{2-}]_m}{[Ca^+]_s[CO_3^{2-}]_s} \tag{10.60}$$

In turn, S is related to ΔpH, defined as follows:

$$\Delta pH = pH_{sat} - pH_{meas} = -0.5 \log S \tag{10.61}$$

In laboratory experiments where pH was carefully controlled, Berner and Morse[19] showed that dissolution rates of calcium carbonate in seawater depend strongly on ΔpH, for which a key value is 0.15. At ΔpH < 0.15, dissolution rates are very slow; rates increase rapidly (and linearly) at ΔpH > 0.15. This trend was used to explain numerous observations showing that $CaCO_{3(s)}$ occurs in marine sediment to water column depths up to ~6000 m, even though ocean waters below ~500–1000 m depth typically are unsaturated with respect to calcite. This indicates that $CaCO_{3(s)}$ (produced mostly biogenically) in supersaturated surface waters does not all dissolve as it settles through a substantial column of unsaturated seawater. In situ measurements of $CaCO_{3(s)}$ dissolution rates using samples of polished calcite spheres,[20] powdered calcite, marine sediment, and foraminifera (marine planktonic animals with $CaCO_3$ shells), suspended in mesh bags in the oceans have shown similar trends:[19] low rates in unsaturated waters until depths of ~3800–4000 m, where ΔpH reaches ~0.15, after which dissolution (and ΔpH) increase rapidly with depth. The depth at which dissolution rates begin to increase has been termed the "chemical lysocline." Berner and Morse[19] suggested that the change beginning at ΔpH = 0.15 reflects a change in the rate-controlling step. They also found that phosphate ions inhibit calcite dissolution and that a larger ΔpH is required to induce dissolution as the concentration of phosphate (P_i) increases. They speculated that P_i binds strongly to kinks on the calcite surface, which are assumed to be the preferred sites for dissolution. They proposed that P_i binding prevents detachment of the crystal ions at a

kink, thus immobilizing it and inhibiting dissolution. If all the kinks are immobilized by bound P_i, dissolution can proceed only by formation of new kinks, a slower process than kink migration.

Plummer et al.[18] studied the relative importance of the three mechanisms involved in $CaCO_3$ dissolution:

$$CaCO_{3(s)} + H_2O \rightleftharpoons Ca^{2+} + HCO_3^- + OH^- \qquad \text{(water-catalyzed)} \qquad (10.62)$$

$$CaCO_{3(s)} + H^+ \rightleftharpoons Ca^{2+} + HCO_3^- \qquad \text{(acid-catalyzed)} \qquad (10.63)$$

$$CaCO_{3(s)} + H_2CO_3^* \rightleftharpoons Ca^{2+} + 2HCO_3^- \qquad \text{(CO_2-catalyzed)} \qquad (10.64)$$
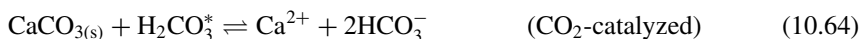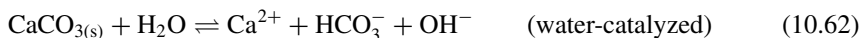
The overall dissolution rate, R_{dis} (mmol cm^{-2} s^{-1}), is the sum of the three rate processes:

$$R_{dis} = k_{H_2O}[H_2O] + k_{H^+}[H^+] + k_{H_2CO_3^*}[H_2CO_3^*] \qquad (10.65)$$

The relative importance of the three processes was determined as a function of pH and P_{CO_2} (Figure 10.7). It is clear that under typical environmental conditions only the water-catalyzed process is important. The acid-catalyzed process dominates only at pH $<\sim$ 5.5, and the CO$_2$-catalyzed process only at $P_{CO_2} > 0.1$ atm (far higher than ambient conditions even in soils).
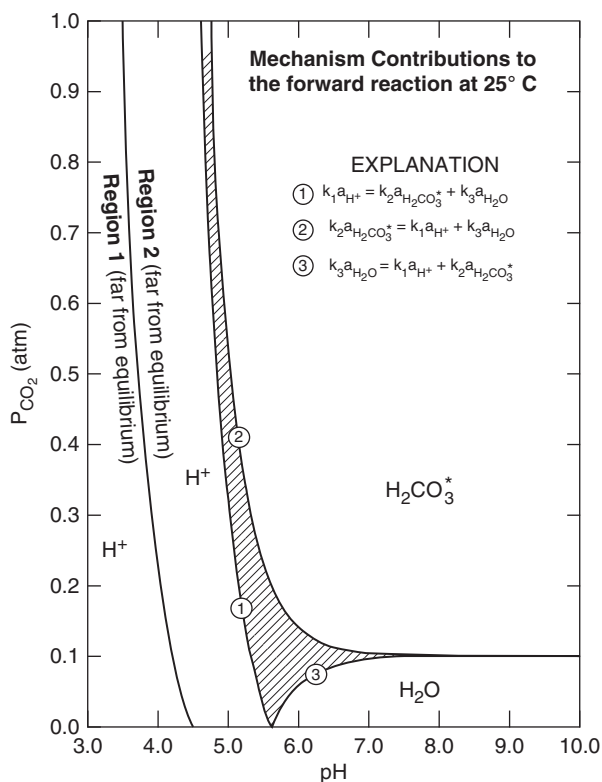
Figure 10.7 Regions of pH and P_{CO_2} where each of the three mechanisms in calcite dissolution is dominant. Lines show boundaries where the contribution from one mechanism balances the sum of the other two. All three mechanisms contribute significantly in the gray area. Reprinted from Plummer et al.[18] (public domain).

As solutions approach saturation, precipitation becomes important, and the net reaction is the difference between the forward (dissolution) and reverse (precipitation) reactions:

$$R_{net} = k_{H_2O}[H_2O] + k_{H^+}[H^+] + k_{H_2CO_3^*}[H_2CO_3^*] - k_p[Ca^{2+}][HCO_3^-], \qquad (10.66)$$

where k_p is the rate constant for $CaCO_{3(s)}$ formation, expressed in terms of the bulk reactants. Plummer et al.[18] developed a sophisticated mechanistic model describing $CaCO_3$ dissolution and precipitation in terms of three solution layers: an adsorption layer (A) at the $CaCO_3$ surface, a hydrodynamic boundary layer (B), and the bulk solution (C). Ions in the A layer (assumed to be only a few molecules thick) are loosely bound to reactive sites (kinks) on the $CaCO_3$ surface and have restricted mobility compared with ions in the B layer. Unfortunately, the model cannot used to predict rates of dissolution or precipitation under environmentally relevant conditions because some terms cannot be measured. For example, at near-equilibrium conditions, where both processes (precipitation and dissolution) are significant components of R_{net}, one cannot assume that $[H_2CO_3^*]$ in layer A is the same as that in bulk solution (C), and there are no reliable ways to measure the difference.

Problems

10.1. Given that K_{s0} for AgCl is $10^{-9.75}$:

    (a) What is the solubility of AgCl in mol/L in pure water, and what is the concentration of Ag^+ in mg/L?

    (b) If the chloride content of seawater is 19.4 parts per thousand, what is the solubility of Ag^+ in seawater? Note you may ignore activity corrections even though they would be significant.

    (c) Correct the solubility product to a concentration basis using a value of 0.69 as an estimate for the activity coefficients of Cl^- and Ag^+ in seawater. Compare the result to your answer in part (b).

10.2. K_{s0} for gypsum ($CaSO_4 \cdot 2H_2O$) is $10^{-4.61}$, and K_{s0} for anhydrite ($CaSO_4$) is $10^{-4.36}$. Which mineral phase controls the solubility of Ca^{2+} in brine containing Ca^{2+} and SO_4^{2-}? Suppose a piece of sheetrock (drywall), which essentially is gypsum covered by paper, fell off a truck during a rainstorm, broke into pieces and landed in a parking lot in a depression filled with rainwater. What is the maximum concentration of Ca^{2+} and SO_4^{2-} that could occur in the water if it reaches equilibrium with the gypsum in the sheet?

10.3. Consider the equilibrium conditions calculated in Example 7.9 for calcite exposed to an atmosphere of $10^{-3.5}$ atm of CO_2. Is the system defined by these results supersaturated with respect to any other calcium mineral phase or phases? Why or why not? Suppose there were some kinetic constraints on the precipitation of calcite. If the system became closed to the atmosphere and its pH were raised to 9.0, would any other mineral precipitate? If so, what would precipitate?

10.4. Cr^{III}, the least toxic form of the element chromium, forms hydroxide complexes that control its solubility in water.

(a) Determine the pH of minimum solubility for Cr^{III} and the total concentration of Cr_T^{III} at this pH. Use MINEQL+ or another computer equilibrium program in multirun mode over the pH range of 1–13. Assume an initial Cr_T^{III} of 1×10^{-2} M and a fixed ionic strength of $I = 0.1$. Plot your output and edit the log C axis to an appropriate scale to illustrate the species composition changes over the pH range.

(b) Based on the results in (a), describe how the speciation of Cr^{III} changes as a function of pH. Explain why the line for $Cr(OH)_{3(aq)}$ increases with pH up to a value of about 4.0 and then remains constant up to pH 13. What fraction of the Cr_T^{III} is present as $Cr(OH)_{3(aq)}$ at the pH of minimum solubility for Cr^{III}?

10.5. (Courtesy of Dan Giammar). Lead phosphate minerals are relatively insoluble, and the addition of phosphate to lead-contaminated soils has been proposed as a means of *in situ* lead remediation. For an aqueous system with $TOTPb = 10^{-6}$ M, $TOTPO_4 = 10^{-4}$ M, and $TOTCl = 10^{-4}$ M, answer parts (a)–(c) below. You can assume that the system is free of dissolved carbonate species, and you can exclude Pb^{II} complexes with Cl^- from your calculations. Consider only the following three solids: chloropyromorphite, $Pb_5(PO_4)_3Cl_{(s)}$ (CPY); hydroxypyromorphite, $Pb_5(PO_4)_3OH_{(s)}$ (HPY); and lead hydroxide, $Pb(OH)_{2(s)}$. Solubility products the three solids are

$$CPY \rightleftharpoons 5Pb^{2+} + 3PO_4^{3-} + Cl^- \qquad K_{s0} = 10^{-84.4},$$

$$HPY \rightleftharpoons 5Pb^{2+} + 3PO_4^{3-} + OH^- \qquad K_{s0} = 10^{-76.8},$$

$$Pb(OH)_{2(s)} + 2H^+ \rightleftharpoons Pb^{2+} + 2H_2O \qquad {}^*K_{s2} = 10^{8.15}.$$
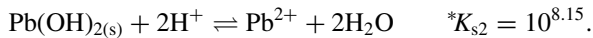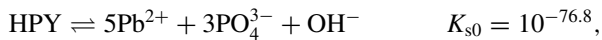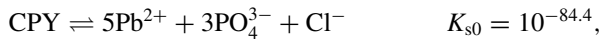
(a) According to the Gibbs phase rule, is it possible for all three solids to coexist?

(b) Plot $[Pb^{2+}]$ versus pH for the conditions of (i) no solid, (ii) equilibrium with only chloropyromorphite, (iii) only hydroxypyromorphite, and (iv) only lead hydroxide.

(c) Based on your result to parts (a) and (b), plot the total dissolved lead in the system. On this same plot, identify which solids are present for different pH regions.

(d) Use MINEQL+ or another computer equilibrium program to rerun this problem for total Pb, Cl, and P concentrations corresponding to 1 g/L chloropyromorphite. Plot the total dissolved lead versus pH and identify pH regions where various solids are present. Briefly explain why this problem would be difficult by hand; that is, why are you glad that you could use MINEQL+ for this?

10.6. (Courtesy of Dan Giammar) Water containing 1×10^{-5} M dissolved cadmium and 0.01 M Cl^- is treated with 1 mM NaHS to precipitate $CdS_{(s)}$. At pH 7, what is the equilibrium dissolved Cd after treatment? Assume that $CdS_{(s)}$ precipitates and

that NaHS dissociates completely to Na^+ and HS^-. Consider only the following reactions:

$$H_2S \rightleftharpoons HS^- + H^+ \qquad\qquad pK_{a1} = 7.02$$

$$HS^- \rightleftharpoons S^{2-} + H^+ \qquad\qquad pK_{a2} = 17.3$$

$$CdS_{(s)} \rightleftharpoons Cd^{2+} + S^{2-} \qquad\qquad \log K = -31.66$$

$$Cd^{2+} + Cl^- \rightleftharpoons CdCl^+ \qquad\qquad \log K = 1.98$$

$$Cd^{2+} + 2Cl^- \rightleftharpoons CdCl_{2(aq)} \qquad\qquad \log K = 2.6$$

$$Cd^{2+} + 3Cl^- \rightleftharpoons CdCl_3^- \qquad\qquad \log K = 2.4$$
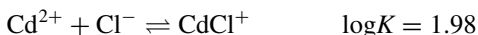
10.7. (Courtesy of Dan Giammar) $FeCl_{3(s)}$ is often added as a flocculant to water in treatment plants. For the problems below, assume that ferrihydrite, $Fe(OH)_{3(s)}$, is the only solid that forms.

(a) Briefly describe how ferric chloride additions help in water treatment.
(b) Determine the pH and dissolved iron concentration if 10^{-4} M $FeCl_3$ were added to pure water.
(c) If a water initially had an alkalinity of 150 mg/L as $CaCO_3$ and a pH of 8.3 (assume that all the alkalinity is from dissolved inorganic carbon), what are the pH and dissolved iron concentration at equilibrium? Treat the water as a closed system with respect to CO_2 exchange. Comment on whether or not strong base should be added with the $FeCl_{3(s)}$.

10.8. (Courtesy of Dan Giammar) Prepare pC-pH plots of dissolved mercury (II) (Hg^{II}) speciation for the two cases described below. Prepare these plots using a spreadsheet; you can check your answers using MINEQL+. Show for the pH range of 1–13 and log C range of -12 to -2. For each case assume that the only solid that can precipitate is $Hg(OH)_{2(s)}$, and note in your answer whether or not the solid precipitates.

(a) $TOTHg^{II} = 10^{-3}$ M
(b) $TOTHg^{II} = 10^{-3}$ M and $TOTCl = 10^{-1}$ M
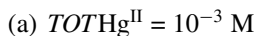
10.9. You have the following data on a lake contaminated with nickel:

$$pH = 9.2; [F^-] = 8.69 \times 10^{-4} \text{ M}; [PO_4^{3-}] = 1.28 \times 10^{-8} \text{ M}$$

The lake is open to the atmosphere, and $P_{CO_2} = 10^{-3.5}$ atm.

(a) Given the following information, determine which solid phase limits the solubility of Ni^{II}, and calculate the speciation of dissolved nickel when saturation with respect to this solid has been reached.

$$Ni^{2+} + H_2O \rightleftharpoons NiOH^+ + H^+ \qquad\qquad \log{}^*\beta_1 = -9.86$$

$$Ni^{2+} + 2H_2O \rightleftharpoons Ni(OH)_2^\circ + 2H^+ \qquad\qquad \log{}^*\beta_2 = -19$$

$$Ni^{2+} + 3H_2O \rightleftharpoons Ni(OH)_3^- + 3H^+ \qquad \log{}^*\beta_3 = -30$$

$$Ni(OH)_{2(s)} \rightleftharpoons Ni^{2+} + 2OH^- \qquad \log K_{s0} = -15.206$$

$$NiCO_{3(s)} \rightleftharpoons Ni^{2+} + CO_{3-2} \qquad \log K_{s0} = -6.84$$

$$Ni_3(PO_4)_{2(s)} \rightleftharpoons 3Ni^{2+} + 2PO_4^{3-} \qquad \log K_{s0} = -31.3$$

$$NiF_{2(s)} \rightleftharpoons Ni^{2+} + 2F^- \qquad \log K_{s0} = -8.58$$
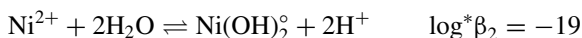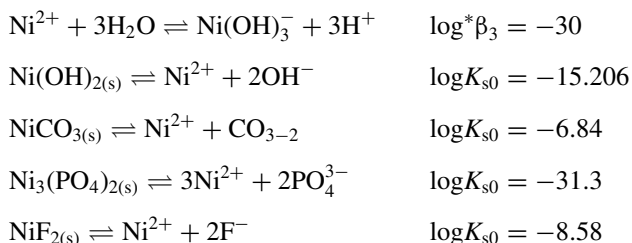
(b) The solubilities of $NiCO_{3(s)}$ and $Ni(OH)_{2(s)}$ are both pH dependent. Only one of the two solids can control the solubility of the system (i.e., be present at all) *except* at the specific pH where the transition of solubility control shifts from one solid to the other. For a closed system with a constant $C_T = 0.1$ M (assume that if precipitation or dissolution of the $NiCO_{3(s)}$ occurs, that the C_T is somehow artificially held constant), determine the pH where $NiCO_{3(s)}$ and $Ni(OH)_{2(s)}$ coexist.

10.10. Based on the information below, what is the total dissolved barium concentration, Ba_T, in

(a) $BaSO_{4(s)}$ added to water at pH 8, and
(b) $BaSO_{4(s)}$ added to a 0.1 M solution of citrate at pH 8.

Assume excess solid is present. Because $BaSO_4$ is the only solid present, for every Ba^{2+} that dissolves, one SO_4^{2-} must dissolve.

Potentially valuable information

$$BaSO_{4(s)} \rightleftharpoons Ba^{2+} + SO_4^{2-} \qquad K_{s0} = 10^{-9}$$

$$Ba^{2+} + H\text{-citrate}^{3-} \rightleftharpoons BaH\text{-citrate}^- \qquad K = 10^{2.4}$$
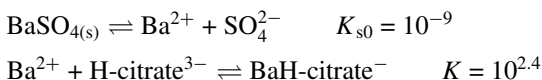
The pK_a values of citric acid (H_4L) are 3.0, 4.4, 6.1, and 16.

10.11. Knowing your love of water chemistry, a favorite relative, who happens to be on the mineralogical naming society, has given you a crystal of $Pb_3(PO_4)_{2(s)}$, which has no common name. Your relative has offered to name the mineral after you (INSERT YOUR NAME HERE-ite) if you can solve the following problem.

An excess of $Pb_3(PO_4)_{2(s)}$ is placed in a solution of 1×10^{-3} M total phosphate (P_T) at pH 8.4. What is the total dissolved lead concentration (Pb_T) at equilibrium? You may assume that any dissolution is not sufficient to change P_T and that the pH is well buffered.

$$Pb^{2+} + H_2O \rightleftharpoons PbOH^+ + H^+ \qquad {}^*\beta_1 = 10^{-7.597}$$

$$Pb^{2+} + 2H_2O \rightleftharpoons Pb(OH)_{2(aq)} + 2H^+ \qquad {}^*\beta_2 = 10^{-17.094}$$

$$Pb^{2+} + 3H_2O \rightleftharpoons Pb(OH)_3^- + 3H^+ \qquad {}^*\beta_3 = 10^{-28.091}$$

$$Pb(OH)_{2(s)} + 2H^+ \rightleftharpoons Pb^{2+} + 2H_2O \qquad {}^*K_{s0} = 10^{8.15}$$

$$H_3PO_4 \rightleftharpoons H_2PO_4^- + H^+ \qquad K_{a1} = 10^{-2.15}$$

$$H_2PO_4^{2-} \rightleftharpoons HPO_4^{2-} + H^+ \qquad\qquad K_{a2} = 10^{-7.2}$$

$$HPO_4^{2-} \rightleftharpoons PO_4^{3-} + H^+ \qquad\qquad K_{a3} = 10^{-12.35}$$

$$Pb_3(PO_4)_{2(s)} \rightleftharpoons 3Pb^{2+} + 2PO_4^{3-} \qquad K_{s0} = 10^{-44.5}$$
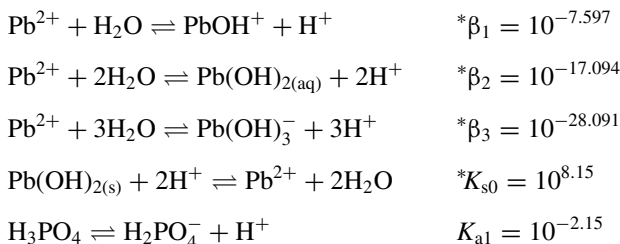
10.12. A chemist with a warped sense of humor developed a new beverage, "CoCO$_3$-Cola," in his position at a soft drink company. Ignoring toxicity and only considering taste and shelf life, he found that the concentration of Co^{2+} must be greater than 3×10^{-5} M and the alkalinity of the solution must be greater than 8×10^{-5} M. There are two possible formulations/storage conditions for "CoCO$_3$-Cola":

(i) closed system, $C_T = 1 \times 10^{-4}$ M (*constant and fixed*), CoCO$_{3(s)}$ is present
(ii) open system, $P_{CO_2} = 10^{-2.2}$ M, CoCO$_{3(s)}$ is present

If both formulations are at pH 6, does either one meet the above criteria?

$$CoCO_{3(s)} \rightleftharpoons Co^{2+} + CO_3^{2-} \qquad \log K_{so} = -9.98$$
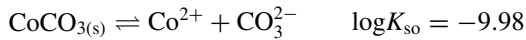
References

1. Benjamin, M. M. 2002. *Water chemistry*, McGraw-Hill, New York.
2. Migdisov, A., A. E. Williams-Jones, L. Z. Lakshtanov, and Y. V. Alekhin. 2002. Estimates of the second dissociation constant of H$_2$S from the surface sulfidation of crystalline sulfur. *Geochim. Cosmochim. Acta* **66**: 1713–1725.
3. Stumm, W., and J. J. Morgan. 1996. *Aquatic chemistry*, 3rd ed., Wiley-Interscience, New York.
4. Plummer, L. N., and E. Busenberg. 1982. The solubilities of calcite, aragonite and vaterite in CO$_2$-H$_2$O solutions between 0 and 90°C and an evaluation of the aqueous model for the system CaCO$_3$-CO$_2$-H$_2$O. *Geochim. Cosmochim. Acta* **46**: 1011–1140.
5. Sherman, L. A., and P. Barak. 2000. Solubility and dissolution kinetics of dolomite in Ca–Mg–HCO$_3$/CO$_3$ solutions at 25°C and 0.1 MPa carbon dioxide. *Soil Sci. Soc. Amer. J.* **64**: 1959–1968.
6. Baker, P. A., and Kastner, M. 1981. Constraints on the formation of sedimentary dolomite. *Science* **213**: 214–216.
7. Wacey, D., W. T. Wright, and A. J. Boyce. 2007. A stable isotope study of microbial dolomite formation in the Coorong Region, South Australia. *Chem. Geol.* 244: 155–174.
8. Deelman, J. C. 1999. Low-temperature nucleation of magnesite and dolomite. *Neues Jahrbuch Mineral.* (**7**): 289–302.
9. Hsu, K. J. 1963. Solubility of dolomite and composition of Florida ground water. *J. Hydrol.* **1**: 288–310.
10. Schwarzenbach, R. P., P. M. Gschwend, and D. M. Imboden. 2003. *Environmental organic chemistry*, 2nd ed., J. Wiley & Sons, New York.
11. Yalkowlsky, S. H., and S. Banerjee. 1992. *Aqueous solubility. Methods of estimation for organic compounds*, Marcel Dekker, New York.
12. Sherman, S. R., D. B. Trampe, D. M. Bush, M. Schiller, C. A. Eckert, A. J. Dallas, J. Li, and P. W. Carr. 1965. Compilation and correlation of limiting activity coefficients of nonelectrolytes in water. *Ind. Eng. Chem. Res.* **35**: 1044–1058.

13. Abraham, H. H., and J. C. McCowan. 1987. The use of characteristic volumes to measure cavity terms in reversed phase liquid chromatography. *Chromatographia* **25**: 243–246.

14. Nielsen, A. E. 1964. *Kinetics of precipitation*, Pergamon Press, Oxford.

15. Nielsen, A. E. 1961. Homogeneous nucleation in barium sulphate precipitation. *Acta Chem. Scand.* **15**: 441–442.

16. Nielsen, A. E. 1986. Mechanisms and rate laws in electrolyte crystal growth from aqueous solution. In *Geochemical processes at mineral surfaces*, J. A. Davis and K. F. Hayes (eds.), ACS Symp. Ser. **323**, Am. Chem. Soc., Washington, D.C., 600–614.

17. Burton, W. K., N. Cabrera, and F. C. Frank. 1951. The growth of crystals and the equilibrium structure of their surfaces. *Philos. Trans. Roy. Soc. Lond.* **A243**: 299–358.

18. Plummer, L. N., T. M. L. Wigley, and D. L. Parkhurst. 1978. The kinetics of calcite dissolution in CO_2-water systems at 5° to 60°C and 0.0 to 1.0 atm CO_2. *Amer. J. Sci.* **278**: 179–216.

19. Berner, R. C., and J. W. Morse. 1974. Dissolution kinetics of calcium carbonate in seawater: IV. Theory of calcite dissolution. *Amer. J. Sci.* **274**: 108–134.

20. Peterson, M. N. A. 1966. Calcite: rates of dissolution in a vertical profile in the central Pacific. *Science* **154**: 1542–1544.

11

■■■ Redox Equilibria and Kinetics

■■■ Objectives and scope

This chapter treats the last of the four major classes of reactions of interest regarding ionic equilibria in natural waters: the coupled processes of oxidation and reduction. Redox processes are important not only for inorganic ions, but they also play prominent roles in the biogeochemical cycles of important biogenic elements (carbon, nitrogen, sulfur, and oxygen) and in transformations of natural organic matter and synthetic organic contaminants in water. After defining important terms and redox processes, we describe how to write and balance redox reactions and how to combine reduction potentials to determine reaction energetics. The relationship between reduction potentials ($E°$ in units of volts) and Gibbs free energy of reaction ($\Delta G°$) is explained, and the related concepts of $p\varepsilon°$ and $p\varepsilon$ as measures of relative electron activity are derived, along with useful analogies between $p\varepsilon$ and pH. Next we develop procedures for displaying redox equilibrium conditions in diagrams and describe how to interpret and use the two major kinds of redox diagrams—pC-$p\varepsilon$ and $p\varepsilon$-pH diagrams. Redox potential is a commonly measured property of natural waters and sediments, but there are severe limitations regarding the interpretation of such data. Reasons for these difficulties are explained as part of a discussion of how redox potentials are measured and what such data mean. The chapter emphasizes the importance of kinetics in describing redox conditions in natural systems. Many redox reactions are very slow, and nonequilibrium conditions are a common feature of the redox status of natural systems. Finally, two mechanisms for redox reactions—inner- and outer-sphere electron exchange—and the implications for kinetic treatment of such processes are described.

Key terms and concepts

- Oxidation, oxidants, oxidizing agents; reduction, reductants, reducing agents; redox reactions as coupled processes
- Electronegativity of elements, electropositive elements
- Reduction potentials; $E°$, E $p\varepsilon°$, $p\varepsilon$, $E_7°$, and $p\varepsilon_7°$ as measures of electron activity; analogies between pH and $p\varepsilon$
- Nernst equation and modified Nernst equation
- Electrochemical cells: anodes (sites of oxidation) and cathodes (sites of reduction)
- pC-$p\varepsilon$ (pC-E_H) and $p\varepsilon$-pH (E_H-pH) diagrams
- Equilibrium potentials, exchange current, electroactive couples, mixed potentials
- Inner and outer sphere electron exchange processes; Marcus cross-correlation

11.1 Introduction

It is difficult to overestimate the importance of redox reactions in controlling the chemistry of natural waters or their importance in water and wastewater treatment. This is especially true if one includes redox processes mediated by microorganisms. It is reasonable to do this because biologically mediated processes involve *chemical* transformations, and many (perhaps most) of those transformations involve redox reactions. Biologically mediated processes drive the redox status of natural waters through oxygen production by the process of photosynthesis and its consumption in the decomposition of organic matter. Indeed, water chemistry is dramatically different in "oxic" waters than in waters where oxygen is absent. The latter may have high concentrations of sulfide, ammonium, soluble iron and manganese, and many other species that are absent or nearly so from oxic waters. Oxygen thus is a key redox variable in water chemistry. Except for the physical process of gravitational settling involved in removing particulate matter from wastewater, the major processes in wastewater treatment are biologically mediated redox reactions. In drinking water treatment, disinfection chemistry mostly involves redox chemistry.

Most of this chapter focuses on redox equilibria—the conditions toward which natural systems tend to go in the absence of further energy inputs. It is important to realize, however, that natural waters generally are ***not*** equilibrium systems with regard to redox reactions. Many redox reactions are very slow, such that nonequilibrium conditions can persist for long periods of time—in some cases indefinitely—in natural waters. Moreover, many redox couples* are not tightly linked with other redox couples, and the net effect is that the different couples in an aquatic system may be in disequilibrium with each other. The often slow kinetics of redox reactions is in contrast to the generally very rapid kinetics of acid-base reactions, and this suggests that redox kinetics is important in water chemistry. One fundamental issue concerning the kinetics of redox reactions is discussed at the end of this chapter, but more detailed discussions on the redox kinetics of specific constituents of natural and engineered aquatic systems are presented in subsequent chapters: Chapter 12 describes the kinetics of redox reactions involving O_2,

---

*In a redox context, a "couple" consists of the oxidized and reduced components of a given half-reaction (see Section 11.2.1 for a definition of "half-reaction.") Examples of some important redox couples in water chemistry include O_2/H_2O, Fe^{III}/Fe^{II}, SO_4^{2-}/HS^-, and NO_3^-/NH_4^+.

Chapter 13 covers oxidation by chlorine compounds, and Chapter 14 treats iron and manganese redox kinetics.

11.2 Fundamentals of redox equilibria

11.2.1 Review of definitions from general chemistry

Oxidation is the loss of electrons by a chemical species; *reduction* is the gain in electrons by a chemical species. *Redox* is shorthand for oxidation-reduction processes (not a crimson-colored bovine!), which always occur as coupled sets of reactions. The *oxidation state* of an atom is the number of missing or extra electrons that it has relative to its elemental form, which by definition has an oxidation state of 0. If there are missing electrons, the oxidation state is positive; if there are extra electrons, it is negative. It is important to note that oxidation state does not necessarily define the chemical species in which the atom exists, nor does it define the charge on the atom (or species in which the atom is found). Instead, it is a "generic identification" for all chemical species in which an element has a given number of electrons.

In the case of simple ions, the oxidation state is easy to assign, and for monoatomic ions it is the same as the charge on the ion. For example, the oxidation state of the ion Na^+ is (+) 1* and is written in Roman numerals by either of the following conventions: (a) in parentheses immediately after the element—Na(I) with no space between the symbols— or (b) as a superscript to the element (Na^I); we use the latter convention in this book. The oxidation states of atoms in more complicated ions or compounds, where electron pairs are shared in covalent bonds, may be more difficult to assign, but the following convention helps to circumvent ambiguities: within molecules and multiatomic ions, the electrons in a bond are formally associated with the more electronegative atom in the bond when calculating oxidation states of elements. *Electronegativity* refers to the tendency of atoms to accept electrons. Highly electronegative elements have a strong tendency to do so and complete their outer electron shell. A rough ranking of atomic electronegativities is **F > O > Cl > S, N >> C > H > metals**. Metals have low electronegativity and often are referred to as *electropositive* elements.

Some elements exist in only one oxidation state (aside from the elemental state), but many elements exist stably in two or more oxidation states depending on the redox status of the system (i.e., its potential, as defined in Section 11.2.3). Carbon, nitrogen, sulfur, and chlorine have many potential oxidation states in environmental systems. Rules for assigning oxidation states of elements in ions and compounds are summarized in Box 11.1. Examples of oxidation states of elements of interest in water chemistry include the following:

C^0 (elemental carbon—graphite, diamond, or fullerenes); C^{IV} (CO_2); C^{-IV} (CH_4)
S^{-II}: sulfide forms; e.g., H_2S, HS^-
S^{IV}: sulfurous forms: SO_2 (sulfur dioxide), H_2SO_3 (sulfurous acid), HSO_3^- (bisulfite), SO_3^{2-} (sulfite)
S^{VI}: sulfuric forms: H_2SO_4, HSO_4^-, SO_4^{2-}

---

*We put the word "plus" in parentheses because it usually is not written but is understood. If the oxidation state is negative, we state that explicitly.

Box 11.1 Rules for assigning oxidation states*

(1) For monoatomic substances, oxidation states are equal to the electronic charge.

(2) Except for metal hydrides, which are not common in environmental systems, H bound in compounds is assumed to have an oxidation state of $+I$.

(3) Oxygen has an oxidation state of $-II$ in all compounds except peroxides, which contain the $-O-O-$ group. Oxygen in peroxide-containing substances has an oxidation state of $-I$.

(4) In covalent compounds, the oxidation state of each atom is the charge remaining when each shared pair of electrons is assigned completely to the more electronegative of the two atoms forming a bond. If an electron pair is shared by two atoms of the same electronegativity (e.g., a $C-C$ bond), the pair is split between the two atoms.

(5) The sum of oxidation states for atoms in multiatomic substances is zero for molecules and equal to the formal charge for ions.

(6) When multiple atoms of the same kind occur in a species (especially C in organic compounds), the element may have an average oxidation state that is a fractional value because different C atoms have different oxidation states (see example of phenol below).

Nitrogen compounds		Sulfur compounds		Carbon compounds	
Substance	Oxidation states	Substance	Oxidation states	Substance	Oxidation states
NH_4^+	$N = -III$, $H = +I$	H_2S	$S = -II$, $H = +I$	CH_4	$C = -IV$
HCN	$N = -III$, $C = +II$, $H = +I$	$S_{8(s)}$	$S = 0$	CH_3OH	$C = -II$
N_2	$N = 0$	$S_2O_3^{2-}$	$S = +II$, $O = -II$	$C_6H_{12}O_6$	$C = 0$
N_2O	$N = +I$, $O = -II$	$S_4O_6^{2-}$	$S_{ave} = +2.5$, $O = -II$	C_6H_5OH	$C_{ave} = -2/3$[†]
NO_2^-	$N = +III$, $O = -II$	SO_3^{2-}	$S = +IV$, $O = -II$	HCOOH	$C = +II$
NO_2	$N = +IV$, $O = -II$	SO_4^{2-}	$S = +VI$, $O = -II$	HCO_3^-	$C = +IV$
NO_3^-	$N = +V$, $O = -II$	SCN^-	$S = -II$, $C = +IV$, $N = -III$		

* Adapted in part from Stumm and Morgan.[1]

† The five carbons in the benzene ring with H attached have an oxidation state of -1; the carbon with the $-OH$ group has an oxidation state of $+1$; the net (average) oxidation state thus is $(-5 + 1)/6 = -4/6$

Hg^0 (elemental), Hg^I (mercurous form), Hg^{II} (mercuric form)
Fe^0 (elemental iron (ferrum)), Fe^{II} (ferrous iron), Fe^{III} (ferric iron), Fe^{VI} (ferrate)
Cl^0 (elemental: Cl_2); Cl^I (hypochlorous forms: HOCl, hypochlorous acid, and OCl$^-$, hypochlorite); Cl^{-I} (chloride, Cl^-)

A **reductant** (also called a **reducing agent**) donates electron(s) to some other species (to an oxidant), in the process becoming more oxidized:

$$\textbf{Reductant}_1 \rightarrow \textbf{Oxidant}_1 + \textbf{\textit{e}}^- \tag{11.1}$$
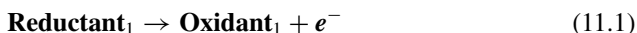
An **oxidant** (also called an **oxidizing agent**) accepts electrons from a reducing agent, in the process becoming more reduced:

$$\textbf{Oxidant}_2 + \textbf{\textit{e}}^- \rightarrow \textbf{Reductant}_2 \tag{11.2}$$

Equations 11.1 and 11.2 are general examples of redox **half-reactions**. For any chemical reaction in solution, there is no net production or consumption of electrons, and thus an oxidation half-reaction always is combined with a reduction half-reaction to yield a complete redox reaction:

$$\textbf{Reductant}_1 + \textbf{Oxidant}_2 \rightarrow \textbf{Oxidant}_1 + \textbf{Reductant}_2 \tag{11.3}$$

11.2.2 Balancing redox reactions

Balancing of redox reactions is based on the fact that free electrons cannot exist in solution and electrons thus must be conserved; i.e., there is no net production or consumption of electrons over the two half-reactions that constitute a balanced complete redox reaction. Balancing redox reactions can be complicated, but if the following steps are followed, one should arrive at a balanced chemical reaction with little difficulty.

1. Identify the principal reactants and products (generally species other than H^+, OH^-, and H_2O) in the oxidation and reduction half-reactions and write the components of each half-reaction without bothering to balance the number of atoms on each side of the equations. Write both half-reactions as reductions; i.e., the oxidized form of the principal reactant is on the left, and the reduced form on the right side of the equation.
2. Balance each half-reaction for atoms other than hydrogen (H) and oxygen (O) by multiplying the principal reactants and products by appropriate integers.
3. Determine the oxidation state of the principal reactant and product in each half-reaction, compute the difference in total oxidation state for each redox couple (taking into account any stoichiometric coefficients for the redox-active species), and add sufficient electrons (e^-) on the left side of each half-reaction to account for this difference.
4. Balance oxygen in each half-reaction by adding enough H_2O on the side deficient in O.
5. Balance hydrogen by adding enough H^+ on the side deficient in H.

6. Check to see that the charge is the same (balanced) on both sides of each half-reaction. If it is not, check steps 2–5 to see where you made an error.
7. Multiply each half-reaction by an appropriate integer so both contain the same number of electrons.
8. Subtract the balanced reduction half-reaction for the substance undergoing oxidation in the overall reaction from the balanced reduction half-reaction for the substance undergoing reduction in the overall reaction and simplify the result.

Several alternatives may apply to the process depending on what information you are provided initially. If the half-reactions are given as balanced entities, you can skip steps 2–5. If the half-reactions are balanced in terms of principal species and electrons (i.e., each half-reaction involves the same number of electrons), you may proceed directly to step 8 and then do steps 4 and 5 on the net reaction.

EXAMPLE 11.1 Balancing ferrous iron oxidation reactions: Dissolved ionic iron exists in anoxic* ground water as the reduced species Fe^{2+}. When such waters are used from drinking water supplies and the water becomes exposed to the atmosphere, the Fe^{2+} is oxidized by O_2 to Fe^{III} (ferric iron), which is insoluble at neutral pH and precipitates as $Fe(OH)_{3(s)}$. Hypochlorous acid (HOCl), a common disinfectant, also oxidizes Fe^{II} very rapidly to Fe^{III}. Write balanced equations for the oxidation of Fe^{2+} to $Fe(OH)_{3(s)}$ by both O_2 and HOCl.

Answer: **(1) Oxygen as oxidant**

	$Fe(OH)_{3(s)} + e^- = Fe^{2+}$	A one-electron change; steps 1–3 complete
	$Fe(OH)_{3(s)} + e^- = Fe^{2+} + 3H_2O$	Step 4 complete
(i)	$Fe(OH)_{3(s)} + 3H^+ + e^- = Fe^{2+} + 3H_2O$	Step 5 complete; reaction balanced; step 6 complete
	$O_2 + e^- = 2H_2O$	Steps 1 and 2 complete
	$(O^0 \leftrightarrow O^{-II})$	Reduction of oxygen is a two-electron change
(ii)	$O_2 + 4H^+ + 4e^- = 2H_2O$	Steps 3, 4–6 complete
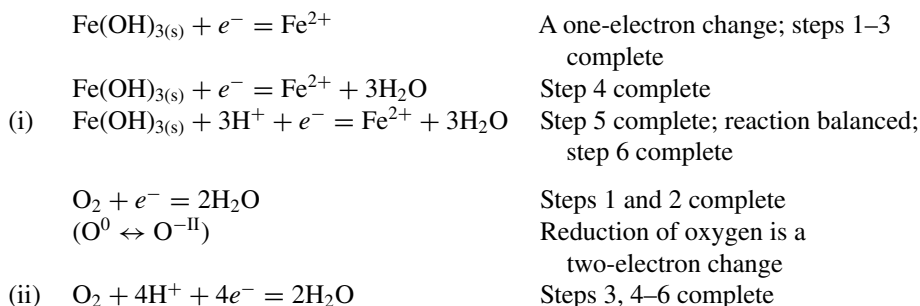
Multiply (i) by the number of electrons in (ii):

(i)′ $4Fe(OH)_{3(s)} + 12H^+ + 4e^- = 4Fe^{2+} + 12H_2O$

Subtract (i)′ from (ii):

Net: $4Fe^{2+} + 12H_2O + O_2 + 4H^+ + 4e^- = 4Fe(OH)_{3(s)} + 12H^+ + 4e^- + 2H_2O$

Simplifying yields

$4Fe^{2+} + O_2 + 10H_2O = 4Fe(OH)_{3(s)} + 8H^+$ Atoms and charges balance

---
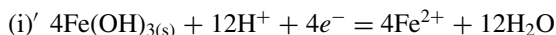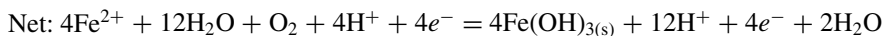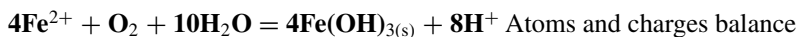
*"Anoxic" means that the water contains no dissolved oxygen (DO). Most ground waters have no or very low DO, which allows the reduced (and typically more soluble) forms of many elements to exist stably as dissolved species in the water.

(2) HOCl as oxidant
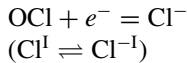
$$OCl + e^- = Cl^-$$ Step 1 and 2 complete
$$(Cl^I \rightleftharpoons Cl^{-I})$$ (Reduction of HOCl to Cl^- is a
    two-electron change)
$$HOCl + 2e^- = Cl^-$$ Step 3 complete
$$HOCl + 2e^- = Cl^- + H_2O$$ Step 4 complete
(iii) $$HOCl + 2e^- + H^+ = Cl^- + H_2O$$ Steps 5 and 6 complete
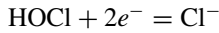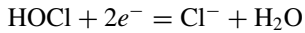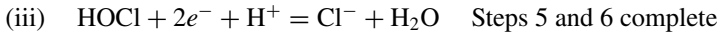
Multiply (i) by number of electrons in (iii):

(i)″ $2Fe(OH)_{3(s)} + 6H^+ + 2e^- = 2Fe^{2+} + 6H_2O$

Subtract (i)″ from (iii):

Net: $2Fe^{2+} + 6H_2O + HOCl + 2e^- + H^+$
    $= 2Fe(OH)_{3(s)} + 6H^+ + 2e^- + Cl^- + H_2O$

Simplifying yields

$$\mathbf{2Fe^{2+} + 5H_2O + HOCl = 2Fe(OH)_{3(s)} + 5H^+ +\ Cl^-}\ \text{Atoms and charges balance}$$
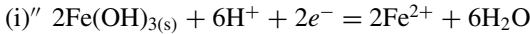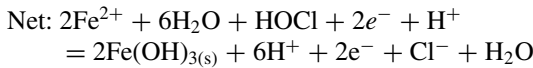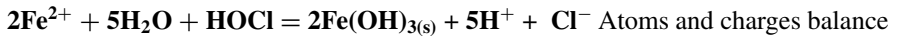
EXAMPLE 11.2 Balancing the nitrification reaction (oxidation of ammonium to nitrate by O$_2$):
Ammonium (NH_4^+) is released into water in the decomposition of natural organic matter
(e.g., cellular material containing proteins) and is oxidized to nitrate (NO_3^-) by bacteria
using dissolved oxygen (DO) in the process of nitrification. Although the reaction does
not occur abiotically, it can be written as a chemical reaction. Write the balanced chemical
reaction.

Answer: From reaction (ii) in Example 11.1, we can write the reduction of oxygen to
water:

(ii) $O_2 + 4H^+ + 4e^- = 2H_2O$
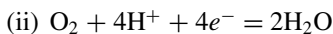
For the reduction of nitrate to ammonium,
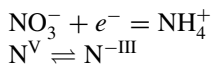
$$NO_3^- + e^- = NH_4^+$$ Steps 1 and 2 complete
$$N^V \rightleftharpoons N^{-III}$$ Reduction of NO_3^- to NH_4^+ is an
    eight-electron change
$$NO_3^- + 8e^- = NH_4^+ + 3H_2O$$ Steps 3 and 4 complete
(iv) $$NO_3^- + 10H^+ + 8e^- = NH_4^+ + 3H_2O$$ Step 5 complete; half-reaction
    balanced; step 6 complete
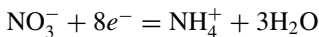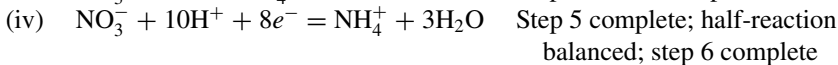
Multiplying (ii) by 2 to get same number of electrons as in (iv) yields

(ii)′ $2O_2 + 8H^+ + 8e^- = 4H_2O$
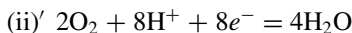
Subtracting (iv) from (ii)′ yields

$$NH_4^+ + 3H_2O + 2O_2 + 8H^+ + 8e^- = NO_3^- + 10H^+ + 8e^- + 4H_2O$$

Simplifying yields

$$NH_4^+ + 2O_2 = NO_3^- + \underline{2H^+ + H_2O} \quad \text{Atoms and charges balance}$$
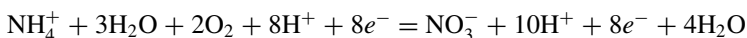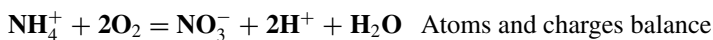
11.2.3 Reduction potential as quantitative measure of redox (equilibrium) tendencies

By convention, half-reactions are written as reductions (as in Eq. 11.2). In a thermodynamic or equilibrium sense, the tendency for any half-reaction, $Ox_1 + e^- = Red_1$, to occur is given by the standard reduction potential, $E°$ (units of volts, V). Table 11.1 provides reduction potentials for important redox couples in natural waters and sediments. A few examples used in the following discussion are as follows:

$O_{2(aq)} + 4e^- + 4H^+ = 2H_2O \quad E° = +1.27$ V
$Cl_{2(aq)} + 2e^- = 2Cl^- \quad\quad\quad E° = +1.36$ V
$H^+ + e^- = \frac{1}{2}H_2 \quad\quad\quad\quad E° = 0.00$ V (by definition)
$Na^+ + e^- = Na \quad\quad\quad\quad E° = -2.72$ V
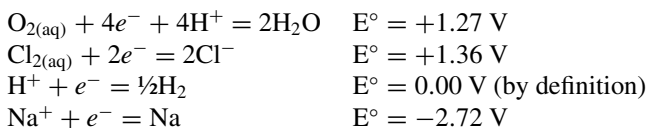
Values of $E°$ apply to standard conditions; i.e., all reactants and products (except e^-) are at unit activity (i.e., 1 M for dissolved species). It is not possible to measure the absolute value of the reduction potential for any single half-reaction because it is not possible to isolate half-reactions. Instead, we measure the difference in reduction potentials between two half-reactions, which taken together constitute a whole reaction (or electric cell). To develop a useful list of standard reduction potentials, we need to define the reduction potential of some half-reaction arbitrarily. For consistency with the convention used to define free energies of formation of ions (see Section 3.11), the standard reduction potential for the $H^+/\frac{1}{2}H_2$ couple is defined to be 0.00 V.

It is important to note that the value of $E°$ for a given half-reaction does not depend on the stoichiometric coefficients for the half-reaction. For example, we may write reduction potentials either as single electron transfers or as multiple electron transfers with appropriate change in stoichiometric coefficients for the other reactants and products, but this has no effect on $E°$. For example, we may write the reduction potential for O_2 as $\frac{1}{4}O_2 + e^- + H^+ = \frac{1}{2}H_2O$, and $E°$ still is +1.27 V. This is not true, however, for $\Delta G°$ of the reaction, which depends on the number of moles, as explained in Section 11.2.4.

In general, the higher the value of $E°$, the stronger is the reactant as an oxidant in a reduction potential half-reaction. Conversely, the more negative the value of $E°$, the stronger the product of a reduction potential half-reaction is as reducing agent. In the above list, O_2 and Cl_2 are both strong oxidants, and Na metal is a strong reductant. O_2 and Cl_2 thus have strong tendencies to react with (oxidize) other species, taking up electrons and moving into their reduced states (H_2O and Cl^-, respectively). In contrast, Na metal has a strong tendency to give up an electron to something else, in the process becoming oxidized Na^+. Another way of saying this is that Na^+ has little tendency to accept an electron and become Na metal; similarly, it is difficult to get H_2O and Cl^- to give up electrons to go to their oxidized states.

It is important to recognize that $E°$ is an equilibrium (thermodynamic) property and is not necessarily the same as the *measured* electrode potential. In fact, many published

Table 11.1 Reduction potentials, $p\varepsilon^\circ$, and log K values for some important redox half-reactions[*]

Reaction	E°(V)	$p\varepsilon^\circ$	$p\varepsilon_7^\circ$	log K
$Ag^+ + e^- = Ag^0_{(s)}$	0.797	13.51	13.51	13.51
$Al^{3+} + 3e^- = Al^0_{(s)}$	−1.686	−28.57	−28.57	−85.71
$AsO_4^{3-} + 2H^+ + 2e^- = AsO_3^{3-} + H_2O$	0.156	2.64	−4.36	5.29
$HOBr + H^+ + 2e^- = Br^- + H_2O$	1.338	22.68	19.18	45.36
$2HOBr + 2H^+ + 2e^- = Br_{2(aq)} + 2H_2O$	1.581	26.80	20.27	53.60
$BrO_3^- + 6H^+ + 6e^- = Br^- + 3H_2O$	1.437	24.35	17.35	146.10
$CO_{2(g)} + 8H^+ + 8e^- = CH_{4(g)} + 2H_2O$	0.170	2.87	−4.13	22.96
$6CO_{2(g)} + 24H^+ + 24e^- = glucose + 6H_2O$	−0.012	−0.20	−7.20	−4.80
$CO_{2(g)} + 4H^+ + 4e^- = CH_2O + H_2O$	−0.071	−1.20	−8.20	−4.80
$CO_{2(g)} + H^+ + 2e^- = HCOO^-$	−0.285	−4.83	−8.33	−9.66
$CH_2O + 2H^+ + 2e^- = CH_3OH$	0.236	3.99	−3.01	7.98
$CH_2O + 4H^+ + 4e^- = CH_{4(g)} + H_2O$	0.410	6.94	−0.06	27.76
$CH_3OH + 2H^+ + 2e^- = CH_{4(g)} + H_2O$	0.584	9.88	2.88	19.76
$Cl_{2(aq)} + 2e^- = Cl^-$	1.392	23.60	23.60	47.20
$HOCl + H^+ + 2e^- = Cl^- + H_2O$	1.481	25.10	21.60	50.20
$ClO_2 + 4H^+ + 5e^- = Cl^- + 2H_2O$	1.495	25.33	19.73	126.67
$ClO_2^- + 4H^+ + 4e^- = Cl^- + 2H_2O$	1.609	27.27	20.26	109.06
$ClO_3^- + 6H^+ + 6e^- = Cl^- + 3H_2O$	1.446	24.50	17.50	147.02
$Co^{3+} + e^- = Co^{2+}$	1.953	33.10	33.10	33.10
$CrO_4^{2-} + 8H^+ + 3e^- = Cr^{3+} + 4H_2O$	1.514	25.66	7.00	77.00
$Cu^{2+} + e^- = Cu^+$	0.160	2.72	2.72	2.72
$Cu^{2+} + 2e^- = Cu^0_{(s)}$	0.339	5.74	5.74	11.48
$Fe^{3+} + e^- = Fe^{2+}$	0.769	13.03	13.03	13.03
$Fe^{2+} + 2e^- = Fe^0_{(s)}$	−0.441	−7.45	−7.45	−14.90
$2H^+ + 2e^- = H_{2(g)}$	0.000	0.00	0.00	0.00
$2H^+ + 2e^- = H_{2(aq)}$	−0.092	−1.55	−8.55	−3.10
$2Hg^{2+} + 2e^- = Hg_2^{2+}$	0.908	15.40	15.40	30.79
$Hg_2^{2+} + e^- = 2Hg_{(l)}$	0.794	13.46	13.46	26.91
$MnO_4^- + 8H^+ + 5e^- = Mn^{2+} + 4H_2O$	1.508	25.56	14.36	127.82
$MnO_{2(s)} + 4H^+ + 2e^- = Mn^{2+} + 2H_2O$	1.227	20.80	6.80	41.60
$Mn^{3+} + e^- = Mn^{2+}$	1.505	25.51	25.51	25.51
$Ni^{2+} + 2e^- = Ni^0_{(s)}$	−0.236	−3.99	−3.99	−7.98
$O_{2(g)} + 4H^+ + 4e^- = 2H_2O$	1.226	20.78	13.78	83.12
$O_{2(aq)} + 4H^+ + 4e^- = 2H_2O$	1.268	21.50	14.50	86.00
$O_{2(aq)} + 2H^+ + 2e^- = H_2O_{2(aq)}$	0.777	13.17	6.17	26.34
$H_2O_{2(aq)} + 2H^+ + 2e^- = 2H_2O$	1.758	29.80	22.80	59.59
$Pb^{4+} + 2e^- = Pb^{2+}$	0.845	14.32	14.32	28.64
$Pb^{2+} + 2e^- = Pb^0_{(s)}$	−0.126	−2.13	−2.13	−4.27
$SO_4^{2-} + 10H^+ + 8e^- = H_2S_{(aq)} + 4H_2O$	0.299	5.08	−3.67	40.67
$SO_4^{2-} + 9H^+ + 8e^- = HS^- + 4H_2O$	0.248	4.21	−3.67	33.68
$SO_4^{2-} + 2H^+ + 2e^- = SO_3^{2-} + H_2O$	0.801	13.58	6.58	27.16
$SeO_4^{2-} + 4H^+ + 2e^- = H_2SeO_3 + H_2O$	1.071	18.16	4.16	36.32
$Zn^{2+} + 2e^- = Zn^0_{(s)}$	−0.760	−12.88	−12.88	−25.76

[*] See Table 11.3 for similar data on nitrogen species. Compiled or calculated from Stumm and Morgan[1] and Benjamin.[2]

E° values were computed from the free energies of formation (G_f°) of the reactants and products in a reaction or half-reaction rather than measured by potentiometric means. As shown below, E° is related to the free energy of reaction, ΔG_r°. When E° is positive, ΔG° is negative, and the reaction is spontaneous.

11.2.4 Relationship of E and E° to other measures of equilibrium

Reduction potentials are directly related to the other common thermodynamic measures of chemical equilibrium. For whole reactions,

$$\Delta G_r^\circ = -n\mathcal{F}\,E_{cell}^\circ, \tag{11.4}$$

where ΔG_r° is in joules per mole ($J\ mol^{-1}$); n is the number of electrons involved in the redox reaction; $\mathcal{F}$ is Faraday's constant (charge per mol of electrons, 96,485 coulombs/mol); and E_{cell}° is in volts.* The equation explains why ΔG° depends on stoichiometric coefficients and E° does not. When multiplying an equation by a constant, n will also increase by the same factor. Thus, when E° is calculated based on ΔG°, the ΔG° is divided by n, giving the same E° value.

Because $\Delta G_r^\circ = -RT \ln K$, we can write

$$\ln K = \left(\frac{n\mathcal{F}}{RT}\right) E_{cell}^\circ. \tag{11.5}$$

The term $2.303RT/\mathcal{F}$ has a value of 0.0591 at 25°C ($2.303 \times 8.314\ J\ K^{-1}\ mol^{-1} \times 298\ K \div 96,485\ coulomb\ mol^{-1} = 0.0591$, which has dimensions of $J\ coul^{-1}$, or V), and so we can write

$$\log K = \frac{n}{0.059} E_{cell}^\circ, \tag{11.6}$$

or

$$\frac{1}{n} \log K = \frac{E_{cell}^\circ}{0.059}. \tag{11.7}$$

11.2.5 The Nernst equation

This fundamental redox equilibrium relationship defines how reduction potentials under any conditions depend on the reduction potential for standard conditions (unit activity)

---

*The units conversion here may not be immediately obvious, but in SI units 1 joule (J) = 1 N·m = 1 kg·m²/s² (in mechanical work terms) or V·A·s (in electrical work terms). Also, A (amperes) = coulomb/s, and thus V (volts) = J coul⁻¹. Combining the mechanical and electrical equivalencies of work, we find that $V = kg\cdot m^2/(A\cdot s^3)$. Thus, $\mathcal{F}E_{cell}^\circ = (coul/mol)\cdot kg\cdot m^2/A\cdot s^3 = (coul/s)\cdot(1/mol)\cdot(kg\cdot m^2/A\cdot s^2) = kg\cdot m^2/s^2\cdot mol$, or $J\ mol^{-1}$.

and the activities of the species on the oxidized and reduced sides of a reduction half-reaction:

$$E = E^\circ + \frac{RT}{n\mathcal{F}} \ln \prod \frac{a_{ox}}{a_{red}}, \tag{11.8}$$

or

$$E = E^\circ + \frac{0.059}{n} \log \prod \frac{a_{ox}}{a_{red}}, \tag{11.9}$$

where

E	=	reduction potential (V) (for $Ox_1 + e^- \rightarrow Red_1$) for a set of activities of reactants and products,
E°	=	standard reduction potential for reaction when all species are at unit activity,
RT	=	thermal energy per mole,
n	=	number of electrons involved in reaction,
$\mathcal{F}$	=	Faraday's constant, and
$\prod$	=	mathematical symbol for multiplication.

For equilibrium constants, the ratio of activities has always been "products over reactants." By convention, it is "oxidized over reduced" or "reactants over products" for redox equations. Writing the Nernst equation as "products over reactants" changes the "plus sign" after E° to a "minus sign."

11.2.6 Cell potentials

When half-reactions are combined, E° for the net reaction, which sometimes is called a "cell," is the algebraic sum of the E°s for the component half-reactions. For example,

$$Cu^{2+} + 2e^- = Cu \qquad E^\circ = +0.34V \tag{11.10a}$$

$$- \underline{(Zn^{2+} + 2e^- = Zn)} - \underline{(E^\circ = -0.76V)} \tag{11.10b}$$

Net:

$$Cu^{2+} + Zn = Cu + Zn^{2+} \qquad E^\circ_{cell} = 1.10V \tag{11.10c}$$
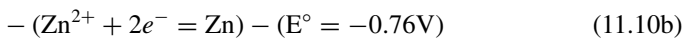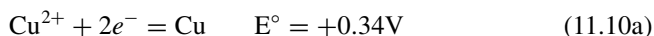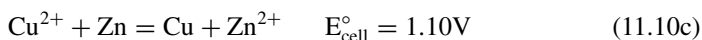
Because E°_{cell} for reaction 11.10c is strongly positive, the reaction is spontaneous as written. In contrast, if we subtract the standard reduction potential for Cu^{2+} (Eq. 11.10a) from that for Zn^{2+} (Eq. 11.10b), the net reaction is the reverse of Eq. 11.10c, and E°_{cell} is -1.10 V, indicating that oxidation of Cu to Cu^{2+} by the reduction of Zn^{2+} to Zn is not spontaneous.

Figure 11.1 Schematic of an electrochemical cell for the Zn/Zn^{2+} and Cu/Cu^{2+} couples.

11.2.7 Electrochemical cells

If the half-reactions constituting a whole redox reaction or cell occur in separate solutions connected as shown in Figure 11.1, we have an electrochemical cell, and the potential (voltage) produced by the cell may be used to do work. The potential for such a cell is defined as

$$E_{cell} = E_{cathode} - E_{anode} = E_c - E_a, \tag{11.11}$$

where E_a and E_c are the reduction potentials (electrode potentials) of the half-reactions, and by convention, the oxidation half-reaction occurs at the *anode* (remember, oxidation and anode both start with vowels), and the reduction half-reaction occurs at the *cathode*.

For the cell defined by Eqs. 11.10a–11.10c, the reduction of Cu^{2+} to Cu is the cathodic reaction, and the oxidation of Zn to Zn^{2+} is the anodic reaction. We also can write the reactions of an electrochemical cell as follows:

$$Zn|ZnSO_4(a_{Zn^{2+}=1.0})||CuSO_4(a_{Cu^{2+}=1.0})|Cu \tag{11.12}$$

ANODE   CATHODE

The single vertical lines in the cell represent a phase change, and the double vertical line represents a liquid junction between the two half cells. As written, the cell is for oxidation of Zn to Zn^{2+} at the anode and reduction of Cu^{2+} to Cu at the cathode. If we want to consider an electrochemical cell going in the opposite direction (Cu oxidation and Zn^{2+} reduction), we would write Eq. 11.12 in exactly the reverse way. Because

Zn^{2+} and Cu^{2+} are at unit activity in the cell defined by Eq. 11.12, the electrode and cell potentials are equal to the standard (E°) potentials.

We are interested in knowing whether the reaction is spontaneous. From the reduction potentials in Table 11.1,

$$Cu^{2+} + 2e^- = Cu, \qquad E° = 0.34V = E_c°$$

$$Zn^{2+} + 2e^- = Zn, \qquad E° = -0.76V = E_a°$$

$$\underline{\underline{E_{cell}}} = E_{cell}° = E_c° - E_a° = 0.34 - -0.76 = \underline{1.10V}$$
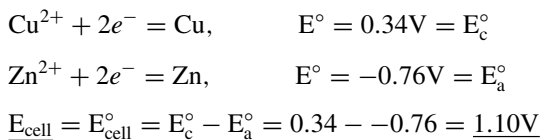
The reaction thus goes strongly to the right (is spontaneous); Cu^{2+} is a better oxidizing agent (it is more readily reduced) than Zn^{2+}, and Zn is a better reducing agent (it is more easily oxidized) than Cu. If the above cell were written backward: $Cu|Cu^{2+}||Zn^{2+}|Zn$, Cu then would be the anode and Zn the cathode, and $E_{cell} = -0.763 - 0.337 = -1.10$ V, which indicates the cell would be nonspontaneous as written.

How long will the reaction proceed? Another way to ask this is, at what activities (or concentrations, if we ignore effects of ionic strength) of Cu^{2+} and Zn^{2+} will the reaction be at equilibrium. The Nernst equation for this cell at equilibrium is

$$E = 1.10 + \frac{0.059}{2} \log \frac{[Cu^{2+}]}{[Zn^{2+}]} = 0$$

$$\log \frac{[Cu^{2+}]}{[Zn^{2+}]} = \frac{-1.10(2)}{0.059} = -37.28, \quad \text{or} \quad \frac{[Cu^{2+}]}{[Zn^{2+}]} = 10^{-37.28} \qquad (11.13)$$

Thus, when the Zn^{2+} concentration is $10^{37.28}$ times that of Cu^{2+}, the reaction will be at equilibrium. In a practical sense, this means that starting with 1 mol/L of Cu^{2+} and 1 mol/L Zn^{2+} in the cathode and anode, respectively, the final concentrations will be ~ 0 mol/L of Cu^{2+} and ~ 2 mol/L Zn^{2+} in the respective cells. At that point, electrons stop flowing, and the battery (for that is what an electrochemical cell is!) is dead.

11.2.8 pε: a measure of free energy of electron transfer

One drawback to using reduction potentials expressed in volts to define the energetics of a redox process is that the units are so familiar that they encourage a false sense that we can measure reduction potentials for any reaction by electrometric means (e.g., a voltmeter). In part to avoid this issue, water chemists often use a related dimensionless term, pε, to quantify reduction potentials. As noted above, the term $2.303RT/n\mathcal{F} = 0.0591$ has units of volts. Dividing E by this quantity thus yields a dimensionless quantity that we call pε:

$$p\varepsilon = \frac{E}{0.0591} \qquad (11.14a)$$

Similarly,

$$p\varepsilon° = \frac{E°}{0.0591}. \qquad (11.14b)$$

Table 11.1 lists values of $p\varepsilon^\circ$ for important redox couples in natural waters and sediment. From Eq. 11.7, it is apparent that $p\varepsilon^\circ$ is directly related to log K. In general,

$$p\varepsilon^\circ = \frac{1}{n}\log K, \tag{11.15}$$

and when $n = 1$,

$$p\varepsilon^\circ = \log K. \tag{11.16}$$

Also, from the relationship between K and ΔG, we can obtain

$$p\varepsilon = -\frac{\Delta G}{nRT\ln 10}, \tag{11.17}$$

$$p\varepsilon^\circ = -\frac{\Delta G^\circ}{nRT\ln 10}. \tag{11.18}$$

Finally, we can rewrite the Nernst equation (Eq. 11.9) in terms of $p\varepsilon$ and $p\varepsilon^\circ$ by dividing all terms by the constant 0.0591, yielding

$$p\varepsilon = p\varepsilon^\circ + \frac{1}{n}\log\prod\frac{a_{ox}}{a_{red}}. \tag{11.19}$$

We refer to Eq. 11.19 as the modified Nernst equation and from here forward use $p\varepsilon$ in preference to E.

Based on Eqs. 11.17 and 11.18, we can interpret $p\varepsilon$ physically as a measure of the free energy involved in the transfer of electrons. Just as pH is a measure of H^+ activity, $p\varepsilon$ is a measure of the relative electron activity; i.e., $p\varepsilon = -\log\{e^-\}$. Also, $p\varepsilon^\circ$ is the negative log of the relative electron activity when all species but e^- are at unit activity. The similarities of the equations related to pH for acid-base reactions and those related to $p\varepsilon$ for redox reactions (Table 11.2) are striking,[1] and they suggest that $p\varepsilon$ is a useful and valuable characteristic of redox conditions, just as pH is an important characteristic of the acid-base status of a water body. For example, a large positive $p\varepsilon$ implies oxidizing conditions (hence low e^- activity), and a low or negative $p\varepsilon$ implies reducing conditions (or high e^- activity).

One can obtain the modified Nernst equation for any half-reaction using the equilibrium constant. As an example, consider the following half-reaction:

$$O_{2(aq)} + 4e^- + 4H^+ = 2H_2O \quad \log K = 86.00 \qquad \text{(Table 11.1)}.$$
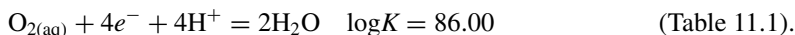
Thus,

$$\log K = \log\frac{1}{\{O_2\}\{H^+\}^4\{e^-\}^4} = -4\log\{e^-\} + \log\frac{1}{\{O_2\}\{H^+\}^4}.$$

Defining $-\log\{e^-\}$ as $p\varepsilon$, and dividing by 4 gives

$$\frac{1}{4}\log K = p\varepsilon + \frac{1}{4}\log\frac{1}{\{O_2\}\{H^+\}^4}.$$

Table 11.2 Analogies between pH and pε*

$pH = -\log\{H^+\}$	$p\varepsilon = -\log\{e^-\}$
General acid-base reaction:	General redox reaction:
(1A) $HA + H_2O = H_3O^+ + A^-$; K_1	(1B) $Fe^{3+} + \frac{1}{2}H_{2(g)} = Fe^{2+} + H^+$; K_1
Reaction 1A is composed of two steps:	Reaction 1B is composed of two steps:
(2A) $HA = H^+ + A^-$; K_2	(2B) $Fe^{3+} + e^- = Fe^{2+}$; K_2
(3A) $H_2O + H^+ = H_3O^+$; K_3	(3B) $\frac{1}{2}H_{2(g)} = H^+ + e^-$; K_3
By thermodynamic convention, $K_3 = 1$	By thermodynamic convention, $K_3 = 1$
Thus, we can write	Thus, we can write
(4A) $K_1 = K_2 = K_2K_3 = \{H^+\}\{A^-\}/\{HA\}$,	(4B) $K_1 = K_2 = K_2K_3 = \{Fe^{2+}\}/\{Fe^{3+}\}\{e^-\}$,
or	or
(5A) $pH = pK + \log\{A^-\}/\{HA\}$.	(5B) $p\varepsilon = p\varepsilon^\circ + \log\{Fe^{3+}\}/\{Fe^{2+}\}$.
Because $pK = -\log K = \Delta G^\circ/2.3RT$,	Because $p\varepsilon^\circ = -\log K = \Delta G^\circ/2.3RT$,
(6A) $pH = \Delta G^\circ/2.3RT + \log\{A^-\}/\{HA\}$.	(6B) $p\varepsilon = \Delta G^\circ/2.3RT + \log\{Fe^{3+}\}/\{Fe^{2+}\}$.
For transfer of one mole of H^+ from acid to water:	For transfer of one mole of e^- to oxidant from H_2:
(7A) $\Delta G = \Delta G^\circ + 2.3RT \log\{A^-\}/\{HA\}$	(7B) $\Delta G = \Delta G^\circ + 2.3RT \log\{Fe^{3+}\}/\{Fe^{2+}\}$

* Abbreviated from Stumm and Morgan.[1]

Using $p\varepsilon^\circ = \frac{1}{n}\log K$ (note that 86 divided by 4 is 21.5, the $p\varepsilon^\circ$ value in Table 11.1 for this reaction) gives the modified Nernst equation for this half-reaction:

$$p\varepsilon^\circ = p\varepsilon + \frac{1}{4}\log\frac{1}{\{O_2\}\{H^+\}^4}; \text{ or } p\varepsilon = 21.5 + \frac{1}{4}\log\{O_2\}\{H^+\}^4$$

There are some important and practical differences between pH and pε. Although H^+ does not exist in aqueous solution any more than free electrons (e^-) do, according to the Brønsted H^+ donor-acceptor concept of acids and bases, H^+ in water is always accepted by a single species, H_2O, to form H_3O^+. In contrast, electrons do not combine with a single species in water. Instead a wide variety of redox couples may be present in the system, and e^- may be present in a wide variety of reduced species. In addition, the kinetics of H^+ exchange across various acids and bases is very rapid, such that equilibrium conditions essentially always apply in systems containing a mixture of acids and bases. In contrast, many redox reactions are very slow. As a result, disequilibrium may occur across mixtures of redox couples in a complicated system. The net effect is that the activity ratios of the oxidized and reduced forms in one redox couple may predict a different pε (or E) than the activity ratios of the oxidized and reduced forms of another couple in the same system. Consequently, pε values should be considered

applicable only to a given redox couple in a natural system and not to the system as a whole.[3]

EXAMPLE 11.3: Write the balanced redox reaction for the net reaction $MnO_4^- + Mn^{2+} = MnO_2$, and determine $E°$, $p\varepsilon°$, and $\log K$ for the cell.

The following half-reactions are involved:

$$MnO_4^- + ne^- = Mn^{2+} \quad E° = 1.51V; \, p\varepsilon° = 25.59$$

$$MnO_2 + ne^- = Mn^{2+} \quad E° = 1.23V; \, p\varepsilon° = 20.85$$

Balanced half-reactions are

$$MnO_4^- + 8H^+ + 5e^- = Mn^{2+} + 4H_2O \quad E° = 1.51V; \, p\varepsilon° = 25.59$$

$$MnO_2 + 4H^+ + 2e^- = Mn^{2+} + 2H_2O \quad E° = 1.23V; \, p\varepsilon° = 20.85$$
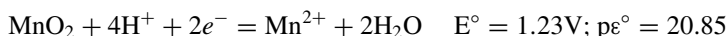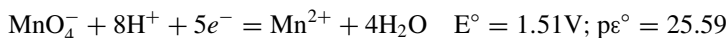
We see we need to multiply the top half-reaction by 2 and the bottom one by 5 to get the same number of electrons (10) in both reactions:

$$2MnO_4^- + 16H^+ + 10e^- = 2Mn^{2+} + 8H_2O \quad E° = 1.51V; \, p\varepsilon° = 25.59$$

$$- (5MnO_2 + 20H^+ + 10e^- = 5Mn^{2+} + 10H_2O) - E° = 1.23V; \, -p\varepsilon° = 20.85$$

Net:

$$2MnO_4^- + 16H^+ + 5Mn^{2+} + 10H_2O = 2Mn^{2+} + 8H_2O + 5MnO_2 + 20H^+$$

or

$$\mathbf{2MnO_4^- + 3Mn^{2+} + 2H_2O = 5MnO_2 + 4H^+} \quad \mathbf{E° = 1.51 - 1.23 = 0.28 \ V};$$

$$\mathbf{p\varepsilon° = 25.59 - 20.85 = 4.74}$$
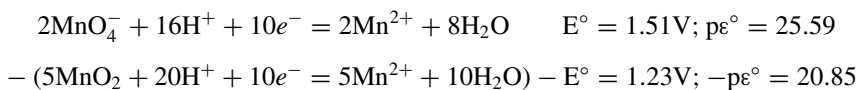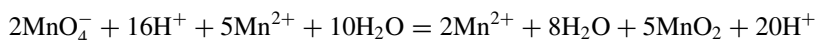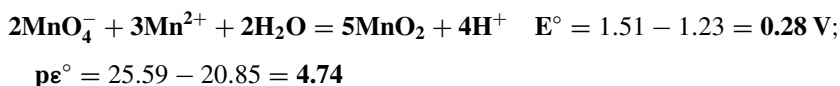
We can compute $\log K$ for the net reaction as follows:

$$\mathbf{\log K = nE°/0.059 = 10 \times 0.28/0.059 = 47.45}$$

11.2.9 $E_7°$ and $p\varepsilon_7°$

The standard conditions that apply to values of $E°$ and $p\varepsilon°$ include $\{H^+\} = 1$, i.e., $pH = 0$, for reactions that involve H^+ or OH^-. This is very unrepresentative of conditions in the natural environment, and values of $E°$ and $p\varepsilon°$ thus are not good predictors of the actual tendency for such redox reactions to proceed. Consequently, an alternative standard state closer to natural conditions is sometimes used to express redox potentials and $p\varepsilon$: $E_7°$ and $p\varepsilon_7°$, which represent conditions where all species are at unit activity (standard state) except pH, which is defined to be at an activity of 1×10^{-7}, i.e., pH 7.00.

The relationship between $p\varepsilon_7^\circ$ and $p\varepsilon^\circ$ can be derived as follows. Consider a general reduction half-reaction:

$$Ox + ne^- + mH^+ \rightarrow Red + \frac{m}{2}H_2O \qquad (11.20)$$
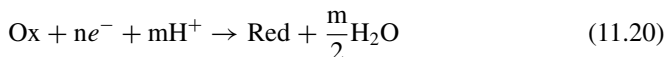
We can write the modified Nernst equation for this reaction as

$$p\varepsilon = p\varepsilon^\circ + \frac{1}{n}\log\frac{\{Ox\}\{H^+\}^m}{\{Red\}}. \qquad (11.21)$$

Taking the H^+ factor out of the log term and converting it to pH yields

$$p\varepsilon = p\varepsilon^\circ + \frac{1}{n}\log\frac{\{Ox\}}{\{Red\}} - \frac{m}{n}pH \qquad (11.22)$$

Because we have defined $p\varepsilon_7^\circ$ as the condition where all species are at unit activity except that pH = 7, we can write from Eq. 11.22

$$p\varepsilon_7^\circ = p\varepsilon^\circ - (7)\frac{m}{n}. \qquad (11.23a)$$

The analogous equation for E_7° is

$$E_7^\circ = E^\circ - 0.059(7)\frac{m}{n}, \qquad (11.23b)$$

where m is the number of protons (on the oxidized side) and n is the number of electrons in the half-reaction.

EXAMPLE 11.4: Convert $p\varepsilon^\circ$ and E° for the half-reactions and the net reaction in Example 11.3 to $p\varepsilon_7^\circ$ and E_7°.

We can apply Eq. 11.23a and b to the two half-reactions and net reaction:

$$MnO_4^- + 8H^+ + 5e^- = Mn^{2+} + 4H_2O \quad E^\circ = 1.51V \quad p\varepsilon^\circ = 25.59$$

$$\mathbf{p\varepsilon_7^\circ = 25.59 - 7 \times 8/5 = 14.39}$$

$$\mathbf{E_7^\circ = 1.51 - 0.059 \times 7 \times 8/5 = 0.85\ V}$$

$$MnO_2 + 4H^+ + 2e^- = Mn^{2+} + 2H_2O \quad E^\circ = 1.23\ V \quad p\varepsilon^\circ = 20.85$$

$$\mathbf{p\varepsilon_7^\circ = 20.85 - 7 \times 4/2 = 6.85}$$

$$\mathbf{E_7^\circ = 1.23 - 0.059 \times 7 \times 4/2 = 0.40\ V}$$

Net:

$$2MnO_4^- + 3Mn^{2+} + 2H_2O = 5MnO_2 + 4H^+ \quad E^\circ = 0.28V; \quad p\varepsilon^\circ = 4.74$$

$$\mathbf{p\varepsilon_7^\circ = 14.39 - 6.85 = 7.54}\ (or \quad p\varepsilon_7^\circ = 4.74 - 7 \times (-4)/10 = 7.54)$$

$$\mathbf{E_7^\circ = 0.85 - 0.40 = 0.45\ V}(or\ E_7^\circ = 0.28 - 0.059 \times 7 \times (-4)/10 = 0.45\ V)$$
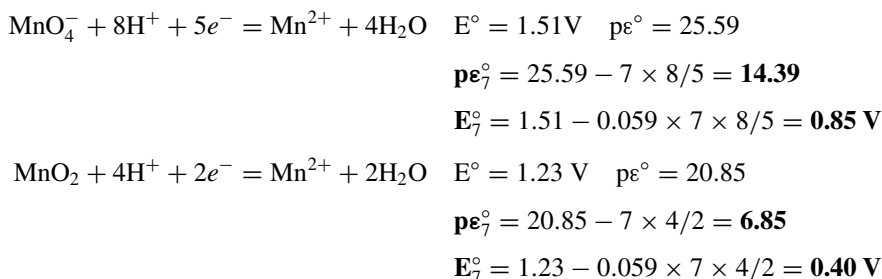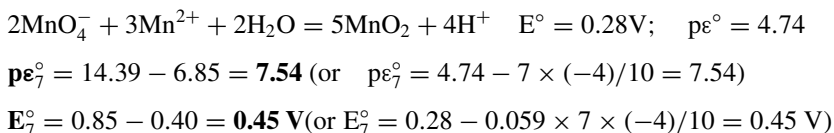
Note that in the net reaction, H^+ is produced rather than consumed, as it is in the two reduction half-reactions, and consequently m $= -4$. It is apparent from the above calculations that large differences can occur between $p\varepsilon°$ and $p\varepsilon_7°$ (and between E° and $E_7°$).

EXAMPLE 11.5 Combining redox half-reactions (by addition or subtraction) to get new half-reactions: We are interested in finding the reduction potential for the following half-reaction: $MnO_4^- + 3e^- = MnO_2$, given the half-reactions and corresponding E° and $p\varepsilon°$ values from Example 11.3:

$$MnO_4^- + 8H^+ + 5e^- = Mn^{2+} + 4H_2O \quad E° = 1.51V \quad p\varepsilon° = 25.59$$

$$MnO_2 + 4H^+ + 2e^- = Mn^{2+} + 2H_2O \quad E° = 1.29V \quad p\varepsilon° = 21.86$$
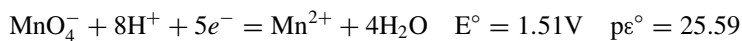
In this case, we see that if we do not balance the half-reactions for number of electrons but directly subtract the second half-reaction from the first, we will get the half-reaction we are looking for:

$$MnO_4^- + 8H^+ + 5e^- = Mn^{2+} + 4H_2O \quad (1)$$

$$- \quad (MnO_2 + 4H^+ + 2e^- = Mn^{2+} + 2H_2O) \quad (2)$$

Net:

$$\mathbf{MnO_4^- + 4H^+ + 3e^- = MnO_2 + 2H_2O} \quad (3)$$
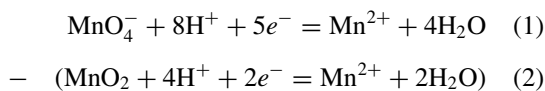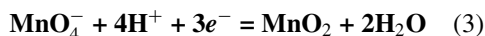
Recall that when we combine two half-reactions to get a whole reaction (i.e., where the number of electrons on the left and right side of the equation are the same, we just subtract the E° and $p\varepsilon°$ values to get the corresponding values for the net reaction. However, in situations like the above, when we are adding (or subtracting) half-reactions to derive an new half-reaction, ***we cannot just subtract the E° and $p\varepsilon°$ values*** to get the corresponding values for the new half-reaction. Instead, we must subtract log K values for the half-reactions, as follows:

(1) $\log K = nE°/0.059 = 5 \times 1.51/0.059 = 127.97$
(2) $\log K = nE°/0.059 = 2 \times (1.29)/0.059 = 43.72$
(3) $\mathbf{\log K_{net}} = 127.97 - 43.72 = \mathbf{84.25}$

Then

$$\mathbf{E°} = (0.059 \times \log K_{net})/n = 84.25 \times 0.059/3 = \mathbf{1.66\ V} \text{ (and } \mathbf{p\varepsilon° = 28.08})$$

11.3   Construction and uses of redox equilibrium diagrams

11.3.1 Introduction

Two types of diagrams are commonly used to display redox equilibria, and both are analogous to the diagrams described in Chapter 7: pC-pε diagrams are analogous to the pC-pH diagrams described in Sections 7.3.2–7.3.4, and pε-pH diagrams are analogous to the log P_{CO_2}-pH diagram described in Section 7.3.6. The following sections describe how to draw and interpret these diagrams.

11.3.2 pC-pε (pC-E_H) diagrams

In general, these are based on the modified Nernst equation (Eq. 11.19) for pC-pε diagrams or the Nernst equation (Eq. 11.9) for pC-E_H diagrams. However, they can be drawn without writing and solving any equations, as we showed for pC-pH diagrams in Table 7.2. We illustrate the basic approach to drawing pC-pε diagrams using the iron redox system, $Fe^0/Fe^{II}/Fe^{III}$ (Figure 11.2) at a total (analytical) concentration of iron of 10^{-2} M. As was the case for pC-pH diagrams, the distinction between concentration and activity generally is ignored in pC-pε diagrams, and we write the Nernst equation in terms of concentration (except for H^+, because pH is a measure of H^+ activity).

The only information we need to draw the diagram is Fe_T and pε° values (from Table 11.1) for the two redox couples: $p\varepsilon_{32}^\circ = 13.03$ for $Fe^{3+} + e^- = Fe^{2+}$, and $p\varepsilon_{20}^\circ = -7.45$ for $Fe^{2+} + 2e^- = Fe^0$. Here we use the convention that subscript numbers represent the oxidation states of the oxidized and reduced species, respectively, in a given redox half-reaction. The steps are as follows.

1. Draw and label the axes as a "fourth quadrant" graph with the x-axis at the top of graph labeled "pε" and the y-axis extended downward labeled "$-\log C$" or "pC."
2. Draw a light horizontal line at -log C_T (pFe_T) = 2.0.
3. Put in system points at pFe_T and pε = $p\varepsilon_{32}^\circ = 13.0$ and pε = $p\varepsilon_{20}^\circ = -7.45$, and mark small notches 0.3 log units below these points.
4. Draw sloping lines that go from the system points (pFe_T, $p\varepsilon_i^\circ$) with slopes equal to the number of electrons involved in change for the half-reaction associated with that pε°. Use positive slopes for oxidized forms (slope = +1 for Fe^{3+} below $p\varepsilon_{32}^\circ$ and slope = +2 for Fe^{2+} below $p\varepsilon_{20}^\circ$) and negative slopes for reduced forms (e.g., slope = −1 for Fe^{2+} above $p\varepsilon_{32}^\circ$). Draw smooth curves for the sloping lines to pass through the notches and meeting the horizontal lines slightly to the right (or left) of the system points.
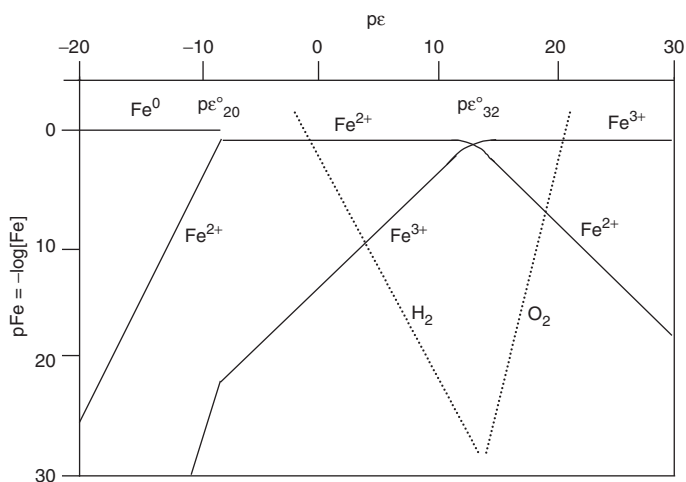
Figure 11.2 pε-pC diagram for $Fe^0/Fe^{II}/Fe^{III}$ at pH 1 and $Fe_T = 10^{-1}$ M showing lines for water reduction to H_2 and oxidation to O_2.

5. Draw horizontal lines for reduced forms that are a solid (elemental) phase (e.g., Fe^0) at log $C_T = 0$ to indicate that the solid has unit activity. In such cases, there is a discontinuity between the line for the solid phase and the next higher oxidation state (Fe^{2+}). In addition, there is no sloping line for solid phase Fe^0 at $p\varepsilon > p\varepsilon^\circ_{20}$ because Fe^0 either is present at unit activity or it is not present at all; the idea of the solid existing at activities < 1 is meaningless.

In some cases, pC-pε diagrams have lines to show the reduction and oxidation of water. These are drawn as follows. First, one must select a pH that the lines will represent. In Figure 11.2, we used pH = 1.0.

Water reduction line:

$$H^+ + e^- = \tfrac{1}{2}H_2; \quad p\varepsilon^\circ = 0; \log K = 0; n = 1 \tag{11.24}$$
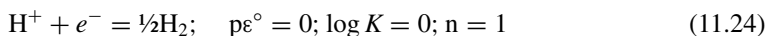
$$p\varepsilon = p\varepsilon^\circ + \log \frac{\{H^+\}}{[H_2]^{0.5}} \quad \text{or} \quad p\varepsilon = \log\{H^+\} - \tfrac{1}{2}\log[H_2] \tag{11.25}$$

Thus,

$$\tfrac{1}{2}\log[H_2] = \log\{H^+\} - p\varepsilon,$$

or

$$\log[H_2] = -2pH - 2p\varepsilon. \tag{11.26}$$

For pH = 1, we have $\underline{\underline{\log[H_2] = -2 - 2p\varepsilon}}$. The line has a slope $= -2$.

Water oxidation line:

$$O_{2(aq)} + 4e^- + 4H^+ = 2H_2O; \, p\varepsilon^\circ = 21.5 \tag{11.27}$$
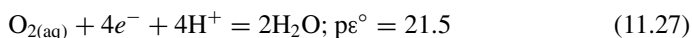
$$p\varepsilon = p\varepsilon^\circ + \tfrac{1}{4}\log \frac{[O_2]\{H^+\}^4}{[H_2O]^2} \tag{11.28}$$

or

$$p\varepsilon = 21.5 + \tfrac{1}{4}\log[O_2] + \log\{H^+\} = 21.5 - pH + \tfrac{1}{4}\log[O_2]$$

Thus,

$$\log[O_2] = 4p\varepsilon - 4(21.5) + 4pH. \tag{11.29}$$

For pH = 1, we have

$$\underline{\underline{\log[O_2] = -86 + 4 + 4p\varepsilon = -82 + 4p\varepsilon.}}$$

The line has a slope of +4, and it is evident that P_{O_2} is vanishingly small at low pε. Note that if we chose to define the water oxidation line in terms of $\{O_{2(g)}\} = 1$, we would use $p\varepsilon^\circ = 20.78$ (Table 11.1).

Whereas pC-pH diagrams often are used to solve acid-base problems, pC-pε diagrams rarely are used for such purposes. Instead, their primary use is illustrative; they show the range of pε over which the reduced and oxidized components of a redox system predominate (under equilibrium conditions) and how they change in activity once they no longer are the dominant redox component.

It is important to note that pC-pε diagrams are abstractions of reality and contain only the species specified by the person constructing the diagram. They do not necessarily reflect equilibrium situations when additional soluble species or solid phases (beyond those specified in constructing the diagram) are present over some range of pε in a natural system. For example, we could choose to ignore the existence of $Fe^0_{(s)}$ in an iron system, in which case the line for Fe^{2+} would extend indefinitely to the left of $p\varepsilon^\circ_{32}$ on the pε axis in Figure 11.2. Another example is shown in Figure 11.3, which compares redox conditions for nitrogen forms in a system where we include N_2 as a redox-active species and a similar system in which N_2 is excluded from consideration. An argument can be made for the latter case because the triple bond in N_2 is very difficult to break, which makes N_2 largely unreactive in natural environments.[*]

Note that in the system where N_2 is allowed to be redox active, NO_2^- is never the dominant species at any pε. Instead, it reaches a maximum value of $\sim 10^{-13.5}$ M at $p\varepsilon = p\varepsilon^\circ$ for the NO_3^-/N_2 couple. This is because $p\varepsilon^\circ$ for the NO_3^-/NO_2^- couple is lower than $p\varepsilon^\circ$ for the NO_3^-/N_2 couple (Table 11.3), and the net effect is that N_2 is dominant at a higher pε than that at which NO_2^- is stable with regard to NO_3^-.

EXAMPLE 11.6 Reduction potential for the NO_2^-/N_2 couple: Values for E°, $p\varepsilon^\circ$, and the corresponding E_7° and $p\varepsilon_7^\circ$ for the NO_2^-/N_2 couple are needed to draw the pε-pC diagram for the nitrogen system but were not given in the source for the other N cycle half-reactions. We can compute the desired values from the NO_3^-/NO_2^- and NO_3^-/N_2 couples as follows. From the half-reactions in Table 11.3, we write

	$p\varepsilon^\circ$	$\log K (= n \times p\varepsilon^\circ)$
$NO_3^- + 6H^+ + 5e^- = \frac{1}{2} N_2 + 3H_2O$	21.05	105.25
$-(NO_3^- + 2H^+ + 2e^- = NO_2^- + H_2O)$	14.15	28.30

Net:

$$NO_2^- + 4H^+ + 3e^- = \frac{1}{2}N_2 + 2H_2O \quad 76.95$$
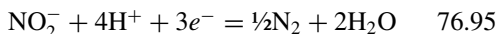
or

$$\tfrac{1}{3}NO_2^- + \tfrac{4}{3}H^+ + e^- = \tfrac{1}{6}N_2 + \tfrac{2}{3}H_2O; \; p\varepsilon^\circ = (\log K)/3 = \underline{\mathbf{25.65}}$$

From Eq. 11.23a, we can write

$$\underline{\mathbf{p\varepsilon_7^\circ}} = p\varepsilon^\circ - 7 \times m/n = 25.65 - 7 \times 4/3 = \underline{\mathbf{16.32}}.$$

---

[*]It is, of course, not completely unreactive; nitrogen-fixing bacteria reduce N_2 to NH_3 and organic N forms, and denitrifying bacteria reduce nitrate to N_2 under anoxic conditions. Nonetheless, N_2 is much less reactive both chemically and biologically than ammonium and nitrate are in aquatic systems. Hence, it is reasonable to consider a system of nitrogen forms excluding N_2 as a "pseudo-equilibrium" system.
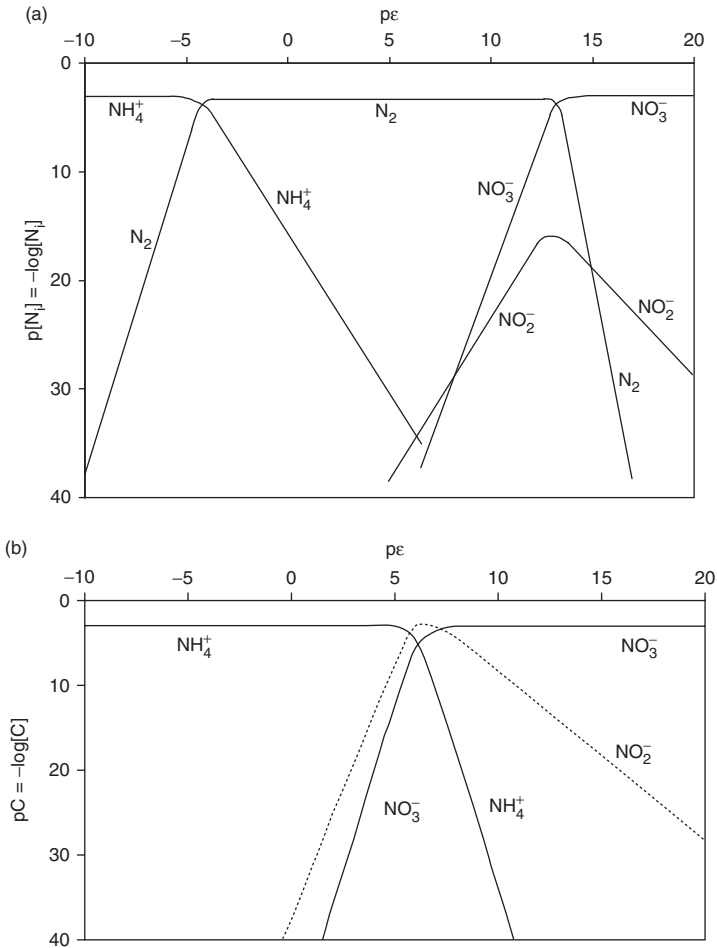
Figure 11.3 pC-pε diagrams for nitrogen at pH 7 and $N_T = 10^{-3}$ M: (a) N_2 included as a redox-active species, drawn in Excel based on based on $p\varepsilon_7^{\circ}$ values in Table 11.3 and slopes calculated from the modified Nernst equation; (b) N_2 excluded as a redox-active species, produced using the MultiRun feature of MINEQL+ (note that MINEQL+ does not have N_2 as a component).

11.3.3 pε-pH diagrams

These diagrams involve two "***master variables***" pH and pε (or pH and E). They are known by a various names: stability-field, predominance-area, pε-pH, E_H-pH, or Pourbaix diagrams,[4] the latter after the Belgian corrosion chemist who developed them and promoted their use. The ***areas*** within a set of lines on such a diagram define a region—a combination of pH and pε values—in which a given redox/acid-base species is the predominant form. Lines on the diagrams represent the combination of pH and pε values where either (a) two species have equal activity, or (b) one species is a soluble (aqueous)

Table 11.3 Reduction potentials for nitrogen processes

Half-reaction*	$p\varepsilon°$	$p\varepsilon_7°$
$NO_3^- + 6H^+ + 5e^- = \tfrac{1}{2}N_{2(g)} + 3H_2O$	+21.05	+13.75
$NO_3^- + 2H^+ + 2e^- = NO_2^- + H_2O$	+14.15	+7.15
$NO_3^- + 10H^+ + 8e^- = NH_4^+ + 3H_2O$	+14.90	+6.15
$NO_2^- + 4H^+ + 3e^- = \tfrac{1}{2}N_2 + 2H_2O$	+26.65	+17.31
$NO_2^- + 8H^+ + 6e^- = NH_4^+ + 2H_2O$	+15.14	+5.82
$N_2 + 8H^+ + 6e^- = 2NH_4^+$	+4.65	−4.68

* Values for half-reactions from Stumm and Morgan[1] except for NO_2^-/N_2 couple, which was computed from the NO_3^-/NO_2^- and NO_3^-/N_2 couples as shown in Example 11.6.

species with an arbitrarily defined activity (e.g., $a = 1$, $a = 10^{-6}$, or whatever one wishes), and the other species is either a solid phase ($a = 1$ by definition), or a gas, where $a_i = 1$ ($P_i = 1$ atm) or a_i is arbitrarily defined, e.g., $P_{O_2} = 0.21$ atm. Both types (a) and (b) have three kinds of lines:

 (i) *Vertical lines*: species are related by pure acid-base reactions; lines are pH dependent and $p\varepsilon$ independent
 (ii) *Horizontal lines*: species are related by pure redox reactions/couples; lines are pH independent and $p\varepsilon$ dependent
 (iii) *Sloping lines*: species are related by a combination of redox and acid-base reactions; lines are both pH and $p\varepsilon$ dependent.

All $p\varepsilon$-pH diagrams have lines for "water reduction" and "water oxidation" that together define the stability field for water itself. As was the case with pC-$p\varepsilon$ diagrams, we normally ignore distinctions between activity and concentration in drawing and interpreting $p\varepsilon$-pH diagrams.

Drawing $p\varepsilon$-pH diagrams requires (i) a compilation of all of the acid-base and redox species to be considered, and (ii) the equilibrium constants ($p\varepsilon°$ or log K) for the acid-base, redox, or combination reactions involving pairs of the compiled species of interest. In cases where one is unable to find a published $p\varepsilon°$ or log K value for a reaction of interest, the required value may be computed from published free energy of formation ($G_f°$) values for the reactants and products of the reaction or may be derived by appropriate combinations of reactions (by addition and/or subtraction), for which $p\varepsilon°$ or log K are known. We illustrate the construction of $p\varepsilon$-pH diagrams using one of the most common redox systems portrayed by these diagrams: the iron system, $Fe^0/Fe^{II}/Fe^{III}$ (Figure 11.4). In particular, we show how the lines for the reduction and oxidation of water (which are common to all $p\varepsilon$-pH diagrams) are constructed and give one example each for constructing vertical, horizontal, and sloping lines. Table 11.4 summarizes the relevant equilibrium constants and equations needed to define the lines on the diagram.

Water reduction line:

$$H^+ + e^- = \tfrac{1}{2}H_2;\ p\varepsilon° = 0;\ \log K = 0;\ n = 1 \qquad (11.24)$$
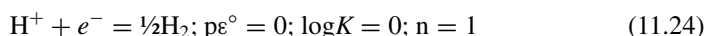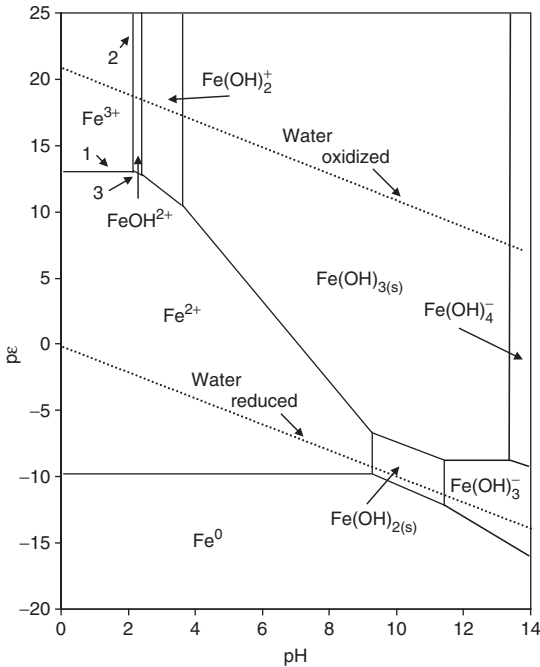
Figure 11.4 pε-pH diagram for the Fe-H_2O system. Lines for soluble Fe species in equilibrium with solid phases represent [Fe_i] $= 1 \times 10^{-5}$ M. Dotted lines are the water-oxidized/water-reduced lines. Equations for labeled lines 1–3 are derived in the text.

Table 11.4 Equilibrium relationships in Fe^0/Fe^{II}/Fe^{III}/H_2O system*

Reaction	Constant	Equation
$Fe^{3+} + e^- = Fe^{2+}$	$p\varepsilon^o = 13.03$	$p\varepsilon = 13.03 + \log\{Fe^{3+}\}/\{Fe^{2+}\}$
$Fe^{2+} + 2e^- = Fe^0$	$p\varepsilon^o = -7.45$	$p\varepsilon = -7.45 + \frac{1}{2}\log\{Fe^{2+}\}$
$Fe^{3+} + 3H_2O = Fe(OH)_{3(s)} + 3H^+$	$\log K = -3.191$	
$Fe(OH)_{3(s)} = Fe^{3+} + 3OH^-$	$\log K_{s0} = -38.80$	
$Fe^{3+} + H_2O = FeOH^{2+} + H^+$	$\log K_1 = -2.19$	$pH = 2.19 + \log\{FeOH^{2+}\}/\{Fe^{3+}\}$
$Fe^{3+} + 2H_2O = Fe(OH)_2^+ + 2H^+$	$\log K = -4.59$	
$FeOH^{2+} + H_2O = Fe(OH)_2^+ + H^+$	$\log K_2 = -2.40$	$pH = 2.40 + \log\{Fe(OH)_2^+\}/\{FeOH^{2+}\}$
$Fe(OH)_{3(s)} + H^+ = Fe(OH)_2^+ + H_2O$	$\log K = -1.39$	$pH = -1.39 - \log\{Fe(OH)_2^+\}$
$Fe(OH)_{3(s)} + H_2O = Fe(OH)_4^- + H^+$	$\log K = -18.40$	$pH = 18.4 + \log\{Fe(OH)_4^-\}$
$Fe(OH)_{3(s)} + 3H^+ + e^- = Fe^{2+} + 3H_2O$	$p\varepsilon^o = 16.22$	$p\varepsilon = 16.22 - \log\{Fe^{2+}\} - 3pH$
$FeOH^{2+} + H^+ + e^- = Fe^{2+} + H_2O$		$p\varepsilon = 15.22 - pH - \log\{Fe^{2+}\}/\{FeOH^{2+}\}$
$Fe(OH)_{3(s)} + H^+ + e^- =$ $\quad Fe(OH)_{2(s)} + H_2O$	$p\varepsilon^o = 2.66$	$p\varepsilon = 2.66 - pH$
$Fe^{2+} + H_2O = FeOH^+ + H^+$	$\log K = -9.40$	$pH = 9.40 + \log\{FeOH^+\}/\{Fe^{2+}\}$
$FeOH^+ + H_2O = Fe(OH)_{2(s)} + H^+$	$\log K = -4.16$	$pH = 4.16 - \log\{FeOH^+\}$
$Fe(OH)_{2(s)} + H_2O = Fe(OH)_3^- + H^+$	$\log K = -15.43$	$pH = 15.43 + \log\{Fe(OH)_3^-\}$
$Fe(OH)_{2(s)} + 2H^+ + 2e^- = Fe^0_{(s)} + 2H_2O$	$p\varepsilon^o = -1.34$	$p\varepsilon = -1.34 - pH$

* Values calculated to be consistent with MINEQL+ ver. 4.6 and Table 11.1; solid phase for Fe^{III} is assumed to be ferrihydrite; that for Fe^{II} is assumed to be amorphous $Fe(OH)_{2(s)}$.

We can rewrite Eq. 11.24 in more explicit terms of water by adding the dissociation of water to it:

$$H^+ + e^- = \tfrac{1}{2}H_2 \qquad \log K = 0$$

$$+[H_2O = H^+ + OH^-] \quad \underline{\log K_w = -14}$$

Net:

$$H_2O + e^- = \tfrac{1}{2}H_2 + OH^- \quad \log K = -14; \; p\varepsilon^\circ = -14$$

$$(\text{Also, } E^\circ = 0.059(-14) = -0.826 \text{ V}) \tag{11.30}$$
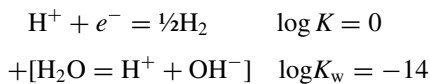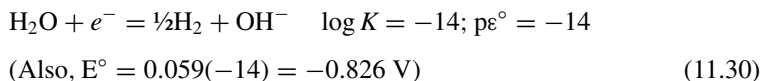
Note: Eqs. 11.24 and 11.30 are equivalent ways of writing the water reduction equilibrium.

From Eq. 11.30:

$$p\varepsilon = p\varepsilon^\circ + \log \frac{\{H_2O\}}{\{H_2\}^{0.5}\{OH^-\}} \qquad \left(\text{Also, } E = E^\circ + 0.059 \; \log \frac{\{H_2O\}}{\{H_2\}^{0.5}\{OH^-\}}\right)$$

Because $a_{H_2O} = 1$, and the water reduction line is defined as the condition where $P_{H_2} = 1$ atm,

$$p\varepsilon = -14 - \log\{OH^-\}, \tag{11.31a}$$

or

$$p\varepsilon = -14 + pOH = -14 + (14 - pH); \tag{11.31b}$$

that is,

$$\underline{p\varepsilon = -pH} \quad (\text{alternatively, } \underline{\underline{E = -0.059pH}}). \tag{11.31c}$$

Water oxidation line:

$$O_{2(g)} + 4e^- + 4H^+ = 2H_2O; \; p\varepsilon^\circ = 20.78 \tag{11.27}$$
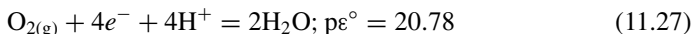
$$p\varepsilon = p\varepsilon^\circ + \tfrac{1}{4}\log \frac{\{O_2\}_{(g)}\{H^+\}^4}{\{H_2O\}} \tag{11.28}$$

If the water oxidation line is defined for $a_{H_2O} = 1$ and $P_{O_2} = 1$ atm, then

$$\underline{\underline{p\varepsilon}} = 20.78 + \tfrac{1}{4}\log\{H^+\}^4 = \underline{\underline{20.78 - pH}}. \tag{11.32a}$$

If we chose to define the line as $\{O_{2(aq)}\} = 1$, then we would use $p\varepsilon^\circ = 21.5$ in Eq. 11.32a, and if the line is for $a_{H_2O} = 1$ and $P_{O_{2(g)}} = 0.21$ atm, the equation becomes

$$\underline{\underline{p\varepsilon}} = 20.78 + \tfrac{1}{4}(\log\{H^+\}^4 + \log 0.21)$$

$$= 20.78 - pH + \tfrac{1}{4}(-0.68) = \underline{\underline{20.61 - pH}}. \tag{11.33b}$$

Horizontal line in the Fe pε-pH diagram:
Line 1

$$Fe^{3+} + e^- = Fe^{2+} \quad p\varepsilon° = 13.03; n = 1$$

$$p\varepsilon = p\varepsilon° + \log \frac{\{Fe^{3+}\}}{\{Fe^{2+}\}} \tag{11.34}$$

Line 1 is where $\{Fe^{3+}\} = \{Fe^{2+}\} = 10^{-5}$. Therefore,

$$\underline{\underline{p\varepsilon = p\varepsilon° = \mathbf{13.03.}}} \tag{11.35}$$

Vertical line in the Fe pε-pH diagram:
Line 2

$$Fe^{3+} + H_2O = FeOH^{2+} \tag{11.36a}$$

$$K_1 = \frac{\{H^+\}\{FeOH^{2+}\}}{\{Fe^{3+}\}\{H_2O\}} = 10^{-2.19} \tag{11.36b}$$

The line is represents the condition

$$\{Fe^{3+}\} = \{FeOH^{2+}\} = 10^{-5}. \tag{11.36c}$$

Therefore,

$$K_1 = \{H^+\} = 10^{-2.19}, \text{ or } \underline{\underline{\mathbf{pH = 2.19}}}. \tag{11.36d}$$

Sloping line in the Fe pε-pH diagram:
Line 3

$$FeOH^{2+} + e^- + H^+ = Fe^{2+} + H_2O; p\varepsilon° = 15.22; n = 1 \tag{11.37a}$$
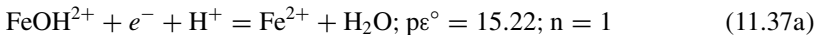
$$p\varepsilon = p\varepsilon° + \log \frac{\{FeOH^{2+}\}\{H^+\}}{\{Fe^{2+}\}\{H_2O\}} \tag{11.37b}$$

This very short line (Figure 11.4) represents the condition $\{FeOH^{2+}\} = \{Fe^{2+}\} = 10^{-5}$. Therefore,

$$p\varepsilon = 15.22 + \log\{H^+\} \text{ or } \underline{\underline{p\varepsilon = 15.22 - pH}} \tag{11.37c}$$

The line has slope of -1. At pH $= 2.19$, $p\varepsilon = 13.03$, which is the intersection of lines 1, 2, and 3. This serves as a check on the accuracy of the calculations for the three lines.

Construction of the rest of the lines in the Fe pε-pH diagram is straightforward using the information in Table 11.4. It should be noted that the assumed activities (or ratios of activities) of the soluble species in pε-pH diagrams affects not only the positions of the lines representing these species, but the even existence of stability fields for

some species. For example, the stability field for $Fe(OH)_{2(s)}$ in Figure 11.4 disappears when the lines delimiting this field are redefined to represent $\{Fe_i\} = 10^{-6}$ instead of 10^{-5} (because the solubility of Fe^{II} exceeds 10^{-6} M at all pH values).

EXAMPLE 11.7: Given the following equations, construct a pε-pH diagram for the sulfur system. Consider only those species listed, and assume $S_T = 10^{-2}$ M. Plot over the pH range 3–12 and pε as appropriate, ignoring ionic strength corrections (i.e., assuming $a_i = c_i$.).

(1) $H_2S = HS^- + H^+$ $pK_a = 7.24$
(2) $SO_4^{2-} + 8H^+ + 6e^- = S_{(s)} + 4H_2O$; $K = 10^{36.2}$
(3) $S_{(s)} + 2H^+ + 2e^- = H_2S$; $K = 10^{4.8}$
(4) $SO_4^{2-} + 8e^- + 9H^+ = HS^- + 4H_2O$; $K = 10^{33.68}$
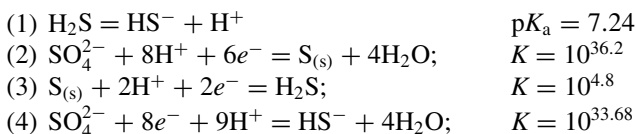
Answer: The line for reaction (1) (see Figure 11.5) is vertical at pH 7.24 and divides H_2S and HS^-. Lines (2)–(4) will be sloping as they contain both electrons and protons. For line (2),

$$10^{36.2} = \frac{1}{[SO_4^{2-}][H^+]^8[e^-]^6}.$$

Taking the logarithm of both sides gives

$$36.2 = -\log[SO_4^{2-}] - 8\log[H^+] - 6\log[e^-].$$

There is only one dissolved species in the equation, and so we take its concentration to be 10^{-2} M.

$$36.2 = -\log(10^{-2}) + 8pH + 6p\varepsilon = 2 + 8pH + 6p\varepsilon$$
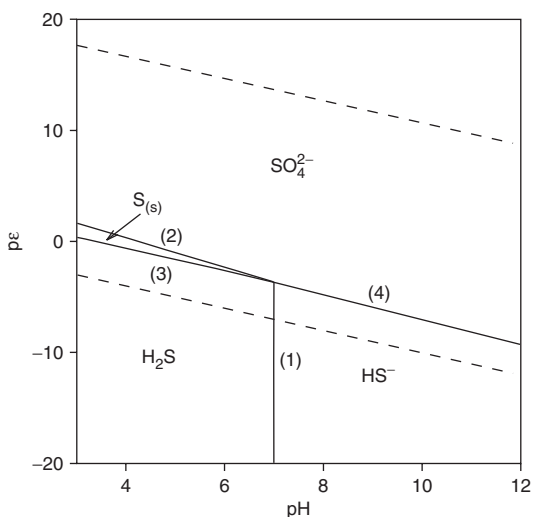
Figure 11.5 pε-pH diagram for the sulfur system with $S_T = 10^{-2}$ M. Lines are labeled as noted in Example 11.7. Dashed lines are the water-oxidized/water-reduced lines, and solid lines define predominance areas of the species displayed.

Rearranging gives

$$p\varepsilon = (34.2/6) - (4/3)pH$$

For line (3), the equilibrium expression is

$$10^{4.8} = \frac{[H_2S]}{[H^+]^2[e^-]^2}.$$

A similar manipulation to the one above gives

$$p\varepsilon = (6.8/2) - pH.$$

For line (4), we have

$$10^{33.68} = \frac{[HS^-]}{[SO_4^{2-}][H^+]^9[e^-]^8}.$$

Here taking the log gives

$$33.68 = \log\frac{[HS^-]}{[SO_4^{2-}]} - 9\log[H^+] - 8\log[e^-].$$

For the case with two aqueous species, we assume that their activities are equal, and so the first term has a value of zero ($\log 1 = 0$). The relevant expression thus is

$$p\varepsilon = (33.68/8) - (9/8)pH.$$

These four lines (along with the water oxidized and water reduced lines) are plotted in Figure 11.5. Note that all four lines should have the same value at pH 7. When substituting into the above equations, you will find that the values vary by up to ~0.1 due to rounding errors. It is left to the reader to figure out why the following equations are not used:

$$S_{(s)} + H^+ + 2e^- = HS^-; \quad \Delta G^0 = 12.05 \text{ kJ/mol}$$
$$SO_4^{2-} + 8e^- + 10H^+ = H_2S + 4H_2O; \quad K = 10^{40.67}$$
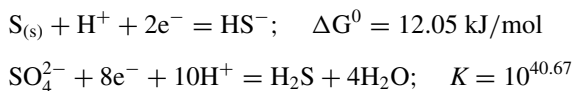
11.3.4 Applications of redox diagrams

It is important to note that pε-pH diagrams also are abstractions of reality and contain only species that result from the input conditions specified by the person who constructed the diagram. They do not necessarily reflect equilibrium situations when additional solid phases and soluble species (beyond those specified in constructing the diagram) might be dominant over some range of pH and pε. For example, Figure 11.4 describes the system $Fe^0/Fe^{II}/Fe^{III}/H_2/H_2O/O_2$, which allows formation of hydroxide and oxide solids of Fe only. The possibility of Fe solid phases with carbonate or sulfide does not exist in the

abstract world represented by the diagram because those components were not included in defining the system on which the diagram is based.

We are at liberty, however, to include a wider variety of components and species in pε-pH diagrams. To do this, we need to specify a total concentration for each additional component, determine the additional species that our principal redox component may form with the component, and assemble the equilibrium constants relating those species to the forms already defined. In the context of the pε-pH diagram for Fe (Figure 11.4), if we add carbonate, we need to specify C_T and find equilibrium constants for solid Fe carbonate phases and soluble complexes (e.g., $FeHCO_3^+$). Only Fe^{II} forms a stable solid phase with carbonate—siderite, $FeCO_{3(s)}$; ferric carbonate is unstable and reacts with water to release CO_2 and form ferric hydroxide. For simplicity, we may choose to ignore soluble complexes; given their small formation constants, they do not become dominant Fe species at any pH. Figure 11.6 illustrates how the pε-pH diagram for the iron system changes when we add carbonate at $C_T = 10^{-3}$ M to the system. The size of the predominance area for $FeCO_{3(s)}$ depends on both the value of C_T and the values of $\{Fe^{2+}\}$ and $\{Fe(OH)_3^-\}$ selected to represent the equilibrium lines.

Although pC-pε and pε-pH diagrams are rarely used to solve numerical problems involving redox equilibria, they are useful to evaluate trends in the speciation of elements across the range of pH and pε in aquatic systems. For example, Figure 11.7 shows pε-pH diagrams for the major elements of interest in biogeochemistry: H, O, C, N, and S. Figure 11.7a illustrates the stability region for water itself and establishes the limits of the stable pε-pH domain for aquatic reactions involving the other elements. The two diagrams for N contrast situations where N_2 is included (Figure 11.7b) and where
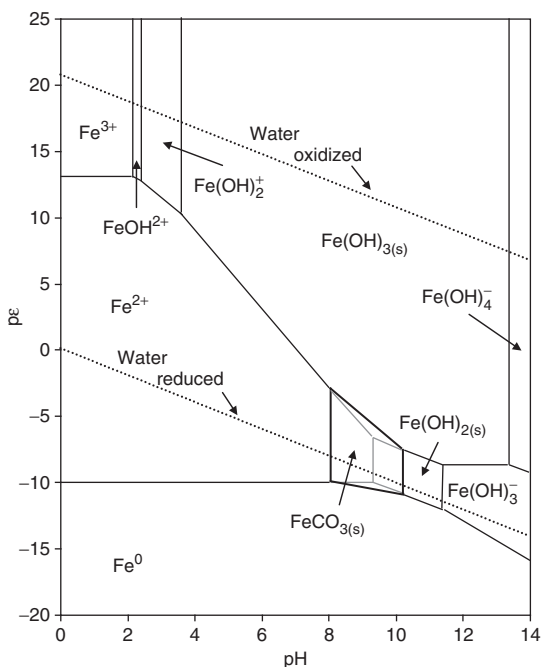
Figure 11.6 pε-pH diagram for Fe system from Figure 11.4 modified to include dissolved carbonate at $C_T = 10^{-3}$ M. Lines for soluble Fe species in equilibrium with solid phases represent $[Fe_i] = 1 \times 10^{-5}$ M. Black lines for $FeCO_{3(s)}$ field show stability region for siderite; gray lines represent portions of diagram for Fe/H_2O system that are no longer dominant.
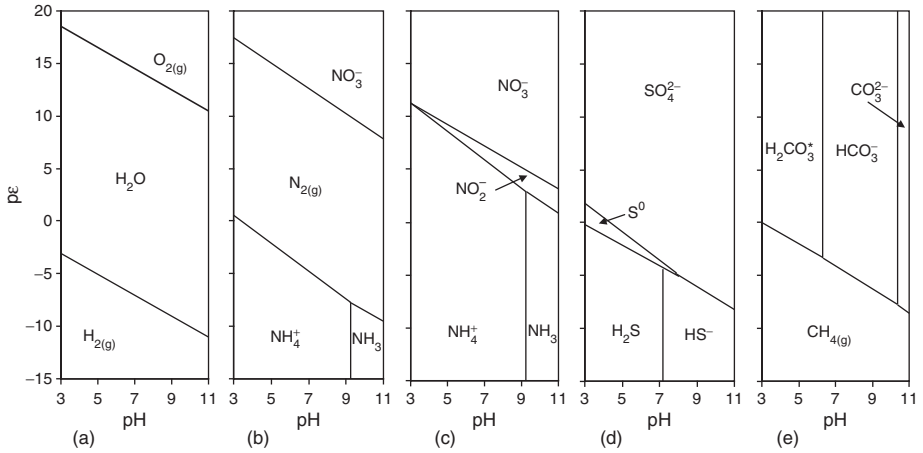
Figure 11.7 pε-pH diagrams for the major biogenic elements: (a) $O_2/H_2O/H_2$; (b) nitrogen including N_2; (c) nitrogen excluding N_2 (assuming it is redox inert); (d) sulfur; (e) carbon. Lines calculated based on pε° values in Tables 11.1 and 11.3. Based on a similar figure in Stumm and Morgan.[1]

it is excluded, i.e., treated as a redox-inert species—or a species very slow to react compared with the other N forms (Figure 11.7c). In the former case, only three redox states form dominant N species over the range of pε and pH, N^V (NO_3^-), N^0 (N_2), and N^{-III}, (NH_4^+/NH_3), and the stability regions for H_2O and NO_3^- hardly overlap. In contrast, when N_2 is excluded from consideration, the stability fields change dramatically, and the domain for NO_3^- extends to lower pε values than before, now including more of the region in which H_2O is stable. In addition, N^{-III} (NH_4^+/NH_3) now is stable at much higher pε values than before, and N^{+III} (NO_2^-, nitrite ion) has a small region of dominance at intermediate pε. Figure 11.7c is more illustrative of the conditions that occur in actual natural waters. Comparison of Figures 11.7c and 11.7d shows that sulfate, the oxidized form of S, is stable to much lower pε values than is the oxidized form of N, NO_3^-. This agrees with what we know about the environmental behavior of these ions: nitrate is reduced to N_2 by microbial denitrification at moderate pε values—as soon as O_2 disappears from the system, but reduction of sulfate to sulfide (also by microbial mediation) occurs only under strongly reducing conditions.

11.4 Measuring redox potentials

As noted in the introduction to this chapter and illustrated in the previous section, the chemical composition of aquatic systems can change dramatically as a function of redox conditions. Moreover, we have seen that equilibrium conditions for all redox couples are defined by a common metric—redox potential, E (or the related variable pε). Because the measurement of redox potential is seemingly straightforward and also fast and inexpensive, environmental scientists and engineers have measured it (often referred to

as E_H rather than E) on numerous water bodies, soils, and sediments for decades.* Many attempts have been reported to interpret the values in terms of the chemical composition of the sample. According to the Nernst equation (Eq. 11.9), if we can measure an equilibrium potential, E, and know E° for the redox couple involved, we can compute the ratio of the oxidized and reduced forms of the couple. Unfortunately, as Morris and Stumm[5] explained many years ago, this cannot be done in natural systems. The reasons transcend technological limitations and instead reflect fundamental scientific limitations. In this section we explain the theoretical basis for measuring redox potentials and the primary reasons why such measurements in natural systems cannot be interpreted quantitatively using the Nernst equation.

For stable readings, a redox reaction must be reversible—which means rapid—at the electrode surface. Noble metals, commonly platinum, are used as redox sensing electrodes to avoid reactions and potentials caused by the electrode itself. The "equilibrium" potential is measured at zero *applied* potential, where the rate of cathodic reduction is equal to the rate of the anodic oxidation, e.g., for Fe^{III}/Fe^{II},

$$\text{Rate of } Fe^{2+} \rightarrow Fe^{3+} + e^- = \text{Rate of } Fe^{3+} + e^- \rightarrow Fe^{2+}. \tag{11.38}$$

If we apply a potential to an electrode higher than the equilibrium potential, which is defined by the ratio of oxidized to reduced species for a redox couple in solution, we can readily understand that the anodic (oxidation) reaction will be promoted, and a net positive current will flow. Conversely, if we apply a potential lower than the equilibrium potential of the couple in solution, cathodic reduction will be promoted, and a net negative current will flow. When no potential is applied and the electrode is allowed to "respond" to the potential defined by the activities of the oxidized and reduced forms in the solution, the electrode "senses" the potential of the redox couple in solution, and no net current flows. These concepts are illustrated by the electrode polarization curves in Figure 11.8a and b. The figure also shows that although there is no *net* current at the equilibrium potential, this does not mean that nothing is happening at the electrode surface. The net zero current is the result of cathodic and anodic currents that are precisely equal in magnitude but opposite in sign. The absolute magnitude of the cathodic or anodic current at the equilibrium potential is called the ***exchange current***, i_0. In general, i_0 depends on the kinetics of half-reactions—i.e., on an intrinsic rate constant, k_0 for the specific redox couple, the concentrations of the oxidized and reduced forms of the couple, Faraday's constant, and the area of the electrode surface (in cm^2):[1,5,6]

$$i_0 = \mathcal{F} A k_0 [Ox]^{1-\alpha} [Red]^\alpha \tag{11.39}$$

The term α in Eq. 11.39, called the *transfer coefficient*, is a measure of the symmetry of the energy barriers for oxidation and reduction; generally, α is thought to be ≈ 0.5. To obtain reproducible potential measurements, the specific exchange current, i_0/A, must be sufficiently large; i.e., greater than $\sim 10^{-7}$ amp/cm^2 for modern potentiometers.[5,6]

---

*E_H is measured in water, soil, and sediment slurries with a pH meter (which is just a potentiometer) and an inert electrode (usually Pt) that reflects the potential of electroactive couple(s) in solution.
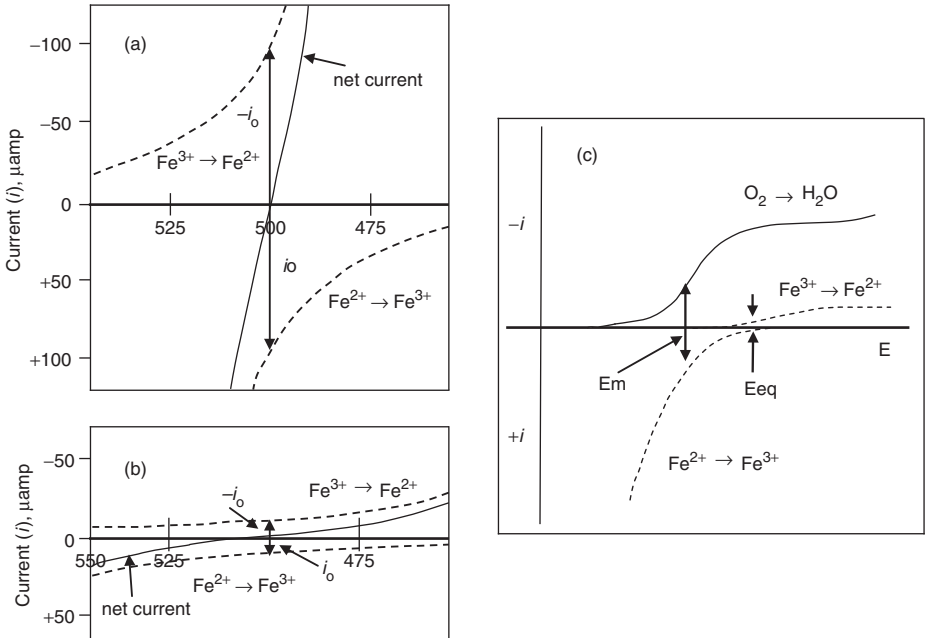
Figure 11.8 (a and b) Electrode polarization curves for $[Fe^{3+}] = [Fe^{2+}]$ at 10^{-3} M (a) and 10^{-4} M (b) showing effect on exchange current, i_0. (c) Electrode polarization curve for Fe^{3+}-Fe^{2+} in the presence of O_2 yields a mixed potential with net O_2 reduction and Fe^{2+} oxidation. Redrawn from Stumm and Morgan,[1] copyright John Wiley & Sons, and used with permission.

The basis for this statement is that the slope of the polarization curve, i.e., $(\Delta i/\Delta E)_{i=0}$ near the equilibrium potential is proportional to i_0:

$$(\Delta i/\Delta E)_{i=0} = -(n\mathcal{F}/RT)i_0 \tag{11.40a}$$

or

$$(\Delta i/\Delta p\varepsilon)_{i=0} = -2.3 n i_0 \tag{11.40b}$$

The slope is important because it indicates the amount by which the potential must shift to get a measurable current—hence, it is related to the sharpness and reproducibility with which one can measure potentials. i_0 exceeds the criterion value for the iron system when $[Fe^{2+}] = [Fe^{3+}] > {\sim}1 \times 10^{-5}$ M (${\sim}0.55$ mg/L),[1,5] but when either ion is below this concentration, i_0/A is $< 10^{-7}$ amp/cm^2, and the measurements are imprecise. Typical values for Fe_T in most waters are much lower than this, and thus it is unlikely that the iron couple could provide reproducible measurements of E_H in most natural waters.

Another issue of concern in natural systems is that the half-reactions giving rise to the cathodic and anodic currents in the electrode polarization curve may not correspond to the same species (e.g., Figure 11.8c). For example, the anodic step might involve

oxidation of Fe^{2+} to Fe^{3+}, but the cathodic step might involve the reduction of O_2 to H_2O, which occurs at equilibrium redox potentials for Fe^{2+}/Fe^{3+} systems. This phenomenon gives rise to *mixed potentials*,[1,5] in which rates of the cathodic and anodic processes are balanced at a potential where the anodic current is from Fe^{2+} oxidation but the cathodic current is from O_2 reduction. Because the anodic and cathodic processes are not simply the reverse of each other, a net redox reaction occurs that causes "drift" in the measured potential.

The above discussion leads to the question: what other electroactive couples are there in aquatic systems? Aside from Fe^{III}/Fe^{II}, there are many possibilities: O_2/H_2O, Mn^{IV}/Mn^{II}, SO_4^{2-}/HS^-, NO_3^-/NH_4^+, but all have slow or negligible kinetics at Pt electrodes—far too slow to yield exchange currents sufficient to give stable readings. Even today, after many years of study, we still do not know what precisely is measured at Pt electrodes when one measures the redox potential of water or sediment samples.[1] Nonetheless, a technical basis for the reasonably stable readings analysts usually obtain has been described,[7] and there often is a semiquantitative agreement between measured E_H and major biogeochemical redox processes.[8] Specifically, in oxygenated systems the measured E_H is high, and in strongly anoxic and reducing conditions (e.g., where sulfide is notably present or where methane is being formed), E_H is low (negative values). Under conditions where oxygen is just absent but nitrate is present, E_H is lower than that in oxygenated systems but higher than that found in strongly anoxic environments. In fact, E_H values have been used as a rough estimate of the nature of the primary electron acceptor in use for microbial metabolism in water/sediment systems.[8] The order of electron acceptor use generally follows the amount of energy (based on thermodynamics, hence redox potentials of the electron acceptor couples) that microbes can obtain in oxidizing organic matter:

Order of use of electron acceptors	Approximate E_H range (mV)
O_2/H_2O	$> +350$
NO_3^-/N_2	$+100$ to $+300$
Mn^{IV}/Mn^{II}	$+50$ to $+250$
Fe^{III}/Fe^{II}	$+100$ to -100
SO_4^{2-}/HS^-	-100 to -200
CO_2/CH_4	< -200

These are only rough estimates, however, and it often is found that a measured potential predicts one set of conditions and measurements reveal another. Lovely and Goodwin[9] noted that microorganisms couple hydrogen oxidation to the reduction of several terminal electron acceptors, and the more electropositive the electron acceptor, the lower the steady state hydrogen concentration (CO_2/CH_4, 7–10 nM; SO_4^{2-}/HS^-, 1–1.5 nM; Fe^{III}/Fe^{II}, 0.2 nM; Mn^{IV}/Mn^{II} or NO_3^-/N_2, <0.05 nM). It has been shown that such measurements often give a different (and more correct) picture of the conditions present than one might infer from simple E_H measurements. For example, according to Chapelle et al.,[10] the combination of E_H and pH measurements in a contaminated aquifer predicted iron-reducing conditions. Measured H_2 concentrations, however, predicted methanogenic and sulfate reducing zones, and these were confirmed by measurement of methane and hydrogen sulfide. Of course, the disadvantage of this method is that measuring H_2 concentrations in groundwater is more labor and

instrument intensive[11] than simply inserting a platinum electrode into a collected sample.[12]

11.5 Redox kinetics

11.5.1 Mechanisms of redox reactions

Many redox reactions occur by bond breaking and making and can be described by conventional kinetic theories, e.g., activated complex or transition state theory (see Section 5.5.3). Most redox reactions involving metal ions in natural waters occur by inner sphere (*is*) electron transfer, in which the two reactants share a common hydration sphere, and the activated complex involves a bridging ligand between the two ions (M-L-M′). Electron transfer in such cases may be achieved by ligand transfer, and these reactions involve bond formation and breaking processes similar to other group transfer and substitution reactions. Acid-base catalysis and complicated mechanisms are common in many of these reactions, many of which are of profound importance in water chemistry. The kinetics of such reactions is described in subsequent chapters.

In contrast, some redox reactions of metal ions occur by outer sphere (*os*) electron transfer, in which the primary hydration spheres remain intact, the ions are separated by at least two water molecules (or other ligands), and only the electron moves between the ions. An *os* mechanism can be inferred if the reaction is much faster than the rates of ligand exchange of the metal ions (see Section 9.7). Because bonds are not made or broken in *os* transfers, conventional theory requires modification, as summarized below.

Electrons move much more rapidly than atoms or nuclei; vibrational periods of atoms are on the order of 10^{-13} s, but electron transitions occur on a timescale of 10^{-15} s. Atoms thus can be regarded as having fixed internuclear distances on the timescale of electron transitions. This raises the question: if electron transitions are so rapid, why are many redox reactions so slow? For aqueous metal ions the answer lies in the fact that the distribution of charge in ions induces structural configurations in the surrounding ligands and solvent.[13] The reactants and products in an electron exchange reaction have different charge distributions and structural configurations, and energy is required to distort the ions to a shape (the transition state) from which they can form product ions spontaneously. The time required to rearrange the solvent/ligands to an equilibrium configuration is long compared with the time of electronic transitions. Water molecules get properly oriented in about 10^{-11} s, about the same as the lifetime of a solvent-reactant cage and $\sim 10^4$ times longer than an electronic transition. Reordering metal-ligand bond lengths requires the time associated with bond vibration ($\sim 10^{-13}$ s). Because transferred electrons are in unfavorable energy states as long as ligands and solvent have the reactant configuration, they return to the donor, and no reaction occurs. For net electron transfer, the ligands and solvent must rearrange to a nonequilibrium configuration intermediate between the reactants and products. This requires energy and is responsible for the slowness of redox processes.

The importance of the above processes is illustrated in the electron exchange reactions of Fe^{II}-Fe^{III} complexes.[14] Metal-water bond lengths in hydrated Fe^{II} are longer

than those in Fe^{III} (an example of electrostriction), leading to a low rate constant for electron exchange (4 M^{-1} s^{-1}). In contrast, metal-ligand bond lengths and molecular orbitals are similar in both ferricyanide and ferrocyanide complexes, and these complex ions have lower hydration energies. Together, these factors lead to a reduced energy barrier and faster rate of electron exchange (3×10^2 M^{-1} s^{-1}).[15]

11.5.2 Advanced topic: the Marcus model for *os* redox reactions

The most widely used model to explain rates of *os* electron transfer was derived by Marcus (e.g., Marcus[16,17]). The model is based on the assumption that E_{act} for electron transfer reactions is the sum of three terms: (1) electrostatic work ω to bring two ions together, (2) energy needed to modify the solvent structure, $\Delta G_{solv}^{\neq}$, and (3) energy needed to change the metal-ligand bond lengths, $\Delta G_{lig}^{\neq}$. Rate constants are formulated in terms of the free energy required for these tasks:

$$k_{AB} = Z_{AB}\exp(-\Delta G_{AB}^{\neq}/RT), \tag{11.41a}$$

where Z_{AB} is the collision frequency of A and B in solution and

$$\Delta G_{AB}^{\neq} = \omega_{elec} + \Delta G_{solv}^{\neq} + \Delta G_{lig}^{\neq}. \tag{11.41b}$$

Electrostatic work is given by Coulomb's law: $\omega_{elec} = z_A z_B e^2 / D_{H_2O} r_{AB}$. For reaction of an ion and neutral molecule, such as O_2, ω_{elec} is zero. Marcus[16] quantified the solvent and ligand energy terms, which led to his "cross-correlation":

$$k_{AB} = (k_{AA}k_{BB}k_{AB}f)^{0.5} \tag{11.42a}$$

or

$$\ln k_{AB} \propto \Delta G_{AB}^{\neq} = 0.5\Delta G_{AA}^{\neq} + 0.5\Delta G_{BB}^{\neq} + 0.5\Delta G_{AB}^{\circ} - 0.5RT \ln f \tag{11.42b}$$

where

$$\ln f = 0.25(\ln K_{AB})^2 / \ln(k_{AA}k_{BB}/Z^2) \tag{11.42c}$$

The factor 0.25 in Eq. 11.42c results from a geometric analysis of the activation barrier for *os* reactions and assumes that potential energy profiles along the reaction coordinate are described by parabolas.[18] Z is the collision frequency factor for uncharged molecules, which Marcus[17] estimated as $10^{12} M^{-1}$ s^{-1}. If $\Delta G_{AB}^{\circ} \approx 0$, the last term in Eq. 11.42b can be ignored. k_{AA} and k_{BB} are rate constants for electron "self-exchange" between the oxidized and reduced states of an element:

$$ox_A + red_A^* \overset{k_{AA}}{=} red_A + ox_A^*; \ ox_B + red_B^* \overset{k_{BB}}{=} red_B + ox_B^* \tag{11.43}$$
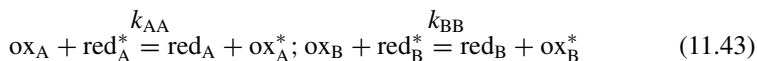
Rate constants for electron self-exchange reactions are determined by isotopic exchange methods and are available for many metal ions[15,19] (Table 11.5). Finally,

Table 11.5 Rate and equilibrium constants for some outer sphere electron transfers,
$A_{ox} + B_{red} \rightarrow A_{red} + B_{ox}$*

Reactants	k_{AA}	k_{BB}	K_{AB}	k_{pred}	k_{obs}
A B					
$Ce^{IV} + Fe(CN)_6^{4-}$	4.4	3.0×10^2	6×10^{12}	7.0×10^6	1.9×10^6
$Ce^{IV} + Mo(CN)_8^{4-}$	4.4	3.0×10^4	6×10^{10}	1.3×10^7	1.4×10^7
$Mo(CN)_8^{3-} + Fe(CN)_6^{4-}$	3.0×10^4	3.0×10^2	1×10^2	2.7×10^4	3.0×10^4
$Ce^{IV} + Fe^{2+}$	4.4	4.0	1×10^{12}	6.0×10^5	1.0×10^3
$Co^{III} + Fe^{2+}$	5.0	4.0	2×10^{18}	6.0×10^7	42
$Co(phen)_3^{3+} + Fe^{II}(cyt\ \mathbf{c})$	40	1.2×10^3	72	2.0×10^3	1.5×10^3
$Co(phen)_3^{3+} + V^{2+}$	40	3.0×10^{-3}	4×10^{10}	3.2×10^4	4.0×10^3
$Fe^{3+} + V^{2+}$	4.0	3.0×10^{-3}	8×10^{16}	1.7×10^6	1.8×10^4
$Fe^{3+} + Co(phen)_3^{2+}$	4.0	40	2×10^6	4.2×10^3	5.3×10^2

* Tabulated from Weston and Schwarz[15] and Chou et al.[20]

K_{AB}, the equilibrium constant for the net redox reaction, $ox_A + red_B = red_A + ox_B$, can be determined from $p\varepsilon°$ values of the half-reactions:

$$\ln K_{AB} = p\varepsilon_A° - p\varepsilon_B° \qquad (11.44)$$

Under some conditions, Marcus theory leads to a simple linear free energy relationship. In a plot of $\ln k$ versus $\ln K$ (or $\Delta G_{AB}°$), the value at the y-intercept (where $\Delta G_{AB}° = 0$) is half the sum of the exchange rate constants k_{AA} and k_{BB} (Eq. 11.42b). For *os* redox reactions of two metal ions and a series of ligands complexed with one cation ($A_{ox}L_i + B_{red} = A_{red}L_i + B_{ox}$), a plot of $\ln k$ versus $\ln K$ (or $\ln k$ versus $\Delta G_{AB}°$ or $p\varepsilon_{AB}°$) has a slope of ~0.5 for small values of $\Delta G_{AB}°$. In such cases, k_{BB} is constant but K_{AB} varies. Exchange rate constants (k_{AA}) for various complexes of A vary somewhat, causing scatter about the line.

The slope in plots of $\ln k$ versus $\ln K$ for *os* electron transfers is 0.5 only when $\Delta G_{AB}°$ is small because factor f (Eq. 11.42c) is no longer ~1 at large $\Delta G°$ values. Linear plots of $\ln k$ versus $\Delta G°$ also are found in some *is* redox reactions, however, and care needs to be taken in inferring redox mechanisms (*is* versus *os*) from the existence of redox LFERs.

The Marcus theory has been verified for a variety of metal-ion redox reactions, but theory-based estimates of rate constants for electron exchange between +2 and +3 charged reactants do not always agree closely with measured values, and k_{obs} usually is smaller than k_{pred} (Table 11.5). Large deviations may indicate that a reaction occurs by an inner sphere mechanism. For example, k_{obs} is ~10^6 lower than k_{pred} for Fe^{II}-Co^{III} exchange, and the reaction probably involves an inner sphere mechanism.[15] Reasons why the "theoretically" faster *os* mechanism does not occur are not always clear, but in some cases, the slowness of *os* exchange reflects inaccessible orbitals.

11.6 Corrosion

Corrosion is the destructive result of chemical reaction of a metal or metal alloy in its environment. It is driven by the transfer of electrons to a suitable oxidant and occurs readily in many aqueous systems. Corrosion thus is a redox process, and it is encountered commonly in engineering practice. For example, cast iron metal pipes used for drinking water distribution systems are exposed to the powerful oxidants chlorine and oxygen. Iron metal, however, is a powerful enough reductant that it reduces water itself and thus is also unstable in anoxic environments (see Figure 11.9). $p\varepsilon$-pH diagrams are used for metals to show the regions where corrosion occurs, i.e., those regions where a solution-phase species predominates. The rate of corrosion essentially is defined by the exchange current density for the electrochemical cell involving the cathodic reaction (O_2 reduction) and the anodic (Fe^0 oxidation) reaction, as illustrated for iron in Figure 11.9. Polarization curves similar to Figure 11.8c are used to relate the potential of the Fe-O_2 cell and current density (hence the kinetics of corrosion). A more complete explanation is beyond our scope, and readers are referred to more appropriate texts (e.g., Jones[21]).

Some metals are protected from further oxidation by their own oxidation products. For example, the oxides of aluminum are insulators, and once an oxide forms on the surface of aluminum metal (i.e., it is "passivated," or a passive film forms), further corrosion is inhibited. Many iron oxides also are insulators, but most environmental conditions are not sufficient to allow formation of a passive layer on iron (fuming nitric acid is an exception). Other metals (e.g., zinc) do not form passive layers under any conditions.

Many conditions accelerate the corrosion processes. For example, contact of two dissimilar metals in an aqueous environment leads to one corroding faster than the other (galvanic corrosion). Additionally, chloride is able to break down passive films, leading to additional corrosion. Bacterial attachment to surfaces is problematic because bacteria release chemicals that promote corrosion (e.g., H^+, H_2S). Methods to limit corrosion include development of noncorrosive alloys, use of coatings (including plastics, porcelains, metals, and paints), and use of a sacrificial anode. In the last case,
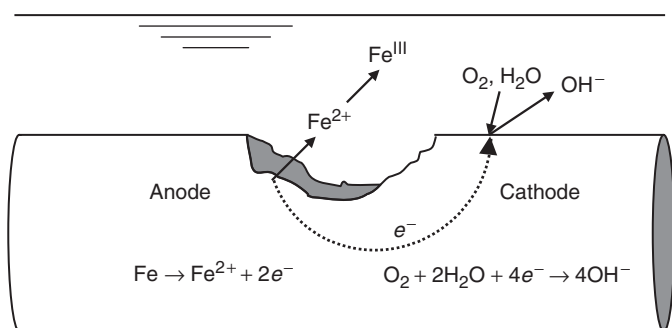
Figure 11.9 Schematic of the cathodic and anodic reactions in the corrosion of an iron pipe.

the metal one wishes to protect is connected to another, more active metal (e.g., iron may be connected to zinc, which provides electrons by its own corrosion to prevent corrosion of the iron); this technique sometimes is called cathodic protection because the protected metal is acting as a cathode. Another method involves the addition of chemical additives to promote precipitation of an insoluble solid on the surface. For example, phosphate addition to drinking water systems is used to precipitate iron phosphates as the iron metal corrodes, and a protective (but not completely so) layer develops. Addition of phosphate, however, provides a nutrient necessary for microbial growth, which is not desired and can lead to further corrosion.

Problems

11.1. The reduction potential for the half-reaction

$$Fe(OH)_{3(s)} + e^- + 3H^+ = Fe^{2+} + 3H_2O$$
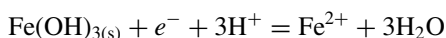
can be computed from the value for the half-reaction $Fe^{3+} + e^- = Fe^{2+}$, which is listed in Table 11.1, K_{s0} for $Fe(OH)_{3(S)} = 10^{-37.11}$ and $K_w = 10^{-14.00}$. Compute $E°$ and $p\epsilon°$ for this half-reaction and convert the value you find to the corresponding values of $E_7°$ and $p\epsilon_7°$.

11.2. Consider the following unbalanced redox reactions. In each case, separate the whole reactions into half-reactions, balance the half-reactions, and combine to yield a balanced whole reaction. Compute the net $E_7°$ and $p\epsilon_7°$ values for the net reactions and indicate whether the reaction is spontaneous as written. Use the values calculated in problem 11.1 for the $Fe(OH)_{3(s)}/Fe^{2+}$ reduction potential. Note: you may wish to verify your answer to problem 11.1 with the instructor before using it in this problem.

(a) $Fe^{2+} + NO_3^- = Fe(OH)_{3(s)} + N_2$
(b) $Fe^{2+} + SO_4^{2-} = Fe(OH)_{3(s)} + H_2S$
(c) $Mn^{2+} + Fe(OH)_{3(s)} = MnO_{2(s)} + Fe^{2+}$

11.3. (a) Write and balance the half-reactions (reductions) for the following redox couples and determine $\Delta G°$ and $E°$ for each half-reaction from the $G_f°$ data in the appendix:

  (i) Pb_3O_4/Pb^{2+}
  (ii) NO_2^-/NH_4^+
  (iii) $HSeO_3^-/SeO_4^{2-}$

(b) Combine each combination of (i)–(iii) [i.e., (i) and (ii), (i) and (iii), (ii) and (iii)] to obtain overall redox reactions. What is $E°$ for each overall reaction? In which direction does each reaction proceed?

(c) Which species is the strongest oxidizing agent?

11.4. Balance redox reaction of toluene oxidation (to carbon dioxide) coupled to iron reduction ($Fe(OH)_{3(s)}$ to Fe^{2+}).

11.5. Given the following two half-reactions,

$$ClO_3^- + 6e^- + 6H^+ = Cl^- + 3H_2O \quad E° = 1.446 \text{ V},$$

$$HOCl + 2e^- + H^+ = Cl^- + H_2O \quad E° = 1.481 \text{ V},$$
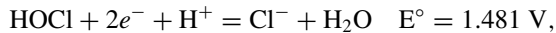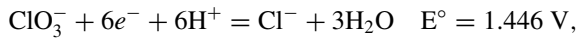
what is $E°$ for the half-reaction representing the oxidation of HOCl to ClO_3^-?

11.6. Bacteria can oxidize acetate to bicarbonate using O_2 at neutral pH according to the stoichiometric relationship:

$$CH_3COO^- + 2O_2 = 2HCO_3^- + H^+$$
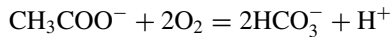
    (a) Compute the standard free energy of reaction, $\Delta G°$, for the reaction using $G_f°$ values in the appendix.

    (b) If $[HCO_3^-] = 2 \times 10^{-3}$, $[CH_3COO^-] = 2 \times 10^{-4}$ M, pH = 8.0, and $P_{O_2} = 0.21$ atm, what is the actual free energy yield of bacteria using this reaction? If the pH is lowered to 4.0, how will this affect your calculations?

11.7. You can construct pC-pε diagrams for certain redox couples using MINEQL+. The program is somewhat limited in the number of components it provides, but for those in the database, the procedure is no more difficult than the earlier pC-pH diagrams you produced. Here you are asked to construct a pC-pε diagram for the nitrogen system, considering the three species: NH_4^+, NO_2^-, and NO_3^-. MINEQL+ does not have redox data for N_2, and you can ignore this species. Construct the diagram using $N_T = 1 \times 10^{-1}$ M for each N form and pH = 7.0, and write a paragraph describing your findings.

    Note: (1) You need to include e^- as a component; it is the very first component listed in the table of components. (2) You will need to do a MultiRun using log K of pε as your multirun variable; MINEQL+ designates this as "logK of pe." For a titration range you have some discretion, but a range of -10 to $+20$ works. (3) The plotting routine in MINEQL+ allows you to draw only one component (NH_4^+, NO_2^-, or NO_3^-) at a time and does not produce all three components on the same diagram, as you need. Therefore, you need to export your log C data for these three species into a spreadsheet or graphing program to produce your diagram.

11.8. What partial pressure of oxygen cannot be exceeded so that the reduction of SO_4^{2-} to HS^- can take place at pH 7?

11.9. Using MINEQL+, determine how the partial pressure (or concentration) of oxygen affects speciation and pε in the Fe^{2+}/Fe^{3+} system. Use 10^{-5} M $Fe(NO_3)_2$ and 10^{-7} M $Fe(NO_3)_3$ as starting concentrations in the system. Be sure to click "e^-" on the components page. This will turn on the "Redox" tab in the Wizard. Set the pH at 7, and run the calculation for dissolved oxygen = 0, 2, 5, and 8 mg/L.

11.10. (Based on a problem in Stumm and Morgan[1]) (a) Determine the solubility (in mol/L) of $Au_{(s)}$ (i.e., calculate Au_T) in seawater in equilibrium with the atmosphere. If the volume of the world's oceans is 1.37×10^9 km^3, how much gold (in kg) can the oceans hold?

Seawater has a pH = 8.1 and $[Cl^-] = 0.545$ M. The following equilibrium constants may be useful:

$$AuCl_2^- + e^- = Au_{(s)} + 2Cl^- \qquad\qquad \log K = 19.2$$

$$AuCl_4^- + 3e^- = Au_{(s)} + 4Cl^- \qquad\qquad \log K = 51.3$$

$$Au(OH)_4^- + 4H^+ + 4Cl^- = AuCl_4^- + 4H_2O \quad \log K = 29.64$$

$$O_{2(g)} + 4H^+ + 4e^- = 2H_2O \qquad\qquad\qquad E^\circ = 1.226 \text{ V}$$
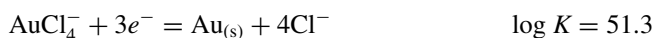
11.11. The potential (E) of the Co^{3+}/Co^{2+} redox couple can be changed by adding the ligand iminodiacetic acid (H_2L). If you have two beakers with solutions containing this redox couple but only enough iminodiacetic acid to create a 10^{-3} M solution in one beaker, to which beaker would you add the iminodiacetic acid to cause the largest change in E?

    Beaker 1: $Co(OH)_{3(s)}$ and $Co_T^{II} = 1 \times 10^{-6}$ M at a pH of 4.5.

    Beaker 2: $Co_T^{III} = 1 \times 10^{-6}$ M and $Co_T^{II} = 1 \times 10^{-6}$ M at a pH of 4.5

    (no solid present)

You may assume that the Co^{II} does not precipitate.

$H_2L = H^+ + HL^-$	$K_{a1} = 10^{-9.8}$
$HL^- = H^+ + L^{2-}$	$K_{a2} = 10^{-12.6}$
$Co^{3+} + e^- = Co^{2+}$	$E^0 = 1.95V$
$Co^{3+} + H_2O = CoOH^{2+} + H^+$	$*\beta_1 = 10^{-1.291}$
$Co^{3+} + L^{2-} = CoL^+$	$K_{1Co(III)} = 10^{30.68}$
$Co(OH)_{3(s)} = Co^{3+} + 3OH^-$	$K_{s0} = 10^{-35.5}$
$Co^{2+} + H_2O = CoOH^+ + H^+$	$*\beta_1 = 10^{-9.697}$
$Co^{2+} + 2H_2O = Co(OH)_2^0 + 2H^+$	$*\beta_2 = 10^{-18.794}$
$Co^{2+} + 3H_2O = Co(OH)_3^- + 3H^+$	$*\beta_3 = 10^{-31.491}$
$Co^{2+} + L^{2-} = CoL^0$	$K_{1Co(II)} = 10^{7.8}$
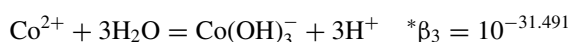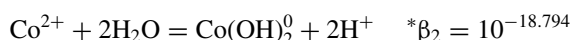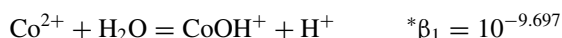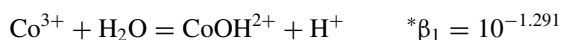
11.12. Using Figure 11.5 (sulfur pε-pH diagram), answer the following questions. Consider H_2S to be only in the aqueous form (i.e., ignore any partitioning according to Henry's law).

(a) You close the system from the atmosphere, and bubble $H_{2(g)}$ at $P = 1$ atm through the system continuously. The pH is 6.5. For the system:

  (i) determine E (what is the potential of the system?)
  (ii) identify the dominant sulfur species
  (iii) calculate the dissolved sulfur speciation

(b) You then open the beaker is open to the atmosphere ($P_{O_2} = 0.21$ atm). The pH is still 6.5 and all hydrogen gas is flushed from the system.

(i) What is the potential of the system?
(ii) What is the most stable sulfur species?

11.13. Given the following reactions draw a pε-pH diagram for aluminum. Assume a concentration of 10^{-6} M for Al_T. For the water reduction line, assume an H_2 pressure of 1 atm, and for water oxidation line, assume an O_2 pressure of 1 atm. Your plot should extend from pH 0 to 14 and pε from -45 to $+18$.

$$Al^{3+} + 3e^- = Al_{(s)} \qquad\qquad E° = -1.66 \text{ V}$$

$$Al_2O_{3(s)} + 6H^+ + 6e^- = 2Al_{(s)} + 3H_2O \quad E° = -1.55 \text{ V}$$

$$AlO_2^- + 4H^+ + 3e^- = Al_{(s)} + 2H_2O \qquad E° = -1.26 \text{ V}$$

$$2Al^{3+} + 3H_2O = Al_2O_{3(s)} + 6H^+ \qquad K = 10^{-11.4}$$

$$Al_2O_{3(s)} + H_2O = 2AlO_2^- + 2H^+ \qquad K = 10^{-29.2}$$
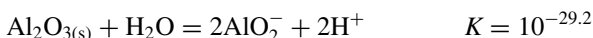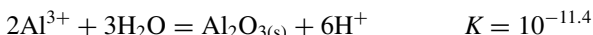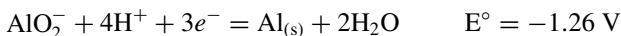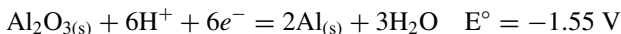
References

1. Stumm, W., and J. J. Morgan. 1996. *Aquatic chemistry*, 3rd ed., Wiley-Interscience, New York.
2. Benjamin, M. M. 2002. *Water chemistry*, McGraw-Hill, New York.
3. Stumm, W. 1978. What is the pε of the sea? *Thalassia Jugoslavica* **14**: 197–208.
4. Pourbaix, M. 1974. *Atlas of electrochemical equilibria in aqueous solutions*, 2nd Engl. ed., Nat. Assoc. Corrosion Engineers, Houston, Tex.
5. Morris, J. C., and W. Stumm. 1967. Redox equilibria and measurements of potentials in the aquatic environment. In *Equilibrium concepts in natural water systems*, W. Stumm (ed.), Adv. Chem. Ser. **67**, Amer. Chem. Soc., Washington, D.C., 270–285.
6. Stumm, W., and J. J. Morgan. 1980. *Aquatic chemistry*, 2nd ed., Wiley-Interscience, New York.
7. Whitfield, M. 1972. The electrochemical characteristics of natural redox cells. *Limnol. Oceanogr.* **17**: 383–392.
8. Graetz, D. A., D. R. Keeney, and R. B. Aspiras. 1973. E_h status of lake sediment-water systems in relation to nitrogen transformations. *Limnol. Oceanogr.* 18: 906–917.
9. Lovely, D. R., and S. Goodwin. 1988. Hydrogen concentrations as an indicator of the predominant electron-accepting reactions in aquatic sediments. *Geochim. Cosmochim. Acta* **52**: 2993–3003.
10. Chapelle, F. H., S. K. Haack, P. Adriaens, M. A. Henry, and P. M. Bradley. 1996. Comparison of E_h and H_2 measurements for delineating redox processes in a contaminated aquifer. *Environ. Sci. Technol.* **30**: 3565–3569.
11. Chapelle, F. H., P. B. McMahon, N. M. Dubrovsky, R. F. Fujii, E. T. Oaksford, and D. A. Vroblesky. 1995. Deducing the distribution of terminal electron-accepting processes in hydrologically diverse groundwater systems. *Water Resources Res.* **31**: 359–371.
12. U.S. Geological Survey. 2009. Field measurements. Reduction-oxidation potential (electrode method). In *National field manual for the collection of water-quality data*, TWRI Book 9, ver 2.2, chap. A6.5 (available online at http://water.usgs.gov/owq/pubs.html, accessed 12/2009).

13. Brezonik, P. L. 1994. *Chemical kinetics and process dynamics in aquatic systems*, CRC Press, Boca Raton, Fla.
14. Amis, E.S. 1966. *Solvent effects on reaction rates and mechanisms*, Academic Press, New York.
15. Weston, R. E., Jr., and H. A. Schwarz. 1972. *Chemical kinetics*, Prentice-Hall, Englewood Cliffs, N.J.
16. Marcus, R. A. 1963. On the theory of oxidation-reduction reactions involving electron transfer. V. Comparison and properties of electrochemical and chemical rate constants. *J. Phys. Chem.* **67**: 853–857.
17. Marcus, R. A. 1981. On the frequency factor in electron transfer reactions and its role in highly exothermic reactions. *Int. J. Chem. Kinetics* **13**: 865–872.
18. Wehrli, B. 1990. Redox reactions of metal ioins at mineral surfaces. In *Aquatic Chemical Kinetics*, W. Stumm (ed.), Wiley-Interscience, New York, 311–336.
19. Proll, P. J. 1972. Reactions in solution between various metal ions of the same element in different oxidation states. In *Comprehensive chemical kinetics*, Vol. 7, C. H. Bamford and C. F. H. Tipper (eds.), Elsevier, Amsterdam, New York, 56–152.
20. Chou, M., C. Creutz, and N. Sutin. 1977. Rate constants and activation parameters for outer-sphere electron-transfer reactions and comparisons with the predictions of Marcus theory. *J. Am. Chem. Soc.* **99**: 5615–5623.
21. Jones, D. A. 1992. *Principles and prevention of corrosion*, Macmillan, Englewood Cliffs, N.J.

This page intentionally left blank

IV

Chemistry of Natural Waters and Engineered Systems

This page intentionally left blank

12

▨ Dissolved Oxygen

▨ Objectives and scope

This is the first of several chapters focusing on aquatic constituents whose chemistry is dominated by redox reactions. Here we discuss the water chemistry of dissolved oxygen (DO), or $O_{2(aq)}$, which plays a critical role in regulating the redox chemistry of solutes in natural waters. DO concentrations are controlled by a wide range of chemical and biological redox processes, as well as by physical factors that affect O_2 solubility and transfer rates across the air-water interface. Spatial and temporal patterns of DO concentrations in surface waters are explained in the context of major driving forces, including solubility factors and gas-transfer kinetics. Finally, redox chemistry is fundamental to the analysis of DO by the classic Winkler titration. Chemical principles underlying DO analysis by instrumental methods (DO electrodes and optodes) also are explained.

▨ Key terms

- Dioxygen, molecular oxygen, dissolved oxygen (DO)
- Triplet and singlet states
- Singlet oxygen, superoxide radical anion, hydroxyl radical
- Haber-Weiss process
- Henry's law; Whitman's two-film gas transfer theory, surface renewal model
- Thermal stratification: epilimnion, thermocline, metalimnion, hypolimnion; hypoxia, supersaturation
- Oxygen sag curve; BOD; Streeter-Phelps model
- Winkler method, iodometric titrations; Clark electrodes; optodes

12.1   Introduction

It is difficult to overstate the importance of molecular oxygen (O_2), also called dioxygen, in regulating the chemistry and biology of natural waters. From a biological perspective, dissolved oxygen, often abbreviated DO, is essential for all higher forms of life in water bodies, and government agencies have established water quality standards for minimum levels of DO in surface waters to protect aquatic life. From a chemical perspective, oxygen is a major indicator of the redox status of a water body, but it does so primarily in a dichotomous fashion. That is, if oxygen is present, even at low concentrations, other redox-sensitive elements are present in their oxidized forms. When it is absent, a range of reduced forms of the elements occurs, but the exact redox potential at which they begin to predominate varies among the elements, as illustrated in Figure 12.1. The chemistry and biology of natural waters thus are dramatically different depending on whether dissolved oxygen (DO) is present or not.

As implied above, the behavior of O_2 in natural waters strongly affects—and is affected by—a wide variety of chemical and biological processes. In addition, DO concentrations in surface waters are controlled by the physical process of air-water gas transfer, as well as the biological process of primary production, which produces O_2, and various chemical and biological processes that consume it. In this chapter we discuss the chemical characteristics of O_2 and explain why it is a relatively reactive molecule. We describe the physical factors affecting oxygen solubility in water and its transfer rates across the air-water interface, as predicted by several kinetic models. Spatial and temporal patterns of DO concentrations in typical lakes and streams are explained in the context of controlling physical, chemical, and biological driving forces. Finally, we explain the redox chemistry involved in the classic Winkler titration used to measure oxygen concentrations in water and the principles underlying measurement of oxygen by instrumental methods (DO electrodes and optodes).

Figure 12.1 Scheme illustrating some important differences in water chemistry resulting from the presence and absence of DO. Placement of reduced forms along the horizontal axis qualitatively reflects the redox potentials at which they begin to predominate.

O_2 present	O_2 absent		
Oxic conditions	Weak anoxia		Strong anoxia
$p\varepsilon \gg 0$	$p\varepsilon \sim 0$		$p\varepsilon \ll 0$
Oxidized solutes and solids:	Reduced solutes		
N NO_3^-	NO_2^-	NH_4^+	
S SO_4^{2-}		S^0	H_2S
C $CO_{2(aq)}$			CH_4
Fe Fe^{III}; e.g., $FeOOH_{(s)}$		Fe^{2+}	
Mn Mn^{IV}; e.g., $MnO(OH)_{2(s)}$	Mn^{2+}		

12.2 Chemistry of molecular oxygen

12.2.1 Electronic structure

Although oxygen and nitrogen are neighbors in the Periodic Table and differ by only one proton (and hence one electron), differences in the reactivities of their molecular forms, O_2 and N_2 (dioxygen and dinitrogen), are dramatic. N_2 (at. no. 7, electron configuration $1s^2\ 2s^2\ 2p^3$) is chemically unreactive, but O_2 (at. no. 8, electron configuration $1s^2\ 2s^2\ 2p^4$) is surprisingly reactive regarding both biotic and abiotic processes. Reasons for the difference in reactivity can be understood by examining electronic structures of the two molecules. Figure 12.2, a molecular orbital diagram of the bonding (p) orbitals in O_2, shows that the two highest orbitals in its ground state each have one electron with parallel spins—making O_2 a triplet state (designated $^3\Sigma_g^-$ by inorganic chemists). In contrast, the ground-state forms of most molecules are singlet states, in which all the electrons exist as pairs in filled orbitals. O_2 thus is unusual in its electronic configuration, and this results in its unusual reactivity; half-filled orbitals are not the most stable configuration for electrons. Because oxygen is highly electronegative, it has very little tendency to give up an electron; instead, it tends to accept an electron into one of the half-filled orbitals, starting the reduction of O_2 to H_2O by a sequence of one-electron transfers. In contrast, ground-state nitrogen, with one less electron in each atom, has three filled bonding orbitals (a σ and two π), making triply bonded dinitrogen (N≡N) a very stable species.

Molecular orbital diagrams of the first two excited states of O_2 also are shown in Figure 12.2. In the first excited state, designated $^1\Delta_g$ and called singlet oxygen ($^1O_2$), the two outer electrons combine to yield a filled π^* orbital (highest occupied molecular orbital, HOMO). The other π^* orbital is unfilled (lowest unoccupied molecular orbital, LUMO) and can accept a pair of electrons. In the second excited state the two outermost electrons again are in separate π^* orbitals, but the electron spins are paired,
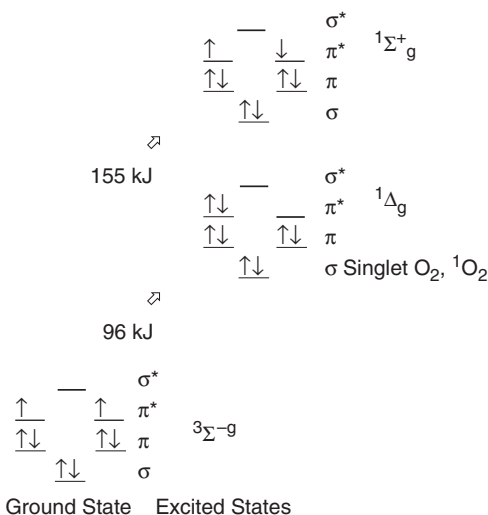
Figure 12.2 Molecular orbital diagram for the p orbitals in ground-state O_2 and its first two excited states.

resulting in another singlet state ($^1\Sigma_g^+$). The first excited state, singlet oxygen, is an important photochemical intermediate. Because the energy difference between it and ground-state O_2 is low (only 94.3 kJ mol^{-1}), it is formed readily by collision of the latter with excited triplet state molecules formed by absorption of a photon of light (see Figure 17.1 for details). $^1O_2$ is reactive because its LUMO can accept an electron pair, but $^1O_2$ is quite selective in its reactivity. As an electrophile, it reacts with electron-rich compounds such as alkenes, aromatic compounds, and reduced sulfur species, but because of its electron configuration, it participates only in reactions involving two-electron transfers. Further discussion of the role of singlet oxygen in photochemistry is provided in Chapters 17–19.

12.2.2 Oxygen reduction: mechanisms and intermediates

As indicated above, complete reduction of ground-state oxygen to water involves the transfer of four electrons:

$$O_2 + 4e^- + 4H^+ \rightarrow 2H_2O \tag{12.1}$$

Several mechanisms are possible. In abiotic autoxidation of reduced species like Fe^{2+} in aquatic systems, O_2 reduction occurs by four one-electron transfers that produce reactive intermediates of oxygen. Biotic reduction of O_2 is mediated by cytochrome enzymes that facilitate transfer of four electrons usually without release of intermediate, partially reduced species of oxygen.[1] In the presence of light and sensitizing agents that produce singlet oxygen, reduction occurs by transfer of electron pairs. The four-step one-electron transfer process is called the **_Haber-Weiss mechanism_**:

$$M^I + O_2 \rightarrow M^{II} + O_2^- \cdot \tag{12.2a}$$

$$(H^+ + O_2^- \cdot \rightleftharpoons HO_2) \qquad pK_a = 4.8 \tag{12.2b}$$

$$M^I + O_2^- \cdot \rightarrow M^{II} + O_2^{2-} \tag{12.2c}$$

$$(2H^+ + O_2^{2-} \rightleftharpoons H_2O_2) \qquad pK_{a1} = 11.7 \tag{12.2d}$$

$$M^I + H_2O_2 \rightarrow M^{II} + \cdot OH + OH^- \tag{12.2e}$$

$$M^I + \cdot OH \rightarrow M^{II} + OH^- \tag{12.2f}$$
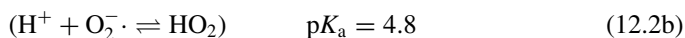
M^I in this sequence represents a generic electron donor, which becomes oxidized to M^{II} in the process. Acid-recombination reactions (Eqs. 12.2b and 12.2d) are in parentheses because they are so are rapid (diffusion-controlled) that they achieve equilibrium essentially instantaneously. The intermediates in O_2 reduction to H_2O are reactive species and also are important in photochemical reactions (Chapter 17).

The product of the first step is superoxide radical anion ($O_2^- \cdot$), so-called because it is an ion with an uneven number of electrons—making it a highly reactive radical. For brevity, we will refer to it simply as "superoxide." It is the acid anion of HO_2, hydroperoxyl radical. Because the pK_a for HO_2 is 4.8, superoxide predominates at circumneutral pH. In the second step of O_2 reduction, superoxide accepts an electron (from M^I) to form the peroxide anion, O_2^{2-} (or HO_2 accepts an electron to become

the hydrogen peroxide anion, HO_2^-). Both species rapidly combine with H^+ to form hydrogen peroxide, H_2O_2. Because $pK_{a1} = 11.7$ for H_2O_2, the anionic forms are not important in natural waters. The rate constant for step 2 (Eq. 12.2c) is $\sim 1 \times 10^7\ M^{-1}\ s^{-1}$ when Fe^{2+} is the reducing agent.[2] Superoxide can act as both an oxidizing and a reducing agent, in the latter process returning to O_2. In fact, Fe^{III} reduction is faster than Fe^{2+} oxidation ($Fe^{III} + O_2^- \cdot \rightarrow Fe^{2+} + O_2; k_2 = 1.5 \times 10^8\ M^{-1}\ s^{-1}$).[2] Effectively, this reaction and the oxidation of Fe^{2+} with O_2 that forms $O_2^- \cdot$ constitute a null cycle. Nonetheless, net reduction of O_2 (and net oxidation of Fe^{2+} or some other reducing agent) occurs because Fe^{2+} competes with Fe^{III} for reaction with superoxide.

An alternative loss mechanism for superoxide and hydroperoxyl is disproportionation (or "dismutation," i.e., self-oxidation/reduction) to H_2O_2 and O_2:

$$2HO_2 \rightarrow H_2O_2 + O_2 \qquad (12.3a)$$

or

$$2O_2^- \cdot + 2H^+ \rightarrow H_2O_2 + O_2 \qquad (12.3b)$$
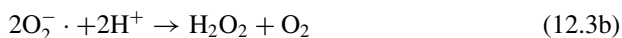
These reactions are catalyzed by dismutase enzymes to control concentrations of highly toxic $O_2^- \cdot$ in cells. The fact that cells have such enzymes suggests that biotic reduction of O_2 is not always a simultaneous four-electron transfer process but partly proceeds sequentially. The equilibrium constant for Eq. 12.3b is very high ($K = 6.2 \times 10^{31}$),[3] but dismutation without enzyme catalysis is slower than direct reaction of $O_2^- \cdot$ with a reducing agent. CDOM (colored (or chromophoric) dissolved organic matter) (aquatic humic matter)[4] and natural organic-Cu complexes[5] also catalyze superoxide dismutation in coastal waters and may control its concentrations in such waters. These processes probably are important in freshwater as well (see Section 17.6.1).

Hydrogen peroxide, the product of the second step in the Haber-Weiss mechanism, is moderately stable and occurs at concentrations of 10^{-8} to 10^{-6} M in many surface waters. It reacts with a variety of reducing agents to form hydroxyl radicals, $\cdot OH$. These are extremely reactive species that react at near diffusion-controlled rates with numerous natural and manmade organic compounds, as well as many inorganic ions.

12.2.3 Energetics of O_2 reduction

Standard reduction potentials and free energies of reaction for one-, two, and four-electron steps in O_2 reduction are summarized in Table 12.1. The standard reduction potential for the O_2/H_2O couple is highly positive, and O_2 thus is a strong oxidizing agent (although not as strong as Cl_2 and $HOCl$ and well-known oxidizing agents, e.g., permanganate and dichromate). The standard reduction potential for the O_2/H_2O_2 couple (0.777 V) is much less than that for the O_2/H_2O couple, and the first step in O_2 reduction (formation of superoxide) actually is endergonic ($\Delta G^\circ = 15.5\ kJ\ mol^{-1}$). As noted above, superoxide is both an oxidizing and a reducing agent. In fact, reduction by $O_2^- \cdot$ likely is the mechanism for Cu^I formation in oxic seawater and also explains the presence of Fe^{2+} in oxic waters. Although we consider O_2 to be a reactive species, the negative $p\varepsilon^\circ$ for the $O_2/O_2^- \cdot$ couple helps to explain the fact that O_2 is relatively stable in the atmosphere and water and that activation by light, enzymes, or transition metal

Table 12.1 E°, pɛ°, and ΔG° values for O$_2$ reduction half-reactions

Reaction	E° (V)	pɛ°	ΔG° (kJ mol^{-1})
$O_{2(g)} + 4e^- + 4H^+ \rightarrow 2H_2O$	1.226	20.74	−473.2
$O_{2(aq)} + 4e^- + 4H^+ \rightarrow 2H_2O$	1.268	21.46	−489.4
$O_{2(aq)} + e^- \rightarrow O_2^- \cdot_{(aq)}$	−0.161	−2.72	15.5
$O_2^- \cdot_{(aq)} + e^- + 2H^+ \rightarrow H_2O_{2(aq)}$	1.719	29.09	−165.9
$H_2O_{2(aq)} + e^- + H^+ \rightarrow \cdot OH_{(aq)} + H_2O$	0.988	16.71	−95.3
$\cdot OH_{(aq)} + e^- + H^+ \rightarrow H_2O$	2.538	42.95	−244.9
$O_{2(aq)} + 2e^- + 4H^+ \rightarrow 2H_2O_{2(aq)}$	0.777	13.15	−149.9
$H_2O_{2(aq)} + 2e^- + 2H^+ \rightarrow 2H_2O$	1.760	29.78	−339.6

catalysts generally is needed to begin the reduction process. On the other hand, E° for the H$_2$O$_2$/H$_2$O couple is substantially higher than that for O$_2$/H$_2$O, and the reduction potential for highly reactive ·OH is higher still.

Some have questioned whether the full oxidizing potential of O$_2$ is exerted in redox reactions involving reduced inorganic ions in natural waters, given that the second intermediate in the reduction sequence, H$_2$O$_2$, often is found at measurable concentrations in natural waters, which implies that the process occurs as two distinct redox couples: O$_2$/H$_2$O$_2$, and H$_2$O$_2$/H$_2$O. Stumm and Morgan[3] concluded that O$_2$/H$_2$O is the operative couple for biologically mediated redox reactions because the enzymatically catalyzed four-electron transfer process is more-or-less synchronous, and Stumm[6] also concluded that it determines the effective pɛ for natural waters, even if the reduction of H$_2$O$_2$ is relatively slow.

12.3 Solubility and gas transfer kinetics

12.3.1 Factors affecting O$_2$ solubility

The solubility of O$_2$ in water is given by Henry's law: solubility is equal to the atmospheric partial pressure of O$_2$ times the Henry's law constant (K_H, units of mol L^{-1} atm^{-1}), which depends on temperature and ionic strength. An alternative convention gives O$_2$ solubility in units of mL/L using ***Bunsen coefficients*** (β), where β is equal to 22,400 $\times K_H$:

$$S_{O_2}(mL/L) = \beta P_{O_2} \tag{12.4}$$

A mole of gas occupies 22,400 cm^3 at STP (standard temperature and pressure), and the units for β thus are cm^3 L^{-1} atm^{-1}. K_H for O$_2$ at 20°C is 1.386×10^{-3} mol L^{-1} atm^{-1}; the corresponding value of β is 31.05 cm^3 L^{-1} atm^{-1}.[5] These values are equivalent to the solubility of O$_2$ in water at 20°C when the pressure of O$_2$ = 1.00 atm. The actual pressure of O$_2$ in the atmosphere is a function of total pressure and the mole fraction (or "mixing ratio") of O$_2$ in air, which is constant at 0.2095. Total pressure varies daily in response to weather conditions, but these variations are small (± ∼1–3% of mean atmospheric pressure at sea level of 101.325 kPa (1013.25 mbar)), except under extreme conditions.

(The lowest sea-level barometric pressure ever measured is 879 mbar during a typhoon in the Pacific Ocean.) Consequently, variations in barometric pressure usually can be ignored in calculating oxygen saturation.

According to Dalton's law of partial pressure, the total pressure of a mixture of gases is the sum of the partial pressures of the individual gases comprising the mixture. This law applies to ideal gases (the atmosphere behaves as ideally) and implies that the individual gases behave independently. It is important to note that the composition of the atmosphere usually is expressed on a dry basis—i.e., exclusive of water vapor, and correction for water vapor in the ambient atmosphere is needed. For example, at 20°C, the vapor pressure of water is 23.98 mbar, or 2.37% of the total (standard) atmospheric pressure. The partial pressure (P_i) of any gas thus is expressed as

$$P_i = \left[P_T - \frac{h_r}{100} VP \right] f_i, \tag{12.5}$$

where P_T is the atmospheric pressure, h_r is the relative humidity, VP is the vapor pressure of water at a given temperature (available in standard tables), and f_i is the mole fraction of the gas in dry air (0.2095 for O_2).

As shown in Figure 12.3 and Table 12.2, O_2 solubility decreases in curvilinear fashion with temperature, from 14.6 mg/L at 0°C to 7.6 mg/L at 30°C—i.e., nearly by half over the range of ambient temperatures. The effect of ionic strength (I) is much smaller, reflecting the fact that nonelectrolytes are affected only moderately by I. Although the trend appears nearly linear (Table 12.2), the relationship actually is exponential and follows the Setschenow relationship (Eq. 4.24). O_2 saturation in seawater is about 20% lower than that in freshwater, and the decrease in O_2 solubility with I (called "salting out") implies that the activity coefficient for O_2 increases with I. Atmospheric pressure
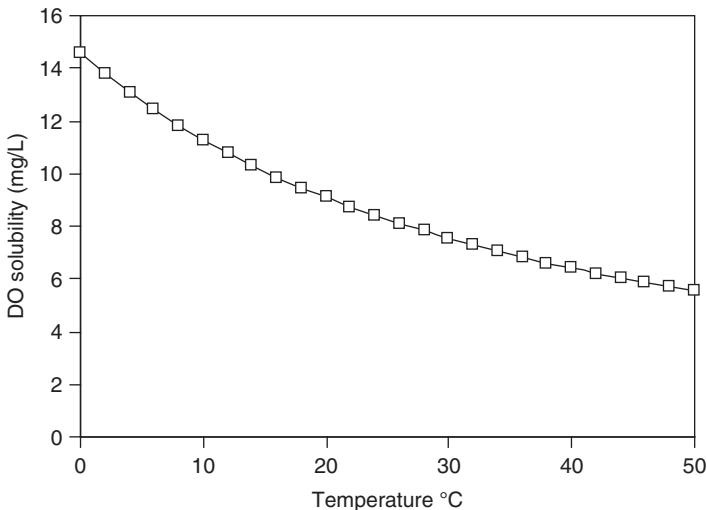
Figure 12.3 Solubility of O_2 versus temperature in water at $I = 0$. Data from *Standard methods*.[7]

Table 12.2 Factors affecting O_2 solubility in water*

A. Temperature

T°C	0	5	10	15	20	25	30
S (mg/L)	14.62	12.77	11.29	10.08	9.09	8.26	7.56

B. Salinity

Salinity ‰	0	10	20	30	35
S (mg/L at 20°C)	9.07	8.55	8.06	7.59	7.37
% of $S_{I=0}$	100	94	89	84	81

C. Elevation above sea level

H above msl[†]	atm	P	S at 20°C
m	ft	mm Hg	mg/L
0	0	760	9.07
305	1,000	732	8.77
610	2,000	704	8.38
1,524	5,000	626	7.49
3,048	10,000	516	6.11

* Values in mg/L for water-saturated air from *Standard Methods*.[7]
† Height above mean sea level.

decreases fairly rapidly with elevation. Consequently, O_2 solubility varies significantly with elevation (Table 12.2). For example, at 20°C, the solubility at 3,000 m (~10,000 ft) is only two-thirds that at sea level.

The solubility of O_2 in water has been determined many times, starting with the measurements of Winkler[8] in 1889–1891 and Fox[9] in 1909, which were the standard values until measurements by Truesdale et al.[10] in 1955 cast doubt on their accuracy. Subsequent studies (e.g., see Carpenter[11] and Murray and Riley[12]) showed that the Truesdale et al. data were flawed, and a careful analysis of those data sets by Weiss[13] yielded values that are widely used today.[14] A polynomial equation was developed by Weiss to calculate O_2 solubility (at sea level) at any temperature and salinity:

$$\ln DO = A_1 + A_2(100/T) + A_3 \ln(T/100)$$
$$+ A_4(T/100) + S \times [B_1 + B_2(T/100) + B_3(T/100)^2], \qquad (12.6)$$

where DO is in mL/L; $A_1 = -173.429$; $A_2 = 249.634$; $A_3 = 143.348$; $A_4 = -21.849$; $B_1 = -0.03310$; $B_2 = 0.01426$; and $B_3 = -0.00170$; T is temperature (K), and S is salinity (g/kg). To convert from units of mL/L to mg/L the former are multiplied by 1.4276. The most accurate data on O_2 solubility today are those of Benson and Krause,[15] who reported data for the temperature range of 0–60°C to three decimal places and an accuracy of ~0.02%, about a factor of 5–10 times better than previous data. Their results are tabulated in *Standard Methods*[7] and are in close agreement with the values of Weiss; over the range of 0–30°C, the two sets consistently are within 0.02 mg/L. Given uncertainties in ambient conditions (e.g., barometric pressure and relative humidity) that affect O_2 solubility and that fact that such factors vary on timescales shorter than that needed for surface waters to reach equilibrium with the atmosphere, the practical

significance of these differences is inconsequential. An alternative polynomial equation presented by Benson and Krause for DO solubility (in mg/L) as a function of temperature (in °C) in freshwaters is

$$\ln S_{O_2}(mg/L) = 139.34410 + (1.575701 \times 10^5/T) + (6.642308 \times 10^7/T^2)$$
$$+ (1.243800 \times 10^{10}/T^3). \tag{12.7}$$

12.3.2 Gas transfer kinetics

O_2 transfer from air to unsaturated water is called reaeration, and transfer from supersaturated solutions to air is called deaeration, degassing, or volatilization. Both processes are described by the same first-order expression, in which the rate of change in gas concentration in water depends on the difference between its actual concentration, [C], in water and its saturation value, $[C]_s$:

$$\frac{d[C]}{dt} = \frac{K_L A}{V}([C]_s - [C]), \tag{12.8}$$

where K_L is the gas transfer coefficient (units of length time^{-1}; e.g., m s^{-1}); A is the surface area of the water body and V is its volume. Note that the units of K_L are the same as velocity (length time^{-1}), and they often are referred to as a "piston velocity." For a given water body, $A/V = 1/\bar{z}$, where $\bar{z}$ = mean depth. The quantity $([C]_s - [C])$ can be denoted as D, the deficit of the gas relative to saturation. (If $[C] > [C]_s$, D is < 0, the water is supersaturated, and gas transfer is from water to air.) Thus, Eq. 12.8 can be rewritten as

$$\frac{d[C]}{dt} = -\frac{dD}{dt} = \frac{K_L}{\bar{z}}D = k_g D, \tag{12.9}$$

where $k_g = K_L/\bar{z}$ is a first-order rate constant (units of t^{-1}). The integrated form of Eqs. 12.8 and 12.9 is

$$\ln \frac{[C]_t - [C]_s}{[C]_0 - [C]_s} = -\ln \frac{D}{D_0} = k_g t. \tag{12.10}$$

The apparent simplicity of Eq. 12.10 is misleading, however, in that the value of the gas transfer coefficient (k_g or $K_L/\bar{z}$) depends on physical conditions, such as wind, wave conditions, and water flow velocity, the effects of which on k_g are difficult to quantify. For rough calculations, published values (Table 12.3) applicable to various kinds of water bodies can be used, but it is apparent from the table that considerable uncertainty results from using such values.

Parameterization of k_g requires a more mechanistic understanding of O_2 transfer than the equations given above provide. A long-standing model for gas transfer is the two-film model developed by Lewis and Whitman[17] in the 1920s. Figure 12.4 illustrates the essential features of the model, which is based on four assumptions:[18] (1) gas transfer in the bulk gas and liquid phases is rapid and controlled by turbulent mixing; (2) transfer through gas and liquid films at the surface is slow (rate limiting) and proceeds by

Table 12.3 Ranges of k_g for various water bodies*

Water body	Range of k_g for O_2 at 20°C $(day^{-1})^{\dagger}$
Small ponds	0.10–0.23
Small, slow streams, large lakes	0.23–0.35
Large, slow streams	0.35–0.46
Large rivers	0.46–0.69
Rapid streams	0.69–1.15
Rapids and waterfalls	> 1.15

*Summarized from Tchobanoglous and Schroeder.[16]
† For other temperatures, $k_{g(T)} \approx k_{g(20)} * 1.024^{(T-20)}$.
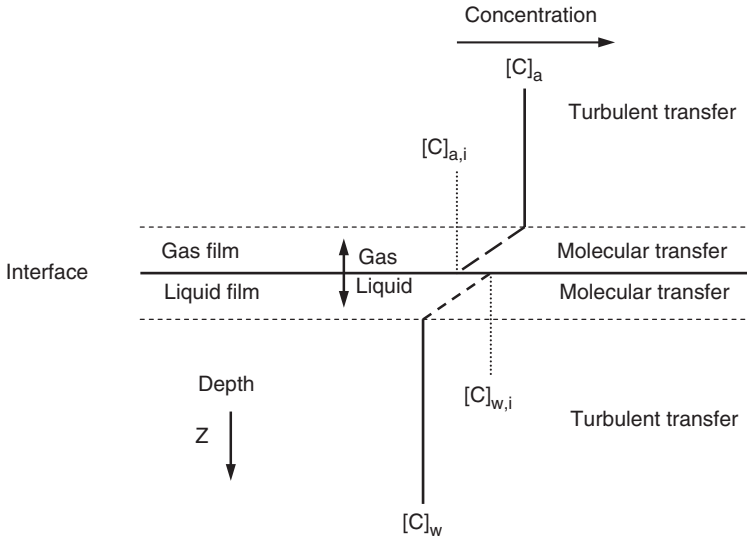
Figure 12.4 Diagram showing essential features of the two-film model for gas transfer.

molecular diffusion (i.e., Fick's law); (3) gas- and liquid-phase concentrations at the interface are assumed to be at equilibrium and defined by Henry's law; and (4) the process is assumed to be at steady state. These assumptions lead to the following expression for the flux of gas across an air-water interface:

$$F = \frac{k_l k_g}{k_l/H + k_g}\left\{\frac{[C]_a}{H} - [C]_w\right\} = K_L\left\{\frac{[C]_a}{H} - [C]_w\right\}, \qquad (12.11)$$

where F is the gas flux (e.g., concentration area^{-1} time^{-1}) across the interface, i.e., from air to water; k_l and k_g are transfer coefficients for the liquid and gas film,

respectively; H is the dimensionless Henry's law constant for the gas of interest; and K_L is defined as

$$\frac{1}{K_L} = \frac{1}{k_l} + \frac{1}{Hk_g},$$ (12.12)

where K_L, k_l, and k_g all have the same (velocity) units. If the gas concentration in air is expressed in pressure, the term RT is added to the numerator of the second term in Eq. 12.12. To convert from flux to change in concentration in the water phase, $(-d[C]_w/dt)$, the left side of Eq. 12.11 is multiplied by A/V (or $1/\overline{z}$). For a given gas, transport through the liquid film may be rate limiting ($k_l \ll k_g$), transfer through the gas film may be limiting ($k_l \gg k_g$), or both may control ($k_l \approx k_g$). Liquid-film control occurs for nonreactive gases such as the major constituents of air (O_2, N_2, Ar); in general, substances diffuse through a gas phase much faster than through a liquid phase of comparable thickness. Gas-film control occurs for reactive gases like NH_3. For such gases, chemical reaction to form another species (e.g., NH_4^+) occurs so rapidly at the air-water interface that the thickness of the liquid diffusion layer (film) is greatly decreased. Conversion of the gas to a nonvolatile form also increases the difference between the interfacial concentration and the equilibrium concentration in the bulk solution. The net effect is to increase the diffusional flux in the liquid film. According to Fick's law, $F = -D_i(\Delta C/\Delta z)$, and gas reactivity increases ΔC and decreases Δz.

There are several troublesome features of the two-film model. First, the idea that steady-state conditions apply at the interface is unrealistic; turbulence is characterized by non-steady conditions, both at large scales (e.g., winds typically have gusts) and smaller scales associated with the air-water interface. Second, it is very difficult to imagine that liquid and gas films can persist on a wind-swept lake or river, where the surface is in continuous motion. Several models have been developed to overcome the limitations of the two-film model. The most common of these is the surface renewal model,[19,20] in which packets of water reside at the interface for varying lengths of time (a Gaussian distribution was assumed in the original version of the surface renewal model) allowing varying amounts of diffusion into the liquid film to occur. The newer, more realistic models lead to the same basic form of transfer equation as the two-film model, but they yield different functional relationships for K_L. For example, K_L in the two-film model scales across different gases in proportion to their molecular diffusion coefficients, D_i, but in the surface renewal model scaling is related to the square root of the reciprocal Schmidt number, Sc, an important parameter in chemical engineering: $K_L \propto (D_i/\nu)^{1/2} = Sc^{-1/2}$, where ν is kinematic viscosity ($m^2\ s^{-1}$).

Wind is a dominant physical factor affecting K_L in lakes and the oceans and is important even in flowing waters, especially large rivers. Many workers thus have developed predictive relationships between wind speed and K_L. Using results from wind tunnel and lake measurements, Liss and Merlivat[21] divided wind speed into three ranges with linear relationships between K_L and U_{10} (wind velocity at a height of 10 m above the water surface). Slopes of the relationships increase piecewise across the three ranges (Figure 12.5). The first break (at $U_{10} = 3.6\ m\ s^{-1}$ (~8 mph)) is thought to represent the transition from a smooth to a rough surface; the second break
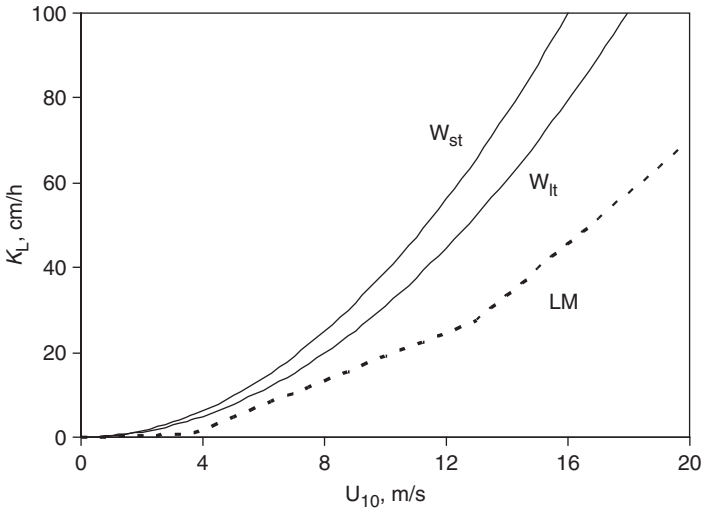
Figure 12.5 Empirical relationships for gas transfer coefficients as a function of wind velocity 10 m above the water surface (U_{10}): LM from Liss and Merlivat[21] based on wind tunnel and field data; W_{lt} from Wanninkhof[23] for long-term (time-averaged) values of U_{10}; W_{st} from Wanninkhof[23] for short-term or instantaneous measurements of U_{10}. Values normalized to Schmidt number, Sc, = 600.

(at $U_{10} = 13$ m s^{-1} (~29 mph)) is thought to represent the transition from a rough surface to breaking waves. It is apparent from the figure that K_L is quite low in the range for smooth surfaces and not very dependent on U_{10} compared with values in the higher ranges.

Based on an analysis of CO_2 gas transfer data for the oceans and for lakes, Wanninkhof and colleagues[22,23] developed quadratic expressions for $K_{L,i}$ for any gas i of the form

$$K_{L,i} = AU_{10}^2 \left(\frac{Sc_i}{660} \right)^{-0.5}, \tag{12.13}$$

where A is an empirical constant that depends on the timescale over which the wind measurements apply, Sc_i is the Schmidt number for gas i, and the factor 660 is the Schmidt number for CO_2 in seawater at 20°C. In freshwater at 20°C, Sc = 600 for CO_2 and 589 for O_2. A has a value of 0.39 for the long-term (time-averaged) wind conditions needed in some field techniques that require timescales of days to measure K_L, and C = 0.31 for short-term or constant wind conditions. When the former value is used, K_L and U_{10} represent long-term (time-averaged) values. Unfortunately, many relationships like those in Figure 12.5 exist in the literature, and differences in predicted values among them are considerable (e.g., see Wanninkhof[23]). Consequently, estimating air-water oxygen transfer rates under field conditions still is subject to much uncertainty.[24]

12.4 Spatial and temporal patterns of DO in natural waters

Much can be learned about surface water bodies by examining temporal and spatial variations in DO. Inferences about water quality, metabolic conditions and chemistry all can be made from appropriately gathered DO data. In this section we describe patterns and profiles of DO in lakes and streams and discuss how they can be interpreted, in some cases quantitatively.

12.4.1 Biological processes affecting DO

Primary production and respiration are the main biological processes affecting DO concentrations in surface waters. The basic equation for these processes is

$$CO_2 + H_2O \underset{R}{\overset{P}{\rightleftharpoons}} CH_2O + O_2, \tag{12.14}$$
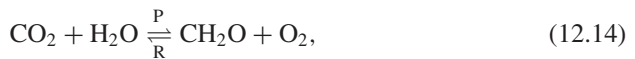
where P stands for primary production and R for respiration; CH_2O is a generic representation of organic matter. Equation 12.14 suggests that P may be measured by the decrease in CO_2 or increase in organic matter or O_2, and respiration may be measured by the decrease in O_2 or organic matter or increase in CO_2. Not all these possibilities are convenient, however. Primary production the oceans and lakes usually is measured by adding ^{14}C tracer in the form HCO_3^- to a sample and determining the amount of ^{14}C incorporated into particulate matter or "seston" after incubation in the light. P and R also can be measured in terms of O_2 changes. The difference between the initial DO and that after incubation in the light gives the net planktonic primary production (NP) in oxygen equivalents. The difference between an initial value and a sample incubated in the dark yields the oxygen equivalents of respiration (R). The difference between the DO in a light bottle (LB) and a dark bottle (DB) after incubation provides the oxygen equivalents of gross primary production (GP). Thus we can write

$$
\begin{aligned}
NP &= LB - IB, \\
R &= IB - DB, \\
GP &= LB - DB = NP + R.
\end{aligned}
\tag{12.15}
$$

In nutrient-rich, biologically productive waters, DO changes of several tenths of a mg/L may occur in incubations of a few hours, but in oligotrophic waters the changes are too small to detect without much longer incubations. In these cases ^{14}C methods are preferred. Conversion from oxygen equivalents of P or R to carbon equivalents requires knowledge of the stoichiometry of the reactions, but as a rough estimate one can assume a one-to-one correspondence of O_2 produced to CO_2 reduced to organic matter.

Although all organisms—plants, animals, microorganisms—respire, of special interest to environmental engineers is the microbial respiration of biodegradable organic matter dissolved or suspended in water and wastewater. This is called biochemical oxygen demand (BOD) and is the major sink for O_2 in many water bodies. BOD, a

classic measure of water quality, is determined by incubating samples in the dark at 20°C and measuring the loss of O_2 versus time. The O_2 consumed over a 5-day incubation (BOD_5) often is used in wastewater treatment studies, but this value gives incomplete information about the total amount of O_2-demanding organic matter in a sample. BOD exertion is modeled as a first-order process:

$$y = L_0\{1 - \exp(-k_1 t)\}, \qquad (12.16)$$

where y is the measured amount of O_2 consumed (BOD exerted) at time t; L_0 is the ultimate first-stage (or carbonaceous) BOD, which is equivalent to the initial concentration of biodegradable organic matter; and k_1 is a first order rate constant for BOD exertion. Today, L_0 and k_1 are fitted to the BOD equation by nonlinear least squares procedures, but before these became widely available (only about 20 years ago) engineers had devised several approximation methods to estimate L_0 and k_1 from measured values of y.[25] The value of k_1 varies depending on the lability (ease of degradation) of organic matter, but typical values for wastewater are in the range 0.1–0.3 day^{-1}. Nitrification (microbial oxidation of NH_4^+ to NO_3^-) also exerts an oxygen demand called nitrogenous BOD. This is treated as a separate process because nitrification tends to be very slow until most carbonaceous BOD has been exerted.

12.4.2 Lakes

Two timescales are of interest for DO in lakes: short term (hours-days) and long term (seasonal-annual). Vertical variations in DO are especially informative of a lake's metabolism. DO changes in the photic zone over the scale of hours are used to estimate rates of P and R. The annual cycle of DO vertical profiles is of interest in lakes that undergo seasonal temperature stratification (Box 12.1). In many such lakes, DO becomes severely or completely depleted in the hypolimnion during summer because the oxygen demand of settling organic particles and bottom sediments exceeds the O_2 supply present when the water becomes isolated from the surface. The DO profiles in Figure 12.6 describe such a situation. The onset of anoxia in the hypolimnion has obvious implications for all types of biota and important effects on water and sediment chemistry. As described in Figure 12.1, anoxia results in gradual loss of nitrate and increased concentrations of ammonium, soluble (reduced) Fe and Mn, sulfide, and methane. In addition, the ferric (hydr)oxide floc that may coat the sediment surface becomes reduced, releasing phosphate into the overlying water. Oxygen depletion also can occur during winter ice cover (Figure 12.6) even though cold temperatures decrease rates of biological and chemical activity.

   In oligotrophic lakes, a metalimnetic DO maximum may occur in summer as a result of phytoplankton growth. The increase in DO over time at 5–7 m in Little Rock Lake (Figure 12.6) illustrates this phenomenon, and maximum levels of chlorophyll also were found at these depths. Light inhibition and nutrient depletion in clear surface waters often limit plankton growth, making water at mid-depth more optimal for plant growth. A wide variety of patterns in DO vertical profiles occurs in lakes and the oceans, reflecting the diversity of these aquatic environments; examples are available elsewhere.[26,27]

Box 12.1 Seasonal patterns of temperature structure in lakes

Many lakes exhibit annual cycles of vertical temperature structure caused by seasonal changes in solar heating. In cool temperate latitudes, lakes have two periods of thermal stratification—in summer and under ice in winter—and two periods (in spring and fall) when the lake is well mixed; such lakes are called *dimictic*. These patterns (Figure 12.6) have important effects on the distribution of DO and related redox-sensitive species. Here we summarize important features of seasonal temperature structure with reference to Figure 12.6.

Starting at near-freezing temperatures after ice-out in spring, solar radiation warms the water from the surface downward. Initially, vertical differences in temperature and density are small, and winds keep the lake mixed as it warms. Eventually, the surface water warms rapidly enough that density differences with cooler water below inhibit vertical mixing, and stable temperature stratification begins. At this point the lake becomes divided into three layers: a warm, well-mixed, nearly isothermal surface layer, the *epilimnion*; a layer of rapid temperature change, the *thermocline* or *metalimnion*; and a bottom layer of colder water, the *hypolimnion*, which is isolated from the epilimnion and atmosphere. The three layers persist until *fall overturn*. Over the summer, the epilimnion becomes deeper and the thermocline more sharply defined. As days get shorter and cooler in late summer and fall, the epilimnion cools and continues to deepen. Eventually, the temperature/density difference with the small hypolimnion becomes sufficiently small that winds break down the thermal structure, and the lake becomes mixed from top to bottom. This condition persists as the water cools to its maximum density at 4°C. With increasingly colder weather, further cooling of the surface water to 0°C leads to weak "inverse stratification"—so-called because the surface water is colder but less dense than the bottom water. When ice cover forms, in November or December, the lack of wind-induced turbulence allows the weak inverse stratification to be maintained until ice-out in spring, when the temperature cycle begins anew.

In warm climates, ice cover does not occur, and the annual cycle consists of a period of stratification during summer and parts of spring and fall and a period of mixing in winter and parts of spring and fall, depending on latitude. Such lakes are called *monomictic*. Lakes whose surface area to depth ratio is too large to allow stable thermal stratification may stratify for short time periods depending on weather. Such lakes are called *polymictic*. Variations of these patterns also exist, reflecting the diversity of environments in which lakes occur.[26,27]

12.4.3 Rivers and streams

Short-term (hourly to daily) changes in DO concentrations can be used to estimate whole-ecosystem metabolism (i.e., primary production and respiration) in flowing waters, as exemplified by the classic studies of Odum[28,29] on Florida springs (Figure 12.7). Because much of the plant life in shallow streams is either attached to surfaces (periphyton) or consists of submerged macroscopic plants, bottle incubations, which measure only
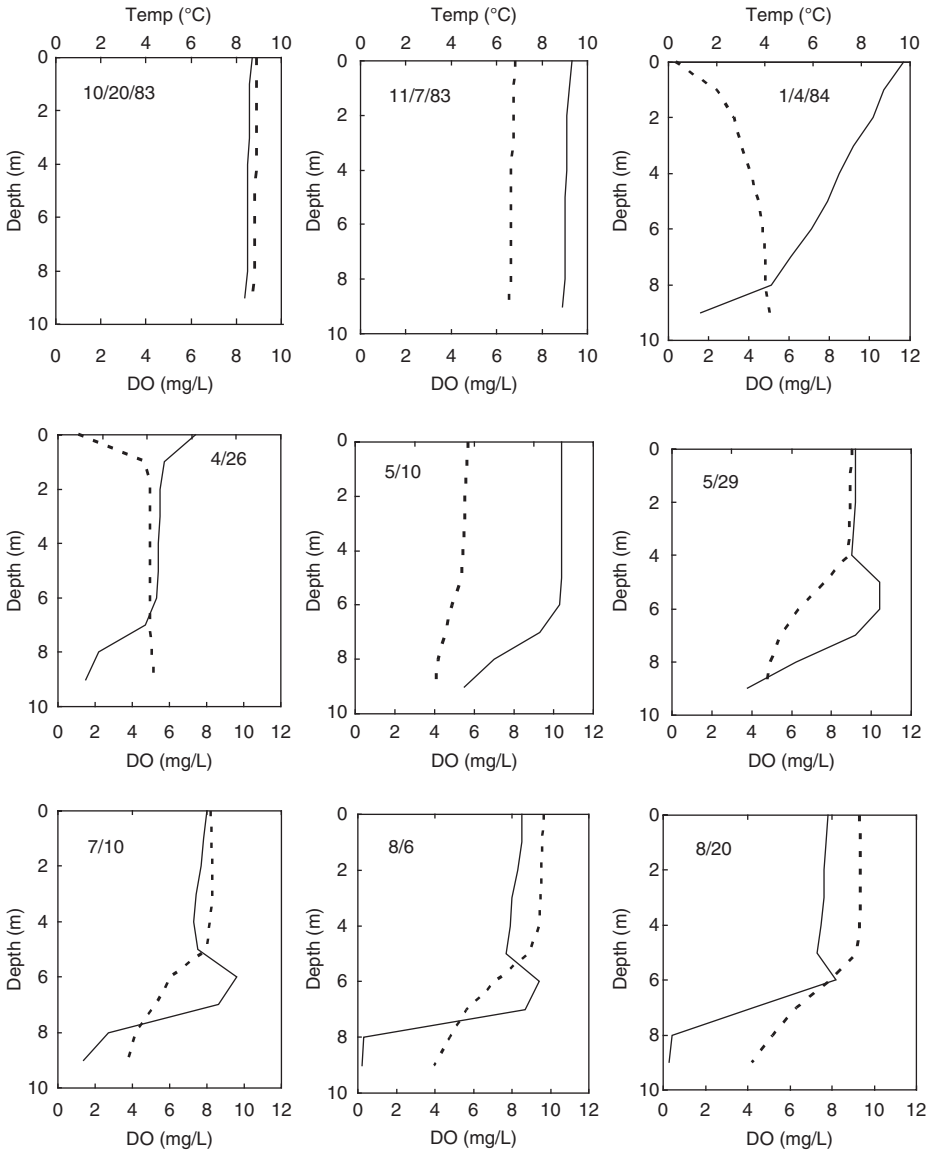
Figure 12.6 Vertical profiles of temperature (dashed lines) and DO (solid lines) in the north basin of Little Rock Lake (Vilas County), Wisconsin, for water year 1984 (October 1983 to the beginning of October 1984). Unpublished data courtesy of T. Kratz, University of Wisconsin-Madison Trout Lake Station.
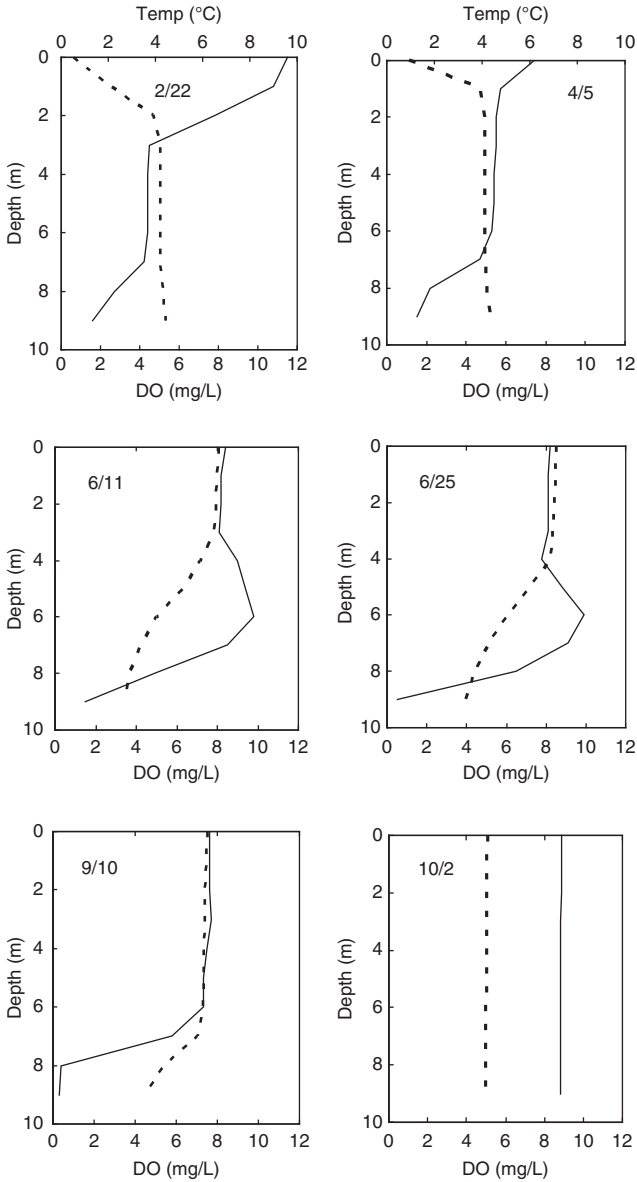
Figure 12.6 Cont'd

planktonic production, are not very useful in streams. A disadvantage of such whole-body approaches is that gas transfer between the atmosphere and water also affects the DO concentration (unless the water is precisely at saturation, which is unlikely), and losses or gains in DO from reaeration or degassing must be taken into account. As described above, oxygen transfer coefficients depend on water surface and wind conditions, adding uncertainty to stream metabolism calculations. The use of tracers like SF_6 can help in estimating more accurate site- and time-specific gas transfer coefficients.[24,30]

Figure 12.7 Estimation of aquatic ecosystem metabolism in a flowing stream—primary production, P, and respiration, R—from diurnal DO measurements. Top: measured DO ~1 km downstream from the stream source, a large spring (left ordinate) and difference (ΔC) between measured DO and constant DO of 2.5 mg/L at spring source (right ordinate). Middle: Accr. = DO accrual (mg/L) at the measurement site from more oxygenated side springs; Resp. = respiration (mg/L) measured in darkened bell jars; Reaer. = DO contribution from reaeration, based on the O_2 deficit and an estimated gas transfer coefficient. Bottom: primary production (P) calculated from ΔC corrected for Accr., Resp., and Reaer.: P = ΔC − Accr. − Reaer. + Resp. Based on a figure in Odum[28] for Silver Springs, Florida, but using hypothetical data.
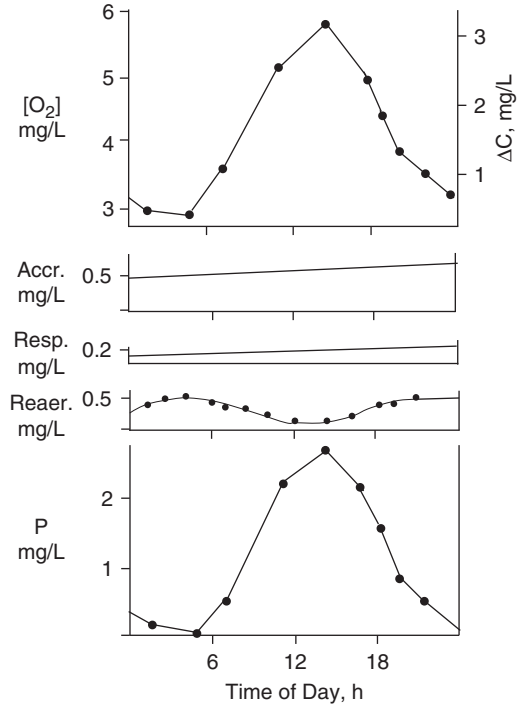
Longitudinal distributions of DO and other water quality characteristics also serve as a surrogate for temporal variations in flowing waters. This concept is useful in rivers and streams with point sources of oxygen demand, e.g., "BOD" from wastewater treatment plant outfalls. If the point-source discharge is relatively constant on a scale of hours to a few days, such that steady-state conditions apply, and if longitudinal mixing is small such that plug-flow conditions apply (see Section 5.4.4), a typical "oxygen sag" curve is established in the river (Figure 12.8), and the DO pattern can be modeled mathematically by the classic Streeter-Phelps equation[31] or one of its derivatives (see Box 12.2).

Of interest regarding the oxygen sag model are the maximum deficit, called D_c, occurring downstream from the point source, and the time of travel (t_c) or distance (x_c) at which this occurs. D_c can be obtained by setting Eq. (2) of Box 12.2 to zero; i.e., D_c occurs when $dD/dt = 0$:

$$D_c = \frac{k_1 L_0}{k_2} \exp(-k_1 t_c) \qquad (12.17)$$

To use Eq. 12.17, we must know the critical time, t_c. This is obtained by differentiating Eq. (3) of Box 12.2, setting the result to zero, and solving for t_c:

$$t_c = \frac{1}{k_2 - k_1} \ln\left[\frac{k_2}{k_1}\left(1 - D_0 \frac{k_2 - k_1}{k_1 L_0} \right) \right] \qquad (12.18)$$

Thus, once we obtain t_c from Eq. 12.18, D_c can be calculated from Eq. 12.17.
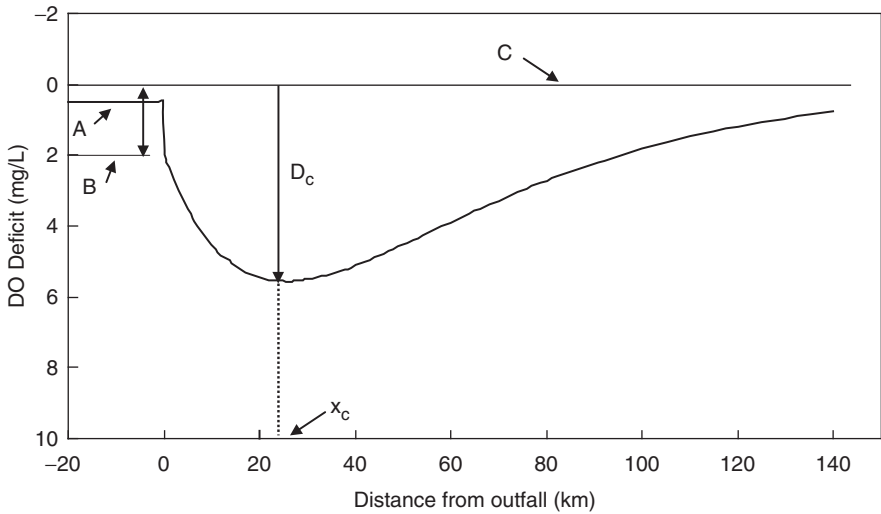
Figure 12.8 Hypothetical oxygen sag curve for a stream receiving a point discharge of BOD. Curve was calculated in Excel using equation (4) of Box 12.2 and the following parameter values: $L_0 = 20$ mg/L; $D_0 = 2$ mg/L; $k_1 = 0.3$ day^{-1}; $k_2 = 0.6$ day^{-1}; v = 0.15 m/s (13 km/day). Line A = DO deficit in stream prior to outfall; line B = initial deficit at outfall; line C = saturation concentration (D = 0) at stream temperature after addition of wastewater.

DO concentrations in the Mississippi River near Minneapolis-St. Paul, Minnesota, during much of the twentieth century (Figure 12.9) show a longitudinal pattern indicative of the oxygen sag curve, and the changes in the pattern over time reflect the positive impacts of improved wastewater treatment on water quality in the river.[32] Today, this stretch of the river fully meets DO standards, even in low-flow conditions, when effluent represents a significant fraction of the river flow. The river also supports an abundant and diverse community of fish, including many game species, but this positive circumstance is tempered by the fact that the fish are contaminated by mercury, PCBs, and possibly other pollutants, such as endocrine disruptors, which has led to the issuance of consumption advisories by public health agencies.

12.5 Analysis of DO

12.5.1 The Winkler method

By far, the oldest analytical method for DO is the Winkler iodometric titration. Developed by a Hungarian chemist, Lajos Winkler, as part of his Ph.D. dissertation in 1888,[33] the Winkler method is still the "gold standard" to which more recent instrumental methods are calibrated. In brief, the method involves conversion of DO to an equivalent amount of iodine through an intermediate step involving Mn^{II} oxidation to Mn^{IV} by O_2 and subsequent reduction of Mn^{IV} by iodide. The iodine is quantified by titration with thiosulfate.

Box 12.2   A model for DO in streams

Stripped to the essentials, O_2 concentrations in streams receiving point sources of O_2-demanding organic matter (Figure 12.8) depend on two rate processes— O_2 consumption by microbial oxidation of the organic matter and atmospheric reaeration. Both processes can be described by first order rate equations: the rate of microbial O_2 consumption is proportional the concentration of oxygen-demanding organic matter, L, and the reaeration rate is proportional to the difference between the solubility of O_2 and its concentration in the water. If we assume plug-flow behavior in the stream, the resulting equation is

$$(1) \quad -\frac{d[O_2]}{dx} = \frac{k_1}{v}L - \frac{k_2}{v}(C_s - C),$$

where k_1 (t^{-1}) is the rate constant for microbial oxygen consumption; x is the distance along the stream; v is the stream velocity (assumed constant); L is the concentration of O_2-demanding organic matter remaining at any time; k_2 is the rate constant for reaeration (t^{-1}); C_s is the saturation concentration of O_2 in the water; and C is the actual concentration. Equation (1) cannot be integrated as written, but if we (i) let $C_s - C = D$, the "oxygen deficit,; (ii) note that x = vt (distance = velocity × time), and (iii) recognize that $-d[O_2]/dt = dD/dt$, we can rewrite Eq. (1) as

$$(2) \quad \frac{dD}{dt} = k_1 L_0 \exp(-k_1 t) - k_2 D,$$

which integrates to

$$(3) \quad D_t = \frac{k_1 L_0}{k_2 - k_1} \{\exp(-k_1 t) - \exp(-k_2 t) + D_0 \exp(-k_2 t),$$

or

$$(4) \quad D_x = \frac{k_1 L_0}{k_2 - k_1} \left\{ \exp\left(-k_1 \frac{x}{v}\right) - \exp\left(-k_2 \frac{x}{v}\right) + D_0 \exp\left(-k_2 \frac{x}{v}\right) \right\},$$

where D_t and D_x are the O_2 deficit at time t or distance x downstream from the entry of a point source of O_2-demanding organic matter having an initial concentration (in the stream) of L_0. Equations (1)–(4) are forms of the "oxygen-sag model" for rivers and streams. Developed by Streeter and Phelps in 1925,[31] the model is of historical relevance as the first water quality model. It is the starting point for later, more complicated DO models and the forerunner for all water quality models used to predict pollutant concentrations in surface waters.

Many variations on the basic method have been developed over the past 120 years, some to overcome chemical interferences, others to adapt the method for special needs. In some published modifications the iodine is measured colorimetrically rather than by titration, but titration methods are the most widely used. *Standard Methods*[7] describes five variations on the basic procedure in its current edition. The most common, the
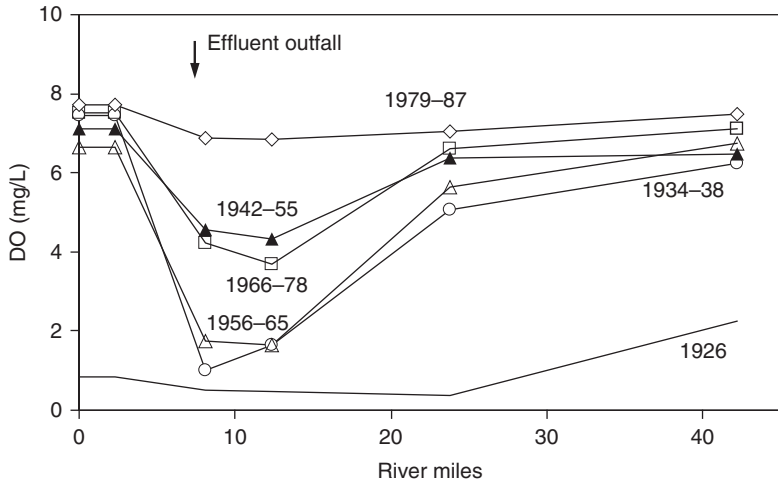
Figure 12.9 Profiles of DO in the Mississippi River near Minneapolis-St. Paul, Minnesota, for various periods of the twentieth century show the classic oxygen sag curve. River mile 0 is in downtown St. Paul; effluent from the main wastewater treatment plant for the urban region is added to the river 2.3 miles downstream. Data were not available at the outfall and DO concentrations at the upstream monitoring site were assumed to hold constant to the outfall. Drawn from data in Johnson and Aasen.[32]

Alsterberg-azide modification, is designed to eliminate potential interference from nitrite and is described below.

The Winkler procedure involves four redox reactions plus a color indicator reaction and uses three reagents plus the titrant and endpoint indicator:

Reaction	Reagents
$\begin{bmatrix} \text{1. } Mn^{2+} + 2OH^- \rightarrow Mn(OH)_{2(s)}(\text{white precipitate}) \\ \text{2. } Mn(OH)_{2(s)} + 0.5O_2 \rightarrow MnO(OH)_{2(s)}(\text{brown precipitate}) \end{bmatrix}$	(1) $MnSO_4$; (2) alkali-azide-iodide
3. $MnO(OH)_{2(s)} + 4H^+ + 3I^- \rightarrow Mn^{2+} + I_3^- + 3H_2O$	(3) concentrated H_2SO_4
4. $I_3^- + 2S_2O_3^{2-} \rightarrow 3I^- + S_4O_6^{2-}$	(4) 0.025 N $Na_2S_2O_3$ (titrant); (5) starch
5. $I_2 + \text{starch} \rightleftharpoons \text{starch-}I_2 \text{ blue complex (color indicator)}$	

The first two reagents are added in the field as soon as samples are collected (Figure 12.10).* Reagent (2) is a solution of strong base (~50% NaOH), sodium azide, and potassium iodide, and it makes the sample highly alkaline. As soon as this reagent and

---

*Our focus is on the chemistry of the procedure rather than physical details of processing samples for DO analysis, but we note that samples must be collected in a way to avoid contact with the atmosphere. This is done by using a submersible pump or cylindrical water samplers (Van Dorn or Kemmerer samplers; see Figure 12.10a,b) that are open on both ends and lowered on a graduated line to the desired depth. They are closed by releasing a weighted "messenger" and hauled to the surface. Water is transferred from the sampler into a special 300-mL glass "DO bottle" (Figure 12.10c) by plastic tubing, and the bottle is overfilled to flush out water that was in contact with the atmosphere when the bottle was being filled. DO bottles have tapered ground-glass stoppers to prevent entrainment of air bubbles when they are sealed.
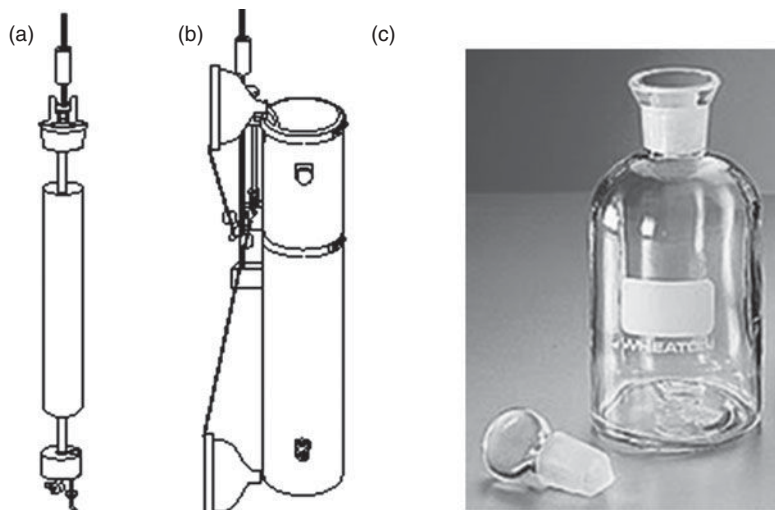
Figure 12.10 Sampling equipment for DO: (a) Kemmerer sampler and (b) Van Dorn sampler used to collect uncontaminated samples at depth in the water column; (c) 300 mL DO glass bottle; note the tapered stopper to minimize contamination by air bubbles.

the $MnSO_4$ are added to a sample, reactions 1 and 2 occur simultaneously. If the sample has no oxygen, only $Mn(OH)_2$ is formed, and the resulting flocculent precipitate is white. If oxygen is present, reaction 2 occurs, and the precipitate has varying shades of brown depending on the oxygen concentration. This step converts $O_{2(aq)}$ to an equivalent amount of oxidized Mn precipitate, which settles to the bottom of the bottle and is relatively stable and safe from contamination by atmospheric O_2. The third step, addition of concentrated sulfuric acid, makes the sample highly acidic, which facilitates reaction 3—oxidation of iodide to iodine and reduction of Mn^{IV} oxyhydroxide back to soluble Mn^{2+}. This step is carried out immediately before the titration step to minimize extraneous reactions of I^- and I_2 with other oxidizing or reducing agents in the sample. The former can react with I^- to form more I_2; the latter (e.g., natural organic matter) can reduce I_2 and produce a negative interference. Enough iodide is added in reagent (2) to ensure that all the Mn^{IV} generated from $O_{2(aq)}$ in the sample is reduced back to Mn^{2+} and also to ensure that the generated I_2 reacts with excess I^- to form the stable tri-iodide complex, I_3^- (I_2 + $I^- \rightleftharpoons I_3^-$). This prevents I_2 loss by volatilization during the titration step. When the sulfuric acid is added, the azide added in reagent (2) destroys any nitrite present in the sample:

$$HN_3 + HNO_2 \rightarrow N_2 + N_2O + H_2O$$
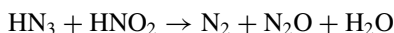
This is important because under acidic conditions nitrite acts in a cyclic (essentially catalytic) fashion to produce I_2; i.e., it is a positive interference:

$$2HNO_2 + 2H^+ + 2I^- \rightarrow 2H_2O + N_2O_2 + I_2$$

$$N_2O_2 + H_2O + \tfrac{1}{2}O_2 \rightarrow 2HNO_2$$
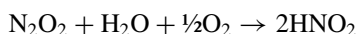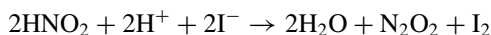
Oxidation of N_2O_2 to HNO_2 by molecular oxygen is relatively slow, and so the interference becomes a larger issue if the titration is delayed after acid addition occurs.

The titration step reduces I_2 to iodide and oxidizes the thiosulfate titrant to tetrathionate ion ($S_4O_6^{2-}$). The endpoint is detected by adding a small amount of starch to the flask just prior to the endpoint. Starch and iodine form an intensely blue colored complex by weak (easily reversible) interactions of I_2 molecules with –OH groups in the coiled glucose polymers. At high concentrations I_2 binding tends to become irreversible, and some oxidation of starch occurs; for this reason starch is not added until near the endpoint—when the solution reaches a pale "straw yellow" color. The endpoint is very sharp; the solution goes from light blue to completely colorless with the last drop of titrant. With reasonable care the regular Winkler procedure can yield accuracies and precision of $\pm\ 0.05$ mg/L (1.6 μM).

Although the Winkler method has been replaced for routine field studies by faster and simpler instrument techniques described in the next sections, it still is widely when highly accurate or precise measurements are needed (e.g., in studies on primary productivity and microbial respiration, especially in oligotrophic environments), and it is commonly used to calibrate the instrumental methods.

12.5.2 Electrode methods for DO

The electrode technique to measure DO was invented by Clark in 1953.[34] Its original purpose was to measure oxygen concentrations in human blood, but the devices were modified for use in natural waters by the early 1960s, and "DO probes," as they commonly are called, gradually came to replace the Winkler method for routine water quality monitoring. Many variations on Clark's design, including micro-probes that can measure DO concentrations in biofilms, have been developed and are available commercially.

Electrometric analysis of O_2 is based on the measurement of current produced when O_2 is reduced at the cathode of an electrode pair (cell) imbedded in plastic and covered by a thin membrane (Figure 12.11). A KCl solution inside the membrane provides electrical
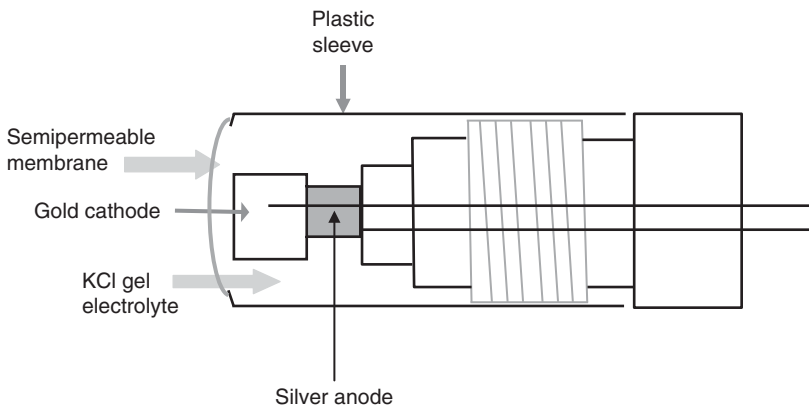
Figure 12.11 Schematic of a Clark-type amperometric electrode for O_2.

contact between the electrodes. The membrane is permeable to gases like oxygen but not to ions. A voltage difference ($\sim$800 mV) is applied such that electrons flow from the cathode to reduce O_2 to H_2O. O_2 consumption at the cathode establishes a concentration gradient between the external solution and the sensor interior causing O_2 to diffuse across the membrane at a rate proportional to the concentration gradient (by Fick's law). If the concentration at the cathode is near zero (a result of rapid reduction), the magnitude of the gradient is proportional to the O_2 concentration in the external solution—or at the solution-side of the membrane. If the solution is well mixed, the concentration at the membrane essentially is the same as the bulk solution concentration.

Clark's original device used a platinum cathode, cellophane membrane, and Ag/AgCl electrode as the anode. Commercial DO probes today use gold or platinum cathodes and silver anodes; KCl in the inner solution causes Ag^+ ions formed at the anode to precipitate as AgCl. Other metals have been used for DO probes, including combinations like lead (anode)/gold (cathode), which produce their own potential (they are galvanic cells) and reduce O_2 without the need to provide a polarizing potential.

Because the membranes of DO probes do not allow redox-sensitive ions to reach the cathode, the probes have few chemical interferences. However, reducible gases like H_2S do penetrate the membranes and poison the electrodes. Convenience aside, DO probes have many shortcomings. The permeability of the membranes and diffusivity of O_2 are temperature dependent. Mixing is an important issue, because the maximum current generated is limited by the rate at which oxygen diffuses through the membrane. Thus, to obtain accurate readings, mixing of the whole solution (which can entrain oxygen and alter the measurement) or mixing near the membrane surface (to minimize the boundary layer and maximize oxygen transfer) is necessary. Some commercial probes have built in stirrers and imbedded thermistors with built-in temperature-compensating algorithms, but variations in temperature still are a source of uncertainty. The accuracy of DO probes is at best a few tenths of a milligram per liter, and precision is similarly modest. Electrode drift and membrane fouling are serious problems when the probes are used for continuous monitoring, especially in biologically rich waters.

12.5.3 Optical methods for DO

Within the past decade optically based solid-state sensors (called ***optodes***) have become commercially available that overcome most of the accuracy and instability problems of electrochemical probes.[35,36] The principle upon which optodes work is luminescence quenching. Complexes of certain heavy metals such as ruthenium, platinum or iridium with organic ligands (e.g., porphyrins) emit red light when excited by blue or blue-green light. The presence of oxygen (O_2) causes a quenching of the luminescence according to the Stern-Volmer relationship (see Chapter 17). Three measurement options can be used to measure this effect: (1) intensity of luminescence, (2) lifetime of luminescence (how quickly it dies out), and (3) phase shift changes—a variation of the lifetime approach in which the excitation light is modulated at a certain frequency (e.g., 5 kHz), and the phase shift of the partially quenched luminescence is detected.[36] Although direct measurement of luminescence intensity is conceptually more straightforward, such measurements are subject to drift, and commercial optodes usually are based on lifetime or phase-shift measurements that require more sophisticated (but readily available) electronics. The sensors are solid-state devices in which the O_2-sensitive "luminophore" (i.e., the
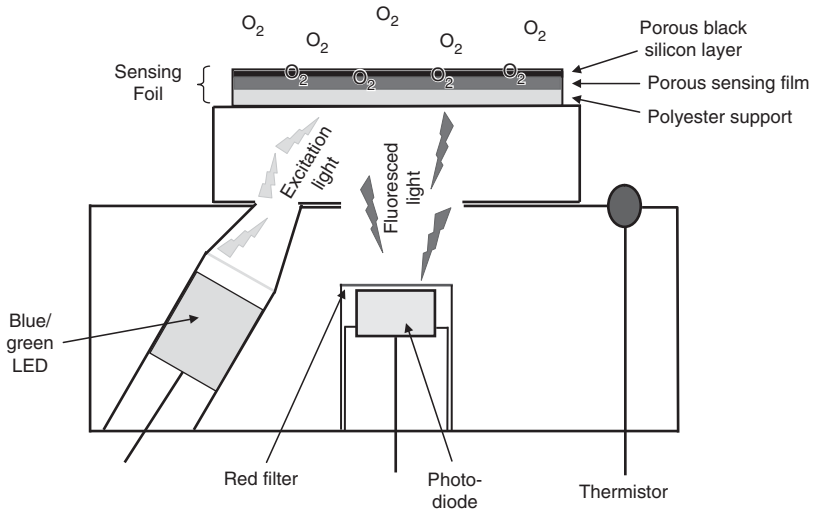
Figure 12.12 Schematic of a typical O_2 optode similar to commercially available optodes of Aanderaa Data Instruments, Bergen, Norway. The three-layer sensing foil contains a gas-permeable black silica layer to minimize stray light reaching the detector, a gas-permeable sensing film containing the luminophore (a fluorescent dye; e.g., an Ru- or Pt-porphyrin complex) embedded in a porous polymer and a polyester support. The source light is a blue-green LED and the photodiode detector is covered with a filter allowing only fluoresced red light to reach the diode. A red LED also may be included in the base for light calibration purposes. (See color insert at end of book for a color version of this figure.)

organically complexed metal) is embedded in a porous polymer matrix (Figure 12.12). In some cases, the foil containing the luminophore is covered by a thin, gas-permeable black silicon layer to minimize interference from ambient light. In contrast to electrode sensors, optodes do not consume O_2, and with proper design their response times are fast ($\leq \sim 1$ s). Reported accuracies of optodes are ± 0.1 mg/L. Because the source and emitted light all are contained within the solid sensor, optical conditions in the water body do not influence measurements, but fouling caused by build-up of biofilms that hinder O_2 diffusion to the sensing surface is a problem for long-term deployments of optodes in natural waters.

The availability of reliable, relatively low-cost DO sensors has enabled environmental scientists and engineers to obtain high frequency DO data under conditions where gathering such data previously was infeasible for reasons of cost, safety or human resource limitations. In turn, this ability has led to the discovery of new phenomena and processes. For example, DO was found to increase during nighttime hours in a small Iowa stream (Figure 12.13a). This curious trend was explained by enhanced rates of reaeration as the stream water cooled (and DO solubility increased) during the night. Nighttime DO increases also have been observed in many lakes where high frequency data collection has been undertaken with buoy-based sensor systems (e.g., Figure 12.13b). Reasons for the increases are still uncertain, but enhanced reaeration caused by higher nighttime wind speeds is a possible explanation. Deployment of stable DO optodes also
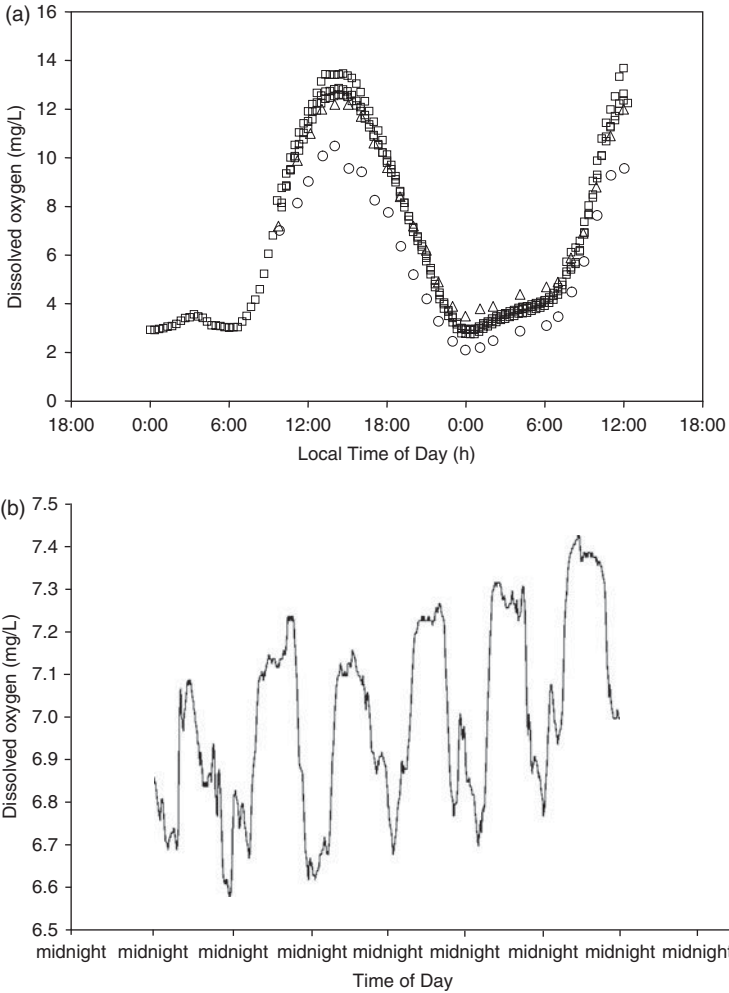
Figure 12.13 (a) High-frequency measurements of DO in a small Iowa stream show peaks during daylight caused by primary production and a consistent nighttime increase starting around midnight. Unpublished data courtesy of J. Schnoor, University of Iowa. (b) Diel oxygen patterns in Sparkling Lake, Wisconsin, showing a consistent secondary increase in DO near midnight. Unpublished data courtesy of T. Kratz, University of Wisconsin-Madison Trout Lake Station. (c) Continuous record of DO in Shingle Creek, Minneapolis, Minnesota, during August 2008 showing large daily variations and violations of state DO standards every night. Unpublished data courtesy of C. Wennen and W. Arnold.
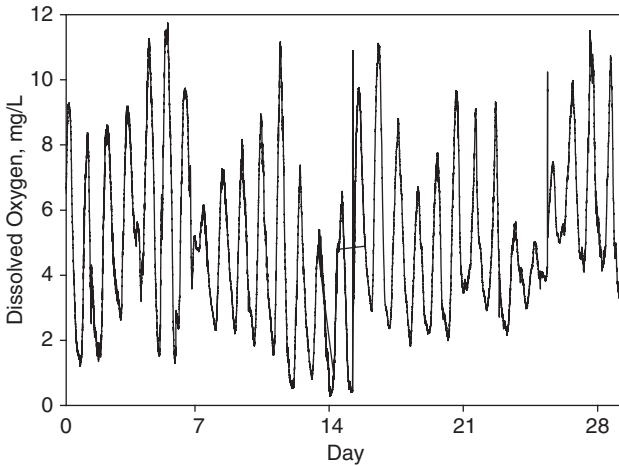
Figure 12.13 Cont'd

enhance opportunities to observe water quality problems in streams and may enhance management approaches. For example, large daily DO variations (far beyond what would be expected from changes in temperature) resulted in nighttime violations of state oxygen standards during low-flow conditions in a small urban stream (Figure 12.13c). The high daily range was attributed to a combination of algal productivity and high sediment oxygen demand. Under typical monitoring protocols (low-frequency, daytime only) necessitated by previous sampling and measurement capabilities, the likelihood of observing these problems would be small.

Problems

12.1. The standard free energy of formation of aqueous methanol, G_f°, is -175.4 kJ/mol.

    (a) Write balanced equations for the oxidation of methanol to water and dissolved carbon dioxide using the following electron acceptor couples: (i) $O_{2(aq)}/H_2O$; (ii) $O_{2(aq)}/H_2O_2$); and (iii) H_2O_2/H_2O.

    (b) Using the data in Table 12.1 calculate ΔG° for each reaction.

    (c) If the methanol concentration in water is 16 mg/L and the pH is 7.0, determine the actual ΔG for each reaction. For $O_{2(aq)}$ assume the water is saturated with respect to atmospheric O_2; for H_2O_2 assume the concentration in the water is 1×10^{-5} M.

12.2. Using information provided in Section 12.2.2, estimate the equilibrium concentration of superoxide radical anion in an oxygen-saturated solution of H_2O_2 at a concentration of 1 μM and pH 7.

12.3. (a) As a field engineer for a consulting firm, you measured the DO concentration in Lake Patagonia, in the Sonoran desert of southern Arizona, and found a value of 7.74 mg/L O_2. The water temperature was 17°C, and

the relative humidity was a typically low 15%. The lake is at an elevation of 3,325 ft above sea level. Determine as accurately as possible whether the oxygen content of the lake water is under or supersaturated with respect to the atmosphere.

(b) If the average wind velocity on the day of sampling was 20 mph and the lake (mean depth of 4 m) was well-mixed thermally, estimate the reaeration coefficient, K_L, and the rate of reaeration.

12.4. The DO concentration in a small pond was found to be 5.2 mg/L at 7 a.m. (near sunrise), and repeated measurements over the day showed a steadily increasing concentration that reached a maximum of 8.3 mg/L at 7 p.m. (near sunset). The water temperature remained constant at 20°C over the day. A sample of pond water taken at 7 a.m. and incubated in a dark bottle for 12 h had a DO content of 3.5 mg/L at 7 p.m.

(a) Estimate the gross and net primary production and respiration rate of the pond water ignoring possible influence of reaeration.

(b) Using the data in Table 12.3 make a first approximation of the effect of reaeration on the values calculated in part (a).

12.5. A microbiologist prepared a growth medium for a bacterial metabolism experiment containing 250 mg of citric acid and 50 mg of NH_4Cl diluted to 1 L. Calculate the ultimate carbonaceous and nitrogenous BOD (in mg/L) of the growth medium.

12.6. A nitrified wastewater effluent has a ultimate carbonaceous BOD of 25 mg/L and enters a receiving water at a constant flow of 20 mgd (million gallons per day).

(a) If the seven-day average 10-year low flow (7Q10) in the stream is 100 cfs (ft^3/s), and the rate coefficient for BOD exertion is 0.15 day^{-1}, is the stream likely to violate the state DO minimum standard of 5.0 mg/L under low-flow conditions? Assume that the stream flow is saturated at the point of the wastewater outfall and that low flow conditions occur during summertime, and do not correct rate coefficients for temperature. Note: you will need to select and justify a value for the reaeration rate coefficient to work this problem.

(b) If the stream velocity is roughly constant at 0.3 ft/s under 7Q10 low-flow conditions in (a), what is the downstream distance at which the minimum DO occurs?

(c) Using a spreadsheet program to solve the Streeter-Phelps equation as a function of time or distance from the outfall and the conditions and results obtained above, develop a graph showing the longitudinal profile of DO in the stream under 7Q10 low-flow conditions.

12.7. (a) Trace the change in oxidation state of the elements involved in the sequence of four reactions shown in Section 12.5.1 for the Winkler determination of DO. How many millimoles of thiosulfate must react in the final step (the titration of I_2 to $2I^-$) for each millimole of O_2 in the original sample?

(b) What is the oxidation state of S in tetrathionate (the product of the I_2-thiosulfate reaction)?

(c) The usual concentration of thiosulfate titrant in the Winkler analysis is 0.025 N. Given that normality was defined in Chapter 1 in terms of a "reactive capacity" with regard to some type of reaction, what is the basis for the normality of thiosulfate in this reaction, and how is this related to the concentration of O_2?

(d) A 100-mL sample of acidified water is withdrawn from a DO bottle after it was processed with the three Winkler reagents ($MnSO_4$, alkaline-azide-iodide, and H_2SO_4) for titration with 0.025 N thiosulfate, and 9.15 mL were required to reach the endpoint (disappearance of blue color from the starch-iodine complex). What was the O_2 concentration in the original sample.

Note: To be exact in computing the DO concentration you need to consider a small volume correction, which results from the fact that the initial two reagents displace a total of 4 mL of sample from the 300 mL DO bottle, thus diluting the sample by a factor of 296/300. The 100 mL sample titrated thus represents only 98.67 mL of original lake water. Addition of the 2 mL of concentrated H_2SO_4 does not have a similar dilution effect because all the O_2 in the water was converted to $MnO(OH)_{2(s)}$ floc which is at the bottom of the bottle and none of it is removed from the bottle when the H_2SO_4 is added.

12.8. Optical methods for DO (so-called "optodes") have become commercially available that overcome many of the drawbacks of electrode-based DO meters. Optical methods provide longer temporal stability and higher accuracy and precision.

(a) Find an article in the literature (post-2000 and not included in the references cited in this chapter) that describes the basis of operation for optical DO measurements and write a synopsis describing how these devices work and their advantages over electrode-based DO measurements.

(b) Although the Winkler method now is used only rarely for routine monitoring, it still is used for work needing high accuracy and/or precision (e.g., measurement of primary production in waters of low biological activity). Find a paper in the recent literature (2005 or later) that used the Winkler method and provide a half-page synopsis focusing on the purposes for which the authors used the method and their reported accuracy. Journals having such articles include: *Environmental Science & Technology*, *Limnology and Oceanography*, *Biogeochemistry*, *Water Research*, and *Journal of Environmental Engineering*, but you are free to use any peer-reviewed journal.

References

1. Nelson, D. L., and M. M. Cox. 2004. *Lehninger principles of biochemistry*, 4th ed., W. H. Freeman Publ., New York.
2. Voelker, B. M., and D. Sedlak. 1995. Iron reduction by photoproduced superoxide in seawater. *Mar. Chem.* **50**: 93–102.

3. Stumm, W., and J. J. Morgan. 1996. *Aquatic chemistry*, 3rd ed., Wiley-Interscience, New York.

4. Goldstone, J. V., and B. M. Voelker. 2000. Chemistry of superoxide radicals in seawater: CDOM associated sink for superoxide in coastal waters. *Environ. Sci. Technol.* **34**: 1043–1048.

5. Voelker, B. M., D. L. Sedlak, and O. C. Zafiriou. 2000. Chemistry of superoxide radicals in seawater: reactions with organic Cu complexes. *Environ. Sci. Technol.* **34**: 1036–1042.

6. Stumm, W. 1978. What is the pε of the sea? *Thalassia Jugoslavica* **14**: 197.

7. Eaton, A. D., L. S. Clesceri, E. W. Rice, and A. E. Greenberg (eds.). 2005. *Standard methods for the examination of water &wastewater*, 21st ed., Am. Publ. Health Assoc., Water Env. Fed., Am. Water Wks. Assoc., Washington, D.C.

8. Winkler, L. 1889. Der Löslichkeit des Sauerstoffs in Wasser. *Berlin. Deut. Chem. Ges.* **22**: 1764–1774.

9. Fox, C. J. 1909. On the coefficients of absorption of nitrogen and oxygen in distilled water and seawater, and of atmospheric carbon dioxide in seawater. *Trans. Faraday Soc.* **5**: 68–87.

10. Truesdale, G. A., A. L. Downing, and G. F. Lowden. 1955. The solubility of oxygen in pure water and seawater. *J. Appl. Chem.* **5**: 53–62.

11. Carpenter, J. H. 1966. New measurements of oxygen solubility in pure and natural water. *Limnol. Oceanogr.* **11**: 264–277.

12. Murray, C. N., and J. P. Riley. 1969. The solubility of gases in distilled and seawater. 2. Oxygen. *Deep-Sea Res.* **16**: 311–320.

13. Weiss, R. F. 1970. The solubility of nitrogen, oxygen and argon in water and seawater. *Deep-Sea Res.* **17**: 721–735.

14. U.S. Geological Survey. 2009. *National field manual for the collection of water-quality data*, TWRI Book 9, ver. 2.2, chap. A5 (available online at http://water.usgs.gov/owq/pubs.html, accessed 12/2009).

15. Benson, B. B., and D. Krause, Jr. 1980. The concentration and isotopic fractionation of gases dissolved in freshwater in equilibrium with the atmosphere. 1. Oxygen. *Limnol. Oceanogr.* **25**: 662–671; and 1984. The concentration and isotopic fractionation of oxygen dissolved in freshwater and seawater in equilibrium with the atmosphere. *Limnol. Oceanogr.* **29**: 620–632.

16. Tchobanoglous, G., and E. D. Schroeder. 1985. *Water quality*, Addison-Wesley, Reading, Mass.

17. Lewis, W. K., and W. G. Whitman. 1924. Principles of gas absorption. *Ind. Eng. Chem.* **16**: 1215–1220.

18. Brezonik, P. L. 1994. *Chemical kinetics and process dynamics in aquatic systems*, CRC Press, Boca Raton, Fla., 275–278.

19. Danckwerts, P. V. 1951. Significance of liquid-film coefficients in gas absorption. *Ind. Eng. Chem.* **43**: 1460–1467.

20. Dobbins, W. E. 1964. BOD and oxygen relationships in streams. *J. Sanit. Eng. Div. ASCE* **90** (SA3): 53.

21. Liss, P. S., and L. Merlivat. 1986. In *The role of air-sea exchange in geochemical cycling*, P. Buat-Menard (ed.), Reidel, Dordrecht, 113–127.

22. Wanninkhof, R., J. R. Ledwell, and W. S. Broecker. 1985. Gas exchange-wind speed relation measured with sulfur hexafluoride on a lake. *Science* **227**, 1224–1226.

23. Wanninkhof, R. 1992. Relationship between wind speed and gas exchange over the ocean. *J. Geophys. Res.* **97**: 7373–7382.

24. Gulliver, J. S. 2007. *Introduction to chemical transport in the environment*, Cambridge University Press, New York.

25. Thomas, H. A., Jr. 1940. Analysis of the biochemical oxygen demand curve. *Sewage Works J.* **12**: 504; and 1950. *Water Sewage Works* **97**: 123; see Brezonik,[18] 69–71, for details on these methods.
26. Hutchinson, G. E. 1955. *Treatise on limnology*, Vol. 1, J. Wiley, New York.
27. Wetzel, R. 2001. *Limnology: lake and river ecosystems*, 3rd ed., Acad. Press, New York.
28. Odum, H. T. 1956. Primary production in flowing waters. *Limnol. Oceanogr.* **1**: 102–117.
29. Odum, H. T. 1957. Primary production measurements in eleven Florida springs and a marine turtle-grass community. *Limnol. Oceanogr.* **2**: 85–97.
30. Watson, A. J., R. C. Upstill-Goddard, and P. S. Liss. 1991. Air-sea gas exchange in rough and stormy seas measured by a dual-tracer technique. *Nature* **349**: 145–147.
31. Streeter, H. W., and E. B. Phelps. 1925. Studies of the pollution and natural purification of the Ohio River. U.S. Publ. Health Serv. Bull. **146**, Washington, D.C.
32. Johnson, D. K., and P. W. Aasen. 1989. The metropolitan wastewater treatment plant and the Mississippi River: 50 years of improving water quality. *J. Minn. Acad. Sci.* **55**: 134–138.
33. Winkler, L. 1888. The determination of dissolved oxygen in water. *Berlin. Deut. Chem. Ges.* **21**: 2843.
34. Clark L. C., R. Wolf, D. Granger, and Z. Taylor. 1953. Continuous recording of blood oxygen tensions by polarography. *J. Appl. Physiol.* **6**: 189–193.
35. There are many articles on optodes in the recent literature, including Klimant, I., V. Meyer, and M. Kohls. 1995. Fibre-optic oxygen microsensors, a new tool in aquatic biology. *Limnol. Oceanogr.* **40**: 1159–1165; Demas J. N., B. A. De Graff, and P. Coleman. 1999. Oxygen sensors based on luminescence quenching. *Anal. Chem.* **71**: 793A–800A; and Glud R. N., A. Tengberg, M. Kühl, P. O. J. Hall, and I. Klimant. 2001. An in situ instrument for planar O_2 optode measurements at benthic interfaces. *Limnol. Oceanogr.* **46**: 2073–2080.
36. Tengberg, A., J. Hovdenes, H. J. Andersson, O. Brocandel, R. Diaz, D. Hebert, T. Arnerich, C. Huber, A. Körtzinger, A. Khripounoff, F. Rey, C. Rönning, J. Schimanski, S. Sommer, and A. Stangelmayer. 2006. Evaluation of a lifetime-based optode to measure oxygen in aquatic systems. *Limnol. Oceanogr.: Methods* **4**: 7–17.

13

Chemistry of Chlorine and Other Oxidants/Disinfectants in Water Treatment

Objectives and scope

This chapter treats the chemistry of oxidants utilized in disinfection and chemical oxidation during water treatment, with emphasis on chlorine gas (Cl_2), its products in water (hypochlorous acid, HOCl, and its conjugate base hypochlorite, OCl^-), and other oxidized forms of chlorine. The inorganic chemistry of these forms—their acid-base and redox properties—and the reactions of chlorine forms with organic compounds are described. Formation mechanisms for disinfection by-products (DBPs) are explained, along with techniques to minimize their occurrence in drinking water. The chapter also briefly summarizes important aspects of the chemical behavior of alternative oxidants/disinfectants, including chlorine dioxide, iodine, and ozone (alone and as a component of so-called advanced oxidation processes).

Key terms and concepts

- Free and combined chlorine forms, chloramines, breakpoint chlorination
- Oxidizing strength of halogens: $Cl_2 > Br_2 > I_2$
- Dechlorination: importance of sulfite (SO_3^{2-})
- Disinfection by-products (DBPs), trihalomethanes (THMs)
- Electrophilic substitution of chlorine into organic compounds such as phenols and N-organic compounds
- Chlorine dioxide, iodine, ozone, and advanced oxidation processes as alternative oxidants/disinfectants

13.1 Introduction

Chlorination of drinking water has been a widespread practice for almost 100 years, and along with treatment and proper disposal of wastewater, it is often credited with saving more lives and halting the spread of communicable diseases more than any other public health or medical advance. The most common drinking water disinfectants, by far, are chlorine gas (Cl_2) and its reaction products in water, $HOCl$ and OCl^-. Other oxidized chlorine forms, however, and some nonchlorine compounds (e.g., ozone) also are used for disinfection and for other water treatment purposes requiring oxidants. The chemistry of these substances is complicated and focused primarily on redox processes. In the case of chlorine species, in particular, there are several important but unintended consequences to their use for drinking water disinfection, including the formation of chlorinated organic byproducts. In this chapter we describe the chemistry of the oxidized forms of chlorine and briefly discuss the chemistry of ozone and other "advanced oxidants" that can serve as replacements for chlorine in drinking water treatment.

13.2 Oxidation states of chlorine

The element chlorine occurs in ions and compounds with a range of formal oxidation states, from $-I$ to $+VII$ (Table 13.1), but as shown by the $p\varepsilon$-pH diagram (Figure 13.1), Cl^- is the only stable form in aqueous solution; i.e., all compounds containing chlorine in oxidation states greater (more positive) than $-I$ are unstable with regard to redox equilibria in water. In general, chlorine compounds with oxidation states greater than $-I$ act as oxidizing agents for organic matter and reduced inorganic ions of Fe, Mn, N, and S. The reactivity of oxidized Cl forms and their availability at low cost makes them useful in treating water. Collectively, Cl_2, $HOCl$, and OCl^- are known as

Table 13.1 Oxidation states of inorganic species of chlorine

State	Name	Species	pK_a	Comments
$-I$	Chloride	Cl^-		Only stable Cl oxidation state in aqueous solution
0	Chlorine	Cl_2		Disproportionates to $+I$ and $-I$ states
$+I$	Hypochlorous acid/hypochlorite	$HOCl/OCl^-$	7.5	Weak acid; common disinfecting agents and good oxidants
$+III$	Chlorous acid/chlorite	$HOClO/ClO_2^-$	2	Acid form highly unstable; ion used as bleaching agent
$+IV$	Chlorine dioxide	ClO_2		Disinfectant; oxidizing agent; radical species
$+V$	Chloric acid/chlorate	$HOClO_2/ClO_3^-$	-1	Strong acid and oxidant
$+VII$	Perchloric acid/perchlorate	$HOClO_3/ClO_4^-$	-7	Very strong acid; powerful oxidant, explosive in concentrated form, important contaminant of groundwater from use in rocket fuels; highly toxic

Figure 13.1 pε-pH diagram for −I, 0, and +I oxidation states of chlorine showing that chloride is the only stable form of chlorine in aqueous solutions. The diagram is constructed assuming all aqueous species contain 1 mM chlorine (i.e., all concentrations are set to 1 mM, except for Cl_2 which is set to 0.5 mM) using $pK_a = 7.5$ for HOCl and pε° values for the chlorine redox couples as follows: 26.89 for $HOCl/\frac{1}{2}Cl_{2(aq)}$, 23.60 for $\frac{1}{2}Cl_{2(aq)}/Cl^-$, 25.25 for $HOCl/Cl^-$, and 20.76 for OCl^-/Cl^-.
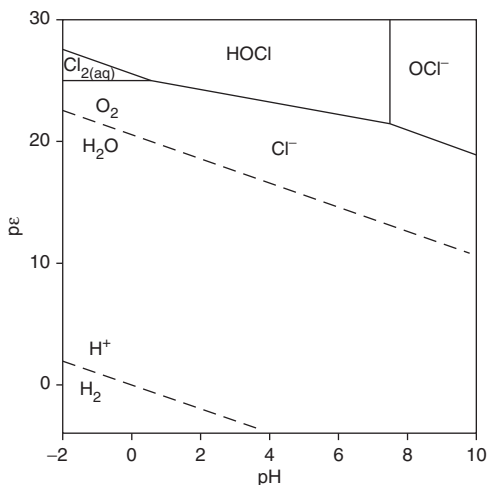
free chlorine. Chlorine (Cl_2) and hypochlorite salts (NaOCl and $Ca(OCl)_2$) are the most common disinfectants in municipal water treatment, but chlorination also is used to oxidize inorganic ions (Fe^{2+}, Mn^{2+}, H_2S, and HS^-) and natural, color-causing organic compounds (humic and fulvic acids (CDOM)), which cause water quality problems to consumers. Chlorine dioxide also is used as a disinfectant and oxidant in industry and occasionally for drinking water.

Advantages of free chlorine species for water treatment include rapid rates of pathogen inactivation (although this is not always the case; e.g., for resistant organisms such as *Cryptosporidium parvum* or *Giardia lamblia*),[1] low cost, and the ability (sometimes with difficulty) to maintain residual levels in distribution systems, thus ensuring continuous disinfection within the system. The dosage added at a drinking water treatment plant is dictated by the desired level of disinfection, which is determined by the concentration of the disinfectant, the contact time, and the rate at which a given target organism is inactivated (see Box 13.1).

Disadvantages of free chlorine arise from the high and nonselective reactivity of free chlorine species, which results in the formation of various disinfection by-products (DBPs), some of which are toxic to humans (see section 13.6.3). Maintenance of a free chlorine residual also is difficult in the presence of organic matter. This problem can be circumvented by adding ammonium, which in its basic form, NH_3, reacts rapidly with free chlorine to form ***combined chlorine***, i.e., ***chloramines***, such as NH_2Cl and $NHCl_2$ (see section 13.5.1). Chloramines are less reactive chemically and also slower acting disinfectants, but this makes them persist for longer periods in distribution systems.

Aside from acting as an oxidant, free chlorine participates in "substitution" reactions with some kinds of organic substances, producing organochlorine compounds, such as chlorophenols, trihalomethanes (THMs, e.g., chloroform), and trichloroacetic acid. The latter two compounds are examples of regulated DBPs. Combined chlorine is less reactive with organic matter than free chlorine. Thus, the addition of ammonium to water prior to chlorination is an important way to minimize formation of undesirable THMs. Unfortunately, combined chlorine is also not without disadvantages. For example,

Box 13.1 Disinfection kinetics

Rates of disinfection are dictated by the Chick-Watson law, which was developed more than 100 years ago:

$$\ln \frac{N}{N_0} = -\alpha C^n t,$$

where N is the number of microorganisms, N_0 is the initial number of microorganisms, C is the concentration of the disinfectant, t is time, α is the inactivation constant, and n is usually assumed to be 1. In 1908, Harriette Chick first showed that bacterial inactivation in the presence of chlorine followed first-order kinetics with respect to the population of bacteria.[2] Later that same year, Herbert Watson expanded the mathematical analysis to include the effect of varying disinfectant concentration.[2] Essentially, the law says that as either C or t is increased, the extent of inactivation will increase. Thus, Ct is a key parameter in disinfection.

a switch from free chlorine to chloramines in Washington, D.C., in 2000 led to unacceptable concentrations of lead in drinking water due to the corrosion of lead pipes and fittings (causing considerable controversy). This is because free chlorine can prevent the corrosion of lead pipes (via formation of a protective lead oxide coating on lead surfaces), whereas combined chlorine is not a strong enough oxidant to do so.[3] Chlorine dioxide, ClO_2, which acts only as an oxidant[1] (and thus does not generate appreciable organic DBP yields), is preferred for disinfection in some countries, although its application is constrained by its generation of ClO_2^- (an example of an inorganic DBP) as a direct reduction product.

Because of the water quality and human health significance of chlorine forms, including chloramines and organochlorine compounds, their chemistry has been studied extensively for several decades, and a large literature exists on the subject.[4] Compared with many other aquatic redox reactions, reactions of chlorine are fast (many have timescales of subseconds to seconds). Many of the reactants and products absorb light in the UV range, and this often is put to advantage in measuring reaction rates. A critical review of the reactivity of chlorine with inorganic and organic species recently was compiled.[5]

The two highest oxidation states of chlorine, chlorate (Cl^V) and perchlorate (Cl^{VII}) are not used in water treatment but are strong oxidants in their acid forms and are commonly used as acids in chemistry laboratories. Sodium chlorate is used industrially to produce ClO_2 for bleaching paper pulp. Perchloric acid is a common reagent and strong oxidant used to oxidize organic matter in analyzing total phosphorus and nitrogen. Perchloric acid is one of the strongest mineral acids. It is considered a "superacid" because it is much stronger than 100% sulfuric acid, and its pK_a is roughly -7! It also is a very strong oxidant (see Box 13.2), and concentrated perchloric acid must be handled carefully because of its explosive hazard. Perchlorate ion is one of the weakest ligands known.

It shows virtually no tendency to form complexes with metal ions and for that reason is the anion of choice to adjust ionic strength in complexation experiments.

Box 13.2   Perchlorate: it *is* rocket science!

The oxidizing strength of perchlorate is used in solid rocket fuels in the form of ammonium perchlorate. This application has led to contamination of ground water in many areas near military and aerospace installations. Unfortunately, perchlorate also is toxic to humans. It interferes with uptake of iodine by the thyroid gland, which is critically important in childhood development and regulation of metabolism, and concern exists about human exposures even to low concentrations in contaminated ground water. Perchlorate recently was discovered in Martian soil and also occurs naturally in some extreme environments on Earth, such as the Atacama Desert in Chile. A federal drinking water standard has not been issued for perchlorate, and in 2008 the U.S. EPA issued a controversial announcement that it would not do so. Nonetheless, the EPA has issued a *recommended* limit of 25 µg/L.

13.3 Hydrolysis of Cl_2

Cl_2 is a highly soluble gas ($H = \frac{P_{Cl_2}}{[Cl_{2(aq)}]} = 10.87$ L-atm/mol at 25 °C)[6] that hydrolyzes rapidly to Cl^-, hypochlorous acid, and its conjugate base hypochlorite ($HOCl/OCl^-$) in water:

$$Cl_2 + H_2O \rightleftharpoons HOCl + H^+ + Cl^- \quad K = 5.18 \times 10^{-4} \ (10^{-3.29}) = k_f/k_r \quad (13.1)$$
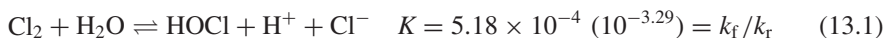
The forward reaction rate constant, k_f, is 22.3 s^{-1}, and the reverse reaction rate constant, k_r, is 4.3×10^4 M^{-2} s^{-1}.[7] The acid/base reaction for $HOCl/OCl^-$ is

$$HOCl \rightleftharpoons H^+ + OCl^- \quad K_a = 3.2 \times 10^{-8}, \quad pK_a = 7.50. \quad (13.2)$$

Equilibrium among these species is pH dependent. The hydrolysis of Cl_2 (eq. 13.1) is a disproportionation reaction (i.e., a self-oxidation and reduction). At freshwater concentrations of Cl^- and pH > 5, the hydrolysis of Cl_2 is nearly complete, and Cl_2 generally is not a significant species in the treatment of drinking or waste water (Example 13.1, Table 13.2). It is apparent from the stoichiometry of eq. 13.1 that the hydrolysis equilibrium depends on the concentration of Cl^- in water. However, over the range of $[Cl^-]$ in fresh waters, this has much less effect on equilibrium composition than pH does. Hypochlorous acid is a weak acid, and HOCl is the predominant species at pH < 7.5; OCl^-, which is a much less effective disinfectant (roughly 400-fold weaker), predominates at higher pH. As Table 13.2 and Figure 13.1 show, Cl_2 becomes predominant at very low pH (< 2). Hydrolysis of Cl_2 is very rapid and essentially complete at neutral pH. Many measurements have been made of the

Table 13.2 Distribution of free chlorine species versus pH at 25°C*

pH	Cl_2	HOCl	OCl^-
2	0.163	0.837	0.0000
3	0.019	0.981	0.0000
4	1.9×10^{-3}	0.998	0.0003
5	1.9×10^{-4}	0.997	0.0032
6	1.9×10^{-5}	0.969	0.031
7	1.5×10^{-6}	0.760	0.240
8	4.7×10^{-8}	0.240	0.760
9	6×10^{-10}	0.031	0.969

* Fraction of total free chlorine at $[Cl^-] = 355$ mg/L (10^{-2} M).

hydrolysis reaction rate. According to Aieta and Roberts,[8] the best estimate for the first-order rate constant at 20°C is 12.2 s^{-1}. Margerum et al.[9] reported a value of 28.6 s^{-1} at 25°C and I = 0.5. The half-life of Cl_2 in water at circumneutral pH is thus short (≤ 0.1 s). E_{act} for the reaction is 60.2 kJ/mol, and the Arrhenius preexponential factor (A) is 6.8×10^{11}. Although HOCl can accept another proton to become H_2OCl^+ at low pH (i.e., < 2) in nonaqueous systems, this species does not appear to occur in water.[10]

EXAMPLE 13.1 Speciation of free chlorine as a function of pH: Using eqs. 13.1 and 13.2, generate a pC-pH diagram for Cl_2, [HOCl], and $[OCl^-]$ from pH 2 to 9 with $[Cl^-] = 10^{-2}$ M, and $Cl_{ox,T} = [Cl_2] + [HOCl] + [OCl^-] = 10^{-3}$ M.

Answer: This is similar to speciation calculations performed in chapters 8–10, but Cl^- is assumed to be constant and thus tracked separately.

Starting with the mass balance

(1) $Cl_{ox,T} = [Cl_2] + [HOCl] + [OCl^-]$,

we need to use eqs. 13.1 and 13.2 to substitute in for two of the three species. Equation 13.1 becomes

(2) $[Cl_2] = \dfrac{[HOCl][H^+][Cl^-]}{K}$,

and 13.2 is rearranged to

(3) $[OCl^-] = \dfrac{K_a[HOCl]}{[H^+]}$.

Substituting into the mass balance gives

(4) $Cl_{ox,T} = \dfrac{[HOCl][H^+][Cl^-]}{K} + [HOCl] + \dfrac{K_a[HOCl]}{[H^+]}$

$= [HOCl]\left(1 + \dfrac{[H^+][Cl^-]}{K} + \dfrac{K_a}{[H^+]}\right)$,

or

$$(5) \quad [\text{HOCl}] = \left(\frac{\text{Cl}_{\text{ox,T}}}{1 + \frac{[\text{H}^+][\text{Cl}^-]}{K} + \frac{K_a}{[\text{H}^+]}} \right).$$
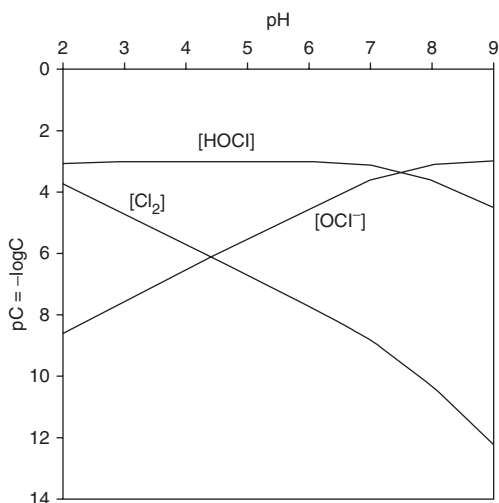
Now the values are plugged into the right hand side of eq. (5) (recall $[\text{Cl}^-] = 10^{-2}$ M and is constant) to solve for [HOCl]. Once this value is known for any pH, eqs. (2) and (3) are used to calculate $[\text{Cl}_2]$ and $[\text{OCl}^-]$ and the plot shown in this example is generated. Concentrations at pH 2 are $[\text{Cl}_2] = 1.63 \times 10^{-4}$ M, $[\text{HOCl}] = 8.37 \times 10^{-4}$ M, and $[\text{OCl}^-] = 2.64 \times 10^{-6}$ M, which gives the same fractions of total free chlorine shown in Table 13.2.

Concentrations of chlorine species in water usually are reported in mg/L as Cl or Cl_2, as described in chapter 1. Conversion between these units and molar units is based on the atomic weight of Cl (35.45) and the redox "reacting capacities" of chlorine in its various forms (i.e., the number of electrons needed to reduce the species to chloride ion). From eqs. 13.1 and 13.2 we now can see why chlorine concentrations reported in mg/L as either Cl or Cl_2 are equivalent: the hydrolysis of Cl_2 produces one HOCl (oxidation state of +I), and it takes two electrons to reduce HOCl to Cl^-. From a redox perspective, the equivalent weight of Cl_2 thus is $70.9 \div 2 = 35.45$, which is the same as that for chlorine atoms ($35.45 \div 1 = 35.45$). Thus, the equivalent weights of Cl_2 and HOCl are the same with respect to Cl. Consequently, 1 mol/L of HOCl is equivalent to 1 mol/L×2 eq/mol×35.45 g/eq $= 70.9$ g/L of Cl_2, or 70.9 g/L of free chlorine (as each chlorine species contains one mole of Cl in the +I oxidation state), as discussed in chapter 1. The same convention may be applied to the measurement of combined chlorine—taking a mole of combined chlorine (again with Cl in the +I oxidation state) to contain one mole of Cl_2.

13.4 Kinetics of chlorination

Many reactions of substrates (S) with chlorine occur via second-order kinetics:[5]

$$\frac{d[S]}{dt} = -k_T[HOCl]_T[S]_T, \qquad (13.3)$$

where $[HOCl]_T = [HOCl] + [OCl^-]$ and $[S]_T$ is the concentration of all forms of S in solution. The apparent rate constant, k_T, will itself depend on the speciation of the hypochlorous acid. To account for the different reactivity of the two species we can write

$$\frac{d[S]}{dt} = -k_1[HOCl][S]_T - k_2[OCl^-][S]_T. \qquad (13.4)$$

Depending on pH, one term may dominate over the other. Furthermore, there also may be multiple acid/base forms of the substrate (e.g., HS and S^- for a monoprotic acid), making the situation more complicated. The speciation of HS may be accounted for as follows:

$$\frac{d[S]}{dt} = -k_1[HOCl][HS] - k_2[OCl^-][HS] - k_3[HOCl][S^-] - k_4[OCl^-][S^-] \quad (13.5)$$

Assuming that contributions of OCl^- to observed reaction kinetics are negligible compared to HOCl (consistent with numerous observations),[4] it can be shown that the apparent rate constant, k_T, can be calculated at any pH using the formula

$$k_T = \frac{k_1[H^+]^2 + k_3[H^+]K_{a,S}}{[H^+]^2 + K_{a,HOCl}[H^+] + K_{a,S}[H^+] + K_{a,HOCl}K_{a,S}}, \qquad (13.6)$$

where $K_{a,S}$ is the equilibrium constant for the HS/S^- system. Accordingly, it turns out that the maximum rate for reaction of HOCl with a simple diprotic acid occurs at $pH = \frac{1}{2}(pK_{a,S} + pK_{a,HOCl})$.

13.5 Inorganic chemistry of aqueous chlorine

13.5.1 Formation and reactions of chloramines

Because of the importance of chloramines in water disinfection, the reaction of chlorine with ammonia to form chloramines and reactions of chloramines have been studied for a long time.[11–15] Reaction rates and product distribution depend on pH, relative concentrations of HOCl and NH_3, time, and temperature. The best studied and simplest reaction is

$$HOCl + NH_3 \rightarrow NH_2Cl + H_2O. \qquad (13.7)$$

Monochloramine, NH_2Cl, is the major product formed under normal conditions of water chlorination in the presence of ammonia/ammonium. When the rate is expressed in terms of total concentrations of reactants (rate $= k_T[Cl]_T[N]_T$), k_T varies with pH,
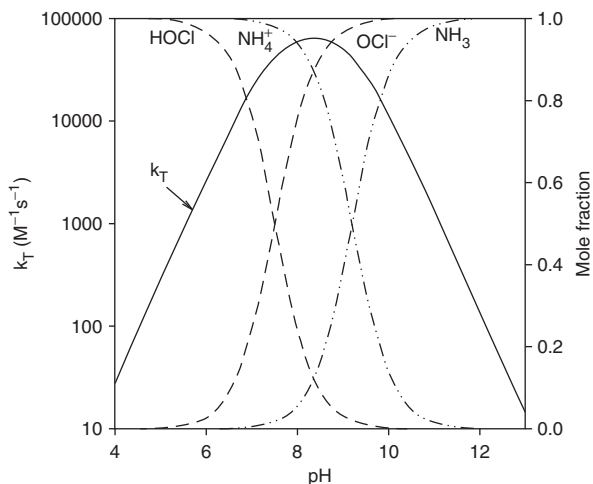
Figure 13.2 pH dependence of the chlorination of ammonia. Based on Deborde and von Gunten.[5]

decreasing under both acidic and basic conditions and reaching a maximum at pH 8.35 (i.e., $pH = \frac{1}{2}(pK_{a,NH_{4+}} + pK_{a,HOCl}) = \frac{1}{2}(7.5 + 9.2))$; see Figure 13.2). This suggests that HOCl and NH_3 are the actual reactants. When the reactants are expressed in terms of these species, the value of k is 4.2×10^6 M^{-1} s^{-1} at 25°C. The reaction has a low E_{act}, 13 kJ/mol,[12] which is in the range of diffusion-controlled processes. The reaction is very rapid and essentially complete in $<< 1$ minute under typical conditions for water chlorination.

Chloramine can be further oxidized via the following reactions:

$$HOCl + NH_2Cl \rightarrow NHCl_2 + H_2O \tag{13.8}$$

$$HOCl + NHCl_2 \rightarrow NCl_3 + H_2O \tag{13.9}$$
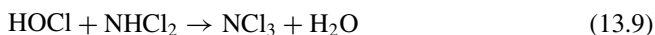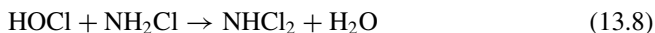
Reactions involving dichloramine (either as reactant or product) are difficult to study because a variety of competing reactions occur simultaneously. The formation of $NHCl_2$ from NH_2Cl and HOCl is much slower (by a factor of $\sim 10^{-4}$) than the formation of NH_2Cl from NH_3 and HOCl because NH_2Cl is a much weaker base than NH_3. Morris and Isaac[12] reported $k = 3.5 \times 10^2$ M^{-1} s^{-1} at 25°C (for the reaction expressed in terms of neutral reactants) and a low E_{act} (17 kJ/mol), but a large range exists for both k and E_{act} in the literature. The reaction of NH_2Cl with HOCl is subject to acid catalysis (in contrast to that for NH_3 with HOCl). Because the reactions producing NH_2Cl and $NHCl_2$ have different sensitivities to pH, the distribution of chloramines from reaction of free chlorine with NH_3 varies with pH. At near neutral pH, NH_2Cl predominates when Cl:N < 1, but at pH < 5.5, formation of $NHCl_2$ becomes competitive. For equimolar concentrations of free chlorine and ammonium at 25°C, the following distributions occur:[15]

pH	% NH_2Cl	% $NHCl_2$
5	13	87
6	57	43
7	88	12
8	97	3
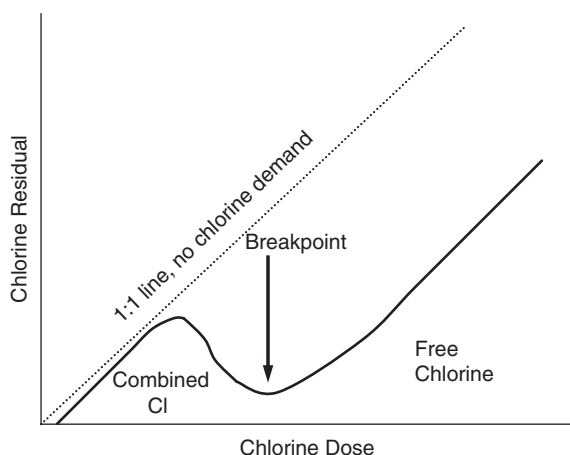
Figure 13.3 General scheme of breakpoint chlorination.

Thus, if one wishes to generate dichloramine, the pH of the solution can be lowered to < 5.5 by addition of acid. Dichloramine also is formed by disproportionation of monochloramine: $2NH_2Cl \rightleftharpoons NHCl_2 + NH_3$. This can be viewed as the chlorination of a monochloramine molecule by a second monochloramine molecule. Because NH_2Cl is a weak chlorinating agent (compared with HOCl), the rate of disproportionation ($k = 5.6 \times 10^{-2}$ M^{-1} s^{-1}) is much slower (factor of $\sim 10^{-4}$) than the reaction between NH_2Cl and HOCl. An additional mechanism complicates the formation of $NHCl_2$ from NH_2Cl: the slow, first-order hydrolysis of NH_2Cl to HOCl and NH_3 (where $K = 1.5 \times 10^{-11}$ M^{-1} at $\mu = 0.5$ M,[16] with respect to the equilibrium HOCl + $NH_3 \rightleftharpoons NH_2Cl + H_2O$). This can be followed by reaction of HOCl with another molecule of NH_2Cl.

13.5.2 Breakpoint chlorination

Di- and trichloramine are unstable in aqueous solution and decompose by several mechanisms. The most important mechanism is a redox process yielding Cl^- and N_2 and thus resulting in a loss of active chlorine. This process, called ***breakpoint chlorination***, is a common practice in water treatment when one wishes to insure the presence of free chlorine residual. As Figure 13.3 illustrates, when ammonium is present, little or no free chlorine exists before the breakpoint, but after the breakpoint, any added chlorine remains in solution as a free residual. The overall stoichiometry of breakpoint chlorination is deceptively simple,

$$3Cl_2 + 2NH_3 \rightarrow N_2 + 6H^+ + 6Cl^-, \qquad (13.10)$$
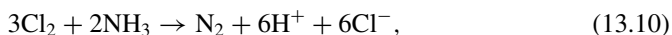
and the breakpoint thus should occur at a molar ratio of Cl_2 added to initial NH_3 present of 1.5. The actual mechanisms whereby the breakpoint process occurs, however, are highly complicated and depend on pH and other solution conditions. Some features of these mechanisms are described in Box 13.3.

Box 13.3   Chemistry of breakpoint chlorination

Loss of $NHCl_2$ from solution is an ***autocatalytic process*** because the products ($HOCl$ and NCl_3) formed in decomposition accelerate further reactions.[13] The presence of NH_4^+ in solution greatly increases $NHCl_2$ stability, however. $NHCl_2$ losses $< 10\%$ in 24 h occurred in solutions prepared by disproportionation of NH_2Cl at pH 3.5–4.0, which yields $NHCl_2$ and NH_4^+, but substantial loss of $NHCl_2$ occurred in < 1 h when NH_4^+ was removed by ion exchange.[13] Inhibition of $NHCl_2$ decomposition by NH_4^+ is explained by its scavenging of $HOCl$, which otherwise would react rapidly with $NHCl_2$, accelerating its decomposition.

Under neutral and basic conditions, decomposition of $NHCl_2$ proceeds by coupled reactions:

(1) $NHCl_2 + HOCl + B \rightarrow NCl_3 + BH^+ + OH^-$,
(2) $NHCl_2 + NCl_3 + OH^- \rightarrow N_2 + 2HOCl + 3Cl^- + H_2O$,
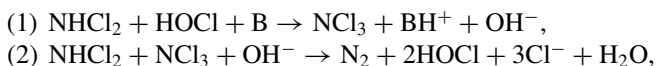
where B stands for a Brønsted base. When $[HOCl]$ is low, reaction (1) is slower than reaction (2), and $[NCl_3]$ remains low. Trichloramine is explosive in pure form but fairly stable in dilute solution. NCl_3 is formed from $NHCl_2$ and $HOCl$ under acidic conditions and is important in breakpoint chlorination. The equilibrium constant reported for this reaction,[14]

(3) $NHCl_2 + HOCl \rightleftharpoons NCl_3 + H_2O$,

is high—1.6×10^8 M^{-1}; this value is based on the ratio of the forward and reverse rate constants. The stability implied by this value is misleading, however, in that NCl_3 reacts with $NHCl_2$ (eq. (2)). Therefore, NCl_3 and $NHCl_2$ do not reach a true equilibrium implied by eq. (3). The decomposition of NCl_3 itself is base catalyzed and fits the rate equation:[14]

(4) $-d[NCl_3]/dt = 2(k_0 + k_1\{OH^-\} + k_{HB}[HB]\{OH^-\} + k_2\{OH^-\}^2)[NCl_3]$
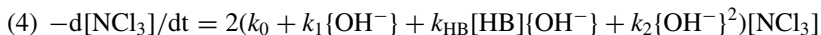
Values of the rate constants at $I = 0.5$ and $25°C$ are $k_0 = 1.6 \times 10^{-6}$ s^{-1}; $k_1 = 8$ M^{-1} s^{-1}; $k_2 = 890$ M^{-1} s^{-1}; k_{HB} (M^{-1} s^{-1}) $= 2.1 \times 10^3$ ($H_2PO_4^-$), 7.6×10^2 ($B(OH)_3$), 128 (HPO_4^{2-}), and 65 (HCO_3^-), where HB is a Brønsted acid. The stoichiometry of trichloramine decomposition is

(5) $2NCl_3 + 6OH^- \rightleftharpoons N_2 + 3OCl^- + 3Cl^- + 3H_2O$.
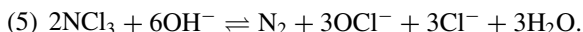
This reaction also has a complicated mechanism and proceeds along two pathways, including the reverse of formation reaction (1):

(6) $NCl_3 + BH^+ + OH^- \rightarrow NHCl_2 + HOCl + B$,
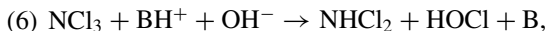
followed by reaction with dichloramine to yield N_2 via eq. (2).

13.5.3 Reactions with other halogen compounds

If bromide ion, Br^-, is present in water, which is common in regions affected by sea salt and brines, chlorine oxidizes it rapidly to HOBr. Similarly, free chlorine *and* free

bromine each oxidize iodide to iodine. This reflects the reduction potentials of the halogens:

$$Cl_{2(g)} + 2e^- \rightleftharpoons 2Cl^- \quad E_H^\circ = 1.36 \text{ V} \tag{13.11a}$$

$$Br_{2(g)} + 2e^- \rightleftharpoons 2Br^- \quad E_H^\circ = 1.07 \text{ V} \tag{13.11b}$$

$$I_{2(aq)} + 2e^- \rightleftharpoons 2I^- \quad E_H^\circ = 0.53 \text{ V} \tag{13.11c}$$
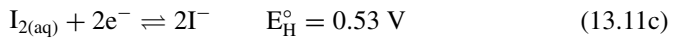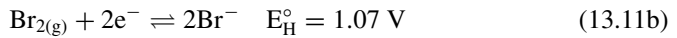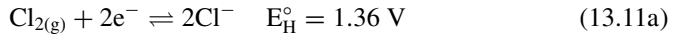
Chlorine thus is the strongest oxidant of the three halogens, and if traces of Br^- or I^- are present in water with free chlorine, they are oxidized stoichiometrically to bromine and iodine species. Section 13.7.1 provides further information on the chemistry of iodine. In addition, the chlorine residual in a water is capable of oxidizing Br^- to bromate ion (BrO_3^-), which is a suspected carcinogen:[17]

$$HOCl + 2e^- + H^+ \rightleftharpoons Cl^- + H_2O \qquad p\varepsilon_7^\circ = 21.60$$

$$BrO_3^- + 6H^+ + 6e^- \rightleftharpoons Br^- + 3H_2O \quad p\varepsilon_7^\circ = 17.35$$

Net:

$$Br^- + 3HOCl \rightleftharpoons 3Cl^- + BrO_3^- + 3H^+ \quad p\varepsilon_7^\circ(net) = 4.25 \tag{13.12}$$
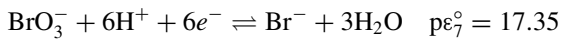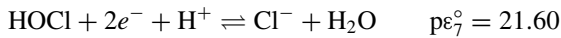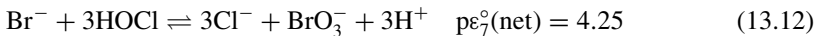
Sunlight-assisted buildup of BrO_3^- to levels as high as 100 ppb (the drinking water standard is 10 ppb) has been reported in reservoirs holding treated, chlorinated drinking water for the City of Los Angeles,[18] but whether reaction with HOCl is directly involved in unclear.

Over a broad range of pH, the reaction rate of chlorine with bromide varies widely (Figure 13.4), but it is nearly constant over the pH range of 3–8 (within which free chlorine is present primarily as HOCl), which includes most natural waters. Second-order rate constants for the reaction of Br^- with OCl^- and HOCl as oxidants[19] are $k = 0.9 \times 10^{-3} \text{ M}^{-1} \text{ s}^{-1}$ and $1.55 \times 10^3 \text{ M}^{-1} \text{ s}^{-1}$, respectively. HOCl thus is more than 10^6 times more reactive with Br^- than is OCl^-. An increase in rate at pH < 3 reflects catalysis by H^+, but reaction with HOCl predominates from pH 3 to ~13. The decrease in k_{obs} at pH >~7 simply reflects the decrease in HOCl at pH > pK_a. Reaction of Br^- with OCl^- is not important in water treatment processes; it dominates only at pH > 13. The reaction also is catalyzed by Brønsted acids, HB, and is thought to proceed in a two-step process through the formation of the intermediate BrCl, which is a strong oxidant:[19]

$$HB + OCl^- + Br^- \rightleftharpoons B^- + OH^- + BrCl(slow) \tag{13.13a}$$

$$BrCl + 2OH^- \rightarrow OBr^- + Cl^- + H_2O(fast) \tag{13.13b}$$
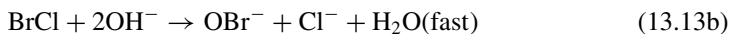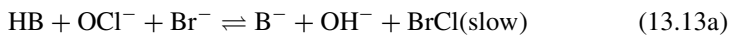
The first step of the mechanism essentially involves transfer of electrophilic Cl^+ to Br^-. Once the intermediate, BrCl, is formed, it reacts rapidly with OH^- ions to form hypobromite and chloride. Overall, the chemistry of HOCl reactions with Br^- is quite complicated. Figure 13.5 summarizes the potential reaction pathways, in addition to comparable pathways resulting from reaction of HOCl with I^-.
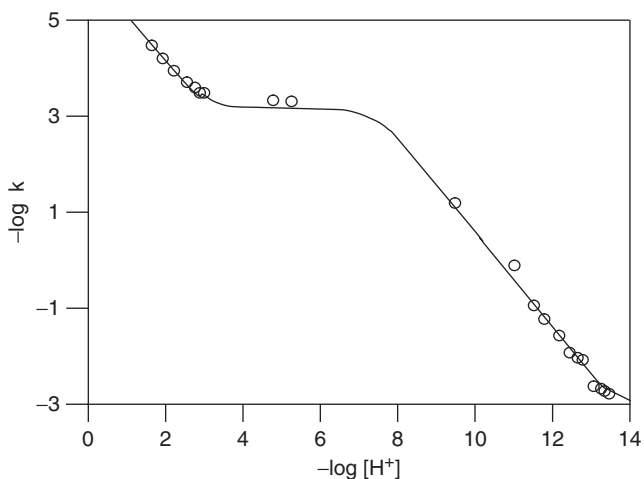
Figure 13.4 Effect of pH on the observed second-order rate constant k_{obs} for oxidation of Br^- by free chlorine at 25°C. Redrawn from Kumar and Margerum[19] and used with permission of the American Chemical Society.

Cl_2 and $HOCl/OCl^-$ also react rapidly with chlorite (ClO_2^-) to form chlorine dioxide (ClO_2) or chlorate (ClO_3^-), and chloride (Cl^-), where $k = 1.3–1.7 \times 10^4$ M^{-1} s^{-1} at 20°C for the reaction of ClO_2^- with Cl_2.[8] ClO_2 is the dominant product of these reactions under acidic conditions, whereas ClO_3^- is the dominant product under circumneutral to alkaline conditions.

13.5.4 Other inorganic species and dechlorination

Chlorine is lost from solution by many reactions, including the breakpoint process described above, oxidation of organic compounds, and oxidation of reduced inorganic species like Fe^{II}, Mn^{II}, HS^-, and CN^-. Oxidation of these three species is advantageous in terms of drinking water treatment in that they are the cause of taste and color issues. When oxidized, Fe and Mn become much less soluble, and thus waters with high concentrations of these species may be dosed with chlorine at the intake end of a treatment plant. These reactions tend to be fast, but Fe^{II} ($k_{HOCl} = 1.7 \times 10^4$ M^{-1} s^{-1})[20] reacts much more rapidly than Mn^{II} ($k_{HOCl} = 6.4 \times 10^{-4}$ M^{-1} s^{-1}).[21] More recently, the presence of arsenic in waters has received attention, with the allowable levels lowered from 50 to 10 ppb. As^V is much more readily removed than As^{III} during conventional drinking water treatment. Thus, HOCl is used to oxidize As^{III} to As^V. The rate of reaction is pH dependent,[22] reflecting increased reactivity of the more deprotonated species of As^{III}: 4.3×10^3 M^{-1} s^{-1} for $As(OH)_3$, 5.8×10^7 M^{-1} s^{-1} for $As(OH)_2O^-$, and 1.4×10^9 M^{-1} s^{-1} for $As(OH)O_2^{2-}$.

Aside from consumption by natural constituents in water, chlorine is purposely removed from water by adding dechlorinating agents, the most common of which is sulfite (SO_3^{2-}). This ion reacts rapidly with free chlorine and most chloramines.
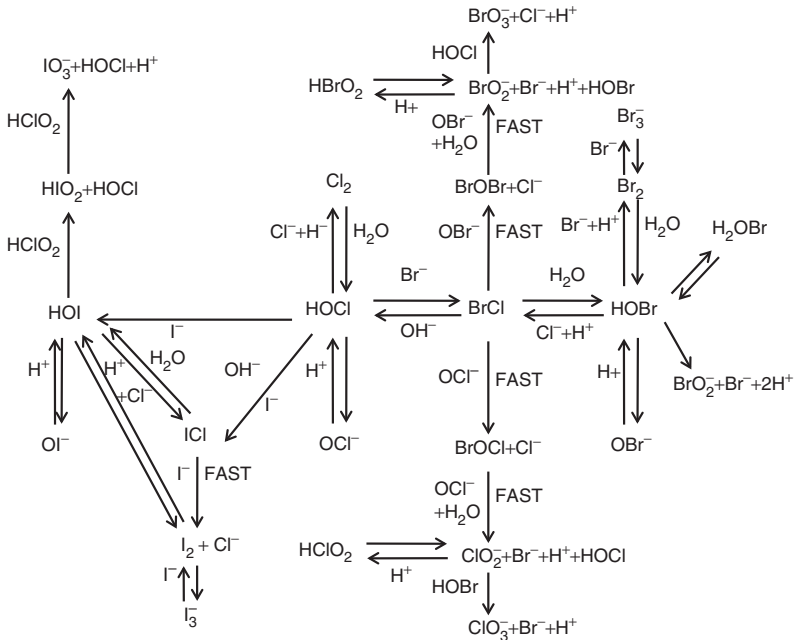
Figure 13.5 Reaction pathways and products of HOCl and Br⁻ or I⁻. (Courtesy of Peter Vikesland, Virginia Polytechnic Institute and State University)

For example, the reaction of bisulfite with hypochlorous acid is:

$$HSO_3^- + HOCl \rightarrow SO_4^{2-} + 2H^+ + Cl^- \tag{13.15}$$
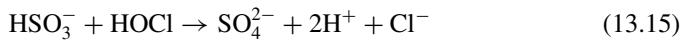
Sulfite (usually added as SO_2 gas; $SO_2 + H_2O \rightarrow H_2SO_3$) is widely used to remove chlorine residuals from waste water effluents before they are released to natural waters because of the toxicity of chloramines to aquatic invertebrates, even at ppb levels.[23]

EXAMPLE 13.2 Apparent chlorination rate constant of a multiprotic substrate: Assuming that only HOCl oxidizes As^{III} species, determine the apparent rate constant for the reaction of $As(OH)_3$ at pH 7 with HOCl. The specific rate constants for reaction with HOCl are as follows:[22]

$$As(OH)_3 \qquad k_1 = 4.3 \times 10^3 M^{-1}s^{-1}$$

$$As(OH)_2O^- \quad k_2 = 5.8 \times 10^7 M^{-1}s^{-1}$$

$$As(OH)O_2^{2-} \quad k_3 = 1.4 \times 10^9 M^{-1}s^{-1}$$
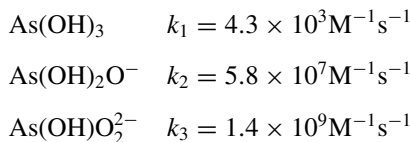
The speciation of $As(OH)_3$ is described by the following equilibrium constants:

$$As(OH)_3 \rightleftharpoons As(OH)_2O^- + H^+ \qquad pK_{a1} = 9.2$$

$$As(OH)_2O^- \rightleftharpoons As(OH)O_2^{2-} + H^+ \quad pK_{a2} = 12.1$$

$$As(OH)O_2^{2-} \rightleftharpoons AsO_3^{3-} + H^+ \qquad pK_{a3} = 12.7$$
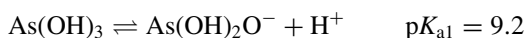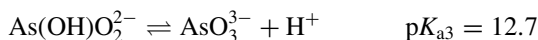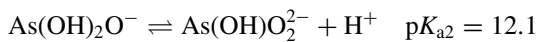
Answer: The overall rate constant will be dependent on both the speciation of the HOCl and the $As(OH)_3$. The specific rate constants need to be multiplied by (i) the fraction of free chlorine present at HOCl, and (ii) the fraction of the total As^{III} present in the protonation state for the specific rate constant. In alpha notation,

$$k_{overall} = k_1 \alpha_{o,HOCl} \alpha_{o,As(OH)_3} + k_2 \alpha_{o,HOCl} \alpha_{1,As(OH)_3} + k_3 \alpha_{o,HOCl} \alpha_{2,As(OH)_3},$$

At pH 7,

$$\alpha_{o,HOCl} = \frac{[H^+]}{[H^+] + K_a} = \frac{10^{-7}}{10^{-7} + 10^{-7.5}} = 0.760.$$

And for the triprotic acid $As(OH)_3$

$$\alpha_{o,As(OH)_3} = \frac{[H^+]^3}{[H^+]^3 + K_{a1}[H^+]^2 + K_{a1}K_{a2}[H^+] + K_{a1}K_{a2}K_{a3}} = 0.9937,$$

$$\alpha_{1,As(OH)_3} = \frac{K_{a1}[H^+]^2}{[H^+]^3 + K_{a1}[H^+]^2 + K_{a1}K_{a2}[H^+] + K_{a1}K_{a2}K_{a3}} = 0.0063$$

$$\alpha_{2,As(OH)_3} = \frac{K_{a1}K_{a2}[H^+]}{[H^+]^3 + K_{a1}[H^+]^2 + K_{a1}K_{a2}[H^+] + K_{a1}K_{a2}K_{a3}} = 4.98 \times 10^{-8}$$

Thus,

$$k_{overall} = 4.3 \times 10^3 (0.76)(0.9937) + 5.8 \times 10^7 (0.76)(0.0063)$$

$$+ 1.4 \times 10^9 (0.76)(4.98 \times 10^{-8})M^{-1}s^{-1}$$

$$= 3.25 \times 10^3 + 2.77 \times 10^5 + 5.30 \times 10^2 M^{-1}s^{-1}$$

$$= 2.81 \times 10^5 M^{-1}s^{-1}$$

Note that even though $As(OH)_2O^-$ only makes up $\sim0.6\%$ of the As^{III} is solution, it dominates the reactivity with the HOCl.

13.6 Reactions of chlorine with organic compounds

13.6.1 Overview

Although studies on the reactions of chlorine with organic compounds go back at least to the early twentieth century, the majority of the most relevant information was stimulated by the discovery in the 1970s that drinking water often is contaminated with chlorinated organic compounds formed as unintended products of chlorination (called disinfection by-products, DBPs) by reaction of chlorine with natural organic

matter and/or synthetic organic contaminants.[4,5,24] Free chlorine reacts with organic functional groups primarily by three types of mechanisms: (1) oxidation of organic functional groups, (2) addition to double bonds, and (3) electrophilic substitution. In the first category, chlorine species are reduced to Cl^-, and chlorinated organic compounds are not formed. The timescale of these reactions varies widely depending on the nature of the organic compound being oxidized. Reactions with organic S and some aromatic and heterocyclic rings are very fast ($t_{1/2} < 1$ s). Oxidation of sulfur groups leads to sulfoxides, sulfones, and sulfonic acids.[5] Oxidation of amines occurs on timescales of minutes to hours. Second-order rate constants for reaction with HOCl are typically on the order of 10^8 M^{-1} s^{-1} for primary amines, 10^7 M^{-1} s^{-1} for secondary amines, and 10^4 M^{-1} s^{-1} for tertiary amines. Figure 13.6 provides ranges of second-order rate constants for the reaction of HOCl with various substrates. Nonselective oxidation of organic matter occurs over minutes to days. In the following sections, some of the more important (but by no means all of the) reactions of chlorine with organic compounds are discussed.

HOCl can add to double bonds to form halohydrins:

$$\text{C=C} + \text{HOCl} \longrightarrow \underset{\text{Cl}}{-\text{C}-\text{C}-} + \text{OH}^- \longrightarrow \underset{\text{Cl} \quad \text{OH}}{-\text{C}-\text{C}-} \tag{13.16}$$
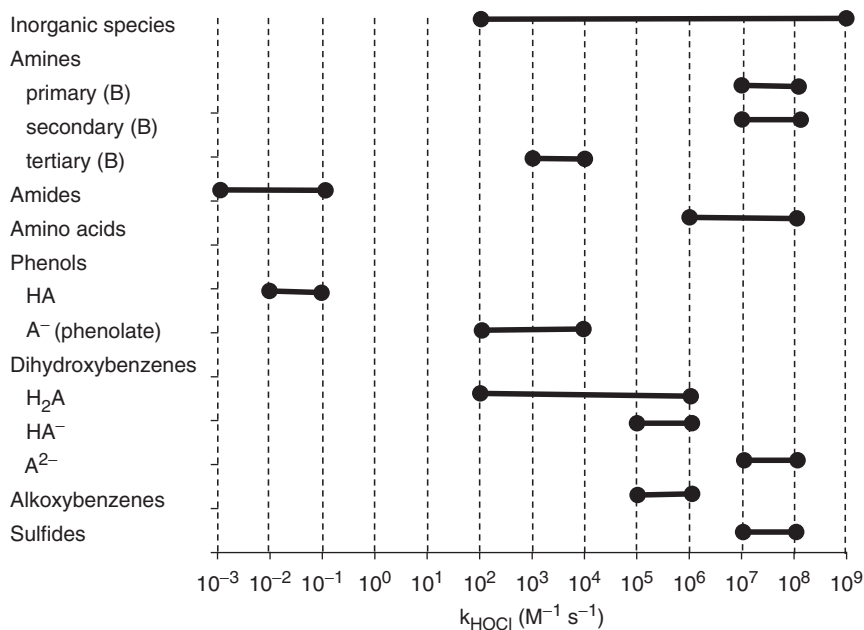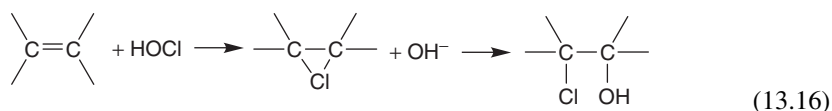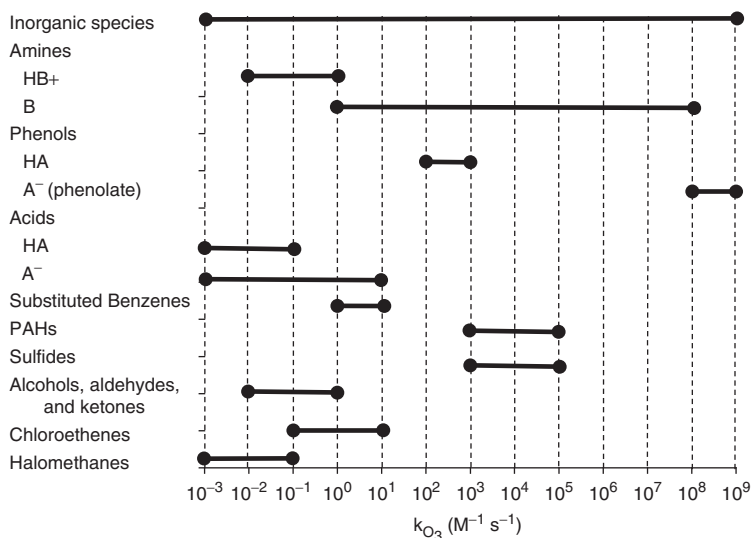

Figure 13.6 Ranges of second-order rate constants for the reaction of various classes of substrates with HOCl. Data summarized from Deborde and von Gunten[5] and references therein.

This could be significant in natural waters containing unsaturated compounds (e.g., plant pigments), but addition reactions are slow unless the double bond is activated by substituent groups. Not much is known about the importance of these reactions in water supplies.

Three types of electrophilic substitution reactions involving chlorine species are of interest: (1) substitution into aromatic compounds such as phenols, (2) reaction with N-containing compounds to form N-chloro-organic compounds, and (3) reaction with natural organic matter to form trihalomethanes (THMs) and haloacetic acids (HAAs). At near neutral pH, all three reactions involve HOCl acting as an electrophilic agent. The Cl atom in HOCl behaves like Cl^+, which is a strong electrophile and combines with a pair of electrons residing on nucleophilic substrates.

13.6.2 Formation of chlorophenols and other chlorobenzenes

Phenolic compounds occur in water contaminated by some industrial activities, and phenolic groups are important in aquatic humic matter. Phenol itself causes taste and toxicity problems, but chlorophenols are much worse. The threshold odor concentration (ThOC) of phenol is $> 1000\,\mu g/L$, but the ThOC of 2-chlorophenol, 2,4-dichlorophenol, and 2,6-dichlorophenol is only $2–3\,\mu g/L$, and the ThOC of 4-chlorophenol is $250\,\mu g/L$. Phenols react readily with free chlorine, and this can lead to serious taste and odor problems in water. Chlorination of phenol was studied as early as 1926 and recognized as an electrophilic attack of HOCl on phenolic anions.[25] In the 1950s, Burtschell et al.[26] identified the reaction products and established a reaction sequence, and Lee and Morris[27,28] determined the kinetics of each step. As Figure 13.7 shows, stepwise substitution of Cl at the *ortho* and *para* positions on the ring yields several monochloro- and dichloro- intermediates with high odor potential (low ThOC) before forming the relatively low-odor compound 2,4,6-trichlorophenol, TCP (ThOC $> 1000\,\mu g/L$). Reaction of TCP with chlorine results in a variety of more oxidized and chlorinated products, including the following:[31]
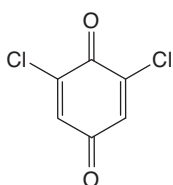
2,6-Dichlorobenzoquinone   2,4,4,6-Tetrachlorocyclohexa-2,5-dienone
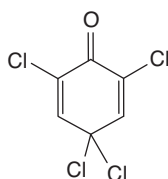
Chlorination also leads to rupture of the ring, eventually leading to the DBPs chloroform and trichloroacetic acid. Phenolic groups in organic matter are chloroform precursors.[29,32]

The reactions fit simple second-order rate expressions of the form

$$-d[Cl]_T = k_T[Cl]_T[Phenol]_T. \qquad (13.14)$$

Subscript $_T$ again refers to total concentrations of the reactants irrespective of acid-base form. Rate constants (k_T) for each step have maximum values in the range pH 7–9 and decrease rapidly on either side of the maximum (Table 13.3).[27] Figure 13.8 illustrates
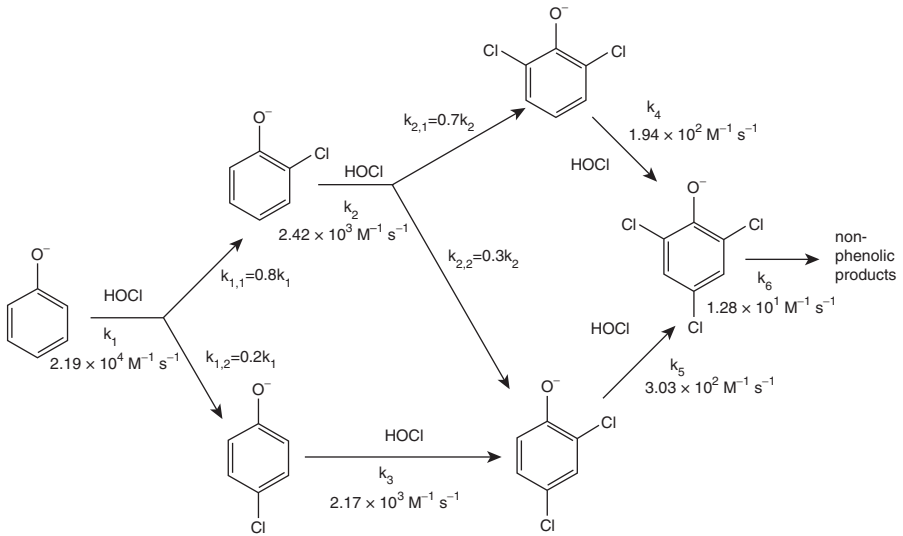
Figure 13.7 Reaction scheme for the chlorination of phenoxide ion (adapted from Burtschell et al.[26] and Lee and Morris[28]) with rate constants and ratio percentages from Gallard and von Gunten[29] and Acero et al.[30] Redrawn from Deborde and von Gunten.[5]

Table 13.3 Rate constants (k_T; M^{-1} s^{-1}) for chlorination of phenols*

pH	Phenol	2-Cl-Phenol	4-Cl-Phenol	2,4-Di-Cl-phenol	2,6-Di-Cl-phenol	2,4,6-Tri-Cl-phenol
5	2.09×10^2	4.03×10^2	9.60×10^1	2.38×10^2	6.32×10^2	1.17×10^2
6	4.82×10^2	1.04×10^3	2.98×10^2	4.02×10^2	1.34×10^3	3.46×10^2
7	2.23×10^3	3.16×10^3	8.93×10^2	1.76×10^3	4.95×10^3	5.16×10^2
8	6.15×10^3	8.15×10^3	1.84×10^3	2.72×10^3	2.19×10^3	1.45×10^2
9	6.14×10^3	3.21×10^3	1.54×10^3	5.48×10^2	2.96×10^2	1.34×10^1
10	2.84×10^3	4.30×10^3	4.15×10^2	6.32×10^1	3.09×10^1	0.905
11	4.73×10^2	4.60×10^1	4.70×10^1	6.37	3.12	0.054
12	4.50×10^1	4.60	4.54	0.636	0.315	1.81×10^{-3}

* T = 25°C; I = 0.02; $[Cl^-] = 10^{-1}$ M. From Lee.[27]

how the concentrations of phenol and the three intermediates with the lowest TOC values change over time in kinetic simulations over the pH range of 6.0–8.0. It is apparent that the disappearance of phenol and concentration profiles of the three intermediates are highly pH dependent and that the chlorophenols exceed their threshold odor values, at least for limited periods of time. The pH of maximum k_T also decreases with increasing acidity of a phenol. This can be explained in terms of changes in the acid-base forms of chlorine and phenols with pH. When rates are expressed in terms of concentrations of HOCl and phenolate, $-d[Cl]_T = k_2[HOCl][PhO^-]$, k_2 is nearly constant over the pH range of 6–12, which suggests that these are the actual reactants. Overall, rate constants for phenolates are $\sim 10^5$ times greater than the corresponding phenols.[29,30] The product
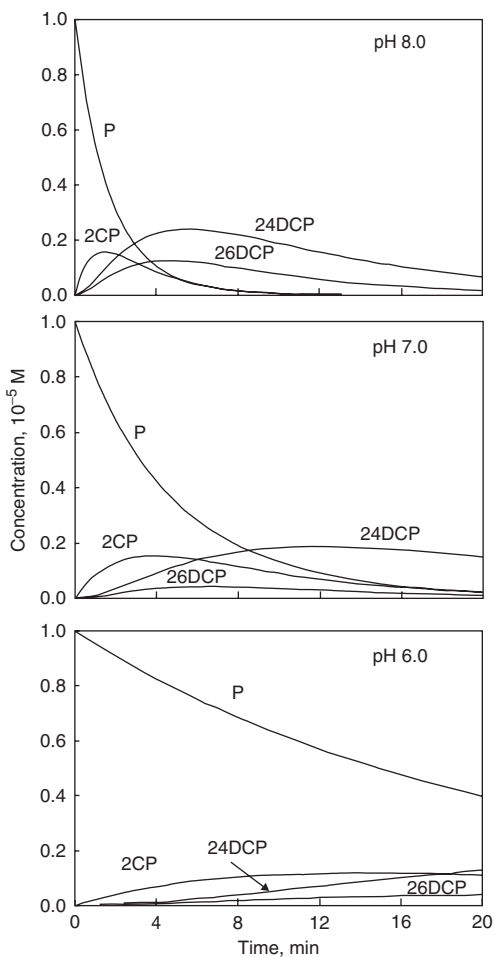
Figure 13.8 Comparison of time courses for reaction of phenol (P) and formation of the three most odorous products of phenol chlorination, 2CP (2-chlorophenol), 24DCP (2,4-dichlorophenol), and 26DCP (2,6-dichlorophenol), at pH 6.0, 7.0, and 8.0 using Acuchem.[33] Rate constants are from Table 13.3. Initial concentrations: phenol $= 1 \times 10^{-5}$ M; HOCl $= 1 \times 10^{-4}$ M.

$k_2 K_a$ (where K_a is the acid dissociation constant of a chlorophenol) is roughly constant and equal to $\sim 10^{-4}$. Electron-withdrawing substitutents that make substituted phenols more acidic tend to decrease reaction rates with electrophilic chlorine.[5,34]

Addition of ammonia to a phenol-containing water prior to chlorination can significantly lower the formation of chlorophenols. For example, at equimolar concentrations of phenol and ammonium, the formation of monochloramine at pH 8 is $\sim 10^3$ times faster than the formation of monochlorophenol. Chloramines can react with phenol to yield the same chlorophenols formed by free chlorine but at much slower rates (days to weeks). Chlorination of benzene requires a stronger electrophile than HOCl and is not important at neutral pH. Aromatic rings must be activated by substituent groups like $-O^-$ to react with HOCl, and the presence of multiple activating groups accelerates these reactions. For example, resorcinol, m-dihydroxybenzene, reacts rapidly with HOCl to form chloroform.[35]

13.6.3 Formation of THMs

The occurrence of chloroform and other THMs in chlorinated drinking water at concentrations up to several hundred micrograms per liter was first explained as the inadvertent chlorination of dissolved natural organic matter in 1974.[35−37] Since then, much has been learned about the factors affecting formation rates of THMs, methods have been developed to minimize their formation or remove them from drinking water, and other DBPs also have been discovered (Box 13.4). Understanding the mechanisms of THM formation is made difficult by the fact that the organic reactant is not a single compound or small set of compounds but a complicated mixture of organic structures, including aquatic humic matter.

The general mechanism of THM formation from natural organic matter (NOM) in water is thought to be related to the classic haloform reaction[36] (Figure 13.9), in which hypohalites react with methylketones, successively replacing hydrogens on the carbon next to the carbonyl group (called the α-carbon), and ultimately forming CHX_3, where X stands for any halide (Cl, Br, I). This reaction has been known since the nineteenth century. It is catalyzed by bases and initially involves proton dissociation from the α-carbon, yielding a carbanion that is subject to electrophilic attack by HOCl or OCl^-. The successive ionization and chlorination steps are increasingly rapid, and cleavage of the fully chlorinated methyl group releases $CHCl_3$. In Figure 13.9, the final step is shown as promoted by either hydroxide or hypochlorite. Traditionally, this reaction is written as proceeding via hydroxide attack. The production of chloroform from acetylacetone (Figure 13.9b) occurs in matter of seconds, but the hydrolysis of trichloroacetone (i.e., the final step) takes hours to days. The rapid production of chloroform from acetylacetone thus is inconsistent with hydroxide mediating the release of chloroform. Hypochlorite is a much more potent nucleophile than hydroxide, and it has been proposed that OCl^- actually mediates the process.[32]

Many studies have shown that simple methylketones cannot be the primary precursors for THMs in drinking water. For example, chlorination of acetone is much too slow to account for THMs at the levels found in drinking water; more active compounds thus must be involved during chlorination. To facilitate formation of the first carbanion intermediate, a compound must have more acidic carbons than those alpha to a single carbonyl group (see Figure 13.9b). Methylene groups between two carbonyl groups are more acidic, and some diketones yield chloroform at rapid rates under the conditions of water chlorination. Other organic compounds that yield carbanions are important precursors in THM formation. Humic substances (fulvic and humic acids) have received much attention, and 1,3-dihydroxybenzene structures found in them are thought to be the key components leading to THM formation.[29]

Production of brominated THMs, such as bromodichloromethane ($CHBrCl_2$) and bromoform ($CHBr_3$), which are found in some drinking waters, can be explained by the rapid reaction of free chlorine with traces of bromide, which occurs in some natural waters, to form HOBr. HOBr is a more effective halogenating agent than is HOCl, and can generate brominated THMs and HAAs via analogous pathways.[51,52]

Although the exact structures of THM precursors are controversial, general categories that give rise to THMs are well known. Aside from humic substances, these include algae and products of algal metabolism, such as pigments and organic nitrogen compounds. THM formation is associated with algal blooms in water supplies, and

---

Box 13.4   HAAs and other DBPs

Only two classes of halogenated DBPs currently are regulated by the U.S. EPA: trihalomethanes and haloacetic acids. The sum of four trihalomethanes (THM_4: $CHCl_3$, $CHBrCl_2$, $CHBr_2Cl$, and $CHBr_3$) must be less than $80\,\mu g/L$ and the sum of five haloacetic acids (HAA_5: chloroacetic acid, dichloroacetic acid, trichloroacetic acid, bromoacetic acid, and dibromoacetic acid) must be less than $60\,\mu g/L$ upon delivery to consumers.[38] HAAs are toxic (they once were used as herbicides) and their presence in drinking water after disinfection thus is of obvious concern. Compared to THMs, much less work has been done to elucidate the mechanisms of HAA formation. Several precursors have been identified, including phenols, which have much higher yields for HAA formation than THM formation, and aliphatic β-dicarbonyl acids.[39]

Although THM and HAA levels are regulated, more than 500 halogenated DBPs have been identified,[40,41] and many more remain unknown and await identification as analytical techniques continue to improve. Among the nonregulated compounds are halonitromethanes, haloacetonitriles, haloketones, haloacetaldehydes, and haloacetamides.[41] Some of these compounds have known biological effects. For example, trichloroacetaldehyde (which in its hydrated form is known as chloral hydrate) leads to unconciousness when ingested in sufficient quantities (thus gangsters would lace drinks with chloral hydrate, i.e., give them a Mickey Finn, or slip them a Mickey, to incapacitate rivals). Note that some DBPs react to form others. For example, trichloroacetonitrile undergoes hydrolysis to form trichloroacetamide, which then hydrolyzes to trichloroacetic acid.

Recent studies have demonstrated that many of the nonregulated DBPs are much more cytotoxic and genotoxic than the regulated THMs and HAAs. Work by Richardson, Plewa, and colleagues[42−45] has demonstrated that nitrogen-containing DBPs (i.e., halonitromethanes, haloacetonitriles, and haloacetamides) are more toxic than halogenated carbonaceous DBPs and that iodine- and bromine-containing DBPs are more toxic than their chlorinated analogues. Concerns have been raised that switching from free chlorine to chloramines to reduce THM and HAA level may increase levels of the more toxic halonitromethanes, haloacetonitriles, and haloacetamides,[41] as well as iodinated DBPs.[45] The compound 3-chloro-4-(dichloromethyl)-5-hydroxy-2(5*H*)-furanone (known as MX for mutagen X) has also been found in chlorinated drinking waters and may account for 20–50% of the total mutagenicity of chlorinated drinking waters.[46,47]

---

preventing algal blooms is one strategy to prevent THMs in drinking water. Other strategies include removing organic precursors by coagulation or adsorption on to activated carbon prior to chlorination, and adding ammonium during chlorination to generate chloramines. Chloramines produce < 3% of the THMs produced by comparable concentrations of free chlorine,[53] but they do produce significant amounts of high molecular-weight chlorinated organic matter in the presence of humic substances.[54] An additional drawback to utilizing chloramines in place of free chlorine (in addition

(a)

$$R-\overset{\overset{\displaystyle O}{\|}}{C}-CH_3 \underset{}{\overset{OH^-}{\rightleftharpoons}} R-\overset{\overset{\displaystyle O^-}{|}}{C}=CH_2 \xrightarrow{+H_2O}_{HOCl}$$

$$HOCl \searrow\ R-\overset{\overset{\displaystyle O^-}{|}}{C}=CHCl \xrightarrow[+H_2O]{OH^-} R-\overset{\overset{\displaystyle O}{\|}}{C}-CH_2Cl \xrightarrow{+OH^-}$$

$$\xrightarrow{+OH^-}\ R-\overset{\overset{\displaystyle O}{\|}}{C}-CHCl_2 \underset{}{\overset{OH^-}{\rightleftharpoons}} R-\overset{\overset{\displaystyle O^-}{|}}{C}=CCl_2 \xrightarrow{+H_2O}_{HOCl}$$

$$R-\overset{\overset{\displaystyle O}{\|}}{C}-OH\ +CHCl_3 \xleftarrow{OH^-\ or\ OCl^-} R-\overset{\overset{\displaystyle O}{\|}}{C}-CCl_3 \xrightarrow{+OH^-}$$

(b)

$$H_3C-\overset{\overset{\displaystyle O}{\|}}{C}-CH_2-\overset{\overset{\displaystyle O}{\|}}{C}-CH_3 \xrightarrow{2HOCl} H_3C-\overset{\overset{\displaystyle O}{\|}}{C}-\overset{\overset{\displaystyle Cl_2}{}}{C}-\overset{\overset{\displaystyle O}{\|}}{C}-CH_3 \xrightarrow{OH^-} CH_3COO^- + {}^-Cl_2C-\overset{\overset{\displaystyle O}{\|}}{C}-CH_3$$

$${}^-Cl_2C-\overset{\overset{\displaystyle O}{\|}}{C}-CH_3 \xrightarrow{HOCl} Cl_3C-\overset{\overset{\displaystyle O}{\|}}{C}-CH_3 \xrightarrow{OH^-\ or\ OCl^-} CH_3COO^- + CHCl_3$$
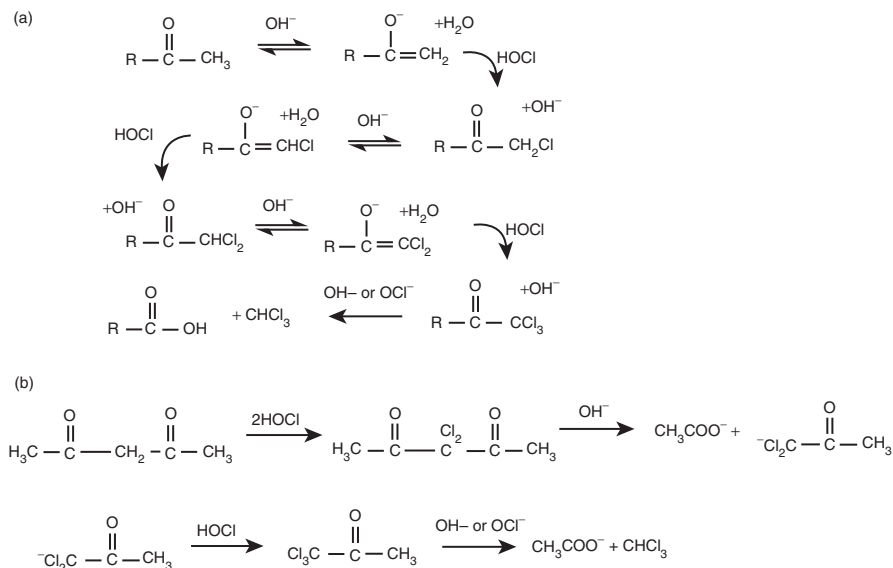
Figure 13.9 (a) General chlorination reaction of aldehydes and ketones to produce chloroform (adapted from Morris[48] and Dore[49]); (b) proposed pathway for acetylacetone chlorination (adapted from deLaat[50]). See text regarding the final hydrolysis step.

to possible enhancement of lead dissolution, as discussed above), can be increases in the formation of iodinated THMs.[55] This can be attributed to the fact that a substantial proportion of I^- is oxidized to iodate, IO_3^-, in the presence of excess free chlorine, whereas in the presence of chloramines, I^- oxidation may instead lead to the accumulation of HOI, which, like HOCl and HOBr, is an effective halogenating agent. This can be particularly problematic, on account of the very low odor thresholds and high toxicity of organic iodinated DBPs.[56]

13.6.4 Reactions with amines and amides

Free chlorine reacts with simple amines to form N-chloramines, analogous to the manner in which it reacts with ammonia. In reactions with amines, the Cl atom initially forms an N–Cl bond, in which the Cl atom maintains its +I oxidation state and thus is still capable of reacting with other substrates via electrophilic mechanisms (generally at much slower rates).[57–59] Formation of CH_3NHCl from HOCl and methylamine is rapid ($\sim60\times$ that of NH_2Cl). Formation of CH_3NCl_2 from CH_3NHCl and HOCl is $\sim10^{-5}$ as fast as formation of CH_3NHCl but still faster than the formation of $NHCl_2$. A correlation between the rate constant for N-chlorination and pK_b, the base dissociation constant for the amine, is another example of a linear free energy relationship (LFER).[9] This relationship agrees with the ideas that (1) the reactions involve electrophilic Cl species and nucleophilic N species, and (2) reactivity toward Cl is correlated with basicity toward H^+.[48] Amides, which are less basic than amines, react much more slowly. For many years it was thought that peptide-N groups, which are very weak bases, are unreactive toward

chlorine, but based on the above LFER and an estimated K_b of 0.1 for peptide N, the rate constant for chlorination of peptide N was estimated to be 13 M^{-1} s^{-1} (small but not negligible), and experimental evidence for the reaction was obtained.[60] Chlorine reacts with amino acids (second-order rate constants of 10^7 to 10^8 M^{-1} s^{-1})[4] to produce mono- and dichloramines and classic breakpoint curves. Decomposition rates of organic chloramines are not fully characterized, but several studies provide insight into the first-order decay rates of simple amino acids and alkyl amines in aqueous systems.[61,62] N-Chlorination of amino acids and primary amines can lead to formation of a diverse array of nitrogenous DBPs including nitriles, nitroalkanes, aldehydes, and cyanogen chloride, many of which are of substantial toxicological concern.[63]

With the recent lowering of allowable THM and HAA levels in drinking water by the U.S. EPA, many utilities have been switching to chloramines as the disinfectant in drinking water distribution systems. Upon this switch, utilities began to detect N-nitrosodimethylamine (NDMA; a known human carcinogen) in their finished drinking water.[64−66] Current data indicate that the reaction of chloramine and dichloramine with dimethylamine, dimethylamine-containing compounds, and potentially other amines leads to formation of NDMA.[67,68] It also has been shown that many nitrosamines are formed upon the chloramination of natural waters or wastewaters.[64,69−71]

13.6.5 Reactions of chlorinated organic compounds with sulfite (dechlorination)

Many organic chloramines react rapidly (timescale of seconds to minutes) with sulfite, but chlorinated amino-N groups of some peptides react more slowly (timescales of hours) under environmental conditions.[72] Some chlorinated by-products formed when Cl_2 reacts with humic substances are of concern as mutagens. Addition of sulfite to chlorinated water reduces its mutagenic activity and destroys some of these compounds by nucleophilic dehalogenation.[73] Many mutagens are electrophiles, and thus it makes sense that they are destroyed by a nucleophile like sulfite. The mechanism involves sulfite attack of the electrophilic carbon to which Cl is attached, resulting in reductive dehalogenation (displacement of –Cl by –H) and oxidation of sulfite to sulfate. Reactions are first order in the chlorinated compound and sulfite; second-order rate constants for the most reactive compounds are in the range of 10–100 M^{-1} s^{-1}. Rates increase with pH over the range of 6.1–8.5, probably because of increasing ionization of HSO_3^- to SO_3^{2-} (pK_{a2} = 7.18); bisulfite is a much weaker nucleophile than sulfite. In light of these characteristics, a cautionary note is pertinent: if one is interested in identifying DBPs, one must be sure that dechlorinating the solution with sulfite does not destroy the compounds being studied!

13.7 Other disinfectants

While free and combined chlorine have proven to be robust and effective disinfectants for drinking water and wastewater treatment, the formation of DBPs and the ineffectiveness of chlorine against some pathogens (e.g., cysts of *Cryptosporidium*) and some organic micropollutants (e.g., pesticides and pharmaceuticals) have led to the development of various alternative disinfection/oxidation techniques.

13.7.1 Other halogens

Chlorine dioxide sometimes is used as a disinfectant (often for residual maintenance within distribution systems), as well as to remove tastes and odors and oxidize iron and manganese in public water supplies, on account of its oxidative selectivity and its high reactivity toward Fe^{II} and Mn^{II}.[74] Its main advantage is that it acts strictly as an oxidant and does not produce a substantial amount of chlorinated organic compounds. The chemical properties of ClO_2 otherwise are similar to chlorine, and similar analytical procedures are used to analyze both forms. At high pH ($\sim$12), ClO_2 is converted to chlorite (ClO_2^-) and chlorate (ClO_3^-), a disproportionation reaction of Cl^{IV} to Cl^{III} and Cl^V:

$$2ClO_2 + H_2O \rightarrow ClO_2^- + ClO_3^- + H^+ \tag{13.18}$$
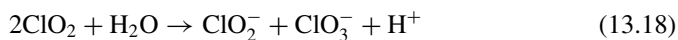
The reaction is not reversed when the solution pH is returned to near neutral. The maximum allowable level of chlorite in drinking water is 1 mg/L.[38] Direct reaction of substrates with ClO_2 proceeds via second-order kinetics.

Iodine (in tablet form) is used to disinfect personal water supplies in remote situations and sometimes in swimming pools. It has a safety advantage over chlorine in transporting the chemicals to remote areas and also has two potential advantages for use in swimming pools: less potential to cause eye irritation and easier maintenance of iodine residuals, because it is less reactive than free chlorine toward organic matter. Iodine has been used only to a limited extent in public water treatment. A brief but failed experimental application occurred in Gainesville, Florida, in the 1970s. In this case iodine reacted with organic matter in the treated water or coatings on pipes in the distribution system, causing a noticeably unpleasant taste and odor problem. The experiment was terminated quickly, to the chagrin of the water treatment chemists who had proposed the experiment.

The chemistry of iodine in water is similar to that of chlorine, but hydrolysis of I_2 to form HOI and IO^- is much less complete than that of Cl_2 at neutral pH. Four forms exist in water treated with iodine: primarily I_2 and I_3^-, and small amounts of HOI and OI^- (see Figure 13.5; together they are referred to as iodine residual). The second species, triiodide ion, is formed by reaction of I_2 with excess I^-. Iodine is added as to water in the elemental form (I_2) or produced in water by adding an iodide salt and an oxidant like chlorine; recall that iodine is a weaker oxidizing agent than chlorine.

13.7.2 Ozone

Ozone, a strong oxidant and powerful disinfectant, is used to treat drinking water in countries where chlorine tastes are considered unacceptable (e.g., much of western Europe). It is a more selective oxidant toward organic compounds than chlorine, reacting only with unsaturated bonds, reduced sulfur atoms, amines, and activated aromatic rings (e.g., phenols). Ozonation is practiced widely in industrial waste treatment and is used to remove tastes and odors in some public drinking water supplies. As concerns increase about the undesirable characteristics of chlorination, especially its tendency to form organochlorine compounds, ozone is becoming more popular for disinfecting public

water supplies in the United States. Ozone, however, is so reactive that a residual does not remain in the distribution system. Because U.S. regulations state that a disinfectant residual must be present, ozonation is usually followed by chloramination, which may lead to formation of nitrogen-containing halogenated DBPs (see Box 13.4). The inability of chlorine to effectively inactivate protozoan spores is a factor in the conversion to ozone by some water utilities. The City of Milwaukee, which uses Lake Michigan as a water source, converted to ozonation, which is more effective against protozoa and their spores, after a major incident involving the protozoan *Cryptosporidium* affected several hundred thousand users of this water supply in 1993. and More than 30 deaths were attributed to the outbreak. The source of *Cryptosporidium* in the water was never determined for certain. Initially it was speculated that it originated from farm animals in the watershed of the Milwaukee River, which flows into the lake near the city's water intake, but genotyping of the strain associated with the outbreak suggested a human (sewage) source.[75]

Ozone is unstable in water, and so it must be generated in the gas phase at the site of use—usually by electric discharge techniques—and subsequently dissolved into a water to be treated. Its decomposition in pure water generally involves free radicals (including O_3^-, O_2^-, or $\cdot OH$) and proceeds through chain mechanisms which vary in complexity depending on the composition of the aqueous matrix (Figure 13.10).[76,77] Under neutral-to-alkaline conditions, decomposition of O_3 in pure water follows a chain mechanism initiated by the hydroxide ion, OH^-. Additional studies have indicated that O_3 may decompose in water at acidic pH via thermal dissociation to O and O_2.[78] This process is relatively slow at room temperature. Ozone solutions thus are relatively stable at low pH, and loss rates increase rapidly with increasing pH. In systems containing organic compounds or other scavengers, ozone chain decomposition may also be mediated by radical processes initiated by direct reaction with such dissolved constituents (e.g., dissolved organic matter).[79] This can involve single electron transfer or homolytic oxygen transfer processes:

$$O_3 + S \rightarrow O_3^-, \tag{13.19}$$

$$O_3 + S \rightarrow O_2^- + \; S^+ - O\cdot, \tag{13.20}$$
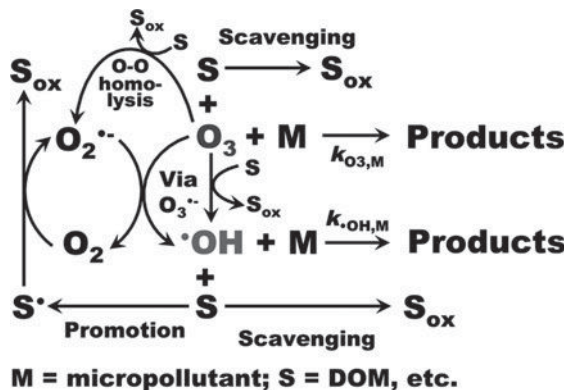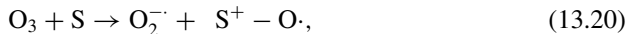
Figure 13.10 Reactions of ozone and hydroxyl radical with organic contaminants follow complicated pathways. Courtesy of Michael Dodd, University of Washington, based on information in von Gunten[76] and Buffle and von Gunten.[79] (See color insert at end of book for a color version of this figure.)

where S represents a generic substrate. The ozonide radicals, O_3^- and O_2^-, so produced may serve to propagate a radical chain decomposition of O_3 by processes similar to those occurring in pure water.[76] Consequently, ozone decomposition in natural waters can be much faster than anticipated solely based on direct reactions with dissolved constituents.

Many studies have been conducted on the reactions of O_3 and its decomposition products in drinking water, wastewater, and natural water.[76–87] O_3 reacts directly with a variety of organic and inorganic compounds but is highly selective regarding the functional groups it attacks. Direct reactions of O_3 with organic compounds almost invariably are second-order processes, and rate constants are available for many compounds.

Second-order rate constants for reactions of O_3 with unsaturated aliphatics and neutral aromatic compounds vary by six orders of magnitude depending on the degree of activation by substituent groups (Figure 13.11). Electron-withdrawing groups such as $-Cl$. Groups $-C=O$, and $-NO_2$ substantially decrease reactivity, but electron-donating groups such as $-CH_3$, $-COCH_3$, or NH_2 may substantially increase reactivity. In the case of $-OH$-substituted aromatic compounds (phenols), which exhibit acid-base speciation in pH range of natural waters, the degree of activation/deactivation by the $-OH/-O^-$ group depends strongly on pH: anionic phenolate forms may be up to 8 orders of magnitude more reactive toward O_3 than neutral phenol forms (Figure 13.11). In general, rate constants for organic acids and bases increase with pH if the site of attack by O_3 is conjugated with the acid/base functional groups, and the deprotonated forms react more quickly than the protonated conjugates. Amines thus also exhibit tremendous pH dependency in reactivity toward O_3. Neutral amine species have rate constants ranging from 10^3 to 10^7 M^{-1} s^{-1} (depending on the degree and type of substitution),

Figure 13.11 Ranges of second-order rate constants for the reaction of various classes of substrates with O_3. Ozone data summarized from Brezonik[34] with original data sources.[83–85]

but their protonated forms are effectively nonreactive. Ozone also may react very rapidly with reduced sulfur compounds such as sulfides, thiols, and thioethers. Because many pharmaceuticals and personal care products (which are ubiquitous micropollutants in municipal wastewaters) contain such reactive moieties,[88] much recent research has focused on investigating their reactions with chlorine and ozone, particularly in the context of wastewater treatment.[89−93] Many of these compounds have acid-base chemistries, and reaction rates with ozone thus are pH dependent.

Ozone also reacts readily with reduced inorganic chemicals,[76,94] often at comparable rates to the reaction with chlorine (see Figures 13.6 and 13.11). A notable exception is ammonia, which is essentially unreactive with ozone. An important ozone reaction is that with bromide, which leads to bromate formation.[95] In the presence of ozone, bromide is oxidized to OBr^-. The OBr^- is then oxidized by ozone to BrO_2^-, and this species in turn reacts with ozone to form BrO_3^-. In the presence of hydroxyl radicals and ozone, bromide is oxidized to a bromine radical that then reacts with ozone to ultimately form bromate.

The radical chain decomposition processes identified above also yield the hydroxyl radical ($^.OH$) as an intermediate product, and so $^.OH$ nearly always is present during aqueous ozonation.[80,81] Thus, $^.OH$, which is itself a very powerful oxidant and highly reactive toward many substrates,[96] often is responsible for the destruction of pollutants during ozonation (Figure 13.10). Therefore, when one desires to study the direct kinetics of reactions between ozone and organic substrates, a $^.OH$ radical scavenger (e.g., t-butanol) should be added to prevent $^.OH$ from influencing the kinetics measurements. Although ozone is present at much higher concentrations than hydroxyl radicals during aqueous ozonation processes, $^.OH$ may be responsible for a considerable proportion of substrate oxidation if substrates are recalcitrant to O_3 itself. The dominant transformation pathway of a given substrate thus is a function of oxidant concentrations and the respective second-order rate constants for direct reaction of the substrate with O_3 and $^.OH$:

$$\frac{dS}{dt} = -k_{O_3,S}[O_3][S] - k_{.OH,S}[^.OH][S] \tag{13.21}$$

Ozone is a major product of photochemical reactions in the atmosphere, but it is not formed by photochemical reactions in natural waters, except as a very minor product in nitrate photolysis. Its main source in natural waters likely is absorption from the atmosphere, but atmospheric levels are low. Polluted urban air contains ∼100–200 ppb O_3, and rural air normally is several orders of magnitude lower. The solubility of O_3 in water, however, is almost 10× greater than that of O_2 (12.2 vs. 1.35 mmol L^{-1} atm^{-1}); Henry's law constants (H) at 25°C are 0.082 and 0.74 atm m^3 mol^{-1}, for O_3 and O_2, respectively. An order-of-magnitude estimate for the rate of O_3 transfer from the atmosphere into water bodies[34] is 0.01–0.1 mol m^{-2} yr^{-1}. Thus atmospheric inputs are quite small (but perhaps not negligible), especially in remote areas. Relatively little is known about the importance of O_3 as a reactant in natural waters, although it is hypothesized to play an important role in driving halogen cycling at the ocean surface.[97]

EXAMPLE 13.3 Ozonation of trimethylamine: (a) Determine the apparent second-order rate constant for the reaction of trimethylamine (TMA; $(CH_3)_3N$) with ozone and

hydroxyl radical at pH 8 given the following information:

$$\text{TMAH}^+ \rightleftharpoons \text{TMA} + \text{H}^+ \quad pK_a = 9.9$$
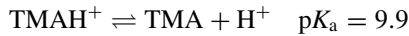
Species	$k_{O_3}(\text{M}^{-1}\,\text{s}^{-1})$	$k_{\cdot\text{OH}}(\text{M}^{-1}\,\text{s}^{-1})$
TMAH$^+$	~ 0	4×10^8
TMA	4.1×10^6	1.3×10^{10}

Answer: The apparent rate constant for each oxidant will depend on the speciation of the TMA:

(1) $k_{app} = \alpha_0 k_{HB^+} + \alpha_1 k_B$

At pH 8,

(2) $\alpha_0 = \dfrac{[\text{H}^+]}{[\text{H}^+] + K_a} = \dfrac{10^{-8}}{10^{-8} + 10^{-9.9}} = 0.988$

and $\alpha_1 = 0.012$.
   Thus,

(3) $k_{O_3,app} = (0.987)(0) + 0.012(4.1 \times 10^6) = 4.9 \times 10^3\ \text{M}^{-1}\,\text{s}^{-1}$

(4) $k_{\cdot\text{OH},app} = (0.987)(4 \times 10^8) + 0.012(1.3 \times 10^{10}) = 5.5 \times 10^8\ \text{M}^{-1}\,\text{s}^{-1}$

(b) Calculate the pseudo-first-order rate constant for the loss of TMA at pH at an ozone concentration of 50 μM and a ratio of $[\text{OH}]:[O_3]$ of 10^{-8}. Assume the hydroxyl radical and ozone concentrations are constant.

Answer: Recall that a pseudo-first-order rate constant is a second-order rate constant times a concentration which is constant. Thus,

(5) $k_{ozone} = (4.9 \times 10^3)(50 \times 10^{-6}) = 0.245\ \text{s}^{-1}$,

(6) $k_{hydroxyl} = (5.5 \times 10^8)(50 \times 10^{-6})(10^{-8}) = 2.75 \times 10^{-4}\text{s}^{-1}$.

Although the second-order rate constant for the reaction of ˙OH is greater than that of O_3, the difference in the steady-state concentrations of the two species make ozone the oxidant primarily responsible for the disappearance of TMA.

13.7.3 Advanced oxidation techniques

Advanced oxidation processes (AOPs)—which are designed primarily for pollutant oxidation, rather than disinfection—rely on the production of highly reactive and nonselective hydroxyl radicals.[98,99] As ozone produces ˙OH upon its decomposition, some AOPs rely on accelerating the production of ˙OH from ozone; e.g., UV light photolyzes ozone to various intermediates, including ˙OH. The combination of ozone and UV light can be effective in oxidizing organic contaminants, and reactor systems have been developed to take advantage of this fact. The effectiveness of photolytic

ozonation results from the photolysis of O_3 at 254 nm to yield H_2O_2, which itself is photolyzed to yield $\cdot OH$. Reaction with the conjugate base of H_2O_2, the hydroperoxide ion, HO_2^- ($pK_a = 11.6$), further accelerates the decomposition of O_3 at circumneutral to alkaline pH. In fact, two additional means of generating $\cdot OH$ for water treatment include the direct combinations of O_3 with H_2O_2 and UV with H_2O_2. Interest in the latter process for micropollutant oxidation has grown rapidly in recent years, partly on account of its potential for application in wastewater reuse and drinking water treatment schemes already using UV light for disinfection.

Problems

13.1. The Arizona winter residence of Professor Rheam, a retired paper chemist, has an in-ground swimming pool (dimensions 40×16 ft; average depth 4.5 ft). Never known for his knowledge of redox chemistry or dexterity, Rheam took a gallon of household bleach to the pool area in an effort to remove some rust spots, and in his haste to get the job done, he tipped over the jug of bleach. It all flowed into the swimming pool before he was able to retrieve it. Assume the jug was full and that its strength was 5% NaOCl, which is typical for household bleach.

   (a) Was Rheam's intended use of the bleach—to remove rust spots—likely to be successful?
   (b) Rheam did a quick calculation in his head and decided that the amount of bleach that entered the pool would not pose a hazard to swimmers, and he did not mention it to his guests, who swam in the pool later that afternoon. Assume that the bleach was completely mixed in the pool water in a matter of minutes. By how much did the chlorine residual increase (in mg/L as Cl_2), and was Rheam justified in his initial calculation?

13.2. If the swimming pool in problem 13.1 had accumulated ammonium at a concentration of 0.14 mg/L as N prior to the bleach spill, would the additional free chlorine been sufficient to achieve the breakpoint reaction with the ammonium? What would the likely concentrations of free and combined chlorine be in the pool after the chlorine reacted with the ammonium? (Assume the initial chlorine residual in the pool was negligible; Rheam was not a very good pool caretaker).

13.3. What is the equilibrium speciation of free chlorine forms ($HOCl$, OCl^-, and $Cl_{2(aq)}$) at pH 5.0 in a water containing 35 mg/L of Cl^-?

13.4. A ground water used as a drinking water supply has a pH of 7.0 and a concentration of dissolved arsenic, all present as As^{III}, of 100 μg/L, well above the drinking water standard. The first unit in the treatment plant is prechlorination in a flash mixer—essentially a CFSTR—which has a water residence time of 2 minutes. If chlorine is added at a dose sufficient to maintain a constant concentration of 1.5 mg/L of free chlorine residual what is the estimated concentration of dissolved As^{III} in the outlet from the flash mixer? How does the answer change for water at pH 6 or pH 8.

13.5. Use Acuchem to simulate the time-course for appearance and disappearance of the various chlorophenols produced in the chlorination of phenol at pH 5 and pH 9. Assume initial concentrations of 1.5 mg/L for phenol and 5 mg/L for free chlorine. Plot your results and discuss the differences between the time-courses at the two pH values. What chlorophenol compounds exceed their threshold odor concentrations and for what duration?

13.6. Using the rate constants given in the chapter, calculate the fraction of HOCl/OCl$^-$ that would react with NH$_4^+$/NH$_3$ and the fraction that would react with As^{III} at pH 8, if 50 mL of a 10 µM solution of HOCl$_T$ was added directly to 50 mL of a solution containing total ammonia/ammonium at 100 µM as N, and As^{III} at 1 µM, assuming ideal and instantaneous mixing.

13.7. Given the following information for the formation and destruction of chloramine, perform an Acuchem simulation of monochloramine decay at a constant of pH 8 with a total carbonate (C$_T$) concentration of 2 mM in a closed system. You may assume that the initial concentrations of free chlorine and ammonia are zero, but you will need to consider their speciation as you construct your model (because the fractions in the OCl$^-$ and NH$_4^+$ forms are not reactive).

HOCl + NH$_3$ → NH$_2$Cl + H$_2$O	$k_1 = 1.5 \times 10^{10}$ M^{-1} h^{-1}
NH$_2$Cl + H$_2$O → HOCl + NH$_3$	$k_2 = 7.6 \times 10^{-2}$ h^{-1}
HOCl + NH$_2$Cl → NHCl$_2$ + H$_2$O	$k_3 = 1.0 \times 10^6$ M^{-1} h^{-1}
NHCl$_2$ + H$_2$O → HOCl + NH$_2$Cl	$k_4 = 2.3 \times 10^{-3}$ h^{-1}
NH$_2$Cl + NH$_2$Cl → NHCl$_2$ + NH$_3$	$k_5 = k_d$
NHCl$_2$ + NH$_3$ → NH$_2$Cl + NH$_2$Cl	$k_6 = 2.2 \times 10^8$ M^{-2} h^{-1}
NHCl$_2$ + H$_2$O → I	$k_7 = 4.0 \times 10^5$ M^{-1} h^{-1}
I + NHCl$_2$ → HOCl + products	$k_8 = 1.0 \times 10^8$ M^{-1} h^{-1}
I + NH$_2$Cl → products	$k_9 = 3.0 \times 10^7$ M^{-1} h^{-1}
NH$_2$Cl + NH$_2$Cl → products	$k_{10} = 55$ M^{-1} h^{-1}
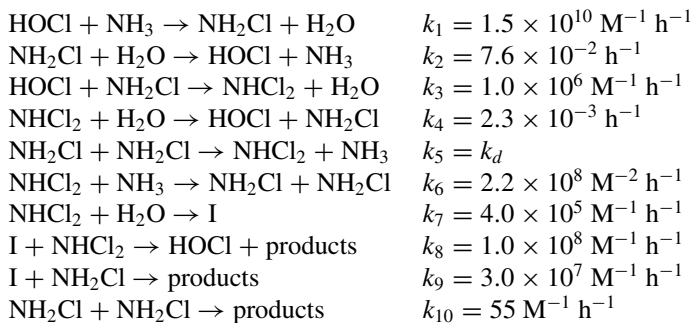
"I" is an unknown intermediate (with initial concentration of zero).

$$k_d = k_a[\text{H}^+] + k_b[\text{H}_2\text{CO}_3^*] + k_c[\text{HCO}_3^-] \text{ with } k_a = 2.5 \times 10^7 \text{ M}^{-2}\text{h}^{-1},$$

$$k_b = 4 \times 10^4 \text{ M}^{-2}\text{h}^{-1}, \text{ and } k_c = 800 \text{ M}^{-2}\text{h}^{-1}$$

All information is from Vikesland et al.[100]

References

1. U.S. EPA. 1999. Alternative disinfectants and oxidants guidance manual. EPA 815-R-99-014, Washington, D.C.
2. Chick, H. 1908. An investigation of the laws of disinfection. *J. Hygiene* **8**: 92–158; Watson, H. E. 1908. A note on the variation of the rate of disinfection with concentration of disinfectant. *J. Hygiene* **8**: 536–542.

3. Edwards, M., S. Triantafyllidou, and D. Best. 2009. Elevated blood lead in young children due to lead-contaminated drinking Water: Washington, DC, 2001–2004. *Environ. Sci. Technol.* **43**: 1618–1623; Renner, R. 2006. Mis-lead. *Environ. Sci. Technol.* **40**: 4333–4334; Edwards, M., and A. Dudi. 2004. Role of chlorine and chloramines in corrosion of lead-bearing plumbing materials. *J. Am. Water Works Assoc.* **96**: 69–81.

4. For example, a series of conferences on chlorination chemistry in the 1970s and 1980s was published in a five-volume series: *Water chlorination: environmental impact and health effects*, Ann Arbor Sci. Publ., Ann Arbor, Mich.: Vol. 1, R. L. Jolley (ed.), 1978; Vol. 2, R. L. Jolley, H. Gorchev, and D. H. Hamilton, Jr. (eds.), 1978; Vol. 3, R. L. Jolley, W. A. Brungs, and R. B. Cummings (eds.), 1980; Vol. 4, R. L. Jolley, W. A. Brungs, J. A. Cotruvo, R. B. Cummings, J. S. Mattice, and V. A. Jacobs (eds.), 1983; Vol. 5, R. L. Jolley, R. J. Bull, W. P. Davis, S. Katz, M. H. Roberts, Jr., and V. A. Jacobs (eds.), Lewis Publ., Chelsea, Mich., 1985.

5. Deborde, M., and U. von Gunten. 2008. Reactions of chlorine with inorganic and organic compounds during water treatment—kinetics and mechanisms: a critical review. *Water Res.* **42**: 13–51.

6. Bartlett, W. P., and D. W. Margerum. 1999. Temperature dependencies of the Henry's Law constant and the aqueous phase dissociation constant of bromine chloride. *Environ. Sci. Technol.* **33**: 3410–3414.

7. Wang, T. X., and D. W. Margerum. 1994. Kinetics of reversible chlorine hydrolysis: temperature dependence and general-acid/base-assisted mechanisms. *Inorg. Chem.* **33**: 1050–1055.

8. Aieta, E. M., and P. V. Roberts. 1985. The chemistry of oxo-chlorine compounds relevant to chlorine dioxide generation. In *Water chlorination*, Vol. 5, 783–794; and 1986. Kinetics of the reaction between molecular chlorine and chlorite in aqueous solution. *Environ. Sci. Technol.* **20**: 50–55.

9. Margerum, D. W., E. T. Gray, and R. P. Huffman. 1978. Chloramine equilibria and the kinetics of disproportionation in aqueous solution. In *Organometals and organometalloids.Occurrence and fate in the environment*, F. E. Brickman and J. M. Bellama (eds.), Symp. Ser. **82**, Am. Chem. Soc., Washington, D.C., 278–291.

10. Cherney, D. P., S. E. Duirk, J. C. Tarr, and T. W. Collette. 2006. Monitoring the speciation of aqueous free chlorine from pH 1 to 12 with Raman spectroscopy to determine the identity of the potent low-pH oxidant. *Appl. Spectrosc.* **60**(7): 764–772.

11. Weil, I., and J. C. Morris. 1949. Kinetic studies on the chloramines. I. The rates of formation of monochloramine, N-chlormethylamine and N-chlordimethylamine. *J. Am. Chem. Soc.* 71: 1664–1671; and Kinetic studies on the chloramines. II. The base strength of N-chloro dialkylamines and of monochloramine. *J. Am. Chem. Soc.* 71: 3123–3126.

12. Morris, J. C., and R. A. Isaac. 1983. A critical review of kinetic and thermodynamic constants for the aqueous chlorine-ammonia system. In *Water chlorination*, Vol. 4, 49–62.

13. Hand, V. C., and D. W. Margerum. 1983. Kinetics and mechanisms of the decomposition of dichloramine in aqueous solution. *Inorg. Chem.* **22**: 1449–1456.

14. Kumar, K., R. W. Shinness, and D. W. Margerum. 1987. Kinetics and mechanisms of the base decomposition of nitrogen trichloride in aqueous solution. *Inorg. Chem.* **26**: 3430–3434.

15. Jolley, R. L., and J. H. Carpenter. 1983. A review of the chemical and environmental fate of reactive oxidant species in chlorinated water. In *Water chlorination*, Vol. 4, 3–47.

16. Gray, E. T., Jr., D. W. Margerum, and R. P. Huffman. 1978. Chloramine equilibria and the kinetics of disproportionation in aqueous solution. In *Organometals and organometalloids. Occurrence and fate in the environment*, F. E. Brinkman and J. M. Bellama (eds.), Am. Chem. Soc. Washington, DC., 264–277.

17. Margerum, D. W., and K. E. H. Hartz. 2002. Role of halogen(I) cation-transfer mechanisms in water chlorination in the presence of bromide ion. *J. Environ. Monit.* **4**: 20–26.

18. Kemsley, J. 2007. Bromate in Los Angeles water. *C&E News*, Dec. 24: 9.

19. Kumar, K., and D. W. Margerum. 1987. Kinetics and mechanism of general-acid-assisted oxidation of bromide by hypochlorite and hypochlorous acid. *Inorg. Chem.* **26**: 2706–2711.

20. Folkes, L. K., L. P. Candeias, and P. Wardman. 1995. Kinetics and mechanisms of hypochlorous acid reactions. *Arch. Biochem. Biophys.* **323**: 120–126.

21. Hao, O. J., A. P. Davis, and P. H. Chang. 1991. Kinetics of manganese(II) oxidation with chlorine. *J. Environ. Eng.* **117**: 359–374.

22. Dodd, M. C. N. Duy Vu, A. Ammann, V. Chieu Le, R. Kissner, H. V. Pham, T. H. Cao, M. Berg, and U. von Gunten. 2006. Kinetics and mechanistic aspects of As(III) oxidation by aqueous chlorine, chloramines, and ozone: relevance to drinking water treatment. *Environ. Sci. Technol.* **40**: 3285–3292.

23. Bedner, M., W. A. MacCrehan, and G. R. Helz. 2004. Making chlorine greener: investigation of alternatives to sulfite for dechlorination. *Water Res.* **38**: 2505–2514.

24. Richardson, S. D. 2003. Disinfection by-products and other emerging contaminants in drinking water. *TrAC Trends Anal. Chem.* **22**: 666–684.

25. Soper, F. G., and G. F. Smith. 1926. The halogenation of phenols. *J. Chem. Soc.* **129**: 1582–1591.

26. Burtschell, R. H., A. A. Rosen, F. M. Middleton, and M. B. Ettinger. 1959. Chlorine derivatives of phenol causing taste and odor. *J. Am. Water Works Assoc.* **51**: 205–213.

27. Lee, G. F. 1967. Kinetics of reactions between chlorine and phenolic compounds. In *Principles and applications of water chemistry*, S. D. Faust and J. V. Hunter (eds.), J. Wiley, New York, 54–72.

28. Lee, G. F., and J. C. Morris. 1962. Kinetics of chlorination of phenol: chlorophenolic tastes and odors. *Int. J. Air Wat. Poll.* **6**: 419–431.

29. Gallard, H. and U. von Gunten. 2002. Chlorination of phenols : kinetics and formation of chloroform. *Environ. Sci. Technol.* **36**: 884–890.

30. Acero, J. L., P. Piriou, and U. von Gunten. 2005. Kinetics and mechanisms of formation of bromophenols during drinking water chlorination: assessment of taste and odor development. *Water Res.* **39**: 2979–2993.

31. Smith, J. G., S.-F. Lee, and A. Netzer. 1976. Model studies in aqueous chlorination: the chlorination of phenols in dilute aqueous solution. *Water Res.* **10**: 985–990.

32. Arnold, W. A., J. Bolotin, U. von Gunten, and T. B. Hofstetter. 2008. Evaluation of functional groups responsible for chloroform formation during water chlorination using compound specific isotope analysis. *Environ. Sci. Technol.* **42**: 7778–7785.

33. Braun, W., J. T. Herron, and D. K. Kahaner. 1988. Acuchem: a computer program for modeling complex chemical reaction systems. *Int. J. Chem. Kinetics* **6**: 51–62.

34. Brezonik, P. L. 1994. *Chemical kinetics and process dynamics in aquatic systems*, Lewis Publ., CRC Press, Boca Raton, Fla.

35. Rook, J. J. 1976. Haloforms in drinking water. *J. Am. Water Works Assoc.* **68**: 168–172.

36. Rook, J. J. 1974. Formation of haloforms during chlorination of natural waters. *Water Treatment Exam.* **23**(pt. 2): 234–243.

37. Bellar, T. A., J. J. Lichtenberg, and R. C. Kroner. 1974. The occurrence of organohalides in chlorinated drinking water. *J. Am. Water Works Assoc.* **66**: 703–706.

38. U. S. EPA. 1998. National primary drinking water regulations: disinfectants and disinfection byproducts; final rule. *Fed. Reg.* **63**(241): 69389–69476.

39. Dickenson, E. R. V., R. S. Summers, J. P. Croué, and H. Gallard. 2008. Haloacetic acid and trihalomethane formation from the chlorination and bromination of aliphatic β-dicarbonyl acid model compounds. *Environ. Sci. Technol.* ***42***: 3226–3233.

40. Weinberg, H. S., S. W. Krasner, S. D. Richardson, and A. D. Thurston, Jr. 2002. The occurrence of disinfection by-products (DBPs) of health concern in drinking water: results of a nationwide DBP occurrence study. U.S. EPA, EPA/600/R-02/068 (available at http://www.epa.gov/Athens/publications/reports/EPA_600_R02_068.pdf, accessed 10/2009).

41. Krasner, S. W., H. S. Weinberg, S. D. Richardson, S. J. Pastor, R. Chinn, M. J. Sclimenti, G. D. Onstad, and A. D. Thruston, Jr. 2006. Occurrence of a new generation of disinfection byproducts. *Environ. Sci. Technol.* **40**: 7175–7185.

42. Plewa, M. J., M. G. Muellner, S. D. Richardson, F. Fasano, K. M. Buettner, Y. Woo, A. B. McKague, and E. D. Wagner. 2008. Occurrence, synthesis, and mammalian cell cytotoxicity and genotoxicity of haloacetamides: an emerging class of nitrogenous drinking water disinfection byproducts. *Environ. Sci. Technol.* **42**: 955–961.

43. Plewa, M. J., E. D. Wagner, P. Jazwierska, S. D. Richardson, P. H. Chen, and A. B. McKague. 2004. Halonitromethane drinking water disinfection byproducts: chemical characterization and mammalian cell cytotoxicity and genotoxicity. *Environ. Sci. Technol.* **38**: 62–68.

44. Plewa, M. J., E. D. Wagner, S. D. Richardson, A. D. Thurston, Jr., Y. Woo, and A. B. McKague. 2004. Chemical and biological characterization of newly discovered iodoacid drinking water disinfection byproducts. *Environ. Sci. Technol.* **38**: 4713–4722.

45. Richardson, S. D., F. Fasano, J. J. Ellighton, F. G. Crumley, K. M. Buettner, J. J. Evans, B. C. Blount, L. K. Silvia, T. J. Waite, G. W. Luther, A. B. McKague, R. J. Miltner, E. D. Wagner, and M. J. Plewa. 2008. Occurrence and mammalian cell toxicity of iodinated disinfection byproducts in drinking water. *Environ. Sci. Technol.* 42: 8330–8338.

46. Kronberg, L., B. Holmbom, M. Reunanen, and L. Tikkanen. 1988. Identification and quantification of the Ames mutagenic compound 3-chloro-4-(dichloromethyl)-5-hydroxy-2(5H)-furanone and of its geometric isomer (E)-2-chloro-3-(dichloromethyl)-4-oxobutenoic acid in chlorine-treated humic water and drinking water extracts. *Environ. Sci. Technol.* **22**: 1097–1103.

47. Onstad, G. D., H. S. Weinberg, and S. W. Krasner. 2008. Occurrence of halogenated furanones in US drinking waters. *Environ. Sci. Technol*. **42**: 3341–3348.

48. Morris, J. C. 1978. The chemistry of aqueous chlorine in relation to water chlorination. In *Water chlorination*, vol. 1, 21–33.

49. Dore, M. 1989. *Chimie des oxydants et traitement des eau. Edition technique et documentation*, Lavoisier, Paris.

50. DeLaat, J., M. Merlet, and M. Dore. 1982. Chlorination of organic compounds: chlorine demand and reactivity in relationship to the trihalomethane formation. Incidence of ammoniacal nitrogen. *Water Res.* **16**: 1437–1450.

51. Richardson, S. D. A. D. Thruston, C. Rav-Acha, L. Groisman, I. Popilevsky, O. Juraev, V. Glezer, A. B. McKague, M. J. Plewa, and E. D. Wagner. 2003. Tribromopyrrole, brominated acids, and other disinfection byproducts produced by disinfection of drinking water rich in bromide. *Environ. Sci. Technol.* **37**: 3782–3793.

52. Acero, J. L., P. Piriou, and U. von Gunten. 2005. Kinetics and mechanisms of formation of bromophenols during drinking water chlorination: assessment of taste and odor development. *Water Res.* **39**: 2979–2993.

53. Norwood, D. L., J. D. Johnson, R. F. Christman, J. R. Hoss, and M. J. Bobenreith. 1980. Reactions of chlorine with selected aromatic models of aquatic humic material. *Environ. Sci. Technol.* **14**: 187–190.

54. Fleischacker, S. J., and S. J. Randtke. 1983. Formation of organic chlorine in public water supplies. *J. Am. Water Works Assoc.* **75**: 132–138.

55. Bichsel, Y., and U. von Gunten. 2000. Formation of iodo-trihalomethanes during disinfection and oxidation of iodide containing waters. *Environ. Sci. Technol.* **34**: 2784–2791.

56. Richardson, S. D., F. Fasano, J. J. Ellington, F. G. Crumley, K. M. Buettner, J. J. Evans, B. C. Blount, L. K. Silva, T. J. Waite, G. W. Luther, A. B. McKague, R. J. Miltner, E. D. Wagner, and M. J. Plewa. 2008. Occurrence and mammalian cell toxicity of iodinated disinfection byproducts in drinking water. *Environ. Sci. Technol.* **42**: 8330–8338.

57. Snyder, M. P., and D. W. Margerum. 1982. Kinetics of chlorine transfer from chloramine to amines, amino acids, and peptides. *Inorg. Chem.* **21**: 2545–2450.

58. Yoon, J., and J. N. Jensen. 1993. Distribution of aqueous chlorine with nitrogenous compounds: chlorine transfer from organic chloramines to ammonia. *Environ. Sci. Technol.* **27**: 403–409.

59. Isaac, R. A., and J. C. Morris. 1985. Transfer of active chlorine from chloramine to nitrogenous organic compounds. 2. Mechanism. *Environ. Sci. Technol.* **19**: 810–814.

60. Ayotte, R. C., and E. T. Gray, Jr. 1985. Chlorination of the peptide nitrogen. In *Water chlorination*, Vol. 5, 797–806.

61. Hand, V. C., M. P. Snyder, and D. W. Margerum. 1983. Concerted fragmentation of N-chloro-α-amino acid anions. *J. Am. Chem. Soc.* **105**: 4022–4025.

62. Antelo, J. M., F. Arce, and M. Parajo. 1996. Kinetic study of the decomposition of N-chloramines. *J. Phys. Org. Chem.* **9**: 447–454.

63. Joo, S. H., and W. A. Mitch. 2007. Nitrile, aldehyde, and halonitroalkane formation during chlorination/chloramination of primary amines. *Environ. Sci. Technol.* **41**: 1288–1296.

64. Najm, I., and R. R. Trussell 2001. NDMA formation in water and wastewater. *J. Am. Water Works Assoc.* **93**: 92–99.

65. Choi, J., and R. L. Valentine. 2002. Formation of N-nitrosodimethylamine (NDMA) from reaction of monochloramine: a new disinfection byproduct. *Water Res.* **36**: 817–824.

66. Mitch, W. A., and D. L. Sedlak. 2002. Formation of N-nitrosodimethylamine (NDMA) from dimethylamine during chlorination. *Environ. Sci. Technol.* **36**: 588–595.

67. Mitch, W. A., J. O. Sharp, R. R. Trussell, R. L. Valentine, L. Alvarez-Cohen, and D. L. Sedlak. 2003. N-Nitrosodimethylamine (NDMA) as a drinking water contaminant: a review. *Environ. Eng. Sci.* **20**: 389–404.

68. Schreiber, I. M., and W. A. Mitch. 2006. Nitrosamine formation pathway revisited: the importance of chloramine speciation and dissolved oxygen. *Environ. Sci. Technol.* **40**: 6007–6014.

69. Mitch, W. A., and D. L. Sedlak. 2004. Characterization and fate of N-nitrosodimethylamine precursors in municipal wastewater treatment plants. *Environ. Sci. Technol.* **38**: 1445–1454.

70. Mitch, W. A., A. C. Gerecke, and D. L. Sedlak. 2003. A N-nitrosodimethylamine (NDMA) precursor analysis for chlorination of water and wastewater. *Water Res.* **37**: 3722–3741.

71. Walse, S. S., and W. A. Mitch. 2008. Nitrosamine carcinogens also swim in chlorinated pools. *Environ. Sci. Technol.* **42**: 1032–1037.

72. Stanbro, W. D., and M. J. Lenkevich. 1982. Slowly dechlorinated organic chloramines. *Science* **215**: 967–968.

73. Croué, J. P., and D. Reckhow. 1989. Destruction of chlorination byproducts with sulfite. *Environ. Sci. Technol.* **23**: 1412–1419.

74. Hoigné, J., and H. Bader. 1994. Kinetics of reactions of chlorine dioxide (OClO) in water. 1. Rate constants for inorganic and organic compounds. *Water Res.* **28**: 45–55.

75. Hrudey, S. E. and E. J. Hrudey. 2004. *Safe drinking water: lessons from recent outbreaks in affluent countries*. IWA Publ., London, p. 242.

76. von Gunten, U. 2003. Ozonation of drinking water: part I. Oxidation kinetics and product formation. *Water Res.* **37**: 1443–1467.

77. Hoigné, J., and H. Bader. 1978. Ozone and hydroxyl radical-initiated oxidations of organic and organometallic trace impurities in water. In *Organometals and organometalloids. Occurrence and fate in the environment*, F. E. Brinckman and J. M. Bellama (eds.), ACS Symp. Ser. **82**, Am. Chem. Soc., Washington, D.C., 292–313; Hoigné, J. 1998. Chemistry of

aqueous ozone and transformation of pollutants by ozonation and advanced oxidation processes. In *The handbook of environmental chemistry*, J. Hrubec (ed.), Springer-Verlag, Berlin, 83–141.

78. Sehested, K. H. Corfitzen, J. Holcman, and E. J. Hart. 1998. On the mechanism of the decomposition of acidic O_3 solutions, thermally or H_2O_2-initiated. *J. Phys. Chem. A* **102**: 2667–2672.

79. Buffle, M.-O., and U. von Gunten. 2006. Phenols and amine induced HO· generation during the initial phase of natural water ozonation. *Environ. Sci. Technol.* **40**: 3057–3063.

80. Buffle, M.-O., J. Schumacher, E. Salhi, M. Jekel, and U. von Gunten. 2006. Measurement of the initial phase of ozone decomposition in water and wastewater by means of a continuous quench-flow system: application to disinfection and pharmaceutical oxidation. *Water Res.* **40**: 1884–1894.

81. Nöthe, T., H. Fahlenkamp, and C. von Sonntag. 2009. Ozonation of wastewater: rate of ozone consumption and hydroxyl radical yield. *Environ. Sci. Technol.* **43**: 1590–1595.

82. Glaze, W. H. 1987. Drinking-water treatment with ozone. *Environ. Sci. Technol.* **21**: 224–230.

83. Hoigné, J., and H. Bader. 1976. The role of hydroxyl radical reactions in ozonation processes in aqueous solution. *Water Res.* **10**: 377–386.

84. Butkovic, V., L. Klasinc, M. Orhanovic, J. Turk, and H. Guesten. 1983. Reaction rates of polynuclear aromatic hydrocarbons with ozone in water. *Environ. Sci. Technol.* **17**: 546–548.

85. Hoigné, J., and H. Bader. 1983. Rate constants of reactions of ozone with organic and inorganic compounds in water-–I: Non-dissociating organic compounds; II: Dissociating organic compounds. *Water Res.* **17**: 173–183; 185–194.

86. Staehelin, J., and J. Hoigné. 1982. Decomposition of ozone in water: rate of initiation by hydroxide ions and hydrogen peroxide. *Environ. Sci. Technol.* **16**: 676–681.

87. Gurol, M. D., and P. C. Singer. 1982. Kinetics of ozone decomposition: a dynamic approach. *Environ. Sci. Technol.* **16**: 377–383.

88. Richardson, S. D. 2009. Water analysis: emerging contaminants and current issues. *Anal. Chem.* **81**: 4645–4677.

89. Pinkston, K. E., and D. L. Sedlak. 2004. Transformation of aromatic ether- and amine-containing pharmaceuticals during chlorine disinfection. *Environ. Sci. Technol.* **38**: 4019–4025.

90. Deborde, M., S. Rabouan, H. Gallard, and B. Legube. 2004. Aqueous chlorination kinetics of some endocrine disruptors. *Environ. Sci. Technol.* **38**: 5577–5583.

91. Huber, M. M., S. Canonica, G.-Y Park, and U. von Gunten. 2003. Oxidation of pharmaceuticals during ozonation and advanced oxidation processes. *Environ. Sci. Technol.* **37**: 1016–1024.

92. Dodd, M. C., M.-O. Buffle, and U. von Gunten. 2006. Oxidation of antibacterial molecules by aqueous ozone: moiety-specific reaction kinetics and application to ozone-based wastewater treatment. *Environ. Sci. Technol.* **40**: 1969–1977.

93. Dodd, M. C., and C.-H. Huang. 2004. Transformation of the antibacterial agent sulfamethoxazole in reactions with chlorine: kinetics, mechanisms, and pathways. *Environ. Sci. Technol.* **38**: 5607–5615.

94. Hoigné, J., H. Bader, W. R. Haag, and J. Staehelin. 1985. Rate constants of reactions of ozone with organic and inorganic compounds in water. 3. Inorganic compounds and radicals. *Water Res.* **19**: 993–1004.

95. von Gunten, U. 2003. Ozonation of drinking water: part II. Disinfection and by-product formation in presence of bromide, iodide or chlorine. *Water Res.* **37**: 1469–1487.

96. Buxton, G. V., W. P. Greenstock, W. P. Helman, and A. B. Ross. 1988. Critical review of rate constants for reactions of hydrated electrons, hydrogen atoms, and hydroxyl radicals (OH/O^-) in aqueous solution. *J. Phys. Chem. Ref. Data* **17**: 513–886.

97. Martino, M., G. P. Mills, J. Woeltjen, and P. S. Liss. 2009. A new source of volatile organoiodine compounds in surface seawater. *Geophys. Res. Lett.* **36**: L01609; doi: 10.1029/2008GL036334.

98. Peyton, G. R., and W. H. Glaze. 1987. Mechanism of photolytic ozonation. In *Photochemistry of environmental aquatic systems*, R. G. Zika and W. J. Cooper (eds.), ACS Symp. Ser. **327**, Am. Chem. Soc., Washington, D.C., 76–88.

99. Legrini, O., E. Oliveros, and A, M. Braun. 1993. Photochemical processes for water treatment. *Chem. Rev.* **93**: 671–698.

100. Vikesland, P. J., K. Ozekin, and R. L. Valentine. 2001. Monochloramine decay in model and distribution system waters. *Water Res.* **35**: 1766–1776.

14

An Introduction to Surface Chemistry and Sorption

Objectives and scope

This chapter focuses on the role of surfaces associated with suspended particles and bottom sediments—pervasive components of aquatic systems—in affecting concentrations of all types of solutes. The nature of surfaces and interfaces and the forces involved in attracting or repelling solutes (and other surfaces) is described with emphasis on the important role of their electrical charge (electrostatic interactions). The excess energy found at surfaces, called surface or interfacial tension, is described and its origins explained. The accumulation (or binding) of solutes on surfaces is called sorption, and the chapter describes various models and mathematical expressions to quantify this important process, including the basic Freundlich and Langmuir models and more complicated models developed to overcome limiting assumptions of the two basic models. The classic Gouy-Chapman model of the electrical double layer is described, along with more modern extensions, and the chapter concludes with an explanation of surface complexation models—a more chemically oriented approach to describing and quantifying the interactions between solutes and surfaces.

Key terms and concepts

- Sorbate, sorbent, sorption, adsorption, absorption
- Surface and interfacial tension
- Surface charge and its origins: isomorphic substitution and ionizable surface functional groups
- pH of point of zero charge, pH_{PZC}
- Surface complexation and surface sites as ligands

- Freundlich equation, Langmuir equation, Brunauer-Emmet-Teller (BET) equation
- Electric double layer, diffuse double layer, double layer thickness (κ^{-1}), Gouy-Chapman theory
- Constant charge, constant potential, and constant capacitance models
- Stern layer, triple-layer model

14.1 Introduction

Numerous reactions in natural waters involve surfaces—reactions with sediments at the bottoms of lakes and streams and interactions between solutes and solid particles suspended in the water column. Suspended solids include inorganic substances, such as aluminosilicate clays, and metal (hydr)oxides, carbonates, and sulfides, as well as particulate organic matter—detritus from dead microbes, living microorganisms, and remains of terrestrial organisms. Solid-solution interactions control the aqueous concentrations of many natural constituents in water and are especially important in understanding controls on concentrations of pollutants such as heavy metals, anthropogenic organic compounds, and various nutrients. It is difficult to overestimate the importance of surface processes in environmental water chemistry. Indeed, these processes may be considered to be a defining feature of natural water chemistry, and they are critically important in a host of water engineering reactions, including sorption of organic contaminants onto activated carbon, coagulation of suspended solids in drinking water, and many processes involved in remediating contaminated ground water. Oxides and hydrous metal oxides are key scavengers of toxic metals in the environment, and sorption is perhaps more important to the fate and transport of such metal ions than is dissolution/precipitation. Redox-active metal oxides like Fe and Mn dissolve when they become reduced and can release previously sorbed quantities of toxic metals.

For many decades, the approach used to develop an understanding of solid-solution interactions focused on the physics of solid surfaces and was based on the concept that nearly all surfaces of interest in aquatic systems are electrically charged. This includes clay minerals, hydrous oxides, natural organic matter, microbial cells, and most other natural solids. Most of the research on this topic was aimed at quantifying how surface charge (1) varies as a function of the nature of the solid and the composition of the solution and (2) affects the ways that solutes are attracted to or repelled from surfaces. Although refinements in knowledge continue to occur, the basic physics of these processes has been understood for many decades. Over the past few decades, increasing emphasis has been placed on treating surface sites where sorption of ions occurs as *ligands*. The idea of surface-solute interactions as **surface complexation reactions** has facilitated a more "chemical approach" to understanding sorption processes.[1] The underlying physics resulting from the charges and electric fields at surface-aquatic interfaces still must be considered, but now they become complications that affect the chemical equilibria rather than the primary focus of solid-solution (surface) equilibria.

The subject of this chapter is a mature and highly complicated topic, and we cannot provide a complete development in this text. Instead, our goals are more modest. First, we describe the nature of solid surfaces for typical (electrically charged) natural solids,

focusing on the origin of the charge, how it changes with solution conditions such as pH, and the nature of surface tension and molecular-level forces at interfaces. Second, we describe important relationships that chemists and engineers use to quantify interactions between solutes in aqueous solutions and solid surfaces—sorption isotherms—and provide practical examples of their use in understanding the behavior of important solutes in aquatic systems. In addition to describing older, well-known empirical and semitheoretical models for sorption, we introduce more recent approaches developed to overcome limitations of the earlier models. Third, we explain the physics of the surface-solution interface and how the presence of a charged surface disrupts the electroneutrality of the solution near the interface, giving rise to an electrical "double layer." Finally, we describe how knowledge of the underlying physics and chemistry is useful in developing a better understanding of various processes with emphasis on sorption.

14.2 Surfaces, surface charge, and forces at interfaces

14.2.1 Nature of solid-water interfaces

The surfaces involved in solid-water interfaces in aquatic systems (e.g., suspended or bottom sediments) are very diverse, but they can be grouped into two broad categories—hydrophilic and hydrophobic—reflecting the nature of the solutes they attract. Examples of hydrophilic surfaces include mineral solids, such as hydrous oxides of Fe and Al, aluminosilicate clays, and carbonate and sulfide minerals, all of which are rich in electronegative atoms and polar or ionizable surface sites. The structures of hydrophobic surfaces have low polarity and include organic detritus (natural organic matter, NOM) from decomposing organisms, microbial cells, biofilms, and "black carbon" particles from incomplete combustion of wood and fossil fuels. Purely hydrophobic surfaces are rare in natural systems, however. Microbial cells and organic detritus have ionic or ionizable functional groups on their surfaces that behave as hydrophilic sites. Even black carbon particles, which are similar chemically but much smaller in size to commercial activated carbon, have some ionic functional groups that can attract and form bonds with ionic solutes. As the above remarks imply, the nature of the solutes attracted to surfaces and the forces involved in binding solutes to the surfaces differ substantially for the two types of surfaces.

14.2.2 Origin of surface charges

Because electrical charge is such a defining property of surfaces, even nominally hydrophobic ones, our first task is to describe the nature and origin of the charge. Surface charges on solids of interest in environmental water systems arise in two primary ways: by isomorphic substitution in the crystalline lattice of the solid (permanent charge) and by the presence of ionizable functional groups on the surface of the solid (variable charge).

In the case of *isomorphic substitution*, metal centers of lower charge than the primary metal center decrease the amount of positive charge in hydrous oxides, leading to a net negative charge. For example, substitution of Al for Si atoms in the tetrahedral (silica) layer and of Mg for Al atoms in the octahedral (aluminum oxide) layer of clay

minerals (see Section 15.5 for further information on their structures) leads to an intrinsic negative charge in these layers, e.g.,

$$\left[\begin{array}{c} \text{HO} \\ \text{Si} \\ \text{HO} \end{array} \quad \text{O} \quad \text{Si} \quad \text{O} \quad \text{Al} \quad \text{O} \quad \text{Si} \quad \begin{array}{c} \text{OH} \\ \text{OH} \end{array} \right]^{-1}_{....}$$

(14.1)

This accounts for a significant proportion of the charge associated with such minerals. The substituted metals (e.g., Al for Si) sometimes are called lattice imperfections.

Ionizable functional groups that occur on surfaces include oxide and hydroxide, carboxylic acid (–COOH), amino (–NH$_2$), phosphate (–OPO(OH)$_2$), thiol (–SH), and other acid-base groups. The charge on the particles depends on the degree of proton transfer (ionization), and hence on the pH of the medium. Examples include the silanol group on the surface of silica and siloxanes (aluminosilicates) and (hydr)oxide groups on iron and aluminum, e.g.,

$$\overset{\text{p}K_{a1}}{\equiv\text{Si–OH} \rightleftharpoons \equiv\text{Si–O}^- + \text{H}^+}$$

(14.2a)

$$\overset{\text{p}K_{a1}}{\equiv\text{Fe–OH}_2^+ \rightleftharpoons} \overset{\text{p}K_{a2}}{\equiv\text{Fe–OH} + \text{H}^+ \rightleftharpoons \equiv\text{Fe–O}^- + \text{H}^+}$$

(14.2b)

The symbol $\equiv$ is used to indicate that the rest of the coordination sites on Fe are attached to the solid lattice; in general, $\equiv$M indicates a metal center attached to a solid surface. Equation 14.2b implies that the FeOH group is "half in solution and half out,"[2] and also shows that Fe is amphoteric (or amphiprotic)—it can act as both an acid and a base. Many oxide and hydroxide surfaces behave similarly (see Figure 14.1). Organic surfaces may be amphoteric because different functional groups can be ionized as a function

Figure 14.1 Surface charge versus pH for some common solids. From Stumm[1], copyright 1992 by John Wiley & Sons, and used with permission.

of pH, e.g., protolysis of amino and carboxylate functional groups of amino acids in proteins:

$$RCH(NH_3^+)COOH \rightleftharpoons RCH(NH_3^+)COO^- + H^+ \rightleftharpoons RCH(NH_2)COO^- + H^+ \quad (14.3)$$
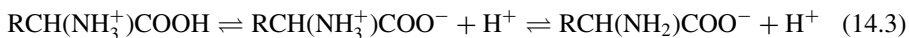
A third source for surface charge related to protolysis is the reaction of ionizable surface sites with ligands (surface complexation reactions), which is called **specific adsorption**. For example, phosphate ions may bind to an aluminum hydroxide surface, replacing an OH^- group and transforming a surface site from being uncharged to being negatively charged:

$$\equiv Al - OH + HPO_4^{2-} \rightleftharpoons \equiv Al - OPO_3^{2-} + H_2O \quad (14.4)$$
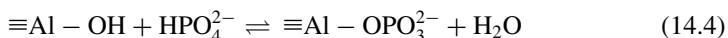
A fourth source for surface charge is the sorption of charged solutes such as surfactant molecules that have a nonpolar "tail" and an ionic functional group (see Figure 6.9) onto otherwise uncharged surfaces.

14.2.3 pH$_{PZC}$

The protonation sequence shown in Eq. 14.2 suggests that at high pH values in solution surfaces should have a net negative charge and at low pH they should have a net positive charge. At the transition between positive and negative charge, there should be some pH where the net charge is zero. The **pH of point of zero charge**, **pH$_{PZC}$**, is the pH at which the net particle charge becomes zero, and it is an important parameter in describing the behavior of surfaces. It is important to realize that we are not implying that the surface has no charges at pH$_{PZC}$. Instead, the number of positive (protonated) sites is equal to the number of negative (deprotonated) sites; pH$_{PZC}$ sometimes is called the isoelectric point and it is the pH at which particles do not migrate in an electric field. Another important feature of pH$_{PZC}$ is that it represents the pH of minimum stability of colloidal particles in suspension. At pH values away from pH$_{PZC}$, the charged surfaces, whether positive (at pH $<$ pH$_{PZC}$) or negative (at pH $>$ pH$_{PZC}$), tend to repel each other, tending to keep particles in suspension, but at or near pH$_{PZC}$, particles more readily collide, agglomerate, and precipitate. The actual value of pH$_{PZC}$ varies widely among inorganic particles, depending on the intrinsic acidity of surface functional groups, as shown in Table 14.1. For example, silica and many clays are negatively charged except at low pH values not normally found in natural waters; surface charges on Fe and Mn (hydr)oxides change from positive to negative in the circumneutral pH range, and MgO is positively charged except at pH greater than found in natural systems.

It is important to note that pH$_{PZC}$ is not necessarily the pH of zero net proton charge, pH$_{ZNPC}$, because specific adsorption of ions other than H^+ and OH^- may contribute to surface charge (e.g., Eq. 14.4). If the net charge contributed by surface complexes is zero, then pH$_{PZC}$ = pH$_{ZNPC}$.[1] In the special case that H^+ and OH^- are the only ions affecting surface charge, the pH$_{PZC}$ is equal to the average of the pK_a values for the protonated and neutral forms of the surface sites (e.g., pK_{a1} and pK_{a2} in Eq. 14.2b), or pH$_{PZC}$ = 0.5(pK_{a1} + pK_{a2}). For example, acidity constants for zinc sulfide, ZnS$_{(s)}$, have

Table 14.1 Values of pH_{PZC} for some common oxides, clays, and other minerals*

Substance	pH_{PZC}
SiO_2	2.0
Albite (Na feldspar)	2.0
Feldspars	2.0–2.4
Montmorillinite (clay)	2.5
$\delta-MnO_2$	2.8
Kaolinite (clay)	4.6
$\alpha-Al(OH)_3$	5.0
TiO_2	6.2
Fe_3O_4	6.5
$\beta-MnO_2$	7.2
$\alpha-FeOOH$	7.8
$\gamma-AlOOH$	8.2
$\alpha-Fe_2O_3$	8.5
$Fe(OH)_{3(am)}$	8.5
$\alpha-Al_2O_3$	9.1
CuO	9.5
MgO	12.5

*Values are approximate and were determined by different investigators using various methods. From Stumm[1] and Benjamin.[2]

been reported as[3]

$$\equiv ZnSH^+ \rightleftharpoons \; \equiv ZnS + H^+; \qquad pK_{a1}^s = 6.91, \qquad (14.5a)$$

$$\equiv SZn + H_2O \rightleftharpoons \; \equiv SZnOH^- + H^+; \qquad pK_{a2}^s = 10.28. \qquad (14.5b)$$
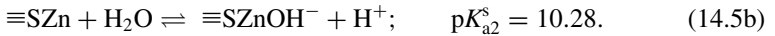
The superscript "s" denotes an equilibrium constant involving a solid surface. Accordingly, pH_{PZC} would be $(6.91 + 10.28)/2$, or 8.6.[1] Similarly, apatite, has two primary surface groups, $\equiv Ca–OH_2^+$ and $\equiv P–OH$:

$$\equiv P–OH \rightleftharpoons \; \equiv P–O^- + H^+; \qquad pK_{a1}^s = 6.6 \qquad (14.6a)$$

$$\equiv Ca–OH_2^+ \rightleftharpoons \; \equiv Ca–OH + H^+; \quad pK_{a2}^s = 9.7 \qquad (14.6b)$$
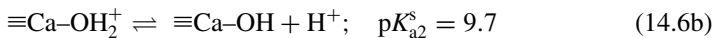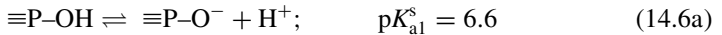
Thus we predict $pH_{PZC} = 8.15$. The literature shows a wide range of pH_{PZC} values for apatite, but a widely quoted value is 8.5 from Bell et al.[4]

One common method to determine pH_{PZC} is to conduct acid-base titrations of the surface in solutions at different ionic strengths. Ionic strength (I) has no effect on the value of pH_{PZC}, but for reasons related to the electric double layer and its compression as I increases (described later in this chapter), I does affect the charge-pH relationship when the surface has a net charge, causing the shape of titrations curves to change (become more compressed) with increasing I. Figure 14.2 illustrates this trend for titrations of a lake sediment at three concentrations of NaCl. The curves intersect at $pH = 4.1$, which is called the pH_{PZSE} (pH of the point of zero salt effect). This often is interpreted as the
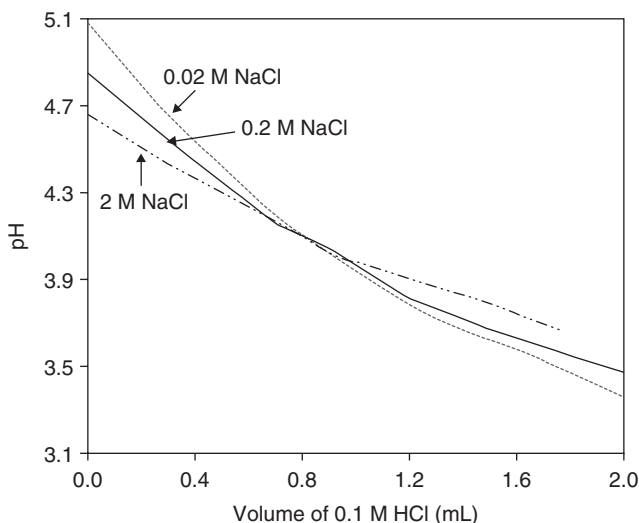
Figure 14.2 Acid-base titrations of sediment from Little Rock Lake, Wisconsin, at three ionic strengths intersect at a common pH value of 4.1, pH_{PZSE}, often interpreted as the pH_{PZC} of the sediment. Redrawn from Detenbeck and Brezonik.[5]

pH_{PZC} of the sediment, although certain assumptions beyond the scope of this text must be fulfilled for this to be strictly true.

14.2.4 Forces at interfaces

Five types of attractive or repulsive forces may be involved in the interactions of atoms and ions at interfaces:

  (i) chemical forces (covalent bonds);
 (ii) long-range electrical (electrostatic) forces;
(iii) dipole-dipole interactions, called orientation energy;
(iv) London-van der Waals forces (induced dipoles); and
 (v) hydrogen bonding.

The forces vary considerably in strength and distances over which they are effective, but all are electrical in the sense that they involve the electron clouds surrounding atoms, ions, and molecules. Chemical forces are by far the strongest, typically $>>$ 50 kJ/mol, but are effective over only very short distances, i.e., only by merging the electron clouds of adjacent atoms. Long-range electric forces are defined by Coulomb's law, $F = -z_1 z_2 / x^2$, where z_i is the charge on particle i and x is the distance between charged particles. The skewed distributions of electron clouds in dipolar molecules that result from the presence of atoms of differing electronegativities produce weak interactions between molecules called orientation energy (< 8 kJ/mol). The oscillating nature of electronic clouds even in nonpolar molecules induces attractive dipoles in adjacent molecules called dispersion or London-van der Waals forces. These are larger

than orientation energy ($\sim 8 - 40$ kJ/mol) and are inversely proportional to the sixth power of distance over small distances between two atoms. Finally, hydrogen bonding occurs when an H atom on one molecule is attracted to an unshared pair of electrons on another molecule, as described for water in Chapter 1. Hydrogen bond strengths are in the same range as London-van der Waals interactions ($\sim 8 - 40$ kJ/mol), but they occur at preferred molecular orientations (see Figures 1.3 and 1.4 for water), in contrast to the symmetric nature of London-van der Waals forces.

Interfaces represent inherent discontinuities between two phases, and this inevitably results in an imbalance of forces on molecules at interfaces. Consider a water-mineral interface, for example. A water molecule at the interface is subject to attractive forces from adjacent water molecules, which results in a net attraction of the molecule into the bulk water phase. This tends to reduce the number of water molecules at the surface and increases intermolecular distances. Work must be done to bring molecules from the interior (bulk water phase) to the surface and to increase the area of the surface (or interface). The minimum work required to create a surface dA is γdA, where γ is the interfacial Gibbs free energy, commonly called the surface tension (units of N/cm or J/cm^2):

$$\gamma = \left(\frac{\delta G}{\delta A} \right)_{T,P,n} \tag{14.7}$$

Both London-van der Waals forces and hydrogen bonding contribute to the surface tension of water: $\gamma_{H_2O} = \gamma_L + \gamma_H$, with $\sim 30\%$ from γ_L and 70% from γ_H.[6] Table 14.2 summarizes data on total surface tension, γ_T, and the contribution from London-van der Waals forces, γ_L, for some common substances.

The interfacial tension between two phases depends on the surface tensions of the individual phases in the following way. If γ_1 and γ_2 are the surface tensions (with respect to a vacuum) of the two phases, the *interfacial tension*, γ_{12}, is the net effect of attractive forces (hydrogen-bonding and London-van der Waals forces) in the bulk of each phase

Table 14.2 Total attractive forces, γ_T, at interfaces and contributions from London-van der Waals forces*

	γ_T	γ_L
Substance	10^{-7} J/cm^2	10^{-7} J/cm^2
Water	72.8	21.8
Mercury	484	200
n-Hexane	18.4	18.4
Carbon tetrachloride	26.9	—
Paraffin wax	—	25.5
Polyethylene	—	35.0
Graphite	—	110
Anatase (TiO$_2$)	—	91
Rutile (TiO$_2$)	—	143
Ferric oxide	—	107
Silica	—	123

*Dashes indicate data not available; summarized from Stumm.[1]

and attractive forces across the interface, which usually are just London-van der Waals forces:

$$\gamma_{12} = \gamma_1 + \gamma_2 - 2(\gamma_{1,L}\gamma_{2,L})^{1/2} \qquad (14.8)$$

The last term in Eq. 14.8, the geometric mean of the London-van der Waals forces, is interpreted as a measure of the interfacial attraction resulting from attractive forces between adjacent dissimilar phases. Values of γ_L can be used to predict the adsorbent properties of solids because γ_L is a measure of the available energy at a solid surface for interaction with adjacent media. The low values of γ_L for paraffin and polyethylene in Table 14.2, for example, agree with our knowledge that these are weak adsorbents. In contrast, the oxides and graphite, with larger values of γ_L, are much stronger adsorbents.

14.3 Basic sorption processes and models

14.3.1 Definitions

The process whereby solutes partition onto solid surfaces or into solid matrices in general is called *sorption*. When the solute attaches only to the solid surface, the process is called *adsorption*, and when the solute enters into the solid matrix, it is called *absorption*. Because it often is difficult to distinguish between the two processes, the generic term "sorption" often is used. Solutes that undergo sorption to surfaces/into matrices are called *sorbates*, and the sorbing surfaces/solids are called *sorbents*. In this section we describe the process of sorption and various mathematical models used to quantify the process.

14.3.2 Freundlich model

This is the oldest model used to quantify relationships between concentrations of substances in solution and the extent to which they sorb onto surfaces. It was developed in 1909 as an empirical way to explain the sorption of gases onto solid surfaces (Box 14.1). As Freundlich noted,[7] the basic model is the equation for a parabola and usually is expressed as

$$X = K_F P^{1/n}, \qquad (14.9)$$

where X = amount of sorbate sorbed per mass of sorbent (e.g., $\mu g/g$), P is the equilibrium partial pressure of the gas sorbate (e.g., in atm), K_F is called the Freundlich constant, and n is an empirical factor. As coefficients in an empirical model, K_F and n, have no intrinsic meaning, and as an empirical expression the equation requires very few assumptions about the process. Data are fit to the equation by plotting the log X versus log P; the y-intercept yields K_F and the slope of the fitted line yields n. (Modern computer software allows one to perform a nonlinear regression of the data to determine K_F and n.) For solutes in liquids sorbing to surfaces, the expression is the same except that P is replaced by C, the equilibrium sorbate concentration in molar or mass units (Figure 14.3a). Freundlich noted that the equation holds for gases only over a limited

Box 14.1   Herbert Freundlich

A founding father of colloid and surface chemistry and the developer of the sorption equation that bears his name, Herbert Max Finlay-Freundlich was in many ways a Renaissance man. Born in 1880 in Charlottenberg (near Berlin), he was one of seven children in a well-educated family; his younger brother Erwin was a famous astronomer. (Finlay is their Scottish mother's name.) Herbert Freundlich initially was interested in a career as a pianist and composer, but a visit to a prominent music teacher in Munich discouraged him from such a career unless he could be at least as good as Brahms! Freundlich then selected physical chemistry for his life's work, studying in Munich and then with Ostwald in Leipzig, where he received his Ph.D. in 1903. However, he continued to compose—mostly chamber music for strings, piano and voice (for a list of his music compositions and their availability, see http://www.herbert-freundlich.com/). When his wife died in 1917, he abruptly ended his avocation of composer. In his "day job," he was on the faculty of universities in Leipzig and Braunschweig and was a professor and director of the Kaiser Wilhelm Institute for Physical Chemistry and Electrochemistry in Berlin from 1919 to 1934, when he was forced to resign because of his Jewish ancestry. He moved to London, where he worked at University College, and then to the United States. He was a Distinguished Service Professor at the University of Minnesota from 1938 until his death in 1941.

Freundlich published an important book *Kapillarchemie* (*Capillary Chemistry*) in 1909.[7] Later editions were translated into English. Capillary chemistry was the forerunner of colloid and surface chemistry, and the name reflects the use of capillaries to study surface tension phenomena. Freundlich recognized the inadequacy of the name capillary chemistry in his book and suggested that *Grenzflächenchemie*, literally "boundary surface chemistry" or "interfacial chemistry," would be a more appropriate name. Freundlich's 1909 book introduced his isotherm equation to quantify the sorption of gases onto solid surfaces, and in the century since its introduction, it has been used widely to quantify sorption phenomena of all sorts. His more than 200 papers and several books include important contributions spanning the range of colloid chemistry and technology.

range of P. Because of its empirical foundation, the equation is not held in as high a regard as sorption equations based on physical models, such as the Langmuir model, which we discuss next.

14.3.3 Langmuir model

This model also was developed to explain sorption of gases onto solid surfaces, and like the Freundlich equation, it has been used widely to quantify sorption of solutes from aqueous solution. Developed less than a decade after the Freundlich model, the Langmuir model is based on two critical assumptions about the surface and the sorption process.[8,9]
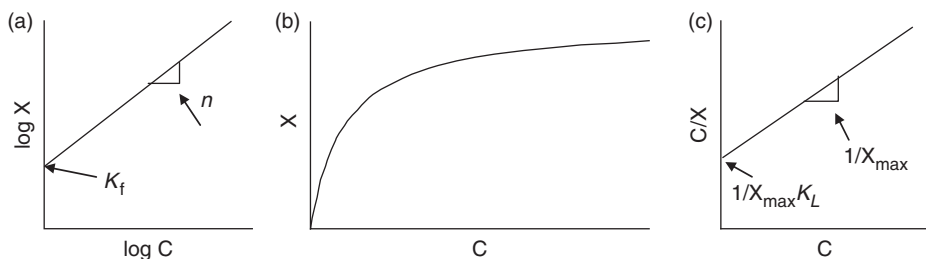
Figure 14.3 (a) Log-log plot of Freundlich isotherm; (b) amount sorbed (X) per unit of sorbent versus equilibrium concentration of sorbate (C) based on the Langmuir equation (eq. 14.10) yields a hyperbolic plot; (c) rearrangement of Langmuir equation to eq. 14.11 and plot of C/X versus C yields a linear plot if the data fit the Langmuir equation.

First, all sorption sites on the surface are assumed to be identical—i.e., they have equal binding strengths with a given sorbate. Second, only a monolayer of sorbate can be adsorbed to the solid; once all sites are occupied by sorbate molecules, no more sorption can occur. The model was developed from simple kinetic principles (Box 14.2). For sorption of solutes from aqueous solution, the basic isotherm is expressed as

$$X = \frac{X_{max}K_L C}{1 + K_L C}, \tag{14.10a}$$

where X and C are the same as for Eq. 14.7, X_{max} is the maximum sorption capacity ($\mu g/g$), and K_L is a binding constant related to the energy of sorption ($L/\mu g$). A plot of X versus C is a hyperbola, as shown in Figure 14.3b (the same as plots of the Michaelis-Menten and Monod equations described in Chapter 5, Box 5.3). Note that at small values of C (such that $K_L C \ll 1$), equation 14.10a simplifies to

$$X = X_{max}\,K_L C = K_d\,C. \tag{14.10b}$$

In Eq. 14.10b, the sorbed concentration thus is a just a linear function of concentration. The Freundlich isotherm also collapses to this form when $n = 1$. In this case, K_d is the solid-water distribution or solid-water partitioning coefficient. When organic compounds are present at low concentration (or are not very soluble) in water, their sorption to sediments or other materials may collapse to this form, which is discussed further in Chapter 19.

To determine the coefficients of the Langmuir model, Eq. 14.10 historically was rearranged by inverting both sides and then multiplying by C to obtain

$$\frac{C}{X} = \frac{1}{X_{max}K_L} + \frac{C}{X_{max}}. \tag{14.11}$$

A plot of C/X (y-axis) versus C (x-axis) is a straight line if data fit the Langmuir model (Figure 14.3c). The slope of the line is $1/X_{max}$, and the y-intercept is $1/X_{max}K_L$. It should be noted that Eq. 14.11 results in a plot of a variable (C) and a function of the same variable (C/X), which leads to the possibility of spurious self-correlation.[5,10]

Caution thus should be observed in using the transformed equation. A better alternative is to fit the sorption data directly to the untransformed Langmuir equation by nonlinear regression analysis, computer programs for which now are widely available.

Box 14.2 Kinetic derivation of the Langmuir equation

Consider a gas, A, at pressure P_A. The rate of sorption of A to a surface will be proportional to the product P_A times the fraction of the surface available for sorption (i.e., the fraction *not* covered by A, $1 - \theta_A$, where θ_A is the fraction of the surface that is covered by A):

(1) $R_{adsorption} = k_{ad}P_A(1 - \theta_A)$

The rate of desorption depends only on the concentration or number of molecules of A adsorbed to the surface:

(2) $R_{desorption} = k_{de}\theta_A$

At equilibrium the two rates are equal:

(3a) $R_{adsorption} = R_{desorption}$,

or

(3b) $k_{ad}P_A(1 - \theta_A) = k_{de}\theta_A$

Solving for θ_A, the fraction of sites occupied by A, we obtain

(4) $\theta_A = \dfrac{k_{ad}P_A}{k_{de} + k_{ad}P_A}$.

If we divide numerator and denominator by k_{de}, we obtain

(5) $\theta_A = \dfrac{\frac{k_{ad}}{k_{de}}P_A}{1 + \frac{k_{ad}}{k_{de}}P_A} = \dfrac{K_L P_A}{1 + K_L P_A}$,

where $K_L = k_{ad}/k_{de}$ is the equilibrium constant for adsorption of A to the surface. The fraction of surface sites occupied by A can be replaced by the ratio of the equivalent mass, m_A, or volume, v_A, of gas A actually adsorbed to the surface to either the mass, $m_{A,max}$, or the volume, $v_{A,max}$, that would be adsorbed if all surface sites were covered by a monolayer of A:

(6) $\theta_A = \dfrac{m_A}{m_{A,max}} = \dfrac{v_A}{v_{A,max}}$

For example,

(7) $m_A = \dfrac{m_{A,max}K_L P_A}{1 + K_L P_A}$.

For convenience, in actual studies, m_A and $m_{A,max}$ are divided by the total mass of sorbent in the system to yield X_A and $X_{A,max}$ (e.g., μg sorbed per g sorbent).

14.3.4 Applications of the Langmuir model

The basic Langmuir model provides good fits for an amazing variety of sorption phenomena, including sorption of cations to clays, metal ions to oxides, phosphate to soils and suspended and bottom sediments, and hydrophobic organic compounds to activated carbon and to organic matter in sediments. Here we provide several examples that illustrate the applicability of this basic sorption model to two diverse sorbates: phosphate ions and hydrophobic organic compounds.*

Excessive loadings of phosphorus are a major cause of eutrophication in lakes, reservoirs, rivers, and estuaries. In addition to external sources of P, water quality managers must be concerned about the bottom sediments, which often have large reservoirs of P. Several mineral forms as well as organic P in are found in bottom sediments (see Chapter 16), but some is present as inorganic phosphate ions (P_i) sorbed onto sediment surfaces. P_i is of special interest because it may be released (desorbed) readily and represents a potentially available P source for algal growth. Sorption of P_i by sediments and soils has been studied by many workers, and data typically are fit to the Langmuir equation. Figure 14.4a shows good fits to this model for organic-rich and sandy-silt sediments from two eutrophic lakes in Florida.[11] A broad range was found for the fitted parameters—a factor of 8 for K_L and a factor of 16 for X_{max} (Table 14.3).

Similarly, the simple Langmuir model yielded good fits of P_i sorption to soils from a Midwestern agricultural river basin (Table 14.4).[12,13] Samples in this study were selected to represent the diversity of soils in the basin and included silts, clays and loams (e.g., range of pH: 4.9–8.1; range of organic content, 2.4–6.2%). In contrast to the lake sediment results in Table 14.3, the soil sorption data show only a small range in X_{max} (< factor of two) and K_L (factor of ~3), but they did exhibit wide ranges in EPC (equilibrium phosphorus concentration; see below) and the fraction of sorbed P_i that could be desorbed in a subsequent aqueous extraction. X_{max} was not found to be related to any basic soil properties (probably because of the low range of measured values), but

Table 14.3 Summary of Langmuir sorption parameters for P_i to sediments from Lake Okeechobee and Lake Apopka, Florida*

Site	NAI-P[†]	X_{max}	K_L	r^2
O10	12	27.4	4.3	0.964
O11	35	91.0	7.5	0.964
O13	6	6.5	20.8	0.941
A5	108	108	34.6	0.998

*From Brezonik and Pollman.[11]
†NAI-P = nonapatite inorganic content of sediment, a measure of the maximum P_i initially sorbed to the sediment.

*Computer equilibrium programs like MINEQL+ can be used to solve sorption problems involving both the Freundlich and Langmuir equations, but the simplicity of these equations also allows one readily to solve such problems by hand or by use of spreadsheet programs.
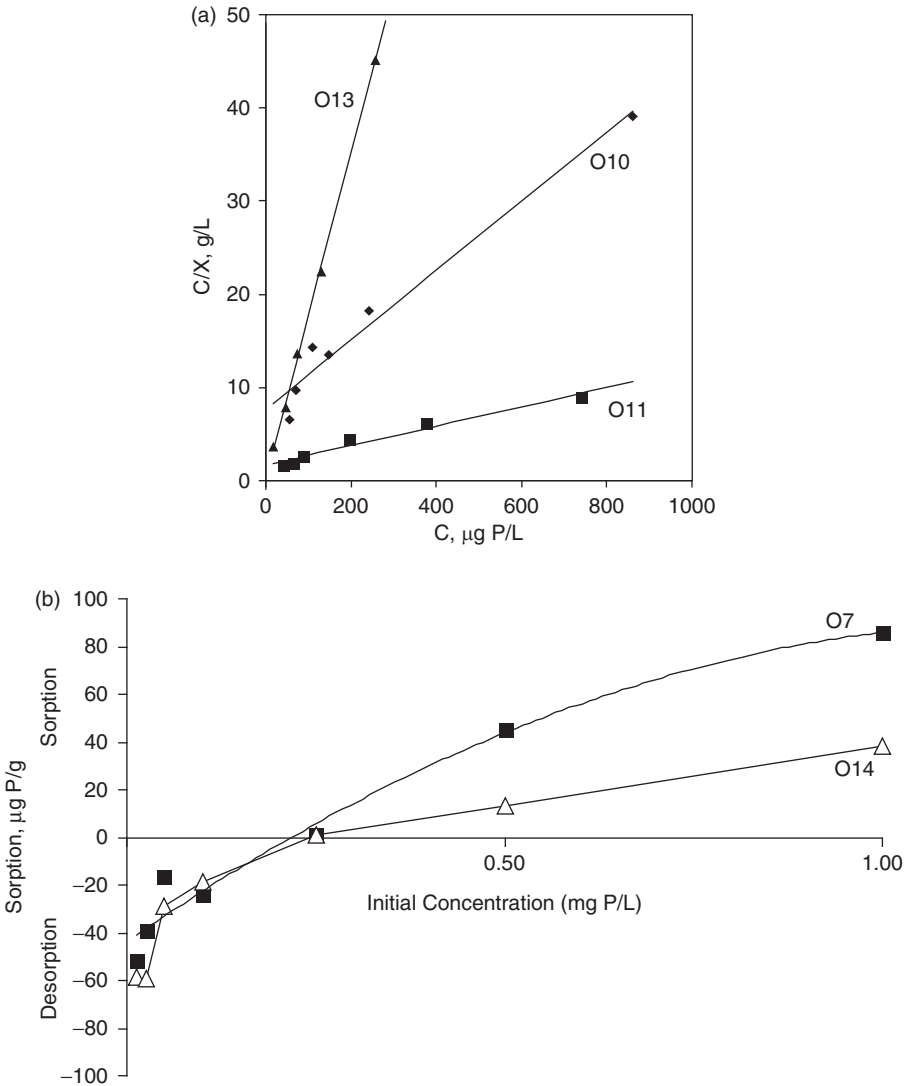
Figure 14.4 (a) Langmuir plots of phosphate sorption to sediments from Lake Okeechobee, Florida. (b) Sorption and desorption of P_i versus initial P_i concentration for two sediments from Lake Okeechobee, Florida. Equilibrium phosphate concentration (EPC) occurs where lines cross the x-axis (no net sorption): 225 μg/L for site O7 and 235 μg/L for site O14 (both highly organic "mud zone" sites). Both (a) and (b) redrawn from Brezonik and Pollman.[11]

K_L was correlated with soil pH, and clay and organic content. In addition, the product $X_{max} K_L$, called sorptivity, was found to be the best predictor of the availability of soil P for algal growth. Overall, the above results support the idea that the Langmuir model is broadly applicable to soils and sediments.

One complication associated with studying sorption/desorption of P_i by sediments and soils is that ambient samples already contain some sorbed P_i that must be taken into

Table 14.4 Summary of Langmuir sorption-desorption parameters for P_i to 25 soil samples from the Minnesota River Basin*

	$r^{2\dagger}$	X_{max}	K_L	EPC	Sorptivity‡	Desorbability
	mg/kg	10^{-3}	L/µg	µg/L	L/kg	%
Minimum	0.976	180	1.22	44	303	9
Maximum	0.998	335	3.67	1904	859	87
Average	0.990	241	2.17	483	506	30
CV (%)§	1	15	39	94	33	57

*Summarized from Fang et al.[12]
†Coefficient of determination.
‡Sorptivity $= X_{max}K_L$.
§Coefficient of variation.

account to apply the Langmuir equation properly. A modified form of the equation that does this[11,14] is

$$\frac{C_o + \frac{\Delta X}{V}}{X_o - \frac{\Delta X}{m}} = \frac{1}{X_{max}K_L} + \frac{C_o + \frac{\Delta X}{V}}{X_{max}}, \tag{14.12}$$

where C_0 is the initial P_i concentration in solution (µg/L) for a given sample, X_0 is the initial P_i present on the sediment or soil (µg/g (dry weight) of sediment), ΔX is the mass of P (µg) released from the sediment or soil in an experiment, V is the volume of solution (L), m is the (dry) mass (g) of sediment or soil in the experiment, and other terms are as defined for Eq. 14.10.

An additional sorption parameter used in studies of P sorption to soils[12–14] and sediments[11] is the EPC, defined as the inorganic P concentration in solution at which no net sorption or desorption would occur when a sediment or soil is equilibrated with that solution. The EPC of a sediment sample can be determined by plotting the incremental amount of P sorbed or desorbed versus the initial inorganic P concentration, as illustrated in Figure 14.4b. The EPC occurs where the curve for P sorbed/desorbed crosses the x-axis. The EPC is a useful parameter in describing the tendency of a sediment to act as a source or sink for inorganic P to the overlying water. Essentially, a sediment acts as a source if its EPC exceeds the actual concentration of inorganic P in the overlying water, and it acts as a sink if its EPC is lower than the water column concentration. For systems where the Langmuir model applies, it can be shown that the EPC is related to Langmuir parameters:[13]

$$\text{EPC} = \frac{X_0}{K_L(X_{max} - X_0)} \tag{14.13}$$

EPC thus is inversely proportional to the binding constant, K_L, and its value approaches infinity as X_0 approaches X_{max}.

Sorption is also a means to remove organic contaminants from water. Activated carbon, which has a high affinity for organic compounds, is a common sorbent this purpose. It is used to remove contaminants from ground water being treated by pump-and-treat methods and to remove taste and odor compounds during drinking water treatment.
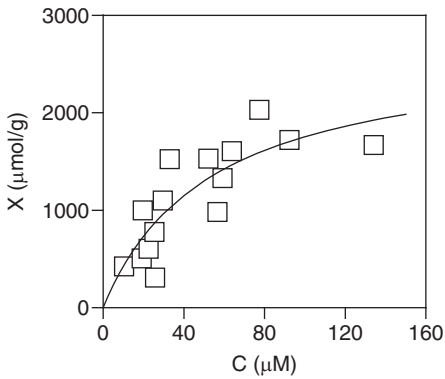
Figure 14.5 Sorption of 1,2,4-trichlorobenzene to powdered activated carbon. The Langmuir isotherm fit is $X_{max} = 3000 \pm 1000\ \mu\text{mol/g}$ and $K_L = 0.02 \pm 0.02\,\text{L}/\mu\text{mol}$ (line). From Surdo et al.,[15] copyright American Chemical Society, and used with permission.

Sorption of a representative organic contaminant, 1,2,4-trichlorobenzene, to powdered activated carbon is shown in Figure 14.5.[15] The model fit was performed using a nonlinear regression. Note that the affinity of the 1,2,4-trichlorobenzene for the solid is high and the capacity of the activated carbon is large (3000 µmol/g = 544,050 µg/g = 0.54 g/g!), which demonstrates the usefulness of activated carbon as a sorbent.

14.4 Beyond the basic Langmuir model: extensions to overcome its limiting assumptions

The explicit assumptions made in developing the Langmuir model, plus the fact that the simple model does not account for any electrostatic factors, limit the model's applicability even for some commonly encountered sorption conditions, as well as limit its ability to provide fits over wide ranges of solution conditions. Several extensions of the basic Langmuir model, as well as some radically different models, have been developed over the past 80 years to provide better fits and better explanations for specific kinds of sorption phenomena. The most important of these are described in the following sections.

14.4.1 BET model

The assumption of monolayer coverage is reasonable for the binding of ions to charged surfaces but is less so for physical adsorption (by van der Waals forces) of hydrophobic solutes to hydrophobic surfaces. Brunauer, Emmet, and Teller[16] developed the following multilayer physical adsorption model based on the Langmuir model:

$$\frac{P}{V(P_{vp} - P)} = \frac{1}{aV_m} + \frac{a - 1}{aV_m} \times \frac{P}{P_{vp}}, \qquad (14.14)$$

where V is the volume of gas adsorbed at pressure P, P_{vp} is the vapor pressure of the gas at the experimental temperature (i.e., the pressure required to condense the gas to liquid), V_m is the volume of gas adsorbed at monolayer coverage, and a is a constant. The value

of a is approximately equal to $\exp\{(E_1 - E_{gl})/RT\}$, where E_1 is the heat of adsorption for the first monolayer and E_{gl} is the heat of condensation of the gas to the liquid state. A plot of the left side of Eq. 14.14 versus P/P_{vp} yields a slope, S, of $(a-1)/aV_m$ and y-intercept, I, of $1/aV_m$, from which a and V_m can be computed; $V_m = 1/(S+I)$, and a $= (S+I)/I$. If one knows the molecular diameter of the gas, one can compute the surface area of the adsorbent from V_m, if one assumes close packing of the gas on the surface. The BET model also is widely applied to sorption of solutes in liquid solutions to solid surfaces.

14.4.2 Extension of the Langmuir model to multiple adsorbates: a competitive Langmuir model

In many real-world cases, more than one solute capable of adsorption is present in solution. If we continue to assume that there is only one kind of site on the surface, $\equiv$S, the Langmuir model can be extended as follows. Assume there are two sorbates, A and B, competing for surface sites, and their binding constants are K_A and K_B. Following the surface complexation approach of Benjamin,[2] we will write the equilibrium expressions for sorbed A and B as surface complexes. For convenience, we will use concentration-based equilibrium constants, which apply at a given ionic strength, because it is difficult to determine the activity of surface-bound species. Thus, we have

$$K_A = \frac{[\equiv SA]}{[\equiv S][A]}, \tag{14.15a}$$

$$K_B = \frac{[\equiv SB]}{[\equiv S][B]}, \tag{14.15b}$$

We can obtain the ratio of the concentrations of complexed A and B by combining the above equations:

$$\frac{[\equiv SB]}{[\equiv SA]} = \frac{K_B[B]}{K_A[A]} \tag{14.16}$$

We also can write a mass balance equation for surface sites:

$$TOT \equiv S = [\equiv S] + [\equiv SA] + [\equiv SB] \tag{14.17}$$

By algebraic manipulation of Eqs. 14.15a, 14.15b, 14.16, and 14.17, we can obtain the following equation:

$$[\equiv SA] = \frac{K_A[A]}{1 + K_A[A] + K_B[B]} TOT \equiv S \tag{14.18}$$

Dividing both sides of Eq. 14.18 by the concentration of adsorbent ($TOT \equiv S$) yields an adsorption equation for adsorbent A in the presence of competing adsorbent B:

$$X_A = \frac{K_A[A]}{1 + K_A[A] + K_B[B]} X_{max} \tag{14.19a}$$

It is readily apparent that an analogous equation can be written for the sorption of B:

$$X_B = \frac{K_B[B]}{1 + K_A[A] + K_B[B]} X_{max}$$ (14.19b)

Finally, Equations 14.19a and 14.19b can be extended to the general case of n adsorbents competing for the surface sites. For the ith adsorbent:

$$X_i = \frac{K_i[C_i]}{1 + \sum\limits_{i=1}^{n} K_i[C_i]} X_{max}$$ (14.20)

Comparing Eq. 14.20 with the basic Langmuir equation (Eq. 14.10) shows that the numerators are the same and the denominator differs by having the sum of the $K_i[C_i]$ terms rather than a single term. Addition of each competing sorbent j to a system will increase the denominator term and thus decrease the fraction of surface sites occupied by adsorbent i by an amount depending on the magnitude of K_j and $[C_j]$.

14.4.3 Sorption to surfaces with multiple discrete binding sites

The next level of complexity in sorption modeling is to consider surfaces that are not uniform but have multiple types of binding sites, each of which is characterized by a binding constant for a given adsorbent. The simplest system for this analysis is a surface with two types of sites—strong sites and weak sites—and a single adsorbent A. In such systems there generally is a relatively small number of the strong binding sites and a larger number of sites that bind A more weakly.[2] The sorption equation for the two-site case is:

$$X_{A,s} + X_{A,w} = X_{A,tot} = \frac{X_{max,s} K_{A,s}[A]}{1 + K_{A,s}[A]} + \frac{X_{max,w} K_{A,w}[A]}{1 + K_{A,w}[A]}$$ (14.21a)

where subscripts s and w denote the stronger and weaker sites, respectively. The total sorption of A thus is the sum of the sorption by the two types of sites, each defined by a Langmuir term. Equation 14.21a can be generalized to surfaces having n types of sites:

$$X_{A,tot} = \sum_{i=1}^{n} X_{A,i} = \sum_{i=1}^{n} \frac{X_{max,i} K_{A,i}[A]}{1 + K_{A,i}[A]},$$ (14.21b)

or

$$\Theta_A = \frac{\sum X_{A,i}}{\sum X_{max,i}} = \sum_{i=1}^{n} \frac{K_{A,i}[A]}{1 + K_{A,i}[A]},$$ (14.21c)

where Θ_A is a macroscopic binding parameter for A defined by summing the amount of sorption of A over all sites. Although it is relatively straightforward to write the equations for these more complicated systems, it is another matter to obtain the parameter values to use the equations. As Eqs. 14.21b and 14.21c show, for each new site we have two additional parameters to estimate. Even for the simplest (two-site) case, the ease of estimating the four parameters, $X_{max,s}$, $X_{max,w}$, $K_{A,s}$, and $K_{A,w}$, depends on their relative

magnitudes. If the weak sites are much more abundant than the strong sites, which is generally the case, an experiment covering a suitable range of [A] to define the weak-site binding may miss the influence of strong-site binding altogether, as shown by the hypothetical data for two-site sorption in Figure 14.6. Only at very low concentrations of [A] would one see that the data do not fit a simple one-site model. The number of sites needed to fit data to this model may reflect the range of sorption values as much as the actual sorption site characteristics. For example, in applying this model to metal binding by humic matter, Dzombak et al.[17] found that the number of binding sites needed was equal to the orders of magnitude of metal concentration included in a titration; each 10-fold increase in bound metal concentration required addition of another binding site.

14.4.4 Continuous distribution models

In part because of the parameter estimation difficulties associated with multiple discrete-site sorption models, especially when the number of sites is large than ~ 2, some have proposed that binding sites can be modeled as having a continuous distribution of energies. A general form of the Langmuir model that uses a continuous distribution of binding energies[17] is

$$\Theta = \frac{\sum X_i}{\sum X_{max,i}} = \int_{-\infty}^{+\infty} N(K) \frac{KC}{1 + KC} dK, \qquad (14.22)$$

where $N(K)$ is a probability function for site concentrations as a function of binding energy. Whether Eq. 14.22 can be integrated easily and applied to actual sorption data depends on the nature of $N(K)$. Perdue and Lytle[18] developed an equation based on Eq. 14.22 that assumes site concentrations are normally distributed in "log K space" (see Chapter 18, Eq. 18.9). Unfortunately, the equation cannot be integrated analytically but can be evaluated by numerical methods; "quasi-normal" functions that can be integrated analytically also are available.[5] This approach has been used to model metal binding by humic matter,[18] and others have used it to model sorption processes.[5,19]

Figure 14.6 Two-site Langmuir model using hypothetical parameter values. Site 1, $X_{max,1} = 1 \times 10^{-4}$ mol/g and $K_{L,1} = 200$ L/mol; site 2, $X_{max,2} = 1 \times 10^{-5}$ mol/g and $K_{L,2} = 2 \times 10^4$ L/mol (i.e., site 2 is 100 times stronger but one-tenth as abundant as site 1). Inset shows results at low values of X and [A]. The figures were drawn using Excel to solve eq. 14.10 at multiple values of [A]. Based on a similar analysis by Benjamin.[2]
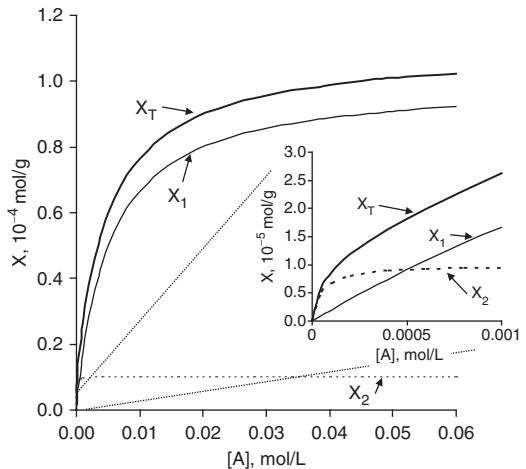
It is interesting to note that if we assume the density of sites having a given of K decreases geometrically as K increases, the probability function in Eq. 14.22 becomes $N(K) = \alpha K^{-n}$, where α and n are constants and $0 \leq n \leq 1$. This leads to an integral with a simple closed-form solution that is essentially the same as the Freundlich equation:[2]

$$\Theta = \frac{\sum X_i}{\sum X_{max,i}} = \int_0^{K_{max}} \alpha K^{-n} \frac{K[A]}{1 + K[A]} dK = \int_0^{K_{max}} \frac{\alpha K^{1-n}[A]}{1 + K[A]} dK = K_f[A]^n, \qquad (14.23)$$

where $K_f = \alpha RT\pi/\sin(n\pi)$. Note that the exponent on [A] in this derivation is n, whereas in Freundlich's original equation (Eq. 14.9) and in most books the exponent is expressed as $1/n$. Except for implications on the exact magnitude of n, the two forms are mathematically equivalent.

14.4.5 A sorption model for soil and sediment that accounts for electrostatic factors

The change in the charge on surfaces caused by sorption/desorption of ions affects the free energy change of these reactions. For example, consider the sorption of negatively charged inorganic phosphate (P_i) to an oxide surface. Regardless of the initial status of the surface (positive, neutral, or negative, depending on pH), as P_i continues to sorb to surface sites, the surface charge will decrease, becoming increasingly negative, and electrostatic repulsion will make it more difficult—less favorable energetically— for additional ions to sorb (see the reaction of P_i with an aluminum oxide surface in Eq. 14.4). The binding strength, and thus the apparent binding constant, will decrease with increasing extent of surface coverage, even if the binding sites are otherwise uniform with one intrinsic binding constant. The mathematics describing this was worked out decades ago by polymer chemists, who face the same situation in the deprotonation of polymeric acids, and is related to the electric double-layer theory described later in this chapter. Overall, this leads to rather complicated expressions. A Langmuir-based model by Barrow[20] accounting for electrostatic effects in P_i sorption by soils divided the binding term into two components: an intrinsic (Langmuir-like) constant, K_{int}, and an exponential term, $\exp[-z_i\mathcal{F}\Psi/RT]$, representing electrostatic effects:

$$\Theta = \frac{X}{X_{max}} = \frac{1}{\sigma_{\Psi_0}\sqrt{2\pi}} \int_{\Psi_0-5\sigma}^{\Psi_0+5\sigma} \frac{(\alpha_2\gamma P_{i,T})K_{int}\exp[-z_2\mathcal{F}\Psi/RT]}{(1+(\alpha_2\gamma P_{i,T})K_{int}\exp[-z_2\mathcal{F}\Psi/RT])} \exp[((\overline{\Psi}_0 - \Psi_0)/\sigma)^2]d\Psi_0$$

$$(14.24)$$

Previously undefined terms in Eq. 14.24 are Ψ_0 = initial electrostatic potential (V) in the plane of sorption (in the absence of any sorption); σ_{Ψ_0} = standard deviation of Ψ_0; $\overline{\Psi}_0$ = mean electrostatic potential (V); Ψ = actual electrostatic potential in the plane of sorption; α_2 = ionization fraction of HPO_4^{2-}, the assumed sorbing species (this is important for P_i, but $\alpha = 1$ if the sorbing species is in the same ionic form regardless of pH); $P_{i,T}$ = total (analytical) concentration of inorganic phosphate; γ = activity coefficient of sorbing; z_i = charge on sorbing ion; and $\mathcal{F}$ = Faraday's constant. In all cases, Ψ represents the difference in potential between the plane of sorption and bulk solution.

The above model assumes the P_i binding sites have a uniform intrinsic binding energy, but Ψ_{a0}, the electrostatic potential in the absence of bound P_i, is described by a normal distribution. Barrow also assumed that Ψ decreases linearly as surface coverage increases: $\Psi = \Psi_0 - m_1\Theta$, where m_1 is the rate of change in surface potential with respect to fraction of sites occupied (Θ). The model thus has five fitted parameters: Ψ_0, $\sigma_{\Psi_0}, K_{int}, X_{max}$, and m_1, which can cause problems if one attempts to fit raw sorption data to the unconstrained equation using a nonlinear least-squares fitting routine. In applying the model to P_i sorption by soils, Barrow[20] simplified the problem by using values of K_{int}, X_{max}, and m_1, reported for goethite (α-FeOOH), correcting X_{max} for surface area. In applying the model to P_i sorption by lake sediment, Detenbeck and Brezonik[5,19] used K_{int} for P_i sorption to goethite and fit the other four parameters by a nonlinear Marquardt fitting routine.

14.4.6 A cautionary tale: not all data on phosphate sorption to sediment fit the Langmuir equation!

Although phosphate sorption to soils and sediments often fits a simple Langmuir isotherm (Section 14.3.4), this is not always the case, as Detenbeck and Brezonik[5,19] showed in a study of phosphate binding to sediment from Little Rock Lake, an oligotrophic, acid-sensitive, softwater lake in northern Wisconsin. An initial plot of P_i sorption data for pelagic sediment showed moderately good fit on a direct Langmuir plot of X versus C (Figure 14.7a), and a plot using the linear transformation (C/X vs. C; Eq. 14.11) showed very good fit (Figure 14.7b). Further analysis, however, showed that the apparent fit in the latter plot resulted from a spurious self-correlation. An alternative form of the Langmuir equation uses a plot of X/C versus X to linearize the data,* and a replot of the data based on this form (Figure 14.7c) shows clearly that the data do not fit a linear pattern. Further application of the sorption data to more complicated models described in previous sections showed a good fit to the electrostatic model of Barrow[20] and the normal distribution model of Perdue and Lytle[18] (Figure 14.7d). Natural sediments are highly heterogeneous materials and may contain a variety of inorganic substances (aluminosilicate clays, Al and Fe oxides, $CaCO_3$) to which P_i can sorb. Given this situation, we should not attempt to infer too much about the actual number of binding sites and structural aspects of P_i binding to sediments even when we are able to fit experimental data to a given model.

14.4.7 Effects of pH: sorption envelopes and edges

Because of the role of pH in determining the charge density (and even the sign of the charge) of surfaces, it is easy to imagine that pH plays an important role in the extent of sorption by ions. For example, at low pH, surfaces will be positively charged, and sorption of anions will be favored, but at high pH (generally $> pH_{PZC}$) electrostatic repulsion will prevent anionic adsorption. This gives rise to the concept of adsorption envelopes and edges. Plots of the extent of surface coverage by an anion versus pH

---

*Further algebraic manipulation of Eq. 14.10 yields $X/C = X_{max}K_L - K_LX$, and thus a plot of X/C versus X also should yield a straight line with slope $= -K_L$ and y-intercept $= X_{max}K_L$, if the data fit the Langmuir equation.
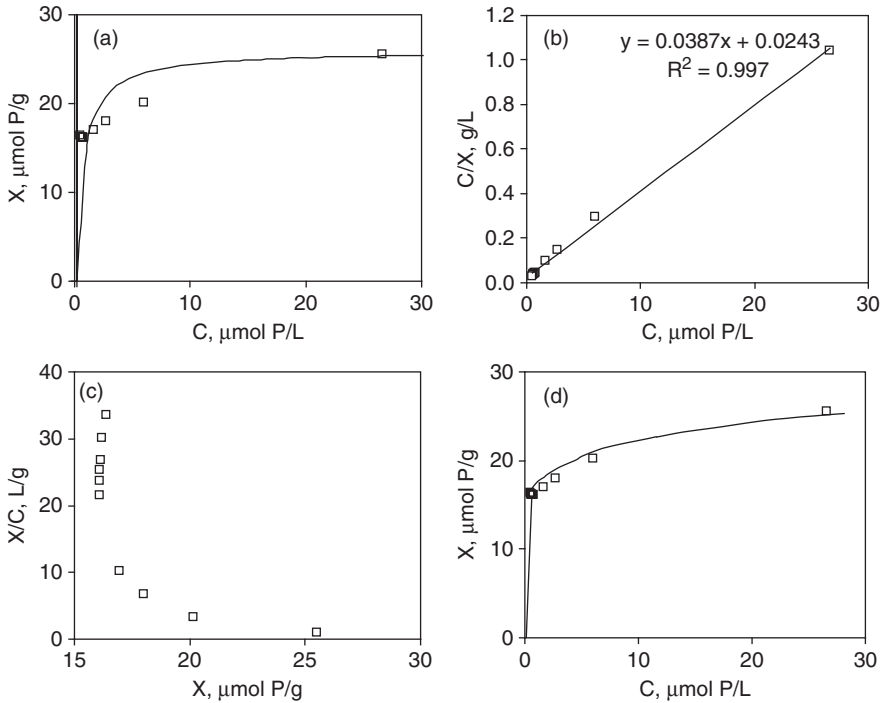
Figure 14.7 Sorption of phosphate (P_i) at pH 4.5 to pelagic sediment from Little Rock Lake, Wisconsin. (a) Langmuir plot shows actual data points and curve obtained from line of best fit in linearized plot (b), according to eq. 14.11. Line of best fit shows apparently excellent fit and yields $X_{max} = 25.84 \mu$mol P/g and $K_L = 1.59$ L/μmol P, but alternative linearized plot (c) shows that the plot in (b) is the result of a spurious self-correlation. Good fit of the data was achieved using Barrow's electrostatic model (d), and the Perdue-Lytle normal distribution model gave virtually the same line as that for the Barrow model in (d). Redrawn from Detenbeck and Brezonik.[5]

(sorption envelopes) generally show a rapid decrease at some intermediate pH (perhaps in the vicinity of pH_{PZC}), and cations tend to show a rapid increase at some intermediate pH. The sorption curve itself usually is referred to as the **sorption edge**. Surface complexation models allow one to model the adsorption edge quantitatively. Usually, one must consider several reactions and acid-base species for the adsorbing ion. In the case of phosphate sorption to amorphous ferric hydroxide (ferrihydrite; Figure 14.8), the following equilibria apply:[22]

Reaction		$\log K_{int}$	
$\equiv FeOH + 3H^+ + PO_4^{3-} \rightleftharpoons \equiv FeOPO_3H_2 + H_2O$		32.08	(14.25a)
$\equiv FeOH + 2H^+ + PO_4^{2-} \rightleftharpoons \equiv FeOPO_3H^- + H_2O$		26.39	(14.25b)
$\equiv FeOH + H^+ + PO_4^{2-} \rightleftharpoons \equiv FeOPO_3^{2-} + H_2O$		20.73	(14.25c)
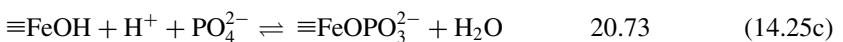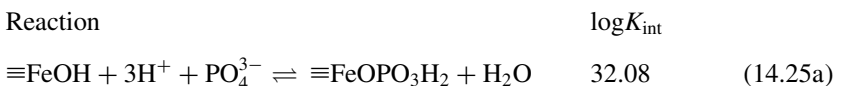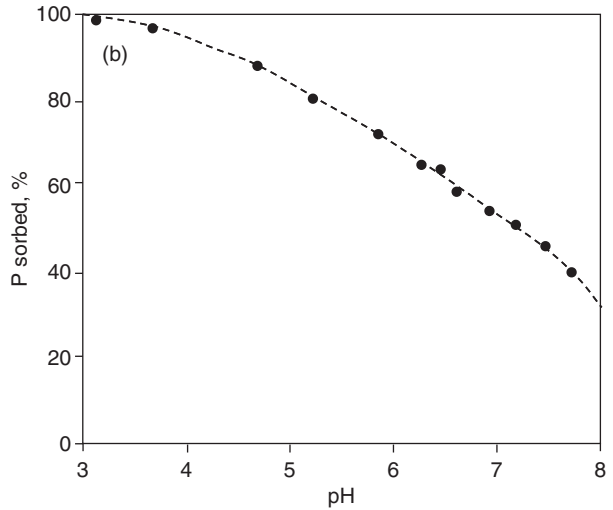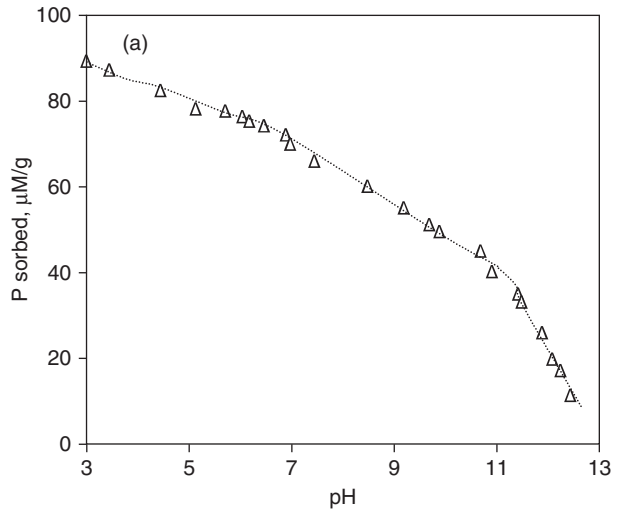
Figure 14.8 Sorption edges for phosphate sorption versus pH: (a) original envelope of Hingston et al.[21] for goethite; (b) edge of Gustafsson[22] for ferrihydrite. Dotted and dashed lines indicate trends in the data and are not fitted curves. Note difference in units for y-axes. Both (a) and (b) redrawn from original figures.

The reactions are written as formation reactions in the familiar format used in MINEQL+. A body of such reactions and associated constants was developed by Dzombak and Morel.[23] The effects of surface charge make realistic surface complexation models complicated, and we defer further description of such models until after the next section, which explores the physics of charged surfaces.

14.5 Advanced topic: physics of the electric double layer

14.5.1 Constant charge and constant potential surfaces

The electric charge on a surface and the potential difference between the surface and bulk solution are related properties. We can distinguish two basic models for these

properties: (1) ***constant charge surfaces***: in this model, the charge on the surface is fixed and independent of solution composition, and (2) ***constant potential surfaces***: in this case, the surface potential remains constant and is not affected by the presence of "indifferent" electrolytes (i.e., ions that do not interact with surface sites). The former model applies to minerals in which the charge results solely from isomorphic substitution; for example, clays have constant charges. The term constant potential surface may be a little misleading in that the surface potential actually can be controlled externally in such systems either by applying an external potential (in the case of metal electrodes) or by fixing the bulk solution concentration of solutes whose reaction with the surface gives rise to the potential. The latter situation occurs whenever we can formulate a reaction between the surface of a solid and constituents in solution; e.g.,

$$Ag_{(s)} \rightleftharpoons \underline{Ag}^+ + e^-, \tag{14.26a}$$

$$FeOOH_{(s)} + \underline{H}^+ \rightleftharpoons FeOOH_2^+{}_{(s)}, \tag{14.26b}$$

$$SiO_{2(s)} + \underline{OH}^- \rightleftharpoons SiO_2OH^-{}_{(s)}, \tag{14.26c}$$
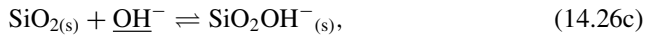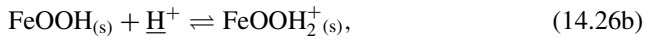
where the potential-determining ion is underlined. Constant potential surfaces are common in electrochemistry and colloid chemistry, and also in environmental systems. Because H^+ and OH^- are common potential-determining ions, metal oxides (or metal (hydr)oxides) can be viewed as having constant potential surfaces at constant pH in solution.

The electrical potential drop between the surface and bulk solution, Ψ_0, is related to the free energy change, ΔG, involved in changing the composition of the solution from the given value to a reference state at which $\Psi_0 = 0$, which in fact is the surface potential when it has no net charge (i.e., at pH_{PZC}). For example, for a metal hydroxide, we can write

$$\equiv Me-OH + OH^- \rightleftharpoons \equiv Me-O^- + H_2O, \tag{14.27a}$$
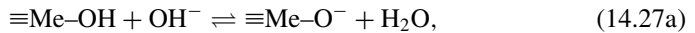
$$-\Delta G = \mathcal{F}\Psi_0 = RT\ln\frac{\{OH_o^-\}}{\{OH^-\}}, \tag{14.27b}$$

where $\{OH_o^-\}$ is the activity of OH^- at the point of zero charge. Ideally, for a unit change in pH, Eq. 14.27b indicates that Ψ_0 should vary by 59 mV at 20°C.

Many systems have more than one potential-determining species. In addition, many solids have both constant charge and constant potential surfaces present simultaneously.[6] For example, in clays, the potential on the face is produced by fixed charge resulting from isomorphic substitution in the lattice, but the potential at edges (where Si-O and Al-O bonds are discontinuous) is fixed by H^+ and OH^- as potential-determining ions.

14.5.2 The Gouy-Chapman theory

In this section we describe in quantitative terms the nature of the electric double layer that occurs at charged surfaces. We already have an understanding of the nature and origin of the charge on the surface itself (see Section 14.2.2): the charge is exerted on the plane of the surface. In contrast, the opposing charge in the solution is not all focused at the surface. Because dissolved ions are subject not only to coulombic attraction/repulsion

but also to thermal motion, it is distributed diffusely in the solution near the surface, giving rise to a ***diffuse double layer*** (Figure 14.9a), in which the charge density in solution decreases rapidly with distance from the surface. Gouy and Chapman early in the twentieth century independently developed a theory to quantify this phenomenon. The theory is based on three main assumptions:[1] (1) ions are considered as point charges and they interact with the surface only by coulombic forces, (2) the surface is treated as a uniform infinite plane of charge, and (3) water is treated as a uniform continuum with a constant dielectric constant, **D**. The potential Ψ_x in the diffuse layer at distance x from the surface is proportional to the energy, $W_{i,x}$, required to bring ion i from an infinite distance (effectively from the bulk solution) to point x in the diffuse layer and is given by

$$W_{i,x} = z_i \mathcal{F} \Psi_x. \tag{14.27}$$

The model includes the following qualitative features:

(1) The net charge in solution is equal in magnitude and opposite in sign to the charge on the surface.
(2) Net double-layer charge is reflected by disturbance in of electroneutrality close to the surface and is represented by the total area between the two concentration curves in Figure 14.9b, i.e., the charge resulting from the surplus of cations, σ_+, and from the deficiency of anions, σ_-, in the diffuse double layer. (If the surface were positively charged instead of negatively charged, as shown in the figure, signs on the curves would be reversed.)
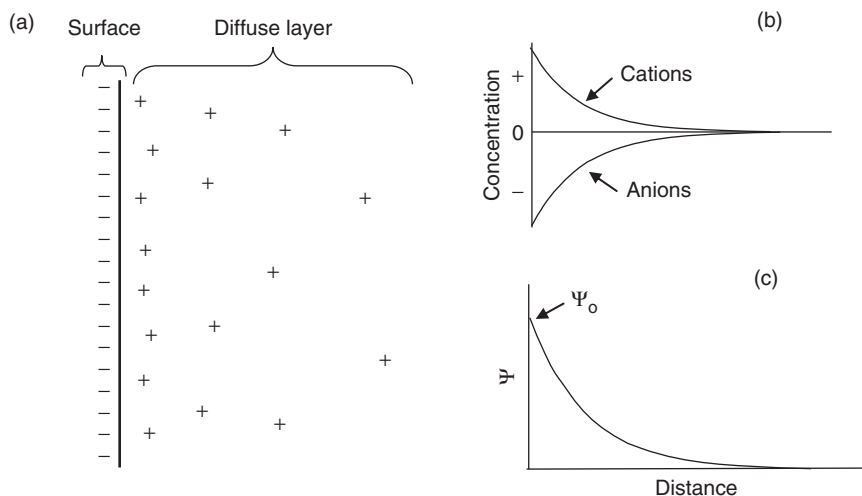
Figure 14.9 (a) Schematic of electrical double layer for a negatively charged surface. For clarity, only the net excess of counter positive charges is shown in the diffuse layer. (b) Concentration of excess positive charges and deficiency of negative charges in diffuse layer decrease exponentially with distance from the surface. (c) Electrical potential (Ψ) decreases exponentially with distance from the surface; Ψ_0 is the surface potential relative to the bulk solution.

(3) The potential Ψ declines exponentially with distance from the surface (Figure 14.9c).

(4) At low ionic strength (I), the disturbance of electroneutrality extends farther into solution; i.e., the thickness of the diffuse double layer is a function of I.

The Gouy-Chapman theory quantifies these features and predicts two important parameters: Ψ_0, the surface potential, and κ^{-1} (reciprocal kappa), the thickness of the diffuse double layer, expressed in cm or nm.

From (2), the charge density in the diffuse layer, q, is given by

$$q = z\mathcal{F}(n_+ - n_-), \tag{14.28}$$

where q is the charge density (coul/cm^3), $\mathcal{F}$ is Faraday's constant (96,485 coul/mol of electrons), and n_+ and n_- are the local cation and anion concentrations in mol/cm^3, and z is the valence of the ions. In turn, n_+ and n_- are given by

$$n_+ = n_{+(x=\infty)} \exp\left(\frac{-z\mathcal{F}\Psi_x}{RT}\right); \quad n_- = n_{-(x=\infty)} \exp\left(\frac{-z\mathcal{F}\Psi_x}{RT}\right). \tag{14.29}$$

The potential Ψ is related to the charge (q) by Poisson's equation:

$$\frac{d^2\Psi}{dx^2} = -\frac{q}{DD_o}, \tag{14.30}$$

where D is the relative permittivity of water (80.1 (dimensionless) at 20°C; also called the dielectric constant of water), and D_o is the permittivity in a vacuum (8.854×10^{-14} coul V^{-1} cm^{-1}).

Combining Eqs. 14.28–14.30 leads to the Gouy-Chapman **double-layer equation**:[1]

$$\frac{d^2\Psi}{dx^2} = -\frac{\kappa^2 \sinh(z\mathcal{F}\Psi/RT)}{2\mathcal{F}/RT} \tag{14.31}$$

Recall that sinh $x = (e^x - e^{-x})/2$. Parameter κ in the above equation is the reciprocal of the double-layer thickness (units of cm^{-1}). To be precise, κ^{-1} is the "characteristic distance" for decay of Ψ—the distance at which Ψ is $1/e^{th}$ of Ψ_0 (i.e., $0.3679 \times \Psi_0$). The theory expresses κ as a function of I:

$$\kappa = \left(\frac{2\mathcal{F}^2 I \times 10^3}{DD_o RT}\right)^{1/2}, \tag{14.32}$$

where all terms are as defined previously. For water at 20°C, the double-layer thickness (in cm) is

$$\kappa^{-1} = 2.8 \times 10^{-8} I^{-1/2}. \tag{14.33}$$

For freshwaters (I $= 10^{-4}$ to 10^{-2}), κ^{-1} has a range of $\sim$3–30 nm, and for seawater, $\kappa^{-1} = \sim 0.33$ nm, which is about the thickness of a hydrated ion. The double layer thus is *not* diffuse in seawater. This gives rise to the **Helmholtz model**, a simplified double-layer model (DLM) that treats the double layer as a two-layer capacitor and actually predates the Gouy-Chapman theory (see next section).

14.5.3 Beyond the Gouy-Chapman model: advances in double-layer theory

The Gouy-Chapman model led to improved understanding of many behavioral facets of charged particles in aquatic systems, but its underlying assumptions limit its accuracy. Many advances have been made in the century since it was developed to overcome its limitations, starting in 1924 with the Stern model.[24] This model divided the diffuse layer into two parts (Figure 14.10): a "compact layer" of ions adsorbed at the surface, called the ***Stern layer***, and a diffuse layer beyond that, called the Gouy layer, in which ions are attracted by nonspecific (electrostatic) adsorption. Ions in the Stern layer are considered to be attracted to the surface by "specific adsorption" by bonding mechanisms beyond electrostatic forces, but the precise mechanisms were not well defined. According to Stumm,[1] adsorbed ions in the Stern layer are considered to be in a plane separated from the solid by a "short distance," but H^+ and OH^- are considered to be incorporated in the solid.

The ***triple-layer model*** (***TLM***),[25,26] a more recent development based on a physical model similar to the Stern model, has been used for more than 20 years mainly to describe metal binding to oxide surfaces (Figure 14.11). The TLM is more explicit about the nature of binding in the compact layer; it includes adsorbed ions that bind directly to surface oxide groups as "inner-sphere" complexes—meaning that the adsorbed ion must lose at least its water of hydration on the side bonded to the surface—and adsorbed ions that retain their waters of hydration, are separated from the surface by at least one water molecule, and thus form weaker outer-sphere complexes.[2] The former adsorbates are in the surface or "0" plane; the latter are in a plane still within the compact layer called the
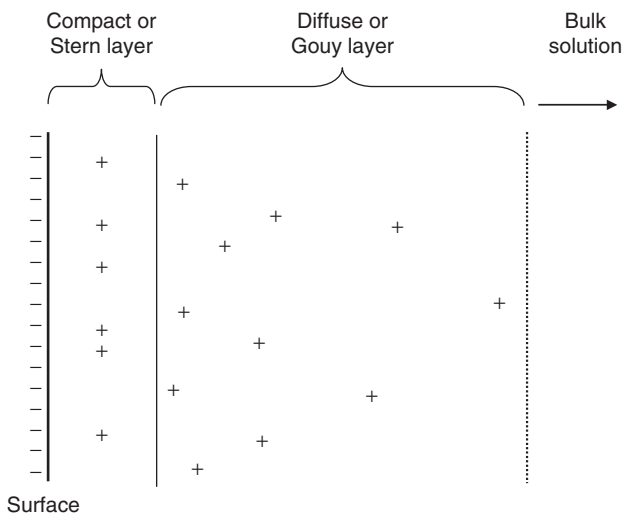
Figure 14.10 Stern modification of double-layer model (DLM) showing compact (or Stern) layer, in which specific adsorption satisfies some of the surface charges and the diffuse (or Gouy) layer satisfies the remainder. As in Figure 14.9, only the net excess of positive charges is shown in the electrical double layer.
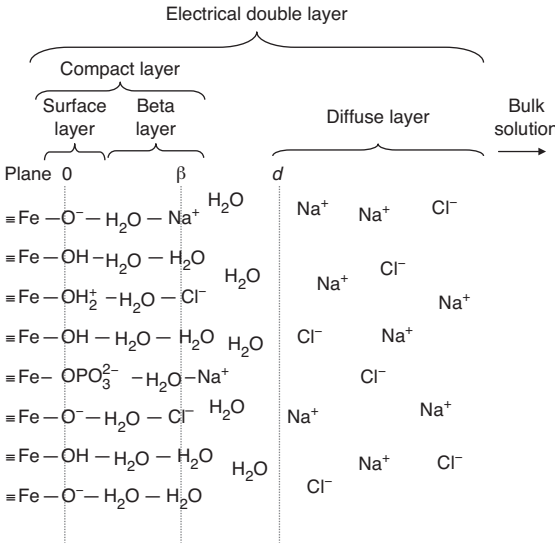
Figure 14.11 Schematic of triple-layer model (TLM) for a ferric hydroxide surface. Surface oxygen groups are in the 0 plane and part of the surface layer. The compact layer is divided into two zones—the surface layer and β layer. Specific adsorption (inner sphere binding) is shown for a phosphate group, and outer sphere binding is indicated by the Na^+ and Cl^- ions in the β plane, which are separated from the surface oxygen groups by a layer of water. An additional water layer separates the β plane from the d plane that demarcates the start of the diffuse layer, which has an excess of cations to balance the negative charge of the surface not satisfied in the compact layer. Based on a similar figure in Benjamin.[2]

β plane, and the limit of the compact layer and start of the diffuse layer is called the *d* plane (Figure 14.11).

All the interfacial models involving charged surfaces agree on the nature of the charge-potential (σ-Ψ) relationships in the Gouy layer (if one is present). They also agree that potential decreases exponentially with distance from the surface (Ψ-x relationships) within that layer, at least when $\Psi <\sim 25$ mV, which is typically the case.[1] There are significant differences, however, among models in treatment of σ-Ψ and Ψ-x relationships in the compact layer. Figure 14.12 shows these differences for three common models. Unfortunately, direct physical observations at this scale are elusive, and these differences remain an unresolved controversy.

14.5.4 Capacitance in the double layer and a constant capacitance model

The ratio between charge and potential is called capacitance; in general, $C = \sigma/\Psi$, where C is capacitance in units of farads (F or coul/V) or F/m^2 if σ is expressed on an areal basis, coul/m^2. In the TLM, capacitance is viewed as decreasing linearly within each of the two parts of the compact layer, reflecting the different slopes in potential change between the 0 and β planes and the β and *d* planes (Figure 14.12):

$$C_1 = \frac{\sigma_0}{\Psi_0 - \Psi_\beta}; \quad C_2 = \frac{\sigma_\beta}{\Psi_d - \Psi_\beta}, \tag{14.34}$$

where the subscripts represent the charge and potential values at the o, β, and *d* planes, respectively. Capacitance values in compact layers are not known with much precision,
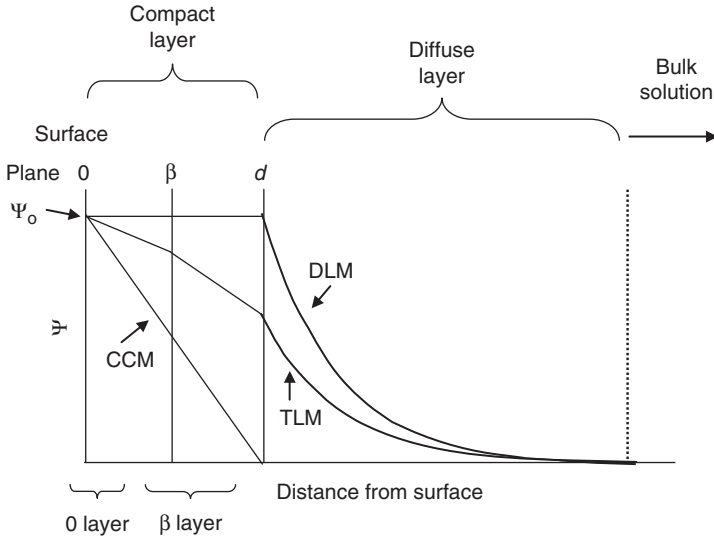
Figure 14.12 Variation of potential Ψ with distance from the surface for three diffuse-layer models: CCM, constant capacitance model; DLM, double-layer model; TLM, triple-layer model. Based on a similar figure in Benjamin.[2]

but typical values used in adsorption modeling are 1–3 F/m^2 for C_1 and 0.2–1 F/m^2 for C_2.[2]

When the double layer is highly compressed, as in high ionic strength solutions, essentially all the potential drop between the surface and bulk solution occurs in the compact layer, which acts as a parallel plate condenser. This is known as both the Helmholtz model, which was derived before the Gouy-Chapman theory, and the **constant capacitance model** (**CCM**). The CCM often is used in surface complexation modeling, and this makes sense for two reasons. First, in surface complexation models the amount of charge that a surface can develop is restricted to the number of surface sites (charges based on isomorphic substitution in the solid lattice are not considered). Second, the binding energy of surface complexes is relatively high, and specific adsorption thus should be the prime mechanism for satisfying charged surface sites.

Capacitance also can be defined in terms of the ratio of permittivity to distance, d, across the two plates of a parallel plate condenser,[1] and for the electric double layer d can be approximated by κ^{-1}:

$$C = \frac{DD_o}{d} = \frac{DD_o}{\kappa^{-1}} = DD_o\kappa \qquad (14.35)$$

If we assume a constant capacitance for a double-layer system, the surface charge is proportional to the surface potential through the constant capacitance: $\sigma_0 = \Psi_0 \times C$. This condition holds when σ_0 is small or when the double layer is compressed (at high I). More generally, from the fact that κ^{-1} is inversely proportional to $I^{1/2}$, we can see that increasing I should result in increasing capacitance (C), which is equivalent

to increasing the ratio of surface charge to surface potential (σ/Ψ_0). This tells us that the responses of constant charge and constant potential surfaces to changing I will be different. If σ is constant, Ψ_0 decreases with increasing I, but if Ψ_0 is constant, σ increases with increasing I.

14.6 Advanced topic: surface complexation models

14.6.1 Overview

Modeling the sorption of ions to charged surfaces must take into account the physical principles described in the previous section. The models described in that section, however, focus on the physics of the systems and are somewhat unsatisfying from a chemical perspective. Surface complexation models are a blend of the (by now) familiar chemical principles of complex formation equilibria and the physics of charged surfaces. In brief, these models treat ion-surface interactions as reactions between ligands and metal ions, as shown for ferric hydroxide and phosphate in Eq. 14.25. In that case, the sorbing ion acts as the ligand and the solid contains the central metal ion, but when dissolved metal ions react with oxide surfaces, the surface site acts as the ligand. In either case, the reactions can be described by conventional equilibrium (formation) constants ($K_{\mathrm{f,int}}$).[†] Applying these constants to solve problems in real systems requires that the effects of surface charge be taken into account. This is not as simple as it might seem because we lack data on critically important parameters for most natural surfaces. This is an active area of research in environmental chemistry, however, and we can expect further advances in understanding and expansion of basic data in coming years.

Computer-based equilibrium modeling programs like MINEQL+ and VMINTEQ include several versions of adsorption and surface complexation models, which makes the models more accessible and easier to apply to solving practical problems. It is important to emphasize, however, that the models involve many assumptions and that uncertainties exist in the applicability of various parameter values to specific surfaces. Consequently, one should interpret the results with caution and view them as illustrative of trends rather than an exact portrayal of reality.

MINEQL+ includes four surface complexation models that differ only in the way they treat the interfacial electric layer; all use the same approach to describe the complexation of ions to surface sites as the program uses to solve other equilibrium problems. The models are (1) constant capacitance model (CCM), (2) double-layer model (DLM), (3) DLM for FeOH, and (4) triple-layer model (TLM). VMINTEQ has a larger suite of models and options, including the four listed above plus a Stern model and a version of the CD-MUSIC (charge distribution-multisite complexation) model,[29] which is similar to the TLM but differs in the way it distributes charge over two surface planes. Several models in both programs provide options for modeling

---

[†]In some cases the metal ion-surface interactions are even more complicated and involve redox reactions. For example, when Fe^{II} sorbs onto Fe^{III} (hydr)oxides like goethite (α-FeOOH), hematite (α-Fe$_2$O$_3$), and ferrihydrite (Fe(OH)$_3$), it forms an inner sphere complex and transfers an electron to the iron oxide lattice, becoming a surface Fe^{III} surface group (as measured by Mossbauer spectroscopy)[27] that cannot be desorbed and is released only upon a digestion process. The electron is apparently quite mobile within the oxide, and the particles are able to reduce nitrobenzene[27] and oxidize arsenic from As^{III} to As^{V}.[28]

Table 14.5 Components and terms defined in MINEQL+ to run surface complexation models*

Term	Definition
Coul.	$= \exp(-\mathcal{F}\Psi/RT)$; a coulombic correction factor used to relate concentrations of species at a surface to their corresponding bulk solution concentrations. This is achieved by multiplying the mass action expression for the formation of a surface complex by Coul. raised to the power of Δz, which is the change in the charge of the surface site resulting from the adsorption reaction. Δz is calculated by the program from the stoichiometry of the adsorption reaction.
Fe(st)OH	Strong binding site component in the two layer FeOH model
Fe(wk)OH	Weak binding site component in the two layer FeOH model
PSI0	Potential in the surface or 0 plane (Ψ_0); used in the TLM
PSIB	Potential in the beta (β) plane (Ψ_β); used in the TLM
SOH	Surface hydroxide component in the TLM
S(st)OH	Strong binding surface hydroxide component in the generic DLM
S(wk)OH	Weak binding surface hydroxide component in the generic DLM
SC(st)OH	Strong binding surface hydroxide component in the CCM
SC(wk)OH	Weak binding surface hydroxide site used in CCM

*All these terms are selected from the initial *Select Components* table in MINEQL+.

surface sites as being homogeneous (the so-called 1-pK approach) or having two types of sites (strong and weak; the so-called 2-pK approach). We present an introduction to the models in MINEQL+ below, but except for details in application, the basic concepts apply to the models in VMINTEQ.

14.6.2 The MINEQL+ approach to surface complexation models: examples

MINEQL+ defines a few additional components and terms to enable use of the models, and these are explained in Table 14.5. Two factors further complicate the use of the models: (1) not all components one may need are defined in the program, requiring redefinition of some of the extra "null components" provided in the initial table of components, and (2) the program's thermodynamic database has very few entries for surface complex reactions, and consequently such information must be entered by the user. This normally is done in the "Type II Aqueous Species" tableau, and reactions producing surface complexes are added as if they were dissolved complexes, as described in Tables 7.3 and 9.7. The formation constants for surface complexes usually are obtained from experimental data using nonlinear least-squares fitting programs; FITEQL[30] is widely used for this purpose in sorption research.

A simple simulation that one can do with the models is an acid-base titration of a surface. Figure 14.13 shows the results of such an exercise for a TiO$_2$ surface using the CCM and the following conditions: I = 0.01; TiO$_{2(s)}$ = 12.07 g/L; specific surface area = 20 m^2/g; site density = 0.4 mmol/g. Running this problem in MINEQL+ involves the procedure summarized in Table 14.6a. Concentrations of *TOT*H$^+$ in the system and *TOT*H$^+$ adsorbed on the TiO$_2$ surface versus pH are produced as output (Figure 14.13a) that can be viewed within the program by its "GraphIT" routine, and model output

Table 14.6 Instructions for running three surface complexation examples in MINEQL+*

(a) *Acid-base titration of TiO$_2$ suspension using the CCM*

1. Select **SC(wk)OH** and **Coul.** from the *Select Components* table in MINEQL+ and scan the thermodynamic database.
2. Create thermodynamic data for protonated and deprotonated surface sites in the *Type II – Aqueous species* tableau by pressing the insert button to define the new species and fill in the tableau as shown below:

Name	H2O	H(+)	Coul.	SC(wk)OH	Log K
SC(wk)OH-H (+1)	**0**	**1**	**1**	**1**	**3.11**
SC(wk)OH-OH (−1)	**0**	**−1**	**−1**	**1**	**−8.66**

   Insertion of the above information adds the following surface reactions to the database:

$$SC_{wk}\text{–}OH + H^+ \rightleftharpoons SC_{wk}\text{–}OH_2^+, \qquad \log K = 3.11$$
$$SC_{wk}\text{–}OH \rightleftharpoons SC_{wk}\text{–}O^- + H^+, \qquad \log K = -8.66$$
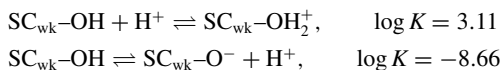
   The log K values are from literature cited in the MINEQL+ user manual.
3. In the *Calculation Wizard* insert a value of **0.00483** for the molar concentration of SC(wk)OH; this is based on a surface site density of 0.4 mmol/g and solids concentration of 12.07 g/L.
4. In the *RunTime Manager* click *MultiRun* and select **Titration** as the type of calculation, **Log K of pH** as the type of variable, starting and ending values of **4.0** and **10.0**, and **25** as the number of points.
5. In the *RunTime Manager* set I = **0.01**. Click the *Adsorption Model* box menu and select **Const. Capacitance**. Then click the options button and fill in the following values: surface area = **20 m^2/g**; solids concentration = **12.07 g/L**; and capacitance = **0.72 F/m^2**. (All values are as recommended in the MINEQL+ manual.)
6. Supply a name for your output file and click run. In the *Output Manager* click *Graph It*, set the *Component* menu to H+ and *Units* to **Conc (M)**, and press *Plot* to see a graph similar to Figure 14.13a.

(b) *Sorption edge for Zn^{2+} using two layer FeOH model*

1. Select **Fe(st)OH**, **Fe(wk)OH**, **Coul.**, **Fe^{3+}**, and **Zn^{2+}** from the *Select Components* table.
2. In the *Calculation Wizard* insert concentrations of components Fe^{3+} = 1.79E–4 and Zn^{2+} = 3.02E-6. Fe^{3+} is fixed because the model uses conventions in Dzombak and Morel,[23] as described in the text. Concentrations of Fe(st)OH and Fe(wk)OH are calculated from the given site densities,[23] as described in the text.
3. In the *RunTime Manager* click *MultiRun* and select **Titration** as the type of calculation, **Log K of pH** as the type of variable, starting and ending values of **4.0** and **9.0**, and **21** as the number of points. Also, fix I at **0.01**, and select **2-layer FeOH** from the *Adsorption Model* menu. There are no other options for this model.
4. Supply a name for your output file and click run. In the *Output Manager* click *Graph It*, set the *Component* menu to Zn(2+) and *Units* to **% Total**, and press *Plot* to see a graph similar to Figure 14.14a.

Table 14.6 Cont'd

(c) *Sorption edge for Pb^{II} on γ-Al$_2$O$_3$ using the TLM.*

1. Select the following components from the *Select Components* table: **SOH**, **PIS0**, **PSIB**, **Na+**, **Cl$^-$**, (and default components **H2O** and **H$^+$**).
2. In the *Type II – Aqueous species* tableau insert the following information to define new species SOH$_2^+$, SO$^-$, SO$^-$–Pb^{2+}, and SO$^-$–PbOH:

Actual Species	Name		H2O	H(+)	SOH	PSI0	PSIB	Pb(2+)	Log K
SOH$_2^+$	**SOH2**	**(+1)**	0	1	1	1	0	0	5.7
SO$^-$	**SOH−OH**	**(−1)**	0	−1	1	−1	0	0	−11.5
SO$^-$−Pb^{2+}	**SOH–PbOH**	**(+1)**	0	−1	1	−1	2	1	−5.0
SO$^-$−PbOH	**SOH–Pb(OH)2**		0	−2	1	−1	1	1	−10.3

3. In the *Calculation Wizard* input the following concentrations: Pb(2+) = **2.9E-4**; Na(+) = Cl(−) = **0.1**; SOH = **1.82E-2**; PSI0 = PSIB = **1.3E-3**. (Note: the total site concentration SOH is based on the calculation:

$$8 \text{ sites/nm}^2 \div 6.02 \times 10^{23} \text{sites/mol} \times 10^{18} \text{nm}^2/\text{m}^2 \times 1371\text{m}^2/\text{L} = 1.82 \times 10^{-2}\text{mol/L}$$

The values for PSI0 and PSIB are from the MINEQL+ manual and were obtained by trial and error.
4. In the *RunTime Manager* click *MultiRun*, select **Titration** as the type of calculation, **Log K of pH** as the type of variable, starting and ending values of **4.0** and 7.**0**, and **16** as the number of points. Also, fix I at **0.1**, and select **Triple Layer** from the *Adsorption Model* menu. In the options menu for this model insert a surface area of 1371 m²/g and a solids concentration of 1 g/L. The default capacitance values can be left unaltered.
5. Supply a name for your output file and click run. In the *Output Manager* click *Graph It*, set the *Component* menu to Pb(2+) and *Units* to **% Total**, and press *Plot* to see a graph similar to Figure 14.15a.

---

*These examples are adapted from the MINEQL+ users manual, Lessons 11, 12b, and 13 in Chapter 18.[31]

accessed from the "Output Manager" screen can be downloaded into text files for insertion into spreadsheets for further analysis and plotting. For example, output data on the concentrations of surface sites occupied by H$^+$ and OH$^-$ are plotted in Figure 14.13b. From the intersection of the lines one can readily determine the pH$_{PZC}$ for TiO$_2$ is ∼5.9, which is close to the value of 6.2 reported in Table 14.1.

Adsorption of heavy metal ions on oxide surfaces has been a long standing interest of environmental engineers, and soil scientists because of the water quality implications of such processes. In addition to quantifying the extent of adsorption under specific solution conditions, we are interested in evaluating how the extent of sorption changes with pH— i.e., the nature of the sorption edge. Figure 14.14 shows results from a simulation of Zn^{2+} adsorption onto ferric hydroxide as a function of pH using the two-layer FeOH model in MINEQL+. Solution conditions were I = 0.01 (KNO$_3$) and *TOT*Zn = 3.02 × 10^{-6} M. This model option in MINEQL+ relies on conventions used by Dzombak and Morel[22] to develop a database for a two-layer sorption model for hydrous ferric oxide. As a result,
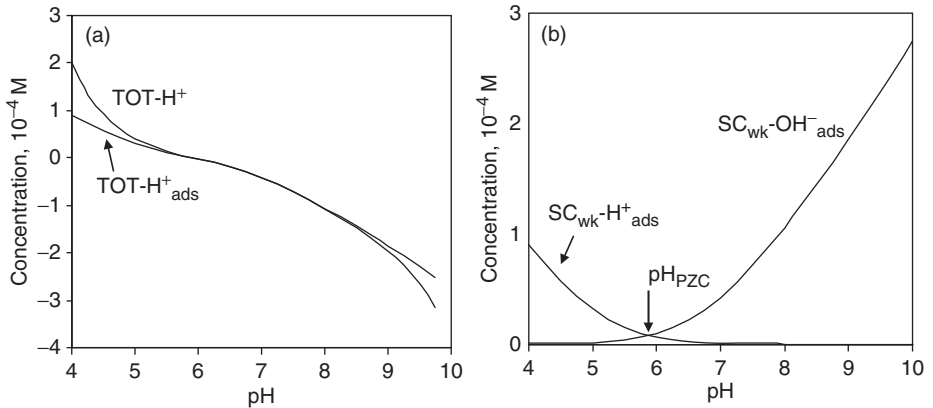
Figure 14.13 Simulated acid-base titration of TiO_2 surface using constant capacitance model in MINEQL+. (a) TOT–H^+ and TOT–H^+_{ads} versus pH; (b) concentrations of surface sites covered by H^+ and OH^- versus pH. Note that pH_{PZC} is found easily from the intersection of these two lines. See text for parameter values used in the simulation.

the MINEQL+ model has limited options with regard to surface characteristics. For example, the specific surface area is fixed at 600 m^2/g, and the solids concentration is fixed at 1.79×10^{-4} M Fe (virtually all present as $Fe(OH)_{3(s)}$), or 18.9 mg/L as $Fe(OH)_3$. Two binding sites are included in the model: a strong site with a density of 0.005 mol/mol Fe, and a more abundant weak site with a density of 0.2 mol/mol Fe. Procedures for running the problem in MINEQL+ are summarized in Table 14.6b.

Figure 14.14a shows a fairly sharp sorption edge for Zn^{2+} under the specified conditions; the fraction of Zn sorbed increases from nearly 0 at pH 5.5 to almost 100% at pH 8.5. The capacity of computer equilibrium programs like MINEQL+ to solve complicated problems is illustrated by the model output in Figure 14.14b, which shows the equilibrium speciation of Zn as a function of pH in the solution, as well as the speciation of Zn on the ≡FeOH surface. Although concentrations of all soluble hydroxo-complexes of Zn increase with pH, they never dominate the speciation because sorption onto the ≡FeOH surface is a more important reaction mechanism. Although the strong sites are more important in Zn sorption at low pH, they become saturated by pH 6.75, and further sorption involves the weaker sites. About half of *TOT*Zn is sorbed at pH 7.25. At high pH, where nearly all the Zn is sorbed, weak sites dominate the speciation of sorbed Zn because of their much greater (40-fold) abundance.

Another heavy metal of environmental interest is lead. Figure 14.15 shows the results of a third simulation with the MINEQL+ sorption models—this one using the TLM to evaluate the effect of pH on Pb^{2+} sorption to γ-Al_2O_3. Input conditions include: γ-Al_2O_3 surface area = 1371 m^2/L; I = 0.1 (NaCl) and *TOT*Pb = 2.9×10^{-4} M. MINEQL+ procedures to solve problems using the TLM differ from those used for the CCM and DLM; Table 14.6c summarizes the steps for this simulation. It is important to emphasize that considerable judgment is required in selecting values of certain input parameters for the TLM, and as the MINEQL+ user manual[31] indicates, results depend on the selection of initial values for some parameters. The model is not for
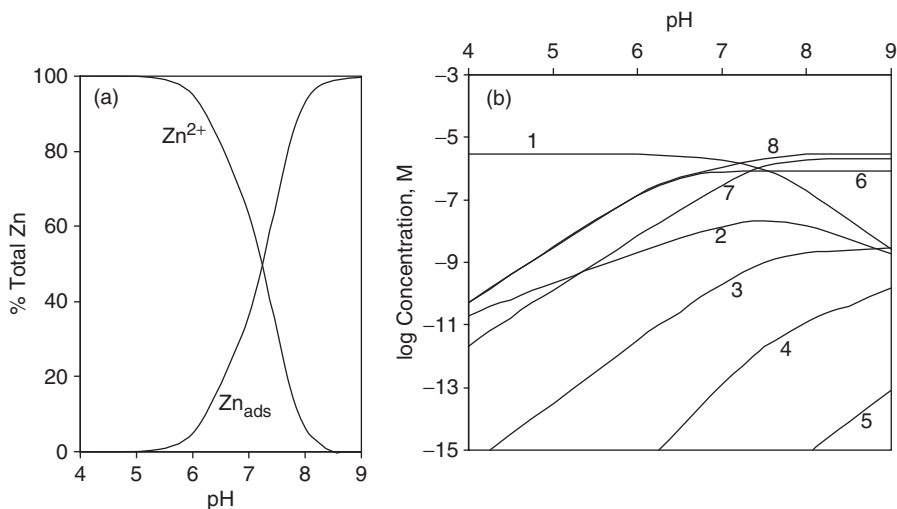
Figure 14.14 Sorption of Zn^{2+} onto ferric hydroxide versus pH modeled using the DLM in MINEQL+. (a) Zn^{2+} sorption edge and percent free Zn^{2+} versus pH. (b) Speciation of Zn in the system: 1, Zn^{2+}; 2, $ZnOH^+$; 3, $Zn(OH)_2^0$; 4, $Zn(OH)_3^-$; 5, $Zn(OH)_4^{2-}$; 6, $\equiv Fe\text{-}O_{st}\text{-}Zn$; 7, $\equiv Fe\text{-}O_{wk}\text{-}Zn$; 8, $TOT Zn_{ads}$; subscripts "st" and "wk" refer to strong and weak binding sites of ferric hydroxide. Based on an example in the MINEQL+ users manual supplied by D. Dzombak, Carnegie-Mellon University. System conditions: I = 0.01; $TOT Fe = 1.79 \times 10^{-4}$ M; $TOT Zn = 3.02 \times 10^{-6}$ M; specific surface area of $Fe(OH)_{3(s)} = 600$ m^2/g; strong binding site density = 0.005 mol/mol Fe; weak binding site density = 0.2 mol/mol Fe. See text for details on other parameter values.

beginners, and its proper application in research on new systems requires a level of expertise in surface chemistry beyond that which we have attempted to provide in this chapter.

The sorption edge for Pb^{II} in this system is sharp, with most of the change in the percent of $TOT Pb^{II}$ adsorbed occurring between pH 5 and 6 (Figure 14.15a). In terms of Pb^{II} speciation, sorption of the less protonated form, $-Pb(OH)_2^0$, overall is more important than that of the positively charged species, $-PbOH^+$ (Figure 14.15a). With regard to speciation of the Al surface, hydroxo sites, $\equiv Al\text{-}OH$ and $\equiv Al\text{-}OH_2^+$, dominate over the entire pH range of the simulation (Figure 14.15b), even at pH > 6, when all the Pb^{II} is adsorbed, and deprotonated sites ($\equiv Al\text{-}O^-$) are not important over the pH range of the simulation. The log C-pH diagram in Figure 14.15c shows the speciation of Pb^{II} both in solution and on the Al surface and demonstrates that chloro-complexes are important for Pb^{II} in solution, with $PbCl^+$ being the dominant species (higher than Pb^{2+}). The log C-pH diagram also shows that the dominance between $-Pb(OH)_2^0$ and $-PbOH^+$ as sorbed species switches at pH $\sim$5.6.

Finally, the aqueous chemistry of molybdate is of some interest because Mo is an essential element for both plants and animals and has been found to be limiting for primary production in some cases. Gustafsson[22] recently studied the sorption of molybdate (MoO_4^{2-}) experimentally and modeled the results using versions of the two layer FeOH model and the CD-MUSIC model. He found that the sorption edge
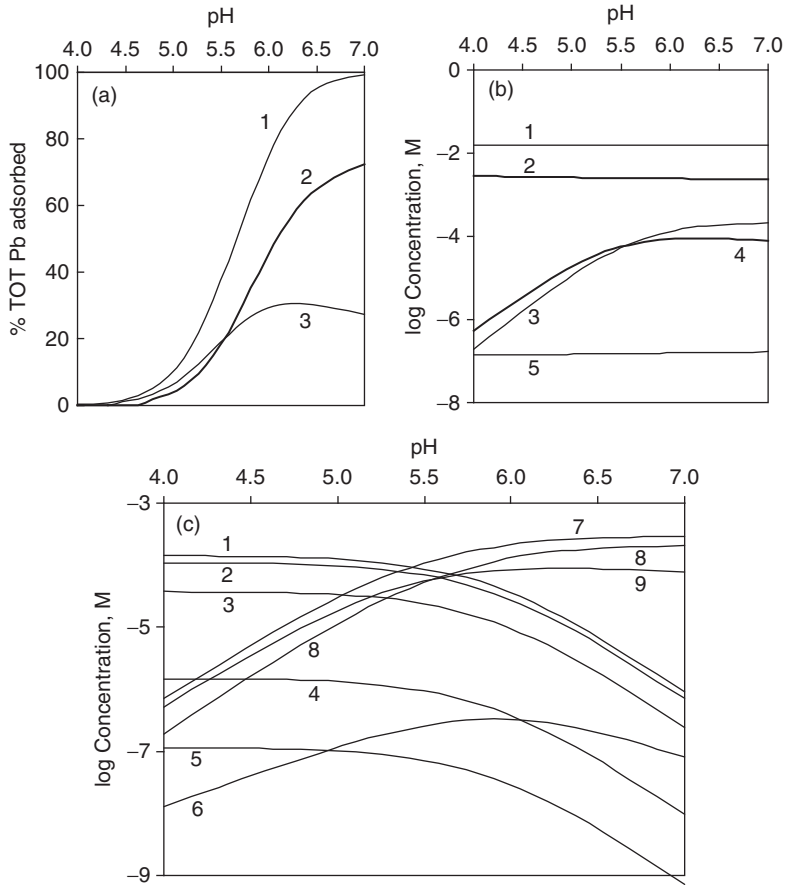
Figure 14.15 Sorption of Pb^{2+} onto γ-Al_2O_3 (surface area of 1371 m^2/L) in 0.1 M NaCl versus pH modeled using the TLM in MINEQL+. Initial Pb^{II} = 2.9×10^{-4} M. (a) Pb^{II} sorption edge versus pH: 1, percent $TOT$$Pb^{II}$ adsorbed; 2, percent adsorbed as $\equiv$Al-OH-Pb(OH)$_2$; 3, percent adsorbed as $\equiv$Al-OH-PbOH$^+$. (b) Speciation of Al(OH)$_3$ surface sites: 1, $\equiv$Al-OH; 2 $\equiv$Al-OH$_2^+$; 3, $\equiv$Al-OH-PbOH$^+$; 4, $\equiv$Al-OH-PbOH$_2^+$; 5, $\equiv$Al-O$^-$. (c) Speciation of Pb^{II} in the system: 1, PbCl$^+$; 2, Pb^{2+}; 3, PbCl$_2^0$; 4, PbCl$_3^-$; 5, PbCl$_4^{2-}$; 6, PbOH$^+$; TOTPb$_{ads}$; 8, $\equiv$Al-OH-PbOH$_2^+$; 9, $\equiv$Al-OH-PbOH$^+$. Based on an example in the MINEQL+ users manual; see text for details on parameter values.

for a 50 μM molybdate solution moved to higher pH values with increasing TOTFe concentrations (which agrees with basic mass action principles), and for TOTFe = 0.3 mM, the edge was centered near pH 6.5; i.e., about 50% of the Mo was sorbed to $\equiv$FeOH sites at that pH. He also found that for good model fits to the experimental data it was necessary to include two acid-base forms of molybdate a sorbing species: $H_2MoO_4^0$ and either $HMoO_4^-$ or MoO_4^{2-}, and best fits were achieved with MoO_4^{2-}. Figure 14.16 shows the results of a similar modeling effort using the MINEQL+ two layer FeOH model. Because of the limited flexibility of the MINEQL+ model, which fixes TOTFe
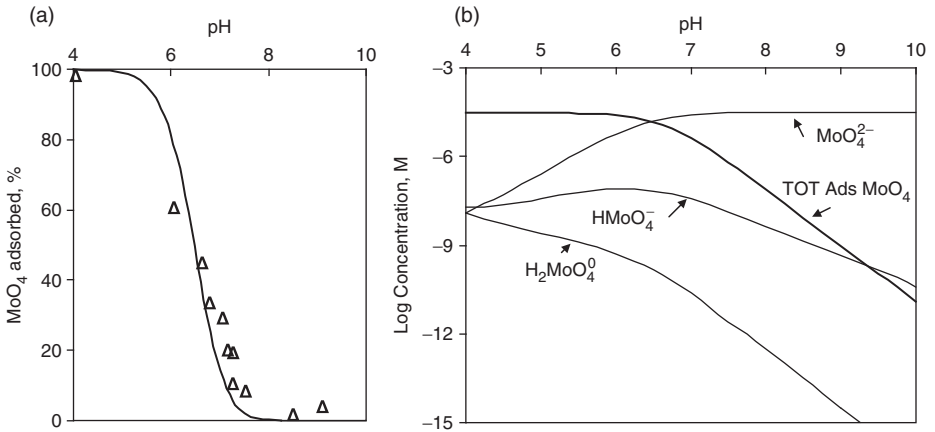
Figure 14.16 (a) Sorption edge for molybdate on ferric hydroxide based on the MINEQL+ two-layer FeOH model. Triangles represent experimental adsorption data from Gustafsson[22] for 50 μM molybdate on ferrihydrite (0.3 mM as Fe) in 0.01 M NaNO$_3$. (b) Log C-pH diagram of modeled results for dissolved acid-base species of molybdate and total adsorbed molybdate.

at 0.18 mM, we used a lower concentration of molybdate, 30 μM. As the sorption edge curve in Figure 14.16a shows, the model fits the experimental data nicely.

Problems

14.1. Which of the following sorbents would bind trichloroethylene most strongly?

(a) Graphite or paraffin
(b) Activated carbon or silica

Would your answers change if the sorbate were mercuric ion (Hg^{2+})? If so, how? Explain your answers and describe the nature of the binding forces likely to be important.

14.2. You are trying to remove p-nitrophenol (p$K_a = 7.2$) from water using activated carbon. Would you expect the removal to be more effective at pH 6 or pH 9? Explain your answer.

14.3. Sketch possible molecular structures of (a) Cu^{2+} and (b) phosphate (HPO$_4^{2-}$) binding to ferric oxide surface sites for both inner sphere and outer sphere binding. Note: For inner sphere binding several possible structures exist.

14.4. The Langmuir binding constant, K_L, for phosphate sorption to a lake sediment was found to be 20×10^{-3} L/μg. What would the EPC be for sediment-water suspensions if 25% of the sediment binding sites were bound by phosphate? How would your answer change if 50% or 75% of the binding sites were bound by phosphate?

14.5. The following data were obtained in an experiment to determine the phosphorus (phosphate) sorption characteristics of sediment from a lake. Solutions were buffered to maintain constant pH of 7.0 and constant ionic strength of $I = 0.01$. The total amount of sediment in each flask was 1.25 g (dry wt.), and the volume of the solution was 100 mL. $P_{i,eq}$ is the amount of dissolved phosphate-P remaining in solution after equilibration with the sediment.

$P_{i,init}$ (μg/L)	60	100	125	240	450	850
$P_{i,eq}$ (μg/L)	40	65	90	195	388	765

Determine whether the data fit the Langmuir and Freundlich isotherms and determine the parameters of the sorption equations. Which of the two models would you select to portray the sorption results?

14.6. The data below was collected from a study of the sorption of chloroform onto a novel organic-based sorbent. Fit the data to both the Freundlich and Langmuir isotherms. Which isotherm better describes the data? Under what conditions would you recommend the use of this sorbent?

X (mg/L)	0.87	1.21	1.51	1.6	2	2.21	2.29	2.36	2.58
C (mg/L)	0.05	0.25	0.75	1	3	5	6	7	11

14.7. Based on the isotherm shown in Figure 14.5, what dosage of activated carbon would be necessary to remove 99% of 1,2,4-trichlorobenzene from a solution initially containing 1.5 μM of 1,2,4-trichlorobenzene? 150 μM of 1,2,4-trichlorobenzene?

14.8. The surface potential Ψ_0 of an aluminum oxide surface was found to be 21 mV.

(a) What is the free energy ΔG that would be required to bring the solution to the condition where Ψ_0 would be zero?
(b) If the solution pH = 7.25, what is the pH at the oxide surface?

14.9. Develop a graph that shows how the thickness of the double layer, κ^{-1}, varies over the range of ionic strength, $I = 0.0001$ to $I = 1.0$. At what ionic strength does the double layer essentially cease being a "diffuse layer"?

14.10. Determine the sorption edges for Cu^{II} and Cd^{II} on $Fe(OH)_3$ using the two-layer $Fe(OH)_3$ model in MINEQL+. In both cases plot the % of *TOT*Cu that is adsorbed and the quantity (100 – %Cu adsorbed) versus pH. Compare your graphs to Figure 14.14a and discuss why the sorption edges differ for the three metal ions.

References

1. Stumm, W. 1992. *Chemistry of the solid-water interface*, Wiley-Interscience, New York.
2. Benjamin, M. M. 2002. *Water chemistry*, McGraw-Hill, New York.

3. Rönngren, L., S. Sjöberg, Z. Sun. W. Forsling, and P. W. Schindler. 1991. Surface reactions in aqueous metal sulfide systems. *J. Coll. Interf. Sci.* **145**: 396–404.

4. Bell, L. C., A. M. Posner, and J. P. Quirk. 1973. The point of zero charge of hydroxyapatite and fluorapatite in aqueous solution. *J. Coll. Interf. Sci.* **42**: 250–261.

5. Detenbeck, N. E., and P. L. Brezonik. 1991. Phosphorus sorption by lake sediments. 1. Comparison of equilibrium models. *Environ. Sci. Technol.* **25**: 395–403.

6. Stumm, W., and J. J. Morgan. 1996. *Aquatic chemistry*, 3rd ed., Wiley-Interscience, New York.

7. Freundlich, H. 1909. *Kapillarchemie*, Akad. Verlags., Leipzig.

8. Langmuir, I. 1916. The constitution and fundamental properties of solids and liquids. Part I. Solids. *J. Am. Chem. Soc.* **38**: 2221–2295.

9. Langmuir, I. 1918. The adsorption of gases on plane surfaces of glass, mica and platinum. *J. Am. Chem. Soc.* **40**: 1361–1403.

10. Kenney, 1982. Beware of spurious self-correlations! *Wat. Resour. Res.* **18**: 1041–1048.

11. Brezonik, P. L., and C. D. Pollman. 1999. Phosphorus chemistry and cycling in Florida lakes: global issues and local perspectives. In *Phosphorus biogeochemistry in subtropical ecosystems*, K. R. Reddy, G. A. O'Connor, and C. L. Schelske (eds.), Lewis Publ./CRC Press, Boca Raton, Fla., 69–110.

12. Fang, F., P. L. Brezonik, D. J. Mulla, and L. K. Hatch. 2005. Characterization of soil algal bioavailable phosphorus in the Minnesota River Basin. *Soil Sci. Soc. Am. J.* **69**: 1016–1025.

13. Fang, F., P. L. Brezonik, D. J. Mulla, and L. K. Hatch. 2002. Estimating runoff phosphorus loss in the Minnesota River Basin. *J. Environ. Qual.* **31:** 1918–1929.

14. Väänänen, R. J. Hristov, N. Tanskanen, H. Hartikainen, M. Nieminen, and H. Ilvseniemi. 2008. Phosphorus sorption properties in podzolic forest soils and soil solution phosphorus concentration in undisturbed and disturbed soil profiles. *Boreal Environ. Res.* **13**: 553–567.

15. Surdo, E. M., E. L. Cussler, P. J. Novak, and W. A. Arnold. 2009. Geomembranes containing powdered activated carbon have the potential to improve containment of chlorinated aromatic contaminants. *Environ. Sci. Technol.* **43**: 8916–8922.

16. Brunauer, S., P. H. Emmet, and E. Teller. 1938. Adsorption of gases in multimolecular layers. *J. Am. Chem. Soc.* **60**: 309–319.

17. Dzombak, D. A., W. Fish, and F. M. M. Morel. 1986. Metal-humate interactions. 1. Discrete ligand and continuous distribution models. *Environ. Sci. Technol.* **20**: 669–675.

18. Perdue, E. M., and C. R. Lytle. 1983. A distribution model for binding of protons and metal ions by humic substances. *Environ. Sci. Technol.* **17**: 654–660.

19. Detenbeck, N. E., and P. L. Brezonik. 1991. Phosphorus sorption by lake sediments. 2. Effects of pH and other solution variables. *Environ. Sci. Technol.* **25**: 403–409.

20. Barrow, N. J. 1983. A mechanistic model for the sorption and desorption of phosphate by soil. *J. Soil Sci.* **34**: 733–750.

21. Hingston, F. J., R. J. Atkinson, A. M. Posner, and J. P. Quirk. 1967. Specific adsorption of anions. *Nature* **215**: 1459–1461.

22. Gustafsson, J. P. 2003. Modelling molybdate and tungstate adsorption to ferrihydrite. *Chem. Geol.* **200**: 105–115.

23. Dzombak, D. A., and F. M. M. Morel. 1990. *Surface complexation modeling—hydrous ferric oxide*, J. Wiley, New York.

24. Stern, O. 1924. Theory of the electrolytic double layer. *Z. Electrochem.* **30**: 508–516.

25. Yates, D. E., S. Levine, and T. W. Healy. 1974. Site-binding model of the electrical double layer at the oxide/water interface. *J. Chem. Soc. Faraday Trans.* **70**: 1807–1818.

26. Davis, J. A., R. O. James, and J. O. Leckie. 1978. Surface ionization and complexation at the oxide/water interface: I. Computation of electrical double layer properties in simple electrolytes. *J. Colloid Interf. Sci.* **63**: 480–499; Davis, J. A., and J. O. Leckie. 1978. Surface ionization and complexation at the oxide/water interface: II. Surface properties of

amorphous iron oxyhydroxide and adsorption of metal ions. *J. Colloid Interf. Sci.* **67**: 90–107.

27. Williams, A. G. B., and M. M. Scherer. 2004. Spectroscopic evidence for Fe(II)-Fe(III) electron transfer at the iron oxide-water interface. *Environ. Sci. Technol.* **38**: 4782–4790.

28. Amstaetter, K., T. Borch, P. Larese-Casanova, and A. Kappler. 2010. Redox transformation of arsenic by Fe(II) activated goethite (α-FeOOH). *Environ. Sci. Technol.* **44**: 102–108.

29. Hiemstra, T., and W. H. Van Riemsdijk. 1996. A surface structural approach to ion adsorption: the charge distribution (CD) model. *J. Colloid Interface Sci.* **179**: 448–508.

30. Herbelin, A. L., and J. C. Westall. 1999. FITEQL 4.0: a computer program for determination of chemical equilibrium constants from experimental data. Report 99–01. Dept. of Chemistry, Oregon State Univ., Corvallis.

31. Environmental Research Software. 2007. MINEQL+ users manual, ver. 4.6., Hallowell, Maine.

15

Aqueous Geochemistry II

The Minor Elements: Fe, Mn, Al, Si; Minerals and Weathering

Objectives and scope

In this chapter we apply the concepts and tools developed in Chapters 3–5 and 7–11 to analyze the behavior of three important metals (Fe, Mn, Al) and one nonmetal (Si) in natural waters. Although their aquatic concentrations usually are lower than those of the seven major ions described in Chapter 2, these four elements have very rich chemistries involving acid-base, complexation, solubility, and (for Fe and Mn) redox processes, and they greatly influence the chemical and biochemical quality of aquatic systems. The three metals have practical interest to environmental engineers because of their roles in water treatment processes. Al and Si also are important as aluminosilicates, the major constituents of rocks and clay minerals. An introduction to the structural characteristics of these important substances is provided, and the chapter concludes by describing the mechanisms and factors controlling their degradation by weathering in soils and watersheds. This complicated process has major implications for the chemical composition of aquatic systems.

Key terms

- Iron oxidation states: Fe^0 (zero valent iron), Fe^{II} (ferrous), Fe^{III} (ferric), Fe^{VI} (ferrate)
- Manganese oxidation states: Mn^{II} (manganous), Mn^{III}, Mn^{IV} (manganic), Mn^{VI} (manganate), Mn^{VII} (permanganate)
- Important minerals: siderite ($FeCO_3$), goethite (α-FeOOH), manganite (γ-MnOOH), gibbsite (γ-$Al(OH)_3$)
- Autoxidation, autocatalysis, reductive dissolution

- Primary minerals; feldspars: albite, plagioclase, anorthite; olivine; pyroxenes and amphiboles: diopside and hornblende; micas (biotite)
- Secondary minerals (clays): two layer (kaolinite), three layer (illite, smectites, montmorillinite)
- Mineral weathering

15.1 Introduction

Although the elements and substances that are the focus of this chapter have somewhat disparate chemistries, several important threads link them together, making them an appropriate subject for this chapter. The elements Al, Si, Fe, and Mn are abundant in the Earth's crust but because of their reactivities and generally low solubilities, they are not major solutes in natural waters. Nonetheless, their reactions are important in defining the chemistry and biology of natural waters. They also are among the most important elements in the fields of soil science and geochemistry. Many aspects of the chemical behavior of Fe and Mn are parallel, and there also are important similarities between Fe and Al regarding hydrolysis. In addition, each element has significant influences on the behavior of other important elements in aquatic chemistry.

15.2 Iron and manganese

15.2.1 Comparative overview of chemical characteristics

We consider iron and manganese together because of their generally similar chemical characteristics and geochemical behavior. The basic properties of the elements (Table 15.1) illustrate these similarities, as well as some differences. The elements are neighbors in the first row of transition metals in the Periodic Table, and so similarities in behavior are to be expected. Both elements have several important oxidation states, and the stability of the reduced states increases with decreasing pH. The reduced ($+$II) states are relatively soluble in water but are stable only in the absence of O_2. The oxidized states, Fe^{III}, Mn^{III}, and Mn^{IV}, have very different acid-base, complexing and hydrolyzing properties than the reduced states. For both elements, the oxidized states are insoluble at neutral pH because of strong tendencies to form hydroxo or oxo species. As a result, they occur only as minor constituents in natural waters despite their abundance in the Earth's crust.

Both elements have complicated and generally parallel biogeochemical cycles that include chemical and photochemical reactions and microbial processes. Abiotic oxidation of the $+$II states by O_2 is strongly pH dependent, with much lower rates at low pH. Aerobic bacteria can oxidize the $+$II states of both elements and obtain energy for growth. Because the elements are constituents of enzymes that control key metabolic processes, both are biologically essential. Solubility constraints on their availability in oxic surface waters make them, especially Fe, potentially limiting for phytoplankton growth. Both elements cause problems in drinking water—taste issues for Fe, staining of plumbing fixtures for both. Because of their complicated behavior and importance for chemical (and biological) water quality, a rich literature exists on their aquatic behavior.

Table 15.1 Chemical and geological properties of iron and manganese[*]

Property	Manganese	Iron
Global abundance	10th (0.085%)	4th (5%)
Major minerals	Pyrolusite, MnO_2; manganite, γ-MnOOH; hausmanite, Mn_3O_4; rhodochrosite, $MnCO_3$	Hematite, Fe_2O_3; magnetite, Fe_3O_4; limonite, FeOOH; siderite, $FeCO_3$; pyrite, FeS_2; troilite, FeS
Biological importance	Essential; low toxicity; Mn^{II} is energy source for some bacteria at circumneutral pH	Essential; not toxic in natural waters; Fe^{II} is energy source for some acidophilic bacteria; may limit primary production in oceans and some lakes
Atomic number	25	26
Atomic weight	54.938	55.847
Isotopic abundance (%)	55 (100)	54 (5.8), 56 (91.7), 57 (2.2), 58 (0.3) (^{54}Fe is not stable, but $t_{1/2} > 10^{22}$ y)
Principal radioisotope	54 ($t_{1/2} = 312$ d)	55 ($t_{1/2} = 2.73$ y)
Outer electron configuration of element	$4s^2 3d^5$	$4s^2 3d^6$
Electronegativity[†]	1.55	1.83
Most common oxidation states in natural waters	II, III, IV	II, III
Redox potentials[§] (V)	(III–II) 1.60 (II–0) −1.18 (IV–II) 1.20	(III–II) 0.771 (II–0) −0.44
For oxidation state II:		
Coordination numbers[‡]	4, <u>6</u>, 7, 8	4, 5, <u>6</u>, 8
Complexing strength	Very weak (no ligand field stabilization energy)	Generally weak, but strong with N ligands (e.g., CN^-)
Ionic radius (A°)	0.80	0.76
$-\log K_{1a}$ for $M^{II}(H_2O)_6^{2+}$	10.6	9.5
Electron configuration	$4s^0 3d^5$ $(t_2^3) e_g^2$	$4s^0 3d^6$ $(t_2^4 e_g^2)$
For oxidation state III:		
Coordination numbers[§]	5, <u>6</u>, 7	3, 4, 5, <u>6</u>, 7, 8
Isoelectronic with	—	Mn^{II} (d^5)
Complexing strength	Forms metastable complexes with some organic ligands that decompose by redox processes	Low affinity for N ligands; higher affinity for O ligands (e.g., PO_4^{3-}) and halides (except F^-)
$-\log K_{1a}$ for $M^{III}(H_2O)_6^{3+}$	0.4	3.05
For oxidation state IV:		
Coordination numbers[§]	4, <u>6</u>	—
Complexing strength	No soluble complexes	

[*] Modified from Brezonik.[1]
[†] Pauling scale.
[‡] The most common coordination number is underlined.
[§] Potentials in volts for reduction half-reactions are indicated in parentheses.

The above similarities not withstanding, information on one element does not provide much quantitative insight into the behavior of the other. Even from some qualitative perspectives, the two elements behave quite differently. For example, Fe has only one important oxidized state in natural waters (Fe^{III}), but Mn has two (Mn^{III} and Mn^{IV}). Mn is toxic to organisms at moderate concentrations. Fe is not toxic at levels found in natural waters, although excessive levels of Fe intake can be toxic to humans. Bacterial oxidation of Fe occurs at low pH as well as circumneutral pH, but bacterial oxidation of Mn occurs only at circumneutral pH. Abiotic oxidation of Fe^{2+} occurs even at low pH (albeit slowly), but abiotic oxidation of Mn^{2+} apparently does not occur at pH much below 7.

15.2.2 Inorganic equilibrium chemistry

Useful insights into the aqueous inorganic chemistry of Mn and Fe can be gleaned by comparing the pε-pH diagram for Mn (Figure 15.1) with that for Fe (Figure 11.4). From a thermodynamic perspective, Mn^{II} is more stable toward oxidation than is Fe^{II}, as shown by the stability regions of the oxidized and reduced states of the elements in the diagrams and the higher reduction potentials for Mn^{III} and Mn^{IV} than for Fe^{III} (Table 15.1). Another way of saying this is that the oxidized states of Mn are stronger oxidizing agents than Fe^{III}. The upper pε limits of the stability regions for the reduced states decrease with increasing pH, reflecting enhanced stability of the oxidized states from the hydrolysis reactions that form hydroxo and oxo species. The lower pε limits for the +II states of both elements extend below the stability region for water, indicating that the elemental forms, Fe^0 and Mn^0, are not stable in water. Instead, they are oxidized to the +II states by reducing H_2O to H_2.

Iron has an oxidation state higher than Fe^{III}, but it does not occur naturally. Ferrate, Fe^{VI} (FeO_4^{2-}), is a very strong oxidant ($E°$ for the Fe^{VI}/Fe^{III} couple is ~2.2 V—higher than that of permanganate, chromate, and ozone). Solid forms of ferrate tend to be unstable. This has limited the use of ferrate as an oxidant, but commercial production of a stable potassium ferrate solid was initiated in 2009. Ferrate is more stable in solution and can be formed readily at the point of use by reaction of ferric chloride and chlorine at high pH. Use of ferrate for disinfection and oxidation of contaminants in wastewater was studied for many years but generally considered to be uneconomical. A renewed interest in using ferrate for water treatment has developed because of the desire to find effective disinfectants that do not produce the byproducts associated with chlorine. With the development of methods to produce solid ferrate and solutions containing ferrate, it is considered an "emerging" technology.[2]

For the Fe^{III} state, the aquated ion, Fe^{3+}, is dominant only at low pH (Figure 11.4); soluble hydroxo-complexes dominate over a narrow pH range, and insoluble $Fe(OH)_{3(s)}$ is the dominant form over a wide range of pH. Soluble $Fe(OH)_4^-$ becomes dominant at high pH. Hydrolysis is much less important for Fe^{II}; Fe^{2+} is the dominant species up to pH > 7. The difference in hydrolyzing tendency is evident in pC-pH diagrams for Fe^{II} and Fe^{III} (Figure 15.2). $Fe(OH)_{3(s)}$ limits Fe^{III} solubility even in the acidic pH range, and Fe^{III} has a minimum solubility of ~$10^{-9.2}$ M at pH 8.5. In contrast, substantial hydrolysis of Fe^{II} does not occur below pH 7, and its minimum solubility (~$10^{-7.5}$ M) does not occur until pH 10.
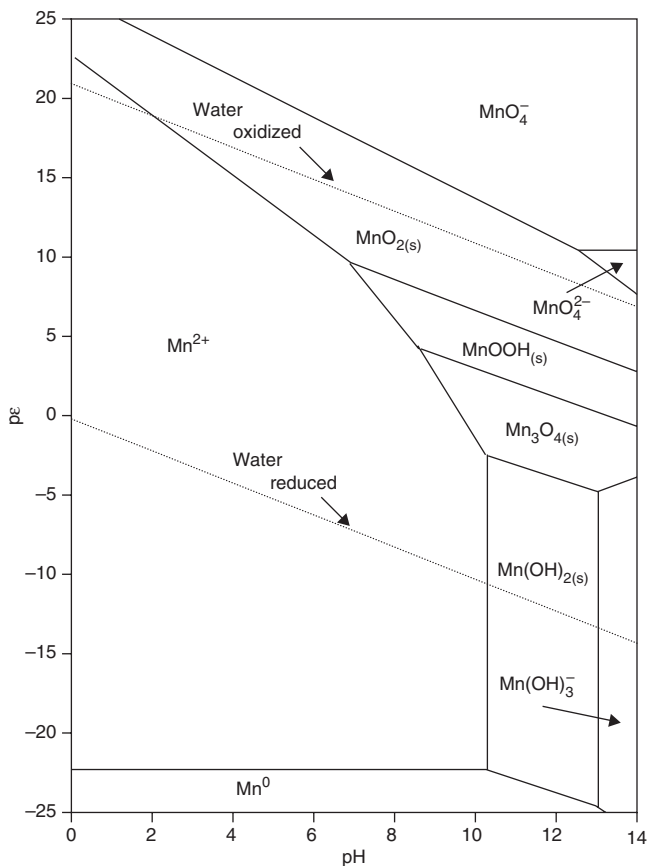
Figure 15.1 pε-pH diagram for manganese in the absence of ions like carbonate or sulfide that form alternative stable mineral phases.

The most oxidized states of Mn (Mn^{VI}, manganate, and Mn^{VII}, permanganate) are important chemical reagents and are used as oxidants in commercial applications. They do not occur naturally, and are not discussed further here. Neither of the oxidized Mn states that occur in natural systems (Mn^{IV}, Mn^{III}) is soluble—either as free ions or complexes. Mn^{IV} has no important hydroxo- or oxo-complexes and occurs as $MnO_{2(s)}$ in natural systems. The stable form of Mn^{III} in water is manganite (γ-$MnOOH_{(s)}$). Mn^{III} does not have many important inorganic complexes, but it forms a metastable species with pyrophosphate that stabilizes the Mn^{III}, which in oxic systems otherwise is oxidized fairly rapidly to Mn^{IV}. Metastable Mn^{III} complexes also exist with some organic ligands such as citrate and EDTA.[3] These complexes decompose by electron transfer reactions that reduce Mn^{III} to Mn^{II} (and oxidize the organic ligand). Timescales for decomposition at neutral pH are on the order of a few minutes for EDTA and ~30 h for citrate and 60 days for pyrophosphate.[3]

Many Fe^{II} and Mn^{II} salts are relatively soluble, but the carbonate salts of both metals have low solubility (log K_{s0} = −10.58 and −10.24, respectively, for rhodochrosite,
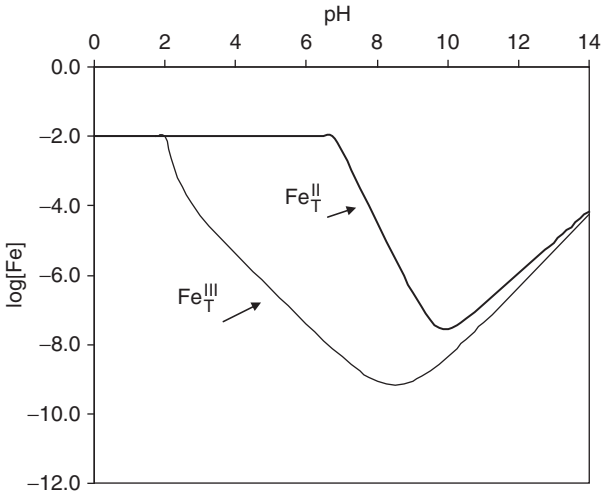
Figure 15.2 Comparison of solubility of $Fe^{II}(OH)_{2(s)}$ and $Fe^{III}(OH)_{3(s)}$. Maximum $Fe_T = 10^{-2}$ M for Fe^{II} and Fe^{III}. Speciation not shown for soluble forms of Fe^{III} or Fe^{II}; see Figures 10.3 and 10.4 for Fe^{II} and Figure 7.5 for Fe^{III}.

$MnCO_{3(s)}$, and siderite, $FeCO_{3(s)}$). Concentrations of the reduced ions may be controlled by CO_3^{2-} in anoxic waters.[4] In general, carbonates are the controlling phase for many divalent metal ions at intermediate pH values, but at higher pH values, hydroxide controls metal ion solubility (see the discussion on carbonate and hydroxide controls for magnesium ion in Section 10.4.3 and Examples 10.5 and 10.6). Some uncertainties exist in the formation constants for soluble complexes of Fe^{2+} and Mn^{2+} with HCO_3^- and CO_3^{2-}, which could influence the concentrations of the metal ions under conditions of control by carbonate.

15.2.3 Autoxidation of Fe^{II} and Mn^{II}

The higher stability of Mn^{II} compared with Fe^{II} is reflected in the oxidation kinetics of the elements. Although Fe^{II} autoxidation decreases rapidly with pH, it does occur at measurable rates in acidic solutions. In contrast, Mn^{II} oxidation is exceedingly slow—from a practical perspective nonexistent—at low pH. The mechanisms of electron transfer to O_2 also are different for the two elements.[5] Fe^{II} reacts with O_2 by an outer sphere process, and O_2 does not bond with Fe during the reaction. In contrast, Mn^{II} reacts with O_2 by an inner sphere mechanism, in which O_2 forms a π–σ bond with Mn^{II} before electron transfer.[6] The differences are related to the orbital electron configurations of the elements (Figure 15.3). Mn^{II} has one electron in each of its five d orbitals (a stable situation); Fe^{II}, with an extra d electron, has one filled and four half-filled d orbitals.

Fe^{II} oxidation kinetics.   Unraveling the kinetics of Fe^{II} autoxidation is one of the success stories of water chemistry. This is one of the most studied reactions in the annals of the field, reflecting its complexity and importance. Some bacteria oxidize Fe^{II} to obtain energy; bacterial oxidation is especially important in acidic systems (pH $<\sim$4), such as acid mine drainage, where the primary Fe^{II} form is Fe^{2+}, but microaerophilic bacteria such as *Gallionella* and *Leptothrix* are able to conduct the reaction at anoxic-oxic interfaces. Chemical oxidation is the primary mechanism at neutral pH. Stumm and

(a) Fe^{2+} autoxidation
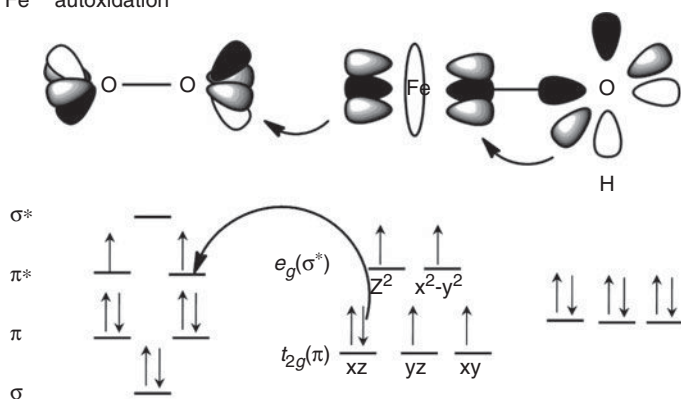
(b) Mn^{2+} autoxidation
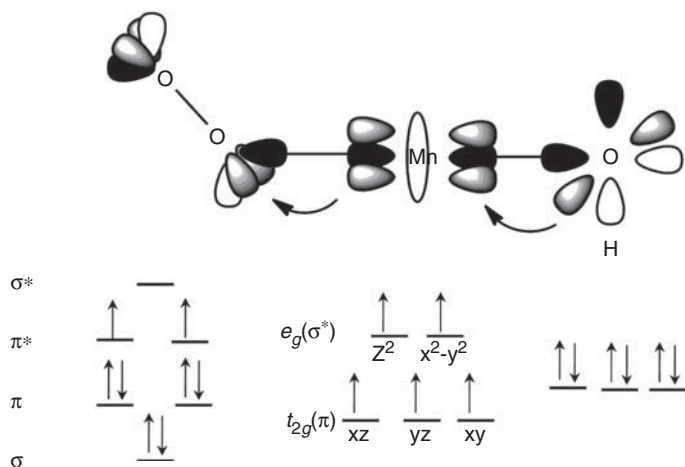
Figure 15.3 Molecular orbital diagrams for autoxidation of Fe^{2+} (a) and Mn^{2+} (b). Outer-sphere electron transfer from Fe $\pi(d_{xz})$: (a t$_{2g}$ (π) orbital), to O$_2$ π^* is possible for Fe^{2+}, and OH$^-$ bound to Fe^{2+} enhances the rate by transferring electron density, stabilizing product Fe^{III}. Outer-sphere transfer is not possible for Mn(H$_2$O)$_6^{2+}$, which has perfect octahedral symmetry, because (1) transfer from Mn $e_g(\sigma^*)$ to O$_2\pi^*$ has unfavorable symmetry (π-to-π transfers are favored in outer-sphere mechanisms), and (2) transfer from Mn $\pi(t_{2g})$ to O$_2\pi^*$ is energetically unfavorable because the t_{2g} orbital is not the HOMO of Mn^{2+}. Binding of OH$^-$ to Mn^{2+} distorts the octahedral symmetry and rearranges the d orbital energies, donating electron density and increasing the basicity of Mn. This allows O$_2$ binding by an e_g to π bond and facilitates electron transfer to O$_2$. Drawn in ChemBioDraw Ultra 12.0 based on diagrams in Luther.[6]

Lee[7] were among the first (in 1961) to study the abiotic reaction under natural water conditions. They established the form of the rate equation, measured the rate constant, and evaluated the effects of solution conditions on reaction rates. As they and many later workers found, the reaction is first order in Fe^{II} and P_{O_2} and second order in $\{OH^-\}$ at near neutral pH values:

$$-\frac{d[Fe^{II}]}{dt} = k_{Fe}[Fe^{II}]P_{O_2}\{OH^-\}^2 \tag{15.1}$$

Ferric iron is insoluble at neutral pH, and the initial oxidation products are lepidocrocite (γ-FeOOH) and amorphous FeOOH, which age to form goethite (α-FeOOH). Stumm and Lee[7] reported that Fe^{III} hydrolysis products catalyze Fe^{II} oxidation; that is, the reaction is autocatalytic. Many subsequent studies confirmed and expanded upon their results (for a review, see Brezonik[1]). Important findings include the following: (1) the rate constant varies little over the range of ambient temperatures, once one corrects for changes in O_2 solubility and K_w (which affects $\{OH^-\}$ at constant pH);[8] and (2) many anions affect the rate of oxidation, some inhibiting it and others accelerating it.

The insensitivity of k_{Fe} to temperature indicates that observed E_{act} is nearly zero in the ambient range. Because the reaction is not an elementary (single-step) reaction it is difficult, however, to translate this information into knowledge about the reaction mechanism. Anions that inhibit oxidation are assumed to form Fe^{II} complexes that are less reactive toward O_2 than is free Fe^{2+} (Example 15.1). Cl^- and SO_4^{2-} are in this category, but their Fe^{II} complexes are so weak that they do not affect Fe^{II} oxidation in freshwaters. High concentrations of these ions in seawater help to explain the much higher ($\sim$20 $\times$) rate of Fe^{II} oxidation at a given pH in freshwater than seawater.[9] In contrast, millimolar concentrations of fluoride and phosphate, which form strong Fe^{II} complexes, catalyze its oxidation.[1] Tannic and humic acid hinder oxidation, probably by forming unreactive or less reactive complexes, but citrate accelerates the rate.[9,10] It is interesting to note that citrate also reduces Fe^{III} by a photochemical mechanism involving ligand-to-metal charge transfer (LMCT) process (see Section 17.7.2).

EXAMPLE 15.1 Modeling the inhibition of Fe^{II} oxidation by organic ligands: The inhibiting effect of organic acid ligands, L^-, can be explained by the formation of unreactive $Fe^{II}L$ complexes:[10,11]

(1) $Fe^{2+} + L^- \underset{k_d}{\overset{k_f}{\rightleftharpoons}} FeL^+$
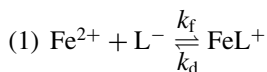
We can simulate the effects of varying pH, L_T, and values of the rate constants for formation and dissociation of FeL^{-n+2} complexes (where $-n$ is the charge on L) on rates of Fe^{II} autoxidation using Acuchem or similar programs. In the following example (see Figure 15.4), we use $L_T = 5 \times 10^{-6}$ M and initial $Fe_T^{II} = 1 \times 10^{-5}$ M.

For complexation reactions, the stability constant is the ratio of the formation and dissociation rate constants, $K_f = k_f/k_d$. Varying k_d at fixed k_f is equivalent to varying K_f. $K_f = 1 \times 10^6 = k_f/k_d$, where $k_f = 1$ s^{-1} applies to the reaction $Fe^{2+} + L^- \rightarrow FeL^+$ and $k_d = 1 \times 10^6$ M^{-1} s^{-1} applies to the reverse reaction. We assume that only free Fe^{2+} undergoes oxidation; values of the pseudo-first-order rate constant, k'_{Fe}, computed from $k_{Fe} = 1.3 \times 10^{12}$ M^{-2} atm^{-1} s^{-1} are 0.027 s^{-1} at pH 7.5 and 2.7 s^{-1} at pH 8.5.
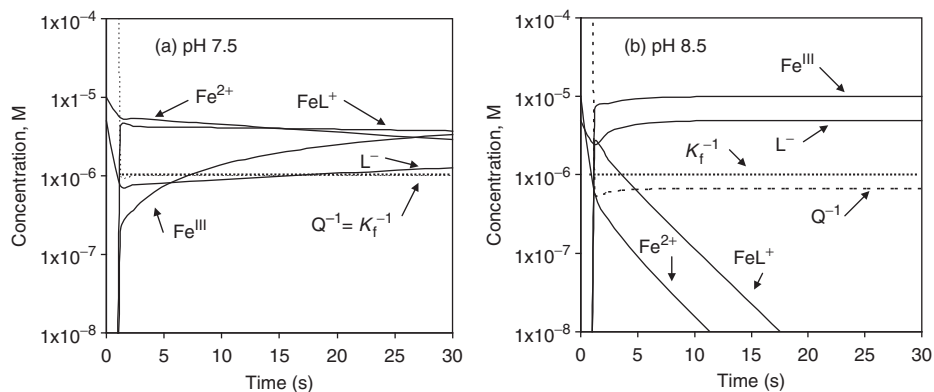
Figure 15.4 Simulated kinetics of Fe^{II} oxidation in the presence of a ligand (L^-) that forms an unreactive complex with Fe^{2+} at pH 7.5 (a) and pH 8.5 (b). Simulations were performed in Acuchem using conditions described in Example 15.1 and by Pankow and Morgan.[10] At pH 7.5 and 8.5, the primary species being oxidized actually is $Fe(OH)_2^0$, not Fe^{2+}, but the simulations should hold if we assume that equilibrium between Fe^{2+} and $Fe(OH)_2^0$ is very rapid (near diffusion control). Discontinuities in concentrations shown at the beginning of the simulations are artifacts of the initial integration time-step.

The reaction quotient, $Q = [FeL^+]/[Fe^{2+}][L^-]$, was calculated versus time and plotted as $1/Q$ to fit on the graphs; when $Q = K_f$, equilibrium prevails.

Increasing L_T may lower the oxidation rate by (1) decreasing $[Fe^{2+}]$ or (2) decreasing the rate of Fe^{2+} release from the complex. A simulation at pH 7.5 (Figure 15.4a) illustrates the first effect. Oxidation is sufficiently slow and complex dissociation so rapid that the reaction quotient, $Q = [FeL^{-n+2}]/[Fe^{2+}][L^{n-}]$, remains constant and equal to K_f over the reaction time. Equilibrium between free and complexed Fe^{II} is maintained, and the decrease in the oxidation rate caused by L^{n-} can be predicted from K_f. At pH 8.5, however, oxidation of free Fe^{II} is so rapid that dissociation of FeL^{-n+2} does not keep pace with the loss of free Fe^{II}. Q deviates from K_f (Figure 15.4b) and reaches a nonequilibrium "steady-state" value.

Autocatalysis of Fe^{II} oxidation was verified in a laboratory study[8] at pH 7.2 and I = 0.5. A two-term expression: $d[Fe^{II}]/dt = (k_1 + k_2[Fe^{III}])[Fe^{II}]$, where k_1 and k_2 are pseudo-first- and second-order rate constants applicable at a given pH and P_{O_2}, was found to fit the data. In contrast, no evidence for autocatalysis was found in a eutrophic English lake, at natural $TOTFe^{III}$ levels up to several mg/L,[11] but the rate was enhanced when high concentrations of synthetic amorphous Fe^{III} hydroxide were added. Natural Fe^{III} hydroxides may have lower activity than synthetic materials because of natural organic matter may sorb onto natural particles. Autocatalysis thus may not be important in many natural waters.

A wide range has been reported for k_{Fe}, but a value of 2×10^{13} M^{-2} atm^{-1} min^{-1} is widely accepted for 20°C in media without inhibiting or accelerating agents.[11] Pseudo-first-order rate constants, k'_{Fe}, applicable to a given pH and $P_{O_2} = 0.21$ atm often are used ($k'_{Fe} = k_{Fe}\{OH^-\}^2 P_{O_2}$). Values are $\sim10^{-1.2}$ day^{-1} ($10^{-4.4}$ min^{-1}) at pH 5
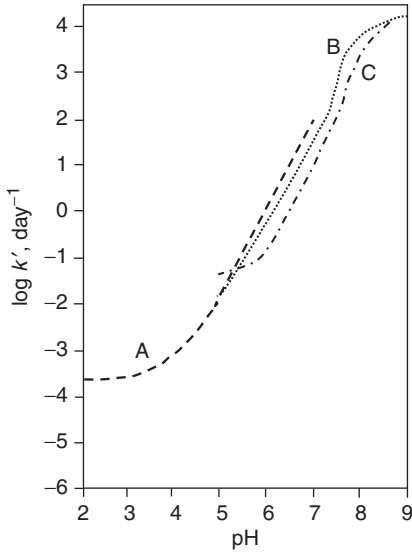
Figure 15.5 Effect of pH on the observed rate constant for Fe^{2+} oxidation by O_2. Curve A from Singer and Stumm[12] for freshwater; curve B from Millero et al.[13] for freshwater; curve C from Millero et al.[13] for seawater.

(representative of lakes impacted by acid deposition), $10^{1.6}$ day^{-1} at pH 7.0, and $\sim 10^{3.8}$ day^{-1} (~ 4.3 min^{-1}) at pH 8.0. Corresponding half-lives range from 11.5 days at pH 5 to < 10 s at pH 8.0.

The lower pH limit for the slope 2 in plots of log k_{Fe} versus pH is of interest relative to predicting abiotic oxidation rates in acidic environments, such as streams and lakes affected by acid mine drainage or acid deposition. Singer and Stumm[12] found a slope of 2 down to pH 4.5 and a decrease thereafter until k_{Fe} became constant at pH $< \sim 3$ (Figure 15.5). Millero et al.[13] found second order dependency on $\{OH^-\}$ from pH 5.0 to 8.0 at 25°C in freshwater but lower pH dependency at pH < 6 in seawater (Figure 15.5). In contrast, Emmenegger et al.[14] found that Fe^{II} oxidation rates reached a plateau at pH $\leq \sim 7.3$ in Greifensee, a eutrophic, hardwater Swiss lake, and suggested this may reflect Fe^{II} binding with natural organic ligands.

A mechanism explaining the strong effect of pH on Fe^{II} oxidation was first described in the mid-1980s when Millero et al.[13,15] showed that the effect results from the greatly differing reactivities of Fe^{2+} and its hydrolysis products toward O_2. In the absence of other ligands, $[Fe^{II}]_T$ is given by

$$[Fe^{II}]_T = [Fe^{2+}] + [FeOH^+] + [Fe(OH)_2^0] + [Fe(OH)_3^-]. \qquad (15.2)$$

Substituting Eq. 15.2 and k'_{Fe} as defined above for k_{Fe} into rate Eq. 15.1 yields an expression in terms of the individual hydrolysis species of Fe^{II}:

$$-d[Fe^{II}]_T/dt = k'_{Fe}[Fe^{II}]_T = k'_0[Fe^{2+}] + k'_1[FeOH^+] + k'_2[Fe(OH)_2] + k'_3[Fe(OH)_3^-] \qquad (15.3)$$

The equation can be rewritten in terms of α values and $[Fe^{II}]_T$:

$$-d[Fe^{II}]_T/dt = \{k'_0\alpha_0 + k'_1\alpha_1 + k'_2\alpha_2 + k'_3\alpha_3\}[Fe^{II}]_T \qquad (15.4)$$

where α_i is the fraction of Fe^{II} in the ith state of deprotonation (see Section 7.2.5). As described in Section 15.2.1, Fe^{2+} has a low tendency to hydrolyze, and concentrations of the hydrolyzed forms are small compared $[Fe^{2+}]$ (see Figure 10.3). Nonetheless, Fe^{2+} is much less reactive toward O_2 than is $FeOH^+$, which is much less reactive than $Fe(OH)_2^0$. By a fitting procedure, Millero et al.[13] extracted values of the k_i' from their experimental data and found $k_0' = 1 \times 10^{-6}$ min^{-1}, $k_1' = 1.7$ min^{-1}, and $k_2' = 10^{5.63}$ min^{-1}. Because of experimental limitations at high pH, where oxidation is so rapid, a value could not be obtained for k_3'. Although $Fe(OH)_2^0$ occurs only at very low concentrations, even at pH 7–9, it contributes most to the oxidation rate at pH $>\sim 5$; that is, $k_2'\alpha_2$ is the largest term in Eq. 15.4 (see Example 15.2). Because dlog$[Fe(OH)_2^0]$/dpH (and dlogα_2/dpH) $= 2$ up to pH ~ 9.2, where $Fe(OH)_{2(s)}$ begins to precipitate, the slope of log k_{Fe}' versus pH is 2. As Example 15.2 indicates, Fe^{2+} is the most important reactant ($k_0'\alpha_0$ is the largest term) below pH 3, and the rate is low but independent of pH because $\alpha_0 \approx 1$.

EXAMPLE 15.2 Effect of pH on forms of Fe^{II} that control the autoxidation of Fe_T^{II}: If we assume that Eq. 15.5 defines the rate of Fe^{II} oxidation (i.e., the reactants are only Fe^{2+} and the hydroxo-complexes of Fe^{II}), we can use MINEQL+ to quantify the contributions of Fe^{II} species to the total rate of oxidation. From MINEQL+ for $Fe_T^{II} = 1 \times 10^{-5}$ M, we find the following:

pH	log$[Fe^{2+}]$	log$[FeOH^+]$	log$[Fe(OH)_2^0]$	log$[Fe(OH)_3^-]$
2	−5.00	−12.5	−21.6	−28.1
3	−5.00	−11.4	−19.5	−25
5	−5.00	−9.4	−15.5	−19
7	−5.00	−7.41	−11.5	−13
8	−5.02	−6.42	−9.52	−10
9	−5.15	−5.55	−7.65	−7.15

Because we do not have an accurate estimate for k_3', we will ignore contributions of $Fe(OH)_3^-$ to the overall rate. Using these values and the k_i' given in the text, we find the following:

pH	k_0' $[Fe^{2+}]$ + k_1' $[FeOH^+]$ + k_2' $[Fe(OH)_2^0]$	=	Rate (M min^{-1})
2	**1 × 10^{-11}** + 10$^{-12.27}$ + 10$^{-15.97}$	=	1.0 × 10^{-11}
3	**1 × 10^{-11}** + 10$^{-11.17}$ + 10$^{-13.87}$	=	1.7 × 10^{-11}
5	1 × 10^{-11} + **10$^{-9.17}$** + 10$^{-9.87}$	=	8.1 × 10^{-10}
7	1 × 10^{-11} + 10$^{-7.18}$ + **10$^{-5.87}$**	=	1.4 × 10^{-6}
8	1 × 10^{-11} + 10$^{-6.19}$ + **10$^{-3.89}$**	=	1.3 × 10^{-4}
9	1 × 10^{-11} + 10$^{-5.32}$ + **10$^{-2.02}$**	=	9.6 × 10^{-3}

The boldface numbers indicate the species that dominates the reaction at a given pH. For example, Fe^{2+} dominates at pH 2 and contributes the most to the rate at pH 3, although $FeOH^+$ accounts for 40% of the rate at pH 3. At pH 5, the $[FeOH^+]$ term, which increases with pH with a slope of 1, dominates, and $[Fe(OH)_2^0]$ accounts for $\sim 20\%$ of the rate. At pH 7.0, $Fe(OH)_2^0$, which increases with pH with a slope of 2, accounts for $\sim 95\%$ of the

rate, and FeOH$^+$ accounts for the rest. At pH 8, [Fe(OH)$_2^0$] accounts for 99.5% of the overall rate, and at pH 9, it constitutes 99.95%.

A more comprehensive analysis of the effects of Fe^{II} speciation on rates of its oxidation was reported by King,[16] who found that (1) ferrous carbonate species dominate the speciation in waters with carbonate alkalinity >~1 meq/L and (2) the Fe(CO$_3$)$_2^{2-}$ complex is the most kinetically active species in such waters at pH > 6. Rate constants derived by King for Fe^{II} carbonate and hydroxide species are summarized in Table 15.2, along with Fe^{II} speciation information and contributions of various species to the overall oxidation rate. He also accounted for the negative effects of complexation by Cl$^-$ and SO$_4^{2-}$ on Fe^{2+} by assuming that those complexes have negligible reactivity. Overall, King considered that nine species affect the Fe^{II} oxidation rate: Fe^{2+}, FeCl$^+$, FeSO$_4^0$, FeOH$^+$, Fe(OH)$_2^0$, FeHCO$_3^+$, FeCO$_3^0$, FeCO$_3^0$, Fe(CO$_3$)$_2^{2-}$, and FeCO$_3$OH$^-$. At any given pH and C$_T$, not all terms were important, and species with low rate constants (e.g., FeCl$^+$ and FeSO$_4^0$) affect the overall rate by decreasing the α values for more reactive species. Overall, King's results (Table 15.2) indicate that carbonate has important effects on Fe^{II} oxidation in waters with moderate to high alkalinity.

Table 15.2 Speciation of Fe^{II} and effects of autoxidation rate in presence of carbonate*

(a) α values[†]

Sample	C$_T$	pH	Fe^{2+}	FeOH$^+$	Fe(OH)$_2^0$	FeHCO$_3^-$	FeCO$_3^0$	Fe(CO$_3$)$_2^{2-}$	Fe(CO$_3$)OH$^-$
1	1.20E-3	7.541	0.537	0.0054	1.48E-6	0.0162	0.439	5.75E-5	3.19E-3
2	2.00E-3	7.516	0.435	0.0040	1.05E-6	0.0211	0.536	1.16E-4	3.76E-3
3	5.00E-3	7.475	0.272	0.0022	5.19E-7	0.0299	0.691	3.78E-4	4.68E-3
4	1.00E-2	7.457	0.177	0.0013	2.99E-7	0.0352	0.780	9.20E-4	5.39E-3
5	2.00E-2	7.695	0.067	0.0008	3.22E-7	0.0233	0.893	4.24E-3	1.17E-2
6	3.33E-2	7.889	0.030	0.0006	3.41E-7	0.0155	0.921	1.29E-2	2.04E-2
7	5.33E-2	8.057	0.014	0.0004	3.41E-7	0.0104	0.908	3.43E-2	3.07E-2

(b) Formation and rate constants   (c) Contributions of species to overall rate ($\alpha_i k_i$)

Species	log K$_f^{‡}$	log k§	Sample	Fe(OH)$_2^0$	Fe(CO$_3$)$_2^{2-}$	Fe(CO$_3$)OH$^-$	$\sum$[¶]	k$_{meas}$
Fe^{2+}	—	−4.6	1	0.0731	0.0355	0.0266	0.135	0.151
FeOH$^+$	4.60	2.62	2	0.0502	0.0693	0.0305	0.150	0.199
Fe(OH)$_2^0$	7.50	7.72	3	0.0230	0.21	0.0350	0.268	0.245
FeHCO$_3^-$	1.47	< 1.9	4	0.0122	0.4690	0.0372	0.518	0.525
FeCO$_3^0$ (aq)	5.69	< 1.4	5	0.0117	1.92	0.714	2.646	1.698
Fe(CO$_3$)$_2^{2-}$	7.45	5.82	6	0.0111	5.23	0.1120	5.353	4.898
Fe(CO$_3$)OH$^-$	9.97	4.0	7	0.0098	12.2	0.1570	12.367	16.595

* Compiled from King.[16]
† Fraction of total Fe^{II} present as indicated species at the given pH and C$_T$.
‡ Formation constants from King[16] except for hydroxo species, which were calculated from data in MINEQL+.
§ Second-order rate constants (first order in Fe^{II} and O$_2$) at a given pH and C$_T$ in M^{-1} min^{-1} at I = 0.
¶ Sum of the three $\alpha_i k_i$ columns to the left, which represent the dominant terms in a rate equation analogous to eq. 15.4 for the conditions of King's experiments.

The reduction of O_2 in Fe^{II} autoxidation follows the Haber-Weiss mechanism; that is, O_2 reduction proceeds by four one-electron transfers (Section 12.2.2), yielding three reactive intermediates: superoxide ($O_2^- \cdot$), hydrogen peroxide, and hydroxyl radicals (HO·). The rate-limiting step most likely is reaction with O_2 itself, because all the intermediates are highly reactive. However, the extent to which the reactive oxygen intermediates play a role in Fe^{II} oxidation is not certain; their high reactivities mean that they may react with other species as well. For example, Emmenegger et al.[14] compared the amount of Fe^{II} oxidation attributable to O_2 and H_2O_2 in Greifensee, Switzerland, for typical summer conditions (pH 8.0–8.5, $[O_2] = 3 \times 10^{-4}$ M, and $[H_2O_2] = 50$–200 nM, and half-lives for Fe^{II} of 7–60 s) and found that O_2 was always the more important oxidant (by $2\times$ to $30\times$) under the range of those conditions.

Kinetics of Mn^{II} oxidation.   Most of the information on this subject was developed by Morgan and his students starting in the 1960s.[17] The rate equation for Mn^{II} oxidation is similar to that for Fe^{II} at pH $\geq \sim 7$: first order in Mn^{II} and O_2, second order in OH^-), but Mn^{II} oxidation yields a mixture of Mn^{III} and Mn^{IV}. Morgan[17] reported that the reaction is not stoichiometric and that x in the product MnO_x ranges from 1.3 to 1.9 (x = 1.5 corresponds to Mn^{III}, and x = 2.0 to Mn^{IV}). More recent studies[18–20] agree that the initial oxidation product is Mn^{III} (γ-MnOOH, manganite). Dissolved Mn levels in oxic natural waters often are in equilibrium with this species (see Section 15.2.5 for an example). Nonetheless, manganite is unstable and disproportionates:

$$2MnOOH + 2H^+ \rightarrow MnO_2 + Mn^{2+} + 2H_2O \tag{15.5}$$

ΔG for this reaction is -105 kJ/mol at the pH and dissolved Mn concentration in seawater.[20] MnOOH thus is only an intermediate in the formation of the stable Mn^{IV} product, MnO_2.

A mechanism involving the formation of dissolved $Mn^{II}(OH)_2^0$ followed by a rate-limiting, one-electron transfer from O_2 was proposed[18] to explain the rate dependence on $\{OH^-\}^2$:

$$Mn(OH)_2^0 + O_2 \rightarrow MnOOH_{(s)} + HO_2 \cdot, \tag{15.6}$$
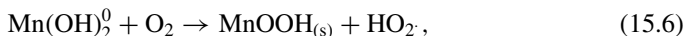
with a proposed transition state of HO–Mn–O—H—$O_{2(aq)}$. Although $Mn(OH)_2^0$ exists only at very low concentrations in solution, similar structures could be formed at the surface of precipitated product.

A major difference between Fe^{II} and Mn^{II} oxidation is that the former is only weakly autocatalytic, but the latter is strongly so. Morgan[17] described Mn^{II} oxidation by a two-term rate equation with an uncatalyzed and a catalyzed term, at constant pH, P_{O_2}, and temperature:

$$-d[Mn^{II}]/dt = k'_{Mn1}[Mn^{II}] + k'_{Mn2}[Mn^{II}][MnO_x] \tag{15.7}$$

Experiments to evaluate the rate coefficients of Eq. 15.7 under conditions where the autocatalytic term was thought to be negligible[17] yielded 4×10^{12} M^{-2} atm^{-1} day^{-1} for k_{Mn1} (i.e., $k'_{Mn1}/[O_2][OH^-]^2$). A large range for k_{Mn2} (defined similarly) is found in the literature: 2.4×10^{14} to 3.2×10^{19} M^{-3} atm^{-1} day^{-1}. The range actually may reflect

differences in the catalytic activity of Mn oxides formed under different conditions rather than poor measurement accuracy.[1]

Several lines of evidence suggest that the first term in Eq. 15.7 and the reported value of k'_{Mn1} are not accurate. The electronic structure of Mn^{2+} described in Figure 15.3 indicates that an outer sphere electron transfer process is not possible for the octahedrally symmetric $Mn(H_2O)_6^{2+}$ ion.[6] In support of this theory-based conclusion, a laboratory study by Diem and Stumm[21] suggests that homogeneous oxidation of Mn^{II} either does not occur or is extremely slow (timescale of decades) in solutions undersaturated with respect to $MnCO_{3(s)}$ and $Mn(OH)_{2(s)}$ and lacking microorganisms or other solids. In an experiment demonstrating impressive patience, these authors incubated Mn^{II} solutions fitting these conditions for up to seven years, and no loss of dissolved Mn^{II} was found. Measurable oxidation occurred only in solutions supersaturated with respect to a solid Mn^{II} phase. The solutions Morgan used to establish the two-term autocatalytic rate law are thought to have been supersaturated with respect to $MnCO_3$ or $Mn(OH)_2$ and probably had Mn^{II} solid phases.[21] The reaction of Mn^{II} with O_2 apparently occurs much more readily when Mn^{II} is present as $MnCO_{3(s)}$, $Mn(OH)_{2(s)}$, or surface complexes of hydrous oxides, such as shown below, than when it is $Mn_{(aq)}^{2+}$:

$$\begin{aligned} &\equiv Me - O_\backslash \\ &\qquad\qquad Mn^{II} \\ &\equiv Me - O^{/} \end{aligned} \qquad (15.8)$$
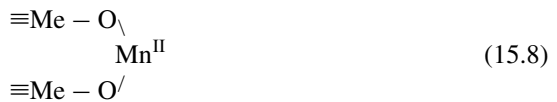
where $Me = Fe^{III}$, Mn^{III}, or Mn^{IV}.

High values of E_{act} (110–120 kJ/mol) were reported for Mn^{II} oxidation on iron oxide surfaces, but these values include the effects of temperature on Mn^{II} sorption. When this was factored out, E_{act} for surface-bound Mn^{II} was only 35–50 kJ/mol,[20] comparable to the E_{act} found in Morgan's initial study.[17] Ligands that form soluble Mn^{II} complexes decrease Mn sorption to oxide surfaces and decrease Mn^{II} oxidation rates. Pyrophosphate ($P_2O_7^{4-}$), a strong complexing agent, greatly depresses the oxidation rate, but the extent apparently is greater than can be accounted for by complex formation.[22]

15.2.4 Reductive dissolution of Fe and Mn (hydr)oxides: abiotic and biotic mechanisms

Compared with the extensive literature on Fe^{II} and Mn^{II} oxidation, that on the reduction of insoluble Fe^{III} and $Mn^{III,IV}$ (hydr)oxides to soluble +II forms is sparser and much more recent—despite the fact that reduction is just as important as oxidation in the cycles of these elements. This situation is explainable by the greater difficulties in studying reduction reactions because the reactants are solids. Aside from basic questions about rates and environmental factors affecting rates, questions of interest include (1) what are the reducing agents, and how do they operate; and (2) are the reactions abiotic or microbial, and if the latter, how do microbes transfer electrons to solids they cannot bring inside their cells? Rapid increases in dissolved (i.e., reduced) Fe and Mn are observed in lakes once their bottom waters become anoxic, indicating that reduction of Fe and Mn (hydr)oxides is rapid (timescale of days rather than months), but not much is known about environmental factors affecting reduction rates.

Abiotic reduction: a surface complexation process.   Progress in elucidating mechanisms of reduction has focused on complexation of dissolved reductants on surface sites on the metal (hydr)oxides. Such surface complexes can be characterized by stability constants (like those for complexes in solution). Substantial evidence exists to show that the major reducing agent for reductive dissolution of Fe and Mn (hydr)oxides in aquatic systems is natural organic matter. In fact, one way to view the redox cycles of Fe and Mn is that they act as catalysts for the oxidation of organic matter by O_2. NOM oxidation causes reductive dissolution of the metal (hydr)oxides, and the dissolved (reduced) metal ion products are reoxidized by O_2 in solution. NOM plays a direct role in abiotic reactions and an indirect role as carbon and energy sources for microbially mediated reductive dissolution, in which the metal (hydr)oxides act as microbial electron acceptors. Photoreduction of Fe and Mn (hydr)oxides also occurs in natural systems, by mechanisms that involve surface complexation and charge-transfer processes (Section 17.7.2).

Organic reducing agents of metal (hydr)oxides have two essential characteristics: (1) functional groups that form surface complexes with metal ion centers and (2) electron-rich groups that donate electrons to the metal ion, transforming the organic moiety to a radical. Compounds with these properties include phenols, thiols, and organic acids, which occur widely in aquatic humic material and sediment organic matter. Inorganic sulfide also can reduce Mn oxides. Both outer (*os*) and inner sphere (*is*) surface complexes may be formed, as illustrated for Mn^{III}(hydr)oxide complexes with phenolate:[23]

$$\text{Outer sphere: } \equiv Mn^{III} - OH + {}^-OPhen \rightarrow \ \equiv Mn^{III} - OH - \ {}^-OPhen \qquad (15.9)$$

$$\text{Inner sphere: } \equiv Mn^{III} - OH + HOPhen \rightarrow \ \equiv Mn^{III} - OPhen + H_2O \qquad (15.10)$$
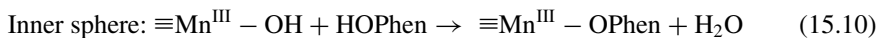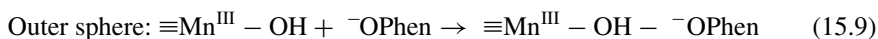
In *os* complexes, the ligand is separated from the metal's primary coordination sphere by an $-OH$ or $-H_2O$ ligand. In *is* complexes, the ligand replaces a ligand (typically $-OH$) in the metal's coordination sphere. Strong inhibition of dissolution by adsorption of other ions supports the surface complexation model for reductive dissolution of metal (hydr)oxides. The extent of the charge on (hydr)oxide surface sites depends on pH (see Chapter 14); surface protonation equilibria describe this quantitatively, e.g.,

$$\equiv Mn^{III}OH_2^+ \rightarrow \ \equiv Mn^{III}OH + H^+, \ K_{a1(sfc)}, \qquad (15.11)$$

$$\equiv Mn^{III}OH \rightarrow \ \equiv Mn^{III}O^- + H^+, \ K_{a2(sfc)}. \qquad (15.12)$$
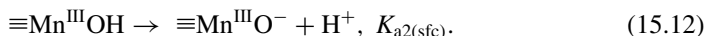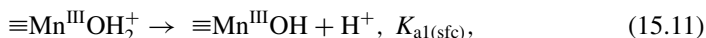
In the absence of adsorption by charged ligands, oxide surfaces have a net positive charge when the completely protonated sites ($\equiv Mn^{III}OH_2^+$) outnumber the deprotonated sites ($\equiv Mn^{III}O^-$), and a net negative charge when the opposite is true.

Possible mechanisms for reductive dissolution of metal (hydr)oxides by *os* and *is* surface complexes are given in Table 15.3. Limiting cases for the mechanisms and the effects of pH and ligand concentration on rates of metal mobilization were examined by computer simulation (Example 15.3). Experimental verification of such simulations is hindered by the lack of methods to measure actual speciation on (hydr)oxide surfaces. As a result, it is not possible to measure rate constants for the elementary steps, and the values used in simulations must be considered estimates at best.

Table 15.3 Inner- and outer-sphere mechanisms for reductive dissolution of trivalent metal oxide surfaces ($\equiv Me^{III}OH$) by phenols (HOP)*

Inner sphere	Outer sphere
(1) Precursor complex formation	
$\equiv Me^{III}OH + HOP \underset{k_{-1}}{\overset{k_1}{\rightleftharpoons}} \equiv Me^{III}OP + H_2O$	$\equiv Me^{III}OH + HOP \underset{k_{-1}}{\overset{k_1}{\rightleftharpoons}} \equiv Me^{III}OH - HOP$
(2) Electron transfer	
$\equiv Me^{III}OP \underset{k_{-2}}{\overset{k_2}{\rightleftharpoons}} \equiv Me^{II}OP^+$	$\equiv Me^{III}OH{-}HOP \underset{k_{-2}}{\overset{k_2}{\rightleftharpoons}} \equiv Me^{II}OH^-HOP^+$
(3) Release of oxidized organic product	
$\equiv Me^{II}OP^+ + H_2O \underset{k_{-3}}{\overset{k_3}{\rightleftharpoons}} \equiv Me^{II}OH_2 + OP^+$	$\equiv Me^{II}OH{-}HOP^+ \underset{k_{-3}}{\overset{k_3}{\rightleftharpoons}} \equiv Me^{II}OH_2 + OP^+$
(4) Release of reduced metal ion	
$\equiv Me^{II}OH_2 + 2H^+ \underset{k_{-4}}{\overset{k_4}{\rightleftharpoons}} \equiv Me^{III}OH + Me^{2+}$	$\equiv Me^{II}OH_2 + 2H^+ \underset{k_{-4}}{\overset{k_4}{\rightleftharpoons}} \equiv Me^{III}OH + Me^{2+}$

* Adapted from Stone and Morgan.[23]

EXAMPLE 15.3 Simulation of metal oxide reductive dissolution by an inner sphere mechanism*:

Case I. Consider the following simplification of the inner sphere mechanism in Table 15.3. Assume that all steps except complex formation are irreversible and that release of reduced metal and oxidized organic products is rapid compared with complex formation and electron transfer. Because reduced metal is released as soon as it forms, $[\equiv Me^{II}OP^+]$ and $[\equiv Me^{II}OH_2]$ are negligible, and the mass balance for surface sites (S_T) simplifies to

(1) $S_T = [\equiv Me^{III}OH] + [\equiv Me^{III}OP]$.

Rates of metal release are proportional to the number of sites complexed by phenolate ions, OP^-:

(2) $d[Me^{2+}]/dt = k_2[\equiv Me^{III}OP]$

In turn, $[\equiv Me^{III}OP]$ depends on relative rates of adsorption, desorption, and electron transfer:

(3) $d[\equiv Me^{III}OP]/dt = k_1[HOP][\equiv Me^{III}OH] - k_{-1}[\equiv Me^{III}OP] - k_2[\equiv Me^{III}OP]$

If phenol concentration, [HOP], is constant, Eq. (3) can be integrated by solving Eq. (1) for $[\equiv Me^{III}OH]$ and substituting into Eq. (3) to yield

(4) $[\equiv Me^{III}OP] = S_T \left[\dfrac{k_1[HOP]}{k_1[HOP] + k_{-1} + k_2} \right] (1 - \exp\{-k_1[HOP] + k_{-1} + k_2)t\}).$

Substituting Eq. (4) into Eq. (2) yields a rate equation for metal ion solubilization in terms only of rate constants and a measurable solution condition, [HOP]. According to

Eq. (4), when t $\gg$ τ, the characteristic time, $[\equiv Me^{III}OP]$ reaches a steady-state value:

(5) $[\equiv Me^{III}OP]_{ss} = S_T k_1[HOP]/(k_1[HOP] + k_{-1} + k_2)$,

where τ is the reciprocal of the rate coefficient term, $(k_1[HOP] + k_{-1} + k_2)$. At steady-state, the release rate of Me^{II} is

(6) $d[Me^{2+}]/dt = k_2[\equiv Me^{III}OP]_{ss} = k_1 k_2 S_T[HOP]/(k_1[HOP] + k_{-1} + k_2)$.

Electron transfer thus is rate-limiting when $k_2 \ll k_1[HOP] + k_{-1}$; adsorption is limiting when $k_1[HOP] \ll k_{-1} + k_2$.

    To simulate this case by Acuchem, we need to estimates of k_1, k_{-1}, k_2, and k_4. Rate constants k_{-2}, k_{-3}, and k_{-4} are negligible by the assumption that steps (2)–(4) are irreversible. Constant k_3 can be combined with k_4 because of the assumption that both steps (3) and (4) are rapid compared with steps (1) and (2), and k_4 must be large compared with k_1 and k_2. We also need initial values for $[HOP]$ and S_T, which (initially) is equal to $[\equiv Me^{III}OH]$.

Case II. Alternatively, release of reduced metal ions may be rate limiting. If the other conditions of case I are the same, reaction 4 of Table 15.3 must be included in the analysis. The mass balance on surface sites then becomes

(7) $S_T = [\equiv Me^{III}OH] + [\equiv Me^{III}OP] + [\equiv Me^{II}OH_2]$.

This case also requires values for k_1, k_{-1}, k_2, and k_4, but here k_4 is small compared with k_1 and k_2.

    Simulations by Acuchem are straightforward once values of the rate coefficients, $S_{T,0}$ and $[HOP]_0$ are estimated. The simulations for both cases (Figure 15.6) show that $[\equiv Me^{II}OH_2]$ reaches a steady-state that accounts for only a small portion of S_T when k_4 is large (case I, metal release not rate limiting). When k_4 is small (case II), $[\equiv Me^{II}OH_2]$ continues to increase, eventually accounting for most of S_T.

* Adapted from Stone and Morgan.[23]

Microbial reduction.   Many types of bacteria (>18 genera) can reduce Fe and Mn (hydr)oxides, including aerobes, facultative anaerobes and strict anaerobes. Important taxa in this regard include *Shewanella putrefaciens*, a marine facultative anaerobe also found in soil, and anaerobic *Geobacter metallireducens* and related species, widely found in freshwater sediments, which oxidizes organic matter using ferric oxides as the electron acceptor and has been used extensively in recent studies on microbial fuel cells. Some fungi also are able to reduce Fe and Mn oxides.[24] For some microbes activity is inhibited by O_2 and/or NO_3^-, but these thermodynamically preferred electron acceptors have no effects on other microbes. Microbial reduction could involve enzymatic reactions in the electron transport system, other reductase enzymes, or could involve nonenzymatic reactions with organic compounds produced by cellular metabolism. How enzymatic reduction would occur is uncertain. Although bacterial cells can be found on metal (hydr)oxide surfaces, transport of amorphous solid (hydr)oxides into cells does not seem possible. If enzymes are involved, they must be extracellular or bound to surface membranes. Some iron-reducing bacteria use nitrate reductase,
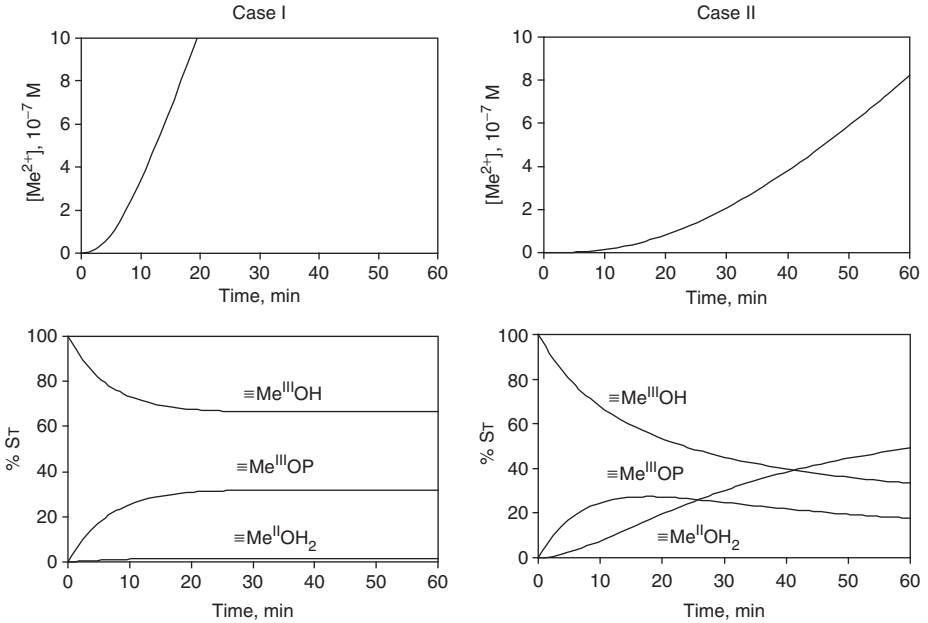
Figure 15.6 Simulation by Acuchem of Me^{2+} release from Me^{III}(hydr)oxide for cases I and II of Example 15.3. HOP adsorption/desorption and electron transfer are rate limiting in case I; Me^{2+} release is rate limiting in case II. Values used in simulations: $S_T = 5 \times 10^{-6}$ M (= $[\equiv Me^{III}OH]_0$); $[HOP] = 1 \times 10^{-4}$ M; $k_1 = 500$ M^{-1} min^{-1}; $k_{-1} = k_2 = 0.05$ min^{-1}; and $k_4 = 1$ min^{-1} in case I and 0.01 min^{-1} in case II. Based on a similar figure in Stone and Morgan.[23]

a soluble enzyme. Whether cells obtain energy by coupling the reduction to ATP formation also is uncertain.[25] Cells could grow using Fe or Mn (hydr)oxides as electron acceptors without obtaining energy from the reduction because energy can be obtained by "substrate-level phosphorylation," as occurs in fermentation. Metal reduction then would simply be a means to eliminate excess electrons. Use of microbial inhibitors demonstrated that microbial reduction is important for the dissolution of Fe (hydr)oxides in anaerobic sediments, but results were inconclusive for Mn. More details on microbial reduction of Fe and Mn are available elsewhere.[24]

15.2.5 Patterns of Fe and Mn in lakes

The distribution of dissolved Fe and Mn in lake waters varies seasonally and vertically depending on redox and pH conditions. For example, vertical profiles of dissolved Fe and Mn in dimictic lakes show classic "inverse clinograde" patterns (Figure 15.7) during summer stratification—low concentrations in oxic surface waters and higher concentrations in anoxic hypolimnia. Similar patterns are found for phosphate, reflecting a linkage between the iron and phosphate cycles in lakes. Phosphate ions sorb onto Fe^{III} (hydr)oxides and form insoluble Fe^{III} phosphate compounds. The $Fe(OH)_{3(s)}$ floc forms a protective barrier at the sediment-water interface at the bottom of lakes, limiting the release of phosphate from sediments. When the overlying water goes anoxic during
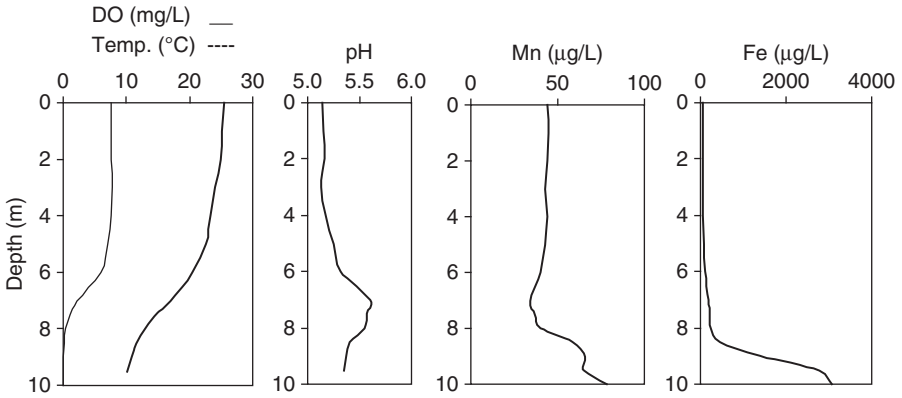
Figure 15.7 Midsummer (July 22, 1987) vertical profiles of dissolved Fe and Mn in Little Rock Lake, Wisconsin, along with temperature, dissolved oxygen, and pH profiles. Unpublished data of C. E. Mach and the author (P.L.B.).
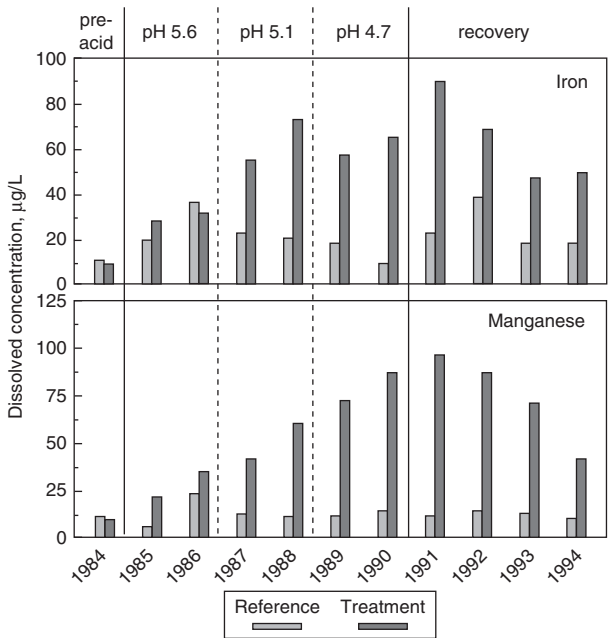
Figure 15.8 Annual average dissolved Fe and Mn concentrations in surface water of the treatment and reference basins of Little Rock Lake, Wisconsin, during an acidification and recovery experiment. From Brezonik et al.,[27] © Springer, and used with permission.

summer stratification, the floc undergoes reductive dissolution, and the protective barrier disappears, allowing more rapid release of phosphate.

Concentrations of Fe and Mn also tend to be higher in lakes with lower pH; this is illustrated by an increase in dissolved concentrations as pH was lowered in an acidification experiment in Little Rock Lake, Wisconsin (Figure 15.8).[26–28] The Fe increases reflect increased solubility of Fe^{III} at lower pH, as well as slower oxidation
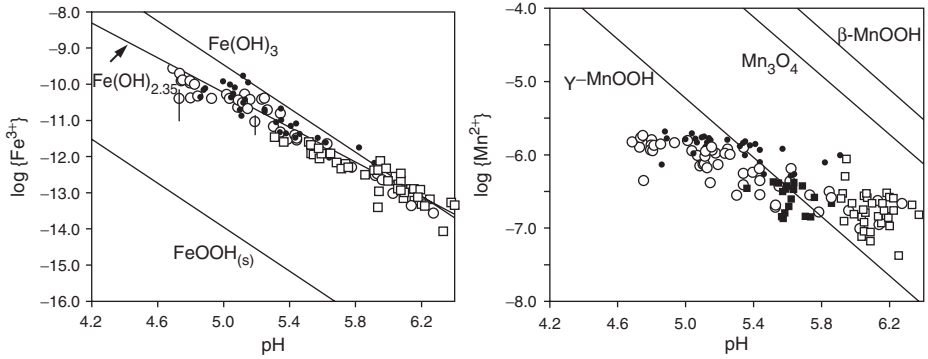
Figure 15.9 Calculated activity of Fe^{3+} (a) and Mn^{2+} (b) versus pH in Little Rock Lake, Wisconsin, superimposed on Fe^{3+} and Mn^{2+} solubility lines for selected Fe and Mn minerals corrected to 10°C and I $= 1.55 \times 10^{-4}$ (annual averages for Little Rock Lake). Squares, reference basin; open circles, treatment basin during acidification; closed circles, treatment basin during recovery phase. From Brezonik et al.,[27] who provided details on the calculations, © Springer, and used with permission.

of Fe^{2+} at lower pH, allowing Fe^{2+} produced in the anoxic hypolimnion to remain in the oxic water column as a metastable species. Dissolved Fe decreased at pH 4.7–4.9, illustrating the need for caution in extrapolating trends in pH or other potentially controlling variables. The decline may reflect Fe precipitation by humic matter; color and dissolved organic carbon also declined in this pH range.[27]

In situ observations sometimes can be used to infer the mineral(s) controlling metal concentrations in water bodies. For example, Fe and Mn in Little Rock Lake appear to be controlled by amorphous ferric hydroxide with a stoichiometry of $Fe(OH)_{2.35}$ and manganite (γ-MnOOH), respectively, as plots of dissolved Fe and Mn versus pH (Figure 15.9) suggest. The lower than expected Fe:hydroxide ratio may reflect inclusion of other anions or the presence of mixed oxidation states of Fe.[29] Slow oxidation kinetics likely is the reason for the scatter in $\{Mn^{2+}\}$ and slope < 2 in Figure 15.9.

15.2.6 Iron in groundwater

Because iron minerals are present in aquifer materials, iron is commonly present in ground water. Levels are low if the ground water is oxic because ferric iron is essentially insoluble. If the water is anoxic, however, iron is reduced to the ferrous form, which is much more soluble. Iron causes problems when the groundwater is pumped and used for drinking water. Upon exposure to oxygen the ferrous iron is oxidized to ferric iron, which precipitates, causing stains on plumbing fixtures and clothes. It can also block pipes. The water also is often colored and has a metallic taste. The obvious solution to this problem is to precipitate the iron. This can be performed by exposing the water to air or chlorine in a reaction chamber and either allowing the iron oxide to settle or removing it via filtration. This is easily done at municipal water treatment plants, but harder for someone with an individual well. In this case, water softeners (via ion exchange) or other commercial oxidation/filtration products are available for onsite removal of iron.

15.3 Aluminum

15.3.1 Introduction: sources and significance

After oxygen and silicon, aluminum (at. no. 13, at. wt. 27) is the third most abundant element (8.3%) in the Earth's crust. Al has a high affinity for oxygen, and its mineral forms almost exclusively are oxides and aluminosilicates, in which Al also is bonded to oxygen. Gibbsite, the stable form of $Al(OH)_{3(s)}$ (γ-$Al(OH)_3$), occurs widely in nature. It has exists two common forms—crystalline and microcrystalline—and also occurs as two polymorphs of $AlO(OH)$, diaspore and boehmite, as well as Al_2O_3, corundum. Together, these forms comprise bauxite, the ore from which Al metal is obtained. In water, Al hydrolyzes readily, and its solubility at near neutral pH is limited by the formation of $Al(OH)_{3(s)}$. The solubility of crystalline gibbsite is $\sim 10^{-7.35}$ M (~ 1 μg/L) at pH 7, but amorphous $Al(OH)_3$ is much more soluble ($10^{-4.84}$ M or ~ 0.4 mg/L). The solubility of both forms increases rapidly below pH 5. For example, Al_T in equilibrium with gibbsite is $10^{-5.06}$ M (0.22 mg/L) at pH 4.5 and $10^{-3.66}$ M (5.9 mg/L) at pH 4.0.

In spite of the normally low Al concentrations in natural waters, Al chemistry is important, especially in engineered systems, for several reasons. First, dissolved Al ions are toxic to fish and other aquatic animals, and this is of concern in acidic waters, where Al solubility is high (e.g., see Figure 15.10). The mechanism of toxicity to fish is thought to be precipitation of $Al(OH)_{3(s)}$ at the higher pH on gill surfaces, and this prevents absorption of O_2. Second, Al in water raises human health concerns because it has been associated with Alzheimer's disease. Human exposures to Al via drinking water are thought to be small, but use of low-pH water in cooking utensils made of aluminum may be an issue. Third, the hydrolyzing strength of aluminum is of great practical use. Alum, aluminum sulfate ($Al_2(SO_4)_3 \cdot 10H_2O$), hydrolyzes in water to form
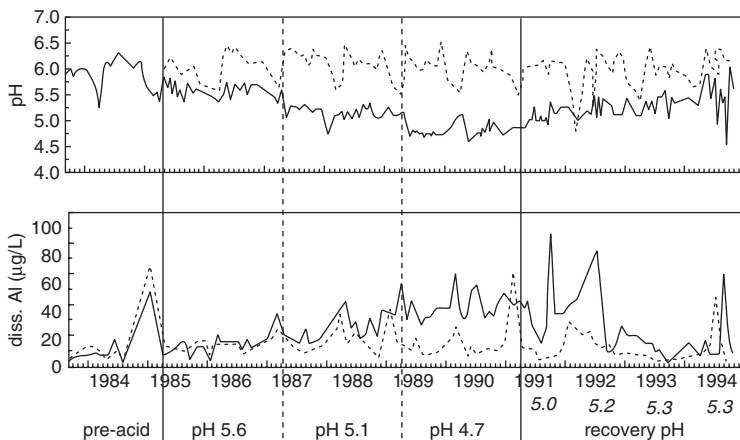
Figure 15.10 Temporal trends in pH and dissolved Al in Little Rock Lake, Wisconsin, during a whole-lake acidification experiment. Solid lines, treatment basin; dashed lines, reference basin. From Brezonik et al.,[27] © Springer, and used with permission.

$Al(OH)_{3(s)}$ and is a widely used coagulant to remove organic color and turbidity from surface waters in drinking water treatment. Alum also is used to remove phosphate from wastewater, and lake treatments with alum are a common means of controlling eutrophication in small lakes of recreational importance.

Al is not redox active; its only oxidation state is +III. This causes Fe and Al (hydr)oxides to behave differently with regard to phosphate cycling in lakes. Ferric (hydr)oxide undergoes reductive dissolution when lake hypolimnia go anoxic, allowing release of phosphate from sediments, but this does not occur when sediments are covered with a layer of $Al(OH)_{3(s)}$. Alum treatment thus is potentially effective in controlling internal cycling of phosphorus in lakes. The main reactions of interest in the inorganic chemistry of Al in natural waters are hydrolysis, dissolution/precipitation of Al (hydr)oxides and aluminosilicates, and a few complexation reactions. Aluminosilicate dissolution is described in Section 15.5, and removal of phosphate by alum treatment is covered in Section 16.4.2. The other reactions are discussed below.

15.3.2 Al hydrolysis equilibria

The main equilibria in the hydrolysis and precipitation of Al are listed in Table 15.4. When Al precipitates, a metastable phase, amorphous (gel-like) $Al(OH)_3$ is formed; this crystallizes to stable gibbsite only slowly. Solubility equilibria for Al are complicated by various polymorphs and metastable phases that have different solubilities. In addition, Al hydrolysis readily produces multinuclear, oligomeric or polymeric complexes such as $Al_7(OH)_{17}^{4+}$ and $Al_{13}(OH)_{34}^{5+}$. These important intermediates in coagulation are thought to have structures like the following:[4]
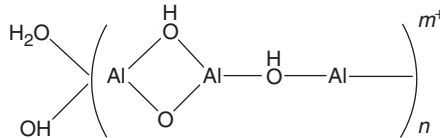
Table 15.4 Equilibria for reactions involved in Al hydrolysis[*]

Reaction	Log K_{eq}
$Al^{3+} + H_2O \rightleftharpoons AlOH^{2+} + H^+$	$\log K_1 = -4.997$
$Al^{3+} + 2H_2O \rightleftharpoons Al(OH)_2^+ + 2H^+$	$\log \beta_2 = -10.094$
$Al^{3+} + 3H_2O \rightleftharpoons Al(OH)_{3(aq)}^0 + 3H^+$	$\log \beta_3 = -16.791$
$Al^{3+} + 4H_2O \rightleftharpoons Al(OH)_4^- + 4H^+$	$\log \beta_4 = -22.688$
Gibbsite	
$Al(OH)_{3(gibbsite)} + 3H^+ \rightleftharpoons Al^{3+} + 3H_2O$	$\log{}^* K = 8.29$
Microcrystalline gibbsite	
$Al(OH)_{3(micr\ gib)} + 3H^+ \rightleftharpoons Al^{3+} + 3H_2O$	$\log{}^* K = 9.35$
Amorphous Al(OH)$_3$	
$Al(OH)_{3(am)} + 3H^+ \rightleftharpoons Al^{3+} + 3H_2O$	$\log{}^* K = 10.8$

[*] All values from MINEQL+ except for microcrystalline gibbsite.[5]

Figure 15.11 Solubility diagrams for amorphous $Al(OH)_3$ and crystalline gibbsite. The diagrams were prepared using MINEQL+ and the equilibrium constants in Table 15.4.

Multinuclear hydrolysis products affect the surface charge of colloids differently than Al^{3+} does; they absorb specifically by ligand exchange with $-OH$ groups and can reverse the surface charge.[4]

Solubilities of the end-member forms of aluminum hydroxide, $Al(OH)_{3(am)}$ and crystalline gibbsite, are shown as a function of pH in Figure 15.11. The results for $Al(OH)_{3(am)}$ are representative of conditions that occur in engineered systems when alum is added to water or when the pH is raised in acidic solutions containing Al^{3+}; the initial precipitation product is $Al(OH)_{3(am)}$. The plot for gibbsite is more reflective of natural systems, where gibbsite is a common mineral phase. Indeed, concentrations of Al in Little Rock Lake[27] appeared to be controlled by equilibrium with a gibbsite phase during an acidification experiment that lowered the pH from ~6.0 to ~4.7 (Figure 15.12).

15.3.3 Al complex formation: equilibria and kinetics

Aside from the strong tendency of Al to form hydroxo-complexes, Al otherwise tends to form weak complexes, befitting its status as a Class A (hard) metal, and the coordination chemistry of dissolved Al in natural waters is generally not important. Reaction with fluoride is an exception, however. Al^{III} forms strong complexes with F^-, ($\beta_1 = 10^7$, $\beta_2 = 10^{12.6}$), and the complexed forms dominate even when both Al^{III} and F^- are present at micromolar concentrations (Example 15.4).

EXAMPLE 15.4 Al-F equilibria in waters affected by acid deposition: Calculate the equilibrium concentrations of all Al^{III} and F^- species in water at pH 4.5 when both Al_T and $F_T^- = 100 \mu g/L$.

Answer: Using MINEQL+ in single-run mode at fixed pH = 4.5, converting the concentrations of Al and F^- to molar values (3.7×10^{-6} and 5.3×10^{-6} M, respectively), and inserting them as components, we find that >99% of Al_T is in fluoride complexes. The dominant form of Al is AlF_2^+ (62%), AlF_3^0 accounts for 33%, and AlF^{2+} for 4%. Table 15.5 summarizes the output of the equilibrium calculations from MINEQL+.

Figure 15.12 Calculated Al^{3+} activity in Little Rock Lake versus pH superimposed on lines for $\{Al^{3+}\}$ in equilibrium with three gibbsite phases. Squares, reference basin; open circles, treatment basin during acidification; closed circles, treatment basin during recovery phase. From Brezonik et al.,[27] © Springer, and used with permission.

Table 15.5 Summary of MINEQL+ output for Al-F equilibria at pH 4.5

ID Species	Conc. (M)	Log C
Type I components		
8 Al^{3+}	3.460E-10	−9.461
34 F^-	4.250E-05	−4.372
Type II complexes		
4300 $Al(OH)_2^+$	2.630E-11	−10.580
4400 $Al(OH)_{3(aq)}$	1.660E-13	−12.780
4500 $Al(OH)_4^-$	6.700E-15	−14.174
4600 $AlOH^{2+}$	1.060E-10	−9.974
6400 $H_2F_{2(aq)}$	1.040E-11	−10.982
6500 HF_2^-	3.190E-10	−9.496
6600 $HF_{(aq)}$	1.970E-06	−5.705
62100 AlF_2^+	2.310E-06	−5.636
62200 $AlF_{3(aq)}$	1.220E-06	−5.914
62300 AlF^{2+}	1.410E-07	−6.852
62400 AlF_4^-	2.600E-08	−7.585

The water-exchange rate constant for Al^{3+}, $k_{-H_2O} = \sim 10$ s^{-1}) is among the lowest of common metal ions—about 10^{-5} to 10^{-8} as fast as most metal ions of interest in natural waters (see Figure 9.18). Indeed, only the kinetically inert Cr^{3+} ($k_{-H_2O} = 10^{-6}$ s^{-1}) and Co^{3+} ($k_{-H_2O} = \sim 10^{-1}$ s^{-1}) have slower water exchange rates. Consequently, formation rates of Al^{3+} complexes should be substantially slower than those for most metals (because k_f is correlated with k_{-H_2O}). This was found to be the case for AlF_2^+ by Plankey et al.,[30] who described a formation process involving four pathways based on the Eigen mechanism. The formation mechanism for this complex is complicated because the acid-base speciation of both Al^{3+} and F^- varies within the pH region of interest. Formation rates of AlF_2^+ are pH-sensitive, decreasing rapidly below pH 5, reaching a minimum at pH ~ 3, and increasing slowly at lower pH values. Equilibrium may not be reached for several hours at low temperature and pH ~ 3, but under conditions more typical of acidic lakes and streams, half-lives are on the order of seconds to a few minutes.

15.4 Silica

15.4.1 Sources and significance

Silicon (at. no. 14, at. wt. 28) is second only to oxygen in abundance (25.7%) in the Earth's crust. It exists almost exclusively as tetravalent oxides in various mineral forms of silicon dioxide (silica, SiO_2), metal silicates like olivine, $(Mg,Fe)_2SiO_4$, which is important in the Earth's mantle, and in combination with Al as aluminosilicate minerals. In all cases, Si occurs in a tetrahedral coordination structure with oxygen atoms. Silica has four common polymorphs (Table 15.6), and all have low solubility (S) in water. The least soluble form, quartz ($S = 1.1 \times 10^{-4}$ M or 6.6 mg/L as SiO_2 at 25°C), is about 5% as soluble as the most soluble form, amorphous silica. Although concentrations of silica usually are reported in mg/L of SiO_2, it occurs in water as the hydrated species $Si(OH)_{4(aq)}$. Quartz, the most common mineral in continental crust, exists in many varieties: agate, amethyst, milky quartz, chalcedony, and many others, including colored, translucent, and transparent forms that result from trace impurities and variations in microcrystalline structure. Silica reactions are important in many geochemical processes—from high temperature water-rock reactions deep in the Earth's crust to low temperature weathering processes in soils and near-surface rocks. Silica is significant in natural waters as a biogenic element

Table 15.6 Thermodynamic data for silica forms

Species	G_f° (kJ/mol)	Log K^*	Log $K(T)^*$
Quartz	−855.86	−3.958	$1.881 - 2.028 \times 10^{-3}T - 1560/T$
α-Cristobalite	−855.06	−3.348	$-0.0321 - 988.2/T$
β-Cristobalite	—	−2.919	$-0.2560 - 793.6/T$
Amorphous silica	−849.92	−2.716	$0.338 - 7.889 \times 10^{-4}T - 840.1/T$
$Si(OH)_{4(aq)}$	−1315.45		

* For the reaction $SiO_{2(s)} + H_2O \rightleftharpoons Si(OH)_{4(aq)}$; K is equivalent to the molar solubility of the mineral. Data from Rimstidt and Barnes.[31]

(essential for diatoms), and it causes problems (e.g., pitting of turbine blades) in industrial situations.

Except for the dissolved gases O_2 and N_2, silica is usually the most abundant nonelectrolyte in natural waters. Concentrations in fresh and saline waters vary from < 1 mg/L to tens of mg/L (see Tables 2.3 and 2.6). Dissolved silica is not very reactive chemically, but some algae (in freshwaters, primarily diatoms) require silica for their cell walls, called frustules. Diatom blooms can deplete water of silica, limiting further growth of these algae. If this occurs before nitrogen and phosphorus are depleted, growth of undesirable cyanobacteria (often called blue-green algae, although they are prokaryotic bacteria rather than eukaryotic cells) may be stimulated. Concentrations of dissolved silica usually are much lower than allowed by the solubility of $SiO_{2(am)}$ but may exceed the solubility of quartz. In general, there is little relationship between observed and equilibrium concentrations for any of the silica polymorphs because the kinetics of silica dissolution/precipitation at ambient temperatures is quite slow, especially for the crystalline forms. In fact, the main source of silica in natural waters is weathering of aluminosilicate minerals and the dissolution of "biogenic silica" (primarily silica from diatom frustules).

15.4.2 Silica equilibrium chemistry

Solid silica-water reactions are simple examples of mineral dissolution and precipitation reactions. The reactions are hydration/dehydrations:

$$SiO_{2(s)} + 2H_2O \rightleftharpoons Si(OH)_{4(aq)} \tag{15.13}$$
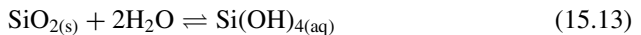
The equilibrium constant for Eq. 15.13 is $K = \{Si(OH)_{4(aq)}\}/\{SiO_{2(s)}\}\{H_2O\}^2$. In dilute solutions at ambient temperatures, the activities of silica and water and the activity coefficient of $Si(OH)_{4(aq)}$ are unity. K thus is equal to the molar solubility of silica. Over the range of temperatures at which silica-water reactions have been studied (0–300°C), solubility varies widely. High concentrations are possible under geothermal conditions. At 250°C quartz solubility is $10^{-2.16}$ M (415 mg/L as SiO_2), that is, 63 times that at 25°C. Similarly, the solubility of amorphous silica at 250 °C is $10^{-1.68}$ M (1253 mg/L), almost 11 times that at 25°C ($10^{-2.716}$ M or 115 mg/L).

Over the pH range of most natural waters, $Si(OH)_4$ is undissociated, but dissolved silica is a weak acid: $pK_{a1} = 9.84$ (see Table 8.2). Under alkaline conditions some dissolved silica thus exists as the acid anion $SiO(OH)_3^-$. The value for pK_{a2} (13.17) is sufficiently high that more highly charged silica species are not important in natural waters. Polynuclear species like $Si_4O_6(OH)_6^{2-}$ occur at high pH, as defined by the following relationship:[4]

$$4Si(OH)_{4(aq)} = Si_4O_6(OH)_6^{2-} + 2H^+ + 4H_2O, \quad \log K = -12.57 \tag{15.14}$$
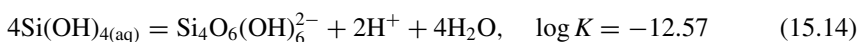
The dissociation of silica enhances its solubility at high pH (Figure 15.13). There is some uncertainty about the kinds and exact importance of multinuclear Si species like that defined by Eq. 15.14, but according to Stumm and Morgan,[4] there is no doubt about their existence.
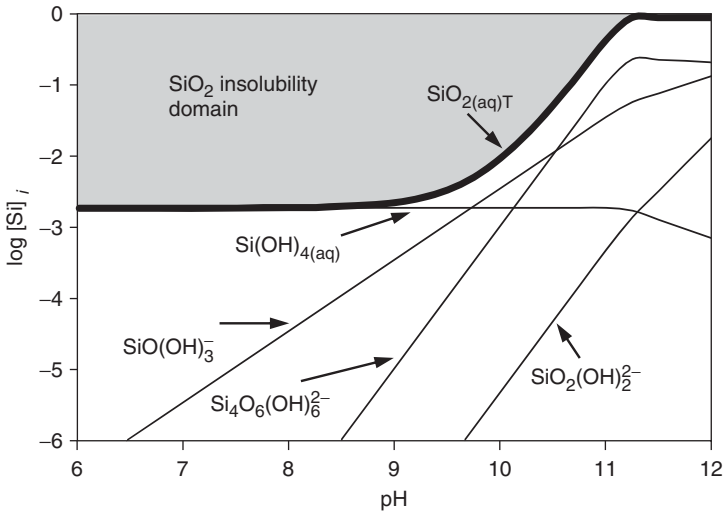
Figure 15.13 Solubility of silica in water over the pH range of 6–12. Calculated by MINEQL+ with Eq. 15.14 added to the thermodynamic database.

15.4.3 Kinetics of silica-water reaction

Reversible first-order rate equations can be used to develop a rate expression for the dissolution and precipitation of silica in water.[31] The reactions are pH independent at circumneutral pH, and the change in $[Si(OH)_4]$ over time is the difference between the dissolution and precipitation:

$$\mathbf{R} = -\frac{d[Si(OH)_4]}{dt} = (A/V)\{k_d - k_p[Si(OH)_4]\} \tag{15.15}$$

where A = surface area of silica in the system and V = volume of water; A/V is called the extent of the system. The rate of dissolution of solid silica is assumed to be equal to the rate constant for dissolution (k_d) times the surface area of silica (A); the rate of precipitation is assumed to be first order in dissolved silica. Equation 15.15 implies that precipitation and dissolution occur simultaneously. Dissolution thus occurs even in supersaturated solutions but is less rapid than precipitation. Because $K = k_d/k_p$ for reaction 15.13, we can rewrite the above equation as

$$-\frac{d[Si(OH)_4]}{dt} = \frac{A}{V}k_d\left(1 - \frac{[Si(OH)_4]}{K}\right) = \frac{A}{V}k_d(1 - S), \tag{15.16}$$

where $S = [Si(OH)_4]/K$ is the degree of saturation. If we divide both sides of Eq. 15.16 by K, we get

$$-\frac{dS}{dt} = \frac{A}{V}k_p(1 - S) \tag{15.17}$$

Table 15.7 Kinetic constants for silica-water reactions*

	Log k_d	Log $k_p(T)$	E_{act}
Quartz	−13.38	$1.174 - 2.028 \times 10^{-3}T - 4158/T$	71.9
α-Cristobalite	−12.77	$-0.739 - 3586/T$	68.6
β-Cristobalite	−12.35	$-0.963 - 3586/T$	64.8
Amorphous silica	−11.99	$-0.369 - 2.89 \times 10^{-4}T - 3438/T$	62.7
	Log k_p	Log $k_p(T)$	E_{act}
All phases	−9.43	$-0.707 - 2598/T$	49.7

* k_d and k_p in s^{-1}; E_{act} in kJ/mol. From Rimstidt and Barnes.[31]

because we defined $[Si(OH)_4]/K$ to be S, and $k_d/K = k_p$. This equation can be integrated to

$$\ln\left(\frac{1 - S}{1 - S_0}\right) = -k_p t \tag{15.18}$$

If $S_0 = 0$; that is, $[Si(OH)_4]_0 = 0$, Eq. 15.18 simplifies to

$$\ln(1 - S) = -k_p t. \tag{15.19}$$

Therefore, plots of $\ln((1 - S)/(1 - S_0))$ or $\ln(1 - S)$ versus time should yield a straight line with slope of k_p, and this relationship should hold whether the starting solution is supersaturated or undersaturated! Under the latter conditions, Rimstidt and Barnes[31] observed an initial steep slope that was interpreted as evidence for a surface layer of higher solubility, which dissolved more rapidly than bulk quartz. In terms of solubility and dissolution kinetics the layer behaved like amorphous silica.

Rimstidt and Barnes[31] also found that k_p was the same for quartz and amorphous silica; that is, the rate of precipitation of dissolved silica is independent of the nature of the precipitating phase (Table 15.7). From the law of microscopic reversibility and $K = k_d/k_p$, it is apparent that k_d is proportional to K and thus to the solubility of the solid phase. This implies that E_{act} for dissolution *decreases* with increasing solubility of the solid phase. The values of k_d and E_{act} in Table 15.7 agree with these statements. Rates of silica dissolution and precipitation are very slow below 100°C (10^{-13}–10^{-12} s^{-1} at 25°C) but higher by up to 10^3 under geothermal conditions. For example, at A/V = 100, a solution would reach equilibrium in < 15 h at 300°C, but it would need almost 6 years at 25°C. The relatively high E_{act} values for silica dissolution/precipitation indicate that the rate-limiting step is a chemical reaction (breakage of a covalent Si–O bond)[32] rather than physical diffusion of reactants or products.

15.5 Aluminosilicate minerals and weathering reactions

Aluminosilicate minerals are complicated structurally and chemically, and the kinetics of their dissolution (weathering) is correspondingly complex. This section provides an introduction to the topic; more detailed treatments are available elsewhere.[1,4,33−37]

15.5.1 Classification and structures

An amazing diversity of structures exists among the silicate and aluminosilicate minerals. Nonetheless, all the structures are based on the same fundamental "unit cells" shown in Figure 15.14a: tetrahedral silicon oxide and octahedral aluminum oxide units. (Some substitution of other metal ions may occur in both the tetrahedral and octahedral cells.) The diversity of structures reflects the variety of ways in which the units are linked together—in particular, the number of oxygen atoms in a unit cell that are shared with other cells. For silicates, there are five main types of linkages (Table 15.8 and Figure 15.14b), ranging from isolated tetrahedra with no oxygen sharing (called *nesosilicates*) to a continuous three-dimensional framework of tetrahedra in which all four oxygens are shared (called *tectosilicates*). Although all five types are important in geology and common in the Earth's crust, two types, the tectosilicates and phyllosilicates, are especially important for the chemistry of natural waters. The tectosilicates are the most abundant silicates (and aluminosilicates) in rocks and the most common primary minerals subject to weathering in catchments. They include various quartz minerals and their polymorphs and the aluminosilicate feldspars. Other types of primary mineral silicates, including olivine, amphiboles such as hornblende, phyllosilicates such as the magnesium silicates, talc and serpentine, and micas such as biotite and muscovite are important sources of iron and manganese, and as a group these so-called mafic minerals are common in basalts and gabbro. The phyllosilicate group also includes the very important secondary minerals, aluminosilicate clays.

The feldspars are divided into two overlapping classes (Figure 15.15): alkali feldspars and plagioclase. The latter include sodium feldspar (albite) and calcium feldspar (anorthite), but as the figure shows, these end members form a complete range of mixtures. In contrast, there is little interchange between Na and K feldspars. Feldspars constitute slightly more than half of the minerals in granitic rocks and slightly less than half the minerals in basalt. They are formed at high temperature and pressure deep in the
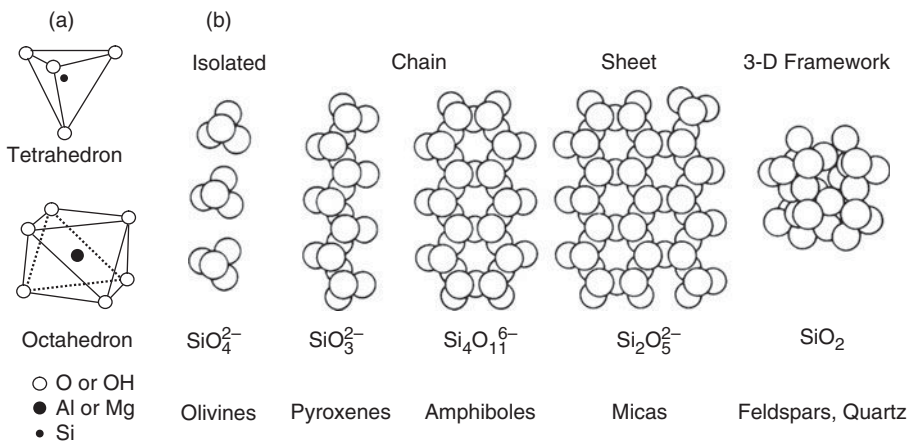
Figure 15.14 (a) Tetrahedral structure of Si units in silicates and octahedral structure of Al and Mg units. (b) Principal silicate structures in soil and rock minerals. Part (b) from Sposito[38].

Table 15.8 Major categories of silicate and aluminosilicate structures

Type of linkages of the Si-O tetrahedra	Examples
Nesosilicates (Gr. *nesos*, island): no shared oxygens; *isolated* SiO_4 tetrahedra held together by cations like Mg^{2+}	**Olivine**: Mg_2SiO_4; Fe_2SiO_4 (garnets, zircon, topaz)
Cyclosilicates (Gr. *kyklos*, circle or ring): separate *rings* of 3, 4, or 6 tetrahedra formed by sharing two oxygen atoms	**Beryl**: $Al_2Be_3Si_6O_{18}$ (emeralds, tourmaline)
Inosilicates (Gr. *inos*, thread): single (*s*) or double (*d*) *chains* of tetrahedra formed by sharing two oxygen atoms	**Pyroxene** (*s*): $CaMgSi_2O_6$ (diopside) **Amphiboles** (*d*): $NaCa_2Mg_5Fe_2Al\text{-}Si_7O_{22}(OH)$ (hornblende)
Phyllosilicates (Gr. *phyllon*, leaf): continuous *sheets* in a hexagonal network formed by sharing three oxygen atoms	**Talc**: $Mg_3Si_4O_{10}(OH)_2$ **Serpentine**: $Mg_3Si_2O_6(OH)_4$ **Clay minerals**: e.g., $Al_2Si_2O_5(OH)_4$ (kaolinite) **Micas**: e.g., biotite, $K(Mg,Fe)_3AlSi_3O_{10}(F,OH)_2$, muscovite, $K_2[Al_2Si_6]Al_4O_{20}(OH)_4$
Tectosilicates (Gr. *tekton*, builder): continuous *3-D framework* of tetrahedral formed by sharing all four oxygen atoms	**Quartz**: SiO_2 **Feldspars**: orthoclase, $KAlSi_3O_8$; albite, $NaAlSi_3O_8$; anorthite, $CaAl_2Si_2O_8$
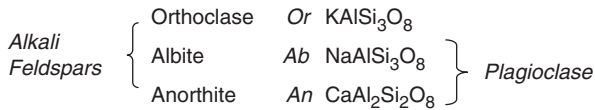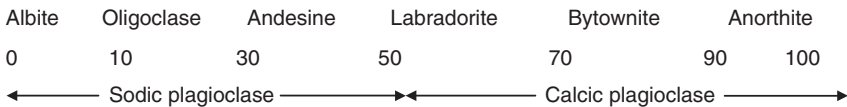
Figure 15.15 Classification of the feldspar minerals.

Earth's crust and tend to decompose (weather) when exposed to water and acids under ambient conditions.

Clay minerals are formed from feldspars by the complicated process of weathering, and they degrade by further weathering, ultimately releasing cations, dissolved silica and aluminum ions to solution. Because of the low solubility of aluminum, most of it winds up as solid gibbsite (aluminum oxide). Clays are layered structures consisting of tetrahedral silica sheets and octahedral gibbsite (aluminum oxide) or brucite (magnesium hydroxide) sheets. The silica tetrahedra are connected in an open hexagonal pattern, and the octahedra of the gibbsite or brucite layer lie sideways in a closest packed arrangement

Table 15.9 Main types of clay minerals*

Structure	Characteristics	Examples
Two-layer (T-O)[†]	Little isomorphous substitution; small cation exchange capacity (CEC); nonexpanding	Kaolinite Halloysite
Three-layer (T-O-T) Expanding (*smectites*)	Some Al substitution for Si in T-sheet; Mg, Fe, Zn, or Li for Al or Mg in O-sheet; large CEC; swell in water	Montmorillinite Vermiculite
Three-layer (T-O-T) Nonexpanding (*Illites*)	One-fourth of Si replaced by Al in T-sheet; similar O-sheet substitutions; small CEC	Micas (biotite, muscovite)

* Chlorites, three-layer aluminosilicates (T-O-T) with alternating octahedral brucite and gibbsite layers, sometimes are grouped with the clay minerals. They are nonswelling materials with low CEC.
[†]T = tetrahedral; O = octahedral

(a)

Tetrahedral (Si) layer

Octahedral (Al or Mg) layer

(b)

1 : 1 LAYER

Al, Mg

Si

2 : 1 LAYER

Si

Al

Si
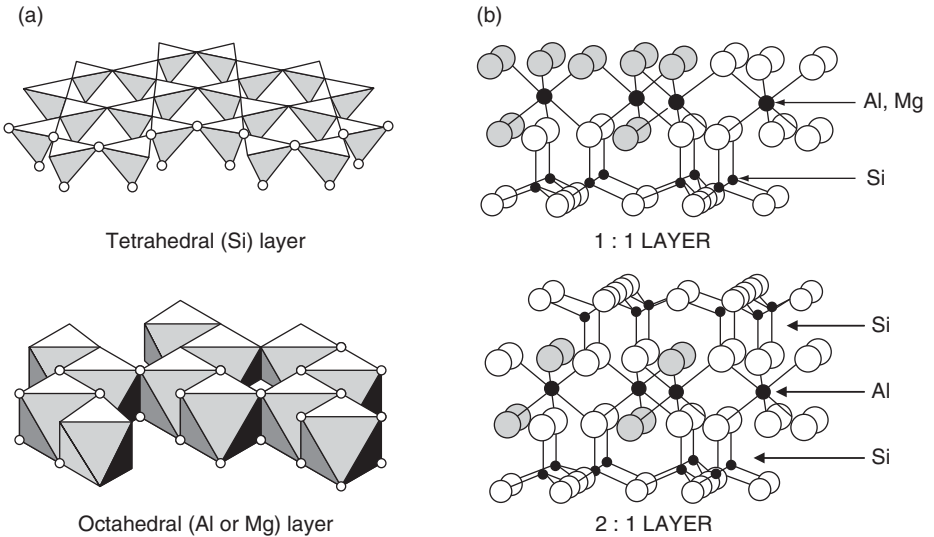
Figure 15.16 (a) Open hexagonal pattern of silica tetrahedral layer in clays and close-packed pattern of octahedral Al layer; (b) structures of 1:1 and 2:1 layer clays showing the sharing of oxygen atoms (open spheres) between the tetrahedral and octahedral layers. Modified from Sposito[38].

(see Figure 15.16). As indicated in Table 15.9, the sheets are stacked in two-layer units (T-O) or three-layer units (T-O-T), and the oxygen atoms at the vertices of the silica tetrahedra (T) are also part of the octahedral (O) layer.[22] There are three main categories of clays (Table 15.9 and Figure 15.16): two-layer, expanding three-layer, and nonexpanding three-layer clays. As summarized in Table 15.9, the three categories have very different properties.

The stabilities of aluminosilicates vary widely. Jackson et al.[39] ranked common minerals in order of their reactivity and proposed a weathering sequence: hornblende > Ca-feldspar > K-feldspar > Na-feldspar > montmorillinite > mica > kaolinite. In general, more stable (less soluble) minerals weather more slowly,[40] another example where thermodynamic and kinetic trends are in agreement.

15.5.2 Aluminosilicate phase equilibria

The solubility of silicate and aluminosilicate minerals in water is complicated by at least four factors. First, the reactions are slow, such that equilibrium is seldom reached in aquatic systems. Second, the rates and equilibria depend in complicated ways on various solution conditions. Third, the dissolution processes typically are incongruent, meaning that other solid phases may be formed as products. Finally, because of the first three factors, reliable equilibrium constants are not available for many of the minerals. Consequently, most work in recent decades on the behavior of silicates and aluminosilicates in aquatic systems has focused on rates and mechanisms of their weathering reactions rather than on equilibrium conditions, and that is our focus in the remainder of this chapter.*

15.5.3 Weathering processes

Weathering often is portrayed as a heterogeneous acid-base reaction in which dissolved acids react with basic mineral phases. The acids may be strong mineral acids (from acid rain), $H_2CO_3^*$, or natural organic acids. The products are dissolved base cations, bicarbonate and silica, and secondary aluminosilicates (clays). A typical weathering reaction involving a common feldspar is

$$2NaAlSi_3O_8 + 11H_2O + CO_2 \rightarrow 2Na^+ + HCO_3^- + 4Si(OH)_4 + Al_2Si_2O_5(OH)_4.$$

albite   kaolinite

$$(15.20)$$
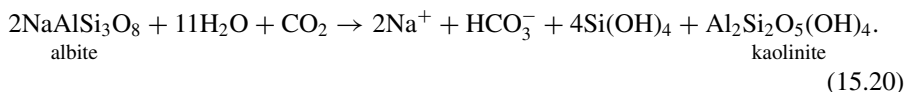
Weathering is a major process in alkalinity generation and the neutralization of acid rain in terrestrial environments, and the uncertainties in determining weathering rates has been an important issue relative to the calculation of critical loads (i.e., maximum acceptable levels) of acid deposition.[41] Aluminosilicate weathering also is a major source of alkalinity and cations in natural waters (see Chapter 2), accounting for 87% of the K^+ and 54% of the Mg^{2+} in global-average river water and smaller but still important fractions of Na^+ (22%) and Ca^{2+} (18%; see Table 2.9).

Aluminosilicate dissolution is difficult to study for many reasons. First, rates are slow at neutral pH and ambient temperatures. Second, rates depend greatly on a variety of solution conditions, especially pH and concentrations of organic ligands that attack reactive sites on mineral surfaces. Third, mineral conditions, including particle size and presence of organic surface coatings affect rates. Finally, the products may change over time—i.e., the reactions do not follow a simple stoichiometry. In addition,

*Examples of how the equilibrium concepts we used earlier to produce solubility diagrams for Fe and Al (hydr)oxides are applied to more complicated aluminosilicate minerals can be found in Stumm and Morgan.[22]

rates depend on the extent to which weatherable mineral surfaces are exposed to so-called "aggressive water," i.e., water with attacking ligands or low pH. This means that flow paths of water through soils are important factors in affecting rates of weathering and export of weathered cations from watersheds. Laboratory experiments on aluminosilicate weathering may be conducted at elevated temperatures to accelerate rates, but greatly elevated temperatures are not necessary. Mechanisms and even the qualitative aspects of weathering do not change greatly in the range 0–50°C.[40] However, uncertainties in measuring E_{act} limit the temperature range over which one can extrapolate rates accurately. Low pH has been used to accelerate dissolution, but unless enough measurements are made to define the typically nonlinear relationship between rate and pH, experiments at low pH are not useful to predict rates at near-neutral pH. The lack of consistent stoichiometry poses problems in understanding aluminosilicate weathering. Many aluminosilicates consist of several layers with structure-forming metal centers (e.g., Al, Si, Fe, Mg) that occur in both octahedral and tetrahedral bonding arrangements. The ease of removing metal ions from the lattice depends on their structural environments.

As the albite reaction (Eq. 15.20) indicates, aluminosilicate weathering involves formation of a second aluminosilicate phase, a clay mineral. The overall reaction actually is the sum of two separate steps: (1) dissolution of albite to form soluble products and (possibly) a disordered solid residue on the mineral surface, and (2) formation of a new mineral phase from some soluble products (and possibly the solid residue). The second step is slow relative to the first, and when weathering reactions are studied in the laboratory, clay minerals are not formed. However, formation of other secondary solid phases may occur in laboratory studies by precipitation of amorphous Al (or Fe) hydroxides or formation of residual solid phases on the mineral surface as partial dissolution of the mineral proceeds. Both processes complicate the interpretation of rate data.

15.5.4 Rate expressions

Many studies (e.g., Aagaard and Helgeson[34] and Berner et al.[42]) have found that aluminosilicate dissolution exhibits parabolic time dependency—i.e., arithmetic plots of amount of silica or cations solubilized versus time are parabolic (or linear in $t^{\frac{1}{2}}$). Mechanistic interpretation of this behavior has been controversial and is still not completely resolved. Parabolic time dependency usually is interpreted as indicating that a process is diffusion limited. Weathering reactions are much too slow for diffusion of reactants to be rate-limiting, but two-stage models fitting parabolic kinetics have been proposed in which initial diffusion of soluble products through a surface layer is rate limiting.[43] The initial stage, which involves incongruent dissolution and the development of a "leached surface layer," is followed by a slower steady-state congruent dissolution stage in which the rate-limiting step is surface-controlled detachment of the central metal ion. An alternative model[35] involves the formation of an "armored precipitate layer," that is, a metal hydroxide such as amorphous $Al(OH)_{3(s)}$, on the mineral surface when the metal's solubility is exceeded by release from the dissolving mineral. A third interpretation[43] is that slower chemical weathering reactions control release rates only after an initial rapid release by ion exchange processes.

Original albite surface

Si   15 Å

28 Å

Si + Al

Fresh albite

Si

Si + Al + Na

Si
+
Al

Si
+
Al

5 Å

20 Å

33 Å
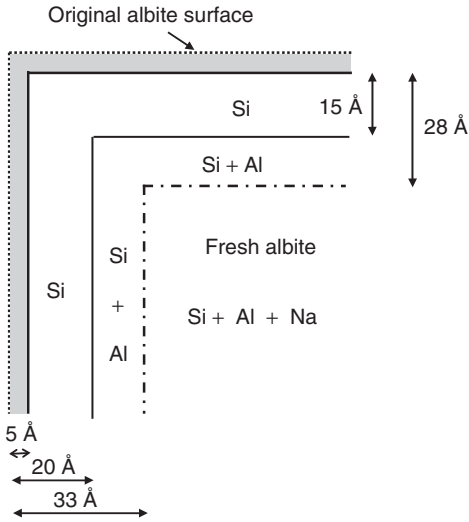
Figure 15.17 Representation of weathering on an albite surface after 500 h of reaction (255 h at pH 5.1 and 245 h at pH 3.1). Shaded area represents the layer in which all components dissolved, and the solid line represents the new surface. Enough additional Na and Al dissolved to yield 15 Å layer with only Si (and O) left. Additional Na leached further within the albite to yield a cation-depleted layer 13 Å thick. Redrawn from Chou and Wollast,[45] © 1984, and used with permission of Elsevier.

In contrast, Berner et al.[42] concluded that parabolic kinetics is an artifact of grinding done on mineral samples to obtain a uniform particle size before experiments are conducted. Berner et al. contended that grinding disrupts grain surfaces and produces ultrafine particles that dissolve more quickly than larger particles with smooth surfaces. The net effect is that the rate of dissolution decreases with time, yielding a parabolic plot. In support of this argument, linear (zero-order) dissolution rates were found when particles were rigorously cleaned to remove fines and treated to remove disrupted surfaces. Additional studies using x-ray spectroscopy failed to detect the presence of a cation-depleted layer thick enough to account for diffusion limitation.[44] Nevertheless, later studies by others[45] found evidence for an initial cation-leaching stage in albite dissolution experiments designed to avoid artifacts from grinding and secondary precipitation; parabolic kinetics was induced repetitively just by changing the pH in a reactor where dissolved product concentrations were kept below saturation. The results were explained by a model in which incongruent weathering released soluble cations and some Si and Al, leaving a residual (secondary mineral) layer on the weathered surface. The thicknesses of the layers from which components were released were calculated by mass balance from the amounts of Al, Si, and Na released to solution, the surface area available for dissolution and molar volume of albite (Figure 15.17).

15.5.5 Mechanisms of surface-controlled aluminosilicate dissolution

Aluminosilicates do not weather by spontaneous breakdown of lattice constituents to dissolved species. Instead, surface acid-base and coordination reactions, like those described earlier for the reductive dissolution of Fe and Mn (hydr)oxides, play key roles.[4] These reactions occur preferentially at surface sites with excess free energy, i.e., crystal defects, kinks, and etch pits (see Section 10.10.3). H^+-promoted dissolution is a

two-step process:

Fast

$$\equiv| -OH +H^+ \rightarrow \equiv| -OH_2^+ \qquad (15.21a)$$

Slow

$$\equiv| -OH_2^+ \rightarrow Me(H_2O)^+ + \equiv| - \qquad (15.21b)$$
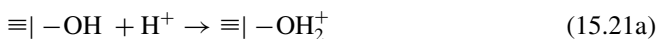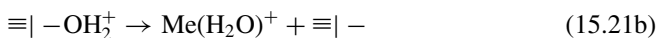
$\equiv|-OH$ is a reactive site on a hydrous metal oxide or aluminosilicate with a functional OH group, and Me is a central metal ion (Al, Si, Fe, Mn). In the first step, H^+ from the solution protonates a surface $-OH$ group, weakening the $Me-O$ bonds that hold the metal ion in the mineral lattice and promoting detachment of an activated coordination complex. The detachment process renews the surface for further attack and dissolution. Figure 15.18 shows how reaction sequence 15.21 applies to an aluminum oxide surface.

More than one H^+ must be added to reacting sites to weaken lattice bonds sufficiently for detachment to occur. Dissolution rates are thought to be proportional to the degree of surface protonation to the z power, where z is the valence of Me, $\mathbf{R}_{dis} \propto [\equiv| - OH_2^+]^z$. Surface protonation can be viewed as an adsorption reaction. At very low pH in the bulk solution (high $\{H^+\}$), the surface may become saturated with H^+, and the rate may be independent of pH. At intermediate pH values, protonation is described by the Freundlich isotherm:

$$\log[\equiv| - OH_2^+] = n \ \log \{H^+\} + \log K_{ads}, \qquad (15.22)$$

where n is the slope of the isotherm and K_{ads} (the y-intercept) is the adsorption equilibrium constant. Over the pH range where Eq. 15.22 applies, the dissolution rate depends on the bulk solution $\{H^+\}$ in the following way: $\mathbf{R}_{dis} \propto \{H^+\}^m$, where m = nz. Stumm et al.[46] found that m = 0.4, n = 0.13, and z = 3.1 for dissolution of aluminum oxide, and Schnoor[43] found m = 0.5 for a soil sample containing 25% albite, 5% orthoclase, and 10% mica. Surface-controlled mineral dissolution by H^+ attack thus leads to fractional order dependence of the rate on solution $\{H^+\}$.

Mineral dissolution by ligand attack occurs by a similar mechanism:

Fast

$$\equiv| -OH + HA \rightarrow \equiv| -A + H_2O \qquad (15.23a)$$

Slow

$$\equiv| -A \rightarrow \equiv| - + M(A)^{(z-1)+} \qquad (15.23b)$$
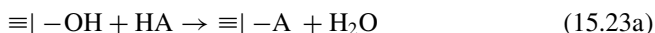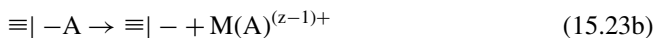
The strength of complex formation by HA affects the rate of dissolution, and rates are proportional to the concentration of the ligand in solution. Based on our knowledge of factors affecting the strength of complex formation by bidentate ligands (see Section 9.3.2), we predict that ligands forming five- and six-membered rings, such as oxalate, malonate, and salicylate, are more effective in promoting dissolution than are ligands forming seven-membered rings. In addition, monodentate ligands such as
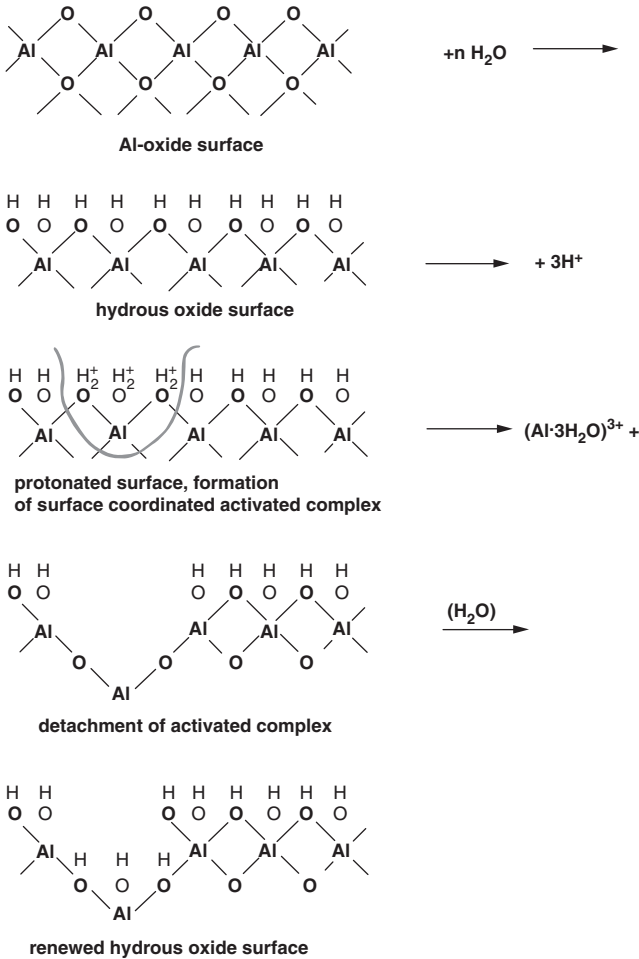
Figure 15.18 Schematic of an aluminum oxide surface undergoing dissolution by protonation and hydrolysis. Dissolution occurs when an Al center becomes sufficiently protonated to release $(Al \cdot 3H_2O)^{3+}$. From Schnoor,[43] © John Wiley and Sons, and used with permission.

benzoate that form weak complexes should be much less effective. These trends were found to apply to dissolution of δ-Al_2O_3.[47] If binding of the ligand on the surface follows an adsorption isotherm, the dissolution rate may be fractional order in [HA], and if the pK_a of HA is in the pH range of interest for dissolution, the concentration of HA will be depend on pH at fixed total ligand concentration.

Overall, the mechanisms of H^+- and ligand-promoted dissolution lead to a two-term rate expression:

$$\mathbf{R}_{dis} = k_{H^+}\{H^+\}^m + k_{HA}[HA^-]^{m'} \tag{15.24}$$

At low pH, H^+ attack predominates, and at high pH, ligand attack predominates if ligands that promote dissolution are present. Under such conditions, dissolution becomes pH-independent if [HA] is not pH dependent. The pH where the change occurs varies among minerals and depends on the nature and concentration of the ligand(s). For example, dissolution of orthoclase (potassium feldspar) is H^+ dependent below pH 5 and pH independent in the range 5–10.[34] Plots of $\mathbf{R}_{dis}$ versus pH can have complicated shapes, depending on the soluble product being measured, as shown for the dissolution of kaolinite (Figure 15.19). The difference between the release rates for Si and Al indicates that dissolution is not stoichiometric for reaction times of 10–15 days. However, when a dissolution-promoting ligand (oxalate) was added, dissolution rates increased at a given pH, and release rates were the same for both elements.

The effects of P_{CO_2} on weathering rates is a potentially important issue relative to global climate change because of the importance of silicate weathering on the global carbon budget. Stephens[48] concluded that P_{CO_2} had no direct influence on weathering rates of volcanic ash soils at Mammoth Mountain, California, under conditions of low pH, but it had indirect effects by changing the pH and concentrations of organic acids in the soil solution. In contrast, Navarre-Sitchler and Thyne[49] used catchment mass balances on drainage water from a series of Sierra Nevada canyons with differing levels of P_{CO_2} in their source (spring) waters, and they found a fractional-order dependency
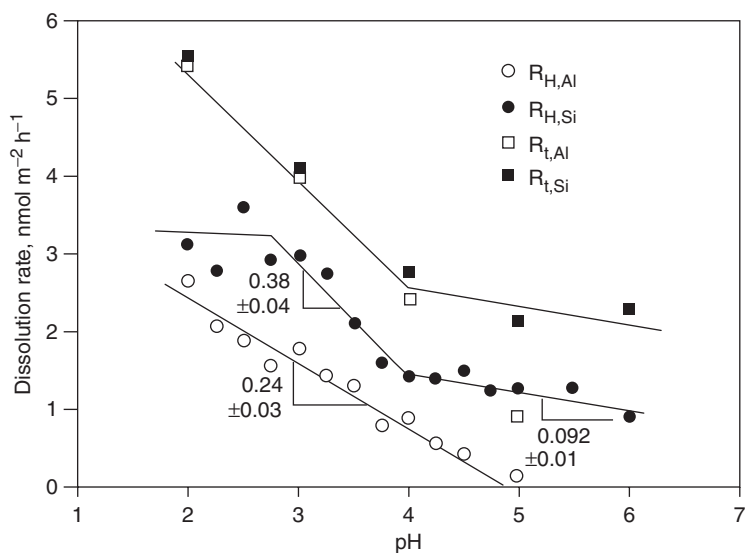
Figure 15.19 Kaolinite dissolution rates depend on the product being measured (the reaction is not stoichiometric). Si release is higher than Al release over laboratory experiments of 10–15 days. Data points with subscript H are for solutions in which only H^+ is involved in promoting dissolution; those with subscript t include effects of oxalate in addition to H^+. From Stumm and Wieland,[36] © John Wiley and Sons, and used with permission.

(rate $\propto P_{CO_2}^{0.45}$) for plagioclase weathering. It should be noted that P_{CO_2} values can be much higher in soils ($10\times$ to $100\times$) than the ambient atmosphere.

15.5.6 Comparison of field and laboratory weathering rates

Dissolution rates can be measured reliably in laboratory experiments (Table 15.10). Such studies have greatly enhanced our understanding of the mechanisms of aluminosilicate weathering. Reliable catchment-scale measurements of aluminosilicate weathering also have been made for a variety of natural systems (Table 15.10) using mass balance measurements of annual fluxes of cations and/or silica in streams draining catchments with uniform geological composition. Inputs of major cations from atmospheric deposition are subtracted from mass export rates, which are determined as the product of hydrologic outflow and cation concentrations in the outflow. Cation contributions from human activities (e.g., fertilizer) and losses due to changes in biomass may need to be

Table 15.10 Comparison of field and laboratory weathering rates[*]

Mineral or watershed	Weathering rate				
	$mol\ Si$ $m^{-2}y^{-1}$	$mol\ M^{n+}$ $m^{-2}y^{-1}$	Cation measured	Reference	Comments
Laboratory studies					
Albite	1.6E-4	8.0E-4	Na^+	50	25°C, pH 4, $P_{CO_2} = 1$ atm
Oligoclase	1.6E-4	5.3E-5	Na^+	50	25°C, pH 4, $P_{CO_2} = 1$ atm
Anorthite		1.0E-5	Na^+	50	25°C, pH 4, $P_{CO_2} = 1$ atm
Orthoclase		2.1E-5	Na^+	50	25°C, pH 4, $P_{CO_2} = 1$ atm
Muscovite	8.0E-6			51	
Gibbsite		8.1E-5	Al^{3+}	52	pH 3.2, 25°C
Kaolinite	1.1E-5	1.1E-6	Al^{3+}	53	pH 5
	1.2E-5	7.9E-6	Al^{3+}	36	pH 4
Field (watershed) studies					
Bear Crk., Maine	2.8E-7			43	Plagioclase, biotite, hornblende
Filson Crk., Minn.	1.6E-7			53	Plagioclase, biotite, hornblende
Cristallina, Switzerland	1.9E-6			54	Plagioclase, biotite, hornblende
Trnavka R., Czk.					
Forested catchment		2.8E-7	Na^+	55	Oligoclase
Agricultural catchment		1.3E-6	Na^+	55	Oligoclase
Elbe R. basin					
In 1892		1.6E-7	Na^+	55	Oligoclase
In 1976		5.0E-7	Na^+	55	

[*] Recalculated from original literature based on a table in Brezonik.[1]

taken into account. Sampling must be frequent enough to capture short-term hydrologic events that may dominate the water and ion budgets.*

Unfortunately, a scale discontinuity problem has limited our ability to compare rates at the two scales. Extrapolation of laboratory measurements to the field scale is problematic because successful laboratory experiments generally are obtained by eliminating organic or oxide coatings and ensuring that water is present at nonlimiting rates. However, these complicating factors likely limit mineral weathering rates in watersheds. As a result, laboratory results are poor predictors of field rates,[52,53] and the former often are higher than the latter by factors of 10 to 10^3. Down-scaling of catchment-scale rates to the units used for laboratory rates (e.g., moles of cations solubilized per square meter of mineral surface per unit time) also is problematic, in part because of the difficulty in estimating the actual surface area of minerals exposed to water in a catchment. Other complicating factors in down-scaling field-based rates include (1) old minerals with smooth surfaces and few defects may dominate in field conditions, whereas fresh surfaces with more reactive kinks and edges may dominate in laboratory studies;[51] (2) NOM, Al (hydr)oxide, and amorphous aluminosilicate[56] coatings occur on mineral surfaces in natural systems but are absent in cleanly prepared laboratory samples; (3) high dissolved Al levels in soil-water may inhibit aluminosilicate dissolution;[41] and (4) unsaturated flow conditions and macropores, which provide a rapid pathway for percolating water in soils, tend to limit the exposure of weatherable minerals to water.

Weathering rates measured on European catchments having a high-sodium plagioclase (oligoclase) as the major mineral[51] were estimated to range from 1.6×10^{-7} to 1.3×10^{-6} mol m^{-2} y^{-1}, much lower than weathering rates measured on oligoclase in the laboratory (5.4×10^{-5} mol m^{-2} y^{-1}).[46] Similar discrepancies have been noted in other comparisons of laboratory and field weathering rates based on cation and silica export.[1,33,41] Laboratory-based rates generally are much higher than field-based rates. The differences are too large to be accounted for by differences in temperature or P_{CO_2} but may be explained by the factors described in the previous paragraph. Malmstrom et al.[59] found that the scale dependency of weathering rates could be explained by several empirically derived "scaling factors" from bulk-average physical-chemical data for temperature, pH, mineral content, hydrologic flow path, and particle size distribution. Small but consistent variations in these parameters were found across three observation scales (batch, large columns and field), but the general applicability of their scaling factors or even their approach seems not to have been evaluated.

Finally, a simple but useful way to view mineral weathering rates is that they are controlled either by hydrologic factors or by surface reaction kinetics. Support for this view is provided by a plot of areal export rates for dissolved silica versus the ratio of hydrologic flow rate to mass of soil (Figure 15.20). At flow rate:mass ratios less than

---

*One important limitation of the traditional catchment mass balance approach is that the number of ions for which export data are available is small, typically six (Al, Mg, Ca, Na, K, SiO$_2$). This limits the number of mass balance equations that can be written to solve for weathering rates of different minerals in a catchment using mineral stoichiometry and matrix algebra techniques.[56] Many catchments have a much greater diversity of weatherable mineral phases. Recent studies have overcome this problem by measuring a variety of trace metals found in minerals and measurable in catchment outflows; e.g., see Price et al.[57] for details on this approach and its limitations.
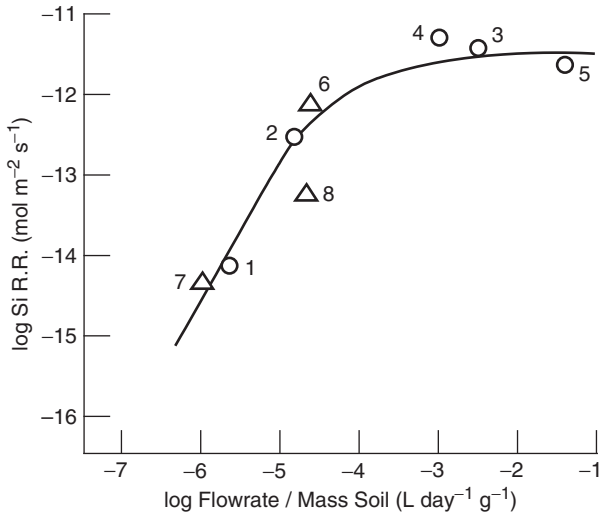
Figure 15.20 Weathering rate expressed in terms of dissolved Si release versus the logarithm of the hydrologic outflow rate from catchments normalized to the mass of soil. Triangles from laboratory studies; circles from field measurements. From Schnoor,[43] © John Wiley and Sons, and used with permission.

$\sim 10^{-4}$ L day^{-1} g^{-1}, the areal export rate for silica depends strongly on hydrologic flow rate, but at ratios above this critical value, export approaches a value between 10^{-12} and 10^{-11} mol m^{-2} s^{-1}. The critical ratio corresponds to a hydraulic flushing rate of approximately one volume of water per volume of soil per day. According to Schnoor,[43] this may represent a limit above which surface chemical reaction controls weathering rates and below which hydrologic control is dominant. Laboratory studies generally are conducted at flow rates above the critical value and thus yield rates corresponding to the asymptotic range. Variations in hydrologic conditions and uncertainties related to the area of water-exposed mineral surfaces in the field may cause field rates to be orders of magnitude lower than those measured in the laboratory.

References

1. Brezonik, P. L. 1994. *Chemical kinetics and process dynamics in aquatic systems*, CRC Press, Boca Raton, Fla.
2. Batarseh, E. S., D. R. Reinhart, and L. Daly. 2007. Liquid sodium ferrate and Fenton's reagent for treatment of mature landfill leachate. *J. Environ. Eng.* **113**: 1042–1050; Sharma, V. K. 2008. *Ferrates. Synthesis, properties and applications in water and wastewater treatment*, ACS Symp. Ser. **985**, Oxford Univ. Press, New York.
3. Klewicki, J. K., and J. J. Morgan. 1998. Kinetic behavior of Mn(III) complexes with pyrophosphate, EDTA, and citrate. *Environ. Sci. Technol.* **32**: 2916–2922.
4. Stumm, W., and J. J. Morgan. 1996. *Aquatic chemistry*, 3rd ed., Wiley-Interscience, New York.
5. Wehrli, B. 1990. Redox reactions of metal ions at mineral surfaces. In *Aquatic chemical kinetics*, W. Stumm (ed.), Wiley-Interscience, New York, 311–336.
6. Luther, G. W., III. 1990. The frontier-molecular orbital theory approach in geochemical processes. In *Aquatic chemical kinetics*, W. Stumm (ed.), Wiley-Interscience, New York, 173–198.
7. Stumm, W., and G. F. Lee. 1961. Oxygenation of ferrous iron. *Ind. Eng. Chem.* **53**: 143–146.

8. Sung, W., and J. J. Morgan. 1980. Kinetics and product of ferrous iron oxygenation in aquatic systems. *Environ. Sci. Technol.* **14**: 561–568.

9. Davison, W., and G. Seed. 1983. The kinetics of the oxidation of ferrous iron in synthetic and natural waters. *Geochim. Cosmochim. Acta* **47**: 67–79.

10. Theis, T. L., and P. C. Singer. 1974. Complexation of iron(II) by organic matter and its effect on iron(II) oxygenation. *Environ. Sci. Technol.* **8**: 569–573.

11. Pankow, J. F., and J. J. Morgan. 1981. Kinetics for the aquatic environment. *Environ. Sci. Technol.* **15**: 1155–1164.

12. Singer, P. C., and W. Stumm. 1970. Acidic mine drainage: the rate-determining step. *Science* **167**: 1121–1123.

13. Millero, F. J., S. Sotolongo, and M. Izaguirre. 1987. The oxidation kinetics of Fe(II) in seawater. *Geochim. Cosmochim. Acta* **51**: 793–801.

14. Emmenegger, L., D. W. King, L. Sigg, and B. Sulzberger. 1998. Oxidation kinetics of Fe(II) in a eutrophic Swiss lake. *Environ. Sci. Technol.* **32**: 2990–2996.

15. Millero, F. J. 1985. The effect of ionic interactions on the oxidation of metals in natural waters. *Geochim. Cosmochim. Acta* **49**: 547–553.

16. King, D. W. 1998. Role of carbonate speciation on the oxidation rate of Fe(II) in aquatic systems. *Environ. Sci. Technol.* **32**: 2997–3003.

17. Morgan, J. J. 1967. Chemical equilibria and kinetic properties of manganese in natural waters. In *Principles and applications of water chemistry*, S. D. Faust and J. V. Hunter (eds.), Wiley, New York, 561–622.

18. Kessick, M. A., and J. J. Morgan. 1975. Mechanism of manganese autoxidation in aqueous solution. *Environ. Sci. Technol.* **9**: 157–159.

19. Grill, E. V. 1982. Kinetic and thermodynamic factors controlling manganese concentrations in oceanic waters. *Geochim. Cosmochim. Acta* **46**: 2435–2446.

20. Davies, S. H. R., and J. J. Morgan. 1989. Manganese(II) oxidation kinetics on metal oxide surfaces. *J. Coll. Interface Sci.* **129**: 63–77.

21. Diem, D., and W. Stumm. 1984. Is dissolved Mn^{2+} being oxidized by O_2 in the absence of Mn-bacteria or surface catalysts? *Geochim. Cosmochim. Acta* **48**: 1571–1573.

22. Stumm, W., and J. J. Morgan. 1970. *Aquatic chemistry*, J. Wiley, New York.

23. Stone, A. T., and J. J. Morgan. 1988. Reductive dissolution of metal oxides. In *Aquatic surface chemistry*, W. Stumm (ed.), Wiley-Interscience, New York, 221–254.

24. Ehrlich, H. L. 1996. *Geomicrobiology*, 3rd ed., Marcel Dekker, New York; Ghiorse, W. 1986. In *Environmental microbiology of anaerobes*, A. J. B. Zehnder (ed.), Wiley-Interscience, New York, 305–331.

25. Arnold, R. G., T. M. Olson, and M. R. Hoffmann. 1986. Kinetics and mechanism of dissimilative Fe(III) reduction by *Pseudomonas* sp. 200. *Biotech. Bioeng.* **28**: 1657–1671.

26. Brezonik, P. L., J. G. Eaton, T. M. Frost, P. J. Garrison, T. K. Kratz, C. E. Mach, J. H. McCormick, J. A. Perry, W. A. Rose, C. J. Sampson, B. C. L. Shelley, W. A. Swenson, and K. E. Webster. 1993. Experimental acidification of Little Rock Lake, Wisconsin: chemical and biological changes over the pH range 6.1 to 4.7. *Canad. J. Fish. Aquat. Sci.* **50**: 1101–1121.

27. Brezonik, P. L., C. E. Mach, and C. J. Sampson. 2003. Geochemical controls for Al, Fe, Mn, Cd, Cu, Pb, and Zn during experimental acidification and recovery of Little Rock Lake, WI, USA. *Biogeochem.* **62**: 119–143.

28. Mach, C. E. 1992. The aquatic chemistry of aluminum, iron, manganese, cadmium, copper, lead, and zinc in an experimentally-acidified seepage lake. Ph.D. thesis, University of Minnesota, Minneapolis.

29. Fox, L. 1988. The solubility of colloidal ferric hydroxide and its relevance to iron concentrations in river water. *Geochim. Cosmochim. Acta* 52: 771–777.

30. Plankey, B. J., H. H. Patterson, and C. S. Cronan. 1986. Kinetics of aluminum fluoride complexation in acidic waters. *Environ. Sci. Technol.* **20**: 160–165.

31. Rimstidt, J. D., and H. L. Barnes. 1980. The kinetics of silica-water reactions. *Geochim. Cosmochim. Acta* **44**: 1683–1699.

32. Lasaga, A. C., and G. V. Gibbs. 1990. Ab initio quantum-mechanical calculations of surface reactions—a new era? In *Aquatic chemical kinetics*, W. Stumm (ed.), Wiley-Interscience, New York, 259–289.

33. Stumm, W. 1992. *Chemistry of the solid-water interface*, Wiley-Interscience, New York.

34. Aagaard, P., and H. C. Helgeson. 1982. Thermodynamic and kinetic constraints on reaction rates among minerals and aqueous solutions. I. Theoretical considerations. *Amer. J. Sci.* **282**: 237–285.

35. Helgeson, H. C., W. M. Murphy, and P. Aagaard. 1984. Thermodynamic and kinetic constraints on reaction rates among minerals and aqueous solutions. II. Rate constants, effective surface area, and hydrolysis of feldspars. *Geochim. Cosmochim. Acta* **48**: 2405–2432.

36. Stumm, W., and E. Wieland. 1990. Dissolution of oxide and silicate minerals: rates depend on surface speciation. In *Aquatic chemical kinetics*, W. Stumm (ed.), Wiley-Interscience, New York, 367–400.

37. White, A. F., and S. L. Brantley. 1995. Chemical weathering rates of silicate minerals; an overview. *Rev. Mineral. Geochem.* **31**: 1–22. (Note: the entire volume contains review articles on this topic.)

38. Sposito, G. 1989. *The chemistry of soils*, Oxford University Press, New York.

39. Jackson, M. L., S. A. Tyler, A. C. Willis, G. A. Burbeau, and R. P. Pennington. 1948. Weathering sequence of clay-size minerals in soils and sediments. I. Fundamental generalizations. *J. Phys. Colloid Chem.* **52**: 1237–1260.

40. Nesbitt, H. W., and G. M. Young. 1984. Prediction of some weathering trends of plutonic and volcanic rocks based on thermodynamic and kinetic considerations. *Geochim. Cosmochim. Acta* **48**: 1523–1534.

41. Langan, S. M. Hodson, D. Bain, M. Hornung, B. Reynolds, J. Hall, and L. Johnston. 2001. The role of mineral weathering rate determinations in generating uncertainties in the calculation of critical loads of acidity and their exceedance. *Water Air Soil Pollut. Focus* **1**: 299–312.

42. Berner, R. A., E. L. Sjoberg, M. A. Velbel, and M. D. Krom. 1980. Dissolution of pyroxenes and amphiboles during weathering. *Science* **207**: 1205–1206.

43. Schnoor, J. L. 1990. Kinetics of chemical weathering: a comparison of laboratory and field weathering rates. In *Aquatic chemical kinetics*, in W. Stumm (ed.), Wiley-Interscience, New York, 475–504.

44. Holdren, G. R., Jr., and R. A. Berner. 1979. Mechanism of feldspar weathering— I. Experimental studies. *Geochim. Cosmochim. Acta* **43**: 1161–1171.

45. Chou, L., and R. Wollast. 1984. Study of the weathering of albite at room temperature and pressure with a fluidized bed reactor. *Geochim. Cosmochim Acta* **48**: 2205–2217.

46. Stumm, W., G. Furrer, and B. Kunz. 1983. The role of surface coordination in precipitation (heterogeneous nucleation) and dissolution of mineral phases. *Croat. Chim. Acta* **56**: 593–611.

47. Furrer, G., and W. Stumm. 1986. The coordination chemistry of weathering: I. Dissolution kinetics of δ-Al_2O_3 and BeO. *Geochim. Cosmochim. Acta* **50**: 1847–1860.

48. Stephens, J. C. 2002. Response of soil mineral weathering to elevated carbon dioxide. Ph.D. thesis, California Institute of Technology, Pasadena.

49. Navarre-Sitchler, A., and G. Thyne. 2007. Effects of carbon dioxide on mineral weathering under earth surface conditions. *Chem. Geol.* **243**: 53–63.

50. Busenberg, E., and C. V. Clemency. 1976. The dissolution kinetics of feldspars at 25°C and 1 atm CO_2 partial pressure. *Geochim. Cosmochim Acta* **40**: 41–49.

51. Lin, F.-C., and C. V. Clemency. 1981. The kinetics of dissolution of muscovites at 25°C and 1 atm CO_2 partial pressure. *Geochim. Cosmochim. Acta* **45**: 571–576.

52. Bloom, P. R. 1983. Kinetics of gibbsite dissolution in nitric acid. *Soil Sci. Soc. Am. J.* **47**: 164–168.

53. Siegel, D. I., and H. O. Pfannkuch. 1984. Silicate dissolution influence on Filson Creek chemistry northeastern Minnesota. *Geol. Soc. Am. Bull*. **95**: 1446–1453.

54. Giovanoli, R., J. L. Schnoor, L. Sigg, W. Stumm, and J. Zobrist. 1989. Chemical weathering of crystalline rocks in the catchment area of acidic Ticino lakes, Switzerland. *Clays Clay Min*. **36**: 521–529.

55. Pačes, T. 1983. Rate constants of dissolution derived from the mass balance in hydrological catchments. *Geochim. Cosmochim. Acta* **47**: 1855–1863.

56. Bowser, C. J., and B. F. Jones. 2002. Mineralogic controls on the composition of natural waters dominated by silicate hydrolysis. *Amer. J. Sci.* **32**: 582–662.

57. Price, J. R., N. Heitman, J. Hull, and D. Szymanski. 2002. Long-term average mineral weathering rates from watershed geochemical mass balance methods: using mineral modal abundances to solve more equations in more unknowns. *Chem. Geol.* **254**: 36–51.

58. Nugent, M. A., S. L. Brantley, C. G. Pantano, and P. A. Maurice. 1998. The influence of natural mineral coatings on feldspar weathering. *Nature* **395**: 588–591.

59. Malmström, M. E., G. Destouni, S. A. Banwart, and B. H. E. Strömberg. 2000. Resolving the scale dependence of mineral weathering rates. *Environ. Sci. Technol.* **34**: 1375–1378.

16

Nutrient Cycles and the Chemistry of Nitrogen and Phosphorus

Objectives and scope

This chapter discusses the chemistry of the primary nutrient elements, nitrogen and phosphorus, in the context of their cycles in the environment. The concept of nutrient cycling is described, and examples of ways to portray nutrient cycles are presented at molecular, landscape, and global scales. Cycling of N and P in aquatic systems is linked through biotic stoichiometry—that is, the ratio of elements in organisms, which for N:P is ∼16:1 on an atom basis). Implications of this stoichiometry on N and P cycles and related useful relationships are described. Nutrients are beneficial insofar as biological production is desirable in ecosystems, but excess N and P concentrations cause water quality problems. Methods to remove them from wastewater and to control concentrations in aquatic systems (especially lakes) by chemical means are described. Some overarching factors complicating nutrient analysis and a summary of methods used for nutrient analyses conclude the chapter.

Key terms and concepts

- Molecular, organism, ecosystem, and landscape scales of nutrient cycles; seasonal nutrient cycles
- Ammonium and ammonia, nitrate, Kjeldahl N, TON, DON
- Denitrification, nitrification, nitrogen fixation, N assimilation
- Orthophosphate, SRP, condensed phosphates, inositol phosphate (IP)
- Phosphorus fractionation in sediments by sequential extractions
- Liebig's law, Redfield ratio

601

16.1 Introduction

16.1.1 Overview

Aside from carbon, oxygen, and hydrogen, organisms—both plants and animals—require approximately a dozen elements as "nutrients" to grow. These include N, P, S, Fe, Mn, Ca, Mg, K, and several heavy metals (Cu, Co, Zn, Mo, and a few others). The major ions are abundant in water relative to plant needs and are not limiting factors for plant growth in typical water bodies. Similarly, the heavy metals are needed only in trace amounts, and even though their concentrations are low in natural waters, their availability is not thought to limit plant growth in most natural waters. Iron is an exception and is limiting for plant growth in wide areas of the oceans. Nitrogen and phosphorus* often are referred to as "macronutrients" because they are needed in relatively large proportions compared with the other elements. The average C:N:P composition of algae is 106:16:1 by atoms or about 40:7:1 by weight, and N and P each constitute more than ~1% of algal biomass. Concentrations of these elements in water and soils generally are low—at least relative to the needs of plants for growth, and they are the nutrients that most commonly limit primary production—plant growth—in the natural environment. Nitrogen and phosphorus thus are of central importance in nutrient chemistry, and they are the focus of this chapter.

Given the close links between these elements and the biological processes of primary production and decomposition of organic matter in aquatic systems, it should come as no surprise that understanding of how these elements behave in aquatic systems requires more than knowledge of their molecular-level chemistry. The subject encompasses aspects of environmental microbiology, aquatic ecology, soil science, and many related fields. Moreover, the aquatic cycles are but subsets of larger cycles encompassing landscapes and ultimately the global biosphere. Although details of the broader perspectives of nutrient cycles are beyond our scope, a few comments and key references are included below because a basic understanding of these broader perspectives is essential for environmental scientists and engineers. After a brief description of these larger scales, our focus in this chapter is on the chemical behavior of nitrogen and phosphorus, including inorganic and organic forms of the elements and briefly on their analytical chemistry. Important spatial and temporal patterns in the concentrations of the important inorganic forms of N and P in surface waters are described, and chemical methods of removing the elements from wastewater and lake water are presented.

16.1.2 Nutrient cycles: types and scales

Nutrient cycles are portrayed in numerous ways depending on the aspects one wishes to emphasize and the spatial scale of interest. The finest scale—***molecular***—focuses on transformations among the chemical species (inorganic and organic) and oxidation

---

*Note that the correct spelling of the element is ***phosphorus***. *Phosphorous* is not correct in either American or British English, although one sees this misspelled form all too often in both the popular press and scientific papers. The word "phosphorous" is an adjective referring to the trivalent form of the element. Phosphorous acid is H_3PO_3 (actually $HP(O)(OH)_2$; $pK_{a1} = 1.3$, $pK_{a2} = 6.7$). It is toxic at low concentrations and is used to control microbial plant diseases, but it is not considered important in natural waters.
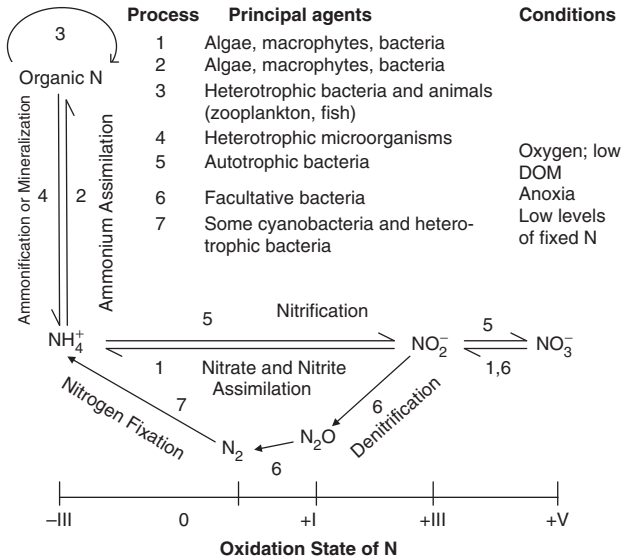
Figure 16.1 Molecular-scale nitrogen cycle diagram. Key to transformations, all of which are biologically mediated: (1) nitrate and nitrite assimilation, (2) ammonium assimilation, (3) heterotrophic conversion of organic N, (4) ammonification (also called N mineralization), (5) nitrification, (6) denitrification, (7) nitrogen fixation.

states of a nutrient element. Figure 16.1 illustrates a molecular-level view of the nitrogen cycle and provides the names, agents, and conditions for common N-cycle transformations in aquatic and terrestrial systems. All the processes shown in Figure 16.1 are mediated primarily or exclusively by organisms in the biosphere. Important abiotic transformations in the nitrogen cycle occur primarily in the atmosphere, and some photochemical reactions involving nitrate that occur in aquatic systems are described in Chapter 17. Numerous N-containing organic compounds are involved at the cellular level, but molecular-level N cycles generally lump all organic N into one or two pools (total organic N (TON) or particulate (PON) and dissolved (DON) organic N). The molecular-level phosphorus cycle is much simpler than the nitrogen cycle. The only important inorganic P form is orthophosphate; it becomes organic P by microbial assimilation, and organic P mineralizes to become orthophosphate.

At the *organism* scale, nutrient cycle representations focus on transfer between inorganic and organic states of nutrient elements and movement of an element through a food web, e.g., uptake by plants, transfer to higher trophic levels by herbivorous and carnivorous animals, and return to inorganic forms by macroscopic and microbial degraders and decomposers. The *ecosystem* scale expands on this perspective by including the cycling of nutrients between abiotic (e.g., water and sediment) and biotic components in an aquatic or terrestrial ecosystem. The *landscape* level incorporates all the above cycling processes plus transport and transformation processes within and between the terrestrial, aquatic and atmospheric phases of a landscape. The spatial scale

of landscape cycles may range from small catchments or watersheds to regions, states, continents or even the entire globe. Figure 16.2 is an example of a broad-based landscape-level N cycle showing linkages between atmospheric, terrestrial, and aquatic portions of the cycle.[1] The diagram illustrates many influences of human activities on the nitrogen cycle. In particular, fixation of nitrogen by industrial processes (mainly for fertilizer) and by fossil fuel combustion contribute significant amounts of "new nitrogen" to the pool of N available for cycling.

At the global scale, nutrient cycle diagrams usually are highly aggregated and simplified presentations that provide estimates of (1) the amounts of an element in a few major reservoirs (e.g., global atmosphere, the oceans, terrestrial biota) and (2) transfer rates (input and output) of the element between reservoirs. Such diagrams thus are "budgets" and can be considered as simple mass balance models.

Many examples of global nitrogen budgets have been published, including some early rough estimates before the middle of the twentieth century.[2] Söderlund and Svensson[3] were the first to present a detailed estimate of the impacts of human activities on the global N cycle. A highly cited analysis by Vitousek et al.[4] stressed the profound distortion of the natural N cycle caused by industrial N_2 fixation (almost entirely for fertilizer) and to a lesser extent by inputs of nitrogen oxides from fossil fuel burning. A recent example of a global N cycle that quantifies the human and natural inputs[5] is shown in Figure 16.3. Although human activities still account for a small proportion of the reactive N cycling in the oceans, more than half of the riverine loadings and 75% of the atmospheric loadings to the oceans are attributed to human activities, and industrial fixation is a larger N source to terrestrial systems than is biological fixation. Galloway et al.[6] argued that the circulation of anthropogenically derived reactive (i.e., fixed) N through the atmosphere, hydrosphere, and biosphere has numerous consequences— called the "nitrogen cascade." Some of the consequences are positive and intentional (e.g., increased agricultural production), but many, e.g., eutrophication, air pollution (smog, acid deposition), and contributions to global warming, are unintended and undesirable.

Similar input-output models have been developed for nutrient dynamics at regional scales[7] (e.g., Figure 16.4), and they can be considered a bridge between nutrient cycle diagrams and compartment-based mathematical models based on mass balance principles. The tools of chemical reactor analysis can be used to extract quantitative information about the behavior of the element (e.g., residence times in a given reservoir). In such cases, the reservoirs are treated as well-mixed compartments, and losses are modeled as first-order processes. Simulations with such models can be used to address "what if" questions and analyze scenarios for managing fluxes of the element through the system.[7] For example, the nitrogen budget in Figure 16.4 showed that N inputs to ground water were greater than withdrawals, resulting in nitrate contamination of the aquifer. The analysis proposed a way to account for the nitrate in ground water used to irrigate fields, thereby reducing the quantity of fertilizer needed and reducing costs while improving the aquifer.

16.1.3 Similarities and differences between N and P cycles

Representations of the N and P cycles at organism, ecosystem, and landscape scales are similar. Both elements are essential for plant growth and move through food webs and
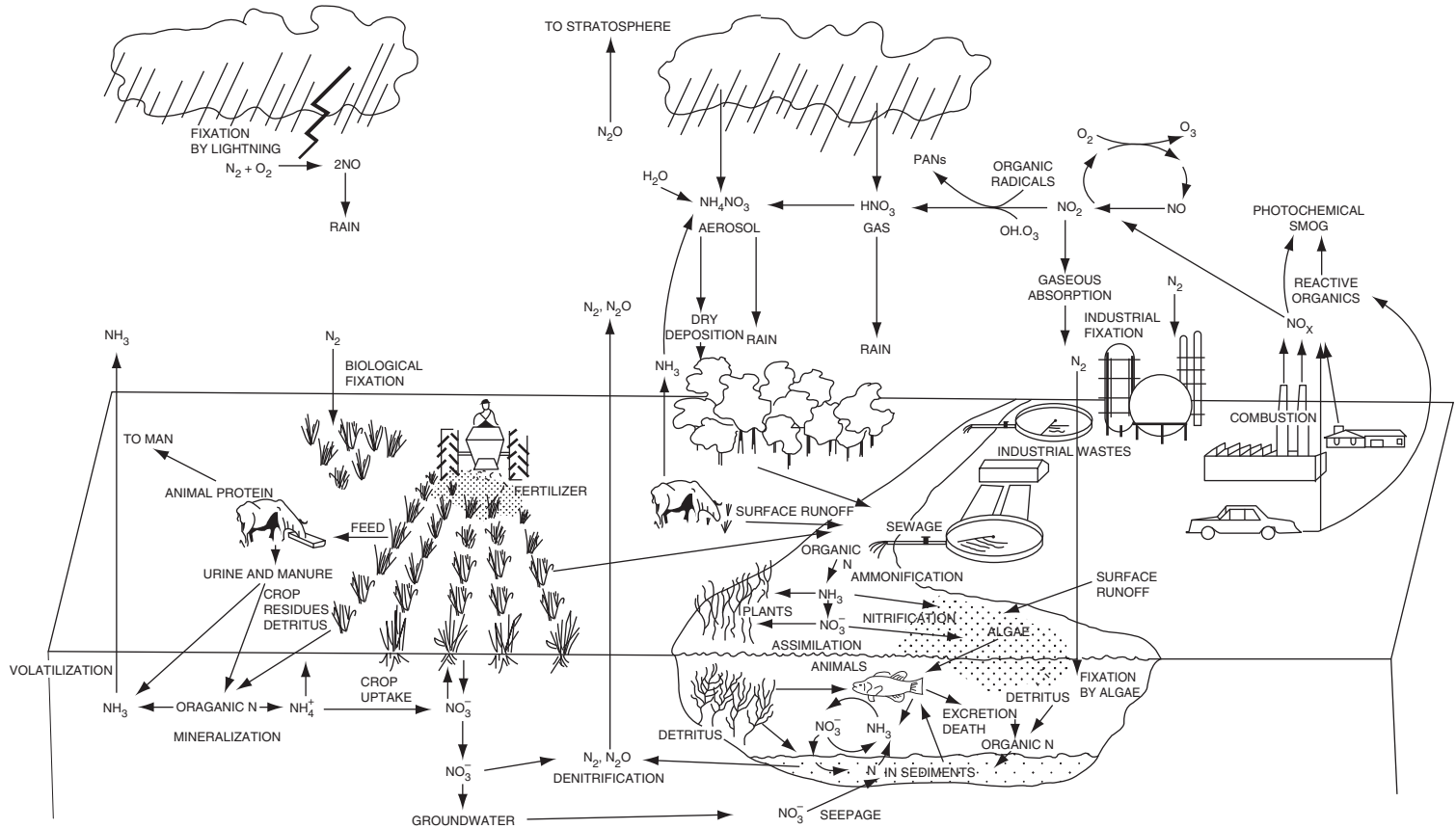
Figure 16.2 Landscape-level representation of the nitrogen cycle illustrating natural and human activities that affect nitrogen fluxes. Used with permission from *Nitrates: An Environmental Assessment*, 1978, by the National Academy of Sciences, courtesy of the National Academies Press, Washington, D.C.
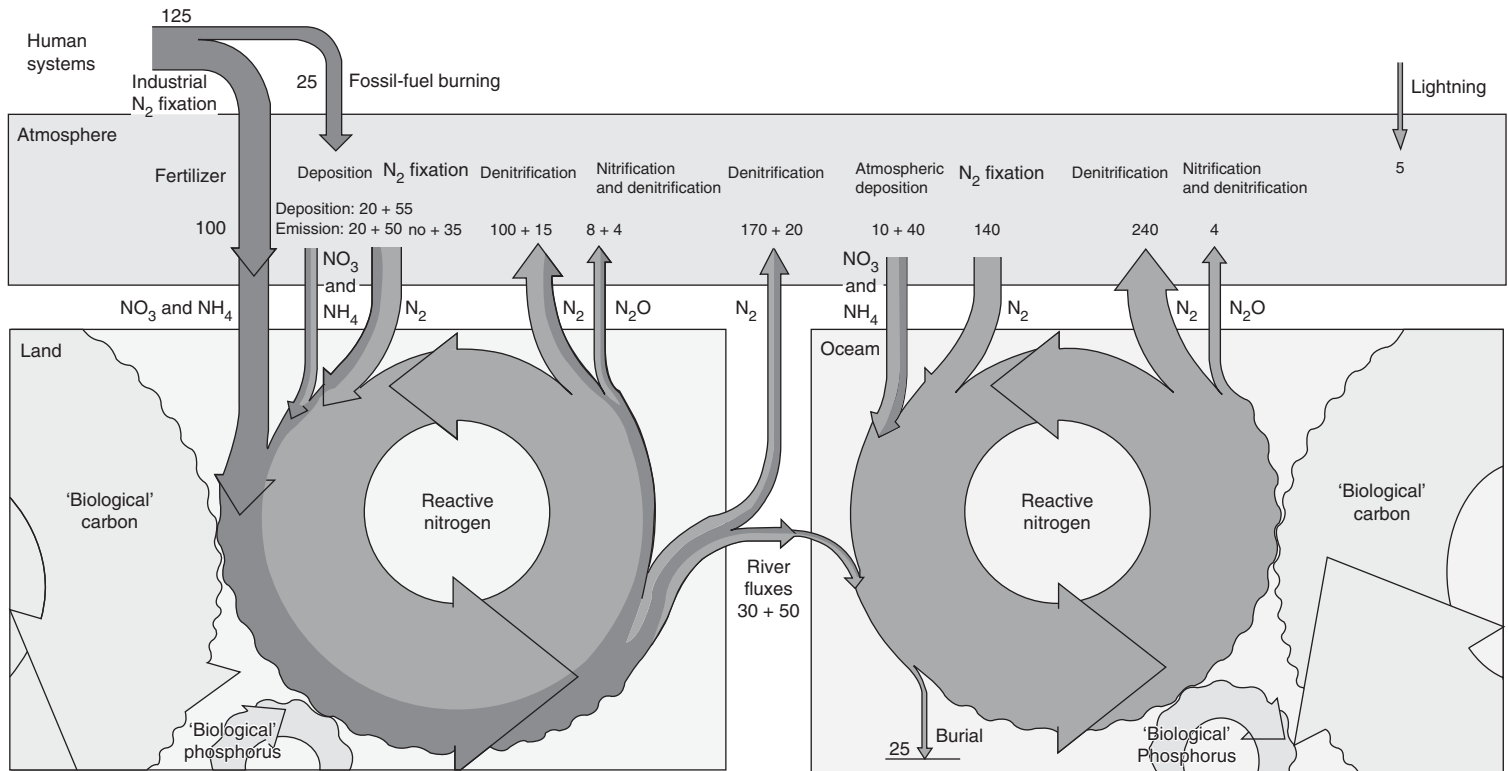
Figure 16.3 Global nitrogen budget showing relative importance of human (darkest gray shade) and natural (middle gray shade) fluxes on land and in the oceans. Reprinted from Gruber and Galloway[4] by permission from Macmillan Publishers Ltd: *Nature* **451**: 293–6, copyright 2009. (See color insert at end of book for a color version of this figure.)
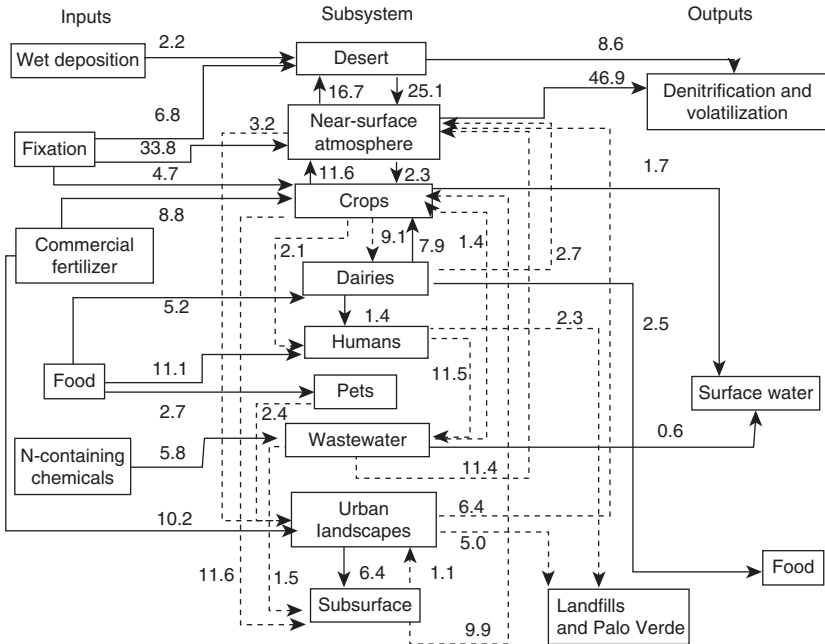
Figure 16.4 Nitrogen mass balance for central Arizona, including Phoenix, showing inputs, internal transfers, and outputs, in Gg/yr. "Palo Verde" sink is a nuclear power plant that uses wastewater for cooling water, which is evaporated to dryness. The resulting salts are stored permanently. From Baker et al.,[7] © Springer, and used with permission.

ecosystems in similar—although not identical—ways. Differences between the cycles at these scales primarily reflect differences at the molecular scale—that is, the many differences in the chemistry of the two elements. Phosphorus has only one important oxidation state (P^V) in natural systems, and the P cycle thus involves no redox processes. In contrast, biologically mediated redox processes dominate N cycle transformations. Phosphorus has no volatile forms, and atmospheric processes are simple and usually not important. Although atmospheric deposition is a P source for aquatic systems, most of the P in rain and dry-fall is derived from local wind-blown suspension of soil and plant debris. Nitrogen has several important gaseous and volatile forms, and significant chemical transformations occur in the atmosphere. The scales of atmospheric N transport are hundreds to thousands of kilometers, in contrast to scales of meters to a few kilometers for P. Phosphorus, however, has a much more complicated mineral chemistry than N. Solubility constraints on P concentrations in natural systems result from the formation of solid phases with several cations (Fe, Al and Ca); in contrast, nearly all salts of inorganic N forms are very soluble. Finally, dissolved inorganic P participates in complexation and acid-base reactions to a greater extent than do inorganic N forms.

Pronounced variations occur over time and space in inorganic N and P concentrations in aquatic systems, as a result of changes in temperature, light, and dissolved oxygen, which promote or retard plant growth and decomposition over the course of a year.

These variations are referred to as the "seasonal or annual cycle" of N or P. Typically, these conditions reflect low rates of primary production (and associated nutrient assimilation) during fall and winter. Rates of nutrient mineralization and continued inputs of inorganic nutrients from external sources and recycling from bottom sediments combine to replenish stocks of inorganic N and P during this period, producing maximum concentrations of inorganic N and P in surface waters in late winter or early spring. Conditions become more favorable for photosynthesis in spring (longer daylight, higher temperatures, and high nutrient concentrations), resulting in a rapid depletion of inorganic N and P. Minimum concentrations are maintained during summer because conditions favorable to plant production remain high. Figure 16.5 illustrates these trends for nitrate and ammonium; orthophosphate shows similar seasonal trends. The seasonal cycle of temperature that produces vertical stratification and loss of oxygen from the bottom waters in summer (see Figure 12.6) also has strong effects on vertical patterns of N and P forms, as illustrated for inorganic nitrogen forms in Figure 16.6a and phosphate in Figure 16.6b. The nitrogen profiles show an initial increase in nitrite and nitrate in the hypolimnion, especially at mid-depths, caused by nitrification of ammonium produced from decomposition of settling PON, followed by loss of both ions, mostly
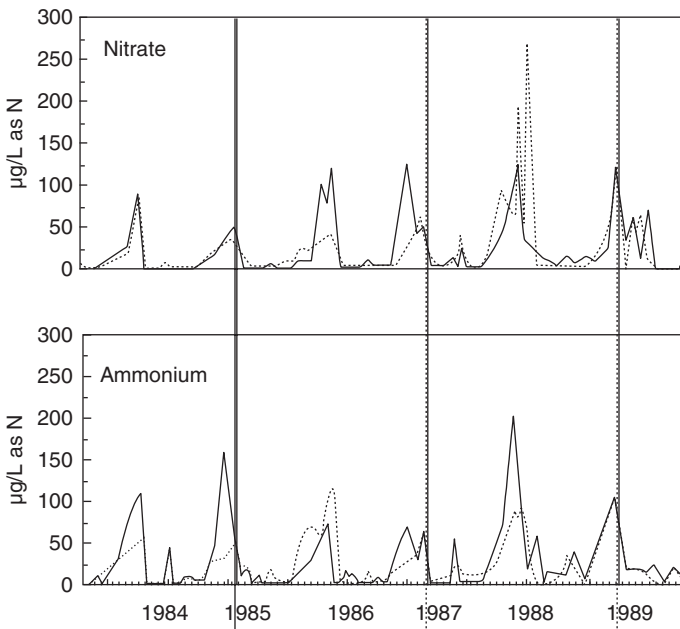
Figure 16.5 Seasonal patterns of nitrate and ammonium in surface waters of Little Rock Lake, a soft-water oligotrophic lake in northern Wisconsin. Solid line, treatment basin; dotted line, reference basin. Vertical lines for alternate years show the beginning of ice-free conditions and beginning of two-year cycles for the treatment basin in a whole-basin acidification experiment at target pH values of 5.5, 5.1, and 4.7 (left to right). From Sampson and Brezonik,[8] © Springer, and used with permission.
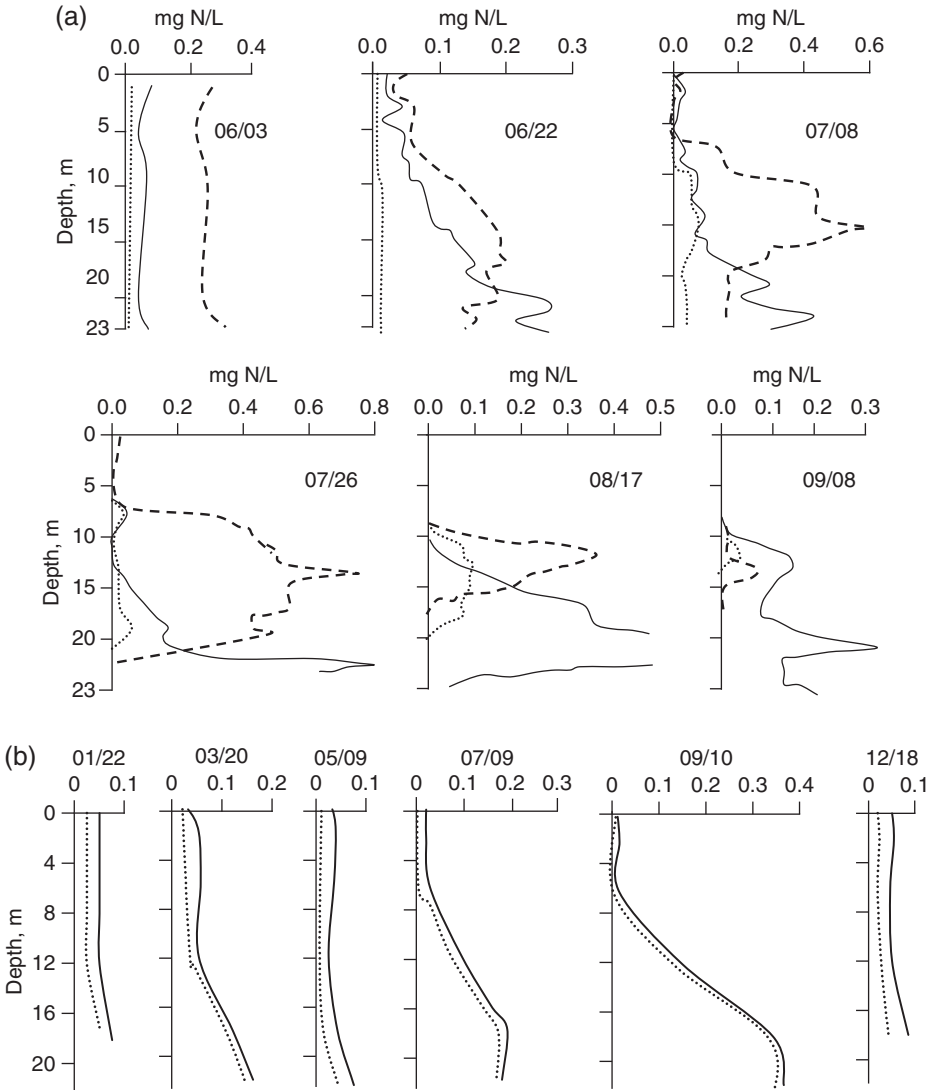
Figure 16.6 (a) Depth profiles of ammonium (solid lines), nitrite (dotted lines), and nitrate (dashed lines) in Lake Mendota, Madison, Wisconsin, in summer 1966 (unpublished data of the author [P.L.B.]); (b) selected depth profiles of soluble reactive phosphate (SRP; dotted lines) and total P (TP; solid lines) in Lake Harriet, Minneapolis, Minnesota, in 1991 (unpublished data of K. Jensen and the author [P.L.B.]).

to N_2 by denitrification as the hypolimnion became anoxic starting at the sediment-water interface in July and gradually moving upward.[9] Increases in ammonium in the hypolimnion reflect a combination of release from the bottom sediments once the bottom water became anoxic and mineralization of particulate organic matter sinking into the hypolimnion from the surface waters.

Seasonal variations in concentrations are not indicative of the dynamic timescale of N and P cycle reactions, however. Isotope tracer studies over the past half-century have demonstrated that N and P forms are much more dynamic than that; half-lives of dissolved inorganic pools of P may be as short as seconds to minutes during maximum algal growth, and turnover times of inorganic N often are on the scale of minutes to hours.[10]

16.2 Chemistry of nitrogen and phosphorus

16.2.1 Overview

Nitrogen occurs in compounds with oxidation states from –III to +V (Table 16.1). The two end-members, nitrate and ammonium, are the most important inorganic N forms in aquatic systems. Some intermediate oxidation states are important in atmospheric transformations. Phosphorus occurs in only in the oxidation state +V, except for some synthetic phosphonates (see Table 6.3) that are found as trace pollutants in the environment. The following sections summarize the basic chemical characteristics of nitrogen and phosphorus forms found in aquatic environments.

16.2.2 Ammonium/ammonia (NH_4^+/NH_3)

Ammonium ion* is a very weak acid ($pK_a = 9.25$); ammonia, its conjugate form, is a moderately strong base ($pK_b = 4.75$). NH_3 is very soluble in water and is a gas at room temperature (b.p. $= -33.3°C$). Its air-water transfer is controlled by the gas film because once NH_3 reaches the air-water interface it reacts, essentially instantly, with water to form NH_4^+. The liquid film thus does not have a concentration gradient in NH_3. All simple ammonium salts are very soluble except struvite, $MgNH_4PO_4$, precipitation of which has been proposed to remove both N and P from wastewater (see Section 16.4.3). With a pair of valence electrons available for sharing, NH_3 forms complexes with many metal ions, but stability constants generally are small (see Section 9.1.1). Complex formation is not important at the pH and concentrations in natural waters but can be important in industrial wastes.

NH_3 (un-ionized ammonia) is toxic to fish, and state water quality standards commonly limit its concentration in surface waters to 0.01 mg/L as N. Concentrations of NH_3 depend on total ammonium concentration, pH, and temperature. Although most plants can use either nitrate or ammonium equally well for growth, use of NH_4^+ is advantageous because it is at the oxidation state of organic N and no redox reactions are needed. Assimilation of NH_4^+ releases H^+ and thus decreases the alkalinity of water. NH_3 is photooxidized in the atmosphere, but in spite of early suggestions that this reaction occurs in seawater,[11] it is not an important process in aquatic systems. NH_3 is oxidized by ozone,[12] but the rate constant is much too low (~ 20 M^{-1} s^{-1}) for the reaction to be

---

*A word on nomenclature: most of inorganic N^{-III} is ionic at the pH of natural waters. Thus, it is proper to refer to it as *ammonium*, as is the convention in most sciences. We use this term for both the ion and total $[NH_4^+] + [NH_3]$. Water quality scientists and environmental engineers, however, often use the term *ammonia* to refer to the total.

Table 16.1 Oxidation states of nitrogen

Oxid. State	Compound(s)	Name(s)	Comments
−III	NH_4^+/NH_3	Ammonium/ammonia	Weak acid/moderately strong base
−II	N_2H_4	Hydrazine	Used in rocket fuel; not found in nature
−I	NH_2OH	Hydroxylamine	Intracellular intermediate in nitrification; explosively reactive, unstable species
0	N_2	Dinitrogen	Major component of atmosphere (78%); chemically unreactive
+I	N_2O	Nitrous oxide	Greenhouse gas produced in denitrification; called "laughing gas" because in past use as an anesthetic, it made people giddy
+II	NO	Nitric oxide	Major air pollutant; a free radical
+III	HNO_2, NO_2^-	Nitrous acid, nitrite	Weak acid; biologically and chemically unstable; usually low in concentration
+IV	NO_2, N_2O_4	Nitrogen dioxide	Formed from NO in air; a radical; $NO + NO_2$ is called NO_x
+V	HNO_3, NO_3^-	Nitric acid, nitrate	Strong acid; stable form in oxic water; a very weak ligand

important under environmental conditions or even in ozonation reactors. NH_3 reacts with hydroxyl radicals ($\cdot OH$) at a much higher rate ($\sim 1 - 8 \times 10^7 \, M^{-1} \, s^{-1}$),[12] but this still is 1–2 orders of magnitude slower than $\cdot OH$ rate constants with many organic molecules, which thus act as scavenging agents for $\cdot OH$ and minimize its reaction with NH_3. NH_3 reacts with HOCl to form chloramines, which are important in water disinfection (see Chapter 13).

16.2.3 Nitrogen gases

N_2 is chemically unreactive in natural waters; the $N\equiv N$ triple bond is very stable. In natural waters N_2 is transformed to "fixed N" forms only by certain nitrogen-fixing blue-green algae (cyanobacteria) and some heterotrophic bacteria, and the concentration of N_2 is controlled primarily by equilibrium with the atmosphere. K_H (see equation 6.1) values for N_2 are about half those for O_2, but because N_2 is almost four times as abundant in the atmosphere, saturation values in water are higher than those of O_2 (Table 16.2). The ratio of the concentration of N_2 to that of the inert noble gas Ar ($[N_2]/[Ar]$) has been used as an integrative estimate of the extent to which denitrification of nitrate increases the concentration of N_2 in anoxic waters.[14]

Nitrous oxide (N_2O) is an intermediate in denitrification. Acetylene blocks the enzymatic reduction of N_2O to N_2, and this provides the basis for the "acetylene block" method[15,16] to measure denitrification rates. Because of the high background of N_2 in the environment, it is difficult to measure small amounts of N_2 production in incubated samples and measurement of N_2O production is easier and more accurate. (The background concentration of N_2O in natural waters is low, limited by its low

Table 16.2 Solubility, S and S′, of N_2 in water*

	T (°C)	0	10	20	25	30
K_H	mol L^{-1} atm^{-1}	1.06×10^{-3}	8.39×10^{-4}	6.96×10^{-4}	6.44×10^{-4}	6.00×10^{-4}
β	cm^3 L^{-1} atm^{-1}	23.74	18.81	15.59	14.42	13.45
S	mg/L	23.0	18.1	14.9	13.6	12.6
S′	mL/L	18.4	14.5	11.9	10.9	10.1

*Calculated from values in Weiss.[13] S and S′ for water-saturated air (100% relative humidity) at total pressure (P) = 1.00 atm.

partial pressure in the atmosphere, which is ~320 ppb.) N_2O is a potent greenhouse gas (~300× stronger than CO_2), and increases in atmospheric N_2O (by ~0.25% per year) are a subject of concern. The increasing atmospheric N_2O is assumed to be caused by increasing global rates of denitrification, which in turn are assumed to be to be a consequence of the global increases in fixed N resulting from industrial N fixation for fertilizer.

Nitric oxide (NO) and nitrogen dioxide (NO_2) are important air pollutants produced primarily by fossil fuel combustion. Both are free radicals and thus moderately reactive. The two gases usually are measured together and the sum is called NO_x. In the atmosphere these gases lead to the formation of photochemical smog, and they are oxidized to nitric acid vapor ($HNO_{3(g)}$) by a complicated series of reactions.[17] Only trace quantities of the two gases occur in natural waters from photochemical reduction of NO_3^- and NO_2^- and partitioning from polluted air.

16.2.4 Nitrate and nitrite

Nitrite (NO_2^-) is chemically and biologically unstable. It is the least abundant inorganic N ion, usually found at levels of a few micrograms per liter as N or less. Exceptions occur in zones of active nitrification or denitrification, and its presence in high concentrations indicates disruptions in these multi-step reactions. Nitrous acid (HNO_2) is a weak acid, pK_a = 3.29. It is toxic to organisms and causes ***methemoglobinemia*** in humans, a syndrome of concern for infants, in whom nitrite combines with hemoglobin to form *methemoglobin*, which cannot transport O_2. Nitrite levels seldom are high enough to cause the syndrome even in sensitive populations, but nitrate is reduced to nitrite in the nonacidic stomachs of infants, causing the syndrome. As a result, state drinking water (maximum) standards for nitrate are 10 mg/L as N, which is sufficient to protect sensitive individuals. Nitrite can react with amines to form carcinogenic nitrosamines, but there is no evidence that nitrite (and nitrate) levels found in drinking waters are sufficient to cause cancer in humans, although dietary consumption of nitrite (e.g., in processed meats) remains a concern.[1,18]

Nitrate* (NO_3^-), the most oxidized (+V) form of N, is the anion of the strong acid HNO_3 (pK_a = −1.30). All nitrate salts are very soluble, and nitrate is one of the weakest ligands in water. It is not a strong chemical oxidant in dilute solution.

*Another word on nomenclature: There is only one kind of inorganic nitrate in natural waters, NO_3^-. Therefore, it is not correct to use the plural form "nitrates," which is common practice in some circles.

Until the 1970s, nitrate was thought to be chemically unreactive in aquatic systems and subject only to biological transformations. Nitrate is not quite as strong an electron acceptor as O_2, and oxidation of organic matter by O_2 yields more energy than oxidation by NO_3^-. O_2 thus is the preferred microbial electron acceptor, and denitrification does not occur until O_2 is depleted, at least in microzones where microbes live. Nitrate is now known to be photochemically active in water, and its photoreduction produces hydroxyl radicals, ·OH (see Chapter 17). Nitrate is the most important source of ·OH in many water bodies, especially those affected by agricultural drainage, where $[NO_3^-]$ may exceed 1 mM.

16.2.5 Organic nitrogen

Individual compounds within the total organic N (TON) fraction of water are not routinely measured, but the fraction often is divided operationally into particulate and dissolved organic N (PON and DON) based on separation by a specified pore-size filter (usually 0.45–0.7 μm). PON in surface waters is mostly from planktonic organisms and organic detritus—partly decomposed cells and cellular components—and thus contains amide N in proteins and peptides. Heterocyclic organic N is present in PON from purines and pyrimidines in nucleic acids, some amino acids (see Figure 6.8), and pyrrole groups in chlorophyll. Studies on organic N in surface waters dating back to the mid-1920s[19] show that DON is mostly macromolecular and contains a significant fraction of amino and amide N. Although organic N concentrations in wastewater are much higher than in natural water bodies, the source is similar (microorganisms), and the composition also is likely to be similar. A much more recent study on seawater,[20] using the sophisticated tools that modern science affords, also concluded that most of the high-molecular-weight DON (HMWDON; material retained by a 1-kDa pore-size ultrafiltration membrane, which is ∼30% of the total DON), is amide N. Two distinct fractions were found: half of the HMWDON in surface waters of the open ocean was present as N-acetyl amino polysaccharides (e.g., chitin, poly-H-acetyl-glucosamine, a component of the exoskeletons of many organisms, including crustaceans and cephalopods, e.g., squids and octopuses).
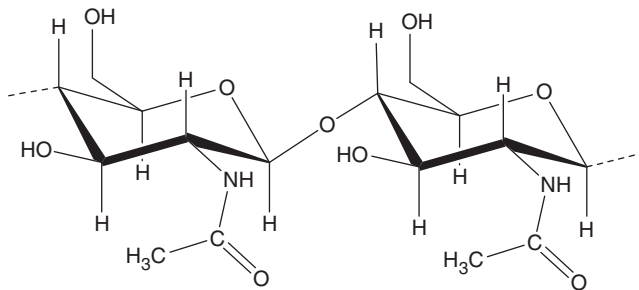
Structure of chitin showing two of the N-acetyl glucosamine units that form the polymer

The other half of the HMWDON was present as amides that resist both chemical hydrolysis and biological degradation. In deep waters, nearly all the HMWDON was

present in the latter fraction, which is thought to be derived from protein N that interacted with other DOM in a way that protects it from chemical hydrolysis or microbial attack.[20]

Low-molecular-weight organic N compounds, especially those involved in metabolic activity—such as free amino acids—are too bio-reactive to build up to high levels in water bodies, but dissolved free amino acids (DFAAs) do occur at low concentrations (usually nM range) in lakes and seawater.[21–23] For example, ten amino acids were found in Lake Mendota, Wisconsin,[21] at mean concentrations ranging from 4.2 nM (lysine and tyrosine) to 12.6 nM (alanine) and 18.8 nM (serine). Others[22,23] also have found the latter two compounds to be among the most abundant DFAAs. Concentrations in Lake Mendota did not vary much with season or depth and appeared to be controlled by bacterial uptake. High concentrations ($\sim 100-400$ nM) of some DFAAs (serine, glycine and lysine) were found in eutrophic Upper Klamath Lake, Oregon.[22] In aggregate, DFAAs constitute only a small fraction ($\leq 1-2\%$) of the DON,[23,24] but studies have shown that they are actively involved in bacterial metabolism in fresh and marine waters.[22,23,25]

Reactions of organic compounds containing amino and amine groups with chlorine and ozone are of interest and concern because of the diverse array of potentially toxic products that are formed, as described in Sections 13.6.4 and 13.7.2. Some structural characteristics and metal-binding properties of organic N in natural organic matter (NOM) and humic substances are discussed in Chapter 18.

16.2.6 Orthophosphate

Phosphoric acid is a triprotic acid (pK_a values of 2.15, 7.20, and 12.38), and the predominant forms of orthophosphate in water at circumneutral pH are $H_2PO_4^-$ and HPO_4^{2-}. Phosphate ions have a tetrahedral shape, with the P atom at the center:

$$
\begin{array}{c}
\text{O} \\
\| \\
{}^-\text{O}-\!\!\!\overset{}{\text{P}}\!\!\!-\text{O}^- \\
| \\
\text{O}^-
\end{array}
\qquad \mathbf{PO_4^{3-}\ ion}
$$
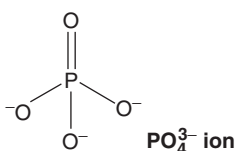
Only the exterior O atoms participate in chemical reactions. Phosphate can contribute to the alkalinity of natural waters, but typical inorganic P concentrations are so small compared with carbonate forms that the contribution is negligible. For example, an orthophosphate concentration of 31 μg/L as P (i.e., 1×10^{-6} M) would be considered a high concentration in a lake, but it would contribute only ~1 μeq/L to alkalinity (if the pH were > pK_{a2},). This is a negligible amount even in acid-sensitive lakes. Many phosphate salts are insoluble, including those of the trivalent metal ions Fe^{3+} and Al^{3+}, as well as various calcium salts, and this fact is put to use in removing phosphate from wastewater and lakes (see Section 16.4.2). Although phosphate can serve a ligand with many metal ions (through oxygen linkages), the complexes are not especially strong and not important in natural water chemistry.

16.2.7 Condensed phosphates

These chemicals are formed by linking orthophosphate ions together by successively removing H_2O molecules:
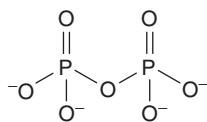
Pyrophosphate

$pK_{a2} = 2.4$; $pK_{a3} = 6.6$;

$pK_{a4} = 9.3$
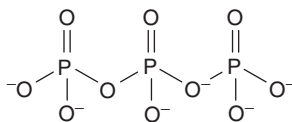
Tripolyphosphate

$pK_{a3} = 2.3$; $pK_{a4} = 6.5$;

$pK_{a5} = 9.2$
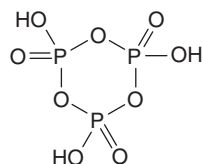
Trimetaphosphate

$pK_{a3} = 2.1$

Condensed phosphates are important as "builders" in detergents to buffer pH and complex Ca^{2+} and Mg^{2+} preventing them from precipitating the surfactant. They hydrolyze by chemical and microbially mediated (enzymatic) mechanisms to form orthophosphate on timescales of hours to days[26] and thus represent potentially bioavailable P. Concerns about the eutrophication of lakes receiving wastewater with high TP concentrations led several states to ban their use (or restrict allowable concentrations) in laundry detergents in past decades, but condensed phosphates still are used in dishwasher detergents. Such phosphate bans have decreased TP concentrations in raw wastewater by a third to a half.

16.2.8 Dissolved organic phosphorus (DOP)

As in the case of organic N, specific organic P components are not measured routinely, but efforts have been made to determine the major components of DOP.* One popular approach uses enzymes that hydrolyze specific kinds of phosphate esters (e.g., monoesterases; diesterases; alkaline and acid phosphatases; phytase).[27−29] For example, the soluble enzyme alkaline phosphatase (APase) releases orthophosphate from phosphomonoesters. Many studies have shown that APase and APase-hydrolyzable DOP occur in lakes, but the studies have not provided much information on the nature of the organic structures to which the phosphate is attached. Use of ^{31}P nuclear magnetic resonance spectroscopy recently was proposed to characterize dissolved and particulate P in natural waters, and initial results showed the presence of phosphomonoesters and phosphodiesters, phosphonates, and inositol phosphate (IP).[30]

   Aquatic DOP is partly macromolecular and includes such decomposition products of microbial cells as sugar phosphates, phosphoproteins, phospholipids, and phosphonucleotides (remnants of nucleic acids). Most low-molecular-weight DOP compounds found in cells are too bioavailable to remain in water very long. Inositol (hexahydroxycyclohexane) phosphates (IPs), which comprise a significant fraction of

---

*Phosphorus-containing pesticides are common contaminants in aquatic systems, but they occur at very low concentrations and do not contribute significantly to total DOP or TP concentrations.

the DOP in soils and possibly in aquatic systems, are important exceptions. Inositol has several stereoisomers, but the *myo* form (see below) is the most common in nature. From one to six phosphate groups may be attached to the ring; inositol hexa*kis*phosphate (IP$_6$; also called phytic acid or phytate) is the major storage form for P in plants and is thought to be the major form of organic P in soils:[31,32]
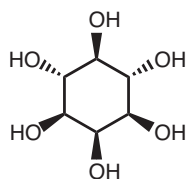
Myo-inositol
(hydrogen atoms not shown for clarity)

Myo-inositol (axial form)
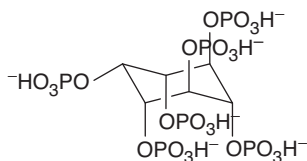
Partially (half) deprotonated myo-inositolhexakisphosphate (IP$_6$)*

The dominance of IP$_6$ in aquatic systems is less certain; studies indicating a predominance of the lower esters (IP$_{1-4}$)[34] were criticized because the extraction process may have degraded higher esters (IP$_{5-6}$).[32] The relative contributions of terrestrial and internal production of IPs to aquatic systems also is uncertain. Although terrestrial sources seem obvious given the importance of IPs in soils, strong binding of highly charged IP species to clays and iron oxides in soils limits their mobility. Some aquatic macrophytes can synthesize IPs, but the importance of IPs in phytoplankton is still unknown.[32] Whether IPs constitute the majority of total P in lake sediments[32,35] also is considered unconfirmed, and further studies are needed on these compounds.

The enzyme phytase hydrolyzes orthophosphate from inositol and some other phosphomonoesters. Herbes et al.[29] reported that 50% of the DOP in lake water could be hydrolyzed by this enzyme. The lack or low activity of phytase in nonruminants is a principal reason for the high levels of IP$_6$ in animal manure,[32] and this may play a role in the accumulation of IPs in soils. As indicated above, major uncertainties exist regarding the role of IPs in aquatic P cycling. The bioavailability of IPs to algae is not clear, and IPs may be more important as a means of long-term storage of P than as active source of P for algal growth. For a recent review of IPs in soil and aquatic systems, see Turner et al.[32]

16.2.9 Particulate P (PP)

This fraction is even more heterogeneous than DOP because it also includes inorganic phosphate forms. Orthophosphate sorbed onto suspended clays and precipitates of Ca, Al, and Fe phosphates are important in rivers and impoundments with high levels of inorganic suspended solids, but inorganic PP is of minor importance in most lakes, where PP is composed mostly of planktonic organisms and detrital P from decomposing

*IP$_6$ has 12 ionizable protons with pK_as ranging from 1.1–2.1 (pK_{a1-6}) to 5.7–7.6 (pK_{a-9}) and 10.0–12.0 (pK_{a10-12}).[33]

organisms. It presumably consists of the organic biomolecules described for DOP. Much of the P in runoff from agricultural and urban lands is associated with inorganic particulate forms, and control of soil erosion is a major factor in controlling P losses from such landscapes.

16.2.10 Sediment P

The chemical forms and distribution of P in sediments affect the rates and mechanisms of P cycling between sediments and overlying water. Many mineral and organic forms of varying chemical lability and bioavailability are found in aquatic sediments: phosphate associated with ion exchange sites, phosphate sorbed onto or occluded in iron and aluminum hydroxides, and phosphate bound in minerals, such as apatite. Sequential extraction schemes developed for soils[36−38] and later adapted for use on lake sediments[39,40] have been used widely to fractionate soil/sediment phosphorus (Table 16.3). Not all fractions are present in every sediment; for example, the Ca fraction is not found in soft-water environments. The fractions determined by these techniques are "operationally defined," but the amounts in particular fractions have been related to the potential for P release from lake sediments under various conditions[41] and to the bioavailability of soil P.[42] For example, P released from sediments under anoxic conditions is related to the reductant-soluble fraction, which largely represents iron-bound P.[43] This finding led to the development of methods[44,45] to calculate the alum dose needed to immobilize loosely bound and iron-bound P, which together are called "mobile P," in sediments and to control internal P loading in eutrophic lakes.

The above concepts also have led to the development of single-extractant soil tests, such as Bray P,[46] Mehlich-III P,[47] and Olsen P,[48] which are widely used to assess the concentrations of "bioavailable phosphorus" in agricultural soils in order to determine appropriate doses of fertilizer P. These extraction procedures also are used to assess the potential for P losses to runoff in agricultural catchments.[42,49]

Table 16.4 lists solubility product values of common phosphate minerals. Although apatite is the thermodynamically stable P phase with Ca, it is slow to form in natural waters, and more soluble Ca-P minerals, for which solubility is illustrated as a function of pH in Figure 16.7, actually may control P concentrations. Fluorapatite occurs commonly in phosphate mineral deposits and also is important in tooth enamel. Some uncertainty

Table 16.3 Extraction scheme for P fractionation in lake sediments*

Reagent	Fraction
1 M NH$_4$Cl	Loosely bound (ion exchangeable)
0.11 M Na$_2$S$_2$O$_4$ (sodium dithionate) + 0.11 M NaHCO$_3$	Iron bound
0.1 M NaOH	Al bound
0.5 M HCl	Ca bound (apatite)
Ignition at 500°C	Organic bound

*Based on Psenner et al.[40] and Williams et al.[39]

Table 16.4 Common phosphate minerals and their solubility products*

Mineral name	Formula	$-Log\ K_{s0}$
Hydroxyapatite	$Ca_5(PO_4)_3OH$	58.33
Fluorapatite	$Ca_5(PO_4)_3F$	59.5
Strengite	$FePO_4 \cdot 2H_2O$	26.4
Variscite	$AlPO_4$	20.07
	$CaHPO_4$	6.90
	$CaHPO_4 \cdot 2H_2O$	6.62
	$\beta\text{-}Ca_3(PO_4)_2$	28.92
	$Ca_4H(PO_4)_3 \cdot 3H_2O$	34.71
Struvite	$MgNH_4PO_4$	12.6

*Values from MINEQL+ except for fluorapatite.[46]
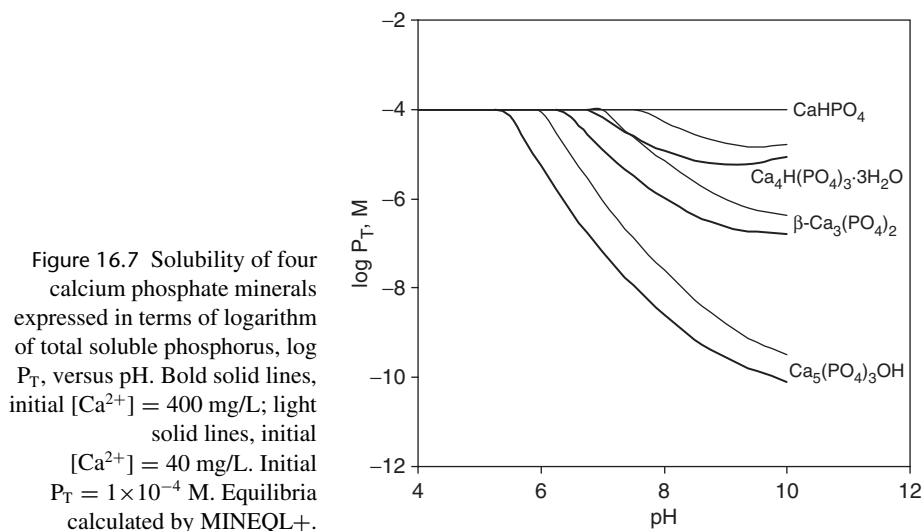
Figure 16.7 Solubility of four calcium phosphate minerals expressed in terms of logarithm of total soluble phosphorus, log P_T, versus pH. Bold solid lines, initial $[Ca^{2+}] = 400$ mg/L; light solid lines, initial $[Ca^{2+}] = 40$ mg/L. Initial $P_T = 1 \times 10^{-4}$ M. Equilibria calculated by MINEQL+.

exists regarding K_{s0} for fluorapatite, but it is widely accepted that it is less soluble than hydroxyapatite.[50] Phosphate forms mineral phases with Fe^{III}, Al, Mg, and many heavy metals.

16.3 Nutrient stoichiometry: from Liebig's limiting law to ecological theories

Organisms are extremely complicated assemblages of organic compounds and macro-molecules. As such, it is not surprising that their elemental composition is not restricted to a single stoichiometry. Nonetheless, as mentioned at the beginning of this chapter, there is an optimal N:P ratio of ~16:1 by atoms (7 by weight) in microorganisms. Similarly, the carbon content of microbial cells typically is related to the N and P content in a

ratio of 106:16:1 (C:N:P). This is called the ***Redfield ratio*** after the oceanographer who in 1934 found that plankton in the oceans have a fairly constant N:P ratio of 16:1 and that the N:P ratio throughout the oceans (even in deep waters) also has this value.[51] Redfield's insight was that this is not just happenstance but causal. More recent analyses[52] have explained the similarity of the ratios as resulting partly from the fact that residence times of the two elements in the oceans ($\sim 10^4$ yr) are about an order of magnitude longer than the mixing time of the oceans ($\sim 10^3$ yr). The Redfield ratio is considered to be an "emergent property" of the system that reflects interactions among many nutrient-cycling processes.[52]

Although the elemental composition of higher organisms is fairly rigidly defined, individual species of phytoplankton exhibit compositional plasticity and can adjust their cellular N:P ratio over a range of ~ 6:1 to 60:1 depending on the relative availability of N and P in the growth medium. The average N:P ratio at the phytoplankton community level is less variable, however, and there is little evidence that the optimal ratio across species differs substantially from the Redfield ratio.

The "fuzzy" stoichiometry of N and P has broader implications for the behavior of these elements in the environment. First, it provides an important link between the two cycles. Although many processes within each cycle can be studied without reference to the other cycle, a holistic understanding of N cycling in a system requires knowledge about P cycling in that system and vice versa. Second, stoichiometry provides a basis to determine which nutrient limits plant growth in an aquatic system. The concept of ***limiting nutrients*** goes back to the mid-nineteenth century when Liebig developed his famous ***law of the minimum***, which says that the element present in least amount *relative to its need* is the "limiting nutrient," i.e., the nutrient that limits the amount or rate of plant growth in the system. The ratio of inorganic forms of N and P at the end of ice-cover in lakes has been used to evaluate which element will limit the amount of algal biomass that can be produced in subsequent springtime blooms. Simple plots of TN:TP and inorganic N:P (Figure 16.8) also have been used to infer which element limits plant growth in lakes. Such information has implications for lake management and controlling the consequences of eutrophication, as well as scientific value. For example, it makes little sense to develop expensive engineering operations to decrease the loading of one of the nutrients to a water body if it does not limit algal production in the water body or cannot be decreased sufficiently to become limiting. Finally, the newly emerging area of ***ecological stoichiometry***[54] considers how the balance of elements affects organisms and the way they interact in ecosystems—that is, how the elemental content of organisms affects behavior over the range of subcellular to global scales—and is an active area for research in aquatic ecology.

16.4   Engineering controls on nutrients in natural waters

16.4.1   Introduction

From an ecological perspective, nutrients are beneficial substances because they are essential for plant growth and ecosystem productivity. High nutrient concentrations in waters affected by human activities, e.g., water bodies affected by agricultural and urban runoff and municipal wastewater, cause changes in ecosystem structure and function
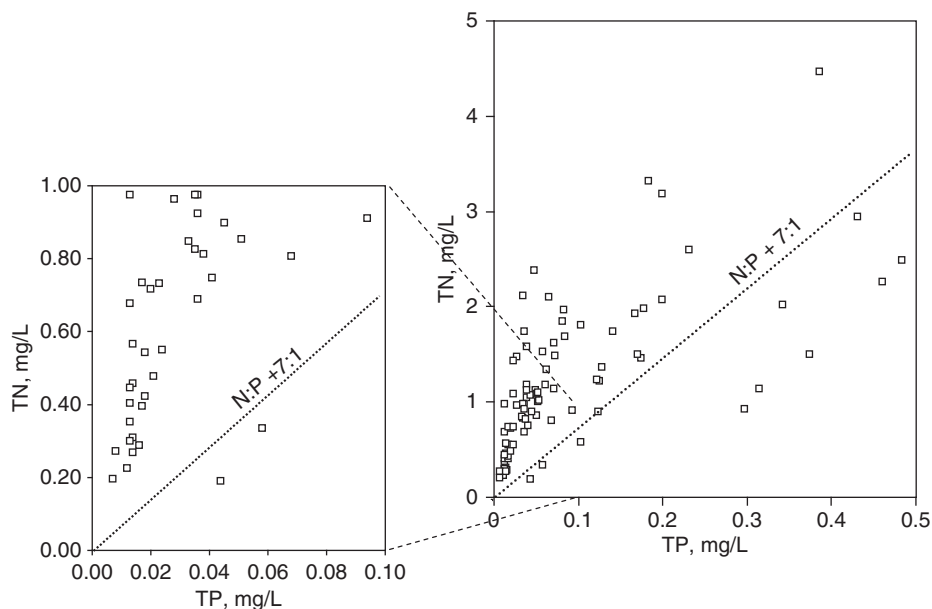
Figure 16.8 TN versus TP for 101 Florida lakes. A simple interpretation is that points above the N:P = 7:1 lines indicate potential P limitation; those below the lines indicate potential N limitation. Drawn from data in Baker et al.[53]

that often are undesirable to humans—unsightly algal blooms, taste and odor problems, and loss of aesthetics. They also may cause anoxic conditions in bottom waters and induce undesirable changes in the composition of plankton and fish communities in lakes, promoting the dominance of cyanobacteria and loss of desirable game fish. In coastal waters, the problem of hypoxia is a result of excess nutrient loading from rivers. Environmental engineers, who generally are charged with fixing such problems, thus tend to regard N and P as problem elements that need to be controlled or eliminated from wastewater and stormwater.

Conventional wastewater treatment systems based on physical and biological treatment processes are not designed for effective nutrient removal from wastewater, but they can be modified to obtain high removal rates biologically. For example, addition of reactors into the treatment stream to promote aerobic nitrification of ammonium to nitrate and subsequent denitrification of nitrate to N_2 under anoxic conditions can produce high removal rates for nitrogen.* In addition, growth conditions for the microbial community in activated sludge systems can be manipulated to induce "luxury uptake" of phosphorus, that is, bacterial storage of phosphate in amounts far greater than their immediate metabolic needs, allowing effective P removal from the water into the biosolids.[56] Phosphorus removal from wastewater by chemical precipitation still is a

---

*Nitrogen also can be removed by air-stripping by preventing nitrification and converting the accumulated NH_4^+ to NH_3 at high pH.[55] This has the potential of converting a water pollution problem to an air pollution problem, however. For this and economic reasons, air stripping is not commonly practiced.

common practice, however, and is described in textbooks on physical-chemical treatment processes.[55] The following sections provide a perspective on the underlying chemistry.

16.4.2 Chemical precipitation of phosphate

Phosphate ion forms insoluble or sparingly soluble salts with many metal ions. For P removal from natural waters and wastewater, the most important metal ions are Ca^{2+}, Fe^{3+}, and Al^{3+} (Table 16.4). Ca^{2+} forms at least four mineral phases with phosphate, and in all cases, phosphate solubility at a fixed Ca_T decreases with pH (Figure 16.7). Apatite is the least soluble (thermodynamically most stable) phosphate mineral with calcium. Equilibrium P_T values are low even at circumneutral pH; e.g., $P_T = 10^{-7.6}$ M (~ 0.8 µg/L as P) at pH 8 and $[Ca^{2+}] = 1 \times 10^{-3}$ M (40 mg/L). Unfortunately, the kinetics of apatite precipitation are relatively slow, and the more soluble minerals $Ca_3(PO_4)_{2(s)}$ and $Ca_4H(PO_4)_3 \cdot H_2O_{(s)}$ are thought to be the controlling phases when slaked lime ($Ca(OH)_2$) is added to water. Addition of lime raises the pH, and inputs of acid (or CO_2) are necessary to return the water to an acceptable pH range before it can be released to receiving waters. This adds to the treatment costs. For economic reasons, lime treatment is not practiced widely in wastewater treatment for phosphate removal.

Ferric iron and aluminum both react with phosphate to form insoluble $M^{III}PO_4$ salts with minimum solubility at pH < 7, and the differences in their behavior are relatively minor compared with the similarities. Both metal ions have strong tendencies to hydrolyze, and formation of the metal hydroxides competes at higher pH values. This causes the solubility of P_T to increase once the metal hydroxide begins to precipitate (Figure 16.9a,b). For $AlPO_4$, P_T reaches a minimum of $10^{-5.18}$ M at pH 5.75. For $FePO_4$, P_T reaches a minimum of $10^{-5.7}$ M at pH 4.25. For ease of comparison, the solubility domains of $AlPO_4$ and $FePO_4$ are graphed together in Figure 16.9c. Although Fe^{III} yields lower equilibrium P_T concentrations, its pH range for effective removal is lower, and water treated this way would need to be neutralized by base before release to receiving waters. Coupled with the typically greater cost of $FeCl_3$ compared to alum ($Al_2(SO_4)_3 \cdot 14H_2O$), this factor makes alum the usually preferred chemical for P removal.

Alum also is used to treat lakes directly. The goal in these situations is a long-term decrease in P recycling from the bottom sediments, that is, a decrease in "internal loading" of P, which is achieved by forming a flocculent barrier of aluminum hydroxide on the sediment surface. The barrier prevents P release from the sediment even when the overlying water becomes anoxic. Treatment of lake water with ferric chloride would not produce similar benefits because the ferric hydroxide/ferric phosphate floc would undergo reductive dissolution when the bottom waters became anoxic.

It is important to recognize that the results in Figure 16.9 do not tell the entire story for phosphate removal by alum or ferric chloride because they do not include the effects of the coprecipitating $Al(OH)_3$ or $Fe(OH)_3$ floc. The solid-phase $AlPO_4$ and $FePO_4$ produced in the removal processes consist of very small particles that are not readily removed by gravitational settling. Formation of the metal hydroxide flocs is essential for effective P removal because the fine $AlPO_4$ or $FePO_4$ particles become entrapped in and removed by the settling floc.[57] Sorption of phosphate ions onto the large surface areas of the metal hydroxide flocs also contributes to P removal. Although the exact contributions of sorption and coprecipitation to P removal are difficult to predict, several lines of evidence suggest they are important. First, large excesses in alum or ferric chloride
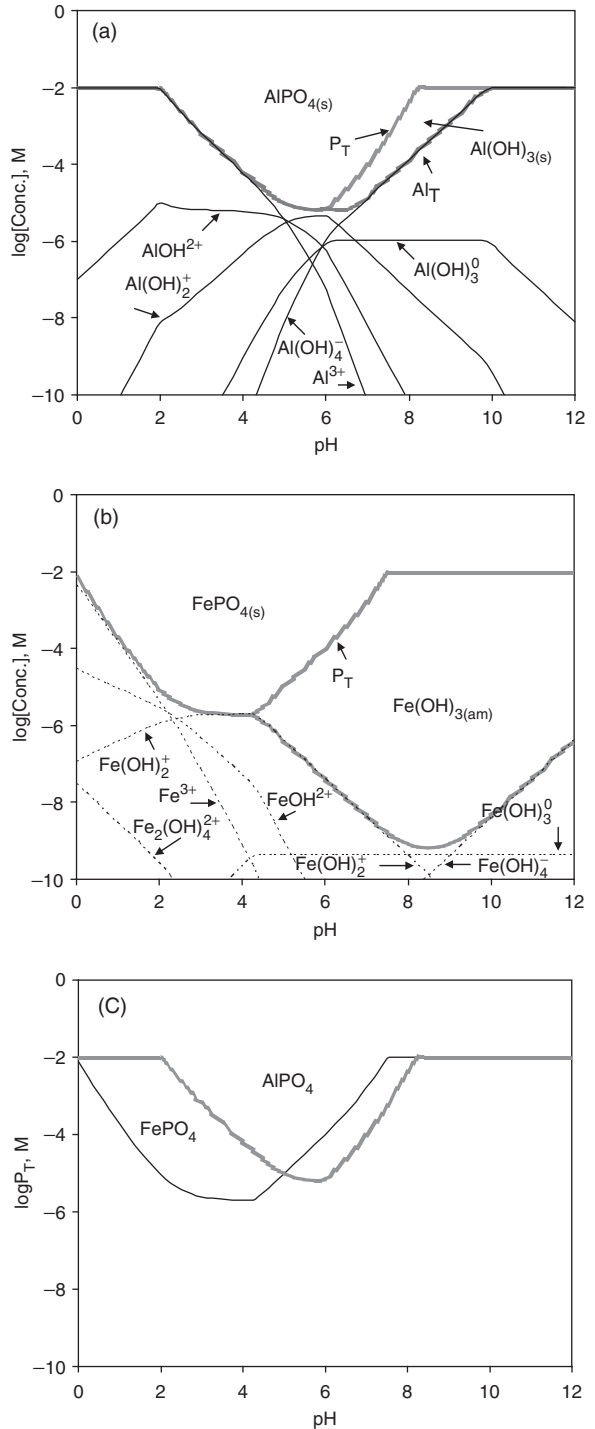
Figure 16.9 (a) Solubility of $AlPO_4$ and amorphous $Al(OH)_3$ versus pH calculated by MINEQL+ for initial Al^{3+} and PO_4^{3-} concentrations of 1×10^{-2} M, showing concentrations of soluble Al complexes; (b) similar plot for $FePO_4$ and amorphous $Fe(OH)_3$; (c) comparison of solubility domains of $AlPO_4$ and $FePO_4$ from graphs in (a) and (b).

(beyond the stoichiometric requirements for formation of the metal phosphates) are needed for effective P removal.[41] Second, P concentrations below those predicted from the solubility of $AlPO_4$ can result when water is treated with alum, pointing to sorption of phosphate ions onto the Al hydroxide floc as an additional removal mechanism.

16.4.3 Struvite: can one mineral control two nutrients?

As noted earlier, nearly all ammonium salts are highly soluble, but struvite, $MgNH_4PO_4$, $pK_{s0} = 11.6$, is an intriguing exception. Could it be used to remove both N and P from wastewater, solving two problems simultaneously? The answer, unfortunately, is no; the mineral is too soluble to achieve N and P reductions to levels needed to control eutrophication in water bodies, as the following analysis shows. Under some circumstances, however, struvite formation can achieve substantial removal of phosphate.[58]

The solubility of struvite depends strongly on pH; all three ions that comprise the mineral undergo acid-base reactions. Because the fraction of P present as PO_4^{3-} increases with pH but the fraction of N present as NH_4^+ decreases as pH rises above pK_a, we can surmise that struvite solubility will have a minimum at an intermediate pH and increase on either side of pH_{min}. Solving the relevant equilibrium relationships to determine pH_{min} manually could be challenging, but as Example 16.1 shows, use of the concept of α (see Section 7.2.5) makes it simple.

EXAMPLE 16.1 Use of α values to evaluate struvite solubility: Construct a diagram for the solubility of struvite as a function of pH and determine the pH of minimum solubility (pH_{min}).

Answer: The concentration-based solubility product for struvite, $^cK_{s0}$, is

(1) $^cK_{s0} = [Mg^{2+}][NH_4^+][PO_4^{3-}]$.

For simplicity we ignore activity corrections, but if ionic strength is constant, these can be embedded in the value of $^cK_{s0}$. Concentrations of all three ions vary with pH: Mg^{2+} hydrolyzes to $MgOH^+$; NH_4^+ dissociates to NH_3; and PO_4^{3-} accepts protons to form HPO_4^{2-}, $H_2PO_4^-$, and H_3PO_4. It is useful to rewrite Eq. (1) in terms of total analytical concentrations, Mg_T, N_T, and P_T by using α relationships:

(2a) $\alpha_{Mg,0} = [Mg^{2+}]/Mg_T = [Mg^{2+}]/([Mg^{2+}] + [MgOH^+])$

or

(2b) $\alpha_{Mg,0} = \dfrac{[H^+]}{[H^+] + K_{1,hyd}}$

(3a) $\alpha_{N,0} = [NH_4^+]/N_T = [NH_4^+]/([NH_4^+] + [NH_3])$

or

(3b) $\alpha_{N,0} = \dfrac{[H^+]}{[H^+] + K_a}$

(4a) $\alpha_{P,3} = \dfrac{[PO_4^{3-}]}{P_T} = \dfrac{[PO_4^{3-}]}{[H_3PO_4] + [H_2PO_4^-] + [HPO_4^{2-}] + [PO_4^{3-}]}$

or

(4b) $\alpha_{P,3} = \dfrac{K_{a1}K_{a2}K_{a3}}{[H^+]^3 + [H^+]^2 K_{a1} + [H^+]K_{a1}K_{a2} + K_{a1}K_{a2}K_{a3}}$

Equation (1) thus becomes

(5) $^c K_{s0} = \alpha_{Mg,0} Mg_T \cdot \alpha_{N,0} N_T \cdot \alpha_{P,3} P_T$,

or

(6) $K' = \dfrac{^c K_{s0}}{\alpha_{Mg,0}\alpha_{N,0}\alpha_{P,3}} = Mg_T \cdot N_T \cdot P_T$

K', the conditional solubility product for struvite, depends on pH because the α values are pH dependent. We can calculate α values at as many pH values as desired by inserting Eqs. 2b, 3b, and 4b in a spreadsheet; values of the constants in the α values are $K_{1,hyd} = 10^{-11.4}$, $K_a = 10^{-9.25}$, $K_{a1} = 10^{-2.15}$, $K_{a2} = 10^{-7.20}$, and $K_{a3} = 10^{-12.38}$. Once the α values are known, we can use Eq. (6) to calculate K' over the pH range of interest and plot the results (see Figure 16.10).

The figure shows that $pH_{min} = 10.25$ for struvite, and K' is 4.11×10^{-10} at this pH; the equilibrium ion product, $Mg_T \cdot N_T \cdot P_T$, cannot go lower than this value. We can compare this value to the ion product for typical concentrations in municipal wastewater (line A, Figure 16.10). If treatment converts all the N and P in raw wastewater (which is largely organic N and P) to ammonium and orthophosphate, then the actual concentration product (ACP) would be 9×10^{-10} M, which is only slightly above saturation. At best, only a small fraction of the initial phosphate and an even smaller fraction of the initial ammonium would precipitate before ACP and K' were equal. Moreover, the pH would need to be close to pH_{min} for precipitation to occur, and because the driving force for precipitation is small, the kinetics of precipitation will be slow.

We could promote precipitation by adding Mg^{2+} to the wastewater, increasing it to 1×10^{-2} M (Figure 16.10, line B). Struvite precipitation now could occur over a broader pH range, but the maximum removal still would occur at pH_{min}. In theory, slightly more

Figure 16.10 Conditional solubility product, $K' = Mg_T \cdot N_T \cdot P_T$, for struvite, $MgNH_4PO_4$, versus pH. Minimum solubility occurs at pH 10.25. Line A: actual concentration product (ACP) for typical wastewater, $Mg_T = 10^{-3}$ M, $N_T = 3 \times 10^{-3}$ M, $P_T = 3 \times 10^{-4}$ M. Line B: ACP for same N_T and P_T but $Mg_T = 10^{-2}$ M. Line C: ACP for sludge digester supernatant, $Mg = 10^{-2}$ M, $N_T = 10^{-2}$ M, $P_T = 3 \times 10^{-3}$ M.
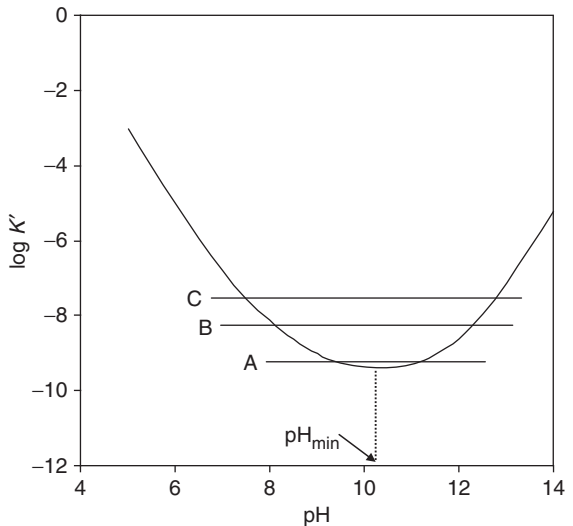
than 90% of the initial P could be removed if the above assumptions held, but because the initial N is $10\times$ the initial P, only a small fraction ($<10\%$) of the N would be removed.

A more favorable situation for N and P removal applies to the supernatant from anaerobic sludge digesters in wastewater treatment facilities, which may have ammonium and phosphate concentrations ten-fold higher than typical raw wastewater (Figure 16.10, line C). Indeed, precipitation in such conditions can produce thick scales of struvite in pipes of such facilities.[57,58]

16.5 Chemical analysis of nutrient forms

16.5.1 Overview

Chemical analysis of nutrients in water is complicated for many reasons. Because concentrations range over several orders of magnitude, even in the same water body at different locations and times of year, methods must be able to cover a *wide range*. Because low concentrations ($< 1\mu$ M) are of interest, methods must have *high sensitivity*. Because of the variability described earlier, sampling must be *frequent*, usually at several locations and depths, to adequately characterize a water body. In addition, nutrient studies must deal with *several inorganic species of N and P*, as well as particulate and dissolved organic forms. The latter factors place a premium on *fast methods* that are easy to perform. Finally, because the chemical *species are labile* (subject to microbial uptake/release and loss to chemical reaction or to container walls), sample preservation also is a problem. These concerns led to the widespread use of automated samplers and automated wet-chemical techniques—autoanalyzers and flow-injection systems—especially for inorganic forms of N and P.

Growing recognition over the past decade of the limitations that current analytical methods pose on understanding the behavior of nutrients in complex aquatic systems, has led to an interest in developing better sensors to measure nutrients in aquatic environments. Of special interest are sensors suitable for continuous (or high frequency) in situ measurements, thus obviating the need for sample collection and preservation. The ideal sensor would be a solid-state device needing no chemical reagents and having the following characteristics: high reliability, high specificity for the analyte (avoiding interferences from other solutes), low cost, large range, low detection limit, rapid response suitable for unattended high-frequency or continuous measurements, low power requirements, and low potential for fouling and drift. Sensors fulfilling all or nearly all these requirements are available for physical characteristics like temperature and conductivity and a few chemical analytes like pH and dissolved oxygen (the optodes described in Section 12.5.3), but such sensors not yet available for any nutrient form. Nonetheless, advances have been made in developing in situ sensors or instruments that meet some of the above ideals, and brief descriptions are included in the following sections.

16.5.2 Inorganic nitrogen

Dissolved ammonium/ammonia is determined commonly by a colorimetric method involving the so-called Berthelot reaction of NH_3 with hypochlorite (OCl^-) and phenol

(1) $NH_3 + OCl^-$ ⟶ $NH_2Cl + OH^-$

(2) NH_2Cl + [benzene ring]—O^- ⟶ O=[ring]=NCl

(3) O=[ring]=NCl + [benzene ring]—O^- ⟶

O=[ring]=N—[ring]—O^-

Indophenol blue, $\lambda_{max} = 630$ nm
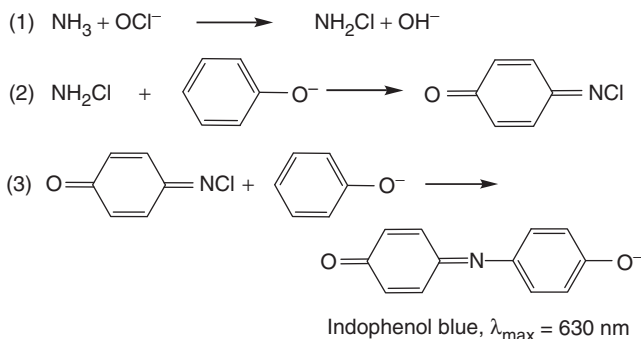
Figure 16.11 Indophenol reaction for analysis of ammonium in water.

at pH $\sim$11 to form an intensely blue-colored indophenol (Figure 16.11).[59,60] The method has a low detection limit (< 1 μM) and wide range. The method has been known since the nineteenth century, but refinements made $\sim$30 years ago[59] improved its reliability. Ammonium also can be measured by a potentiometric electrode method in which the pH is raised to $\sim$11. This converts the NH_4^+ to NH_3, which diffuses across a semipermeable membrane enclosing a pH-sensing electrode.[60] The NH_3 raises the solution pH inside the membrane. The method can detect ammonium over a wide range (0.01–100 mg/L as N or $\sim$10^{-6}–10^{-2} M) and has potential for use in continuous monitoring systems. Currently, it is not widely used because of reliability and precision issues. Older wet-chemical methods for ammonium involve distillation from samples at alkaline pH into boric acid and measurement by acid-base titration or colorimetric analysis.[60] Although these methods have adequate accuracy and sensitivity, they are slow and require large sample volumes.

A highly reliable and sensitive colorimetric method is available for nitrite, ironically the least important inorganic N form. With a detection limit of $\sim$1 μg/L as N, the method involves the reaction of HNO_2 formed from NO_2^- at low pH with sulfanilamide to produce a diazonium salt that reacts with N-(1-naphthyl)-ethylenediamine dihydrochloride at pH 2.0–2.5 to form a reddish-purple diazo dye (Figure 16.12).[60] Many methods for nitrate analysis are based on the reduction of NO_3^- to NO_2^- by passing a sample through a column of metal filings (e.g., Cd or amalgamated Cd filings).[60] The resulting NO_2^- is analyzed by the above reaction. In routine studies, nitrite usually is not measured separately because it is such a minor component of the inorganic N pool, but the sum nitrate + nitrite-N is measured. Several potentiometric (ion-selective) electrodes are available for nitrate,[60] but they have relatively poor sensitivity (detection limit $\sim$10^{-5} M) and some interferences from other common ions. They can be used where nitrate levels are high, e.g., agricultural drainage waters. The chemistry of nitrate (low reactivity, weakness as a ligand) would appear to limit the prospects that nitrate ion-selective electrodes can be developed into reliable sensors for the low levels (10^{-7} to 10^{-5} M) found in many natural waters.

Nitrate has a strong and relatively narrow absorption maximum in the low UV range ($\lambda_{max} = 213$ nm), offering a potential for measurement by UV spectrophotometry.
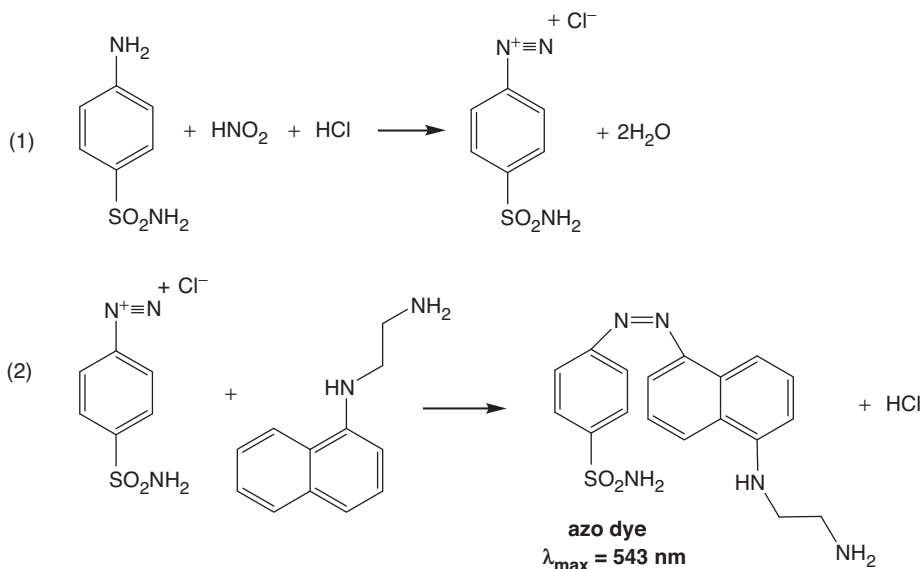
Figure 16.12 Sequence for analysis of nitrite by diazotization reaction to form a red azo dye.

Unfortunately, NOM and especially humic materials strongly absorb light broadly over the UV range. In the past this restricted the usefulness of the method to waters with very low dissolved organic carbon (DOC) concentrations. UV nitrate sensors have been developed that provide high-frequency measurements on coastal waters and agricultural drainage waters.[61] Because the UV spectrum for NOM absorbance generally is a simple exponential function of wavelength, it is possible to develop algorithms to correct for NOM absorbance at 213 nm by measuring its absorbance at higher wavelengths (where NO_3^- does not absorb light).[62]

Finally, nitrate can be measured along with the major and minor anions, Cl^-, SO_4^{2-}, and F^-, by ion chromatography (IC). This method has several advantages: it requires little or no sample preparation and reagents and provides data simultaneously on all the above ions. The detection limit for nitrate by IC ($\sim$0.01 mg/L as N) is adequate for most routine studies on streams and rainfall, but for studies on nitrogen cycle dynamics in oligotrophic systems, detection limits need to be about a factor of 10 lower. Because very high concentrations of anions in seawater require sample dilution for analysis by IC, the method does not have the sensitivity needed for marine samples.

16.5.3 Organic N and P

In routine studies only the total organic N is measured, and specific organic N compounds are not measured individually. Samples may be filtered, typically through 0.4–0.7 μm pore-size glass fiber or membrane filters, and organic N can be measured on the operationally defined particulate and dissolved fractions. For many decades, the *Kjeldahl* method, which dates back to the mid-nineteenth century, was the standard for organic

N analysis.[60] This involved digesting samples containing concentrated H_2SO_4, a salt (K_2SO_4) added to raise the boiling point of the acid, and a catalyst of selenium, mercury or copper. After the water was removed by boiling, the temperature of the concentrated acid increased enough to hydrolyze and oxidize the organic matter, releasing organic N as NH_4^+. After addition of alkali (NaOH), the NH_3 was distilled from the digestate and analyzed by titration or colorimetry. If NH_4^+ was not distilled from the sample before digestion, the NH_4^+ measured after digestion was the sum of the organic N plus the original NH_4^+, which was called ***total Kjeldahl nitrogen***. There are many shortcomings to the Kjeldahl method, including the large consumption of toxic and hazardous reagents, its time-consuming nature, involving many steps that provide opportunities for error, and low sensitivity. Although Kjeldahl analysis can give satisfactory results on samples with high organic N concentrations, such as wastewater and sediment samples, it is not well suited for analysis of most natural waters.

A much better technique involves oxidation by alkaline persulfate, which converts all the nitrogen in a sample to nitrate.[60,63] Samples are autoclaved, and the nitrate formed from the organic N and ammonium can be analyzed by ion chromatography or the Cd reduction/diazotization method described above. An advantage of the alkaline persulfate method for TN is that the same autoclaved sample can be used for analysis of TP.[64]

16.5.4 Orthophosphate

The most widely used method for orthophosphate in water is the Murphy-Riley[65] single-reagent, ascorbic acid version of the "molybdenum blue" spectrophotometric procedure. Under acidic conditions orthophosphate reacts with ammonium molybdate to form a yellow phosphomolybdate complex that is reduced by stannous chloride or ascorbic acid to a heteropoly-molybdenum blue (HMB) complex:

$$H_3PO_4 + 12(NH_4)_2MoO_4 + 2H^+ \rightarrow (NH_4)_3PO_4 \cdot 12MoO_3 + 21NH_4^+ + 12H_2O$$

<div align="center">yellow</div>

$$(16.1)$$

$$(NH_4)_3PO_4 \cdot 12MoO_3 + \text{reducing agent} \rightarrow \text{molybdenum blue complex}$$

<div align="center">blue$-$purple; $\lambda(max) = 690$ and 800 nm</div>

$$(16.2)$$
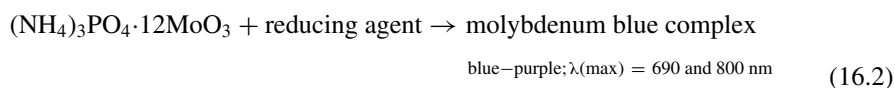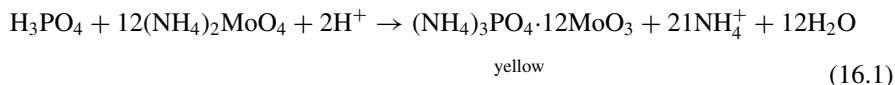
The yellow phosphomolybdate complex can be used to measure high concentrations of P (> 10 mg/L), but because natural water concentrations are much lower, the reduction step almost always is done. The existence of HMB complexes has been known since the late eighteenth century, but the complete structures of these very large and unusual complexes were elucidated only in the past 20 years.[66,67] Called "big wheel" structures, HMBs are nanostructures with an external diameter of 3.8 nm (Figure 16.13) comprising 14 units, each with 11 Mo atoms, and a formula of $Mo_{154}O_{462}H_{14}(H_2O)_{70}^{14-}$, not including the hetero-atoms (in this case, phosphate). The HMBs contain more than 700 atoms and have a molecular mass $> 24,000$ Da. The nature of the HMBs produced with orthophosphate depends on the nature of the reducing agent. Stannous chloride produces complexes with an unstable color, but ascorbic acid, in combination with a small amount of antimonyl tartrate, produces stable complexes with a 1:1 ratio of Sb:P in the complex. The blue-purple color is very intense, and the detection limit using a 5-cm light path is ~1 µg/L as P or ~0.03 µM.[60]
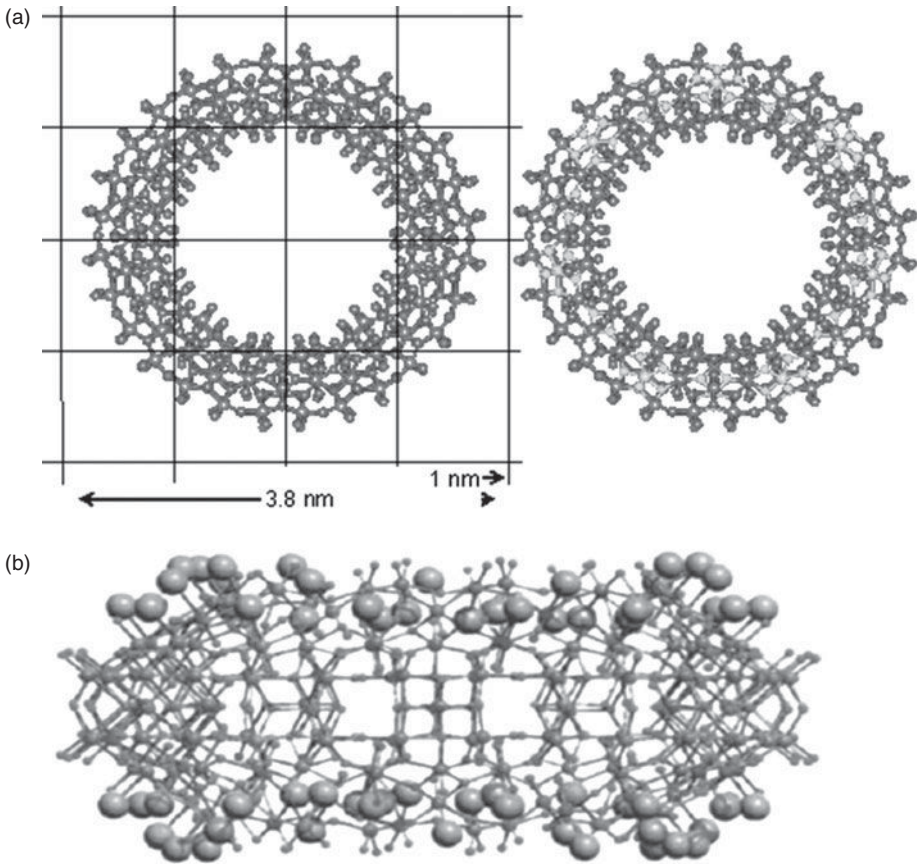
Figure 16.13 (a) Structure of the torus-shaped, nano-sized molybdenum blue complex. The 14 pentagonal (Mo)Mo$_5$ groups, highlighted in light gray on the right, alternate between the two sides of the wheel (seven on each side). From http://www.lsbu.ac.uk/water/giant.html; original authors: Müller et al.[67] (b) Side view of molybdenum blue complex. From Müller et al.,[66] copyright Wiley-VCH Verlag GmbH & Co. KGaA, reproduced with permission. (See color insert at end of book for a color version of this figure.)

Because the acid molybdate reagent may desorb P from suspended matter, samples are filtered before analysis. Also, some labile organic P compounds may be hydrolyzed to yield orthophosphate under the low-pH conditions of the analysis.[68] Consequently, in water quality studies the results usually are called "soluble reactive phosphate" (SRP) rather than orthophosphate. Hydrolysis of labile P, however, is not thought to be important except at low orthophosphate concentrations (near the detection limits). Arsenate interferes stoichiometrically in the analysis of SRP, and this has caused problems in past studies of phosphate in lake waters.[69] The interference can be removed by reducing arsenate to arsenite by adding sulfite before starting the analysis. Silica reacts similarly with ammonium molybdate, but it does not interfere in the analysis of phosphate because its reaction with molybdate requires a higher pH ($\sim$1) than phosphate

does (pH = 0.45). Interference of phosphate in the analysis of silica is removed by adding oxalic acid, which destroys the phosphomolybdate complex but does not affect the silicomolybdate complex.[60]

Solid-state ion-selective electrodes for phosphate have been described based on cobalt phosphate and aluminum phosphate sensing membranes.[70] The devices have detection limits of 10^{-6}–10^{-5} M, which is too high for use on most lakes and streams, where orthophosphate often is in the 10–100 nM range, but they have been used in studies on phosphate removal from wastewater.[71] Microelectrode versions, including MEMS devices (electrodes "on a chip") have been developed but are not yet commercially available.

Problems

16.1. Based on the solubility data for N_2 in Table 16.2, is $\Delta H°$ for the phase transfer constant with temperature or temperature dependent? Is the reaction endothermic or exothermic? Estimate the enthalpy of reaction at 25°C.

16.2. A eutrophic lake is treated with alum to lower its phosphorus concentration and provide a barrier to decrease phosphorus recycling from the bottom sediment. The Al is added as alum ($Al_2(SO_4)_3 \cdot 14H_2O$) at a dose of 8.0 mg/L as Al.

    (a) Write balanced chemical equations for the reactions that happens when the alum is added (as a slurry) to lake water to produce aluminum hydroxide and aluminum phosphate.

    (b) If a lake has a moderate alkalinity of 60 mg/L as $CaCO_3$, what would the resulting alkalinity and pH be as a result of adding alum to the lake water at the above dose if the lake acted as a closed system? Would you expect there to be a problem with treating the lake by this method?

16.3. (a) Sketch a pC-pH diagram for 1×10^{-4} M phosphorous acid (H_3PO_3) over the pH range of 0–9.

    (b) Show the acid-base speciation of the three main inorganic N forms—ammonium/ammonia, nitrite, nitrate—and orthophosphate on one pC-pH diagram over the pH range of 1–13. Assume $N_T = 1 \times 10^{-3}$ in each case and $P_T = 10^{-4}$ M.

16.4. Typical municipal wastewater has TN and TP concentrations of ~40 and ~6 mg/L, respectively, and the carbonaceous biochemical oxygen demand (BOD) is roughly 250 mg/L. If you assume that the organic matter causing the BOD has an oxidation state equivalent to carbohydrates, estimate the TOC concentration and compare the C:N:P ratio of typical wastewater to the Redfield ratio.

16.5. (a) Write the balanced chemical reaction for the following nitrogen cycle reactions:

      (i) nitrification of ammonium to nitrite using molecular oxygen
     (ii) nitrification of nitrite to nitrate using molecular oxygen
   (iii) denitrification of nitrate to N_2 using succinic acid (see Figure 6.10 for structure) as the carbon/energy source

(b) If a wastewater effluent has an ammonium concentration of 12 mg/L as N, what is its nitrogenous BOD; that is, how much O_2 (in mg/L) would be required to oxidize the ammonium to nitrate?

16.6. Mg^{2+} can form the mineral struvite, $MgNH_4PO_4$, $K_{s0} = 10^{-12.4}$, in water with high concentrations of ammonium and phosphate. Anaerobic sludge digesters can reach ammonium and phosphate concentrations high enough to precipitate struvite in pipes draining sludge digesters, sometimes leading to a build-up of scale and causing flow restrictions. Consider an anaerobic sludge liquor with an ionic strength $= 0.01$ containing the following concentrations: $Mg_T = 120$ mg/L (as Mg); ammonium (N_T) $= 125$ mg/L as N; and phosphate (P_T) $= 50$ mg/L as P.

(a) Determine the pH range over which the solution is supersaturated with respect to struvite, i.e., the pH range over which the ion product,
IP $= [Mg^{2+}][NH_4^+][PO_4^{3-}]$, $>^c K_{s0}$.
(b) Determine the pH of minimum solubility of struvite.
(c) Determine how much (what percentage) of the initial phosphorus and nitrogen could precipitate from the sludge liquor at the pH of minimum solubility.

Notes: (1) This problem could be solved manually using α values, as described in Example 16.1, but you should use MINEQL+ or an alternative computer equilibrium program in multi-run mode. Evaluate saturation conditions over the pH range of 4.0–13.0 including the correction for ionic strength.

(2) MINEQL+ does not have a value of K_{s0} for struvite in its database. You need to insert this and the stoichiometry of the solid by clicking the "dissolved solids" button on the "tableau switch" menu that appears after closing the tableau for Type II-Aqueous Species. Recall that K values in MINEQL+ are formation constants. The formation constant for struvite is log $K = 12.4$.

(3) You can determine the pH range in which struvite solubility is exceeded by examining the column for struvite in any of component groups for Mg^{2+}, NH_4^+, or PO_4^{3-}, and finding when the log concentration reaches zero (activity $= 1$).

16.7. Lake Apopka is a shallow, hypereutrophic lake near Orlando in central Florida. A major water source for the lake is Apopka Spring, which supplies calcareous Floridan Aquifer water from a dolomitic limestone formation, on the SW side of the lake (see Table 2.3 for water chemistry data on the spring). Based on an analysis of water from the spring "boil" (i.e., the source water as it emerges from the aquifer), which yielded a total dissolved P concentration of ~100 μg/L (as P), some limnologists have concluded that the spring is a significant source of phosphorus to the lake. Uncertainty exists about the validity of this estimate because water from the boil could have been mixed ("contaminated") with P-rich water from the lake. Based on the data in Table 2.3, estimate the total dissolved inorganic P concentration that the spring water would have if it were in equilibrium with hydroxyapatite ($Ca_5(PO_4)_3OH$, $K_{s0} = 10^{-44.33}$). What would the equilibrium concentration in the spring water be if the water were at pH 8.3? How do your answers agree with the measured concentration? What explanations can you offer for the difference?

Note: To solve this problem, you can use a manual algebraic approach or MINEQL+. In either case, you should correct for ionic strength. If you use MINEQL+, make calcite and aragonite Type VI species to prevent their precipitation. You do not know the exact concentration of PO_4^{3-} to add as the component in this problem, but all you need is to add enough to exceed the solubility of hydroxyapatite. Adding an amount in the range of the state-reported concentration of total dissolved P, the problem will work. The amount of Ca^{2+} in the water is in great excess compared with P that the little amount lost by precipitation as hydroxyapatite will not materially change the equilibrium concentration of Ca^{2+} in the lake (i.e., the amount you add in the problem definition). Alternatively, you can make hydroxyapatite a fixed (Type III) species and then you do not need to impose an initial concentration of phosphorus.

16.8. Before the wastewater treatment plant for the cities of Minneapolis-St. Paul, Minnesota, began to nitrify its effluent, total dissolved ammonium concentrations in the Mississippi River downstream of the plant frequently exceeded 1 mg/L as N. Depending on pH, this could cause the water to exceed the state water quality standard for un-ionized ammonia (NH_3), which is 0.02 mg/L as N. If the river water had a temperature of 25°C, a pH of 7.0, and a total ammonium concentration of 1.0 mg/L as N, and an ionic strength of 4×10^{-3}, would the un-ionized ammonia standard be exceeded? What if the pH instead were 8.0?

16.9. The purpose of the following exercise is to introduce you to online databases for water chemistry and do a brief analysis of water chemistry trends. The assignment is intentionally open-ended. The example used here is the effect of wastewater treatment on nitrogen forms and concentrations in the Mississippi River downriver of the outfall for the main treatment plant for Minneapolis-St. Paul, Minnesota. The Metro plant started to nitrify its effluent in the late 1980s to avoid dissolved oxygen problems in the river from the nitrogenous BOD of high ammonium inputs and to avoid violations of the un-ionized ammonia standard (see previous problem). Instructors may wish to substitute a local site with a similar water quality problem.

One of the most extensive databases for water quality and chemistry data for U.S. waters is maintained by the U.S. Geological Survey (http://waterdata.usgs.gov/nwis). In addition to providing real-time stage and flow data on many streams and other continuous measurements, the site provides historical information on water chemistry for more than 370,000 sites across the country. To find chemistry data for a given water body, click the "water quality" button on the home page and the "field/lab samples" button on the next page. To find the sites on a water body with data, check "state/territory" under site location list and "site name" under the site identifier list on this page and hit submit. On the resulting pull-down menu and type "Mississippi River" in the site name box. Submitting this request gives a page listing 76 Mississippi River sites with data. Scroll the list to the Nininger site (05331570) and request the data for it. Nininger is the closest U.S. Geological Survey site (~13 km) downriver from the Minneapolis-St. Paul treatment plant outfall with nutrient data. It is just upriver from Spring Lake, an impoundment formed by Lock and Dam #2 near Hastings, Minnesota.

Retrieve the data by clicking the button for "Table of data (default attributes)" and submit, which retrieves all data for the period of record. Examine the file to get an idea for the range of variables and measurement frequencies over time. Focus on the columns for nitrogen species. There are two for "ammonia" (00608 and 00610) and two for nitrate (00618 and 00620), which differ only in that one set was for filtered samples and the other for unfiltered samples. Here you can ignore the distinction and assume that the two columns labeled "ammonia" are valid measures of total ammonium plus ammonia-N ($NH_4^+ - N + NH_3 - N$) and the two for nitrate are equally valid measures of nitrate concentrations (expressed as N). Menu-driven instructions in the web site help extract the columns of interest, save them and export them to a separate spreadsheet. You may wish to combine the two columns for each N species in the separate spreadsheet and plot the data to show temporal trends. You should write a page of text describing what you find upon inspecting the data. Is there any indication of lower ammonium or higher nitrate concentrations over time? Comment of the frequency of the sample collection over time and why you think it has changed. Procedures for using the Web site are reasonably straightforward, but you should not expect to get everything correct the first time you try! Also, Web site formats change frequently, and the above instructions may not fit exactly to the Web site in the future.

References

1. National Research Council. 1978. Nitrates: an environmental assessment. Panel report, National Academy of Sciences, Washington, D.C.
2. Hutchinson, G. E. 1944. Nitrogen in the biogeochemistry of the atmosphere. *Amer. Scient.* **32**: 178–195.
3. Söderlund, R., and B. H. Svensson. 1976. The global nitrogen cycle. In *Nitrogen, phosphorus and sulfur—global cycles*, B. H. Svensson and R. Söderlund (eds.), SCOPE Rept. **7**, Ecol. Bull., Stockholm, 23–73.
4. Vitousek, P. M., et al. 1997. Human alteration of the global nitrogen cycle: sources and consequences. *Ecol. Appl.* **7**: 737–750.
5. Gruber, N., and J. N. Galloway. 2008. An Earth-system perspective of the global nitrogen cycle. *Nature* **451**: 293–296.
6. Galloway, J. N., J. D. Aber, J. W. Erisman, S. P. Seitzinger, R. W. Howarth, E. B. Cowling, and B. J. Crosby. 2003. The nitrogen cascade. *BioScience* **53**: 341–356.
7. Baker, L. A. D. Hope, Y. Xu, J. Edmonds, and L. Lauver. 2001. Nitrogen mass balance for central Arizona-Phoenix (CAP ecosystem). *Ecosystems* **4**: 582–602.
8. Sampson, C. J., and P. L. Brezonik. 2003. Responses of nutrients to experimental acidification and recovery in Little Rock Lake, USA. *Water Air Soil Pollut.* **142**: 39–57.
9. Brezonik, P. L., and G. F. Lee. 1968. Denitrification as a nitrogen sink in Lake Mendota, Wis. *Environ. Sci. Technol.* **2**: 120–125.
10. Dugdale, V. A., and R. C. Dugdale. 1965. Nitrogen metabolism in lakes. III. Tracer studies of the assimilation of inorganic nitrogen sources. *Limnol. Oceanogr.* **10**: 53–57.
11. Rakestraw, N., and A. Hollaender. 1936. Photochemical oxidation of ammonia in sea water. *Science* **84**: 442–443.
12. Hoigne, J., and H. Bader. 1978. Ozonation of water: kinetics of oxidation of ammonia by ozone and hydroxyl radicals. *Environ. Sci. Technol.* **12**: 79–84.

13. Weiss, R. F. 1970. The solubility of nitrogen, oxygen and argon in water and seawater. *Deep-Sea Res.* **17**: 721–735.

14. Benson, B. B., and P. D. M. Parker. 1961. Nitrogen/argon and nitrogen isotope ratios in aerobic sea water. *Deep-Sea Res.* **7**: 237–253; Richards, F. A., and B. B. Benson. 1961. Nitrogen/argon and nitrogen isotope ratios in two anaerobic environments, the Cariaco Trench in the Caribbean Sea and Dramsfjord, Norway. *Deep-Sea Res.* **7**: 254–264; Eyre, B. D., S. Rysgaard, T. Dalsgaard, and P. B. Christensen. 2002. Comparison of isotope pairing and N_2:Ar methods for measuring sediment denitrification. *Estuar. Coasts* **25**: 1077–1187.

15. Yoshinari, T., and R. Knowles. 1976. Acetylene inhibition of nitrous oxide reduction by denitrifying bacteria. *Biochem. Biophys. Res. Comm.* **69**: 705–710.

16. Messer, J. J., and P. L. Brezonik. 1983. Comparison of denitrification rate estimation techniques in a large, shallow lake. *Water Res.* **17**: 631–640.

17. Hobbs, P. V. 2000. *Introduction to atmospheric chemistry: a companion text to basic physical chemistry for the atmospheric sciences*, Cambridge Univ. Press, Cambridge.

18. Coss, A., K. P. Cantor, J. S. Reif, C. F. Lynch, and M. H. Ward. 2004. Pancreatic cancer and drinking water and dietary sources of nitrate and nitrite. *Am. J. Epidemiol.* **159**: 693–701.

19. Peterson, W. H., E. B. Fred, and B. H. Domgalla. 1925. The occurrence of amino acids and other organic nitrogen compounds in lake water. *J. Biol. Chem.* **43**: 287–295; Domogalla, B. P., C. Juday, and W. H. Peterson. 1925. The forms of nitrogen in certain lake waters. *J. Biol. Chem.* **43**: 269–285.

20. Aluwihare, L. I., D. J. Repeta, S. Pantoja, and C. G. Johnson. 2005. Two chemically distinct pools of organic nitrogen accumulate in the ocean. *Science* **308**: 1007–1010.

21. Gardner, W. S., and G. F. Lee. 1975. The role of amino acids in the nitrogen cycle of Lake Mendota. *Limnol. Oceanogr.* **20**: 379–388.

22. Burnison, B. K., and R. Y. Morita. 1974. Heterotrophic potential for amino acid uptake in a naturally eutrophic lake. *Appl. Microbiol.* **27**: 488–495.

23. Tranvik, L. J., and N. O. G. Jørgensen. 1995. Colloidal and dissolved organic matter in lake water: carbohydrate and amino acid composition and ability to support bacterial growth. *Biogeochem.* **30**: 77–97.

24. Tuschall, J. R., and P. L. Brezonik. 1980. Characterization of organic nitrogen in natural waters: its molecular size, protein content, and interactions with heavy metals. *Limnol. Oceanogr.* **25**: 495–504.

25. Hobbie, J. E., C. C. Crawford, and K. L. Webb. 1968. Amino acid flux in an estuary. *Science* **159**: 1463–1464.

26. Clesceri, N. L., and G. F. Lee. 1965. Hydrolysis of condensed phosphates. I. Non-sterile environment; II. Sterile environment. *Int. J. Air Water Poll.* **9**: 723–742; 743–751.

27. Francko, D. A., and R. T. Heath. 1979. Functionally distinct classes of complex phosphorus compounds in lake water. *Limnol. Oceanogr.* **24**: 463–473.

28. Monbet, P., I. E. McKelvie, A. Saefumillah, and P. J. Worsfold. 2007. A protocol to assess the enzymatic release of dissolved organic phosphorus in waters species under environmentally relevant conditions. *Environ. Sci. Technol.* **41**: 7479–7485.

29. Herbes, S. E., H. E. Allen, and K. H. Mancy. 1975. Enzymatic characterization of soluble organic phosphorus in lake water. *Science* **187**: 432–434.

30. Cade-Menun, B. J., J. A. Navaratnam, and M. R. Walbridge. 2006. Characterizing dissolved and particulate phosphorus in water with ^{31}P nuclear magnetic resonance spectroscopy. *Environ. Sci. Technol.* **40**: 7874–7880.

31. Harrison, A. F. 1987. *Soil organic phosphorus. A review of the world literature*, CAB International, Oxford, UK.

32. Turner, B. L., M. J. Papházy, P. M. Haygarth, and I. D. Mckelvie. 2002. Inositol phosphates in the environment. *Phil. Trans. R. Soc. Lond. B* 2002 **357**: 449–469.

33. Costello, A. J., T. Glonek, and T. C. Myers. 1976. ^{31}P nuclear magnetic resonance-pH titrations of *myo*-inositol hexaphosphate. *Carbohydr. Res.* **46**: 159–171.

34. Weimer, W. C., and D. E. Armstrong. 1979. Naturally occurring organic phosphorus compounds in aquatic plants. *Environ. Sci. Technol.* **13**: 826–829.

35. Sommers, L. E., R. F. Harris, J. D. H. Williams, D. E. Armstrong, and J. K. Syers. 1972. Fractionation of organic phosphorus in lake sediments. *Soil Sci. Soc. Am. Proc.* **36**: 51–54.

36. Chang, S. C., and M. L. Jackson. 1957. Fractionation of soil phosphorus. *Soil Sci.* **84**: 133–144.

37. Peterson, G. W., and R. B. Corey. 1966. A modified Chang and Jackson procedure for routine fractionation of inorganic soil phosphates. *Soil Sci. Soc. Amer. Proc.* **30**: 563–565.

38. Sharpley, A. N., and S. J. Smith. 1985. Fractionation of inorganic and organic phosphorus in virgin and cultivated soils. *Soil Sci. Soc. Amer. J.* **49**: 127–130.

39. Williams, J. D. H., J. K. Syers, R. F. Harris, and D. F. Armstrong. 1971. Fractionation of inorganic phosphate in calcareous lake sediments. *Soil Sci. Soc. Amer. Proc.* **35**: 250–255.

40. Psenner, R., B. Bostrom, M. Dinka, K. Petterson, R. Puckso, and M. Sager. 1988. Fractionation of phosphorus in suspended matter and sediment. *Arch. Hydrobiol. Suppl.* **30**: 98–103.

41. Pilgrim, K. M., B. J. Huser, and P. L. Brezonik. 2007. A method for comparative evaluation of whole-lake and inflow alum treatment. *Water Res.* **41**: 1215–1224.

42. Fang, F. P. L. Brezonik, D. Mulla, and L. K. Hatch. 2005. Characterization of soil algal bioavailable phosphorus in the Minnesota River Basin. *Soil Sci. Soc. Amer. J.* **69**: 1016–1025.

43. Nurnberg, G. K. 1988. Prediction of phosphorus release rates from total and reductant-soluble phosphorus in anoxic lake sediments. *Can. J. Fish. Aquat. Sci.* **45**: 453–462.

44. Rydin, E., and E. B. Welch. 1999. Dosing alum to Wisconsin lake sediments based on in vitro formation of aluminum bound phosphate. *Lake Reserv. Manage.* **15**: 324–331.

45. Rydin, E., B. Huser, and E. B. Welch. 2000. Amount of phosphorus inactivated by alum treatments in Washington lakes. *Limnol. Oceanogr.* **45**: 226–230.

46. Sims, J. T. 1993. Environmental soil testing for phosphorus. *J. Prod. Agric.* **6**: 501–507.

47. Mehlich, A. 1984. Mehlich 3 soil test extractant: a modification of Mehlich 2 extractant. *Commun. Soil Sci. Plant Anal.* **15**: 1409–1416.

48. Olsen, S. R., C. V. Col, F. S. Watanabe, and L. A. Dean. 1954. Estimation of available phosphorus in soils by extraction with sodium bicarbonate, USDA Circ. 939, U.S. Government Printing Office, Washington, D.C.

49. Sharpley, A. N., W. W. Troeger, and S. J. Smith. 1991. The measurement of bioavailable phosphorus in agricultural runoff. *J. Environ. Qual.* **20**: 235–238.

50. Wier, D. R., S. H. Chien, and C. A. Black. 1972. Transformation of hydroxyapatite to fluorapatite. *Soil Sci. Soc. Am. J.* **36**: 285–288.

51. Redfield, A. C. 1934. On the proportions of organic derivatives in sea water and their relation to the composition of plankton. In *James Johnstone Memorial Volume*, R. J. Daniel (ed.), Liverpool Univ. Press, Liverpool, 176–192.

52. Falkowski, P. G., and C. S. Davis. 2004. Natural proportions. *Nature* **431**: 131.

53. Baker, L. A., P. L. Brezonik, and C. R. Kratzer. 1981. Nutrient loading-trophic state relationships in Florida lakes, Publ. 56, Wat. Res. Res. Ctr., Univ. of Florida, Gainesville.

54. Sterner, R. W., and J. J. Elser. 2002. *Ecological stoichiometry: the biology of the elements from molecules to the biosphere*, Princeton Univ. Press, Princeton, N.J.

55. Sincero, A. P., and G. A. Sincero. 2003. *Physical-chemical wastewater treatment*, CRC Press, Boca Raton, Fla.

56. Mino, T., M. C. van Loosdrecht, and J. J. Heijnen. 1998. Microbiology and biochemistry of the enhanced biological phosphate removal process. *Water Res.* **32**: 3193–3207.

57. Snoeyink, V. L., and D. Jenkins. 1980. *Water chemistry*, J. Wiley & Sons, New York.

58. Le Corre, K. S., E. Valsami-Jones, P. Hobbs, and S. A. Parsons. 2009. Phosphorus recovery from wastewater by struvite crystallization: a review. *Crit. Rev. Environ. Sci. Technol.* **39**: 433–477.

59. Solorzano, L. 1969. Determination of ammonia in natural waters by the phenolhypochlorite method. *Limnol. Oceanogr.* **14**: 799–801.

60. Eaton, A. D., L. S. Clesceri, E. W. Rice, and A. E. Greenberg (eds.). 2005. *Standard methods for the examination of water & wastewater*, 21st ed. Amer. Pub. Health Assoc., Amer. Water Works Assoc., Water Environ. Fed., Washington, D.C.

61. Finch, M. S., D. J. Hydes, C. H. Clayson, B. Weigl, J. Dakin, and P. G. William. 1998. A low power ultraviolet spectrophotometer for measurement of nitrate in seawater: introduction, calibration and initial sea trials. *Anal. Chim. Acta* **377**: 167–177.

62. Crumpton, W. G., T. M. Isenhard, and P. D. Mitchell. 1992. Nitrate and organic N analyses with second-derivative spectroscopy. *Limnol. Oceanogr.* **37**: 907–913.

63. D'Elia, C. F., P. A. Steudler, and N. Corwin. 1977. Determination of total nitrogen in aqueous samples using persulfate digestion. *Limnol. Oceanogr.* **22**: 760.

64. Valderrama, J. C. 1981. The simultaneous determination of total nitrogen and total phosphorus in water using peroxodisulfate oxidation. *Water Res.* **17**: 1721–1726.

65. Murphy, J., and J. P. Riley. 1962. A modified single solution method for the determination of phosphate in natural waters. *Anal. Chim. Acta* **27**: 31–36.

66. Müller, A., J. Meyer, E. Krickemeyer, and E. Diemann. 1996. Molybdenum blue: a 200 year old mystery unveiled. *Angew. Chem. Int. Ed. Engl.* **35**: 1206–1208.

67. Müller, A., S. K. Das, V. P. Fedin, E. Krickemeyer, C. Beugholt, H. Bögge, M. Schmidtmann, and B. Hauptfleisch. 1999. Rapid and simple isolation of the crystalline molybdenum-blue compounds with discrete and linked nanosized ring-shaped anions. *Z. Anorg. Allg. Chem.* **625**: 1187–1192.

68. Rigler, F. 1968. Further observations inconsistent with the hypothesis that the molybdenum blue method measures orthophosphate in lake water. *Limnol. Oceanogr.* **13**: 7–13.

69. Goulden, P., and P. J. Brooksbank. 1974. Automated phosphate analysis in the presence of arsenic. *Limnol. Oceanogr.* **19**: 704–707.

70. Xiao, D., H. Y. Yuan, and R. Q. Yu. 1995. Surface-modified cobalt-based sensor as a phosphate-sensitive electrode. *Anal. Chem.* **67**: 288–291.

71. Wang, J. J., and P. D. Bishop. 2005. Development of a phosphate ion-selective microelectrode and its use in the enhanced biological phosphorus removal (EBPR) process. *Environ. Technol.* **26**: 381–388.

17

█ Fundamentals of Photochemistry and Some Applications in Aquatic Systems

█ Objectives and scope

This chapter describes the basic physical and chemical processes involved in photochemistry, including both direct and indirect photochemical reactions in natural waters and engineered systems. The kinetics of both kinds of photochemical reactions is summarized along with the main factors affecting the quantity and spectral quality of light at the water surface and within water bodies. The chemistry of important reactive photo-intermediates is summarized, and we briefly describe some important photochemical reactions of dissolved inorganic substances in aquatic systems. Finally, the basic model for semiconductor photochemical reactions is presented, along with potential applications of such reactions in water and wastewater treatment.

█ Key terms and concepts

- Photophysical and photochemical processes, direct and indirect photolysis, quantum yield
- Sensitizing agents (sensitizers), receptors, scavenging agents and probes
- Inorganic photo-intermediates: singlet oxygen, hydroxyl radical, superoxide radical anion, hydrated electron (e_{aq}^-)
- Beam and diffuse attenuation coefficients
- Fenton's reagent
- Ligand-to-metal charge transfer (LMCT) mechanisms
- Semiconductor photochemistry, e^-/h^+ formation, valence band and conduction band, band gap energy

17.1 Introduction: importance of photochemical processes

Aquatic photochemistry is a relatively new part of the field of water chemistry.[1] Early papers on this topic date to the mid-1970s, but most of our knowledge on this topic dates from the 1980s and more recent decades. Although the importance of photochemical reactions in aquatic systems is still a work in progress, we do know that these processes are important in breaking down petroleum and crude oil present in water from spills and leaks. Also, many otherwise refractory organic contaminants that absorb visible or UV light are degraded in aquatic systems by photochemical reactions. Natural organic matter (NOM), especially aquatic humus, undergoes photochemical transformations, and this is an important part of the global carbon cycle. Additionally, photochemical breakdown of organic matter leads to release of nutrients (e.g., ammonium).[2] NOM also serves as a ***sensitizing agent*** for indirect photochemical reactions in freshwater systems. The process of sensitization involves the formation of highly reactive inorganic intermediates such as singlet oxygen ($^1O_2$) and hydroxyl radicals ($\cdot OH$), as well as organic radicals and radical anions. In turn, these intermediates can react with a wide variety of organic contaminants, including those that do not absorb UV or visible light in the range occurring in natural waters and thus cannot undergo direct photochemical reactions. These reactive intermediates also react with/break down organic matter itself.

Photochemistry also affects inorganic substances. For example, $\cdot OH$ is produced photochemically from nitrate and nitrite, and the redox cycles of both Fe and Mn involve photochemical reactions. Aquatic photochemical transformations are not limited to solutes. Oxide particles of Fe and Mn can undergo photo-induced reductive dissolution, and various metal oxides and sulfides that act as semiconductors can photocatalyze reactions of compounds adsorbed to their surfaces. Some of these minerals are found in natural systems, and others are of potential interest for engineered treatment systems.

This chapter describes the physical and chemical processes involved in aquatic photochemistry, including direct and indirect photochemical reactions and the chemistry of reactive photo-intermediates involved in the latter reactions. We also describe the kinetics of aquatic photochemistry and briefly summarize some important photochemical reactions of dissolved inorganic substances in aquatic systems. The basic mechanism involved in semiconductor photochemical reactions is described, along with potential applications in water and wastewater treatment. Discussion of photochemical transformations of NOM is deferred to Chapter 18, and photochemical reactions of organic contaminants in natural waters are treated in Chapter 19.

17.2 Photophysical and photochemical processes

The amount of energy in a photon of UV or visible light is significant; that should come as no surprise to anyone who has sat on a beach too long and gotten sunburned! At 300 nm, for example, one photon has the energy of 6.65×10^{-19} joules or ~ 400 kJ mol^{-1} of photons—that is, per einstein (Ei). At 400 nm, a mole of photons is equivalent to 300 kJ. These energies are large relative to the activation energies needed for chemical reactions and close to the bond energies for C–H, C–C, and C–Cl: 413, 348, and 330 kJ/mol, respectively. For midday, midsummer conditions at latitude 40° (Philadelphia, USA, Naples, Italy, or Beijing, China, in the northern hemisphere) solar radiation in the

range 300–400 nm provides a flux at the Earth's surface of 8.9×10^{19} photons m^{-2} s^{-1} or $\sim$0.54 Ei m^{-2} h^{-1}. Extending the range to 300–500 nm yields a flux of 4.2×10^{20} photons m^{-2} s^{-1}, or 2.5 Ei m^{-2} h^{-1}. This light, if all absorbed in the top meter of water, would be equivalent to $\sim$25 mEi L^{-1} h^{-1}; that is, 25 mmol/L of photons per hour would be available to induce photochemical reactions.

The first step in any photochemical reaction is the absorption of a photon of light; a necessary condition for a photochemical reaction is that at least one substance must be able to absorb light in the UV-visible range. Ground-state molecules normally have even numbers of electrons (they are not free radicals), and the spins of the electrons are paired, meaning that ground states typically are singlet states (^1S_o). Absorption of a photon by molecule S raises an orbital electron from its ground state into a higher orbital (higher energy state) and produces an excited singlet state (e.g., $^1S^*$). The excited electron can return to the ground state by a variety of processes, as summarized below.

First, the fate of excited electrons includes a variety of ***photophysical processes*** (Figure 17.1, Table 17.1)—electron transitions into various energy states and emission of light energy by fluorescence or phosphorescence—that do not produce chemical change.[3] The excited (and ground) states have a range of rotational and vibrational states, and molecules in solution have essentially a continuous range of vibrational and rotational energies associated with each electronic (orbital) state. Excess vibrational or rotational energy is lost rapidly by thermal equilibration, which drops the state to its
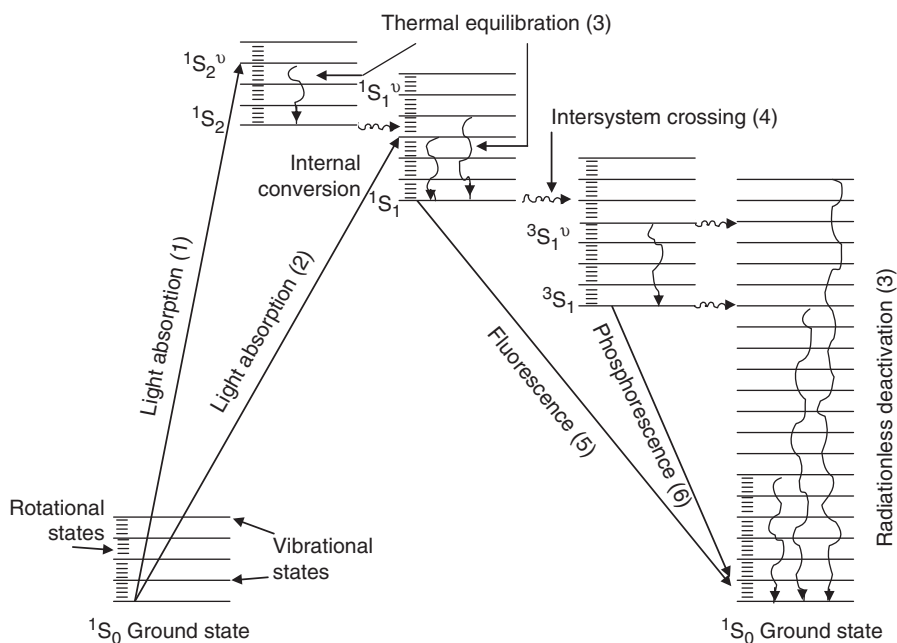
Figure 17.1 Photoactivation of a molecule in its singlet ground state and its return to ground state by photophysical processes. Numbers in parentheses refer to processes/reactions listed in Table 17.1; superscript υ indicates a vibrationally excited electronic state. Redrawn based on a figure in Adamson.[3]

Table 17.1 Major types of photophysical processes and photochemical reactions

Photophysical processes

Reaction	Description	Number (in text)
$S_o + h\nu \to {}^1S^*$	Light absorption; excitation	(1,2)
${}^1S^* \, or \, {}^3S^* \to S_o$	Radiationless deactivation	(3)
${}^1S^* \to {}^3S^*$	Intersystem crossing	(4)
${}^1S^* \to S_o^v + h\nu$	Fluorescence	(5)
${}^3S^* \to S_o^v + h\nu$	Phosphorescence	(6)
${}^3S^* + P \to S_o + {}^3P^*$	Sensitization	(7)
${}^3S^* + Q \to S_o(+Q^*)$	Quenching of S^* and radiationless	(8)
$\qquad {}^*Q \to Q$	$\qquad$ deactivation of quenching agent Q	
${}^3S^* + O_2 \to S_o + {}^1O_2$	Formation of singlet oxygen	(9)
${}^1O_2 + Q \to O_2 + {}^3Q$	Quenching of singlet oxygen by Q	(10)
${}^3Q \to Q$	and radiationless deactivation of Q	

Photochemical reactions

Reaction	Description	Number (in text)
$S^* \to$ Products, or	Direct photolysis (may involve several steps	(11)
$\qquad S^* + R \to \; \to$ Products	$\qquad$ and other ground-state reactants)	
${}^3S^* + HR \to SH\cdot + R\cdot$	Hydrogen transfer—first step in	(12)
	$\qquad$ photosensitized oxidation of HR by free	
	$\qquad$ radical mechanism	
${}^1O_2 + R_{ene} \to RO_2$ or	Addition of singlet oxygen to organic	(13)
$\qquad {}^1O_2 + R \to R'O + R''O$	$\qquad$ molecule with C=C bond (R_{ene})	
${}^3S^* + O_2 \to S_{ox} + O_2\cdot^-$	Oxidation of light-absorbing sensitizer	(14)
	$\qquad$ molecule by O_2, yielding superoxide	
	$\qquad$ radical anion	
${}^3S^* + R \to S + R^*$	Energy transfer from sensitizer	(15)
$\qquad R^* \to \to$ Products	$\qquad$ to produce excited species that then	
	$\qquad$ reacts to form product(s)	

[*]Adapted from Brezonik.[1]

lowest energy level. In turn, this state can pass into a vibrationally excited level of a lower excited state by a process known as "internal conversion." Excited singlet states may fluoresce—emit a photon of a higher wavelength (lower energy) than was absorbed and thereby return to the ground state. Most excited singlet states are very short-lived (half-lives $< 10^{-9}$ s) and do not persist long enough to react with aqueous solutes. Singlet states are converted to longer lived triplet states (${}^3S^*$) by the process of "intersystem crossing," in which the spin of an electron is inverted so that two electrons have parallel spins. Most photochemical reactions involve excited triplet states. Triplet states can undergo the same processes described above. If a triplet state emits a photon, the process is called phosphorescence, and the molecule returns to its ground singlet state. "Radiationless deactivation," another way for excited states to return to the ground state, converts the excess energy to vibrational energy (heat) of the molecule and its neighboring solvent molecules. Finally, an excited molecule may transfer its excess energy to a receptor molecule, R, exciting it to R^*, and R^* may react chemically or return to the ground state by the mechanisms described above. An important example of energy transfer is the formation of singlet oxygen ${}^1O_2$, the first excited state of O_2. Ground-state O_2, which

with its two unpaired electrons is unusual in being a triplet (see Chapter 12), is very efficient in capturing the energy of excited triplet states because the energy difference between it and $^1O_2$ is small—only $\sim$96 kJ/mol.

Second, the excited state S* can induce *photochemical processes*—that produce structural transformations in the molecule and form other compounds by a variety of bond rearrangements that may involve other solutes and/or solvent molecules. Chemical reaction of the light-absorbing molecule (S) is called direct photolysis (Table 17.1, reaction 11). Chemical reactions of receptor molecules (R) that get excited (to R*) by collision with an excited sensitizer molecule (S*) or reactions of molecules that react with R* are called indirect photolysis or photosensitized reactions. This mode of reaction is important because it enables organic compounds that cannot undergo direct photolysis (because they do not absorb light at wavelengths available in the aquatic systems) to be photodegraded indirectly. Excited sensitizer molecules can interact with receptor molecules in several ways to produce indirect photochemical reactions (Table 17.1). S* can extract a hydrogen atom from R producing a reactive free radical R· (Table 17.1, reaction 12); it can donate an electron to ground-state O_2 to produce highly reactive superoxide radical anion O_2^-·, which then can oxidize other species (reaction 14); or it can transfer its energy to another species, creating R*, which then reacts to form other products (reaction 15). In addition to inducing the transformation of a receptor molecule, the first two types of reactions also result in transformation of the sensitizer itself. The reaction of singlet oxygen formed from S* (Table 17.1, reaction 9) with electron-rich compounds like olefins (reaction 13) is another indirect photochemical reaction.

Some receptor substances react directly with excited sensitizer molecules, as reaction 11 (Table 17.1) shows, but most indirect photolysis reactions proceed through the sequence illustrated in Figure 17.2, in which excited sensitizers (S*) directly form highly reactive transient intermediates, which then react with the substances of interest. The most important sensitizers in natural waters are natural organic matter, NOM (especially aquatic humic and fulvic acids), nitrate and iron. The reactive intermediates mostly are inorganic free radicals or radical ions ($^1O_2$ is an exception) formed from water or O_2, but organic radicals formed from NOM also can be important. Aside from reacting with substances of interest, transient intermediates disappear by several other mechanisms shown in Figure 17.2. Scavenging and quenching agents may cause them to dissipate or be transformed to other intermediates before they react with substances of interest. In the case of $^1O_2$, collision with water or nonreactive solutes may dissipate their excess energy by radiationless deactivation (producing heat). Because intermediates usually have very low concentrations, it is impractical to measure them directly, and reagents with a high specificity for a given intermediate (called probes) are used to measure their steady-state concentrations (see Section 17.6.2).

17.3 Kinetics of photochemical reactions

17.3.1 Direct photolysis

In one sense, kinetic descriptions of direct photolysis are straightforward, at least when rates are measured in terms of reactant loss. In general, such reactions are first order in the light-absorbing reactant. A major complicating factor, however, is that direct photolysis
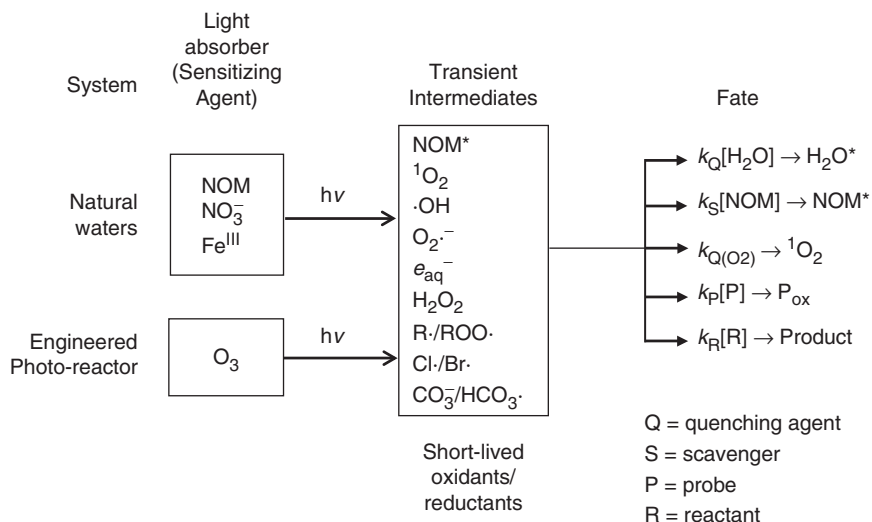
Figure 17.2 Scheme of photosensitized reactions in natural and engineered aquatic systems showing the diversity of photosensitizing agents and alternative reaction pathways for transient intermediates. Only the last pathway leads to chemical reaction with the compound of interest.

rates also depend on light intensity, and as we show below, this is difficult to model exactly.

Two fundamental laws of photochemistry provide the underpinnings for kinetic descriptions of photochemical reactions. The ***Grotthus-Draper law*** (first law of photochemistry) states that only light that is absorbed can produce chemical change; the ***Stark-Einstein law*** (second law of photochemistry) states that one molecule is activated for each photon absorbed by a system. These laws lead to the simple idea that rates of direct photolysis are proportional to the number of photons absorbed per unit time, $I_a(\lambda)$, times the fraction of absorbed photons that produces chemical change, which is called the ***quantum yield***, Φ_d:

$$\text{Rate}_\lambda = I_a(\lambda)\Phi_d, \tag{17.1}$$

where (λ) indicates a wavelength-dependent variable. Φ_d reflects the fact that only some absorbed photons produce chemical change and that competing photophysical processes also return unstable excited molecules to the stable ground state. It is often assumed that this coefficient is not wavelength-dependent. When measurements and calculations are performed with the same spectrum of light, this assumption is valid. When measuring using single-wavelength light sources, and extrapolating to other wavelengths or spectra, the assumption should be checked. In turn, light absorption is proportional to the concentration of light absorbing compounds, e.g., [S] in mol/L, at least at low [S]:

$$I_a(\lambda) = k_{a(\lambda)}[S], \tag{17.2}$$

where $k_{a(\lambda)}$ is a wavelength-dependent rate coefficient for light absorption called the "specific light absorption rate constant." Substitution of Eq. 17.2 into Eq. 17.1 shows that direct photolysis is a first order process, and the overall rate constant at a given λ, $k_{d(\lambda)}$, is $k_{a(\lambda)}\Phi_d$ (units of t^{-1}):

$$\text{Rate}_{(\lambda)} = k_{a(\lambda)}\Phi_d[S] = k_{d(\lambda)}[S] \qquad (17.3)$$

$k_{a(\lambda)}$ depends on the molar absorptivity of S at a given wavelength, $\varepsilon_{(\lambda)}$, and the amount of light available at λ. For natural waters, available light is defined by a complicated term, the **scalar irradiance**, $E_0(\lambda, z)$, which depends on λ, depth (z), and solar angle. A more complete description and derivation of the scalar irradiance function is provided elsewhere.[1,4,5] For near-surface conditions in natural waters, the following relationship holds between $k_{a(\lambda)}$ and $E_0(\lambda, z)$:

$$k_{a(\lambda)} = 2.303 E_0(\lambda, 0)\varepsilon_\lambda \qquad (17.4)$$

$E_0(\lambda, 0)$ is the scalar irradiance just below the water surface. This term has units of mEi cm^{-2} s^{-1} if ε_λ, the molar absorptivity of S has units of M^{-1} cm^{-1}. The molar absorptivity is obtained from **Beer's law**, $A_\lambda = \varepsilon_\lambda l[S]$, where A_λ is the absorbance measured by spectrophotometer, l is the cell path length (cm), and [S] is molar concentration of S. The observed rate constant for direct photolysis is obtained by integrating (or summing) over the wavelengths of light absorbed by S:

$$k_d = 2.303\Phi_d \int_{\lambda_1}^{\lambda_2} E_0(\lambda, 0)\varepsilon_\lambda d\lambda = \Phi_d \sum_\lambda k_{a(\lambda)} \qquad (17.5)$$

Scalar irradiance and ε vary substantially with λ in aquatic environments, and a useful plot involves these two components of $k_{a(\lambda)}$ versus λ. The overlap of the ε curve for a reactant with the irradiance curve indicates the potential for a low or high rate of photon absorption by a reactant in a water body (Figure 17.3).

Determining photolysis rate constants by Eq. 17.5 is difficult because of the need to evaluate the integral containing E_0 and ε. Sometimes direct photolysis rate constants are calibrated in terms of total solar radiation (R_T) at the Earth's surface, e.g.,,

$$\text{Rate} = \frac{k_{obs}}{R_T}[S] = k'_d[S]. \qquad (17.6)$$

$k'_d = k_{obs}/R_T$ has units of s$^{-1} \div$ (mEi cm^{-2} s^{-1}), or cm^2 mEi^{-1}. This works for compounds that absorb in the visible and UV-A regions (> 320 nm) because light intensity in this range varies little with solar angle or cloud cover.[4] Examples include nitrosamines, PAHs, and iron cyanide complexes. The approach is not valid for compounds that absorb primarily in the UV-B (280–320 nm), because the spectral quality of this light varies with solar angle. The spectral character of UV and visible light also varies with depth in water bodies because of selective absorbance of light by water and natural solutes. As a result, photolysis rates vary in complicated ways with depth in water bodies.
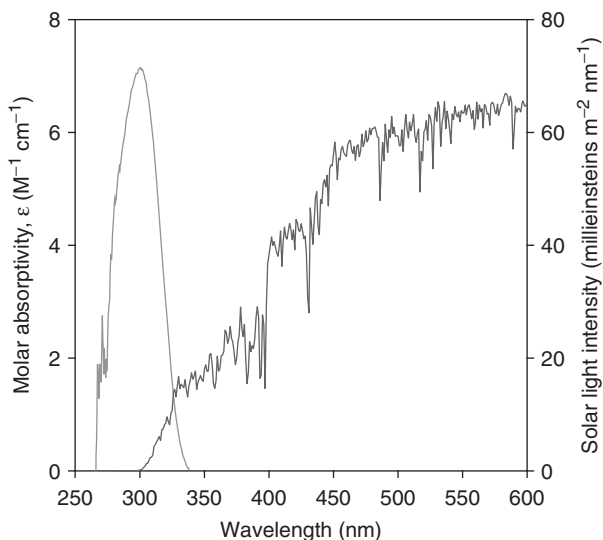
Figure 17.3 Absorptivity of NO_3^- and intensity of solar radiation at water surface (scalar irradiance, $E°$) showing the spectral overlap of NO_3^- and the solar spectrum. (see eq. 17.4).

A final factor to consider in predicting rates of direct photolysis is the role of quenching agents (Table 17.1, reaction 8) on quantum yields. The ***Stern-Volmer equation*** can be used to obtain the quenching rate constant of $^3S^*$ from experimental data:

$$\frac{\Phi_d^o}{\Phi_d^q} = 1 + k_{3S^*} \tau_o [Q], \tag{17.7}$$

where Φ_d^o and Φ_d^q are quantum yields for direct photolysis in the absence and presence of quenching agent Q, respectively; k_{3S^*} is the rate constant for quenching of $^3S^*$ by Q (Table 17.1, reaction 8); and τ_o is the characteristic lifetime of $^3S^*$ in the absence of Q. It is apparent from Eq. 17.7 that the importance of quenching on Φ decreases as the lifetime of $^3S^*$ decreases and also as [Q] decreases. Dissolved oxygen is an important quenching agent in aquatic systems because its concentration is high and the energy it needs to absorb to become excited to $^1O_2$ is small. Rate constants for quenching by O_2 (Table 17.1, reaction 9) are $\sim 2 \times 10^9$ M^{-1} s^{-1}, (close to diffusion-limited) and in O_2-saturated waters (~ 0.3 mM), the product, $k_{O_2} \times [O_2]$, is $\sim 6 \times 10^5$ s^{-1}. Quenching by O_2 thus has significant effects on Φ for direct photolysis when τ_o is greater than ~ 1–2×10^{-7} s. Of course, $^1O_2$, the product of quenching by O_2, itself may induce a reaction (Table 17.1, reaction 13).

17.3.2 Indirect photolysis

Comprehensive kinetic models are not available for most indirect photolysis reactions. In addition to the complications involved in quantifying light conditions, the number of transient intermediates that may participate and the many reactions they can undergo complicates development of such models. Consequently, kinetic models of indirect photochemical processes in natural waters usually are very incomplete. Indirect

photolysis rates of most organic contaminants are described simply in terms of second order rate constants for reaction of the contaminant with a given transient intermediate (e.g., ·OH, $^1O_2$). Predicting rates of photosensitized reactions under ambient conditions in natural water usually involves estimates of the time-averaged (e.g., 24-h average) or maximum (midday) concentration of the photo-intermediate, and often these estimates are limited to the surface layer in a water body.

17.4 Factors affecting light intensity in natural waters

As described previously, the main difference between rate equations for photolysis and those for thermal reactions is the need to account for rates of light absorption for photochemical reactions. Although both reactant and environmental parameters affect light absorption (Eq. 17.4), the main reactant parameter, ε_λ, is easily measured by spectrophotometry. In contrast, $E_0(\lambda)$, the measure of available light, depends on many factors and is difficult to predict exactly. The spectral quality and intensity of light vary with solar angle, cloud cover, water column depth, and concentrations and composition of solutes and particles in the water. The difficulties in predicting light intensity are especially large in the UV-B range (280–320 nm) where many organic pollutants have their absorption maxima. Irradiance at the Earth's surface decreases rapidly below 320 nm because of the stratospheric ozone layer, and almost no solar radiation < 295 nm reaches the Earth's surface. Light intensity in the UV-B range also decreases more rapidly with increasing solar angle than does light in the UV-A (320–400 nm) and visible regions.

Some solar radiation that enters the top of the Earth's atmosphere is scattered by aerosols and absorbed by molecules, and some is transmitted to the Earth's surface. Scattering increases with decreasing wavelength, and this scattered, short-wavelength light illuminates the sky causing its blue color. Light at the Earth's surface consists of radiation directly from the sun (R_d) and radiation scattered from the sky (R_s). (Note, other texts give these terms and I_d and I_s. Here we chose R for "radiation" to avoid confusion with $I_{a(\lambda)}$ as defined in Eq. 17.1.) $G(\lambda)$, the total irradiance (sun + sky) at the Earth's surface, and $E_0(\lambda,0)$, total scalar irradiance just below the water surface, vary with season, latitude, and time of day in well-understood ways and can be modeled using computer codes.[4,6,7] Cloud cover affects the intensity of surface light but has smaller effects on its spectral quality than one might think. In fact, clouds transmit UV radiation slightly better than visible light,[4,8] and the reduction in UV radiation at the Earth's surface thus is roughly proportional to the reduction in total radiation caused by clouds.

Factors affecting the spectral quality of light as a function of depth in the water column include the nature and concentrations of light-scattering particles and light-absorbing NOM, as well as absorbance by water itself. These factors are understood relatively well,[4,9] but temporal variations in their importance make predictions for a given water body difficult.

Light attenuation in water increases at both extremes of the UV-visible spectrum and reaches a minimum in the range ∼470–490 nm; that is, blue light is the most transparent. UV light penetrates water farther than is commonly thought, and the depth of the photic zone (the region in which UV-mediated photolysis may occur) can be relatively large.[10]

The bottom of the photic zone often is defined as the depth at which light intensity is 1% of incident light. Defined this way, the photic zone of mid-ocean water, which has low concentrations of UV-absorbing dissolved organic carbon (DOC) and light-scattering particles, ranges from $\sim$ 30 m at 320 nm (top of the UV-B range) to $\sim$160 m near 500 nm and < 20 m above 600 nm. From ***Lambert's law***,

$$E(\lambda, z) = E_0(\lambda, 0)\exp(-K_\lambda z), \tag{17.8}$$

we can show that the photic zone depth defined as above is equal to $4.6/K_\lambda$, where K_λ is the diffuse attenuation coefficient of the water at λ. Variations in K_λ with λ depends on the nature and concentrations of light-scattering and light-absorbing material in the water.

The photic zone in most freshwaters is much less than that of mid-ocean waters—often a few meters or even less in turbid waters. Light attenuation by particle scattering varies with λ, but less than absorbance by NOM does. Absorbance by humic matter increases exponentially with decreasing λ in the low visible and UV regions (see Section 18.6.1). Plant pigments from phytoplankton absorb strongly in the UV region and have two peaks of absorbance in the visible region: broadly in the range $\sim$400–500 nm and a narrower peak near $\sim$660 nm. Light absorbance in natural waters thus depends on relative concentrations of aquatic humus and plant pigments, but both substances cause rapid increases in light absorption as λ decreases below 500 nm, the range with sufficient energy to induce photochemical reactions.

Measurement of light attenuation in natural waters is complicated, even ignoring complications of wavelength variations. Two approaches are used, but they measure different phenomenon and yield different attenuation coefficients. ***Beam attenuation coefficients*** (α_λ) measure light transmittance through water using a conventional spectrophotometer. Beam attenuation is caused by a combination of molecular absorption and particle scattering. Most scattering occurs in a forward direction in natural waters but not exactly in the same direction as the beam. Consequently, most forward scattered light does not reach the spectrophotometer's detector, and thus

$$\alpha_\lambda \approx a_\lambda + s_\lambda, \tag{17.9a}$$

where a is the absorption coefficient and s the total scattering coefficient.

In contrast, ***diffuse attenuation coefficients*** (K_λ) are determined from measured solar irradiance versus depth in a water body. K_λ is obtained from the slope of ln(irradiance) versus depth: $G_\lambda(z) = G_\lambda(0)\exp(-K_\lambda z)$. Values of K_λ always are smaller than α_λ because irradiance measured with a light meter includes forward scattered light.[11,12] Several empirical relationships have been derived for K_λ:[12]

$$K_\lambda \approx \alpha_\lambda - s_{f\lambda}, \tag{17.9b}$$

$$K_\lambda \approx D_\lambda a_\lambda + s_{b\lambda}, \tag{17.9c}$$

where s_f and s_b are the forward and back components of s and D_λ is a "distribution function," the ratio of mean path length of light in a layer to the layer's actual thickness. Note that all the coefficients defined in Eqs. 17.9a, 17.9b, and 17.9c are wavelength dependent.

In particle-free water, α_λ should be equal to K_λ, but even in very clear ocean waters, $\alpha_\lambda >$ K_λ in the UV.[11] Because forward-scattered light can induce photochemical reactions, K_λ is the best measure of light penetration in natural waters, especially turbid waters.

17.5 Calculation models for direct photolysis

Because light intensity varies with time of day, season, latitude, elevation of the water body, depth in the water, and the thickness of the ozone layer, calculation of ambient photolysis rates from laboratory-measured rate constants is tedious. The above factors also need to be taken into account in comparing ambient measurements for different times and places. GCSOLAR[6,12] a personal computer-based model, computes rates direct photolysis and $t_{1/2}$ of pollutants in water bodies as a function of the amount of light absorbed in a given depth of water, which depends on the attenuation coefficient and the path length taken by light beams. Path lengths of light in water differ for sun and sky radiation, and GCSOLAR takes this into account. The model applies to waters with low suspended solids, where light attenuation occurs primarily by absorption. In essence, GCSOLAR calculates $k_{a(\lambda)}$ for two limiting conditions; along with Φ and the reactant concentration, $k_{a(\lambda)}$ defines the rate of direct photolysis.

(I) System absorbs all solar radiation available for direct photolysis.   In this case, $\alpha_\lambda l_d$ and $\alpha_\lambda l_s > 2$, where l_d and l_s are the path lengths for sun and sky radiation, respectively. Under these conditions, $k_{a(\lambda)}$ is given by

$$k_{a(\lambda)} = \frac{(R_{d\lambda} + R_{s\lambda})\varepsilon_\lambda}{jz\alpha_\lambda} = \frac{W_\lambda\varepsilon_\lambda}{jz\alpha_\lambda}, \tag{17.10}$$

where j is a conversion factor ($j = 6.02 \times 10^{20}$ when [S] is in M and light intensity is in photons cm^{-2} s^{-1}; $j = 1$ if light intensity is in mEi cm^{-2} s^{-1}), and W_λ is the intensity of sun + sky radiation on a horizontal plane below the surface of a water body. W_λ is computed from the total irradiance at the Earth's surface, G_λ, by taking reflection into account. It is related to scalar irradiance by the formula: $E_0(\lambda) = W_\lambda D_\lambda/j$, where D_λ, the distribution function defined in Eq. 17.9. In effect, Eq. 17.10 defines rate constants for direct photolysis in water bodies deep enough to absorb all incident light. Under these conditions, wavelength-specific rate constants are proportional to the total irradiance entering the water times the molar absorptivity of the compound and inversely proportional to the light attenuation coefficient and water column depth over which photolysis occurs.

(II) Near-surface conditions.   When $\alpha_\lambda l_d$ and $\alpha_\lambda l_s$ are $<\sim0.02$, $k_{a(\lambda)}$ is independent of α_λ and is given by

$$k_{a(\lambda)} = 2.303\varepsilon_\lambda \frac{(R_{d(\lambda)}l_d + R_{s(\lambda)}l_s)}{jz} = 2.303\varepsilon_\lambda \frac{Z_\lambda}{j}. \tag{17.11}$$

Equation 17.11 applies when less than $\sim5\%$ of the incident light is absorbed. According to Eq. 17.11, $k_{a(\lambda)}$ is depth independent, but the depth to which it applies depends on the light attenuation rate. Comparison of Eq. 17.11 with Eq. 17.4 shows that $Z_\lambda/j = E_0(\lambda, 0)$.
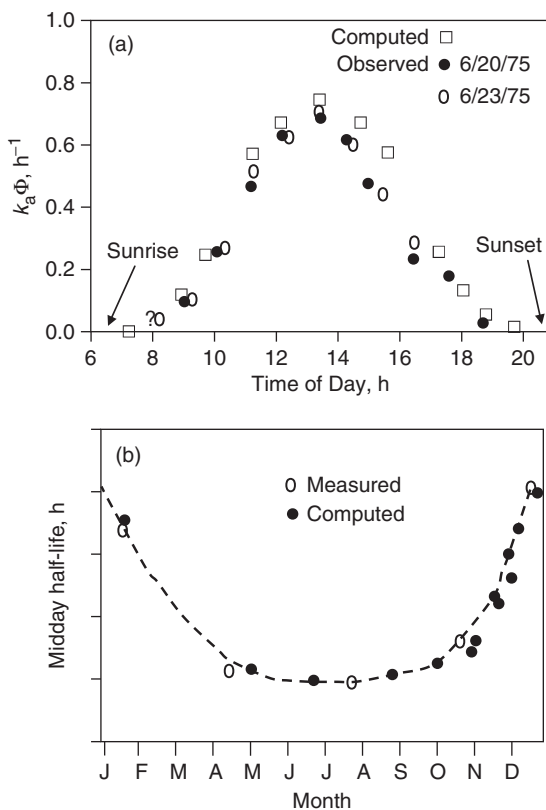
Figure 17.4 Measured rates of direct photolysis versus rates computed by GCSOLAR model: (a) photolysis of DMDE (1,1-bis(4-methoxyphenyl)-2,2-dichloroethene), an analog of DDT (dichlorodiphenyltrichloroethane), versus time of day; (b) photolysis of DMDE versus month of year at Athens, Georgia. From Zepp and Cline,[4] © American Chemical Society, and reproduced with permission.

Tabulated values of W_λ and Z_λ for midday and midseason clear sky conditions at 40°N latitude are available,[4,6] (values for other latitudes and seasons are also available),[5] and GCSOLAR produces output of $W(\lambda)$, $Z(\lambda)$, and k_a and models direct photolysis rates at specified latitudes, longitudes, elevations, seasons, and times of day. As Figure 17.4 shows, computed rates compare well with measured rates for several compounds. One difficultly with GCSOLAR is that it must be run from a DOS prompt, which is becoming more difficult to do on modern PCs. An alternative is to perform the calculation in a spreadsheet. SMARTS (A Simple Model of the Atmospheric Radiative Transfer of Sunshine),[7] a spreadsheet-based macro, can be used to generate the necessary solar irradiance spectrum at any longitude/latitude, date and time and under a variety of atmospheric conditions. If the ε_λ and Φ_d are known, the $k_{a(\lambda)}$ and k_d can be calculated. An additional advantage of SMARTS is that it allows calculation of irradiance at each individual wavelength, rather than over wavelength intervals (i.e., GCSOLAR divides up the solar spectrum into 39 intervals).

Note that GCSOLAR applies to waters where light attenuation by scattering is less important than that by absorption. When scattering is dominant, D_λ increases with depth, as light becomes increasingly diffuse; the net effect should be to increase photolysis rates. Miller and Zepp[12] evaluated the effects of suspended sediments on D_λ in laboratory experiments and found that the ratio D_{ss}/D_{dw} (subscripts "ss" and "dw" refer to suspended

sediments and distilled water) varied from 1.06 to 1.69 for six rivers and ponds. In contrast, D_{ss}/D_{dw} was near the expected value of unity for a nonscattering humic acid solution. They concluded that, on average, photolysis was about a third faster in turbid water than in clear water.

17.6 Inorganic photochemistry of natural waters

17.6.1 Inorganic intermediates produced by photolysis

Some inorganic ions can undergo direct photolysis in natural waters, but this is not a major sink for any major or minor inorganic species. It *is* important, however, as a source of reactive photo-intermediates that play key roles in indirect photolysis. Nitrate, bicarbonate, bromide, dissolved O_2, and water itself all undergo such reactions. The important free radicals, radical anions, and other reactive photo-intermediates produced from water or dissolved oxygen include: superoxide anion, $\cdot O_2^-$; hydroxyl radical, $\cdot OH$; hydroperoxyl radical, $HO_2\cdot$; hydrogen peroxide, H_2O_2; hydroperoxide ion, HO_2^-; singlet oxygen, $^1O_2$; and the hydrated electron, e_{aq}^-. Other reactive intermediates, such as carbonate ion radical, CO_3^-, and nitric oxide, NO, are formed from inorganic ions (carbonate and nitrate/nitrite). Table 17.2 lists reactions that form these species in water. This section describes the chemistry of important inorganic photo-intermediates in natural waters, including sources and reactions of the intermediate and typical concentrations (where known) in natural waters.

Superoxide, $O_2^-\cdot$.   Formed by several mechanisms (Table 17.2, reactions 1–3; also see Section 12.2.2), this radical anion is a key first step in the reduction of O_2 to water. Because $pK_a = 4.8$, little $HO_2\cdot$ (hydroperoxyl, the conjugate acid of $O_2^-\cdot$) is present at circumneutral pH when superoxide is formed, even though the acid-recombination reaction is extremely fast—such that equilibrium conditions apply. $O_2^-\cdot$ is highly toxic, and many cells have dismutase enzymes that degrade it to H_2O_2 and O_2 (a disproportionation reaction; i.e., simultaneous oxidation and reduction). Not much is known about the concentrations of $O_2^-\cdot$ in freshwaters, but Voelker and Sedlak[13] estimated a steady-state concentration of 7 nM in seawater in the absence of scavenging trace metals (e.g., Fe, Mn, Cu) at summertime, mid-latitude light conditions. Inclusion of Fe at 0.1 nM decreased $[O_2^-\cdot]_{ss}$ to 0.4–2 nM. We can infer the presence of $O_2^-\cdot$ in freshwaters from the fact that the product of its reduction, H_2O_2, is widely found in surface waters, during daylight hours. $O_2^-\cdot$ rapidly oxidizes many metal ions, but it also can reduce other metal ions, in the process returning to ground-state O_2. For example, the formation of Cu^+ in seawater is thought to occur by reaction of Cu^{II} with $O_2^-\cdot$.

Hydrogen peroxide.   Hydrogen peroxide has been found in seawater, rain, lakes, and sewage lagoons at concentrations up to 10^{-5} M.[14,15] Concentrations of H_2O_2 increase in many waters when they are illuminated and decrease in the dark, supporting the idea that it is formed by photochemical reactions. H_2O_2 in rainfall may arise from absorption (by rain droplets) of H_2O_2 preformed in the atmosphere. Alternatively, it may arise by aqueous reactions of O_3 and other reactive species in rain droplets. The most likely mechanisms for H_2O_2 formation in surface waters involve photochemical reduction

Table 17.2 Reactions producing inorganic photo-intermediates

Formation of superoxide radical ion, $O_2^{-\cdot}$

(1) Charge transfer in photoexcited sensitizer-O_2 complexes:

$$S + O_2 + h\nu \rightarrow [S^{*\cdots}O_2] \rightarrow S_{ox} + O_2^{-\cdot}$$

(S = photosensitizer (reducing agent), e.g., DOM, Fe^{2+})

(2) Photoionization:

$$DOM + h\nu \rightarrow DOM^+ + e_{aq}^-; e_{aq}^- + O_2 \rightarrow O_2^{-\cdot}$$
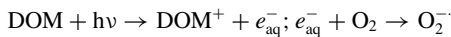
(3) Semiconductor pathways:

$$TiO_2 + h\nu \rightarrow TiO_2^+ + e^- \rightarrow\rightarrow O_2^{-\cdot}$$
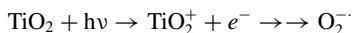
Formation of hydroperoxyl

(4) $>C{=}O + h\nu \xrightarrow{ROH} [>C{-}O^{\cdot}]^* \xrightarrow{O_2} >C{-}OH \rightarrow >C{=}O + {}^{\cdot}OOH$

Formation of H_2O_2

(5) $S + O_2 + h\nu \rightarrow S_{ox} + O_2^{-\cdot}$ (i.e., reaction 1, 2, or 3)
(6) $O_2^{-\cdot} + H^+ \rightarrow HO_2\cdot$
(7) $2HO_2^{\cdot} \rightarrow H_2O_2 + O_2$ (catalyzed by superoxide dismutase)

or

(8) $HO_2^{\cdot} + R + H^+ \rightarrow H_2O_2 + R_{ox}$ (R = reducing agent)

Photolysis of H_2O_2

(9) $H_2O_2 + h\nu \rightarrow 2{\cdot}OH$ ($\lambda < 300$ nm)
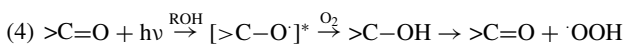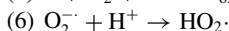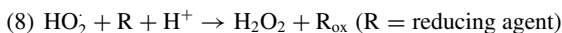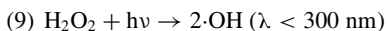
Nitrate and nitrite photolysis

(10) $NO_3^- + h\nu \rightarrow NO_2^- + O(^3P)$ ($\lambda_{max} = 302$ nm)
(11) $O(^3P) + O_2 \rightarrow O_3$

or

(12) $NO_3^- + h\nu \rightarrow NO_2 + {\cdot}O^-$ ($\lambda_{max} = 302$ nm)
(13) ${\cdot}O^- + H^+ \rightarrow {\cdot}OH$
(14) $NO_2^- + h\nu \rightarrow NO + {\cdot}O^-$
(15) ${\cdot}O^- + H_2O \rightarrow {\cdot}OH + OH^-$
     (Net14 + 15)$NO_2^- + H_2O + h\nu \rightarrow NO + {\cdot}OH + OH^-$) ($\lambda \approx 300$–370 nm)

(16) $HNO_2 + h\cdot \rightarrow NO + OH$;
(17) $NO + {\cdot}OH \rightarrow HNO_2$ (16 + 17 = a null cycle)
(18) $NO + HO_2^{\cdot} \rightarrow NO_2 + {\cdot}OH$
(19) $NO_2^- + O_3 \rightarrow NO_3^- + O_2$
(20) $2NO + 0.5O_2 + H_2O \rightarrow 2H^+ + 2NO_2^-$
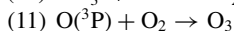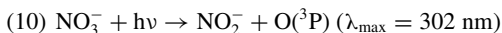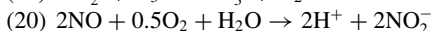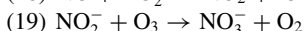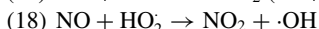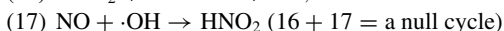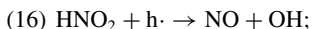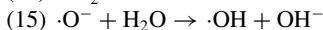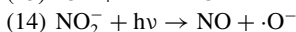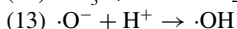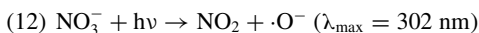
Table 17.2 Cont'd

Production of radicals by ·OH

(21) $·OH + Br^- \rightarrow ·Br + OH^-$
(22) $·Br + Br^- \rightarrow Br_2^- ·$
(23) $·OH + HCO_3^- \rightarrow HCO_3 + OH^-$
(24) $·OH + DOM \rightarrow OH^- + organocations \rightarrow\rightarrow oxidation\ products$

Production of aquated electron from organic matter

(25) $DOM + h\nu \rightarrow DOM^+ + e_{aq}^-$

Iron photolysis

(26) $FeOH^{2+} + h\nu \rightarrow Fe^{2+} + ·OH$
(27) $Fe^{III} + O_2^- · \rightarrow Fe^{2+} + O_2$
(28) $Fe^{2+} + H_2O_2 \rightarrow FeOH^{2+} + ·OH$ (Fenton's reaction)

Ozone photolysis

(29) $O_3 + H_2O + h\nu \rightarrow H_2O_2 + O_2$

of dissolved O_2 by Fe^{II}, Mn^{II}, or NOM to produce $O_2^-·$, which accepts another electron (step 2 of the Haber-Weiss mechanism; see Section 12.2.2) or disproportionates to H_2O_2 and O_2 (Table 17.2, reactions 5–7). Support for the latter mechanism is the finding that the enzyme superoxide dismutase, which catalyzes the disproportionation of $O_2^-·$, accelerates H_2O_2 production.[16] H_2O_2 is a fairly weak oxidant but does reacts with many organic compounds, including phenols, unsaturated fatty acids, and organic N and S compounds.[17] The fate of H_2O_2 in surface waters is not well known, but it is thought to be consumed biologically. H_2O_2 photolyzes ($\lambda < 300$ nm) to ·OH radicals, but this is not an important source of ·OH in natural waters.

Hydroxyl radical, ·OH.   This highly reactive species is a key intermediate in photochemical smog formation and the stratospheric ozone cycle. Over the past two decades evidence has mounted to demonstrate its importance in aquatic photochemistry. It is formed in many ways (Table 17.2), including photolysis of H_2O_2, NO_3^- and NO_2^-, and NOM; decomposition of O_3; reaction of NO with ·OOH; photoreduction of $FeOH^{2+}$; and reaction of Fe^{2+} and H_2O_2 (Fenton's reagent). The relative importance of these mechanisms varies among water bodies, but photolysis of NOM, photoreduction of nitrate, and reactions of iron are thought to be the main sources in freshwaters.[18]

   Production rates of ·OH in the eutrophic Swiss lake Greifensee were found to be about 1,000 times slower than production rates of $^1O_2$ in the same lake,[19] but the mean lifetime of ·OH radicals, $\sim 10^{-5}$ s, was comparable to that of $^1O_2$. ·OH concentrations in Greifensee were estimated to be $\sim 1 - 3 \times 10^{-16}$ M, based on measurements with the probe butyl chloride, and Mill et al.[20] found an average of $\sim 10^{-17}$ M for several

eutrophic surface waters using the probe cumene. Based on low production rates and low $[\cdot OH]_{ss}$, Haag and Hoigne[19] concluded that $\cdot OH$ is not important as a reactant for organic contaminants in water bodies, but more recent studies indicate that $\cdot OH$ production rates from nitrate photolysis ($\sim 2 \times 10^{-12}$ to 2×10^{-11} M s^{-1} or $\sim 7 \times 10^{-9} - 10^{-8}$ M h^{-1}) are sufficient to make $\cdot OH$ important in the photodegradation of organic contaminants (also see Chapter 19). The importance of nitrate photolysis as a source of $\cdot OH$ was first shown by studies with benzene, which reacts with $\cdot OH$ to form phenol.[21] Phenol production in samples from German lakes was correlated with $[NO_3^-]$ and inversely correlated with [DOC]. The authors thus concluded that NO_3^- photolysis was a more important source of $\cdot OH$ than was NOM; $[\cdot OH]_{ss}$ was estimated to be 5×10^{-16} M.

$\cdot OH$ is highly reactive both in air and water and is much more reactive and less selective than $^1O_2$. Rate constants for reactions of $\cdot OH$ with many organic compounds and inorganic ions are known, and many are near the diffusion-limited value. The principal aquatic sinks for $\cdot OH$ are dissolved organic matter (DOM), which plays a dual role as both source and sink for $\cdot OH$, and HCO_3^-, which reacts with it to form $CO_3^- \cdot$. Rate constants for $\cdot OH$ scavenging by DOM were found to be fairly consistent ($2.3 \pm 0.77 \times 10^4$ (mg C/L)$^{-1}$ s^{-1}),[18] suggesting that the importance of NOM as a $\cdot OH$ sink can be estimated simply from the DOC concentration. In seawater Br$^-$ is a sink for $\cdot OH$. It forms $\cdot Br$, which reacts rapidly reacts with another Br$^-$ to form $Br_2^- \cdot$. The latter species decays by reaction with various carbonate species.[22]

Singlet oxygen.   Singlet oxygen is formed by collision of ground state O_2 with excited triplet states of sensitizers (reaction 9, Table 17.1). It was proposed to act as a photo-intermediate in aquatic systems in 1970,[23] and the first measurements of $^1O_2$ in natural waters date to 1977.[24] Triplet state energies of organic contaminants (150–350 kJ mol^{-1})[7] are higher than that of $^1O_2$ (96 kJ mol^{-1}). Energy transfer to O_2 thus is efficient; γ_{O_2}, the fraction of collisions of triplet sensitizers with O_2 that produce $^1O_2$, is near unity. The rate constant for $^1O_2$ formation ($k_9 = \sim 2 \times 10^9$ M^{-1} s^{-1}; Table 17.1) is within a factor of ten of the diffusion-controlled limit. Humic matter is thought to be an important sensitizing agent for $^1O_2$ in surface waters.[25]

Most photo-produced $^1O_2$ is quenched to ground state O_2 by water before it can cause chemical reactions. The water-quenching rate constant for $^1O_2$, k_q, is 2.5×10^5 s^{-1}, and the lifetime (τ) of $^1O_2$ in water is short; $\tau = 1/k_q = 4 \times 10^{-6}$ s.[26] Maximum rate constants for reactions of $^1O_2$ with organic contaminants are 10^7–10^8 M^{-1} s^{-1}, and given their low concentrations (and the very high concentration of water), quenching by water is the predominant fate of $^1O_2$. The fraction of $^1O_2$ that does react represents significant sinks for some compounds (see Chapter 19). Concentrations of $^1O_2$ in surface waters range from $\sim 10^{-15}$ to $\sim 10^{-12}$ M for midday conditions. For example, values of 2–20×10^{-13} M were reported for waters in the southeastern United States, and highest concentrations were found in highly colored waters.[24] Concentrations of 0.3–5×10^{-14} M per mg/L of DOC were reported for Swiss waters under midday, spring-to-fall sunlight conditions.[27] These concentrations, however, are in the bulk aqueous phase. Recent work using probe molecules of varying hydrophobicity has shown that concentrations can be much greater within the NOM matrix.[28] NOM serves as both a source and sink for $^1O_2$, and thus concentrations within the NOM matrix are higher than those in the bulk water (measured using a hydrophilic probe, such as furfuryl alcohol). Hydrophobic contaminants associated with NOM thus may "see" $^1O_2$ concentrations

greater than hydrophilic pollutants do. Concentrations of $^1O_2$ are sufficient to oxidize some highly reactive organic contaminants in a few hours, but half-lives of most organic contaminants are much longer.[27]

Hydrated electrons.   This highly reactive and very short-lived species, symbolized e_{aq}^-, is a photo-intermediate formed from colored NOM[29,30] (Table 17.2, reaction 25). Recent studies resolved earlier discrepancies between the low quantum yields reported using the probe 2-chloroethanol[31] and higher values obtained by laser flash photolysis, and apparent quantum yields for e_{aq}^- formation from colored NOM indeed are low $(6 \times 10^5 – 1.3 \times 10^{-4})$.[32] Steady-state concentrations also are very low ($\sim 10^{-17}$ M per mg DOC/L),[31] and the lifetime of the hydrated electron is very short (< 1 ns).[33] This means that e_{aq}^- travel only very short distances between formation and reaction (or decay). The Einstein-Smoluchowski equation defines this distance as $(2D\tau)^{1/2}$, where D is the diffusion coefficient and τ is the lifetime of the species. For $\tau = 1$ ns and $D = 10^{-5}$ cm^2 s^{-1} (a reasonable value for small ions), the distance e_{aq}^- travel before reaction is $\sim$1.4 nm. Consequently, not all e_{aq}^- produced by photoactivation leave the molecule in which they were produced but some react or recombine within the NOM. Nonetheless, e_{aq}^- can play a role in degrading organic contaminants even if it does not leave the NOM; e_{aq}^--mediated decomposition of mirex, a chlorinated pesticide, sorbed to humic molecules was reported to be significant.[34]

The e_{aq}^- that escapes from NOM molecules has several fates. It reacts with O_2 to produce superoxide (Table 17.2, reaction 2) at diffusion-controlled rates ($k = 2 \times 10^{10}$ M^{-1} s^{-1}). It reacts with nitrate nearly as fast ($8–11 \times 10^9$ M^{-1} s^{-1}), producing nitrite, and also with electrophilic chlorinated and cationic organic compounds. Because O_2 concentrations generally are much higher than those of nitrate and organic contaminants, the principal fate of e_{aq}^- in solution is formation of superoxide (and then H_2O_2). This reaction, however, likely accounts for only a small fraction of the photochemically produced H_2O_2 in surface waters.[31]

17.6.2 Scavenging reagents: probes for reactive intermediates

Except for NO, which is relatively stable, and H_2O_2, which is only moderately reactive, the photo-intermediates described in the previous section are highly reactive. Although this makes them potentially important for indirect photolysis, their high reactivity results in typically very low (10^{-11} to 10^{-18} M) steady-state concentrations, which makes it difficult to measure them directly. Although techniques like pulsed laser spectroscopy[29,30] enable direct observation of some photo-intermediates, the most common way to measure them is through their reaction with *scavenging reagents* or *probes* (Table 17.3). To be useful as a probe, a molecule should have the following characteristics: it *should not* undergo direct photolysis, quench sensitizer triplets, or react with radical intermediates other than the one of interest; it *should* have a high rate constant for reaction with the species of interest and yield a single, stable product (or a few products) that can be measured easily.

If k_p, the second-order rate constant for reaction with the reactive intermediate of interest, is known for reaction of probe P with a photo-intermediate, X_{IP}, and if the

Table 17.3 Probe reagents used for photochemical intermediates

Intermediate	Reagent	Measured product
·OH	Benzene	Phenol
	Benzoic acid	Primarily salicylic acid
	Cumene (isopropylbenzene)	Side-chain and ring oxidation products
	Bromide	Br_2^-
	Thiocyanate (SCN^-)	SCN_2^-
	Butyl chloride	Loss of probe*
	p-chlorobenzoic acid	Loss of probe*
	Pyridine	Hydroxypyridine, other polar compounds
O_2^-·	NH_2OH	NO_2^-
$^1O_2$	2,5-Dimethylfuran	Diacetylethylene, H_2O_2
	Furfuryl alcohol	6-Hydroxy(2H)pyran-3(6H)-one, H_2O_2
	Disulfoton	Corresponding sulfoxide
	Histidine	Loss of probe*
	Tryptophan	Loss of probe*
	1,4-Diazabicyclo-[2.2.2]octane	None (quenches $^1O_2$)
	β-Carotene	None (quenches $^1O_2$)
e_{aq}^-	2-Chloroethanol	Chloride
	NO_3^-	NO_2^-
ROO·	Pyridine	Pyridine N-oxide
	Cumene	Side-chain oxidation products

*Probe loss measured because complex mixture of products is formed.

production and loss rates of X_{IP} are constant, the steady-state concentration of X_{IP} can be calculated from the following equations:

$$d[P]/dt = k_P[X_{IP}]_{ss}[P] = k_{exp}[P] \quad \text{where } k_P[X_{IP}]_{ss} = k_{exp}, \tag{17.12a}$$

or

$$[X_{IP}]_{ss} = k_{exp}/k_P, \tag{17.12b}$$

where k_{exp} is the experimentally measured pseudo-first order loss rate of the probe molecule. For Eq. 17.12 to apply, [P] must be low enough that it does not affect $[X_{IP}]_{ss}$ or the lifetime of X_{IP}. Steady-state production and loss of X_{IP} is a reasonable assumption for incubations of natural water samples under constant light conditions.

A wide variety of compounds has been used as probes for ·OH. For probes like butyl chloride, which forms multiple products with ·OH, loss of the probe is measured, but it usually is more desirable (and more sensitive) to measure a product of the probe with the intermediate. Concentrations of $^1O_2$ in natural waters also are measured by probes. Early studies used 2,5-dimethylfuran (DMF), which reacts with $^1O_2$ to yield diacetylethylene and H_2O_2 as the principal oxidation products, but furfuryl alcohol (FFA) now is commonly used. It reacts with $^1O_2$ to form a single organic product plus

H_2O_2, and H_2O_2 does not react with FFA. Both DMF and FFA react rapidly with $^1O_2$ (rate constants are 6.3×10^8 and 1.2×10^8 M^{-1} s^{-1}, respectively). Use of furans to trap $^1O_2$ has been criticized because some can be oxidized by species other than $^1O_2$ (e.g., H_2O_2). A range of other probes has been used for $^1O_2$ (Table 17.3), but none has achieved the popularity of DMF and FFA.

17.6.3 Photochemistry of inorganic nitrogen species

Photochemical oxidation of ammonia in seawater and soils was proposed as far back as the 1930s,[35] but convincing evidence for this was lacking until a 1970 laboratory study[23] showed that $^1O_2$ can oxidize ammonia to nitrite and nitrate. Nonetheless, the importance of photochemical oxidation of ammonia in water still is poorly understood. The photochemical activity of oxidized nitrogen forms is better documented. Zafiriou and coworkers[36] showed that both ions are photoactive. For nitrite, the principal reaction (Table 17.2, reactions 14, 15) forms nitric oxide, NO, and $\cdot$OH. The quantum yield of $\cdot$OH from NO_2^- varies with λ—from 0.015 to 0.08 over the range of 298–371 nm.[37] NO and $\cdot$OH radicals can recombine to form a null cycle, but $\cdot$OH in seawater is scavenged by Br^-, HCO_3^- or NOM (reactions 21–24, Table 17.2) allowing NO to accumulate at rates $> 10^{-12}$ $M\,h^{-1}$ during daylight. NO levels can reach 10^{-11} M or higher—five times the equilibrium concentration at the partial pressure of NO in marine air. Photolysis of NO_2^- thus may make the sea a *source* of atmospheric NO. Rapid reactions consume NO at night, but reaction with O_2 to produce NO_2^- (Table 17.2, reaction 20) is too slow to account for the loss of NO in the dark. Reactions with other radicals are likely. Net photolysis of NO_2^- in the photic zone of seawater under midsummer, mid-latitude conditions averages $\sim$10% per day.[38] Comparable studies on freshwaters are lacking, but it is reasonable to expect that similar processes occur. Nitrite concentrations in freshwaters usually are very low and represent a very small fraction of the inorganic N in surface waters (see Chapter 16), but the concentrations are generally not lower than those in the oceans.

Nitrate absorbs UV-B light ($\lambda_{max} = 302$ nm), and its main reaction upon absorbing a photon is production of NO_2^- plus either $\cdot O^-$ or ground-state atomic oxygen, $O(^3P)$ (Table 17.2, reactions 10, 12).[39] $\cdot O^-$ reacts rapidly with H^+ to yield $\cdot$OH, and O(3P), which is much less reactive, reacts with O_2 to form O_3. In turn, O_3 reacts with NO_2^- or decomposes to $\cdot$OH. The rate of $\cdot$OH photoproduction from nitrate by reactions 12 and 13 (Table 17.2) is $k_d[NO_3^-] = k_a \Phi_d[NO_3^-]$ (Eq. 17.3), where k_a is the wavelength-integrated light absorption coefficient and Φ_d is the quantum efficiency for $\cdot$OH production. According to Zepp et al.,[39] $\Phi_d = 0.013$–0.017 over the range of 20–30°C, and k_a (obtained from the UV absorbance spectrum of NO_3^- and seasonally varying solar irradiance) has a midday, midsummer value of 1.78×10^{-5} s^{-1} at 40° N. For these conditions, the near-surface production rate of $\cdot$OH from NO_3^- thus is $\sim 2.7 \times 10^{-7}$ $[NO_3^-]$. A reasonable range of $[NO_3^-]$ in most freshwaters is 10^{-6}–10^{-4} M (14–1400 µg/L as N), but summertime concentrations in streams draining row-crop agricultural areas in the Midwest of 10–20 mg/L as N (0.7–1.4 mM) are common. Rates of nitrate-induced $\cdot$OH production under these conditions are $\sim 2.7 \times 10^{-13}$ to 2.7×10^{-11} M/s for most freshwaters and up to $\sim 2.7 \times 10^{-10}$ M/s ($\sim 10^{-6}$ M/h) for high-nitrate agriculture waters. Net photolysis of nitrate to nitrite has been observed in seawater spiked with nitrate[40] but not at ambient nitrate levels. In general, photochemical reactions of nitrate

and ammonium in aquatic systems are more important for the radical intermediates they produce than for net consumption or transformation of the inorganic N ions.

17.6.4 Ozone

Although ozone is a major photochemical product in the atmosphere, it is not formed photochemically in surface waters, except to a minor extent in nitrate photolysis. Its main source in water bodies is absorption from the atmosphere, but atmospheric levels are low. Polluted urban air contains $\sim$100–200 ppb O_3, and rural air is orders of magnitude lower. The solubility of O_3 in water is greater than that of O_2 (12.2 vs. 1.35 mmol L^{-1} atm^{-1} at 25°C; Henry's law constants, H = 0.082 and 0.74 atm m^3 mol^{-1}, respectively). The deposition velocities of O_3 to natural water surfaces are not well known, but using a range of $\sim$0.1–0.5 cm/s estimated by analogy to similar gases we estimate that O_3 transfer from the atmosphere into water bodies is on the order of 0.01–0.1 mol m^{-2} yr^{-1}.

Little is known about the importance of ozone as a reactant in natural waters, but many studies have been conducted on the reactions of O_3 added to drinking water and wastewater by itself or in combination with UV light for disinfection and contaminant oxidation (see Chapter 13).

17.7 Iron photochemistry

17.7.1 Reactions of inorganic Fe with inorganic photo-intermediates

As described in Chapters 12 and 15, Fe^{II} autoxidation by the Haber-Weiss mechanism produces H_2O_2. Although this is not a photochemical process per se, it is significant for aquatic photochemistry in two ways. First, the oxidation product Fe^{III} is photochemically active; specifically, FeOH^{2+} can undergo direct photoreduction to produce Fe^{2+} and ·OH radicals, and Fe^{III} forms in general react rapidly with superoxide to form Fe^{2+} and O_2 (Table 17.2, reactions 26, 27). In fact, k_2 for reduction of Fe^{3+} by $O_2^- \cdot$ (1.5×10^8 M^{-1} s^{-1}) is higher than k_2 for Fe^{2+} oxidation by $O_2^- \cdot$ (1×10^7 M^{-1} s^{-1}). This affects Fe speciation in seawater such that during daylight most of the dissolved Fe is present as Fe^{2+} rather than Fe^{III}.[13] The relative importance of $O_2^- \cdot$ as a reducing agent for Fe^{III} versus oxidation of Fe^{2+} is pH dependent, however. The acid form of superoxide, HO$_2 \cdot$ (hydroperoxyl radical), becomes more abundant at low pH (pK_a = 4.8), thus accelerating superoxide dismutation (Table 17.2, reaction 7), effectively lowering $[O_2^- \cdot]_{ss}$ to the point that it no longer controls Fe speciation.

Second, unreacted Fe^{2+} reacts rapidly with H_2O_2 (produced by Fe^{II} oxidation or superoxide dismutation) to form ·OH and Fe^{3+} (Table 17.2, reaction 28), and as noted above, the Fe^{3+} is photoactive. Together, Fe^{2+} and H_2O_2 are known as Fenton's reagent. The combination is a highly effective oxidant, sometimes used in engineered photoreactors. Fenton's reagent could be produced in humic-rich waters, which often have high Fe concentrations. Hypolimnetic waters of low-alkalinity, oligotrophic lakes also can have Fe concentrations as high as several milligrams per liter (see Figure 15.7). Because water clarity is high in such lakes, light may penetrate to depths where Fe concentrations are high.

17.7.2 Photoreduction of Fe^{III} complexes with organic acids

Dissolved Fe^{III} species complexed with organic (carboxylic) acid ligands are involved in an important direct photo-redox process in which Fe^{III} is reduced to Fe^{2+} and the carboxyl group is oxidized to CO_2; that is, the acid undergoes decarboxylation by a ***ligand-to-metal charge transfer*** (***LMCT***) mechanism. Reduction of ferric ion and decarboxylation of EDTA by this mechanism has been known since 1963,[41] and photodecomposition of Fe^{III}-NTA complexes was reported nine years later.[42] The net reaction with NTA is

$$\begin{array}{c}
CH_2 - COO \\
| \\
N - CH_2 - COO - Fe^{III} \xrightarrow{h\nu} HN(CH_2COOH)_2 + HCHO + CO_2 + Fe^{2+}, \quad (17.13) \\
| \\
CH_2 - COO
\end{array}$$
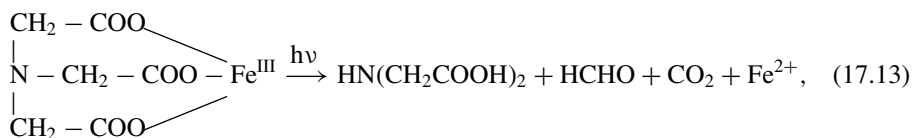
where $HN(CH_2COOH)_2$ is iminodiacetic acid and HCHO is formaldehyde. Fe^{2+} is reoxidized to Fe^{III} by dissolved O_2, which is rapid at neutral and alkaline pH. The net reaction thus involves oxidation of NTA by O_2, with Fe^{III} as a cyclic catalyst that is photoreduced (Eq. 17.13) and thermally oxidized.

The LMCT process involves photon absorption by a metal-ligand complex, promoting an electron from an occupied orbital of the ligand to an unoccupied orbital of the metal ion (Figure 17.5).[43] If the absorptivity of the complex is high, such transitions
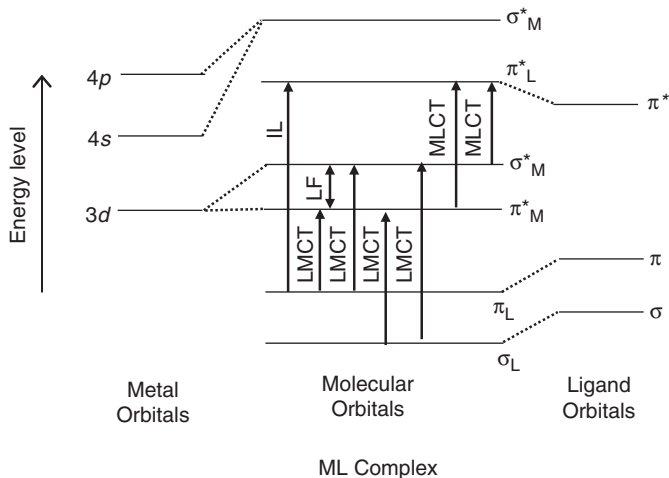
Figure 17.5 Molecular orbital energy diagram showing electronic transitions for octahedral metal-ligand complexes of first row transition metals. Key: p, s, d = second (angular) quantum numbers; σ and π are sigma and pi-type MOs; subscripts "M" and "L" indicate molecular orbitals derived from metal and ligand atomic orbitals, respectively. IL = internal ligand transition; LF = ligand-field transition—the splitting energy Δ between the e_g and $t_{2g}d$-orbitals of M in an octahedral field; LMCT = ligand-to-metal charge transfer; MLCT = metal-to-ligand charge transfer. Redrawn and modified from Balzani and Carassiti.[43]

have high probabilities because the orbitals have unlike spins. Iron is ideal for charge-transfer reactions because it is fairly abundant in aquatic systems, has two oxidation states, forms strong complexes (especially Fe^{III}), and has a charge-transfer absorption region at near-UV wavelengths that penetrate water fairly well. Some other transition metal ions have similar properties: Cu^{II}-Cu^{I}, Co^{III}-Co^{II}, $Mn^{III,IV}$-Mn^{II}, and significant rates of NTA photooxidation were found for Cu^{II}-NTA complexes irradiated at 350 nm.[44]

Photolysis of Fe^{III}-EDTA proceeds stepwise (Figure 17.6) through several intermediates including ED3A, EDDA, imidodiacetic acid (IMDA), and glycine. The overall reaction is faster at lower pH, and the relative importance of the intermediates also varies with pH.[45] Photoreduction of Fe^{III} also has been demonstrated for citric acid and several other mono- and dicarboxylic acids.[46] Tannic acid also reduces Fe^{III}, but this reaction does not require light. In some respects, the Fe^{III}-carboxylate redox process is not surprising; reduction of Fe^{III} by oxalic acid, $2Fe^{III} + C_2O_4^{2-} \rightarrow 2Fe^{II} + 2CO_2$, has been used for many decades as a *chemical actinometer* to measure light intensity and quantum efficiencies.
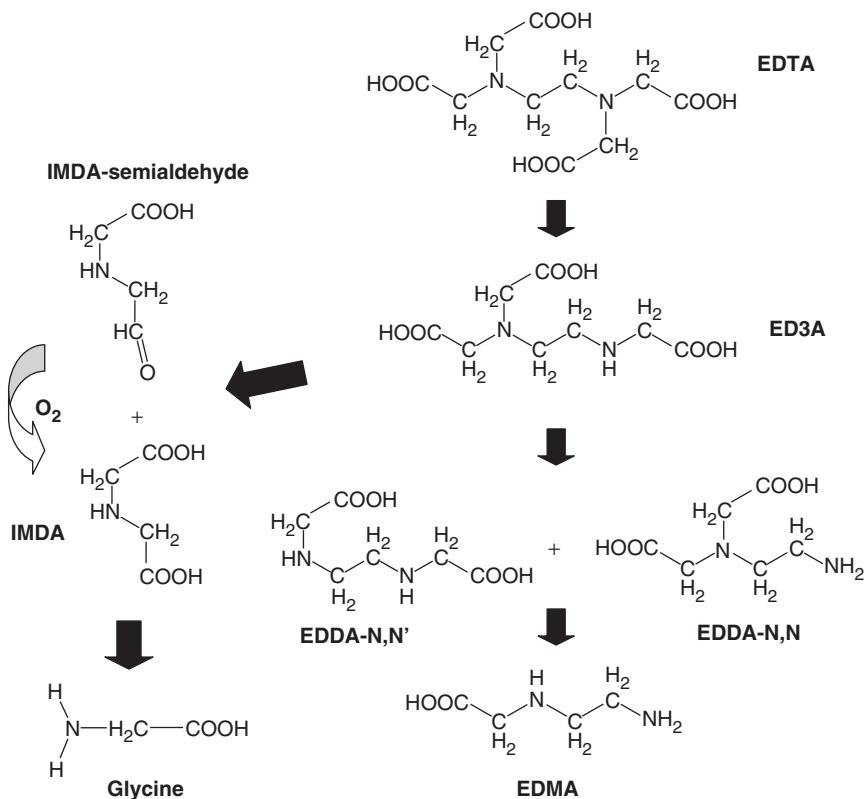
Figure 17.6 Degradation pathways for Fe^{III}-EDTA inferred from concentrations of EDTA and its photodegradation products in presence of Fe^{III} versus time. Intermediate IMDA-semialdehyde was not detected experimentally. Redrawn and modified from Lockhart and Blakely.[45]

Carboxyl groups are common in NOM and aquatic humic matter (AHM), and photoreduction of Fe^{III} by AHM and subsequent reoxidation of Fe^{II} by dissolved O_2 was demonstrated in highly colored surface waters.[46,47] O_2 consumption rates associated with this iron photo-cycle were found to be as high as 0.12 mg L^{-1} h^{-1}.[46] The process may be important in the chemical decomposition of AHM, in solubilizing Fe, and as a sink for dissolved O_2. Rates of O_2 consumption in humic-rich swamp water increased proportional to the amount of added Fe^{III} and DOC concentration and hyperbolically with light intensity. Methylation of carboxyl groups on AHM isolates caused a substantial decrease in the rate of O_2 consumption,[46] supporting the hypothesis that O_2 consumption in colored waters occurs by a charge-transfer iron-cycle mechanism involving iron complexed to carboxyl groups.

If charge-transfer decarboxylation is important, one would expect the carboxyl content of AHM to decrease with increasing exposure to sunlight. The initial study of this process[46] reported a molar ratio of CO_2 produced to O_2 consumed of 2.0 in a colored lake in Florida, supporting a net stoichiometry of $RCOOH + \frac{1}{2}O_2 \rightarrow ROH + CO_2$ (with the cyclic Fe^{III} reduction and Fe^{II} oxidation canceling out). However, more recent studies on colored river waters in Georgia by Xie et al.[47] indicate the process is more complicated and that it does not result in a *net* decrease in the carboxyl concentration of AHM. Instead, they found molar ratios of CO_2 produced to O_2 consumed from 0.8 to 2.5, and concentrations of carboxyl groups in the NOM decreased only slightly (and sometimes increased). Xie et al. concluded that the photodecarboxylation process involves a simultaneous regeneration of carboxyl groups, possibly by oxidative cleavage of aromatic rings, and proposed a net reaction of the following stoichiometry:

$$C_xH_yO_z(COOH)_m + aO_2 \xrightarrow{\text{metals, }h\nu} bCO_2 + cH_2O_2 + C_{x-b}H_{y'}O_{z'}(COOH)_{m-b}(COOH)_b$$

$$(17.14)$$
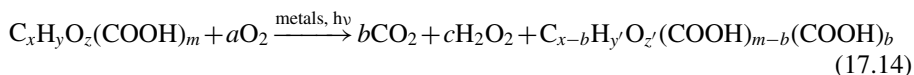
17.8 Photochemistry of suspended oxide particles

At least two kinds of photochemical reactions in aquatic systems involve particles: (1) iron and manganese oxides undergo reductive dissolution at least partly by an LMCT process involving surface complexes of organic acids; and (2) some metal oxides and sulfides photocatalyze redox reactions of organic solutes.[48] In the former case, the organic acid complexed to the oxide absorbs light energy and transfers an electron to the metal ion to which it is complexed. In the latter case, the particles behave as semiconductors, and when they absorb light, the resulting excited states produce a charge separation (electrons and holes, e^-/h^+) that form oxidizing or reducing sites on the particle surface.

17.8.1 Charge-transfer photoreductive dissolution

Reductive dissolution of ferric (hydr)oxides can occur photochemically by an LMCT process analogous to that described above.[49] Elevated levels of dissolved Fe^{2+} occur in solutions containing Fe (hydr)oxide particles and citrate or AHM illuminated in the near UV ($\lambda_{max} = 360$ nm). Iron (hydr)oxide polymorphs vary widely with respect to photo-redox properties. For example, photodissolution occurs with both lepidocrocite

(γ-FeOOH) and amorphous ferric (hydr)oxide, but the latter is much more photoactive. The variations appear to reflect differences in crystal and surface structure rather than differences in surface area or band gap energy (see next section for a definition of this term). Insoluble $Mn^{III,IV}$ oxides also are reduced to Mn^{2+} by humic and fulvic acids.[50,51]

For example, Waite et al.[51] explained the photoreductive dissolution of $MnO(OH)_2$ by fulvic acid (FA) as a four step model in which FA is sorbed rapidly to the oxide surface and forms a surface complex that undergoes electron-transfer by an LMCT mechanism:

(1) Adsorption

$$\equiv Mn^{IV}OH + FA \rightleftarrows \ \equiv Mn^{IV}FA + H_2O \tag{17.15a}$$

(2) Electron transfer

$$\equiv Mn^{IV}FA \rightarrow \ \equiv Mn^{IV}OMn^{II}FA_{ox} \tag{17.15b}$$

(3) Ligand exchange

$$\equiv Mn^{IV}OMn^{II}FA_{ox} + H_2O \rightarrow \ \equiv Mn^{IV}OMn^{II}OH_2^+ + FA_{ox}^{2-} \tag{17.15c}$$

(4) Detachment

$$\equiv Mn^{IV}OMn^{II}OH_2^+ + H^+ \rightleftarrows \ \equiv Mn^{IV}OH + Mn^{2+} + H_2O \tag{17.15d}$$
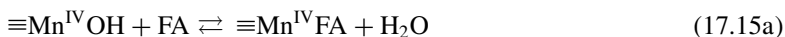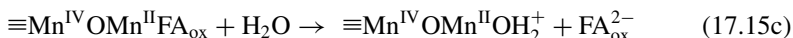
Recall that $\equiv$ means the species shown is part of the mineral surface. Electron transfer was assumed to be the rate-limiting step; steps (1) and (4) are rapid sorption/desorption processes, and step (3) is a rapid ligand-exchange. Not all reduced Mn necessarily desorbs in step (4). The production of Mn^{II} is first order in concentration of surface complex:

$$d[Mn^{II}]_T/dt = k_r[S\equiv Mn^{IV}FA], \tag{17.16}$$

where subscript T stands for total Mn^{II}, both free and adsorbed, and $[S\equiv Mn^{IV}A]$ is the concentration of Mn^{IV}-fulvic acid surface complex. If FA sorption is a rapid "preequilibrium step," the rate becomes

$$d[Mn^{II}]_T/dt = k_f K^c[\equiv Mn]_T \left[\frac{[FA]_T}{1 + K^c[FA]_T} \right], \tag{17.17}$$

where $[\equiv Mn]_T$ is the total concentration of Mn^{IV} oxide surface sites and K^c is the conditional formation constant for surface complexes ($K^c = [\equiv Mn^{IV}FA]/[Mn^{IV}OH][FA]$). Dissolution rates increased linearly with concentration of Mn oxide particles and hyperbolically with [AHM], and rates were higher in the light. These findings are significant in that they expand the domain of water bodies where photo-redox reactions of Fe and Mn can occur; both elements exist primarily as (hydr)oxide particles in oxic surface waters.

Initial photo-redox studies of Fe and Mn oxides focused on the importance of the process in solubilizing Fe and Mn rather than on the organic ligands, but the findings also

were interpreted as an LMCT process involving electron transfer from adsorbed organic ligands to $\equiv Fe^{III}$ on the oxide surface. As described above, this leads to decarboxylation of organic acids. Subsequent studies found that the reaction occurs in iron-rich mountain streams, confirmed the LMCT mechanism, and identified some organic products.[52] Organic compounds that induce the photo-redox process include carboxylic acids, amino acids, and mercapto acids, which form inner-sphere complexes with Fe^{III} on the oxide surfaces. Adsorbed amines, alcohols, and glycols that do not form such complexes, however, also induce photodissolution of Fe (hydr)oxides.

Ferric (hydr)oxides are photoactive even when organic ligands are not present. Irradiation of organic-free suspensions of γ-FeOOH and hematite (α-Fe$_2$O$_3$) with near-UV light increased [Fe^{2+}] in solution.[49] A possible mechanism is charge-transfer from a bound hydroxide to an excited surface lattice $\equiv Fe^{III}$:[53]

$$\equiv Fe^{III}(:OH^-) + h\nu \rightarrow\ \equiv Fe^{III*}(:OH^-) \rightarrow\ \equiv Fe^{II} + \cdot OH \qquad (17.18)$$
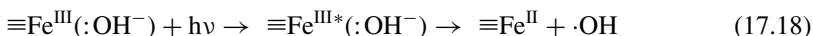
Fe^{II} dissociates rapidly from the lattice, and the mechanism thus produces Fenton's reagent in solution. An alternative mechanism is a semiconductor model, in which electrons and holes photo-generated in the Fe oxide semiconductor lattice migrate to surface sites, respectively producing $\equiv Fe^{II} + OH^-$ and $\equiv Fe^{III} + \cdot OH$ (see next section for details on the semiconductor mechanism). Although it is not possible to distinguish this model from the first mechanism based on analysis of the products alone, very short diffusion lengths of electrons and holes in Fe oxides[53] argue against the semiconductor mechanism. Although the $\cdot OH$ produced in photoreduction of iron (hydr)oxides could be generated from surface reactions (e.g., Eq. 17.18), it also could be generated in solution from autoxidation of Fe^{2+} by the Haber-Weiss mechanism. Using benzoic acid as a $\cdot OH$ probe and comparing production rates of Fe^{2+} and $\cdot OH$, Cunningham et al.[53] concluded that most of the $\cdot OH$ is produced by oxidation of Fe^{2+} in solution.

17.8.2 Semiconductor photochemistry

The photocatalytic activity of metal oxides has been a topic of interest for many decades. For example, Rao and Dhar[35] proposed in 1931 that ammonia is oxidized photochemically on soil particles, but strong evidence and a mechanism were lacking. Production of H$_2$O$_2$ by illuminated ZnO suspensions was reported in 1953, and compounds like formate and oxalate increased H$_2$O$_2$ production rates,[54] but it was not until 1972 that Fujishima and Honda[55] reported the oxidation of H$_2$O on illuminated TiO$_2$. Although related reduction of water to produce H$_2$ could not be achieved without supplying additional energy, this work stimulated much research on the photocatalytic activity of metal oxide semiconductor/liquid systems. Much of this work was aimed at converting light energy into useful chemical energy by splitting water to generate H$_2$ and O$_2$. Research toward this goal led to the finding that semiconductor oxides can photocatalyze thermodynamically feasible but kinetically slow chemical reactions, including those of organic and inorganic pollutants.

Mechanistically, semiconductor photo-redox catalysis is explained by the Gerischer-Willig model[56] (Figure 17.7). Photon absorption by the solid promotes an electron to an excited state and leads to charge separation—formation of a free electron and positive hole (or e^-/h^+ pair). The ground state is referred to as the *valence band* (VB) and the

(a)

Si : Si : Si : Si
·· ·· ·· ··
Si : Si : Si : Si
·· ·· ·· ··
Si : Si : Si : Si
·· ·· ·· ··
Si : Si : Si : Si

Perfect crystal

mobile electron

Si : Si : Si :/Si
·· ·· ·· ·/·
Si : Si : As : Si
·· ·· ·· ··
Si : Si : Si : Si
·· ·· ·· ··
Si : Si : Si : Si

n-type

hole

Si : Si : Si : Si
·· ·· ·· · ·
Si : Si : B : Si
·· ·· ·· ··
Si : Si : Si : Si
·· ·· ·· ··
Si : Si : Si : Si

p-type

(b)

E

Conduction Band

E_{CB}

E_{BG}

Valence Band

E_{VB}

(c)

E

E_{CB}

E_{VB}

n-type semiconductor

A/A^+

Solution

E_{CB}

E_{VB}

Interface

A/A^+

Semiconductor Solution

$h\nu$

$E_{CB} \leftarrow e^-$

h^+

E_{VB}

$A \leftarrow A^+$
$\leftarrow e^-$

Further reaction

Electron
transfer

$E_{CB}\ e^- \uparrow$

$h^+ \mapsto$

E_{VB}

A/A^+

depletion layer

Figure 17.7 (a) Semiconductors derived from silicon: pure Si crystals are not semiconductors, and all atoms in the crystal have completed bonds; n-type semiconductors have atoms with more valence electrons than Si (e.g., arsenic) present as impurities, providing mobile electrons to the crystal; impurities in p-type semiconductors (e.g., boron) have fewer valence electrons than Si, creating an electron deficiency (or positive holes, h^+). (b) Electron bands in semiconductors: E_{VB} = highest ground state orbitals, or *valence band*; E_{CB} = lowest unoccupied (excited) orbitals, or *conduction band*; the difference, $E_{CB} - E_{VB} = E_{BG}$, the band gap energy. Absorption of light energy $\geq E_{BG}$ promotes electrons from the ground state to excited state. (c) Immersion of an n-type semiconductor in an electrolyte solution results in a charge-transfer equilibration that causes bending of CB and VB at the semiconductor surface, thus posing a barrier against further charge transfer. Absorption of photon creates an e^-/h^+ pair at the semiconductor surface. The electron migrates inward in the nearly empty CB, and the hole migrates toward the surface, acting as an oxidizing agent for reactant A, sorbed on surface. Redrawn based on figures in Brezonik[1] and Fox.[57]

excited state as the ***conduction band*** (CB). The energy difference, E_{bg}, between the bands, in eV or wavelength of light energy, is called the ***band gap energy***. VB and CB correspond to the highest occupied (ground state) molecular orbitals and lowest unoccupied orbitals of the material. When a semiconductor is in a solution containing a redox couple, charge transfer occurs across the interface to equilibrate potentials, and the resulting electrical field causes band bending from the lattice interior to the interface. This facilitates charge separation in electron-rich n-type semiconductors. When an e^-/h^+ pair forms by photon absorption in a semiconductor, the electron migrates toward the crystal interior in the almost empty conduction band, and the hole migrates to a surface site, where it acts as an oxidizing agent, accepting an electron from an adsorbed solute. The buildup of electrons in the semiconductor interior does not continue indefinitely, however. These electrons have three possible fates: they may migrate to other surface sites that act as reducing agents for sorbed species; they may discharge at a cathode in a photoelectrochemical cell; or they may cause photoreductive dissolution of the semiconductor.

The following attributes affect the effectiveness of semiconductors as photo-redox catalysts:

(i)   CB and VB band positions, that is, potentials (in V) of the e^- and h^+ (reducing and oxidizing) sites;

(ii) E_{bg}, the band gap energy, which determines λ_{max} for semiconductor excitation;

(iii) the rate of charge transfer to/from the semiconductor from/to the aqueous species (interfacial charge-transfer kinetics);

(iv) stability of the semiconductor toward photoreductive or photooxidative dissolution; and

(v)   sorption characteristics of the surface and reactants, for example, proximity of sorption sites to oxidizing or reducing sites at the interface.

Most of these attributes vary with solution conditions like pH and ionic strength.[57] Table 17.4 lists band positions and E_{bg} for some semiconductor photocatalysts, and Table 17.5 lists oxidation potentials for organic compounds containing various functional groups. Comparison of the semiconductor band positions with redox potentials for the compounds suggests that redox reactions of various organic compounds should be catalyzable by several semiconductors. Most of the semiconductors do not occur in natural waters, but some of the oxides are found in suspended and bottom sediments.

Engineers have studied the possibilities of using semiconductor photo-redox catalysts in reactors to treat waters with organic contaminants for over two decades,[58] but commercial applications have been slow to develop. Early work showed that cyanide and sulfite could be photooxidized using TiO_2, and complete photodegradation of chlorinated C_1 and C_2 compounds—chloroform, carbon tetrachloride, dichloroethane, and perchloroethylene—on illuminated TiO_2 has been demonstrated. More complicated organic compounds, including pentachlorophenol, benzene, biphenyl, dioxins, PCBs, aromatic hydrocarbons, dodecylbenzene sulfonate, and 2,4,5-T also are photodegradable on TiO_2 (for more detailed reviews, see Brezonik[1] and Hoffmann et al.[58]). In all cases, O_2 was the oxidant; it or another oxidant must be present to trap electrons produced by photoactivation and minimize e^-/h^+ recombination. Other semiconductors, including ZnO, CdS, SnO_2, and WO_3, have been studied, but TiO_2 generally is the most efficient catalyst for oxidation reactions.

Table 17.4 Band positions and band gap energies of some semi-conductor photocatalysts[*]

Semi-conductor	VB[†]	CB[†]	BGE[†]		
	V	V	eV	nm[§]	pH
TiO$_2$ (anatase)	+3.0	0.0	3.0	413	1.0
SnO$_2$	+3.8	+0.3	3.5	354	1.0
Fe oxides[‡]	+1.94–2.1		2.0	585–640	12.0
α−Fe$_2$O$_3$ (hematite)			2.34	530	—
α−FeOOH (goethite)			2.64	470	—
ZnO	+2.9	−0.1	3.0	413	1.0
WO$_3$	+2.9	+0.2	2.7	459	1.0
CdS	+2.0	−0.4	2.4	517	1.0
CdSe	+1.4	−0.3	1.7	729	1.0
GaAs	+0.7	−0.7	1.4	886	1.0
GaP	+1.1	−1.2	2.3	539	1.0
SiC	+1.6	−1.4	3.0	413	1.0

[*]Tabulated from Fox.[57]
[†]VB, valence band; CB, conduction band; BGE, band gap energy.
[§]Maximum wavelength with enough energy to allow e^-/h^+ formation.
[‡]Fe oxides represents the range for α- and γ-Fe$_2$O$_3$ and α-, ß-, γ, and
δ−FeOOH; values for hematite and goethite are for dry solids.

Table 17.5 Oxidation potentials of some organic compounds[*]

Compound	Oxid. potential (V vs. SCE)[†]
Acetic acid	1.60
N,N-Dimethylacetamide	1.02
4-Aminoaniline	0.18
Anthracene	1.09
1,3-Butadiene	2.31
Triethylamine	0.66
4-Methyl-heptane-2,6-dione	1.56
2,6-Di-*tert*-butyl-4-methylphenol	1.21
Pyridine (C$_5$H$_5$N)	1.82
Pyrrole (C$_4$H$_4$N)	0.76
Thiophene (C$_4$H$_4$S)	1.84

[*]Tabulated from Fox.[57]
[†]SCE = saturated calomel electrode; measured in acetonitrile.

One drawback to TiO$_2$ is its large bandgap energy, 3.2 eV, which means that it is photoactivated primarily by UV light (λ_{max} = 387 nm). Recent studies using doped particles have extended the range into visible wavelengths.[59,60] Other factors aside, semiconductors with smaller bandgap values and higher λ_{max} are preferred so that sunlight can be used as the light source. CdS (λ_{max} = 517 nm) is effective in oxidizing sulfur-containing compounds, including H$_2$S and thiols, as well as phenols and EDTA, but unfortunately it undergoes oxidative dissolution in photocatalytic reactors, producing (so far unresolvable) toxic concentrations of cadmium, especially at low pH.

Rates of photocatalytic oxidation usually increase hyperbolically with concentration of the compound being oxidized, suggesting that (1) oxidation rates are proportional to the surface area of catalyst covered by the compound and (2) compound-surface interactions can be described by the Langmuir equation. Oxidation rates with TiO_2 and CdS as photocatalysts are first order in O_2[61] and light intensity,[62] and variations with pH are consistent with pH effects on compound adsorption to CdS surfaces.[63] Reaction of adsorbed compounds is thought to occur with holes at the CdS surface. In contrast, adsorption and reaction between holes and organic compounds is not always found with TiO_2, and indirect photocatalytic mechanisms involving ·OH have been proposed for photooxidation of phenol[63] and 2,4,5-T[64] on TiO_2.

Photocatalytic production of H_2O_2 and organic peroxides has been observed in illuminated suspensions of TiO_2, ZnO, and desert sand in the presence of O_2 and organic electron donors.[65] Values of $[H_2O_2]_{ss}$ as high as 10^{-4} M were measured in ZnO suspensions, and high yields were obtained only when electron donors were adsorbed to the oxide surfaces. Organic peroxides also were found in acetate-containing ZnO suspensions, and additional reactions likely are induced by the peroxides. Adsorbed donors (D) are assumed to react with a valence band hole ($D + h_{vb}^+ \rightarrow D^{·+}$), which inhibits e^-/h^+ recombination and permits CB electrons to react with O_2 to form peroxides, e.g., ($O_2 + 2e_{cb}^+ + 2H_2O \rightarrow 2H^+ + H_2O_2$).

Photocatalysts also have applications beyond chemical destruction. The reactive oxygen species produced are also capable of acting as disinfectants (by oxidizing bacteria and other microorganisms).[66,67] This has potential applications in the solar disinfection of water or the production of antibacterial coatings. Of course, there is also concern that human exposure to such reactive nanoparticles could have unanticipated, adverse effects.[68]

Problems

17.1. You are investigating two compounds proposed for use as herbicides: Dlonra and Kinozerb. An obvious concern is that they may be persistent in the environment. You conduct photolysis tests by exposing aqueous solutions of the compounds to sunlight on the same day at the same time, and find that each degrades with a nearly identical rate constant. In searching the literature, you find values of the quantum yields: 1.18×10^{-4} for Dlonra and 0.71 for Kinozerb. Propose and justify an explanation for these findings.

17.2. Using equation 17.7 and the information provided in the text, demonstrate graphically how the concentration of dissolved oxygen and/or the characteristic lifetime of the triplet state influence the observed quantum yield of a compound.

17.3. The planet Brite does not turn about its axis, and thus receives continuous light from its distant star (known as Kcirtap) on the habitable side of the planet. The Britelians are thus great photochemists, and are studying the degradation of Mailliw, which is used on planet Brite as a cleaning agent. They found that it degrades with a rate constant of 9.66×10^{-4} s^{-1} upon exposure to light from Kcirtap. Given the following information, determine the quantum yield of

the compound. The Absorbance of Mailliw was measured in a 1-cm path-length cell at a concentration of 50 µM.

Wavelength nm	Scalar irradiance mEi cm^{-2} s^{-1}	Absorbance
300	1.00E-08	0.60
301	5.00E-08	0.50
302	1.00E-07	0.40
303	1.50E-07	0.35
304	2.00E-07	0.25
305	2.50E-07	0.25
306	3.00E-07	0.30
307	3.50E-07	0.35
308	4.00E-07	0.41
309	4.50E-07	0.47
310	5.00E-07	0.53
311	5.50E-07	0.60
312	6.00E-07	0.53
313	6.50E-07	0.47
314	7.00E-07	0.41
315	7.50E-07	0.35
316	8.00E-07	0.30
317	8.50E-07	0.25
318	9.00E-07	0.19
319	9.50E-07	0.15
320	1.00E-06	0.11
321	1.05E-06	0.09
322	1.10E-06	0.07
323	1.15E-06	0.05
324	1.20E-06	0.03
325	1.25E-06	0.01

17.4. The steady-state concentration of hydroxyl radical ($[\cdot OH]_{ss}$) can be determined in photolysis experiments using a variety of probe compounds, including 1-butyl chloride, which has a known rate constant for reaction with $\cdot OH$ of 3×10^9 M^{-1} s^{-1}.[19] Because butyl chloride forms a variety of products in reacting with $\cdot OH$, loss of reactant is measured rather than formation of a specific product. In an experiment with samples of agricultural runoff high in nitrate concentration (a source of $\cdot OH$) 1.8 mM of the probe compound were spiked into the samples in quartz bottles and incubated at constant light conditions for exactly 2.0 h. Analysis of the butyl chloride remaining at the end of the incubation by a headspace method[18] yielded the following results:

Sample	1	2	3	4
[butyl chloride, mM]	0.9	1.1	1.2	1.5

Estimate the value of $[\cdot OH]_{ss}$ in each of the samples. Which sample likely had the highest nitrate concentration?

17.5. The photodegradation of Fe-EDTA complexes occurs by an LMCT process and follows the general pathway shown in Figure 17.6. Simulate the formation and loss of the various intermediates as a function of time using Acuchem. Rate constants for the various steps are not known with great accuracy, but the following values will produce simulations generally similar to concentration-time plots reported by Lockhart and Blakely:[45]

(1) EDTA $\rightarrow$ ED3A, $k_1 = 3.2$;
(2) ED3A $\rightarrow$ EDN$'$, $k_2 = 0.8$;
(3) ED3A $\rightarrow$ EDAN, $k_3 = 0.8$;
(4) EDN$'$ $\rightarrow$ EDMA, $k_4 = 0.5$;
(5) EDAN $\rightarrow$ EDMA, $k_5 = 0.5$;
(6) ED3A $\rightarrow$ 2 IMDA, $k_6 = 0.8$;
(7) IMDA $\rightarrow$ GLY, $k_7 = 0.5$.

All rate constants are pseudo-first order in units of d^{-1}. Use an initial concentration of 1.5×10^{-3} M for EDTA and assume that it is all complexed by Fe^{III}. You can assume constant light conditions and constant Fe_T concentrations in this exercise. Compare your results to those of Lockhart and Blakely. You may wish to vary the values of some of the rate constants to determine effect on the shapes of the concentration-time plots. The concentration-time plots reported by Lockhart and Blakely do not appear to fit pseudo-first-order kinetics exactly for all intermediates. Do not frustrate yourself trying to reproduce their plots exactly; this probably cannot be done using the simple pseudo-first-order model you will use.

References

1. Brezonik, P. L. 1994. *Chemical kinetics and process dynamics in aquatic systems*, CRC Press, Boca Raton, Fla.
2. Bushaw, K. L., R. G. Zepp, M. A. Tarr, D. Schulz-Jander, R. A. Bourbonniere, R. E. Hodson, W. L. Miller, D. A. Bronk, and M. A. Moran. 1996. Photochemical release of biologically available nitrogen from aquatic dissolved organic matter. *Nature*: **381**: 404–407.
3. Adamson, A. W. 1979. *A textbook of physical chemistry*, 2nd. ed., Academic Press, New York, 1979.
4. Zepp, R. G., and D. M. Cline. 1977. Rates of direct photolysis in aquatic environment. *Environ. Sci. Technol.* **11**: 359–366.
5. Leifer, A. 1988. *The kinetics of environmental aquatic photochemistry. Theory and practice*, Am. Chem. Soc., Washington, D.C.
6. Center for Exposure Assessment Modeling. 1999. GCSOLAR, ver. 1.2, U.S. EPA, Athens, Ga. (available at www.epa.gov/ceampubl/swater/gcsolar/).
7. Gueymard, C. 2001. Parameterized transmittance model for direct beam and circumsolar spectral irradiance. *Solar Energy* **71**: 325–346; Gueymard, C. 1995. SMARTS, a simple model of the atmospheric radiative transfer of sunshine: algorithms and performance assessment, Prof. Paper FSEC-PF-270-95, Florida Solar Energy Ctr., Cocoa, Fla.
8. Spinhirne, J. D., and A. E. S. Green. 1978. Calculation of the relative influence of cloud layers on received ultraviolet and integrated solar radiation. *Atmos. Environ.* **12**: 2449–2454.

9. Smith, R. C., and K. S. Baker. 1978. Optical classification of natural waters. *Limnol. Oceanogr.* **23**: 260–267; Baker, K. S., and R. C. Smith. 1982. Bio-optical classification and model of natural waters. *Limnol. Oceanogr.* **27**: 500–509.

10. Smith, R. C., and K. S. Baker. 1979. Penetration of UV-B and biological effect of dose-rates in natural waters. *Photochem. Photobiol.* **29**: 311–323.

11. Zepp, R. G. 1980. Assessing the photochemistry of organic pollutants in aquatic environments. In *Dynamics, exposure, and hazard assessment of toxic chemicals*, R. Haque (ed.), Ann Arbor Science Publ., Ann Arbor, Mich., 69–110.

12. Miller, G. C., and R. G. Zepp. 1979. Effects of suspended sediments on photolysis rates of dissolved pollutants. *Water Res.* **13**: 453–459.

13. Voelker, B. M., and D. L. Sedlak. 1995. Iron reduction by photoproduced superoxide in seawater. *Mar. Chem.* **50**: 93–102.

14. Hoigne, J. 1990. Formulation and calibration of environmental reaction kinetics: oxidations by aqueous photooxidants as an example, In *Aquatic chemical kinetics*, W. Stumm (ed.), Wiley-Interscience, New York, 43–70.

15. Cooper, W. J., R. G. Zika, R. G. Petasne, and J. M. C. Plane. 1988. Photochemical formation of hydrogen peroxide in natural waters exposed to sunlight. *Environ. Sci. Technol.* **22**: 1156–1160.

16. Cooper, W. J., and R. G. Zika. 1983. Photochemical formation of hydrogen peroxide in surface and ground waters exposed to sunlight. *Science* **220**: 711–712.

17. Cooper, W. J., R. G. Zika, R. G. Petasne, and A. M. Fischer. 1989. Sunlight-induced photochemistry of humic substances in natural waters: major reactive species. In *Aquatic humic substances; influence on fate and treatment of pollutants*, P. MacCarthy and I. H. Suffet (eds.), Adv. Chem. Ser. **219**, Am. Chem. Soc., Washington, D.C., 333–362.

18. Brezonik, P. L, and J. Fulkerson. 1998. Nitrate-induced photolysis in natural waters: controls on concentrations of hydroxyl radical photo-intermediates by natural scavenging agents. *Environ. Sci. Technol.* **32**: 3004–3010.

19. Haag, W. R., and J. Hoigne. 1985. Photo-sensitized oxidation in natural waters via ·OH radicals. *Chemosphere* **14**: 1659–1671.

20. Mill, T., D. G. Hendry, and H. Richardson. 1980. Free-radical oxidants in natural waters. *Science* **207**: 886–887.

21. Russi, H., D. Kotzias, and F. Korte. 1982. Photoinduzierte Hydroxylierungsreaktionen organischer Chemikalien in natürlichen Gewässern—Nitrate als potentielle OH-radikalquellen. *Chemosphere* **11**: 1041–1048.

22. Zafiriou, O. C., M. B. True, and E. Hayon. 1987. Consequences of OH radical reaction in sea water: formation and decay of Br_2^- ion radical; and True, M. B., and O. C. Zafiriou. 1987. Reaction of Br_2^- produced by flash photolysis of sea water with components of the dissolved carbonate system. In *Photochemistry of environmental aquatic systems*, R. G. Zika and W. J. Cooper (eds.), ACS Symp. Ser. **327**, Am. Chem. Soc., Washington, D.C., 89–105 and 106–115.

23. Joussot-Dubien, J., and A. Kadiri. 1970. Photosensitized oxidation of ammonia by singlet oxygen in aqueous solution and in seawater. *Nature* **227**: 700–701.

24. Zepp, R. G., N. L. Wolfe, G. L. Baughman, and R. C. Hollis. 1977. Singlet oxygen in natural waters. *Nature* **267**: 421–423.

25. Frimmel, F. H., H. Bauer, J. Putzien, P. Murasecco, and A. M. Braun. 1987. Laser flash photolysis of dissolved aquatic humic material and the sensitized production of singlet oxygen. *Environ. Sci. Technol.* **21**: 541–545.

26. Rogers, M. A. J., and P. J. Snowden. 1982. Lifetime of oxygen (O2(1.DELTA.g)) in liquid water as determined by time-resolved infrared luminescence measurements. *J. Am. Chem. Soc.* **104**: 5541–5543.

27. Haag, W. R., J. Hoigne, E. Gassmann, and A. M. Braun. 1984. Singlet oxygen in surface waters. Part I: furfuryl alcohol as a trapping agent. *Chemosphere* **13**: 631–640; Haag, W. R., and J. Hoigne. 1986. Singlet oxygen in surface waters. 3. Photochemical formation and steady-state concentrations in various types of waters. *Environ. Sci. Technol.* **20**: 341–348.

28. Latch, D. E., and K. McNeill. 2006. Microhetergeneity of singlet oxygen distributions in irradiated humic acid solutions. *Science* **311**: 1743–1747.

29. Hoigne, J., B. C. Faust, W. R. Haag, F. E. Scully, Jr., and R. G. Zepp. 1989. Aquatic humic substances as sources and sinks of photochemically produced transient reactants. In *Aquatic humic substances; influence on fate and treatment of pollutants*, P. MacCarthy and I. H. Suffet (eds.), Adv. Chem. Ser. **219**, Am. Chem. Soc., Washington, D.C., 363–381.

30. Fischer, A. M., D. S. Kliger, J. S. Winterle, and T. Mill. 1985. Direct observation of phototransients in natural water. *Chemosphere* **14**: 1299–1306.

31. Zepp, R. G., A. M. Braun, J. Hoigne, and J. A. Leenheer. 1987. Photoproduction of hydrated electrons from natural organic solutes in aquatic environments. Environ. Sci. Technol. 21: 485–490.

32. Wang, W., O. C. Zafiriou, I.-Y. Chan, R. G. Zepp, and N. V. Blough. 2007. Production of hydrated electrons from photoionization of dissolved organic matter in natural waters. *Environ. Sci. Technol.* **41**: 1601–1607.

33. Breugem, P., P. van Noort, S. Velberg, E. Wondergem, and J. Zijlstra. 1986. Steady state concentrations of the phototransient hydrated electron in natural waters. *Chemosphere* **15**: 717–724.

34. Burns, S. E., J. P. Hassett, and M. V. Rossi. 1997. Mechanistic implications of the intrahumic dechlorination of mirex. *Environ. Sci. Technol.* **31**: 1365–1371.

35. Rao, G. G., and N. R. Dhar. 1931. Photosensitized oxidation of ammonia and ammonium salts and the problem of nitrification in soils. *Soil Sci.* **31**: 379–384.

36. Zafiriou, O. C., M. McFarland, and R. H. Bromund. 1980. Nitric oxide in seawater. *Science* **207**: 637–639.

37. Zafiriou, O. C., and R. Bonneau. 1987. Wavelength-dependent quantum yield of OH radical formation from photolysis of nitrite ion in water. *Photochem. Photobiol.* **45**: 723.

38. Zafiriou, O. C. 1983. Natural water photochemistry. In *Chemical oceanography*, Vol. 8, J. P. Riley (ed.), Academic Press, London, 339–379.

39. Zepp, R. G., J. Hoigne, and H. Bader. 1987. Nitrate-induced photooxidation of trace organic chemicals in water. *Environ. Sci. Technol.* **21**: 443–450.

40. Zafiriou, O. C., and M. B. True. 1979. Nitrate photolysis in seawater by sunlight. *Mar. Chem.* **8**: 33–42.

41. Lambert, J. L., C. E. Godsey, and L. M. Seitz. 1963. Preparation and photodecomposition of the complex acid hydrogen aquoethylendiaminetetraacetatoferrate(III). *Inorg. Chem.* **2**: 125–127.

42. Trott, T., R. W. Henwood, and C. H. Langford. 1972. Sunlight photochemistry of ferric nitrilotriacetate complexes. *Environ. Sci. Technol.* **6**: 367–368.

43. Balzani, V., and V. Carassiti. 1970. *Photochemistry of coordination compounds*, Academic Press, New York.

44. Langford, C. H., M. Wingham, and V. S. Sastri. 1973. Ligand photooxidation in copper(II) complexes of nitrilotriacetic acid. Implications for natural waters. *Environ. Sci. Technol.* **7**: 820–822.

45. Lockhart, H. B., Jr., and R. V. Blakely. 1975. Aerobic photodegradation of Fe(III)-(ethylenedinitrilo)tetraacetate (ferric EDTA). Implications for natural waters. *Environ. Sci. Technol.* **9**: 1035–1038.

46. Miles, C. J., and P. L. Brezonik. 1981. Oxygen consumption by a photochemical ferrous-ferric catalytic cycle. *Environ. Sci. Technol.* **15**: 1089–1095.

47. Xie, H., O. C. Zafiriou, W.-J. Cai, R. G. Zepp, and Y. Wang. 2004. Photooxidation and its effects on the carboxyl content of dissolved organic matter in two coastal rivers in the southeastern United States. *Environ. Sci. Technol.* **38**: 4113–4119.

48. Sulzberger, B. 1990. Photoredox reactions at hydrous metal oxide surfaces: a surface coordination chemistry approach. In *Aquatic chemical kinetics*, W. Stumm (ed.), Wiley-Interscience, New York, 401–436.

49. Waite, T. D., and F. M. M. Morel. 1984. Photoreductive dissolution of colloidal iron oxide: effect of citrate. *J. Colloid Interface Sci.* **102**: 121–137.

50. Sunda, W. G., S. A. Huntsman, and G. R. Harvey. 1983. Photoreduction of manganese oxides in seawater and its geochemical and biological implications. *Nature* **301**: 234–236.

51. Waite, T. D., I. C. Wrigley, and R. Szymczak. 1988. Photoassisted dissolution of a colloidal manganese oxide in the presence of fulvic acid. *Environ. Sci. Technol.* 22: 778–785.

52. McKnight, D. M., B. A. Kimball, and K. E. Bencala. 1988. Iron photoreduction and oxidation in an acidic mountain stream. *Science* **240**: 637–640.

53. Cunningham, K. M., M. C. Goldberg, and E. R. Weiner. Mechanisms for aqueous photolysis of adsorbed benzoate, oxalate, and succinate on iron oxyhydroxide (goethite) surfaces. *Environ. Sci. Technol*. **22**: 1090–1097.

54. Markin, M. C., and K. J. Laidler. 1953. A kinetic study of photo-oxidations on the surface of zinc oxide in aqueous suspensions. *J. Phys. Chem.* **57**: 363–369; Rubin, T. R., J. G. Calvert, G. T. Rankin, and W. M. MacNevin. 1953. Photochemical synthesis of hydrogen peroxide at zinc oxide surfaces. *J. Am. Chem. Soc.* **75**: 2850–2853.

55. Fujishima, A., and K. Honda. 1972. Electrochemical photolysis of water at a semiconductor electrode. *Nature* **238**: 37–38.

56. Gerischer, H., and F. Willig. 1976. Reaction of excited dye molecules at electrodes. *Top. Curr. Chem.* **61**: 31–84.

57. Fox, M. A. 1983. Organic heterogeneous photocatalysis: chemical conversions sensitized by irradiated semiconductors. *Acct. Chem. Res.* **16**: 314–321.

58. Hoffmann, M. R., S. T. Martin, W. Choi, and D. W. Bahnemann. 1995. Environmental applications of semiconductor photocatalysis. *Chem. Rev.* **95**: 69–96.

59. Livraghi, S., M. R. Chierotti, E. Giamello, G. Magnacca, M. C. Paganini, G. Cappelletti, and C. L. Bianchi. 2008. Nitrogen-doped titanium dioxide active in photocatalytic reactions with visible light: a multi-technique characterization of differently prepared materials. *J. Phys. Chem. C* **112**: 17244–17252.

60. He, Z.-Q., X. Xu, S. Song, L. Xie, J.-J. Tu, J.-M. Chen, and B. Yan. 2008. A visible light-driven titanium dioxide photocatalyst co-doped with lanthanum and iodine: an application in the degradation of oxalic acid. *J. Phys. Chem. C* **112**: 16431–16437.

61. Davis, A. P., and C. P. Huang. 1990. The removal of substituted phenols by a photocatalytic oxidation process with cadmium sulfide. *Water Res.* **24**: 543–550.

62. Tunesi, S., and M. A. Anderson. 1987. Photocatalysis of 3,4-DCB in TiO_2 aqueous suspensions; effects of temperature and light intensity; CIR-FTIR interfacial analysis. *Chemosphere* **16**: 1447–1456.

63. Davis, A. P., and C. P. Huang. 1991. The photocatalytic oxidation of sulfur-containing organic compounds using cadmium sulfide and the effect on CdS photocorrosion. *Water Res.* **25**: 1273–1278.

64. Barbeni, M., M. Morello, E. Pramauro, E. Pelizzetti, M. Vicenti, E. Borgarello, and N. Serpone. 1987. Sunlight photodegradation of 2,4,5-trichlorophenoxy-acetic acid and 2,4,5,trichlorophenol on TiO_2. Identification of intermediates and degradation pathway. *Chemosphere* **16**: 1165–1179.

65. Kormann, C., D. W. Bahnemann, and M. R. Hoffmann. 1988. Photocatalytic production of hydrogen peroxides and organic peroxides in aqueous suspensions of titanium dioxide, zinc oxide, and desert sand. *Environ. Sci. Technol.* **22**: 798–806.

66. Wei, C., W. Y. Lin, Z. Zainal, N. E. Williams, K. Zhu, A. P. Kruzic, R. L. Smith, and K. Rajeshwar. 1994. Bactericidal activity of TiO_2 photocatalyst in aqueous media: toward a solar-assisted water disinfection system. *Environ. Sci. Technol.* **28**: 934–938.
67. Wolfrum, E. J., J. Huang, D. M. Blake, P.-C. Maness, Z. Huang, and J. Fiest. 2002. Photocatalytic oxidation of bacteria, bacterial and fungal spores, and model biofilms components to carbon dioxide on titanium dioxide-coated surfaces. *Environ. Sci. Technol.* **36**: 3412–3419.
68. Long, T. C., N. Saleh, R. D. Tilton, G. V. Lowry, and B. Veronesi. 2006. Titanium dioxide (P25) produces reactive oxygen species in immortalized brain microglia (BV2): implications for nanoparticle neurotoxicity. *Environ. Sci. Technol.* **40**: 4346–4352.

18

▬ Natural Organic Matter and Aquatic Humic Matter

▬ Objectives and scope

This chapter focuses on the composition and behavior of natural organic matter (NOM) in aquatic systems. The chemical, ecological and engineering significance of these substances is described, along with the rich terminology associated with NOM and its fractions. Emphasis is given to aquatic humic matter (AHM)—fulvic and humic acids— which represent the bulk of NOM in many surface waters. We describe methods to isolate, fractionate and chemically characterize NOM and AHM. A historical perspective is provided to illustrate the changing views on the chemical structure of AHM over time, and its spectral, acid-base, and metal-binding properties are explained.

▬ Key terms and concepts

- NOM, DOM, DOC
- Aquatic humic matter (AHM), humic, fulvic and tannic acid, chromophoric dissolved organic matter (CDOM)
- Autochthonous and allochthonous organic matter
- Effluent organic matter (EfOM); soluble microbial products (SMP)
- NOM fractionation; AHM extraction; XAD and DAX resins; size-exclusion chromatography; ^{13}C NMR
- SUVA, E_4:E_6, spectral slope
- Discrete binding site and continuous distribution models for AHM, Scatchard analysis
- Polyelectrolyte effects and electrostatic models for AHM

18.1 Introduction

Natural organic matter (*NOM*) is of central importance in understanding the acid-base chemistry, behavior of metal ions, and photochemistry of natural waters, and it has important ecological and water quality implications for the treatment and domestic use of water. NOM contains many substances of both internal and terrestrial origin. Even if we exclude synthetic organic chemicals, which are the focus of Chapter 19, many human activities, including the use of water to transport and treat human wastes and agricultural and other land-management practices, add organic matter to natural waters. Although research has been conducted on NOM for decades, the materials still are not completely understood because of their structural diversity, amorphous nature, and high complexity. This chapter provides a broad look at the nature and behavior of NOM. Because of the critical importance of humic matter in the chemistry of natural waters, special focus is given to these substances.

18.2 Chemical, ecological, and engineering importance

Overall, NOM and *aquatic humic matter* (hereafter, *AHM*) play many roles in aquatic chemistry and affect the behavior of many inorganic solutes. As explained in Chapter 8, NOM, and especially AHM, affects pH and alkalinity and provides pH buffering. Anionic sites on NOM account for the typical anionic deficit found in major ion analyses of surface waters. NOM, and especially AHM, complexes minor metals, such as Fe, and trace metals, such as Cu, Hg, and Zn, which has implications for their bioavailability and toxicity. To the extent that complexation retains metals in solution that otherwise would sorb onto solids or precipitate, NOM is an important transport agent for metals in biogeochemical cycles. As a material with hydrophobic components, AHM also is important as a sorbent and transport agent for nonpolar organic contaminants in water. Given that AHM absorbs UV and visible light, it is not surprising that AHM plays important roles in aquatic photochemistry. As we saw in Chapter 17, it is a major sensitizing agent and important source of $^1O_2$, ·OH, and other reactive radicals. Photochemical processes also transform NOM (e.g., by inserting polar oxygenated groups), which has implications for the availability of NOM as a substrate for microorganisms.

NOM also affects aquatic ecology. Some examples were noted above—effects on pH, metal bioavailability, and toxicity. AHM obviously affects light penetration and reduces the depth of the photic zone (the region with enough light for net primary production), and it also protects organisms from harmful UV radiation. High AHM levels in rivers like Florida's Suwannee River and St. Johns River limit the distribution of submersed aquatic plants. Similarly, high AHM in bog lakes can limit phytoplankton growth to the upper meter (or so) of the water column. AHM also affects thermal properties of water bodies. For example, high AHM levels favor a higher position for the thermocline; absorption of light in the upper layers warms the surface water more quickly in spring, but because light does not penetrate far into the water column, cooler conditions prevail at depth. Finally, AHM changes the spectral distribution of light, and this may affect species composition in submersed aquatic plant and phytoplankton communities.

Understanding the nature and behavior of NOM has great practical importance to environmental engineers concerned with treating water for various uses, including for drinking water. NOM exerts a chlorine demand, making it more difficult to disinfect water safely. As explained in Chapter 13, some components of NOM, especially AHM and algal exudates in eutrophic water bodies, are precursors for trihalomethanes, haloacetic acids, and other disinfection by-products (DBPs). In addition, some components of NOM cause fouling of membranes that are used increasingly in desalination and drinking and wastewater treatment.

18.3 NOM fractions and terminology

NOM and the related term **DOM** were defined in Chapter 6 as natural organic matter in natural waters and the dissolved fraction thereof. Although DOM does not exclude synthetic organic compounds dissolved in natural water samples, in most aquatic systems DOM is a subset of NOM because concentrations of synthetic organic compounds are so low both individually (usually $\ll 1\mu g/L$; often $\leq \sim 1$ ng/L) and in aggregate. NOM constitutes a diverse mixture of organic substances, and the associated terminology is extensive and sometimes confusing. Below we describe important classes of NOM and related terms.

DOC is the carbon fraction of DOM. Laboratories do not measure DOM concentrations directly but measure DOC concentrations, usually by combusting or oxidizing a sample at high temperatures in the presence of a catalyst or by UV light and a strong chemical oxidant (e.g., perchlorate) and measuring the resulting CO_2. The fraction of DOM that is DOC depends on the oxidation state (or oxygen content) of the DOM; in most cases DOC is 30–50% of DOM by weight.

The terms **allochthonous** and **autochthonous** refer to the origin of organic material. The former term indicates the material has a terrestrial origin (from partially biodegraded natural vegetation). The latter means the material was formed in a water body by microbial metabolism or partial decomposition of algal biomass. NOM often is divided into **hydrophobic** and **hydrophilic** fractions. Peptides and carbohydrates are in the hydrophilic fraction; AHM usually is placed in the hydrophobic fraction, but this should be understood as a relative term, as discussed below. A fraction of intermediate polarity, **transphilic** organic matter,[1] is used in some studies on NOM in water treatment.[2]

AHM is an important NOM component in surface waters—indeed, the main component in brown stained waters of lakes, wetlands, and streams that drain forested landscapes. Humic matter consists of **humic acid(s)** (**HA**), **fulvic acid(s)** (**FA**), and **humin**. Originally, these fractions were defined operationally by soil scientists based on the solubility of soil organic matter in acid and base extractions. The International Humic Substances Society (IHSS) defines HA as the fraction of organic matter extracted from soil under basic conditions (0.1 M NaOH) that is insoluble in strong acid (pH 1). FA is defined as the fraction of alkali-extracted organic matter that is soluble across the entire pH range, and humin is the organic residue not soluble at high or low pH.[3] These classes are broad and structurally ill-defined, but FA is smaller and more highly charged than HA. AHM consists primarily of FA; humin is not important in aquatic systems because of its lack of solubility in water. AHM usually is extracted from water samples by acidification to pH 2 and adsorption onto a moderately nonpolar resin.

AHM is extracted from the resin with strong base, and HA can be separated from FA by precipitating HA at pH 1. HA and FA are *relatively hydrophobic* at low pH when the acidic groups all are protonated, but even then they are not hydrophobic enough to repel water. At higher pH values, AHM is quite hydrophilic (especially FA). The terms thus are relative, and pH has a large effect. Details on separation and fractionation schemes for NOM and AHM are given in Section 18.4.

The chemical nature of AHM and its components, HA and FA, is described in Section 18.5. Here we simply note that both are mixtures of complicated organic (carboxylic and phenolic) acid molecules with both aromatic and aliphatic components, as well as N and S functional groups. FA is relatively small—nearly all recent reports give an average molecular weight (MW) less than 1,000 daltons (Da) for aquatic FA. There is widespread agreement that HA is larger than FA. A reasonable estimate for its average MW is a few thousand daltons, but there seems to be a wide distribution of size in HA molecules, making the concept of an "average" HA molecule less useful. The aromatic component of HA and FA has many phenolic groups, and methoxy (CH_3O-) groups also are common. HA is relatively more hydrophobic, and it has less oxygen and more aromatic components than FA.

Aquatic scientists also use other terms for AHM. Some limnologists use the German ***Gelbstoffe*** (literally, *yellow substances*). ***CDOM*** (for chromophoric [or colored] dissolved organic matter) is used by oceanographers and more recently by freshwater scientists. CDOM is determined by spectrophotometry. Increasingly, CDOM is the term preferred by aquatic scientists. Although CDOM and AHM generally refer to the same substances, they are not identical because different analytical techniques are involved in defining and measuring them.

The term ***tannic acid*** also is used, mostly in the popular literature, to refer to AHM, but this is not correct. Although tannic acid is humic-like in structure and likely is a component of some AHM, it is a commercial product derived from oak or sumac trees. It consists of related compounds based on gallic acid glycosides—glucose esters of gallic acid[4] (Figure 18.1)—rather than the more diverse mixture that we know AHM to be.

A term of recent use is ***EfOM*** (***effluent organic matter***), which (as it implies) is DOM in wastewater effluent. Interest in this fraction has increased as more water is recycled and reused. A related term, ***SMP*** (***soluble microbial products***), is a major fraction of EfOM. Recent studies have characterized EfOM and SMP and their behavior in water treatment processes.[6-8] SMP is defined as the pool of organic chemicals released into solution from microbial metabolism and biomass decay.[9] It has been studied in wastewater treatment plants and laboratory bioreactors fed with simple organic substrates such as glucose. Numerous components of SMP have been identified, including polysaccharides, proteins, nucleic acids, organic acids, amino acids, antibiotics, steroids, extracellular enzymes, and structural components of cells, but generalizations about their relative abundance in SMP are not available. The MW distribution of SMP is broad and bimodal, with one fraction in the low range (< 1 kDa) and another in the range > 100 kDa, each accounting for 25–30% of the total. In addition, some SMP behaves like humic matter.[9]

EfOM is derived from three main sources: (1) NOM of the drinking water from which the effluent came, (2) SMP from biological processing of wastewater, and (3) synthetic organic compounds added to water as a result of human activity, e.g., antibiotics, pharmaceuticals and personal care products (PPCPs), surfactants, pesticides, and DBPs from chlorination of the water. Although the last group is only a small fraction of the
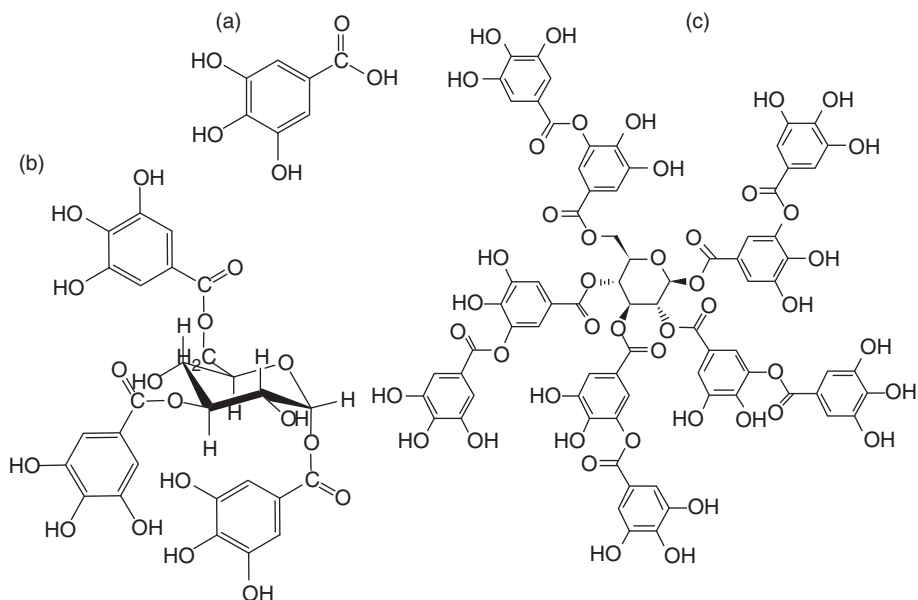
Figure 18.1 Gallic acid (a) and two forms of tannic acid: ester of three gallic acid molecules with glucose, reported by Yang et al.[5] (b) and ester of five digallic acid molecules with glucose (c) $C_{76}H_{52}O_{46}$; CAS Registry no. 1401-55-4; MW 1701.2 Da). Digallic acid is two gallic acid molecules esterified to each other.

total EfOM, it is important in terms of toxicity and bioactivity; some of these compounds act as endocrine disrupters in fish and are of concern because of potential impacts on humans. Concentrations of individual PPCPs in treated wastewater effluent generally are in the sub- to low microgram per liter range. In contrast, the NOM and SMP fractions are in the milligram per liter range. EfOM components are distributed over a wide range of molecular sizes—from small sugars and amino acids through dissolved macromolecules and on to colloidal material and suspended particles (Figure 18.2)—but some studies indicate that EfOM is mostly in the low MW range. EfOM has more hydrophilic material than NOM (Figure 18.3),[10] more polysaccharides and proteins, and lower UV absorbance per unit of DOC.[8] Alum coagulation is less effective in removing EfOM from water, because of its hydrophilic character,[6] than in removing NOM. A few studies have been reported on metal-binding by EfOM and the effects of physical-chemical and biological treatment on EfOM, but much remains to be done to characterize this material.

18.4 Fractionation and characterization methods for NOM

18.4.1 Separation and fractionation methods

Many methods have been used to concentrate and extract NOM from natural waters (Table 18.1), and all have problems and limitations. The first four methods in the table are mostly of historical interest and were used in early studies on NOM. Ultrafiltration (UF) has the advantage of separating NOM from inorganic solutes and concentrating the
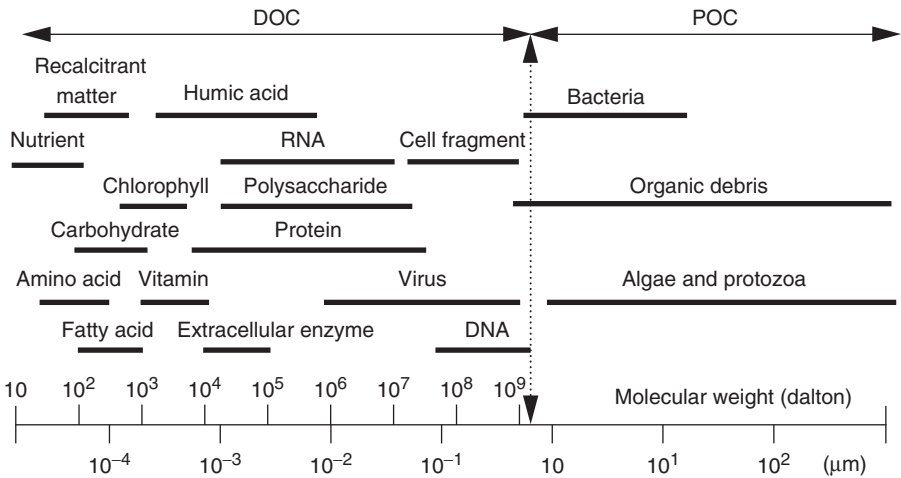
Figure 18.2 Size ranges of EfOM components. POC, particulate organic carbon. From Shon et al.,[6] © Taylor & Francis, and used with permission.
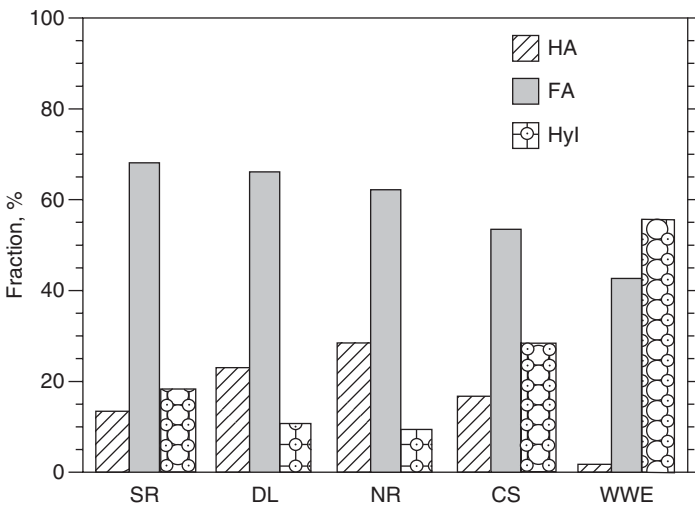
Figure 18.3 Distribution of DOC in HA, FA, and hydrophilic fractions (HyI) in four NOM samples and one EfOM sample: SR = Suwannee River, GA; DL = Drummond Lake, Virginia; NR = Newport River, North Carolina; CS = Cypress Swamp, Delaware; WWE = wastewater effluent from Wilmington, Delaware, treatment plant. From Ma et al.,[10] © Elsevier, and used with permission.

Table 18.1 Extraction methods for NOM and AHM from water

Method	Principle	Comments
Freeze concentration	Solutes remain in solution as water is slowly frozen	Slow and tedious
Activated carbon (AC)	Nonionic sorption	AC requires extensive cleaning; not all NOM sorbs to AC; some sorbs so strongly it cannot be removed
Coprecipitation	Alum and ferric chloride form hydrous oxide flocs that trap or sorb organic matter	Concentrates tend to have high salt residues
Evaporation at reduced P	Removes water from all solutes at moderately elevated temperatures	Concern that higher temperature may affect NOM; salts still must be removed
Reverse osmosis (RO)	Solvent water is forced through RO membrane at high P; all solutes retained	Salts must be removed from concentrated NOM
Ultrafiltration	Retains solutes on membranes of various (nominal) sizes	Cannot separate smallest organic molecules from salts; size fractions only approximate
XAD resins	Sorption onto resins of varying hydrophobicity	Most widely accepted method for separating AHM (HA and FA) from water; XAD resin needs thorough cleaning before use
DEAE-cellulose	Anionic NOM molecules retained on cationic exchange sites	Widely used to separate anionic biomolecules (e.g., proteins)
C_{18} solid-phase extraction columns	Retention on column of hydrophobic organic sorbent	New method; good for relatively hydrophobic NOM but recovered fraction may not include compounds recovered by more traditional methods

material in various molecular size ranges, but even the smallest pore size membranes are unable to separate small organic molecules (MW < a few hundred daltons) from inorganic solutes. Reverse osmosis is a nonselective concentration method, and for some studies additional steps must be taken to remove salts from the organic concentrate.

Sorption onto porous resins has been the most widely used technique to concentrate AHM from natural waters acidified to pH 2 for several decades. Acidification protonates the AHM and makes it more hydrophobic. The resins commonly used are porous absorbents composed of cross-linked polymers of methyl methacrylate. Depending on their exact composition, the resins have a range of polarity. XAD-8 (or DAX-8),* the resin

---

*XAD-8, the original resin used for AHM extraction, has not been available commercially for many years, but some laboratories still have supplies. DAX-8, an equivalent resin[11] made of the same polymer (poly(methyl methacrylate)), is commercially available (Supelco Inc.). We use the terms XAD-8 and DAX-8 interchangeably.

used by the IHSS to prepare aquatic reference materials,[3] is considered to be moderately polar and sorbs moderately polar materials (i.e., less polar than carbohydrates or highly charged molecules). If this resin is considered as the standard, then by definition, AHM is relatively more hydrophobic than extracts obtained with 0.1 M NaOH (the standard technique to obtain humic substances from soils). Details on extraction procedures can be found elsewhere.[3,12]

One alternative extraction method used in studying metal-complexing properties of NOM concentrates anionic NOM molecules on DEAE-cellulose.[13,14] DEAE stands for diethylaminoethyl–, $(C_2H_5)_2N^+HC_2H_5-$, which is attached to cellulose by ether linkages. DEAE-cellulose is positively charged at neutral pH and acts as a weak anion exchanger. It is used in biochemistry to separate proteins and other anionic macromolecules that bind so strongly to conventional anion exchange resins that they cannot be removed. The exchange sites on DEAE-cellulose are sparse enough that binding with macromolecules is easily reversible by increasing the eluant pH. Because binding by DEAE-cellulose is ionic rather than by adsorption, organic acids with a wide range of polarity may be obtained using this method.

A new method for isolating a relatively hydrophobic fraction of DOM uses sorption to C_{18} octadecyl groups covalently bonded to a silica support, similar to the stationary phases used in reverse-phase chromatography, under acidified (pH 2–3) conditions.[15] The C_{18} method likely extracts a less polar (or relatively more hydrophobic) DOM fraction than does DAX-8. The separated components are eluted with methanol or a similar solvent. An advantage of this approach over the other methods is that the C_{18} comes packaged as solid phase extraction cartridges or filter disks, allowing one to use the medium with a minimum of preparation. The small capacities of the disks and cartridges limit the amount of DOM that can be extracted, however. The method thus is ideal for isolating small quantities of relatively hydrophobic DOM for further characterization.

Several procedures have been used to fractionate NOM collected by the methods listed in Table 18.1. Leenheer[16] developed a sequential process using XAD and ion exchange columns to divide NOM into "hydrophilic" and "hydrophobic" fractions (see earlier caution on use of these terms), each of which was further divided into acidic, basic, and neutral subgroups. FA and HA are in the hydrophobic base and hydrophobic acid fractions. A simpler approach by Ma et al.[10] (Figure 18.4) is suited to NOM concentrated by reverse osmosis.

Further characterization of NOM isolates by MW or size distribution is a common practice. Two methods are used: ultrafiltration (UF) and size-exclusion chromatography (SEC). UF divides NOM molecules into discrete classes based on passage through or retention by membranes with increasingly smaller nominal pore sizes; UF membranes with pore sizes ranging from $> 10^5$ Da to as small as 100 Da are available. This technique has the advantage of allowing enough material to be collected in a given size class for further chemical characterization. SEC separates molecules based on their size-dependent ability to penetrate the interstices of cross-linked polymeric stationary phases of chromatographic columns; it separates substances in reverse order of molecular size. Molecules too large to penetrate any of the stationary phase are restricted to the smaller "void volume" of mobile phase outside the matrix, and they elute faster than smaller molecules that penetrate varying fractions, depending on their size, of the "internal volume" of mobile phase in the stationary phase matrix. Early size-exclusion matrices

```
┌─────────────────────────────┐
│   DOM concentrate from RO    │
└─────────────────────────────┘
              │
              ▼
┌─────────────────────────────┐
│ Acidify to pH 1; HA precipitation │
└─────────────────────────────┘
           Filtration
        │                    │
   Solid│                    │Filtrate
        ▼                    ▼
┌──────────────────┐  ┌──────────────────┐
│ Acid and DI water wash │  │   Adjust to pH 2   │
└──────────────────┘  └──────────────────┘
        │                    │
        ▼                    ▼
┌──────────────────┐  ┌──────────────────┐
│ Freeze dry: Humic Acid │  │ Supelite™ DAX-8 resin │
└──────────────────┘  └──────────────────┘
```
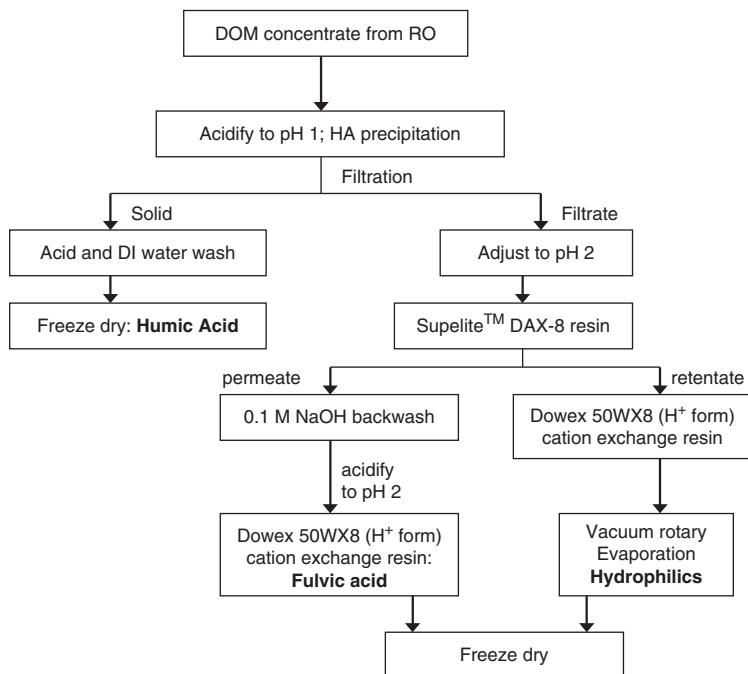
Figure 18.4 Fractionation scheme for NOM. RO = reverse osmosis; DI = deionized. Redrawn from Ma et al.,[10] © Elsevier, and used with permission.

were gels, e.g., Sephadex™ , made of cross-linked glucose polymers (dextrans), and polyacrylamides, that were compressible and thus unsuitable for use at the high pressures employed in high-performance liquid chromatography (HPLC). Rigid size-exclusion matrices suitable for HPLC were developed later.[17,18]

Both UF and SEC have limitations in terms of their ability to characterize the MW distribution of NOM, and results from the methods are considered approximate. Whether a molecule can penetrate a UF pore or the interstices of a SEC matrix depends on the shape of the molecule, e.g., whether it is spherical, spaghetti-like, densely packed, or loose and flocculent. In addition, UF membranes and SEC matrices are not chemically inert (some are worse than others in this regard); ionic groups near or in the pores or interstices may repel solute molecules or may bind them, violating the assumption that the matrices are inert and yielding erroneous estimates of MW. Nonetheless, when properly done both methods yield MW values for DOM that are consistent.[18,19]

18.4.2 Methods for the chemical characterization of AHM

The chemical composition of NOM and AHM is difficult to characterize for two reasons: (1) the complicated nature of individual macromolecules and (2) the large number of compounds in any given sample or even in any fraction obtained by common fractionation methods.[10,16] Although scientists have not given up on determining exact structures of individual molecules, most characterization work has focused on the

aggregate properties of NOM or its major fractions (e.g., HA, FA, hydrophilic acids). A short list of these properties includes elemental composition (C, H, O, N, S), MW (average and distributional characteristics), concentration of acidic functional groups (determined by acid-base titration), and the nature and abundance of functional groups attached to the basic carbon skeleton. Spectroscopic methods used for functional group analysis include: infrared (IR) absorbance, ^{13}C nuclear magnetic resonance (NMR) spectroscopy, and more recently, two-dimensional fluorescence excitation-emission spectroscopy.

Much of the progress made in the past quarter century to understand the chemical nature of AHM can be attributed to solid-state ^{13}C NMR with very rapid spinning of the sample in the NMR magnetic field, along with cross-polarization called solid-state "CP-MAS NMR." Solid-state NMR is needed for adequate sensitivity because of the low (1%) natural abundance of ^{13}C. Cross-polarization involves energizing protons with radio frequency waves to enhance the signal from ^{13}C, which has an inherently low NMR signal. Details on the underlying physical principles for this method are beyond our scope, but briefly, NMR measures the resonance energy of atomic nuclei exposed to strong magnetic fields. Except for ^{2}D, only nuclei with an odd-numbered atomic mass (i.e., ^{13}C, and ^{1}H, but not ^{12}C) respond to the magnetic field. Exactly where resonance occurs within an NMR spectrum depends on the "molecular environment" in which carbon atoms exist; for example, a ^{13}C atom in an aliphatic chain resonates at a slightly different frequency than one in an aromatic ring, and a carboxyl ^{13}C atom resonates at a different frequency than a ^{13}C atom in an alcohol group.

Interpretation of NMR spectra is analogous to the way we interpret other kinds of spectroscopy. The spectra are in ppm of *chemical shift* in radio frequency of the ^{13}C nuclear spin resonance relative to the ^{13}C in a standard, tetramethylsilane. Frequencies where peaks occur provide information on the nature of the carbon group[20] (Table 18.2), and peak size indicates the abundance of carbon in a given molecular environment. Quantifying the amount of a given type of carbon from NMR spectra is difficult, and results are regarded as only semi-quantitative. More recently, the advent of two-dimensional NMR, such as total correlation spectroscopy, which correlates the proton and ^{13}C NMR spectra of a sample, has aided in the interpretation of NMR spectra by allowing more precise identification of functional groups.[21]

For well over 30 years, gas chromatographic separation coupled with mass spectrometry (GC-MS) for detection and analysis has been the most widely used and

Table 18.2 Assignment of carbon type in ^{13}C NMR spectra*

Chemical shift range, ppm	Carbon type
0–50	Aliphatic C (alkanes)
50–60	Methoxy C (C−O−); amino acid C
60–95	All other C−O (carbohydrates)
96–110	Anomeric C (polysaccharides)
110–142	Aromatic C
142–160	Phenolic C
160–190	Carboxylic C (−COOH)
210–230	Carbonyl C (−C=O)

* Summarized from Malcolm.[20]

most powerful technique to identify organic contaminants in environmental samples. Lack of volatility prevents the application of GC-MS techniques to NOM (and AHM) analysis, and problems with coupling HPLC with mass spectrometry have limited the usefulness of LC-MS. Major technical advances in the past decade have greatly improved the usefulness of mass spectrometry for the analysis of nonvolatile or low-volatile compounds. First, new techniques, such as electrospray ionization[22] and atmospheric pressure photoionization,[23] have been developed to ionize polar or low or nonvolatile compounds and transfer them efficiently into mass spectrometers. Both positive and negative ions can be formed, and little or no fragmentation of the compounds occurs; i.e., the ions largely represent the singly charged parent compounds. Second, impressive advances in mass spectrometry, such as high-field Fourier-transform ion cyclotron resonance mass spectrometry (FT-ICR MS),[23−25] have eliminated (or at least minimized) the need for preliminary chromatographic separation by providing extremely high-resolution measurement of the mass-to-charge (m/z) ratios of relatively high-MW ionic species. Measurement of m/z with up to six decimal-place accuracy is possible. Details of how the instrument does this are beyond our scope, but with such instruments scientists can distinguish between compounds of nominally the same MW that differ in isotopic or elemental composition and determine the exact elemental formula of molecules. For example, consider three molecules with a nominal mass of 574 Da that differ slightly in isotopic and elemental composition:

Compound	MW (Da)
$^{12}C_{20}H_{36}O_{18}N$	574.1619
$^{12}C_{19}{}^{13}CH_{35}O_{18}N$	574.1574
$^{12}C_{20}H_{36}O_{16}SN$	574.1442

For the first compound, we assume that only the most abundant isotope is present for all the elements. In the second compound we have one ^{13}C atom replacing a ^{12}C atom and one less H atom, possibly reflecting the presence of a semiquinone structure (see Section 18.5.2), and in the third compound a sulfur atom replaces two oxygen atoms. Exact atomic masses used to calculate the MWs are from a NIST Web site,[26] which reports values to more than six decimal places The MWs of the three compounds differ in the second decimal place, which is easily observable with FT-ICR MS. Studies reported in the past few years using these techniques have greatly expanded our understanding of the chemical nature of AHM.

18.5 Origin and structure of AHM

18.5.1 Alternative views on the origin and nature of AHM

Many hypotheses have been proposed over past decades as alternatives on the origin and nature of AHM.[27] A short list includes the following:

- AHM is the degradation product of plants versus AHM is formed by polymerization of monomers.
- AHM is derived from terrestrial plants (allochthonous origin) versus AHM is formed from phytoplankton or aquatic macrophyte biomass (autochthonous origin).

- The precursor materials for AHM are insoluble lignin and woody tissue versus more soluble tannin and flavin components of plants.
- AHM is colloidal, versus AHM consists of small molecules in solution.
- All AHM is basically the same, versus the nature of AHM depends on its origin.
- The N, S, P, carbohydrates, and amino acids found in AHM are innate constituents versus impurities from imperfect extraction/fractionation schemes.

Controversies about these views reflect the tendency of past scientists to phrase theories as dichotomies—i.e.,, the origin (or nature) of AHM is "this" rather than "that." A more nuanced view today is that few issues about AHM can be decided as "either-or" propositions; "both, depending on circumstances" is more realistic. For example, an early viewpoint considered freshwater AHM simply as solubilized soil humic materials. The broader current view is that soil and aquatic humic materials often have a common precursor—vegetation—but formation reactions can take place in soil, organic litter, natural waters and sediments. Scientists also agree that AHM in bogs consists mostly of decomposition products of terrestrial plants, but there is strong evidence that they are not just the residuals of incomplete degradation of insoluble macromolecules such as lignin. *Synthetic* reactions, some involving photochemical activation, are involved in condensing monomers from lignin degradation and tannins and flavonoids from leaves and bark into new molecules of AHM and linking smaller molecules into larger ones.[*]

The classical model for the origin of freshwater AHM emphasizes allochthonous sources. Isolation of AHM from lakes in Antarctica,[29–31] however, where terrestrial plants do not occur, makes it clear that at least some freshwater AHM is autochthonous, and many other studies support the autochthonous origin of some AHM. According to one recent study,[32] autochthonous DOM (from Esthwaite Water, an English lake) is less light absorbing, less fluorescent, and more hydrophilic and possesses fewer proton-dissociating groups than does allochthonous material.

Several mechanisms have been proposed for autochthonous production of AHM, including transition metal-catalyzed polymerization of phenols,[33] enzyme-catalyzed polymerization of phenols,[34] and the reaction between amino acids and sugars called the "browning" reaction, which forms Schiff bases[35] that undergo rearrangement to form complex melanoidins (high-MW heterogeneous polymers). Several studies have suggested that enzymatic coupling of phenols with aromatic pollutants[25] may be important in binding organic pollutants to AHM.[36]

For decades some contended that the N, S, and P found in elemental analyses of HA and FA extracts from aquatic sources was the result of inadequate selectivity in extraction methods for these materials, and the possibility that they are innate components of AHM was discounted.[†] Given what we now know about the diversity of reactions in which

---

[*]For an interesting perspective on potential chemical mechanisms for the synthesis of NOM (and AHM) from simple precursor molecules, readers should consult the work of Cabaniss and coworkers,[28] who developed a stochastic biogeochemical model for the formation, transformation and mineralization of NOM using an "agent-based" computer modeling approach.

[†]This is not the case in soil science, however, where N has long been considered a part of HA and FA. It was considered a key component in the "lignoprotein theory" of origin for soil HA proposed by Waksman ~90 years ago. N in soil humic matter has been studied for a long time and is mostly peptide N. If protein fragments are part of humic substances, S likely is present, given that several common amino acids contain S. Phosphate groups are part of soil HA and FA but are very low in aquatic AHM.

AHM participates, the presence of these elements in AHM molecules now is widely accepted. Indeed AHM derived from Antarctica has N and S abundances up to an order of magnitude of higher than AHM from predominantly terrestrial environments.[37] In addition, high-resolution MS analyses have verified the presence of these elements in AHM molecules. Typical concentrations of N and S are in the range of ~0.2–3%.

18.5.2 The structure of AHM: historical perspective

The long road to our current knowledge on the chemical structure of AHM is paved with controversies and false or dead-end pathways. Early studies assumed that AHM was macromolecular or colloidal, but an important study by Shapiro[38] in the 1950s concluded that AHM consists of low-MW aliphatic acids (~300–450 Da). Subsequent studies by Black and coworkers[39] contradicted this view and suggested that AHM is much larger—mostly colloidal—and also mostly aromatic. Support for the macromolecular view (size range of 1–100 kDa) was provided by studies in the 1960s and 1970s using SEC with Sephadex[40] and Biogel, a polyacrylamide. The inference that AHM was mostly aromatic was supported by studies that identified hydroxyl- and methoxy-substituted aromatic compounds as the nearly exclusive products of partial oxidative degradation of AHM.[41] Structural models thus emphasized these components (Figure 18.5).

Beginning in the 1970s, various studies cast doubt on the "aromatic macromolecule" model. Inferring the size of complicated molecules from elution patterns with size exclusion gels was found to be difficult[18,42] because AHM molecules interact chemically with the gels, and elution depends on several factors besides MW. Anionic sites on gels repel anionic solutes, decreasing their ability to penetrate gel interstices and accelerating their passage through the column. This produces erroneously high estimates of size. Conversely, aromatic compounds sorb onto gel surfaces, which retards their movement through columns and leads to low estimates of size. Estimates of AHM molecular size published in the 1970s generally are not thought to be reliable, but more recent studies found that artifacts can be minimized by using a nonreactive salt (NaCl) solution at an ionic strength of 0.1 as the eluant and a high-pressure size-exclusion silica column that has low hydrophobicity and minimal ion exchange capacity.[18,43] Use of polystyrene sulfonate random coils rather than globular proteins as size-calibrating standards also was found to be a key to obtaining molecular sizes for humic substances that agreed with results from other methods, such as ultracentrifugation and vapor pressure osmometry—a colligative property method.[43]

Another controversy about the structure of AHM concerns the apparent change in molecular size depending on solution conditions like pH and ionic strength. Results from SEC indicated that size (MW) increased as pH increased. Aggregation of smaller molecules into large ones often has been posited to explain this, but experimental artifacts involving changes in the way AHM molecules interact with the matrices used in SEC also could explain the trend. Based on this trend, Schnitzer and Khan[44] proposed that soil humic matter consists of small monomers held together by pH-dependent hydrogen bonds (Figure 18.5b), but this was not a universally accepted perspective.
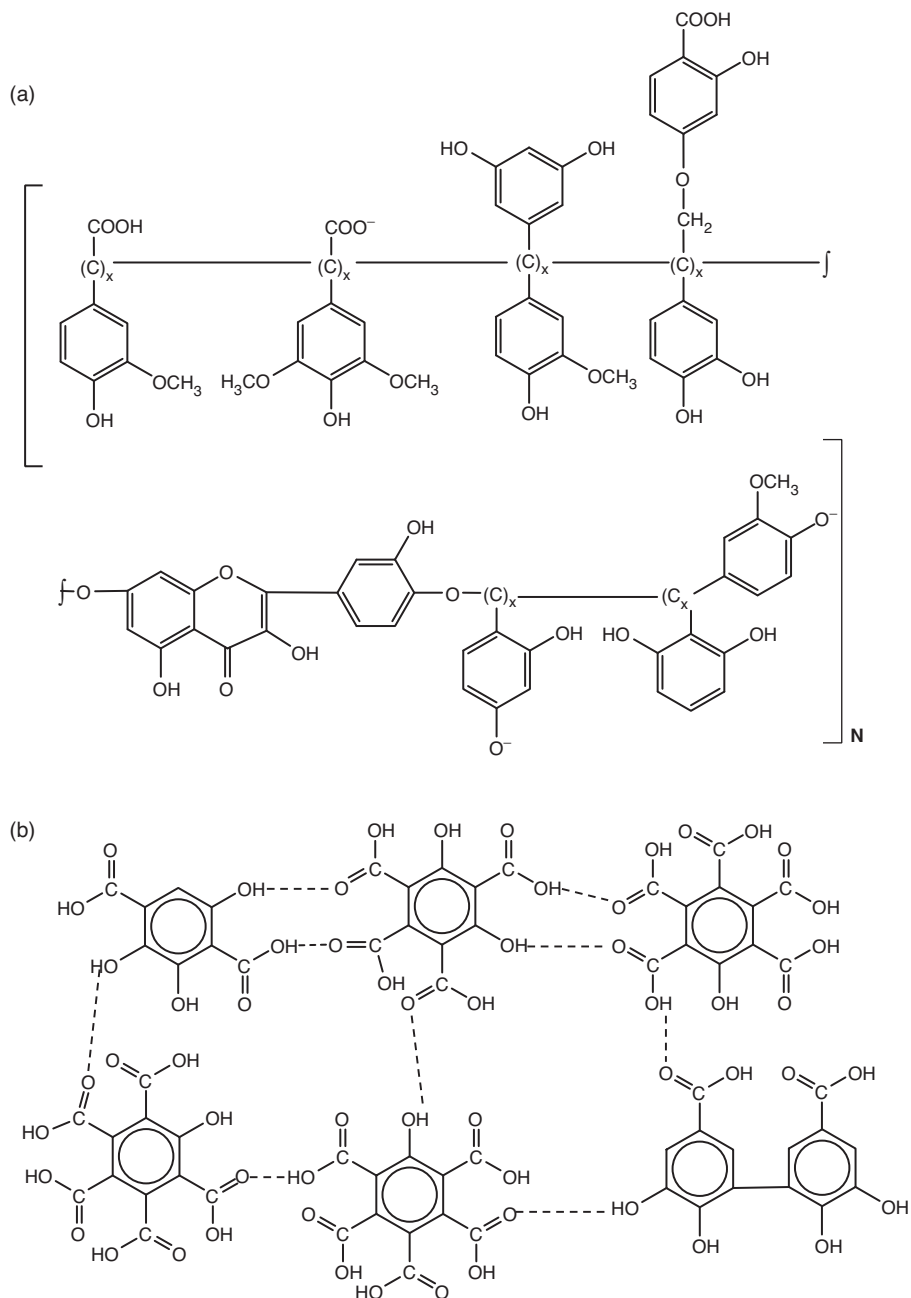
Figure 18.5 (a) Hypothetical structure for AHM proposed by Christman and Ghassemi[41] based on partial oxidation (by alkaline permanganate) and identification of products by thin-layer chromatography; (b) structure proposed by Schnitzer and Khan[44] for soil humic substances emphasizing hydrogen bonding of small monomers.

18.5.3 Structure of AHM: modern perspective

Several lines of evidence support the current view that AHM is relatively small—$MW_{ave} \approx 800$–1000 for aquatic FA (with a range of $\sim$300 to about 10^4 Da) and $\sim$2000–3000 for aquatic HA (with a range of $<\sim$1000 to $\sim$5$\times$10^4 Da).[45] In addition, numerous ^{13}C NMR studies[12] indicate that aquatic and soil humic matter contains much more aliphatic carbon than earlier degradation studies indicated. Only 11–20% of the carbon atoms in aquatic FA is aromatic, and $\sim$30% of the carbon in HA is aromatic.[29,45] The core structure of AHM thus appears to be aliphatic. This leads us to ask: how can the NMR and degradation data be reconciled? The inferences based on degradation data likely are erroneous. Although aromatic compounds predominated in the products of oxidative degradation, yields were only a few percent of the starting material.[41] Even relatively mild oxidants like alkaline permanganate destroy most aliphatic portions of AHM molecules but leave aromatic rings intact. One exception is the use of gentle oxidation at moderate-temperature (300°C) with tetramethyl ammonium hydroxide, which derivatizes acidic functional groups to form more hydrophobic methoxy adducts.[46] GC-MS analysis of derivatives from this procedure revealed higher amounts of aliphatic structures than those derived using more destructive oxidation methods.[47]

The relatively low aromatic content of AHM is illustrated by the solid-state ^{13}C CP-MAS NMR spectra of extracts from a low-pH bog in northern Minnesota using both XAD-8 and DEAE-cellulose (Figure 18.6). Based on the ratios of peak areas in the ranges 110–160 ppm (Table 18.2) to the total spectrum area over the range 0–230 ppm, the XAD-8 isolate had an aromatic content (including phenolic C) of only 26%, and the
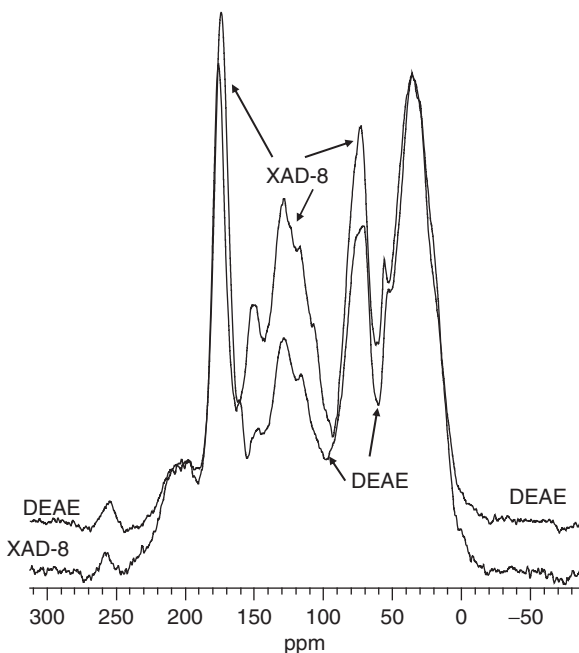
Figure 18.6 Solid-state CP-MAS ^{13}C NMR spectra for NOM extracted by XAD-8 and DEAE-cellulose from bog S2 in Marcell Experimental Forest, in north-central Minnesota. Spectra were obtained on a 400-MHz instrument. From Khwaja[48] with permission.

DEAE-cellulose isolate had an even lower aromatic content (16%). In contrast, based on normalized peak areas in the range of 160–190 ppm the DEAE-cellulose isolate had a higher carboxylic content than the XAD-8 isolate (20 vs. 14%).[48] These results are consistent with the separation mechanisms attributed to the extractants: XAD-8, a nonionic sorbent, preferentially extracted more aromatic components, and DEAE-cellulose, a weak anion exchanger, extracted more carboxylic acid components.

Current thinking among aquatic scientists supports the importance of aggregation of relatively small monomers in forming larger molecules of AHM[49] and in the changing behavior of AHM with pH. However, recent evidence based on NMR and mass spectrometric data indicates that the molecules being aggregated are larger than the monomers in Schnitzer and Khan's proposed structures (Figure 18.5b; MW values of 214–314 Da) by factors of $\sim$2–4.

Recent high-resolution FT-ICR MS studies demonstrate that AHM in a given extract contains thousands of individual compounds. For example, Hockaday et al.[23] identified more than 6,000 molecular species for which they were able to assign unique elemental formulas in C_{18}-extracted DOM (which is probably more hydrophobic than AHM extracted by other methods) from a dark-water lake in the Great Dismal Swamp, Virginia (Figure 18.7). The MW range for the compounds was 250 to 825. Similarly, using a direct injection technique (i.e., no extraction or pre-concentration step), Sleighter et al.[24] identified 1535–2139 unique elemental formulas in DOM from a small Pennsylvania stream (the range was due to variations in analytical techniques) over the m/z range 225–700, and 8–16 individual peaks were detected per nominal mass (Figure 18.8).

The huge quantities of data produced by FT-ICR MS have posed some challenges in data analysis and interpretation. One commonly used approach involves plotting the elemental composition inferred from individual peaks on *van Krevelen diagrams*, which have been used by geochemists to classify major kinds of NOM based on the atomic
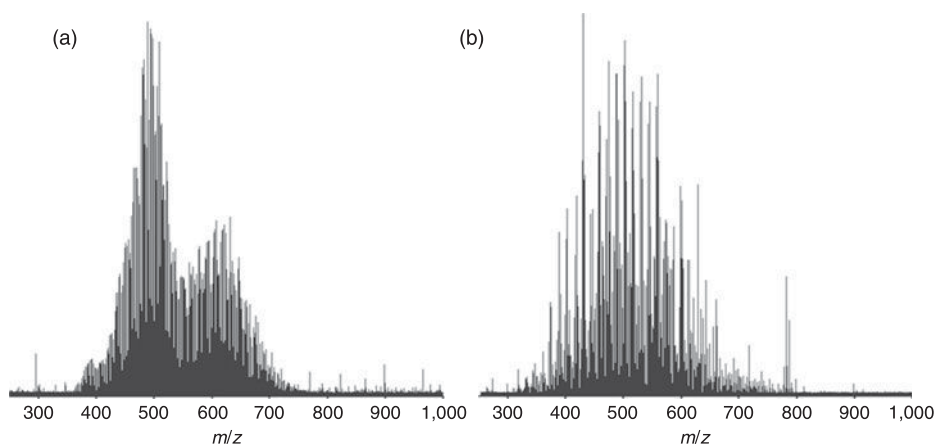
Figure 18.7 FT-ICR positive ion mass spectra for C_{18}-extracted DOM from Lake Drummond, Great Dismal Swamp, Virginia, obtained with atmospheric pressure photoionization (a) and electrospray (b) sources. From Hockaday et al.,[23] © American Society of Limnology & Oceanography, and used with permission.
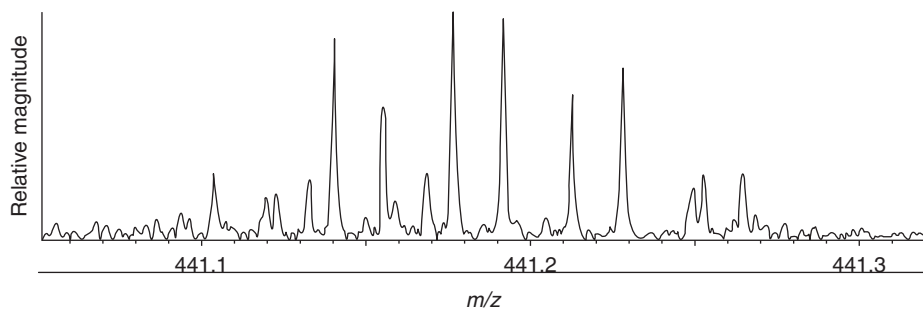
Figure 18.8 Negative-ion FT-ICR mass spectrum expanded at nominal mass 441 for DOM from a Pennsylvania stream. From Sleighter et al.,[24] © Elsevier, and used with permission.

ratios of H:C and O:C in the substances. Figure 18.9a shows that a variety of classes of organic compounds have distinct (nonoverlapping) regions on such diagrams,[50] and Figure 18.9b shows a typical van Krevelen plot for FT-ICR MS data on an aquatic NOM sample.[51] Changes in elemental composition resulting from various chemical reactions, such as hydrogenation, hydration, and oxidation/reduction, plot as vectors on van Krevelen diagrams, allowing one to discern structural relationships among the thousands of compounds in a given sample.

Given the huge number of unique compounds in a given sample of AHM, probably the best we can do in terms of drawing structures of AHM is to show "typical" molecules based on measured aggregate properties like elemental stoichiometry, MW, percent aromatic carbon, and density of major functional groups (e.g., $-COOH$, $C-OH$, $C=O$). Figure 18.10 shows one such hypothetical structure for a moderately sized AHM molecule of allochthonous origin based on these characteristics.

One hypothesized structure of autochthonous marine AHM differs from classical and modern models of freshwater AHM and soil humic matter. AHM from the Sargasso Sea was found to be largely aliphatic, and a free-radical autoxidation mechanism (Figure 18.11) was proposed that involves the cross-linking of unsaturated lipids excreted by algae.[53] The process is accelerated by light and transition metals. Field experiments with triglyceride esters of the unsaturated fatty acid trilinolein yielded FA-like material when seawater from which natural humic material had been removed was incubated in sunlight, and the IR spectrum of the products was similar to that of FA extracted from seawater. Marine FA was proposed to consist of two to four cross-linked fatty acid chains and have a MW of 900–1200 Da. Continued autoxidation of the FA was thought to involve two opposing pathways: (1) cleavage by sunlight-produced $^1O_2$ to produce low-MW acids and aldehydes (the major pathway), and (2) further cross-linking to form less soluble HAs (a minor pathway).[53] Not all AHM in seawater is autochthonous, however; in coastal areas it is primarily of riverine (terrestrial origin), and there is evidence that some of the marine AHM even in oceanic regions distant from land has a terrestrial origin.[54] Whether it is of autochthonous or allochthonous origin, AHM apparently represents a minor portion of the high MW DOM (defined as the fraction retained by a UF membrane with cutoff size of 1 kDa) in the open ocean (far from land); Aluwihare et al.[54] showed that 50–80% of the material in this fraction was acyl
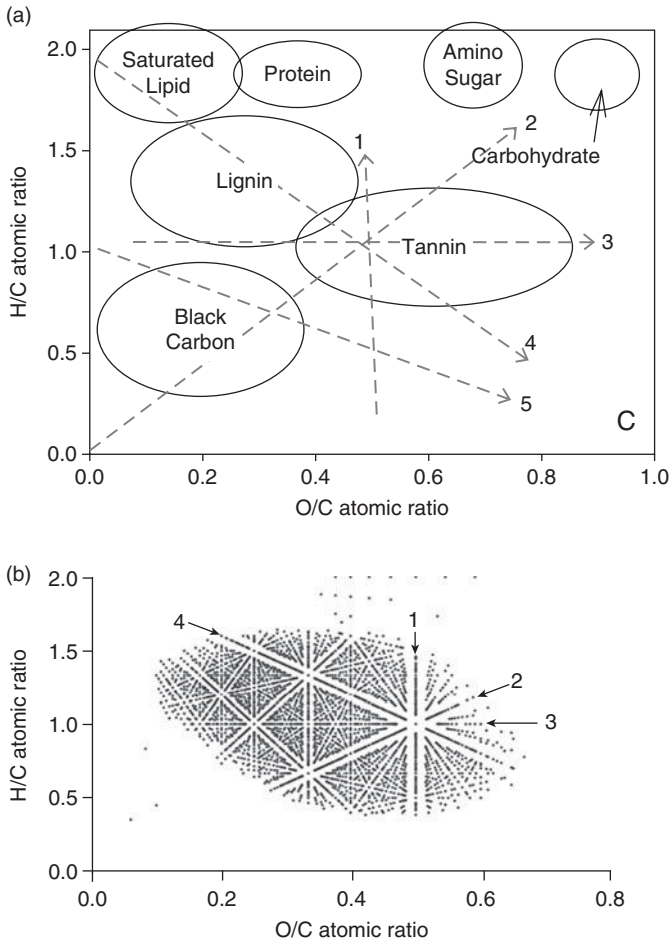
Figure 18.9 Van Krevelen diagrams showing approximate H/C and O/C regions for various classes of DOM (a) and locations H/C and O/C ratios for individual peaks measured by FT-ICR MS (b) on McDonalds Branch, a blackwater stream in the Pinelands of New Jersey. In both diagrams the numbered arrows indicate directions of changes in the ratios resulting from specific chemical processes: 1, hydrogenation/dehydrogenation; 2, hydration/condensation; 3, oxidation/reduction; 4, methylation/demethylation or alkyl chain elongation; 5, carboxylation/decarboxylation. (Intercept and slope for 5 depends on structure of the base molecule). (a) modified from Grannas et al.[50] and (b) modified from Kim et al.[51] with permission of the American Chemical Society.
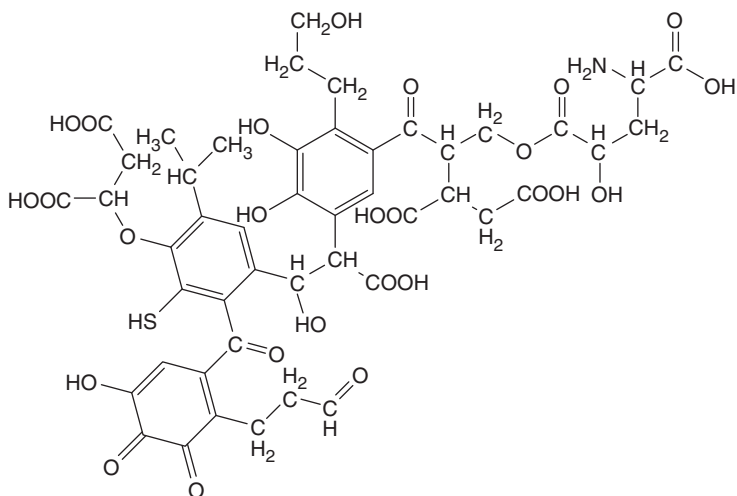
Figure 18.10 Hypothetical structure of a "typical" AHM molecule that has many of the characteristics found by modern chemical measurements: MW = 1060 Da; elemental composition, $C_{47}H_{50}O_{25}NS$; aromatic C = 39% of total C; 1.3% N; 3% S. Based on a structure proposed for XAD-extracted SRFA by Leenheer et al.[52]

polysaccharide, a biopolymer rich in carbohydrates, acetate, and lipid. AHM was most abundant (up to 49% of total C) in estuaries, coastal waters, and deep water, suggesting both marine and terrestrial sources.

18.5.4 AHM and quinones

Aromatic rings with multiple –OH groups (polyphenols) are readily oxidized to form quinones; e.g.,

$$\text{hydroquinone} \longrightarrow \text{1,4-benzoquinone} + 2H^+ + 2e^-, \tag{18.1a}$$

$$\text{catechol} \longrightarrow \text{1,2-benzoquinone} + 2H^+ + 2e^-. \tag{18.1b}$$
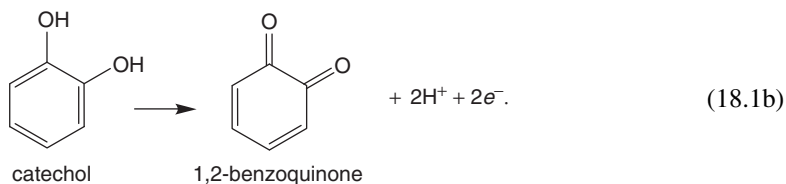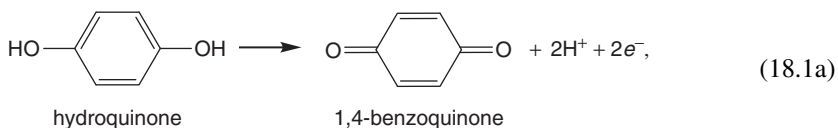
Given the abundance of polyphenols in humic substances, we might expect to find quinones in humic matter, and evidence for this goes back many decades.[55] The importance of these structures in the behavior of humic materials is a recent finding, however.[56]
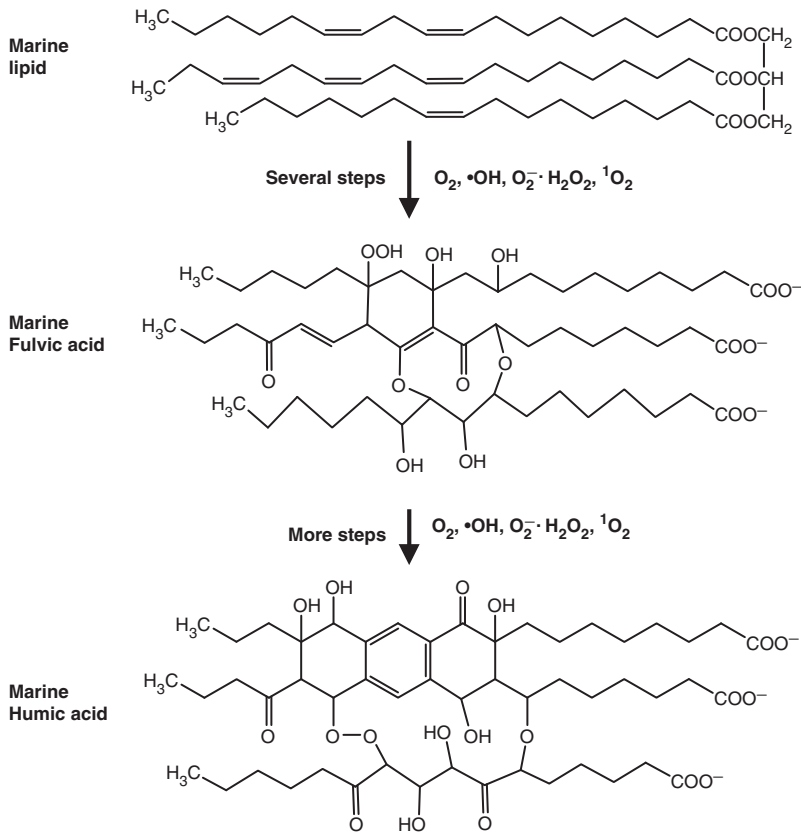
Figure 18.11 Proposed structures of marine FA and HA and autoxidation formation mechanism from lipids excreted by marine algae. Redrawn from Harvey et al.[53]

Reduction of quinones to hydroquinones, which occurs by both electrochemical and biological processes, is a two-electron change, but it can proceed stepwise by two one-electron transfers, forming free radical semiquinones as intermediates:
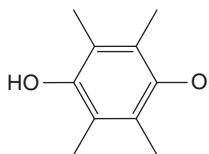
Although simple semiquinones are unstable free radicals, large semiquinone structures, in which the unpaired electron is sufficiently delocalized, are stable under environmental conditions. This occurs in complex humic molecules, and free radicals thought to be semiquinones have been detected in both soil and aquatic humic substances using electron spin resonance spectroscopy.[57] Many studies support the idea that AHM-based quinones are the electron-accepting components when bacteria (e.g., *Geobacter metallireducens*) reduce humic substances. Microbial reduction was found

to increase the abundance of semiquinones in AHM.[56] An interesting characteristic of quinones/hydroquinone couples (including those found in AHM) is that their redox reactions are highly reversible, and studies have shown that quinones in humic substances (HS) act as electron shuttles in the microbial reduction of insoluble ferric (hydr)oxide (ferrihydrite):

$$(18.2)$$
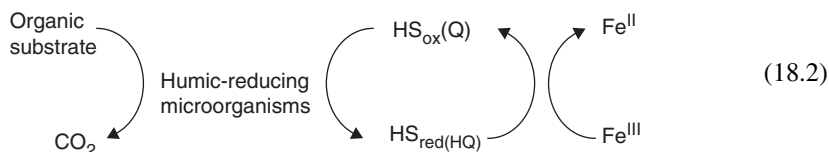
This process has been shown to accelerate the microbial reduction of insoluble Fe^{III} oxides and may provide an explanation for how microorganisms transfer electrons to insoluble iron oxides.[58] Quinone/hydroquinone reduction potentials are readily measurable. $E^{\circ\prime}$ values of -137 to -225 mV have been reported for model compounds that were kinetically the most active in ferrihydrite reduction.[58] Other recent studies were able to reduce and oxidize these quinone-like moieties electrochemically[37,59] and corroborated many of the observations reported for microbially dominated systems.

18.6 Spectral and photochemical characteristics of AHM: UV-visible absorbance

As we have shown, AHM is a heterogeneous mixture of many structures produced by several mechanisms. Nonetheless, AHM from various sources has fairly constant physical-chemical properties and similar structural features. A property relevant to photochemical activity and useful in characterizing the behavior of AHM is its UV-visible absorbance. Soil humic extracts, AHM extracts, and filtered samples of water containing CDOM have simple spectra characterized by increasing absorbance, A, as wavelength (λ) decreases (Figure 18.12a), and many workers have noted that the spectra can be linearized (approximately) by plotting the natural logarithm of A versus wavelength (Figure 18.12b). Statistical fits of the data, as measured by regression r^2 values (Table 18.3) are good, but plots of ln A versus wavelength generally show some simple or S-shaped curvature over the range of 250–500 nm.

Zepp and Schlotzhauer[60] were the first to report that the fitted coefficients of the exponential equation for absorbance spectra of humic material fall in a narrow range. They used an equation of the form

$$e_\lambda = a\, \exp(-s_e(\lambda - 450)), \qquad\qquad (18.3)$$

where e_λ is the λ-dependent extinction coefficient: $e_\lambda = A_\lambda / C_o l$, where A_λ is absorbance at λ, C_o is the DOC concentration in mg/L, and l is light path in m. Inspection of Eq. 18.3 shows that at 450 nm coefficient $a = e_\lambda$. For 11 samples from freshwater and marine sources, coefficient a had a mean (± 1 SD) of 0.60 ± 0.28, and coefficient s_e, called the spectral slope—a measure of the steepness of the spectrum—had a mean (± 1 SD) of 0.0145 ± 0.0014. Several samples of FA had a mean s_e of 0.0138 ± 0.009, but
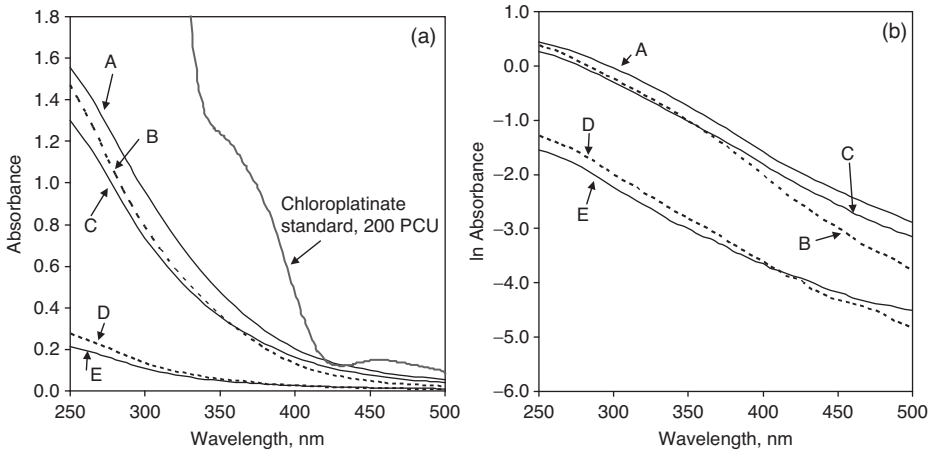
Figure 18.12 (a) UV-visible absorbance spectra for chloroplatinate color standard at 200 PCU and some samples of aquatic humic matter: A, XAD-8 extract from Bog S2, Marcell Forest, Itasca County, Minnesota; B, IHSS SRFA; C, Upper St. Johns River, Florida; D, Lake Itasca, Minnesota; E, St. Croix River, Minnesota-Wisconsin. Samples D and E at ambient concentrations (see Table 2.6); DOC of A, B, and C: 35, 40, and 35 mg/L, respectively. (b) Natural logarithm of absorbance versus wavelength approximately linearizes the AHM spectra. For clarity, trend lines are not shown, but slopes, s_e, are in Table 18.3; $r^2 > 0.99$ for all regressions except E (0.985).

Table 18.3 Spectral data on some NOM/humic extracts and natural waters

Sample*	$s_e^\dagger$	A_{254}	$SUVA_{254}^\S$	Color PCU§
L. Itasca	0.0148	0.266	5.9	63
Miss. R. 1	0.0113	0.189	2.1	79
Miss. R. 2	0.0144	0.224	2.2	58
Miss. R. 3	0.0146	0.167	1.6	42
Miss. R. 4	0.0144	0.120	1.4	29
Minn. R.	0.0148	0.240	2.1	58
St. Croix R., Minn.-Wisc.	0.0126	0.207	4.1	71
Hodstradt L., Wisc.	0.0160	0.029	1.1	4
St. Johns R., Fla.	0.0145	1.261	3.6	373
Minneapolis drinking water	0.0115	0.112	2.2	12
Metro wastewater primary effluent	0.0089	0.475	0.8	323
Metro wastewater final effluent	0.0111	0.208	1.5	96
Bog S2 XAD extract	0.0144	0.862	4.5	394
IHSS SRFA	0.0177	1.416	3.5	247

* See Table 2.6 for locations of first seven samples; Hodstradt L. is an acid-sensitive, clear-water lake in Oneida County, Wisc.; St. Johns R. sample from upper river, west of Cocoa Beach, Fla.; Metro wastewater from Minneapolis-St. Paul, Minn.
$^\dagger s_e$ from ln absorbance versus wavelength over range 250–500 nm; the lnA versus wavelength plot for Metro primary was notably curved.
§ SUVA$_{254}$ calculated from eq 18.4 and color from eq 18.6.

commercial HA had a mean s_e of only 0.0102 ± 0.0002. Others have reported similar results, and s_e generally has a small range within a given study. However, agreement between studies is not always good; the range of s_e for 20 studies is ~ 0.01–0.024.[61] Twardowski and coworkers[61] concluded that most of the variation between studies could be explained by differences in the spectral ranges used to fit the equation (e.g., Zepp and Schlotzhauer[60] used 300–500 nm; others have used 250–450, 350–650, and 290–600 nm, and nearly all of the 20 studies used a different range). Not all the variation in s_e should be attributed to measurement differences, however. Variations in s_e within individual studies have been correlated with changes in the origin (autochthonous vs. allochthonous) and chemical composition of CDOM, such as the ratio of FA and HA in CDOM.[62] The results in Figure 18.12b (obtained on one instrument using identical procedures) show a range of 0.0126 to 0.0177 for s_e among the five samples, and s_e values for waters from the Mississippi River series described in Table 2.6 also yielded a similar range for s_e (Table 18.3), but the central tendency of the colored waters is near 0.014.

It should be noted that absorbance spectra of AHM samples vary with pH. In general, absorbance increases with pH,* but there are more subtle effects, including shifts in the size and position of absorbance shoulders sometimes observed around 280 nm, which are attributed to the presence of carboxyphenols.[63] Weak acid chromophores often have differences in absorbance depending of the fraction of the acid that is ionized. Because of the effect of pH on absorbance, some have proposed that the color of water be measured at a standard pH.[64] Although this tightens the relationship between measured color (or absorbance) and concentration of CDOM, it makes the measurement a less accurate indicator of the actual color perceived by observers at the ambient pH of a water body.

Normalized absorbance (A) values at variety of wavelengths are used to characterize or quantify CDOM. For example, A at 254 or 280 nm divided by the light path length (l) of the spectrophotometer cell in meters (rather than centimeters) and by the DOC concentration (in mg/L) of a water sample is called *specific ultraviolet absorbance*, or *SUVA*; e.g.,[65]

$$\text{SUVA}_{254} \ (\text{L mg}^{-1} \ \text{m}^{-1}) = \text{A}_{254}/l \cdot \text{DOC}. \tag{18.4}$$

This parameter is widely used as an indicator of the aromatic content of DOM;[66] Weishaar et al.[67] reported an r^2 of 0.97 for the relationship:

$$\% \text{ aromaticity} = 6.52 \times \text{SUVA}_{254} + 3.63 \tag{18.5}$$

Percent aromaticity was determined from ^{13}C NMR spectra. These workers concluded that SUVA is not a good predictor of the reactivity of DOM with chlorine or its potential to form halomethanes, but Kitis et al.[68] reported the opposite conclusion. The low SUVA of DOM in the Mississippi River samples in Table 8.3 compared to values for headwaters of the river (Lake Itasca) and for IHSS Suwannee River FA (SRFA), St. Johns River and St. Croix River suggest that DOM in the Mississippi River in Minneapolis-St. Paul

---

*A similar phenomenon occurs when lemon juice is added to tea—a noticeable lightening in color occurs as the juice acidifies the tea.

region has a low aromatic content, perhaps because its NOM is influenced human activity.

SUVA$_{280}$ has been found to be correlated with the MW of HA and FA, and similar correlations to aromaticity have been reported.[43] The ratio of absorbance at 465 and 665 nm, measured at a standard pH of 8.3, is called the E4/E6 ratio and has been used by soil scientists as a measure of the degree of "humification" and condensation undergone by organic matter,[12,69] but it is not widely used for aquatic samples because absorbance values at the higher wavelength are low and subject to precision problems.

The standard method[14] to measure color in freshwaters is by visual comparison to a chloroplatinate standard. Results are expressed in platinum-cobalt color units (PCUs; also called Hazen units), where 1 PCU = 1 mg/L of Pt in the form of $PtCl_6^{2-}$; cobalt chloride is added to the chloroplatinate to obtain a hue similar to that of humic substances. This method has several shortcomings, including the imprecision inherent in visual (i.e., by human eye) comparisons of samples to a small number of chloroplatinate standards. Consequently, many laboratories measure absorbance on a spectrophotometer, but there is no standard wavelength for such measurements. This is problematic because the chloroplatinate standard has a different spectral curve than aquatic humic substances (Figure 18.12a). Consequently, results expressed in PCUs will depend on the wavelength at which the measurements are made. Cuthbert and del Giorgio[70] proposed that absorbance be measured at 440 nm because they found a good correlation between absorbance at that wavelength and visual estimates of color. An equation relating absorbance at 440 nm (A_{440}) to color in PCU based on their approach is

$$\text{Color (PCU)} = 42A_{440}/l - 0.2, \tag{18.6}$$

where l is the cell path length in meters. Hongve and Åkesson[71] later showed that a chloroplatinate solution of 100 PCU and a solution of FA that had the same color intensity and hue by visual comparison had identical absorbance only at 410, 450–460, and 490–500 nm. On this basis they proposed that spectrophotometers should be calibrated with chloroplatinate at 410 nm, and color of samples should be measured at the same wavelength. This has the added advantage that absorptivity of CDOM is higher at 410 than at 440 nm, which increases the measurement sensitivity.

Marine scientists usually report CDOM absorptivity (e.g., A/l, m^{-1}) at a specific wavelength (e.g., 412 or 440 nm) directly.* They also use fluorescence (excitation wavelength of ∼330–340 nm and emission measured at 450 nm) to quantify CDOM. They generally do not convert absorbance or fluorescence values to an equivalent CDOM concentration in mg/L or mol C/L. Fluorescence results usually are expressed in relative units based on calibration to a standard fluorescing compound like quinine.[73]

The fluorescence of humic substances has been known for decades.[55] In addition to its use to estimate relative concentrations of CDOM in natural waters, quenching

---

*Polychlorinated organic acids, including 2,4-dichlorobenzoic acid and compounds similar to PCBs (2-chloro-4-(2′,4′,6′-trichlorophenyl)-benzoic acid, recently were found[72] at micrograms per liter concentrations in both coastal and open ocean waters. Because of their high molar extinction coefficients, they are thought to account for at least a few percent (perhaps more) of the absorbance of seawater in the range of 300–400 nm; they thus are significant components of marine CDOM. The compounds apparently are of natural, biological (in situ) origin. Whether such compounds occur in freshwaters is not yet known.

of humic fluorescence by paramagnetic heavy metal ions like Cu^{2+} has been used as to quantify metal-humate complexation.[74,75] Fluorescence also has been used to characterize the DOC in lakes as being allochthonous (i.e., more aromatic or "humic") versus autochthonous (i.e., more aliphatic).[76] Fluorescence spectroscopy has been used recently to develop a better understanding of the chemical nature of AHM and, more generally, of NOM.[77–80] Modern fluorescence spectra are presented as three-dimensional plots called emission-excitation matrices, in which the excitation wavelength λ_{ex} is plotted on the y-axis, and the emission wavelength λ_{em} is plotted on the x-axis, and the intensity of emission (amount of fluoresced light) is plotted on the z-axis. For ease in interpreting the data, emission intensity usually is plotted on the λ_{ex} versus λ_{em} matrix as a series of isolines of intensity (Figure 18.13). Interpretation of such spectra is not easy, but the locations and shapes of the peaks on the matrix provide information on the nature of the structural groups causing the fluorescence. A multivariate statistical procedure, parallel factor analysis (PARAFAC), was developed[81,82] to relate spectra for aquatic DOM with spectra of model compounds and to identify the components
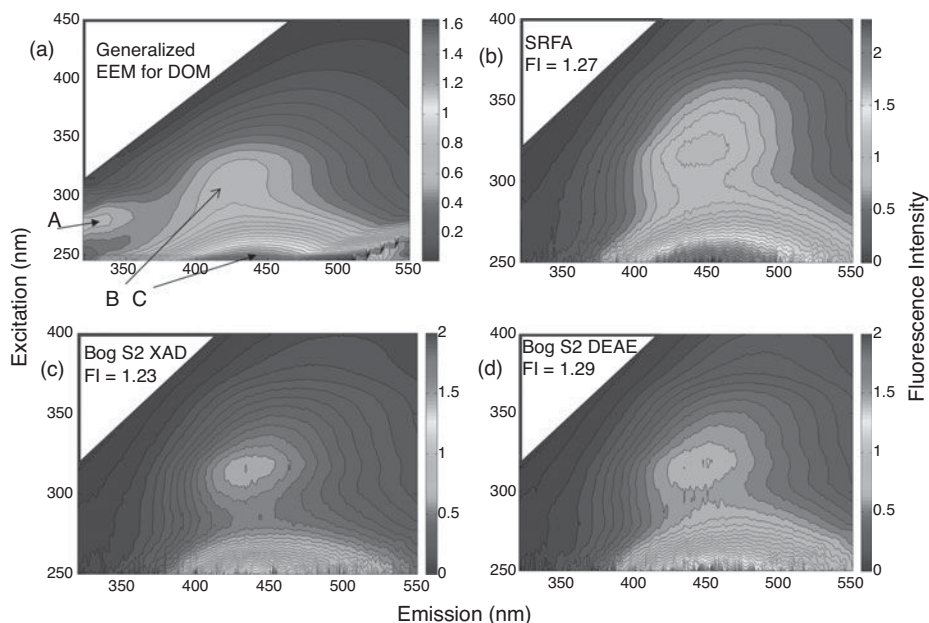
Figure 18.13 Excitation-emission matrices (EEMs) of fluorescence spectra for dissolved NOM: (a) typical NOM showing location of characteristic fluorescence peaks for protein-like material (A) and humic-like material (B and C); (b) IHSS Suwannee River fulvic acid; and (c) XAD-8 extract and (d) DEAE-cellulose extract, both of NOM from Bog S2, Marcell Experimental Forest, Itasca County, Minnesota. FI = fluorescence index calculated according to McKnight et al.[78] EEMs collected on a Fluorolog-321 (Horiba Scientific) in ratio mode using a CCD detector and integration time of 0.2 s; post-processing (inner filter correction, blank subtraction, excitation and emission correction) done following Cory et al., *Limnol. Occeanogr.: Methods* **8**: 67–78 (2010). Spectra courtesy of Rose Cory (University of North Carolina). (See color insert at end of book for a color version of this figure)

of AHM that contribute to fluorescence. By this approach quinone and semiquinone structures, as well as fluorescing amino acids (e.g., typtophan and tyrosine), in aquatic humic substances have been identified as components.[79] Unfortunately, the PARAFAC method is instrument-specific and difficult to apply; details on the use of PARAFAC were described by Stedmon and Bro.[82]

18.7   Acidity and metal complexation behavior of AHM

18.7.1 Acid-base and metal-binding properties of AHM

The density of carboxyl groups on NOM, and especially AHM, is high enough that they can account for a significant fraction of the anions in natural waters—particularly soft waters with high CDOM levels. The strong correlation between calculated "anion deficits" and measured DOC concentrations in soft-water lakes of the Upper Great Lakes region (Figure 18.14) provides support for two important ideas: (1) unmeasured carboxyl groups on NOM account for the "missing" anions and (2) NOM has a fairly constant density of anionic carboxyl groups per unit DOC. The slope of the trend line suggests that on average each milligram per liter of DOC contributed 6.62 µeq/L of anions. This is not equivalent to the total concentration of carboxyl groups in DOC but represents the average concentration of *deprotonated* carboxyl groups in the waters.

Carboxyl groups are major ligands in AHM (although not the only ones), and their concentration in AHM thus is of interest regarding both the acid-base and complexation chemistry in natural waters. Carboxyl concentrations of AHM measured by titration on a wide variety of samples are relatively constant (within a factor of $\sim$2). For example, Oliver et al.[83] reported a mean carboxyl content of 10.5 ($\pm$1.7) µeq/mg organic C in AHM from 19 streams, lakes, wetlands, and ground waters across North America. Eshelman and Hemond[84] reported a value of 7.5 µeq/mg of DOC in surface and ground water from
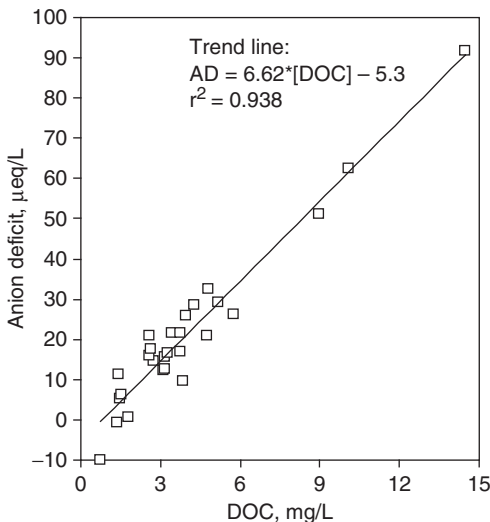
Figure 18.14 Observed relationship between calculated anion deficit (AD) and DOC concentration for 26 soft-water lakes in the Upper Great Lakes region (northern Minnesota and Wisconsin and Upper Michigan. Anion deficit was calculated as the difference between the sums of measured major cations (Ca^{2+}, Mg^{2+}, Na^+, and K^+) and anions (HCO_3^-, Cl^- and SO_4^{2-}), all in µeq/L, at the ambient pH, which ranged between 4.7 and 6.3 among the lakes. Unpublished data of the author (P.L.B.) and K. Webster from U.S. EPA-funded study on long-term trends in acid-sensitive lakes.

Massachusetts. Henriksen and Seip[85] found a value of 5.5 μeq/mg for surface waters in Norway and Scotland. A range of 4.8–9.4 μeq/mg was reported for bog waters from a range of locations.[86,87] Thus, it appears reasonable to say that DOM has ∼5–10 μeq of carboxyl groups per mg organic carbon.

A thorough review of the literature by Ritchie and Perdue[88] yielded this summary:

	Carboxyl groups μeq/g	Phenolic groups μeq/g
FA	4.8–6.6	1.4–4.1
HA	3.2–4.8	1.4–3.4
NOM samples	5.2–8.3	2.1–3.8

The above values are expressed on a dry, ash-free weight basis. Because AHM is ∼50% C by weight, the numbers should be multiplied by two for comparison with the earlier results in the paragraph. IHSS SRFA has a carboxyl content of 11.4 and SRHA has a content of 9.6 μeq/mg C.

Base (alkalimetric) titrations of AHM extracts (or acidified water containing AHM from which CO_2 has been purged) do not yield sharp inflection points expected for titrations of acids with a single pK_a. Instead, broad curves are obtained indicative of mixtures of acids with multiple pK_a values. The range of pK_a, of course, reflects the fact that AHM carboxyl groups are not all in the same molecular environments. The acidity of individual groups varies with the proximity of electron-withdrawing groups that diffuse the negative charges of deprotonated $-COO^-$ groups and electron-donating groups that intensify the charges. For a perspective on this phenomenon, consider that the pK_a values in Table 18.4 for benzoic acid and some mono-, di- and tri- hydroxy-substituted derivatives, which are all reasonable structures for aromatic carboxyl groups on AHM, have a range of 2.5 units. It is instructive to see how the –OH position

Table 18.4 pK_a values for benzoic acid and some hydroxy-, thio-, and amino- substituted derivatives*

Compound	pK_a
Benzoic acid	4.20
o-Hydroxybenzoic acid (salicylic acid)	2.97
m-Hydroxybenzoic acid	4.06
p-Hydroxybenzoic acid	4.48
2,5-Dihydroxybenzoic acid	2.97
3,4-Dihydroxybenzoic acid	4.48
3,5-Dihydroxybenzoic acid	4.04
3,4,5-Trihydroxybenzoic acid (gallic acid)	4.48
2,4,6-Trihydroxybenzoic acid	1.68
2-Mercaptobenzoic acid	8.09
2-Aminobenzoic acid	4.78
3-Aminobenzoic acid	4.55
3,4-Diaminobenzoic acid	4.75
2-(Methylamino)benzoic acid	5.29

* Values from NIST.[89]

affects pK_a. For example, pK_a for *o*-hydroxybenzoic acid (salicylic acid) is 1.23 units lower than that of benzoic acid, but pK_a for *m*-hydroxybenzoic acid is only 0.14 units lower, and pK_a for the *para*-substituted compound is 0.28 units higher.[89] The pK_a for 3,4,5-trihydroxybenzoic acid (gallic acid) also is 0.28 units higher than that of benzoic acid, but pK_a of 2,4,6-trihydroxybenzoic acid is much lower than any of the other listed compounds. In contrast, electron-donating groups like $-SH$ and $-NH_2$ decrease the acidity of the carboxyl group and cause higher pK_a values (see Chapter 19). If we consider that aliphatic carboxylic acid groups also are present in AHM, it is easy to imagine that the K_a values of AHM carboxyl groups could have a range of four or more log units. The same idea applies to phenolic groups, which are abundant in AHM; $pK_a = 9.99$ for phenol itself, but substituted phenols with strong electron-withdrawing groups have pK_a values up to several units lower, and those with electron donating groups may have higher pK_a values.

18.7.2 Advanced topic: modeling acidity and metal binding functions for AHM

The literature on this subject over the past $\sim$30 years is extremely rich, reflecting both the importance of NOM and AHM in trace heavy metal speciation and the difficulties encountered in understanding and modeling these processes. Some heavy metals, such as Cu and Hg, are strongly associated with organic ligands in natural waters, and the concentrations of the free metal ions are very low. In such cases, equilibrium modeling using only inorganic ligands does not yield accurate speciation results. In addition to measurement difficulties associated with quantifying metal binding to NOM, the fact that NOM is such a mixture of substances—leading to uncertainties about the chemical nature of the relevant ligand groups—has posed great difficulties in developing realistic but tractable approaches to modeling these processes. Our goal in the following sections is to describe the basic approaches that have been developed to model proton and metal binding by AHM rather than to focus on measurement techniques or findings from metal binding studies on specific NOM samples.

The simplest approach to modeling the acidity and metal binding properties of AHM is to assume that there is one discrete site with one pK_a value (and one stability constant value for each metal ion). Despite the desirable simplicity of this approach and its ease of application to equilibrium programs like MINEQL+, it is clear from the previous section that it is not realistic; AHM titrations show broad inflection ranges across many pH units (or many units of log[M]), implying that a range of pK values exists— or that the apparent pK changes with degree of ionization. Oliver et al.[83] concluded that the value of pK_a is correlated with pH and proposed an empirical approach to estimate pK_a:

$$pK_a = 0.96 + 0.90\text{pH} - 0.039(\text{pH})^2 \tag{18.7}$$

The empirical nature of Eq. 18.7 is unattractive, but the idea that K_a is a function, not a constant, is a useful advance in thinking. Two broad approaches have been used to develop more realistic models of AHM acidity and metal binding: (1) multiple discrete site models and (2) continuous distribution models.

18.7.2.1 Discrete-site approaches for binding metal ions and protons

In this case, AHM is treated as a collection of n monoprotic acids, where n is assumed to be finite and usually a fairly small number. An important additional assumption is that metal binding is associated with these sites. Such models require $2n$ parameters: the $pK_{a,i}$ and concentration (C_i) or "site density" of each kind of site in the AHM (or NOM). Obtaining these data for $n > 2$ is problematic, but if we consider AHM to be a mixture of just two sites—a strong site (ss) and weak site (ws), values of pK_{ss}, pK_{ws}, C_{ss} and C_{ws} can be obtained from a ***Scatchard plot*** analysis[90] of an acid-base titration.

Scatchard plots (Figure 18.15) have been used both for acid-base and metal complexation modeling. For metal binding studies, AHM samples are titrated with the metal ion of interest at fixed pH. Usually, the free metal ion is measured as a function of added metal in these titrations, but in some studies the concentration of the complexed metal, a competing ligand, or other approaches are used.[75] In Figure 18.15, $M = H^+$ for acid-base titrations or M^{n+} for complexometric titrations with ligand L; M_f is the free metal ion or H^+, and L_T is the total concentration of ligand sites. The ratio $[ML]/L_T$ is given the symbol $\bar{v}$, and Scatchard's approach plots $\bar{v}/M_f$ versus $\bar{v}$. Because this is a plot of a function of a variable versus the variable itself, it suffers from the danger of spurious self-correlation described in Chapter 14.

Scatchard plots for titrations of M^{n+} (or H^+) versus L yield straight lines if L has only one kind of binding site (hence one K_f), and the slope of the plot gives the negative value of K_f (Figure 18.15a). If the ligand has two or more different binding sites (with different K_f values), the plot is hyperbolic (Figure 18.15b), and the slopes of the asymptotes yield $K_{f,ss}$ and $K_{f,ws}$. Hyperbolic plots are found when metal-binding titration data for AHM are analyzed by Scatchard plots. If L has more than two sites and more than two binding constants, the plots still are hyperbolic, and unfortunately one cannot tell from the shape of the curve whether $n = 2$ or $n > 2$. Some workers have used instantaneous values of
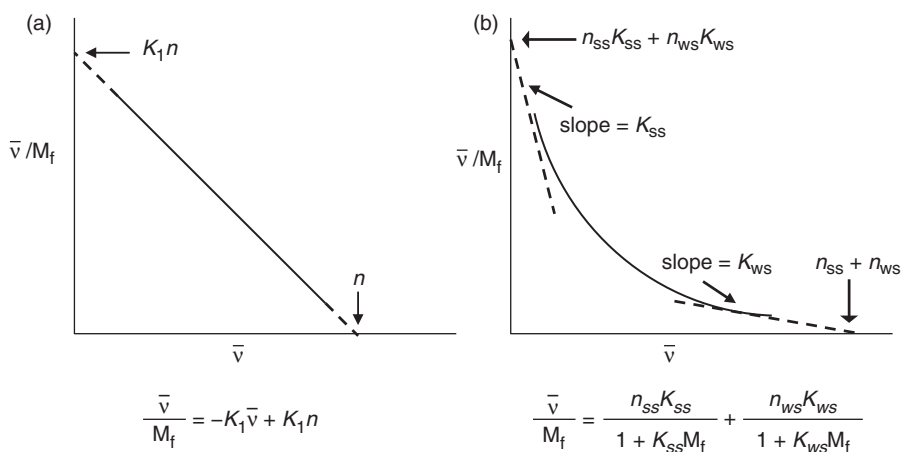
Figure 18.15 Plots used in Scatchard analyses. (a) Identical, independent binding sites. (b) Two classes of independent sites. See text for notation; equations below figures define the lines in the sketches.

the slope along the hyperbolic curve as measures of the instantaneous binding constant associated with a given ratio of [ML]/L_T, but this is not mathematically correct, and only the two asymptotic slopes have physical meaning as measures of K_f.

The general equation from which Scatchard plots and the corresponding equations in Figure 18.15 were derived is

$$M_T = M_f + \sum_{i=1}^{n} \frac{K_i M_f L_T}{1 + K_i M_f}. \tag{18.8}$$

Readers should note the similarity of Eq. 18.8 to the equations used to solve complexation equilibrium problems in Chapter 9 (e.g., Examples 9.1–9.3) and to the multisite Langmuir model (Chapter 14). Titration data can be fit to this equation by nonlinear least squares routines without the strict limitation that n be 2 or less, and Turner et al.[91] found that this approach gave the best results of five different methods for modeling data from Cu and Pb titrations of an FA sample. Typical values for pK_{a1} and pK_{a2} used in two-site models for AHM are ~4.0 and 5.5–6.0. Some have suggested that the strong sites are salicylic acid (o-hydroxybenzoic acid) groups, which form six-membered rings (chelates) with metal ions, and that the weak sites are phthalic acid groups, which form seven-membered rings with metal ions:[92,93]
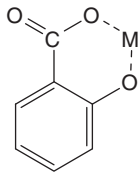
A metal salicylate complex   A metal phthalate complex
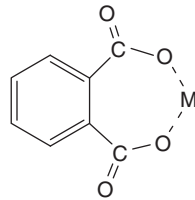
Recall that the optimum ring size for bidentate ligands is five, and six-member rings generally form stronger complexes than do seven-member rings. Also, note that pK_a for salicylic acid is lower than the typical value of pK_{a1} reported for AHM. Although this structural model has some attractive features, it is not likely that the structures of metal-AHM complexes fit into just two categories.

Discrete binding models can be extended to n kinds of binding sites with n pK_a or log K_f values. This makes physical sense, given what we know about AHM. Early efforts modeled this idea by choosing a large number of pKs over a range of ~3.5–6.5 and dividing the AHM equally among those sites. However, in a sense, this is worse than an empirical relationship in that it lacks an experimental basis.

18.7.2.2 Continuous distribution models

Although the number of different acidic or metal-binding sites in a given AHM sample is finite, information presented above (Sections 18.5.3 and 18.7.1) suggests that n could be a very large number. In that case, it may be useful and reasonable to model pK_a or log K_f as a *continuous function*. The question is: what is the nature of that function (or its distribution

Figure 18.16 Normal or Gaussian distribution curve: μ_κ = mean of κ; σ = standard deviation of κ; 68% of the area under the curve falls within the region $\mu_\kappa \pm 1\sigma$ and 95% falls within $\mu_\kappa \pm 2\sigma$.
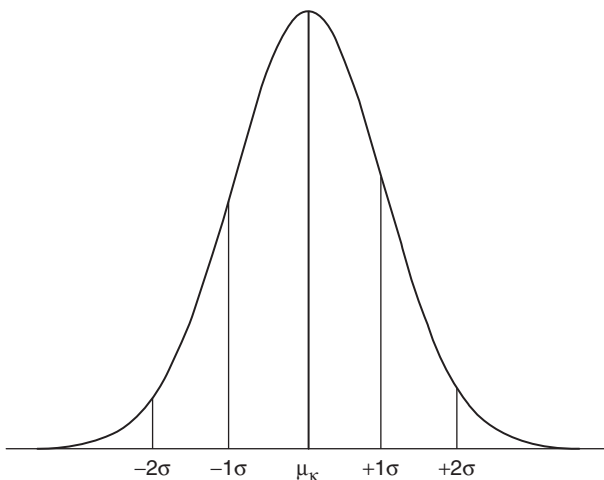
in log K space)? There are, of course, many alternatives. Perdue et al.[94] proposed that pK for AHM could be modeled as a normal (Gaussian) distribution (Figure 18.16):

$$N(\kappa) = \frac{L_i}{L_T} = \frac{1}{\sigma\sqrt{2\pi}} \exp\left[-\frac{1}{2}\left(\frac{\mu - \kappa}{\sigma}\right)^2\right], \tag{18.9}$$

where $N(\kappa)$ = distribution function, μ = mean of κ, where $\kappa = \log K_a$, and σ = standard deviation of κ. Only the top half (right side) of the normal distribution is important in affecting AHM speciation. This model has the advantage of mathematical parsimony because only two coefficients (μ and σ) need to be extracted from experimental data. Although normal or log-normal distributions are common in nature, there is no physical (experimental) basis to assume that $\log K_a$ (or $\log K_f$) is normally distributed in AHM— a major disadvantage of this approach. Nonetheless, Perdue et al.[94] showed that this model accurately described proton binding by AHM from the Satilla River in Georgia between pH 4 and 10. The computer program VMINTEQ has a routine to simulate DOM binding of protons and metals by a Gaussian model.

To avoid arbitrary specification of the distribution of $\log K_a$, some have fit experimental data from acid-base and metal complexation titrations of AHM using an "affinity spectrum approach," which assumes no particular distribution for $\log K$.[95] In general,

$$\bar{v} = \frac{[ML]}{L_T} = \int_{-\infty}^{+\infty} N(\kappa)\frac{10^\kappa[H^+]}{1 + 10^\kappa[H^+]}d\kappa \tag{18.10}$$

where $\bar{v}$ = macroscopic binding parameter or formation function and $\kappa = \log K$. Unfortunately, several studies[91,96] reported instabilities in calculations by this method and/or an inability to obtain interpretable results.

Better success has been obtained using the nonlinear least squares optimization program FITEQL,[97] used widely for surface acidity and complexation titrations (Chapter 14), to fit experimental titration data for AHM extracts. For example, Lu and Allen[98] found that at least three sites (and three log K_a values) were needed to fit data on alkalimetric titrations (i.e., titrations with strong base) of DOM samples from the Suwannee River, Georgia, Drummond Lake, Virginia, and Newport River, North Carolina. A four-site model with four pK_a values was better (Table 18.5). Similarly, four sites were needed to fit Cu^{II} titration data for the same samples (Table 18.5), and log K'_f values for conditional stability constants were in the general range of 5–11. In general, the strongest sites (log $K'_4 = {\sim}11$) had the lowest site densities in the DOM, and the weakest sites (log $K'_1 = {\sim}5.5$–6.0) had the highest site densities.

As others have found, the total binding site density (L_T) found for Cu^{II}, $\sim$4.55 mmol/g C, was similar to the density of phenolic sites in the DOM but much lower than the site density for total acidity in the DOM ($\sim$13–14 mmol/g C). Cu^{II} complexation by the DOM increased by a factor of $\sim$10 per pH unit, even at pH > 8. Based on this finding and the similarity of L_T to the phenolic content of the DOM samples, Lu and Allen[98] concluded that Cu^{II} binding was to phenolic groups rather than carboxyl groups, which tends to agree the soft-acid character of Cu^{II}, but they stated that the possibility of chelation involving both phenolic and carboxylate groups could not be distinguished by their model formulation. The high values of the fitted formation constants in Table 18.5 do suggest chelate formation rather than binding by monodentate ligands. It must be noted that statistical fit of the data to the model is not proof that there are only four binding sites for protons and Cu^{II} in the DOM or that the binding of Cu^{II} necessarily involves phenolic groups. All one can state for certain is that the model fits the data well

Table 18.5 Acidity constants, Cu^{II} conditional stability constants and site densities of a FITEQL-fit four-site DOM model*

A. Acidity constants and site densities

Source	(mmol/g C)			$(L_{i,H}$, mmol/g C$)^{\dagger}$			
	Carboxylic	Phenolic	Total	pK_{a1}	pK_{a2}	pK_{a3}	pK_{a4}
Suwannee R., Ga.	9.37	4.21	13.58	4.1	4.0	1.7	3.0
Newport R., N.C.	8.95	4.20	13.15	4.2	3.5	1.6	2.9
Drummond L., Va.	10.18	3.87	14.05	4.9	4.0	1.5	2.6

B. Cu^{II} conditional stability constants and site densities at pH 7.0

Source	Log K'_1	Log K'_2	Log K'_3	Log K'_4	(mmol/g C)			
					$L_{1,T}$	$L_{2,T}$	$L_{3,T}$	$L_{4,T}$
Suwannee R.	5.95	6.92	8.43	10.51	3.71	0.98	0.29	0.071
Newport R.	5.80	7.33	8.94	11.64	3.49	1.22	0.39	0.096
Drummond L.	5.49	7.04	8.69	11.51	3.68	1.05	0.31	0.084

* Tabulated from Lu and Allen.[98]
† $L_{i,H}$ = site density for the ith site ($I = 1$ to 4; $pK_{a1} = 3.3$; $pK_{a2} = 4.8$; $pK_{a3} = 6.8$; $pK_{a4} = 9.6$).

and is not inconsistent with the proposed molecular (structural) model. In this respect, the limitation in our ability to infer molecular structures is analogous to the difficulties faced in trying to infer reaction mechanisms from the rate equations that kinetic data fit. It should be noted that the ratio of metal to AHM for Cu and other minor metals that bind strongly to AHM is such that only the strong sites are important in real systems, and consequently these systems usually can be described, at least over narrow ranges, using simpler models.

18.7.2.3 Electrostatic model

Even if all the acidic (binding) sites in a macromolecule are chemically the same and have the same intrinsic binding energy (one intrinsic pK_a), the observed pK_a will vary as a result of electrostatic effects as the net charge of the macromolecule increases when it becomes more deprotonated.[93] This phenomenon is analogous to the electrostatic effects on charged surfaces (Chapter 14). Application of this concept to AHM-metal binding was developed from principles in polymer chemistry and leads to the general expression

$$K_{cond} = K_{int} \exp(2\omega zZ), \tag{18.11}$$

where K_{int} is an "intrinsic" K (for uncharged AHM molecules), and K_{cond} is the conditional (observed) K at some degree of deprotonation of AHM. Z is the charge on AHM, and z = charge on combining ion (= +1 for H^+). ω, the "electrostatic interaction factor," is defined as

$$\omega = \frac{e^2}{2\boldsymbol{D}rkT} \left(1 - \frac{\kappa r}{1 + \kappa a} \right), \tag{18.12}$$

where e = charge on the electron; $\boldsymbol{D}$ = dielectric constant; $\mathbf{k}T$ = thermal energy per molecule; κ = Debye parameter (radius of sphere of charge)$^{-1}$, analogous to thickness of the diffuse double layer; r = radius of AHM molecule; and a = $\sum$(r+ closest approach of counter ion). Although the model accounts for the well-known electrostatic effects involved in ionization of macromolecules, AHM-specific parameters for the model are difficult to estimate. By itself, the model does not account for the heterogeneity of AHM molecules—meaning that it needs to be combined with one of the continuous-distribution or multiple discrete-site models described above—and this makes parameter estimation even more problematic.

18.7.2.4 Models combining multiple discrete site and electrostatic effects

Models that combine the concept of K_{obs} varying from electrostatic effects and the heterogeneity of functional groups (several discrete sites with different K_{int} values) are complicated and have many adjustable parameters that need to be estimated (a generally undesirable feature). Early versions of such models were published in the late 1980s.[99] WHAM,[100] a computerized version of this type of model, now is widely used to model metal binding by AHM (e.g., Lu and Allen[98] and Cory et al.[101]) and also has been used as the basis for modeling the kinetics of Zn adsorption to soils.[102] In its default version, there are two classes of acidic sites (A and B), each having equal densities of four subgroups

with different pK_a values (and metal binding constants). Default values are provided for the electrostatic parameters, and the model assumes a diffuse layer surrounding the humic molecules has a different ionic composition than the bulk solution (as is the case for charged surfaces in Chapter 14).

18.7.3 Binding of soft metals by humic substances: role of S and N groups

Not all metal binding by humic materials involves carboxylate and phenolic groups. As noted earlier, AHM and soil humic matter contains small amounts (up to 1–3%) of nitrogen and sulfur. The latter element plays an especially important role in binding of soft metal ions like Hg^{2+} and methyl mercuric ion $(MeHg^+)$. As a soft (Class B) metal, Hg generally forms much stronger complexes with sulfur ligands than with oxygen ligands. X-ray absorption near-edge spectroscopy (XANES) studies[103] have shown that as much as 50% of the sulfur in humic substances occurs in reduced oxidation states (S_{re}), such as thiols (RSH), thioethers (RSR), and disulfides (RSSR). Studies using extended x-ray absorption fine structure spectroscopy (EXAFS) have shown that S_{re} groups in soil organic matter and aquatic organic matter form complexes with Hg^{2+} and $MeHg^+$.[104−106] Although concentrations of S_{re} ligands in humic substances are low compared to those of carboxylate groups ($\sim$0.3–1 μmol S_{re} per mg C vs. 5–10 μeq −COOH per mg C), there still is a huge surplus of S_{re} relative to concentrations of total Hg and $MeHg^+$ in aquatic systems (Hg_T generally is a few nanograms per liter in lakes and wetlands (picomolar), and $MeHg^+$ is usually a small fraction of that).[107]

Wide ranges have been reported for stability constants of Hg^{2+} and $MeHg^+$ with soil and aquatic humic substances. Results from different studies are difficult to compare because of differences in analytical methods, calculation models and reporting units. Nonetheless, recent studies performed under conditions of low $Hg:S_{re}$ loadings that simulate ambient conditions and favor the measurement of complexes with the strongest sites show that Hg forms very strong complexes with humic matter. For example, Khwaja et al.[108] found evidence for binding of Hg^{2+} to bidentate thiol sites with some participation of a third weak-acid group (presumably a thiol), and they reported K_f was in the range $1-2 \times 10^{38}$. Stability constants for $MeHg^+$-humic complexes are lower but still strong; representative values are 6.4×10^9 for IHSS SRFA[109] and 7.5×10^{10} for an organic soil.[109,110]

Finally, most metal-binding studies with Cu^{II} and AHM have assumed the Cu binds with oxygen-containing ligand sites. A study by Woolard et al.[111] found, however, that a hypothetical FA generated by a program called RANDOM2, which produces AHM model structures in a manner similar to the agent-based model of Cabaniss et al.,[28] was not able to reproduce experimentally observed Cu-NOM interactions when nitrogen-containing sites were excluded. When N-containing ligands were included in the RANDOM2 calculations to synthesize an FA mixture, the speciation patterns obtained with MINTEQA2 predicted that Cu-NOM complexes accounted for 80–100% of the Cu at natural levels of FA, in agreement with experimental results. Binding to the FA was primarily through 1,2-propylenediamine and 2,3-diaminopropanoic acid binding sites.

The complexities and subtleties revealed in recent studies of metal binding by NOM suggest that this will be a fertile research area for years to come.

18. Chin, Y. P., and P. M. Gschwend. 1991. The abundance, distribution, and configuration of porewater organic colloids in recent sediments. *Geochim. Cosmochim. Acta* **55**: 1309–1317.

19. Everett, C. R., Y.-P. Chin, and G. R. Aiken. 1999. High pressure size exclusion chromatography analysis of dissolved organic matter isolated by tangential flow ultrafiltration. *Limnol. Oceanogr.* **44**: 1316–1322.

20. Malcolm, R. L. 1990. Variations between humic substances isolated from soils, stream waters and ground waters as revealed by ^{13}C NMR spectroscopy. In *Humic substances in soil and crop sciences*, P. MacCarthy, C. E. Clapp, R. L. Malcolm, and P. R. Bloom (eds.), Am. Soc. Agron., Soil Sci. Soc. Am., Madison, Wisc.

21. Simpson, A. 2001. Multidimensional solution state NMR of humic substances: a practical guide and review. *Soil Sci.* **166**: 795–809.

22. Kebarle, P., and M. Pesche. 2000. On the mechanism by which the charged droplets produced by electrospray lead to gas phase ions. *Anal. Chim. Acta* **406**: 11–35.

23. Hockaday, W. C., J. M. Purcell, A. G. Marshall, J. A. Baldock, and P. G. Hatcher. 2009. Electrospray and photoionization mass spectrometry for the characterization of organic matter in natural waters: a qualitative assessment. *Limnol. Oceanogr. Meth.* **7**: 81–95.

24. Sleighter, R. L., C. G. A. McKee, and P. G. Hatcher. 2009. Direct Fourier transform mass spectral analysis of natural waters with low dissolved organic matter. *Org. Geochem.* **40**: 119–125.

25. Hertkorn, N., M. Frommberger, M. Witt, P. B. Koch, P. Schmitt-Koplin, and E. M. Perdue. 2009. Natural organic matter and the event horizon of mass spectrometry. *Anal. Chem.* **80**: 8908–8919.

26. NIST. 2009. Atomic weights and isotopic compositions for all elements (available at http://physics.nist.gov/cgi-bin/Compositions/stand_alone.pl), accessed November 2009.

27. Brezonik, P. L. 1994. *Chemical kinetics and process dynamics in aquatic systems*, Lewis Publ.-CRC Press, Boca Raton, Fla.

28. Cabaniss, S. E., G. Marey, L. Leff, P. A. Maurice, and R Wetzel. 2005. A stochastic model for the synthesis and degradation of natural organic matter. Part I. Data structures and reaction kinetics; 2007. Part II. Molecular property distributions. *Biogeochem.* **76**: 319–347; **86**: 269–286.

29. McKnight, D. M., G. R. Aiken, and R. L. Smith. 1991. Aquatic fulvic acids in microbially based ecosystems: results from two desert lakes in Antarctica. *Limnol. Oceanogr.* **36**: 998–1006.

30. McKnight D. M., E. D. Andrew, S. A. Spaulding, and G. R. Aiken. 1994. Aquatic fulvic acids in algal-rich Antarctic ponds, *Limnol. Oceanogr.* **39**: 1972–1979.

31. Brown A., D. M. McKnight, Y. P. Chin, E. Roberts, and M. Uhle. 2004. Chemical characterization of dissolved organic material in Pony Lake, a saline coastal pond in Antarctica. *Marine Chem.* **89**: 327–337.

32. Gondar, D., S. A. Thacker, E. Tipping, and A. Baker. 2008. Functional variability of dissolved organic matter from the surface water of a productive lake. *Water Res.* **42**: 81–90.

33. Larson, R. A., and J. M. Hufnal, Jr. 1980. Oxidative polymerization of dissolved phenols by soluble and insoluble inorganic species. *Limnol. Oceanogr.* **25**: 505–512.

34. Bollag, J.-M. 1983. Cross-coupling of humus constituents and xenobiotic substances. In *Aquatic and terrestrial humic materials*, R. F. Christman and E. T. Gjessing (eds.), Ann Arbor Science Publ., Ann Arbor, Mich., 127–141.

35. Steinberg, C., and U. Muenster. 1985, Geochemistry and ecological role of humic substances in lake water. In *Humic substances in soil, sediment, and water*, G. R. Aiken, D. M. McKnight, R. L. Wershaw, and P. MacCarthy (eds.), Wiley, New York, 105–145.

36. Wolf, D. C., and J. P. Martin. 1976. Decomposition of fungal mycelia and humic-type polymers containing carbon-14 from ring and side-chain labeled 2,4-D and chlorpropham. *Soil Sci. Soc. Am. J.* **40**: 700–704.

37. Fimmen, R. L., R. M. Cory, Y.-P. Chin, T. D. Trouts, and D. M. McKnight. 2007. Probing the oxidation–reduction properties of terrestrially and microbially derived dissolved organic matter. *Geochim. Cosmochim. Acta* **71**: 3003–3015.

38. Shapiro, J. 1957. Chemical and biological studies on the yellow organic matter of lake water *Limnol. Oceanogr.* **2**: 161–179; and 1964. Effect of yellow organic acids on iron and other metals in water *J. Am. Wat. Works Assoc.* **56**: 1062–1082.

39. Black, A. P., and R. F. Christman. 1963. Characteristics of colored surface waters. *J. Am. Wat. Works Assoc.* **55**: 753–770; and 1963. Chemical characteristics of fulvic acids. *J. Am. Wat. Works Assoc.* **55**: 897–916.

40. Gjessing, E. T. 1965. Use of "Sephadex" gel for the estimation of molecular weight of humic substances in natural water. *Nature* **208**: 1091–1092.

41. Christman, R. F., and M. Ghassemi. 1966. Chemical nature of organic color in water. *J. Am. Water Works Assoc.* **58**: 723–741; Ghassemi, M., and R. F. Christman. 1968. Properties of the yellow organic acids of natural waters. *Limnol. Oceanogr.* **13**: 583–597.

42. Swift, R. S., and A. M. Posner. 1971. Gel chromatography of humic acid. *J. Soil Sci.* **22**: 237–249.

43. Chin, Y. P., G. Aiken, and E. O'Loughlin. 1994. Molecular weight, polydispersity, and spectroscopic properties of aquatic humic substances. *Environ. Sci. Technol.* **28**: 1853–1858.

44. Schnitzer, M., and S. U. Khan. 1978. *Soil organic matter*, Elsevier Publ., Amsterdam.

45. Wershaw, R. L., and G. R. Aiken. 1985. Molecular size and weight measurements of humic substances. In *Humic substances*, Aiken et al. (eds.), 477–492; Wershaw, R. L. 1985. Application of nuclear magnetic resonance spectroscopy for determining functionality in humic substances. In *Humic substances*, Aiken et al. (eds.), 561–582; Hatcher, P. G., I. A. Breger, L. W. Dennis, and G. E. Maciel. 1983. Solid-state ^{13}C NMR of sedimentary humic substances; new revelations on their chemical composition. In *Aquatic and terrestrial humic materials*, R. F. Christman and E. T. Gjessing (eds.), Ann Arbor Science Publ., Ann Arbor, Mich., 37–82.

46. Mannino, A., and H. R. Harvey. 2000. Terrigenous dissolved organic matter along an estuarine gradient and its flux to the coastal ocean. *Org. Geochem.* **31**: 1611–1625.

47. Frazier S. W., K. O. Nowack, K. M. Goins, F. S. Cannon, L. A. Kaplan, and P. G. Hatcher. 2003. Characterization of organic matter from natural waters using tetramethylammonium hydroxide thermochemolysis GC-MS. *J. Anal. Appl. Pyrol.* **70**: 99–128.

48. Khwaja, A. 2004. Photochemistry of dissolved organic matter and its interactions with methylmercury and inorganic mercury. Ph.D. dissertation, University of Minnesota, Minneapolis.

49. Reemtsma, T., A. These, A. Springer, and M. Linscheid. 2008. Differences in the molecular composition of fulvic acid size fractions detected by size-exclusion chromatography–on line Fourier transform ion cyclotron resonance (FTICR-) mass spectrometry. *Water Res.* **42**: 63–72.

50. Grannas, A. M., W. C. Hockaday, P. G. Hatcher, L. G. Thompson, and E. Mosley-Thompson. 2006. New revelations on the nature of organic matter in ice cores. *J. Geophys. Res.* **111**: D04304, doi: 10.1029/2005JD006251.

51. Kim, S., R. W. Kramer, and P. G. Hatcher. 2003. Graphical method for analysis of ultrahigh-resolution broadband mass spectra of natural organic matter, the van Krevelen diagram. *Anal. Chem.* **75**: 5336–5344.

52. Leenheer, J. A., G. K. Brown, P. MacCarthy, and S. E. Cabaniss. 1998. Models of metal binding structures in fulvic acid from the Suwannee River, Georgia. *Environ. Sci. Technol.* **32**: 2410–2416.

53. Harvey, G. R., D. A. Boran, L. A. Cheasl, and J. M. Tokar. 1983. The structure of marine fulvic and humic acids. *Mar. Chem.* **12**: 119–132.
54. Aluwihare, L. I., D. J. Repeta, and R. F. Chen. 2002. Chemical composition and cycling of dissolved organic matter in the Mid-Atlantic Bight. *Deep-Sea Res. II* **49**: 4421–4437.
55. Schnitzer, M., and R. Riffaldi. 1972. The determination of quinone groups in humic substances. *Soil Sci. Soc. Am. J.* **36**: 772–777.
56. Scott, D. T., D. M. McKnight, E. L. Blunt-Harris, S. E. Kolesar, and D. R. Lovely. 1998. Quinone moieties act as electron acceptors in the reduction of humic substances by humics-reducing microorganisms. *Environ. Sci. Technol.* **32**: 2984–2989.
57. Senesi, N., and C. Steelink. 1989. Application of ESR spectroscopy to the study of humic substances. In *Humic substances II. In search of structure*, M. Hayes, P. MacCarthy, R. Malcolm, and R. Swift (eds.), J. Wiley and Sons, New York, 373–408.
58. Wolf, M., A. Kappler, J. Jiang, and R. U. Meckenstock. 2009. Effects of humic substances and quinones at low concentrations on ferrihydrite reduction by *Geobacter metallireducens*. *Environ. Sci. Technol.* **43**: 5679–5685.
59. Kappler A., and S. B. Haderlein. 2003. Natural organic matter as reductant for chlorinated aliphatic pollutants. *Environ. Sci. Technol.* **37**: 2714–2719.
60. Zepp, R. G., and P. F. Schlotzhauer. 1981. Comparison of photochemical behavior of various humic substances in water III. Spectroscopic properties of humic substances. *Chemosphere* **10**: 479–486.
61. Twardowski, M. S., E. Boss, J. L. Sullivan, and P. L. Donaghay. 2004. Modeling the spectral shape of absorption by chromophoric dissolved organic matter. *Mar. Chem.* **89**: 69–88.
62. Carder, K. L., R. G. Steward, G. R. Harvey, and P. B. Ortner. 1989. Marine humic and fulvic acids: their effects on remote sensing of ocean chlorophyll. *Limnol. Oceanogr.* **34**: 68–81.
63. Baes, A. U., and P. R. Bloom. 1990. Fulvic acid ultraviolet-visible spectra: influence of solvent and pH. *Soil Sci. Soc. Am. J.* **54**: 1248–1254.
64. Singley, J. E., R. H. Harris, and J. S. Maulding. 1966. Correction of color measurements to standard conditions. *J. Am. Water Wks. Assoc.* **58**: 455–457.
65. U.S. EPA 2005. Determination of total organic carbon and specific UV absorbance in source water and drinking water. Method 415.3, EPA/600/R-05/055 (available at http://www.epa.gov/nerlcwww/m_415_3Rev1_1.pdf).
66. Traina, S. J., J. Novak, and N. E. Smeck. 1990. An ultraviolet absorbance method of estimating the aromatic content of humic acids. *J. Environ. Qual.* **19**: 151–153.
67. Weishaar, J. R., G. R. Aiken, B. A. Bergamaschi, M. S. Fram, R. Fujii, and K. Mopper. 2003. Evaluation of specific ultraviolet absorbance as an indicator of the chemical composition and reactivity of dissolved organic carbon. *Environ. Sci. Technol.* **37**: 4702–4708.
68. Kitis, M., T. Karanfil, A. Wigton, and J. E. Kilduff. 2002. Probing reactivity of dissolved organic matter for disinfection by-product formation using XAD-8 resin adsorption and ultrafiltration fractionation. *Water Res.* **36**: 3834–3848.
69. Chen Y., N. Senesi, and M. Schnitzer. 1977. Information provided on humic substances by E4/E6 ratios. *Soil Sci. Soc. Am. J.* **41**: 352–358.
70. Cuthbert, I. D., and P. del Giorgio. 1992. Toward a standard method of measuring color in freshwater. *Limnol. Oceanogr.* **37**: 1319–1326.
71. Hongve, D., and G. Åkesson. 1996. Spectrophotometric determination of water colour in Hazen units. *Water Res.* **30**: 2771–2775.
72. Repeta, D. J., N. T. Hartman, S. John, A. D. Jones, and R. Goericke. 2004. Structure elucidation and characterization of polychlorinated biphenyl carboxylic acids as major constituents of chromophoric dissolved organic matter in seawater. *Environ. Sci. Technol.* **38**: 5373–5378.

73. Chen, R. F., and G. B. Gardner. 2004. High-resolution measurements of chromophoric dissolved organic matter in the Mississippi and Atchafalaya River plume regions. *Mar. Chem.* **89**: 103–125.

74. Saar, R. A., and J. H. Weber. 1977. Comparison of spectrofluorometry and ion-selective electrode potentiometry for determination of complexes between fulvic acid and heavy-metal ions. *Anal. Chem.* **52**: 2095–2100.

75. Tuschall, J. R., Jr., and P. L. Brezonik. 1982. Complexation of heavy metals by aquatic humus: a comparative study of five analytical methods. In *Aquatic and terrestrial humic materials*, R. F. Christman and E. Gjessing (eds.), Ann Arbor Science Publ., Ann Arbor, Mich., 275–294.

76. Donahue, W. F., D. W. Schindler, S. J. Page, and M. P. Stainton. 1998. Acid-induced changes in DOC quality during an experimental whole-lake manipulation. *Environ. Sci. Technol.* **32**: 2954–2960.

77. Coble P. 1996. Characterization of marine and terrestrial DOM in seawater using excitation-emission matrix spectroscopy. *Marine Chem.* **51**: 325–346.

78. McKnight, D. M., E. W. Boyer, P. K. Westerhoff, P. T. Doran, T. Kulbe, and D. T. Andersen. 2001. Spectrofluorometric characterization of dissolved organic matter for indication of precursor organic material and aromaticity. *Limnol. Oceanogr.* **46**: 38–48.

79. Cory, R. M., and D. M. McKnight. 2005. Fluorescence spectroscopy reveals ubiquitous presence of oxidized and reduced quinones in dissolved organic matter. *Environ. Sci. Technol.* **39**: 8142–8149.

80. Mladenov, N., P. Hunstman-Mapila, P. Wolski, W. R. L. Masamba, and D. M. McKnight. 2008. Dissolved organic matter accumulation, reactivity, and redox state in ground water of a recharge wetland. *Wetlands* **28**: 747–759.

81. Stedmon C., and S. Markager. 2005. Resolving the variability in dissolved organic matter fluorescence in a temperate estuary and its catchment using PARAFAC analysis. *Limnol. Oceanogr.* **50**: 686–697.

82. Stedmon, C. A., and R. Bro. 2008. Characterizing dissolved organic matter fluorescence with parallel factor analysis: a tutorial. *Limnol. Oceanogr. Meth.* **6**: 572–579.

83. Oliver, B. G., E. M. Thurman, and R. L. Malcolm. 1983. The contribution of humic substances to the acidity of colored natural waters. *Geochim. Cosmochim. Acta* **47**: 2031–2035.

84. Eshelman, K. N., and H. F. Hemond. 1985. The role of organic acids in the acid-base status of surface waters at Bickford watershed, Massachusetts. *Water Resour. Res.* **21**: 1503–1510.

85. Henriksen, A., and H. M. Seip. 1980. Strong and weak acids in surface waters of southern Norway and southwestern Scotland. *Water Res.* **14**: 809–813.

86. Gorham, E., S. J. Eisenreich, J. Ford, and M. V. Santlemann. 1985. The chemistry of bog waters. In *Chemical processes in lakes*, W. Stumm (ed.), Wiley-Interscience, New York, 339–363.

87. McKnight, D. M., E. M. Thurman, R. L. Wershaw, and H. F. Hemond. 1985. Biogeochemistry of aquatic humic substances in Thoreau's Bog, Concord, Massachusetts. *Ecol.* **66**: 1339–1352.

88. Ritchie, J. D., and E. M. Perdue. 2003. Proton-binding study of standard and reference fulvic acids, humic acids, and natural organic matter. *Geochim. Cosmochim. Acta* **67**: 85–96.

89. NIST. 2004. NIST critically selected stability constants of metal complexes. In *NIST Standard Reference Database*, 46 ver. 8.0, A. E. Martell and R. M. Smith (eds.), Gaithersburg, Md.

90. Scatchard, G. 1949. The attraction of proteins for small molecules and ions. *Ann. N. Y. Acad. Sci.* **51**: 660–672.

91. Turner, D. R., M. S. Varney, M. Whitfield, R. F. C. Mantoura, and J. P. Riley. 1986. Electrochemical studies of copper and lead complexation by fulvic acid. I. Potentiometric measurements and a critical comparison of metal binding models. *Geochim. Cosmochim. Acta* **50**: 289–297.

92. Snoeyink, V. L., and D. Jenkins. 1980. *Water chemistry*. J. Wiley & Sons, New York.

93. Wilson, D. E., and P. Kinney. 1977. Effects of polymeric charge variations on the proton-metal ion equilibria of humic materials. *Limnol. Oceanogr.* **22**: 281–289.

94. Perdue, E. M., J. H. Reuter, and R. S. Parrish. 1984. A statistical model of proton binding by humus. *Geochim. Cosmochim. Acta* **48**: 1257–1263.

95. Thakur, A. K., P. J. Munson, D. L. Hunston, and D. Rodbard. 1980. Characterization of ligand-binding systems by continuous affinity distributions of arbitrary shape. *Anal. Biochem.* **103**: 240–254.

96. Fish, W. D. A. Dzombak, and F. M. M. Morel. 1986. Metal-humate interactions. 2. Application and comparison of models. *Environ. Sci. Technol.* **20**: 676–683.

97. Herbelin, A. L., and J. C. Westall. 1999. FITEQL: a computer program for determination of chemical equilibrium constants from experimental data. Dept. of Chemistry, Oregon State Univ., Corvallis, Ore.

98. Lu, Y., and H. E. Allen. 2002. Characterization of copper complexation with natural dissolved organic matter (DOM)—link to acidic moieties of DOM and competition by Ca and Mg. *Water Res.* **36**: 5083–5101.

99. Ephraim, J., S. Alegret, A. Mathuthu, M. Bicking, R. L. Malcolm, and J. A. Marinsky. 1986. A united physicochemical description of the protonation and metal ion complexation equilibria of natural organic acids (humic and fulvic acids). 1. Analysis of the influence of polyelectrolyte properties on protonation equilibria in ionic media: fundamental concepts; 2. Influence of polyelectrolyte properties and functional group heterogeneity on the protonation equilibria of fulvic acid; 3. Influence of polyelectrolyte properties and functional heterogeneity on the copper ion binding equilibria in an Armadale Horizons Bh fulvic acid sample. *Environ. Sci. Technol.* **20**: 349–354; 354–366; 367–376.

100. Tipping, E. 1994. WHAM—a chemical equilibrium model and computer code for waters, sediments, and soils incorporating a discrete site/electrostatic model of ion-binding by humic substances. *Comput. Geosci.* **20**: 973–1023.

101. Cory, N., C. N. Andrén, and K. Bishop. 2007. Modelling inorganic aluminium with WHAM in environmental monitoring. *Appl. Geochem.* **22**: 1196–1201.

102. Shi, Z., D. M. DiToro, H. E. Allen, and D. L. Sparks. 2008. A WHAM-based kinetics model for Zn adsorption and desorption to soils. *Environ. Sci. Technol.* **42**: 5630–5636.

103. Xia, K., F. Weesner, W. F. Bleam, P. R. Bloom, U. L. Skyllberg, and P. A. Helmke. 1998. XANES studies of oxidation states of sulfur in aquatic and soil humic substances. *Soil Sci. Soc. Amer. J.* **62**: 1240–1246.

104. Qian, J., U. L. Skyllberg, W. Frech, W. F. Bleam, P. R. Bloom, and P. E. Petit. 2002. Bonding of methyl mercury to reduced sulfur groups in soil and stream organic matter as determined by x-ray absorption spectroscopy and binding affinity studies. *Geochim. Cosmochim Acta* **66**: 3873–3885.

105. Yoon, S.-J., L. M. Diener, P. R. Bloom, E. A. Nater, and W. F. Bleam. 2005. X-ray absorption studies of CH_3Hg^+-binding sites in humic substances. *Geochim. Cosmochim. Acta* **69**: 1111–1121.

106. Skyllberg, U., P. R. Bloom, J. Qian, C. M. Lin, and W. F. Bleam. 2006. Complexation of mercury(II) in soil organic matter: EXAFS evidence for linear two-coordination with reduced sulfur groups. *Environ. Sci. Technol.* **40**: 4174–4180.

107. Hines, N. A., and P. L. Brezonik. 2007. Input-output analysis of mercury forms for a small lake in northern Minnesota. *Biogeochem.* **84**: 265–284.

108. Khwaja, A. R., P. R. Bloom, and P. L. Brezonik. 2006. Binding constants of divalent mercury (Hg^{2+}) in soil humic acids and soil organic matter. *Environ. Sci. Technol.* **40**: 844–849.
109. Khwaja, A. R., P. R. Bloom, and P. L. Brezonik. 2010. Binding strength of methylmercury to aquatic NOM. *Environ. Sci. Technol.* **44**: 6151–6156.
110. Karlsson, T., and U. L. Skyllberg. 2003. Bonding of ppb levels of methylmercury to reduced sulfur groups in soil organic matter. *Environ. Sci. Technol.* **37**: 4912–4918.
111. Woolard, C. D., and P. W. Linder. 1999. Modelling of the cation binding properties of fulvic acids: an extension of the RANDOM algorithm to include nitrogen and sulphur donor sites. *Sci. Tot. Environ.* **226**: 35–46.

19

◼ Chemistry of Organic Contaminants

◼ Objectives and scope

This chapter describes the processes that dictate the fate of organic chemicals in environmental systems. The equilibrium partitioning of organic chemicals between environmental phases (air, water, soil/sediment, biota) is presented, as are means to predict the relevant equilibrium constants based on chemical structure using publically available software. The main reactions that lead to transformations of organic chemicals are presented, and the structural features that make a compound susceptible to such reactions are highlighted. The kinetics of the reactions and means to predict kinetic rate constants are also presented.

◼ Key terms and concepts

- Henry's law constant, H
- Octanol-water partition coefficient, K_{ow}
- Solid-water partition coefficient, K_d
- Organic-carbon water partition coefficient, K_{oc}
- Hammett relationship
- Substitution/elimination reactions
- Hydrolysis
- Reduction and oxidation reactions
- Photolysis
- Linear free energy relationships (LFERs) and quantitative structure-activity relationships

19.1 Introduction

Organic chemicals are used in numerous industrial, commercial, and household applications. Examples include solvents, detergents, pesticides (including herbicides and insecticides), flame retardants, dyes, and pharmaceuticals. The number of inorganic chemicals aquatic chemists must deal with may appear to be very large, but it pales in magnitude compared to the virtually infinite number of organic compounds. New compounds are continuously being synthesized and brought to market. Thus, there is a steady stream of potentially new environmental pollutants. The environmental chemistry of organic compounds is a very rich subject that cannot be completely covered in a single book chapter. This chapter covers only the fundamentals of environmental organic chemistry, but it provides enough information for readers to become familiar with the major concepts controlling the fate of organic contaminants in aquatic systems, as summarized in Figure 19.1. For more details about the topics covered in this chapter, the reader is referred to Schwarzenbach et al.[1] The text by Larson and Weber[2] is also an excellent resource focused on reaction mechanisms.

Before beginning this chapter, readers should review the structures of organic molecules (Chapter 6), the concept of vapor pressure (Chapters 3 and 4), and solubility (Chapter 10). Although there are methods to predict the vapor pressure and aqueous solubility of organic compounds, readers are referred to other texts to learn about these methods.[1,3] For many organic compounds that are commonly studied and/or detected, compilations of vapor pressure, aqueous solubility, and other partitioning coefficients are available.[1,4,5]

Much of this chapter is devoted to *neutral* organic compounds (i.e., nonionic compounds). Some of the compounds considered are ionizable (e.g., phenols and amines), and the acid-base speciation of these compounds and the effects on partitioning and reactivity need to be carefully considered. The chapter is divided into three main parts: (1) a summary of major classes of contaminants by type (or use) and/or structure, (2) partitioning of organic contaminants among environmental phases, and (3) reactions that lead to transformation of organic contaminants. Although biological reactions are also important, they are beyond the scope of this text. Some (but certainly not all) of the mechanisms of biologically mediated transformations, however, are analogous to the reaction mechanisms discussed herein. Means to predict partition coefficients and reaction rate constants also are presented.

Some of the prediction methods can be performed using commercially available and publicly available software. In this chapter, EPI Suite[6] and SPARC,[7] both of which available from the U.S. EPA, are used. The program EPI (Estimation Programs Interface) Suite estimates many parameters, including the Henry's law constant, octanol-water partition coefficient, organic carbon-water partition coefficient, bioconcentration factors (BCFs), and hydrolysis rate constants, as well as solubility and vapor pressure (although the last two features are not discussed in this chapter). EPI Suite also contains a database of experimentally measured values for some parameters. We use SPARC to estimate the pK_a of organic acids, but it also has other capabilities. The input to these programs is a CAS (Chemical Abstract Service) registry number or SMILES structure (Simplified Molecular Input Line Entry System; often such notation can be found online or generated using structure drawing programs) of the chemical. EPI Suite can also take the chemical name as input.
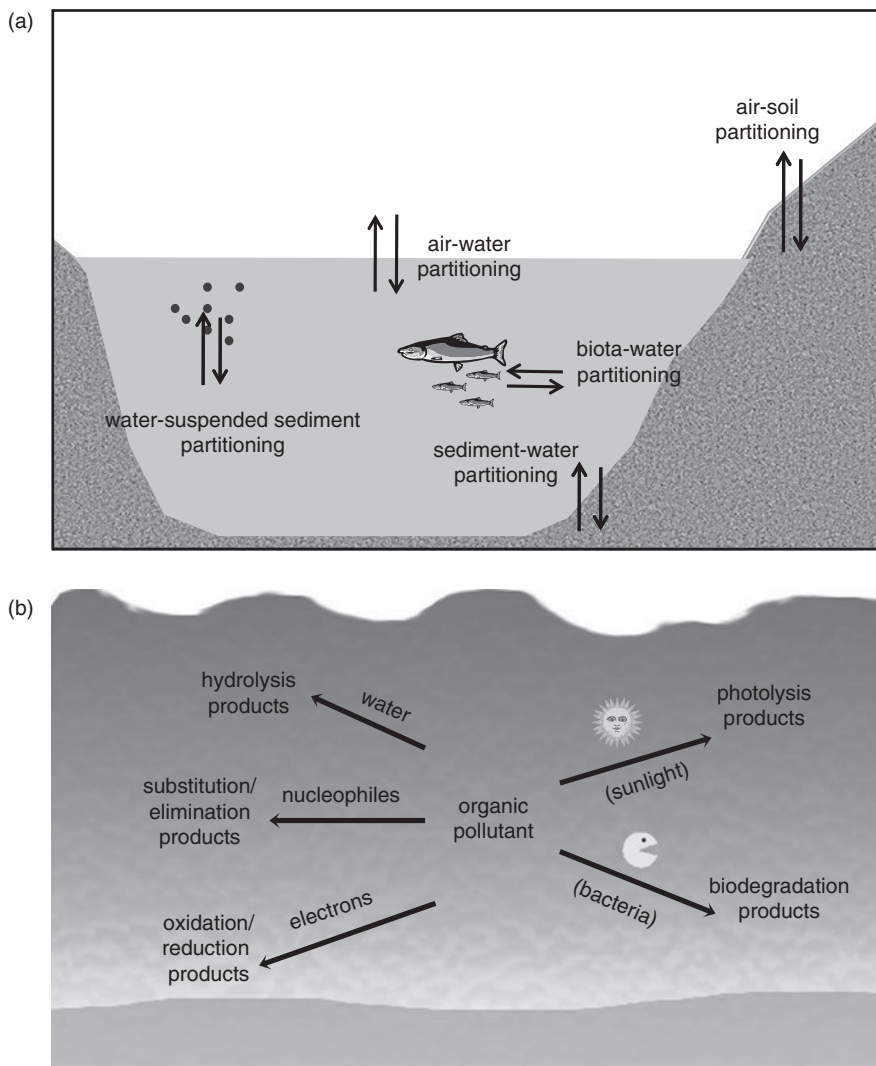
Figure 19.1 Schematics showing the partitioning of organic compounds among environmental matrices (a) and the potential reactions leading to transformation of organic contaminants in aquatic systems (b). (See color insert at end of book for a color version of this figure.)

19.2 Classes of organic contaminants

This section is intended to give readers a feel for the range of chemical structures present in organic contaminants and the ways in which they reach the environment. The list of classes described below is by no means exhaustive, and certainly several important contaminants (e.g., the fuel oxygenate methyl-t-butyl ether) are not included.

19.2.1 Halogenated solvents and related species

This class of compounds includes chlorinated methanes, ethanes, and ethylenes, many of which are or were used as solvents. Improper disposal of these compounds has led to the contamination of ground water at many locations. For example, trichloroethylene (TCE), a common degreasing agent, and tetrachloroethylene (also known as perchloroethylene, PCE or PERC), a dry-cleaning solvent, are commonly detected at Superfund and other contaminated sites. Carbon tetrachloride (CCl_4) is also a common ground-water contaminant.

trichloroethylene   tetrachloroethylene   carbon tetrachloride
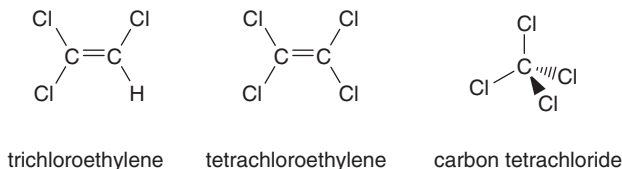
Similar compounds are also of concern in other systems. Fumigants used to control pests in crop fields are halogenated compounds and include methyl bromide (bromomethane) and chloropicrin (trichloronitromethane). Many halogenated disinfection by-products (DBPs) in drinking water and wastewater are also small, halogenated molecules with structure X_3C-R, where X is chlorine, bromine or iodine, and $-R$ can be $-H$ (halomethanes), $-COOH$ (haloacetic acids), $-CN$ (haloacetonitriles), $-NO_2$ (halonitromethanes), $-CHO$ (haloaldehydes), or $-COCH_3$ (haloketones).[8]

19.2.2 Benzenes, phenols, and aromatic amines

Compounds with benzene as the core structure (e.g., benzene, toluene, ethylbenzene and xylenes, together known as BTEX) are major components of gasoline. Pentachlorophenol is a common wood preservative (e.g., for telephone poles). Aromatic amines (or anilines) are common chemical intermediates, dyes, and the degradation products of nitroaromatic compounds.

meta-xylene   pentachlorophenol   aniline
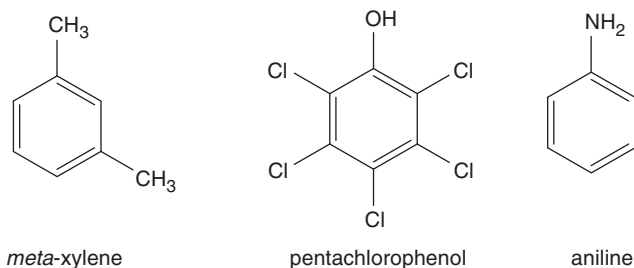
19.2.3 Herbicides, insecticides, and explosives

These three classes of pollutants are commonly introduced into the environment both purposefully (e.g., to control a pest problem) and accidentally (e.g., spills) and contain a huge range of structures. Nitroaromatic compounds are common as herbicides

(e.g., trifluralin, dinoseb), in explosives (trinitrotoluene, TNT), and are present in some insecticides (parathion):
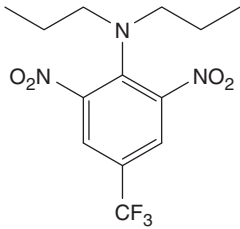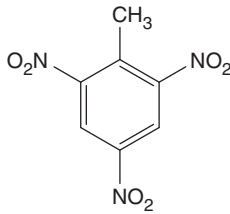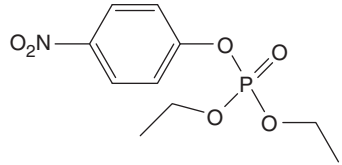
| trifluralin | TNT | parathion |

Atrazine (triazine class) and alachlor (chloroacetanilide class) are examples of other common herbicides. Two common herbicides are glyphosate (commonly known as Roundup®) and 2,4-dichlorophenoxyacetic acid (2,4-D), both used by suburbanites at war with dandelions. Both glyphosate and 2,4-D have acidic functional groups that are deprotonated at ambient pH, leading to a charged molecule in aquatic systems.
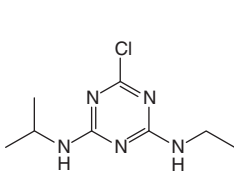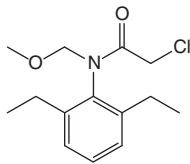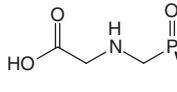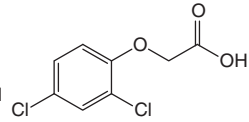
| atrazine | acetochlor | glyphosate | 2,4-dichlorophenoxyacetic acid |

Insecticides encompass a large range of structures. Two examples are malathion (an organophosphate, a class to which parathion also belongs) and oxamyl (a carbamate).
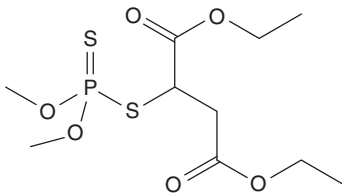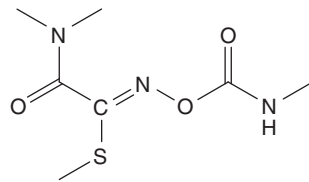
| malathion | oxamyl |

19.2.4 Polycyclic aromatic hydrocarbons

As stated in Chapter 6, these common environmental pollutants arise largely from incomplete combustion of fossil fuels and wood. They are also components of tar and coal. Recent work has demonstrated that a major source of PAHs to the environment is

asphalt sealants.[9,10] Three example structures of PAHs are shown below.
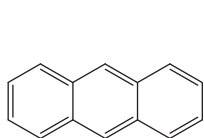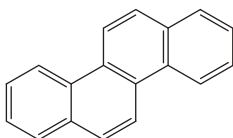
anthracene   chrysene   benzo[a]pyrene
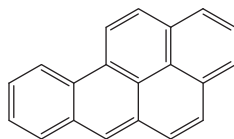
19.2.5 Persistent organic pollutants

Persistent organic pollutants (POPs) are compounds that bioaccumulate, pose a risk to human health, and do not breakdown in the environment (or do so exceedingly slowly). The Stockholm Convention on Persistent Organic Pollutants is an international treaty that defined POPs, and signatories agree to eliminate the production of POPs, minimize unintentional sources, and clean up and safely manage remaining stockpiles and wastes. (Although the U.S. has signed the treaty, it has not been ratified by Congress.) The 12 compounds (or compounds classes, known as the "dirty dozen") specifically designated as POPs by the treaty are the pesticides aldrin, chlordane, DDT, dieldrin, endrin, heptachlor, mirex, and toxaphene. Also listed are hexachlorobenzene, PCBs, and polychlorinated dibenzodioxins/furans (PCDD/Fs). All of these are chlorinated compounds.

Polychlorinated biphenyls (PCBs) are a suite of 209 congeners. These compounds were widely used as dielectric fluids and coolants due to their chemical, biochemical, and thermal stability. These properties also make them very persistent in the environment and commonly found as sediment contaminants. Polychlorinated dioxins are some of the most toxic compounds known. They are also highly regulated. They are formed during incineration processes, chloralkali processes, and other chemical processing industries. The positions of the chlorines have dramatic effect on the toxicity of the congener.[11]

New pollutants that display similar behavior to POPs also have been found. For example, polybrominated diphenyl ethers (PBDEs) are flame retardants found in polyurethane foams in furniture and in electronic devices. In the late 1990s, the widespread prevalence of these compounds in the environment, in biota, and in humans became apparent,[12] and their use is being phased out. They have been dubbed the "new PCBs" because of their apparent environmental persistence. The difference, however, is that while the introduction of PCBs to the environment was largely caused by industrial releases, PBDE releases can be traced largely to their use in consumer products. A general PBDE structure is shown below. PBDE congeners may contain anywhere from 1 to 10 bromine atoms.
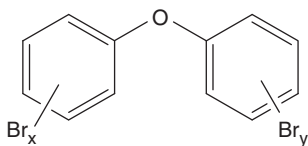
General structure of
polybrominated diphenyl ethers

19.2.6 Perfluorinated chemicals

Perfluorinated chemicals are another group of chemicals largely used for consumer products. The two major compounds found in the environment are perfluorooctanoic acid (PFOA) and perfluorooctane sulfonic acid (PFOS). PFOS was added to the Stockholm Convention in 2009. PFOS was the key ingredient in the stain repellant Scotchgard™ until the product was reformulated in 2000 following concerns about PFOA and PFOS in the environment. These compounds are also used in fire fighting foams and in the production of fluorinated polymers (e.g., Teflon®). They have been found to bioaccumulate and are resistant to degradation in the environment.
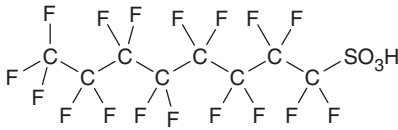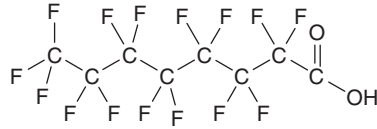
perfluorooctane sulfonic acid (PFOS)   perfluorooctanoic acid (PFOA)

19.2.7 Pharmaceuticals and personal care products

Pharmaceuticals and personal care products (PPCPs) comprise another class of environmental pollutants with wide range of structures/functional groups. These compounds, which include cleaning agents, antibiotics, antibacterials, hormones, prescription medications, nonprescription medications, and fragrances enter the environment with treated wastewater effluent. The study that "put these pollutants on the map" was the 1999–2000 survey conducted by the U.S. Geological Survey in which 82 organic wastewater contaminants were detected in streams and rivers around the United States.[13]

19.3 Air-water partitioning (Henry's law)

When a compound is released into the environment, one possible transfer process is between air and water. Recall from Chapter 6 that

$$H S_w = P, \tag{6.2}$$

so the Henry's law constant H $(= K_H^{-1})$ equals P/S_w and has units of atm·L mol^{-1} or bar·L mol^{-1}. The "dimensionless" form is

$$H' = \frac{C_a}{S_w}, \tag{6.4}$$

with $C_a = P/RT$ for ideal gases (which is generally a reasonable assumption), and T is the temperature at which the Henry's law constant was measured/reported (usually 25°C). Because the vapor pressure (and to a lesser extent, the solubility) are temperature dependent, Henry's law constant is also highly temperature dependent.

The aqueous solubility (S_w) can be replaced with the concentration in water because the equilibrium relationship will hold whether or not the compound is at the solubility limit:

$$H' = \frac{C_a}{C_w}, \tag{19.1}$$

This form of the Henry's law constant is also known as the air-water partitioning coefficient, and is also given the symbol K_{aw}.

19.3.1 Experimental measurements of Henry's law constants

Air-water partitioning coefficients have been measured for many (but by no means all!) organic contaminants. Compilations of measured values are available.[4,5,14,15] Henry's law constants are also important in dynamic system, for they are an important component of predicting the rate at which compounds volatilize from water to air. Such predictions are important in calculating rates of air/water exchange in the environment or in engineered applications such as air stripping.

Measurement of a Henry's law constant is performed in either a static or dynamic system. In a static system with known volumes of air and water, a known amount of compound is introduced, the system is allowed to equilibrate, the concentration is measured in one phase, and the amount in the other is determined by difference. Multiple equilibrations are usually performed. One such method is the equilibrium partitioning in closed systems (EPICS) method.[16] In this case, a series of vials (usually at least five) with varying air-water ratios are prepared and the same mass of contaminant is spiked into each vial. The Henry's law constant is then determined from the relationship[16]

$$H' = \frac{V_{w2} - rV_{w1}}{rV_{a1} - V_{a2}} \tag{19.2}$$

where V_{wi} is the volume of water in vial number i, V_{ai} is the volume of air in vial number i, and r is the ratio of peak areas measured via gas chromatography (which is assumed to be directly proportional to concentration) detected in the air phase of the two vials ($area_1/area_2$). Note that with five vials, there are a total of 10 combinations of two vials that can be used to obtain an average H'.

In any system in which partitioning occurs between two (or more) phases, it is always possible to calculate the fraction of a compound that will be in each phase if one knows the appropriate equilibrium constants and the volume of each phase. Using the air-water system as an example, the total mass, M_T, in the system is

$$M_T = C_a V_a + C_w V_w, \tag{19.3}$$

where C_a and C_w are the concentrations in the air and water and V_a and V_w are the volumes of these two phases. The fraction in the air thus is

$$f_w = \frac{C_a V_a}{C_a V_a + C_w V_w}. \tag{19.4}$$

Dividing numerator and denominator by C_w gives

$$f_a = \frac{\dfrac{C_a}{C_w} V_a}{\dfrac{C_a}{C_w} V_a + \dfrac{C_w}{C_w} V_w} = \frac{H' V_a}{H' V_a + V_w},$$ (19.5)

and similarly,

$$f_w = \frac{V_w}{H' V_a + V_w}.$$ (19.6)

Note that $f_w + f_a = 1$. Clearly, either a large Henry's law constant or a large air volume will lead to more of the compound being in the air phase, and a small Henry's law constant or large water volume will lead to the compound being predominantly in the aqueous phase.

Dynamic methods also are used to measure Henry's law constants, in which water containing the compound of interest is stripped of the compound using a flow of air. (In some methods, the water may also be flowing.) Such methods depend on the flow rate of the liquid and/or gas, and enough contact time must be allowed between the liquid and gas to ensure that equilibrium between the phases is achieved.

19.3.2 Estimation of Henry's law constants

If one knows the vapor pressure and solubility of a compound, the easiest way to estimate a Henry's law constant is via Eq. 6.2. In the absence of such data, a structure-activity relationship can be used, which only requires knowledge of the chemical structure. One such relationship is the bond contribution method developed by Meylan and Howard.[17] In this method, each compound is viewed as the sum of the bonds that form the compound. Each bond is assumed to have a specific contribution to the air-water partitioning. Some will increase the Henry's law constant (hydrophobic groups) and some will decrease it (hydrophilic groups). By setting the sum of the bond contributions equal to the logarithm of the Henry's law constant, a least squares fit can be performed to give a value for the contribution of each bond to Henry's law constants. The values calculated by this method are estimates, and depending on the compound class, average errors compared to experimental values range from 0.06 (alkanes and alcohols) to 0.485 (haloalkenes) log units.[17]

The U.S. EPA software EPI Suite performs estimates using the HENRYWIN™ model. HENRYWIN provides the value estimated from (1) the bond contribution method of Meylan and Howard,[17] (2) the group contribution method of Hine and Mookerjee,[18] and (3) vapor pressure and solubility data. The experimental value also is reported if it is contained in the EPI Suite database. All of these values are reported in units of atm·m^3/mol (requiring multiplication by 1000 L/m^3 to give the same units described above with Eq. 6.2) and thus represent H (not H') values. All of these values are for 25°C, and corrections must be applied as described in Chapter 3 (and Chapter 10) to obtain values at other temperatures. Effects of salt (which decreases solubility and thus increases the H') are handled as described in Chapter 4.

EXAMPLE 19.1 Measurements and estimations, part 1: Determine the Henry's law constants of the following three compounds using the vapor pressure and solubility data given. Compare the answers to the predicted values (bond method) and experimental values given by EPI Suite.

Compound	CAS no.	Vapor pressure (atm)	Solubility (mol/L)
Toluene	108-88-3	0.037	0.006
Trichloroethene	79-01-6	0.099	0.0083
2,4,6-Trichlorphenol	88-6-2	9.9×10^{-7}	7.1×10^{-4}
Alachlor	15972-60-8	2×10^{-8}	8.9×10^{-4}

Answer: Because EPI Suite gives values in atm·m^3 mol^{-1}, we will use

$$H = P/S_w$$

for the Henry's law constant, with S_w needing to be in mol/m^3 rather than mol/L. For toluene, this gives

$$0.037 \text{atm} \div (0.006 \text{mol/L} \times 1000 \text{L/m}^3) = 6.17 \times 10^{-3} \text{atm·m}^3/\text{mol}.$$

A comparison of these values with those calculated by EPI Suite and literature values (from the EPI Suite database) are given below.

Compound	P/S_w	EPI Suite estimate	Experimental value
Toluene	6.17×10^{-3}	5.95×10^{-3}	6.64×10^{-3}
Trichloroethene	1.19×10^{-2}	2.3×10^{-2}	9.85×10^{-3}
2,4,6-Trichlorphenol	1.39×10^{-6}	2.28×10^{-7}	2.6×10^{-6}
Alachlor	2.25×10^{-8}	2.23×10^{-8}	na

For all of these compounds, the three values are generally within a factor of 2, with the EPI Suite estimate for 2,4,6-trichlorophenol being the exception. Here we consider 2,4,6-trichlorophenol only in the neutral form.

19.4 Octanol-water, organic carbon-water, sediment-water, and biota-water partitioning

The octanol-water partition coefficient is

$$K_{ow} = \frac{C_o}{C_w}. \tag{6.5}$$

K_{ow} was originally used to evaluate pharmaceutical transport through the intestinal wall and distribution within the body, and it has been found to be useful in predicting the partitioning of chemicals into sediments (sorption) and into biota (bioconcentration). As described in Chapter 6, means of experimental measurement include shake flasks, column methods, and reverse-phase liquid chromatography.

Estimation methods for K_{ow} break the molecules into fragments (e.g., single atoms or groups of atoms, such as $>C<$ (a carbon with four single bonds to elements other than hydrogen), $-CH_3$, $-NH_2$, $-Cl$), and each fragment is assigned a contribution to K_{ow}.[19] For each fragment, there may be different constants/contributions depending on whether the fragment is bound to an aliphatic, olefinic, or aromatic group. These contributions were determined via regression from a large number of compounds with known K_{ow} values called a training set. There also are correction factors for certain structural features. For a complete list of the fragment constants and factors used by the KOWWIN[TM] model in EPI Suite see Meylan and Howard[19]. The form of the regression equation is as follows:

$$\log K_{ow} = \Sigma(f_i n_i) + \Sigma(c_j n_j) + 0.229 \tag{19.7}$$

(number of structures = 2447, r^2 = 0.982, standard deviation = 0.217, mean error = 0.159), where f_i is the fragment constant for fragment i, c_j is the correction factor for structural feature j, and n_i and n_j are the number of times the fragment i appears in the molecule and the number of times correction j is needed.

EXAMPLE 19.2 Measurements and estimations, part 2: Determine the log K_{ow} values of toluene, trichloroethene, 2,4,6-trichlorophenol, and alachlor using EPI Suite and compare them to the experimental values in the EPI Suite database.

Answer: A comparison of these values with those calculated by EPI Suite and literature values (from the EPI Suite database) are compiled in the following table:

Compound	Log K_{ow}: EPI Suite estimate	Log K_{ow}: experimental value
Toluene	2.54	2.73
Trichloroethylene	2.47	2.42
2,4,6-Trichlorophenol	3.45	3.69
Alachlor	3.37	3.52

The largest difference (on a log scale) between the two values is for toluene (0.19 log units). Converting to actual K_{ow} values (347 vs. 537) demonstrates that this is actually a rather large difference, and one must consider such potential errors when using estimated values.

Of course, the environment does not contain octanol as a phase, so if we are to use K_{ow} to predict partitioning to soils or sediments, we need another parameter. The one used

most commonly is the organic carbon-water partitioning coefficient:

$$K_{oc} = \frac{C_{oc}}{C_w} \qquad (19.8)$$

C_{oc} is the concentration of the compound of interest associated with the organic carbon fraction of the soil or sediment (in units of mol/kg of organic carbon). Thus, K_{oc} has units of liters per kilogram. Octanol serves as a "surrogate" for C_{oc} and it is assumed that a behavior of a compound in octanol is similar to its interaction with soil/sediment organic matter. The fraction of organic carbon (f_{oc} = mass of organic carbon/total mass of solid on a dry weight basis) is measured by oxidizing a sample of the solid and measuring the CO_2 evolved. The K_{oc} is not measured directly. Instead, partitioning to the whole solid is measured:

$$K_d = \frac{C_s}{C_w}, \qquad (19.9)$$

where C_s is the concentration of the contaminant per mass of solid phase (mol/kg), giving the solid-water partition coefficient, K_d, units of L/kg. The relationship between K_d and K_{oc} is

$$K_d = f_{oc}K_{oc}. \qquad (19.10)$$

K_d is often determined by putting a known volume of water, a known mass of sterile sediment, and known mass of contaminant into a vial, sealing it, and allowing it to equilibrate. The concentration in the water is measured, and the concentration sorbed to the sediment (C_s) is determined by difference or extracted and measured. This is usually performed for a range of contaminant concentrations or at various solid:water ratios to generate an isotherm (a plot of C_s vs. C_w; see Chapter 14). The slope of the line is the value of K_d. (Although it is possible to get a K_d value from a single measurement by dividing C_s by C_w, this is not how it is done in practice.) The K_d value is divided by f_{oc} to give K_{oc}. In the discussion here, we assume that the isotherm is linear (or that the contaminant concentrations are low enough to be in the linear range of the Langmuir isotherm). Clearly if experiments show this to be a poor assumption, a more appropriate model should be used (see Chapter 14).

Values of K_d are site specific; that is, the value of K_d measured depends on the source of the soil/sediment and how much organic carbon it contains. Normalizing by the fraction of organic carbon to give K_{oc} puts different soils/sediments from different sites on a common basis, and K_{oc} values for different soils and sediments are close to one another (usually within an order of magnitude).

Because K_{ow} values are readily available, there are many reported correlations between K_{oc} and K_{ow} for the reasons stated earlier. These may be divided up by compound class; the following are some examples:[1]

Alkylated and chlorinated benzenes and PCBs

$$\log K_{oc} = 0.74 \log K_{ow} + 0.15 \ (n = 32; \ r^2 = 0.96) \qquad (19.11a)$$

PAHs

$$\log K_{oc} = 0.98 \log K_{ow} - 0.32 \ (n = 14; r^2 = 0.98) \qquad (19.11b)$$

Chlorinated phenols (neutral form)

$$\log K_{oc} = 0.89 \log K_{ow} - 0.15 \ (n = 10; r^2 = 0.97) \qquad (19.11c)$$

Relationships for other compound classes are also available, but they include a small number of compounds, have a low r^2 value, or both.[1] EPI Suite also uses two methods to estimate K_{oc} in the KOCWIN^{TM} module. One is a relationship with K_{ow}^{20} and the other uses a molecular connectivity index.[21] In both cases, separate correlations are used for nonpolar and polar compounds. Various correction factors are applied to the polar compounds.

EXAMPLE 19.3 Measurements and estimations, part 3: Compare the K_{oc} values generated for anthracene from Eq. 19.11a above to those given by EPI Suite.

Answer: Starting with $\log K_{ow} = 4.45$ for anthracene, we get

$$\log K_{oc} = 0.98(4.45) - 0.32 = 4.04 \ \text{ or } \ K_{oc} = 10,990$$

EPI Suite gives two answers. The molecular connectivity index method gives $\log K_{oc} = 4.214$ ($K_{oc} = 16,360$) and the K_{ow} method gives $\log K_{oc} = 3.862$ ($K_{oc} = 7,274$). Obviously these answers range over a factor of 2, and your final answer in partitioning problems (e.g., fraction of a given compound present in soil/sediment vs. water) will depend on which you choose.

Such predictions assume that the partitioning into organic material in soils and sediments dominates the fate of organic compounds. Although this is true for many neutral organic compounds under many conditions, there are other processes that are also important in sediment water partitioning. Organic compounds may sorb to mineral surfaces via hydrophobic interactions, formation of electron donor-acceptor complexes, via electrostatic interactions, or a bonding with the surface. Even for neutral organic compounds these processes can be important. For example, in a low-organic carbon soil, being sorbed on a mineral surface may provide a more "hydrophobic" environment for a highly hydrophobic compound than being surrounded by water molecules. In matrices dominated by clays, K_d is dominated by electron donor-acceptor interactions for nitroaromatic compounds,[22] and the K_d of tetracycline antibiotics, which are charged in aqueous solution, is dominated by electrostatic interactions with clays and minerals, even when organic carbon is present.[23] The reader is referred to other texts for further information on these sorption processes.[1]

Partitioning into biota (bioconcentration) also can be related to K_{ow}. The uptake of contaminants by algae in particular is important in that this leads to increased exposure to the contaminants higher in the food chain, e.g., fish. Like the relationships developed for K_{oc}, correlations between K_{ow} and bioconcentration assume that the contaminant's

behavior in the octanol phase and the organism (typically the lipid phase) are similar. Again, EPI Suite can estimate the bioconcentration factor (BCF):

$$BCF = \frac{C_{organism}}{C_w} \qquad (19.12)$$

using a relationship of the form $\log BCF = a \log K_{ow} + b +$ corrections. The concentration in the organism ($C_{organism}$) is given in mol/kg-wet weight for the values computed by EPI Suite. Note that in the literature the reported BCF often is normalized to the lipid fraction, which increases the factor a by approximately twofold. For organisms higher in the food chain, the concentration in the organism often exceeds that expected if it were in equilibrium with its environment. This is because the rate at which the organism ingests the contaminant contained in its food is faster than it can process/excrete it. This process is known as *biomagnification*.

EXAMPLE 19.4 A sealed world: You have used a rapid drying, tightly binding adhesive to fix the terrarium home of your pet frog, Aqua. In doing so, you accidently completely seal the top, and for some reason, you bought a terrarium with a solid lid. The adhesive you used contains a large amount of toluene, and you are curious as to the amount that poor Aqua will absorb at equilibrium. You estimate that you put 1 g of toluene in the terrarium, that it contains 5 L of air, 1 L of water, 1 kg of sediment (dry weight, with a fraction of organic carbon of 0.03), and the 100-g Aqua. Using the parameters generated by EPI Suite, determine the mass of toluene in Aqua at equilibrium.

Answer: To solve this problem, the values of H', K_{oc}, and BCF are needed. For toluene, EPI Suite gives

$$H = 5.95 \times 10^{-3} atm \cdot m^3 mol^{-1} = 5.95 \ atm \cdot L/mol.$$

Using R = 0.0821 L·atm mol^{-1} K^{-1} and T = 298.15,

$$H' = H/RT = 0.24,$$
$$K_{oc} = 234 \ L/kg,$$
$$BCF = 29.39 L/kg \text{ (wet weight)}.$$

Using the f_{oc} of 0.03, we can calculate $K_d = 0.03 \times 234 = 7.02$ L/kg. Now we need to expand Eq. 19.3 to include more phases:

$$M_T = C_a V_a + C_w V_w + C_s M_s + C_{frog} M_{frog}$$

C_s and M_s are the concentration in the sediment and mass of the sediment, and C_{frog} and M_{frog} are the concentration in the frog and mass of the frog. These two concentrations are on a mass/kg basis. We want the fraction in Aqua, which would be

$$f_{frog} = \frac{C_{frog} M_{frog}}{C_a V_a + C_w V_w + C_s M_s + C_{frog} M_{frog}}.$$

Dividing through by C_w gives

$$f_{frog} = \cfrac{\dfrac{C_{frog}}{C_w} M_{frog}}{\dfrac{C_a}{C_w} V_a + \dfrac{C_w}{C_w} V_w + \dfrac{C_s}{C_w} M_s + \dfrac{C_{frog}}{C_w} M_{frog}} = \cfrac{(BCF) M_{frog}}{H'V_a + V_w + K_d M_s + (BCF) M_{frog}}.$$

Substituting the above values gives

$$f_{frog} = \frac{29.39 \text{ L/kg} \times 0.1 \text{ kg}}{0.24 \times 5 \text{ L} + 1 \text{ L} + 7.02 \text{ L/kg} \times 1 \text{ kg} + 29.39 \text{ L/kg} \times 0.1 \text{ kg}} = 0.24$$

Thus, 24% of the toluene (or 0.24 g) will be in Aqua at equilibrium, which is a concentration of 0.0024 g toluene/g frog. You had better hope that this level is not toxic to poor Aqua (or that you have a hammer handy to smash open the terrarium to save him ... unless performing this calculation took too long).

19.5 The Hammett relationship and the effect of pH on partitioning

Several aromatic organic chemical structures have acidic/basic functional groups, including benzoic acids, phenols, anilines, and pyridines. As seen for the following substituted benzoic acids, the ring substituents influence the pK_a values (also see Table 18.4).

$pK_a = 4.19$ 4.35   3.97   3.48
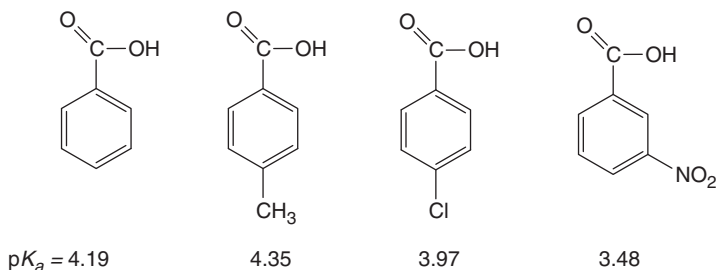
Electron donating groups (alkyl and amine groups) increase the pK_a (i.e., decrease the acidity) of benzoic acid and electron withdrawing groups (halogens, haloalkyl groups, ethers, aldehydes, ketones, and nitro-, cyano-, and sulfur-containing groups) lower the pK_a . A simplified explanation is that the electron withdrawing substituents stabilize the negative charge whereas the electron donating substituents have the opposite effect. It turns out that effect on the pK_a of different substituents on the benzoic acid ring can be expressed with the following equation, known as the Hammett relationship:

$$pK_a = pK_{aH} - \sum_j \sigma_j, \tag{19.13}$$

where σ_j is known as the Hammett constant for substituent j and pK_{aH} is, in this case, the value for benzoic acid with only hydrogen substituents on the aromatic ring.

A more general form of the equation applicable to aromatic structures beyond benzoic acid is

$$pK_a = pK_{aH} - \rho \sum_j \sigma_j, \tag{19.14}$$

where ρ is the susceptibility factor that quantifies how a substituent influences the pK_a of the structure of interest (e.g., phenol) relative to benzoic acid. Again, pK_{aH} is the value for the appropriate structure with only hydrogen substituents. For benzoic acid, ρ is defined as 1. By plotting $\log K_a$ versus the σ values (determined for benzoic acid) for other structures, the value of ρ is determined. Table 19.1 gives Hammett constants for suite of substituents and susceptibility factors for a few common organic acid structures. Note that only values for *meta* and *para* substituents are given, but apparent *ortho* substituent constants are also available for some specific structures (phenols, anilines; see Schwarzenbach et al.[1] and references therein). In general, *ortho*-substituent constant values are not given due to complicating steric hindrance effects.

The Web-based application SPARC (SPARC Performs Automated Reasoning in Chemistry), developed by the U.S. EPA,[7] uses a more complicated approach and can calculate pK_a values for a wide range of organic structures.

EXAMPLE 19.5 Estimation of pK_a values: Compare the pK_a values obtained from the Hammett relationship and SPARC for the following compounds:

4-Chlorobenzoic acid, CAS no. 74-11-3
4-Methylaniline, CAS no. 106-49-0
4-Methoxypyridine, CAS no. 620-08-6

Answer: For each compound, the appropriate equation is

$$pK_a = pK_{aH} - \rho \sum_j \sigma_j.$$

Using the data in Table 19.1, for benzoic acid and Cl in the *para* position the pK_a for 4-chlorobenzoic acid is

$$pK_a = 4.19 - 1(0.22) = 3.97.$$

Similarly, the values for 4-chloroaniline and 4-chloropyridine are

$$pK_a = 4.63 - 2.90(-0.16) = 5.09,$$
$$pK_a = 5.25 - 5.90(-0.24) = 6.67.$$

The values generated by SPARC, 3.75, 5.11, and 6.02 for 4-chlorobenzoic acid, 4-methylaniline, and 4-methoxypyridine, respectively, are close for the first two compounds but not very similar to the third.

Table 19.1 Selected Hammett substituent constants and susceptibility factors*

Substituent j	$\sigma_{j,\text{meta}}$	$\sigma_{j,\text{para}}$	Acid structure	pK_{aH}	ρ
–H	0.00	0.00	benzoic acid	4.19	1.00
–CH₃	−0.06	−0.16			
–CH₂CH₃	−0.06	−0.15			
–C(CH₃)₃	−0.10	−0.20		4.55	0.21
–CH=CH₂	0.08	−0.08			
–C₆H₅	0.06	0.01			
–CH₂Cl	0.12	0.18		3.17	0.30
–CCl₃	0.40	0.46			
–CF₃	0.44	0.57			
–F	0.34	0.05		4.30	0.49
–Cl	0.37	0.22			
–Br	0.40	0.23			
–I	0.35	0.18		9.90	2.25
–OH	0.10	−0.36	phenol –OH		
–OCH₃	0.11	−0.24(−0.12)†			
–OC(=O)CH₃	0.36	0.31		4.63	2.90
–C(=O)H	0.36	0.22(1.03)	aniline –NH₃⁺		
–C(=O)CH₃	0.38	0.50(0.82)			
–C(=O)OCH₃	0.33	0.45(0.66)		5.25	5.90
–CN	0.62	0.67(0.89)	pyridine –NH⁺		
–NH₂	−0.04	−0.66			
–NO₂	0.73	0.78(1.25)			
–SH	0.25	0.15			
–SO₂CH₃	0.68	0.72			
–SO₃⁻	0.05	0.09			

*Adapted from Schwarzenbach et al.[1] and references cited therein.

† Values in parentheses are used if the substituent has a direct resonance interaction with the acid functional group of a phenol, aniline, or pyridine.

Acid-base speciation plays an important role in partitioning. The *neutral* form of a compound generally dominates the partitioning between air and water, octanol and water, or organic carbon and water. (Ionic compounds may partition to sediments and contribute to an overall K_d, but it is reasonable to assume that the contribution to organic carbon-water partitioning is minimal in most cases.) Thus, the partition coefficient must be corrected for the fraction of a compound in the neutral form.

Consider, for example, the K_{ow} of a phenol, which we will denote as ArOH. The distribution coefficient is

$$D_{ow} = \frac{C_{o,ArOH}}{C_{w,ArOH} + C_{w,ArO^-}}, \qquad (19.15)$$

where D is used to denote that this is not a K_{ow} of the neutral molecule, but rather a distribution coefficient that takes into account the speciation as a function of pH. If we assume that only the neutral form enters the octanol (thus only ArOH appears in the numerator) but both the neutral and ionic forms exist in the water, we can divide the numerator and denominator by $C_{w,ArOH}$ and get

$$D_{ow} = \frac{C_{o,ArOH}/C_{w,ArOH}}{(C_{w,ArOH} + C_{w,ArO^-})/C_{w,ArOH}} = K_{ow}\frac{C_{w,ArOH}}{C_{w,ArOH} + C_{w,ArO^-}} = \alpha_0 K_{ow} \quad (19.16)$$

Thus, to obtain D_{ow} we merely need to multiply K_{ow} by the fraction of the phenol in the neutral form. At the pK_a, the K_{ow} value of the phenol thus is reduced by 50%, and one log unit above pK_a the value of K_{ow} is reduced by 90%. Note that for anilines and pyridines, the neutral form is the basic form of the molecule, so that in Eq. 19.16 α_0 is replaced by α_1.

19.6 Substitution and elimination reactions

The remainder of the chapter discusses transformation reactions involving organic compounds. The goal is not to present an exhaustive list of all potential reactions of all compounds but rather to describe the "structural cues" one should look for that may indicate a specific reaction is possible. A more exhaustive treatment of possible reactions of organic contaminants in aquatic systems is given by other texts.[1,2]

Let us first consider the example of the rate of hydrolysis (i.e., reaction with water) at pH 7 of three isomers of butyl chloride:

$t_{1/2}$ = ~1 year	$t_{1/2}$ = ~40 days	$t_{1/2}$ = ~30 seconds
n — butyl chloride	*sec*-butyl chloride	*tert*-butyl chloride
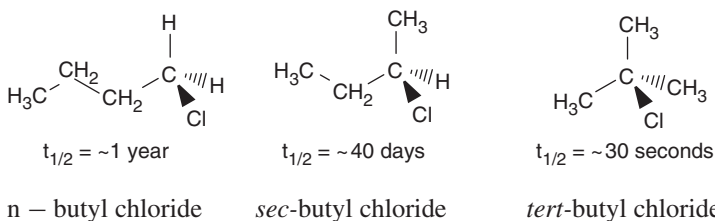
These compounds all have the same formula, but obviously very different stabilities in water. What is different about the isomers? The difference is obviously in the arrangements of the carbons, and this must be responsible for the differences in reactivity.

19.6.1 S_N1 and E_1

These are substitution (S_N1) and elimination (E_1) reactions that involve a compound with a good leaving group (generally a halogen or other chemical group stable in water as an anion) and a nucleophile (a "nucleus loving" reactive species). The structural cues for these two reactions are (1) a good leaving group, as described above, and (2) a tertiary carbon center. A tertiary carbon is a carbon single bonded to three other carbons (the fourth bond is to the leaving group), such as the tertiary-butyl chloride (or t-butyl chloride) above. For these particular substitution (S_N1) and elimination (E_1) reactions, the leaving group leaves spontaneously, yielding a carbocation that is quasi stable in water (but not in organic solvents):
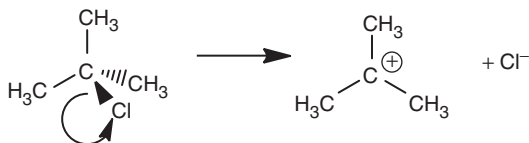
The reason that the tertiary structure is important is that the three surrounding carbons aid in stabilizing the positive charge. Carbocations react with any available nucleophile, and in aqueous systems, water is by far the most abundant nucleophile:
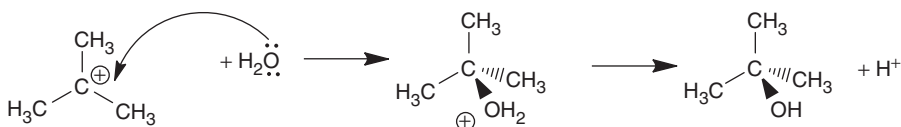
Water is a weak nucleophile. If a stronger nucleophile is present at a high enough concentration (see below for discussion of nucleophile strength), it can outcompete water for the carbocation to form a substituted derivative. In the presence of a strong base OH^- (also a moderately strong nucleophile), an elimination reaction occurs. The distinguishing feature of an elimination reaction is the formation of a carbon-carbon double bond. The strong base abstracts a hydrogen atom, forming the conjugate acid (in this case water) from the carbocation, and the electron in the bond that was holding the hydrogen forms a carbon-carbon double bond.
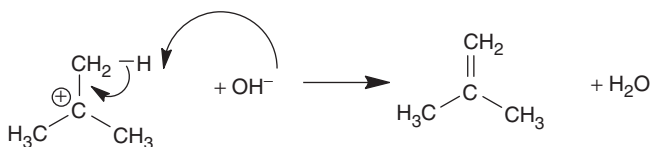
Because the leaving group departs before any further interactions occur, the reaction kinetics of S_N1 and E_1 reactions depends upon the concentration of the substrate and not the nucleophile; i.e., the rate limiting step is the formation of the carbocation:

$$dC/dt = -k[\text{reactant}] \tag{19.17}$$

The reaction is first order, and this is the origin of the "1" in S_N1 and E_1. Changing the pH or nucleophile concentration will not affect the reaction kinetics. To determine whether the reaction leading to the disappearance of the compound is S_N1 or E_1, one must identify the reaction products and the order of the reaction.

19.6.2 S_N2 and E_2

Methyl and primary carbons (e.g., CH_3Cl or n-chlorobutane shown above) with a good leaving group, also undergo substitution reactions, but for these structures, the nucleophile "pushes" out the leaving group. In other words, the reaction is "concerted" with the nucleophile (Nu^- below) forming a new bond and the bond of the leaving group breaking at the same time:
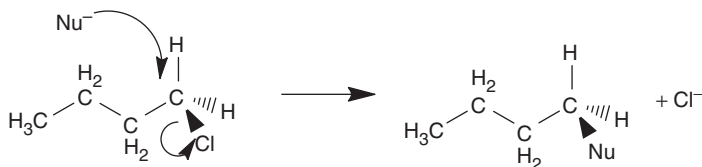
The corresponding elimination (E_2) reaction requires an H-atom on the neighboring carbon. Again, the elimination reaction occurs with strong bases that are able to pull off the proton, leading to concerted formation of a double bond and release of the leaving group:
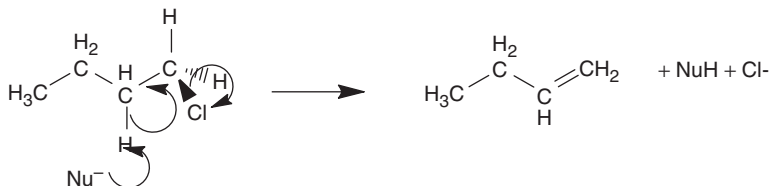
Several important features allow one to distinguish S_N1 from S_N2 and E_1 from E_2. The first is the kinetics. Because the reactions are concerted, the kinetics depends on concentrations of both the substrate and the nucleophile, giving a second-order reaction (and thus the "2" in S_N2 and E_2):

$$dC/dt = -k[\text{reactant}][\text{nucleophile}] \qquad (19.18)$$

Thus, if changing the concentration of the nucleophile alters the rate of reaction, this is strong evidence that the S_N2 or E_2 mechanisms are operating.

Additionally, S_N2 reactions result in inversion of chiral compounds (see Chapter 6) from one enantiomer to the other:

Note that in the reaction above, the "X" and "Nu" substituents cannot be overlain, indicating that the chirality of the two compounds is opposite. Specialized chromatography columns allow separation of enantiomers and can be used to verify such changes.

What about secondary carbons? Depending on the specific substituents and structure of the molecule, the reaction mechanisms of these structures may be close to either an S_N1 or S_N2. Classifying any reaction as a purely S_N1 or S_N2 is a bit misleading, however, for there is spectrum of "S_N1-ness" to "S_N2-ness." Thorough investigation of the reaction kinetics and reaction products is necessary to determine which mechanisms are important and to what extent.

19.6.3 Swain-Scott model for strength of nucelophiles

The reactions discussed above require the presence of a nucleophile. As stated earlier nucleophiles are "nucleus-loving" species and have either a negative charge or a lone-pair of electrons that can be used to form a bond (see Chapter 1). In S_N1 reactions, water is the nucleophile that attacks the carbocation because it is most abundant. While water is abundant, it is not a very strong nucleophile, and so other nucleophiles are also important in these reactions. The Swain-Scott model is a correlation that compares the "strengths" of different nucleophiles (relative to water) and predicts the second-order rate constants for reactions with contaminants.[24] The model has the form

$$\log \frac{k_{\text{Nuc}}}{k_{\text{H}_2\text{O}}} = n \cdot s. \tag{19.19}$$

In this expression, $k_{\text{H}_2\text{O}}$ is the second-order rate constant for the S_N2 reaction of the substrate with water (our reference reaction), k_{Nuc} is the second-order rate constant for reaction with the nucleophile of interest, n is the nucleophilicity (strength) of the nucleophile, and s is the substrate constant, a measure of the sensitivity of the molecule to attack. Values of n (Table 19.2) were originally measured for methyl bromide, and by convention $s = 1$ for methyl bromide. For other substrates and leaving groups, it is generally assumed that s is equal to 1, but this may not always be a good assumption.[25] Note that as n increases, the concentration of the nucleophile needed to be competitive with water decreases. (see example 19.6). This is because rates of S_N2 reactions depend on the rate constant and the concentration of the nucleophile.

EXAMPLE 19.6 S_N2 reactions of methyl bromide in seawater: In seawater at pH 8, which nucleophile will have the highest pseudo-first-order rate constant (relative to water) with CH_3Br? Consider H_2O, OH^-, Cl^-, SO_4^{2-}, and Br^- as nucleophiles.

Answer: Rearranging Eq. 19.19 gives the following:

$$\frac{k_{\text{Nu}}}{k_{\text{H}_2\text{O}}} = 10^{n \cdot s}$$

Table 19.2 Values of *n* from environmentally relevant nucleophiles*

Nucleophile	n
H_2O	0
NO_3^-	1.0
F^-	2.0
SO_4^{2-}	2.5
CH_3COO^-	2.7
Cl^-	3.0
HCO_3^-	3.8
HPO_4^{2-}	3.8
Br^-	3.9
OH^-	4.2
I^-	5.0
CN^-	5.1
HS^-	5.1
S_4^{2-}	7.2

* Adapted from Schwarzenbach et al.[1] and Larson and Weber[2] and references therein.

To obtain a comparison of pseudo-first-order rate constants, we multiply both sides of the equation by [Nu]/[H2O]:

$$\frac{k_{Nuc}[Nu]}{k_{H_2O}[H_2O]} = 10^{n \cdot s} \frac{[Nu]}{[H_2O]}$$

Using $s = 1$ and [H2O] 55.6 M, we can now use the data in Table 9.6B and *n* values in Table 19.2 to compare pseudo-first-order rate constants relative to water.

Nucleophile	[Nu] in mol/L	$10^{n \cdot s} \dfrac{[Nu]}{[H_2O]}$
H_2O	55.6	1
OH^-	10^{-6}	2.85×10^{-4}
Cl^-	0.546	9.82
SO_4^{2-}	0.0282	0.16
Br^-	0.067	9.57

Note that even though their concentrations are much lower, Cl^- and Br^- are each ~10-fold more important that water in the S_N2 reaction of methyl bromide in seawater. Of course, reaction with Br^- just leads to methyl bromide, so this loss process would be impossible to track unless the bromine atom in the CH_3Br was labeled isotopically. It is also important that to note that all these reactions occur simultaneously and that some of the products formed will also be subject to S_N2 reaction by other nucelophiles.

19.7 Ester and acid-derivative hydrolysis

This reaction is relevant to compounds with the general structure:

$$
\begin{array}{c}
X \\
\| \\
Z \\
R' \diagup \quad \diagdown L
\end{array}
$$
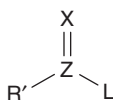
The atom "Z" may be C, P, or S, and the atom X is O, S, or N-R (with R being a carbon-centered group). "L" is the leaving group, and must be something that is stable as an anion in aqueous solution. It is typically of the form $-OR$, $-SR$, or $-NR_1R_2$ (where R_1 or R_2 are carbon centered groups or hydrogen). Obviously, this reaction is important for a range of structures, which we will call "acid derivatives." If $Z = C$, $X = O$, and $L = OH$, the above structure is a carboxylic acid, and changing these substituents makes the structure a derivative of the carboxylic acid. Our description of this reaction will focus on esters ($Z = C$, $X = O$, $L = -OR$), but the same general mechanisms are relevant to thioesters ($Z = C$, $X = O$, $L = -SR$), amides ($Z = C$, $X = O$, $L = -NR_1R_2$), carbonates ($Z = C$, $X = O$, $L = -OR_1$, and $R' = -OR_2$), carbamates ($Z = C$, $X = O$, $L = -OR$, and $R' = -NR_1R_2$), and ureas ($Z = C$, $X = O$, $L = -NR_1R_2$, and $R' = -NR_3R_4$). When $Z = S$, the reactions are generally similar to $Z = C$, but when $Z = P$, there are more possibilities for reaction because P is pentavalent (see Schwarzenbach et al.[1] and references therein).

Ester hydrolysis, which is a type of nucleophilic substitution reaction, occurs via a neutral mechanism as well as acid- and base-catalyzed mechanisms (see below). Thus, the overall pseudo-first-order hydrolysis rate is (modified from eq. 5.55b)

$$ k_h = k_A[H^+] + k_N + k_B[OH^-], \tag{19.20} $$

with $k_N = k_{H_2O}[H_2O]$.

The neutral reaction is the slowest of the three, and so rates are slowest at circumneutral pH and accelerate as pH increases or decreases (see Figure 5.13). Note that some structures are not subject to the acid-catalyzed reaction.

The structure of the molecule influences the magnitude of the second-order rate constants in Eq. 19.20. For example, lower pK_a values for the leaving group L result in faster hydrolysis rates. Because pK_a values can be related to Hammett constants (for aromatic leaving groups) and analogous Taft constants[3] (for aliphatic ones), we can use substituent constants and steric factors (that quantify size/atom crowding effect) to predict rate constants. It turns out that steric and electronic factors on the group R' also influence the rate and can be quantified. Simple plots of log k versus pK_a may be used to predict rate constants; a similar but more complicated relationship is used in EPI Suite via the HYRDOWIN[TM] routine.[26]

From a mechanistic standpoint, the base-catalyzed mechanism is most straightforward. A hydroxide attacks the carbonyl carbon, leading to a tetrahedral intermediate (Figure 19.2a). In the neutral mechanism, water is the nucleophile. The mechanism is similar to the base-catalyzed one, but the diol intermediate has two potential decomposition pathways leading to the final product (Figure 19.2b). In the acid-catalyzed

mechanism (Figure 19.2c), the carbonyl oxygen is protonated, making the carbonyl carbon more susceptible to attack by water.

Although these reactions are important in transforming contaminants, the same reaction mechanism also can lead to contaminant sequestration. For example, it has been shown that anilines (aminobenzenes) attack carbonyl groups in natural organic matter leading to binding of the anilines in the natural organic matter matrix.[27]

19.8 Oxidation and reduction

As with the inorganic species discussed in Chapter 11, oxidation and reduction of organic compounds involves electron transfer and changes in oxidation state. Because many synthetic organic chemicals are designed to be stable in oxic environments, abiotic oxidation reactions of pollutants are not particularly common. An exception is the oxidation of phenols, phenolic acids, and anilines by manganese oxides.[28] Oxidation of most other organic pollutants in the environment is mediated by reactive oxygen species generated by the interaction of light with dissolved substituents (see Chapter 17 and Section 19.9). In engineered systems, oxidation of organic pollutants may occur during ozonation or chlorination (see Chapter 13).

Several common functional groups in organic contaminants are susceptible to reduction, however. There must, of course, be a source of electrons (a reductant) to mediate the transformation. Bacteria may use organic pollutants as electron acceptors. Additionally, bacteria may produce reductants that act outside the cell (extracellularly) such at porphyrins, corrinoids, and enzymes that are able to reduce pollutants. Vitamin B_{12}, which contains a cobalt center, is a common example. Abiotic reductants include sulfide, quinone moieties in organic matter, minerals (ferrous iron bearing oxides, metal sulfides), and reduced metal ions, such as ferrous iron, Fe^{II}. Ferrous iron is a much more potent reductant when it is associated with/sorbed to a mineral surface or oxygen bearing ligands, e.g., carboxylate groups, because these forms of Fe^{II} have much lower reduction potentials than the simple hydrated form. In recent years, the reactions of organic contaminants with zero-valent metals (particularly Fe^0) also have received considerable study because many of the reactions occur relatively quickly and thus can be used in groundwater remediation applications.[29]

The two most common reduction reactions are dehalogenations and reduction of aromatic nitro groups. The mechanisms and kinetics of these reactions are the primary focus of this section, but we also briefly describe a few other reactions.

19.8.1 Dehalogenations

Carbon-halogen bonds are susceptible to reduction, resulting in release of the halogen atom as an ion. Note that while S_N1, S_N2, E_1, and E_2 reactions also involve removal of halogens, these *are not reduction reactions* because there is no transfer of electrons and thus no change in oxidation state of the molecule. Chlorinated compounds are the most common halogenated pollutants, but the same reactions also occur for brominated and iodinated compounds. In fact, the reactions of brominated and iodinated compounds occur more rapidly than those of chlorinated ones, and bromine is preferentially removed over chlorine.[2,30]

(a)
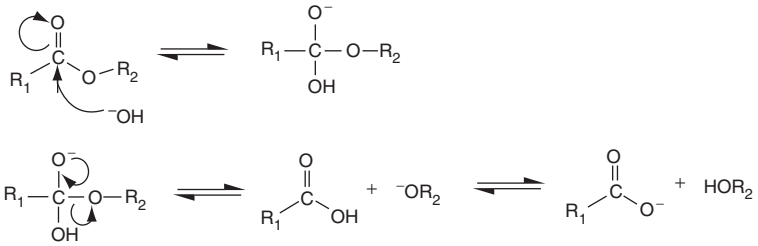
(b)
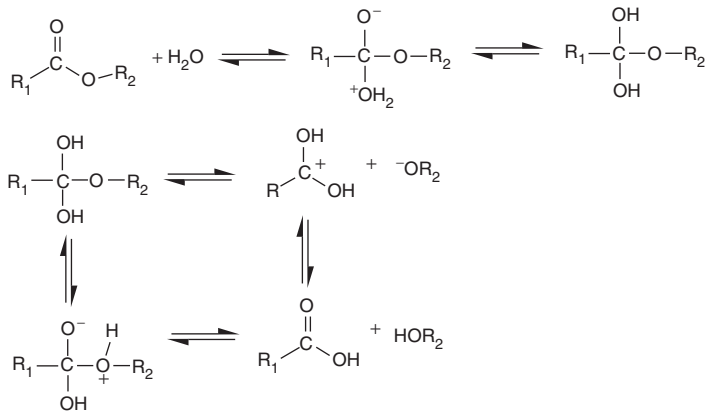
(c)
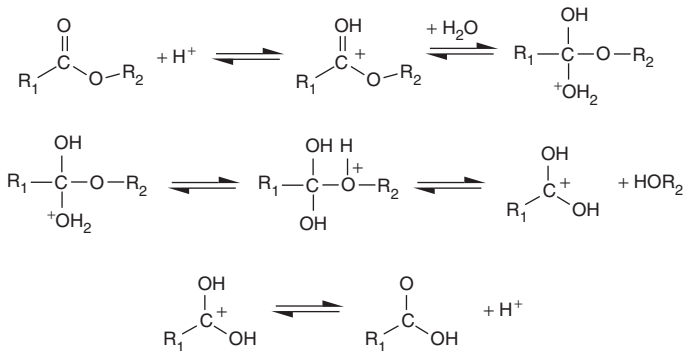
Figure 19.2 Mechanisms for the hydrolysis of esters (or acid derivatives): (a) the base-catalyzed mechanism, (b) the neutral mechanism, and (c) the acid-catalyzed mechanism.

The first reductive dehalogenation reaction is *hydrogenolysis*. This is simply the replacement of a halogen by hydrogen, as shown in the following half-reaction:

$$CCl_3\text{–}CCl_3 + 2e^- + H^+ \longrightarrow CCl_3\text{–}CCl_2H + Cl^-$$
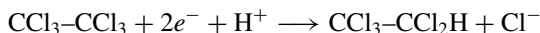
Note that Cl has an oxidation state of –I, and hydrogen of +I; the oxidation state of right-hand carbon thus goes from +III to +I. The reaction needs to be coupled to another half-reaction in which a reductant serves as the electron source.

For compounds containing an α, β pair of halogen atoms (i.e., halogens on adjacent carbon atoms), ***reductive β-elimination*** (or vicinal dehalogenation; "vicinal" means the functional groups are on adjacent carbon atoms) is possible and tends to occur preferentially over hydrogenolysis:
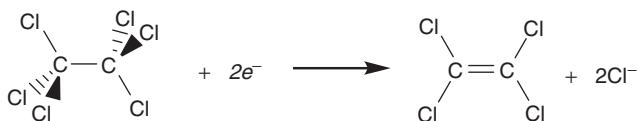
Also possible is *reductive α-elimination*, when two halogens are present on the same carbon:
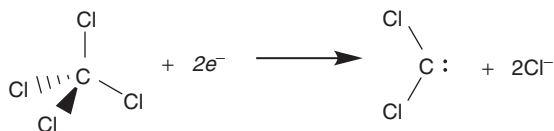
The carbene (:CX$_2$) product formed is highly reactive. The dichlorocarbene shown here undergoes hydrolysis to form formate (or the dehydrated form, carbon monoxide). In general, if an α, β-pair of halogens is present, reductive β-elimination will occur, even if reductive α-elimination is possible (e.g., 1,1,1,2-tetrachloroethane undergoes β-elimination over α-elimination).

The reactions shown above occur for halogenated methanes, ethanes, and ethylenes, all of which are common groundwater pollutants. The ethylenes form acetylenes upon reductive β-elimination. The hydrogenolysis and reductive β-elimination pathways found for chlorinated ethanes and ethylenes with zinc metal are shown in Figure 19.3. Obviously, the ratio of reductive elimination to hydrogenolysis influences the distribution of daughter products. Note that an additional reduction reaction is shown in Figure 19.3, namely, *hydrogenation*. In this reaction, two electrons and two protons are added to a multiple carbon-carbon bond, reducing the bond order by one (in this case, carbon-carbon triple bonds are converted to carbon-carbon double bonds).

Reductive dehalogenation reactions also occur for other halogenated aliphatic molecules, such as lindane (γ-hexachlorocyclohexane) and DDT (which has a –CCl$_3$) group. Hydrogenolysis reactions also occur for various other halogenated compounds, such as DBPs (haloacetic acids, haloacetonitriles, halonitromethanes).[30,32] Dehalogenation of aromatic compounds is also possible, but requires either extreme conditions for abiotic reactions or bacteria. All reductive dehalogenation reactions are irreversible (thus the unidirectional arrows in the reactions shown above).
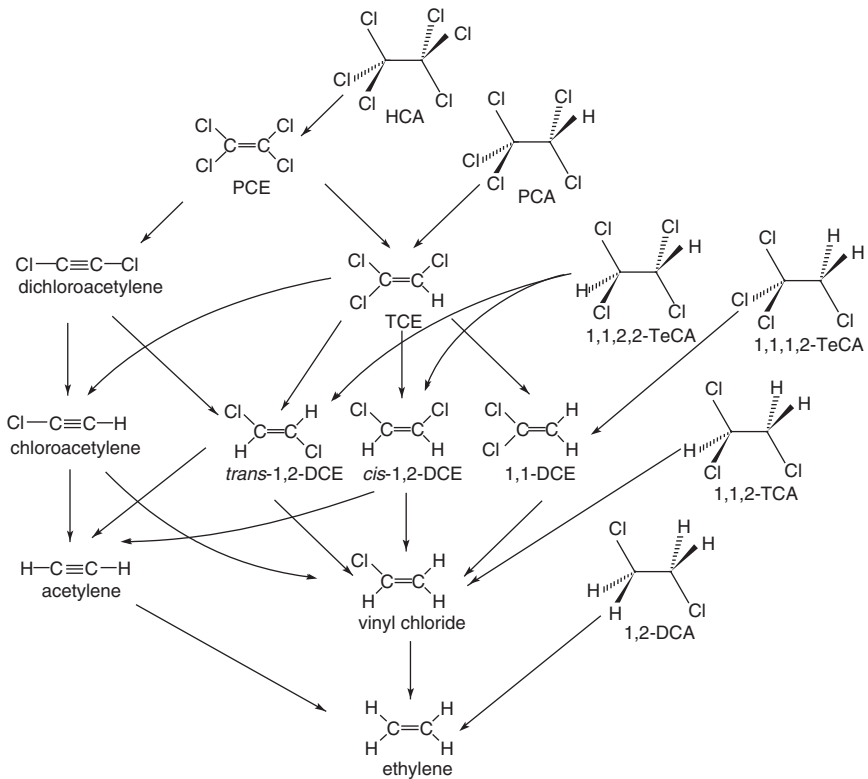
Figure 19.3 Observed hydrogenolysis and reductive β-elimination pathways for the reactions of chlorinated ethanes and chlorinated ethylenes with zinc metal. Hydrogenolysis and hydrogenation of the chlorinated acetylenes are also shown. Reproduced with permission from Arnold et al.[31] © 1999 Elsevier B.V.

19.8.2 Nitro reduction

Nitroaromatic compounds are reduced to anilines via the following sequence:
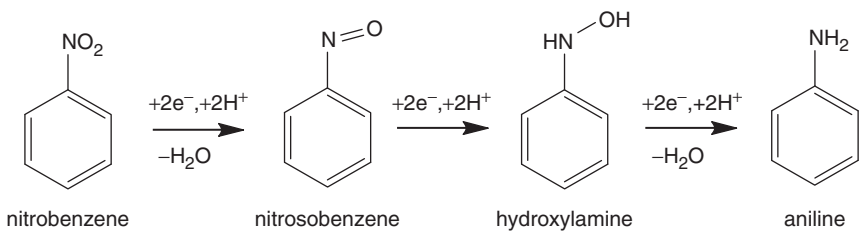
This is a simplification of the reaction mechanism, which actually consists of a series of one-electron transfers, protonations/deprotonations, and dehydrations.[33] Note that for polynitroaromatic compounds, such as TNT, each sequential reduction of a nitro group occurs more slowly than the previous one because amino groups are electron

donating and thus slow the reaction (see Section 19.8.4). Although aliphatic nitro groups are generally not readily susceptible to reduction, some other nitro groups (e.g., those in the nitramine explosives RDX (hexahydro-1,3,5-trinitro-1,3,5-triazine) and HMX (octahydro-1,3,5,7-tetranitro-1,3,5,7-tetrazocine)) are readily reduced.[34] It also should be noted that other reduction reactions of substituted nitroaromatic compounds may occur. For example, the reduction of trifluralin proceeds via multiple pathways, including nitro-reduction, dealkylation, and cyclization.[35]

19.8.3 Other reductions

A few other common compound classes undergo reduction reactions.[2] Aromatic azo compounds are common in dyes:
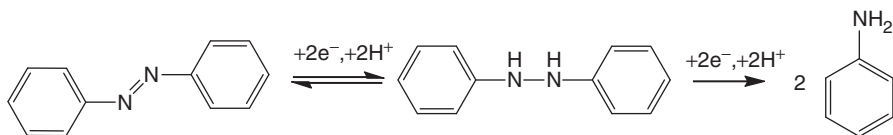
Sulfoxide groups, which are common in agrochemicals, can be reduced to thioethers, and the reaction is reversible:
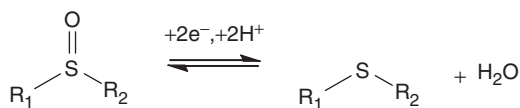
Quinones are reduced to hydroquinones via a semiquinone radical, and again, the reactions are reversible (see Eq. 18.1a). Although quinone functional groups are uncommon in contaminants, this reaction is important in the reduction of pollutants in the presence of natural organic matter. The quinone groups in organic matter may serve as an "electron shuttle" between bacteria and organic pollutants (see Chapter 18).

Carbamate pesticides also have been shown to be susceptible to reduction, with ferrous iron serving as the reductant:[36]
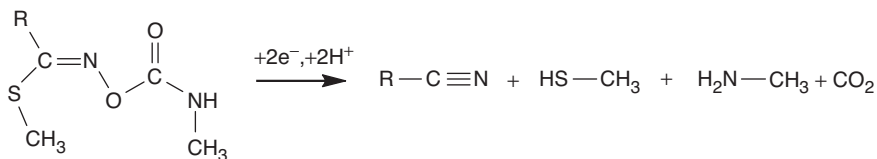
19.8.4 Kinetics and thermodynamics of reduction reactions and linear free energy relationships

The kinetics of reduction reactions are generally second order overall (first order in the reductant and first order in the contaminant) at constant pH:

$$\frac{dC}{dt} = -k[\text{reductant}][C] \tag{19.21}$$

If the reductant is in excess (or is rapidly regenerated), this is reduced to a pseudo-first-order expression with a pseudo-first-order rate constant of $k_{obs} = k[\text{reductant}]$. If the reaction takes place on a surface, more complicated chemical kinetic expressions that account for competition for reactive sites may be required (see Chapter 14). As is indicated in the reactions above, protons are involved in most reduction reactions. Thus, rates of reduction reactions may have a dependence on proton concentration, but it is not necessarily a first-order dependence. In many studies/situations, this complication is overcome by conducting experiments in buffered media where the proton concentration is constant, but often this dependence does need to be considered.

Like the reactions described in Chapter 11, reduction potentials (E°) for the overall reactions can be determined by adding E° values for the half reactions of the reductant and oxidant (i.e., pollutant). These then can be corrected for pH and concentration of other species (e.g., chloride) using the Nernst equation to get a value of E. It is often difficult, however, to measure reduction potentials of contaminants (and essentially impossible for irreversible reactions). Measurements and estimates of reduction potentials are available for the first electron transfer of nitrobenzenes, and compounds with electron withdrawing groups on the ring have more positive potentials than those with electron donating groups.[37] Reduction potential values have been calculated for various dehalogenations (both one-electron transfers to form an alkyl radical and halogen anion and two-electron transfers—hydrogenolysis and reductive elimination—shown above).[38] Also, it has been found that some reactions between a reductant and a contaminant that should occur spontaneously do not without the presence of an electron transfer mediator (e.g., quinones).[1] That said, reduction potentials have proven to be useful tools in predicting contaminant reactivity.

Marcus theory, which was introduced in Chapter 11 (see Section 11.5.2), can be used to relate the rate constants for electron reactions to the driving force (i.e., E or ΔG). For the reduction of nitroaromatic compounds and for dehalogenation reactions, plotting the logarithm of the measured pseudo-first-order rate constant versus reduction potential has proven effective in predicting rate constants (Figure 19.4).[39,40] Some caveats must be mentioned about these linear free energy relationships. First, Marcus theory was derived for outer sphere mechanisms, and reduction reactions (especially dehalogenations) often are inner sphere. Second, such relationships often are specific to the reductant and solution conditions used in the experiments. Third, for a given reductant, correlations may apply only to a given reaction mechanism (e.g., hydrogenolysis and reductive elimination reactions plot on different lines; see Figure 19.4c) or for a given class of compounds (e.g., ethanes and ethylenes may require separate correlations, as would bromoethanes versus chloroethanes). For dehalogenations, reasonable predictions also can be made using other parameters such as the energy of the lowest unoccupied molecular orbital (E_{LUMO}), and bond dissociation energies of the carbon-halogen bond. It is likely, however, that these parameters are co-correlated with the reduction potential.[38]

EXAMPLE 19.7 Possible reaction pathways of 1,2-dibromoethane: You are responsible for the remediation of a site that has ground water contaminated with 1,2-dibromoethane. It has been suggested that you consider chemical reduction as a treatment method. What are
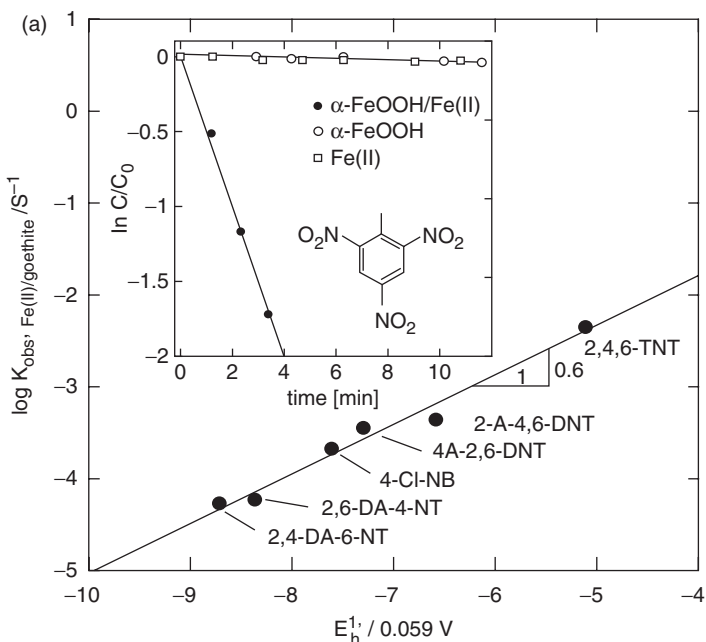
Figure 19.4 Linear free energy relationships that can be used to predict the rate of reduction of organic contaminants. (a) A plot of log k versus one-electron reduction potential for TNT, its reduction products , and 4-chloro-nitrobenzene (4-Cl-NB) by ferrous iron associated with goethite. The inset shows the kinetics of reduction of TNT and control experiments. (b) A plot of log k (a surface area normalized rate constant) versus one-electron reduction potential (for the reaction $R\text{-}Cl + e^- \rightarrow R^\cdot + Cl^-$) for the reduction of chlorinated ethylenes. (c) Plots of log k (a surface area normalized rate constant) versus two-electron reduction potential the hydrogenolysis and reductive β-elimination reactions of chlorinated ethylenes. Panel (a) is reproduced with permission from Hofstetter et al.[39] Copyright 1999 American Chemical Society. (b) and (c) are reproduced with permission from Arnold and Roberts.[40] © 1998 American Chemical Society.

the possible reaction products? The ground water has a pH of 8.
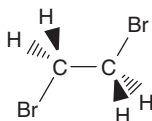
Answer: This compound may form a hydrogenolysis product (1-bromoethane; $H_3C\text{-}CH_2Br$) or a reductive β-elimination product (ethylene; $H_2C{=}CH_2$). Nucleophilic substitution and elimination reactions must also be considered. An S_N2 reaction with
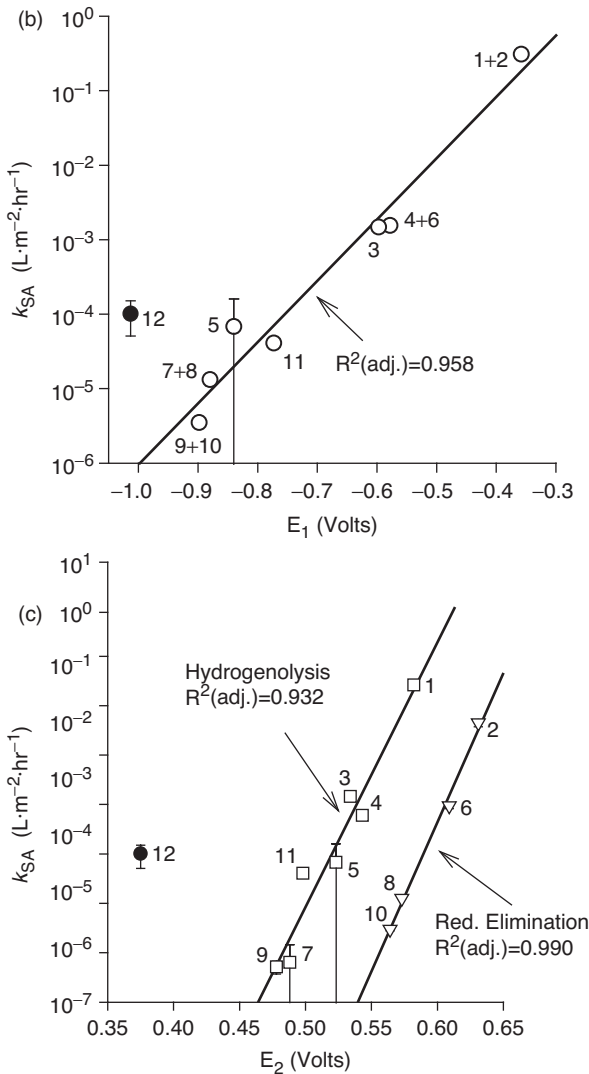
Figure 19.4 Cont'd

OH$^-$ would lead to a bromoethanol, but the more likely reaction with the strong base OH$^-$ is an E$_2$ reaction, which would lead directly to bromoethylene. Because brominated compounds are reduced more readily than chlorinated ones, this compound is reduced much more readily than its chlorinated counterpart, 1,2-dichloroethane.

19.9 Photolysis

The fundamentals of photolysis were introduced in Chapter 17. Here additional information is presented about direct and indirect photolysis of organic contaminants.

19.9.1 Direct photolysis of organic contaminants

For direct photolysis of an organic contaminant to occur, it must absorb photons in the solar spectrum (i.e., $\lambda > 290$ nm). This is easily tested using a UV-visible spectrophotometer. Recall from Chapter 17 that the relevant equations for direct photolysis are

$$k_{a(\lambda)} = 2.303 E_0(\lambda, 0) \varepsilon_\lambda \tag{17.4}$$

and

$$k_d = 2.303 \Phi_d \int_{\lambda_1}^{\lambda_2} E_0(\lambda, 0) \varepsilon_\lambda d\lambda = \Phi_d \sum_\lambda k_{a(\lambda)} \tag{17.5}$$

Where $E_0(\lambda,0)$ is the scalar irradiance just below the water surface, and ε_λ is the molar absorptivity of the compound at a given wavelength. The observed rate constant for direct photolysis (k_d) is obtained by summing over the wavelengths of light absorbed by the compound of interest. Critical to determining the rate of the reaction in natural systems is determining the quantum yield (Φ_d). Currently, the quantum yield cannot be predicted from chemical structure and must be measured experimentally. This is done using chemical actinometry. Using a light source with known intensity at each wavelength (either sunlight at a specific date and time or a lamp), one uses a chemical with known quantum yield (the actinometer) to determine the quantum yield of the compound of interest. The reactions are run side by side. The rate constant for the actinometer is

$$k_{act} = 2.303 \Phi_{act} \int_{\lambda_a}^{\lambda_b} E_0(\lambda, 0) \varepsilon_{\lambda, act} d\lambda \tag{19.22}$$

Note that the actinometer is integrated over a different wavelength range (λ_a to λ_b) than the compound, because the range of wavelengths each absorbs may be different. Taking a ratio of Eqs. 17.5 and 19.22 and rearranging gives

$$\Phi_d = \Phi_{act} \frac{k_d \int_{\lambda_a}^{\lambda_b} E_0(\lambda, 0) \varepsilon_{\lambda, act} d\lambda}{k_{act} \int_{\lambda_1}^{\lambda_2} E_0(\lambda, 0) \varepsilon_{\lambda, d} d\lambda} \tag{19.23}$$

where the subscript "d" is added to the molar absorptivity of contaminant so as not to confuse the molar absorptivity of the contaminant and the actinometer. Finally, it is important to choose actinometers for which light absorption is in roughly the same region as the contaminant and the reaction kinetic timescales are comparable.

Common actinometers are the *p*-nitroanisole-pyridine and p-nitroacetonphenone-pyridine system.[41] The quantum yield of the reaction (and thus photolysis rate) of each

system can be tuned by adjusting the concentration of pyridine. With the quantum yield and appropriate information about light intensity, it is possible to calculate the rate constant for the degradation of any pollutant using the calculation models presented in Chapter 17 (see Section 17.5).

19.9.2 Indirect photolysis of contaminants

The production of photoreactive intermediates was covered in Chapter 17. Here, we consider how a few of these intermediates react with organic contaminants.

Hydroxyl radical.   Estimates of the steady-state concentration of the hydroxyl radical ($[\cdot OH]_{ss}$) in sunlit surface waters range from $\sim 10^{-15}$ to 10^{-18} M, with 10^{-16} M a "typical" value. The exact steady state concentration depends on the concentrations of $\cdot OH$ sources (e.g., nitrate and NOM) and quenchers (e.g., NOM, carbonate), and thus on rates of formation and decay. Hydroxyl radical is a relatively nonselective oxidant, and many substrates react at close to diffusion-controlled rates (second-order rate constants of 5×10^9 to 1×10^{10} M^{-1} s^{-1}). Thus, at the surface of any sunlit surface water, one can assume a loss rate of a compound due to reactions with $\cdot OH$ of $\sim 10^{10}$ M^{-1} $s^{-1} \times 10^{-16}$ $M = \sim 10^{-6}$ s^{-1}, which represents a half life of ~ 8 days. The overall loss rate is slower than this because of light attenuation in the water column. Compounds without a readily extractable H-atom or with multiple electron withdrawing groups react more slowly (10^7 to 10^8 M^{-1} s^{-1}), however. A compilation of rate constants of organic pollutants with $\cdot OH$ is maintained by the Notre Dame Radiation Laboratory.[42]

Singlet oxygen.   Singlet oxygen is present at higher steady-state concentrations (10^{-12} to 10^{-14} M) than hydroxyl radical, but it is a much more selective oxidant. Singlet oxygen, largely produced via the quenching of excited triplet organic matter by ground state (triplet) oxygen, reacts with conjugated double bonds (such as those present in dienes and furans), electron-rich double bonds (e.g., alkenes with electron donating substituents), sulfides, aromatic amines, and phenols. Rate constants are typically of order 10^4 to 10^8 M^{-1} s^{-1}. The reaction rate may depend on pH because electrophilic $^1O_2$ reacts more rapidly with the deprotonated forms of anilines and phenols. Again, a database of rate constants is available from the Notre Dame Radiation Laboratory.[42]

Triplet organic matter.   In recent years, aquatic photochemists have found that triplet dissolved organic matter (^3DOM or $^3DOM^*$) may directly react with contaminants rather than simply generating other reactive intermediates. When a photon is absorbed by DOM, it is first put into an excited singlet state and then undergoes intersystem crossing (ISC) to the lower-energy but longer-lived excited triplet state:
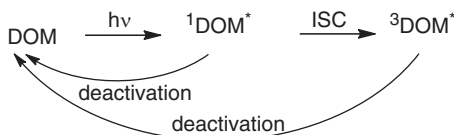
Both excited states can be deactivated to the ground state. For the triplet organic matter, one deactivation pathway is interaction with oxygen (a ground state triplet) to give singlet
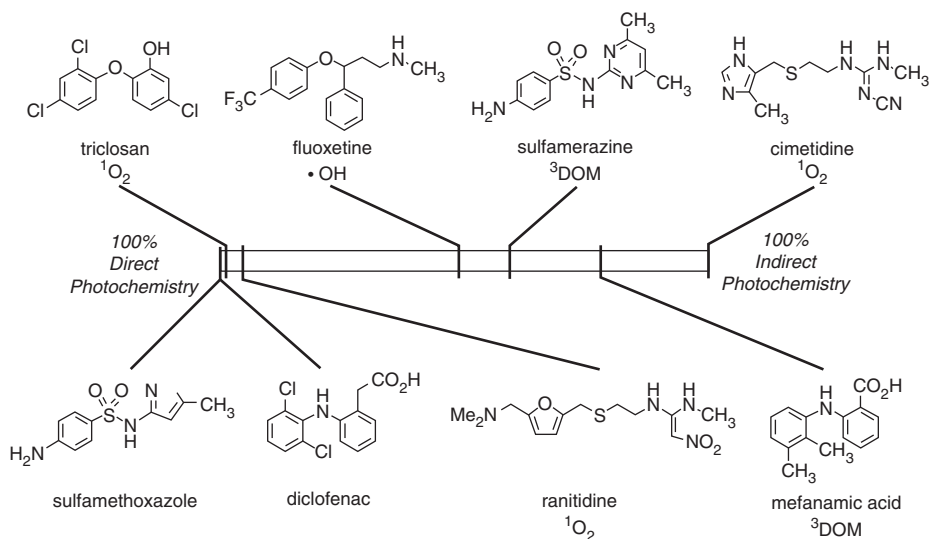
Figure 19.5 The importance of direct and indirect photolysis in the transformation of selected pharmaceutical compounds. Reproduced with permission from Arnold and McNeill.[45] © 2007 Elsevier B.V.

oxygen. Classes of compounds shown to react with triplet dissolved organic matter include alkyl and methoxy phenols[43] and various phenyl amines, including phenyl urea herbicides, sulfa antibiotics, and the antiinflammatory mefenamic acid.[44] It is difficult to determine the steady-state concentration of ^{3}DOM or second-order rate constants of the reactions, but mounting evidence suggests that this pathway is an important sink for some classes of contaminants.

For compounds that do not absorb solar photons, indirect photolysis processes are the only relevant photolysis processes in natural water. A frequently cited rule of thumb is that indirect photolysis is unimportant for compounds that are able to undergo direct photolysis, but there are many situations where both processes are important. As Figure 19.5 shows for a selection of pharmaceutical compounds, it is possible for direct photolysis to dominate, for indirect photolysis to dominate, or for both processes to be responsible for the loss of a compound in sunlit surface waters.

EXAMPLE 19.8 Direct or indirect photolysis?: Triclosan (shown below) is the antibacterial compound found in liquid hand soaps and one of the most commonly detected personal care products in surface waters.[13] The anionic form is subject to direct photolysis, and Buth et al.[46] found that under midsummer sunlight at 45° N latitude, the rate of light absorbance and quantum yield for the anion are

$$2.303 \int_{295 \text{ nm}}^{340 \text{ nm}} E_0(\lambda, 0)\varepsilon_\lambda d\lambda = 3.84 \times 10^{-3} \text{ s}^{-1}$$

and $\Phi_d = 0.35$

An earlier study measured reaction rate constants with hydroxyl radical and singlet oxygen as well:[47]

$$k_{OH} = 5.4 \times 10^9 M^{-1} s^{-1}$$

$$k_{1_{O_2}} = 1.1 \times 10^8 \ M^{-1} s^{-1}$$

The reaction with singlet oxygen is only relevant for the anionic form. Estimate the relative importance of direct and indirect photolysis processes in the loss of triclosan at pH 8.
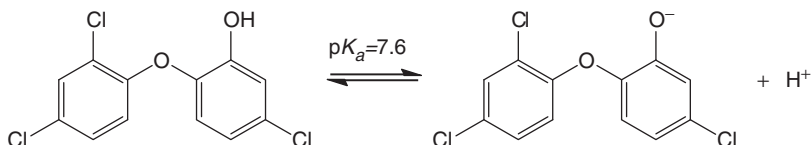
Answer: Direct photolysis and singlet oxygenation are only relevant for the anion. First, we must determine the fraction of the triclosan present in the anionic form at pH 8:

$$\alpha_1 = \frac{K_a}{[H^+] + K_a} = \frac{10^{-7.6}}{10^{-8} + 10^{-7.6}} = 0.72$$

Accounting for the fraction in the anionic form yields a rate constant for direct photolysis of

$$k_d = (0.35)(3.84 \times 10^{-3})(0.72) = 9.7 \times 10^{-4} s^{-1} = 3.5 \ h^{-1}.$$

Assuming concentrations of 10^{-16} M for $\cdot OH$ and 10^{-12} M for $^1O_2$,

$$k_{obs\text{-}hydroxyl} = (5.4 \times 10^9 M^{-1} s^{-1})(10^{-16} \ M) = 5.4 \times 10^{-7} s^{-1} = 0.002 h^{-1},$$

$$k_{obs\text{-}singlet\ oxygen} = (1.1 \times 10^8 M^{-1} s^{-1})(0.72)(10^{-12} M) = 7.9 \times 10^{-5} s^{-1} = 0.3 h^{-1}.$$

Note that the rate constant for $^1O_2$ also contains the 0.72 factor to account for the fraction in the anionic form. Clearly, the direct photolysis component is much more important than indirect photolysis, but reaction with singlet oxygen is responsible for ~8% of the photolysis of triclosan.

19.10 Summary

Chemical structure is a key to predicting the behavior of an organic pollutant in the environment. The tools presented in this chapter allow prediction of (1) the distribution of a chemical among environmental compartments (air, water, soil/sediment, biota) at equilibrium, (2) potential reaction pathways (substitution/elimination, hydrolysis, oxidation/reduction, photolysis), and (3) in some cases, the rate constants for the

reactions. Obviously, the power to make these predictions based solely on chemical structure (without any experiments!) is very useful. To conclude this chapter, the behavior of two chemicals is compared using these tools.

EXAMPLE 19.9 A phone call in the middle of the night: Two trucks carrying chemicals have a minor fender-bender near a roadside lake. Although no one is injured and the damage is minor, both trucks have sprung small leaks, and their payloads are being slowly spilled into the lake. One truck is carrying methylparaben and the other 1,2-dibromo-3-chloropropane. Having read this chapter, you are now the local expert on the fate of organic pollutants, and the sheriff calls you to evaluate the risk the spill poses. Use the tools in this chapter to determine (1) the fraction of the compound in air, water, and sediment at equilibrium and (2) potential reactions of the two compounds. Assume a ratio of 10 L:1 L:0.1 kg for air:water:sediment. From prior measurements, you know the pH of the water is 7.87 and the f_{oc} of the sediment is 0.05. The sediment is anaerobic, and thus reductants are present.

Answer: The first thing to do is determine the two chemical structures. Using the name lookup feature in EPI Suite, you find
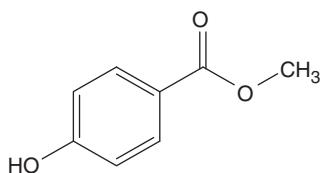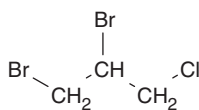
methylparaben   1,2-dibromo-3-chloropropane

Let's take one compound at a time, starting with methylparaben. EPI Suite gives the following information:

$$H = 3.61 \times 10^{-9} \text{atm·m}^3/\text{mol} = 3.61 \times 10^{-6} \text{atm·L/mol}$$

Using R = 0.0821 L·atm mol^{-1} K^{-1} and T = 298.15,

$$H' = H/RT = 1.47 \times 10^{-7},$$
$$K_{oc} = 129 \text{L/kg},$$

and thus

$$K_d = f_{oc}\, K_{oc} = 0.05 \times 129 = 6.45 \text{ L/kg}.$$

This compound is a phenol and thus is subject to acid-base chemistry. Using SPARC, you find the pK_a is 7.87. Because the pH and pK_a are equal, half of the compound is

the anionic form, and H' and K_{oc} are multiplied by 0.5 to determine the equilibrium distribution (see Eq. 19.16). The fraction in the water is

$$f_w = \frac{C_w V_w}{C_a V_a + C_w V_w + C_s M_s} = \frac{V_w}{\dfrac{C_a}{C_w} V_a + V_w + \dfrac{C_s}{C_w} M_s} = \frac{V_w}{H' V_a + V_w + K_d M_s}$$

$$= \frac{1}{(1.47 \times 10^{-7})10 + 1 + (6.45)0.1} = 0.67$$

Similarly,

$$f_a = \frac{H' V_a}{H' V_a + V_w + K_d M_s} = \frac{(1.47 \times 10^{-7})10}{(1.47 \times 10^{-7})10 + 1 + (6.45)0.1} = 9 \times 10^{-7},$$

and by difference, $f_{sed} = 0.33$. Thus, two-thirds of the methylparaben will be in water, and one-third in the sediment.

Now it is time to evaluate the potential reactions. Note that these reactions are relevant only for the *fraction in the aqueous phase*. Thus all rate constants below need to be multiplied by the fraction in the water (or the half-lives need to be divided by the fraction in the water).

(1) There is no good leaving group on a primary or tertiary carbon, and so substitution/elimination reactions will not occur.

(2) Methylparaben has an ester group and thus is subject to ester hydrolysis. EPI Suite predicts a half-life at pH 8 of 3.45 years (for the base-catalyzed reaction). Dividing by 0.67 gives 5.15 years.

(3) The compound is a phenol, and thus there may be oxidation processes mediated by minerals that are relevant. There is no functional group susceptible to reduction.

(4) To determine whether it is subject to direct photolysis, a UV-visible absorbance spectrum is needed. This is available via the NIST Chemistry WebBook.[48] A small amount of absorbance occurs at wavelengths > 290 nm, and so direct photolysis is a possibility. The phenolate form likely absorbs more solar light. The rate of direct photolysis, however, cannot be predicted without a quantum yield.

(5) Phenols also react with singlet oxygen and triplet organic matter. All compounds react with $^{\cdot}$OH. Although methylparaben is not in the Notre Dame Radiation Laboratory database,[42] 4-hydroxybenzoate is, and $k_{\cdot OH} = 6 \times 10^9$ M^{-1} s^{-1}. For singlet oxygen, 2-hydroxybenzoate is in the database, with $k = 1.4 \times 10^5$ M^{-1} s^{-1}. Taking account of the fraction in the anionic form for the singlet oxygen rate constant gives an estimated "effective" rate constant of 0.7×10^5 M^{-1} s^{-1}. If steady state concentrations of $^{\cdot}$OH and $^1O_2$ are 10^{-16} M and 10^{-12} M, respectively, the overall pseudo-first-order rate constant for the two processes is 6.7×10^{-7} s^{-1} giving a half-life of ~ 12 days (when the sun is shining), with a night-corrected value of 18 days.

The same exercise is now performed for the 1,2-dibromo-3-chloropropane. Using the information from EPI Suite:

$$H = 1.47 \times 10^{-4} \text{ atm} \cdot \text{m}^3 \text{mol}^{-1} (\text{experimental value}) = 1.47 \times 10^{-1} \text{atm} \cdot \text{L mol}^{-1}$$

Using $R = 0.0821$ L atm mol^{-1} K^{-1} and T = 298.15,

$$H' = H/RT = 6 \times 10^{-3}.$$

$K_{oc} = 370$ L/kg for the K_{ow} method. The MCI method is 115 L/kg, and the choice of the other value is arbitrary.

$$K_d = f_{oc} \, K_{oc} = 0.05 \times 370 = 18.5 \text{ L/kg}$$

There is no acid-base chemistry to consider. The fraction in the water is

$$f_w = \frac{V_w}{H'V_a + V_w + K_d M_s} = \frac{1}{(6 \times 10^{-3})10 + 1 + (18.5)0.1} = 0.34$$

Similarly,

$$f_a = \frac{H'V_a}{H'V_a + V_w + K_d M_s} = \frac{(6 \times 10^{-3})10}{(6 \times 10^{-3})10 + 1 + (18.5)0.1} = 0.02$$

and by difference, $f_{sed} = 0.64$. Thus, almost two-thirds of the 1,2-dibromo-3-chloropropane will be in the sediment and most of the remainder in the water.

Again, reactions are only relevant for the *fraction in the aqueous phase*

(1) The bromine and chlorine are good leaving groups. S_N2 and E_2 reactions are likely. In either case, bromine is the preferred leaving group over chlorine. We would need the reaction rate constant with water to use the Swain-Scott model.
(2) Ester hydrolysis is not relevant.
(3) Both hydrogenolysis and reductive β-elimination are possible.
(4) This compound does not absorb light of wavelength greater than 290 nm, and consequently, direct photolysis is not relevant.
(5) Reaction with ·OH is relevant. The Notre Dame Radiation Laboratory database[42] gives a value of 4.1×10^9 M^{-1} s^{-1} for 1,3-dibromopropane.

In comparing the two chemicals, we see that different fractions are present in air/water/sediment and the reactions that have the potential to transform the contaminants are quite different. This is hopefully not surprising given the differences in their chemical structures.

▢ Problems

19.1. A graduate student needs to know the dimensionless Henry's law constant of acetylene at 60°C for his Ph.D. research. He dissolves some acetylene gas in water by shaking water and acetylene together in a large syringe. He then transfers 1-mL aliquots to a series of 12.5 mL autosampler vials, along with a varying volume of additional acetylene-free water. Each autosampler vial thus contains an identical total mass of acetylene, but a varying air:water ratio. He then analyzes the acetylene content in the headspace using gas chromatography after equilibrating the vials in an oven at 60°C. His results are shown below:

Sample no.	Volume water (mL)	Peak area (μV-sec)
1	1	295919
2	2	297659
3	4	304339
4	6	312801
5	8	316176

Use Eq. 19.2 to determine H' for acetylene at 60°C and compare this value to that determined by EPI Suite for 25°C. (You will need to convert to "dimensionless" form to allow the comparison.) Does the relative magnitude of the two values make sense? Explain why or why not.

19.2. Use EPI Suite to determine the log(Henry's law constant), log K_{ow}, and log K_{oc} parameters for the following sets of compounds:

Set 1	Set 2
Benzene	phenol
Toluene	4-Chlorophenol
Ethylbenzene	Aniline
Propylbenzene	4-Chloroaniline
Butylbenzene	Benzene
Pentylbenzene	4-Chlorobenzene
Xylene	

From the data sets you generate, determine the contribution of methyl groups ($-CH_3$), methylene groups ($-CH_2-$), and chloro groups ($-Cl$) to log(Henry's law constant), log K_{ow}, and log K_{oc}.

19.3. Your environmental consulting firm WecleanH2O has a project to remove phenol and benzene from contaminated ground water. You have decided to use activated carbon as a sorbent. Your technician, Ofan Miztaken, determined the required activated carbon dose (c_{solid}) to be 1500 g/L. Based on the information below, is the calculation correct? Assume noncompetitive adsorption.

Initial benzene concentration: 1 mmol/L
Target final concentration: 0.0001 mmol/L
Initial phenol concentration: 2 mmol/L
Target final concentration: 0.05 mmol/L

Phenol sorption is treated with a Langmuir isotherm: $X_{max} = 10^{-4}$ mol/g, $K_L = 150$ L/mol. Benzene sorption is treated via a linear isotherm with $K = 25$ L/g.

19.4. The K_{ow} of parathion, a once common organophosphorus pesticide, is $10^{3.81}$, and the Henry's law constant H' is $10^{-4.8}$. To simulate a model world, you have 10 L of water, 250 mL of octanol, and 50 L of air in a sealed flask. What fraction of the parathion will be in the aqueous phase?

19.5. Nitroaromatic compounds are widely used as intermediates in the manufacture of pesticides, dyes, and explosives. Thus, they are commonly detected ground-water pollutants. One such compound is 4-nitrotoluene (4-NT), and one degradation product of 4-NT is 4-aminotoluene (4-AT):

4-NT   4-AT
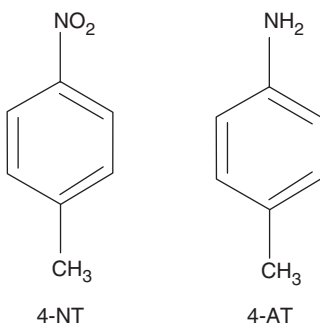
Using a handy reference book, you find the following information about the two compounds.

Species	Log K_{ow}	pK_a	Solubility
4-NT	2.37	na	0.44 g/L
4-AT	1.39	5.1	6.5 g/L

(a) A site has been contaminated with 4-NT, and through natural processes, 4-AT is now also present. The soil at the site is 35% organic matter, and there are 3 g of soil per mL of water where the contaminants are located. You determine that aqueous concentration of 4-NT is 0.13 g/L and that

of 4-AT is 0.05 g/L. What are the concentrations 4-NT and 4-AT in the soil assuming that it is in equilibrium with the water?

(b) You measure the pH of the water at the site and find that it is 3.5. Qualitatively explain how this information could change your answers to part (a).

19.6. The odor threshold of 4-chlorophenol is 30 ppm$_v$ (i.e., 30 μL 4-chlorophenol per liter of air). If you have 10 L of water at pH 6 in equilibrium with 2 L of water, at what aqueous concentration of 4-chlorophenol will the odor threshold be exceeded? Repeat the problem for pH 10.

19.7. Repeat example 19.4 for (a) DDT and (b) 4-chlorobenzoic acid. Use EPI Suite to obtain the appropriate equilibrium constants. The pH of the water is 8.2.

19.8. Benzoyl chloride undergoes reaction with either water or hydroxide.

(a) Sketch the mechanisms of these two reactions.

(b) If the reaction of hydroxide occurs 10^6 times faster than that with water, what is the substrate constant if a Swain-Scott type relationship applies to this reaction?
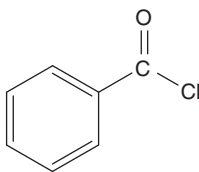
benzoyl chloride

19.9. Arnold and Roberts[40] determined the following surface-area-normalized pseudo-first-order rate constants (all in $L\,m^{-2}\,h^{-1}$) for the reduction of dichloroethylenes and their degradation products with zero-valent zinc:

cis-Dichloroethylene → vinyl chloride	$k_1 = 5.2 \times 10^{-7}$
cis-Dichloroethylene → acetylene	$k_2 = 3.0 \times 10^{-6}$
trans-Dichloroethylene → vinyl chloride	$k_3 = 6.4 \times 10^{-7}$
trans-Dichloroethylene → acetylene	$k_4 = 1.3 \times 10^{-5}$
1,1-Dichloroethylene → vinyl chloride	$k_5 = 4.1 \times 10^{-5}$
Vinyl chloride → ethylene	$k_6 = 1.0 \times 10^{-4}$
Acetylene → ethylene	$k_7 = 5.0 \times 10^{-4}$

Use Acuchem to plot concentration versus time for the six chemical species for a zinc to water ratio of 50 m^2/L.

19.10. Select three organic pollutants (one a phenol, one a chlorinated pollutant, and one containing a sulfur atom), and find the rate constants for their reaction with hydroxyl radical and singlet oxygen in the Notre Dame Radiation Laboratory database[42] or another source. Compare the relative importance of hydroxyl radical and singlet oxygen as indirect photolysis processes for average steady-state concentrations of these oxidants in sunlit surface waters.

References

1. Schwarzenbach, R. P., P. M. Gschwend, and D. M. Imboden. 2003. *Environmental organic chemistry*, 2nd ed., J. Wiley & Sons, New York.

2. Larson, R. A., and E. J. Weber. 1994. *Reaction mechanisms in environmental chemistry*, Lewis Publ., Boca Raton, Fla.

3. Lyman, W. J., W. F. Reehl, and D. H. Rosenblat. 1990. *Handbook of chemical property estimation methods*, Amer. Chem. Soc., Washington, D.C.

4. Mackay, D. M., W. Y. Shiu, and K.-C. Ma. 1992–1997. *Illustrated handbook of physical-chemical properties and environmental fate for organic chemicals*, Vols. 1–5, Lewis Publ., Chelsea, Mich.

5. Syracuse Research Corporation. 2010. Interactive PhysProp database demo (available at http://www.syrres.com/what-we-do/databaseforms.aspx?id=386, September, 2010).

6. U.S. EPA. 2010. Estimation Programs Interface Suite™ for Microsoft® Windows, ver. 4.00 (available at http://www.epa.gov/oppt/exposure/pubs/episuite.htm, September, 2010).

7. Hilal, S., S. W. Karickhoff, and L. A. Carreira. 1995. A rigorous test for SPARC's chemical reactivity models: estimation of more than 4300 ionization pK_a's. *Quant. Struc. Act. Rel.* **14**: 348–355; University of Georgia. 2010. SPARC v4.5. Available at http://sparc.chem.uga.edu/sparc/, September, 2010).

8. Krasner, S. W., H. S. Weinberg, S. D. Richardson, S. J. Pastor, R. Chinn, M. J. Sclimenti, G. D. Onstad, and A. D. Thruston. 2006. Occurrence of a new generation of disinfection byproducts. *Environ. Sci. Technol.* **40**: 7175–7185.

9. Mahler, B. J., P. C. Van Metre, T. J. Bashara, J. T. Wilson, and D. A. Johns. 2005. Parking lot sealcoat: an unrecognized source of urban polycyclic aromatic hydrocarbons. *Environ. Sci. Technol.* **39**: 5560–5566.

10. Yang, Y., P. C. Van Metre, B. J. Mahler, J. T. Wilson, B. Ligouis, M. M. Razzeque, D. J. Schaffer, and C. J. Werth. 2010. Influence of coal-tar sealcoat and other carbonaceous material on polycyclic aromatic hydrocarbon loading in an urban watershed. *Environ. Sci. Technol.* **44**: 1217–1223.

11. Van den Berg, M., L. S. Birnbaum, M. Denison, M. De Vito, W. Farlad, M. Feeley, H. Fiedler, H. Hakansson, A. Hanberg, L. Haws, M. Rose, S. Safe, D. Schrenk, C. Tohymaa, A. Tritcher, J. Tuomisto, M. Tysklind, N. Walker, and R. E. Peterson. 2006. The 2005 World Health Organization reevaluation of human and mammalian toxic equivalency factors for dioxins and dioxin-like compounds. *Toxicol. Sci.* **93:** 223–241.

12. Hites, R. A. 2004. Polybrominated diphenyl ethers in the environment and in people: a meta-analysis of concentrations. *Environ. Sci. Technol.* **38**: 945–956.

13. Kolpin, D. W., E. T. Furlong, E. M. Thurman, S. D. Zaugg, L. B. Barber, and H. T. Buxton. 2002. Pharmaceuticals, hormones, and other organic wastewater contaminants in U.S. streams, 1999–2000: a national reconnaissance. *Environ. Sci. Technol.* **36**: 1202–1211.

14. Staudinger, J., and P. V. Roberts. 1996. A critical review of Henry's law constants for environmental applications. *Crit. Rev. Environ. Sci. Technol.* **26**: 205–297.

15. Staudinger, J., and P. V. Roberts. 2001. A critical compilation of Henry's law constant temperature dependence relations for organic compounds in dilute aqueous solutions. *Chemosphere* **44**: 561–576.

16. Gossett, J. M. 1987. Measurement of Henry's law constants for C1 and C2 chlorinated hydrocarbons. *Environ. Sci. Technol.* **21**: 202–208.

17. Meylan, W. M., and P. H. Howard. 1991. Bond contribution method for estimating Henry's law constants. *Environ. Toxicol. Chem.* **10**: 1283–1293.

18. Hine, J., and P. J. Mookerjee. 1975. The intrinsic hydrophilic character of organic compounds. Correlations in terms of structural contributions. *J. Org. Chem.* **40**: 292–298.

19. Meylan, W. M., and P. H. Howard. 1995. Atom/fragment contribution method for estimating octanol-water partition coefficients. *J. Pharm. Sci.* **84**: 83–92.

20. Doucette, W. J. 2000. Soil and sediment sorption coefficients. In *Handbook of property estimation methods, environmental and health sciences*, R. S. Boethling and D. Mackay (eds.), Lewis Publ., Boca Raton, Fla.

21. Meylan, W. M., P. H. Howard, and R. S. Boethling. 1992. Molecular topology/fragment contribution method for predicting soil sorption coefficients. *Environ. Sci. Technol.* **26**: 1560–1567.

22. Haderlein, S. B., and R. P. Schwarzenbach. 1993. Adsorption of substituted nitrobenzenes and nitrophenols to mineral surfaces. *Environ. Sci. Technol.* **27**: 316–332.

23. Figueroa, R. A., A. Leonard, and A. A. MacKay. 2004. Modeling tetracycline antibiotic sorption to clays. *Environ. Sci. Technol.* **38**: 476–483.

24. Swain, C. G., and C. B. Scott. 1953. Quantitative correlation of relative rates. Comparison of hydroxide ion with other nucleophile reagents toward alkyl halides, esters, epoxides, and acyl halides. *J. Am. Chem. Soc.* **75**: 141–147.

25. Lippa, K. A., and A. L. Roberts. 2005. Correlation analyses for bimolecular nucleophilic substitution reactions of chloroacetanilide herbicides and their structural analogs with environmentally relevant nucleophiles. *Environ. Toxicol. Chem.* **24**: 2401–2409.

26. Mill, T., W. Haag, P. Penwell, T. Pettit, and H. Johnson, H. 1987. Environmental fate and exposure studies development of a PC-SAR for hydrolysis: esters, alkyl halides and epoxides. EPA Contract No. 68-02-4254, SRI International, Menlo Park, Calif.

27. Weber, E. J. D. L. Spidle, and K. A. Thorn. 1996. Covalent binding of aniline to humic substances. *Environ. Sci. Technol.* **30**: 2755–2763.

28. Stone, A. T., and J. J. Morgan. 1984. Reduction and dissolution of manganese(II) and manganese(IV) oxides by organics. 1. Reaction with hydroquinone. *Environ. Sci. Technol.* **18**: 450–456; Stone, A. T. 1987. Reductive dissolution of manganese(III/IV) oxides by substituted phenols. *Environ. Sci. Technol.* **21**: 979–988; Ulrich, H.-J., and A. T. Stone. 1989. Oxidation of chlorophenols adsorbed to manganese oxide surfaces. *Environ. Sci. Technol.* **23**: 421–428; Lehmann, R. G., H. H. Cheng, and J. B. Harsh. 1987. Oxidation of phenolic acids by soil iron and manganese oxides. *Soil Sci. Soc. Amer. J.* **51**: 352–356; Laha, S., and R. G. Luthy. 1990. Oxidation of aniline and other primary aromatic amines by manganese dioxide. *Environ. Sci. Technol.* **24**: 363–373.

29. Gillham, R. W., and S. F. O'Hannesin. 1994. Enhanced degradation of halogenated aliphatics by zero-valent iron. *Ground Wat.* **32**: 958–967; Matheson, L. J., and P. G. Tratnyek. 1994. Reductive dehalogenation of chlorinated methanes by iron metal. *Environ. Sci. Technol.* **28**: 2048–2053; Agrawal, A., and P. G. Tratnyek. 1996. Reduction of nitro aromatic compounds by zero-valent iron metal. *Environ. Sci. Technol.* **30**: 153–160; Scherer, M. M., B. A. Balko, D. A. Gallagher, and P. G. Tratnyek. 1998. Correlation analysis of rate constants for dechlorination by zero-valent iron. *Environ. Sci. Technol.* **32**: 3026–3033; Arnold, W. A., and A. L. Roberts. 2000. Pathways and kinetics of chlorinated ethylene and chlorinated acetylene reaction with Fe(0) particles. *Environ. Sci. Technol.* **34**: 1794–1805.

30. Hozalski, R. M., L. Zhang, and W. A. Arnold. 2001. Reduction of haloacetic acids by Fe^0: implications for treatment and fate. *Environ. Sci. Technol.* **35**: 2258–2263.

31. Arnold, W. A., W. P. Ball, and A. L. Roberts. 1999. Polychlorinated ethane reaction with zero-valent zinc: pathways and rate control. *J. Contam. Hydrol.* **40**: 183–200.

32. Chun, C. L., R. M. Hozalski, and W. A. Arnold. 2005. Degradation of drinking water disinfection byproducts in the presence of synthetic goethite and magnetite. *Environ. Sci. Technol.* **39**: 8525–8532; Chun, C. L., R. M. Hozalski, and W. A. Arnold. 2007. Degradation of disinfection byproducts by carbonate green rust. *Environ. Sci. Technol.* **41**: 1615–1621.

33. Lund, H. 2001. Cathodic reduction of nitro and related compounds. In *Organic electrochemistry*, 4th ed., H. Lund and O. Hammerich (eds.), Marcel Dekker, New York,

379–409; Hartenbach, A., T. B. Hofstetter, M. Berg, J. Bolotin, and R. P. Schwarzenbach. 2006. Using nitrogen isotope fractionation to assess abiotic reduction of nitroaromatic compounds. *Environ. Sci. Technol.* **40**: 7710–7716.

34. Larese-Casanova, P., and M. M. Scherer. 2008. Abiotic transformation of hexahydro-1, 3,5-trinitro-triazine (RDX) by green rusts. *Environ. Sci. Technol.* **42**: 3975–3981.

35. Klupinski, T. P., and Y.-P. Chin. 2003. Abiotic degradation of triflualin by Fe(II): kinetics and transformation pathways. *Environ. Sci. Technol.* **37**: 1311–1318.

36. Bromilow, R. H., G. G. Briggs, M. R. Williams, J. H. Smelt, L. G. M. T. Tuinstra, and W. A. Traag. 1986. The role of ferrous ions in the rapid degradation of oxamyl, methomyl, and aldicarb in anaerobic soils. *Pestic. Sci.* **17**: 535–547; Strathmann, T. J., and A. T. Stone. 2001. Reduction of carbamate pesticides oxamyl and methomyl by dissolved Fe^{II} and Cu^{I}. *Environ. Sci. Technol.* **35**: 2461–2469.

37. Schwarzenbach, R. P., R. Stierli, K. Lanz, and J. Zeyer. 1990. Quinone and iron porphyrin mediated reduction of nitroaromatic compounds in homogeneous aqueous solutions. *Environ. Sci. Technol.* **24**: 1566–1574; Meisel, D., and P. Neta. 1975. One-electron redox potentials of nitro compounds and radiosensitizers. Correlation with spin densities of their radical anions. *J. Am. Chem. Soc.* **97**: 5198–5203; Neta, P., and D. Meisel. 1976. Substituent effects on nitroaromatic radical anions in aqueous solution. *J. Phys. Chem.* **80**: 519–424; Wardman, P. 1977. The use of nitroaromatic compounds as hypoxic cell radiosensitizers. *Curr. Top. Radiat. Res. Q.* **11**: 347–398; Kemula, W., and T. M. Krygowski. 1979. In *Encyclopedia of electrochemistry of the elements* Vol. 8, A. J. Bard and M. Lund (eds.), Marcel Dekker, New York.

38. Totten, L. A., and A. L. Roberts. 2001. Calculated one- and two-electron reduction potential and related molecular descriptors for reduction of alkyl and vinyl halides in water. *Crit. Rev. Environ. Sci. Technol.* **31**: 175–221.

39. Hofstetter, T. B., C. G. Heijman, S. B. Haderlein, C. Holliger, and R. P. Schwarzenbach. 1999. Complete reduction of TNT and other (poly)nitroaromatic compounds under iron-reducing subsurface conditions. *Environ. Sci. Technol.* **33**: 1479–1487.

40. Arnold, W. A., and A. L. Roberts. 1998. Pathways of chlorinated ethylene and chlorinated acetylene reaction with Zn(0). *Environ. Sci. Technol.* **32**: 3017–3025.

41. Dulin, D., and T. Mill. 1982. Development and evaluation of sunlight actinometers. *Environ. Sci. Technol.* **16**: 815–820.

42. Notre Dame Radiation Laboratory. 2010. Radiation Chemistry Data Center http://www.rad.nd.edu/, March 2010.

43. Canonica, S., U. Jans, K. Stemmler, and J. Hoigne. 1995. Transformation kinetics of phenols in water: photosensitization by dissolved natural organic material and aromatic ketones. *Environ. Sci. Technol.* **29**: 1822–1831.

44. Gerecke, A. C. S. Canonica, S. R. Mueller, M. Schaerer, and R. P. Schwarzenbach. 2001. Quantification of dissolved natural organic matter (DOM) mediated phototransformation of phenylurea herbicides in lakes. *Environ. Sci. Technol.* **35**: 3915–3923; Boreen, A. L., W. A. Arnold, and K. McNeill. 2005. Triplet-sensitized photodegradation of sulfa drugs containing six-membered heterocyclic groups: identification of an SO_2 extrusion product. *Environ. Sci. Technol.* **39**: 3630–3638; Werner, J. J., K. McNeill, and W. A. Arnold. 2005. Environmental photodegradation of mefenamic acid. *Chemosphere* **58**: 1339–1346.

45. Arnold, W. A., and K. McNeill. 2007. Transformation of pharmaceuticals in the environment: photolysis and other abiotic processes. In *Comprehensive analytical chemistry*, Vol. 50: *Analysis, fate and removal of pharmaceuticals in the water cycle*, M. Petrovic and D. Barcelo (eds.), Elsevier, Amsterdam, 361–385.

46. Buth, J. M., M. Grandbois, P. J. Vikesland, K. McNeill, and W. A. Arnold. 2009. Aquatic photochemistry of chlorinated triclosan derivatives: potential source of polychlorodibenzo-p-dioxins. *Environ. Toxicol. Chem.* **28**: 2555–2563.

47. Latch, D. E., J. L. Packer, B. L. Stender, J. VanOverbeke, W. A. Arnold, and K. McNeill. 2005. Aqueous photochemistry of triclosan: formation of 2,4-dichlorophenol, 2,8-dichlorodibenzo-p-dioxin and oligomerization products. *Environ. Toxicol. Chem.* **24**: 517–525.
48. NIST. 2010. NIST Chemistry WebBook: NIST Standard Reference Database no. 69 (available at webbook.nist.gov/chemistry), September, 2010.

Appendix

Free Energies and Enthalpies of Formation of Common Chemical Species in Water[*]

Substance	G_f°	H_f°
	$(kJ\ mol^{-1})$	$(kJ\ mol^{-1})$
Aluminum (Al)		
Al^{3+}	−489.4	−531.0
$AlOH^{2+}$	−698	
$Al(OH)_2^+$	−911	
$Al(OH)_{3(aq)}^0$	−1115	
$Al(OH)_4^-$	−1325	
$Al(OH)_3$(amorphous)	−1139	
$Al(OH)_3$(gibbsite)	−1155	−1293
$AlOOH_{(s)}$(boehmite)	−922	−1000
$Al_2Si_2(OH)_4$(kaolinite)	−3799	−4120
$CaAl_2Si_2O_8$ (anorthite)	−4017.3	−4243
$NaAlSi_3O_8$ (albite)	−3711.7	−3935.1
Arsenic (As)		
H_3AsO_4	−766	−898.7
$H_2AsO_4^-$	−748.5	−904.5
$HAsO_4^{2-}$	−707.1	−898.7
AsO_4^{3-}	−636.0	−870.3
$H_2AsO_3^-$	−587.4	

Continued

758

Cont'd

Substance	G_f°	H_f°
	(kJ mol^{-1})	(kJ mol^{-1})
Barium (Ba)		
Ba^{2+}	−560.7	−537.6
$BaSO_{4(s)}$	−1362	−1473
Boron (B)		
H_3BO_3	−968.7	−1072
$B(OH)_4^-$	−1153.3	−1344
Bromine (Br)		
$Br_{2(l)}$	0	0
$Br_{2(aq)}$	3.93	−2.59
Br^-	−104.0	−121.5
$HOBr_{(aq)}$	−82.2	−113.0
BrO^-	−33.5	−94.1
Carbon (C)		
C (graphite)	0	0
C (diamond)	3.93	−259.0
$CO_{2(g)}$	−394.37	−393.5
$H_2CO_{3(aq)}$ (true)	−607.1	
$H_2CO_3^*$	−623.2	−699.7
HCO_3^-	−586.8	−692.0
CO_3^{2-}	−527.9	−677.1
$CH_{4(g)}$	−50.75	−74.8
$CH_{4(aq)}$	−34.39	−89.04
$CH_3OH_{(aq)}$	−175.4	−245.9
$HCOOH_{(aq)}$	−372.3	−425.4
$HCOO^-$	−351.0	−425.6
$HCN_{(aq)}$	119.7	107.1
CN^-	172.4	150.6
$CH_3COOH_{(aq)}$	−396.6	−485.8
CH_3COO^-	−369.4	−486.0
Calcium (Ca)		
Ca^{2+}	−553.54	−542.83
$CaOH^+$	−718.4	
$Ca(OH)_{2(aq)}^0$	−868.1	−1003
CaO (calcium oxide)	−604.2	
$Ca(OH)_{2(s)}$ (portlandite)	−898.4	−986.0
$CaCO_3$ (calcite)	−1128.8	−1207.4
$CaCO_{3(s)}$ (aragonite)	−1127.8	−1207.4
$CaMg(CO_3)_2$ (dolomite)	−2161.7	−2324.5
$CaSO_{4(s)}$ (anhydrite)	−1321.7	−1434.1
$CaSO_4 \cdot 2H_2O$ (gypsum)	−1797.2	−2022.6
$Ca_5(PO_4)_3OH$ (apatite)	−6338.4	−6721.6

Continued

Cont'd

Substance	G_f° (kJ mol^{-1})	H_f° (kJ mol^{-1})
Cadmium (Cd)		
Cd^{2+}	−77.58	
$CdOH^+$	−284.5	
$Cd(OH)_{2(aq)}^0$	−392.2	
$Cd(OH)_3^-$	−600.8	
$CdCl^+$	−224.4	−240.6
$CdCl_{2(aq)}^0$	−340.1	−410.2
$CdCl_3^-$	−487.0	−561.0
$CdCO_{3(s)}$	−699.4	−750.6
Chlorine (Cl)		
$Cl_{2(l)}$	0	0
$Cl_{2(aq)}$	6.9	−23.4
Cl^-	−131.3	−167.2
$HOCl_{(aq)}$	−79.9	−120.9
ClO^-	−36.8	−107.1
$ClO_{2(aq)}$	117.6	74.9
ClO_2^-	17.1	−66.5
ClO_3^-	−3.35	−99.2
ClO_4^-	−8.62	−129.3
Chromium (Cr)		
Cr^{3+}	−215.5	−256.0
$HCrO_4^-$	−764.8	−878.2
CrO_4^{2-}	−727.9	−881.1
$Cr_2O_7^{2-}$	−1301	−1490
Cobalt (Cr)		
Co^{2+}	−54.4	−58.2
Co^{3+}	−134	−92
$Co(OH)_{2(aq)}$	−369	−518
$Co(OH)_{2(s)}$	−450	−
Copper (Cu)		
Cu^+	50.0	71.7
Cu^{2+}	65.5	64.8
$Cu(OH)_{2(aq)}^0$	−249.1	−395.2
$HCuO_2^-$	−258	
CuS	−53.6	−53.1
CuO (tenorite)	−129.7	−157.3
$CuCO_3 \cdot Cu(OH)_2$ (malachite)	−893.7	−1051.4
Fluorine (F)		
F^-	−278.8	−332.6
$HF_{(aq)}$	−296.8	320
HF_2^-	−578.1	−650

Cont'd

Substance	G_f° $(kJ\ mol^{-1})$	H_f° $(kJ\ mol^{-1})$
Hydrogen (H)		
$H_{2(aq)}$	17.57	−4.18
$H^+_{(aq)}$	0	0
$H_2O_{(l)}$	−237.18	−285.83
$H_2O_{(g)}$	−228.57	−241.8
$H_2O_{2(aq)}$	−131.4	−191.1
$HO^-_{2\ (aq)}$	−67.4	−160.3
Iodine (I)		
$I_{2(aq)}$	16.4	22.6
I^-	−51.6	−55.2
I^-_3	−51.5	−51.5
$HOI_{(aq)}$	−99.2	−138
IO^-	−38.5	−107.5
$HIO_{3(aq)}$	−132.6	−211.3
IO^-_3	−128.0	−221.3
Iron (Fe)		
Fe^{2+}	−78.87	−89.1
$FeOH^+$	−277.3	
Fe^{3+}	−4.6	−48.5
$FeOH^{2+}$	−229.4	−324.7
$Fe(OH)^+_2$	−438	
$Fe(OH)_{2(s)}$	−486.6	−569
$Fe(OH)_{3(s)}$ (amorph.)	−699	
α-FeOOH (goethite)	−488.6	−559.3
α-Fe_2O_3 (hematite)	−742.7	−824.6
Fe_3O_4 (magnetite)	−1012.6	−1115.7
$FeCO_3$ (siderite)	−666.7	−737.0
FeS (pyrite)	−160.2	−171.5
FeS_2 (marcasite)	−158.4	−169.4
Lead (Pb)		
Pb^{2+}	−24.39	−1.67
$PbOH^+$	−226.3	
$Pb(OH)^-_3$	−575.7	
$Pb(OH)_{2(s)}$	−452.2	
$PbO_{(s)}$	−187.9	−217.3
$PbO_{2(s)}$	−217.4	−277.4
$PbS_{(s)}$	−98.7	−100.4
$PbCO_{3(s)}$	−625.5	−699.1
$PbSO_{4(s)}$	−813.2	−920

Continued

Cont'd

Substance	G_f°	H_f°
	$(kJ\ mol^{-1})$	$(kJ\ mol^{-1})$
Magnesium (Mg)		
Mg^{2+}	−454.8	−466.8
$MgOH^+$	−626.8	
$Mg(OH)_{2(aq)}^0$	−769.4	−926.8
$Mg(OH)_{2(s)}$ (brucite)	−833.5	−924.5
Manganese (Mn)		
Mn^{2+}	−228.0	−220.7
$Mn(OH)_{2(s)}$	−616	
Mn_3O_4 (hausmannite)	−1281	
α-MnOOH (manganite)	−557.7	
$MnO_{2(s)}$ (pyrolusite)	−465.1	−520.0
$MnCO_3$ (rhodochrosite)	−816.0	−889.3
Mercury (Hg)		
Hg_2^{2+}	153.6	172.4
Hg^{2+}	164.4	171.0
$HgOH^+$	−52.3	−84.5
$Hg(OH)_{2(aq)}^0$	−274.9	−355.2
HgO_2^-	−190.3	
$HgCl^+$	−5.44	−18.8
$HgCl_{2(aq)}^0$	−173.2	−216.3
$HgCl_3^-$	−309.2	−388.7
$HgCl_4^{2-}$	−446.8	−554.0
Nitrogen (N)		
$N_2O_{(g)}$	104.2	82.0
$NH_{3(g)}$	−16.48	−46.1
$NH_{3(aq)}$	−25.57	−80.29
NH_4^+	79.37	−132.5
$HNO_{2(aq)}$	−42.97	−119.2
NO_2^-	−37.2	−104.6
$HNO_{3(aq)}$	−111.3	−207.3
NO_3^-	−111.3	−207.3
Nickel (Ni)		
Ni^{2+}	−45.6	−54.0
$NiO_{(s)}$	−211.6	−239.7
$NiS_{(s)}$	−86.2	−84.9

Cont'd

Substance	G_f°	H_f°
	$(kJ\ mol^{-1})$	$(kJ\ mol^{-1})$
Oxygen (O)		
$O_{2(aq)}$	16.32	−11.71
$O_{3(g)}$	163.2	142.7
OH^-	−157.3	−230.0
Phosphorus (P)		
PO_4^{3-}	−1018.8	−1277.4
HPO_4^{2-}	−1089.3	−1292.1
$H_2PO_4^-$	−1130.4	−1296.3
$H_3PO_{4(aq)}$	−1142.6	−1288.3
Sulfur (S)		
$SO_{2(g)}$	−300.2	−296.8
$SO_{3(g)}$	−371.1	−395.7
$H_2S_{(g)}$	−33.56	−20.63
$H_2S_{(aq)}$	−27.87	−39.75
HS^-	12.05	−17.6
S^{2-}	85.8	33.0
HSO_3^-	−527.8	−626.2
SO_3^{2-}	−486.6	−635.5
$H_2SO_{3(aq)}$	−537.9	−608.8
HSO_4^-	−756.0	−887.3
SO_4^{2-}	−744.6	−909.2
Silicon (Si)		
$Si(OH)_{4(aq)}$	−1316.7	−1468.6
SiO_2 (amorphous)	−850.73	−903.49
SiO_2 (α, quartz)	−856.67	−910.94
SiO_2 (α, cristobalite)	−855.88	−909.48
SiO_2 (α, tridymite)	−855.29	−909.06
Sliver (Ag)		
Ag^+	77.12	105.6
$AgBr_{(s)}$	−96.9	−100.6
$AgCl_{(s)}$	−109.8	−127.1
$AgI_{(s)}$	−66.2	−61.84
$Ag_2S_{(s)}$	−40.7	−29.4
$AgOH^0_{(aq)}$	−92	
$Ag(OH)_2^-{}_{(aq)}$	−260.2	
$AgCl^0_{(aq)}$	−72.8	−72.8
$AgCl_2^-$	−215.5	−245.2

Cont'd

Substance	G_f° (kJ mol^{-1})	H_f° (kJ mol^{-1})
Zinc (Zn)		
Zn^{2+}	−147.0	−153.9
$ZnOH^+$	−330.1	
$Zn(OH)_{2(aq)}^0$	−522.3	
$Zn(OH)_3^-$	−694.3	
$Zn(OH)_4^{2-}$	−858.7	
$Zn(OH)_{2(s)}$	−553.2	−641.9
$ZnCl^+$	−275.3	
$ZnCl_{2(aq)}^0$	−403.8	
$ZnCl_3^-$	−540.6	
$ZnCl_4^{2-}$	−666.1	
$ZnCO_3$ (smithsonite)	−731.6	−812.8

*The data in this appendix have been compiled (with one exception noted below) from a more extensive appendix in Stumm, W., and J. J. Morgan, 1996, *Aquatic chemistry*, 3rd ed., Wiley-Interscience, New York. Stumm and Morgan compiled the data primarily from four sources: (1) Wagman, D. D., et al., Selected values of chemical thermodynamic properties, U.S. National Bureau of Standards (now NIST), Tech. Notes 270-3 (1968), 270–4 (1969), 270–5 (1971); (2) Robie, R. R., et al., Thermodynamic properties of minerals and related substances at 298.15 K and 1 bar (10^5 Pascals) pressure and at higher temperatures, U.S. Geol. Surv. Bull. No. 1452, Washington, D.C. (1978); (3) Bard, A. J., et al., *Standard potentials in aqueous solution*, Marcel Dekker, New York (1985); and (4) in a few cases, unspecified other sources. The value given here for CaO is from Garrels, R. M., and C. L. Christ, *Solutions, minerals and equilibria*, Harper & Row, New York (1965). Errors caused by the difference in reference pressure between 1 bar and 1 atm (1 bar = 0.987 atm) are negligible, but Stumm and Morgan noted that the quality of the original data is highly variable and they did not claim to have critically selected the "best" data. Values for oxides and (hydr)oxides of Fe^{III} are particularly uncertain and depend on the method of preparation and age of the surfaces. One should not expect that using the G_f° values listed here to calculate an equilibrium constant will yield the exact values reported in the text, in the MINEQL+ database, or in other sources.

Subject Index

Absorptivity (ϵ_λ), 643–645, 647, 648, 657, 695
Acetic acid, 156, 232–235, 237, 238, 258, 269
Acetylene, structure, 191
    block, method, 611
Acids and bases, 32, 50, 268–305
    acidity constants, 32, 212, 213, 612,
        614, 616
    acid/base neutralizing capacity
        (ANC/BNC), 282–284, 302
    amphiprotic and amphoteric, 33, 522
    Arrhenius concept, 269
    Brønsted concept, 32, 269–271
    buffering capacity/intensity, 277, 282,
        283, 302
    carbonate system, 33, 222–229, 283,
        284, 292–295
    carboxylic, 24, 37, 194, 209–211
    catalysis, 182, 183
    conjugate acid-base pairs, 269–270
    diprotic systems, 229–231, 250, 251
    hard and soft, 317–319, 323, 369
    ion product of water, 33, 268, 269
    ionization fraction (α), 228–232, 292, 298
    kinetics, 32, 81, 174, 304–305
    Lewis concept, 269–271
    organic compounds, 727–730
    metal ions as acids, 270
    polyprotic, 229

    strength, 32, 271, 272
    strong acids and bases, 271
    titrations, 276–282, 285–287
    weak, 271
    weathering as acid-base reaction, 49,
        301, 589
Acid sensitive lakes, 289, 291, 302, 578, 582
Acid mine drainage, 302
Acid rain, 47, 49, 299, 302
Acidity, mineral and CO_2, 289, 290
    Constants. *See* Equilibrium, constants,
        acidity
    metal oxidation, effects of, 301
Actinometer, chemical, 658, 744
Activated carbon, 532, 533, 678
Activated complex, 175, 176
Activation energy, 167–169, 487, 565,
    571, 638
    enthalpy of activation, 177, 178, 184
    entropy of activation, 177–180, 184
    free energy of activation, 177–178,
        184, 395
Activity, 31, 94, 117–119
    and chemical potential, 94
    definition, 31
    and fugacity, 117, 118
    and ion association model, 126, 128
    and ionic strength, 119–129, 132